Practical Medicinal Chemistry with Macrocycles

Practical Medicinal Chemistry with Macrocycles

Design, Synthesis, and Case Studies

Edited by

Eric Marsault

University of Sherbrooke
Sherbrooke, Quebec, Canada

Mark L. Peterson

Cyclenium Pharma Inc.
Montreal, Quebec, Canada

WILEY

Contents

Foreword

Cyclic structures have always fascinated artists and scientists. In chemistry, the restriction of conformational space by cyclization has stimulated and inspired the understanding of three-dimensional molecular structure and the development of new shapes and entities. When our laboratory started research on conformational analysis of peptides about 40 years ago, we soon realized that the high flexibility of linear peptides results in a complex mixture of conformations. Cyclic peptides are conformationally more restricted and accordingly topologically more defined, and when their structures mimic receptor-interacting conformations, they become not only super-active but also selective for different receptor subtypes.

Nature has used these principles as well. Many biologically important peptides are macrocycles, which possess not only high affinity, but also relatively high stability against enzymatic degradation, and some are even orally available. The simultaneous optimization of synthetic ligands for both activity and bioavailability has become an exciting goal, which is often reached in a stepwise procedure where first activity is optimized; then chemical modifications are introduced to increase oral bioavailability. One successful example of this approach is the conversion of a cyclic hexapeptide with somatostatin activity into a derivative with oral availability *in vivo* via multiple N-methylations while retaining its biological activity. To my knowledge, the reverse process—using an orally permeable scaffold and introducing functionalities required for biological function—has not been achieved yet. Many groups in the world are investigating cyclic scaffold models to understand their intestinal permeability, but their simultaneous functionalization to interact with a biological target remains to be realized.

Above and beyond peptides, many organic molecules form macrocycles with interesting biological properties. It is both surprising and limiting that scientists engaged in non-peptidic macrocycles and peptidic macromolecules live in different scientific worlds and do not exchange information more extensively. Recently, finally, the two communities are joining forces through the rising interest in therapeutic compounds that go beyond Lipinski's rule of five (the so-called bRo5, or beyond Rule of five, compounds). This empirical rule, which segregates compounds with molecular weight above 500 out of the oral bioavailability zone, was derived from a comprehensive study of orally available drugs. An alternative rule by Veber *et al.* added another important property, that is, the importance of rigidity in a molecule. Nevertheless, a "freely rotatable bond" is difficult to define, particularly in the context of macrocycles, where endocyclic bonds are not fully free to rotate but definitely more flexible than in smaller rings. We know that barriers to internal rotations or inversions vary strongly depending on the structural context. Both of the previous rules have been utilized as exclusive criteria in drug development and greatly reduced the interest of the pharmaceutical industry in macrocycles, at least for peptides, for a long period.

However, research in macrocyclic chemistry continued to advance in synthetic methods, conformational studies, and investigation of their role for controlling biological functions. Finally, very recently, the pharmaceutical industry rediscovered macrocycles. It was realized that such molecules not only open new areas for pharmacological treatment of diseases, but also raise hope that some of the problems in their stability and bioavailability might be overcome. Nature has shown us that molecules with sizes between proteins and small molecules can be orally available and, importantly, that this size range is a particularly good fit for targets requiring extended surface areas exemplified by protein–protein interactions. In addition, the criterion of oral availability is not an absolute requirement since more and more drug products are effectively administered by other routes. Indeed, pharmacists know very well that oral administration is not always the best choice since intestinal uptake can strongly vary as a function of patient and situation. As a result, accurate dosage control is more difficult.

Inspiration for new drug molecules often comes from natural compounds, such as secondary metabolites in living organisms that are bioavailable to be efficacious, as well as from regulatory proteins interacting with other

biomolecules. Peptide chemists realized long ago that loop regions in proteins, because of their exposed spatial arrangement (rigidity), are often critical determinants of interaction with other biomolecules and that these loops can be mimicked by cyclic peptides. Conformational control in cyclic peptides can be achieved by introduction of D-amino acids at distinct positions. Similarly, nature and medicinal chemists often modulate the conformation of non-peptides by controlling chirality at certain positions.

Increasing knowledge in biochemical pathways that control physiological conditions or disease states increases the demand for interference by medium-sized molecules like macrocycles. Compared to small molecules, medium-sized entities offer new ways to interact with protein–protein interaction surfaces. Hence, we are looking into an exciting future that will fill the gaps in medicinal applications, with macrocycles already positioned as privileged structures in this regard.

As a result, this book has collected a number of exciting contributions written by experts in the field of macrocycles. It is very timely in light of the aforementioned interest in macrocycles and covers a broad range of topics. These include chemical and biological synthesis, diversity generation, challenges specific to macrocycles, conformational analysis, design and realization of constraints for medium-sized molecules, and multiple examples of therapeutic applications of various classes of macrocycles.

The principles and the dimensions covered in this book on macrocycles, owing to their universal nature and to the practical way they are addressed, are also very relevant for medicinal chemistry applied to other classes of molecules. As a result, I feel this book should belong in the personal library of all medicinal chemists.

(NB: References to the concepts and works cited previously can be found all along the various chapters covered by this book.)

Prof. Dr. Horst Kessler
Institute for Advanced Studies and
Center for Integrated Protein Science
Department of Chemistry
Technische Universität München
Munich, Germany

Introduction

Macrocycles are Great Cycles. This was the title of a review we wrote in 2011 to reflect the increasing attention being then given by medicinal chemists toward this unique compound class. Six years later, the interest has only grown, which strongly indicates that the macrocycle field is not just another trend that becomes hot, generates frenetic activity, then rapidly vanishes or dissipates into irrelevance—quite the contrary. Macrocycles of very diverse chemical classes continue to generate a high level of interest from the drug discovery community, with an impressive number already in or entering the clinic. When we started working over 15 years ago at one of the pioneering companies in this area, NéoKimia (later Tranzyme Pharma), formed to realize the vision of Prof. Pierre Deslongchamps regarding libraries of conformationally defined and chemically diverse macrocyclic molecules, there was only one other company (Polyphor) primarily focused on using macrocycles for drug discovery purposes, and few academics had research focused on these structures. At the time, we met with considerable skepticism that such molecules could ever be effective synthetic drugs. Now, that situation has changed dramatically, with over 30 companies involved in pursuing macrocycles as a key aspect of their R&D, while the number of scientific papers on the topic has exploded. As a result, we felt it would be very timely to assemble a reference book on the medicinal chemistry of macrocycles. From the onset, we wanted this to be a practical guide targeting both experts and their teams, as well as neophytes.

Accordingly, this book is directed to both scientists engaged in drug discovery with macrocycles and those contemplating the use of macrocycles yet have no previous experience with this chemical class. We did not cover allied topics in macrocyclic chemistry, even if they could have some pharmaceutical relevance, including molecular recognition, supramolecular architectures, host–guest molecules, metal chelators, or chromatographic stationary phases.

Macrocycles actually are, in several ways, a polarizing molecular class. On the one hand, they attract researchers for their extraordinary potential to tackle difficult targets, their versatility as scaffolds for diversity generation, and the multiple opportunities they provide to optimize lead compounds. On the other hand, macrocycles can elicit untoward feelings because of notions—often outdated—on the challenges of synthesis, scale-up, diversification, or optimization of drug-like properties. Granted, macrocycles are often more synthetically challenging than traditional small molecules yet have definitely proven their worth to tackle difficult pharmacological target classes. In that sense, macrocycles can be considered as "high hanging molecules for high hanging targets."

In this volume, we have aimed to capture the important aspects of macrocycles as they pertain to medicinal chemistry. This ranges from critical challenges inherent to the class, to an analysis of the various subclasses of macrocycles and where they currently fit in drug discovery, through proven or exploratory methods to make and characterize them, and, finally, to further stimulate ideas of scientists interested in macrocycle drug discovery, several case studies from diverse compound classes and therapeutic indications. Throughout the preparation, we pressed individual authors to keep their contributions as hands-on and practical as possible—within the context of a reference book—to serve as a valuable information source or starting point depending on the reader's objectives. As a result, the book is separated into four main sections.

Part I focuses on challenges specific to macrocycles. The goal is to communicate what makes macrocycles special or distinctive in the context of drug discovery. In Chapter 1, Zaretsky and Yudin single out critical aspects related to the key transformation inherent in the synthesis of all macrocycles, that is, the cyclization process. The fact that this reaction is unimolecular brings significant challenges but also many opportunities. In Chapter 2, Craik, Kaas, and Wang give a detailed, hands-on description of the methods available to characterize and elucidate the structure of macrocycles, largely inspired from their extensive works on natural

macrocyclic peptides, which have been structurally elucidated, synthesized, and diversified in all forms and sizes. Finally, in Chapter 3, Price, Mathiowetz, and Liras share their expertise, and that of their broad network of academic collaborators, on the current understanding of permeability and oral absorption of macrocycles and the ways to improve these important properties. This has been—and remains—an area of intense investigation in an effort to "crack the code," assuming there is one, of structure–permeability relationships in macrocycles. These works relate mostly to macrocyclic peptides and have been the genesis of efforts to understand what is now commonly known as the beyond-Rule-of-5 (bRo5) class.

Part II is devoted to covering the main chemical classes of macrocycles and their potential in drug discovery, as these constitute the knowledge base for medicinal chemists and the starting points of their future efforts. In Chapter 4, this begins with naturally inspired macrocycles by Wessjohann, Bartelt, and Brandt. Chapter 5, from Bockus and Lokey, is devoted to macrocyclic peptides, which constitute one of the two main classes of macrocycles from natural and unnatural origins. Since diversity generation is an integral tool in drug discovery, with high-throughput screening of compound libraries providing the initiation point for most projects, we subsequently move to two chapters specifically aimed at exploring and expanding the chemical diversity of macrocycles. In Chapter 6, Qian, Dougherty, and Pei describe existing chemical approaches to macrocycle libraries. Vitali and Fasan in Chapter 7 then extensively review hybrid chemistry/biology strategies used for diversity generation. Indeed, these approaches, despite limitations inherent to the biological machinery employed, have exploded the numbers of compounds accessible and become a rapidly evolving mainstream method for massive diversity generation. Finally, in Chapter 8, Leitch and Tavassoli expand on the role of macrocycles specifically as modulators of protein–protein interactions (PPI), a target class for which small molecules have generally performed poorly and for which macrocycles have emerged as privileged scaffolds owing to their unique combination of large molecular surface area, conformational restriction, and spatial display of pharmacophores.

Part III, the synthetic toolbox, makes available to the reader the many and diverse synthetic methods useful to construct macrocycles. In Chapter 9, Biron, Vézina-Dawod, and Bédard describe the various methods for making macrocyclic peptides. Gaddam, Mallurwar, Konda, Khatravath, Aeluri, Mitra, and Arya exemplify in Chapter 10 the use of ring-closing metathesis (RCM), a method that nowadays needs no introduction since it became the subject of the Nobel Prize in Chemistry in 2005, to build specific pharmacologically relevant structural types of macrocycles investigated in their myriad synthetic efforts toward diversity generation. Owing to the numerous excellent reviews and books devoted to RCM, we decided not to provide yet another review on the topic here but rather to exemplify the actual use of RCM in diversity generation. In Chapter 11, Pehere and Abell describe Huisgen cycloadditions in the context of macrocyclization. Subsequently, Ronson, Unsworth, and Fairlamb describe the various and versatile Pd-catalyzed approaches employed for the synthesis of macrocycles in Chapter 12, whereas in Chapter 13, Santandrea, Bédard, de Léséleuc, Raymond, and Collins summarize the numerous other strategies used to make macrocycles. As a testimony to chemists' creativity, this chapter presents a broad range of methods, leading to a wealth of macrocyclic structures. In Chapter 14, Wessjohann, Neves Filho, Puentes, and Morejón relate several multicomponent reactions (MCR) applied to the macrocyclization reaction. Finally, since efficient large-scale synthesis is one of the limiting steps to advance compounds into clinical development and macrocycles were perceived, at least 15 years ago as we recounted earlier, as molecules too difficult to prepare to be exploited as pharmaceutical agents, Kong presents in Chapter 15 several methods successfully applied to macrocycle synthesis at manufacturing scale. Although a number of these are proprietary and the subject of carefully guarded know-how, this chapter exemplifies how creative synthetic methods can deliver multi-kilogram quantities of macrocycles.

Finally, Part IV is dedicated to case studies of macrocycles in clinical development or approved as drugs. In Chapter 16, as an introduction to this section, Stotani and Giordanetto summarize the various classes of macrocycles and the individual compounds of each in clinical development. In Chapter 17, Terrett relates the discovery of XIAP antagonists stemming from DNA-encoded technologies. In Chapter 18, Yamazaki, Lam, and Johnson then share their experience in the discovery of lorlatinib, an inhibitor of the ALK kinase able to tackle resistant forms of the kinase, including those found in brain metastases. In Chapter 19, Hoveyda, Fraser, Marsault, Gagnon, and Peterson provide a detailed account of the efforts leading to TZP-102, a ghrelin receptor agonist for the treatment of hypomotility disorders. Finally, in Chapter 20, Pereira, Wu, Majuru, Schneider, and Pradeep describe the research that led to the identification of solithromycin, a very interesting example of a macrocyclic natural product derivative optimized through semisynthesis. The experienced reader will notice that no chapter is devoted to one of the targets that has benefited most from the particular attributes of macrocycles and provided the largest number of macrocyclic development candidates, that is, the hepatitis C virus NS3/4A protease. Similarly to RCM,

this has been covered extensively in previous reviews; thus, we made an editorial choice not to do so yet again. By no means does this indicate a lack of relevance of this particular inhibitor class, which has been one of the initial and most fertile playgrounds of macrocycle drug discovery. Readers are instead referred to the abundance of existing publications on the topic.

As editors, we gave individual authors considerable freedom to express their creativity within the themes that were entrusted to them, delve into their own experiences—good and bad—and provide the reader with hands-on examples and make choices for what was most relevant to their topic. As a result, some examples may be cited in more than one chapter, which is more a testimony to the broad impact of some works across various dimensions of macrocycle drug discovery, rather than simple editorial redundancy.

We sincerely hope that this book will prove useful and instructive for a broad variety of individuals, from novices looking to understand the ins and outs of macrocycle drug discovery to experienced practitioners willing to expand their knowledge on specific aspects of this exciting field.

Finally, we wish to sincerely thank all the coauthors who devoted numerous hours of their precious time and generously shared their knowledge and expertise on this stimulating topic. The book is the result of their collective hard work and dedication.

About the Contributors

Andrew D. Abell

Dr. Abell graduated from the University of Adelaide with B.Sc. (Hon) and Ph.D. degrees and then undertook a postdoctoral fellowship at the University of Cambridge. He held a professorship at the University of Canterbury before returning to the University of Adelaide in 2007, where he is currently a professor of chemistry and node director of the ARC Centre of Excellence for Nanoscale BioPhotonics. His research interests are concerned with understanding the fundamental link between the chemical structure and shape of key bioactive molecules and their biological function. While his work is very much driven by fundamental science, he has always had a keen interest in pursuing associated commercial opportunities. The seed for this was sown with a sabbatical leave working as a visiting scientist, consultant, and senior Fulbright fellow with SmithKline Beecham (now GSK) in Philadelphia. In Australia, he co-founded an Adelaide-based company (Calpain Therapeutics) to develop macrocyclic protease inhibitors as a potential treatment for cataract and other conditions. He served as the Head of School of Chemistry and Physics at the University of Adelaide and is a recent recipient of the Royal Australian Chemical Institute Adrien Albert Prize and the Alexander R. Matzuk Prize and Lecture in Drug Discovery (Baylor College of Medicine, Houston).

Madhu Aeluri

Madhu Aeluri was born in Telangana, India, in 1987. He completed his B.Sc. in 2007 and M.Sc. with specialization in organic chemistry in 2009 from Osmania University. He obtained his Ph.D. in chemistry in 2014 from the University of Hyderabad under the guidance of Professor Prabhat Arya at Dr. Reddy's Institute of Life Sciences (affiliated to University of Hyderabad). After the completion of his doctoral studies, he served as an associate scientific officer at GVK Biosciences Pvt Ltd., Hyderabad, for 2 years. Currently, he is working as a postdoctoral fellow in Professor Prabhat Arya's research group. His research interests are the synthesis of natural product-inspired and natural product-derived small molecules hunting for small molecule modulators of protein–protein interactions.

Prabhat Arya

Prabhat Arya was born in 1958 and grew up on the University of Delhi campus where he received his undergraduate and graduate training. Following postdoctoral tenures at Cambridge and McGill Universities, he joined the National Research Council of Canada in Ottawa and worked with this organization for nearly 20 years. Later, he also had a short stint at the Ontario Institute of Cancer Research helping build the Medicinal Chemistry Program. In July 2009, he decided to follow an adventurous path and moved back to India with the objectives of establishing an integrated chemical biology program and thoroughly connecting his academic program to society and the business world. For him, this has been an exciting journey and a good learning path so far. He enjoys spending time with students and teaching *Stereoselective Organic Synthesis* to a wider audience in India. Overall, his research is focused on developing synthesis methods that allow building a chemical toolbox with compounds that are closer to bioactive natural products. These compounds can be classified as natural product-inspired and hybrid natural products. The ultimate interest is in addressing challenging biological questions related to protein–protein interactions and pathways with an extensive use of small molecules emerging from his group. Prior to moving back to India (*that he does not regret so far*), he was also an adjunct professor at the

Department of Biochemistry of McGill University, OHRI in Ottawa, and the Department of Chemistry and the Department of Biochemistry, Microbiology and Immunology of the University of Ottawa.

Richard Bartelt

Richard Bartelt was born in Wilhelm-Pieck-Stadt Guben, Germany, in 1987. He studied biochemistry at the Martin Luther University Halle-Wittenberg, received his bachelor's degree in 2011 on the topic of "3D-QSAR of Substrates of the Human Amino Acid Transporter hPAT2," and continued his studies until 2014. Under the supervision of Prof. Wessjohann and docent Dr. Brandt, he prepared his master's thesis—"Homology Modelling of Prenylating Enzymes and Elucidation of Their Catalytic Mechanism"—at the Department of Bioorganic Chemistry, Leibniz Institute of Plant Biochemistry (IPB), Halle. Since then, he has focused on chemoinformatic analyses of macrocycles in the same research group.

Anne-Catherine Bédard

Anne-Catherine Bédard was born in Québec, Canada, in 1987. She received her B.Sc. in Biopharmaceutical Sciences from the University of Ottawa in 2010 and her Ph.D. from the Université de Montréal under the supervision of Prof. Shawn K. Collins in 2015. She is currently an NSERC postdoctoral fellow in the laboratories of Prof. Tim F. Jamison at MIT.

François Bédard

François Bédard has completed a B.Sc. in Biochemistry and an M.Sc. in Pharmaceutical Sciences at Université Laval. He then commenced his Ph.D. studies in pharmaceutical sciences under the guidance of Prof. Éric Biron and Prof. Ismail Fliss at the Institute of Nutraceuticals and Functional Foods at Université Laval in 2014. As a Fonds de recherche du Québec – Nature et technologies (FRQNT) scholar, he is currently working on the synthesis, characterization, and pharmacokinetic studies of antimicrobial peptides from the bacteriocin family. His research interests include the synthesis and applications of natural cyclic peptides with antimicrobial activities and the design and development of antimicrobial peptide mimetics.

Éric Biron

Éric Biron obtained his Ph.D. in Chemistry under the direction of Prof. Normand Voyer at Université Laval, Canada, on the design and synthesis of functional peptidic nanostructures as artificial ion channels and DNA intercalators. After his Ph.D. in 2003, he moved to the Technische Universität München in the laboratory of Prof. Horst Kessler as a postdoctoral Alexander von Humboldt fellow. During his stay, he worked on the synthesis of N-methylated peptide macrocycles and studied the effects of multiple N-methylations on the conformation and activity of bioactive cyclic peptides. Upon conclusion of his postdoctoral studies, he returned to Québec and joined the Faculty of Pharmacy at Université Laval as a junior research scholar from the Fonds de recherche du Québec en Santé (FRQS). His research program focuses on the design and synthesis of cyclic peptides and macrocyclic peptidomimetics with antimicrobial activities and the development of new strategies to prepare and screen combinatorial macrocycle libraries. Prof. Biron is currently an associate professor at the Faculty of Pharmacy of Université Laval and a researcher at the Laboratory of Medicinal Chemistry at the Centre de recherche du Centre hospitalier universitaire de Québec in Québec City, Canada.

Andrew T. Bockus

Andrew T. Bockus earned his B.A. in Chemistry from Skidmore College in 2008 where he engaged in enzymology research with Professor Michelle Frey. In the following year as an instructor of English at China University of Petroleum in Beijing, Andrew joined the lab of Professor Scott Lokey at the University of California, Santa Cruz, to study the structure–permeability relationships of cyclic peptides, completing

his Ph.D. in 2015. He continued his academic career postdoctoral work at Trinity University, where he taught undergraduate courses and studied the molecular recognition of peptides and proteins by synthetic hosts under the guidance of Professor Adam Urbach. Andrew currently works on the development of cyclic peptide therapeutics at Circle Pharma, Inc.

Wolfgang Brandt

Wolfgang Brandt studied chemistry at the Martin Luther University Halle-Wittenberg in Halle (Germany), where he received his degree in Chemistry in 1979 and his Ph.D. in 1982 for studies on "structure–activity relationships of auxins" under the supervision of Professor Alfred Barth. From 1985 to 1986, he was a scientific coworker at the Institute of Neurobiology and Brain Research Academy of Science of the GDR (then East Germany) in Magdeburg. In 1987, he became head of the research group "Molecular Modeling—Drug Design" at the Department of Biochemistry/Biotechnology of the University of Halle. In 1992, he was on sabbatical leave at the Clinical Research Institute of Montreal, Canada (Prof. Dr. P. W. Schiller). He received his "Habilitation" (Asst. Prof.) in 1997. In August 2001 he moved to the Department of Bioorganic Chemistry headed by Prof. Ludger Wessjohann at the Leibniz Institute of Plant Biochemistry in Halle as a group leader for computational chemistry. His research interests cover all fields of computational chemistry and molecular modeling. He has published over 170 scientific papers, books, and some licensed patents.
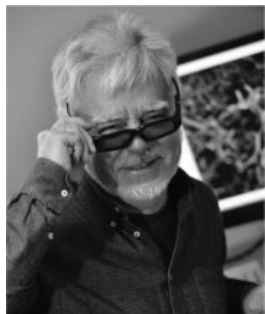
Shawn K. Collins

Shawn K. Collins obtained a B.Sc. degree from Concordia University in 1996 and his Ph.D. at the University of Ottawa (Prof. A. G. Fallis) in 2001. After an NSERC postdoctoral fellowship with Professor L. E. Overman (University of California, Irvine), he joined the faculty at Université de Montréal in September 2003 and was promoted to Full Professor in 2015. Professor Collins' research group is interested in the development of novel synthetic methods, particularly involving catalysis, photochemistry, and continuous flow methods.

David J. Craik

David J. Craik obtained his Ph.D. in Organic Chemistry from La Trobe University in Melbourne, Australia, and undertook postdoctoral studies at Florida State and Syracuse Universities before taking up a lectureship at the Victorian College of Pharmacy in 1983. He was appointed Professor of Medicinal Chemistry and Head of School in 1988. He then moved to University of Queensland in 1995 to set up a new biomolecular NMR laboratory and is currently an NHMRC senior principal research fellow and group leader in IMB. His research focuses on applications of circular proteins, toxins, and NMR in drug design. He is also a fellow of the Australian Academy of Science and has received numerous awards for his research, including the Ralph F. Hirschmann Award from the American Chemical Society. He is an author of more than 600 scientific papers and has trained 60 Ph.D. students.

Patrick G. Dougherty

Patrick G. Dougherty completed his B.S. in Chemistry and Biochemistry at Florida State University in 2013. He joined the Pei group at the Ohio State University in 2014. His research currently focuses on integrating chemical biology and computational chemistry approaches for macrocyclic drug discovery and lead optimization against therapeutically relevant intracellular PPIs.

Ian J. S. Fairlamb

Ian J. S. Fairlamb was appointed as lecturer in York in 2001, following a Ph.D. with Dr. J. M. Dickinson in Manchester (1996/1999) and postdoctoral research with Prof. G. C. Lloyd-Jones in Bristol (2000/2001). He was a Royal Society URF (2004/2012) and promoted to Full Professor in 2010. He leads a talented research group interested in catalysis, mechanism, and synthesis. Recent work includes Pd and Mn catalyst and

ligand design, involvement of higher-order Pd species (e.g., nanoparticles), and exploitation of mechanistic understanding in purine and amino acid C–H functionalization. He has interests in the application of Pd and Au catalysis in macrocyclic ring synthesis, for example, phacelocarpus 2-pyrone A.

Rudi Fasan

Rudi Fasan was born in Italy and studied pharmaceutical chemistry at the University of Padua, where he received his undergraduate degree (B.S.) with the highest honors in 1999. In 2001, he joined the group of Prof. John A. Robinson at the University of Zurich (Switzerland) as a graduate student, working on the design and synthesis of beta-hairpin protein epitope mimetics. In 2005, he joined Prof. Frances H. Arnold's group at the California Institute of Technology as a Swiss National Science Foundation postdoctoral fellow, working on the directed evolution of P450 enzymes for alkane oxidation. Dr. Fasan began his independent career as a member of the Department of Chemistry of the University of Rochester in 2008 and was promoted to the rank of Associate Professor in 2014. His research interests lie in the area of bioorganic chemistry, chemical biology, protein engineering, biocatalysis, and chemoenzymatic synthesis. His research group currently focuses on the synthesis, evolution, and application of macrocyclic peptides and organo-peptide hybrids for targeting and modulation of cancer-related protein–protein interactions and on the design and investigation of engineered and artificial metalloenzymes for selective late-stage C–H functionalization and for asymmetric synthesis of carbon–carbon and carbon–heteroatom bonds. His awards include a Swiss National Science Foundation Graduate Fellowship (2001–2005) and Postdoctoral Fellowship (2005–2007), the 2007 Friedrich-Weygand Outstanding Graduate Research Award, University of Rochester's Multidisciplinary Research Award (2011) and University Award (2016), and the 2014 Tetrahedron Young Investigator Award for Bioorganic and Medicinal Chemistry.

Graeme L. Fraser

Graeme L. Fraser has more than 20 years of industry experience in both management and technical positions. Previously, Graeme was V.P. of Drug Discovery at Tranzyme Pharma (Sherbrooke, Canada) where he led the discovery and preclinical development activities for a pipeline of GPCR-small molecule programs. Earlier, he managed preclinical development activities at Viron Therapeutics Inc. (London, Canada) and led specific GPCR target validation activities at Astra Pain Control AB (Södertälje, Sweden, and Montreal, Canada). In total, he has directed research activities for three products currently in clinical development. Graeme received a Ph.D. from McGill University (Montreal, Canada) and is an author of over 50 publications and research abstracts, including 9 patents and 2 IND filings.

Jagan Gaddam

Jagan Gaddam was born in Telangana, India (1984). He was awarded a bachelor's degree in life sciences from Osmania University, Hyderabad (2005) and a master's degree in organic chemistry (2008) from Kakatiya University. He joined Professor Prabhat Arya's research group in 2011 at Dr. Reddy's Institute of Life Sciences of the University of Hyderabad for doctoral studies. His research interests are in the synthesis of natural product-inspired macrocycles and in building natural product-derived macrocyclic toolbox. His Ph.D. research is mainly focused on stereoselective synthesis of neopeltolide-inspired macrocycles.

René Gagnon

René Gagnon earned his Ph.D. in Organic Chemistry in 1993 from University Laval (Québec). He then joined the team of Stanley M. Roberts at University of Exeter (United Kingdom) as a postdoctoral fellow working on enzymatic catalyze in organic synthesis. In 1995, at the Armand-Frappier Institute, he was implicated in biosynthesis studies on taxol and related analogues. He moved in 1996 to Sherbrooke to be part of Prof. Pierre Deslongchamps team. In 1998, he was mandated to build the analytical group of a new promising drug discovery company called Neokimia (founded by Prof. Deslongchamps). He was appointed in 2003 as head manager of the analytical division of Tranzyme Pharma (resulting from the Tranzyme and Neokimia merger). Over the years, he was implicated in various fields related to drug

discovery, such as chemical library analysis, drug substance and drug product analysis, pharmacokinetic and stability studies, and purification and formulation of chemical entities. From 2007 to 2011, he was an associate professor at the genetic biomedical department of the CHUS working on pediatric diseases. From 2011 to 2015, he managed the mass spectrometry facility at the Chemistry Department of the University of Sherbrooke, where, since 2015, he joined its steering committee and also became the manager of the teaching laboratories.

Fabrizio Giordanetto

Fabrizio Giordanetto graduated with first-class honors in medicinal chemistry in 2000 from the University of Genova (Italy). He completed his Ph.D. in Computational Medicinal Chemistry in 2003 at the University of London (United Kingdom) while working for the chemistry unit of Pharmacia (Pfizer) in Nerviano (Italy). In 2004, he joined the Medicinal Chemistry Department of AstraZeneca in Mölndal (Sweden) where he grew professionally to the position of Principal Scientist and Preclinical Project Leader. Since 2013, he has been Director of Medicinal Chemistry for Taros GmbH, a research-based SME in Dortmund (Germany), where he leads proprietary and third-party medicinal chemistry activities. During his career, he worked on several drug discovery projects resulting in multiple clinical candidates spanning oncology and cardiovascular indications and has more than 80 peer-reviewed publications, book chapters, and international patents.

Hamid R. Hoveyda

Hamid R. Hoveyda obtained his Ph.D. from the University of British Columbia (Vancouver, Canada) followed by a stint at Harvard University as an NSERC postdoctoral fellow. He began his industrial career at the Affymax Research Institute (CA, USA) working on applications of diversity-oriented synthesis in drug discovery. In 2001, he joined Neokimia Inc. (Sherbrooke, Canada), which later became known as Tranzyme Pharma, where

he contributed initially to the platform HTS library technology and was subsequently in charge of lead optimization efforts across several projects including the ghrelin project that culminated in two clinical candidates (ulimorelin, TZP-102) as potential GI therapeutics. Since September 2007, he has led medicinal chemistry efforts on various GPCR targets at Euroscreen (Belgium) that has resulted, inter alia, in the discovery of ESN364 clinical candidate, an NK3R antagonist currently in phase IIa for the treatment of sex-hormone disorders. His scientific contributions thus far have been captured in over 50 publications and patents.

Ted W. Johnson

During his undergraduate studies at the University of California, Irvine, as a Chemistry major, Ted performed research under the direction of Professor Harold Moore where he worked on the synthesis of quinone antitumor/antifungal agents, completing the synthesis of nanaomycin D and making progress toward the total synthesis of griseusin A. He received his B.S. degree in Chemistry in 1994. During his graduate studies at the University of California–Los Angeles with Professor Michael Jung, he completed the total synthesis of 7-deoxy-xestobergsterol A, xestobergsterol A, and several potent antihistamine unnatural analogues. He simultaneously carried out synthetic studies toward the synthesis of eleutherobin, a potent antitumor compound. He was awarded the Saul Winstein Fellowship, the Gregory Research Fellowship, and the Distinguished First-Year Graduate Student Award. Ted received his Ph.D. in 1999. As an NIH postdoctoral fellow at Harvard University with Prof. E.J. Corey, Ted completed the total synthesis of putative pseudopteroxazole, a potent antituberculosis compound, showcasing an unprecedented diastereoselective intramolecular imidoquinone Diels–Alder reaction. During his studies and ongoing 15 years as a medicinal chemist at Pfizer in La Jolla, California, Ted published many high-profile patents and publications. He won the American Chemical Society Young Investigator Award in 2011 and the Pfizer Global Medicinal Chemistry Award in 2013. Most notably, he was the co-project leader of the ALK program and co-designed lorlatinib, which is currently a kinase inhibitor in phase 2 clinical trials for the treatment of ALK positive non-small cell lung cancer (NSCLC). Notably,

lorlatinib was designed to be potent against drug resistant mutants of ALK and also penetrate the central nervous system, a major challenge in kinase inhibitor space. Ted continues to work at Pfizer, La Jolla, in the Oncology Department.

Quentin Kaas

Quentin Kaas obtained his Chemical Engineering degree in 2001 from the École Nationale Supérieure de chimie de Montpellier (ENSCM) and his Ph.D. degree in chemical biology in 2005 from the University of Montpellier II. He conducted 1 year of postdoctoral research in the Laboratory of Immunoinformatics of Professor Marie-Paule Lefranc in Montpellier, studying antigen/receptor interactions. He was then awarded an Australian postdoctoral fellowship by the Australian Research Council to undertake 3 years of postdoctoral research on plant cyclic peptide structure–activity relationships in the laboratory of Professor David J. Craik at the Institute for Molecular Bioscience of the University of Queensland, Australia. He is currently working in that laboratory where he focuses on structural bioinformatics and computational modeling studies of toxins extracted from plants and animals. He has developed and currently maintains the only database specialized on sequences and structures of cone snail toxins, ConoServer (http://www.conoserver.orgMacrocyclesDavidCraikManuscript_revised.doc).

Mahender Khatravath

Mahender Khatravath was born in Telangana, India (1988). He received his B.Sc. degree from Osmania University in 2008 and M.Sc. degree with specialization in organic chemistry from M.N.R. P.G. College (affiliated to Osmania University) in 2010. He joined as a doctoral student at the Dr. Reddy's Institute of Life Sciences, University of Hyderabad, under the supervision of Professor Prabhat Arya and obtained his Ph.D. in Chemistry (2016). Currently, he is working as a national postdoctoral fellow under the supervision of Dr. Srinivasa Reddy at the National Chemical Laboratory, Pune. His research focuses on stereoselective synthesis of substructures of eribulin and related macrocyclic compounds.

Saidulu Konda

Saidulu Konda was born in Telangana, India (1985). He received his B.Sc. degree from Osmania University in 2007 and M.Sc. degree with specialization in organic chemistry from M.N.R. P.G. College (affiliated to Osmania University) in 2010. He received his Ph.D. degree from Hyderabad Central University in 2016. Presently, he is working as an associate scientist at GVK Biosciences Private Limited, Hyderabad.

Jongrock Kong

Jongrock Kong obtained his bachelor's degree from Sungkyunkwan University and master's degree from Pohang University of Science and Technology (POSTECH) in the Republic of Korea. In 2002, he started his graduate studies with Professor Michael J. Krische at the University of Texas at Austin, where he studied hydrogen-mediated reductive C–C bond formation. After the completion of his Ph.D. in 2007, he moved to Princeton University for a postdoctoral fellowship with Prof. David W. MacMillan and worked on enantioselective α-arylation of aldehyde via organo-SOMO catalysis. In 2009, he joined the Process Research Department at the Merck Research Laboratories in Rahway, NJ, where he has been focusing on the development of robust processes for drug candidates.

Justine L. Lam

Dr. Justine L. Lam is a senior principal scientist at Pfizer Worldwide Research and Development in the department of pharmacokinetics, dynamics and metabolism (San Diego, CA). She received her Ph.D. degree in pharmaceutical sciences and pharmacogenomics from the University of California in San Francisco, under the guidance of Professor Leslie Z. Benet. Since joining Pfizer in 2006, she provided DMPK strategies to projects in all stages of drug discovery and development.

As a member of AAPS and ISSX, Dr. Lam's expertise and research interests are in the area of drug transporters and their impact on drug disposition, metabolism, and drug–drug interaction. Her most recent research is focusing on the drug transporters in the blood–brain barrier and their impact on brain penetration.

Eilidh Leitch

Eilidh Leitch is currently a third-year Ph.D. student in the Tavassoli group at the University of Southampton, United Kingdom. Previously, Eilidh received her B.Sc. in Biochemistry and M.Sc. in Oncology, both at the University of Nottingham, United Kingdom. Eilidh then went on to work at Sygnature Discovery in Nottingham, within the bioscience department, providing assay development and routine screening as part of the integrated drug discovery model. Eilidh's Ph.D. studies focus on the development, identification, and characterization of cyclic peptide inhibitors of a metabolic protein–protein interaction target through the utilization of SICLOPPS.

Mylène de Léséleuc

Mylène de Léséleuc was born in Hull, Québec, Canada, in 1989. In 2011, she received her B.Sc. in Chemistry from the University of Ottawa and pursued her graduate studies (Ph.D.) at the Université de Montréal under the supervision of Prof. Shawn K. Collins. She is currently a senior research scientist at OmegaChem in Laval, Québec.

Spiros Liras

Spiros Liras is the Vice President of Medicinal Chemistry and Head of the Cardiovascular, Metabolic, and Endocrine Diseases (CVMET) Medicinal Chemistry at Pfizer Worldwide Research and Development. Prior to joining CVMET, Spiros was Senior Director of Medicinal Chemistry in Neuroscience at Pfizer. In Neuroscience, Spiros was involved in research aiming to deliver treatments for addiction, depression, schizophrenia, cognition, and Alzheimer's disease. Spiros joined Pfizer medicinal chemistry in 1994 after completing postdoctoral research in organic synthesis at the University of Texas, Austin. Spiros obtained a Ph.D. in organic chemistry in 1990 from Iowa State University.

Shingai Majuru

Shingai Majuru is the Executive Director of Oral Drug Product Development at Cempra, Inc., Chapel Hill, North Carolina. He has 20 years of experience in the pharmaceutical industry. His areas of expertise include formulation development, clinical supplies manufacture, technology transfer, process scale-up, process validation, and drug delivery technology development. He earned a B. Pharm. (Hons) degree and a Masters in Medicine from Department of Pharmacy of the University of Zimbabwe. He is also a holder of an M.Sc. and Ph.D. in Pharmaceutics from the College of Pharmacy of the University of Iowa. Shingai obtained an M.B.A. from Ancell School of Business of Western Connecticut State University.

Naveen Kumar Mallurwar

Naveen Kumar Mallurwar was born in Telangana, India (1985). He obtained his bachelor's degree in 2005 and master's degree with specialization in organic chemistry in 2007 from Kakatiya University. He received his Ph.D. degree from the University of Hyderabad in 2016 under the supervision of Professor Prabhat Arya at Dr. Reddy's Institute of Life Sciences of said university. His research interests are the synthesis of natural product-derived hybrid macrocycles and natural product-inspired macrocycles.

Eric Marsault

Eric Marsault obtained his Ph.D. at McGill University (Montreal, QC, Canada) in 1996 with the late Prof. George Just and then worked as a visiting scientist for Sanofi (Milan, Italy) prior to moving to Université de Sherbrooke (QC, Canada) as a postdoctoral fellow with Prof. Pierre Deslongchamps.

He joined Neokimia (which later became Tranzyme Pharma) in 2000, where he worked as a researcher, group leader, and then director of the medicinal chemistry department. During this time, he took an active role in maturing the first platform enabling high-throughout parallel synthesis of macrocycles that delivered up to 40 000 macrocyclic peptidomimetics and became the core of the company. Based on these, several drug discovery programs were established, aimed primarily at GPCR targets, leading to the identification of several preclinical candidates, including clinical candidates ulimorelin and TZP-102.

In 2009, he joined the Department of Pharmacology of Université de Sherbrooke as a professor, where he now focuses on the development of new molecules to validate emerging drug targets in the context of academic drug discovery, with a particular focus on peptidomimetics and macrocycles targeting GPCRs and transmembrane serine proteases for cardiovascular diseases, pain, and infectious diseases. He is coauthor of more than 50 publications and co-inventor of more than 30 patents. Since 2013, he is also the chairman of the Institut de pharmacologie de Sherbrooke.

Alan M. Mathiowetz

Alan M. Mathiowetz is currently the Director of Computational Chemistry in the Cardiovascular, Metabolic, and Endocrine Diseases (CVMET) Medicinal Chemistry Department within Pfizer Worldwide Research and Development. Alan obtained a B.A. in Chemistry at Rice University and a Ph.D. from the California Institute of Technology in Pasadena, California. Alan has worked in a number of technology and therapeutic areas within Pfizer, with an emphasis on structure-based design and virtual screening, *in silico* modeling and physical property analyses, and therapeutics targets for type II diabetes and obesity.

Prasenjit Mitra

Prasenjit Mitra researches on the regulation of cellular metabolism and energy homeostasis at the interface of diabetes and cancer. He has obtained his Ph.D. at the Indian Institute of Chemical Biology, Kolkata, India, and postdoctoral research at UMass Medical School, Worcester, MA, USA. Currently, he is working as a principal research scientist at the Dr. Reddy's Institute of Life Sciences located in the University of Hyderabad campus.

Micjel Chávez Morejón

Micjel Chávez Morejón was born in Pinar del Río, Cuba, in 1985. He earned his Bachelor in Chemistry Science from the University of Havana in 2009, in the field of antimicrobial peptide mimetics. He received his Master of Science in Organic Chemistry in 2011 from the Faculty of Chemistry, University of Havana, on the topic of "Multicomponent synthesis of polycationic peptidomimetic peptide–peptoid hybrids." In 2012, he joined the Ph.D. program of the Leibniz Institute of Plant Biochemistry, Halle (Saale), in collaboration with the Martin Luther University Halle-Wittenberg, Germany, and University of Havana, Cuba. Under the supervision of Prof. Wessjohann and Prof. Rivera, he focused on the development of new multicomponent reaction strategies for the synthesis of cyclic lipopeptides, inspired by natural products.

Ricardo A. W. Neves Filho

Ricardo Antonio Wanderley Neves Filho was born in Recife/PE, Brazil, in 1984. He received his B.Sc. and M.Sc. degrees from the Federal University of Pernambuco (UFPE) in 2006 and 2008, respectively. In 2010, he moved to Germany and enrolled in the Ph.D. program in the Division of Organic Chemistry of the Martin Luther University Halle-Wittenberg, while working at the Leibniz Institute of Plant Biochemistry under the supervision of Prof. Wessjohann. In 2015, he finished his Ph.D. research that focused on the development of reagents for multicomponent reactions and their applications in the synthesis of natural products.

Ashok D. Pehere

Ashok Pehere received his B.Sc. and M.Sc. (Organic Chemistry) at the University of Pune, India. He was a research chemist at Merck Pharmaceutical in Mumbai, India, in 2002–2008, then received his Ph.D. at the University of Adelaide, Australia, under the direction of Professor Andrew D. Abell. This was followed by postdoctoral research at the University of Minnesota, USA, under the

direction of Professor Thomas R. Hoye and Professor Marc A. Hillmyer, working on Diels–Alder reactions of furans and polymer synthesis. Currently working at UT MD Anderson Cancer Center, his research interest is related primarily to the design, synthesis, and characterization of cyclic peptide and new macromolecular materials.

Dehua Pei

Dr. Dehua Pei obtained his bachelor's degree in chemistry from Wuhan University, China, and Ph.D. in Organic Chemistry in 1991 from the University of California in Berkeley. After a postdoctoral fellowship at Harvard Medical School, he joined the faculty of Ohio State University in 1995 and is currently a professor of chemistry and biochemistry. His current research interests include the development of new combinatorial chemistry methods for macrocycle synthesis and screening, discovery of novel cyclic cell-penetrating peptides, and integration of the aforementioned two areas to develop macrocyclic inhibitors against challenging drug targets, such as intracellular protein–protein interactions.
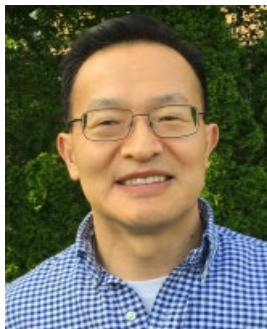
David Pereira

David Pereira received a B.S. in Biochemistry from Virginia Tech in 1981. He conducted research on pyrrolizidine and indole carbamates as potential antineoplastic agents at Virginia Commonwealth University and earned a Ph.D. in Medicinal Chemistry in 1985. From 1985 to 1988, he was a postdoctoral scientist in the laboratory of Professor Nelson Leonard at the University of Illinois. David has been a research scientist in the pharmaceutical industry for over 25 years and has held senior management positions at Cempra, Inc., since 2006.

Mark L. Peterson

Prior to co-founding Cyclenium in December 2013, Dr. Peterson was the Vice President of IP and Operations at Tranzyme Pharma where he led the chemistry R&D efforts during the technology development stage of the company and the initiation of its GPCR drug discovery programs. He later focused on building and maintaining an extensive portfolio of over 120 patents and applications protecting Tranzyme's pioneering technology and pharmaceutical product candidates. Previously with Monsanto and Advanced ChemTech, he has productively worked in a wide variety of research areas, including structure-based design, solid phase organic chemistry, combinatorial libraries, synthesis automation, heterocycles, unnatural amino acids, peptides, and peptidomimetics. A native of Wisconsin, he received his Ph.D. in Organic Chemistry from Washington State University (asymmetric synthesis) and conducted postdoctoral research at the University of Minnesota (antiviral carbocyclic nucleosides) prior to starting his industrial career. He is author or coauthor of over 90 publications and abstracted presentations and three book chapters, as well as coinventor on over 25 patents.

Lovy Pradeep

Lovy Pradeep obtained her Ph.D. in Biochemistry/ Biophysics in the field of protein folding and stability in 2004. She continued her academic research in protein folding and misfolding diseases at Baker Labs in Cornell University and later addressed the binding of small molecules to nicotinic acetylcholine receptors (nAChRs) using electrophysiology techniques, directed toward understanding Alzheimer's disease. Lovy joined Cempra in 2013 and is the holder of RAC and PMP globally recognized certifications. She is currently the Senior CMC Program Manager and continues to work on several aspects of the various solithromycin dosage forms.

David A. Price

David A. Price currently holds the position of Senior Director of Medicinal Chemistry in the Cardiovascular, Metabolic, and Endocrine Diseases (CVMET) department within Pfizer Worldwide Research and Development. David obtained a B.Sc. (First-Class Hons.) and Ph.D. from the University of Nottingham, United Kingdom, after which he carried out postdoctoral research at Colorado State University with Prof. Al Meyers. During his tenure with Pfizer, David has worked on projects to develop drugs for a wide variety of diseases including HIV/AIDS, hepatitis C, respiratory diseases, and, most recently, type II diabetes and obesity.

Alfredo R. Puentes

Alfredo R. Puentes was born in Pinar del Rio, Cuba, in 1983. He obtained his B.Sc. (*summa cum laude*) from the Faculty of Chemistry, University of Havana, Cuba. He obtained his master's degree under the guidance of Prof. Wessjohann (Halle) and Prof. Rivera (Havana) in 2014. Currently, he is a Ph.D. student at the Department of Bioorganic Chemistry of Leibniz Institute of Plant Biochemistry (IPB) in Halle (Saale), Germany, in a cooperative study between Halle and Havana, studying new beta-turn inducers with synthetic application in macrocyclization reactions.

Ziqing Qian

Dr. Ziqing "Leo" Qian obtained his Ph.D. in 2014 from the Ohio State University under the guidance of Dr. Dehua Pei. Currently, he is a postdoctoral researcher in the same group. His research interests include the development of cyclic cell-penetrating peptides for drug delivery and cell-permeable macrocycles as intracellular PPI inhibitors.
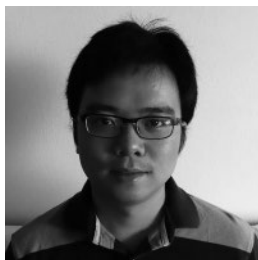
Michaël Raymond

Michaël Raymond was born in Rimouski, Québec, Canada, in 1989. In 2011, he received his B.Sc. in Chemistry from the University of Ottawa and is pursuing his graduate studies (Ph.D.) at the Université de Montréal under the supervision of Prof. Shawn K. Collins.

Thomas O. Ronson

Thomas O. Ronson was born and brought up in Bristol in the southwest of England. He completed his undergraduate studies at the University of Oxford in 2011, having carried out a Part II project in the group of Professor Jeremy Robertson. He then moved to the University of York to pursue a Ph.D. under the joint supervision of Professors Ian J. S. Fairlamb and Richard J. K. Taylor, working toward the total synthesis of unusual macrocyclic natural products using novel palladium catalysts. Following the completion of his Ph.D. studies in 2015, he moved to the University of

Antwerp where he currently works as a postdoctoral researcher in the group of Professor Bert Maes.

Jeffrey Santandrea

Jeffrey Santandrea was born in Montréal, Québec, Canada, in 1990. In 2012, he received his B.Sc. in Chemistry from the Université de Montréal and is currently pursuing his graduate studies (Ph.D.) at the Université de Montréal under the supervision of Prof. Shawn K. Collins.

Stephen E. Schneider

Stephen E. Schneider was formally introduced to chemistry at the North Carolina School of Science and Math by Dr. Lawrence Knecht. He received his B.S. degree from the University of North Carolina at Chapel Hill, where he performed research for Professors Bruce Erickson and Alex Tropsha and was initiated into Alpha Chi Sigma. He earned a Ph.D. in Organic Chemistry from the University of Texas in Austin in 1999 under the supervision of Professor Eric V. Anslyn. Stephen began his career as a process chemist at Trimeris, Inc., and is currently Executive Director, Chemistry at Cempra, Inc.

R. Scott Lokey

R. Scott Lokey did undergraduate research in organometallic chemistry with Professor Nancy Mills at Trinity University and received his Ph.D. at the University of Texas, Austin, working under Professor Brent Iverson, where his research centered on the synthesis of molecules that fold into protein-like shapes in water and bind to specific DNA sequences. He did postdoctoral research at Genentech, where he worked on the synthesis of bioactive cyclic peptides, and then at Harvard Medical School and the Institute of Chemistry and Cell Biology with Professors Timothy Mitchison and Marc Kirschner on chemical biology approaches to the study of the actin cytoskeleton. He joined the faculty of the Department of Chemistry and Biochemistry at UCSC in 2002, where his research group focuses on the relationship between molecular structure and drug-like

properties, especially cell permeability. Professor Lokey is also the director of the UCSC Chemical Screening Center, a high-throughput screening facility dedicated to early-stage lead discovery, especially against infectious agents and neglected disease targets. He lives in Santa Cruz where he and his family enjoy trips to the beach and hiking among the redwoods.

Silvia Stotani

Silvia Stotani graduated with first-class honors in Medicinal Chemistry in 2012 from the University of Rome (Italy). While working as a quality control chemist for Baxter in Rieti (Italy), she started a second-level master's degree on the "design and development of drugs" at the University of Pavia (Italy). For her master's project, she joined the Drug Design Department of Professor Dömling at the University of Groningen (the Netherlands), where she spent 5 months as a master's student and the other 6 months as a research assistant. She is currently a Ph.D. student at Taros GmbH in Dortmund (Germany), for the European Marie Curie Integrate ETN project in antibacterial drug discovery.

Ali Tavassoli

Ali is a professor of chemical biology at the University of Southampton, United Kingdom. His team's efforts are focused on the identification of cyclic peptide inhibitors of protein–protein interactions and their development for use as tools in cell biology and as the starting point for new therapeutics. Ali is currently the Chair of the Royal Society of Chemistry's "Chemical Biology and Bioorganic Group."

Nicholas K. Terrett

Nick Terrett is currently the Scientific Associate Vice President and European Chemistry Lead for Merck Sharp & Dohme GmbH based in Kriens, Switzerland. Prior to this role, he was the Chief Scientific Officer for Ensemble Therapeutics, a biotech company based in Cambridge, Massachusetts, USA. In this role, he focused on the discovery of novel macrocyclic molecules with affinity for significant oncology targets. Using a DNA-encoded library synthesis platform, Ensemble has generated libraries of novel and drug-like synthetic macrocycles that have been screened against enzymes and challenging protein–protein interaction disease targets. In addition to the discovery of the novel IAP antagonists described in Chapter 17, other successes with this technology approach have been the discovery of novel antagonists of the oncology targets IDO and USP9x and IL17 antagonists for treating inflammation. Before Ensemble, much of Nick's career was at Pfizer both in the United Kingdom and the United States where, among other activities, he was lead chemist and inventor for the program that discovered sildenafil (marketed as Viagra™ and Revatio™). Nick has an M.A. and Ph.D. in Organic Chemistry from the University of Cambridge.

William P. Unsworth

William P. Unsworth completed his Ph.D. at the University of Oxford under the supervision of Prof. Jeremy Robertson before accepting an EPSRC-funded postdoctoral post at the University of York to work with Prof. Richard J. K. Taylor. He then moved on to a Research Fellow position, also at the University of York, before starting his present post as a Leverhulme Trust Early Career Research Fellow. His research interests include diversity-oriented synthesis, transition metal catalysis, dearomatizing spirocyclization reactions, and total synthesis. A major focus of his group currently is the development of versatile and scalable methods to assemble medium-sized rings and macrocycles using ring expansion reactions.

Simon Vézina-Dawod

Simon Vézina-Dawod received his B.Sc. in Chemistry from Université Laval. After completing an M.Sc. in Pharmaceutical Sciences in 2014 at the same university, he joined the laboratory of Prof. Biron as a Ph.D. student in pharmaceutical sciences. He is currently working on the development of new peptoid synthesis methodologies and the design and synthesis of macrocyclic peptidomimetics. His research interests principally involve the design and synthesis of complex mono- and polycyclic peptides and the development of new approaches to prepare and screen combinatorial macrocycle libraries.

Francesca Vitali

Francesca Vitali received a B.S. in Chemistry from La Sapienza University in Rome, in 1999 under the supervision of Prof. Claudio Ercolani. She earned her Ph.D. in Bioorganic Chemistry from Prof. John Robinson's group at the University of Zurich, working on the synthesis of peptide precursors and cytochrome P450 enzymes involved in the biosynthesis of the antibiotic vancomycin. She then joined the Swiss Federal Institute of Technology (ETH) in Zurich as a postdoctoral fellow associated with the research groups of Prof. Frederic Allain and Prof. Kurt Wüthrich and worked on the development of cell-free expression methods for segmental isotope labeling of RNA-binding proteins. In 2005, she joined Prof. Thomas Poulos' group at the University of California, Irvine, to work on applying expressed protein ligation techniques for isotope labeling of redox enzymes. Since 2009, she has worked as a senior scientist in Prof. Fasan's laboratory at the University of Rochester focusing on the development of novel chemobiosynthetic strategies for the synthesis of biologically active macrocyclic peptides.

Conan K. Wang

Conan K. Wang is currently a postdoctoral researcher at the Institute for Molecular Bioscience of the University of Queensland in Brisbane, Australia. Conan completed a Bachelor of Engineering at the University of New South Wales in Sydney and then a doctorate at the University of Queensland. He moved to the University of Science and Technology in Hong Kong on an NHMRC exchange fellowship before his return to Australia. His general research area is cyclic peptide drugs with specific interests on the application of NMR and X-ray crystallography to guide the design of peptide drug leads. Lately, he has focused on improving the bioavailability of cyclic peptide drugs and exploring their potential in the treatment of neurological disorders. Conan has authored more than 30 papers on cyclic peptides and the use of biophysical techniques to characterize their structure and function.
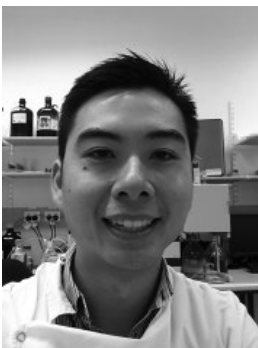
Ludger A. Wessjohann

Professor Wessjohann studied chemistry in Hamburg (Germany), Southampton (United Kingdom), and Oslo (Norway, under the guidance of Prof. Skattebøl). He earned his doctorate in 1990 with Prof. de Meijere in Hamburg. After a short period as a lecturer in Brazil, he became a postdoctoral Feodor-Lynen fellow of the Alexander von Humboldt foundation with Prof. Paul Wender at Stanford University (USA) to work on the total synthesis of Taxol®. After an assistant professorship in Munich (LMU, 1992–1998), he was appointed as the Chair of Bioorganic Chemistry at the Vrije Universiteit Amsterdam (NL) to work on organometallic chemistry and biocatalysis. Since 2001, he is the director of the Department of Bioorganic Chemistry at the Leibniz Institute of Plant Biochemistry (IPB) in Halle (Germany) and, in parallel, holds the Chair of Natural Product Chemistry of the Martin Luther University Halle-Wittenberg. In 2010, he was appointed the Managing Director of the IPB (www.ipb-halle.de).

Prof. Wessjohann focuses on the discovery, synthesis, and application of natural products and bioactive derivatives thereof. He was the first to look into the chemoinformatics of macrocycles and to study their efficient synthesis by multiple multicomponent reactions. He has over 300 publications and 25 patent applications and is co-founder of five companies, the latest being Ontochem IT Solutions. He is a member of many boards and commissions including the Brazilian Academy of Science and received numerous scholarships, prices, and honors, for example, Microsoft IT Founders Award, honorary membership of the Argentinean Soc. of Synth. Org. Chem. and the 2016 Leibniz Drug of the Year award.

Sara Wu

Sara Wu received a B.S. in Applied Chemistry from the University of Science and Technology of China in 1988. Her Ph.D. in Medicinal Chemistry was from the University of Kansas in 1997 with research on enzyme inhibition kinetics and mechanisms with Professor John V. Schloss. She did her postdoctoral research on the pre-formulation and degradation mechanisms of anticancer drug candidates with Professor Valentino J. Stella in the Pharmaceutical Chemistry department also at the University of Kansas from 1997 to 1998. Since October 1998, Sara has been working for various pharmaceutical companies on drug pre-formulation and formulation development including

Eisai, Wyeth, and, presently, Cempra, Inc. Sara is currently the Executive Director of Drug Product Development.

Shinji Yamazaki

Dr. Shinji Yamazaki is currently an associate research fellow in the Department of Pharmacokinetics, Dynamics, and Metabolism (PDM) at Pfizer Worldwide Research and Development (San Diego, CA). He received his Ph.D. degree in Pharmaceutical Science at Tokyo University of Pharmacy and Life Sciences (Tokyo, Japan) under the supervision of Professor Tadashi Watabe. Before joining Pfizer Worldwide Research and Development in 2003, he has over 15 years of international experience in pharmaceutical industry to provide leaderships in drug discovery and development.

Dr. Yamazaki is a scientific leader with a strong background in ADME/PK characterization of clinical candidate drugs *in vitro* and *in vivo*. His current research activities are devoted to the investigation of pharmacokinetic–pharmacodynamic modeling, translational pharmacology, *in vitro*-to-*in vivo* extrapolation of pharmacokinetics, physiologically based pharmacokinetic modeling, and so on. He serves on the editorial board of Drug, Metabolism, and Disposition and has authored and coauthored over 40 peer-reviewed articles and book chapters in this field.

Andrei K. Yudin

Professor Andrei K. Yudin obtained his bachelor in science degree at Moscow State University and his Ph.D. degree at the University of Southern California under the direction of Professors G. K. Surya Prakash and George A. Olah. He subsequently took up a postdoctoral position in the laboratory of Professor K. Barry Sharpless at the Scripps Research Institute. In 1998, he started his independent career at the University of Toronto. He received early tenure, becoming an associate professor in 2002, and an early promotion to the rank of Full Professor in 2007.

Prof. Yudin is one of the pioneers in the design of new chemical transformations. Currently, the main focus of research in the Yudin group is to develop a bridge between basic chemistry research and drug discovery. In addition to significant fundamental discoveries, his lab is making tangible contributions to the chemical industry. In 2009, Sigma-Aldrich used his method and created a wide range of reagents now known as the Yudin amino aldehydes. These powerful molecules are being used to solve some of the long-standing problems of complex molecule synthesis. Prof. Yudin and his students have made molecules that effectively mimic secondary structures such as beta-turns, beta-sheets, and alpha-helices in various contexts.

Among Professor Yudin's awards are the CSC Award in Combinatorial Chemistry, the 2004 Amgen New Faculty Award, the 2010 CSC Merck-Frosst Therapeutic Center Award, the 2010 Rutherford Medal of the Royal Society of Canada, the 2011 University of Toronto Inventor of the Year Award, and the 2015 Bernard Belleau Award in Medicinal Chemistry. Professor Yudin is a fellow of the Royal Society of Canada. He is currently the Editorial Board Chair of the Royal Society of Chemistry journal *Organic & Biomolecular Chemistry*.

Serge Zaretsky

Serge Zaretsky was born in Moscow, Russia, and grew up in Toronto, Canada. He received his B.Sc. in Biochemistry from McGill University (Montreal, Canada) in 2009. There, he performed research in the Tsantrizos group, the Moitessier group, and the Stone Pain Lab. He then joined the University of Toronto (Toronto, Canada) in order to pursue a Ph.D. in Organic Chemistry under the supervision of Prof. Andrei Yudin. His graduate research focused on mechanistic studies and the development of multicomponent peptide macrocyclization techniques. A major element of his studies was the application of cyclic peptides in the fields of chemical biology and medicinal chemistry. Since graduating in 2014, he went on to work in the field of process chemistry at Alphora Research Inc. (Toronto, Canada) and then at Bristol-Myers Squibb (New Brunswick, New Jersey, USA), where he presently works in the Chemical & Synthetic Development department as a member of the reaction sciences group.

Part I

Challenges Specific to Macrocycles

1

Contemporary Macrocyclization Technologies

Serge Zaretsky and Andrei K. Yudin

Lash Miller Chemical Laboratories, University of Toronto, Toronto, Ontario, Canada

1.1 Introduction

In medicinal chemistry, macrocycles occupy the "middle space" between small organic molecules and proteins (Figure 1.1). By virtue of displaying the features of both small molecules *and* proteins, macrocycles have the potential to harness both the exquisite specificity of biological drugs and the synthetic tractability of small molecule drugs [1–3].

Macrocycles encompass a tremendous variety of molecules. Barring the requirement of a suitably large ring size (conventionally over 12 atoms), the constituents of the ring can vary. Macrocycles can be based on primarily aliphatic backbones as exemplified by macrolides [1, 4] or on heteroatom-based scaffolds as exemplified by macrocyclic polyethers [5]. No macrocycle discussion could be whole without mentioning the central role of cyclic peptides (see also Chapters 3, 4, and 9). Cyclic peptides are employed by nature and chemists in a variety of settings, and these molecules are particularly noteworthy for their modular assembly from amino acid building blocks [6–8]. The relative ease of synthesis, both chemical and biological, makes cyclic peptides highly sought-after molecules in drug discovery [9].

Having a constrained backbone enables macrocycles to pre-organize for effective binding to ligands and host molecules; however, the requirements for effective pre-organization have to be considered; simply having a constrained molecule does not always ensure binding [10, 11]. Moreover, the manner in which binding elements of a macrocycle are presented in three dimensions can change dramatically with the macrocycle ring size. The overall effect is ring size-dependent binding affinity and specificity between macrocycles and their hosts or guests [12–17].

In addition to binding affinity gains, macrocycles possess a number of pharmacokinetic advantages when compared with their linear counterparts. This aspect is particularly important for peptides as the linear forms often exhibit very poor cellular permeability and are proteolytically labile, and as a result linear peptidic drugs have to be injected or use advanced formulation techniques and cell-penetration tags for efficacy [18, 19]. Cyclic peptides, on the other hand, can prearrange their peptidic backbone and amino acid side chains such that polar surface character is minimized and the formation of internal hydrogen bonds is facilitated (Figure 1.2) [20–22]. This area of research continues to be actively pursued with concentrated efforts on establishing a rationale for peptide modification toward improved cellular permeability with cyclic peptides [23–26]. An additional differentiation is that macrocycles can be more metabolically stable than their linear counterparts [9]. For example, cyclic peptides are not subject to exopeptidases and generally can resist endopeptidases [27, 28].

Perhaps the most significant and enabling feature of macrocyclic drugs with respect to small molecule therapeutics is their intricate three-dimensional structure. Whereas conventional small molecule therapeutics favor achiral and aromatic (i.e., heterocyclic) substituents, macrocycles offer a robust framework that takes advantage of multiple sp^3 centers to furnish large and unique binding surfaces [29]. Accordingly, macrocycles have been pinned as a privileged class of molecules to modulate protein–protein interactions, which is a difficult, yet growing, target space in drug design [2, 3, 9].

1.2 Challenges Inherent to the Synthesis of Macrocycles

The benefits of macrocycles are vast, especially when compared with their linear analogues, but there are some challenges inherent to their synthesis and isolation. The synthetic challenges are rooted in the conformational difficulties of tying the "ends" of a molecule together,
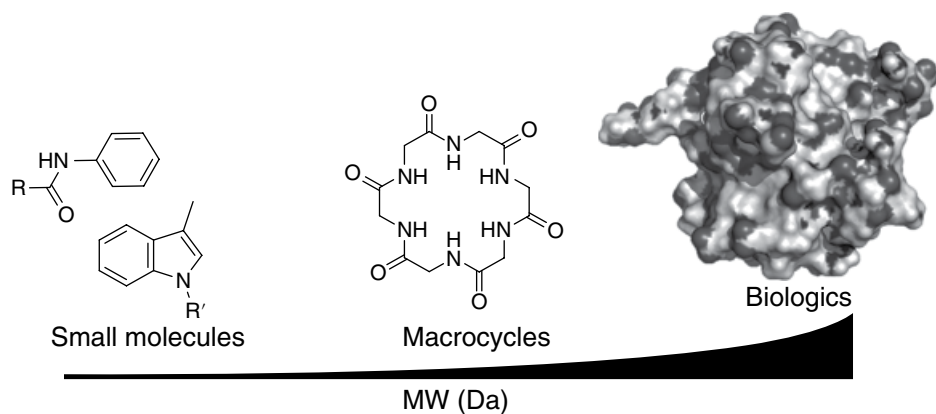
Figure 1.1 Macrocycles are at the intersection of small molecules and biological drugs chemical space.
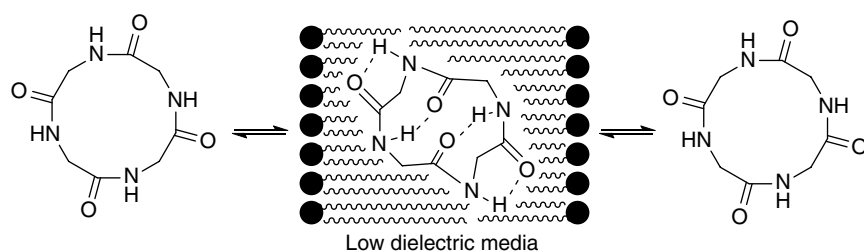
Figure 1.2 Lokey's conformational hypothesis for passive membrane permeability of peptide macrocycles.

irrespective of the nature of the cyclization chemistry (amide, ester, alkene formation, etc.).

In the case of smaller macrocycles (around 12 atoms), transannular strain significantly impacts the cyclization rate. This form of strain energy arises from the clash of backbone atom substituents, such as C—H groups in simple cycloalkanes or side-chain atoms in more complex cycles, within the ring of the forming molecule. Seminal studies by Illuminati, Gali, and Mandolini have shown that ring-closing transition state energies are elevated for ring sizes ranging between 7 and 13 atoms with 8–10 atom ring sizes being most affected [30]. In addition to transannular strain, additional detrimental factors to the kinetic rate arise from bond angle and length deformations and unfavorable eclipsed conformations, all of which are increasingly alleviated in larger rings (>12 atoms) [31, 32].

When considering ring closure kinetics, it is instructive to use effective molarity (EM), the ratio between the intramolecular and intermolecular rates, as a guide to reactivity [33]. The proximity of the two reactive ends in an intramolecular cyclization reaction greatly facilitates the coupling of the two partners versus the intermolecular case. Strain energy impacts the EM as outlined previously for ring sizes of 8–11 atoms, but as the strain energy diminishes with ring size for macrocycles, so too does the EM. For medium and large macrocycles, the main concern becomes the lack of a proximity effect, which, without forcing features (e.g., Thorpe–Ingold effect),

makes the cyclization-conducive conformation an entropically challenging one to reach [34].

In an effort to create a macrocyclization reaction, the effectiveness of the desired transformation has to be balanced with the cyclization ability. A fast cyclization reaction is required to limit side reactions, but if the cyclization-conducive conformation is not readily attainable, then intermolecular reactivity can predominate. For example, the synthesis of cyclic peptides can be complex, and methodology is often not transferrable between sequences and ring sizes [35]. Conventional approaches for peptide cyclization often suffer from oligomerization side reactions unless performed at high dilution. The difficulty in cyclic peptide synthesis stems from the tendency for carboxylic acid activation chemistry to disfavor the cyclization-conducive conformation by negating the peptide termini's ion pair interaction (Scheme 1.1). The consequence is a highly sequence-dependent equilibrium between conformation **2** and **3**, which can affect the expected EM of the system and result in intermolecular reactivity. Research into methods that maintain the stabilizing zwitterionic interaction of peptide ends has recently emerged [36–39].

Schmidt and Langner's work on sequence dependency in forming 15-membered cyclic peptide rings clearly illustrates the challenges faced in this process [40]. Depending on the amide linkage that was formed in the ring-closing reaction, the researchers noted a wide variability in reaction selectivity, with some cases even
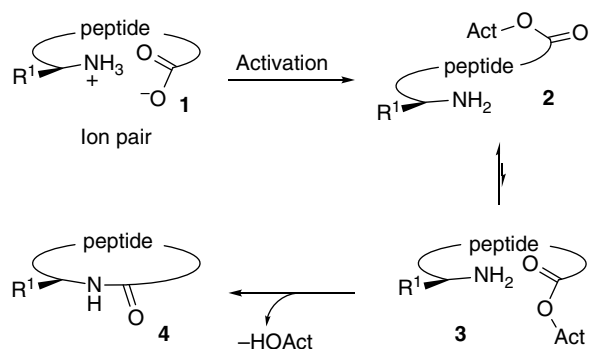
Scheme 1.1 Carboxylic acid activation disfavors the cyclization-conducive conformation **3**.
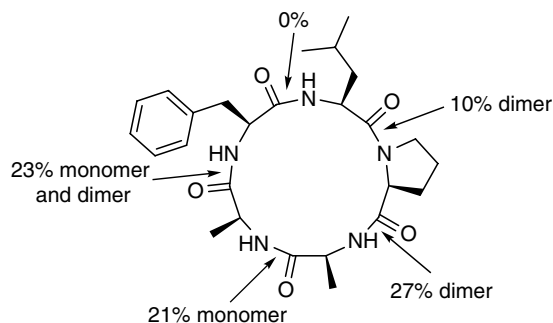
Figure 1.3 The site of retrosynthetic ring disconnection can greatly affect the yield and selectivity of the forward process.

Scheme 1.2 Carboxylic acid side-reaction pathways by way of oxazolone intermediate (a), ketene formation (b), and Curtius rearrangement of acyl azides (c).

forming the cyclodimer as the predominant product (Figure 1.3). For a successful cyclization reaction, the linear substrate has to be carefully selected and the cyclization site considered, as the substrate-dependent cyclization reaction can fail or simply result in isolation of cyclodimers [35, 41].

In order to ensure sufficient selectivity for cyclic monomers, macrocyclization reactions are often performed at high dilution. By decreasing the concentration to the mM and μM range, bimolecular reactivity can be diminished such that the desired monomer cyclization takes place. However, at low concentrations, the desired chemistry also tends to be significantly slowed, and side reactions other than oligomerization may arise [42–45]. The necessity for low concentration may be afforded by working on solid phase, which ensures pseudo-high dilution through physical separation of the reactive species (Section 1.5).

In carboxylate activation chemistry, there is a propensity for C-terminal amino acid epimerization if the nucleophilic coupling is not kinetically competitive [46]. Epimerization results from amide *O*-attack on the active ester to generate an oxazolone intermediate (Scheme 1.2a). In the presence of base, oxazolone **6** can be deprotonated to form **7**, which is stabilized due to aromaticity, with subsequent reprotonation racemizing

the amino acid stereocenter to give **8**. For acyl halides (Scheme 1.2b), the highly activated nature of the functional group can invoke an alternate epimerization pathway through ketene formation as well as provoking hydrolysis [47]. While acyl azides pose less risks for epimerization, a side-product pathway exists through the Curtius rearrangement (Scheme 1.2c) [46].

In the synthesis of peptides, an additional side product may arise from diketopiperazine (DKP) formation. Under conditions where the first amide bond is able to readily adopt a *cis* conformation, the amine at the N-terminus may fold and react onto the second amide to form a six-membered ring [48]. This rearrangement is termed cyclol formation and leads to cleavage of the second amide bond, thereby forming a DKP and a truncated linear peptide. For example, in a study by Titlestad [49], cyclization of sarcosine oligopeptides, from Sar$_3$ to Sar$_8$, was accompanied by formation of sarcosine DKPs in 14–30% yield (Scheme 1.3).

After successfully forming a macrocycle, the isolation and purification of the final product can provide further challenge. As macrocycles tend to be higher in molecular weight than small molecules, conventional techniques such as crystallization and flash column silica chromatography are often ineffective. An additional consideration is that the macrocyclization step can often be the last or

Scheme 1.3 Cyclol formation in a peptide macrocyclization can lead to DKP formation.
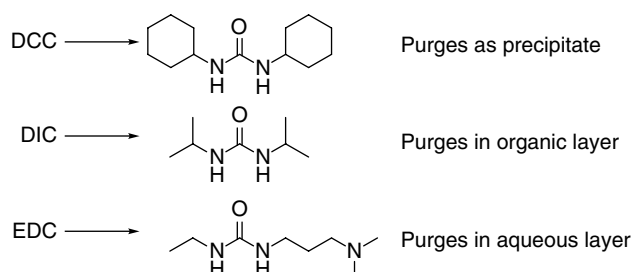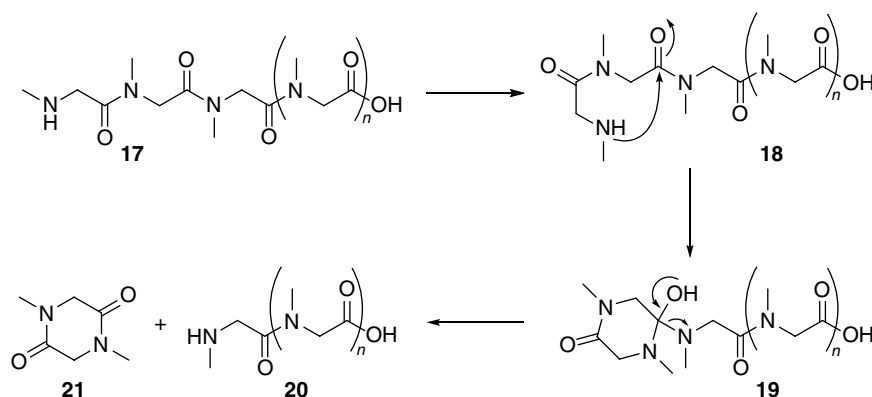
Figure 1.4 Selective solubility of the activating agent by-product simplifies isolation.

penultimate step of a synthesis, and particular attention will need to be paid to purging of cyclization by-products, toxic solvents such as DMF, and transition metals. In certain cases, activation chemistry by-products can be purged by taking advantage of selective solubility (Figure 1.4) [47]. Similarly, cyclization on solid phase can greatly simplify the isolation of macrocycles (Section 1.5 and Chapter 9) [50–53].

Replacing toxic organic solvents by aqueous conditions can significantly reduce safety hazards and costs of a chemical process. Propylphosphonic anhydride (T3P®)[1] has gained considerable exposure as an efficient and more benign alternative in carboxylic acid activation chemistry [54]. For example, in the cyclization toward cycloaspeptide E, the cyclization of **22** was found to be low yielding (10–15%) with DPPA activation, and predominantly the Curtius rearrangement product **23** was observed (Scheme 1.4) [55]. Switching to T3P dramatically increased the yield to 67%.

In spite of the efficient means of isolating macrocycles from the cyclization reagent by-products, purification of the final compounds can be quite challenging. As the macrocycles tend to have very similar chemical features to their linear precursors and reaction side products, high performance liquid chromatography purification is

often required. Reversed-phase HPLC purification remains a crucial method for purifying macrocyclic compounds, but it is not efficient and can be difficult to implement on scale.

1.3 Challenges in Macrocycle Characterization

In the realm of macrocycle characterization, routine techniques are often used at their limit or they can be even completely ineffective. For example, the simple TLC experiment, a standard technique of organic chemistry, can be wholly ineffective for many classes of macrocycles. The same reasons that make purification of macrocycles difficult, specifically their high molecular weight and complexity along with substantial homogeneity between side products and precursors, also significantly complicate their structural analysis (Table 1.1). Chapter 2 is devoted to the practical aspects of macrocycle structural analysis.

High-resolution mass spectrometry (HRMS) is another core analytical technique that presents challenges in the field of macrocycles. This method is routinely used as a substitute for elemental analysis in proving compound identity. For small molecules with a molecular weight below 500 Da, routine HRMS performed on time-of-flight (TOF) mass spectrometers can provide ppm resolution for analytes and enable a diagnostic identity of the elemental composition [56]. As molecular weight increases, the permutations for the compound formula increase dramatically, such that above 1000 Da, HRMS data can no longer reliably deliver exact masses for the elemental composition [56]. As an added challenge to chemists working with macrocycles, broad chemistry journals continue to require HRMS analysis for macrocycles and large molecules, yet, ultimately, HRMS data is not a reliable method for elemental composition for such structures.

---

1 T3P is a registered trademark of Archimica GmbH.

Scheme 1.4 T3P® proves successful in a difficult macrocyclization to cycloaspeptide E (**24**).
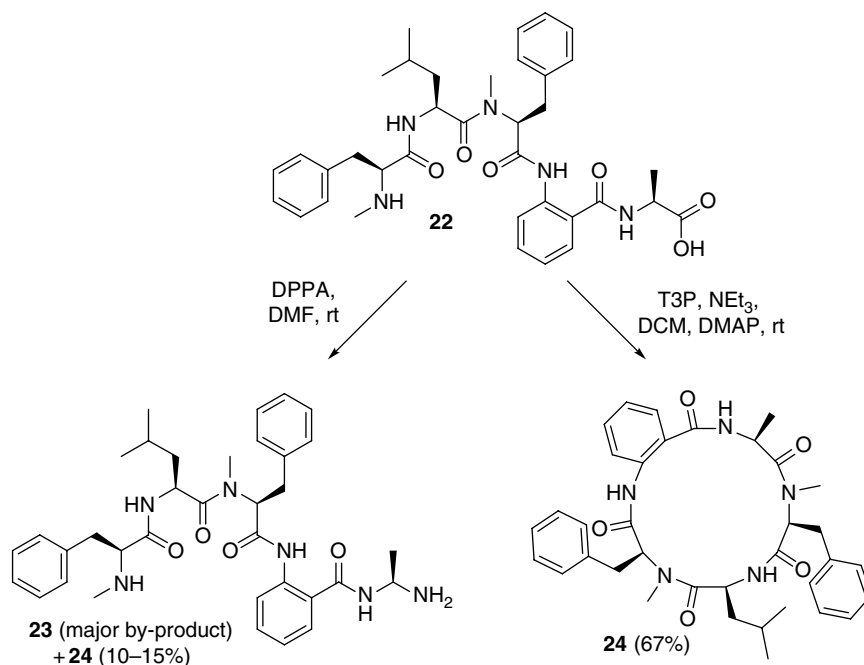
Table 1.1 Common structural analysis techniques and their applications to macrocycles.

Technique	Diagnostic features	Issues with macrocycles
Chromatography	Separation of chemical species by polarity and/or functional groups	Difficult separations necessitate HPLC and alternate solid phases
MS	Identity by mass and elemental composition with HRMS	Resolution limited for exact masses as molecules reach and exceed 1000 Da
NMR	Functional groups and atom identity; structural analysis for connectivity and solution-phase conformations	Challenging solubility can limit amount of signal; complex spectra of overlapping peaks from similar functional groups requires high-field NMR; multiple conformers lead to additional sets of peaks
Crystallography	Structural analysis in the solid state	Poor crystallinity and prone to aggregation; methods not transferable

An additional consequence for mass spectrometry with macrocycles is that, due to their ring structure, macrocycles can be difficult to fragment in a predictable manner with methods such as collision-induced dissociation (CID) [57, 58]. This phenomenon is most apparent for macrocyclic peptides or peptidomimetics. Whereas linear peptides can be easily fragmented at their amide bonds and sequenced by CID/MS^2, cyclic peptides do not fragment into informative ions and can lead to scrambled sequences by rearrangement. Recent advances in *de novo* sequencing of cyclic peptides by mass spectrometry have focused on multiple tandem mass spectrometry methods [59, 60], statistical analysis [61, 62], and library encoding [63, 64].

A synthetic work-around has been to chemically linearize the molecules first, such as using cyanogen bromide to cleave peptides at methionine residues (Scheme 1.5a), although that raises issues of its own regarding the integrity of the molecule through the process. Likewise, this approach requires the obligatory presence of a methionine residue in the ring [65]. More recently, a linearization-sequencing technique using weak amides has been reported for certain macrocyclic compounds (Scheme 1.5b) [66]. Furthermore, CID/MS^2 can be instrumental in the unambiguous assignment of a cyclodimer [M$_2$+2H]$^{2+}$ from the isobaric non-covalent dimer [2M+2H]$^{2+}$ [67].

An enabling mass spectrometry tool for macrocycles is ion mobility–mass spectrometry, which can enable conformational analysis of molecules in the gas phase [68]. Examples of cyclic and lasso peptide analyses have been reported [69, 70].

NMR is a fundamental technique that is often used for characterizing macrocyclic molecules and is, unfortunately, also associated with certain caveats for these structures. The high similarity and number of functional groups and atom types in a macrocycle may greatly complicate simple 1D ^{1}H and ^{13}C NMR analysis due to

(a)

(b)
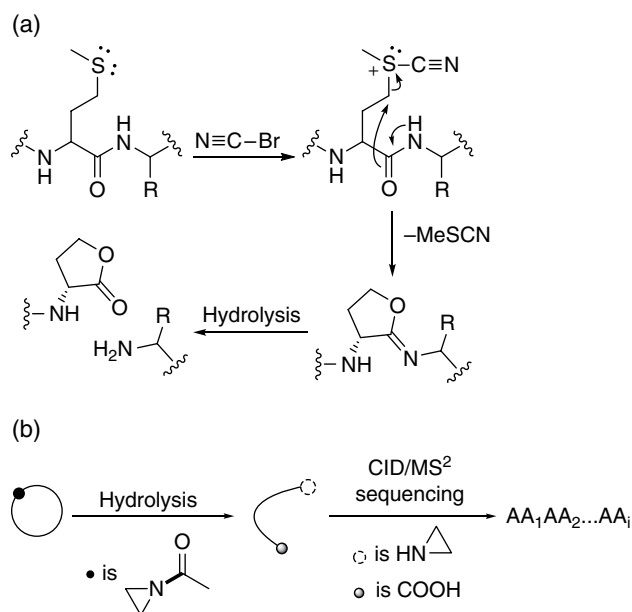
Scheme 1.5 Linearization of peptides by cyanogen bromide at methionine residues (a) and selective hydrolysis of weak aziridine amides (b).

Figure 1.5 QM calculations enable high predictability of macrocyclic NMR chemical shifts.

overlapping peaks. This issue also greatly limits the ability to differentiate between cyclic monomers, dimers, and higher order oligomers using NMR spectroscopy. Accordingly, 2D hetero- and homonuclear NMR is vital to deconvoluting congested signal areas and assigning chemical peaks. A further complication arises from the fact that changes in the chemical shift and splitting patterns can result from the constrained ring structure of the macrocycle. As an analogy, characterization and assignment of macrocyclic molecules by NMR can be the basis of whole studies in natural product research [71–73].

These structural effects on NMR chemical shifts also make prediction software error-prone. Simple increment-based NMR prediction software, such as available in ChemDraw,[2] ACD,[3] and Mnova,[4] cannot compute effectively the chemical shifts of macrocycles due to their conformational flexibility and effects [74]. Quantum mechanical (QM) calculations offer an alternative to predicting chemical shifts in macrocycles [75]. However, such approaches are time-consuming. An initial conformational search and geometry optimization is crucial to generating a statistically relevant aggregate of chemical shift values (Figure 1.5). Moreover, conformational modeling of peptides requires macrocycle-specific algorithms

to effectively sample the conformational space of these molecules (Chapter 2) [76, 77].

1.4 Macrocyclization Methods

Development of new macrocyclization methods continues to be an active area of research [2, 42, 78, 79]. Part III of this book is entirely devoted to macrocyclization methods. Method development can be for the most part separated between the search for novel ring-closing reactions and improvements of established methods. In polyfunctionalized macrocycles, the myriad of choices for the type of ring-closing reaction can dramatically affect macrocyclization yield. For example, in efforts to make the natural product macrocycle Riccardin C, three main macrocyclization routes were envisioned and realized with a variety of efficiencies (Figure 1.6) [80]. The palladium(0) cross-coupling of two aryl species led to the macrocycle in only 37% yield. Coupling of the benzylic positions was accomplished in modest (30–50%) to excellent yield (92%) by Wittig or McMurry chemistry, depending on the choice of cyclization site. The work on Riccardin C and analogues is illustrative of the importance of choosing the right bond for a ring-closing reaction. Indeed, since there was no evident strategy that would *a priori* confer high selectivity for the macrocyclic product, only one site for macrocyclization proved effective.

Carboxylic acid coupling chemistry to form amides and esters is a staple technique in macrocyclization. As previously discussed (Section 1.2), this transformation has well-defined side-product pathways that lead to oligomerization (e.g., cyclodimers) and impurities such as epimerization at the C-terminus of peptides. Foregoing the importance of selecting an appropriate site for the ring-closing reaction in a macrocycle (Figure 1.3), the next point of optimization in carboxylic acid chemistry lies in the selection of an appropriate coupling agent.

At its core, a coupling agent removes an equivalent of water in the reaction of a carboxylic acid with an amine

---

2 PerkinElmer, Inc., Waltham, MA, USA.
3 Advanced Chemistry Development, Inc., Toronto, Ontario, Canada.
4 Mnova NMRPredict Desktop; Mestrelab Research, Santiago de Compostela, Spain.
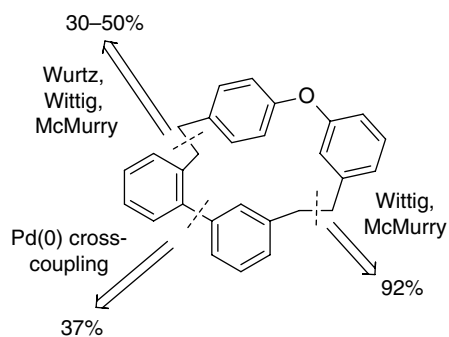
Figure 1.6 Site selection and chemistry both affect the macrocyclization efficiency toward Riccardin C.
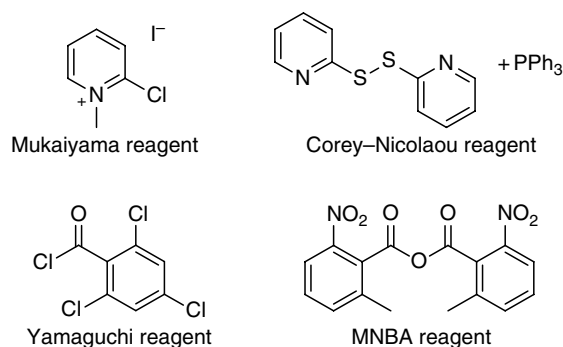
Figure 1.7 Common carboxylate activation agents for macrolactonization.
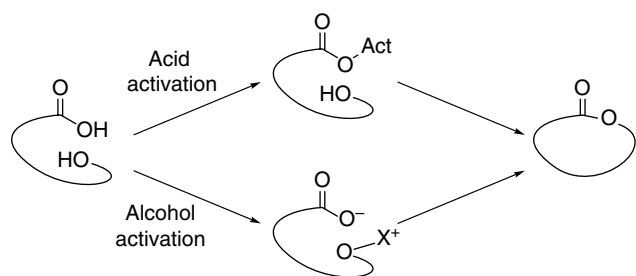
Scheme 1.6 Macrolactonization by acid or alcohol activation.

or hydroxyl-containing partner. Carbodiimides, such as DCC, are the prototypical class of compounds that activate carboxylic acids toward amides and esters (Figure 1.4) [47]. Additives such as the common HOAt and HOBt are used to temper reactivity through active ester formation and reduce the amount of side products, particularly epimers [81]. Phosphonium and uronium derivatives of the additives combine the carboxylic acid activation and active ester formation properties and are often utilized in carboxylic acid macrocyclization [82]. A wide selection of other agents for formation of the amide bond, primarily developed for peptide chemistry, is also available [82].

Macrolactonization, while appearing to have great similarities to macrolactamization, offers a number of unique pathways and opportunities for ring formation. In addition to the shared carboxylic activation pathways, in which the alcohol is the nucleophile, the reaction may proceed by alcohol activation where the carboxylate becomes the nucleophile (Scheme 1.6) [83]. Formative works in the acid activation stream have been the Corey–Nicolaou reaction [84], Mukaiyama esterification [85], Yamaguchi esterification [86], and Shiina macrolactonization [87], among others (Figure 1.7) [83, 88]. The Yamaguchi reagent and 2-methyl-6-nitrobenzoic anhydride (MNBA) in the Shiina reaction are used with DMAP catalysis. Research into modifications and improvements of these reagents has seen continued development [83].
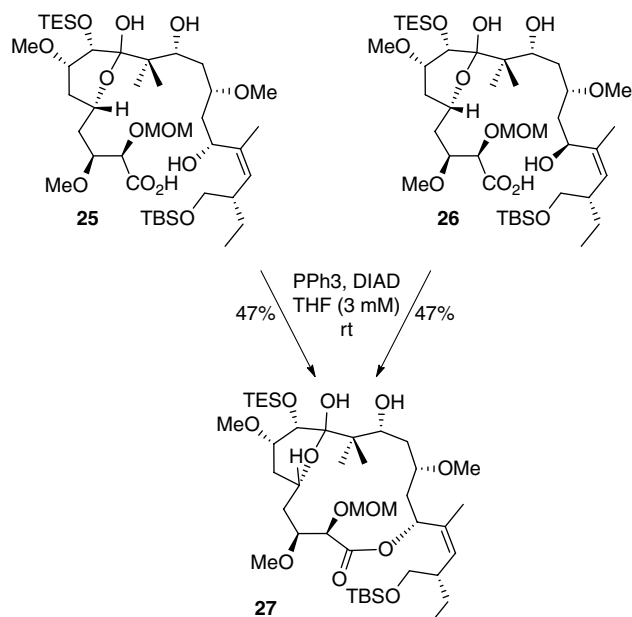
Scheme 1.7 Configuration-dependent mechanistic switching in the Mitsunobu reaction toward **27**, a derivative of peloruside A.

The preferred method of macrolactonization through the alcohol activation pathway is the Mitsunobu reaction [83]. Drawbacks of this methodology include the formation and removal of triphenylphosphine oxide and reduced azodicarboxylate by-products. Nucleophilic displacement in the Mitsunobu reaction conventionally proceeds with inversion of stereochemistry at the electrophilic carbon; however, retention of configuration has also been reported, suggesting that care needs to be exercised with this convention in the macrocyclic framework. In their work on the total synthesis of peloruside A (Scheme 1.7), De Brabander and coworkers observed the formation of **27** from either epimer **25** or **26** [89]. The retention of stereochemistry from **25** to **27** was hypothesized to happen through an acyloxy-phosphonium intermediate that would predominate if
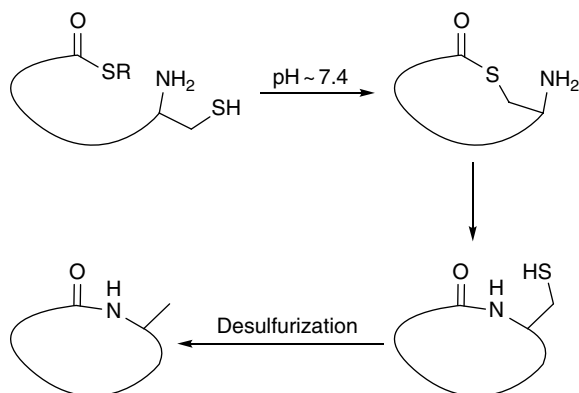
Scheme 1.8 Peptide cyclization by NCL and desulfurization to effectively ligate at an alanine residue.
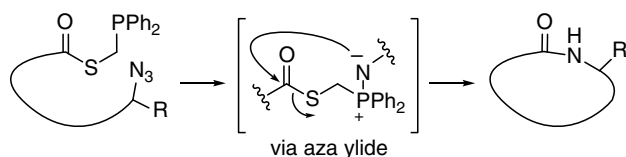
Scheme 1.9 Peptide cyclization by traceless Staudinger ligation.

the alkoxyphosphonium intermediate was prevented from forming due to conformational effects [90].

Native chemical ligation (NCL) offers an opportunity to form amide bonds with thiol surrogates of carboxylic acids [91]. Initial reports on the use of NCL for peptide macrocyclization emerged from the Muir and Tam groups in 1997 (Scheme 1.8) [92, 93]. This reaction was notable for its ability to accommodate unprotected peptides. Additional methods to expand the substrate scope and remove the limitations of the N-terminal cysteine residue were reported shortly thereafter [94, 95]. A related report for the thia zip reaction, a cascade thiolactone formation and ring expansion by thiolactone exchange, offered a conceptually powerful method for end-to-end cyclization of large unprotected peptides [96, 97].

Staudinger ligation has further diversified the range of substrates for ligation of deprotected peptides [98, 99]. The traceless Staudinger cyclization reported by Kleineweischede and Hackenberger employed a bifunctional azidopeptide phosphinothioester (Scheme 1.9), which, in the presence of base, underwent an acyl transfer reaction through an aza-ylide intermediate [100]. This development removed the constraint of having an N-terminal cysteine residue and has also been utilized in the synthesis of difficult medium-sized cyclic peptides [101].

Additional ligation strategies have included the serine–threonine ligation [102], intein-mediated cyclization [103], and others (Chapters 9 and 13) [104–106]. For early stage drug discovery, the split-intein strategy has been applied in SICLOPPS to generate vast libraries of genetically encoded peptides (Chapter 8) [8, 107, 108].

Thiols have been extensively exploited in the synthesis of macrocycles, more specifically through the macrocyclization utilizing disulfide bonds (Scheme 1.10a) [109]. Disulfide-bridged macrocycles are inspired by numerous biological entities that take advantage of this moiety to form cyclic peptides, bicycles, and higher order structures [109–112]. While cysteine residues in peptides pose some challenges due to oxidation issues, protecting group strategies can greatly limit side reactions, and, along with selective deprotection strategies, disulfide bonds can be formed on both partially protected and fully deprotected peptides. Concomitant cysteine deprotection and disulfide oxidation is also possible [113]. Moreover, the orthogonal nature of disulfide bond formation makes this technique of macrocyclization compatible with biosynthesis [109, 114]. Disulfide formation has been interfaced with phage display of peptides to biosynthetically produce and select for cyclic peptides from libraries of more than 10^{13} compounds (see Chapters 7 and 8) [115].

The reducing environment of cells and an overall desire for more stable bonds has led to research into alternative linkages for cysteine molecules [116]. Notable examples include thioether formation (Scheme 1.10b) [117, 118] and multiple cysteine alkylation with 1,3,5-tris(bromomethyl)benzene (Scheme 1.10c) [119]. Furthermore, by using mutated aminoacyl tRNA synthetases, it has been possible to incorporate a broad variety of non-proteinogenic amino acids and explore additional bioorthogonal methods for macrocyclization [115, 116]. Techniques based on oxidative coupling of benzylamine and 5-hydroxyindole groups (Scheme 1.11a) [120], intramolecular Michael addition (Scheme 1.11b) [121], and copper(I)-catalyzed azide–alkyne cycloaddition (CuAAC) (also known as click chemistry; Scheme 1.11c) have been reported for cyclization of peptidic molecules [122].

In addition to applications for macrocyclization of biosynthetically derived peptides, CuAAC has been also applied to synthetic peptides and non-peptidic macrocyclization. Along with the synthetic ease of introducing azide and alkyne functionalities into molecules, the 1,2,3-triazole moiety has been identified as a privileged scaffold for drug design [123, 124]. A wide variety of synthetic macrocycles have been formed using CuAAC and employing peptide [125], steroid [126], carbohydrate [127–129], and various other scaffolds (Chapter 11) [130–132].

Recently, macrocyclization by CuAAC has been utilized with flow chemistry [133]. In addition to the benefits of low-residency time and the ability to tune reactant concentration as needed, such processes have been highlighted as having a significant *green chemistry* advantage through the use of simple copper tubing as catalyst

Scheme 1.10 Cysteine-based macrocyclization technique for peptides.

(a)

(b)

(c)
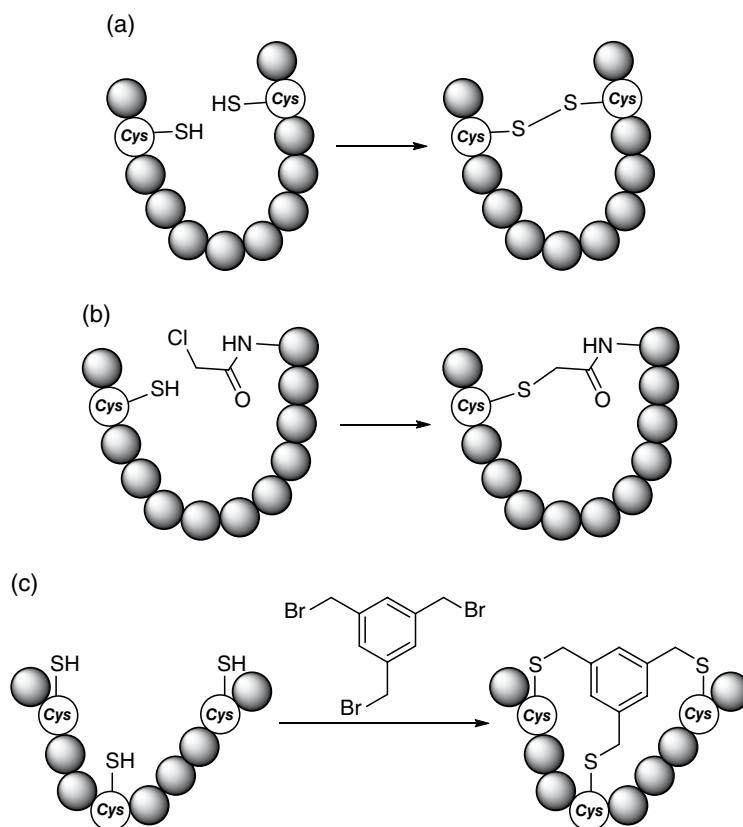
Scheme 1.11 Macrocyclization of biosynthetic peptides with non-proteinogenic amino acids.

(a)

(b)

(c)
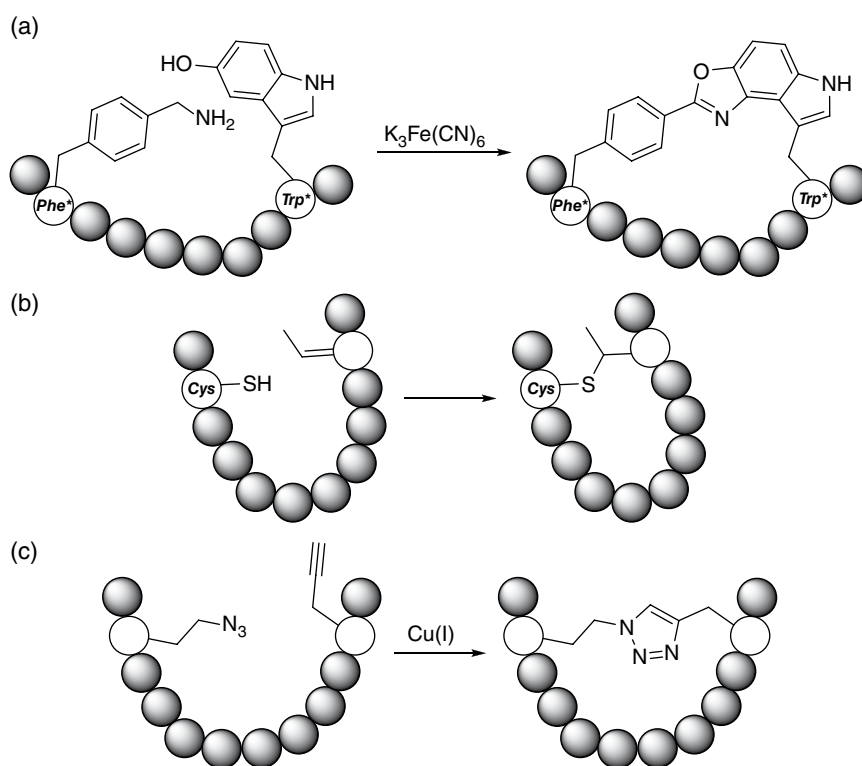
source. Bogdan and James have reported a method for *in flow* CuAAC macrocyclization to generate a 5-iodo-1,2,3-triazole in the cyclization linker. An interesting feature of this methodology was that the cyclization event not only closed the ring but also enabled further diversification by subsequent palladium-catalyzed cross-coupling (Scheme 1.12). The *in flow* macrocycle synthesis by CuAAC was also used to assess the thermodynamics of the reaction in the context of decreasing ring size [134]. Notable changes in geometry and ring strain were observed as ring size was decreased from 14 to 10 atoms, with the CuAAC chemistry being able to tolerate up to 21 kcal/mol of strain energy before forming primarily oligomeric side products.

Many methods exist for C—C bond forming macrocyclization, enabling a wide variety of connectivity to be established (for an extensive review, see Chapters 12 and 13) [79]. Organometallic cross-coupling [135, 136], Diels–Alder reaction [137], and Ni-catalyzed reductive coupling are a select number of the transformations available to chemists (Scheme 1.13) [138, 139]. Just as in carboxylic acid chemistry (Chapter 9), the macrocyclization by C—C bond formation has to be performed at high dilution to avoid oligomerization [42]. Additionally, high temperatures can be required to access the desired reactivity.

Ring-closing metathesis (RCM) is also a very important C—C bond forming technique for macrocyclization and has been widely used to form a variety of unsaturated rings (Chapter 9) [140]. Most commonly achieved with ruthenium catalysis, RCM is driven by the expulsion of ethylene to form a diverse range of challenging rings [141]. However, in certain cases, a sustained reaction can be observed with formation of a ring–chain equilibrium [44]. The reversibility of RCM can be used to form the thermodynamically favored product as seen in the "self-editing" example published by Smith and coworkers (Scheme 1.14) [142].

RCM plays an important role in the formation of "stapled" peptides. First conceived in 1998 [143], stapled peptides are linear peptides that, once connected by an alkyl or alkene linker [144], possess stabilized alpha-helical conformations in solution [145]. A key development to this technique was the introduction of α,α-disubstituted olefin-bearing amino acids at the *i* and *i* + 4 or *i* + 7 positions of the peptide to take advantage of the periodicity of amino acid side-chain projection in peptide alpha helices (Scheme 1.15) [144]. It has also proven possible to establish multiple staples into a single peptide to further rigidify the helical nature [146]. Stapled peptides have been pursued in a range of indications and diseases including difficult to target extra- and intracellular PPIs [147], as well as a number of clinical trials [145, 148].

The example of stapled peptides highlights the notion of using an external conformational element to direct a productive macrocyclization [35]. Template-driven reactivity has been used in a wide variety of macrocyclization reactions to pre-organize difficult to cyclize substrates and increase reaction concentration [42]. Non-covalent pre-organization strategies have included the use of metal, organic and inorganic anions, arene-interaction, and hydrogen-bonding templates [42]. The use of covalent
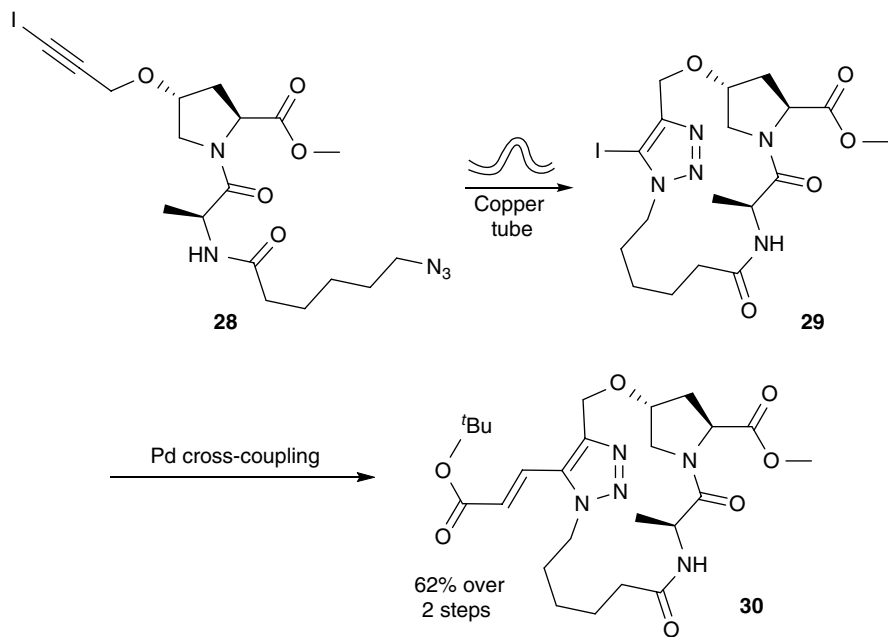
Scheme 1.12 In flow CuAAC-mediated macrocyclization and subsequent diversification by palladium-catalyzed cross-coupling.

Scheme 1.13 Macrocyclization by C—C bond formation with the Stille coupling (a), Diels–Alder reaction (b), and Ni-catalyzed reductive coupling (c).

(a)

31 → Pd(Ph$_3$P)$_4$ (0.05 eq) / LiCl (3.0 eq) / THF (1 mM), Δ, 6 h → **32** (76%)

(b)

33a → La(OTf)$_3$ (0.1 eq) / PhMe (10 mM), 100 °C, 4 h → **33b** (79%)

(c)

34 → Ni(cod)$_2$ (0.2 eq) / Bu$_3$P (0.4 eq) / Et$_3$B, PhMe (50 mM), 60 °C, 14 h → **35** (44%, >10 : 1 dr)

36 → 35 mol% [Ru] / PhH (20 mM), 55°C, 1 h → **37** (70%)
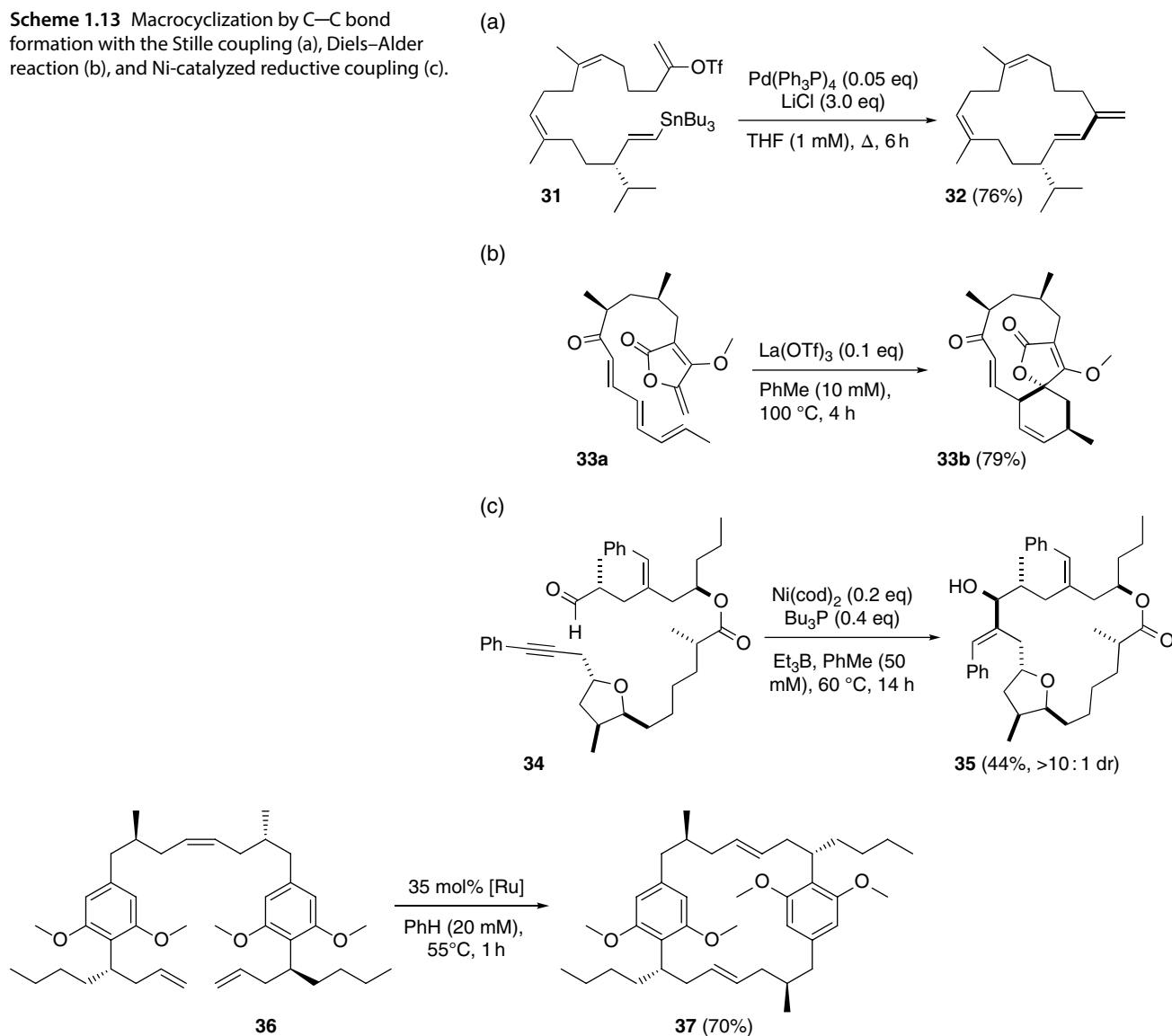
Scheme 1.14 "Self-editing" in RCM to produce a single rearranged thermodynamic product.

Scheme 1.15 Stabilized alpha-helical peptide derived from stapled peptides by RCM.

[Ru] RCM
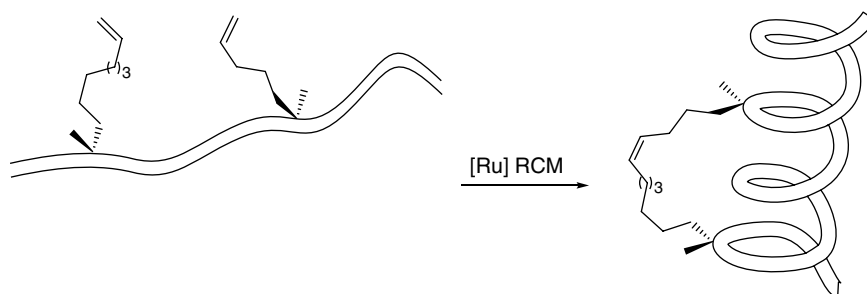
templates through ester and imine linkages has enabled the synthesis of challenging large rings [149–151].

In the field of macrocyclization, the ability to integrate additional functionality to the cyclization linker is highly sought after [152]. One possible way of achieving this multi-faceted synthesis is to employ a multicomponent reaction (MCR) for the macrocyclization (Chapter 14) [153]. In such an event, at least three components are united with a corresponding increase in molecular complexity. The Ugi reaction [154], a multicomponent
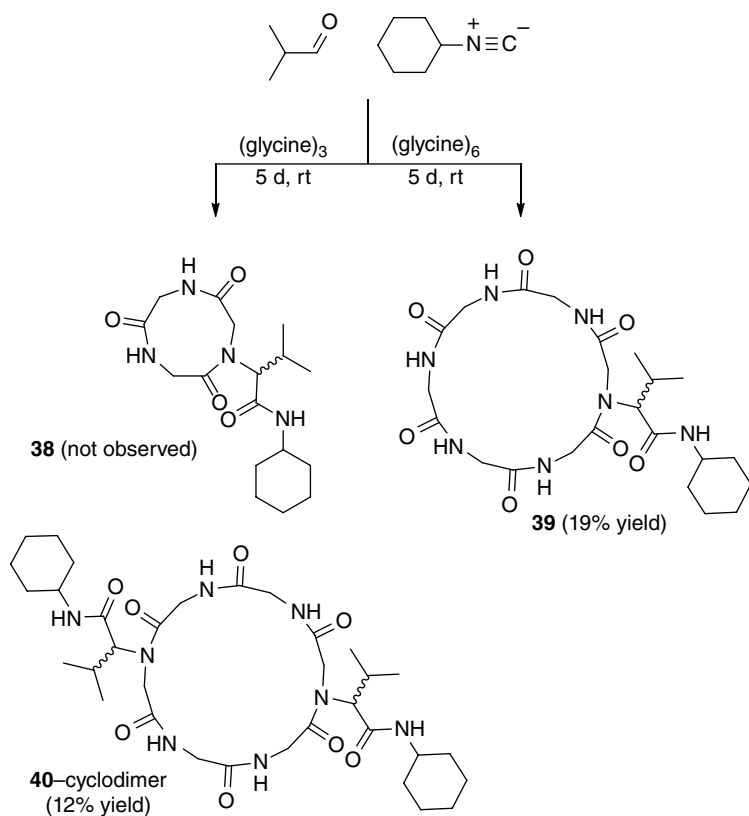
Scheme 1.16 Macrocyclization by Ugi MCR.

coupling of an amine, aldehyde, carboxylic acid, and iso-cyanide, was first attempted on a peptide by Götz and coworkers [155]. While the reaction of a glycine tripep-tide was not successful, the 18-membered ring from (glycine)$_6$ was successfully isolated (Scheme 1.16).

In their continued efforts, the Wessjohann group has harnessed the utility of the cyclodimerization process by forming macrocycles with multiple Ugi reactions, termed multiple multicomponent macrocyclizations (MiBs) [156]. Using bifunctional building blocks such as diamines and diacids, consecutive MCRs were per-formed on a range of substrates to demonstrate the wide variety of ring sizes and types that can be efficiently cyclized in this manner (Scheme 1.17) [157].

The Yudin group has been interested in mechanisms that would reroute the regular process of an Ugi MCR and yield a divergent set of products (Scheme 1.18) [39]. When the amine and aldehyde components were com-bined in the form of amphoteric aziridine aldehyde dimers **42**, a disrupted Ugi reaction took place with pep-tides and isocyanides to yield aziridine-containing cyclic peptides **46**. In subsequent studies, the analysis of side products and substrate-dependent reactivity suggested the involvement of an imidoanhydride intermediate **44** in the reaction pathway of the disrupted Ugi reaction [158]. The importance of this intermediate within the

macrocyclization pathway, in addition to side-product formation, remains a subject of further investigation. Formation of imidoanhydride intermediates has also been postulated by Zhu and coworkers in their work on three-component macrocyclization with 5-iminooxazo-lines [159–161].

The aziridine ring embedded within the cyclization linker of **46** has been investigated as a point for late-stage functionalization by nucleophiles (Scheme 1.18) [133]. Thiol [13, 39, 162], thioacid [163], azide [164, 165], and hydrogenolysis ring opening conditions have been demonstrated for this class of molecules [163]. The ability to install thiol or azide functionality allows for further diversification by Michael addition to maleimides and CuAAC, respectively (Scheme 1.19) [164].

1.5 Cyclization on the Solid Phase

Due to the difficult nature of purifying macrocycles, cyclization on the solid phase can be a crucial technique to preferentially isolate successfully cyclized substrates. Loading substrates on solid phase can partially mimic the effects of high dilution by physically separating the individual molecules and dramatically enhancing intra-molecular processes. The result of this has been observed

Scheme 1.17 Multiple multicomponent macrocyclizations (MiBs).
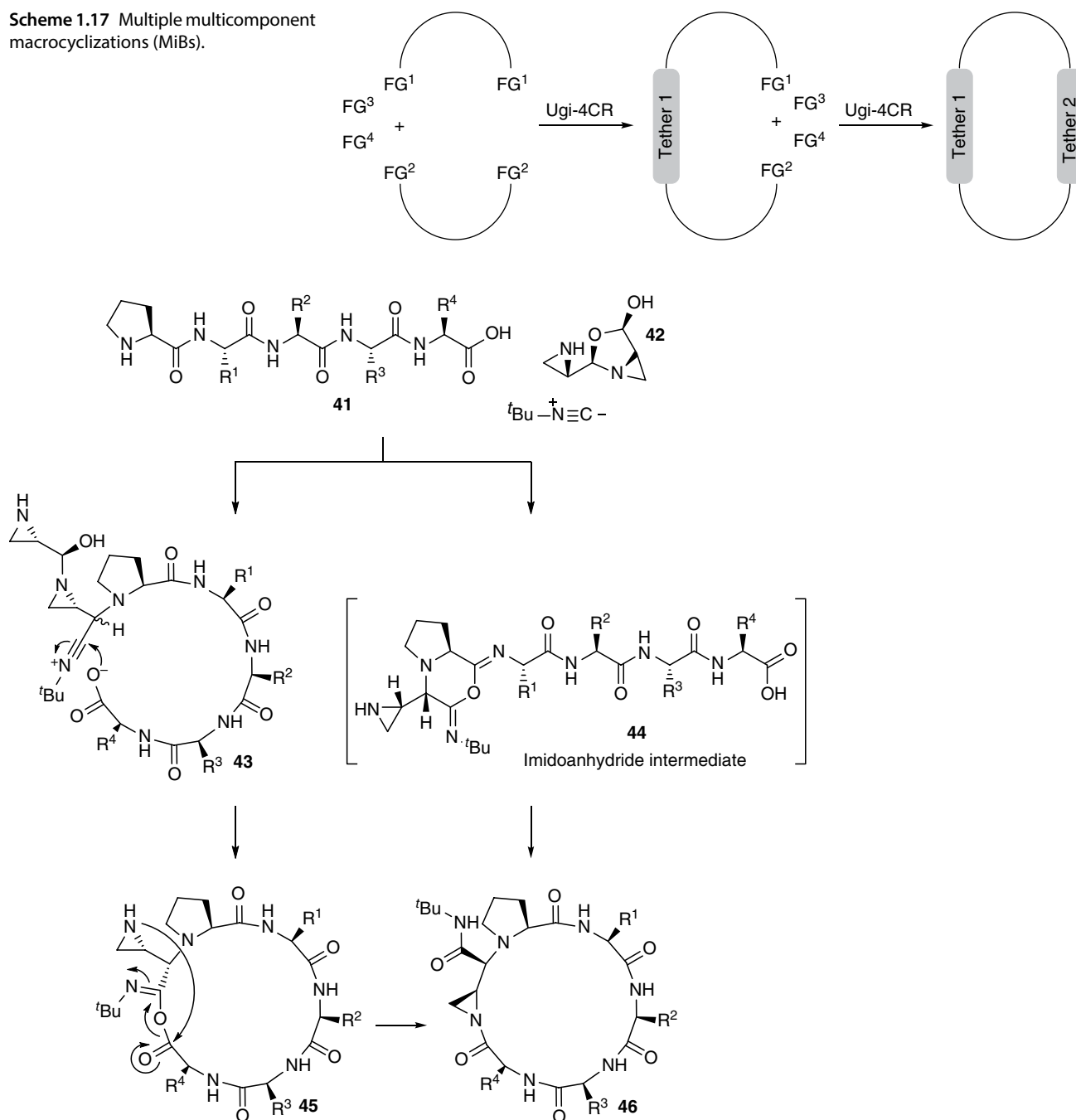
Scheme 1.18 Macrocyclization by the disrupted Ugi MCR with aziridine aldehyde dimers, peptides, and isocyanides.

as high cyclization efficiency with reduced formation of oligomers, although this is not always the case [166].

As an alternative, there has been considerable research into solid phase immobilized coupling agents for peptide synthesis (Scheme 1.20) [167]. A variety of polymer-supported carbodiimide, *N*-hydroxysuccinimide, and uronium/phosphonium reagents have been reported. The use of immobilized reagents greatly simplifies the isolation of products from the reaction mixture otherwise

problematic to separate (Figure 1.4). In addition to solid phase immobilized reagents for macrolactamization, solid phase chemistry has been used to immobilize bases for alkylative macrolactonization, phosphines for Mitsunobu chemistry, and palladium catalysts for Tsuji–Trost alkylation [168].

When substrates are immobilized instead of reagents, careful manipulation of protecting groups has to be considered, as well as choice of anchoring groups.

For example, in conventional solid phase peptide synthesis, the C-terminal carboxylate is anchored on the resin and the peptide is assembled in a C-to-N fashion along the peptide backbone amides to minimize epimerization. For a peptide to be macrocyclized along the backbone, while on solid phase, the peptide has to
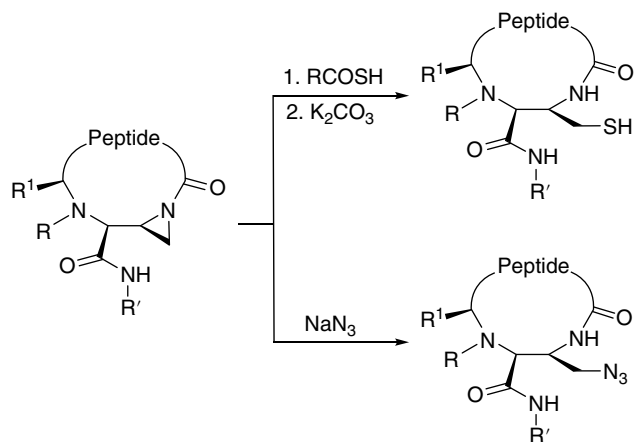
Scheme 1.19 Late-stage functionalization for peptide conjugates by aziridine ring opening.
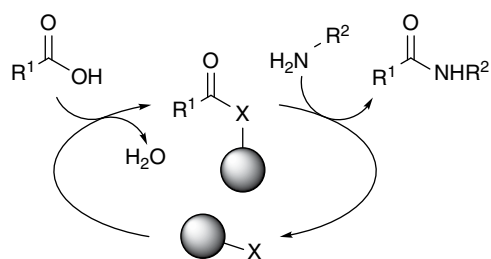
Scheme 1.20 Immobilized coupling reagents for amide bond formation.
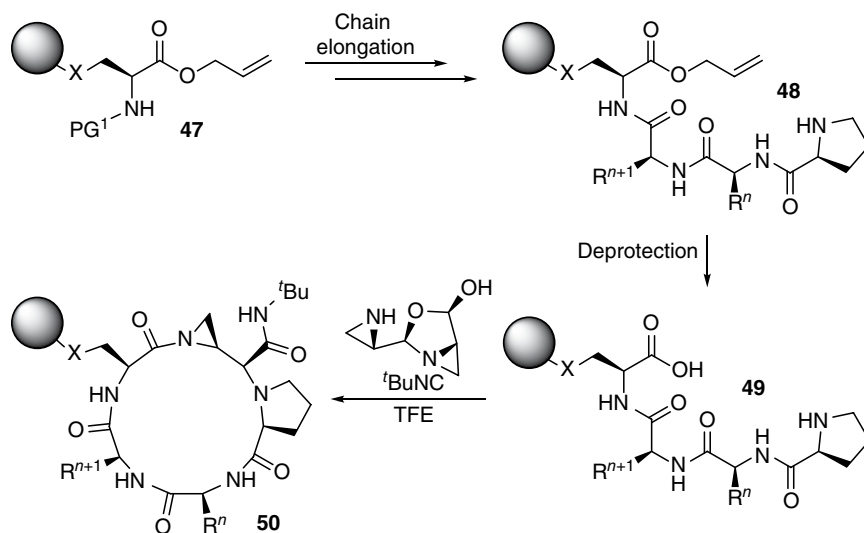
be anchored to the resin by a side chain [169]. Orthogonal protecting groups (e.g., allyl/alloc in Fmoc-based peptide chemistry) allow for selective deprotection of the C-terminal carboxylate without cleavage from the resin [170]. For example, the Yudin and Marsault groups used a side-chain immobilized amino acid allyl ester as a pivotal anchor in demonstrating macrocyclization on solid phase with the disrupted Ugi MCR (Scheme 1.21) [50].

Additional macrocyclization chemistries demonstrated on the solid phase have included S_N2 processes [171], Heck reaction [172], and CuAAC [125]. The mild and tolerant nature of the CuAAC reaction has actually enabled the cyclization of deprotected peptides on solid phase [166].

When macrocyclization of a substrate is followed by release from the solid phase, the process is called cyclative release or cleavage, and it is enabling from the standpoint of cleaving only the successfully macrocyclized compounds, simplifying purification [173]. The use of an amine-bearing tether, orthogonally protected by a Ddz group, enabled cyclative release of 14–22 peptidomimetic macrocycles from thioester-immobilized peptides (Scheme 1.22a) [52, 174]. Changing the substrate anchor to an olefin-containing linker enabled cyclative release by RCM of similar tripeptidomimetic substrates (Scheme 1.22b). Additional methods have been reported for backbone cyclative release chemistry based on Suzuki coupling [175], sulfur ylides [176], azidopeptidylphosphoranes [177], and oxidative cleavage of aryl hydrazides [178].

Cyclative release has been employed for the synthesis of cycle-tail motif depsipeptides by acylphenyldiazene activation [179]. The cyclative release strategy avoided epimerization issues in analogous syntheses and afforded

Scheme 1.21 Macrocyclization by the disrupted Ugi MCR on solid phase.

Scheme 1.22 Cyclative release strategies for macrocyclic peptidomimetics.

(a)

1. Ddz cleavage
2. Cyclative release
3. Bts cleavage
4. Side-chain deprotection

(b)

1. RCM cyclative release
2. Deprotection

X = O, NH
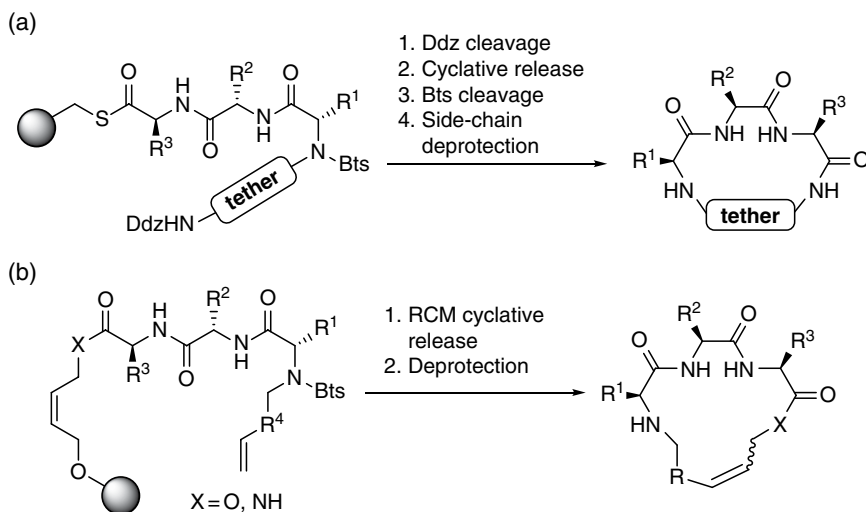
products without contamination by excess coupling reagents. Simplifying the isolation of peptides from cyclization reagents can be especially important for particularly toxic cyclization reagents. Barany and coworkers reported the use of resin-bound Ellman's reagent for cyclative release of cysteine disulfide macrocycles (Scheme 1.23) [180]. The resin-bound reagent is a more practical alternative to thallium (III) trifluoroacetate chemistry for disulfide formation.

1.6 Summary

Macrocycles comprise a broad and functionally rich class of molecules in medicinal chemistry. As therapeutics, macrocycles are particularly noted for their stability and ability to disrupt difficult targets like protein–protein interactions (Chapters 8 and 17) [2]. Crucially, macrocycles can, in certain cases, be made orally bioavailable (Chapter 3), which opens new opportunities for therapeutic intervention, such as those detailed in Part IV. As macrocycles have progressed to the forefront of pharmaceutical interest, considerable effort has been committed to improve and devise new methods for macrocyclization. Contemporary efforts have focused on solid phase methods to enable easier product recovery, yield improvements of established reactions and novel synthetic processes, and use of template-driven macrocyclization to enable greater selectivity. However, since this is a unimolecular reaction, substrate-dependent reactivity continues to characterize—and often limit—this particular reaction, regardless of methodologies new and old, which creates the need for a better understanding of the underlying chemical processes and kinetics. As computational methods improve, the future holds promise

Capture
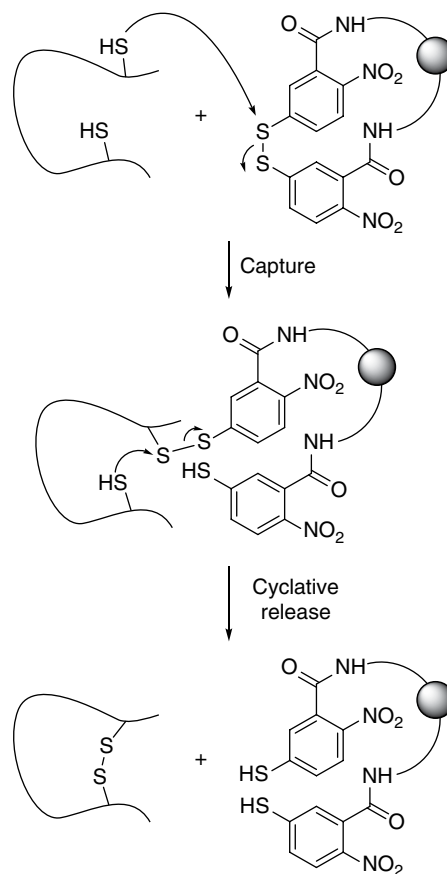
Cyclative release

Scheme 1.23 Cyclative release by disulfide formation. Source: Gonthier *et al*. [168]. Reproduced with permission of Springer.

for a clearer view of the mechanistic underpinnings in macrocyclization reactions and a chance to surpass the inherent challenges.

References

1 Mallinson, J.; Collins, I. Macrocycles in New Drug Discovery. *Future Med. Chem.* **2012**, *4*(11), 1409–1438.

2 Marsault, E.; Peterson, M. L. Macrocycles Are Great Cycles: Applications, Opportunities, and Challenges of Synthetic Macrocycles in Drug Discovery. *J. Med. Chem.* **2011**, *54*(7), 1961–2004.

3 Driggers, E. M.; Hale, S. P.; Lee, J.; Terrett, N. K. The Exploration of Macrocycles for Drug Discovery: An Underexploited Structural Class. *Nat. Rev. Drug Discov.* **2008**, *7*(7), 608–624.

4 Gaynor, M.; Mankin, A. Macrolide Antibiotics: Binding Site, Mechanism of Action, Resistance. *Curr. Top. Med. Chem.* **2003**, *3*(9), 949–960.

5 Rychnovsky, S. D. Oxo Polyene Macrolide Antibiotics. *Chem. Rev.* **1995**, *95*(6), 2021–2040.

6 Uhlig, T.; Kyprianou, T.; Martinelli, F. G.; Oppici, C. A.; Heiligers, D.; Hills, D.; Calvo, X. R.; Verhaert, P. The Emergence of Peptides in the Pharmaceutical Business: From Exploration to Exploitation. *EuPA Open Proteom.* **2014**, *4*, 1–12.

7 Verzele, D.; Madder, A. Patchwork Protein Chemistry: A Practitioner's Treatise on the Advances in Synthetic Peptide Stitchery. *ChemBioChem* **2013**, *14*(9), 1032–1048.

8 Joo, S. H. Cyclic Peptides as Therapeutic Agents and Biochemical Tools. *Biomol. Ther. (Seoul)* **2012**, *20*(1), 19–26.

9 Yudin, A. K. Macrocycles: Lessons from the Distant Past, Recent Developments, and Future Directions. *Chem. Sci.* **2015**, *6*(1), 30–49.

10 Udugamasooriya, D. G.; Spaller, M. R. Conformational Constraint in Protein Ligand Design and the Inconsistency of Binding Entropy. *Biopolymers* **2008**, *89*(8), 653–667.

11 Llinàs-Brunet, M.; Bailey, M. D.; Bolger, G.; Brochu, C.; Faucher, A. M.; Ferland, J. M.; Garneau, M.; Ghiro, E.; Gorys, V.; Grand-Maître, C.; Halmos, T.; Lapeyre-Paquette, N.; Liard, F.; Poirier, M.; Rhéaume, M.; Tsantrizos, Y. S.; Lamarre, D. Structure-Activity Study on a Novel Series of Macrocyclic Inhibitors of the Hepatitis C Virus NS3 Protease Leading to the Discovery of BILN 2061. *J. Med. Chem.* **2004**, *47*(7), 1605–1608.

12 Piekielna, J.; Kluczyk, A.; Gentilucci, L.; Cerlesi, M. C.; Calo', G.; Tomböly, C.; Łapiński, K.; Janecki, T.; Janecka, A. Ring Size in Cyclic Endomorphin-2 Analogs Modulates Receptor Binding Affinity and Selectivity. *Org. Biomol. Chem.* **2015**, *13*(21), 6039–6046.

13 Roxin, Á.; Chen, J.; Scully, C. C. G.; Rotstein, B. H.; Yudin, A. K.; Zheng, G. Conformational Modulation of in Vitro Activity of Cyclic RGD Peptides via Aziridine Aldehyde-Driven Macrocyclization Chemistry. *Bioconjug. Chem.* **2012**, *23*(7), 1387–1395.

14 Hoveyda, H. R.; Marsault, E.; Gagnon, R.; Mathieu, A. P.; Vézina, M.; Landry, A.; Wang, Z.; Benakli, K.; Beaubien, S.; Saint-Louis, C.; Brassard, M.; Pinault, J.-F.; Ouellet, L.; Bhat, S.; Ramaseshan, M.; Peng, X.; Foucher, L.; Beauchemin, S.; Bhérer, P.; Veber, D. F.; Peterson, M. L.; Fraser, G. L. Optimization of the Potency and Pharmacokinetic Properties of a Macrocyclic Ghrelin Receptor Agonist (Part I): Development of Ulimorelin (TZP-101) from Hit to Clinic. *J. Med. Chem.* **2011**, *54*(24), 8305–8320.

15 Chen, K. X.; Njoroge, F. G.; Arasappan, A.; Venkatraman, S.; Vibulbhan, B.; Yang, W.; Parekh, T. N.; Pichardo, J.; Prongay, A.; Cheng, K.-C.; Butkiewicz, N.; Yao, N.; Madison, V.; Girijavallabhan, V. Novel Potent Hepatitis C Virus NS3 Serine Protease Inhibitors Derived from Proline-Based Macrocycles. *J. Med. Chem.* **2006**, *49*(3), 995–1005.

16 Cherney, R. J.; Wang, L.; Meyer, D. T.; Xue, C.-B.; Wasserman, Z. R.; Hardman, K. D.; Welch, P. K.; Covington, M. B.; Copeland, R. A.; Arner, E. C.; DeGrado, W. F.; Decicco, C. P. Macrocyclic Amino Carboxylates as Selective MMP-8 Inhibitors. *J. Med. Chem.* **1998**, *41*(11), 1749–1751.

17 Hancock, R. D. Chelate Ring Size and Metal Ion Selection. The Basis of Selectivity for Metal Ions in Open-Chain Ligands and Macrocycles. *J. Chem. Educ.* **1992**, *69*(8), 615–621.

18 Bechara, C.; Sagan, S. Cell-Penetrating Peptides: 20 Years Later, Where Do We Stand? *FEBS Lett.* **2013**, *587*(12), 1693–1702.

19 Maher, S.; Brayden, D. J. Overcoming Poor Permeability: Translating Permeation Enhancers for Oral Peptide Delivery. *Drug Discov. Today Technol.* **2012**, *9*(2), e113–e119.

20 Bockus, A. T.; McEwen, C. M.; Lokey, R. S. Form and Function in Cyclic Peptide Natural Products: A Pharmacokinetic Perspective. *Curr. Top. Med. Chem.* **2013**, *13*(7), 821–836.

21 Rezai, T.; Bock, J. E.; Zhou, M. V.; Kalyanaraman, C.; Lokey, R. S.; Jacobson, M. P. Conformational Flexibility, Internal Hydrogen Bonding, and Passive Membrane Permeability: Successful in Silico Prediction of the Relative Permeabilities of Cyclic Peptides. *J. Am. Chem. Soc.* **2006**, *128*(43), 14073–14080.

22 Rezai, T.; Yu, B.; Millhauser, G. L.; Jacobson, M. P.; Lokey, R. S. Testing the Conformational Hypothesis of Passive Membrane Permeability Using Synthetic Cyclic Peptide Diastereomers. *J. Am. Chem. Soc.* **2006**, *128*(8), 2510–2511.

23 Hewitt, W. M.; Leung, S. S. F.; Pye, C. R.; Ponkey, A. R.; Bednarek, M.; Jacobson, M. P.; Lokey, R. S. Cell-Permeable Cyclic Peptides from Synthetic Libraries

Inspired by Natural Products. *J. Am. Chem. Soc.* **2015**, *137*(2), 715–721.

24 Craik, D. J.; Fairlie, D. P.; Liras, S.; Price, D. The Future of Peptide-Based Drugs. *Chem. Biol. Drug Des.* **2013**, *81*(1), 136–147.

25 Chatterjee, J.; Laufer, B.; Kessler, H. Synthesis of N-Methylated Cyclic Peptides. *Nat. Protoc.* **2012**, *7*(3), 432–444.

26 Alex, A.; Millan, D. S.; Perez, M.; Wakenhut, F.; Whitlock, G. A. Intramolecular Hydrogen Bonding to Improve Membrane Permeability and Absorption in beyond Rule of Five Chemical Space. *Med. Chem. Commun.* **2011**, *2*(7), 669–674.

27 Madala, P. K.; Tyndall, J. D. A.; Nall, T.; Fairlie, D. P. Update 1 of: Proteases Universally Recognize Beta Strands in Their Active Sites. *Chem. Rev.* **2010**, *110*(6), PR1–PR31.

28 Horswill, A. R.; Benkovic, S. J. Cyclic Peptides, A Chemical Genetics Tool for Biologists. *Cell Cycle* **2005**, *4*(4), 552–555.

29 Lovering, F.; Bikker, J.; Humblet, C. Escape from Flatland: Increasing Saturation as an Approach to Improving Clinical Success. *J. Med. Chem.* **2009**, *52*(21), 6752–6756.

30 Illuminati, G.; Mandolini, L. Ring Closure Reactions of Bifunctional Chain Molecules. *Acc. Chem. Res.* **1981**, *14*(4), 95–102.

31 Karaman, R. Proximity vs. Strain in Intramolecular Ring-Closing Reactions. *Mol. Phys.* **2010**, *108*(13), 1723–1730.

32 Galli, C.; Mandolini, L. The Role of Ring Strain on the Ease of Ring Closure of Bifunctional Chain Molecules. *Eur. J. Org. Chem.* **2000**, *2000*(18), 3117–3125.

33 Collins, J. C.; James, K. Emac: A Comparative Index for the Assessment of Macrocyclization Efficiency. *Med. Chem. Commun.* **2012**, *3*(12), 1489–1495.

34 Jung, M. E.; Piizzi, G. Gem-Disubstituent Effect: Theoretical Basis and Synthetic Applications. *Chem. Rev.* **2005**, *105*(5), 1735–1766.

35 White, C. J.; Yudin, A. K. Contemporary Strategies for Peptide Macrocyclization. *Nat. Chem.* **2011**, *3*(7), 509–524.

36 Brown, H. A.; Waymouth, R. M. Zwitterionic Ring-Opening Polymerization for the Synthesis of High Molecular Weight Cyclic Polymers. *Acc. Chem. Res.* **2013**, *46*(11), 2585–2596.

37 Guo, L.; Lahasky, S. H.; Ghale, K.; Zhang, D. N-Heterocyclic Carbene-Mediated Zwitterionic Polymerization of N-Substituted N-Carboxyanhydrides toward Poly(α-Peptoid)s: Kinetic, Mechanism, and Architectural Control. *J. Am. Chem. Soc.* **2012**, *134*(22), 9163–9171.

38 Londregan, A. T.; Farley, K. A.; Limberakis, C.; Mullins, P. B.; Piotrowski, D. W. A New and Useful Method for the Macrocyclization of Linear Peptides. *Org. Lett.* **2012**, *14*(11), 2890–2893.

39 Hili, R.; Rai, V.; Yudin, A. K. Macrocyclization of Linear Peptides Enabled by Amphoteric Molecules. *J. Am. Chem. Soc.* **2010**, *132*(9), 2889–2891.

40 Schmidt, U.; Langner, J. Cyclotetrapeptides and Cyclopentapeptides: Occurrence and Synthesis. *J. Pept. Res.* **1997**, *49*(1), 67–73.

41 Davies, J. S. The Cyclization of Peptides and Depsipeptides. *J. Pept. Sci.* **2003**, *9*(8), 471–501.

42 Martí-Centelles, V.; Pandey, M. D.; Burguete, M. I.; Luis, S. V. Macrocyclization Reactions: The Importance of Conformational, Configurational, and Template-Induced Preorganization. *Chem. Rev.* **2015**, *115*(16), 8736–8834.

43 Crane, E. A.; Scheidt, K. A. Prins-Type Macrocyclizations as an Efficient Ring-Closing Strategy in Natural Product Synthesis. *Angew. Chem. Int. Ed.* **2010**, *49*(45), 8316–8326.

44 Monfette, S.; Fogg, D. E. Equilibrium Ring-Closing Metathesis. *Chem. Rev.* **2009**, *109*(8), 3783–3816.

45 Casadei, M. A.; Galli, C.; Mandolini, L. Ring-Closure Reactions. 22. Kinetics of Cyclization of Diethyl (ω-Bromoalkyl)malonates in the Range of 4- to 21-Membered Rings. Role of Ring Strain. *J. Am. Chem. Soc.* **1984**, *106*(4), 1051–1056.

46 Joullié, M. M.; Lassen, K. M. Evolution of Amide Bond Formation. *Arkivoc* **2010**, *2010*(8), 189–250.

47 Montalbetti, C. A. G. N.; Falque, V. Amide Bond Formation and Peptide Coupling. *Tetrahedron* **2005**, *61*(46), 10827–10852.

48 Fischer, P. M. Diketopiperazines in Peptide and Combinatorial Chemistry. *J. Pept. Sci.* **2003**, *9*(1), 9–35.

49 Titlestad, K. Cyclic Peptides of Sarcosine. Syntheses and Conformation. *Acta Chem. Scand. B* **1975**, *29*(2), 153–167.

50 Treder, A. P.; Hickey, J. L.; Tremblay, M.-C. J.; Zaretsky, S.; Scully, C. C. G.; Mancuso, J.; Doucet, A.; Yudin, A. K.; Marsault, E. Solid-Phase Parallel Synthesis of Functionalised Medium-to-Large Cyclic Peptidomimetics through Three-Component Coupling Driven by Aziridine Aldehyde Dimers. *Chem. Eur. J.* **2015**, *21*(25), 9249–9255.

51 Khan, S. N.; Kim, A.; Grubbs, R. H.; Kwon, Y.-U. Ring-Closing Metathesis Approaches for the Solid-Phase Synthesis of Cyclic Peptoids. *Org. Lett.* **2011**, *13*(7), 1582–1585.

52 Marsault, E.; Hoveyda, H. R.; Gagnon, R.; Peterson, M. L.; Vézina, M.; Saint-Louis, C.; Landry, A.; Pinault, J.-F.; Ouellet, L.; Beauchemin, S.; Beaubien, S.; Mathieu, A.; Benakli, K.; Wang, Z.; Brassard, M.; Lonergan, D.; Bilodeau, F.; Ramaseshan, M.; Fortin, N.; Lan, R.; Li, S.; Galaud, F.; Plourde, V.; Champagne, M.; Doucet, A.; Bhérer, P.; Gauthier, M.; Olsen, G.; Villeneuve, G.; Bhat, S.; Foucher, L.; Fortin, D.; Peng, X.; Bernard, S.; Drouin, A.; Déziel, R.; Berthiaume, G.; Dory, Y. L.;

Fraser, G. L.; Deslongchamps, P. Efficient Parallel Synthesis of Macrocyclic Peptidomimetics. *Bioorg. Med. Chem. Lett.* **2008**, *18*(16), 4731–4735.

53 Grubbs, R. H.; Chang, S. Recent Advances in Olefin Metathesis and Its Application in Organic Synthesis. *Tetrahedron* **1998**, *54*(18), 4413–4450.

54 Waghmare, A. A.; Hindupur, R. M.; Pati, H. N. Propylphosphonic Anhydride (T3P®): An Expedient Reagent for Organic Synthesis. *Rev. J. Chem.* **2014**, *4*(2), 53–131.

55 Lewer, P.; Graupner, P. R.; Hahn, D. R.; Karr, L. L.; Duebelbeis, D. O.; Lira, J. M.; Anzeveno, P. B.; Fields, S. C.; Gilbert, J. R.; Pearce, C. Discovery, Synthesis, and Insecticidal Activity of Cycloaspeptide E. *J. Nat. Prod.* **2006**, *69*(10), 1506–1510.

56 Russell, D. H.; Edmondson, R. D. High-Resolution Mass Spectrometry and Accurate Mass Measurements with Emphasis on the Characterization of Peptides and Proteins by Matrix-Assisted Laser Desorption/ Ionization Time-of-Flight Mass Spectrometry. *J. Mass Spectrom.* **1997**, *32*(3), 263–276.

57 Chawner, R.; Holman, S. W.; Gaskell, S. J.; Eyers, C. E. Peptide Scrambling During Collision-Induced Dissociation Is Influenced by N-Terminal Residue Basicity. *J. Am. Soc. Mass Spectrom.* **2014**, *25*(11), 1927–1938.

58 Wysocki, V. H.; Tsaprailis, G.; Smith, L. L.; Breci, L. A. Mobile and Localized Protons: A Framework for Understanding Peptide Dissociation. *J. Mass Spectrom.* **2000**, *35*(12), 1399–1406.

59 Mohimani, H.; Yang, Y.-L.; Liu, W.-T.; Hsieh, P.-W.; Dorrestein, P. C.; Pevzner, P. A. Sequencing Cyclic Peptides by Multistage Mass Spectrometry. *Proteomics* **2011**, *11*(18), 3642–3650.

60 Ngoka, L. C. M.; Gross, M. L. Multistep Tandem Mass Spectrometry for Sequencing Cyclic Peptides in an Ion-Trap Mass Spectrometer. *J. Am. Soc. Mass Spectrom.* **1999**, *10*(8), 732–746.

61 Mohimani, H.; Kim, S.; Pevzner, P. A. A New Approach to Evaluating Statistical Significance of Spectral Identifications. *J. Proteome Res.* **2013**, *12*(4), 1560–1568.

62 Liu, W.-T.; Ng, J.; Meluzzi, D.; Bandeira, N.; Gutierrez, M.; Simmons, T. L.; Schultz, A. W.; Linington, R. G.; Moore, B. S.; Gerwick, W. H.; Pevzner, P. A.; Dorrestein, P. C. Interpretation of Tandem Mass Spectra Obtained from Cyclic Nonribosomal Peptides. *Anal. Chem.* **2009**, *81*(11), 4200–4209.

63 Kavan, D.; Kuzma, M.; Lemr, K.; Schug, K. A.; Havlicek, V. CYCLONE: A Utility for De Novo Sequencing of Microbial Cyclic Peptides. *J. Am. Soc. Mass Spectrom.* **2013**, *24*(8), 1177–1184.

64 Joo, S. H.; Xiao, Q.; Ling, Y.; Gopishetty, B.; Pei, D. High-Throughput Sequence Determination of Cyclic Peptide Library Members by Partial Edman Degradation/Mass Spectrometry. *J. Am. Chem. Soc.* **2006**, *128*(39), 13000–13009.

65 Liang, X.; Girard, A.; Biron, E. Practical Ring-Opening Strategy for the Sequence Determination of Cyclic Peptides from One-Bead-One-Compound Libraries. *ACS Comb. Sci.* **2013**, *15*(10), 535–540.

66 Zaretsky, S.; Rai, V.; Gish, G.; Forbes, M. W.; Kofler, M.; Yu, J. C. Y.; Tan, J.; Hickey, J. L.; Pawson, T.; Yudin, A. K. Twisted Amide Electrophiles Enable Cyclic Peptide Sequencing. *Org. Biomol. Chem.* **2015**, *13*(27), 7384–7388.

67 Piekielna, J.; Kluczyk, A.; Perlikowska, R.; Janecka, A. Cyclic Pentapeptide Analogs Based on Endomorphin-2 Structure: Cyclization Studies Using Liquid Chromatography Combined with on-Line Mass Spectrometry and Tandem Mass Spectrometry. *Peptides* **2014**, *55*, 32–40.

68 Lanucara, F.; Holman, S. W.; Gray, C. J.; Eyers, C. E. The Power of Ion Mobility-Mass Spectrometry for Structural Characterization and the Study of Conformational Dynamics. *Nat. Chem.* **2014**, *6*(4), 281–294.

69 Jeanne Dit Fouque, K.; Afonso, C.; Zirah, S.; Hegemann, J. D.; Zimmermann, M.; Marahiel, M. A.; Rebuffat, S.; Lavanant, H. Ion Mobility-Mass Spectrometry of Lasso Peptides: Signature of a Rotaxane Topology. *Anal. Chem.* **2015**, *87*(2), 1166–1172.

70 Ruotolo, B. T.; Tate, C. C.; Russell, D. H. Ion Mobility-Mass Spectrometry Applied to Cyclic Peptide Analysis: Conformational Preferences of Gramicidin S and Linear Analogs in the Gas Phase. *J. Am. Soc. Mass Spectrom.* **2004**, *15*(6), 870–878.

71 Adusumalli, S. R.; Yudin, A. K.; Rai, V. Cyclic Peptides. In *Natural Lactones and Lactams*; Janecki, T., Ed.; Wiley-VCH Verlag GmbH & Co. KGaA: Weinheim, Germany, **2013**; pp 321–369.

72 Takada, Y.; Umehara, M.; Katsumata, R.; Nakao, Y.; Kimura, J. The Total Synthesis and Structure–Activity Relationships of a Highly Cytotoxic Depsipeptide Kulokekahilide-2 and Its Analogs. *Tetrahedron* **2012**, *68*(2), 659–669.

73 Lang, G.; Kalvelage, T.; Peters, A.; Wiese, J.; Imhoff, J. F. Linear and Cyclic Peptides from the Entomopathogenic Bacterium *Xenorhabdus nematophilus*. *J. Nat. Prod.* **2008**, *71*(6), 1074–1077.

74 Willoughby, P. H.; Jansma, M. J.; Hoye, T. R. A Guide to Small-Molecule Structure Assignment through Computation of (^{1}H and ^{13}C) NMR Chemical Shifts. *Nat. Protoc.* **2014**, *9*(3), 643–660.

75 Zaretsky, S.; Hickey, J. L.; St. Denis, M. A.; Scully, C. C. G.; Roughton, A. L.; Tantillo, D. J.; Lodewyk, M. W.; Yudin, A. K. Predicting Cyclic Peptide Chemical Shifts Using Quantum Mechanical Calculations. *Tetrahedron* **2014**, *70*(42), 7655–7663.

76 Watts, K. S.; Dalal, P.; Tebben, A. J.; Cheney, D. L.; Shelley, J. C. Macrocycle Conformational Sampling with MacroModel. *J. Chem. Inf. Model.* **2014**, *54*(10), 2680–2696.

77 Bonnet, P.; Agrafiotis, D. K.; Zhu, F.; Martin, E. Conformational Analysis of Macrocycles: Finding What Common Search Methods Miss. *J. Chem. Inf. Model.* **2009**, *49*(10), 2242–2259.

78 Peterson, M. L. The Synthesis of Macrocycles for Drug Discovery. In *Macrocycles in Drug Discovery*; Levin, J., Ed.; Royal Society of Chemistry: London, **2015**; pp 398–486.

79 Yu, X.; Sun, D. Macrocyclic Drugs and Synthetic Methodologies toward Macrocycles. *Molecules* **2013**, *18* (6), 6230–6268.

80 Harrowven, D. C.; Kostiuk, S. L. Macrocylic Bisbibenzyl natural Products and Their Chemical Synthesis. *Nat. Prod. Rep.* **2012**, *29*(2), 223–242.

81 Knorr, R.; Trzeciak, A.; Bannwarth, W.; Gillessen, D. New Coupling Reagents in Peptide Chemistry. *Tetrahedron Lett.* **1989**, *30*(15), 1927–1930.

82 El-Faham, A.; Albericio, F. Peptide Coupling Reagents, More Than a Letter Soup. *Chem. Rev.* **2011**, *111*(11), 6557–6602.

83 Parenty, A.; Moreau, X.; Campagne, J.-M. Macrolactonizations in the Total Synthesis of Natural Products. *Chem. Rev.* **2006**, *106*(3), 911–939.

84 Corey, E. J.; Kirst, H. A. New Method for the Synthesis of Macrolides. *J. Am. Chem. Soc.* **1972**, *94*(2), 667–668.

85 Mukaiyama, T.; Usui, M.; Saigo, K. The Facile Synthesis of Lactones. *Chem. Lett.* **1976**, *5*(1), 49–50.

86 Inanaga, J.; Hirata, K.; Saeki, H.; Katsuki, T.; Yamaguchi, M. A Rapid Esterification by Means of Mixed Anhydride and Its Application to Large-Ring Lactonization. *Bull. Chem. Soc. Jpn.* **1979**, *52*(7), 1989–1993.

87 Shiina, I.; Kubota, M.; Ibuka, R. A Novel and Efficient Macrolactonization of ω-Hydroxycarboxylic Acids Using 2-Methyl-6-Nitrobenzoic Anhydride (MNBA). *Tetrahedron Lett.* **2002**, *43*(42), 7535–7539.

88 Li, W.; Schlecker, A.; Ma, D. Total Synthesis of Antimicrobial and Antitumor Cyclic Depsipeptides. *Chem. Commun.* **2010**, *46*(30), 5403.

89 Liao, X.; Wu, Y.; De Brabander, J. K. Total Synthesis and Absolute Configuration of the Novel Microtubule-Stabilizing Agent Peloruside A. *Angew. Chem. Int. Ed.* **2003**, *42*(14), 1648–1652.

90 McNulty, J.; Capretta, A.; Laritchev, V.; Dyck, J.; Robertson, A. J. The Role of Acyloxyphosphonium Ions and the Stereochemical Influence of Base in the Phosphorane-Mediated Esterification of Alcohols. *Angew. Chem. Int. Ed.* **2003**, *42*(34), 4051–4054.

91 Dawson, P.; Muir, T.; Clark-Lewis, I.; Kent, S. Synthesis of Proteins by Native Chemical Ligation. *Science* **1994**, *266*(5186), 776–779.

92 Camarero, J. A.; Muir, T. W. Chemoselective Backbone Cyclization of Unprotected Peptides. *Chem. Commun.* **1997**, *15*, 1369–1370.

93 Tam, J. P.; Lu, Y.-A. Synthesis of Large Cyclic Cystine-Knot Peptide by Orthogonal Coupling Strategy Using Unprotected Peptide Precursor. *Tetrahedron Lett.* **1997**, *38*(32), 5599–5602.

94 Yan, L. Z.; Dawson, P. E. Synthesis of Peptides and Proteins without Cysteine Residues by Native Chemical Ligation Combined with Desulfurization. *J. Am. Chem. Soc.* **2001**, *123*(4), 526–533.

95 Shao, Y.; Lu, W.; Kent, S. B. H. A Novel Method to Synthesize Cyclic Peptides. *Tetrahedron Lett.* **1998**, *39*(23), 3911–3914.

96 Hemu, X.; Qiu, Y.; Tam, J. P. Peptide Macrocyclization through Amide-to-Amide Transpeptidation. *Tetrahedron* **2014**, *70*(42), 7707–7713.

97 Tam, J. P.; Lu, Y. A.; Yu, Q. Thia Zip Reaction for Synthesis of Large Cyclic Peptides: Mechanisms and Applications. *J. Am. Chem. Soc.* **1999**, *121*(18), 4316–4324.

98 Nilsson, B. L.; Kiessling, L. L.; Raines, R. T. Staudinger Ligation: A Peptide from a Thioester and Azide. *Org. Lett.* **2000**, *2*(13), 1939–1941.

99 Saxon, E.; Armstrong, J. I.; Bertozzi, C. R. A "Traceless" Staudinger Ligation for the Chemoselective Synthesis of Amide Bonds. *Org. Lett.* **2000**, *2*(14), 2141–2143.

100 Kleineweischede, R.; Hackenberger, C. P. R. Chemoselective Peptide Cyclization by Traceless Staudinger Ligation. *Angew. Chem. Int. Ed.* **2008**, *47*(32), 5984–5988.

101 Ha, K.; Monbaliu, J.-C. M.; Williams, B. C.; Pillai, G. G.; Ocampo, C. E.; Zeller, M.; Stevens, C. V.; Katritzky, A. R. A Convenient Synthesis of Difficult Medium-Sized Cyclic Peptides by Staudinger Mediated Ring-Closure. *Org. Biomol. Chem.* **2012**, *10*(40), 8055–8058.

102 Lam, H.; Li, X. Serine/Threonine Ligation in Cyclizing Peptides. *Synlett* **2014**, *25*(10), 1339–1344.

103 Camarero, J. A.; Kimura, R. H.; Woo, Y.-H.; Shekhtman, A.; Cantor, J. Biosynthesis of a Fully Functional Cyclotide Inside Living Bacterial Cells. *ChemBioChem* **2007**, *8*(12), 1363–1366.

104 Tailhades, J.; Patil, N. A.; Hossain, M. A.; Wade, J. D. Intramolecular Acyl Transfer in Peptide and Protein Ligation and Synthesis. *J. Pept. Sci.* **2015**, *21*(3), 139–147.

105 Macmillan, D.; De Cecco, M.; Reynolds, N. L.; Santos, L. F. A.; Barran, P. E.; Dorin, J. R. Synthesis of Cyclic Peptides through an Intramolecular Amide Bond Rearrangement. *ChemBioChem* **2011**, *12*(14), 2133–2136.

106 Clark, R. J.; Craik, D. J. Native Chemical Ligation Applied to the Synthesis and Bioengineering of Circular Peptides and Proteins. *Biopolymers* **2010**, *94*(4), 414–422.

107 Foster, A. D.; Ingram, J. D.; Leitch, E. K.; Lennard, K. R.; Osher, E. L.; Tavassoli, A. Methods for the Creation of Cyclic Peptide Libraries for Use in Lead Discovery. *J. Biomol. Screen.* **2015**, *20*(5), 563–576.

108 Lennard, K. R.; Tavassoli, A. Peptides Come Round: Using SICLOPPS Libraries for Early Stage Drug Discovery. *Chem. Eur. J.* **2014**, *20*(34), 10608–10614.

109 Northfield, S. E.; Wang, C. K.; Schroeder, C. I.; Durek, T.; Kan, M.-W.; Swedberg, J. E.; Craik, D. J. Disulfide-Rich Macrocyclic Peptides as Templates in Drug Design. *Eur. J. Med. Chem.* **2014**, *77*, 248–257.

110 Chung, B. K. W.; Yudin, A. K. Disulfide-Bridged Peptide Macrobicycles from Nature. *Org. Biomol. Chem.* **2015**, *13*(33), 8768–8779.

111 Craik, D. J.; Swedberg, J. E.; Mylne, J. S.; Cemazar, M. Cyclotides as a Basis for Drug Design. *Expert Opin. Drug Discovery* **2012**, *7*(3), 179–194.

112 Craik, D. J.; Čemažar, M.; Wang, C. K. L.; Daly, N. L. The Cyclotide Family of Circular Miniproteins: Nature's Combinatorial Peptide Template. *Biopolymers* **2006**, *84*(3), 250–266.

113 Andreu, D.; Albericio, F.; Solé, N. A.; Munson, M. C.; Ferrer, M.; Barany, G. Formation of Disulfide Bonds in Synthetic Peptides and Proteins. In *Peptide Synthesis Protocols*; Pennington, M. W., Dunn, B. M., Eds.; Humana Press: Totowa, **1994**; Vol. *35*, pp 91–170.

114 Bulaj, G. Formation of Disulfide Bonds in Proteins and Peptides. *Biotechnol. Adv.* **2005**, *23*(1), 87–92.

115 Passioura, T.; Katoh, T.; Goto, Y.; Suga, H. Selection-Based Discovery of Druglike Macrocyclic Peptides. *Annu. Rev. Biochem.* **2014**, *83*(1), 727–752.

116 Jongkees, S. A. K.; Hipolito, C. J.; Rogers, J. M.; Suga, H. Model Foldamers: Applications and Structures of Stable Macrocyclic Peptides Identified Using In Vitro Selection. *New J. Chem.* **2015**, *39*(5), 3197–3207.

117 Goto, Y.; Ohta, A.; Sako, Y.; Yamagishi, Y.; Murakami, H.; Suga, H. Reprogramming the Translation Initiation for the Synthesis of Physiologically Stable Cyclic Peptides. *ACS Chem. Biol.* **2008**, *3*(2), 120–129.

118 Sako, Y.; Goto, Y.; Murakami, H.; Suga, H. Ribosomal Synthesis of Peptidase-Resistant Peptides Closed by a Nonreducible Inter-Side-Chain Bond. *ACS Chem. Biol.* **2008**, *3*(4), 241–249.

119 Heinis, C.; Rutherford, T.; Freund, S.; Winter, G. Phage-Encoded Combinatorial Chemical Libraries Based on Bicyclic Peptides. *Nat. Chem. Biol.* **2009**, *5*(7), 502–507.

120 Yamagishi, Y.; Ashigai, H.; Goto, Y.; Murakami, H.; Suga, H. Ribosomal Synthesis of Cyclic Peptides with a Fluorogenic Oxidative Coupling Reaction. *ChemBioChem* **2009**, *10*(9), 1469–1472.

121 Goto, Y.; Iwasaki, K.; Torikai, K.; Murakami, H.; Suga, H. Ribosomal Synthesis of Dehydrobutyrine- and Methyllanthionine-Containing Peptides. *Chem. Commun.* **2009**, *23*, 3419–3421.

122 Sako, Y.; Morimoto, J.; Murakami, H.; Suga, H. Ribosomal Synthesis of Bicyclic Peptides via Two Orthogonal Inter-Side-Chain Reactions. *J. Am. Chem. Soc.* **2008**, *130*(23), 7232–7234.

123 Haider, S.; Alam, M. S.; Hamid, H. 1,2,3-Triazoles: Scaffold with Medicinal Significance. *Inflamm. Cell Signal.* **2014**, *1*, e95.

124 Agalave, S. G.; Maujan, S. R.; Pore, V. S. Click Chemistry: 1,2,3-Triazoles as Pharmacophores. *Chem. Asian J.* **2011**, *6*(10), 2696–2718.

125 Ingale, S.; Dawson, P. E. On Resin Side-Chain Cyclization of Complex Peptides Using CuAAC. *Org. Lett.* **2011**, *13*(11), 2822–2825.

126 Echemendía, R.; Concepción, O.; Morales, F. E.; Paixão, M. W.; Rivera, D. G. The CuI-Catalyzed Alkyne–Azide Cycloaddition as Direct Conjugation/ Cyclization Method of Peptides to Steroids. *Tetrahedron* **2014**, *70*(20), 3297–3305.

127 Billing, J. F.; Nilsson, U. J. C2-Symmetric Macrocyclic Carbohydrate/Amino Acid Hybrids through Copper(I)-Catalyzed Formation of 1,2,3-Triazoles. *J. Org. Chem.* **2005**, *70*(12), 4847–4850.

128 Bodine, K. D.; Gin, D. Y.; Gin, M. S. Highly Convergent Synthesis of C3- or C2-Symmetric Carbohydrate Macrocycles. *Org. Lett.* **2005**, *7*(20), 4479–4482.

129 Bodine, K. D.; Gin, D. Y.; Gin, M. S. Synthesis of Readily Modifiable Cyclodextrin Analogues via Cyclodimerization of an Alkynyl–Azido Trisaccharide. *J. Am. Chem. Soc.* **2004**, *126*(6), 1638–1639.

130 Chouhan, G.; James, K. CuAAC Macrocyclization: High Intramolecular Selectivity through the Use of Copper-Tris(Triazole) Ligand Complexes. *Org. Lett.* **2011**, *13*(10), 2754–2757.

131 Wenzel Torne, C.; Meldal, M. Dipolar Cycloaddition Reactions in Peptide Chemistry. In *Organic Azides: Syntheses and Applications*; Bräse, S., Banert, K., Eds.; John Wiley & Sons, Ltd: Chichester, **2010**; pp 285–310.

132 Meldal, M.; Tornøe, C. W. Cu-Catalyzed Azide–Alkyne Cycloaddition. *Chem. Rev.* **2008**, *108*(8), 2952–3015.

133 Bogdan, A. R.; James, K. Efficient Access to New Chemical Space Through Flow-Construction of Druglike Macrocycles through Copper-Surface-Catalyzed Azide-Alkyne Cycloaddition Reactions. *Chem. Eur. J.* **2010**, *16*(48), 14506–14512.

134 Bogdan, A. R.; Jerome, S. V.; Houk, K. N.; James, K. Strained Cyclophane Macrocycles: Impact of Progressive Ring Size Reduction on Synthesis and Structure. *J. Am. Chem. Soc.* **2012**, *134*(4), 2127–2138.

135 Ronson, T. O.; Taylor, R. J. K.; Fairlamb, I. J. S. Palladium-Catalysed Macrocyclisations in the Total Synthesis of Natural Products. *Tetrahedron* **2015**, *71*(7), 989–1009.

136 Peng, L.; Zhang, F.; Mei, T.; Zhang, T.; Li, Y. Studies on Novel Macrocyclization Methods of Cembrane-Type Diterpenoids: A Stille Cyclization Approach to (±)-Isocembrene. *Tetrahedron Lett.* **2003**, *44*(31), 5921–5923.

137 Zapf, C. W.; Harrison, B. A.; Drahl, C.; Sorensen, E. J. A Diels-Alder Macrocyclization Enables an Efficient Asymmetric Synthesis of the Antibacterial Natural Product Abyssomicin C. *Angew. Chem. Int. Ed. Engl.* **2005**, *117*(40), 6691–6695.

138 Colby, E. A.; O'Brien, K. C.; Jamison, T. F. Total Syntheses of Amphidinolides T1 and T4 via Catalytic, Stereoselective, Reductive Macrocyclizations. *J. Am. Chem. Soc.* **2005**, *127*(12), 4297–4307.

139 Colby, E. A.; O'Brien, K. C.; Jamison, T. F. Synthesis of Amphidinolide T1 via Catalytic, Stereoselective Macrocyclization. *J. Am. Chem. Soc.* **2004**, *126*(4), 998–999.

140 Fürstner, A.; Langemann, K. Macrocycles by Ring-Closing Metathesis. *Synthesis* **1997**, *1997*(7), 792–803.

141 Fogg, D.; Conrad, J. Ruthenium-Catalyzed Ring-Closing Metathesis: Recent Advances, Limitations and Opportunities. *Curr. Org. Chem.* **2006**, *10*(2), 185–202.

142 Smith, A. B.; Adams, C. M.; Kozmin, S. A.; Paone, D. V. Total Synthesis of (−)-Cylindrocyclophanes A and F Exploiting the Reversible Nature of the Olefin Cross Metathesis Reaction. *J. Am. Chem. Soc.* **2001**, *123*(25), 5925–5937.

143 Blackwell, H. E.; Grubbs, R. H. Highly Efficient Synthesis of Covalently Cross-Linked Peptide Helices by Ring-Closing Metathesis. *Angew. Chem. Int. Ed.* **1998**, *37*(23), 3281–3284.

144 Schafmeister, C. E.; Po, J.; Verdine, G. L. An All-Hydrocarbon Cross-Linking System for Enhancing the Helicity and Metabolic Stability of Peptides. *J. Am. Chem. Soc.* **2000**, *122*(24), 5891–5892.

145 Walensky, L. D.; Bird, G. H. Hydrocarbon-Stapled Peptides: Principles, Practice, and Progress. *J. Med. Chem.* **2014**, *57*(15), 6275–6288.

146 Bird, G. H.; Madani, N.; Perry, A. F.; Princiotto, A. M.; Supko, J. G.; He, X.; Gavathiotis, E.; Sodroski, J. G.; Walensky, L. D. Hydrocarbon Double-Stapling Remedies the Instability of a Lengthy Peptide Therapeutic. *Proc. Natl. Acad. Sci. U. S. A* **2010**, *107*(32), 14093–14098.

147 Cromm, P. M.; Spiegel, J.; Grossmann, T. N. Hydrocarbon Stapled Peptides as Modulators of Biological Function. *ACS Chem. Biol.* **2015**, *10*(6), 1362–1375.

148 Sawyer, T. K. AILERON Therapeutics. *Chem. Biol. Drug Des.* **2009**, *73*(1), 3–6.

149 Albrecht, M.; Fröhlich, R. Nontemplated versus Templated Synthesis of a 56-Membered Macrocycle. *Synlett* **2007**, *2007*(14), 2295–2297.

150 Höger, S. Highly Efficient Methods for the Preparation of Shape-Persistent Macrocyclics. *J. Polym. Sci. A Polym. Chem.* **1999**, *37*(15), 2685–2698.

151 Höger, S.; Meckenstock, A.-D.; Pellen, H. High-Yield Macrocyclization via Glaser Coupling of Temporary Covalent Templated Bisacetylenes. *J. Org. Chem.* **1997**, *62*(14), 4556–4557.

152 Wessjohann, L.; Rhoden, C.; Rivera, D.; Vercillo, O. E. Cyclic Peptidomimetics and Pseudopeptides from Multicomponent Reactions. In *Topics in Heterocyclic Chemistry*; Orru, R. V. A., Ruijter, E., Eds.; Springer: Berlin/Heidelberg, **2010**; Vol. *23*, pp 199–226.

153 Wessjohann, L. A.; Neves Filho, R. A. W.; Puentes, A. R.; Morejon, M. C. Macrocycles from Multicomponent Reactions. In *Multicomponent Reactions in Organic Synthesis*; Zhu, J., Wang, Q., Wang, M.-X., Eds.; Wiley-VCH Verlag GmbH & Co. KGaA: Weinheim, Germany, **2015**; pp 231–264.

154 Ugi, I. The α-Addition of Immonium Ions and Anions to Isonitriles Accompanied by Secondary Reactions. *Angew. Chem. Int. Ed.* **1962**, *1*(1), 8–21.

155 Failli, A.; Immer, H.; Götz, M. The Synthesis of Cyclic Peptides by the Four Component Condensation (4 CC). *Can. J. Chem.* **1979**, *57*(24), 3257–3261.

156 Wessjohann, L. A.; Rivera, D. G.; Vercillo, O. E. Multiple Multicomponent Macrocyclizations (MiBs): A Strategic Development toward Macrocycle Diversity. *Chem. Rev.* **2009**, *109*(2), 796–814.

157 Wessjohann, L. A.; Filho, R. A. W. N.; Rivera, D. G. Multiple Multicomponent Reactions with Isocyanides. In *Isocyanide Chemistry: Applications in Synthesis and Material Science*; Nenajdenko, V. G., Ed.; Wiley-VCH Verlag GmbH & Co. KGaA: Weinheim, Germany, **2012**; pp 233–262.

158 Zaretsky, S.; Hickey, J. L.; Tan, J.; Pichugin, D.; St. Denis, M. A.; Ler, S.; Chung, B. K. W.; Scully, C. C. G.; Yudin, A. K. Mechanistic Investigation of Aziridine Aldehyde-Driven Peptide Macrocyclization: The Imidoanhydride Pathway. *Chem. Sci.* **2015**, *6*(10), 5446–5455.

159 Pirali, T.; Tron, G. C.; Masson, G.; Zhu, J. Ammonium Chloride Promoted Three-Component Synthesis of 5-Iminooxazoline and Its Subsequent Transformation to Macrocyclodepsipeptide. *Org. Lett.* **2007**, *9*(25), 5275–5278.

160 Bughin, C.; Zhao, G.; Bienaymé, H.; Zhu, J. 5-Aminooxazole as an Internal Traceless Activator of C-Terminal Carboxylic Acid: Rapid Access to Diversely Functionalized Cyclodepsipeptides. *Chem. Eur. J.* **2006**, *12*(4), 1174–1184.

161 Zhao, G.; Sun, X.; Bienaymé, H.; Zhu, J. Activation of a Terminal Carboxylic Acid by an Internal Oxazole: A Novel Synthesis of Macrocyclodepsipeptide. *J. Am. Chem. Soc.* **2001**, *123*(27), 6700–6701.

162 Rotstein, B. H.; Rai, V.; Hili, R.; Yudin, A. K. Synthesis of Peptide Macrocycles Using Unprotected Amino Aldehydes. *Nat. Protoc.* **2010**, *5*(11), 1813–1822.

163 Zaretsky, S.; Scully, C. C. G.; Lough, A. J.; Yudin, A. K. Exocyclic Control of Turn Induction in Macrocyclic Peptide Scaffolds. *Chem. Eur. J.* **2013**, *19*(52), 17668–17672.

164 Zaretsky, S.; Tan, J.; Hickey, J. L.; Yudin, A. K. Macrocyclic Templates for Library Synthesis of Peptido-Conjugates. In *Methods in Molecular Biology (Springer): Peptide Libraries*; Derda, R., Ed.; Springer Science+Business Media: New York, **2015**; Vol. *6*, pp 67–80.

165 Chung, B. K. W.; Hickey, J. L.; Scully, C. C. G.; Zaretsky, S.; Yudin, A. K. Bicycle Synthesis through Peptide Macrocyclization Using Aziridine Aldehydes Followed by Late Stage Disulfide Bond Installation. *Med. Chem. Commun.* **2013**, *4*(7), 1124–1128.

166 Turner, R. A.; Oliver, A. G.; Lokey, R. S. Click Chemistry as a Macrocyclization Tool in the Solid-Phase Synthesis of Small Cyclic Peptides. *Org. Lett.* **2007**, *9*(24), 5011–5014.

167 Cherkupally, P.; Ramesh, S.; de la Torre, B. G.; Govender, T.; Kruger, H. G.; Albericio, F. Immobilized Coupling Reagents: Synthesis of Amides/Peptides. *ACS Comb. Sci.* **2014**, *16*(11), 579–601.

168 Gonthier, E.; Breinbauer, R. Solid-Supported Reagents and Catalysts for the Preparation of Large Ring Compounds. *Mol. Divers.* **2005**, *9*(1–3), 51–62.

169 Kim, J.; Hong, I.-K.; Kim, H.-J.; Jeong, H.-J.; Choi, M.-J.; Yoon, C.-N.; Jeong, J.-H. Efficient Macrocyclization for Cyclicpeptide Using Solid-Phase Reaction. *Arch. Pharm. Res.* **2002**, *25*(6), 801–806.

170 Isidro-Llobet, A.; Alvarez, M.; Albericio, F. Amino Acid-Protecting Groups. *Chem. Rev.* **2009**, *109*(6), 2455–2504.

171 Feng, Y.; Pattarawarapan, M.; Wang, Z.; Burgess, K. Solid-Phase SN2 Macrocyclization Reactions to form β-Turn Mimics. *Org. Lett.* **1999**, *1*(1), 121–124.

172 Akaji, K.; Teruya, K.; Akaji, M.; Aimoto, S. Synthesis of Cyclic RGD Derivatives via Solid Phase Macrocyclization Using the Heck Reaction. *Tetrahedron* **2001**, *57*(12), 2293–2303.

173 Nicolaou, K. C.; Pastor, J.; Winssinger, N.; Murphy, F. Solid Phase Synthesis of Macrocycles by an Intramolecular Ketophosphonate Reaction. Synthesis of a (dl)-Muscone Library. *J. Am. Chem. Soc.* **1998**, *120*(20), 5132–5133.

174 Marsault, E.; Hoveyda, H. R.; Peterson, M. L.; Saint-Louis, C.; Landry, A.; Vézina, M.; Quellet, L.; Wang, Z.; Ramaseshan, M.; Beaubien, S.; Benakli, K.; Beauchemin, S.; Déziel, R.; Peeters, T.; Fraser, G. L. Discovery of a New Class of Macrocyclic Antagonists to the Human Motilin Receptor. *J. Med. Chem.* **2006**, *49*(24), 7190–7197.

175 Li, W.; Burgess, K. A New Solid-Phase Linker for Suzuki Coupling with Concomitant Macrocyclization: Synthesis of β-Turn Mimics. *Tetrahedron Lett.* **1999**, *40*(36), 6527–6530.

176 La Porta, E.; Piarulli, U.; Cardullo, F.; Paio, A.; Provera, S.; Seneci, P.; Gennari, C. Cyclative Cleavage via Solid-Phase Supported Stabilized Sulfur Ylides: Synthesis of Macrocyclic Lactones. *Tetrahedron Lett.* **2002**, *43*(5), 761–766.

177 Ahsanullah; Rademann, J. Cyclative Cleavage through Dipolar Cycloaddition: Polymer-Bound Azidopeptidylphosphoranes Deliver Locked Cis-Triazolylcyclopeptides as Privileged Protein Binders. *Angew. Chem. Int. Ed. Engl.* **2010**, *49*(31), 5378–5382.

178 Rosenbaum, C.; Waldmann, H. Solid Phase Synthesis of Cyclic Peptides by Oxidative Cyclative Cleavage of an Aryl Hydrazide Linker: Synthesis of Stylostatin 1. *Tetrahedron Lett.* **2001**, *42*(33), 5677–5680.

179 Shigenaga, A.; Moss, J. A.; Ashley, F. T.; Kaufmann, G. F.; Janda, K. D. Solid-Phase Synthesis and Cyclative Cleavage of Quorum Sensing Depsipeptide Analogues by Acylphenyldiazene Activation. *Synlett* **2006**, *4*, 0551–0554.

180 Annis, I.; Chen, L.; Barany, G. Novel Solid-Phase Reagents for Facile Formation of Intramolecular Disulfide Bridges in Peptides under Mild Conditions 1, 2. *J. Am. Chem. Soc.* **1998**, *120*(29), 7226–7238.

2

A Practical Guide to Structural Aspects of Macrocycles (NMR, X-Ray, and Modeling)

David J. Craik, Quentin Kaas and Conan K. Wang

Institute for Molecular Bioscience, The University of Queensland, Brisbane, Queensland, Australia

2.1 Background

As is apparent from the recent literature [1–4] and other chapters in this book, macrocycles have attracted a great deal of attention over the last decade because of their wide range of applications in drug design and agriculture, as well as their potential uses as molecular probes, diagnostics, or imaging agents. In this chapter, we focus on the structural aspects of macrocycles and discuss state-of-the-art methods for determining their structures, as well as the implications of these structures for the functions and biophysical properties of macrocycles. We have focused the discussion mainly on examples from our own laboratory, where we examine disulfide-rich peptides from plants and animals with applications in drug design and agriculture. However, the structural techniques described in these examples are broadly applicable to a wide range of other macromolecules.

To provide a foundation for the discussion, Table 2.1 shows selected classes of macrocyclic peptides, along with their sizes and structural features of representative examples from each class [3, 5–55]. Our emphasis is on peptidic molecules (i.e., peptides or closely related molecules that have a high content of amino acids), and readers are referred to other recent reviews that have covered non-peptidic macrocycles in more detail for coverage of those classes of macrocycles [1, 56–59].

2.1.1 Classes of Macrocycles Covered

In their general order of size, the smallest examples we cover here include synthetic monocyclic peptides (including pentapeptides and hexapeptides) [3, 5–12]; naturally occurring monocyclic peptides (e.g., antamanide [13, 14]; members of the orbitide family [15–19]; and cyclosporine A [20–24]); protein epitope mimetics (PEMs), which are synthetic β-hairpin-type peptides often built on a D-Pro/L-Pro template [25–29]; synthetic "bicycles" typically
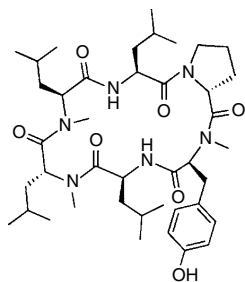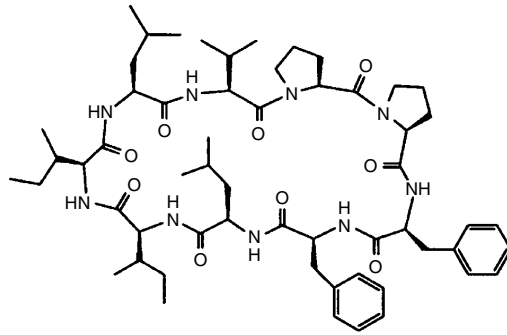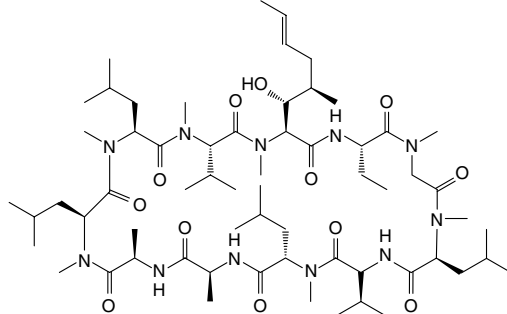
of 500–1500 Da molecular weight that contain two covalent cycles [30–35]; and sunflower trypsin inhibitors of 14 amino acids with a single disulfide bond [36–39]. The slightly larger, and more disulfide-rich, examples we cover include cyclized conotoxins with two or more disulfide bonds [39–41]; θ-defensins, which comprise three disulfide bonds and 18 amino acids [42–45]; and cyclotides of around 30 amino acids with three disulfide bonds in a knotted configuration [46–50]. Finally, the circular bacteriocins are the largest macrocycles that we will mention here. These head-to-tail bacterial products are around 60–80 amino acids in size [51–55].
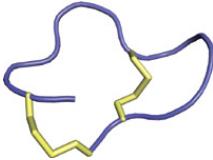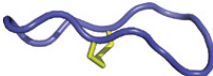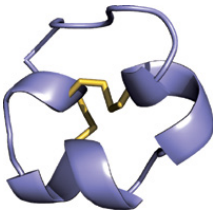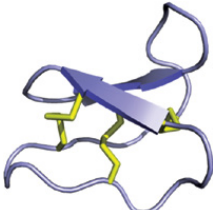
Many of the naturally occurring macrocycles described herein are ribosomally synthesized, and a recent article provides an excellent overview of the biosynthesis and nomenclature of these and other ribosomally synthesized peptides [60]. In this chapter, we do not consider internal cycles formed by disulfide bonds as leading to the definition of a molecule as "macrocyclic." Rather we focus on head-to-tail (e.g., cyclotides) or side chain-to-tail (e.g., lasso peptides [61] and a melanocortin receptor antagonist called MT-II [62]) macrocyclization. We make this arbitrary definition since disulfide bonds can be broken via reduction, and our focus is on more "permanent" covalent approaches to macrocyclization. Nevertheless, many of the molecules we discuss do contain disulfide bonds and thus have extra layers of cyclization, and hence rigidity, built into them. The disulfide bonds provide additional stabilization and make disulfide-rich cyclic peptides a particularly interesting class of molecules to study.

2.1.2 Applications of Macrocycles in Drug Design and Agriculture and the Role of Structural Information in These Applications

Interest in macrocycles from a drug design perspective derives mainly from the wide range of pharmaceutically relevant activities that cyclic peptides have been reported
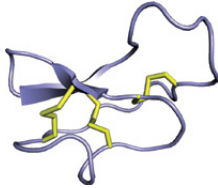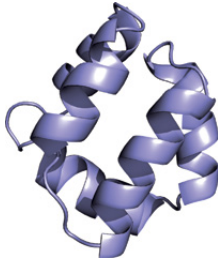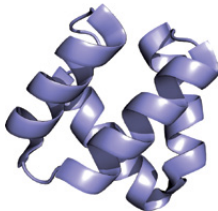
Table 2.1 Selected classes of macrocyclic peptides with their sizes and structural features of representative examples.

Peptide class	Size (a.a.)	No. SS bond	Example	Structure	Comments	References
Synthetic cyclic peptides	5–10	0	Somatostatin analogue			[3, 5–12]
Naturally occurring monocyclic peptides	5–12	0	Cyclolinopeptide A		Orbitide derived from flax plants	[13–19]
Cyclosporine A	11	0	Cyclosporine A		N-methylated natural product	[20–24]

Protein epitope mimetics (PEMs)	10–16	0	L-22		Peptides often built on a D-Pro/L-Pro template	[25–29]
Bicycles	13–17	2	UK504		Cyclized with disulfide bonds or other cross-linkages, creating two cycles	[30–35]
Sunflower trypsin inhibitors	14	1	SFTI-1		Derived from sunflower seeds	[36–39]
Cyclized conotoxins	16–22	2	Cyclic Vc1.1		Chemically cyclized peptide reengineered from Vc1.1 from the venom of *Conus victoriae*	[39–41]
Theta-defensins	18	3	RTD-1		Originally discovered in rhesus macaque (*Macaca mulatta*) leukocytes	[42–45]
Cyclotides	28–37	3	Kalata B1		Ultra-stable cyclic peptides from plants of the Rubiaceae, Violaceae, Cucurbitaceae, Solanaceae, and Fabaceae	[46–50]

(*Continued*)

Table 2.1 (Continued)

Peptide class	Size (a.a.)	No. SS bond	Example	Structure	Comments	References
		3	MCoTI-I/II		Derived from seeds of *Momordica cochinchinensis*	[49, 50]
Circular bacteriocins	60–78	0	AS-48		Derived from *Enterococcus*	[51–55]
	64	0	NKR-5-3B		In *Enterococcus faecium* isolated from Thai fermented fish	[55]

to have and the higher relative stability and bioactivity of these molecules compared with topologically "linear" molecules. Although peptides are widely regarded as excellent drug leads, in the past there have been reservations in the pharmaceutical industry about their potential for practical applications as drugs because of their perceived poor stability (due to susceptibility to proteolytic degradation) and low oral bioavailability. Cyclization appears to be a relatively robust and general way of improving the stability of peptides, thus ameliorating the first of these limitations. Furthermore, there are now several cases where cyclic peptides have been reported to have oral bioactivity in animal disease models in which the corresponding linear peptides were not orally active [40, 63], thus offering promise for at least a partial solution to the bioavailability problem. However, detailed pharmacokinetic studies have not been reported for these cases. Their oral activity might reflect exceptional potency and stability rather than intrinsic bioavailability, and further work is necessary to examine this possibility. Cyclosporine A (see Table 2.1 for structure) is perhaps the best known and most studied example of an orally bioavailable macrocyclic peptide, where *F*% (oral bioavailability) has been quantitatively reported to be 30% (see Chapter 3 for an in-depth discussion on the bioavailability of macrocycles) [64].

Cyclosporine A is an interesting example of a macrocyclic peptide because it comprises nonstandard amino acids, such as N-methylated amino acids and D-amino acids, that control its conformation and thus affect its activity. In fact, cyclosporine A is the first example of the full use of NOE in peptide conformational analysis [24, 65] (the use of NOE information in structure determination will be discussed later). In general, additional structural constraints, such as those imparted from disulfide bonds or nonstandard amino acids, can further improve the biopharmaceutical properties of the macrocyclic peptide [66–68]. For example, a D-Trp was incorporated into a cyclic somatostatin analogue to stabilize a βII′ turn that was initially identified from the structure of a disulfide-constrained analogue. One of the optimized analogues displayed improved metabolic stability and had a long duration of action as well as oral activity [66]. An extension of the use of D-amino acids as conformational constraints is captured in the approach of "spatial screening," which involves systematic conversion of individual residues to their opposite enantiomeric form to tease out preferred conformations that might enhance selectivity and/or activity [69]. From the examples briefly mentioned here and others discussed in other chapters, it is clear that macrocycles can often act as templates that can be optimized to become potent bioactive molecules.

The potential pharmaceutical activities of macrocyclic peptides cover a vast spectrum, from anticancer to cardiovascular diseases, as well as from metabolic diseases to inflammatory and infectious diseases. The activities may be present in naturally occurring peptides or may be engineered or "grafted" into a macrocyclic peptide, as, for example, has been widely reported for cyclotides [70, 71].

There is also increasing interest in peptides as bioactives for agricultural applications. For example, cyclotides have been reported to have insecticidal [72, 73], antiviral [74], antimicrobial [75], nematocidal [76–79], and molluscicidal activities [80], all of which could be relevant to the protection of crop plants from microbes, pathogens, or herbivorous pests (Figure 2.1). In the case of the antimicrobial (i.e., antibacterial and antiviral) activities, the tested microbes were not direct plant pathogens, and the activities were relatively weak, and so it is not clear yet whether these activities are agriculturally relevant. However, for the various other pesticidal activities, cyclotides are relatively potent and show promise for applications involving either external delivery (e.g., via spraying) or in transgenic plants.

Other reported activities for cyclotides suggest additional potential industrial applications, including antifouling [81] and possibly as imaging agents. For such applications, the relatively high cost of cyclotides is currently a limitation, and other shorter cyclic peptides such as orbitides might be more cost-effective. Perhaps the most readily realized industrial application of other classes of cyclic peptides could be the use of cyclic bacteriocins as food preservatives [51–55].

Structural studies of macrocyclic peptides have played a vital role in facilitating their pharmaceutical, agricultural, and other industrial applications. Determining the structures of these macrocycles has, for example, allowed the bioactive insecticidal regions of cyclotides to be found [82] and has allowed regions of their structures to be identified that can be modified to increase nematocidal activity without perturbing the stability of the framework [83]. Structural studies have guided the design of cyclic conotoxins [84, 85] and chlorotoxins [86], which have been used to improve the biopharmaceutical properties of these disulfide-rich venom-derived peptides. Furthermore, the structures of macrocycles in complex with their receptors have provided mechanistic insights into activity; for example, the structure of the cyclotide MCoTI-II bound with trypsin has helped to unravel its mechanism of inhibition [87, 88]. Given the vital role of structure in exploiting macrocyclic peptides, we now provide a more detailed introduction on the structural methods that have been applied.
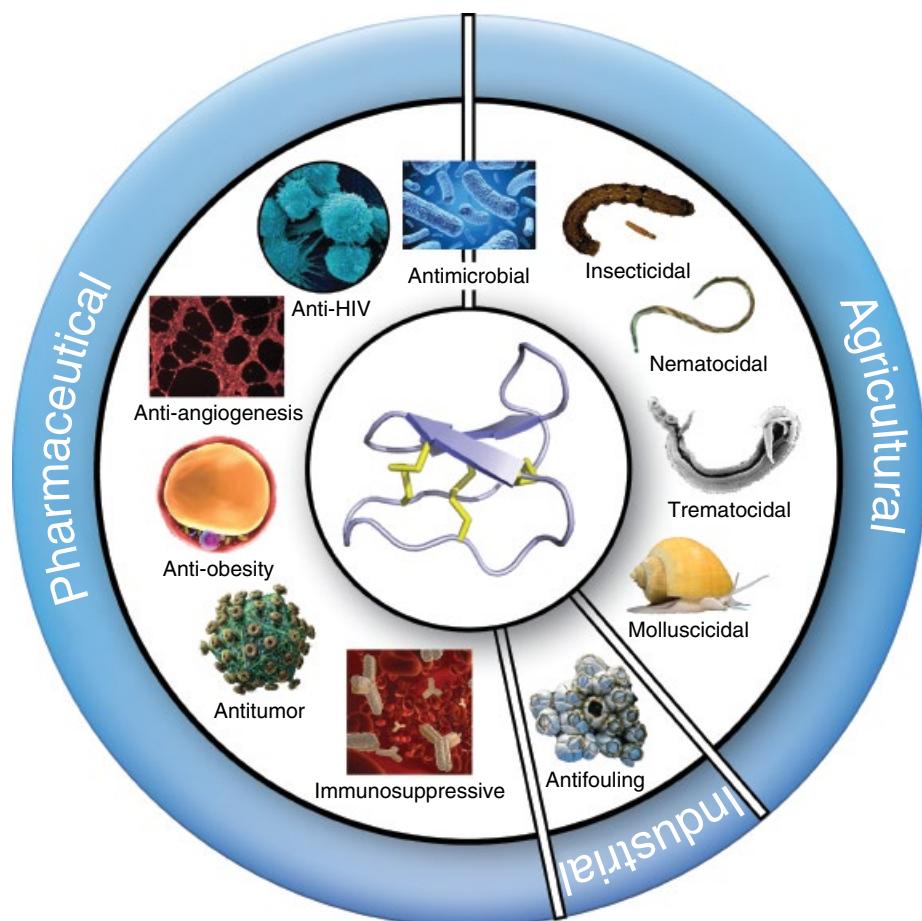
Figure 2.1 Pharmaceutical, agricultural, and industrial applications of cyclotides. The range of potential applications of cyclotides is illustrated schematically by showing the relevant target organisms. (*See insert for color representation of the figure.*)

2.1.3 Experimental Techniques (NMR and X-Ray)

Disulfide-rich peptides are notoriously difficult to crystallize, and, hence, most work on their structures has been done using either nuclear magnetic resonance (NMR) or molecular modeling. To illustrate this trend, we note that among a large and well-studied class of disulfide-rich peptides, namely, the conotoxins [89, 90], there have been approximately 175 structures reported to date, of which more than 95% were derived from NMR and only 11 from X-ray [91–99]. The advent of racemic crystallography [100] has recently opened the door for crystallographic studies of such molecules, and this advance is covered in Section 2.2.4. Notwithstanding this development, the focus of most of the discussion in this chapter is on NMR structures.

From an experimental perspective, macrocycles are particularly amenable to NMR analysis because their spectra are relatively uncomplicated and can be readily assigned without the need for isotopic labeling, at least for peptides up to approximately 50 amino acids, which includes most of the classes of macrocycles referred to in

Table 2.1, apart from the circular bacteriocins, but even these have been solved using homonuclear NMR methods. Additionally, with NMR, the effects of the solution conditions (e.g., pH, cosolvents, membrane mimics such as micelles, bicelles, or vesicles) and temperatures can be resolved and thus, arguably, can be used to study peptides in physiologically or industrially more relevant conditions than crystals. In particular, the conformations of small peptides, which have a relatively large surface-to-core ratios, typically depend strongly on the environment. In such cases, the conformation in solution might differ from that in a crystalline state [101, 102]. On the other hand, peptides with a well-stabilized core will have crystal and NMR solution structures that are generally very similar. For example, this is clearly the case for kalata B1, which has a dense cystine core [39].

2.1.4 Modeling Studies

Molecular modeling also plays an important role in the studies of the structures of macrocycles, in large part by providing a methodology for examining the interaction of these molecules with their target receptors. These
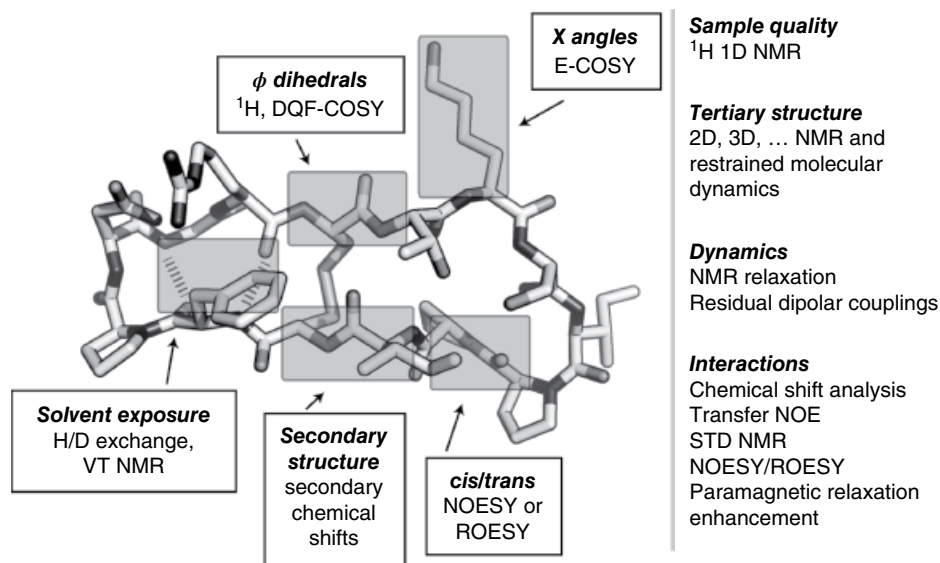
Figure 2.2 Structural information on macrocycles that can be derived from NMR experiments. The types of structural information are mapped onto the structure of SFTI-1 (PDB: 1JBL), which is used here as an example of a macrocyclic peptide. Additional information and the NMR experiments that can be used are shown on the right. This figure is adapted from one in an article by Yudin [2]. Source: http://pubs.rsc.org/en/content/articlehtml/2015/sc/c4sc03089c. Used under CC BY-NC 3.0, https://creativecommons.org/licenses/by-nc/3.0/

targets include membranes, nucleic acids, enzymes, or protein-based cellular or cell surface receptors. Such modeling studies are covered in Section 2.3. Modeling approaches have also contributed very greatly to the studies of the macrocycles themselves, including the prediction of their structures and associated surface properties such as charge distributions and hydrophobicity, as well as their dynamics, particularly in cases where the desired structural information cannot be easily determined using NMR or X-ray crystallography or where there are limits on the physical amount of the macrocycle accessible for experimental studies.

2.2 Experimental Studies of Macrocycles

In this section, we describe experimental approaches to the structure determination of representative classes of macrocycles. As noted earlier, most experimental studies have utilized NMR, but X-ray crystallography has been used in some cases.

2.2.1 NMR Experiments and Parameters That Yield Structural Information

NMR experiments for deriving structural information on various molecular classes, ranging from small molecules to proteins, are now routinely applied in many laboratories. Importantly, many of these experiments can be used to interrogate the structures of macrocyclic

compounds without the need for isotopic labeling, as is typically required for the NMR structure determination of larger proteins. Figure 2.2 outlines some of the types of structural data that can be obtained using NMR, along with the techniques used to provide these data. The range of techniques used depends to some extent on the type of molecule being studied. Small macrocycles are covered in a recent excellent review on NMR of peptides [103]. Here, we will also describe structural analyses of cyclic disulfide-rich peptides. These molecules typically have well-defined secondary and tertiary structures and thus resemble proteins in many ways and so are more amendable to the procedures used for protein structure determination than those used for more flexible peptides. As further guides, we refer readers to textbooks and reviews on the principles of NMR, some of which provide general perspectives [104–107] and others that highlight specific challenges pertaining to particular classes of macrocycles, such as circular and knotted peptides [108].

An initial assessment of the conformation of a macrocycle, or indeed its suitability for structural analysis by NMR, can be obtained from its 1D NMR spectrum by observing the nature of the peaks, that is, their number, dispersion, and chemical shifts. Sample optimization (concentration, pH, solvent, temperature) is sometimes required to improve spectral quality. In the case of cyclosporine A, for example, spectra in methanol show more peaks than expected for a conformationally homogeneous sample. In chloroform, however, the molecule exhibits predominantly one conformation [109, 110]. In our laboratory, we

use 1D spectra to predict whether disulfide-rich peptides (either naturally occurring or engineered analogues) are well folded into a single conformation, with wide dispersion of amide NH peaks being an indicator that the correct disulfide connectivity has formed.

A wide range of NMR parameters provide structural information. Backbone and side-chain dihedral angles can be derived from scalar coupling constants, ^3J, via the Karplus equation [111]. For example, the backbone angle ϕ can be obtained from $^3J_{\text{NH–H}\alpha}$, which is most accurately measured from highly digitized 1D ^{1}H spectra or, in cases of spectral overlap, from 2D double quantum filtered correlation spectroscopy (DQF-COSY) spectra. We note that the use of $^3J_{\text{NH-H}\alpha}$ alone for identifying the dihedral angle can sometimes be ambiguous due to the nature of the Karplus equation. In such scenarios, exclusion of certain possibilities can be achieved by measuring additional couplings such as $^3J_{\text{NH-C}\beta}$ and $^3J_{\text{H}\beta\text{–N}}$ [112]. The side-chain χ_1 can be derived from accurate measurement of $^3J_{\text{H}\alpha\text{–H}\beta}$ and the intensity of relevant NOEs. Another approach to derive dihedral angle information is using the program TALOS+, which predicts dihedral angles (e.g., backbone ϕ and ψ) from ^{1}H, ^{13}C, and ^{15}N chemical shifts [113]. The program exploits the dependence of the chemical shift on the local geometry of the selected nucleus and a growing knowledge base of assigned chemical shifts. Overall, TALOS+ provides valuable information that complements experimentally derived parameters for a range of macrocyclic peptides.

The hydrogen bond network of macrocycles can be monitored using hydrogen/deuterium exchange (H/D exchange) and variable temperature (VT) NMR experiments. The readouts from these experiments (i.e., exchange rates and amide temperature coefficients, respectively) have been used as indicators of intramolecular hydrogen bonding based on the fact that they identify amide protons that are shielded in some way, most commonly via their participation in intramolecular hydrogen bonds. For example, in a recent study we showed a correlation between the temperature coefficients of amide protons with their solvent exposure calculated from molecular dynamics (MD) simulations for a diverse set of macrocyclic peptides [8]. Although the results from H/D exchange experiments generally agree with those from variable temperature NMR (VT NMR), in some cases there are inconsistencies [114], reflecting the fact that a combination of effects is in play. For example, temperature-dependent conformational changes may distort temperature coefficient values. Aside from these limitations, VT NMR experiments can be more robust than H/D exchange because they are less sensitive to variations in the solvent environment (e.g., pH).

Correlations reflecting through-space interactions can be obtained from NOE spectroscopy (NOESY) or rotating-frame Overhauser spectroscopy (ROESY) spectra, and, from these, quantitative measures of interatomic distances can be derived. A prerequisite for this is the assignment of spectra, which is typically done using the sequential assignment methodology [115] based on information from both total correlation spectroscopy (TOCSY) and NOESY (or ROESY) spectra, with NOESY favored for cyclic disulfide-rich peptides bigger than 12 amino acids. Heteronuclear couplings can also be used to assist in making stereospecific assignments [103]. For smaller macrocycles, ROESY rather than NOESY is often used because possible nulling of the NOE intensity can occur depending on the correlation time of the molecule (τ_c, which is dependent on its size) and the operating frequency of the spectrometer (ω_o): when $\omega_o\tau_c \approx 1$, the enhancement is negligible. This phenomenon is illustrated by examples where, to obtain interatomic distances for a cyclic hexapeptide of approximately 600 Da, a ROESY experiment was required [10–12], whereas for SFTI-1, a cyclic 14-residue peptide of approximately 1500 Da, a NOESY experiment was sufficient [36]. If the potential artifacts affecting ROE to distance conversions are taken into account (i.e., correcting for offset effects and TOCSY contributions), accurate distances can be obtained from ROESY spectra [103]. An alternative to using ROESY is to lower the sample temperature (thus modulating τ_c) and use NOESY, as was done for the case of cyclosporine A [116]. Aside from being used to derive quantitative interatomic distances, NOEs can also be interpreted qualitatively. For example, the presence or absence of NOEs between Hα–Hα and Hα–HN (Hα–Hδ for Pro) can be used as an indicator of the *cis/trans* configuration of peptide bonds [5, 46].

The secondary structure of macrocyclic peptides can be gauged from deviations of chemical shifts from random coil values. These deviations are referred to as secondary chemical shifts and can be very useful as a first tool in the analysis of macrocyclic structures. Despite their small size, secondary structure elements are not uncommon in cyclic peptides as cyclization often stabilizes local structure. A series of consecutive positive secondary Hα chemical shifts along a peptide sequence is indicative of β-sheet secondary structure, whereas negative secondary Hα chemical shifts are indicative of α-helical structure. By contrast, secondary shifts close to zero are indicative of flexible or random coil-like structure. We use the random coil chemical shifts reported by Wishart for these calculations [117]. Secondary chemical shifts are also useful as markers for comparison with reported structures to identify structural similarities and make inferences regarding tertiary structure.

Angles between bond vectors and an external reference coordinate system can be obtained from residual dipolar couplings (RDCs), which can be used to refine

calculated structures. For example, the structure of cyclosporine A in chloroform was refined using RDCs [21]. To measure RDCs, samples need to be partially aligned in the appropriate medium as dipolar couplings average to zero when samples are in isotropic solution.

NMR is also a powerful technique for studying interactions of cyclic peptides with molecular partners. Analysis of changes in chemical shifts or peak widths from titration experiments can provide information on binding affinity and the interaction interface, as described in Section 2.2.3.

2.2.2 Protocols for 3D Structural Determination Using NMR

Structure determination by NMR is essentially a process of identifying structural descriptors (using experiments such as those described previously) and the construction of models that best fit those descriptors. The general procedure for macrocycles illustrated in Figure 2.3 involves sample preparation, acquisition of NMR parameters to determine structural restraints, application of those restraints to build structural models, and validation of the models. Here, we focus on peptides of fewer than 50 amino acids (see Table 2.1), the structures of which can be elucidated using natural abundance spectra and homonuclear NMR experiments. For newcomers to this field looking for tutorials, we recommend two excellent articles that describe the process, one for a cyclic somatostatin analogue [118] and another for the ω-conotoxin MVIIA, a 25-residue peptide [119]. For larger molecules, complications arising from overlapping peaks often necessitate enriched samples and the use of heteronuclear multidimensional NMR experiments. There are numerous textbooks that describe

these experiments [105, 107]. In cases when 2D homonuclear spectra are well resolved, such as in the case of the 64-residue circular bacteriocin NKR-5-3B, structural elucidation can be completed without the need for sample enrichment [55]. The standard protocol used for 3D structure determination using NMR is given in Scheme 2.1.

For natural abundance spectra, we typically use samples of concentration 0.5–1.0 mM, but the optimal concentration will depend on the sensitivity of the spectrometer and the behavior of the sample. For example, in the case of the 18-amino acid θ-defensin retrocyclin-2, broad spectral peaks were observed at 2.6 mM in aqueous solution, which was attributed to oligomer formation; much sharper lines and improved spectra were observed upon lowering the concentration to 0.5 mM [42]. Along with optimization of the sample concentration, other conditions such as temperature, pH, and solvent may need to be modified to improve spectral quality. We already mentioned the example of cyclosporine A, in which changes in solvent improved conformational homogeneity and, hence, spectral clarity. The effect of sample conditions on spectral quality can be easily monitored using 1D spectra.

Spectral assignment can be achieved using the methodology of Wüthrich [115]. Although complete assignment can be achieved using only ^{1}H spectra, we find that a ^{13}C-HSQC spectrum is often useful for guiding assignments, particularly for resolving ambiguities in assignment of side-chain protons. A unique and definitive feature of backbone cyclic peptides is the presence of NOE connectivities from the last residue to the first, confirming their backbone cyclic nature.

Once assignments are complete, a range of NMR experiments can be used to identify structural descriptors.

Figure 2.3 Structure determination of macrocycles by NMR. (a) Flowchart of the general process of structure determination, which can vary depending on the size of the macrocycle. Specific features of structure determination for macrocyclic peptides compared with linear peptides are highlighted in the gray box on the bottom right of the figure. (b) Overlay of the 20 lowest energy structures of kalata B1 (PDB: 1NB1).

(a)

Macrocycle

<5 kDa — Natural abundance and homonuclear methods

>5 kDa — Sample enrichment and heteronuclear methods

NMR spectroscopy, 1D, 2D, etc.

Spectral assignment

Collection of conformational constraints

Calculation of initial structures

Structure refinement

Validation and deposition

(b)

Differences vs. linear
* nOes connecting "last" to "first" residue
* Inclusion of cyclic backbone constraint
* Manual manipulation to visualize cyclic backbone
* Manual manipulation to obtain validation statistics

Step 1 — Prepare sample.

(a) Prepare a 1 mM sample in 90% v/v H_2O, 10% v/v/ D_2O. Adjust solution conditions, that is, solvent composition, pH, or concentration if necessary for solubility or to improve spectral quality. Add an internal standard such as 4,4-dimethyl-4-silapentane-1-sulfonic acid (DSS).

(b) Note: Generally, for small cyclic peptides less than 50 amino acids, spectra can be acquired at natural abundance and do not require sample enrichment. This protocol is for small cyclic peptides.

Step 2—NMR spectroscopy.

(a) Acquire 1D ^1H, 2D ^1H–^1H TOCSY, NOESY (or ROESY depending on peptide size), and ^{13}C-HSQC (heteronuclear single quantum coherence spectroscopy). Note: Parameters may need to be optimized to account for artifacts, for example, those arising from spin diffusion.

(b) Acquire DQF-COSY, and perform a VT NMR experiment.

(c) Perform an H/D exchange experiment and acquire E-COSY and NOESY spectra.

Step 3—Spectral assignment.

(a) Assign cross-peaks in TOCSY and NOESY (and ^{13}C-HSQC) spectra. Note: NOEs between the "last" and "first" residues should be present.

Step 4—Collect conformational restraints.

(a) Integrate NOESY cross-peaks to obtain peak volumes for distance restraints, analyze 1D ^1H or DQF-COSY spectra to obtain coupling constants for backbone dihedral angle restraints (use TALOS+ as well), analyze E-COSY and NOESY spectra for side-chain angle restraints, and interpret VT NMR and H/D exchange experiments for H-bond restraints.

Step 5—Calculate initial structures.

(a) Run CYANA to obtain initial structures. Note: Additional "artificial" restraints may be needed to enforce backbone cyclization.

Step 6—Refine structures.

(a) Cross-check with restraints to resolve violations.

(b) Refine structures further in CNS.

Step 7—Validate and deposit.

(a) Run validation software, for example, PROCHECK and MolProbity. Note: Validation software typically expects linear biomolecules, and cyclic peptides may need to be "permuted" to obtain statistics across the cyclization point. Furthermore, manual editing of the coordinate file may be required to visualize cyclic peptides properly.

Scheme 2.1 Protocol for NMR Structure Determination of Cyclic Peptides.

These restraints are input to software such as CYANA [120] and CNS [121] along with the peptide sequence for model calculation and subsequent refinement. For backbone cyclic peptides, it is necessary to incorporate additional restraints to enforce cyclization *in silico*. For small cyclic peptides with few restraints, MD simulations have been used to further refine the calculated structures [5, 103].

A subset of the generated models is typically selected to represent the final structure, rather than just the lowest energy structure. It is imperative that the models are validated in some way. This is usually achieved by noting the number of violations and the root-mean-square deviation (RMSD) of the models to assess agreement between the models and experimentally observed parameters. Even with apparent agreement between the models and experimental data, there is still a need to be cautious in interpreting the models. This is particularly the case for compact macrocyclic peptides that exhibit overlapping cross-peaks in 2D ^1H NOESY spectra. Microcin J25, for example, was originally reported to have a backbone cyclic structure [122] but was later

shown to form a "lasso"-like structure [123]. In another example, the disulfide connectivity of kalata B1 was incorrectly deduced by Skedjal *et al.* [124] based on assumptions about NOEs between Cys residues. Our original structure [125] was subsequently shown to be correct. In both examples, chemical experiments (e.g., chemical modification of the termini and selective reduction and alkylation experiments) were beneficial for structure validation [123, 126].

Programs such as PROCHECK [127] and MolProbity [128] provide further metrics to assess the quality of the models, such as their Ramachandran statistics. A challenge for cyclic peptides is that cyclic backbones are sometimes not recognized in validation programs and are not represented properly in visualization software. For example, Ramachandran statistics for the "first" and "last" residues of a cyclic peptide are not generated by typical validation software because the input peptide is assumed to be acyclic and φ/ψ angle pairs are not calculated for terminal residues. For cyclic peptides, it is necessary to run the validation software twice, once with the calculated structure and a second time with an *in silico*

permuted version to obtain a complete analysis of the structure. Inspection of the final structures and noting stereoelectronic preferences can also provide an indication of structural quality. For example, in small cyclic peptides in solution, the carbonyl bond of a constituent amino acid has been observed to favor a *syn* orientation with respect to the CαH bond of the following amino acid due to steric and dipole orientation preferences [6].

2.2.3 Dynamic Aspects of Structures (NMR Relaxation)

NMR is a powerful technique to study the dynamics of molecules in solution, and the available experiments cover a broad range of timescales [129]. Here, we focus on nuclear spin relaxation to study dynamics on the ps−ns timescale. The physical processes captured in this time window include bond vibration, side-chain rotamer interconversion, random coil and loop motions, and backbone torsion angle rotation. These motions have been implicated as important for ligand affinity [130], allosteric effects [131], and conformational entropy [132–135].

Studies of NMR relaxation rely on the relation between site-specific observables and metrics of motion (Figure 2.4). The observables include the longitudinal (T_1) and transverse (T_2) relaxation times and the heteronuclear

nuclear Overhauser effect (hNOE). These observables are related to the spectral density function $J(\omega)$, which is formulated by metrics that describe motion, such as S^2, the square of the generalized order parameter, which in turn describes the amplitude of motion. The most commonly used parameterization of $J(\omega)$ into motional parameters is given by the model-free formalism [136]. It is named "model-free" because there is no structural model used to describe the nature of the motion, unlike approaches proposed before it. This approach assumes that internal motion is independent of, and much faster than, overall molecular rotation [137, 138].

Acquisition of the relevant spectra for proteins is often accomplished using isotopically enriched samples because of the use of heteronuclear experiments. For example, Camarero and coworkers used ^{15}N-enriched MCoTI-II to study its backbone dynamics [87], and we used ^{15}N-enriched HTD-2 to study its molecular flexibility [45]. However, if sufficiently high concentrations of the macrocycle can be used without violating the assumptions of the model-free approach, natural abundance measures can be performed, particularly for ^{13}C measurements because the ^{13}C nucleus is more sensitive than the ^{15}N nucleus. For example, we recorded ^{13}C relaxation measurements of MCoTI-II at natural abundance [88]. It is recommended to acquire relaxation experiments in triplicate and at multiple field strengths
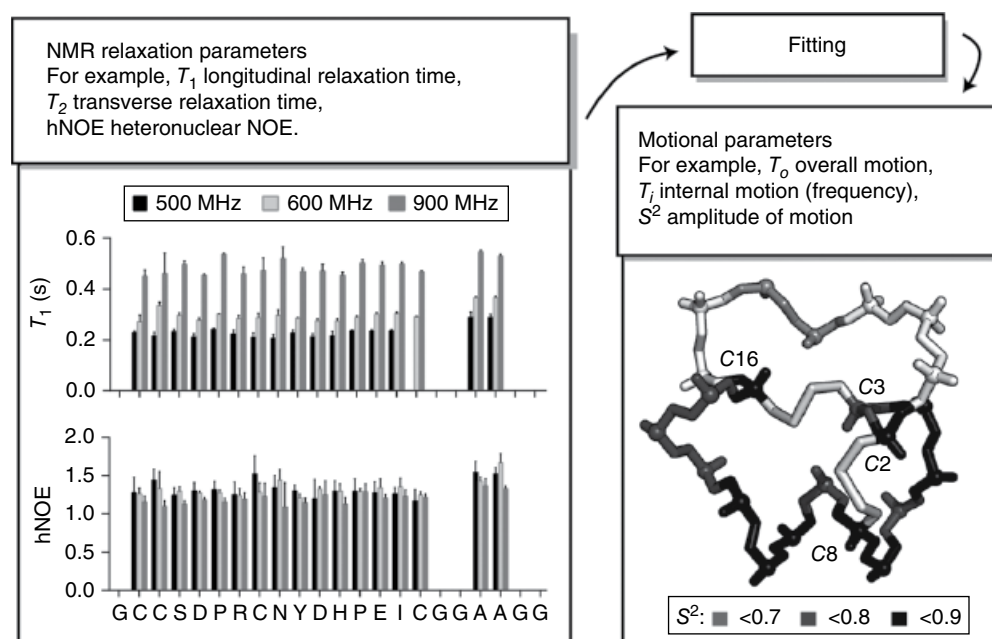
Figure 2.4 Analysis of dynamics by NMR relaxation. The general process involves acquisition of relaxation parameters such as T_1 (longitudinal relaxation time), T_2 (transverse relaxation time), and hNOE (heteronuclear NOE), followed by fitting of the relaxation parameters to motional parameters such as T_o (overall correlation time), T_i (internal correlation time), and S^2 (square of the generalized order parameter). Experimental data and the fitted S^2 values mapped onto the structure of cyclic Vc1.1 are shown as an example of the process. Source: Wang *et al.* [121]. Reproduced with permission of American Chemical Society.

to ensure reliability in the fitted parameters. Several programs are available for fitting of the relaxation data to motional parameters, including Model-free [139] and Relax [140].

2.2.4 X-Ray Studies of Macrocycles

As with NMR, the general procedure for crystallography widely used to elucidate the structures of small molecules and proteins can be adopted to solve the structures of macrocycles. The procedure involves obtaining diffraction-quality crystals by screening and optimization, acquisition and processing of diffraction datasets, generation of the electron density map, and model building and refinement. This process, as it applies to peptides, has been explained in detail in a recent review [141].

The first challenge in X-ray crystallography is to grow crystals that diffract to a high resolution. Small macrocycle crystals ($\lesssim 1\,kDa$) can be grown in organic solvents, much like small organic molecules. For example, the nine-residue cyclic peptide cyclolinopeptide A was crystallized from methanol/isopropanol [15]. Larger macrocycle crystals can be grown in an aqueous solution with various buffers, pH ranges, salts, additives, and cryogenic protectants, much like protein crystals. For example, to crystallize a β-amyloid (Aβ)-derived cyclic peptide, Nowick and coworkers screened at $10\,mg/ml$ using three commercially available screens (Hampton PEG/Ion, Crystal Screen, and Index) and observed crystal growth in several different conditions after 24 h. They subsequently optimized one of the conditions and were able to harvest crystals from a final reservoir solution of 0.1 M HEPES at pH 7.5 with 25% Jeffamine M-600 at pH 7.0 [141, 142].

Diffraction data can be collected using in-house X-ray diffractometers or at a synchrotron. Once collected, the data is first indexed to identify the unit cell dimensions and the space group, and then integrated, scaled, and merged into a single reflection file. Many software packages are available for this, including iMosflm [143], HKL2000 [144], and XDS [145]. Solving the structure of the macrocycle from the processed diffraction data is equivalent to solving the "phase problem." Essentially, the problem (described in detail in textbooks [146, 147]) relates to the identification of the phase information, which is lost during the diffraction experiment, but is required to generate the electron density map that provides a representation of the crystallized structure. In principle, the problem can be solved by directly estimating the phases (i.e., direct methods), which is feasible for small molecules (<1000 atoms), but becomes intractable for larger molecules, such as most peptides and proteins. Two common approaches to address the phase problem are anomalous diffraction and molecular replacement.

Nowick and coworkers have taken advantage of chemical methods to incorporate a *p*-iodophenylalanine into their cyclic peptides; the heavy atom iodine attached to the *para* position of the aromatic ring enables phase determination by single anomalous diffraction experiments [141].

Initial attempts to solve the phase problem are often followed by iterative rounds of model building and structure refinement to more accurately determine the phases and generate a complete electron density map. The program Coot [148] can be used to manipulate the model and the program Phenix [149] to refine the model and electron density map. For backbone cyclic peptides, it is necessary to artificially incorporate additional restraints to enforce cyclization during refinement. The program eLBOW in the Phenix software suite can be useful for creating library files for unnatural amino acids. As with NMR, there are still challenges related to structure visualization, validation, and deposition for macrocyclic peptides.

As we noted already, one of the main challenges in X-ray crystallography is growing diffraction-quality crystals. It has been proposed that racemic crystallography (i.e., crystallization from a mixture of equal proportions of L- and D-enantiomers) can be used to overcome the crystallization bottleneck [100]. The theory of racemic crystallography as it applies to proteins and, by analogy, peptides was investigated by Wukovitz and Yeates [150], who were interested in explaining the distinct space group preferences of protein crystals. In the course of their studies, they predicted that proteins would crystallize with ease if they could be made in racemic form. Essentially, their hypothesis was based on the fact that a racemic mixture has access to a greater number of ways that it can pack to form crystals. Chiral samples can only access chiral space groups, comprising 65 of the total of 230 space groups, whereas a racemic mixture has access to all space groups.

Kent and coworkers demonstrated that facile crystal formation can occur from a racemic mixture for peptides that have previously been considered recalcitrant [100]. To address the phase problem, it should be noted that anomalous contributions are not observed in a centrosymmetric space group, so the appropriate atom for anomalous dispersion methods should only be incorporated into one enantiomer. Furthermore, as racemic mixtures can result in the formation of centrosymmetric crystals, Kent and coworkers also demonstrated that structures can be solved by direct methods [151] (normally not feasible for peptides as noted previously), because all reflections from centrosymmetric crystals have quantized phases (e.g., in RBR'$_2$, all phases are 0 or π).

We have shown that racemic crystallography can indeed be used for facile crystallization of cyclic peptides by growing crystals of BTD-2, SFTI-1, cyclic Vc1.1, and
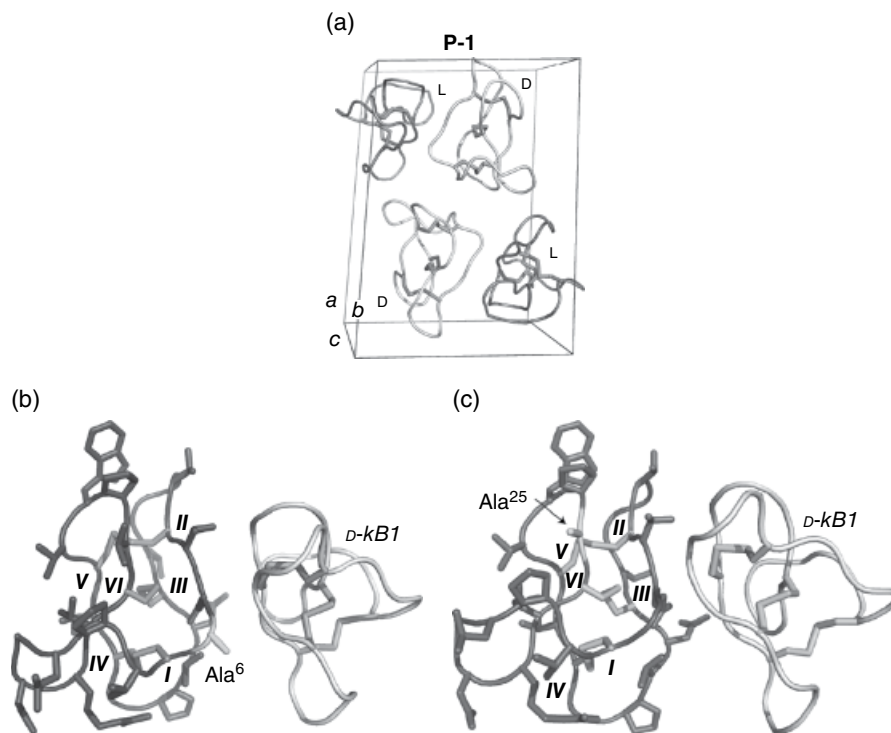
Figure 2.5 Racemic and quasi-racemic structures of kalata B1. (a) Packing of the L- and D-enantiomers of kalata B1 in the unit cell. The L- and D-enantiomers are labeled with L and D, respectively. (b, c) quasi-racemic structures of kalata B1 composed of a mutant of L-kalata B1 (i.e., [G6A]kalata B1 and [V25A]kalata B1) colored in dark gray and D-kalata B1 colored in light gray. The side chains and the positions of the Cys residues for the L-enantiomer are labeled with Roman numerals.

kalata B1 from their racemic mixtures [39, 152]. For example, racemic crystals of kalata B1 were obtained from 14% w/v (+/−)-2-methyl-2,4-pentanediol and 4% v/v 1,3-propanediol. An initial model was obtained by molecular replacement using the NMR structure of kalata B1 as the initial search model and refined to give the final structure of the racemate as shown in Figure 2.5a. We have also shown that analogues of kalata B1 are amenable to quasi-racemic crystallography, in which crystals are grown from a mixture of one enantiomer, in this case D-kalata B1, with an analogue of its other enantiomer, in this case either L-[G6A]kalata B1 or L-[V25A]kalata B1 (Figure 2.5b and c).

2.2.5 Macrocycle–Receptor Interactions (NMR and X-Ray)

To make inferences regarding function from structure, it is beneficial to study how macrocycles interact with their environment: this may include interactions by self-association, with membranes, nucleic acids, or a protein partner. NMR or X-ray crystallography can be used to investigate such molecular interactions and, when used in combination, provides a wealth of information. The types of information on molecular interactions that can

be obtained using NMR include binding affinity, location of residues at or near the interaction interface, bound conformation of the macrocycle, geometry of the macrocycle–target complex, and information on conformational dynamics [153]. X-ray crystallography can be used to obtain a high-resolution structure of large macrocycle–target complexes.

Binding affinities between a macrocycle and its target can be calculated by monitoring certain NMR parameters (e.g., chemical shifts, T_2 relaxation times, and diffusion coefficients) over the course of a titration. In general, NMR is best suited for this when the interaction is governed by moderate or weaker binding affinities, rather than tightly bound complexes. During the titration experiment, changes in particular NMR signals can help identify atoms at the binding interface or allosteric effects from binding. As an example, Arseniev and coworkers studied the binding of kalata B1 to dodecylphosphocholine (DPC) micelles using NMR [154]. They observed changes in molecular diffusion coefficient and chemical shifts for particular atoms as a concentrated solution of DPC micelles was titrated into a solution of kalata B1, allowing them to estimate binding affinity and identify residues of kalata B1 at the kalata B1–DPC micelle interface. The contact residues were further

(a)

(b)

(c)

(d)
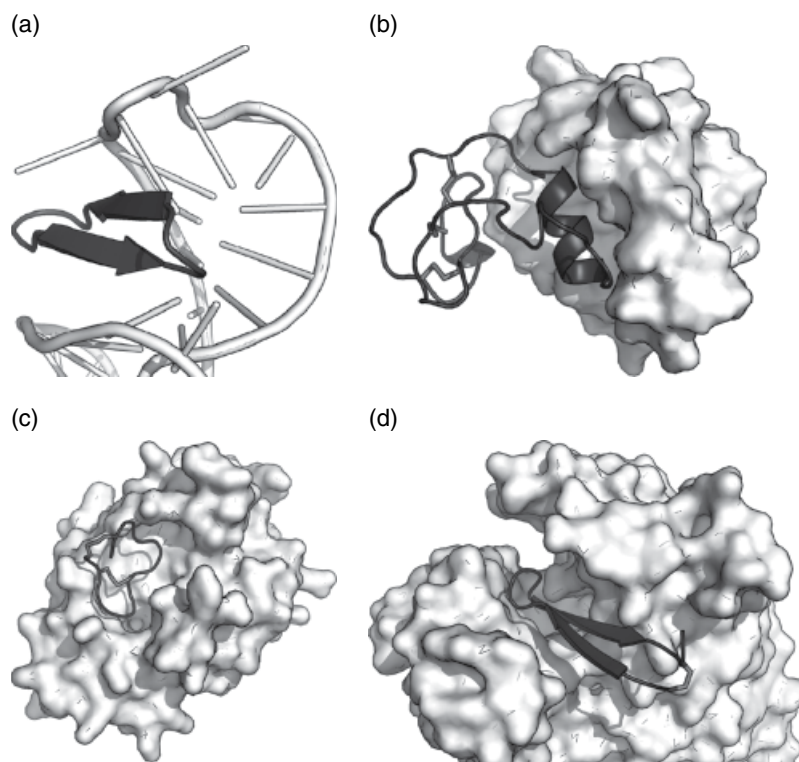
Figure 2.6 Examples of complex structures involving macrocyclic peptides. (a) NMR complex structure of a PEM with HIV-1 TAR RNA. (b) NMR complex structure of a grafted MCoTI-I with the p53-binding domain of HDM2. (c and d) Complex structures of a bicyclic peptide and a thioester cyclized peptide to their protein targets solved by X-ray crystallography.

confirmed using paramagnetic probes that insert into the DPC micelle and broaden the signals of atoms nearby. We showed that similar experiments could be used to study the binding of other cyclotides to DPC micelles and identify novel modes of interaction [155].

In the case of tightly bound complexes, NMR can be used to determine the complete structure of protein–ligand complexes using similar methodology to that employed to determine protein structures themselves. This typically involves sample enrichment and the use of higher dimensional and isotope-edited techniques, as described in more detail elsewhere [105, 107]. One of the earliest examples of an NMR structure of a cyclic peptide bound to its protein target is that of the cyclosporine A–cyclophilin complex [156]. Other examples of complex structures involving cyclic peptides include a cyclic peptide mimetic bound to HIV-1 TAR RNA [25] (Figure 2.6a) and a reengineered MCoTI-I bound to the p53-binding domain of Hdm2 (Figure 2.6b) [71].

The structure of a macrocycle–target complex can also be solved by X-ray crystallography. The main difference between such studies and those of single molecules is how the samples are prepared. Complexes of small molecules bound to a protein can be achieved by soaking protein crystals into a reservoir containing the small molecule ligand. In principle, this approach also can be applied for small macrocycles, but, for larger macrocycles, this

approach may be limited by their ability to diffuse into the crystal. The alternative is to crystallize a mixture of the macrocycle with the target or the purified complex. In work by Heinis and coworkers, complexes of bicyclic peptides with their protein target were crystallized by directly mixing a mixture of the two components with the crystallization condition (Figure 2.6c) [33]. For the crystallization of the MCoTI-II–trypsin complex, the complex was first isolated from unbound components using size exclusion chromatography before crystallization [88]. Interestingly, cyclic peptides bound to a target may stabilize the conformation of the protein partner and thereby facilitate crystallization (Figure 2.6d) [157, 158].

2.3 Molecular Modeling of Macrocyclic Peptides

A range of molecular modeling methods has been used to study macrocycles, as summarized in Figure 2.7. The most extensively modeled classes of cyclic peptides are (i) those that form nanotubes, which have applications as antibacterials and drug delivery agents, and (ii) a wide range of natural and synthetic cyclic peptides that are highly heterogeneous in sizes, chemical nature, and activities. One example of the latter that have been modeled are the type

Figure 2.7 Molecular modeling methods used to study cyclic peptides. The methods are in black boxes and are linked by dashed lines to their applications, which are in white boxes. As apparent from this diagram, molecular dynamics (MD) methods are the most versatile. All the methods are described in the text. MM, molecular mechanics; MMPBSA, molecular mechanics/Poisson–Boltzmann surface area; QM, quantum mechanics; REMD, replica-exchange molecular dynamics.
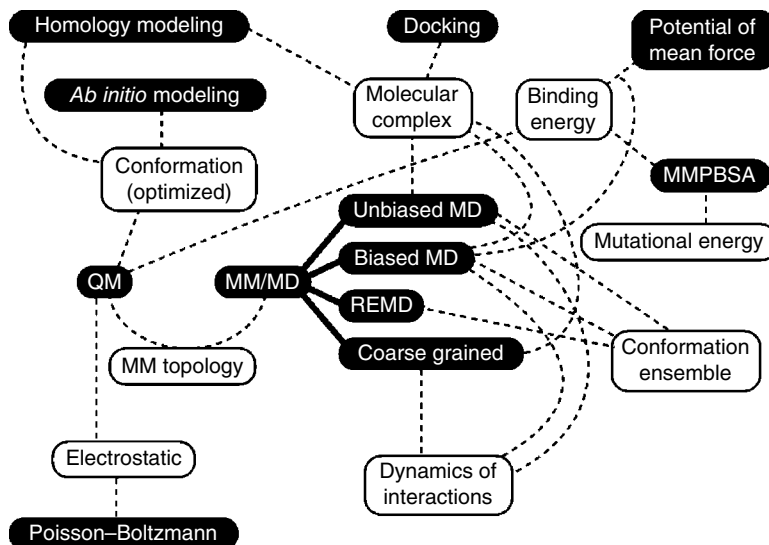
IIc bacteriocins [159], which, as noted earlier, are backbone cyclic peptides of bacterial origin of approximately 60 residues in size, which display antibacterial activity. Another example is the contryphan family of disulfide cyclic peptides [160], which are expressed in the venom of marine cone snails and inhibit ion channels. Despite typically comprising only 8 residues, contryphans have as many as 5 posttranslational modifications, considerably increasing their chemical diversity beyond the 20 standard amino acids. With respect to synthetic peptides, numerous studies have used molecular modeling to design cyclic peptides by (i) grafting active peptides into a cyclic scaffold, (ii) designing cyclic peptides *de novo*, or (iii) cyclizing linear peptides.

In the first part of this section, an overview of the main modeling methods is provided, as well as a discussion on challenges to the modeling of cyclic peptides. In the second part, *in silico* methods employed to study the monomeric structure of cyclic peptides, including their dynamics and electrostatic properties, are described. Finally, approaches to model the activity of cyclic peptides including their multimeric states (e.g., nanotubes) and interactions with molecular targets are discussed. Molecular modeling is a rapidly evolving field and we will mainly focus on studies from the last 5 years.

2.3.1 Methods and Challenges in Modeling Cyclic Peptides

Depending on its size, the number of atoms in a peptide is comparable either to a small molecule or to a protein, and peptides have been studied using techniques applicable to both small and large ensembles of atoms, that is, using quantum mechanics (QM) and molecular mechanics (MM) methods.

2.3.1.1 Quantum Mechanics

Analyzing cyclic peptides using QM is fundamentally not different from analyzing linear peptides or small molecules. Most QM studies of macromolecules employ density functional theory (DFT) methods. Recently, some studies used correlated-wave methods, such as second-order Møller–Plesset 2 (MP2) theory, which are more accurate than DFT methods, but previously were not applicable to peptides due to their high computational cost. A new approach called divide–expand–consolidate (DEC) was developed to compute the correlation energy for "large molecular" systems (~50 amino acids) by fragmenting the calculations into small subsets of local orbitals [161]. The precision and applicability of this new method need to be further validated. Notably, no cyclic peptide has as yet been modeled using this strategy.

DFT methods are well characterized and represent a good compromise between accuracy and computational cost. DFT methods decompose the system energy into four components: kinetic, external potential, exchange, and correlation energies. The most popular DFT method is B3LYP, which incorporates Hartree–Fock (HF) functions to compute the exchange energy. As a striking example of the difference in computational cost of the various QM methods, an energy computation that was recently reported to take about 1 h using the B3LYP method took 50 days with the coupled cluster with singles and doubles (CCSD) method, which is one of the most accurate QM functionals [162]. It should be noted that in contrast to CCSD, the B3LYP method fails to accurately describe dispersion interactions, which are important for representing π–π interactions. Nevertheless, a range of other interactions, such N—H···O hydrogen bonds or cation–π, are well predicted by both

CCSD and B3LYP. Some empirical correction functions have been proposed to correct for the deficient dispersion energy of B3LYP, for example, the correction proposed by Du *et al*. [163]. A range of academic software is available to carry out B3LYP QM of small peptides, including Firefly (ex GAMESS), Spartan, and Orca, but the most popular and complete software package is Gaussian, which is commercially available.

QM molecular orbitals are modeled as a linear combination of basis functions, which are made up of a linear combination of Gaussian functions. The 6-31G basis set family (6-31G, 6-31G*, 6-31+G*, and 6-31+G(d,p)) is the most commonly used for representing organic compounds. These basis sets have six Gaussian functions for each atom, and the valence orbitals are represented by two basis functions, which display three or one Gaussian functions, respectively. The 6-31G basis set can have additional diffuse functions (+) and polarized functions (*), and the type of functions used to augment the description of heavy atoms (d) and hydrogen atoms (p) is indicated between parentheses. Diffuse functions are important for taking into account weak bonds, such as hydrogen bonds, and polarization functions are important for representing covalent bonds.

Due to computational limitations, the largest systems that can be studied using B3LYP are of about 100 atoms, that is, approximately 10 amino acid residues. Semiempirical QM methods, which use some of the HF methods combined with a range of empirical values, are far less computationally demanding and can be used with larger molecules. The semiempirical QM methods AM1 and PM3, which are implemented in a range of software packages such as MOPAC, ADF, and SQM, are commonly used to optimize geometries and predict electronic properties. Larger peptides, as well as proteins, need to be represented using MM, which does not take into account the creation and destruction of covalent bonds. Chemical reactions occurring in the active site of large proteins can be studied using the QM/MM scheme, in which atoms taking part in the chemical reaction are modeled at the QM level and the remaining part of the system is modeled at the MM level.

2.3.1.2 Molecular Mechanics

MM represents atoms as hard spheres covalently connected by springs to form molecules. Contrary to QM, MM employs a large number of parameters to represent molecules; the ensemble of these parameters and associated energy functions are referred to as the force field. A force field typically contains information to restrain covalent bonds, angles, dihedral angles, and improper dihedral angles (restraining geometry associated with hybridization), as well as to compute nonbonded interactions. MM approximates the interactions between atoms using classical physics, significantly simplifying the computation.

Besides the all-atom force fields, for example, Amber [164], Charmm [165], and OPLS [166], some force fields use interaction centers that represent several atoms, effectively reducing the number of interactions to consider and therefore computational time. The united-atom force fields, for example, GROMOS [167], represent carbon atoms and covalently linked aliphatic and aromatic hydrogen atoms by a single center. Coarse-grained force fields, such as Martini [168], represent several heavy atoms and linked hydrogen atoms by a single center. The united-atom force fields have comparable accuracy to all-atom force fields, whereas coarse-grained force fields can only approximate the details of molecular interactions. The benefit of coarse-grained force fields is that they are more suited to the modeling of medium- and large-size molecular systems over a long timescale.

Because of its low computational cost, MM can be used to model the dynamics of large molecular systems, that is, carry out MD simulations. Several academic MD packages specializing in biomolecules exist, the most popular being Gromacs [169], Amber [170], Charmm [171], and NAMD [172]. All of the packages have their strengths and weaknesses, with the NAMD MD engine having the best scaling abilities with the number of central processing units. The Amber package provides the most convenient suite of tools and third-party programs to analyze MD simulations, as well as to prepare topology files, which contain the parameters used to represent the molecules to be simulated. The standard protocol used to conduct MD simulations on cyclic peptides in explicit solvent is given in Scheme 2.2 [173–176].

The main challenge in representing cyclic peptides using MM is the generation of molecular topologies. All major MD packages have dedicated scripts and software that automate the creation of topologies for linear proteins, but the creation of side-chain and backbone cyclic peptides is less straightforward. The Amber, Charmm, and NAMD packages provide graphical interfaces in which bonds, angle, and dihedral angle restraints based on atom types can be easily created. This strategy works well for backbone cyclic peptides but should be used cautiously when generating topologies for side-chain cyclic peptides (aside from disulfide bonded cyclic peptides), because force fields often do not have parameters for connecting all atom types. Gromacs does not have a graphical interface, requiring manual editing of topology files to cyclize peptides through their backbone or side chains. Whatever the method used to modify topologies, it is strongly recommended to always check manually that the correct topologies have been created for cyclic peptides.

1—Build an initial structure.

(a) Determine experimentally the conformation of the cyclic peptide (Section 2.2) or predict it (Section 2.3).
(b) If required, embed the peptides in or locate them near a membrane bilayer patch, which needs to be built using standard MD package tools or other software such as VMD [154], Charmm-GUI [155], or insane [156].

2—Prepare topologies.

(a) Derive force field parameters for nonstandard residues not included in the chosen force field. Several tools listed in Table 2.2 can help determine these parameters.
(b) Use standard MD package to prepare topologies of cyclic peptides and other molecules (altogether called solute) for the chosen force field. Consider the ionization state of side chains, for example, using a pK_a prediction algorithm, such as propka3 [157].
(c) Modify the topologies to "cyclize" cyclic peptides (Section 2.3.1.2).

3—Solvate.

(a) Minimize the energy of the system in vacuum.
(b) Decide a shape and size of the box with periodic boundary conditions to include the system. Systems with a membrane should employ a triclinic or hexagonal box, whereas systems without a membrane component often fit better in an octahedron or dodecahedron box. The solute molecule should be at least 1 nm away from the side of the box.
(c) Add water molecules of a type compatible with the chosen force field using standard MD package tools. Replace a number of water molecules by sodium and chloride ions to reach a chosen salt concentration and neutralize the system.

4—Equilibrate the system at a given temperature.

(a) Minimize the system using periodic boundary conditions.
(b) Run an MD simulation with solute atom positions strongly restrained. If there is a membrane, monitor the equilibration of the membrane to decide the length of the simulation. This first simulation will generate initial atom velocities to be used in the following simulations. The velocities are initially randomly set accordingly to a statistical distribution of velocities at a given temperature, usually 300 K. A thermostat algorithm, often the Berendsen or Nosé–Hoover thermostat, is used to keep the atom velocity distribution according to the chosen temperature.
(c) Run a series of MD simulations in which the position restraints are progressively released.

5—Production run for a given time.

(a) Run an MD simulation without restraint for a given time. The MD frames and associated energies are typically recorded every 2 ps.

6—Analysis.

(a) Analyze the log files and monitor the evolution of pressure, temperature, and energy of the system to evaluate if it has reached equilibrium. Consider extending the simulation if not.
(b) Analyze the evolution of the conformation of the cyclic peptides during the production run simulation by monitoring the evolution of some specific distances or their atom RMSD from the initial frame.
(c) Monitor the evolution of membrane characteristics, interaction energies, contacts, distances, and/or angles that are relevant to the system under study.

Scheme 2.2 Molecular Dynamics (MD) Simulation Protocol for Cyclic Peptides.

Table 2.2 Online and stand-alone tools helping generate topologies and force field parameters for nonstandard amino acids.

Software	Force field	Access
ATB	Gromacs	http://atb.uq.edu.au
Vienna-PTM	Gromacs	http://vienna-ptm.univie.ac.at/
PRODRG	Gromacs	http://davapc1.bioch.dundee.ac.uk/cgi-bin/prodrg
AnteChamber	Amber	Stand-alone, part of Ambertools
ACPYPE	Amber, Charmm, and Gromacs	http://webapps.ccpn.ac.uk/acpype
SwissParam	Charmm and Gromacs	http://www.swissparam.ch
SwissSidechain	Charmm and Gromacs	http://www.swisssidechain.ch
CHARMMing	Charmm	http://www.charmming.org

Side-chain cyclic peptides often use nonstandard amino acid side chains to create the ring structure, and the force fields need to be amended to consider nonstandard residues. New force field parameters can be obtained either from those for similar chemical entities or by using QM or semiempirical computations. A range of software and online resources are also available to help derive new residue topologies and force field parameters (Table 2.2). The most recently developed tools, such as ATB [177] and ACPYPE [178], are the most convenient to use. ACPYPE uses Ante Chamber, from the AmberTools package [170], to generate topologies and parameters for the general Amber force field (GAFF) and then converts them into Charmm or Gromacs force fields. AnteChamber uses by default partial charges computed at the semiempirical level AM1-BCC. ATB first optimizes the geometry at the HF/STO-3G QM level or semiempirical AM1 or PM3 levels and then at the more accurate B3LYP/6-31G*level, which is then used to estimate the partial charges carried by each atom. The Vienna-PTM database provides access to pre-computed Gromacs topologies and force field parameters for 260 posttranslational modifications of amino acids [179].

2.3.2 Conformation, Dynamics, and Electrostatics of Cyclic Peptides

As noted already, the structures of cyclic peptides are frequently determined using NMR spectroscopy, but, in some instances, structures can also be generated reliably using molecular modeling. For example, the structures of peptide variants resulting from the substitution of a single side chain in a peptide with a known experimental structure can be generated reliably by homology modeling, for example, using MODELLER [180] or RosettaCM [181], or by side-chain prediction algorithms, such as SCWRL [182]. Although algorithms relying on backbone structural alphabets, such as Rosetta [183] or I-TASSER [184], have been successfully used to generate *ab initio* conformations of proteins, structures of peptides are typically more difficult to predict.

2.3.2.1 NMR Spectroscopy Combined with MD Simulations

The study of peptide conformations by NMR involves deriving distance restraints that are then employed in simulated-annealing MD simulations to determine the coordinates of each atom. Therefore, peptide structures generated from NMR data are molecular models that are informed by experimental data. Unrestrained MD simulations are often used in parallel with NMR data to study

the dynamics of peptides [185]. MD simulations are routinely used to study dynamics on the femtosecond (fs) to microsecond (μs) timescale, and NMR relaxation data or amide temperature coefficients probe hydrogen atoms binding to backbone nitrogen (HN) atoms on a similar timescale.

Figure 2.8 gives an overview of the timescales of various protein motions compared with the timescale of MD simulations, as well as NMR and circular dichroism experiments. In a recent study, it was shown that the solvent exposure of NH atoms in cyclic peptides was strongly correlated with amide temperature coefficients measured using NMR spectroscopy, bridging results from MD simulations and NMR experiments [8]. MD simulations were also instrumental in resolving seemingly conflicting data from NMR NOE and circular dichroism experiments on a side-chain cyclic β-peptide [185]. Circular dichroism suggested that the peptide had helical content, which seemed incompatible with interatomic distances suggested by the NOE experiment. A series of long MD simulations suggested that the ensemble of conformations adopted by the peptide could explain the measurements from the two experimental techniques, which assess the structural properties on
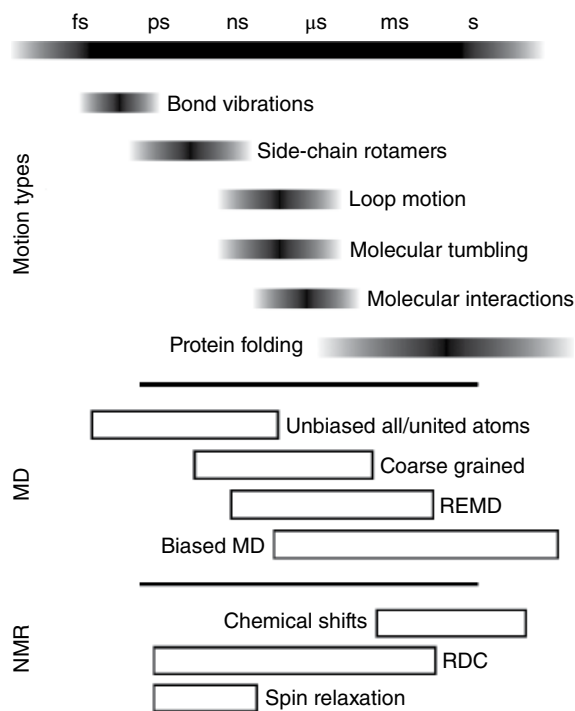
Figure 2.8 Timescales of protein motion types, MD simulations, and nuclear magnetic resonance (NMR) experiments. All MD simulation methods have a time step of a few femtoseconds (fs), and the figure shows for each of them the timescale of the process that typically simulate. ns, nanosecond; ps, picosecond; REMD, replica-exchange molecular dynamics; RDC, residual dipolar coupling.

different timescales. It should be noted that cosolvents, such as DMSO, are often used when studying peptides by NMR spectroscopy, and reproducing this solvent composition in the systems studied by MD simulation helps correlate with experiments [186]. The radial distribution function between the DMSO oxygen and each NH atom measured during MD simulations was, for example, used to interpret NH shielding observed by NMR spectroscopy [186].

2.3.2.2 Studying Large Conformational Ensembles and Folding

Peptides adopting multiple conformations in solution can be difficult to study by NMR, and MD simulations can provide insights about the ensemble of conformations dynamically adopted by these peptides. Three main strategies are employed in MD simulations to efficiently explore conformational space: MD simulations at high temperature [187], replica-exchange MD simulations (REMD), and biased MD simulations.

The REMD approach involves performing several MD simulations in parallel, but at different temperatures, and allowing simulations that display similar potential energies to swap their temperatures based on a probability function. REMD simulations can be easily prepared and run with the Gromacs package. The parameters specific to REMD simulations are the number of parallel simulations, their temperature, and the average frequency at which temperature is exchanged. A web server (http://folding.bmc.uu.se/remd) can be used to help determine an initial set of these parameters [188]. In a recent study, the conformational ensembles of cyclic peptide mimics of a β-hairpin were studied using REMD, and a single steric interaction was shown to control shifts between distinct conformation populations [189]. REMD combined with QM computations was able to predict the conformation of a cyclic peptoid nonamer within 1.0 Å backbone RMSD [190]. In that study, QM at the B3LYP level, as well as the higher M052X level, was used to optimize the geometry of different conformations generated by REMD and compute their absolute free energy.

Efficient exploration of the folding energy surface can also be achieved by biasing MD simulations using accelerated MD (aMD) or metadynamics. In the aMD method, a boost potential is added to the energy of the system when this energy falls below a certain value, resulting in a "flooding" of the energy surface and decreasing energy barriers between energy minima. An implementation of aMD is available in the NAMD and Amber engines. Metadynamics extends the aMD concept by using collective variables (CVs) defining the state of the system instead of using the energy only. CVs are user-defined variables that encompass a wide range of parameters, including distances, dihedral angles, contact maps,

RMSD, and radii of gyration. In the metadynamics approach, Gaussians of energies are deposited when the system explores the free energy surface, the coordinates of which are defined by the CVs. The main parameters of a metadynamics MD simulation are the width, height, and frequency of the deposited Gaussians. These parameters need to be optimized for the system to be able to overcome energy barriers in a reasonable time without exploring unrealistic scenario. Metadynamics simulations can easily be carried out with PLUMED, which is a plug-in that functions with all major MD engines [191]. For example, the conformations of small disulfide cyclic contryphans were studied using metadynamics with the omega torsion angle of a proline residue used as a CV to bias the system toward exploring the *cis*/*trans* isomers of this residue [160]. Conformational sampling in that study was further enhanced by simultaneously using replica simulations at different temperatures, that is, REMD. The predicted energy ratio between *cis* and *trans* isomers was comparable to the relative population of the two isomers as measured by NMR [160]. Bias-exchange metadynamics is a variant of the metadynamics approach in which several simulations are run in parallel with a different bias and regularly exchange their coordinates according to a Metropolis criterion, similarly to REMD [192]. This method was used to determine the impact of N-methylation on the conformational ensemble of cyclic hexapeptides harboring the integrin inhibitor RGD motif [193].

2.3.2.3 Electrostatic Characteristics of Cyclic Peptides

The electrostatic potential of peptides is often crucial for their activity. As examples, antimicrobial peptides acting on membranes have a very distinct amphipathic character, and peptides acting as ligands of larger proteins often display complementary electrostatic potentials to those of their target. The unmodified N- and C-termini of linear peptides are charged under physiological conditions and backbone cyclic peptides, which do not display such termini and, therefore, charges, have a different electrostatic signature.

The electrostatic potential of peptides can be computed using QM, most often using DFT B3LYP. QM computations are demanding and, in practice, are only performed to study a limited number of conformations. The Poisson–Boltzmann equation describes the electrostatic potentials around solute, the principle being that ions diffuse around solute, forming homogeneously charged layers that interact with each other. Solvent and ionic effects are therefore treated implicitly with this technique. Solving the Poisson–Boltzmann equation is comparatively more tractable than using QM, even for very large systems such as complexes between peptides

and proteins, DNA, or membrane bilayers. This technique is therefore routinely utilized to analyze biological molecules in solvent environments. Several Poisson–Boltzmann solvers exist, but the most commonly used are APBS [194] and Delphi [195]. The Amber MD engine also has a Poisson–Boltzmann solver implemented internally, allowing rapid computation of electrostatics on a series of frames from an MD simulation [170].

2.3.3 Modeling the Activity of Cyclic Peptides

Relatively few cyclic peptides have been crystallized in complex with their molecular targets, and, thus, molecular modeling is essential to give insights into the activity of cyclic peptides at the atomic level. It should be noted that molecular models are based on a large number of hypotheses and approximations. The aim of a molecular model is to provide guidance in the interpretation of experimental data (e.g., mutational data or change of conditions such as pH) and to help design experiments to further study proposed molecular mechanisms.

2.3.3.1 Cyclic Peptide Interactions with Molecular Targets

The most accurate method to model the binding mode between a peptide and its target is to use information from a crystal structure of a homologous complex [196]. For example, Quimbar *et al.* built a structural model of complexes between cyclic peptide variants and the cancer target matriptase by homology with crystal structures of the native cyclic peptides with trypsin, an enzyme related to matriptase [197]. The binding modes were then refined using unbiased MD simulations, and the nonadditivity of the mutational effects of some side chains was deduced to result from small changes of orientation of the cyclic peptides. In a similar study, differences in the activity of wild-type cyclic peptides targeting trypsin were proposed to arise from varying stabilities of the hydrogen bonding network with the targeted protein [198]. Another case is the discovery of potential peptide inhibitors of protein–protein interactions, which might be candidates for cyclization, by interrogating crystallographic structures of complexes between proteins [199]. A model of the corresponding cyclic peptide bound to its molecular target could be built starting from the crystallographic structure from which the peptide was derived and only modeling the atoms needed for cyclizing the peptide.

In many cases, no experimental structure of a homologous complex is available. Indeed, only about 20 experimental structures of macrocycles bound to proteins have been determined [200]. Molecular models of the complexes therefore have to be generated using a docking technique or MD simulations. Docking proceeds by exploring a large number of orientations and positions of a ligand around a receptor to discover the binding poses of low energy. The most commonly used software for docking peptides is AutoDock [201]. Docking algorithms typically have two main components, the search function and the scoring function. Grid-based fast Fourier transform algorithms can rapidly search rotational and distance space to provide rigid-body docking poses. Some limited elements of flexibility of side chains and the peptide backbone can be incorporated into the search, but many linear peptides are very flexible, making them difficult to study using docking. By contrast, cyclic peptides are more constrained and docking has been successfully used in many cases. To compensate for the limited ability to model flexibility, MD simulations can be performed on top-ranked models to refine the molecular interactions. For example, in a recent study, a range of cyclic peptides was screened for binding to a methyltransferase from dengue virus, and the binding poses of selected peptides were then studied by MD simulations, which was considered as a second screen of the stability of the complexes [202].

MD simulations allow the modeling of molecular interactions without imposing restraints on the conformation of cyclic peptides. The binding process for peptides is often too slow to be simulated within a practical computational time using standard MD simulations, although it is possible in some instances. For example, the binding of the cyclic peptide BPC194 to a lipid bilayer was simulated using unbiased MD, and this simulation suggested that the cyclic peptide is disordered in solution but adopts a β-sheet conformation when bound to the membrane [203]. Simulations of complex formation can be accelerated by using distance and orientation restraints, and complex restraint scenarios can be carried out using the PLUMED plug-in. Another strategy to overcome the limited timescale of standard MD simulations is to use coarse-grained force fields, for example, Martini [168], which decreases the number of interaction centers, allowing high microsecond to millisecond timescale simulations to be achieved. A two-step strategy can be used: first using coarse-grained MD simulations to form initial complexes and then refining the binding modes using all-atom MD simulations. For example, the interaction between the cyclic decapeptide labatidin and a large lipid micelle was studied using this strategy [204].

Molecular models of binding modes can be validated by comparing predicted properties with experimental results. The small number of crystal structures of complexes involving macrocyclic molecules has been recently compared, providing useful statistics for evaluating predicted binding modes of cyclic peptides [200]. A more specific and definitive validation is the ability to accurately

predict binding affinities or explain mutational data. An accurate MM method to predict the free energy of binding of small molecules and peptides involves the computation of the potential of mean force based on umbrella sampling MD simulations. Umbrella sampling proceeds in two steps: the peptide is first rapidly pulled out of the binding pocket using steered MD simulations, and then multiple simulations are carried out starting from different frames extracted from the pulling simulations. If the simulations are long enough, they will explore overlapping states and the energy of unbinding of the peptide can be reconstructed. The high computational cost of this technique prevents its systematic use though. QM can also be used to compute binding energy, but this method is even more computationally demanding. Nevertheless, it has been used with small systems, for example, to suggest that a cyclic decapeptide had preferential interactions with one enantiomer of 1-phenyl-1-propanol [205]. A powerful alternative is to combine QM and MM methods, a technique commonly called QM/MM, by simulating most of the system using MM and computing localized interactions, such as in the binding site, using QM. To our knowledge, QM/MM hybrid methods have not been employed so far to study the binding of macrocycles with large molecular targets.

The impact of substitutions on peptide/target systems can be explained qualitatively by considering the creation or destruction of non-covalent interactions, as well as potential entropic effects. Quantitative energy calculations can also be used to rank the affinity of mutants, potentially providing support for a proposed binding mode. The molecular mechanics/Poisson–Boltzmann surface area (MMPBSA) energy function is a computationally affordable method that predicts the impact of substitutions. It is an end-point free energy function, that is, it only considers the bound and unbound states. Electrostatic interactions with solvent are approximated by solving the Poisson–Boltzmann equation; the internal enthalpy of the solute is provided using an MM force field, and the nonpolar interaction with the solvent is approximated as being proportional to the solvent-accessible surface area (SASA), which is the molecular surface area that is accessible to solvent. The complex is typically simulated using standard MD simulations, and the MMPBSA energies are averaged over several frames extracted from an MD simulation. This method is less accurate at computing free energies than umbrella sampling but can be applied to a large number of substitutions. The binding energies computed by MMPBSA do not typically compare in their absolute values with experiments, but they show good correlations in some cases, for example, in a study of the interaction between two cyclic peptides and an HIV-1 RNA [206] or between disulfide-rich toxin peptides and nicotinic acetylcholine receptors [207, 208]. MMPBSA splits the polar and nonpolar energy terms into interactions between solute molecules and between solvent and solute molecules and has been used to interpret the influence of solvation on cyclic peptide/protein complexes [209].

2.3.3.2 Cyclic Peptide Nanotubes

Cyclic hexa- to decapeptides that auto-assemble into nanotubes are a very active area of research involving molecular modeling. The first cyclic peptide nanotube was designed without computational methodology [210], but a large number of computational studies have since successfully predicted and designed the properties of cyclic peptide nanotubes for specific applications. Cyclic peptide nanotubes form pores in biological and organic membranes and have applications as nanoscale ion filters, for example, for water desalinization or as antibacterial agents, as well as for the transport of small drugs [211] or gases [212]. Cyclic tetrapeptides can auto-assemble into nanomaterials such as nanoporous thin films [213]. The permeation properties of nanotubes can be tailored by changing the size of the pore [214] or the nature of the side chains in the pore to select specific molecules as well as to control flow rate [215, 216]. Molecular explanations for ion selection suggested by molecular modeling include charge repulsion, modification of ion solvation shell [215, 217, 218], and adsorption on the nanotube pore [215]. Simulations suggest that the flow of water molecules in nanotubes is controlled by the diameter of the pore and also by the steric hindrance and electrostatic properties of the cyclic peptide side chains [216].

An initial structure of cyclic peptide nanotubes was elegantly modeled by creating a first stack of cyclic peptides, which were then monitored by MD simulations restraining the atom positions in the plane perpendicular to the nanotube axis, allowing the cyclic peptide to freely rotate and maximizing hydrogen bonding between rings [215]. The stability of nanotubes in water or organic solvent can then be studied using unbiased MD simulations [219] or steered MD simulations in which a force is applied along the axis of the tube [220] or tangentially [213]. The energetic contribution made by each cyclic peptide to the nanotube stability can also be studied using the MMPBSA energy function [221].

Nanotubes are often simulated embedded in a layer of organic solvent or in lipid membranes. For simulating ion conduction, an external electric potential can be applied in a direction orthogonal to the membrane, and the flow of ions diffusing through the nanotube is measured during long MD simulations [215]. Unbiased MD simulations were sufficient to study the diffusion of ethanol in a decapeptide nanotube embedded in a 1-palmitoyl-2-oleoyl phosphatidylethanolamine (POPE) membrane [214].

Some studies used umbrella sampling [211, 212, 214] or the adaptive biasing force method [217] to compute the potential of mean force and determine the energy profiles of molecules passing through cyclic peptide nanotubes [214].

2.3.3.3 Membrane Permeation and Diffusion

The process of insertion of cyclic peptides into biological membranes can be simulated by unbiased MD simulations [203], but the formation of pores or membrane diffusion is often of a timescale incompatible with unbiased MD simulations. The membrane diffusion properties of small cyclic peptides and bicyclic peptides were shown to be correlated with the solvent exposure of backbone amides observed using NMR[11] or during unbiased MD simulations [8, 222], but these studies did not simulate the diffusion process (see also Chapter 3 on cellular permeability and bioavailability of macrocycles).

The formation of pores through membranes is complicated by the fact that various working models of membrane perforation exist, ranging from the formation of toroidal pores comprising a few peptides to the carpet model (or detergent effect) involving a large number of peptides participating in membrane leakage. Three studies have proposed working models of membrane permeation by cyclic peptides. These studies focused on the cyclic decapeptide BPC194 [223], the cyclic bacteriocin AS-48 [159], and the cyclotide kalata B1 [224]. To overcome the timescale limitations of conventional MD simulations, coarse-grained force fields were employed in the latter two studies. By contrast, toroidal pore formation in a dipalmitoyl phosphatidylglycerol (DPPG) membrane by BPC194 could be simulated using multiple 100 ns unbiased all-atom simulations [223]. The possibility to use a small timescale to simulate the poration process probably arose from the larger fluidity of DPPG bilayers compared with cellular membranes, which are better represented by POPC (1-palmitoyl-2-oleoyl phosphatidylcholine)/POPE/POPG (1-palmitoyl-2-oleoyl phosphatidylglycerol) bilayers.

The circular bacteriocin AS-48 comprises 70 residues and exists as a dimer in solution. Insertion of this dimer into membranes was modeled by simulating the auto-formation of a membrane around the dimer [159]. Simulation of the insertion of AS-48 into a preformed bilayer membrane was not attempted because pore formation is on the millisecond timescale, which is beyond the time frame that can be simulated even using coarse-grained MD simulations. The resulting molecular models identified various architectures of water channels, one of which displayed a pore radius compatible with the experimental data.

Coarse-grained MD simulations of kalata B1 suggest that a large number of cyclotides are required to form pores in membranes [224]. Large multimeric "towerlike" assemblies were observed during the simulations. Indeed, an impressive simulation of 350 cyclic peptides bound to the membrane suggested that lipids were extracted from the membrane by these large peptide assemblies. Nevertheless, no poration of the membrane was observed. Interestingly, kalata B1 is known to have stronger affinity for membranes containing phosphatidylethanolamine (PE) lipids [225], but the coarse-grained study did not include this information in the model.

2.3.4 Engineering Cyclic Peptides as Grafting Scaffolds

Cyclic peptides typically are more stable than linear peptides and have been used as scaffolds to display and/or stabilize linear peptides. For example, SFTI-1 has been grafted with an ESDV sequence, which binds to the PDZ2 domain of the postsynaptic density-95 protein [226]. Cyclotides have been used in more than a dozen grafting studies [70], with applications in cancer [227], obesity [228], chronic and inflammatory pain [63], angiogenesis and lymphangiogenesis [229], multiple sclerosis [230], foot-and-mouth disease [231], inflammation disorders [232, 233], cardiovascular disease and wound healing [234], antitumor treatment [71, 197, 235], anti-HIV therapy [236], and chronic myeloid leukemia [237]. The lasso peptide Mcj25 was recently grafted with the RGD turn motif, creating a nanomolar integrin inhibitor with potential anticancer activity [238].

Molecular modeling has been used to help in the design of grafted cyclic peptides by determining if the grafted peptide can be displayed in its active conformation without disrupting the fold of the scaffold. In a recent example, the cyclotide MCoTI-II was grafted with a peptide targeting the ligand binding pocket of Abl kinase, which is the causative agent of chronic myeloid leukemia [237]. In that study, several engineered cyclic peptides were designed *in silico*, differing only in the peptide linkers that connect the grafted active peptide and the cyclotide scaffold. It was shown by MD simulations that the activity of the grafted variants correlated with the ability of the grafted active peptide sequence to adopt a similar conformation to that displayed by the linear active peptide in complex with Abl kinase.

2.4 Summary

NMR and molecular modeling have played and continue to play a vital role in the structural and dynamic characterization of a wide range of macrocycles. These two techniques are highly complementary in that modeling studies obviate the need for physical samples of the macrocycles, but NMR studies provide experimental

data supporting possible structures. Advances in computing techniques have accelerated the pace in which both experimental and modeling structures can be derived, and this trend of ever faster structure determination is expected to continue.

We hope that this chapter has provided some insights for new students and researchers entering the field of structure determination of macrocycles, and we note again that we have drawn examples mainly from our own laboratory for illustrative purposes. The many references cited in this article and schematically illustrated in Table 2.1 provide an overview of the wealth of structures and groups that are actively working in this field.

Acknowledgments

References

1 Marsault, E.; Peterson, M. L. Macrocycles are great cycles: Applications, opportunities, and challenges of synthetic macrocycles in drug discovery. *J. Med. Chem.* **2011**, *54*, 1961–2004.

2 Yudin, A. K. Macrocycles: lessons from the distant past, recent developments, and future directions. *Chem. Sci.* **2015**, *6*, 30–49.

3 White, T. R.; Renzelman, C. M.; Rand, A. C.; Rezai, T.; McEwen, C. M.; Gelev, V. M.; Turner, R. A.; Linington, R. G.; Leung, S. S. F.; Kalgutkar, A. S.; Bauman, J. N.; Zhang, Y.; Liras, S.; Price, D. A.; Mathiowetz, A. M.; Jacobson, M. P.; Lokey, R. S. On-resin N-methylation of cyclic peptides for discovery of orally bioavailable scaffolds. *Nat. Chem. Biol.* **2011**, *7*, 810–817.

4 Heinis, C. Drug discovery: Tools and rules for macrocycles. *Nat. Chem. Biol.* **2014**, *10*, 696–698.

5 Chatterjee, J.; Mierke, D.; Kessler, H. *N*-Methylated cyclic pentaalanine peptides as template structures. *J. Am. Chem. Soc.* **2006**, *128*, 15164–15172.

6 Heller, M.; Sukopp, M.; Tsomaia, N.; John, M.; Mierke, D. F.; Reif, B.; Kessler, H. The conformation of *cyclo*(-D-Pro-Ala$_4$-) as a model for cyclic pentapeptides of the DL$_4$ type. *J. Am. Chem. Soc.* **2006**, *128*, 13806–13814.

7 Nielsen, D. S.; Hoang, H. N.; Lohman, R.-J.; Hill, T. A.; Lucke, A. J.; Craik, D. J.; Edmonds, D. J.; Griffith, D. A.; Rotter, C. J.; Ruggeri, R. B.; Price, D. A.; Liras, S.; Fairlie, D. P. Improving on nature: Making a cyclic heptapeptide orally bioavailable. *Angew. Chem. Int. Ed. Engl.* **2014**, *53*, 12059–12063.

8 Wang, C. K.; Northfield, S. E.; Swedberg, J. E.; Colless, B.; Chaousis, S.; Price, D. A.; Liras, S.; Craik, D. J. Exploring experimental and computational markers of cyclic peptides: Charting islands of permeability. *Eur. J. Med. Chem.* **2015**, *97*, 202–213.

9 Biron, E.; Chatterjee, J.; Ovadia, O.; Langenegger, D.; Brueggen, J.; Hoyer, D.; Schmid, H. A.; Jelinek, R.; Gilon, C.; Hoffman, A.; Kessler, H. Improving oral bioavailability of peptides by multiple N-methylation: Somatostatin analogues. *Angew. Chem. Int. Ed. Engl.* **2008**, *47*, 2595–2599.

10 Wang, C. K.; Northfield, S. E.; Colless, B.; Chaousis, S.; Hamernig, I.; Lohman, R.-J.; Nielsen, D. S.; Schroeder, C. I.; Liras, S.; Price, D. A.; Fairlie, D. P.; Craik, D. J. Rational design and synthesis of an orally bioavailable peptide guided by NMR amide temperature coefficients. *Proc. Natl. Acad. Sci. U. S. A* **2014**, *111*, 17504–17509.

11 Rezai, T.; Yu, B.; Millhauser, G. L.; Jacobson, M. P.; Lokey, R. S. Testing the conformational hypothesis of passive membrane permeability using synthetic cyclic peptide diastereomers. *J. Am. Chem. Soc.* **2006**, *128*, 2510–2511.

12 Beck, J. G.; Chatterjee, J.; Laufer, B.; Kiran, M. U.; Frank, A. O.; Neubauer, S.; Ovadia, O.; Greenberg, S.; Gilon, C.; Hoffman, A.; Kessler, H. Intestinal permeability of cyclic peptides: Common key backbone motifs identified. *J. Am. Chem. Soc.* **2012**, *134*, 12125–12133.

13 Kessler, H.; Müller, A.; Pook, K.-H. Assignment of all proton, carbon, and nitrogen NMR signals of antamanide in chloroform solution. *Liebigs Ann. Chem.* **1989**, *1989*, 903–912.

14 Kessler, H.; Bats, J. W.; Lautz, J.; Müller, A. Conformation of antamanide. *Liebigs Ann. Chem.* **1989**, *1989*, 913–928.

15 Matsumoto, T.; Shishido, A.; Morita, H.; Itokawa, H.; Takeya, K. Conformational analysis of cyclolinopeptides A and B. *Tetrahedron* **2002**, *58*, 5135–5140.

16 Di Blasio, B.; Rossi, F.; Benedetti, E.; Pavone, V.; Pedone, C.; Temussi, P. A.; Zanotti, G.; Tancredi, T. Bioactive peptides: Solid-state and solution conformation of

cyclolinopeptide A. *J. Am. Chem. Soc.* **1989**, *111*, 9089–9098.

17 Quail, J. W.; Shen, J.; Reaney, M. J.; Sammynaiken, R. Cyclo-linopeptide A methanol solvate. *Acta Crystallogr. Sect. E: Struct. Rep. Online* **2009**, *65*, o1913–o1914.

18 Huben, K.; Jewgiński, M.; Pabis, A.; Paluch, P.; Luy, B.; Jankowski, S. The structure of cyclolinopeptide A in chloroform refined by RDC measurements. *J. Pept. Sci.* **2014**, *20*, 901–907.

19 Burnett, P.-G. G.; Jadhav, P. D.; Okinyo-Owiti, D. P.; Poth, A. G.; Reaney, M. J. T. Glycine-containing flaxseed orbitides. *J. Nat. Prod.* **2015**, *78*, 681–688.

20 Borel, J. F.; Feurer, C.; Gubler, H. U.; Stahelin, H. Biological effects of cyclosporin A: A new antilymphocytic agent. *Agents Actions* **1976**, *6*, 468–475.

21 Klages, J.; Neubauer, C.; Coles, M.; Kessler, H.; Luy, B. Structure refinement of cyclosporin A in chloroform by using RDCs measured in a stretched PDMS-gel. *ChemBioChem* **2005**, *6*, 1672–1678.

22 Fesik, S. W.; Gampe, R. T., Jr.; Eaton, H. L.; Gemmecker, G.; Olejniczak, E. T.; Neri, P.; Holzman, T. F.; Egan, D. A.; Edalji, R.; Simmer, R.; Helfrich, R.; Hochlowski, J.; Jackson, M. NMR studies of [U-^{13}C]cyclosporin A bound to cyclophilin: Bound conformation and portions of cyclosporin involved in binding. *Biochemistry* **1991**, *30*, 6574–6583.

23 Weber, C.; Wider, G.; von Freyberg, B.; Traber, R.; Braun, W.; Widmer, H.; Wuthrich, K. The NMR structure of cyclosporin A bound to cyclophilin in aqueous solution. *Biochemistry* **1991**, *30*, 6563–6574.

24 Loosli, H.-R.; Kessler, H.; Oschkinat, H.; Weber, H.-P.; Petcher, T. J.; Widmer, A. Peptide conformations. Part 31. The conformation of cyclosporin a in the crystal and in solution. *Helv. Chim. Acta* **1985**, *68*, 682–704.

25 Davidson, A.; Leeper, T. C.; Athanassiou, Z.; Patora-Komisarska, K.; Karn, J.; Robinson, J. A.; Varani, G. Simultaneous recognition of HIV-1 TAR RNA bulge and loop sequences by cyclic peptide mimics of Tat protein. *Proc. Natl. Acad. Sci. U. S. A* **2009**, *106*, 11931–11936.

26 Srinivas, N.; Jetter, P.; Ueberbacher, B. J.; Werneburg, M.; Zerbe, K.; Steinmann, J.; Van der Meijden, B.; Bernardini, F.; Lederer, A.; Dias, R. L. A.; Misson, P. E.; Henze, H.; Zumbrunn, J.; Gombert, F. O.; Obrecht, D.; Hunziker, P.; Schauer, S.; Ziegler, U.; Käch, A.; Eberl, L.; Riedel, K.; DeMarco, S. J.; Robinson, J. A. Peptidomimetic antibiotics target outer-membrane biogenesis in *Pseudomonas aeruginosa*. *Science* **2010**, *327*, 1010–1013.

27 Robinson, J. A. Design and applications of protein epitope mimetics. *Chimia* **2013**, *67*, 885–890.

28 Robinson, J. A. Protein epitope mimetics as anti-infectives. *Curr. Opin. Chem. Biol.* **2011**, *15*, 379–386.

29 Maltsev, O. V.; Marelli, U. K.; Kapp, T. G.; Di Leva, F. S.; Di Maro, S.; Nieberler, M.; Reuning, U.; Schwaiger, M.; Novellino, E.; Marinelli, L.; Kessler, H. Stable peptides instead of stapled peptides: Highly potent αvβ6-selective integrin ligands. *Angew. Chem. Int. Ed.* **2016**, *55*, 1535–1539.

30 Chen, S.; Heinis, C. Phage Selection of Bicyclic Peptides Based on Two Disulfide Bridges. In *Peptide Libraries*, Derda, R., Ed. Springer: New York, **2015**, Vol. *1248*, pp 119–137.

31 Baeriswyl, V.; Heinis, C. Polycyclic peptide therapeutics. *ChemMedChem* **2013**, *8*, 377–384.

32 Heinis, C.; Winter, G. Encoded libraries of chemically modified peptides. *Curr. Opin. Chem. Biol.* **2015**, *26*, 89–98.

33 Chen, S.; Rentero Rebollo, I.; Buth, S. A.; Morales-Sanfrutos, J.; Touati, J.; Leiman, P. G.; Heinis, C. Bicyclic peptide ligands pulled out of cysteine-rich peptide libraries. *J. Am. Chem. Soc.* **2013**, *135*, 6562–6569.

34 Heinis, C.; Rutherford, T.; Freund, S.; Winter, G. Phage-encoded combinatorial chemical libraries based on bicyclic peptides. *Nat. Chem. Biol.* **2009**, *5*, 502–507.

35 Angelini, A.; Cendron, L.; Chen, S.; Touati, J.; Winter, G.; Zanotti, G.; Heinis, C. Bicyclic peptide inhibitor reveals large contact interface with a protease target. *ACS Chem. Biol.* **2012**, *7*, 817–821.

36 Korsinczky, M. L.; Schirra, H. J.; Rosengren, K. J.; West, J.; Condie, B. A.; Otvos, L.; Anderson, M. A.; Craik, D. J. Solution structures by ^{1}H NMR of the novel cyclic trypsin inhibitor SFTI-1 from sunflower seeds and an acyclic permutant. *J. Mol. Biol.* **2001**, *311*, 579–591.

37 Korsinczky, M. L.; Schirra, H. J.; Craik, D. J. Sunflower trypsin inhibitor-1. *Curr. Protein Pept. Sci.* **2004**, *5*, 351–364.

38 Luckett, S.; Garcia, R. S.; Barker, J. J.; Konarev, A. V.; Shewry, P. R.; Clarke, A. R.; Brady, R. L. High-resolution structure of a potent, cyclic proteinase inhibitor from sunflower seeds. *J. Mol. Biol.* **1999**, *290*, 525–533.

39 Wang, C. K.; King, G. J.; Northfield, S. E.; Ojeda, P. G.; Craik, D. J. Racemic and quasi-racemic X-ray structures of cyclic disulfide-rich peptide drug scaffolds. *Angew. Chem. Int. Ed. Engl.* **2014**, *53*, 11236–11241.

40 Clark, R. J.; Jensen, J.; Nevin, S. T.; Callaghan, B. P.; Adams, D. J.; Craik, D. J. The engineering of an orally active conotoxin for the treatment of neuropathic pain. *Angew. Chem. Int. Ed. Engl.* **2010**, *49*, 6545–6548.

41 Hemu, X.; Taichi, M.; Qiu, Y.; Liu, D.-X.; Tam, J. P. Biomimetic synthesis of cyclic peptides using novel thioester surrogates. *Biopolymers* **2013**, *100*, 492–501.

42 Daly, N. L.; Chen, Y. K.; Rosengren, K. J.; Marx, U. C.; Phillips, M. L.; Waring, A. J.; Wang, W.; Lehrer, R. I.;

Craik, D. J. Retrocyclin-2: Structural analysis of a potent anti-HIV θ-defensin. *Biochemistry* **2007**, *46*, 9920–9928.

43 Trabi, M.; Schirra, H. J.; Craik, D. J. Three-dimensional structure of RTD-1, a cyclic antimicrobial defensin from rhesus macaque leukocytes. *Biochemistry* **2001**, *40*, 4211–4221.

44 Tam, J. P.; Lu, Y.-A.; Yang, J.-L. Marked increase in membranolytic selectivity of novel cyclic tachyplesins constrained with an antiparallel two-β strand cystine knot framework. *Biochem. Biophys. Res. Commun.* **2000**, *267*, 783–790.

45 Conibear, A. C.; Wang, C. K.; Bi, T.; Rosengren, K. J.; Camarero, J. A.; Craik, D. J. Insights into the molecular flexibility of θ-defensins by NMR relaxation analysis. *J. Phys. Chem. B* **2014**, *118*, 14257–14266.

46 Craik, D. J.; Daly, N. L.; Bond, T.; Waine, C. Plant cyclotides: A unique family of cyclic and knotted proteins that defines the cyclic cystine knot structural motif. *J. Mol. Biol.* **1999**, *294*, 1327–1336.

47 Daly, N. L.; Rosengren, K. J.; Craik, D. J. Discovery, structure and biological activities of cyclotides. *Adv. Drug Deliv. Rev.* **2009**, *61*, 918–930.

48 Göransson, U.; Burman, R.; Gunasekera, S.; Strömstedt, A. A.; Rosengren, K. J. Circular proteins from plants and fungi. *J. Biol. Chem.* **2012**, *287*, 27001–27006.

49 Heitz, A.; Hernandez, J. F.; Gagnon, J.; Hong, T. T.; Pham, T. T.; Nguyen, T. M.; Le-Nguyen, D.; Chiche, L. Solution structure of the squash trypsin inhibitor MCoTI-II. A new family for cyclic knottins. *Biochemistry* **2001**, *40*, 7973–7983.

50 Felizmenio-Quimio, M. E.; Daly, N. L.; Craik, D. J. Circular proteins in plants. Solution structure of a novel macrocyclic trypsin inhibitor from *Momordica cochinchinensis*. *J. Biol. Chem.* **2001**, *276*, 22875–22882.

51 Montalbán-López, M.; Sánchez-Hidalgo, M.; Cebrián, R.; Maqueda, M. Discovering the bacterial circular proteins: Bacteriocins, cyanobactins, and pilins. *J. Biol. Chem.* **2012**, *287*, 27007–27013.

52 González, C.; Langdon, G. M.; Bruix, M.; Gálvez, A.; Valdivia, E.; Maqueda, M.; Rico, M. Bacteriocin AS-48, a microbial cyclic polypeptide structurally and functionally related to mammalian NK-lysin. *Proc. Natl. Acad. Sci. U. S. A* **2000**, *97*, 11221–11226.

53 Sánchez-Barrena, M. J.; Martínez-Ripoll, M.; Gálvez, A.; Valdivia, E.; Maqueda, M.; Cruz, V.; Albert, A. Structure of bacteriocin AS-48: From soluble state to membrane bound state. *J. Mol. Biol.* **2003**, *334*, 541–549.

54 Cascales, L.; Craik, D. J. Naturally occurring circular proteins: Distribution, biosynthesis and evolution. *Org. Biomol. Chem.* **2010**, *8*, 5035–5047.

55 Himeno, K.; Rosengren, K. J.; Inoue, T.; Perez, R. H.; Colgrave, M. L.; Lee, H. S.; Chan, L. Y.; Henriques, S. T.; Fujita, K.; Ishibashi, N.; Zendo, T.; Wilaipun, P.; Nakayama, J.; Leelawatcharamas, V.; Jikuya, H.; Craik, D. J.; Sonomoto, K. Identification, characterization, and three-dimensional structure of the novel circular bacteriocin, enterocin NKR-5-3B, from *Enterococcus faecium*. *Biochemistry* **2015**, *54*, 4863–4876.

56 Driggers, E. M.; Hale, S. P.; Lee, J.; Terrett, N. K. The exploration of macrocycles for drug discovery: An underexploited structural class. *Nat. Rev. Drug Discov.* **2008**, *7*, 608–624.

57 Mallinson, J.; Collins, I. Macrocycles in new drug discovery. *Future Med. Chem.* **2012**, *4*, 1409–1438.

58 Chatterjee, M. N.; Kay, E. R.; Leigh, D. A. Beyond switches: Ratcheting a particle energetically uphill with a compartmentalized molecular machine. *J. Am. Chem. Soc.* **2006**, *128*, 4058–4073.

59 Lewandowski, B.; De Bo, G.; Ward, J. W.; Papmeyer, M.; Kuschel, S.; Aldegunde, M. J.; Gramlich, P. M. E.; Heckmann, D.; Goldup, S. M.; D'Souza, D. M.; Fernandes, A. E.; Leigh, D. A. Sequence-specific peptide synthesis by an artificial small-molecule machine. *Science* **2013**, *339*, 189–193.

60 Arnison, P. G.; Bibb, M. J.; Bierbaum, G.; Bowers, A. A.; Bugni, T. S.; Bulaj, G.; Camarero, J. A.; Campopiano, D. J.; Challis, G. L.; Clardy, J.; Cotter, P. D.; Craik, D. J.; Dawson, M.; Dittmann, E.; Donadio, S.; Dorrestein, P. C.; Entian, K. D.; Fischbach, M. A.; Garavelli, J. S.; Goransson, U.; Gruber, C. W.; Haft, D. H.; Hemscheidt, T. K.; Hertweck, C.; Hill, C.; Horswill, A. R.; Jaspars, M.; Kelly, W. L.; Klinman, J. P.; Kuipers, O. P.; Link, A. J.; Liu, W.; Marahiel, M. A.; Mitchell, D. A.; Moll, G. N.; Moore, B. S.; Muller, R.; Nair, S. K.; Nes, I. F.; Norris, G. E.; Olivera, B. M.; Onaka, H.; Patchett, M. L.; Piel, J.; Reaney, M. J. T.; Rebuffat, S.; Ross, R. P.; Sahl, H. G.; Schmidt, E. W.; Selsted, M. E.; Severinov, K.; Shen, B.; Sivonen, K.; Smith, L.; Stein, T.; Sussmuth, R. D.; Tagg, J. R.; Tang, G. L.; Truman, A. W.; Vederas, J. C.; Walsh, C. T.; Walton, J. D.; Wenzel, S. C.; Willey, J. M.; van der Donk, W. A. Ribosomally synthesized and post-translationally modified peptide natural products: Overview and recommendations for a universal nomenclature. *Nat. Prod. Rep.* **2013**, *30*, 108–160.

61 Hegemann, J. D.; Zimmermann, M.; Xie, X.; Marahiel, M. A. Lasso peptides: An intriguing class of bacterial natural products. *Acc. Chem. Res.* **2015**, *48*, 1909–1919.

62 Al-Obeidi, F.; Hadley, M. E.; Pettitt, B. M.; Hruby, V. J. Design of a new class of superpotent cyclic.alpha.-melanotropins based on quenched dynamic simulations. *J. Am. Chem. Soc.* **1989**, *111*, 3413–3416.

63 Wong, C. T. T.; Rowlands, D. K.; Wong, C. H.; Lo, T. W. C.; Nguyen, G. K. T.; Li, H. Y.; Tam, J. P. Orally active peptidic bradykinin B-1 receptor antagonists engineered from a cyclotide scaffold for inflammatory

pain treatment. *Angew. Chem. Int. Ed. Engl.* **2012**, *51*, 5620–5624.

64 Beveridge, T.; Gratwohl, A.; Michot, F.; Niederberger, W.; Nüesch, E.; Nussbaumer, K.; Schaub, P.; Speck, B. Cyclosporin A: Pharmacokinetics alter a single dose in man and serum levels after multiple dosing in recipients of allogenic bone marrow grafts. *Curr. Ther. Res. Clin. Exp.* **1981**, *30*, 5–18.

65 Kessler, H.; Loosli, H.-R.; Oschkinat, H. Peptide conformations. Part 30. Assignment of the 1H-, 13C-, and 15N-NMR spectra of cyclosporin A in CDCl3 and C6D6 by a combination of homo- and heteronuclear two-dimensional techniques. *Helv. Chim. Acta* **1985**, *68*, 661–681.

66 Veber, D. F.; Freidlinger, R. M.; Perlow, D. S.; Paleveda, W. J., Jr.; Holly, F. W.; Strachan, R. G.; Nutt, R. F.; Arison, B. H.; Homnick, C.; Randall, W. C.; Glitzer, M. S.; Saperstein, R.; Hirschmann, R. A potent cyclic hexapeptide analogue of somatostatin. *Nature* **1981**, *292*, 55–58.

67 Aumailley, M.; Gurrath, M.; Müller, G.; Calvete, J.; Timpl, R.; Kessler, H. Arg-Gly-Asp constrained within cyclic pentapoptides strong and selective inhibitors of cell adhesion to vitronectin and laminin fragment P1. *FEBS Lett.* **1991**, *291*, 50–54.

68 Carlos, M.-M.; Florian, R.; Horst, K. Cilengitide: The first anti-angiogenic small molecule drug candidate. Design, synthesis and clinical evaluation. *Anti Cancer Agents Med. Chem.* **2010**, *10*, 753–768.

69 Kessler, H.; Gratias, R.; Hessler, G.; Gurrath, M.; Müller, G. Conformation of cyclic peptides. Principle concepts and the design of selectivity and superactivity in bioactive sequences by "spatial screening". *Pure Appl. Chem.* **1996**, *68*, 1201–1205.

70 Poth, A. G.; Chan, L. Y.; Craik, D. J. Cyclotides as grafting frameworks for protein engineering and drug design applications. *Biopolymers* **2013**, *100*, 480–491.

71 Ji, Y.; Majumder, S.; Millard, M.; Borra, R.; Bi, T.; Elnagar, A. Y.; Neamati, N.; Shekhtman, A.; Camarero, J. A. *In vivo* activation of the p53 tumor suppressor pathway by an engineered cyclotide. *J. Am. Chem. Soc.* **2013**, *135*, 11623–11633.

72 Jennings, C.; West, J.; Waine, C.; Craik, D.; Anderson, M. Biosynthesis and insecticidal properties of plant cyclotides: The cyclic knotted proteins from *Oldenlandia affinis*. *Proc. Natl. Acad. Sci. U. S. A* **2001**, *98*, 10614–10619.

73 Barbeta, B. L.; Marshall, A. T.; Gillon, A. D.; Craik, D. J.; Anderson, M. A. Plant cyclotides disrupt epithelial cells in the midgut of lepidopteran larvae. *Proc. Natl. Acad. Sci. U. S. A* **2008**, *105*, 1221–1225.

74 Gustafson, K. R.; Sowder, R. C. I.; Henderson, L. E.; Parsons, I. C.; Kashman, Y.; Cardellina, J. H. I.; McMahon, J. B.; Buckheit, R. W. J.; Pannell, L. K.; Boyd, M. R. Circulins A and B: Novel HIV-inhibitory macrocyclic peptides from the tropical tree *Chassalia parvifolia*. *J. Am. Chem. Soc.* **1994**, *116*, 9337–9338.

75 Tam, J. P.; Lu, Y. A.; Yang, J. L.; Chiu, K. W. An unusual structural motif of antimicrobial peptides containing end-to-end macrocycle and cystine-knot disulfides. *Proc. Natl. Acad. Sci. U. S. A* **1999**, *96*, 8913–8918.

76 Colgrave, M. L.; Kotze, A. C.; Huang, Y. H.; O'Grady, J.; Simonsen, S. M.; Craik, D. J. Cyclotides: Natural, circular plant peptides that possess significant activity against gastrointestinal nematode parasites of sheep. *Biochemistry* **2008**, *47*, 5581–5589.

77 Colgrave, M. L.; Kotze, A. C.; Ireland, D. C.; Wang, C. K.; Craik, D. J. The anthelmintic activity of the cyclotides: Natural variants with enhanced activity. *ChemBioChem* **2008**, *9*, 1939–1945.

78 Colgrave, M. L.; Kotze, A. C.; Kopp, S.; McCarthy, J. S.; Coleman, G. T.; Craik, D. J. Anthelmintic activity of cyclotides: *In vitro* studies with canine and human hookworms. *Acta Trop.* **2009**, *109*, 163–166.

79 Colgrave, M. L.; Huang, Y. H.; Craik, D. J.; Kotze, A. C. Cyclotide interactions with the nematode external surface. *Antimicrob. Agents Chemother.* **2010**, *54*, 2160–2166.

80 Plan, M. R. R.; Saska, I.; Cagauan, A. G.; Craik, D. J. Backbone cyclised peptides from plants show molluscicidal activity against the rice pest *Pomacea canaliculata* (golden apple snail). *J. Agric. Food Chem.* **2008**, *56*, 5237–5241.

81 Göransson, U.; Sjogren, M.; Svangard, E.; Claeson, P.; Bohlin, L. Reversible antifouling effect of the cyclotide cycloviolacin O2 against barnacles. *J. Nat. Prod.* **2004**, *67*, 1287–1290.

82 Simonsen, S. M.; Sando, L.; Rosengren, K. J.; Wang, C. K.; Colgrave, M. L.; Daly, N. L.; Craik, D. J. Alanine scanning mutagenesis of the prototypic cyclotide reveals a cluster of residues essential for bioactivity. *J. Biol. Chem.* **2008**, *283*, 9805–9813.

83 Huang, Y. H.; Colgrave, M. L.; Clark, R. J.; Kotze, A. C.; Craik, D. J. Lysine-scanning mutagenesis reveals a previously unidentified amendable face of the cyclotide kalata B1 for the optimisation of nematocidal activity. *J. Biol. Chem.* **2010**, *285*, 10797–10805.

84 Clark, R. J.; Craik, D. J. Engineering cyclic peptide toxins. *Methods Enzymol. Protein Eng. Ther. B* **2012**, *503*, 57–74.

85 Clark, R. J.; Akcan, M.; Kaas, Q.; Daly, N. L.; Craik, D. J. Cyclization of conotoxins to improve their biopharmaceutical properties. *Toxicon* **2012**, *59*, 446–455.

86 Akcan, M.; Stroud, M. R.; Hansen, S. J.; Clark, R. J.; Daly, N. L.; Craik, D. J.; Olson, J. M. Chemical re-engineering of chlorotoxin improves bioconjugation properties for tumor imaging and targeted therapy. *J. Med. Chem.* **2011**, *54*, 782–787.

87 Puttamadappa, S. S.; Jagadish, K.; Shekhtman, A.; Camarero, J. A. Backbone dynamics of cyclotide MCoTI-I free and complexed with trypsin. *Angew. Chem. Int. Ed. Engl.* **2010**, *49*, 7030–7034.

88 Daly, N. L.; Thorstholm, L.; Greenwood, K. P.; King, G. J.; Rosengren, K. J.; Heras, B.; Martin, J. L.; Craik, D. J. Structural insights into the role of the cyclic backbone in a squash trypsin inhibitor. *J. Biol. Chem.* **2013**, *288*, 36141–36148.

89 Terlau, H.; Olivera, B. M. Conus venoms: A rich source of novel ion channel-targeted peptides. *Physiol. Rev.* **2004**, *84*, 41–68.

90 Kaas, Q.; Yu, R. L.; Jin, A. H.; Dutertre, S.; Craik, D. J. ConoServer: Updated content, knowledge, and discovery tools in the conopeptide database. *Nucleic Acids Res.* **2012**, *40*, D325–D330.

91 Guddat, L. W.; Martin, J. A.; Shan, L.; Edmundson, A. B.; Gray, W. R. Three-dimensional structure of the α-conotoxin GI at 1.2 Å resolution. *Biochemistry* **1996**, *35*, 11329–11335.

92 Hu, S. H.; Gehrmann, J.; Guddat, L. W.; Alewood, P. F.; Craik, D. J.; Martin, J. L. The 1.1 Å crystal structure of the neuronal acetylcholine receptor antagonist, α-conotoxin PnIA from *Conus pennaceus. Structure* **1996**, *4*, 417–423.

93 Hu, S. H.; Gehrmann, J.; Alewood, P. F.; Craik, D. J.; Martin, J. L. Crystal structure at 1.1 Å resolution of α-conotoxin PnIB: Comparison with α-conotoxins PnIA and GI. *Biochemistry* **1997**, *36*, 11323–11330.

94 Hu, S.-H.; Loughnan, M.; Miller, R.; Weeks, C. M.; Blessing, R. H.; Alewood, P. F.; Lewis, R. J.; Martin, J. L. The 1.1 Å resolution crystal structure of [Tyr15]EpI, a novel α-conotoxin from *Conus episcopatus*, solved by direct methods. *Biochemistry* **1998**, *37*, 11425–11433.

95 Celie, P. H. N.; Kasheverov, I. E.; Mordvintsev, D. Y.; Hogg, R. C.; van Nierop, P.; van Elk, R.; van Rossum-Fikkert, S. E.; Zhmak, M. N.; Bertrand, D.; Tsetlin, V.; Sixma, T. K.; Smit, A. B. Crystal structure of nicotinic acetylcholine receptor homolog AChBP in complex with an α-conotoxin PnIA variant. *Nat. Struct. Mol. Biol.* **2005**, *12*, 582–588.

96 Hansen, S. B.; Sulzenbacher, G.; Huxford, T.; Marchot, P.; Taylor, P.; Bourne, Y. Structures of *Aplysia* AChBP complexes with nicotinic agonists and antagonists reveal distinctive binding interfaces and conformations. *EMBO J.* **2005**, *24*, 3635–3646.

97 Ulens, C.; Hogg, R. C.; Celie, P. H.; Bertrand, D.; Tsetlin, V.; Smit, A. B.; Sixma, T. K. Structural determinants of selective α-conotoxin binding to a nicotinic acetylcholine receptor homolog AChBP. *Proc. Natl. Acad. Sci. U. S. A* **2006**, *103*, 3615–3620.

98 Dy, C. Y.; Buczek, P.; Imperial, J. S.; Bulaj, G.; Horvath, M. P. Structure of conkunitzin-S1, a neurotoxin and Kunitz-fold disulfide variant from cone snail. *Acta Crystallogr. D Biol. Crystallogr.* **2006**, *62*, 980–990.

99 Dutertre, S.; Ulens, C.; Büttner, R.; Fish, A.; van Elk, R.; Kendel, Y.; Hopping, G.; Alewood, P. F.; Schroeder, C.; Nicke, A.; Smit, A. B.; Sixma, T. K.; Lewis, R. J. AChBP-targeted α-conotoxin correlates distinct binding orientations with nAChR subtype selectivity. *EMBO J.* **2007**, *26*, 3858–3867.

100 Yeates, T. O.; Kent, S. B. H. Racemic protein crystallography. *Annu. Rev. Biophys.* **2012**, *41*, 41–61.

101 Kessler, H.; Zimmermann, G.; Förster, H.; Engel, J.; Oepen, G.; Sheldrick, W. S. Does a molecule have the same conformation in the crystalline state and in solution? Comparison of NMR results for the solid state and solution with those of the X-ray structural determination. *Angew. Chem. Int. Ed. Engl.* **1981**, *20*, 1053–1055.

102 Marelli, U. K.; Frank, A. O.; Wahl, B.; La Pietra, V.; Novellino, E.; Marinelli, L.; Herdtweck, E.; Groll, M.; Kessler, H. Receptor-bound conformation of cilengitide better represented by its solution-state structure than the solid-state structure. *Chem. Eur. J.* **2014**, *20*, 14201–14206.

103 Beck, J. G.; Frank, A. O.; Kessler, H. NMR of Peptides. In *NMR of Biomolecules*, Bertini, I.; McGreevy, K. S.; Parigi, G., Eds. Wiley-VCH Verlag GmbH & Co. KGaA: Weinheim, **2012**, pp 328–344.

104 Reid, D. G. *Protein NMR Techniques*, Humana Press: Totowa, **1997**.

105 Palmer III, A. G.; Fairbrother, W. J.; Cavanagh, J.; Skelton, N. J.; Rance, M. *Protein NMR Spectroscopy: Principles and Practices*, Elsevier Academic Press: San Diego, **2007**.

106 Keeler, J. *Understanding NMR Spectroscopy*, John Wiley & Sons, Ltd: Chichester, **2010**.

107 Rules, G. S.; Hitchens, T. K. *Fundamentals of Protein NMR Spectroscopy*, Springer: Dordrecht, **2006**.

108 Craik, D. J.; Daly, N. L. NMR as a tool for elucidating the structures of circular and knotted proteins. *Mol. Biosyst.* **2007**, *3*, 257–265.

109 Ko, S. Y.; Dalvit, C. Conformation of cyclosporin A in polar solvents. *Int. J. Pept. Protein Res.* **1992**, *40*, 380–382.

110 Köck, M.; Kessler, H.; Seebach, D.; Thaler, A. Novel backbone conformation of cyclosporin A: The complex with lithium chloride. *J. Am. Chem. Soc.* **1992**, *114*, 2676–2686.

111 Karplus, M. Vicinal proton coupling in nuclear magnetic resonance. *J. Am. Chem. Soc.* **1963**, *85*, 2870–2871.

112 Schmieder, P.; Kurz, M.; Kessler, H. Determination of heteronuclear long-range couplings to heteronuclei in natural abundance by two- and three-dimensional NMR spectroscopy. *J. Biomol. NMR* **1991**, *1*, 403–420.

113 Shen, Y.; Delaglio, F.; Cornilescu, G.; Bax, A. TALOS+: A hybrid method for predicting protein backbone

torsion angles from NMR chemical shifts. *J. Biomol. NMR* **2009**, *44*, 213–223.

114 Wang, C. K.; Hu, S. H.; Martin, J. L.; Sjogren, T.; Hajdu, J.; Bohlin, L.; Claeson, P.; Goransson, U.; Rosengren, K. J.; Tang, J.; Tan, N. H.; Craik, D. J. Combined X-ray and NMR analysis of the stability of the cyclotide cystine knot fold that underpins its insecticidal activity and potential use as a drug scaffold. *J. Biol. Chem.* **2009**, *284*, 10672–10683.

115 Wüthrich, K. *NMR of Proteins and Nucleic Acids*, John Wiley & Sons, Inc.: New York, **1986**.

116 Kessler, H.; Köck, M.; Wein, T.; Gehrke, M. Reinvestigation of the conformation of cyclosporin A in chloroform. *Helv. Chim. Acta* **1990**, *73*, 1818–1832.

117 Wishart, D.; Bigam, C.; Holm, A.; Hodges, R.; Sykes, B. ^{1}H, ^{13}C and ^{15}N random coil NMR chemical shifts of the common amino acids. I. Investigations of nearest-neighbor effects. *J. Biomol. NMR* **1995**, *5*, 67–81.

118 Kessler, H.; Bats, J. W.; Griesinger, C.; Koll, S.; Will, M.; Wagner, K. Peptide conformations. 46. Conformational analysis of a superpotent cytoprotective cyclic somatostatin analog. *J. Am. Chem. Soc.* **1988**, *110*, 1033–1049.

119 MacLachlan, L. K.; Middleton, D. A.; Edwards, A. J.; Reid, D. G. A Case History: NMR Studies of the Structure of a Small Protein, ω-Conotoxin MVIIA. In *Protein NMR Techniques*, Reid, D. G., Ed. Humana Press: Totowa, **1997**, pp 337–362.

120 Güntert, P.; Mumenthaler, C.; Wüthrich, K. Torsion angle dynamics for NMR structure calculation with the new program DYANA. *J. Mol. Biol.* **1997**, *273*, 283–298.

121 Brunger, A. T.; Adams, P. D.; Clore, G. M.; DeLano, W. L.; Gros, P.; Grosse-Kunstleve, R. W.; Jiang, J. S.; Kuszewski, J.; Nilges, M.; Pannu, N. S.; Read, R. J.; Rice, L. M.; Simonson, T.; Warren, G. L. Crystallography and NMR system: A new software suite for macromolecular structure determination. *Acta Crystallogr. D Biol. Crystallogr.* **1998**, *54*, 905–921.

122 Blond, A.; Péduzzi, J.; Goulard, C.; Chiuchiolo, M. J.; Barthélémy, M.; Prigent, Y.; Salomón, R. A.; Farías, R. N.; Moreno, F.; Rebuffat, S. The cyclic structure of microcin J25, a 21-residue peptide antibiotic from *Escherichia coli*. *Eur. J. Biochem.* **1999**, *259*, 747–756.

123 Rosengren, K. J.; Clark, R. J.; Daly, N. L.; Göransson, U.; Jones, A.; Craik, D. J. Microcin J25 has a threaded sidechain-to-backbone ring structure and not a head-to-tail cyclized backbone. *J. Am. Chem. Soc.* **2003**, *125*, 12464–12474.

124 Skjeldal, L.; Gran, L.; Sletten, K.; Volkman, B. F. Refined structure and metal binding site of the kalata B1 peptide. *Arch. Biochem. Biophys.* **2002**, *399*, 142–148.

125 Saether, O.; Craik, D. J.; Campbell, I. D.; Sletten, K.; Juul, J.; Norman, D. G. Elucidation of the primary and three-dimensional structure of the uterotonic polypeptide kalata B1. *Biochemistry* **1995**, *34*, 4147–4158.

126 Göransson, U.; Craik, D. J. Disulfide mapping of the cyclotide kalata B1: Chemical proof of the cystic cystine knot motif. *J. Biol. Chem.* **2003**, *278*, 48188–48196.

127 Laskowski, R. A.; Rullmannn, J. A.; MacArthur, M. W.; Kaptein, R.; Thornton, J. M. AQUA and PROCHECK-NMR: Programs for checking the quality of protein structures solved by NMR. *J. Biomol. NMR* **1996**, *8*, 477–486.

128 Chen, V. B.; Arendall, W. B., 3rd; Headd, J. J.; Keedy, D. A.; Immormino, R. M.; Kapral, G. J.; Murray, L. W.; Richardson, J. S.; Richardson, D. C. MolProbity: All-atom structure validation for macromolecular crystallography. *Acta Crystallogr. D Biol. Crystallogr.* **2010**, *66*, 12–21.

129 Kleckner, I. R.; Foster, M. P. An introduction to NMR-based approaches for measuring protein dynamics. *Biochim. Biophys. Acta Proteins Proteomics* **2011**, *1814*, 942–968.

130 Tzeng, S.-R.; Kalodimos, C. G. Protein activity regulation by conformational entropy. *Nature* **2012**, *488*, 236–240.

131 Popovych, N.; Sun, S.; Ebright, R. H.; Kalodimos, C. G. Dynamically driven protein allostery. *Nat. Struct. Mol. Biol.* **2006**, *13*, 831–838.

132 Marlow, M. S.; Dogan, J.; Frederick, K. K.; Valentine, K. G.; Wand, A. J. The role of conformational entropy in molecular recognition by calmodulin. *Nat. Chem. Biol.* **2010**, *6*, 352–358.

133 Yang, D.; Kay, L. E. Contributions to conformational entropy arising from bond vector fluctuations measured from NMR-derived order parameters: Application to protein folding. *J. Mol. Biol.* **1996**, *263*, 369–382.

134 Trbovic, N.; Cho, J.-H.; Abel, R.; Friesner, R. A.; Rance, M.; Palmer, A. G. Protein side-chain dynamics and residual conformational entropy. *J. Am. Chem. Soc.* **2009**, *131*, 615–622.

135 Wang, C. K.; Swedberg, J. E.; Northfield, S. E.; Craik, D. J. Effects of cyclization on peptide backbone dynamics. *J. Phys. Chem. B* **2015**, *119*, 15821–15830.

136 Lipari, G.; Szabo, A. Model-free approach to the interpretation of nuclear magnetic resonance relaxation in macromolecules. 1. Theory and range of validity. *J. Am. Chem. Soc.* **1982**, *104*, 4546–4559.

137 Fushman, D.; Cahill, S.; Cowburn, D. The main-chain dynamics of the dynamin pleckstrin homology (PH) domain in solution: Analysis of ^{15}N relaxation with monomer/dimer equilibration 1. *J. Mol. Biol.* **1997**, *266*, 173–194.

138 Bernadó, P.; Åkerud, T.; García de la Torre, J.; Akke, M.; Pons, M. Combined use of NMR relaxation measurements and hydrodynamic calculations to study protein association. Evidence for tetramers of low molecular weight protein tyrosine phosphatase in solution. *J. Am. Chem. Soc.* **2003**, *125*, 916–923.

139 Mandel, A. M.; Akke, M.; Palmer III, A. G. Backbone dynamics of *Escherichia coli* ribonuclease HI: Correlations with structure and function in an active enzyme. *J. Mol. Biol.* **1995**, *246*, 144–163.

140 Bieri, M.; d'Auvergne, E.; Gooley, P. relaxGUI: A new software for fast and simple NMR relaxation data analysis and calculation of ps-ns and μs motion of proteins. *J. Biomol. NMR* **2011**, *50*, 147–155.

141 Spencer, R. K.; Nowick, J. S. A newcomer's guide to peptide crystallography. *Isr. J. Chem.* **2015**, *55*, 698–710.

142 Spencer, R. K.; Kreutzer, A. G.; Salveson, P. J.; Li, H.; Nowick, J. S. X-ray crystallographic structures of oligomers of peptides derived from β2-microglobulin. *J. Am. Chem. Soc.* **2015**, *137*, 6304–6311.

143 Battye, T. G.; Kontogiannis, L.; Johnson, O.; Powell, H. R.; Leslie, A. G. iMOSFLM: A new graphical interface for diffraction-image processing with MOSFLM. *Acta Crystallogr. D Biol. Crystallogr.* **2011**, *67*, 271–281.

144 Otwinowski, Z.; Minor, W. Processing of X-ray Diffraction Data Collected in Oscillation Mode. In *Methods in Enzymology*, Carter Jr., C. W.; Sweet, R. M., Eds. Academic Press: New York, **1997**, Vol. *276*, pp 307–326.

145 Kabsch, W. XDS. *Acta Crystallogr. D Biol. Crystallogr.* **2010**, *66*, 125–32.

146 Rhodes, G. *Crystallography Made Crystal Clear*, Elsevier: Amsterdam, **2006**.

147 Rupp, B. *Biomolecular Crystallography: Principles, Practice, and Application to Structural Biology*, Garland Science: New York, **2010**.

148 Emsley, P.; Lohkamp, B.; Scott, W. G.; Cowtan, K. Features and development of Coot. *Acta Crystallogr. D Biol. Crystallogr.* **2010**, *66*, 486–501.

149 Adams, P. D.; Afonine, P. V.; Bunkoczi, G.; Chen, V. B.; Davis, I. W.; Echols, N.; Headd, J. J.; Hung, L. W.; Kapral, G. J.; Grosse-Kunstleve, R. W.; McCoy, A. J.; Moriarty, N. W.; Oeffner, R.; Read, R. J.; Richardson, D. C.; Richardson, J. S.; Terwilliger, T. C.; Zwart, P. H. PHENIX: A comprehensive Python-based system for macromolecular structure solution. *Acta Crystallogr. D Biol. Crystallogr.* **2010**, *66*, 213–221.

150 Wukovitz, S. W.; Yeates, T. O. Why protein crystals favour some space-groups over others. *Nat. Struct. Mol. Biol.* **1995**, *2*, 1062–1067.

151 Mandal, K.; Pentelute, B. L.; Tereshko, V.; Thammavongsa, V.; Schneewind, O.; Kossiakoff, A. A.; Kent, S. B. H. Racemic crystallography of synthetic protein enantiomers used to determine the X-ray structure of plectasin by direct methods. *Protein Sci.* **2009**, *18*, 1146–1154.

152 Wang, C. K.; King, G. J.; Conibear, A. C.; Ramos, M. C.; Chaousis, S.; Henriques, S. T.; Craik, D. J. Mirror images of antimicrobial peptides provide reflections on their functions and amyloidogenic properties. *J. Am. Chem. Soc.* **2016**, *138*, 5706–5713.

153 Craik, D. J.; Wilce, J. A. Studies of Protein–Ligand Interactions by NMR. In *Protein NMR Techniques*, Reid, D. G., Ed. Humana Press: Totowa, **1997**, Vol. *60*, pp 195–232.

154 Shenkarev, Z. O.; Nadezhdin, K. D.; Sobol, V. A.; Sobol, A. G.; Skjeldal, L.; Arseniev, A. S. Conformation and mode of membrane interaction in cyclotides. *FEBS J.* **2006**, *273*, 2658–2672.

155 Wang, C. K.; Colgrave, M. L.; Ireland, D. C.; Kaas, Q.; Craik, D. J. Despite a conserved cystine knot motif, different cyclotides have different membrane binding modes. *Biophys. J.* **2009**, *97*, 1471–1481.

156 Theriault, Y.; Logan, T. M.; Meadows, R.; Yu, L.; Olejniczak, E. T.; Holzman, T. F.; Simmer, R. L.; Fesik, S. W. Solution structure of the cyclosporin A/ cyclophilin complex by NMR. *Nature* **1993**, *361*, 88–91.

157 Tanaka, Y.; Hipolito, C. J.; Maturana, A. D.; Ito, K.; Kuroda, T.; Higuchi, T.; Katoh, T.; Kato, H. E.; Hattori, M.; Kumazaki, K.; Tsukazaki, T.; Ishitani, R.; Suga, H.; Nureki, O. Structural basis for the drug extrusion mechanism by a MATE multidrug transporter. *Nature* **2013**, *496*, 247–251.

158 Hipolito, C.; Tanaka, Y.; Katoh, T.; Nureki, O.; Suga, H. A macrocyclic peptide that serves as a cocrystallization ligand and inhibits the function of a MATE family transporter. *Molecules* **2013**, *18*, 10514.

159 Cruz, V. L.; Ramos, J.; Melo, M. N.; Martinez-Salazar, J. Bacteriocin AS-48 binding to model membranes and pore formation as revealed by coarse-grained simulations. *Biochim. Biophys. Acta Biomembr.* **2013**, *1828*, 2524–2531.

160 Sonti, R.; Gowd, K. H.; Rao, K. N. S.; Ragothama, S.; Rodriguez, A.; Perez, J. J.; Balaram, P. Conformational diversity in contryphans from *Conus* venom: *cis-trans* isomerisation and aromatic/proline interactions in the 23-membered ring of a 7-residue peptide disulfide loop. *Chemistry* **2013**, *19*, 15175–15189.

161 Kristensen, K.; Hoyvik, I.-M.; Jansik, B.; Jorgensen, P.; Kjaergaard, T.; Reine, S.; Jakowski, J. MP2 energy and density for large molecular systems with internal error control using the Divide-Expand-Consolidate scheme. *Phys. Chem. Chem. Phys.* **2012**, *14*, 15706–15714.

162 Liao, S.-M.; Du, Q.-S.; Meng, J.-Z.; Pang, Z.-W.; Huang, R.-B. The multiple roles of histidine in protein interactions. *Chem. Cent. J.* **2013**, *7*, 44.

163 Du, Q.-S.; Liu, P.-J.; Deng, J. Empirical correction to molecular interaction energies in density functional theory (DFT) for methane hydrate simulation. *J. Chem. Theory Comput.* **2007**, *3*, 1665–1672.

164 Maier, J. A.; Martinez, C.; Kasavajhala, K.; Wickstrom, L.; Hauser, K. E.; Simmerling, C. ff14SB: Improving the accuracy of protein side chain and backbone parameters from ff99SB. *J. Chem. Theory Comput.* **2015**, *11*, 3696–3713.

165 MacKerell, A. D.; Bashford, D.; Bellott, M.; Dunbrack, R. L.; Evanseck, J. D.; Field, M. J.; Fischer, S.; Gao, J.; Guo, H.; Ha, S.; Joseph-McCarthy, D.; Kuchnir, L.; Kuczera, K.; Lau, F. T. K.; Mattos, C.; Michnick, S.; Ngo, T.; Nguyen, D. T.; Prodhom, B.; Reiher, W. E.; Roux, B.; Schlenkrich, M.; Smith, J. C.; Stote, R.; Straub, J.; Watanabe, M.; Wiórkiewicz-Kuczera, J.; Yin, D.; Karplus, M. All-atom empirical potential for molecular modeling and dynamics studies of proteins. *J. Phys. Chem. B* **1998**, *102*, 3586–3616.

166 Robertson, M. J.; Tirado-Rives, J.; Jorgensen, W. L. Improved peptide and protein torsional energetics with the OPLS-AA force field. *J. Chem. Theory Comput.* **2015**, *11*, 3499–3509.

167 Schmid, N.; Eichenberger, A.; Choutko, A.; Riniker, S.; Winger, M.; Mark, A.; van Gunsteren, W. Definition and testing of the GROMOS force-field versions 54A7 and 54B7. *Eur. Biophys. J.* **2011**, *40*, 843–856.

168 de Jong, D. H.; Singh, G.; Bennett, W. F. D.; Arnarez, C.; Wassenaar, T. A.; Schäfer, L. V.; Periole, X.; Tieleman, D. P.; Marrink, S. J. Improved parameters for the Martini coarse-grained protein force field. *J. Chem. Theory Comput.* **2013**, *9*, 687–697.

169 Pronk, S.; Páll, S.; Schulz, R.; Larsson, P.; Bjelkmar, P.; Apostolov, R.; Shirts, M. R.; Smith, J. C.; Kasson, P. M.; van der Spoel, D.; Hess, B.; Lindahl, E. GROMACS 4.5: A high-throughput and highly parallel open source molecular simulation toolkit. *Bioinformatics* **2013**, *29*, 845–854.

170 Case, D. A.; Berryman, J. T.; Betz, R. M.; Cerutti, D. S.; Cheatham III, T. E.; Darden, T. A.; Duke, R. E.; Giese, T. J.; Gohlke, H.; Goetz, A. W.; Homeyer, N.; Izadi, S.; Janowski, P.; Kaus, J.; Kovalenko, A.; Lee, T. S.; LeGrand, S.; Li, P.; Luchko, T.; Luo, R.; Madej, B.; Merz, K. M.; Monard, G.; Needham, P.; Nguyen, H.; Nguyen, H. T.; Omelyan, I.; Onufriev, A.; Roe, D. R.; Roitberg, A.; Salomon-Ferrer, R.; Simmerling, C. L.; Smith, W.; Swails, J.; Walker, R. C.; Wang, J.; Wolf, R. M.; Wu, X.; York, D. M.; Kollman, P. A. *AMBER 2015*, University of California: San Francisco, **2015**.

171 Brooks, B. R.; Brooks, C. L.; Mackerell, A. D.; Nilsson, L.; Petrella, R. J.; Roux, B.; Won, Y.; Archontis, G.; Bartels, C.; Boresch, S.; Caflisch, A.; Caves, L.; Cui, Q.; Dinner, A. R.; Feig, M.; Fischer, S.; Gao, J.; Hodoscek, M.; Im, W.; Kuczera, K.; Lazaridis, T.; Ma, J.; Ovchinnikov, V.; Paci, E.; Pastor, R. W.; Post, C. B.; Pu, J. Z.; Schaefer, M.; Tidor, B.; Venable, R. M.; Woodcock, H. L.; Wu, X.; Yang, W.; York, D. M.; Karplus, M. CHARMM: The biomolecular simulation program. *J. Comput. Chem.* **2009**, *30*, 1545–1614.

172 Phillips, J. C.; Braun, R.; Wang, W.; Gumbart, J.; Tajkhorshid, E.; Villa, E.; Chipot, C.; Skeel, R. D.; Kalé, L.; Schulten, K. Scalable molecular dynamics with NAMD. *J. Comput. Chem.* **2005**, *26*, 1781–1802.

173 Humphrey, W.; Dalke, A.; Schulten, K. VMD: Visual molecular dynamics. *J. Mol. Graph.* **1996**, *14*, 33–38.

174 Wu, E. L.; Cheng, X.; Jo, S.; Rui, H.; Song, K. C.; Dávila-Contreras, E. M.; Qi, Y.; Lee, J.; Monje-Galvan, V.; Venable, R. M.; Klauda, J. B.; Im, W. CHARMM-GUI Membrane Builder toward realistic biological membrane simulations. *J. Comput. Chem.* **2014**, *35*, 1997–2004.

175 Wassenaar, T. A.; Ingólfsson, H. I.; Böckmann, R. A.; Tieleman, D. P.; Marrink, S. J. Computational lipidomics with insane: A versatile tool for generating custom membranes for molecular simulations. *J. Chem. Theory Comput.* **2015**, *11*, 2144–2155.

176 Olsson, M. H. M.; Søndergaard, C. R.; Rostkowski, M.; Jensen, J. H. PROPKA3: Consistent treatment of internal and surface residues in empirical pKa predictions. *J. Chem. Theory Comput.* **2011**, *7*, 525–537.

177 Koziara, K.; Stroet, M.; Malde, A.; Mark, A. Testing and validation of the Automated Topology Builder (ATB) version 2.0: prediction of hydration free enthalpies. *J. Comput. Aided Mol. Des.* **2014**, *28*, 221–233.

178 Sousa da Silva, A.; Vranken, W. ACPYPE: AnteChamber PYthon Parser interfacE. *BMC Res. Notes* **2012**, *5*, 367.

179 Margreitter, C.; Petrov, D.; Zagrovic, B. Vienna-PTM web server: A toolkit for MD simulations of protein post-translational modifications. *Nucleic Acids Res.* **2013**, *41*, W422–W426.

180 Webb, B.; Sali, A. Comparative Protein Structure Modeling Using MODELLER. *Curr. Protoc. Protein Sci.* **2016**, *86*, 2.9.1–2.9.37.

181 Song, Y.; DiMaio, F.; Wang, Y.-R.; Kim, D.; Miles, C.; Brunette, T. J.; Thompson, J.; Baker, D. High-resolution comparative modeling with RosettaCM. *Structure* **2013**, *21*, 1735–1742.

182 Krivov, G. G.; Shapovalov, M. V.; Dunbrack, R. L. Improved prediction of protein side-chain conformations with SCWRL4. *Proteins Struct. Funct. Bioinf.* **2009**, *77*, 778–795.

183 Leaver-Fay, A.; Tyka, M.; Lewis, S. M.; Lange, O. F.; Thompson, J.; Jacak, R.; Kaufman, K. W.; Renfrew, P. D.; Smith, C. A.; Sheffler, W.; Davis, I. W.; Cooper, S.; Treuille, A.; Mandell, D. J.; Richter, F.; Ban, Y.-E. A.;

Fleishman, S. J.; Corn, J. E.; Kim, D. E.; Lyskov, S.; Berrondo, M.; Mentzer, S.; Popović, Z.; Havranek, J. J.; Karanicolas, J.; Das, R.; Meiler, J.; Kortemme, T.; Gray, J. J.; Kuhlman, B.; Baker, D.; Bradley, P. ROSETTA3: An Object-Oriented Software Suite for the Simulation and Design of Macromolecules. In *Methods in Enzymology*, Michael, L. J.; Ludwig, B., Eds. Academic Press: San Diego, **2011**, Vol. *487*, pp 545–574.

184 Yang, J.; Yan, R.; Roy, A.; Xu, D.; Poisson, J.; Zhang, Y. The I-TASSER Suite: Protein structure and function prediction. *Nat. Methods* **2015**, *12*, 7–8.

185 Niggli, D. A.; Ebert, M.-O.; Lin, Z.; Seebach, D.; van Gunsteren, W. F. Helical content of a β^3-octapeptide in methanol: Molecular dynamics simulations explain a seeming discrepancy between conclusions derived from CD and NMR Data. *Chemistry* **2012**, *18*, 586–593.

186 Mierke, D. F.; Kessler, H. Improved molecular dynamics simulations for the determination of peptide structures. *Biopolymers* **1993**, *33*, 1003–1017.

187 García-Aranda, M. I.; Mirassou, Y.; Gautier, B.; Martín-Martínez, M.; Inguimbert, N.; Vidal, M.; García-López, M. T.; Jiménez, M. A.; González-Muñiz, R.; Pérez de Vega, M. J. Disulfide and amide-bridged cyclic peptide analogues of the $VEGF_{81-91}$ fragment: Synthesis, conformational analysis and biological evaluation. *Bioorg. Med. Chem.* **2011**, *19*, 7526–7533.

188 Patriksson, A.; van der Spoel, D. A temperature predictor for parallel tempering simulations. *Phys. Chem. Chem. Phys.* **2008**, *10*, 2073–2077.

189 Razavi, A. M.; Wuest, W. M.; Voelz, V. A. Computational screening and selection of cyclic peptide hairpin mimetics by molecular simulation and kinetic network models. *J. Chem. Inf. Model.* **2014**, *54*, 1425–1432.

190 Butterfoss, G. L.; Yoo, B.; Jaworski, J. N.; Chorny, I.; Dill, K. A.; Zuckermann, R. N.; Bonneau, R.; Kirshenbaum, K.; Voelz, V. A. De novo structure prediction and experimental characterization of folded peptoid oligomers. *Proc. Natl. Acad. Sci. U. S. A* **2012**, *109*, 14320–14325.

191 Tribello, G. A.; Bonomi, M.; Branduardi, D.; Camilloni, C.; Bussi, G. PLUMED 2: New feathers for an old bird. *Comput. Phys. Commun.* **2014**, *185*, 604–613.

192 Piana, S.; Laio, A. A bias-exchange approach to protein folding. *J. Phys. Chem. B* **2007**, *111*, 4553–4559.

193 Paissoni, C.; Ghitti, M.; Belvisi, L.; Spitaleri, A.; Musco, G. Metadynamics simulations rationalise the conformational effects induced by N-methylation of RGD cyclic hexapeptides. *Chem. Eur. J.* **2015**, *21*, 14165–14170.

194 Baker, N. A.; Sept, D.; Joseph, S.; Holst, M. J.; McCammon, J. A. Electrostatics of nanosystems: Application to microtubules and the ribosome. *Proc. Natl. Acad. Sci. U. S. A* **2001**, *98*, 10037–10041.

195 Rocchia, W.; Alexov, E.; Honig, B. Extending the applicability of the nonlinear Poisson–Boltzmann equation: Multiple dielectric constants and multivalent ions. *J. Phys. Chem. B* **2001**, *105*, 6507–6514.

196 Lensink, M. F.; Wodak, S. J. Docking, scoring, and affinity prediction in CAPRI. *Proteins Struct. Funct. Bioinf.* **2013**, *81*, 2082–2095.

197 Quimbar, P.; Malik, U.; Sommerhoff, C. P.; Kaas, Q.; Chan, L. Y.; Huang, Y.-H.; Grundhuber, M.; Dunse, K.; Craik, D. J.; Anderson, M. A.; Daly, N. L. High-affinity cyclic peptide matriptase inhibitors. *J. Biol. Chem.* **2013**, *288*, 13885–13896.

198 Mahatmanto, T.; Mylne, J. S.; Poth, A. G.; Swedberg, J. E.; Kaas, Q.; Schaefer, H.; Craik, D. J. The evolution of *Momordica* cyclic peptides. *Mol. Biol. Evol.* **2015**, *32*, 392–405.

199 Gavenonis, J.; Sheneman, B. A.; Siegert, T. R.; Eshelman, M. R.; Kritzer, J. A. Comprehensive analysis of loops at protein–protein interfaces for macrocycle design. *Nat. Chem. Biol.* **2014**, *10*, 716–722.

200 Villar, E. A.; Beglov, D.; Chennamadhavuni, S.; Porco Jr, J. A.; Kozakov, D.; Vajda, S.; Whitty, A. How proteins bind macrocycles. *Nat. Chem. Biol.* **2014**, *10*, 723–731.

201 Morris, G. M.; Huey, R.; Lindstrom, W.; Sanner, M. F.; Belew, R. K.; Goodsell, D. S.; Olson, A. J. AutoDock4 and AutoDockTools4: Automated docking with selective receptor flexibility. *J. Comput. Chem.* **2009**, *30*, 2785–2791.

202 Tambunan, U. S.; Zahroh, H.; Utomo, B. B.; Parikesit, A. A. Screening of commercial cyclic peptide as inhibitor NS5 methyltransferase of dengue virus through molecular docking and molecular dynamics simulation. *Bioinformation* **2014**, *10*, 23–27.

203 Mika, J. T.; Moiset, G.; Cirac, A. D.; Feliu, L.; Bardají, E.; Planas, M.; Sengupta, D.; Marrink, S. J.; Poolman, B. Structural basis for the enhanced activity of cyclic antimicrobial peptides: The case of BPC194. *Biochim. Biophys. Acta Biomembr.* **2011**, *1808*, 2197–2205.

204 Barbosa, S. C.; Cilli, E. M.; Dias, L. G.; Fuzo, C. A.; Degrève, L.; Stabeli, R. G.; Itri, R.; Ciancaglini, P. Interaction of cyclic and linear Labaditin peptides with anionic and zwitterionic micelles. *J. Colloid Interface Sci.* **2015**, *438*, 39–46.

205 Zhao, H.; Zhu, Y.; Tong, M.; He, J.; Liu, C.; Tang, M. Density functional theory studies on the inclusion complexes of cyclic decapeptide with 1-phenyl-1-propanol enantiomers. *J. Mol. Model.* **2012**, *18*, 851–858.

206 Li, C. H.; Zuo, Z. C.; Su, J. G.; Xu, X. J.; Wang, C. X. The interactions and recognition of cyclic peptide mimetics of Tat with HIV-1 TAR RNA: A molecular dynamics simulation study. *J. Biomol. Struct. Dyn.* **2013**, *31*, 276–287.

207 Yu, R.; Kompella, S. N.; Adams, D. J.; Craik, D. J.; Kaas, Q. Determination of the α-conotoxin Vc1.1 binding site on the α9α10 nicotinic acetylcholine receptor. *J. Med. Chem.* **2013**, *56*, 3557–3567.

208 Yu, R.; Craik, D. J.; Kaas, Q. Blockade of neuronal α7-nAChR by α-conotoxin ImI explained by computational scanning and energy calculations. *PLoS Comput. Biol.* **2011**, *7*, e1002011.

209 Giménez-Oya, V.; Villacañas, Ó.; Obiol-Pardo, C.; Antolin-Llovera, M.; Rubio-Martinez, J.; Imperial, S. Design of novel ligands of CDP-methylerythritol kinase by mimicking direct protein–protein and solvent-mediated interactions. *J. Mol. Recognit.* **2011**, *24*, 71–80.

210 Ghadiri, M. R.; Granja, J. R.; Milligan, R. A.; McRee, D. E.; Khazanovich, N. Self-assembling organic nanotubes based on a cyclic peptide architecture. *Nature* **1993**, *366*, 324–327.

211 Vijayaraj, R.; Van Damme, S.; Bultinck, P.; Subramanian, V. Theoretical studies on the transport mechanism of 5-fluorouracil through cyclic peptide based nanotubes. *Phys. Chem. Chem. Phys.* **2013**, *15*, 1260–1270.

212 Li, R.; Fan, J.; Li, H.; Yan, X.; Yu, Y. Exploring the dynamic behaviors and transport properties of gas molecules in a transmembrane cyclic peptide nanotube. *J. Phys. Chem. B* **2013**, *117*, 14916–14927.

213 Ruiz, L.; VonAchen, P.; Lazzara, T. D.; Xu, T.; Keten, S. Persistence length and stochastic fragmentation of supramolecular nanotubes under mechanical force. *Nanotechnology* **2013**, *24*, 195103.

214 Li, R.; Fan, J.; Li, H.; Yan, X.; Yu, Y. Dynamic behaviors and transport properties of ethanol molecules in transmembrane cyclic peptide nanotubes. *J. Chem. Phys.* **2015**, *143*, 015101.

215 Ruiz, L.; Benjamin, A.; Sullivan, M.; Keten, S. Regulating ion transport in peptide nanotubes by tailoring the nanotube lumen chemistry. *J. Phys. Chem. Lett.* **2015**, *6*, 1514–1520.

216 Ruiz, L.; Wu, Y.; Keten, S. Tailoring the water structure and transport in nanotubes with tunable interiors. *Nanoscale* **2015**, *7*, 121–132.

217 Song, X.; Fan, J.; Liu, D.; Li, H.; Li, R. Molecular dynamics study of Na^+ transportation in a cyclic peptide nanotube and its influences on water behaviors in the tube. *J. Mol. Model.* **2013**, *19*, 4271–4282.

218 Yan, X.; Fan, J.; Yu, Y.; Xu, J.; Zhang, M. Transport behavior of a single Ca^{2+}, K^+, and Na^+ in a water-filled transmembrane cyclic peptide nanotube. *J. Chem. Inf. Model.* **2015**, *55*, 998–1011.

219 Khavani, M.; Izadyar, M.; Housaindokht, M. R. Theoretical design of the cyclic lipopeptide nanotube as a molecular channel in the lipid bilayer, molecular dynamics and quantum mechanics approach. *Phys. Chem. Chem. Phys.* **2015**, *17*, 25536–25549.

220 Vijayaraj, R.; Van Damme, S.; Bultinck, P.; Subramanian, V. Molecular dynamics and umbrella sampling study of stabilizing factors in cyclic peptide-based nanotubes. *J. Phys. Chem. B* **2012**, *116*, 9922–9933.

221 Vijayaraj, R.; Van Damme, S.; Bultinck, P.; Subramanian, V. Structure and stability of cyclic peptide based nanotubes: A molecular dynamics study of the influence of amino acid composition. *Phys. Chem. Chem. Phys.* **2012**, *14*, 15135–15144.

222 Quartararo, J. S.; Eshelman, M. R.; Peraro, L.; Yu, H.; Baleja, J. D.; Lin, Y.-S.; Kritzer, J. A. A bicyclic peptide scaffold promotes phosphotyrosine mimicry and cellular uptake. *Bioorg. Med. Chem.* **2014**, *22*, 6387–6391.

223 Cirac, A. D.; Moiset, G.; Mika, J. T.; Koçer, A.; Salvador, P.; Poolman, B.; Marrink, S. J.; Sengupta, D. The molecular basis for antimicrobial activity of pore-forming cyclic peptides. *Biophys. J.* **2011**, *100*, 2422–2431.

224 Nawae, W.; Hannongbua, S.; Ruengjitchatchawalya, M. Defining the membrane disruption mechanism of kalata B1 via coarse-grained molecular dynamics simulations. *Sci. Rep.* **2014**, *4*, 3933.

225 Henriques, S. T.; Huang, Y. H.; Rosengren, K. J.; Franquelim, H. G.; Carvalho, F. A.; Johnson, A.; Sonza, S.; Tachedjian, G.; Castanho, M. A.; Daly, N. L.; Craik, D. J. Decoding the membrane activity of the cyclotide kalata B1: The importance of phosphatidylethanolamine phospholipids and lipid organization on hemolytic and anti-HIV activities. *J. Biol. Chem.* **2011**, *286*, 24231–24241.

226 Zhang, J.; Yamaguchi, S.; Nagamune, T. Sortase A-mediated synthesis of ligand-grafted cyclized peptides for modulating a model protein-protein interaction. *Biotechnol. J.* **2015**, *10*, 1499–1505.

227 Gunasekera, S.; Foley, F. M.; Clark, R. J.; Sando, L.; Fabri, L. J.; Craik, D. J.; Daly, N. L. Engineering stabilized vascular endothelial growth factor-A antagonists: Synthesis, structural characterization, and bioactivity of grafted analogues of cyclotides. *J. Med. Chem.* **2008**, *51*, 7697–7704.

228 Eliasen, R.; Daly, N. L.; Wulff, B. S.; Andresen, T. L.; Conde-Frieboes, K. W.; Craik, D. J. Design, synthesis, structural and functional characterization of novel melanocortin agonists based on the cyclotide kalata B1. *J. Biol. Chem.* **2012**, *287*, 40493–40501.

229 Getz, J. A.; Cheneval, O.; Craik, D. J.; Daugherty, P. S. Design of a cyclotide antagonist of neuropilin-1 and -2 that potently inhibits endothelial cell migration. *ACS Chem. Biol.* **2013**, *8*, 1147–1154.

230 Wang, C. K.; Gruber, C. W.; Cĕmažar, M.; Siatskas, C.; Tagore, P.; Payne, N.; Sun, G.; Wang, S.; Bernard, C. C.; Craik, D. J. Molecular grafting onto a stable framework yields novel cyclic peptides for the treatment of multiple sclerosis. *ACS Chem. Biol.* **2014**, *9*, 156–163.

231 Thongyoo, P.; Roque-Rosell, N.; Leatherbarrow, R. J.; Tate, E. W. Chemical and biomimetic total syntheses of natural and engineered MCoTI cyclotides. *Org. Biomol. Chem.* **2008**, *6*, 1462–70.

232 Sommerhoff, C. P.; Avrutina, O.; Schmoldt, H. U.; Gabrijelcic-Geiger, D.; Diederichsen, U.; Kolmar, H. Engineered cystine knot miniproteins as potent inhibitors of human mast cell tryptase β. *J. Mol. Biol.* **2010**, *395*, 167–175.

233 Thongyoo, P.; Bonomelli, C.; Leatherbarrow, R. J.; Tate, E. W. Potent inhibitors of β-tryptase and human leukocyte elastase based on the MCoTI-II scaffold. *J. Med. Chem.* **2009**, *52*, 6197–6200.

234 Chan, L. Y.; Gunasekera, S.; Henriques, S. T.; Worth, N. F.; Le, S. J.; Clark, R. J.; Campbell, J. H.; Craik, D. J.; Daly, N. L. Engineering pro-angiogenic peptides using stable disulfide-rich cyclic scaffolds. *Blood* **2011**, *118*, 6709–6717.

235 Glotzbach, B.; Reinwarth, M.; Weber, N.; Fabritz, S.; Tomaszowski, M.; Fittler, H.; Christmann, A.; Avrutina, O.; Kolmar, H. Combinatorial optimization of cystine-knot peptides towards high-affinity inhibitors of human matriptase-1. *PLoS One* **2013**, *8*, e76956.

236 Aboye, T. L.; Ha, H.; Majumder, S.; Christ, F.; Debyser, Z.; Shekhtman, A.; Neamati, N.; Camarero, J. A. Design of a novel cyclotide-based CXCR4 antagonist with anti-human immunodeficiency virus (HIV)-1 activity. *J. Med. Chem.* **2012**, *55*, 10729–10734.

237 Huang, Y.-H.; Henriques, S. T.; Wang, C. K.; Thorstholm, L.; Daly, N. L.; Kaas, Q.; Craik, D. J. Design of substrate-based BCR-ABL kinase inhibitors using the cyclotide scaffold. *Sci. Rep.* **2015**, *5*, 12974.

238 Knappe, T. A.; Manzenrieder, F.; Mas-Moruno, C.; Linne, U.; Sasse, F.; Kessler, H.; Xie, X.; Marahiel, M. A. Introducing lasso peptides as molecular scaffolds for drug design: Engineering of an integrin antagonist. *Angew. Chem. Int. Ed.* **2011**, *50*, 8714–8717.

3

Designing Orally Bioavailable Peptide and Peptoid Macrocycles

David A. Price, Alan M. Mathiowetz and Spiros Liras

Cardiovascular, Metabolic and Endocrine Diseases, Pfizer Worldwide Medicinal Chemistry, Cambridge, MA, USA

3.1 Introduction

There is a resurgence of interest within the drug discovery community in macrocycles. Due to their size and structural complexity, macrocycles may be effective modalities for difficult targets such as protein–protein interactions [1]. A book on the subject of macrocycles would be incomplete without an overview of the contributions that peptides and peptidomimetics have made in this arena. The interest in peptide and peptidomimetic macrocycles stems from several important factors. Peptidomimetic macrocycles could achieve exquisite binding to biological targets of interest. In addition, peptidomimetic macrocycles have the potential for increased safety due to higher pharmacological selectivity and reduced off-target activity [2]. Synthetic accessibility is excellent due to the availability of modular synthetic routes and scalable technologies. However, these modalities often have molecular weights that exceed 500 Da and hydrogen bonding capabilities that move them outside what has been considered oral drug space within the modern pharmaceutical industry [3]. This oral drug space is often referred to as the Rule of Five. The majority of peptide and protein therapeutics are administered *via* parenteral routes due to the low oral bioavailability of these compounds. This low oral bioavailability can be attributed to two major problems: intestinal metabolic degradation by proteases expressed at the enterocytes brush border or released in the gastrointestinal (GI) tract and subsequently poor ability of the peptide/peptidomimetic to cross the gut wall [4]. The ability to design macrocyclic peptides and peptoids that cross this barrier *via* a passive transcellular mode is still a major challenge for the drug discovery community to solve. The strategic and commercial attraction of this field has recently been elegantly reviewed [5]. The peptide/peptidomimetic that successfully navigates this challenge and enters the hepatic portal vein often suffers from a short plasma half-life due to proteolytic degradation and/or renal elimination of the parent. For the sake of clarity, we review cyclic peptides and structurally related peptidomimetics or peptoids together, many of whose challenges and lessons are common to both. Outside the scope of this chapter are orally administered macrocyclic peptides where the site of action is in the gut and low absorption into the systemic circulation is desired. This is an exciting field as demonstrated by the approval of linaclotide in 2012 for the treatment of chronic constipation, and readers are recommended to read further in the literature [6]. Furthermore, macrocycles that are postulated to be absorbed by unknown transporters or receptor-mediated endocytosis mechanisms in the gut are not included in the chapter. The use of ring-closing metathesis methodology, and other α-helix constraining linkers, is of interest to researchers to enable the synthesis of cyclic peptides with defined secondary structure in aqueous solution. However, this alone is insufficient to make the macrocycles cell permeable *via* nonenergy-dependent processes [7]. The risk of taking these compounds into clinical trials as orally administered drugs is therefore high due to potential unforeseen drug–drug interactions, high patient variability, or nonlinear pharmacokinetics in dose escalation studies. Even if the drug did show a strong pharmacokinetic profile, this would be no guarantee of a pharmacodynamic response if the drug still needs to access an intracellular compartment to elicit a physiological effect. The transporters required to access the intracellular compartment could be different than the transporters enabling absorption cross the gut wall. Undoubtedly, there will be advances in this area, but at the present time, these are not part of the chapter. Moreover, conjugation to cell-penetrating peptides or polycationic moieties such as TAT is also outside the scope of this work [8].

The chapter starts with a description of designing peptides that possess improved proteolytic stability and

increased plasma half-life. A section that introduces absorption and *in vitro* means to measure this process follows. Subsequently, the chapter moves into three sections describing differing approaches to enable the macrocycle to cross the gut wall:

1) A brief review of paracellular absorption of macrocycles with a specific focus on the hydrophilic macrocycle desmopressin comprises the initial section. The ability of formulation technology to improve the oral bioavailability of desmopressin and other peptides is also highlighted.

2) A transition is then made into macrocycles that are believed to cross the gut wall in a passive transcellular manner. Various research groups have worked on the concept of hydrogen bond management within macrocycles, which is critical in the prospective design of macrocycles capable of crossing membranes. Using compounds from the literature, we review the utility of macrocyclization, N-methylation, conformational effects, shielding, and internal hydrogen bonding frameworks. Furthermore, hydrogen bond management *via* structural modifications, such as the incorporation of depsipeptide functionality and peptoid fragments, is covered. There is often interplay between these strategies. Within these approaches, a concise discussion is included of the hydrophobic macrocycle cyclosporine (CSA), which is absorbed in a passive transcellular manner and then undergoes P-450-mediated oxidation in the liver to metabolites that are subsequently eliminated. CSA is a fascinating drug that could act as a case history for many components of drug discovery; however, in the interest of space, the reader is directed to a number of excellent reviews already published on CSA [9]. Across the extensive literature on CSA, it has been argued that N-methylation, conformational effects, shielding, and internal hydrogen bonding frameworks all have made contributions to its favorable properties. As our sophistication in macrocycle design grows, it is hoped that we can emulate CSA. This is the most extensive section and includes exciting recently published work that gives a sense of the enormous potential and direction of this field.

3) An opinion is provided on the future directions and challenges that the drug discovery communities need to overcome to realize the full potential of this drug modality.

We acknowledge that it is an oversimplification to assume that compounds cross the gut wall *via* a single mode (paracellular vs. transcellular vs. active transport) [10]. There are compounds that could be classified into more than one section, and they have been considered where the authors decided were most appropriate from the data available and optimal for the flow of the chapter.

3.2 Improving Peptide Plasma Half-Life

Short plasma half-lives of acyclic peptides are due to both fast renal clearance and enzymatic degradation during systemic circulation. A variety of strategies known to prolong plasma residence time of peptide-based drugs have recently been comprehensively reviewed, and readers are encouraged to consult these contributions [11]. In brief, the most common approach is a conjugation of the peptide to macromolecules such as poly(ethylene glycol) (PEG) to limit renal clearance. The need for large, polar conjugating molecules like PEG arises since, as a general rule, substances with a molecular mass <5 kDa, which are not highly bound to plasma proteins, are completely excreted *via* the renal route, whereas molecules with molecular weight >50 kDa are not found in large quantities in the glomerular filtrate. The discovery and development of long-acting glucagon like peptide (GLP)-1 receptor agonists for the treatment of type 2 diabetes mellitus provides a rich case history of differing peptide–macromolecule conjugation strategies to improve exposure. Several research groups have utilized the attachment of the peptide pharmacophore to PEG, long-chain fatty acids, and polylysine expressions. Many of the approaches in GLP-1 have yielded clinical candidates in various stages of development, as well as marketed agents. Conjugation to other long-lived plasma proteins such as antibody fragments or serum albumin have also been reported [12]. It is unfortunate that attachment to macromolecules not only prolong the plasma half-life but invariably also takes the physicochemical properties of the molecule even further from the space required for good absorption postoral administration. Reducing the propensity for enzymatic degradation in the gut lumen, plasma, liver, or kidney has been successfully accomplished using a variety of strategies such as replacement of natural amino acids known to be susceptible to cleavage or modification of the N and C terminus amino acids [13]. The most effective strategy for improving plasma half-life of peptides, while not damaging their potential for absorption, is cyclization [14]. Modes of cyclization include backbone cyclization of the N and C termini, cyclization involving either terminus and side chain, and cyclization between side chains. Backbone cyclization is the most frequently used method for the optimization of half-life as this often preserves the biological activity of the molecule, which is most often predominantly influenced by the side chains. On the other hand, side chain-to-side chain cyclization is

useful when the biological activity of the peptide is heavily influenced by the N and C termini interacting with the target protein [15].

3.3 Absorption, Bioavailability, and Methods for Predicting Absorption

The aspiration of this section is to review literature where the peptide/peptidomimetic is able to cross the gut wall postoral administration, enter the hepatic portal vein, and have sufficient systemic exposure to access the molecular target for engagement and modulation. There is a wealth of literature on macrocyclic peptides that have the potential for oral administration, so it is important to rationalize the priorities given to compounds discussed in this chapter [16]. Due to the difficulty of translating *in vitro* data into accurate prediction of pharmacokinetics in animals and the subsequent translation of animal studies to man, priority has been given to agents where there is sufficient data disclosed in man and preclinical species. Marketed agents such as cyclosporine and desmopressin are examined, followed by compounds in the preclinical phase where there is robust data from rat or dog studies. At the outset, it is worth taking a moment to differentiate between the concepts of "absolute oral bioavailability," "oral bioavailability," and "oral activity." These terms are sometimes used interchangeably in the literature and can cause confusion. Within this chapter, priority is given to compounds that possess absolute oral bioavailability from an assessment of drug concentration in the systemic circulation after oral administration compared to an *intravenous* (*i.v.*) administration of the compound. The term oral bioavailability is used where the drug is found as a parent in the systemic circulation postoral administration, but there is *no intravenous* leg to compare to. Finally, oral activity can be defined for compounds that possess pharmacological activity postoral administration, but there is no measurement of systemic exposure. These oral activity disclosures are often difficult to interpret and so are of limited value, particularly if the dose administered is unusually high. In this chapter, we will endeavor to be clear in the data presented as to the experimental design.

3.3.1 *In Vitro* Assays

Outside of marketed agents or compounds in advanced clinical trials, few examples exist of confirmed absolute bioavailability and comprehensive understanding of properties that influence absorption. In this field, there is a large body of literature investigating relationships between chemical structure, associated physicochemical properties, and cell permeability assessed in multiple *in vitro* assays including Caco-2 cell monolayers [17], PAMPA [18], or Ussing chambers and subsequent development of computational models from this data [19]. Caco-2 cell monolayers have been widely used throughout the literature for the assessment of permeability. Alternative cell lines are also being developed and publications in this chapter often use the RRCK cell line [20]. For papers where there is only *in vitro* data, without the translation into an *in vivo* experiment in preclinical species or man, these contributions are often difficult to put into context. Nonetheless significant papers in this category are highlighted.

There is little agreement in the literature in which *in vitro* assays generate the greatest value in the prediction of gut wall permeability and contribute to oral bioavailability in an *in vivo* study. Recently, a key paper has evaluated two commonly employed *in vitro* models, Caco-2 monolayers and rat intestinal mucosa, regarding their correlation to *in vivo* bioavailability of peptide drugs after oral administration in rat and human [21]. The peptides selected were hydrophilic in nature, and the conclusion is the rat mucosa model is a better prediction model for human oral bioavailability than Caco-2 monolayers. However, the correlation of rat-to-human data was not undertaken due to the limited data set of hydrophilic peptides. Without access to high-quality preclinical *in vivo* pharmacokinetic data, great care must be taken to not over-interpret predictions to man. Due to the technical challenges and expense associated with the use of tissue-based models, many research groups publish work using cultured cell systems such as Caco-2 monolayers or artificial membranes. Although these are valuable contributions, this work needs to be reviewed with care. Developing high throughput, predictive *in vitro* assays is a challenge that we return to in Section 3.5.

3.3.2 Paracellular Absorption

Desmopressin **1** (Figure 3.1) is a synthetic replacement for the pituitary hormone [Arg^8]-vasopressin. A structural comparison of desmopressin to [Arg^8]-vasopressin shows the first amino acid has been deaminated, and the arginine at the eighth position has the opposite configuration to the endogenous hormone. These modifications lead to increased metabolic stability compared to [Arg^8]-vasopressin and so desmopressin possesses a longer half-life in man and therefore an extended duration of action. Desmopressin is prescribed extensively for nocturnal enuresis and is associated with a low incidence of adverse events. Desmopressin has been the agent of choice for patients with diabetes insipidus and, due to its good safety profile, is also prescribed for children with nocturnal enuresis [22]. With high affinity for the vasopressin (V2)
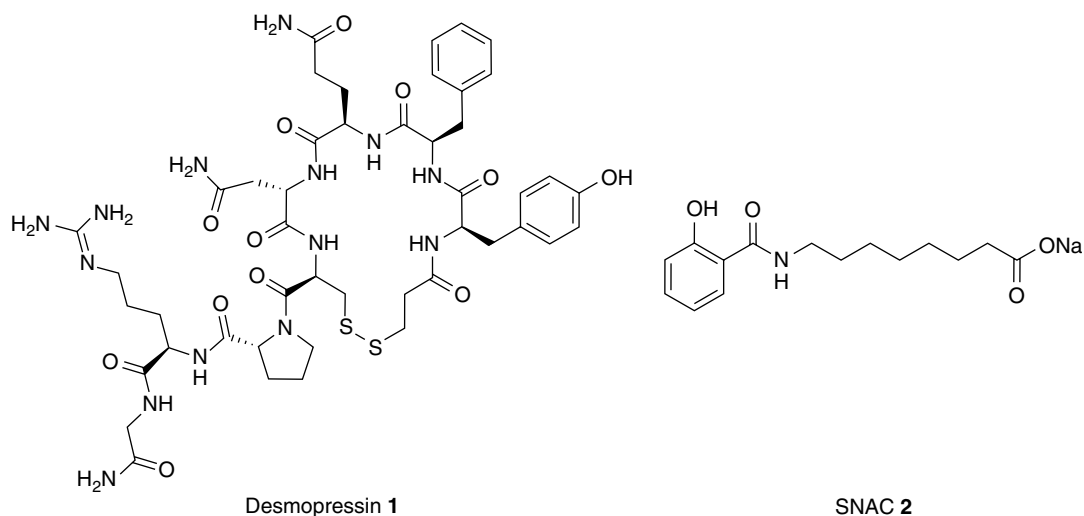
Figure 3.1 Desmopressin **1** and SNAC **2**.

receptors located in the collecting ducts of the kidney and high plasma stability, the dose required is 0.2 mg and is administered orally. Alternative routes of administration such as nasal sprays were removed from the market following patient seizures and, in some cases, death. Desmopressin clearly lies outside the Rule of Five with a molecular weight of 1069 Da and extensive hydrogen bonding potential giving a measured log*D* of −3.5.

The negative log*D* of **1** demonstrates the extreme hydrophilicity of this drug, which is absorbed in a paracellular fashion in the gut and has variable oral bioavailability in the range of 0.08–0.16%. In the case of highly hydrophilic desmopressin, the volume of distribution in man is limited to the body's aqueous compartment, giving a low V_D of 0.3 l/kg and plasma protein binding of 50% [23]. As expected from this physicochemical profile, renal clearance contributes significantly to the elimination of desmopressin, and the drug is excreted in the urine. Desmopressin has a terminal half-life of 1.5–3.0 h and is safe and well tolerated in patients with impaired renal function where there is a longer terminal half-life [23]. Desmopressin is a successful drug driven by the interplay of three factors. The dose required is low, at 0.2–0.6 mg prior to bedtime. The low dose is driven by its exquisite target affinity and there is little risk of solubility-limited absorption of the small dose in the gut. Once in solution, the high hydrophilicity drives paracellular absorption and, because of desmopressin's high molecular weight, this process is inefficient, giving a remarkably low, but sufficient, oral bioavailability [24]. It is generally accepted that for paracellular absorption to be an efficient process, the molecular weight should be <300 Da. The third factor that makes desmopressin a rare example of a marketed,

orally administered peptide macrocycle is its strong safety profile with low rates of reported adverse events.

3.3.3 Tight Junction Modifiers to Improve Paracellular Absorption

There has been a great deal of research into the use of surfactants and tight junction modifiers to improve the paracellular absorption of hydrophilic molecules. The paracellular absorption of peptides/peptidomimetics is especially attractive because the cell junction is deficient in proteolytic activity and is an aqueous environment in which hydrophilic peptides prefer to reside. A full examination of this field is beyond the scope of this work and has been comprehensively reviewed [25]. There are many reports disclosing improved permeability characteristics of molecules using *in vitro* and *ex vivo* models, but human data in the public domain is limited.

It is not surprising that many permeation enhancers are essentially surfactants in nature and are associated with toxicity (reduced cell viability, epithelial damage) due to this mode of action leading to uncontrolled membrane destabilization and cell death. There is also the potential risk for membrane disruption in the gut and, hence, exposure to unnecessary toxins or other bacterial by-products. With all these caveats, medium-chain fatty acids, their salts, and simple derivatives appear to have potential in this field. It is important to emphasize that these are used as food additives and so have a long track record of safety. Indeed, these formulation excipients are listed as generally recognized as safe (GRAS) and have been tested in rats, dogs, and humans to establish safety profiles. Medium-chain fatty acids such as sodium caprate have been reported to improve the oral bioavailability of

desmopressin whose clinical profile was previously discussed. The exact nature of the formulation has not been disclosed, but, in a trial involving 18 patients, a 13-fold improvement in oral bioavailability was seen compared with the standard marketed formulation [26]. Within macrocycle drug space, formulation technologies should be integrated into the overall project strategy. An alternative absorption enhancer has been published and marketed as the Eligen® system (Emisphere Technologies, Roseland, NJ), where delivery agents or "carriers" facilitate the transport of therapeutic macromolecules across biological membranes [27]. The delivery agents are low molecular weight compounds, which interact non-covalently with the active therapeutic agent. The delivery agents have no known pharmacological activity themselves at the intended dose levels and do not carry pharmacokinetic risks such as drug–drug interactions or accumulation. Publications suggest that some conformations of intrinsically membrane-impermeable molecules can be transported across cell membranes, while other conformations are too large or too charged/polar to do so. This technology enables large or highly charged molecules to cross the gut wall *via* passive, transcellular absorption. Once the drug molecule crosses the membrane, the delivery agent dissociates from the drug molecule, which then reestablishes its low energy conformation and returns to its therapeutically active state. Studies have shown that this process does not involve chemical modification of the drug molecule and the integrity of cell membrane and structure are maintained.

An example of the carrier systems developed is the sodium salt of *N*-[8-(2-hydroxybenzoyl)amino]caprylate (SNAC, **2**, Figure 3.1). Mechanistic studies using Caco-2 cells have shown that a co-formulation of SNAC and insulin can demonstrate a tenfold increase in the permeability of insulin and does so without disrupting cell membranes [28]. Confocal microscopy revealed that the insulin was absorbed transcellularly without detectable alterations of the tight junctions between adjacent cells. The authors suggest that SNAC increases the lipophilic surface area of insulin by either inducing conformational changes in the hormone or binding to the surface of insulin to mask hydrophilicity. Separation of insulin from SNAC and analysis using UV spectroscopy and circular dichroism demonstrated no difference in the secondary and tertiary structures from the insulin that was originally formulated [28]. In animal studies and phase I trials, oral administration of this novel insulin formulation led to an increase in insulin levels and the expected decrease in plasma glucose levels. The treatment was also well tolerated and progressed to further clinical trials. However, in phase II, the oral insulin failed to show superior glycemic control over treatment with metformin alone, and there have been no further reports of ongoing

trials. Recent press releases have disclosed a collaboration between Novo Nordisk and Emisphere to apply carrier technology in the development of an orally delivered GLP-1 agonist semaglutide (also known as OG217SC) [29]. At the time of manuscript preparation, this formulation had successfully completed a phase II trial in type 2 diabetic patients. The highest dose was 40 mg and, over a 26 week trial, the drug was safe and well tolerated with the potential for a once daily regimen. Semaglutide is not a macrocycle but is included as an example of the importance of formulation technology in this field [30].

3.3.4 Transcellular Absorption of Macrocycles

3.3.4.1 Cyclization

There are a variety of strategies for the cyclization of peptides utilizing side-chain-to-side-chain constraints or side-chain-to-backbone atoms (either N or C, see Chapter 9) [31]. In backbone cyclization, a macrocycle is formed by covalently connecting backbone atoms (either N or C) of a linear peptide. This approach has the advantage of not modifying the peptide side chains, which may be critical for binding interactions with the target of choice. From an overall drug profile, the opportunity to modify side chains to improve biopharmaceutical properties is essential. There have been many publications on the impact of cyclization of peptides on oral bioavailability, and there is a general agreement that cyclization reduces the proteolytic liabilities by preventing the peptide from assuming an open sawtooth conformation that is required for many proteases to recognize and cleave substrates. The impact of cyclization on the permeability of peptides is a more open question with publications arguing that it assists, while others suggest that the effects are negligible or due solely to improved proteolytic stability rather than permeability. Seminal publications from Borchardt compared linear and cyclic hexapeptides in the molecular weight range of 556–629 Da, and concluded that cyclic peptides have increased permeability due to an increase in lipophilicity. The increase in lipophilicity of these cyclic analogues was suggested to be due to secondary structure involving two beta turns masking hydrogen bonding capabilities. With this increase in lipophilicity, the ability of the cyclic peptide to cross the cell monolayer *via* transcellular transport presumably increased. It is of interest that the molecular radii derived from NMR studies of the linear and cyclized systems are the same, suggesting that it is not a reduction in molecular size that drives an increase in permeability [32]. Unfortunately, the hydrophobic linear peptides were exposed to significant metabolism by cytosolic endopeptidases present in the Caco-2 cells, thus making conclusions on which parameters are driving improved permeability difficult to draw [33]. In all of these publications, work was undertaken

using *in vitro* systems and no compound was progressed to *in vivo* studies to demonstrate these effects in a relevant animal model. Nonetheless, this is an early suggestion of the utility of hydrogen bond management through cyclization and internal hydrogen bonding networks. Moreover, the use of NMR to understand conformation and hydrogen bonding is a testimony to the value of this early research and is reviewed later in the chapter.

Subsequent studies from Hoffman and coworkers using Caco-2 cell monolayers focused on the preparation and understanding of linear and cyclic hydrophilic hexapeptides [34]. They concluded that the absorption mechanism of all 18 analogues in the test set was paracellular regardless of structural or conformational changes. There did appear to be a greater permeability of cyclic systems, but this was attributed to an increase in proteolytic stability, as well as reduction in molecular size. A third research group using an alternative *in vitro* system, consisting of a reporter gene-based assay in HeLa cells, suggested no appreciable difference in permeability between cyclic and linear peptides where the test libraries constructed were designed to have as similar a physicochemical profile as possible [35]. It is a difficult experiment to design where the only variable examined is the cyclic versus acyclic nature of the peptides and all physicochemical parameters are a controlled constant. The final conclusion in this paper was that within the HeLa *in vitro* system, the linear peptides possessed slightly higher permeability than the cyclic peptides.

As the drug discovery community has evolved in its thinking, differing calculated and measured descriptors, other than molecular weight and simple hydrogen bond counts, are being generated to assist in design. A recent paper looking at membrane-permeable compounds that lie outside the Rule of Five space suggests the use of conformational-dependent measures. In particular, the compound's radius of gyration is an alternative to molecular weight and three-dimensional polar surface area (3D-PSA) can replace hydrogen bond donor and acceptor counts [36]. Radius of gyration is a concept often used in the fields of physics and engineering and it is an elegant experiment to apply this into drug design. An experimentally measured parameter as an alternative to molecular weight is to use NMR experiments to determine the diffusion coefficient of different macrocycles. This allows the further design of compounds with differing molecular shapes in solution, which may have an impact on permeability across membranes [37]. Computational model publications describe the development of high throughput chromatographic techniques that could also act as a surrogate for cell-based permeability measurements. For the practicing drug discovery project, these techniques would enable the team to prioritize compounds for subsequent permeability

measurements. A recent paper on this concept uses supercritical fluid chromatography and compares a compound's retention time to the permeability measured in RRCK monolayers [38]. This publication builds on previous disclosures from the same research group using chromatography retention times as a method to detect the intramolecular hydrogen bonding potential of molecules [39]. An alternative methodology to determine the propensity of a compound to form intramolecular hydrogen bonds is comparing the ability of a compound to partition between octanol and water against the ability to partition between toluene and water. Traditionally, partition coefficients have been measured between octanol and water as a mainstay of the prospective design of drug-like molecules. In this paper, the authors suggest that $\Delta\log P_{\text{oct-tol}}$ (difference between $\log P_{\text{octanol}}$ and $\log P_{\text{toluene}}$) may be considered a privileged measured molecular descriptor for intramolecular hydrogen bonds [40].

Within the melanocortin-4 receptor (MC4R) arena, there has been impressive application of backbone cyclization techniques to yield macrocyclic peptides that are claimed to have oral bioavailability as measured in rodent studies [41]. The parent linear peptide Phe-D-Phe-Arg-Trp-Gly NH$_2$ is known to have high potency in activating the MC4R and was the basis for the preparation of a library of macrocycles from which an analogue was selected for further profiling. In comparison to the linear starting point, the macrocycle BL3020-1 (**3**, Figure 3.2) possessed improved resistance in models of intestinal metabolic degradation. Following the progression of **3** to Caco-2 cell monolayers, the macrocycle demonstrated a higher permeability than the starting linear system and permeability equivalent to propranolol, which was included as a control compound. Propranolol is known to traverse the gut wall *via* the transcellular route. The authors suggest that cyclization leads to a compound with increased lipophilicity due to a decrease in the hydrogen bonding potential of the macrocycle. Within the Caco-2 experiments, an asymmetry was seen (A to B was $2x >$ B to A), which could be an indication of transporters playing a role in the apparent permeability. The nature of these transporters was not elucidated or described.

Compound **3** was progressed to an *i.v./p.o.* crossover study in rats to assess the pharmacokinetics after oral administration. The oral bioavailability was found to be 8% with a half-life of 105 min and V_D equal to 2.1 l/kg. A single dose of 0.5 mg/kg in mice led to reduced food consumption that lasted for 5 h, and multiple dose studies were also conducted (0.5 mg/kg) for 12 days and demonstrated reduced weight gain, which was significant compared with that of the control group. While this is an exciting contribution to the field, the results are difficult
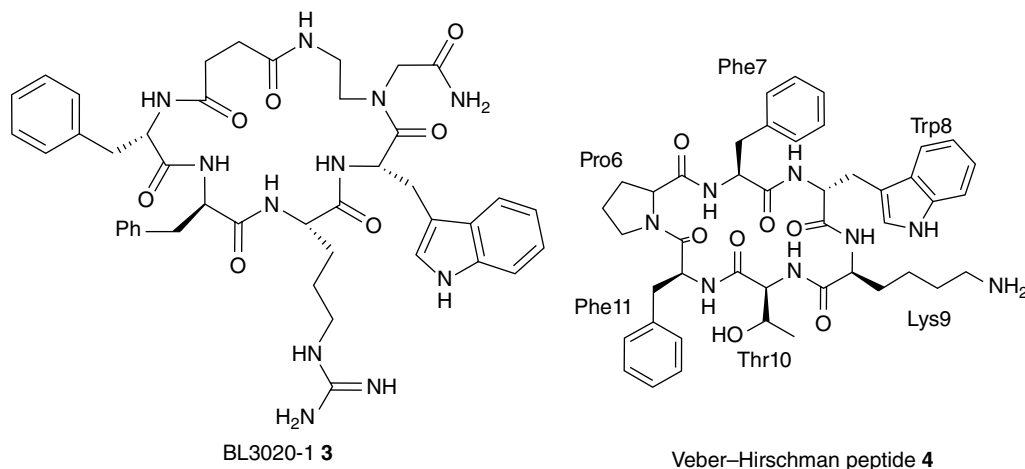
Figure 3.2 BL3020-1 (**3**) and Veber–Hirschman peptide (**4**).

to fully interpret because there is no data showing a pharmacokinetic/pharmacodynamic (PK/PD) relationship established in a single species.

3.3.4.2 N-Methylation

Undoubtedly, the simplest approach to hydrogen bond management is to replace the amide hydrogen with an alkyl group and, in particular, a methyl group [42]. It has been postulated that a combination of macrocyclization, then N-methylation of the resulting cyclic peptide, may be a more general approach to confer the combination of membrane permeability and resistance to hydrolysis required to achieve oral bioavailability [42]. Within this broad strategy, the specific tactics that promote oral bioavailability remain to be determined, and it is clear that only a subset of this chemical space may be desirable. A recent study on cyclic N-methylated somatostatin analogues related to the Veber–Hirschman peptide (**4**, Figure 3.2) generated a library of 30 compounds with varying methylation of the secondary amides contained in the starting macrocycle [43].

Extensive *in vitro* evaluation showed that specific methylation of D-Trp^8, Lys^9, and Phe^{11} gave rise to a large enhancement in membrane permeability in a Caco-2 cell monolayer model, while other methylated derivatives gave no enhancement. This derivative also displayed a reasonable 8% oral bioavailability in rat. Interestingly, the optimized peptide with regard to cell permeability was also the peptide most efficiently cyclized using standard peptide coupling conditions. The authors suggest the linear precursor peptide exhibits a dynamic structure in solution while undergoing some preorganization to bring the N and C termini into close proximity to improve the efficiency of the cyclization reaction. The optimized macrocycle showed no degradation after extensive incubation in rat serum and also was stable in simulated gut

media. Following progression to *in vivo* studies, the compound displayed an oral bioavailability of 9% and a V_D of 3.7 l/kg with an elimination half-life of 74 min. The relatively high oral bioavailability and, in particular, the ability to cross the gut wall were not fully explained and demonstrated the complexity of the pharmacokinetic profile. The high V_D suggests that the compound can distribute effectively into tissues and move out of the plasma compartment. The improvement in permeability was not fully understood, and a variety of experiments failed to demonstrate whether the improvement was due to a transcellular mode or an unexpected active transport mechanism. This research clearly demonstrates the evolution and development of robust *in vitro* transporter assays that needs to take place in macrocyclic drug space in order to understand which *in vitro* systems can be used with greatest predictability of pharmacokinetics for this molecular class in preclinical species or man.

Further research into the concept of N-methylation demonstrates that it may not be an absolute requirement in the design of cyclic orally bioavailable peptides. In a systematic study, cyclic pentaleucine **5** and hexaleucine peptides **6** (Figure 3.3) were prepared with no N-methylation and exhibited cell permeability in a Caco-2 assay and oral bioavailability in the same range as cyclosporine, which was used as a positive control. These compounds contain up to six amide NH protons but are still highly lipophilic due to the selection of leucine. This publication illustrates how complex the field is and how unlikely it is to be able to create a set of "rules" that can guarantee a good pharmacokinetic profile [44]. From NMR studies, the hypothesis for the membrane permeability of **3** is that the leucine side chains enable the shielding of the amide backbone from solvent. In later publications from the same research group, this is also described as a hydrophobic patch on the surface of the macrocycle.
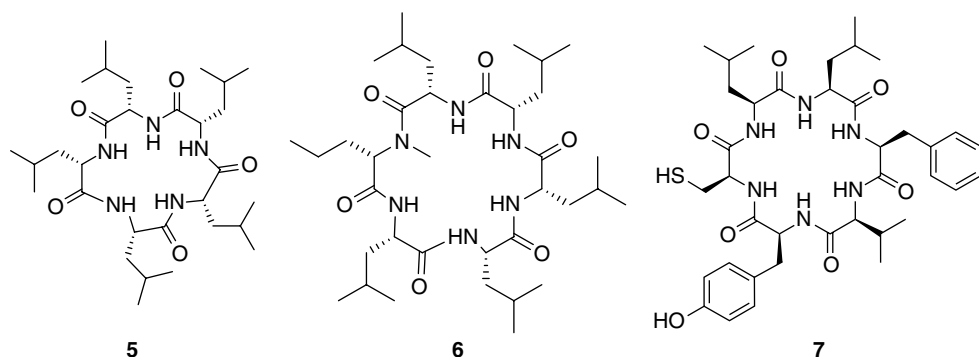
Figure 3.3 Pentaleucine **5**, hexaleucine **6**, and HIF inhibitor **7**.

CSA in hydrophilic environment   CSA conformation from crystallographic and NMR studies
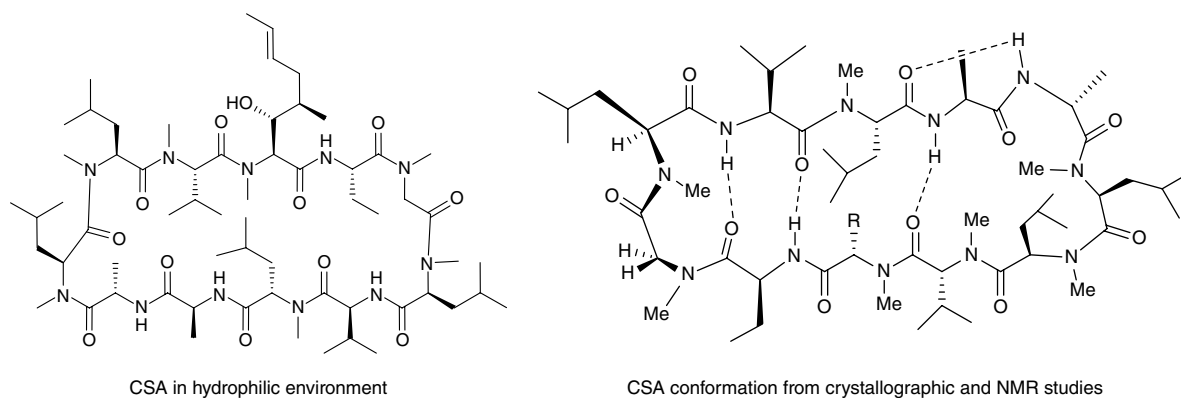
Figure 3.4 Cyclosporin A (CSA, **8**) conformations.

This strategy of shielding will be discussed further later in the chapter. The subtlety of the design features in this field is shown by a simultaneous article on the invention of **7** (Figure 3.3) as an inhibitor of HIF-1 heterodimerization that inhibits hypoxia signaling in cancer cells. To aid the translocation of the macrocycle across the cellular plasma membrane in order to elicit a significant biological effect, a Tat cell-penetrating peptide was conjugated *via* a cysteine residue. Within the hexapeptide, all the side chains are lipophilic in nature, nonetheless, that is insufficient to ensure cell permeability [45]. The comparison of these structures originating from different research groups shows there are no robust rules or guidelines that guarantee the macrocycle to be membrane permeable.

3.3.4.3 Cyclosporine A (CSA)

Cyclosporine A (CSA, **8**, Figure 3.4) is a key component of patient treatment post-organ transplant surgery acting as an immunosuppressant [46]. In addition, CSA has been applied to the treatment of a variety of conditions including psoriasis, dermatitis, rheumatoid arthritis, and Crohn's disease. CSA was originally isolated from the fungus *Tolypocladium inflatum* found in a soil sample obtained by Sandoz scientists and has been an inspiration

for many researchers in differing fields contributing to biomedical research. In addition, groups engaged in the total synthesis of naturally occurring molecules have been intrigued by the complex structure of this 11-amino acid macrocycle, which upon close inspection reveals a single D-amino acid and multiple sites of N-methylation. Indeed, 7 of the 11 available amino acids are N-methylated, contributing to the hydrophobicity of this peptide. Undoubtedly, CSA has driven the evolution of peptide synthesis in the drug discovery community using both solution and solid phase techniques [47]. In addition, the presence of the unusual amino acid (2*S*,3*R*,4*R*,6*E*)-3-hydroxy-4-methyl-2-methylamino-6-octenoic acid is of importance to the pharmacological activity of CSA.

CSA exhibits poor solubility in water and, as a consequence, extensive work has been undertaken to improve the oral bioavailability of the drug due to its poor biopharmaceutical profile [48]. Research comparing two differing formulations of CSA, including the commercially available standard soft gelatin capsule and hard gelatin capsules containing oil/water microemulsions, demonstrated that the hard gelatin capsules possess an improved oral bioavailability. CSA is available in a variety of other formulations including an oral solution and a formulation for *i.v.* administration. The oral absorption of CSA

during chronic administration of soft gelatin capsules is known to be erratic, and it is recommended that patients be monitored at repeated intervals for blood drug levels and subsequent dose adjustments be made in order to avoid toxicity due to high levels and possible organ rejection due to low absorption. The nephrotoxicity of CSA is a particular concern, and drugs that are known to be nephrotoxic in their own right have been suspected of exacerbating that of CSA without altering the exposure. The mechanism of nephrotoxicity of CSA has yet to be fully determined [49]. Following oral administration, the absorption profile is slow and peak concentrations are reached 1–8 h after dosing. Oral bioavailability ranges from <5 to 89% in transplant patients [50]. This is a particularly difficult patient population, and CSA suffers from inter-patient variability that is dependent upon a range of factors including elapsed time after surgery, GI function, and liver disease [51]. Following *i.v.* administration, CSA exhibits multi-compartment behavior with a V_D that ranges from 0.9 to 4.0 l/kg and a moderate to high plasma protein binding of 98% [52]. Elimination of CSA takes place by oxidative metabolism in the liver followed by the excretion of the metabolites in the bile. CSA has transformed the outlook for transplantation from unrelated donors and made many lifesaving organ transplant operations possible; however, the compound possesses flaws from its pharmacokinetics and relatively narrow therapeutic index. CSA has suboptimal pharmacokinetics in terms of its variable absorption profile and displays a number of drug–drug interactions and food effects requiring close monitoring of patients.

There have been extensive studies on the conformation of CSA and how this enables sufficient drug transit across the gut wall for the drug to be administered orally [53]. Using NMR techniques, two major conformations have been observed depending on whether CSA is examined in apolar solvents such as chloroform or bound in an aqueous complex with its putative receptor cyclophilin. The structure of CSA has also been determined from X-ray studies of CSA crystals grown in acetone and has the same conformation as that observed using NMR in chloroform [54]. It has also been shown that the structure of a closely related water-soluble CSA analogue was similar to the cyclophilin-bound conformation [55]. In both the "free" and "bound" conformations, residues 7–11 form a compact antiparallel β-sheet with the remaining residues completing the macrocycle. From the previously mentioned crystallography and NMR studies, the "free" conformation of CSA is distinguished by the presence of a single *cis* peptide bond at MeLeu[9]–MeLeu[10] and four intramolecular hydrogen bonds, as summarized in Figure 3.4. In contrast, the cyclophilin-bound conformation has a *trans* bond at MeLeu[9]–MeLeu[10], while the four amide protons participate in

hydrogen bonds to the protein, and it is suggested that these interact with water molecules in an aqueous environment. Challenges in the NMR analysis of CSA have been overcome, and the NMR spectra of CSA in aqueous solution have generated the hypothesis that permeability is not related to conformational changes but rather to alterations in its hydration state.

3.3.4.4 Conformational Interconversion and H-Bond Networks

Further investigation of CSA and closely related analogues has suggested that passive transcellular absorption is a characteristic of macrocycles that can assume multiple, interconverting conformations with different populations in low and high dielectric environments [56–58]. In the aqueous conditions of the gut, the conformer population will be different from the population in the low dielectric environment of the membrane interior. Thus, membrane permeability is driven by a dominant conformation where intramolecular, transannular hydrogen bonding masks the overall hydrogen bonding potential and thereby reduces the overall hydrophilicity of the system, enabling CSA to cross the gut wall. The conformational flexibility of CSA has intrigued many laboratories, and in addition to the "free" and "bound" conformations described previously, there are a number of "slowly interconverting" conformers in equilibrium in polar solvents such as DMSO, methanol, or methanol/water mixtures. Further, recent disclosures from the same research group reported compound **9** (Figure 3.5), which is often referred to in presentations and publications as the Lokey peptide or 1NMe3. This macrocycle has a physicochemical profile that would be viewed as lying outside of traditional oral drug space. Upon initial inspection, a MW > 750 Da and multiple hydrogen bond donors and acceptors would be expected to limit the ability of compound **9** to cross the gut wall.

Compound **9** was profiled in a range of *in vitro* assays and progressed to an *in vivo* study [59]. The pharmacokinetic profile of **9** in rats was characterized by low clearance and a moderate ability to partition into tissue, leading to a terminal elimination half-life of 2.8 h. Its absolute oral bioavailability (*F*) was determined to be 28%. The ability to understand and predict the influence of intramolecular hydrogen bonding networks on cell permeability is an exciting advance in the field. In addition, the pharmacokinetic data presented, and the computational predictions on synthetic methodology utilizing on-resin methylation as an enabling reaction, are noteworthy. The macrocycles were designed with specific N-methylation patterns to simultaneously reduce the hydrogen bond donor count of the compounds and promote intramolecular hydrogen bonding networks of the remaining protons and carbonyl lone pairs. In this seminal paper, compounds were prepared
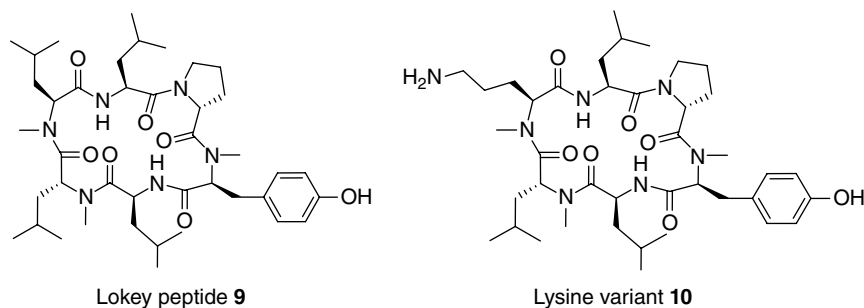
Figure 3.5 The Lokey peptide 1NMe3 **9** and lysine variant **10**.

Lokey peptide **9**   Lysine variant **10**

as pharmacokinetic probes and had no associated pharmacology described. Further disclosures from the same research group investigated replacing a leucine with amino acids that contain a side chain with a functional group that can be ionized at physiological pH. Through the introduction of natural and unnatural residues, it was attempted to modulate permeability and stability *in vitro*. Unfortunately, introduction of any ionizable side chain at a physiological pH proved to compromise either permeability or oxidative stability compared to lead compound **9** [60]. The poor *in vitro* data on lysine analogue **10** were confirmed *in vivo* in rats. Compared to the unionized lead **9**, there was a severe impact on the overall oral bioavailability of **10**. Differing research groups have followed up on these initial reports and ultimately reached similar conclusions [61]. The fine balance between gut wall permeability, microsomal stability, and biopharmaceutical properties is a demanding challenge, and in the current state of the art, there are no unifying rules to design orally bioavailable macrocycles.

The difficulty of designing orally available macrocycles that lie outside the Rule of Five is further demonstrated by research groups that used cyclosporine as the lead, in attempts to eliminate its immunosuppressive properties and implement alternative pharmacology, such as antiviral activity [62]. Other research groups have also published on the approach toward a synthetically tractable cell permeable template that can be modified for the discovery of bioactive peptides [63].

3.3.4.5 Shielding

Natural products other than CSA have also supplied stimulus to the discovery of orally bioavailable macrocycles and attempt to develop general guidelines to rationally apply across projects. The marine natural product sanguinamide A (**11**, Figure 3.6) is a cyclic hexapeptide isolated from the sea slug *H. sanguineus*, and contemporary publications focus on using NMR to understand the macrocycle's conformation and thus improve its pharmacokinetic properties (for a more detailed analysis of natural product cyclic peptides, see Chapter 5) [64]. A combination of biophysical techniques and computational modeling to generate ideas for systematic

modification of the macrocycle is an attractive approach to ensure all analogues provide value to the project. The synthesis of analogues based on sanguinamide A is somewhat challenging, so careful design is required to ensure a return on this synthetic investment. The integration of decreased conformational flexibility, modulation of hydrogen bond strength, and steric effects on hydrogen bonding potential was used to enable improvements. The thiazole heterocycle rigidifies the structure, imposing a single conformation with two strong transannular hydrogen bonds. Notwithstanding its physicochemical properties (MW 721, *c*Log*P* 5.5), sanguinamide A does possess an oral bioavailability of 7% in rats. The authors suggest the oral bioavailability is due to the interplay of three contributing factors: the heterocycle acting as an amide isostere, the presence of transannular hydrogen bonds, and the shielding of the polar amides from solvent by the lipophilic side chains.

Initial modifications of **11** involved N-methylation to reduce the hydrogen bond donor potential, followed by increasing the steric demands of the side chains and introduction of the spatially demanding *t*-butyl motif. Subtle conformational differences within closely related analogues were observed from NMR studies using hydrogen–deuterium exchange. This led to the design of **13**, whereby the *t*-butyl group creates a contiguous hydrophobic patch on the surface of the low energy conformation in solution. Progression of compounds **12** and **13** to *in vivo* studies demonstrated an impressive improvement in oral bioavailability from these modifications. Compound **12** possesses $F = 21\%$, while **13** possesses $F = 51\%$. These modifications were designed prospectively from a comprehensive analysis of conformations and NMR observations to understand solvent-exposed surfaces. It is noteworthy from the NMR studies that there appears to be a more rigid backbone structure present in **13** than in **12**, which opposes some of the arguments made around conformational flexibility of CSA being a requirement for oral bioavailability. The cross comparison of natural products in this area is always of value, and the authors suggest that the proline–isoleucine–proline sequences in sanguinamide A may be a privileged structure. It also appears in other natural

Sanguinamide A **11**   Danamide D **12**   Danamide F **13**
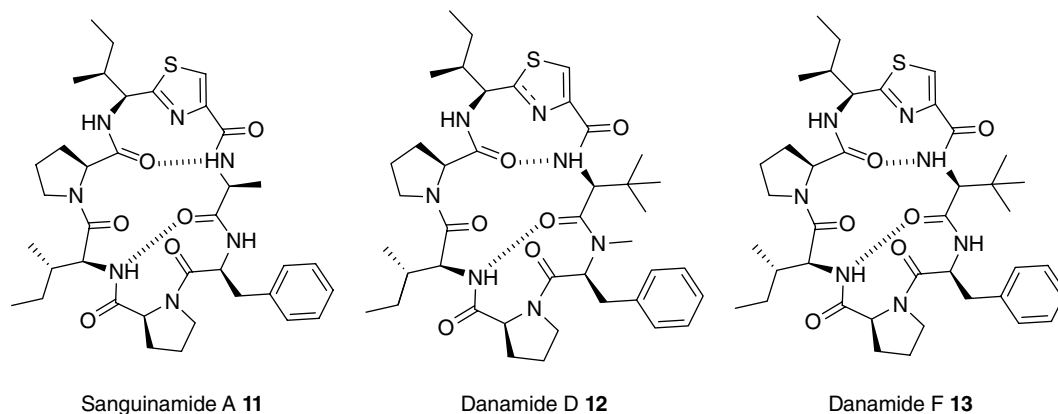
Figure 3.6 Sanguinamide A **11**, danamide D **12**, and danamide F **13**.

products such as dichotomin G and phakellistatin [65]. Further research on sanguinamide from a differing group also confirms the subtle interplay of N-methylation, side chain sterics, and conformation on permeability [66]. As outlined previously, the use of supercritical fluid chromatography retention times may have utility in rank-ordering compounds for progression into *in vitro* cell permeability assays. Within this work, the retention times for sanguinamide A, danamide D, and danamide F correlated with their rank order of cell permeability as measured in an RRCK model. This ordering, however, did not correlate with oral bioavailability, which is influenced by other parameters such as biopharmaceutical properties and stability toward oxidative metabolism. This is a key paper in the field, helping to build upon the concept of steric shielding within the overarching hydrogen bond management strategy. The use of biophysical and analytical techniques, in particular NMR, has been an exciting advance. Once again Borchardt's early use of NMR techniques and their impact should be recognized. A recent paper describes methods to identify solvent-exposed amides in macrocyclic peptides that could be appropriate for N-methylation. Specifically it was reported that measured NMR temperature coefficients can be rationally used to guide N-methylation of amides to improve cyclic peptide permeability. This provides a complementary alternative to methods such as small molecule crystallography for characterizing the structure. With the insights provided by NMR, a macrocyclic peptide was designed that displayed an oral bioavailability of 33% in rats, validating the utility of this approach [67].

3.3.4.6 Additional Strategies for Managing Hydrogen Bond Donors

Depsipeptide Formation Cyclic depsipeptides are formed usually by a C-terminal-to-side-chain cyclization, with serine or threonine residues, to produce a backbone ester
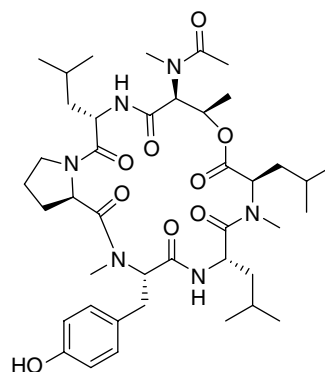
Figure 3.7 An example of a synthetic depsipeptide with favorable cell permeability based on the RRCK assay (3.3×10^{-6} cm/s).

[68]. This is a structural feature of many classes of natural products, which display interesting biological activities and are reported to have attractive cell permeability [69]. A recent study reported the synthesis of a series of depsipeptides resulting from an acid-catalyzed acyl rearrangement of N-methylated, threonine-containing peptide macrocycles. It was found that despite the increase in size and conformational flexibility, the resulting depsipeptides retained or improved permeability relative to their precursor peptide, as measured in the RRCK assay (Figure 3.7). This study suggests that the strategic incorporation of depsipeptide functionality may be an important tool in further diversifying peptide macrocycles while simultaneously enhancing permeability [70].

Peptide-to-Peptoid Transformation Peptoids typically include N-substituted glycine moieties as replacements of amino acid residues and were originally designed as a means to overcome the proteolytic and metabolic instability associated with peptides [71]. In addition, it was determined that peptoids would offer substantially increased structural diversity as analogues of cyclic

peptides, given the abundant availability of amine monomers required for their formation. As N-substituted glycine analogues, peptoids can contribute to overall hydrogen bond donor management, and their strategic incorporation into peptide macrocycles can produce molecules with increased permeability. A recent study reported the permeability of peptoid macrocycles resulting from the systematic replacement of N-methylated residues of benchmark macrocycle 1NMe3 **9** [72]. It was determined that the incorporation of peptoid residues in positions where key hydrogen bond networks were preserved yielded macrocycles that exhibited equal or higher permeability relative to **9**. Furthermore, it was shown that macrocycles with heteroatom-containing peptoid residues could achieve equal or higher permeability relative to **9**. The latter result suggests that peptoid substitutions can be effectively utilized to increase the side-chain diversity of macrocycles while retaining the desired permeability.

3.4 *In Silico* Modeling

Computational modeling of permeability and oral bioavailability has traditionally focused on fundamental properties, such as MW, log*P*, and H-bond donor and acceptor counts, as encompassed in the Rule of Five and was later extended to additional key properties such as polar surface area [73]. These properties can typically be calculated from a 2-D representation of a molecule and are effective discriminators for oral absorption and bioavailability of small molecules [74] but often do not accurately capture the properties of larger molecules. Some larger molecules, especially macrocycles, can adopt 3-D conformations that give them very different effective properties from what would be expected. For example, their 3D-PSAs can be much smaller than their 2-D topological polar surface areas (TPSA), and compact folds allow them to behave more like lower MW compounds. For such Beyond Rule of Five molecules, property guidelines for permeability should be computed from their optimal 3-D conformations. A recent analysis [36] showed that radius of gyration (R_{gyr}) and 3D-PSAs are better discriminators of permeability than MW and TPSA for compounds with MW > 550 Da, with permeability enhanced when the radius of gyration is ≤7 Å and the 3D-PSA is ≤100 Å^2. A comprehensive *in silico* approach to permeability has been introduced by Leung and Jacobson [75]. This physics-based approach computes multiple components of the permeation process, including the adoption of the primary permeating state (often the neutral species), conformational focus on the lowest-energy low-dielectric conformation (LDC), transfer of this LDC conformation from the aqueous into the

membrane environment ($\Delta G_{transfer(LDC)}$), and diffusion barrier in the membrane. This method was applied to a range of different datasets and chemotypes and was shown to provide a good correlation with experimental permeability measure, better than that computed from simple properties such as MW and polar surface area, and often even better than quantitative structure–property relationship methods that have been trained using large datasets and numerous chemical descriptors. For most of the datasets studied, the $\Delta G_{transfer(LDC)}$ term alone gave a good correlation with experimental permeability, providing evidence that the dominant factor in the permeation process is aqueous desolvation of the permeating conformation and insertion into the membrane. This predominant factor roughly correlates with TPSA for small molecules, but for larger molecules it is necessary to utilize 3D-PSA or $\Delta G_{transfer(LDC)}$. These 3-D methods are able to account for the significant impact of stereochemistry, intramolecular hydrogen bonding, and macrocyclization. Several publications have shown the utility of these calculations for peptidic macrocycles. In one study [56], 11 cyclic hexapeptides and heptapeptides were selected for experimental profiling from a virtual library of 448; the resulting experimental PAMPA values correlated very highly ($R^2 = 0.96$) with ΔG_i (another name for $\Delta G_{transfer(LDC)}$). In another study [59], calculation of desolvation energies for a 1024-member cyclic hexapeptide virtual library, differing only by stereochemistry and N-methylation pattern, showed that permeability is highly dependent on stereochemistry and that partial N-methylation is often preferable to per-methylation for providing the most permeable species. One of these optimal partially methylated compounds was the previously mentioned Lokey peptide 1NMe3 **9**. A complementary follow-up study [60] utilized the full physics-based computational approach to calculate the permeability (logP_m) of a series of cyclic peptides with the same template (stereochemistry and N-methylation) of **9** but differing by replacement of one Leucine side chain with a range of natural and unnatural side chains. Here, logP_m correlated well with cell-based permeability for 14 of the 16 compounds studied; the two outliers were high log$D$ peptides with poor recoveries in the assay. These exceptions highlight an important source of experimental error in cell-based permeability measurements and correlation to *in silico* predictions and confirm an important design strategy: one should avoid overreliance upon the desolvation/reduction of polarity to drive permeability as it may lead to overly high log$D$'s and, hence, poorly behaved compounds. Calculations for the threonine-containing analogue from this study showed that intramolecular hydrogen bonding involving a side chain also can be beneficial as it permits more polarity to be incorporated into the compound; the threonine-containing analogue was

measured to have a rat oral bioavailability of 23.8%, approaching that of the parent compound **9**.

3.5 Future Directions

The design parameters for success in macrocycle drug space are by no means well defined and so far have been confined to very small subsets of the available macrocycle chemical space. There is a rapidly growing body of literature in this area; however, it needs to be assessed with a critical eye to ensure that there is consistency and value in the data presented. Moreover, although it is tempting to generalize conclusions obtained on specific systems, so far data indicate that generalization is not viable for these structures. There are few examples of macrocyclic compounds with a clear *in vitro* understanding of both pharmacokinetics and pharmacology linked through to an *in vivo* experiment with a robust PK/PD relationship. Notwithstanding this paucity of data, as further research groups disclose their works, understanding will expand. This has been the case in recent decades for molecules that operate within the Rule of Five. For example, drug discovery organizations have focused on the optimization of compound profiling capacity for Rule of Five-compliant molecules. This has driven generic screening technologies for key pharmacokinetic, pharmacology, and biopharmaceutical parameters. These assay panels are typically composed of kinetic solubility, permeability, lipophilicity, metabolic stability, drug–drug interactions mediated by CYP inhibition, and hERG channel blockade [76, 77]. Currently, high throughput ADME and toxicology screening is well integrated into the drug discovery process and is readily available, in parallel with potency and selectivity against targets. Indeed, many of these assays are now available from commercial vendors on a fee-per-compound basis. An exciting paper has recently been published describing the *in vitro* and *in vivo* pharmacokinetic profiles of a series of macrocyclic decapeptides utilizing high throughput *in vitro* assays that would be available within an industrial setting or from a vendor [78]. The paper does not disclose any associated pharmacology nor any novel insight on prospective macrocycle design but is a clear demonstration of the drug discovery community's commitment to success in this space. In "real-time projects" molecules are optimized not only for pharmacology but also simultaneously for drug-like properties, at least as we currently understand these concepts. The development and validation of these assays was an iterative process with often long learning cycles to ensure the data generated was of value in predictions to preclinical species and man. As research groups wish to operate in macrocycle space, there also will be a need to step back and increase the use of *in vivo*

and *ex vivo* pharmacokinetic experiments to help benchmark key macrocycles and build a useful test set for predictive *in vitro* models. Only with initial knowledge from these more expensive and lower throughput studies will there be sufficient information for discovery teams to design compounds prospectively. Key components for high throughput *in vitro* assays are robust bioanalytical techniques, and this presents another opportunity for innovation and creativity in this arena [79].

File enrichment has been a common strategy across both academic and industrial groups with many organizations possessing compound libraries of potentially millions of compounds either as discrete single compounds or mixtures. These organizations view the composition and quality of their screening file as a competitive advantage [80]. Undoubtedly, the same file enrichment process will occur in macrocycles, and the quality of the corresponding screening library in terms of diversity and coverage of chemical space will be essential. Designing libraries of macrocycles that occupy the "sweet spot" of this chemical space will be another competitive advantage [81]. A recent publication demonstrates the synthesis of a library of diverse membrane-permeable scaffolds using a split pool synthesis approach. The effect of backbone conformation and side-chain shielding on the membrane permeability has been recently studied in the context of a systematic evaluation of a large library of synthetic cyclic hexapeptides (1152 members) [82]. Therein, it was reported that side-chain shielding of backbone amides is as affective at increasing permeability as intramolecular hydrogen bonding. Unfortunately, no absolute bioavailability measurements were provided in the report. The claims for increased permeability were supported instead by *in vitro* measurements in PAMPA and Caco-2 assays. Furthermore, it was suggested that 3D polar solvent-accessible surface areas (SASAs) are superior to intramolecular hydrogen bond counts as predictors of permeability.

A seminal publication demonstrating the value of a high quality screening file was the delivery of ulimorelin (TZP-101, **14**, Figure 3.8) from an initial hit discovered through high throughput screening (see Chapter 19 for follow-up studies leading to TZP-102). Ulimorelin is a potent agonist of the ghrelin receptor and displays 24% oral bioavailability in rats and monkey studies and progressed to phase III clinical trials [83]. An unusual aspect of this compound is the profile displayed post-*i.v.* administration of ^{14}C radio-labelled drug in rats. Following a 30 min infusion, the compound was efficiently excreted in the feces with recovery of 95% of the administered dose. This suggests hepatobiliary elimination is the major route of clearance. Without a full understanding of the transporters and potential species differences that underwrite this effect, it is a risk taking compounds forward
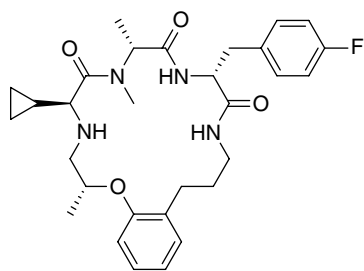
Figure 3.8 Ulimorelin (TZP-101, **14**).

into the clinic. It is to the research organization's credit and commitment to drug discovery that they were willing to take the risk. The use of biophysical techniques such as small molecule crystallography and NMR to characterize the conformation for both potency and optimal pharmacokinetic profile is a superb case history. This work emphasizes the value in the generation of macrocycle libraries that may already possess a profile suitable for rapid optimization of pharmacokinetic properties. The myriad advances in synthetic biology and differing expression technologies combined with *in silico* library design provide a tantalizing taste of the future for this area. Indeed, the combination of computational techniques with the ability to access extremely large numbers of compounds by harnessing expression technology will be a high value breakthrough in this field [84].

In conjunction with the short-term increased use of *in vivo* resources, there will be a need for an earlier relationship with expert formulation groups to assist in the optimal delivery of these compounds. Cyclosporine demonstrates the value that expert formulation researchers bring to improving the bioavailability of nonoptimal drugs. Furthermore, as early engagement with formulation experts increases, a concomitant need arises for technologies to keep pace to deliver the necessary drug substance. There will be innovation required on both solid- and solution-phase synthetic techniques to access the compounds on the scale necessary for regulatory toxicology studies and a smooth transition to the clinic. To enable the rapid progress of macrocycles through clinical trials, the production of crystalline, soluble compounds on scale will be a necessary investment.

Undoubtedly, there will be an increase in macrocycles progressing through the clinic, and unexpected toxicity and pharmacokinetics, as with all compound classes, will cause some molecules to be dropped from trials [85]. This knowledge then will be rapidly cycled back into the discovery stage and researchers will learn from the attrition. This is inevitable and part of the exciting learning curve that the drug discovery community is going to undertake with macrocycles in the next decade.

References

1 Arkin, M. R.; Wells, J. A. Small-molecule inhibitors of protein-protein interactions: progressing towards the dream. *Nat. Rev. Drug Discov.* **2004**, *3*, 301–317.

2 Bose, P. P.; Chatterjee, U.; Hubatsch, I.; Artursson, P.; Govender, T.; Kruger, H. G.; Bergh, M.; Johansson, J.; Arvidsson, P. I. In vitro ADMET and physicochemical investigations of poly-N-methylated peptides designed to inhibit Abeta aggregation. *Bioorg. Med. Chem.* **2010**, *18*, 5896–5902.

3 Lipinski, C. A.; Lombardo, F.; Dominy, B. W.; Feeney, P. J. Experimental and computational approaches to estimate solubility and permeability in drug discovery and development settings. *Adv. Drug Deliv. Rev.* **2001**, *46*, 3–26.

4 Woodley, J. F. Enzymatic barriers for GI peptide and protein delivery. *Crit. Rev. Ther. Drug Carrier Syst.* **1994**, *11*, 61–95.

5 Craik, D. J.; Fairlie, D. P.; Liras, S.; Price, D. The future of peptide-based drugs. *Chem. Biol. Drug Des.* **2013**, *81*, 136–147.

6 Hookway, C.; Buckner, S.; Crosland, P.; Longson, D. Irritable bowel syndrome in adults in primary care: summary of updated NICE guidance. *Brit. Med. J.* **2015**, *350*, h701.

7 de Araujo, A. D.; Hoang, H. N.; Kok, W. M.; Diness, F.; Gupta, P.; Hill, T. A.; Driver, R. W.; Price, D. A.; Liras, S.; Fairlie, D. P. Comparative alpha-helicity of cyclic pentapeptides in water. *Angew. Chem. Int. Ed. Engl.* **2014**, *53*, 6965–6969.

8 Traboulsi, H.; Larkin, H.; Bonin, M. A.; Volkov, L.; Lavoie, C. L.; Marsault, E. Macrocyclic cell penetrating peptides: a study of structure-penetration properties. *Bioconjug. Chem.* **2015**, *26*(3), 405–411.

9 Sweeney, Z. K.; Fu, J.; Wiedmann, B. From chemical tools to clinical medicines: nonimmunosuppressive cyclophilin inhibitors derived from the cyclosporin and sanglifehrin scaffolds. *J. Med. Chem.* **2014**, *57*, 7145–7159.

10 Kell, D. B.; Oliver, S. G. How drugs get into cells: tested and testable predictions to help discriminate between transporter-mediated uptake and lipoidal bilayer diffusion. *Front. Pharmacol.* **2014**, *5*, 231.

11 Werle, M.; Bernkop-Schnurch, A. Strategies to improve plasma half life time of peptide and protein drugs. *Amino Acids* **2006**, *30*, 351–367.

12 Garber, A. J. Novel GLP-1 receptor agonists for diabetes. *Expert Opin. Investig. Drugs* **2012**, *21*, 45–57.

13 Knudsen, L. B.; Nielsen, P. F.; Huusfeldt, P. O.; Johansen, N. L.; Madsen, K.; Pedersen, F. Z.; Thogersen, H.; Wilken, M.; Agerso, H. Potent derivatives of glucagon-like peptide-1 with pharmacokinetic properties suitable for once daily administration. *J. Med. Chem.* **2000**, *43*, 1664–1669.

14 Vlieghe, P.; Lisowski, V.; Martinez, J.; Khrestchatisky, M. Synthetic therapeutic peptides: science and market. *Drug Discov. Today* **2010**, *15*, 40–56.

15 Rozek, A.; Powers, J. P.; Friedrich, C. L.; Hancock, R. E. Structure-based design of an indolicidin peptide analogue with increased protease stability. *Biochemistry* **2003**, *42*, 14130–14138.

16 Marsault, E.; Peterson, M. L. Macrocycles are great cycles: applications, opportunities, and challenges of synthetic macrocycles in drug discovery. *J. Med. Chem.* **2011**, *54*, 1961–2004.

17 Artursson, P.; Palm, K.; Luthman, K. Caco-2 monolayers in experimental and theoretical predictions of drug transport. *Adv. Drug Deliv. Rev.* **2001**, *46*, 27–43.

18 Faller, B. Artificial membrane assays to assess permeability. *Curr. Drug Metab.* **2008**, *9*, 886–892.

19 Goodwin, J. T.; Mao, B.; Vidmar, T. J.; Conradi, R. A.; Burton, P. S. Strategies toward predicting peptide cellular permeability from computed molecular descriptors. *J. Pept. Res.* **1999**, *53*, 355–369.

20 Di, L.; Whitney-Pickett, C.; Umland, J. P.; Zhang, H.; Zhang, X.; Gebhard, D. F.; Lai, Y.; Federico, J. J., 3rd; Davidson, R. E.; Smith, R.; Reyner, E. L.; Lee, C.; Feng, B.; Rotter, C.; Varma, M. V.; Kempshall, S.; Fenner, K.; El-Kattan, A. F.; Liston, T. E.; Troutman, M. D. Development of a new permeability assay using low-efflux MDCKII cells. *J. Pharm. Sci.* **2011**, *100*, 4974–4985.

21 Foger, F.; Kopf, A.; Loretz, B.; Albrecht, K.; Bernkop-Schnurch, A. Correlation of in vitro and in vivo models for the oral absorption of peptide drugs. *Amino Acids* **2008**, *35*, 233–241.

22 Osterberg, O.; Savic, R. M.; Karlsson, M. O.; Simonsson, U. S.; Norgaard, J. P.; Walle, J. V.; Agerso, H. Pharmacokinetics of desmopressin administrated as an oral lyophilisate dosage form in children with primary nocturnal enuresis and healthy adults. *J. Clin. Pharmacol.* **2006**, *46*, 1204–1211.

23 Agerso, H.; Seiding Larsen, L.; Riis, A.; Lovgren, U.; Karlsson, M. O.; Senderovitz, T. Pharmacokinetics and renal excretion of desmopressin after intravenous administration to healthy subjects and renally impaired patients. *Br. J. Clin. Pharmacol.* **2004**, *58*, 352–358.

24 Kramer, S. D. Absorption prediction from physicochemical parameters. *Pharm. Sci. Technol. Today* **1999**, *2*, 373–380.

25 Salamat-Miller, N.; Johnston, T. P. Current strategies used to enhance the paracellular transport of therapeutic polypeptides across the intestinal epithelium. *Int. J. Pharm.* **2005**, *294*, 201–216.

26 Leonard, T. W.; Lynch, J.; McKenna, M. J.; Brayden, D. J. Promoting absorption of drugs in humans using medium-chain fatty acid-based solid dosage forms: GIPET. *Expert Opin. Drug Deliv.* **2006**, *3*, 685–692.

27 Cano-Cebrian, M. J.; Zornoza, T.; Granero, L.; Polache, A. Intestinal absorption enhancement via the paracellular route by fatty acids, chitosans and others: a target for drug delivery. *Curr. Drug Deliv.* **2005**, *2*, 9–22.

28 Malkov, D.; Angelo, R.; Wang, H. Z.; Flanders, E.; Tang, H.; Gomez-Orellana, I. Oral delivery of insulin with the eligen technology: mechanistic studies. *Curr. Drug Deliv.* **2005**, *2*, 191–197.

29 Lau, J.; Bloch, P.; Schaffer, L.; Pettersson, I.; Spetzler, J.; Kofoed, J.; Madsen, K.; Knudsen, L. B.; McGuire, J.; Steensgaard, D. B.; Strauss, H. M.; Gram, D. X.; Knudsen, S. M.; Nielsen, F. S.; Thygesen, P.; Reedtz-Runge, S.; Kruse, T. Discovery of the once-weekly glucagon-like peptide-1 (GLP-1) analogue semaglutide. *J. Med. Chem.* **2015**, *58*, 7370–7380.

30 Moroz, E.; Matoori, S.; Leroux, J. C. Oral delivery of macromolecular drugs: where we are after almost 100years of attempts. *Adv. Drug Deliv. Rev.* **2016**, *101*, 108–121.

31 Hill, T. A.; Shepherd, N. E.; Diness, F.; Fairlie, D. P. Constraining cyclic peptides to mimic protein structure motifs. *Angew. Chem. Int. Ed. Engl.* **2014**, *53*, 13020–13041.

32 Okumu, F. W.; Pauletti, G. M.; Vander Velde, D. G.; Siahaan, T. J.; Borchardt, R. T. Effect of restricted conformational flexibility on the permeation of model hexapeptides across Caco-2 cell monolayers. *Pharm. Res.* **1997**, *14*, 169–175.

33 Knipp, G. T.; Vander Velde, D. G.; Siahaan, T. J.; Borchardt, R. T. The effect of beta-turn structure on the passive diffusion of peptides across Caco-2 cell monolayers. *Pharm. Res.* **1997**, *14*, 1332–1340.

34 Hess, S.; Ovadia, O.; Shalev, D. E.; Senderovich, H.; Qadri, B.; Yehezkel, T.; Salitra, Y.; Sheynis, T.; Jelinek, R.; Gilon, C.; Hoffman, A. Effect of structural and conformation modifications, including backbone cyclization, of hydrophilic hexapeptides on their intestinal permeability and enzymatic stability. *J. Med. Chem.* **2007**, *50*, 6201–6211.

35 Kwon, Y. U.; Kodadek, T. Quantitative comparison of the relative cell permeability of cyclic and linear peptides. *Chem. Biol.* **2007**, *14*, 671–677.

36 Guimaraes, C. R.; Mathiowetz, A. M.; Shalaeva, M.; Goetz, G.; Liras, S. Use of 3D properties to characterize beyond rule-of-5 property space for passive permeation. *J. Chem. Inf. Model.* **2012**, *52*, 882–890.

37 Wang, C. K.; Northfield, S. E.; Swedberg, J. E.; Harvey, P. J.; Mathiowetz, A. M.; Price, D. A.; Liras, S.; Craik, D. J. Translational diffusion of cyclic peptides measured using pulsed-field gradient NMR. *J. Phys. Chem. B.* **2014**, *118*, 11129–11136.

38 Goetz, G. H.; Philippe, L.; Shapiro, M. J. EPSA: a novel supercritical fluid chromatography technique enabling the design of permeable cyclic peptides. *ACS Med. Chem. Lett.* **2014**, *5*, 1167–1172.

39 Goetz, G. H.; Farrell, W.; Shalaeva, M.; Sciabola, S.; Anderson, D.; Yan, J.; Philippe, L.; Shapiro, M. J. High throughput method for the indirect detection of intramolecular hydrogen bonding. *J. Med. Chem.* **2014**, *57*, 2920–2929.

40 Shalaeva, M.; Caron, G.; Abramov, Y. A.; O'Connell, T. N.; Plummer, M. S.; Yalamanchi, G.; Farley, K. A.; Goetz, G. H.; Philippe, L.; Shapiro, M. J. Integrating intramolecular hydrogen bonding (IMHB) considerations in drug discovery using DeltalogP as a tool. *J. Med. Chem.* **2013**, *56*, 4870–4879.

41 Hess, S.; Linde, Y.; Ovadia, O.; Safrai, E.; Shalev, D. E.; Swed, A.; Halbfinger, E.; Lapidot, T.; Winkler, I.; Gabinet, Y.; Faier, A.; Yarden, D.; Xiang, Z.; Portillo, F. P.; Haskell-Luevano, C.; Gilon, C.; Hoffman, A. Backbone cyclic peptidomimetic melanocortin-4 receptor agonist as a novel orally administered drug lead for treating obesity. *J. Med. Chem.* **2008**, *51*, 1026–1034.

42 Chatterjee, J.; Gilon, C.; Hoffman, A.; Kessler, H. N-methylation of peptides: a new perspective in medicinal chemistry. *Acc. Chem. Res.* **2008**, *41*, 1331–1342.

43 Biron, E.; Chatterjee, J.; Ovadia, O.; Langenegger, D.; Brueggen, J.; Hoyer, D.; Schmid, H. A.; Jelinek, R.; Gilon, C.; Hoffman, A.; Kessler, H. Improving oral bioavailability of peptides by multiple N-methylation: somatostatin analogues. *Angew. Chem. Int. Ed. Engl.* **2008**, *47*, 2595–2599.

44 Hill, T. A.; Lohman, R. J.; Hoang, H. N.; Nielsen, D. S.; Scully, C. C.; Kok, W. M.; Liu, L.; Lucke, A. J.; Stoermer, M. J.; Schroeder, C. I.; Chaousis, S.; Colless, B.; Bernhardt, P. V.; Edmonds, D. J.; Griffith, D. A.; Rotter, C. J.; Ruggeri, R. B.; Price, D. A.; Liras, S.; Craik, D. J.; Fairlie, D. P. Cyclic penta- and hexaleucine peptides without N-methylation are orally absorbed. *ACS Med. Chem. Lett.* **2014**, *5*, 1148–1151.

45 Miranda, E.; Nordgren, I. K.; Male, A. L.; Lawrence, C. E.; Hoakwie, F.; Cuda, F.; Court, W.; Fox, K. R.; Townsend, P. A.; Packham, G. K.; Eccles, S. A.; Tavassoli, A. A cyclic peptide inhibitor of HIF-1 heterodimerization that inhibits hypoxia signaling in cancer cells. *J. Am. Chem. Soc.* **2013**, *135*, 10418–10425.

46 Schreiber, S. L.; Crabtree, G. R. The mechanism of action of cyclosporin A and FK506. *Immunol. Today* **1992**, *13*, 136–142.

47 Wu, X.; Stockdill, J. L.; Wang, P.; Danishefsky, S. J. Total synthesis of cyclosporine: access to N-methylated peptides via isonitrile coupling reactions. *J. Am. Chem. Soc.* **2010**, *132*, 4098–4100.

48 Drewe, J.; Meier, R.; Vonderscher, J.; Kiss, D.; Posanski, U.; Kissel, T.; Gyr, K. Enhancement of the oral absorption of cyclosporin in man. *Br. J. Clin. Pharmacol.* **1992**, *34*, 60–64.

49 Kopp, J. B.; Klotman, P. E. Cellular and molecular mechanisms of cyclosporin nephrotoxicity. *J. Am. Soc. Nephrol.* **1990**, *1*, 162–179.

50 Ptachcinski, R. J.; Venkataramanan, R.; Burckart, G. J. Clinical pharmacokinetics of cyclosporin. *Clin. Pharmacokinet.* **1986**, *11*, 107–132.

51 Kahan, B. D.; Welsh, M.; Rutzky, L. P. Challenges in cyclosporine therapy: the role of therapeutic monitoring by area under the curve monitoring. *Ther. Drug Monit.* **1995**, *17*, 621–624.

52 Burckart, G. J.; Starzl, T. E.; Venkataramanan, R.; Hashim, H.; Wong, L.; Wang, P.; Makowka, L.; Zeevi, A.; Ptachcinski, R. J.; Knapp, J. E.; Iwatsuki, S.; Esquivel, C.; Sanghvi, L. A.; Van Thiel, D. H. Excretion of cyclosporine and its metabolites in human bile. *Transplant. Proc.* **1986**, *18*, 46–49.

53 Augustijns, P. F.; Brown, S. C.; Willard, D. H.; Consler, T. G.; Annaert, P. P.; Hendren, R. W.; Bradshaw, T. P. Hydration changes implicated in the remarkable temperature-dependent membrane permeation of cyclosporin A. *Biochemistry* **2000**, *39*, 7621–7630.

54 Rizo, J.; Gierasch, L. M. Constrained peptides: models of bioactive peptides and protein substructures. *Annu. Rev. Biochem.* **1992**, *61*, 387–418.

55 Wenger, R. M.; France, J.; Bovermann, G.; Walliser, L.; Widmer, A.; Widmer, H. The 3D structure of a cyclosporin analogue in water is nearly identical to the cyclophilin-bound cyclosporin conformation. *FEBS Lett.* **1994**, *340*, 255–259.

56 Rezai, T.; Bock, J. E.; Zhou, M. V.; Kalyanaraman, C.; Lokey, R. S.; Jacobson, M. P. Conformational flexibility, internal hydrogen bonding, and passive membrane permeability: successful in silico prediction of the relative permeabilities of cyclic peptides. *J. Am. Chem. Soc.* **2006**, *128*, 14073–14080.

57 Rezai, T.; Yu, B.; Millhauser, G. L.; Jacobson, M. P.; Lokey, R. S. Testing the conformational hypothesis of passive membrane permeability using synthetic cyclic peptide diastereomers. *J. Am. Chem. Soc.* **2006**, *128*, 2510–2511.

58 Whitty, A.; Zhong, M.; Viarengo, L.; Beglov, D.; Hall, D. R.; Vajda, S. Quantifying the chameleonic properties of macrocycles and other high-molecular-weight drugs. *Drug Discov. Today* **2016**, *21*, 712–717.

59 White, T. R.; Renzelman, C. M.; Rand, A. C.; Rezai, T.; McEwen, C. M.; Gelev, V. M.; Turner, R. A.;

Linington, R. G.; Leung, S. S.; Kalgutkar, A. S.; Bauman, J. N.; Zhang, Y.; Liras, S.; Price, D. A.; Mathiowetz, A. M.; Jacobson, M. P.; Lokey, R. S. On-resin N-methylation of cyclic peptides for discovery of orally bioavailable scaffolds. *Nat. Chem. Biol.* **2011**, *7*, 810–817.

60 Rand, A. C.; Leung, S. S.; Eng, H.; Rotter, C. J.; Sharma, R.; Kalgutkar, A. S.; Zhang, Y.; Varma, M. V.; Farley, K. A.; Khunte, B.; Limberakis, C.; Price, D. A.; Liras, S.; Mathiowetz, A. M.; Jacobson, M. P.; Lokey, R. S. Optimizing PK properties of cyclic peptides: the effect of side chain substitutions on permeability and clearance(). *Medchemcomm* **2012**, *3*, 1282–1289.

61 Thansandote, P.; Harris, R. M.; Dexter, H. L.; Simpson, G. L.; Pal, S.; Upton, R. J.; Valko, K. Improving the passive permeability of macrocyclic peptides: balancing permeability with other physicochemical properties. *Bioorg. Med. Chem.* **2015**, *23*, 322–327.

62 Evers, M.; Barriere, J. C.; Bashiardes, G.; Bousseau, A.; Carry, J. C.; Dereu, N.; Filoche, B.; Henin, Y.; Sable, S.; Vuilhorgne, M.; Mignani, S. Synthesis of non-immunosuppressive cyclophilin-Binding cyclosporin A derivatives as potential anti-HIV-1 drugs. *Bioorg. Med. Chem. Lett.* **2003**, *13*, 4415–4419.

63 Beck, J. G.; Chatterjee, J.; Laufer, B.; Kiran, M. U.; Frank, A. O.; Neubauer, S.; Ovadia, O.; Greenberg, S.; Gilon, C.; Hoffman, A.; Kessler, H. Intestinal permeability of cyclic peptides: common key backbone motifs identified. *J. Am. Chem. Soc.* **2012**, *134*, 12125–12133.

64 Nielsen, D. S.; Hoang, H. N.; Lohman, R. J.; Hill, T. A.; Lucke, A. J.; Craik, D. J.; Edmonds, D. J.; Griffith, D. A.; Rotter, C. J.; Ruggeri, R. B.; Price, D. A.; Liras, S.; Fairlie, D. P. Improving on nature: making a cyclic heptapeptide orally bioavailable. *Angew. Chem. Int. Ed. Engl.* **2014**, *53*, 12059–12063.

65 Pettit, G. R.; Cichacz, Z.; Barkoczy, J.; Dorsaz, A. C.; Herald, D. L.; Williams, M. D.; Doubek, D. L.; Schmidt, J. M.; Tackett, L. P.; Brune, D. C.; Cerny, R. L.; Hooper, J. N. A.; Bakus, G. J. Isolation and structure of the marine sponge cell growth inhibitory cyclic peptide phakellistatin 1. *J. Nat. Prod.* **1993**, *56*, 260–267.

66 Bockus, A. T.; Schwochert, J. A.; Pye, C. R.; Townsend, C. E.; Sok, V.; Bednarek, M. A.; Lokey, R. S. Going out on a limb: delineating the effects of beta-branching, N-methylation, and side chain size on the passive permeability, solubility, and flexibility of sanguinamide A analogues. *J. Med. Chem.* **2015**, *58*, 7409–7418.

67 Wang, C. K.; Northfield, S. E.; Colless, B.; Chaousis, S.; Hamernig, I.; Lohman, R. J.; Nielsen, D. S.; Schroeder, C. I.; Liras, S.; Price, D. A.; Fairlie, D. P.; Craik, D. J. Rational design and synthesis of an orally bioavailable peptide guided by NMR amide temperature coefficients. *Proc. Natl. Acad. Sci. U. S. A.* **2014**, *111*(49), 17504–17509.

68 Kitagaki, J.; Shi, G.; Miyauchi, S.; Murakami, S.; Yang, Y. Cyclic depsipeptides as potential cancer therapeutics. *Anticancer Drugs* **2015**, *26*, 259–271.

69 Bockus, A. T.; McEwen, C. M.; Lokey, R. S. Form and function in cyclic peptide natural products: a pharmacokinetic perspective. *Curr. Top. Med. Chem.* **2013**, *13*, 821–836.

70 Schwochert, J.; Pye, C.; Ahlbach, C.; Abdollahian, Y.; Farley, K.; Khunte, B.; Limberakis, C.; Kalgutkar, A. S.; Eng, H.; Shapiro, M. J.; Mathiowetz, A. M.; Price, D. A.; Liras, S.; Lokey, R. S. Revisiting N-to-O acyl shift for synthesis of natural product-like cyclic depsipeptides. *Org. Lett.* **2014**, *16*(23), 6088–6091.

71 Simon, R. J.; Kania, R. S.; Zuckermann, R. N.; Huebner, V. D.; Jewell, D. A.; Banville, S.; Ng, S.; Wang, L.; Rosenberg, S.; Marlowe, C. K.; Spellmeyer, D. C.; Tan, R.; Frankel, A. D.; Santi, D. V.; Cohen, F. E.; Bartlett, P. A. Peptoids: a modular approach to drug discovery. *Proc. Natl. Acad. Sci. U. S. A.* **1992**, *89*, 9367–9371.

72 Schwochert, J.; Turner, R.; Thang, M.; Berkeley, R. F.; Ponkey, A. R.; Rodriguez, K. M.; Leung, S. S.; Khunte, B.; Goetz, G.; Limberakis, C.; Kalgutkar, A. S.; Eng, H.; Shapiro, M. J.; Mathiowetz, A. M.; Price, D. A.; Liras, S.; Jacobson, M. P.; Lokey, R. S. Peptide to peptoid substitutions increase cell permeability in cyclic hexapeptides. *Org. Lett.* **2015**, *17*, 2928–2931.

73 Palm, K.; Stenberg, P.; Luthman, K.; Artursson, P. Polar molecular surface properties predict the intestinal absorption of drugs in humans. *Pharm. Res.* **1997**, *14*, 568–571.

74 Varma, M. V.; Obach, R. S.; Rotter, C.; Miller, H. R.; Chang, G.; Steyn, S. J.; El-Kattan, A.; Troutman, M. D. Physicochemical space for optimum oral bioavailability: contribution of human intestinal absorption and first-pass elimination. *J. Med. Chem.* **2010**, *53*, 1098–1108.

75 Leung, S. S.; Mijalkovic, J.; Borrelli, K.; Jacobson, M. P. Testing physical models of passive membrane permeation. *J. Chem. Inf. Model.* **2012**, *52*, 1621–1636.

76 Singleton, D. H.; Boyd, H.; Steidl-Nichols, J. V.; Deacon, M.; Groot, M. J.; Price, D.; Nettleton, D. O.; Wallace, N. K.; Troutman, M. D.; Williams, C.; Boyd, J. G. Fluorescently labeled analogues of dofetilide as high-affinity fluorescence polarization ligands for the human ether-a-go-go-related gene (hERG) channel. *J. Med. Chem.* **2007**, *50*, 2931–2941.

77 Deacon, M.; Singleton, D.; Szalkai, N.; Pasieczny, R.; Peacock, C.; Price, D.; Boyd, J.; Boyd, H.; Steidl-Nichols, J. V.; Williams, C. Early evaluation of compound QT prolongation effects: a predictive 384-well fluorescence polarization binding assay for measuring hERG blockade. *J. Pharmacol. Toxicol. Methods* **2007**, *55*, 238–247.

78 Fouche, M.; Schafer, M.; Blatter, M.; Berghausen, J.; Desrayaud, S.; Roth, H. J. Pharmacokinetic studies around the mono- and difunctionalization of a bioavailable cyclic decapeptide scaffold. *ChemMedChem* **2016**, *11*, 1060–1068.

79 Hop, C. E.; Cole, M. J.; Davidson, R. E.; Duignan, D. B.; Federico, J.; Janiszewski, J. S.; Jenkins, K.; Krueger, S.; Lebowitz, R.; Liston, T. E.; Mitchell, W.; Snyder, M.; Steyn, S. J.; Soglia, J. R.; Taylor, C.; Troutman, M. D.; Umland, J.; West, M.; Whalen, K. M.; Zelesky, V.; Zhao, S. X. High throughput ADME screening: practical considerations, impact on the portfolio and enabler of in silico ADME models. *Curr. Drug Metab.* **2008**, *9*, 847–853.

80 Fouche, M.; Schafer, M.; Berghausen, J.; Desrayaud, S.; Blatter, M.; Piechon, P.; Dix, I.; Martin Garcia, A.; Roth, H. J. Design and development of a cyclic decapeptide scaffold with suitable properties for bioavailability and oral exposure. *ChemMedChem* **2016**, *11*, 1048–1059.

81 Wang, C. K.; Northfield, S. E.; Swedberg, J. E.; Colless, B.; Chaousis, S.; Price, D. A.; Liras, S.; Craik, D. J. Exploring experimental and computational markers of cyclic peptides: charting islands of permeability. *Eur. J. Med. Chem.* **2015**, *97*, 202–213.

82 Hewitt, W. M.; Leung, S. S.; Pye, C. R.; Ponkey, A. R.; Bednarek, M.; Jacobson, M. P.; Lokey, R. S. Cell-permeable cyclic peptides from synthetic libraries inspired by natural products. *J. Am. Chem. Soc.* **2015**, *137*, 715–721.

83 Hoveyda, H. R.; Marsault, E.; Gagnon, R.; Mathieu, A. P.; Vezina, M.; Landry, A.; Wang, Z.; Benakli, K.; Beaubien, S.; Saint-Louis, C.; Brassard, M.; Pinault, J. F.; Ouellet, L.; Bhat, S.; Ramaseshan, M.; Peng, X.; Foucher, L.; Beauchemin, S.; Bherer, P.; Veber, D. F.; Peterson, M. L.; Fraser, G. L. Optimization of the potency and pharmacokinetic properties of a macrocyclic ghrelin receptor agonist (Part I): development of ulimorelin (TZP-101) from hit to clinic. *J. Med. Chem.* **2011**, *54*, 8305–8320.

84 Townend, J. E.; Tavassoli, A. Traceless production of cyclic peptide libraries in *E. coli*. *ACS Chem. Biol.* **2016**, *11*(6), 1624–1630.

85 Matsson, P.; Doak, B. C.; Over, B.; Kihlberg, J. Cell permeability beyond the rule of 5. *Adv. Drug Deliv. Rev.* **2016**, *101*, 42–61.

Part II

Classes of Macrocycles and Their Potential for Drug Discovery

4

Natural and Nature-Inspired Macrocycles

A Chemoinformatic Overview and Relevant Examples

Ludger A. Wessjohann, Richard Bartelt and Wolfgang Brandt

Department of Bioorganic Chemistry, Leibniz Institute of Plant Biochemistry, Halle (Saale), Germany

4.1 Introduction to Natural Macrocycles as Drugs and Drug Leads

This chapter is dedicated to theoretical analyses and experimental studies of biologically and medicinally relevant macrocyclic compounds (MCs). The connection of pharmacologically active macrocycles to their producer organisms, as well as their biosynthetic pathways, followed by chemoinformatic analyses of structural features will be reviewed. The most important groups of macrocyclic natural products—excluding cyclopeptides (see Chapter 5)—are discussed on the basis of selected examples.

The importance of MCs for drug discovery and development has recently been reviewed by Newman and Cragg [1]. They classified the compounds into a combination of structural and application groups with some extra classes for selected compounds. These were (i) macrolides and peptide-based bioactive compounds with anti-infective and antitumor activities, (ii) ansamycins with antimycobacterial and antibacterial activities, (iii) bryostatins as protein kinase C inhibitors, (iv) epothilones, (v) rapamycin and rapalogs, (vi) peptidic macrocycles, and (vii) buruli toxins. Another detailed classification of macrocyclic drugs into eight families is given in the review of Driggers *et al.* [2] These authors classify MCs into macrolide antibiotics, polyene antifungals, cyclic peptides, avermectin-related compounds, rifampicin- and vancomycin-related ones, α-keto homopropyl amides, and tubulin binders and, specifically in therapeutic fields, antibiotics, antifungals, (other) anti-infectives, immunosuppressors, anticancer compounds, veterinary antiparasitics or antihelminthics, and insecticides. Both, unfortunately, do not provide a clear separation of structural and bioactivity classification (*vide infra*).

In this chapter, the content of these rather extensive publications will not be repeated. Those preceding works already gave a nice overview about structures, functions, and applications of natural MCs. Thus, in the following, we will focus instead on the aspects of structure–activity relationships (SAR) of macrocycles derived from chemoinformatic analyses and related theoretical methods.

The first general chemoinformatic analyses of natural occurring macrocycles were published in 2005 [3] and in 2010 [4] and have recently been extended and repeated based on a larger data set (Bartelt, R., Brandt, W., Haupt, H., and Wessjohann, L. A. Statistical analysis of macrocycles. To be submitted), confirming the previous results. For instance, the distribution of macrocyclic classes in relation to their natural source organisms was analyzed following the pioneering paper of Wessjohann *et al.* [3] (Figure 4.1). Not surprisingly, macrocycles synthesized via the polyketide pathway are most abundant in bacteria, whereas macrocyclic terpenoids were predominantly isolated from plants and animals, with the majority of alkaloids again from plants. Cyclopeptides are common in bacteria but are also found in plants and fungi, and even in animals. They will, however, not be considered here (see Chapter 5). The statistical analysis of macrocycles in relation to their bioactivity profile, especially medicinal applications, reveals that most of the macrocyclic drugs are used as antibacterial and anticancer drugs (Figure 4.2, see also Chapter 16) (Bartelt, R., Brandt, W., Haupt, H., and Wessjohann, L. A. Statistical analysis of macrocycles. To be submitted).

4.2 Biosynthetic Pathways, Natural Role, and Biotechnological Access

A common principle in the biosynthesis of most natural MCs is the primary synthesis of a linear precursor, followed by macrocyclization. Modification of the MC then leads to the final natural product. Often, the linear
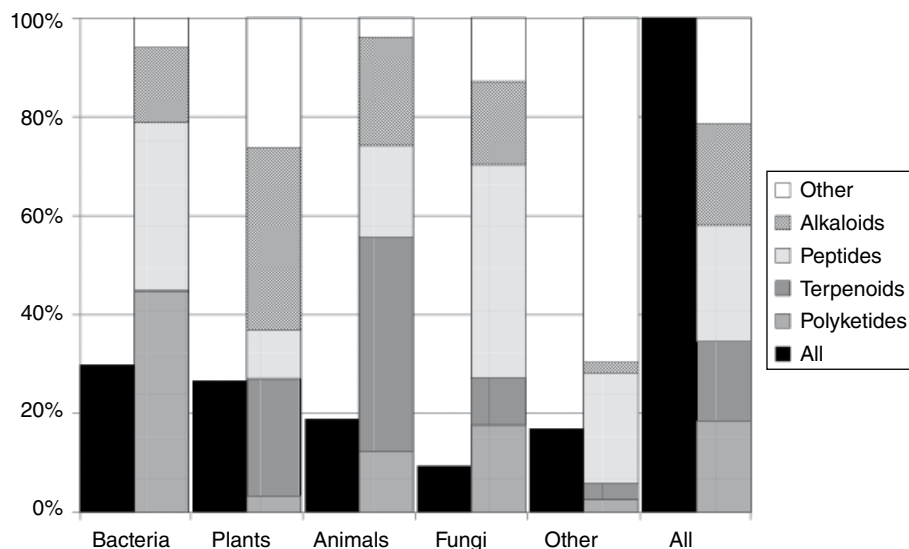
Figure 4.1 Distribution of principal classes of natural products within macrocycles (Bartelt, R., Brandt, W., Haupt, H., and Wessjohann, L. A. Statistical analysis of macrocycles. To be submitted).
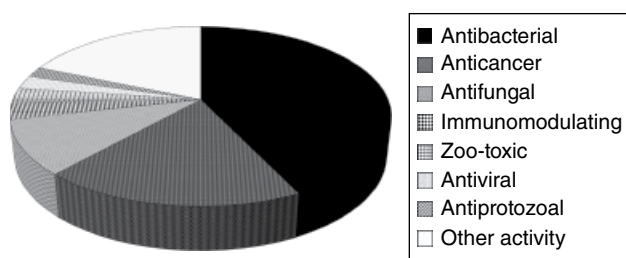

Figure 4.2 Proportional areas of medicinal applications described for macrocyclic drugs (Bartelt, R., Brandt, W., Haupt, H., and Wessjohann, L. A. Statistical analysis of macrocycles. To be submitted).

precursor is a sequentially defined polymer formed by the condensation of diverse monomers. These are derived from common biosynthetic pathways such as amino acids/peptides, acetyl- and malonyl-CoAs/polyketides and fatty acids, terpenoids/polyisoprenes, or sugars/oligosaccharides [3].

Even though the biosynthesis of polyketides has been thoroughly reviewed previously by Kopp and Marahiel [5], features crucial for the macrocyclization are summarized in this chapter. Polyketide macrocycles are produced by polyketide synthase (PKS) protein complexes (Scheme 4.1).

The most prominent type of PKS is the highly modular type I, which is usually encoded in distinct gene clusters [6]. Here, the starter substrate is covalently bound to the active side of the first module of the PKS via a thioester bond. Each module elongates the polyketide chain by one ketide moiety, usually an acetyl, malonyl or methylmalonyl group, by transferring the polyketide chain to the new building block. In contrast to this modular type I PKS, an iterative type I PKS reuses a

catalytic domain multiple times. Final cleavage of the polyketide chain from the protein is catalyzed by a thioesterase (TE) domain, which is usually the last domain of the PKS complex. In most macrocyclic polyketides, macrocyclization is catalyzed during or after this thioester cleavage. However, for the erythromycin PKS, it has been shown that isolated TE domains are not capable of performing the cyclization [7], thus implicating a potential role of other parts of the PKS in macrocyclization. For PKS that produces aromatic polyketide rings, a distinct product template domain has been identified [8, 9], but so far such a domain has not been reported in the context of a macrocyclization. After macrocyclization, the compounds are usually heavily modified by rearrangements, oxidations, glycosylations, acetylations, methylations, etc. [3]

Another common mode of macrocyclization in polyketides is lactam formation between the carboxyl-terminus of the linear precursor and an amine group (Figure 4.3). An example for macrolactamization in polyketides is the group of ansamycin antibiotics, which also occurs in non-ribosomal peptide synthase (NRPS)-derived macrocycles not further discussed here [10]. In ansamycins, usually the starter substrate is an aromatic moiety such as 3-amino-5-hydroxybenzoic acid (AHBA). The terminating TE domain, which is present in many type I PKSs, is missing in the rifamycin and geldanamycin synthase [3, 11]. Macrocyclization is performed by amide formation between the carboxy-terminus of the linear polyketide precursor and the amino group of the aromatic moiety, resulting in the aromatic ring being bridged by the lactam-containing macrocyclic portion. In rifamycin and geldanamycin
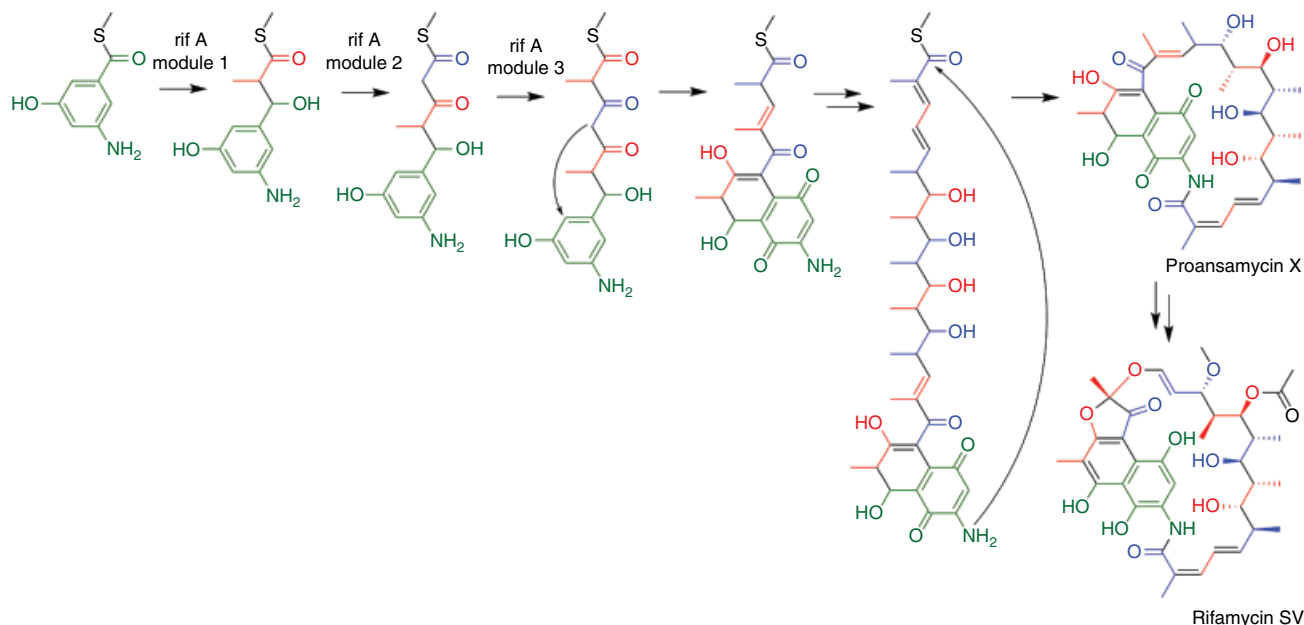
Scheme 4.1 Principal of polyketide synthesis with subsequent macrocyclization. During its biosynthesis the linear precursor is connected via a thioester bond to acyl carrier proteins (ACP, bound to the sulfur – only the bond is shown in the scheme). Modifications and transfer to the next monomer are catalyzed by additional domains of the respective module. The starter unit is gray. (*See insert for color representation of the figure.*)

PKS, this macrolactamization is catalyzed by the distinct enzymes rifF and GdmF, respectively [11, 12].

Aside from this "classical" lactone/lactam macro-cyclization, there are additional, more exotic modes of macrocyclization such as the Diels–Alder cycloaddition in versipelostatin [13].

A special kind of macrocyclic polyketide structure is formed from the combination of polyketides and peptides. These compounds are produced in hybrid PKS–NRPS protein complexes. An example for this type of structure is the antibiotic pristinamycin (Figure 4.3), which is a mixture of pristinamycin I, a cyclodepsipeptide, and pristinamycin II, a hybrid polyketide–peptide macrocycle [14]. Interestingly, the two pristinamycin compounds show a strong cooperative effect. Both compounds bind to the 50S subunit of the bacterial ribosome. However, for the pristinamycin derivatives quinupristin/dalfopristin, it has been shown that the combination is up to 100-fold more potent compared to the respective single compounds [15].

Compared to other oligomeric MCs, macrocyclic terpenoids are rather limited in their sizes, reflecting their biosynthetic origin [4]. Assuming that the whole macrocyclic portion is of terpenoid origin, terpenoid MCs start with sesquiterpenoids (C_{15}, i.e., max C_{12} in the macrocyclic ring) and higher terpenoids. The minimal ring size of a terpenoid macrocycle is further limited by the highly conserved intramolecular electrophilic attack of the mesomeric carbocation of the prenyl chain onto another internal double bond [16]. For example, the smallest macrocycle from the diterpenoid C_{20} precursor geranylgeranyl diphosphate (GGPP) using this mechanism is formed by a C1—C14 ring closure, resulting in cembrene, the most abundant macrocyclic terpenoid skeleton. A variety of cembrene derivatives, called cembrenoids (also cembranoids or cembranolids), have been isolated from soft corals [17, 18], as well as from higher plants [19, 20]. Most of these cembrenoids are the results of (ep)oxidation and further cyclization and rearrangement of the cembrene molecule (Scheme). Some of them have been shown to exhibit antiproliferative activity by modulating microtubule dynamics, as well as neuroprotective, anti-inflammatory, and antimicrobial activity [23–27]. Another structurally similar group of pure terpenoid macrocycles are the verticillenes and norverticillenes [21, 22].

Despite the limitation to a very small set of linear precursors (prenyl diphosphates) and a rather conserved mechanism of macrocyclization, terpenoid macrocycles are actually quite diverse with respect to the resulting structures [17]. Indeed, unlike cyclopeptides in which the variety of monomers creates extreme diversity, the incredible diversity of terpenoids is based on skeletal rearrangements and post-cyclization modifications, which will be further detailed later.

Tightly connected to the biosynthetic pathways of MCs is the biotechnological accessibility of these compounds for pharmacological use. Because the PKS enzyme complexes are usually encoded in gene clusters, the identification, cloning, and expression of PKS genes
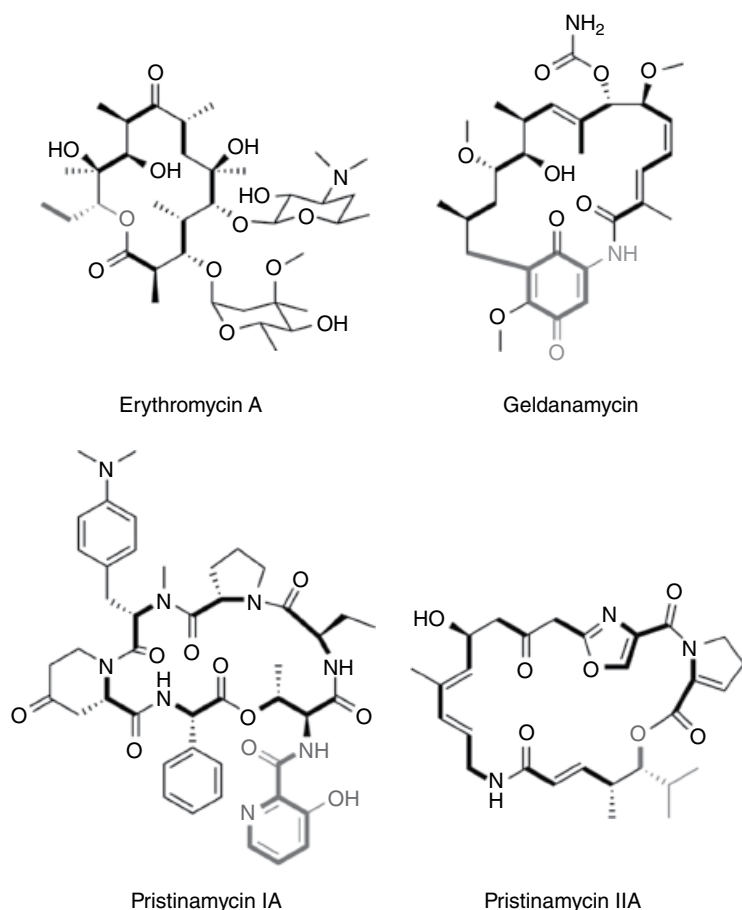
Erythromycin A

Geldanamycin

Figure 4.3 Examples for macrocyclic polyketides. In erythromycin A, ring closure is achieved via lactone formation. In ansamycins/geldanamycins, the macrocycle is formed by amide formation. In both examples, the carboxyl-terminus of the linear precursor is activated as thioester and condensed with an amine or hydroxyl group of the same molecule. Below: Pristinamycin, which is a mixture of pristinamycin I, a cyclodepsipeptide, and pristinamycin II, a hybrid polyketide–peptide macrocycle. Backbone bonds derived from the same building block are marked in bold. The starter substrate is colored gray.

Pristinamycin IA

Pristinamycin IIA

are rather easy considering the size of several hundred kilodaltons of the actual protein complex. In the 1990s, a number of PKS gene clusters have been identified, cloned, and heterologously expressed. Because the modular nature of (bacterial) PKSs was established on both the genetic and the protein level already in the nineties, approaches to artificially designed polyketide compounds by combinatorial domain swapping followed rather quickly [28–30]. Nature itself uses this combinatorial principle during evolution, often initiated by gene duplication and mutation of the distinct modules [31]. Because of the conserved similarity between domains of the same function, it has been possible to develop tools to identify the domains on the gene level and to predict their activity and product structure *in silico*, even up to the absolute configuration of the stereochemical centers generated [32–35].

However, the production of artificial MCs is limited to rearranging the genes and precursors available from biochemistry, or from feeding them in (mutasynthesis). Some compounds with relevant pharmacological activity, such as the anticancer agent spongistatin [36], could not yet be produced successfully by biotechnology and instead are accessed by synthetic means [37]. The "perspective of combinatorial biosynthesis of polyketides,"

nevertheless, is intriguing and was thoroughly reviewed by Wong and Khosla [30].

The largest variety of known macrocyclic terpenoids originates from marine organisms, mostly cnidarians. Because these organisms are hard to grow, in most cases, only the structures of isolated compounds are available. Isolated and cloned synthases of macrocyclic terpenoids are limited to terrestrial plant enzymes [38, 39]. As pointed out previously, and in contrast to macrocyclic peptides and polyketides, the variability of macrocyclic terpenoids is not created by a combinatorial sequence of building blocks, such as amino acids or ketide moieties, but rather by the high reactivity of an intermediate carbocation (see Scheme 4.2) followed by enzymatic diversification [16]. According to the origin of this cation, the enzymes can be classified as type I (cleavage of substrate diphosphate) or type II (protonation of double bond or a therefrom derived epoxide) terpene synthases, which share structural and sequential homology, respectively. The macrocyclic terpenoids are mostly generated by enzymes, which closely resemble typical terpene synthases (terpene cyclases) synthesizing other non-macrocyclic terpenoids. In some cases of terpene synthases leading to polycyclic terpenes, initially a macrocyclic
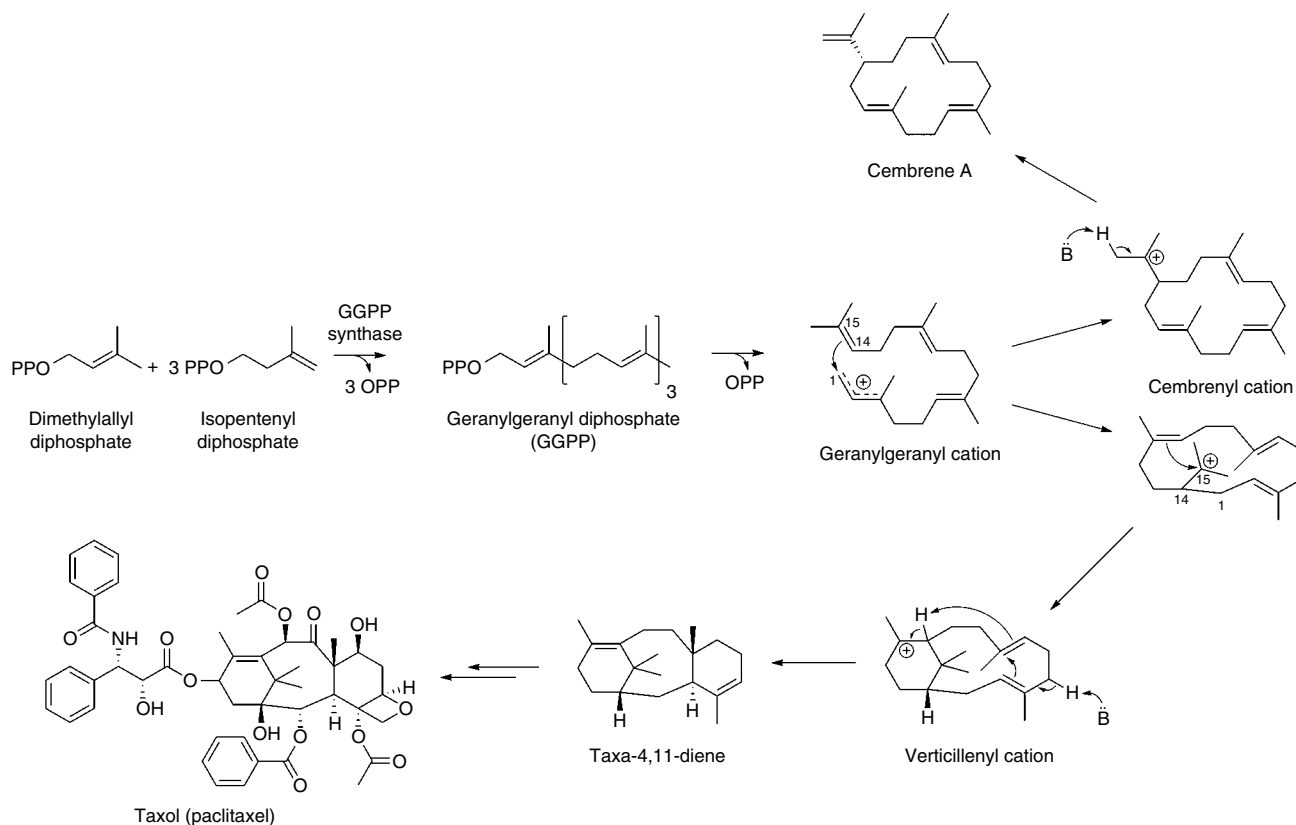
Scheme 4.2 Biosynthesis of cyclic terpenoids. Starting from the isomers isopentenyl diphosphate and dimethylallyl diphosphate, geranylgeranyl diphosphate (GGPP) synthase produces GGPP, which is the substrate of the cembrene and taxadiene synthases. Electrophilic attack of the allylic cation at C-1/C-3 on the double bond at C-14 results in a common intermediate, the macrocyclic cembrenyl cation. Deprotonation leads to cembrene, while within taxadiene synthase, further rearrangements lead to taxadiene, which is modified to taxol later on. Note: Numbering of carbon atoms are according to IUPAC numbering of GGPP; established numberings of cyclic terpenoids may differ. Source: Modified from Chang *et al.* [21] and Nagashima *et al.* [22]. Reproduced with permission of Wiley & the Pharmaceutical Society of Japan.

intermediate is formed, which subsequently is transannularily bridged, thus eliminating the macrocyclic portion of the molecule. An example for this is taxadiene synthase, which performs a macrocyclization of GGPP to yield a macrocyclic verticillen-12-yl cation. Subsequently, this 12-membered macrocyclic reactive intermediate is bridged to taxadiene (Scheme 4.2) [40, 41].

The vast majority of drugs are either natural products or derivatives or mimics thereof. This leads to the very intriguing question: Why do plants, fungi, or microbes produce molecules of pharmacological interest? For the large number of antibiotic and cytotoxic compounds, the answer is rather obvious. Plants, fungi, and microbes are sessile or locally confined and exposed to a large number of threats like nutrient competitors or being fed on by animals or parasites. Therefore, the need to develop strategies to fight these dangers emerged [42]. In 1989, Williams *et al.* [43] compiled several theories why secondary products are biosynthesized. In general, they concluded that survival fitness is increased by producing compounds that bind to receptors in other organisms, provoking certain effects to those organisms.

Already in the nineteenth century, it was described that microorganisms competed against each other [44]. Later, in one of the examined genera, *Penicillium*, the antibacterial agent penicillin was discovered. The occurrence of many antibacterial or antiviral compounds can be explained that way. Even the occurrence of compounds with anticancer activity in plants, bacteria, and fungi can be explained by the toxicity of these compounds at higher doses or after activation by some trigger mechanism, such as enzymatic activation after induction, for example, by a leaf-eating insect.

The benefits for an ascomycete fungus like *Tolypocladium inflatum* to produce immunomodulators, such as cyclosporine, are not as easy to explain. Because most source organisms of pharmacologically active compounds are not well researched within their natural habitat, the actual benefit to the evolutionary fitness of the producer organism remains elusive for many compounds.

However, sometimes the answer may lie on the similarity or evolutionary preservation of certain protein domains and binding sites, serving different contexts in different species or cellular environments [3]. This is demonstrated by the selected following examples of the same natural macrocycle with relevance in different fields of medical applications.

One of the first macrocycles that was approved as a drug was rapamycin (aka sirolimus), discovered in 1975, isolated from the bacterium *Streptomyces hygroscopicus* [45, 46]. First, it was considered as an antifungal antibiotic [45–48]. Now it is used as an immunosuppressive agent to prevent transplant rejection [49], in the treatment of atopic dermatitis [50], as a coronary stent coating [51–53], and in testing for application in anticancer therapies [54–59].

Another class of pharmaceutically relevant macrocycles are the ascomycins, which are used as anti-inflammatory agents [60, 61] or for the treatment of dermatitis [60, 62], with the most prominent examples tacrolimus (also called FK-506, or fujimycin) and pimecrolimus. Tacrolimus was discovered in the soil bacterium *Streptomyces tsukubaensis* in 1987 [61–65]. It is applied in immunotherapy [66–68] and is, as well, relevant for the treatment of atopic dermatitis [62, 68–74]. Pimecrolimus also acts as an anti-inflammatory [75, 76] drug and against dermatitis [77–79].

Other pharmacologically relevant macrocycles are the ansamycins, which include a rather high number of active homologues, including streptovaricin [70, 80, 81], rifabutin [82], rifampicin [82], rifapentine [83–86], and rifaximin [87–90]. These compounds are in clinical use or trials for several applications, such as treatment of infections [91–94], tuberculosis [95–97], and AIDS [98] and in cancer therapy [99–101].

These examples of MCs, already approved either as pharmaceuticals or in clinical testing, illustrate the enormous importance and potency of macrocycle drugs for therapeutic applications, which can sometimes be multiple. **But, how common are macrocycles for such (medicinal) purposes? Are they more abundant than average in bioactive natural compounds? And, if so, why is this so despite the intrinsic (statistical and chemical) difficulty in forming them and in spite of their common violation of the Lipinski rules? All of these are questions for chemoinformatic analyses.**

4.3 QSAR and Chemoinformatic Analyses of Common Features

With ever-increasing sources and amounts of available data and structures of MCs and computational power, the application of chemoinformatics methods [102, 103] can not only rationalize drug design [104] by guiding modifications of macrocyclic structures but may also lead to closer insights into general properties [3, 4], SAR, and understanding of the functional roles of macrocycles within their natural source, as well as for pharmaceutical applications. Synonymous to the expression "chemoinformatics," "cheminformatics" (without an "o") is also in use sometimes. Here, only "chemoinformatics" will be used throughout.

In this section, we will briefly review the outcome of applied theoretical methods, including general chemoinformatic analyses of common features and properties of macrocycles and molecular modeling techniques such as analyses of SAR, docking studies, and molecular dynamics simulations leading to improved properties for specific applications (see also Chapter 2 for additional discussion on modeling).

A general chemoinformatic analysis of macrocycles based on a rather limited set of macrocycles was introduced by Wessjohann *et al.* in 2005 [3] and Brandt *et al.* in 2010 [4]. Therein, a statistical analysis of the number of known natural product macrocycles in dependence of their ring size was displayed (Figure 4.4). In the smaller macrocycles, even-numbered ones are more abundant, as they result from C2-polyketide monomer elongation units [acetyl-CoA, (methyl)malonyl-CoA], whereas, in larger ones, $3n$- and $3n + 1$- sized rings are predominant resulting from cyclic peptides and depsipeptides, respectively. For the latter, the additional atom comes from the alcohol-O of the lactone being at C-3 (β-position of Ser or Thr), that is, with these amino acids contributing four endocyclic atoms.

Furthermore, various common endocyclic structural features were analyzed with respect to abundance versus ring size distribution, including, for example, the number of double bonds, the presence of heteroatoms, or lactone (cf. polyketides and depsipeptides), or lactam (cf. peptides) moieties (Figure 4.5). From such and more elaborated analyses, conclusions about the dependence on biosynthetic origin were statistically analyzed (Figure 4.6) (Bartelt, R., Brandt, W., Haupt, H., and Wessjohann, L. A. Statistical analysis of macrocycles. To be submitted) [3, 4].

Recently, this analysis was repeated using more than 11 000 macrocycles extracted from the dictionary of natural products, corresponding to 4.5% of compounds found in the database of more than 240 000 structures of natural compounds (Bartelt, R., Brandt, W., Haupt, H., and Wessjohann, L. A. Statistical analysis of macrocycles. To be submitted). The result of this enlarged and updated statistical analysis strongly resembles the results of the first publication a decade ago [3]. In particular, oscillation in the distribution of macrocycles was reproduced. At lower ring sizes, even-numbered rings occur predominantly
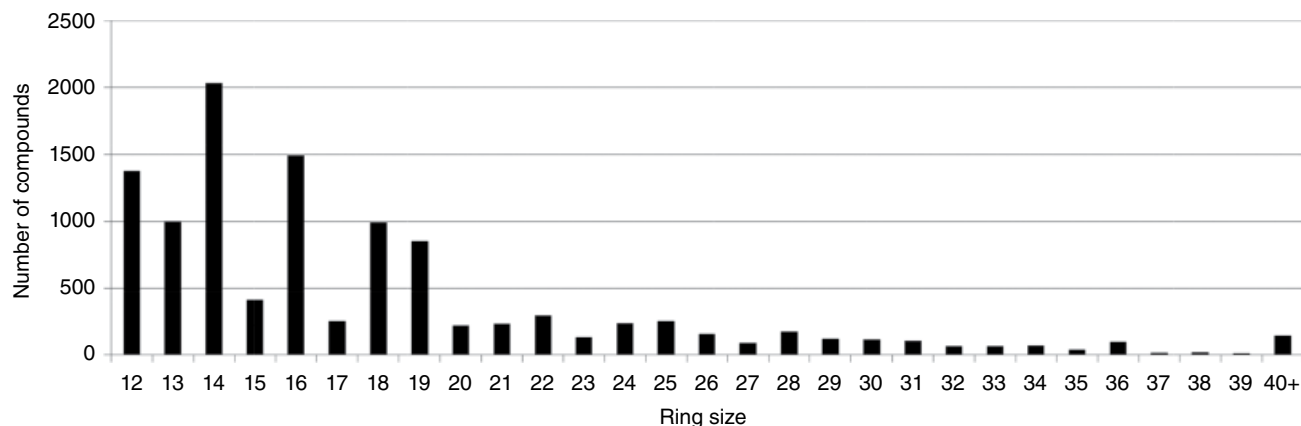
Figure 4.4 Statistical analysis of the abundance of described natural macrocycles with respect to ring size. As expected, the larger the ring, the lower the abundance as a trend. However, with some relevant oscillations, disfavoring, for example, uneven smaller macrocycles (13, 15, 17 members). See text for a detailed discussion [3, 4].

(12-, 14-, 16-, 18-membered rings, Figures 4.4 and 4.5). At higher ring sizes, however, this oscillation changes to a frequency of three, having local maxima at a ring size of $3n/3n + 1$ (21/22-, 24/25-, 28/29-membered rings of cyclopeptides/depsipeptides). The mean molecular weight of these MCs oscillates as well. The reason for this oscillation is that most MCs are biopolymers. Depending on the average number of atoms contributed to the compound by each monomer of the underlying basic pathway, adding another monomer to a macrocyclic ring leads to a more or less fixed increase of the ring size. This implies that most of the smaller macrocycles are built of monomers contributing an even number to the ring size. In contrast, for most medium-sized macrocycles, the monomers seem to contribute three atoms to the macrocycle. These oscillations obviously correlate with their biochemical pathway of origin, mainly the polyketide or terpene synthase pathways for the "smaller," and absolutely and also relatively lighter, macrocycles versus peptide structures with mass-adding side chains for the medium ones (see section 4.2).

Giordanetto and Kihlberg [105] investigated the properties of more than 100 macrocyclic drugs and clinical candidates with respect to their oral bioavailability (see also Chapter 16). An extract of their results is shown in Table 4.1. Herein, only the calculated descriptors of macrocyclic drugs in comparison to small molecule drugs already registered are displayed as an example.

Although the authors emphasize that the current number (34) of orally administered macrocycles is low, they could show that their molecular weights reach up to 1 kDa and the polar surface areas up to 250 Å. Outliers from these values are cyclic peptoids like cyclosporine A and its analogs [106–108] and voclosporin [109, 110]. Due to *N*-alkyl substitutions in the backbone, these have significantly fewer hydrogen bonds and therefore higher

lipophilicities than the other ones studied. Alternatively, the formation of intramolecular hydrogen bonds [106, 107] will result in higher lipophilicity allowing an over-proportional membrane permeability [111, 112], which has already been discussed elsewhere (Figure 4.7) [3, 4, 113].

The functional role of intramolecular hydrogen bonds on ADME properties, especially membrane permeability, was also investigated by Bockus *et al.* (see also Chapter 3) [114]. They could demonstrate that the octanol–water partitioning correlates well with cell permeability. These results were supported by NMR investigations and the measurements of effective log*D*, an HPLC-based predictor of lipophilicity [115], and a supercritical fluid chromatography technique for peptides called EPSA [116, 117].

Another example where increased lipophilicity increases biological activity, whereas more polar moieties reduce it, is also one of the most interesting outcomes of the analysis of SAR of erythromycin-based motilin agonists (Figure 4.8) published by Shaw *et al.* [118].

Other systematic studies of SAR and calculation of lipophilicity-related properties have been performed by Vendeville *et al.* [119], Raboisson *et al.* [120], and Parsy *et al.* [121] for macrocyclic hepatitis C virus (HCV) NS3/4A protease inhibitors (Figure 4.9). Again, these papers show that the introduction of more lipophilic moieties into the macrocycle results in higher bioavailability for the therapeutic application, here targeting the liver.

In 2012, Kopp *et al.* [122] established a modular oxidative ring expansion approach to access a library of MCs defined by them to have at least a 10-membered ring. Based on an analysis and comparison with natural lactones and lactams, such as apicularen A (Figure 4.10a), iriomoteolide 3a, pinolidoxin (Figure 4.10b), fluvirucin A1,

(a)

(b)

(c)
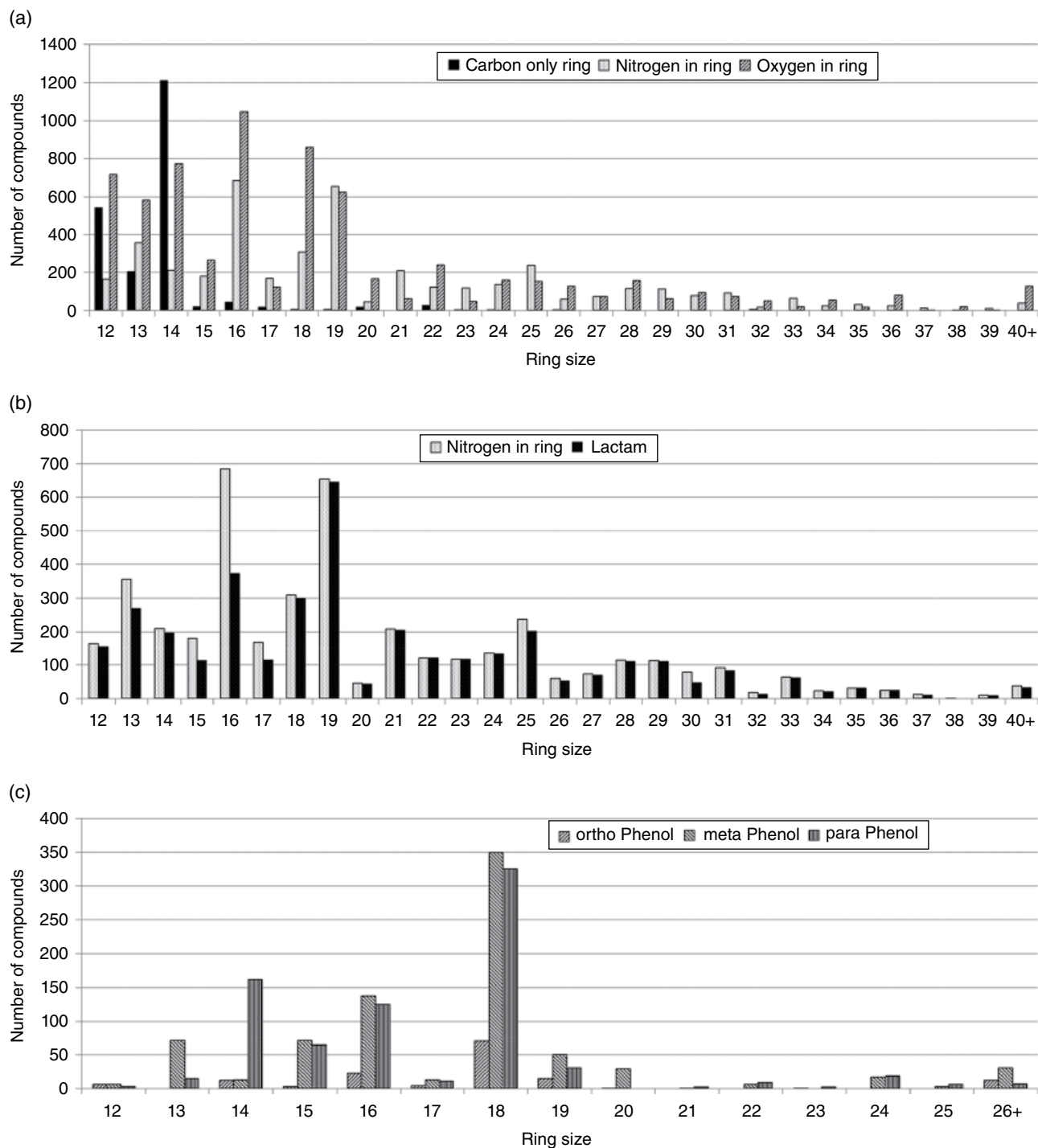
Figure 4.5 (a) Carbon-only rings correlate with abundance of terpenoids, (b) non-lactam nitrogens are predominantly located in smaller macrocycles, (c) analysis of non-lactone oxygens: these are mostly phenol ethers with a dominance of 14-membered cyclopeptide alkaloids [3, 4].

decarestrictine D (Figure 4.10c), and others, they synthesized related macrocycles with different ring sizes (Figure 4.10d). Following their synthetic approach, they performed a chemoinformatic comparison of the synthesized library and a set of macrocyclic and non-macrocyclic drugs, drug-like substances, and natural products, a total of 176 compounds. Principal component analysis (PCA) was performed for 20 descriptors, and principal moment of inertia (PMI) analyses [123] were used to compare the shapes of these compounds.
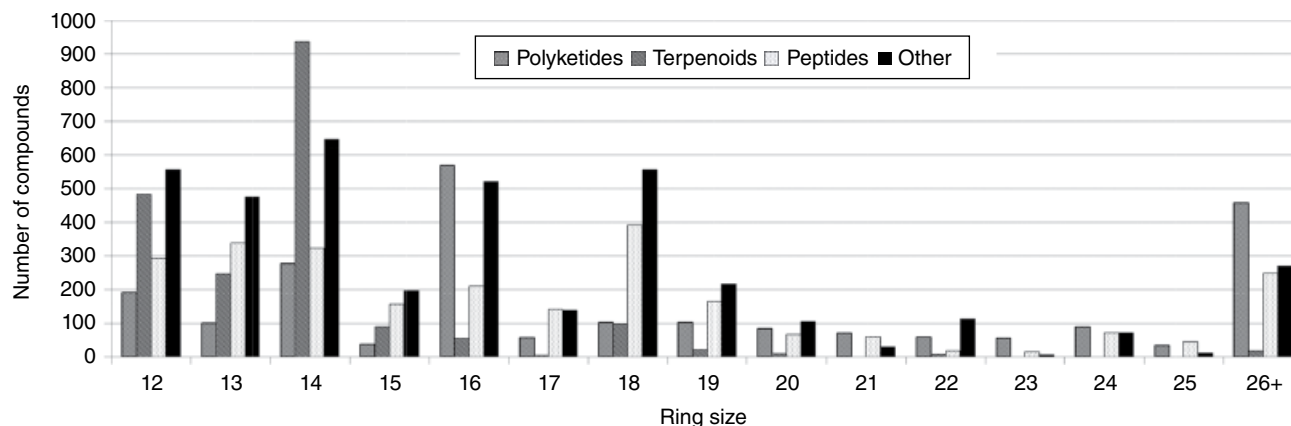
Figure 4.6 Ring size distribution of macrocycles depends on their biosynthetic origin [3, 4].

Table 4.1 Extract of calculated descriptors of registered drugs.

Class	N	HBD	PSA	cLogP	MW
Oral (small drugs)	1589	2	74	2.2	322
Oral (macrocycles)	18	4	212	4.4	852
Parenteral (macrocycles)	45	14	417	0.6	1126

Source: Gasteiger [103]. Reproduced with permission of Wiley.
cLogP, calculated logP; HBD, hydrogen bond donors; MW, molecular mass; N, number of registered drugs; PSA, polar surface area.

Figure 4.7 Conformational changes and changes in hydrogen bonding of "chameleon macrocycles" can overcome the rule of five to some extent. Source: Adapted from Rezai et al. [113]. Reproduced with permission of American Chemical Society.

Figure 4.8 Synthesized and tested erythromycin derivatives with lipophilic and polar substituents (R) investigated by Shaw et al. Source: Shaw et al. [118]. Reproduced with permission of American Chemical Society.

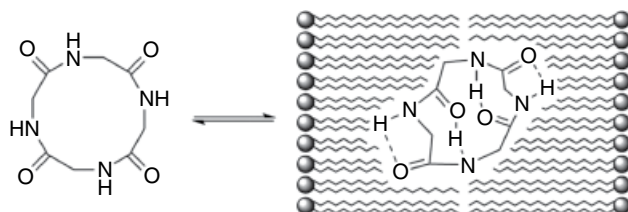From the PCA, they deduced that the parameters describing the hydrophobicity and the aromaticity are the most important ones for a positioning of the compounds in the drug-like library reference sets. For the aim to analyze and characterize the 3D-shaped character of macrocycles, the authors performed a conformational analysis of the compounds using first CORINA [124, 125] and subsequently catConf [126].

All conformations within an energy threshold of 3 kcal/mol over the most favored one were calculated, but only the most stable one was used in the PMI analysis. In this analysis, the compounds were placed in a triangle with regard to rod-, sphere- or disk-like shape. They concluded that—in comparison to the drug reference set—

the MCs, which included approved drugs as well, cluster further from the rod shape but rather have a higher degree of sphere-like character. This may have an impact on the abilities of these compounds to address challenging biological targets like protein–protein interactions [127–129] (see Chapter 8).

It is widely assumed that as a result of macrocyclization, conformational flexibility is reduced in comparison to related noncyclic structures, which should lead to diminished entropy loss when binding such a predefined conformer to a target and thus should enhance affinity [3, 4].

Systematic theoretical conformational analyses of highly flexible organic compounds including macrocycles are rare and still a challenge in computational chemistry, although modern techniques have been developed and applied (Bartelt, R., Brandt, W., Haupt, H., and Wessjohann, L. A. Statistical analysis of macrocycles. To be submitted) [130]. However, there are some examples where conformational flexibility in relation to biological

effects was studied rather systematically. Although there is no relation to a natural product, one nice example was given by Dinsmore *et al.* [131, 132]. They constructed macrocycles as potent inhibitors for farnesyltransferases, potentially relevant as antitumor agents (Figure 4.11). Indeed, the binding affinity of the cyclic compound (i) is about four orders of magnitude higher than that of the related linear one (ii), likely caused by reducing the number of flexible bonds from seven to three.
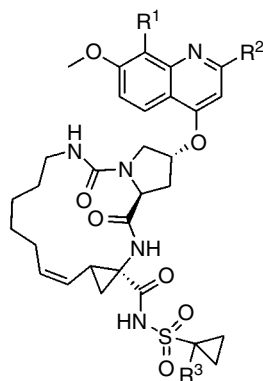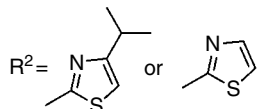
However, simple reduction of structural flexibility does not per se lead to pharmaceutical drug activity; it is the (close to) ideal binding conformation that must be highly populated in the macrocycle to achieve such an improvement (for another case study, see Chapter 18). Thus, even small structural changes leading to the wrong preferred conformer can be detrimental. An example is the influence of ring size by modification of the amino acid residues at several positions of the autoinducer peptide AIP (Figure 4.12), which was studied in relation to gene regulation mechanisms, including virulence factors in *Staphylococcus aureus* [133].

Even minor changes like the insertion of a single methylene bridge in the ring caused an almost complete loss of activity. Comparisons of linear and cyclic compounds and related SAR have also been reported by Gao and Kodadek in 2015 [134]. Rather surprisingly, they could show that macrocyclization in their cases was indeed advantageous but only when the ring contained 17 atoms and not 20 or 23 atoms (Figure 4.13).

4.4 Case Studies: Selected Natural Macrocycles of Special Relevance in Medicinal Chemistry

Besides statistical analyses and prediction of common properties or descriptors by means of chemoinformatic methods, SAR analysis with regard to biological/pharmaceutical activities is another challenging task for which chemoinformatics and molecular modeling can be applied. An overview about quantitative SAR (QSAR) of

$R^1 = $ H, Cl, Me $\quad R^3 = $ H, Me

$R^2 = $

Figure 4.9 Macrocyclic hepatitis C virus NS3/4A protease inhibitors used for SAR studies. Source: Vendeville *et al.* [119], Raboisson *et al.* [120], and Parsy *et al.* [121]. Reproduced with permission of American Chemical Society & Elsevier.

(a)

(b)

(c)

(d)

$X = $ O, NNs $n = $ 1,2,3

$R^1 = $ Ph, $R^2 = $ TBS

Figure 4.10 Based on natural product lactones, (a) apicularen A, (b) pinolidoxin, (c) decarestrictine D, and (d) related artificial macrocycles were synthesized by Kopp *et al.* Source: Kopp *et al.* [122].

Figure 4.11 Structures of macrocycle **1** in comparison to a linear analog **2** according to Dinsmore *et al.* Source: Dinsmore *et al.* [132]. Reproduced with permission of American Chemical Society.

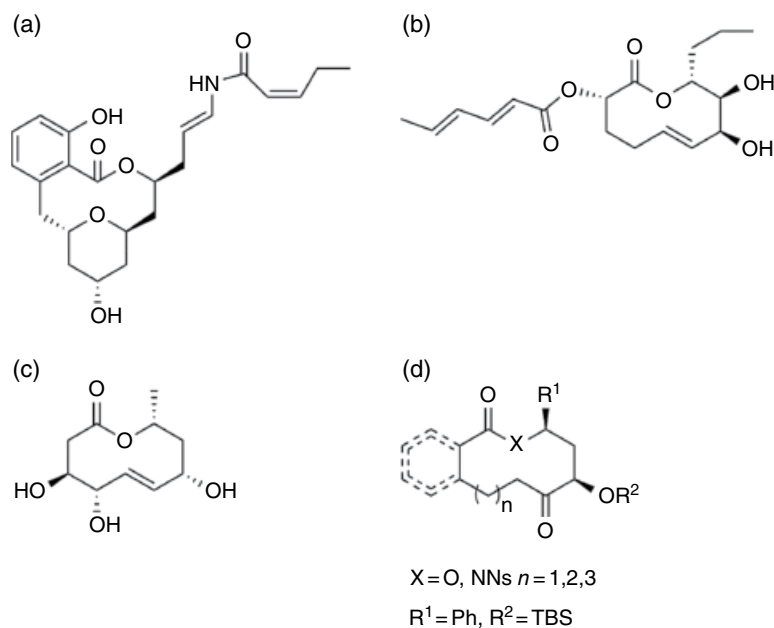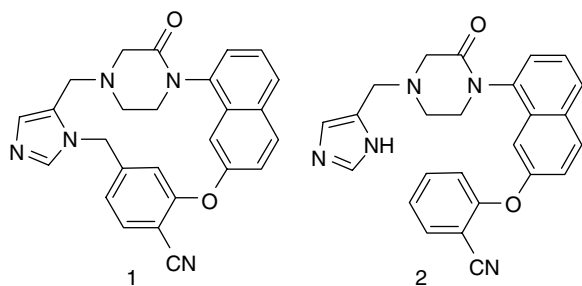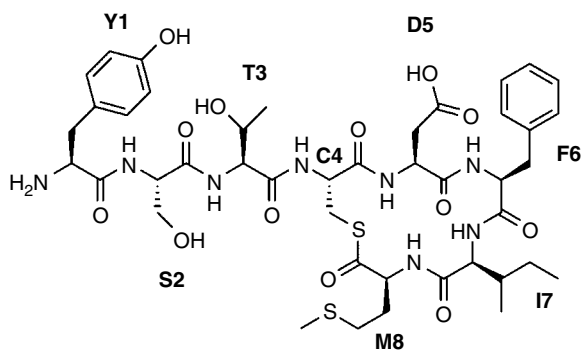**Figure 4.12** Structure of the autoinducer peptide (AIP). The macrocycle was constrained by F6P and I7P substitutions, enlarged by hβ-Met, hβ-Ile, hβ-Phe, hβ-Asp, and others, and reduced by ΔF6 and ΔI7. Source: Johnson *et al.* [133]. Reproduced with permission of Wiley.
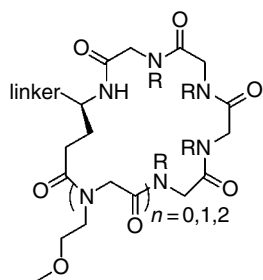

Figure 4.13 Macrocyclic synthetic peptoids ($R = 17$ different amine side chains) with ring sizes 17 ($n = 0$), 20 ($n = 1$), and 23 ($n = 2$) atoms [134].

macrocycles related to drug action was already given by Brandt *et al.* in 2010 [4]. Herein, known aspects of QSAR related to anticancer activities, antibiotics, HIV treatments, and other diseases are reviewed.

Recently, the SAR of heterocycle-containing macrocycles have been discussed by Wahyudi *et al.* [135]. They analyzed natural macrocycles and structural modifications thereof that influence the biological activity with regard to antitumor (e.g., sansalvamide A, sanguinamide

B, mechercharmycin A), antibacterial (thiomuracin and baringolin), and antiparasitic activities (aerocyclamide, balgacycamide, venturamide). Systematically, they analyzed the relationship between biological activity and (i) changing the type of heterocycle, (ii) removing or introducing heterocycles causing more rigid macrocycles, and (iii) altering amino acids by switching chirality, N-methylation, or simply an exchange of the natural amino acid side chains. In their overall conclusion, they emphasize that the preferred conformations are influenced by modifications of the stereochemistry or by changes in rigidity. Further, in their case studies from the inclusion of heterocycles within the cyclic backbone of the macrocycles, conformations, as defined by stereo-elements and rigidity, were the dominant factors for biological activity (or its absence).

The analysis of SAR based on docking studies to target proteins is another valuable tool of molecular modeling or chemoinformatics, although there is still a methodological challenge to predict affinities/activities of large and—despite the macrocyclization—often rather flexible ligands based on theoretical scoring functions [136–141]. A nice example for rational drug design by docking studies and subsequent X-ray structure analysis was given by Tsantrizos *et al.* in 2003 [142]. Based on the known activity of small natural peptides as inhibitors for the HCV NS3 protease, relevant for the treatment of chronic HCV infections, the authors designed *de novo* macrocycles (Figure 4.14). These designed macrocycles (B) exhibited a 2- to 50-fold higher potency in comparison to the linear peptides (A), which led to the development of several related macrocycles now in clinical development [143, 144].

Similar studies, that is, docking and analyses of SAR, have been performed by Hussain *et al.* [145] for the design of anticancer drugs based on actin-binding aplyronines, or natural marine macrolides. However, eventually they could show that the activities of these compounds are not related to the structure of the macrocycle itself but rather to the binding of the extra-cyclic tail. Thus, these studies will not be discussed in more detail here.

Wender *et al.* [146, 147] investigated bryostatin and analogs. Bryostatin 1 (Figure 4.15a) is in clinical trials for the treatment of cancer and Alzheimer's disease. Bryostatins have been obtained from the marine bryozoan *Bugula neritina* [148]. Isolation from natural sources often yields only a very small amount of the active compound, which is not sufficient and economically viable, as is the case here. Synthesis of a bryostatin with many stereocenters requires about 40 steps [149–151]. By means of extensive conformational investigations and comparison with the X-ray structure of bryostatin 1, analogs could be designed (Figure 4.15b)
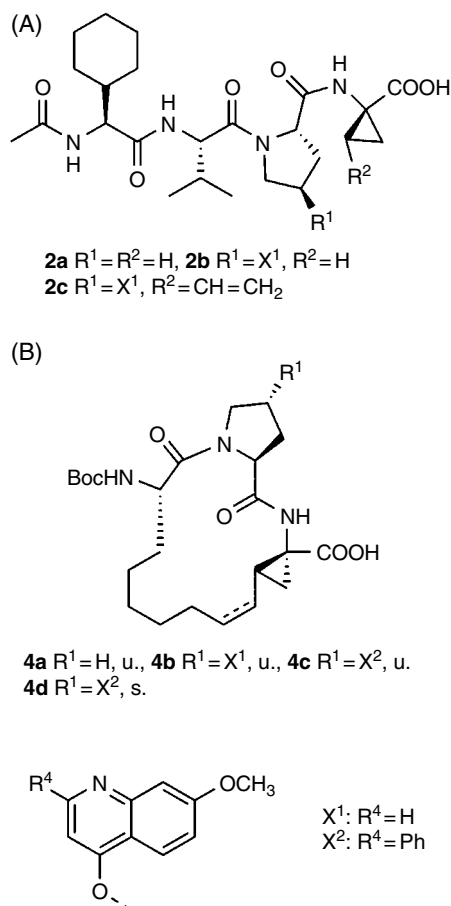
(A)

2a R^1=R^2=H, **2b** R^1=X^1, R^2=H
2c R^1=X^1, R^2=CH=CH$_2$

(B)

4a R^1=H, u., **4b** R^1=X^1, u., **4c** R^1=X^2, u.
4d R^1=X^2, s.

X^1: R^4=H
X^2: R^4=Ph

Figure 4.14 Macrocycles (B, **4**) designed on the basis of linear peptides (A, **2**) as inhibitors for the hepatitis C virus NS3 protease. u.=unsaturated, s.=saturated bridge. IC$_{50}$ values (μM)=**2a** >1000, **2b**=1.4, **2c**=0.047, **4a**=400, **4b**=0.024, **4c**=0.011, **4d**=0.028. Source: Adapted from Tsantrizos *et al.* [142]. Reproduced with permission of Wiley.

(a)   (b)

Spacer domain
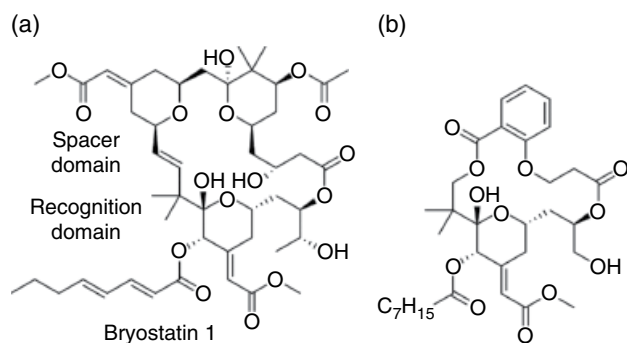
Recognition domain

Bryostatin 1

Figure 4.15 (a) Structure of natural bryostatin (**1**) and (b) a simplified active analog derived by computer-guided design (Source: Adapted from Wender *et al.* [146]). The upper part of the compounds represents the spacer domain, while the lower one, the little changed recognition site.

[146]. Based on the superposition for the structural elements representing the recognition site for binding to the target, protein kinase C, a nice agreement between natural bryostatin 1 and the designed analogs binding mode could be obtained. The measured activity of the analogs binding mode is almost in the same range (K_i (PKCδ and PKC βI) as that of natural bryostatin 1 with **a**=1.1 and 1.0 nM, and for the derivative **b**=18 and 24 nM). However, the gained advantage of the new structure is its relative chemical simplicity (e.g., six stereocenters were removed) in the spacer domain. The authors considered this scaffold as a promising lead for further development.

Binding of bryostatin to protein kinase C delta has been studied by Thangsunan *et al.* [152] with molecular dynamics simulations. Despite the detected formation of several hydrogen bonds between bryostatin and the target enzyme, they could show that backbone fluctuations may influence interactions between a tryptophan and a histidine residue. The authors state that these observed dynamic fluctuations might be of potential benefit for further drug design of new protein kinase inhibitors.

Mitose-inhibiting polyketides that are widely used and tested for anticancer therapy as well as other areas are epothilones and derivatives thereof (Figure 4.16) [154–165]. Epothilones, 16-membered macrocyclic lactones, were discovered by Höfle in 1987 from the myxobacterium *Sorangium cellulosum* [166]. From this time on, many derivatives have been synthesized and tested for biological activity as micro-tubulin stabilizing anticancer agents [167], for example, by the groups of Altmann [168–173], Nicolaou [174–178], and Wessjohann [179–183]. Therein, based on systematic variations of structural elements by chemical synthesis and experimental measurements of their bioactivities, some SAR could be derived. Deeper insights into QSAR, however, could be obtained by docking studies to the protein structure [184] of α,β-tubulin [156, 185–188] and by CoMFA investigations [153].

Navarrete *et al.* [156] investigated the drug resistance of β-tubulin mutations based on molecular modeling studies, including molecular dynamics simulations of
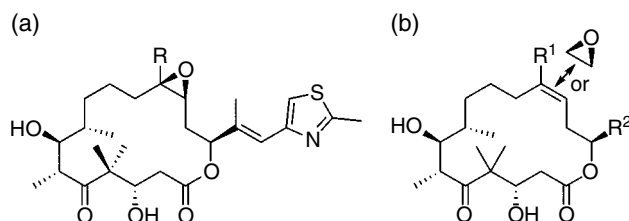
(a)   (b)

Figure 4.16 Structures of (a) epothilone A (R=H), B (R=Me) and (b) basic structure of epothilone derivatives with 68 different substituents R^1 and R^2 used for CoMFA by Yuan *et al.* Source: Yuan *et al.* [153]. Reproduced with permission of Wiley.

tubulin complexes with epothilone B (Figure 4.16a). They could show that tubulin mutations cause both changes in the protein conformations and in the binding arrangements of epothilone in the binding pocket. These results delivered new insights into SAR of epothilones and explained the loss of activity for epothilone B against cancer cells that contain tubulin mutants. These results altogether can now serve as a basis for the rational design of more potent therapeutic tubulin-binding drugs [156].

Yuan *et al*. [153] investigated the SAR of 68 epothilone derivatives (Figure 4.16b) based on docking studies and subsequent CoMFA investigations, resulting in a rather good predictive cross-validated value ($q^2 = 0.784$) between calculated fields and experimental tubulin-polymerization activities. In addition to this correlation, which enables the prediction of the activity for the design of new analogs, they could show that the nitrogen atom of the thiazole ring, which is an essential moiety for activity (Figure 4.16a), can form a hydrogen bond with His[227] of α,β-tubulin.

Docking studies of epothilones to tubulin have also been performed by Kamel and Kolinski [186]. They could show that an alternative docking pose in comparison to the one in the protein X-ray structure (PDB-code 1TVK) [184], that is, interaction of the thiazole nitrogen atom with the backbone NH group of Gly[360] instead of with His[227], may explain additional facets of the SAR.

Finally, an important property of macrocycles in biology and medicine not yet discussed is their ability to selectively complex ions [189]. This property is quite often used for labeling tumor cells [190–192] and in other applications [193], such as in nuclear medicine [194, 195]. Many theoretical calculations have been published to predict the affinity of macrocycles to specific ions, mainly cations [196–201]. Some selected examples are shown in Figure 4.17.
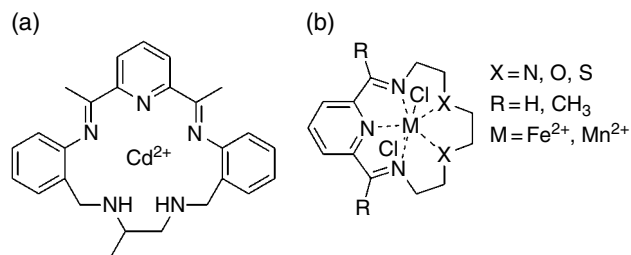

X = N, O, S
R = H, CH$_3$
M = Fe^{2+}, Mn^{2+}

Figure 4.17 (a) Example of a synthetic macrocycle complexing cadmium (and zinc ions) with antibacterial activity. Source: Adapted from Keypour *et al*. [199]. (b) Example of a macrocycle able to complex iron or manganese ions tested for potential use in diagnostics and for antimicrobial activity. Source: Adapted from Gavey *et al*. [196]. Reproduced with permission of Elsevier.

The few examples reviewed here clearly show how chemoinformatics and modeling techniques, such as docking studies, can contribute essential information for drug design to improve their properties (mostly bioavailability or potency) and help to analyze and understand SAR of MCs. Since many of the compound classes or even single compounds are used in more than just one special field of application, there are many open and challenging questions where theoretical methods can help enable further developments in rational drug design. Especially in macrocycles, some additional aspects have to be taken in considerations, such as transannular interactions, inside-out conformational switching, and other complicating factors not found in most linear drugs.

A nice general overview about current challenges in drug development based particularly on natural products including a multitude of macrocycles was given by Newman and Cragg [202, 203] and recently by Cragg *et al*. [204]. The applications of macrocycles for the treatment of many diseases with a focus on cancer are discussed in these papers.

References

1 Newman, D. J. C.; Cragg, G.M. Bioactive Macrocycles from Nature. In *Macrocycles in Drug Discovery*, Levin, J., Ed. The Royal Society of Chemistry: Cambridge, **2013**; Vol. *40*, pp 1–36.

2 Driggers, E. M.; Hale, S. P.; Lee, J.; Terrett, N. K. The exploration of macrocycles for drug discovery—An underexploited structural class. *Nat. Rev. Drug Discov.* **2008**, *7*, 608–624.

3 Wessjohann, L. A.; Ruijter, E.; Garcia-Rivera, D.; Brandt, W. What can a chemist learn from nature's macrocycles?—A brief, conceptual view. *Mol. Divers.* **2005**, *9*, 171–186.

4 Brandt, W.; Haupt, V. J.; Wessjohann, L. A. Chemoinformatic analysis of biologically active macrocycles. *Curr. Top. Med. Chem.* **2010**, *10*, 1361–1379.

5 Kopp, F.; Marahiel, M. A. Macrocyclization strategies in polyketide and nonribosomal peptide biosynthesis. *Nat. Prod. Rep.* **2007**, *24*, 735–749.

6 Otsuka, M.; Ichinose, K.; Fujii, I.; Ebizuka, Y. Cloning, sequencing, and functional analysis of an iterative type I polyketide synthase gene cluster for biosynthesis of the antitumor chlorinated polyenone neocarzilin in "*Streptomyces carzinostaticus*". *Antimicrob. Agents Chemother.* **2004**, *48*, 3468–3476.

7 Gokhale, R. S.; Hunziker, D.; Cane, D. E.; Khosla, C. Mechanism and specificity of the terminal thioesterase domain from the erythromycin polyketide synthase. *Chem. Biol.* **1999**, *6*, 117–125.

8 Crawford, J. M.; Thomas, P. M.; Scheerer, J. R.; Vagstad, A. L.; Kelleher, N. L.; Townsend, C. A. Deconstruction of iterative multidomain polyketide synthase function. *Science* **2008**, *320*, 243–246.

9 Li, Y. R.; Xu, W.; Tang, Y. Classification, prediction, and verification of the regioselectivity of fungal polyketide synthase product template domains. *J. Biol. Chem.* **2010**, *285*, 22762–22771.

10 Felnagle, E. A.; Jackson, E. E.; Chan, Y. A.; Podevels, A. M.; Berti, A. D.; McMahon, M. D.; Thomas, M. G. Nonribosomal peptide synthetases involved in the production of medically relevant natural products. *Mol. Pharm.* **2008**, *5*, 191–211.

11 Floss, H. G.; Yu, T. W. Rifamycin-mode of action, resistance, and biosynthesis. *Chem. Rev.* **2005**, *105*, 621–632.

12 Vetcher, L.; Tian, Z. Q.; McDaniel, R.; Rascher, A.; Revill, W. P.; Hutchinson, C. R.; Hu, Z. Rapid engineering of the geldanamycin biosynthesis pathway by Red/ET recombination and gene complementation. *Appl. Environ. Microbiol.* **2005**, *71*, 1829–1835.

13 Hashimoto, T.; Hashimoto, J.; Teruya, K.; Hirano, T.; Shin-Ya, K.; Ikeda, H.; Liu, H. W.; Nishiyama, M.; Kuzuyama, T. Biosynthesis of versipelostatin: Identification of an enzyme-catalyzed [4+2]-cycloaddition required for macrocyclization of spirotetronate-containing polyketides. *J. Am. Chem. Soc.* **2015**, *137*, 572–575.

14 Mast, Y.; Weber, T.; Golz, M.; Ort-Winklbauer, R.; Gondran, A.; Wohlleben, W.; Schinko, E. Characterization of the "pristinamycin supercluster" of *Streptomyces pristinaespiralis*. *Microb. Biotechnol.* **2011**, *4*, 192–206.

15 Rehm, S. J.; Graham, D. R.; Srinath, L.; Prokocimer, P.; Richard, M. P.; Talbot, G. H. Successful administration of quinupristin/dalfopristin in the outpatient setting. *J. Antimicrob. Chemother.* **2001**, *47*, 639–645.

16 Brandt, W.; Bräuer, L.; Günnewich, N.; Kufka, J.; Rausch, F.; Schulze, D.; Schulze, E.; Weber, R.; Zakharova, S.; Wessjohann, L. Molecular and structural basis of metabolic diversity mediated by prenyldiphosphate converting enzymes. *Phytochemistry* **2009**, *70*, 1758–1775.

17 Hanson, J. R. *Terpenoids and Steroids Volume 12*, RSC publishing: London, **1983**; pp 199–201.

18 Farag, M. A.; Porzel, A.; Al-Hammady, M. A.; Hegazy, M. E.; Meyer, A.; Mohamed, T. A.; Westphal, H.; Wessjohann, L. A. Soft corals biodiversity in the Egyptian Red Sea: A comparative MS and NMR metabolomics approach of wild and aquarium grown species. *J. Proteome Res.* **2016**, *15*, 1274–1287.

19 Haagen-Smit, A. J.; Wang, T. H.; Mirov, N. T. Composition of gum turpentines of pines. XIII. A report on *Pinus albicaulis*. *J. Am. Pharm. Assoc.* **1951**, *40*, 557–559.

20 Roberts, D. L.; Rowland, R. L. Macrocyclic diterpenes—alpha—and beta-4,8,13-duvatriene-1,3-diols from tobacco. *J. Org. Chem.* **1962**, *27*, 3989–3995.

21 Chang, J. Y.; El-Razek, M. H. A.; Shen, Y. C. Verticillane and norverticillane diterpenoids from the formosan soft coral *Cespitularia hypotentaculata*. *Helv. Chim. Acta* **2009**, *92*, 2146–2154.

22 Nagashima, F.; Wakayama, K.; Ioka, Y.; Asakawa, Y. New ent-verticillane diterpenoids from the Japanese liverwort *Jackiella javanica*. *Chem. Pharm. Bull. (Tokyo)* **2008**, *56*, 1184–1188.

23 Ferchmin, P. A.; Andino, M.; Salaman, R. R.; Alves, J.; Velez-Roman, J.; Cuadrado, B.; Carrasco, M.; Torres-Rivera, W.; Segarra, A.; Martins, A. H.; Lee, J. E.; Eterovic, V. A. 4R-cembranoid protects against diisopropylfluorophosphate-mediated neurodegeneration. *Neurotoxicology* **2014**, *44*, 80–90.

24 Nacoulma, A. P.; Megalizzi, V.; Pottier, L. R.; De Lorenzi, M.; Thoret, S.; Dubois, J.; Vandeputte, O. M.; Duez, P.; Vereecke, D.; El Jaziri, M. Potent antiproliferative cembrenoids accumulate in tobacco upon infection with *Rhodococcus fascians* and trigger unusual microtubule dynamics in human glioblastoma cells. *PLoS One* **2013**, *8*, e77529.

25 Thao, N. P.; Luyen, B. T. T.; Ngan, N. T. T.; Song, S. B.; Cuong, N. X.; Nam, N. H.; Kiem, P. V.; Kim, Y. H.; Minh, C. V. New anti-inflammatory cembranoid diterpenoids from the Vietnamese soft coral *Lobophytum crassum*. *Bioorg. Med. Chem. Lett.* **2014**, *24*, 228–232.

26 Yan, N.; Du, Y. M.; Liu, X. M.; Zhang, H. B.; Liu, Y. H.; Zhang, P.; Gong, D. P.; Zhang, Z. F. Chemical structures, biosynthesis, bioactivities, biocatalysis and semisynthesis of tobacco cembranoids: An overview. *Ind. Crop. Prod.* **2016**, *83*, 66–80.

27 Farag, M. A., Al-Mahdy, D. A., Meyer, A., Westphal, H., Wessjohann, L. A. Metabolomics reveal biotic and abiotic elicitor effect on the soft coral *Sarcophyton ehrenbergii* terpenoid content. *Sci. Rep. (Nat.)* **2017**, *7*. doi:10.1038/s41598-017-00527-8.

28 Leadlay, P. F. Combinatorial approaches to polyketide biosynthesis. *Curr. Opin. Chem. Biol.* **1997**, *1*, 162–168.

29 McDaniel, R.; Ebert-Khosla, S.; Hopwood, D. A.; Khosla, C. Rational design of aromatic polyketide natural products by recombinant assembly of enzymatic subunits. *Nature* **1995**, *375*, 549–554.

30 Wong, F. T.; Khosla, C. Combinatorial biosynthesis of polyketides—A perspective. *Curr. Opin. Chem. Biol.* **2012**, *16*, 117–123.

31 Ridley, C. P.; Lee, H. Y.; Khosla, C. Evolution of polyketide synthases in bacteria. *Proc. Natl. Acad. Sci. U. S. A.* **2008**, *105*, 4595–4600.

32 Anand, S.; Prasad, M. V.; Yadav, G.; Kumar, N.; Shehara, J.; Ansari, M. Z.; Mohanty, D. SBSPKS: Structure based sequence analysis of polyketide synthases. *Nucleic Acids Res.* **2010**, *38*, W487–W496.

33 Tae, H.; Kong, E. B.; Park, K. ASMPKS: An analysis system for modular polyketide synthases. *BMC Bioinformatics* **2007**, *8*, 327.

34 Yadav, G.; Gokhale, R. S.; Mohanty, D. Computational approach for prediction of domain organization and substrate specificity of modular polyketide synthases. *J. Mol. Biol.* **2003**, *328*, 335–363.

35 Kitsche, A.; Kalesse, M. Configurational assignment of secondary hydroxyl groups and methyl branches in polyketide natural products through bioinformatic analysis of the ketoreductase domain. *ChemBioChem* **2013**, *14*, 851–861.

36 Bai, R.; Cichacz, Z. A.; Herald, C. L.; Pettit, G. R.; Hamel, E. Spongistatin 1, a highly cytotoxic, sponge-derived, marine natural product that inhibits mitosis, microtubule assembly, and the binding of vinblastine to tubulin. *Mol. Pharmacol.* **1993**, *44*, 757–766.

37 Smith, A. B.; Lin, Q.; Doughty, V. A.; Zhuang, L.; McBriar, M. D.; Kerns, J. K.; Boldi, A. M.; Murase, N.; Moser, W. H.; Brook, C. S.; Bennett, C. S.; Nakayama, K.; Sobukawa, M.; Lee Trout, R. E. Spongipyran synthetic studies. Total synthesis of (+)-spongistatin 2. *Tetrahedron* **2009**, *65*, 6470–6488.

38 Kirby, J.; Nishimoto, M.; Park, J. G.; Withers, S. T.; Nowroozi, F.; Behrendt, D.; Rutledge, E. J.; Fortman, J. L.; Johnson, H. E.; Anderson, J. V.; Keasling, J. D. Cloning of casbene and neocembrene synthases from Euphorbiaceae plants and expression in *Saccharomyces cerevisiae*. *Phytochemistry* **2010**, *71*, 1466–1473.

39 Meguro, A.; Tomita, T.; Nishiyama, M.; Kuzuyama, T. Identification and characterization of bacterial diterpene cyclases that synthesize the cembrane skeleton. *ChemBioChem* **2013**, *14*, 316–321.

40 Lin, X. Y.; Hezari, M.; Koepp, A. E.; Floss, H. G.; Croteau, R. Mechanism of taxadiene synthase, a diterpene cyclase that catalyzes the first step of taxol biosynthesis in *Pacific yew*. *Biochemistry* **1996**, *35*, 2968–2977.

41 Koksal, M.; Jin, Y.; Coates, R. M.; Croteau, R.; Christianson, D. W. Taxadiene synthase structure and evolution of modular architecture in terpene biosynthesis. *Nature* **2011**, *469*, 116–120.

42 Cseke, L. J. K.; Kirakosyan, A.; Kaufman, P. B.; Warber, S.; Duke, J. A.; Brielmann, H. L. *Natural Products from Plants*. 2nd ed.; CRC Press: Boca Raton, **2006**.

43 Williams, D. H.; Stone, M. J.; Hauck, P. R.; Rahman, S. K. Why are secondary metabolites (natural products) biosynthesized? *J. Nat. Prod.* **1989**, *52*, 1189–1208.

44 Duchesne, E. Contribution à l'étude de la concurrence vitale chez les microorganisms antagonisme entre les microbes et les moisissures. thèse de médecine de Lyon n° 59, **1897**.

45 Sehgal, S. N.; Baker, H.; Vezina, C. Rapamycin (Ay-22,989), a new antifungal antibiotic. 2. Fermentation, isolation and characterization. *J. Antibiot.* **1975**, *28*, 727–732.

46 Vezina, C.; Kudelski, A.; Sehgal, S. N. Rapamycin (Ay-22,989), a new antifungal antibiotic. 1. Taxonomy of producing streptomycete and isolation of active principle. *J. Antibiot.* **1975**, *28*, 721–726.

47 Singh, K.; Sun, S.; Vezina, C. Rapamycin (AY-22,989), a new antifungal antibiotic. IV. Mechanism of action. *J. Antibiot. (Tokyo)* **1979**, *32*, 630–645.

48 Sehgal, S. N.; Baker, H.; Eng, C. P.; Singh, K.; Vezina, C. Demethoxyrapamycin (AY-24,668), a new antifungal antibiotic. *J. Antibiot. (Tokyo)* **1983**, *36*, 351–354.

49 McAlister, V. C.; Mahalati, K.; Peltekian, K. M.; Fraser, A.; MacDonald, A. S. A clinical pharmacokinetic study of tacrolimus and sirolimus combination immunosuppression comparing simultaneous to separated administration. *Ther. Drug Monit.* **2002**, *24*, 346–350.

50 Jung, K. E.; Lee, Y. J.; Ryu, Y. H.; Kim, J. E.; Kim, H. S.; Kim, B. J.; Kang, H.; Park, Y. M. Effects of topically applied rapamycin and mycophenolic acid on TNCB-induced atopic dermatitis-like skin lesions in NC/Nga mice. *Int. Immunopharmacol.* **2015**, *26*, 432–438.

51 Prado, G. F., Jr.; Ribeiro, E. E.; Melo, P. H.; Pinton, F. A.; Esteves-Filho, A.; Takimura, C. K.; Mariani, J., Jr.; Kajita, L. J.; Marchiori, G.; Araripe Falcao Bde, A.; Galon, M. Z.; Soares, P. R.; Zalc, S.; Lemos, P. A. Clinical performance of a novel ultrathin strut, low-dose, sirolimus-eluting stent with abluminal-only biodegradable polymeric coating for patients undergoing percutaneous coronary intervention in the daily practice. *Cardiovasc. Diagn. Ther.* **2015**, *5*, 414–419.

52 Wijns, W.; Suttorp, M. J.; Zagozdzon, L.; Morice, M. C.; McClean, D.; Stella, P.; Donohoe, D.; Knape, C.; Ormiston, J. Evaluation of a crystalline sirolimus-eluting coronary stent with a bioabsorbable polymer designed for rapid dissolution: Two-year outcomes from the DESSOLVE I and II trials. *EuroIntervention* **2016**, *12*, 352–355.

53 Lim, K. S.; Park, J. K.; Jeong, M. H.; Bae, I. H.; Nah, J. W.; Park, D. S.; Kim, J. M.; Kim, J. H.; Lee, S. Y.; Jang, E. J.; Jang, S.; Kim, H. K.; Sim, D. S.; Park, K. H.; Hong, Y. J.; Ahn, Y.; Kang, J. C. Effect of stents coated with a combination of sirolimus and alpha-lipoic acid in a porcine coronary restenosis model. *J. Mater. Sci. Mater. Med.* **2016**, *27*, 66.

54 Xu, W.; Bi, Y.; Kong, J.; Zhang, J.; Wang, B.; Li, K.; Tian, M.; Pan, X.; Shi, B.; Gu, J.; Jiang, H.; Kong, X.; Li, Z. Combination of an anti-EGFRvIII antibody CH12 with Rapamycin synergistically inhibits the growth of EGFRvIII + PTEN-glioblastoma *in vivo*. *Oncotarget* **2016**, *7*, 24752–24765.

55 Coppock, J. D.; Vermeer, P. D.; Vermeer, D. W.; Lee, K. M.; Miskimins, W. K.; Spanos, W. C.; Lee, J. H. mTOR inhibition as an adjuvant therapy in a metastatic model of HPV + HNSCC. *Oncotarget* **2016**, *7*, 24228–24241.

56 Santini, D.; Tonini, G. Treatment of advanced renal-cell carcinoma. *N. Engl. J. Med.* **2016**, *374*, 888–889.

57 Zheng, H.; Wang, M.; Wu, J.; Wang, Z. M.; Nan, H. J.; Sun, H. Inhibition of mTOR enhances radiosensitivity of lung cancer cells and protects normal lung cells against radiation. *Biochem. Cell Biol.* **2016**, *94*, 213–220.

58 Zhu, Z.; Pang, B.; Iglesias-Bartolome, R.; Wu, X.; Hu, L.; Zhang, C.; Wang, J.; Gutkind, J. S.; Wang, S. Prevention of irradiation-induced salivary hypofunction by rapamycin in swine parotid glands. *Oncotarget* **2016**, *7*, 20271–20281.

59 Zibelman, M.; Mehra, R. Overview of current treatment options and investigational targeted therapies for locally advanced squamous cell carcinoma of the head and neck. *Am. J. Clin. Oncol.* **2016**, *39*, 396–406.

60 Paul, C.; Ho, V. C. Ascomycins in dermatology. *Semin. Cutan. Med. Surg.* **1998**, *17*, 256–259.

61 Paul, C.; Graeber, M.; Stuetz, A. Ascomycins: Promising agents for the treatment of inflammatory skin diseases. *Expert Opin. Investig. Drugs* **2000**, *9*, 69–77.

62 Luger, T. Treatment of immune-mediated skin diseases: Future perspectives. *Eur. J. Dermatol.* **2001**, *11*, 343–347.

63 Goto, T.; Kino, T.; Hatanaka, H.; Nishiyama, M.; Okuhara, M.; Kohsaka, M.; Aoki, H.; Imanaka, H. Discovery of Fk-506, a novel immunosuppressant isolated from *Streptomyces tsukubaensis. Transplant. Proc.* **1987**, *19*, 4–8.

64 Kino, T.; Hatanaka, H.; Hashimoto, M.; Nishiyama, M.; Goto, T.; Okuhara, M.; Kohsaka, M.; Aoki, H.; Imanaka, H. Fk-506, a novel immunosuppressant Isolated from a *Streptomyces* .1. Fermentation, isolation, and physicochemical and biological characteristics. *J. Antibiot.* **1987**, *40*, 1249–1255.

65 Kino, T.; Hatanaka, H.; Miyata, S.; Inamura, N.; Nishiyama, M.; Yajima, T.; Goto, T.; Okuhara, M.; Kohsaka, M.; Aoki, H.; Ochiai, T. Fk-506, a novel immunosuppressant isolated from a *Streptomyces* .2. Immunosuppressive effect of Fk-506 *in vitro. J. Antibiot.* **1987**, *40*, 1256–1265.

66 Horn, D. G.; Trame, M. N.; Hempel, G. The management of hypertensive emergencies in children after stem cell transplantation. *Int. J. Clin. Pharm.* **2011**, *33*, 165–176.

67 Henze, T.; Janzen, R. W. C.; Schumm, F.; Melms, A.; Sieb, J. P.; Köhler, W.; Heidenreich, F.; Tackenberg, B.; Weber-Schöndorfer, C.; Myasth, A. B. D. Immunotherapy for myasthenia gravis and Lambert-Eaton Myasthenic Syndrome part 1: Drug-Induced immunosuppression. *Aktuel. Neurol.* **2010**, *37*, 505–517.

68 Ruzicka, T.; Bieber, T.; Schopf, E.; Rubins, A.; Dobozy, A.; Bos, J. D.; Jablonska, S.; Ahmed, I.; ThestrupPedersen, K.; Daniel, F.; Finzi, A.; Reitamo, S. A short-term trial of tacrolimus ointment for atopic dermatitis. *N. Engl. J. Med.* **1997**, *337*, 816–821.

69 Garcia, D. P.; Alperte, J. I.; Cristobal, J. A.; Orobia, A. J. M.; Muro, E. M.; Valyi, Z.; del Rio, B. J.; Arnao, M. R. Topical tacrolimus ointment for treatment of intractable atopic keratoconjunctivitis: A case report and review of the literature. *Cornea* **2011**, *30*, 462–465.

70 Balicki, I.; Trbolova, A. Clinical evaluation of tacrolimus eye drops for chronic superficial keratitis treatment in dogs. *Bull. Vet. Inst. Pulawy* **2010**, *54*, 251–258.

71 Numerof, R. P.; Asadullah, K. Cytokine and anti-cytokine therapies for psoriasis and atopic dermatitis. *Biodrugs* **2006**, *20*, 93–103.

72 Pariser, D. Topical corticosteroids and topical calcineurin inhibitors in the treatment of atopic dermatitis: Focus on percutaneous absorption. *Am. J. Ther.* **2009**, *16*, 264–273.

73 Schuller, E.; Oppel, T.; Bornhovd, E.; Wetzel, S.; Wollenberg, A. Tacrolimus ointment causes inflammatory dendritic epidermal cell depletion but no Langerhans cell apoptosis in patients with atopic dermatitis. *J. Allergy Clin. Immunol.* **2004**, *114*, 137–143.

74 Shaw, D. W.; Maibach, H. I.; Eichenfield, L. F. Allergic contact dermatitis from pimecrolimus in a patient with tacrolimus allergy. *J. Am. Acad. Dermatol.* **2007**, *56*, 342–345.

75 Stütz, A.; Grassberger, M.; Meingassner, J. G. Development and pre-clinical aspects of pimecrolimus. *Hautarzt* **2003**, *54*, 405–412.

76 Gupta, A. K.; Chow, M. Pimecrolimus: A review. *J. Eur. Acad. Dermatol. Venereol.* **2003**, *17*, 493–503.

77 Wellington, K.; Jarvis, B. Topical pimecrolimus—A review of its clinical potential in the management of atopic dermatitis. *Drugs* **2002**, *62*, 817–840.

78 Wolff, K.; Stuetz, A. Pimecrolimus for the treatment of inflammatory skin disease. *Expert Opin. Pharmacother.* **2004**, *5*, 643–655.

79 Wollina, U.; Hansel, G.; Koch, A.; Abdel-Naser, M. B. Topical pimecrolimus for skin other disease than atopic dermatitis. *Expert Opin. Pharmacother.* **2006**, *7*, 1967–1975.

80 Lutz, A.; Witz, M. A. Antituberculous action of streptovaricin *in vitro* & *in vivo* in the guinea pig; preventive effect. *Ann. Inst. Pasteur (Paris)* **1958**, *94*, 61–68.

81 Luridiana, N. Streptovaricin, a new antibiotic; effects on Mycobacterium tuberculosis *in vitro*. *G. Ital. Della Tuberc.* **1958**, *12*, 142–146.

82 Crabol, Y.; Catherinot, E.; Veziris, N.; Jullien, V.; Lortholary, O. Rifabutin: Where do we stand in 2016? *J. Antimicrob. Chemother.* **2016**, *71*, 1759–1771.

83 Sterling, T. R.; Scott, N. A.; Miro, J. M.; Calvet, G.; La Rosa, A.; Infante, R.; Chen, M. P.; Benator, D. A.; Gordin, F.; Benson, C. A.; Chaisson, R. E.; Villarino, M. E.; Tuberculosis Trials Consortium. Three months of weekly rifapentine plus isoniazid for treatment of *M. tuberculosis* infection in HIV co-infected persons. *AIDS* **2016**, *30*, 1607–1615.

84 Parvez, M. M.; Jung, J. A.; Shin, H. J.; Kim, D. H.; Shin, J. G. Characterization of 22 anti-tuberculosis drugs for the inhibitory interaction potential on organic anionic transporter polypeptides (OATPs) mediated uptake. *Antimicrob. Agents Chemother.* **2016**, *60*, 3096–3105.

85 Parumasivam, T.; Chan, J. G.; Pang, A.; Quan, D. H.; Triccas, J. A.; Britton, W. J.; Chan, H. K. *In vitro* evaluation of inhalable verapamil-rifapentine particles for tuberculosis therapy. *Mol. Pharm.* **2016**, *13*, 979–989.

86 Juarez-Reyes, M.; Gallivan, M.; Chyorny, A.; O'Keeffe, L.; Shah, N. S. Completion rate and side-effect profile of three-month isoniazid and rifapentine treatment for latent tuberculosis infection in an Urban County Jail. *Open Forum Infect Dis.* **2016**, *3*, 220.

87 Rivkin, A.; Rybalov, S. Update on the management of diarrhea-predominant irritable bowel syndrome: Focus on rifaximin and eluxadoline. *Pharmacotherapy* **2016**, *36*, 300–316.

88 Pandrea, I.; Xu, C.; Stock, J. L.; Frank, D. N.; Ma, D.; Policicchio, B. B.; He, T.; Kristoff, J.; Cornell, E.; Haret-Richter, G. S.; Trichel, A.; Ribeiro, R. M.; Tracy, R.; Wilson, C.; Landay, A. L.; Apetrei, C. Antibiotic and antiinflammatory therapy transiently reduces inflammation and hypercoagulation in acutely SIV-infected pigtailed macaques. *PLoS Pathog.* **2016**, *12*, e1005384.

89 Orr, J. G.; Currie, C. J.; Berni, E.; Goel, A.; Moriarty, K. J.; Sinha, A.; Gordon, F.; Dethier, A.; Dillon, J.; Clark, K.; Richardson, P.; Middleton, P.; Patel, V.; Shawcross, D.; Preedy, H.; Aspinall, R. J.; Hudson, M. The impact on hospital resource utilisation of treatment of hepatic encephalopathy with rifaximin-alpha. *Liver Int.* **2016**, *36*, 1295–1303.

90 Kane, J. S.; Ford, A. C. Rifaximin for the treatment of diarrhea-predominant irritable bowel syndrome. *Expert Rev. Gastroenterol. Hepatol.* **2016**, *10*, 431–442.

91 Motaouakkil, S.; Charra, B.; Hachimi, A.; Nejmi, H.; Benslama, A.; Elmdaghri, N.; Belabbes, H.; Benbachir, M. Colistin and rifampicin in the treatment of nosocomial infections from multiresistant *Acinetobacter baumannii. J. Infect.* **2006**, *53*, 274–278.

92 Wan, Y. C.; Li, T.; Han, Y. D.; Zhang, H. Y.; Lin, H.; Zhang, B. Effect of pregnane xenobiotic receptor activation on inflammatory bowel disease treated with rifaximin. *J. Biol. Regul. Homeost. Agents* **2015**, *29*, 401–410.

93 Ericsson, C. D. Safety and tolerability of the antibacterial rifaximin in the treatment of travellers' diarrhoea. *Drug Saf.* **2006**, *29*, 201–207.

94 Pelosini, I.; Scarpignato, C. Rifaximin, a peculiar rifamycin derivative: Established and potential clinical use outside the gastrointestinal tract. *Chemotherapy* **2005**, *51*, 122–130.

95 Lee, S. S.; Meintjes, G.; Kamarulzaman, A.; Leung, C. C. Management of tuberculosis and latent tuberculosis infection in human immunodeficiency virus-infected persons. *Respirology* **2013**, *18*, 912–922.

96 Figueiredo, R.; Moiteiro, C.; Medeiros, M. A.; da Silva, P. A.; Ramos, D.; Spies, F.; Ribeiro, M. O.; Lourenco, M. C. S.; Junior, I. N.; Gaspar, M. M.; Cruz, M. E. M.; Curto, M. J. M.; Franzblau, S. G.; Orozco, H.; Aguilar, D.; Hernandez-Pando, R.; Costa, M. C. Synthesis and evaluation of rifabutin analogs against Mycobacterium avium and H(37)Rv, MDR and NRP *Mycobacterium tuberculosis. Bioorg. Med. Chem.* **2009**, *17*, 503–511.

97 Albrecht, H.; Horsburgh, C. R.; Vernon, A. A. Clinical studies of rifapentine. *Drugs Today* **1999**, *35*, 29–43.

98 DiPietro, N.; Kamal, M.; Abbott, C.; Baril, J. G.; Barrie, W.; Bart, J.; Bilawski, D.; Cameron, W.; Campbell, J.; Chollette, P.; Conway, D.; Cornelson, B.; Dewet, J.; Etzkorn, W.; Fong, I.; Friedland, L.; Gallimore, I.; Genereux, M.; Gill, J.; Hirsz, A.; Hivon, P.; Ho, V.; Hudson, J.; Ip, H. B.; Johnson, K.; Junod, P.; Karr, G.; Kaufhold, R.; Keystone, D.; Kilby, D.; Klein, A.; Lapchinski, E.; Leger, R.; Li, A.; Logue, K.; MacAulay, D.; MacFadden, D.; Mackie, I.; Maki, A.; Martel, A.; McGinnis, R.; McMillan, B.; McPhail, M.; Merkley, B.; Miller, M.; Minish, K.; Moore, D.; Moore, J.; Nguyen, C.; Poldes, A.; Pomer, E.; Rachlis, A.; Rathwell, A.; Ringnalda, J.; Roedde, S.; Runciman, K.; Schlech, W.; Scott, K.; Shafran, S.; Simor, A.; Sinave, C.; Smaill, F.; Smith, J.; Spencer, P.; Tai, S.; Thompson, B.; Tilley, D.; Toma, E.; Uffen, K.; Walmsley, S.; White, J.; Willoughby, B.; Woodfall, B.; Zayid, D. Rifabutin for the prevention of *Mycobacterium avium* complex bacteraemia in AIDS and HIV-positive patients with CD4 counts ≤200 cells μl 1. *Clin. Drug Invest.* **1996**, *11*, 1–10.

99 Schwock, J.; Pham, N. A.; Cao, M. P.; Hedley, D. W. Efficacy of Hsp90 inhibition for induction of apoptosis and inhibition of growth in cervical carcinoma cells *in vitro* and *in vivo. Cancer Chemother. Pharm.* **2008**, *61*, 669–681.

100 Zhang, H.; Neely, L.; Lundgren, K.; Yang, Y. C.; Lough, R.; Timple, N.; Burrows, F. BIIB021, a synthetic Hsp90 inhibitor, has broad application against tumors with acquired multidrug resistance. *Int. J. Cancer* **2010**, *126*, 1226–1234.

101 Dymock, B. W.; Drysdale, M. J.; McDonald, E.; Workman, P. Inhibitors of HSP90 and other chaperones for the treatment of cancer. *Expert Opin. Ther. Pat.* **2004**, *14*, 837–847.

102 Gasteiger, J. Chemoinformatics: Achievements and challenges, a personal view. *Molecules* **2016**, *21*,151.

103 Gasteiger, J. Some solved and unsolved problems of chemoinformatics. *SAR QSAR Environ. Res.* **2014**, *25*, 443–455.

104 Gasteiger, J. Chemoinformatics in drug design. *Drug Future* **2007**, *32*, 2.

105 Giordanetto, F.; Kihlberg, J. Macrocyclic drugs and clinical candidates: What can medicinal chemists learn from their properties? *J. Med. Chem.* **2014**, *57*, 278–295.

106 Eltayar, N.; Mark, A. E.; Vallat, P.; Brunne, R. M.; Testa, B.; Vangunsteren, W. F. Solvent-dependent conformation and hydrogen-bonding capacity of cyclosporine-a—Evidence from partition-coefficients and molecular-dynamics simulations. *J. Med. Chem.* **1993**, *36*, 3757–3764.

107 Alex, A.; Millan, D. S.; Perez, M.; Wakenhut, F.; Whitlock, G. A. Intramolecular hydrogen bonding to improve membrane permeability and absorption in beyond rule of five chemical space. *Med. Chem. Commun.* **2011**, *2*, 669–674.

108 Hopkins, S.; Scorneaux, B.; Huang, Z. H.; Murray, M. G.; Wring, S.; Smitley, C.; Harris, R.; Erdmann, F.; Fischer, G.; Ribeill, Y. SCY-635, a novel nonimmunosuppressive analog of cyclosporine that exhibits potent inhibition of hepatitis C virus RNA replication *in vitro. Antimicrob. Agents Chemther.* **2010**, *54*, 660–672.

109 Kuglstatter, A.; Mueller, F.; Kusznir, E.; Gsell, B.; Stihle, M.; Thoma, R.; Benz, J.; Aspeslet, L.; Freitag, D.; Hennig, M. Structural basis for the cyclophilin a binding affinity and immunosuppressive potency of E-ISA247 (voclosporin). *Acta Crystallogr. Sect. D* **2011**, *67*, 119–123.

110 Aspeslet, L.; Freitag, D.; Trepanier, D.; Abel, M.; Naicker, S.; Kneteman, N.; Foster, R.; Yatscoff, R. ISA(TX)247: A novel calcineurin inhibitor. *Transplant. Proc.* **2001**, *33*, 1048–1051.

111 White, T. R.; Renzelman, C. M.; Rand, A. C.; Rezai, T.; McEwen, C. M.; Gelev, V. M.; Turner, R. A.; Linington, R. G.; Leung, S. S. F.; Kalgutkar, A. S.; Bauman, J. N.; Zhang, Y. Z.; Liras, S.; Price, D. A.; Mathiowetz, A. M.; Jacobson, M. P.; Lokey, R. S. On-resin *N*-methylation of cyclic peptides for discovery of orally bioavailable scaffolds. *Nat. Chem. Biol.* **2011**, *7*, 810–817.

112 Beck, J. G.; Chatterjee, J.; Laufer, B.; Kiran, M. U.; Frank, A. O.; Neubauer, S.; Ovadia, O.; Greenberg, S.; Gilon, C.; Hoffman, A.; Kessler, H. Intestinal permeability of cyclic peptides: Common key backbone motifs identified. *J. Am. Chem. Soc.* **2012**, *134*, 12125–12133.

113 Rezai, T.; Bock, J. E.; Zhou, M. V.; Kalyanaraman, C.; Lokey, R. S.; Jacobson, M. P. Conformational flexibility, internal hydrogen bonding, and passive membrane permeability: Successful in silico prediction of the relative permeabilities of cyclic peptides. *J. Am. Chem. Soc.* **2006**, *128*, 14073–14080.

114 Bockus, A. T.; Lexa, K. W.; Pye, C. R.; Kalgutkar, A. S.; Gardner, J. W.; Hund, K. C.; Hewitt, W. M.; Schwochert, J. A.; Glassey, E.; Price, D. A.; Mathiowetz, A. M.; Liras, S.; Jacobson, M. P.; Lokey, R. S. Probing the physicochemical boundaries of cell permeability and oral bioavailability in lipophilic macrocycles inspired by natural products. *J. Med. Chem.* **2015**, *58*, 4581–4589.

115 Lombardo, F.; Shalaeva, M. Y.; Tupper, K. A.; Gao, F. ElogD(oct): A tool for lipophilicity determination in drug discovery. 2. Basic and neutral compounds. *J. Med. Chem.* **2001**, *44*, 2490–2497.

116 Goetz, G. H.; Farrell, W.; Shalaeva, M.; Sciabola, S.; Anderson, D.; Yan, J. L.; Philippe, L.; Shapiro, M. J. High throughput method for the indirect detection of intramolecular hydrogen bonding. *J. Med. Chem.* **2014**, *57*, 2920–2929.

117 Goetz, G. H.; Philippe, L.; Shapiro, M. J. EPSA: A novel supercritical fluid chromatography technique enabling the design of permeable cyclic peptides. *ACS Med. Chem. Lett.* **2014**, *5*, 1167–1172.

118 Shaw, S. J.; Chen, Y.; Zheng, H.; Fu, H.; Burlingame, M. A.; Marquez, S.; Li, Y.; Claypool, M.; Carreras, C. W.; Crumb, W.; Hardy, D. J.; Myles, D. C.; Liu, Y. Structure-activity relationships of 9-substituted-9-dihydroerythromycin-based motilin agonists: Optimizing for potency and safety. *J. Med. Chem.* **2009**, *52*, 6851–6859.

119 Vendeville, S.; Nilsson, M.; de Kock, H.; Lin, T. I.; Antonov, D.; Classon, B.; Ayesa, S.; Ivanov, V.; Johansson, P. O.; Kahnberg, P.; Eneroth, A.; Wikstrom, K.; Vrang, L.; Edlund, M.; Lindstrom, S.; Van de Vreken, W.; McGowan, D.; Tahri, A.; Hu, L.; Lenz, O.; Delouvroy, F.; Van Dooren, M.; Kindermans, N.; Surleraux, D.; Wigerinck, P.; Rosenquist, A.; Samuelsson, B.; Simmen, K.; Raboisson, P. Discovery of novel, potent

and bioavailable proline-urea based macrocyclic HCV NS3/4A protease inhibitors. *Bioorg. Med. Chem. Lett.* **2008**, *18*, 6189–6193.

120 Raboisson, P.; de Kock, H.; Rosenquist, A.; Nilsson, M.; Salvador-Oden, L.; Lin, T. I.; Roue, N.; Ivanov, V.; Wahling, H.; Wickstrom, K.; Hamelink, E.; Edlund, M.; Vrang, L.; Vendeville, S.; Van de Vreken, W.; McGowan, D.; Tahri, A.; Hu, L. L.; Boutton, C.; Lenz, O.; Delouvroy, F.; Pille, G.; Surleraux, D.; Wigerinck, P.; Samuelsson, B.; Simmen, K. Structure-activity relationship study on a novel series of cyclopentane-containing macrocyclic inhibitors of the hepatitis C virus NS3/4A protease leading to the discovery of TMC435350. *Bioorg. Med. Chem. Lett.* **2008**, *18*, 4853–4858.

121 Parsy, C.; Alexandre, F. R.; Brandt, G.; Caillet, C.; Cappelle, S.; Chaves, D.; Convard, T.; Derock, M.; Gloux, D.; Griffon, Y.; Lallos, L.; Leroy, F.; Liuzzi, M.; Loi, A. G.; Moulat, L.; Musiu, C.; Rahali, H.; Roques, V.; Seifer, M.; Standring, D.; Surleraux, D. Structure-based design of a novel series of azetidine inhibitors of the hepatitis C virus NS3/4A serine protease. *Bioorg. Med. Chem. Lett.* **2014**, *24*, 4444–4449.

122 Kopp, F.; Stratton, C. F.; Akella, L. B.; Tan, D. S. A diversity-oriented synthesis approach to macrocycles via oxidative ring expansion. *Nat. Chem. Biol.* **2012**, *8*, 358–365.

123 Sauer, W. H. B.; Schwarz, M. K. Molecular shape diversity of combinatorial libraries: A prerequisite for broad bioactivity. *J. Chem. Inf. Comp. Sci.* **2003**, *43*, 987–1003.

124 Sadowski, J.; Rudolph, C.; Gasteiger, J. The generation of 3d-models of host guest complexes. *Anal. Chim. Acta* **1992**, *265*, 233–241.

125 Gasteiger, J.; Rudolph, C.; Sadowski, J. Automatic generation of 3D atomic coordinates for organic molecules. *Tetrahedron Comput. Methodol.* **1990**, *3*, 537–547.

126 catConf 4.5, part of the Catalyst package, Accelrys Inc., San Diego, **2001**.

127 Hall, D. R.; Kozakov, D.; Whitty, A.; Vajda, S. Lessons from hot spot analysis for fragment-based drug discovery. *Trends Pharmacol. Sci.* **2015**, *36*, 724–736.

128 Whitty, A.; Zhou, L. Horses for courses: Reaching outside drug-like chemical space for inhibitors of challenging drug targets. *Future Med. Chem.* **2015**, *7*, 1093–1095.

129 Zerbe, B. S.; Hall, D. R.; Vajda, S.; Whitty, A.; Kozakov, D. Relationship between hot spot residues and ligand binding hot spots in protein-protein interfaces. *J. Chem. Inf. Model.* **2012**, *52*, 2236–2244.

130 Chen, I. J.; Foloppe, N. Tackling the conformational sampling of larger flexible compounds and macrocycles in pharmacology and drug discovery. *Bioorgan. Med. Chem.* **2013**, *21*, 7898–7920.

131 Dinsmore, C. J.; Bergman, J. M.; Bogusky, M. J.; Culterson, J. C.; Hamilton, K. A.; Graham, S. L. 3,8-diazabicyclo[3.2.1]octan-2-one peptide mimetics: Synthesis of a conformationally restricted inhibitor of farnesyltransferase. *Org. Lett.* **2001**, *3*, 865–868.

132 Dinsmore, C. J.; Bogusky, M. J.; Culberson, J. C.; Bergman, J. M.; Homnick, C. F.; Zartman, C. B.; Mosser, S. D.; Schaber, M. D.; Robinson, R. G.; Koblan, K. S.; Huber, H. E.; Graham, S. L.; Hartman, G. D.; Huff, J. R.; Williams, T. M. Conformational restriction of flexible ligands guided by the transferred NOE experiment: Potent macrocyclic inhibitors of farnesyltransferase. *J. Am. Chem. Soc.* **2001**, *123*, 2107–2108.

133 Johnson, J. G.; Wang, B.; Debelouchina, G. T.; Novick, R. P.; Muir, T. W. Increasing AIP macrocycle size reveals key features of agr activation in *Staphylococcus aureus*. *ChemBioChem* **2015**, *16*, 1093–1100.

134 Gao, Y.; Kodadek, T. Direct comparison of linear and macrocyclic compound libraries as a source of protein ligands. *ACS Comb. Sci.* **2015**, *17*, 190–195.

135 Wahyudi, H.; McAlpine, S. R. Predicting the unpredictable: Recent structure-activity studies on peptide-based macrocycles. *Bioorg. Chem.* **2015**, *60*, 74–97.

136 Wang, Y.; Guo, Y. Z.; Kuang, Q. F.; Pu, X. M.; Ji, Y.; Zhang, Z. H.; Li, M. L. A comparative study of family-specific protein-ligand complex affinity prediction based on random forest approach. *J. Comput. Aided Mol. Des.* **2015**, *29*, 349–360.

137 Van Vuong, Q.; Nguyen, T. T.; Li, M. S. A new method for navigating optimal direction for pulling ligand from binding pocket: Application to ranking binding affinity by steered molecular dynamics. *J. Chem. Inf. Model.* **2015**, *55*, 2731–2738.

138 Tripathi, S. K.; Soundarya, R. N.; Singh, P.; Singh, S. K. Comparative analysis of various electrostatic potentials on docking precision against cyclin-dependent kinase 2 protein: A multiple docking approach. *Chem. Biol. Drug Des.* **2015**, *85*, 107–118.

139 Lizunov, A. Y.; Gonchar, A. L.; Zaitseva, N. I.; Zosimov, V. V. Accounting for intraligand interactions in flexible ligand docking with a PMF-based scoring function. *J. Chem. Inf. Model.* **2015**, *55*, 2121–2137.

140 Khamis, M. A.; Gomaa, W.; Ahmed, W. F. Machine learning in computational docking. *Artif. Intell. Med.* **2015**, *63*, 135–152.

141 Khamis, M. A.; Gomaa, W. Comparative assessment of machine-learning scoring functions on PDBbind 2013. *Eng. Appl. Artif. Intel.* **2015**, *45*, 136–151.

142 Tsantrizos, Y. S.; Bolger, G.; Bonneau, P.; Cameron, D. R.; Goudreau, N.; Kukolj, G.; LaPlante, S. R.; Llinas-Brunet, M.; Nar, H.; Lamarre, D. Macrocyclic inhibitors of the NS3 protease as potential therapeutic

agents of hepatitis C virus infection. *Angew. Chem. Int. Edit.* **2003**, *42*, 1355–1360.

143 Avolio, S.; Summa, V. Advances in the development of macrocyclic inhibitors of hepatitis C virus NS3-4A protease. *Curr. Top. Med. Chem.* **2010**, *10*, 1403–1422.

144 Pillaiyar, T.; Namasivayam, V.; Manickam, M. Macrocyclic hepatitis C virus NS3/4A protease inhibitors: An overview of medicinal chemistry. *Curr. Med. Chem.* **2016**, *23*, 3404–3447.

145 Hussain, A.; Melville, J. L.; Hirst, J. D. Molecular docking and QSAR of aplyronine A and analogues: Potent inhibitors of actin. *J. Comput. Aided Mol. Des.* **2010**, *24*, 1–15.

146 Wender, P. A.; Nakagawa, Y.; Near, K. E.; Staveness, D. Computer-guided design, synthesis, and protein kinase C affinity of a new salicylate-based class of bryostatin analogs. *Org. Lett.* **2014**, *16*, 5136–5139.

147 Loy, B. A.; Lesser, A. B.; Staveness, D.; Billingsley, K. L.; Cegelski, L.; Wender, P. A. Toward a biorelevant structure of protein kinase C bound modulators: Design, synthesis, and evaluation of labeled bryostatin analogues for analysis with rotational echo double resonance NMR spectroscopy. *J. Am. Chem. Soc.* **2015**, *137*, 3678–3685.

148 Lopanik, N. B. Chemical defensive symbioses in the marine environment. *Funct. Ecol.* **2014**, *28*, 328–340.

149 Wender, P. A.; Baryza, J. L.; Brenner, S. E.; DeChristopher, B. A.; Loy, B. A.; Schrier, A. J.; Verma, V. A. Design, synthesis, and evaluation of potent bryostatin analogs that modulate PKC translocation selectivity. *Proc. Natl. Acad. Sci. U. S. A.* **2011**, *108*, 6721–6726.

150 Wender, P. A.; Loy, B. A.; Schrier, A. J. Translating nature's library: The bryostatins and function-oriented synthesis. *Isr. J. Chem.* **2011**, *51*, 453–472.

151 Wender, P. A.; Schrier, A. J. Total synthesis of bryostatin 9. *J. Am. Chem. Soc.* **2011**, *133*, 9228–9231.

152 Thangsunan, P.; Tateing, S.; Hannongbua, S.; Suree, N. Structural insights into the interactions of phorbol ester and bryostatin complexed with protein kinase C: A comparative molecular dynamics simulation study. *J. Biomol. Struct. Dyn.* **2016**, *34*, 1561–1575.

153 Yuan, W.; Luan, L. B.; Li, Y. N. CoMFA 3D-QSAR analysis of epothilones based on docking conformation and alignment. *Chin. J. Chem.* **2007**, *25*, 453–460.

154 Trendowski, M. Recent advances in the development of antineoplastic agents derived from natural products. *Drugs* **2015**, *75*, 1993–2016.

155 Ruschel, J.; Hellal, F.; Flynn, K. C.; Dupraz, S.; Elliott, D. A.; Tedeschi, A.; Bates, M.; Sliwinski, C.; Brook, G.; Dobrindt, K.; Peitz, M.; Brüstle, O.; Norenberg, M. D.; Blesch, A.; Weidner, N.; Bunge, M. B.; Bixby, J. L.; Bradke, F. Systemic administration of

epothilone B promotes axon regeneration after spinal cord injury. *Science* **2015**, *348*, 347–352.

156 Navarrete, K. R.; Alderete, J. B.; Jimenez, V. A. Structural basis for drug resistance conferred by beta-tubulin mutations: A molecular modeling study on native and mutated tubulin complexes with epothilone B. *J. Biomol. Struct. Dyn.* **2015**, *33*, 2530–2540.

157 Lopus, M.; Smiyun, G.; Miller, H.; Oroudjev, E.; Wilson, L.; Jordan, M. A. Mechanism of action of ixabepilone and its interactions with the beta III-tubulin isotype. *Cancer Chemoth. Pharm.* **2015**, *76*, 1013–1024.

158 Kern, F.; Dier, T. K. F.; Khatri, Y.; Ewen, K. M.; Jacquot, J. P.; Volmer, D. A.; Bernhardt, R. Highly efficient CYP167A1 (EpoK) dependent epothilone B formation and production of 7-ketone epothilone D as a new epothilone derivative. *Sci. Rep.* **2015**, *5*, 14881.

159 De Luca, A.; D'Alessio, A.; Maiello, M. R.; Gallo, M.; Chicchinelli, N.; Pergameno, M.; Piccirilli, M. S.; Normanno, N. Evaluation of the pharmacokinetics of ixabepilone for the treatment of breast cancer. *Expert Opin. Drug Met.* **2015**, *11*, 1177–1185.

160 Brizuela, M.; Blizzard, C. A.; Chuckowree, J. A.; Dawkins, E.; Gasperini, R. J.; Young, K. M.; Dickson, T. C. The microtubule-stabilizing drug epothilone D increases axonal sprouting following transection injury *in vitro. Mol. Cell. Neurosci.* **2015**, *66*, 129–140.

161 Mukhtar, E.; Adhami, V. M.; Mukhtar, H. Targeting microtubules by natural agents for cancer therapy. *Mol. Cancer Ther.* **2014**, *13*, 275–284.

162 Roemeling, C. A.; Marlow, L. A.; Kennedy, W. P.; Kennedy, G. T.; Copland, J. A.; Menefee, M. E. Preclinical evaluation of the mTOR inhibitor, temsirolimus, in combination with the epothilone B analog, ixabepilone in renal cell carcinoma. *Am. J. Cancer Res.* **2013**, *3*, 390–401.

163 Gokhale, M.; Thakur, A.; Rinaldi, F. Degradation of BMS-753493, a novel epothilone folate conjugate anticancer agent. *Drug Dev. Ind. Pharm.* **2013**, *39*, 1315–1327.

164 Wessjohann, L. Epothilones: Promising natural products with taxol-like activity. *Angew. Chem. Int. Ed.* **1997**, *36*, 715–718.

165 Hause, G.; Lischewski, S.; Wessjohann, L. A.; Hause, B. Epothilone D affects cell cycle and microtubular pattern in plant cells. *J. Exp. Bot.* **2005**, *56*, 2131–2137.

166 Höfle, G. H.; Bedorf, N.; Steinmetz, H.; Schomburg, D.; Gerth, K.; Reichenbach, H. Epothilone A and B—Novel 16-membered macrolides with cytotoxic activity: Isolation, crystal structure, and conformation in solution. *Angew. Chem. Int. Ed.* **1996**, *35*, 1567–1569.

167 Wessjohann, L. A., Scheid, G. Synthetic Access to Epothilones—Natural Products with Extraordinary Anticancer Activity. In *Organic Chemistry Highlights IV* Schmalz, H.-G., Ed. Wiley-VCH: Weinheim, **2000**; pp 251–267.

168 Altmann, K. H. Recent developments in the chemical biology of epothilones. *Curr. Pharm. Design.* **2005**, *11*, 1595–1613.

169 Altmann, K. H.; Cachoux, F.; Caravatti, G.; Isarno, T.; Wartmann, M. Recent developments in the chemistry and biology of epothilones. *Arkivoc* **2006**, *8*, 131–141.

170 Altmann, K. H.; Cachoux, F.; Feyen, F.; Gertsch, J.; Kuzniewski, C. N.; Wartmann, M. Natural products as leads for anticancer drug discovery: Discovery of new chemotypes of microtubule stabilizers through reengineering of the epothilone scaffold. *Chimia* **2010**, *64*, 8–13.

171 Altmann, K. H.; Florsheimer, A.; Bold, G.; Caravatti, G.; Wartmann, M. Natural product-based drug discovery—Epothilones as lead structures for the discovery of new anticancer agents. *Chimia* **2004**, *58*, 686–690.

172 Altmann, K. H.; Gaugaz, F. Z.; Schiess, R. Diversity through semisynthesis: The chemistry and biological activity of semisynthetic epothilone derivatives. *Mol. Divers.* **2011**, *15*, 383–399.

173 Altmann, K. H.; Gertsch, J. Anticancer drugs from nature—Natural products as a unique source of new microtubule-stabilizing agents. *Nat. Prod. Rep.* **2007**, *24*, 327–357.

174 Nicolaou, K. C.; Chen, J. S.; Dalby, S. M. From nature to the laboratory and into the clinic. *Bioorg. Med. Chem.* **2009**, *17*, 2290–2303.

175 Nicolaou, K. C.; Pratt, B. A.; Arseniyadis, S.; Wartmann, M.; O'Brate, A.; Giannakakou, P. Molecular design and chemical synthesis of a highly potent epothilone. *ChemMedChem* **2006**, *1*, 41–44.

176 Nicolaou, K. C.; Rhoades, D.; Wang, Y.; Totokotsopoulos, S.; Bai, R.; Hamel, E. Synthesis and biological evaluation of novel epothilone B side chain analogues. *ChemMedChem* **2015**, *10*, 1974–1979.

177 Nicolaou, K. C.; Ritzen, A.; Namoto, K. Recent developments in the chemistry, biology and medicine of the epothilones. *Chem. Commun.* **2001**, *17*, 1523–1535.

178 Nicolaou, K. C.; Sasmal, P. K.; Rassias, G.; Reddy, M. V.; Altmann, K. H.; Wartmann, M.; O'Brate, A.; Giannakakou, P. Design, synthesis, and biological properties of highly potent epothilone B analogues. *Angew. Chem. Int. Ed.* **2003**, *42*, 3515–3520.

179 Ödman, P.; Wessjohann, L. A.; Bornscheuer, U. T. Chemoenzymatic dynamic kinetic resolution of acyloins. *J. Org. Chem.* **2005**, *70*, 9551–9555.

180 Wessjohann, L. A. Synthesis of natural product based compound libraries. *Curr. Opin. Chem. Biol.* **2000**, *4*, 303–309.

181 Wessjohann, L. A.; Scheid, G. O.; Eichelberger, U.; Umbreen, S. Total synthesis of epothilone D: The nerol/macroaldolization approach. *J. Org. Chem.* **2013**, *78*, 10588–10595.

182 Gabriel, T.; Wessjohann, L. The chromium-Reformatsky reaction: Asymmetric synthesis of the aldol fragment of the cytotoxic epothilons from 3-(2-bromoacyl)-2-oxazolidinones. *Tetrahedron Lett.* **1997**, *38*, 1363–1366.

183 Scheid, G.; Ruijter, E.; Konarzycka-Bessler, M.; Bornscheuer, U. T.; Wessjohann, L. A. Synthesis and resolution of a key building block for epothilones: A comparison of asymmetric synthesis, chemical and enzymatic resolution. *Tetrahedron-Asymmetry* **2004**, *15*, 2861–2869.

184 Nettles, J. H.; Li, H. L.; Cornett, B.; Krahn, J. M.; Snyder, J. P.; Downing, K. H. The binding mode of epothilone A on alpha,beta-tubulin by electron crystallography. *Science* **2004**, *305*, 866–869.

185 Bhonsle, J. B.; Avery, M. A. Prediction of the binding site of paclitaxel, epothilone, and discodermolide on tubulin by docking studies. *Abstr. Pap. Am. Chem. Soc.* **1999**, *218*, U504.

186 Kamel, K.; Kolinski, A. Computational study of binding of epothilone A to beta-tubulin. *Acta Biochim. Pol.* **2011**, *58*, 255–260.

187 Natarajan, K.; Senapati, S. Understanding the basis of drug resistance of the mutants of alpha beta-tubulin dimer via molecular dynamics simulations. *PLoS One* **2012**, *7*, e42351.

188 Shi, G. J.; Wang, Y.; Jin, Y.; Chi, S. M.; Shi, Q.; Ge, M. F.; Wang, S.; Zhang, X. K.; Xu, S. C. Structural insight into the mechanism of epothilone A bound to beta-tubulin and its mutants at Arg282Gln and Thr274Ile. *J. Biomol. Struct. Dyn.* **2012**, *30*, 559–573.

189 Strutt, N. L.; Zhang, H. C.; Schneebeli, S. T.; Stoddart, J. F. Functionalizing pillar[n]arenes. *Acc. Chem. Res.* **2014**, *47*, 2631–2642.

190 Yoo, J. S.; Sohn, Y. S.; Do, Y. K. Synthesis, structures and antitumor activity of the first crown ester-linked bipyridyl platinum complexes. *J. Inorg. Biochem.* **1999**, *73*, 187–193.

191 Brown, S. D.; Plumb, J. A.; Johnston, B. F.; Wheate, N. J. Folding of dinuclear platinum anticancer complexes within the cavity of para-sulphonatocalix[4]arene. *Inorg. Chim. Acta* **2012**, *393*, 182–186.

192 Chaudhary, A.; Shekhawat, G. S.; Singh, R. V. Investigations on new revolutionary fertility inhibitors 9, 10-diaminophenenthrene derivatives of bivalent manganese antifertility, antibacterial, antifungal and percent disease incidence aspects. *Rev. Inorg. Chem.* **2010**, *30*, 113–134.

193 Antunes, P.; Delgado, R.; Drew, M. G. B.; Felix, V.; Maecke, H. Copper complexes of new benzodioxotetraaza macrocycles with potential applications in nuclear medicine. *Inorg. Chem.* **2007**, *46*, 3144–3153.

194 Halime, Z.; Frindel, M.; Camus, N.; Orain, P. Y.; Lacombe, M.; Cherel, M.; Gestin, J. F.; Faivre-Chauvet, A.; Tripier, R. New synthesis of phenyl-isothiocyanate C-functionalised cyclams. Bioconjugation and Cu-64 phenotypic PET imaging studies of multiple myeloma with the te2a derivative. *Org. Biomol. Chem.* **2015**, *13*, 11302–11314.

195 Notni, J.; Simecek, J.; Wester, H. J. Phosphinic acid functionalized polyazacycloalkane chelators for radiodiagnostics and radiotherapeutics: Unique characteristics and applications. *ChemMedChem* **2014**, *9*, 1107–1115.

196 Gavey, E. L.; Pilkington, M. Coordination complexes of 15-membered pentadentate aza, oxoaza and thiaaza Schiff base macrocycles "Old Complexes Offer New Attractions". *Coord. Chem. Rev.* **2015**, *296*, 125–152.

197 Fang, Y. X.; Ao, Y. F.; Wang, D. X.; Zhao, L.; Wang, M. X. Synthesis, structure and transition metal ion complexation property of lariat azacalix[4]pyridines. *Tetrahedron* **2015**, *71*, 2105–2112.

198 Makrlik, E.; Bohm, S.; Vanura, P.; Ruzza, P. Complexation of Li + with antamanide: An experimental and theoretical study. *Monatsh. Chem.* **2014**, *145*, 1051–1054.

199 Keypour, H.; Liyaghati-Delshad, M.; Rezaeivala, M.; Khavasi, H. R. Synthesis and characterization of some new Cd(II) and Zn(II) macrocyclic Schiff base complexes derived from cyclocondensation of three new linear aromatic (N-4) amines and 2,6-diacetylpyridine. Crystal structure and biological activity studies. *J. Iran. Chem. Soc.* **2014**, *11*, 1473–1482.

200 Makrlik, E.; Toman, P.; Vanura, P. Complexation of the thallium cation with dibenzo-30-crown-10: Extraction and theoretical study. *Monatsh. Chem.* **2013**, *144*, 919–923.

201 Makrlik, E.; Dybal, J.; Vanura, P. A combined experimental and theoretical study on the complexation of the ammonium cation with valinomycin. *Monatsh. Chem.* **2010**, *141*, 1191–1194.

202 Newman, D. J.; Cragg, G. M. Natural products as sources of new drugs over the 30 Years from 1981 to 2010. *J. Nat. Prod.* **2012**, *75*, 311–335.

203 Newman, D. J.; Cragg, G. M. Marine-sourced anti-cancer and cancer pain control agents in clinical and late preclinical development. *Mar. Drugs* **2014**, *12*, 255–278.

204 Cragg, G. M.; Grothaus, P. G.; Newman, D. J. New horizons for old drugs and drug leads. *J. Nat. Prod.* **2014**, *77*, 703–723.

5

Bioactive and Membrane-Permeable Cyclic Peptide Natural Products

Andrew T. Bockus[1] and R. Scott Lokey[2]

[1] *Circle Pharma, Inc., South San Francisco, CA, USA*
[2] *Department of Chemistry, University of California Santa Cruz, Santa Cruz, CA, USA*

5.1 Introduction

Cyclic peptide natural products and their synthetic mimics have gained prominence as potential sources of next-generation therapeutics and biological probes [1–4]. The size and structural complexity of these compounds sets them apart from common synthetic drugs, allowing them to access the "undruggable" target space beyond enzymatic active sites and receptor binding pockets to include activities against a variety of nontraditional targets [4]. Although cyclic peptides have molecular weights and polar group counts that exceed the typical parameters for "drug-likeness" [5, 6], many are capable of penetrating cells by passive diffusion, and some, such as cyclosporin A, are orally bioavailable [7]. Passive diffusion offers an advantage over other forms of permeation such as paracellular transport, carrier-mediated transport, and active non-receptor-mediated uptake (e.g., micropinocytosis) because the ability to cross the membrane is dictated by the intrinsic properties of the molecule (e.g., molecular weight, number of intramolecular hydrogen bonds (IMHBs), polar surface area, flexibility, lipophilicity) rather than those of the target tissue or cellular physiology (e.g., size of tight junctions, type of transport proteins, invagination of the membrane in response to surface assemblies). Thus, these natural products may provide insights into the requirements for optimizing the ADME properties of large macrocycles. Further, the stereochemical and conformational complexity of cyclic peptides serves as a model for the design of synthetic scaffolds capable of modulating challenging biological targets such as protein–protein interactions and allosteric binding sites in both extracellular and intracellular space [8–13]. Despite this potential, few efforts have been made to systematically assess the relationship between the structure, pharmacokinetics, and bioactivity of cyclic peptide natural products. This is due in part to the limited number of known passively permeable cyclic peptide and cyclic peptide/polyketide natural products. Therefore the generality of cyclic peptides as orally bioavailable bioactive scaffolds remains an open question.

The few studies that have systematically explored the relationships between structure and permeability in cyclic peptides have been limited to a small subset of methylated (**1**) [14] and non-methylated (**2**) [15] cyclic hexapeptide scaffolds that bear resemblance to baceridin (**3**) [16], segelin I (**4**) [17], and the nocardiamide (**5**/**6**) [18] cyclic hexapeptide natural products (Figure 5.1 and Chapter 3) [19–22]. The work of Lokey and Jacobson [23–27], Fairlie and Craik [28–30], and others has begun to elucidate the structure–permeability relationships of more complex natural products, but the vast majority of these studies have been limited to cyclic penta- and hexapeptides with no observed bioactivity. Thus, the new frontier in understanding structure–permeability relationships in cyclic peptides has moved to the chemical space that encompasses macrocycles of higher molecular weight [31, 32], greater structural complexity, and significant bioactivity.

Here, we first discuss the two-dimensional and three-dimensional (3D) structures of known passively permeable cyclic peptide natural products and then highlight recently discovered cyclic peptide natural products with notable bioactivity that could serve as starting structures for future systematic structural studies to optimize oral absorption.

5.2 Structural Motifs and Permeability of Cyclic Peptide Natural Products

Cyclic peptide natural products have been grouped into four categories based on a broad survey of their structures and known biological functions: (i) charged, (ii) nonpolar,
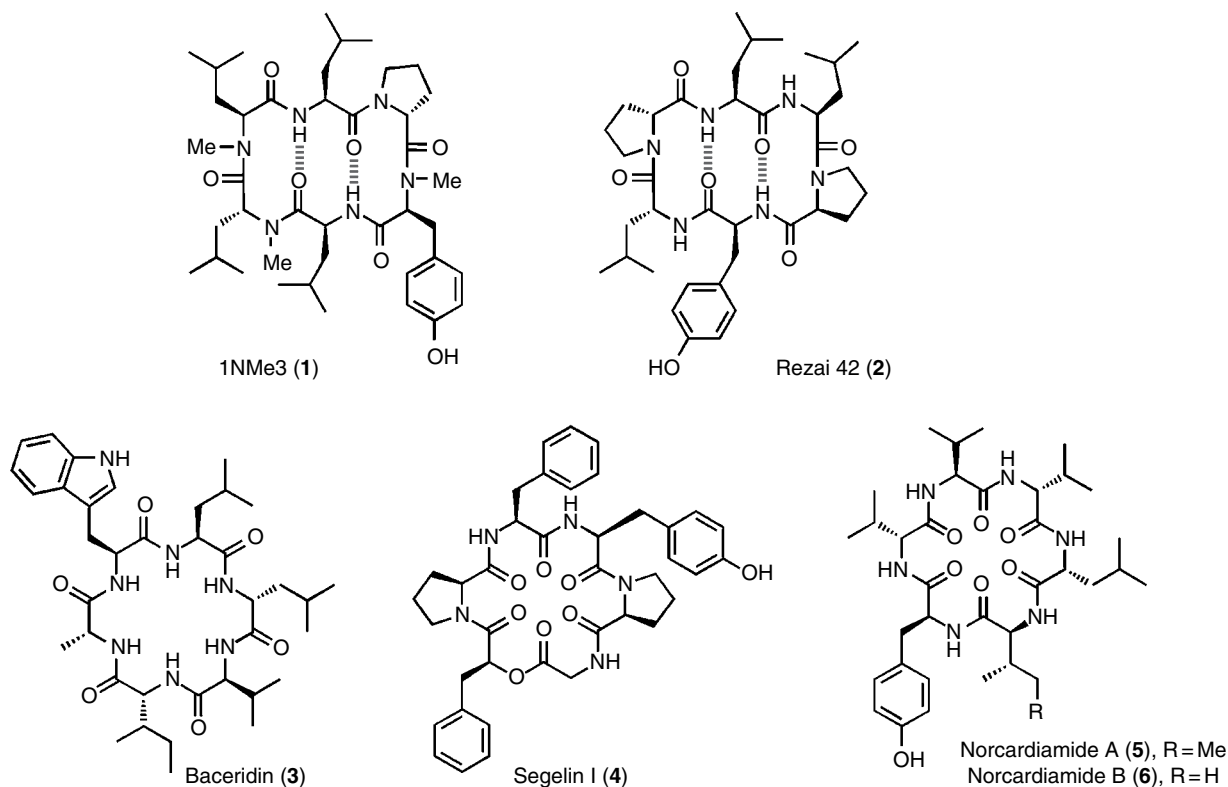
Figure 5.1 Synthetic peptides 1NMe3 (Lokey peptide, **1**) and Rezai 42 (**2**) have inspired numerous studies on cyclic peptide passive permeation. The proteasome inhibitor baceridin (**3**) and three recently discovered cyclic peptides with unknown bioactivity (**4–6**) closely resemble the structures of the Lokey peptides.

(iii) amphiphilic macrocycles, and (iv) cystine knot proteins [33]. Highly charged molecules (both polycationic and polyanionic) function mostly as antimicrobial agents by disrupting bacterial membranes and are unlikely to penetrate eukaryotic cells by passive diffusion. Nonpolar cyclic peptides, on the other hand, contain mostly lipophilic side chains and modifications to the amide backbone (e.g., N-methylation) and have calculated properties that suggest the ability to penetrate eukaryotic cell membranes by passive diffusion [14]. Cyclic peptides of mixed polarity, most of which are amphiphilic, demonstrate antimicrobial activity and have been shown to act against multidrug-resistant bacteria [34]. These charged scaffolds and other cell-penetrating peptides enter cells by mechanisms other than passive membrane diffusion [35]. Cystine knot proteins have unusual topologies stabilized by a network of disulfide bonds [36]. These species have shown remarkable oral activity as well as insecticidal, antiviral, and cytotoxic bioactivities [37]. It is important to note that cystine knot peptides permeate cell membranes by a mechanism distinct from that of passive diffusion [38]. One large charged cyclotide, kalata B1 (Figure 5.2), was recently reported to permeate membranes by accumulating on the surface of HeLa cells, causing an invagination and subsequent endocytosis [39].
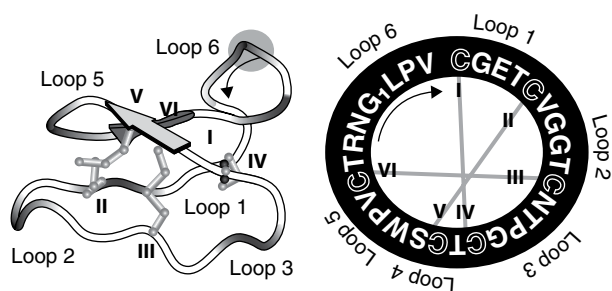

Figure 5.2 Structure of kalata B1. Roman numerals refer to cysteine residues involved in disulfide bonds. Reprinted from Ref. [39] with permission from Elsevier.

A similar route of entry may also be accessed by the highly charged TAT peptides [40, 41].

Cyclic peptides can be further categorized into three main structural subgroups. Homodetic peptides are composed of amide bonds only and usually cyclized from head to tail; heterodetic peptides contain one (or more) non-amide endocyclic bond and are often cyclized between side chains or from a side chain to one of the termini, and complex peptides are comprised of a mixture of homodetic and heterodetic linkages. Homodetic cyclic peptides are usually formed by the condensation

of the N-terminal amine with the C-terminal carboxylic acid [33]. In sequences containing noncanonical residues, ester linkages may also form between an N-terminal alcohol (i.e., lactic acid) and the C-terminal carboxylic acid to generate a lactone ("depsi") linkage [42]. Heterodetic cyclic peptides have a "lariat" structure formed by cyclization of the C-terminal carboxylic acid onto a side chain. This connection is typically made via a lactam linkage through a lysine or ornithine residue or a depsi-linkage through serine or threonine [43]. Heterodetic cyclic peptides can also be capped on their amino termini with a lipid tail of varying length and composition. Alternatively, "lasso" peptides form N-terminal macrocycles with C-terminal tails through lactams between N-terminal glycine or serine and aspartate or glutamate side chains [44]. Compounds in the "complex" category include bicyclic peptides and cyclic peptides with knot topologies [36, 45, 46].

These cyclic molecules, and the biosynthetic pathways that produce them, have been evolutionarily conserved because they offer some advantages to the producing organism [47]. While it is likely that the structural features of natural products have been preserved because they directly modulate ligand–target interactions to create more potent modulators or toxins, these modifications may have survived the test of evolution because they also offer an indirect competitive advantage in terms of their physiochemical properties: the ability to solubilize in aqueous media and to permeate membranes, which is critical for enabling them to reach their target and enable biological activity. An understanding of how the components and conformations of cyclic peptide natural products influence their respective functions, therefore, should further inform the development of cyclic peptide therapeutics with favorable ADME properties.

5.3 Conformations of Passively Permeable Bioactive Cyclic Peptide Natural Products

Although the structures of cyclic peptide natural products have been investigated via NMR and crystallographic studies (Chapter 2), these structures have been considered in the context of permeability only recently [23, 32, 33, 48, 49]. It is likely that the conformational hypothesis of membrane permeation holds true in determining the permeability of these molecules [15]. Numerous cyclic peptide and cyclic peptide/polyketide natural products are flexible and capable of adopting lipophilic conformations containing IMHBs in low dielectric solvent environments. The adoption of IMHB-defined conformations is

just one of a multitude of strategies that may permit the passive permeation of cyclic peptides (for further discussion see Chapter 3). Cyclic peptide natural products often contain other structural motifs such as N-methylation, β-hydroxylation, and β-branched aliphatic side chains that may play a role in compensating for exposed polar surface area and high H-bond donor and acceptor counts [14, 19, 23–25, 28, 29]. The following sections review how the structures of select passively permeable cyclic peptide natural products may allow for their exceptional physicochemical and biological properties, including immunosuppressive, cytotoxic, antiviral, and antibiotic activities, among others.

5.3.1 Flexible Scaffolds

The immunosuppressant cyclosporin A (CsA **7**; Figure 5.3) is an uncharged homodetic undecapeptide containing seven N-methylated amino acids, a D-alanine, and a 2-butenyl-4-methyl-L-threonine (Bmt) residue derived from a polyketide/nonribosomal peptide synthetase pathway [50, 51]. Despite having a molecular weight that is more than twice that of the limit set by Lipinski *et al.* (500 Da) [5] and a calculated octanol–water partition coefficient (cLog$P$) that exceeds a value of 5 in some algorithms (6.92 in ChemAxon; 4.37 in ALOGPS [52]), CsA is passively permeable. The macrocycle exhibits an effective permeability (P_e) of 9.8×10^{-6} cm/s in a parallel artificial membrane permeability assay (PAMPA) and an apparent permeability (P_{app}) of 1.1×10^{-6} cm/s in low-efflux Madin–Darby canine kidney (MDCK-LE) cells [14]. It is also orally bioavailable in rat up to 29% [53].

In chloroform, a low dielectric solvent used to model intra-membrane space, CsA adopts a conformation with four IMHBs [54]. This conformation effectively reduces the number of H-bond donors to one and H-bond acceptors to seven, satisfying Lipinski's parameters for hydrogen bond donors and acceptors [55]. Although CsA is rigid in chloroform, it is quite flexible in water [56]. NMR studies have shown that CsA is capable of accessing multiple conformations in high dielectric environments
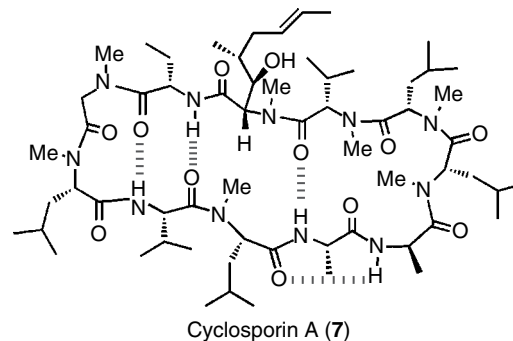

Cyclosporin A (**7**)

Figure 5.3 Solution structure of cyclosporine A in chloroform.

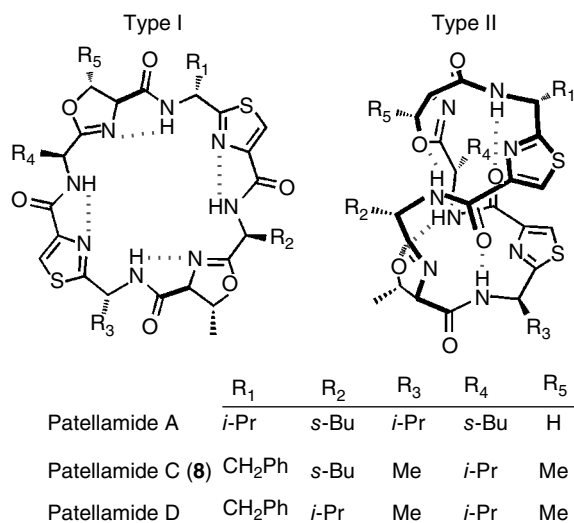|	R₁	R₂	R₃	R₄	R₅
Patellamide A	*i*-Pr	*s*-Bu	*i*-Pr	*s*-Bu	H
Patellamide C (**8**)	CH₂Ph	*s*-Bu	Me	*i*-Pr	Me
Patellamide D	CH₂Ph	*i*-Pr	Me	*i*-Pr	Me

Figure 5.4 Conformations of patellamide.

and binds cyclophilin A in a distinctly different conformation than that observed in chloroform [54, 57–60]. One of these conformations is similar to that of its target-bound crystal structure [60]. This solvent-dependent flexibility may explain why CsA achieves 20 μM solubility in water [61], despite the tendency for larger peptides to exhibit lower solubilities [62].

Patellamide C (**8**; Figure 5.4) ($\log P = 4.12$) [63, 64] is a member of the ascidiacyclamide/lissoclinamide family of bioactive natural products derived from ribosomally synthesized sequences of alternating lipophilic and Ser, Thr, or Cys residues.

These hydroxyl- and sulfhydryl-containing residues are precursors of the oxazoline and thiazoline rings formed by cyclodehydration between the side chain —OH or —SH groups and the neighboring $i - 1$ backbone carbonyl group. Oxidation of the oxazoline and thiazoline rings leads to the corresponding aromatic oxazoles and thiazoles [65]. While the pure patellamide-like peptides seldom contain *N*-methyl groups, consistent with their ribosomal origin, they exhibit multiple IMHBs, either between the 5-membered ring nitrogen lone pair and the neighboring NH group ("open," Type I) or, in some cases, between NH groups and CO groups within the molecule ("closed," Type II) [66]. The adopted solution conformation depends on both the symmetry of the side chains and the polarity of the solvent environment. Patellamides with symmetrical side chains, such as patellamide A, adopt the Type I conformation in polar solvents and the Type II conformation in nonpolar solvents, while members with asymmetrical side chains adopt the Type II conformation irrespective of solvent [67]. Although patellamide D is asymmetrical, favoring a Type II conformation in solution, a crystal structure of Cu₂CO₃–patellamide D in the Type I conformation has

been observed [68]. This conformational flexibility does not necessarily prohibit passive permeation across cell membranes, as demonstrated by the asymmetrical patellamide C ($P_e = 19 \times 10^{-6}$ cm/s), which is more permeable than CsA in the PAMPA assay [23]. Although the biological activity of the patellamides is weak, these molecules demonstrate that IMHBs and conformational flexibility are not reserved for CsA alone and that ribosomal peptides are also capable of passive permeation using conformational alternatives to N-methylation. However, it is not known whether symmetrical patellamides that favor Type I conformers are permeable.

Valinomycin (**9**) ($\log P = 3.07$) is a cytotoxic cyclic depsipeptide that acts as a mitochondrial uncoupler by facilitating the passive diffusion of potassium ions across the mitochondrial inner membrane (Figure 5.5) [69]. This uncharged depsipeptide contains no N-methylated residues but features a considerable enrichment of β-branched residues, which could serve to shield the polar groups from solvent to facilitate its passive diffusion across the mitochondrial membrane [70]. The scaffold also demonstrates ion-dependent conformational flexibility. The *apo*-form of valinomycin crystallized from DMSO adopts a conformation in which three of the NH bonds are solvent-exposed and three engage in IMHBs, while the *apo*-form of valinomycin crystallized from octane shows a rectangular geometry in which all of the amide NH groups are involved in transannular hydrogen bonds. These hydrogen bonds define β-turns between the lactic acid CO groups and the valine NH groups at i and $i + 3$, respectively (Figure 5.5) [71]. In the presence of K⁺, the molecule rearranges to adopt a toroidal geometry using a different arrangement of β-turns in which six of the CO groups point toward the K⁺ in the center of the torus (Figure 5.5) [72], affording a K_d of 1–3 mM in aqueous solution [52]. In both the octane-derived crystal and in the presence of K⁺, all six NH groups are involved in transannular hydrogen bonds. This suggests that valinomycin may be able to adopt lipophilic conformations in both its complexed and uncomplexed forms to afford passive permeation of membranes. Valinomycin is also capable of dissolution in polar solvents [73], as the scaffold may adopt conformations in which the NH groups interact with solvent.

Scytalidamide A (**10**; Figure 5.6) ($\log P = 4.09$) is an uncharged homodetic cyclic heptapeptide from an alga-associated fungus of the genus *Scytalidium*. The compound was found to exhibit moderate cytotoxicity against HCT-116 cells (IC₅₀ 2.7 μM) [74] and has recently been shown to be passively permeable ($P_e = 83 \times 10^{-6}$ cm/s) [23]. In addition to L-amino acids, scytalidamide A contains two N-methylated residues and an α-aminoisobutyric acid, which are both known to serve as turn-inducing elements in helical structures. Vicinal coupling constants
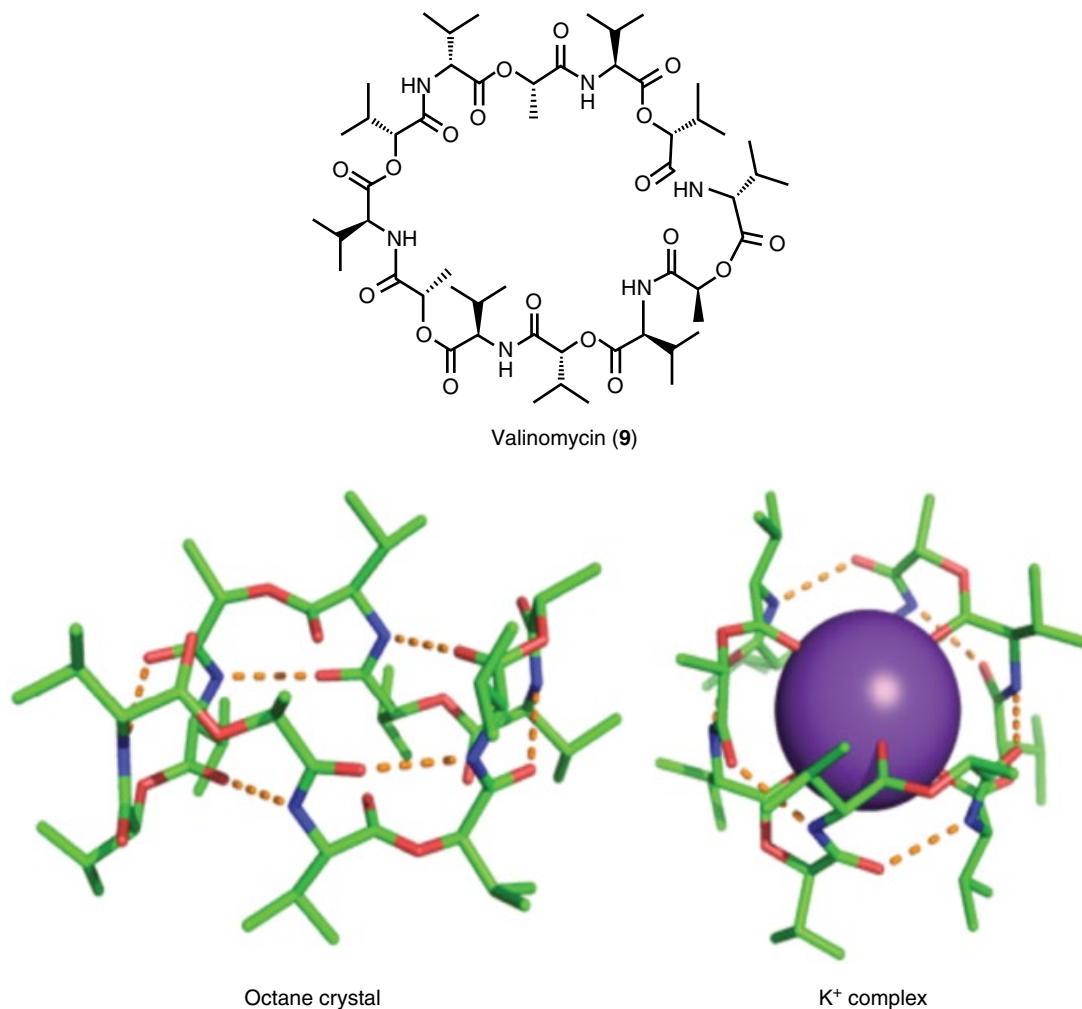
Valinomycin (**9**)

Octane crystal

K⁺ complex

Figure 5.5 Conformations of valinomycin. (*See insert for color representation of the figure*.)
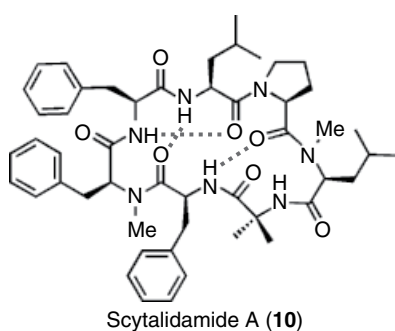

Scytalidamide A (**10**)

Figure 5.6 Scytalidamide A.

($J_{\text{HN-CH}}\alpha \sim 9\,\text{Hz}$) and amide temperature coefficients derived from NMR studies in chloroform suggest that scytalidamide A adopts a single dominant rigid conformer in solution with three IMHBs. Amide temperature coefficient experiments in DMSO, however, have revealed that the scaffold can also adopt a conformation with only two IMHBs [74]. Thus, scytalidamide A, like

CsA and the patellamides, exhibits solvent-dependent flexibility to adopt a rigid IMHB conformer in low dielectric environments.

5.3.2 Structural Analogues

Guangomide A (**11**) and B (**12**) (Figure 5.7) (Alog$P$ = 2.26 and 2.69, respectively) were isolated from a cytotoxic extract of a sponge-derived fungus and found to show weak antibacterial activity against *S. epidermidis* and *E. durans* [75]. The backbones of the uncharged homodetic hexadepsipeptides are N-methylated at two positions and contain two D-amino acids and two α-hydroxyacid residues. Crystallographic [75] and computational [23] studies have shown that both guangomides are capable of adopting two IMHBs to sequester the NH groups from solvent exposure. Interestingly, although the 2-dihydroxyisovaleric acid residue of guangomide A is hydroxylated (an additional H-bond donor and/or acceptor), the peptide demonstrates the same passive permeability as the

non-hydroxylated guangomide B ($P_e = 6.4 \times 10^{-6}$ cm/s) [23]. Crystal structures and *in silico* models of the scaffolds suggest that the additional hydroxyl of guangomide A does not affect permeability because it can engage in an IMHB with a neighboring carbonyl, like the amide NH groups. This β-hydroxy carbonyl motif is found in other passively permeable natural products including CsA (Figure 5.3) [54], rakicidin A (Figure 5.8, Alog*P* = 4.75) [76], didemnins (Figure 5.9), and threonine-containing peptides and may serve to increase backbone and side-chain polarity while maintaining permeability.

Didemnin A (**14**) and B (**15**) (Figure 5.9) (Alog*P* = 3.30 and 3.07, respectively) are uncharged cyclic peptide/
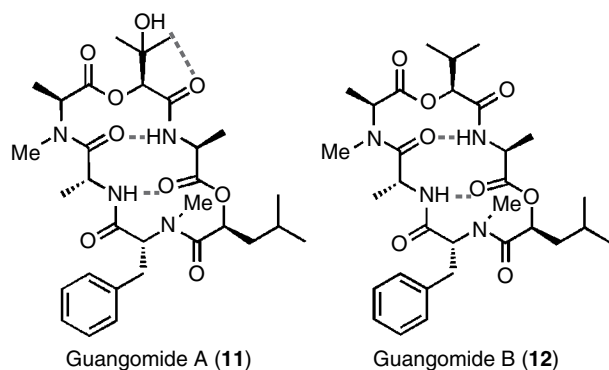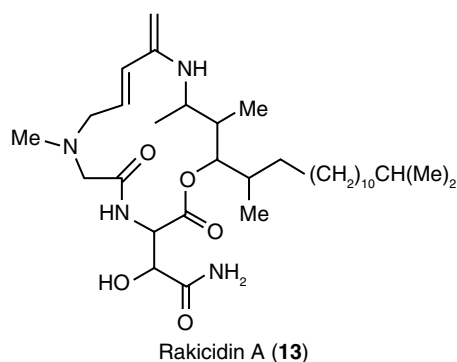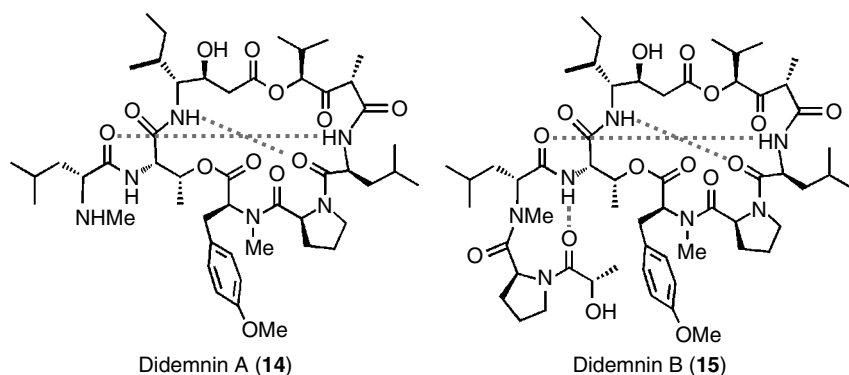
polyketide depsipeptide lariats containing N-methylation and a polyketide/nonribosomal peptide synthetase-derived isostatine amino acid. Didemnin B has been shown to have antiviral, cytotoxic [77] immunosuppressive activities [78], but it has shown high toxicity in patients [79]. Didemnin A, however, exhibits much weaker bioactivity. The crystal and NMR solution structures of didemnin A and B reveal that the structures adopt nearly identical IMHB patterns within the macrocycle [80–82], but, besides the extended lariat tail of didemnin B, there exists another crucial difference between the two analogues that may account for disparities in bioactivity. Didemnin A has a shorter isostatine NH-to-LeuCO H-bond (2.83 Å) than didemnin B (3.02 Å) [81]. In this reference, Hossain *et al.* propose that the "… difference in activity between didemnin A and B may be attributed to features other than the macrocycle conformation. However, the significantly stronger intramolecular hydrogen bonding in didemnin A compared to that in didemnin B suggests a more inflexible macrocyclic ring in didemnin A, and this factor may be relevant to their difference in activity."

The flexibility of didemnin analogues could also be a key factor in target binding, similar to CsA. It is unclear whether the tail of the lariat or the flexibility of the macrocycle is responsible for the differences in bioactivity and permeability. Didemnin A is passively permeable ($P_e = 1.2 \times 10^{-6}$ cm/s), but the permeability of didemnin B has not been reported [23].

The destruxins (Figure 5.10) are a class of cyclic hexadepsipeptides from the fungus *Metarhizium anisopliae*. Their backbones contain non-proteinogenic elements such as a β-amino acid, an α-hydroxy acid, and N-methylation. These compounds are known to have insecticidal and phytotoxic properties and have also been used as antibiotics and V-ATPase inhibitors [83]. The structures of destruxins have been studied since the 1970s, and, although many side-chain analogues have been discovered, the core scaffolds tend to retain similar conformations [23, 84, 85]. In most cases, the non-methylated amide NH groups adopt two β-turn-like transannular

Guangomide A (**11**)   Guangomide B (**12**)

Figure 5.7 Guangomide A and B.

Rakicidin A (**13**)

Figure 5.8 Rakicidin A.

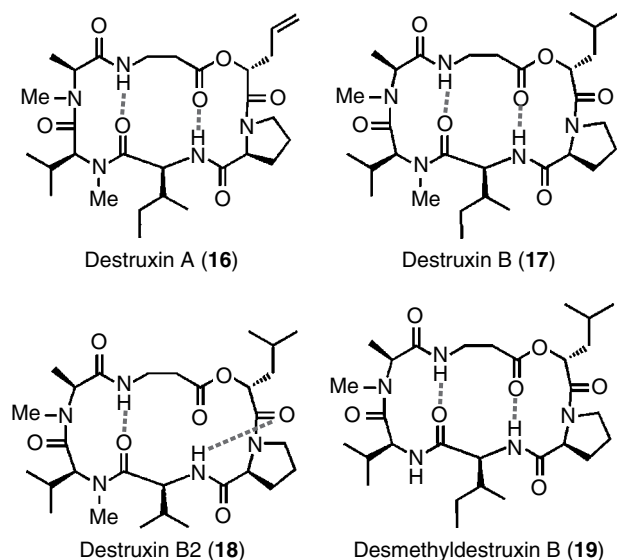Didemnin A (**14**)   Didemnin B (**15**)   **Figure 5.9** Didemnin A and B.

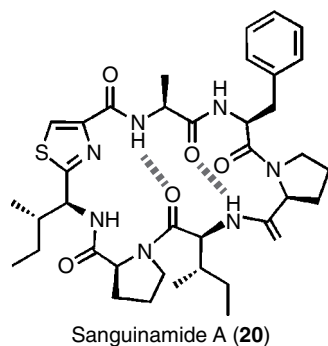Figure 5.10 Structures and IMHB patterns of the destruxins.

Figure 5.11 Sanguinamide A.

hydrogen bonds. Of the four destruxins assessed for passive permeability, destruxin B (17) is the most permeable ($P_e = 5.1 \times 10^{-6}$ cm/s, Alog$P = 2.20$), followed by B2 (18) ($P_e = 1.3 \times 10^{-6}$ cm/s, Alog$P = 1.79$), A (16) ($P_e = 0.51 \times 10^{-6}$ cm/s, Alog$P = 1.85$), and, finally, desmethyl (19) ($P_e = 0.21 \times 10^{-6}$ cm/s, Alog$P = 1.93$) [23]. The data for this series offer insight regarding the effects of side chains and N-methylation on the permeability of a scaffold. 17 and 18 differ by a single side-chain methyl group (Ile vs. Val), the removal of which results in a 75% decrease in permeability, as well as a conformational change. The removal of an aliphatic carbon from the side chain of 16 also decreases permeability relative to 17, even though the modified structure maintains the network of IMHBs. In this scaffold, neither the removal of an aliphatic carbon from a side chain nor the disruption of the IMHB pattern impacts permeability as much as the removal of an *N*-methyl group. 19 is the least permeable analogue in the series, suggesting that N-methylation of solvent-exposed hydrogen bond donors is the most

effective structural modification to alter permeability in this series. Similar structure–permeability relationships have been observed in a series of synthetic analogues of the natural product sanguinamide A (Figure 5.11) [24].

Uncharged homodetic and heterodetic cyclic peptides and hybrid cyclic peptide/polyketides differ in structure and size, but they appear to adopt similar strategies to passively permeate cell membranes. The number of H-bond donors is diminished either by N-methylation or the adoption of IMHB conformers in low dielectric environments, similar to CsA. These molecules demonstrate that the presence of an H-bond donor (OH or NH) only abrogates permeability if the scaffold cannot compensate for its presence by forming a hydrogen bond. While conformational rigidity is beneficial for the stability of IMHBs and is observed in most known synthetic passively permeable cyclic peptides, many cyclic peptide natural products demonstrate solvent-dependent flexibility, adopting rigid conformations only in low dielectric solvents [24]. This "chameleonic" solvent-dependent behavior could be essential in driving the aqueous solubility or target binding of these macrocycles, just as it is for CsA [32]. It should also be noted that the passively permeable cyclic peptides described previously possess Alog$P$ [63, 64] values ranging from 1.8 to 4.12, while peptides subject to alternative modes of membrane permeation, like kalata B1 (Alog$P = -0.45$), tend to fall below this range. Therefore, in the absence of 3D structural data, two-dimensional atomistic lipophilicity calculations could serve as a filter in the initial steps of the determination or design of passively permeable cyclic peptides. As the number of known passively permeable cyclic peptide natural products grows, so does our insight regarding the possibilities and limits for the design of cyclic peptide scaffolds with favorable ADME properties.

5.3.3 Lipophilic (Alog*P* > 3) Peptides and Reported Bioactivities

Based on our current understanding of structure–permeability relationships in cyclic peptides—lipophilicity trends, N-methylation, and IMHB patterns in particular—the compounds described in the following text are likely to exhibit moderate to high passive permeability. The lariat depsipeptide griselimycin (21) (Figure 5.12) has been shown to be 48% orally bioavailable in rats [86]. While it should be noted that passive permeability does not directly translate to oral bioavailability and the 3D structure of griselimycin has not been reported, the hydrophobic nature of this scaffold (Alog$P = 3.16$) suggests it may be capable of passive membrane permeation. Moreover, while nothing is known about the oral bioavailability or permeability of stylissamide G (22) (Alog$P = 3.09$), cordyheptapeptide A (23) (Alog$P = 4.15$),

Griselimycin (**21**)

Stylissamide G (**22**)

Cordyheptapeptide (**23**)

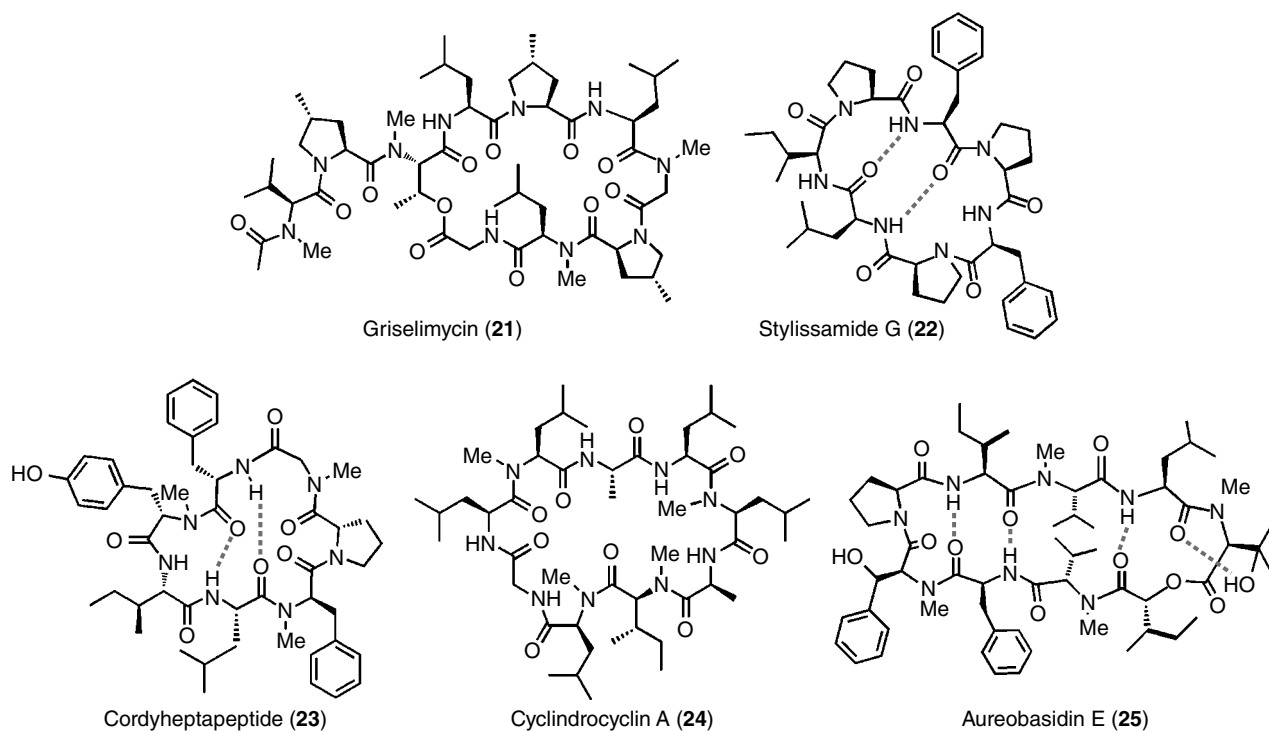Cyclindrocyclin A (**24**)

Aureobasidin E (**25**)

Figure 5.12 Structures and IMHB patterns of cyclic peptides with unknown, but likely, passive permeability.

and cylindrocyclin A (**24**) (Alog$P$ = 3.63) (Figure 5.12), all three structures both fall in an Alog$P$ range that is permissible for passive permeability and adopt low energy conformations with multiple IMHBs. In the crystal structure of the antimalarial **23**, two unmethylated amides are engaged in hydrogen bonds [87]. Amide temperature coefficient studies have shown that **22** adopts a relatively rigid hydrogen bonding conformation in CD_2Cl_2 [88], and **24** [89] is capable of shielding all of its NH groups in $CDCl_3$ (J. A. Schwochert and R. S. Lokey, Unpublished, 2015).

Aureobasidin E (**25**) (Figure 5.12), a close structural relative of aureobasidin A, is a potent antifungal [90–94]. The uncharged nonadepsipeptide is tetra-N-methylated and contains several β-branched residues and has an Alog$P$ value of 4.57. The crystal structure of **25** shows three transannular amide hydrogen bonds, and although the *N*-methyl valine is hydroxylated, the OH is positioned to engage in an IMHB with the N-terminal carbonyl [93]. In DMSO, **25** adopts two conformers, resulting from a cis–trans isomerism about the Pro-Phe amide. Both conformers only have two IMHBs [92]. In chloroform, however, the *cis* conformer is dominant and stabilized by the OH—CO hydrogen bond [95].

Apratoxin A (**26**) and B (**27**) (Figure 5.13) are uncharged homodetic cyclic peptide/polyketide hybrids with Alog$P$ values of 4.95 and 4.72, respectively. Isolated from the marine cyanobacterium *Lyngbya majuscula*, **26** exhibits

potent activity against human solid tumor cell lines (KB IC_{50} = 0.52 nM, LoVo IC_{50} = 0.36 nM) and has shown marginal activity *in vivo* against colon and mammary cancer [96]. More recent studies have shown that **26** modulates co-translational translocation [97], although other evidence points toward a mechanism involving association with Hsp/Hsc70 and subsequent stimulation of chaperone-mediated autophagy of specific client proteins [98]. No IMHBs were observed in the chloroform NMR structure nor molecular dynamics conformers of **26** [96]. The structure of **27**, however, appears to compensate for the loss of an isoleucine *N*-methyl group with the formation of an IMHB [99]. This conformational difference could represent an effective strategy to prevent exposure of NH groups.

5.4 Recently Discovered Bioactive Cyclic Peptide Natural Products

In this section, we highlight select bioactive cyclic peptide natural products discovered between late 2011 and early 2015. These compounds represent a wide variety of structural classes and exhibit a diverse range of bioactivities. Not surprisingly, many of these peptides resemble the better understood passively permeable scaffolds discussed previously in that they also exceed Lipinski's molecular weight limit of 500 Da. Many of the cyclic

Figure 5.13 Structures of apratoxin A and B.

Apratoxin A (**26**)

Apratoxin B (**27**)
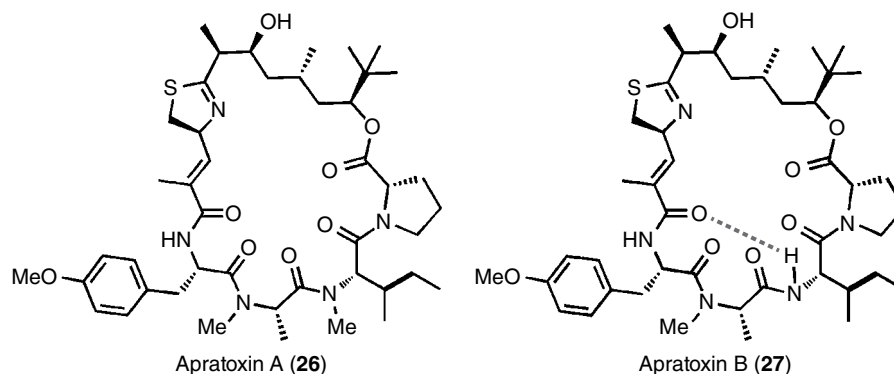
peptides surveyed contain hydrophobic side chains and N-methylated amides, resulting in Alog*P* values between 2 and 5, possibly affording passive membrane permeability. Furthermore, a few structures have been shown in crystal structures to adopt IMHBs, like the scaffolds discussed previously. Others are either heavily charged, polar, or considerably larger than any known passive permeators (>1300 Da), making passive permeation of lipophilic membranes an unlikely mechanism for these molecules. Unless addressed explicitly, the details regarding the cellular permeability of the compounds featured in the following sections are unknown.

The following cyclic peptides have been organized into two major categories: "midsized macrocycles" and "large/complex peptides." Midsized macrocycles include homodetic and heterodetic, charged and uncharged, proteinogenic and non-proteinogenic, and amide- and depsi-linked peptides. The large/complex peptides group includes cystine knot peptides and lantibiotics. Within these two major categories, the display and discussion of these compounds has been organized by bioactivity (cytotoxic, antibacterial, antiviral, antiparasitic, antifungal, protease inhibition, and others).

5.4.1 Midsized Macrocycles

5.4.1.1 Cytotoxics

Vieequeamide A (**28**; Figure 5.14) (Alog*P* = 3.49) was isolated from the cyanobacterium *Rivularia* sp. [100]. The cyclic depsipeptide contains the polyketide synthetase-derived 2,2-dimethyl-3-hydroxy-7-octynoic acid (Dhoya), as well as dual N-methylation and β-branched residues. This molecule is cytotoxic to H460 human lung cancer cells (LD$_{50}$ 60 nM). However, viequeamides B–F, which differ from A at three side-chain positions, are inactive in the same assay. Being a member of the kulolide superfamily, which exhibits a wide variety of activities, viequeamide A and its analogues could serve as strong pool of candidates for further structure–activity and structure–permeability relationship studies.

Cordyheptapeptides C–E (**29–31**; Figure 5.14) were isolated from a fermentation extract of the fungus *Acremonium persicinum* SCSIO [101]. Like cordyheptapeptide A, these new analogues are composed of residues with proteinogenic side chains and three N-methylated amides. The crystal structure of **29** shows 2 IMHBs between the leucine and phenylalanine, which enforce a β-turn about the Tyr-Val, while the D-Phe-L-Pro amide adopts a *cis*-conformation. The three compounds showed differential cytotoxicity against cancer cell lines. While **29** and **31** showed comparable moderate activity against SF-268 and MCF-7 (IC$_{50}$ = 3.0 μM, both) and NCI-H460 (IC$_{50}$ = 4.5 and 11.6 μM, respectively), **30** displayed weaker activity in all cell lines (IC$_{50}$ > 45 μM). Since no difference in activity is observed between **29** and **31**, neither the Val/Ile nor the Phe/Tyr substitution alone can be responsible for the significant reduction of activity of **30**. All three compounds fall in an Alog*P* range (3.28–3.86) permissible for passive membrane permeation. Compound **30**, however, is less lipophilic than both **29** and **31**. Therefore, the differences in physicochemical properties, rather than the K_d of drug–target interactions of this series, may account for the diminished activity of **30**.

Nazumazoles A–C (**32–34**; Figure 5.14) (Alog*P* = 0.41–0.53) were isolated from the sea sponge *Theonella swinhoei* [102]. Each macrocycle is composed of unusual amino acids, including a *cis*-4-methylproline, an alanine oxazole, a formylated β-amino residue, and an α-keto-β-amino residue. The pseudosymmetrical bicycles are tethered together through a disulfide. A mixture of the three compounds exhibited cytotoxicity against P388 murine leukemia cells (IC$_{50}$ = 0.83 μM). Reduction of the ketone diminished activity, as did alkylation of the thiols, suggesting dimerization is necessary for the cytotoxic effect.

Cycloforskamide (**35**; Figure 5.15) (Alog*P* = 2.19) was isolated from the sea slug *Pleurobranchus forskalii* [103]. This cyclic decapeptide shows structural similarity to the patellamides and lissoclinamides, in that it is
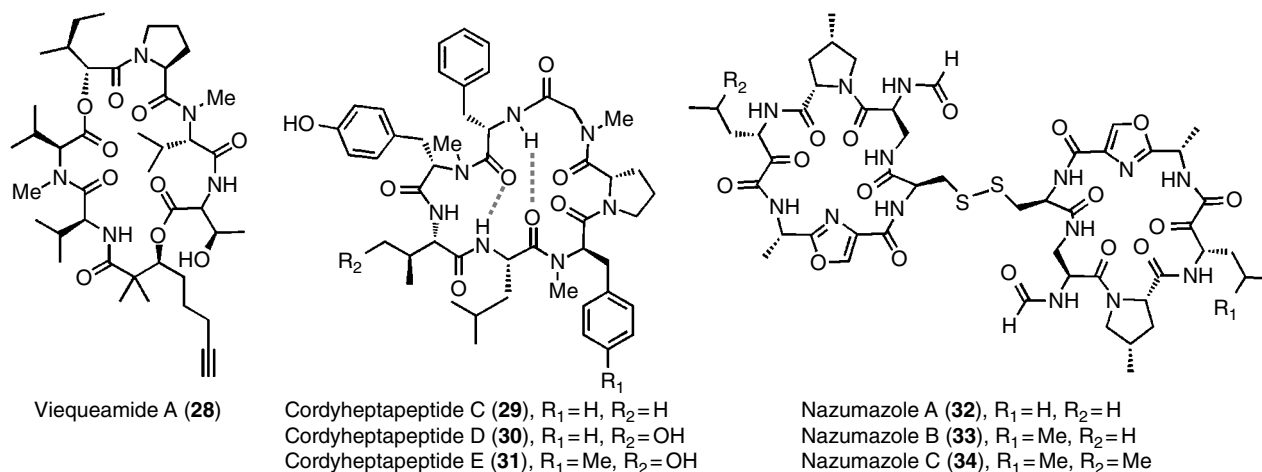
Figure 5.14 Cytotoxic cyclic peptides I.

Viequeamide A (**28**)

Cordyheptapeptide C (**29**), $R_1 = H$, $R_2 = H$
Cordyheptapeptide D (**30**), $R_1 = H$, $R_2 = OH$
Cordyheptapeptide E (**31**), $R_1 = Me$, $R_2 = OH$

Nazumazole A (**32**), $R_1 = H$, $R_2 = H$
Nazumazole B (**33**), $R_1 = Me$, $R_2 = H$
Nazumazole C (**34**), $R_1 = Me$, $R_2 = Me$

rich in aliphatic and β-branched amino acids and thiazolines. The compound was cytotoxic to P388 cells (IC_{50} of 5.8 μM).

Pipecolidepsin A (**36**) and B (**37**) (Figure 5.15) ($AlogP = -1.42$ and -1.15) were isolated from the sponge *Homophymia lamellosa* [104]. The lariat scaffold contains the unusual residues *N*-methyl glutamine, 3-ethoxyasparagine, 4,7-diamino-2,3-dihydroxy-7-oxoheptanoic acid, 3,4-dimethylglutamine, and 2-amino-3-hydroxy-4,5-dimethylhexanoic acid, which forms the depsi-linkage with pipecolic acid. Compound **36** exhibited micromolar to high nanomolar cytotoxicity against multiple cancer cell lines, while the β-hydroxylated **37** was even more potent ($IC_{50} = 10$–40 nM in A-549, MDA-MB-321, and HT-29), showing a 100-fold increase in potency over **36** in the HT-29 cell line. These compounds are large, hydrophilic, charged at physiological pH, and, therefore, unlikely to be passively permeable.

Rubishumanins A (**38**) and B (**39**) (Figure 5.15) ($AlogP = 1.09$ and $1.1.56$) were isolated from the plant *Rubia schumanniana* [105]. These cyclic hexapeptides contain D-alanine, three *N*-methyl amino acids, *O*-methyl tyrosine, and fused tyrosine residues in positions 5 and 6, respectively, that restrain macrocycle conformation. In deuterated pyridine, **38** and **39** each assume a single conformer with a *cis*-amide at $NMeTyr^6$ and a *trans*-amide at $NMeTyr^3$. Both **38** and **39** are active against A-549 (19 and 6 μM, respectively), BCG-823 (2.6 and 1.7 μM), and HeLa (N.D. and 10 μM), comparable with the cytotoxicity of cisplatin.

Minutissamides A–D (**40**–**43**; Figure 5.15) ($AlogP = 0.9$–1.21) were isolated from the cyanobacterium *Anabaena minutissima* [106]. These cyclic peptides are composed of *N*-methyl asparagine, α,β-dehydro-α-aminobutyric acid, and 2-hydroxy-3-amino acid with a long, variably decorated lipophilic tail in addition to

canonical amino acids. All compounds display low micromolar activity against HT-29 cells with IC_{50} of 2.0, 20.0, 11.8, and 22.7 μM for **40**, **41**, **42**, and **43**, respectively.

Mebamides A (**44**) and B (**45**) (Figure 5.16) ($AlogP = 2.60$ and 2.32) were isolated from the green alga *Derbesia marina* [107]. These lariat lipopeptides contain four D-amino acid residues and 3,8-dihydroxy-9-methyldecanoic acid. While neither **44** nor **45** exhibited significant inhibitory activity against HeLa or HL60 cells (**44**, $IC_{50} = 48$ and 19 μM, respectively; **45**, $IC_{50} > 100$ μM on both), **45** significantly induced the adhesion of HL60 cells at 100 μM. The morphological features of HL60 cells incubated with 100 μM of **45** were similar to those of cells treated with 12-*O*-tetradecanoylphorbol-13-acetate, which induces differentiation of HL60 cells into macrophages, prompting the authors to suggest that this peptide also may promote differentiation.

Calyxamides A (**46**) and B (**47**) (Figure 5.16) ($AlogP = 1.42$) were isolated from the sponge *Discodermia calyx* and may derive from the unculturable symbiont *Candidatus Entotheonella* sp. [108]. The diastereomeric lariat cyclic peptides contain a polyketide-derived α,β-unsaturated *O*-methyl serine thiazole moiety, a 5-hydroxytryptophan, and a formylated terminus. **46** and **47** show cytotoxicity against P388 with IC_{50} values of 3.9 and 0.9 μM, respectively.

Trichoramide B (**48**; Figure 5.16) ($AlogP = 1.16$) was isolated from the cyanobacterium *Trichormus* sp. UIC 10339 [109]. This cyclic lipopeptide contains four uncommon amino acids including homoserine, *N*-methylisoleucine, two 3-hydroxyleucines, β-aminodecanoic acid, and several hydroxylated and β-branched moieties. The compound was cytotoxic to MDA-MB-435 and HT-29 cancer cell lines (IC_{50} 0.8 and 1.5 μM, respectively).
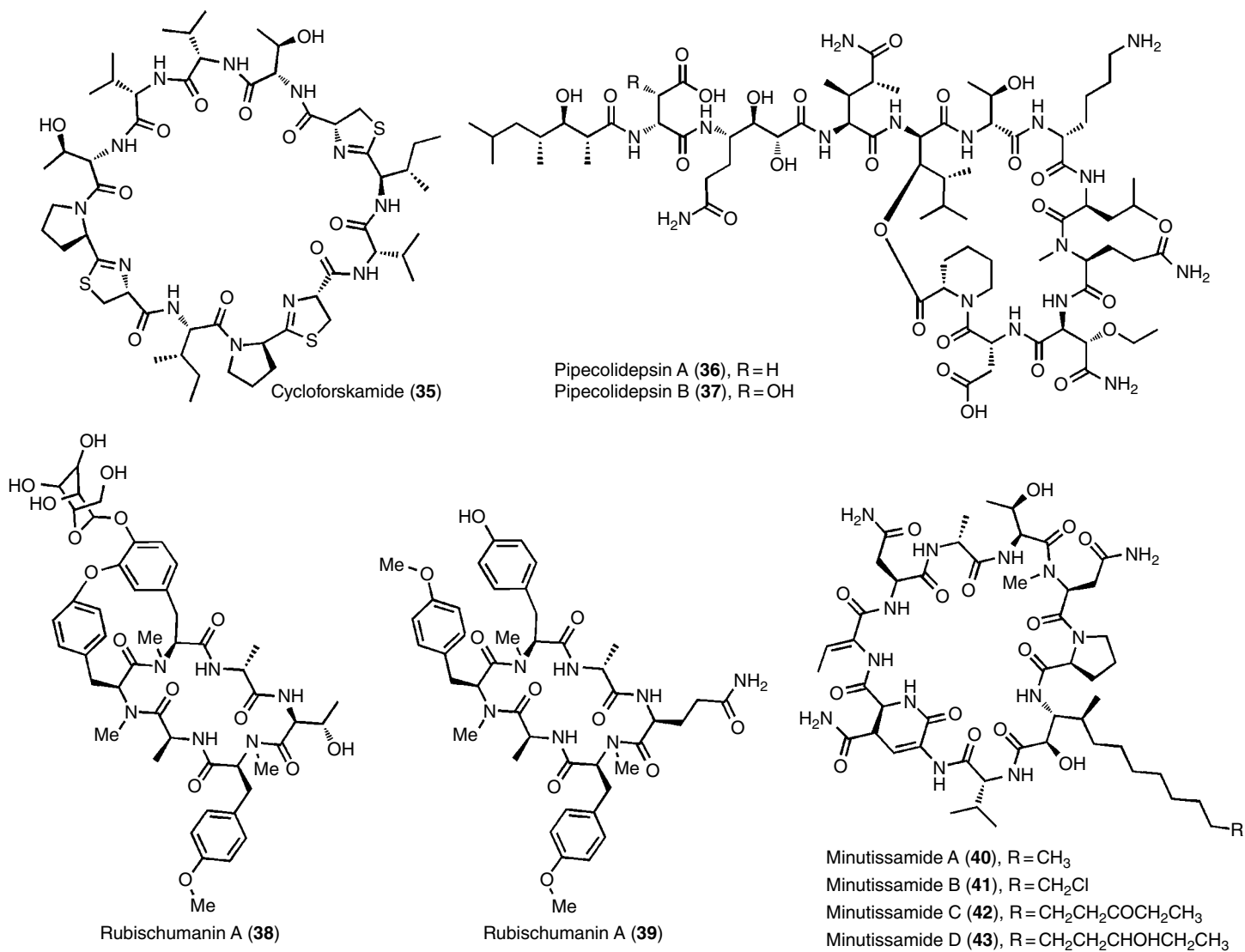
Cycloforskamide (**35**)

Pipecolidepsin A (**36**), R = H
Pipecolidepsin B (**37**), R = OH

Rubischumanin A (**38**)

Rubischumanin A (**39**)

Minutissamide A (**40**), R = CH₃
Minutissamide B (**41**), R = CH₂Cl
Minutissamide C (**42**), R = CH₂CH₂COCH₂CH₃
Minutissamide D (**43**), R = CH₂CH₂CHOHCH₂CH₃

Figure 5.15 Cytotoxic cyclic peptides II.

Mebamide A (**44**), R = A C
Mebamide B (**45**), R = H

Calyxamide A (**46**), *S,S*
Calyxamide B (**47**), *R,R*

Trichoramide B (**48**)

Oleamycin A (**49**)

Kailuin G (**50**), R = H

Kailuin H (**51**), R = Me

Apratoxin H (**52**)

Apratoxin A sulfoxide (**53**)
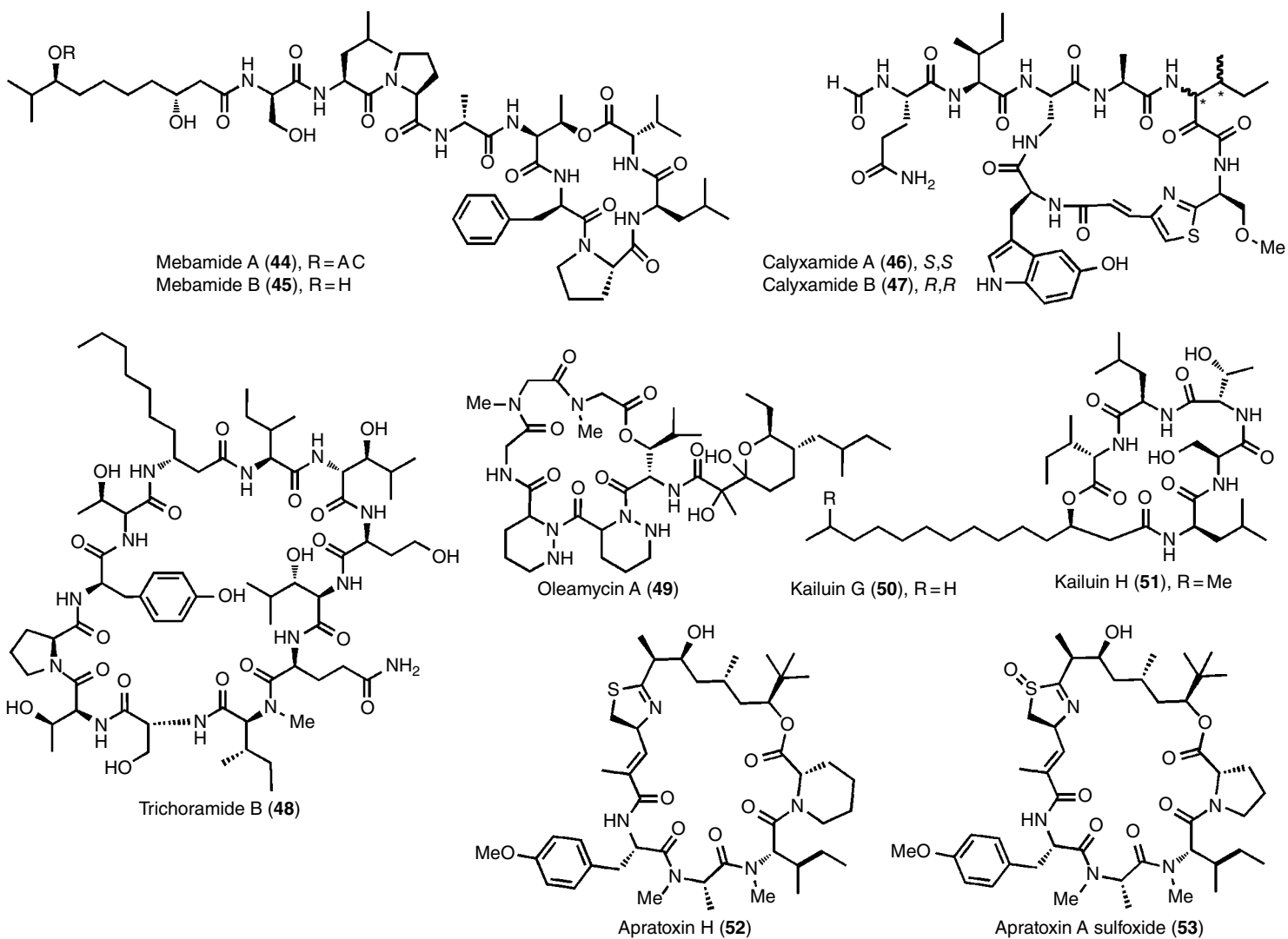
Figure 5.16 Cytotoxic cyclic peptides III.
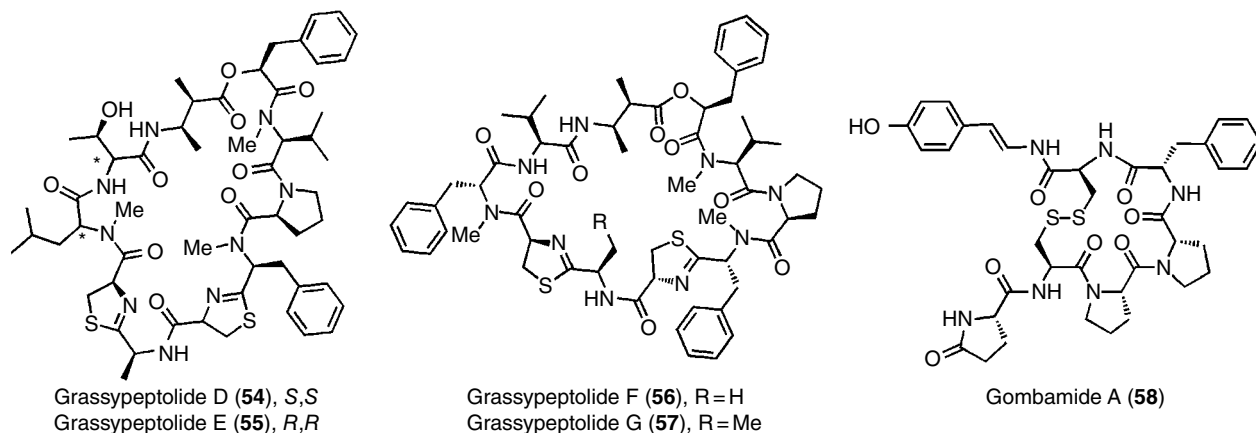
Figure 5.17 Cytotoxic cyclic peptides IV.

Grassypeptolide D (**54**), *S*,*S*
Grassypeptolide E (**55**), *R*,*R*

Grassypeptolide F (**56**), R = H
Grassypeptolide G (**57**), R = Me

Gombamide A (**58**)

Oleamycin A (**49**; Figure 5.16) (Alog*P* = 0.63) was isolated from a culture of *Streptomyces* sp. [110]. The cyclic depsipeptide contains 3-hydroxyleucine, two piperazic acid residues, a sarcosine, and an exocyclic polyketide unit. The peptide exhibited antibacterial activity against *S. aureus* and *M. luteus* (MIC 279 and 36 nM, respectively) and cytotoxic activity against HCT-116 cells (IC$_{50}$ 7.8 nM).

Kailuins G (**50**) and H (**51**) (Figure 5.16) (Alog*P* = 4.63 and 4.56) were isolated from the Gram-negative bacterium *Photobacterium halotolerans* [111]. These lariat lipopeptides are active against HCT-116 cells (IC$_{50}$ 32 and 17 μM, respectively), while the core and lactam are inactive at concentrations greater than 1 mM. These compounds showed weak to no antimicrobial activity.

Apratoxins H (**52**) and A sulfoxide (**53**) (Figure 5.16) (Alog*P* = 5.19 and 3.80) were isolated from the marine cyanobacterium *Moorea producens* [112]. Compound **52** has a pipecolic acid in place of the proline of apratoxin A, while **53** has an oxidized thiazole. These hybrid polyketide–peptides show cytotoxicity against human NCI-H460 lung cancer cells (IC$_{50}$ = 3.4 and 89.9 nM, respectively).

Grassypeptolides D (**54**) and E (**55**) (Figure 5.17) (Alog*P* = 3.87) were isolated from the marine cyanobacterium *Leptolyngbya* species, while F (**56**) and G (**57**) (Alog*P* = 5.19 and 4.99, respectively) came from *L. majuscula* [113, 114]. These cyclic depsipeptides contain a bisthiazole region, a 2,3-dimethyl-3-amino acid, three D-amino acids, and extensive N-methylation. The diastereomers **54** and **55** are cytotoxic to HeLa (IC$_{50}$ 335 and 192 nM, respectively) and murine neuro-2a blastoma cells (IC$_{50}$ 599 and 407 nM). Compounds **56** and **57** show moderate inhibitory activity in the transcription factor AP-1 assay in HEK293 cells (IC$_{50}$ 5.2 and 6.0 μM, respectively), but cytotoxicity was found in the same order of magnitude.
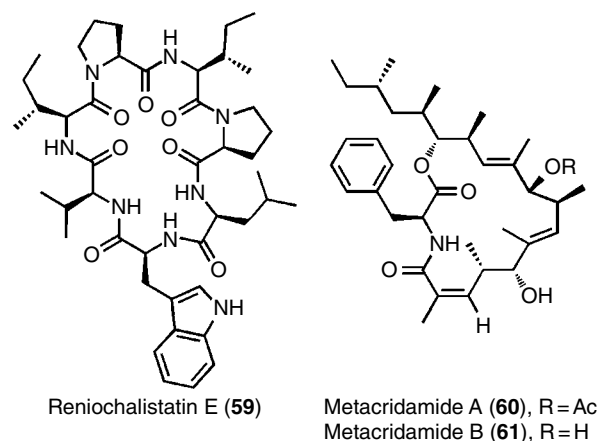

Reniochalistatin E (**59**)

Metacridamide A (**60**), R = Ac
Metacridamide B (**61**), R = H

Figure 5.18 Cytotoxic cyclic peptides V.

Gombamide A (**58**; Figure 5.17) (Alog*P* = 1.47) was isolated from the marine sponge *Clathria gombawuiensis* [115]. This proline-rich cyclic peptide contains the unusual amino acids *p*-hydroxystyrylamide (pHSA), and pyroglutamic acid (pyroGlu). The peptide is cyclized through a disulfide bond, a structure rarely found in sponge-derived compounds. **56** exhibited cytotoxicity against A-549 (LC$_{50}$ = 7.1 μM) and K-562 (6.9 μM) cell lines, as well as moderate inhibition of Na$^+$/K$^+$-ATPase (17.8 μM).

Reniochalistatin E (**59**; Figure 5.18) (Alog*P* = 3.43) was isolated from the marine sponge *Reniochalina stalagmites* [116]. The cyclic heptapeptide is composed completely of proteinogenic amino acids, including three prolines, three aliphatic β-branched amino acids, and a tryptophan. Compound **59** was the only bioactive compound in a series of five analogues isolated (A–E) against melanoma RPMI-8226 and gastric MGCC-803 cells (IC$_{50}$ 4.9 and 9.7 μM, respectively). The tryptophan residue was unique to **59** in the SAR series.

Metacridamides A (**60**) and B (**61**) (Figure 5.18) (Alog*P* = 6.03 and 5.57, respectively) were isolated from the entomopathogenic fungus *Metarhizium acridum* [117]. These cyclic polyketide–peptide hybrids are cyclized through a polyketide-Phe ester. Neither analogues show antimicrobial, phytotoxic, or insecticidal activity, but **60** is cytotoxic to MCF-7, HepG2/C3A, and Caco-2 (IC$_{50}$ 11.0, 10.8, and 6.2 μM, respectively). Compound **61** is active against HepG2/C3A cells (IC$_{50}$ = 18.2 μM) but inactive against other cell lines.

5.4.1.2 Antibacterials

Lassomycin (**62**; Figure 5.19) (Alog*P* = −0.66) was isolated from the soil bacterium *Lentzea kentuckyensis* [118]. The 16-amino acid peptide is genome encoded and cyclized through a Gly^1–Asp^8 side-chain lactam linkage, forming an N-terminal macrocycle and an 8-amino acid C-terminal tail. This peptide had an MIC of 425 nM against *Mycobacterium tuberculosis*. Resistant mutants of *M. tuberculosis* to **62** were mapped to the *clp*C1 gene. **62** was shown to increase ATP hydrolysis by the essential ATP-dependent protease ClpC1 7–10-fold, with an apparent K_d of 0.41 μM, which resembles the MIC of *M. tuberculosis*. The basic cyclic peptide was docked to the acidic N-terminus of the crystal structure of ClpC1 *in silico*, demonstrating an allosteric binding mode.

Streptomonomycin (**63**; Figure 5.19) (Alog*P* = 1.39) was isolated from *Streptomonospora alba* [119]. The 21 amino acid lassopeptide is cyclized through a rare Ser^1–Asp^9 linkage and adopts a conformation in deuterated methanol in which the C-terminal tail (at residues 14–16) threads through the N-terminal macrocycle. This lassopeptide is unusual for its class. It has 5% hydrophilic and 52% hydrophobic residues and an N-terminal Ser in place of the more common Gly or Cys. The compound was inactive against a panel of Gram-negative bacteria and fungi but active against Gram-positive *Bacillus anthracis* (MIC 2–4 μM). Streptomonomycin-resistant *B. anthracis* mutants were enriched in mutations in the walR gene, suggesting **63** may target cell wall metabolism.

Teixobactin (**64**; Figure 5.20) (Alog*P* = 0.45) was discovered in a screen of uncultured bacteria and derives from the soil microbe *Aquabacteria Eleftheria terrae* [120, 121]. The nonribosomal peptide contains a depsi-linkage, an enduracididine, *N*-methylphenylalanine, and four ᴅ-amino acid residues. **64** showed strong antibacterial activity against *C. difficile* (MIC = 4 nM), *B. anthracis* (16 nM), but only modest activity against MSSA (200 μM), MRSA (200 μM), and *M. tuberculosis* (100 μM), and no cytotoxicity against mammalian NIH/3T3 and HepG2 at 80 μM. In mice infected with *S. pneumonia*, the compound caused a 6 log$_{10}$ reduction in c.f.u. in lungs, on par with amoxicillin at 10 mg/kg. No mutants of *S. aureus* or *M. tuberculosis* were obtained, suggesting this peptide could serve in the development of antibiotics that circumvent bacterial resistance.

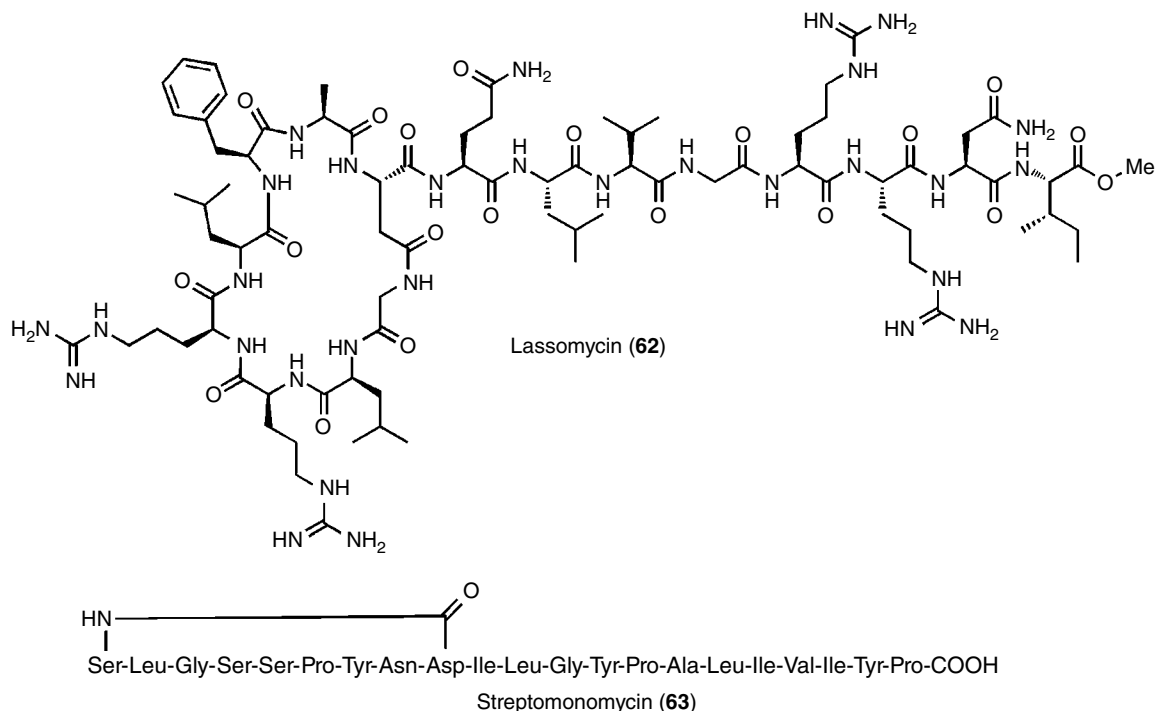NW-G12 (**65**; Figure 5.20) (Alog*P* = −0.32) was isolated from *Streptomyces alboflavus* 313 [122]. This cyclic

Lassomycin (**62**)

Ser-Leu-Gly-Ser-Ser-Pro-Tyr-Asn-Asp-Ile-Leu-Gly-Tyr-Pro-Ala-Leu-Ile-Val-Ile-Tyr-Pro-COOH

Streptomonomycin (**63**)

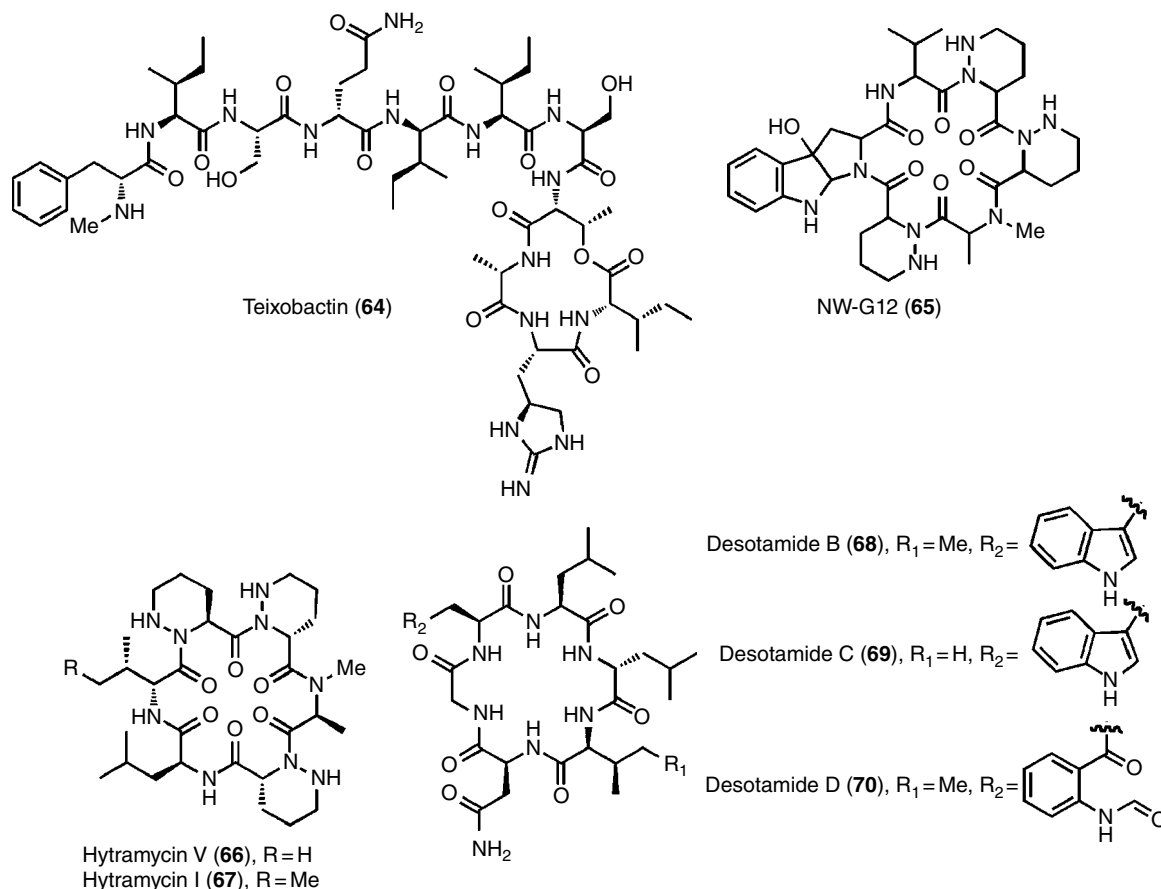**Figure 5.19** Antibacterial cyclic peptides I.

Figure 5.20 Antibacterial cyclic peptides II.

hexapeptide contains piperazic acid, *N*-methylalanine, valine, and hydroxyhexahydropyrroloindole residues. The compound showed antibacterial activity against *B. cerus* (MIC = 4.3 μM), *S. aureus* (MIC = 6.25 μM), and *Bacillus subtilis* (MIC = 6.25 μM), but no activity against *E. coli* or *P. aeruginosa*.

Hytramycins V (**66**) and I (**67**) (Figure 5.20) (Alog*P* = −0.31 and −0.01) were isolated from *Streptomyces hygroscopicus* ECUM 14046 [123]. The cyclohexapeptides differ in a single side chain and each contains three piperazic acid residues and one N-methylated residue. They were found to be weakly active against a panel of monodrug-resistant *M. tuberculosis* (MICs ∼ 10 and 20 μM, respectively).

Desotamides B–D (**68–70**; Figure 5.20) (Alog*P* = 1.44, 0.96, and 0.66, respectively) were isolated from the marine microbe *Streptomyces scopuliridis* SCSIO ZJ46 [124]. These cyclic hexapeptides contain several aliphatic and aromatic non-proteinogenic amino acids. Compound **68**, like the previously discovered desotamide A [125], displayed modest antibacterial activity against *S. pneumoniae*, *S. aureus*, and MRSE (MICs 18, 23, and 46 μM,

respectively). Compounds **69** and **70** were inactive up to 150 μM, demonstrating the essential role of the tryptophan in the observed bioactivity.

Ohmyungsamycins A (**71**) and B (**72**) (Figure 5.21) (Alog*P* = 3.49 and 3.67) were isolated from the marine bacterial strain *Streptomyces* SNJ042 [126]. These lariat depsipeptides contain the unusual amino acids *N*-methyl-4-methoxytryptophan, β-hydroxyphenylalanine, *N,N*-dimethylvaline, and several other *N*-methyl and β-branched amino acids. Both **71** and **72** showed significant cytotoxicity against a panel of cancer cell lines and antibacterial activities. Notably, **71** was more cytotoxic (IC$_{50}$ 300–800 nM) than **72** (IC$_{50}$ 12–17 μM) and also more potent as an antimicrobial against *B. subtilis*, *Kocuria rhizophila*, *Proteus hauseri* (**71**, MIC 1–4 μM; **72**, MIC 8–34 μM). The degree of methylation at the N-terminal alanine obviously influences the bioactivity of this scaffold.

Peptidolipins B–F (**73**; Figure 5.21) (Alog*P* = 6.52–7.13) were isolated from a *Nocardia* sp. from the ascidian *Trididemnum orbiculatum* and differ in lipid chain length and degree of unsaturation [127]. The depsilipopeptides
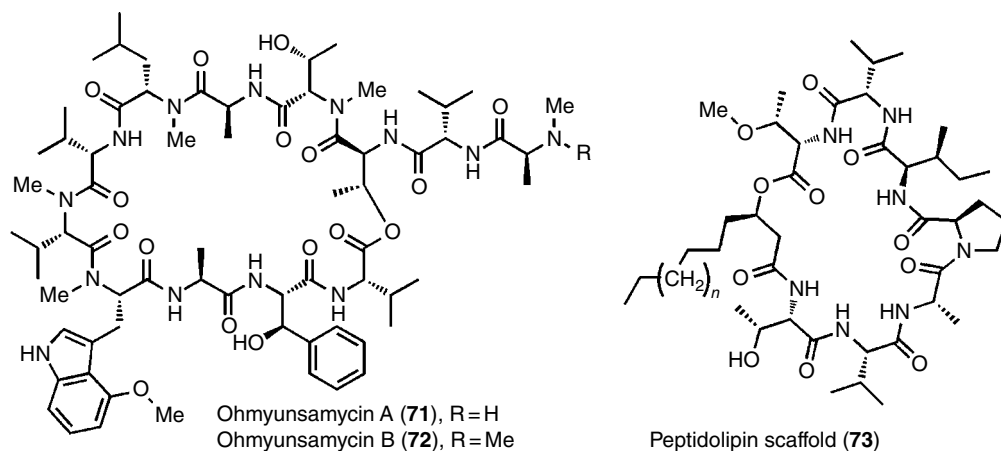
Ohmyunsamycin A (**71**), R = H
Ohmyunsamycin B (**72**), R = Me

Peptidolipin scaffold (**73**)

Figure 5.21 Antibacterial cyclic peptides III.

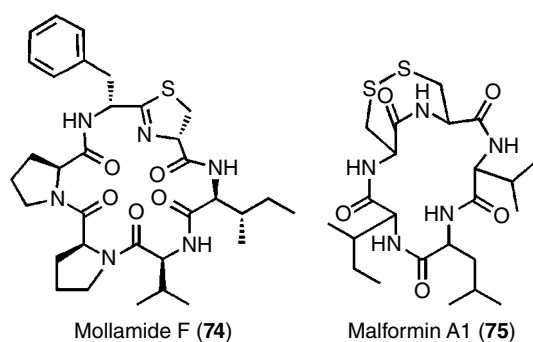

Mollamide F (**74**)

Malformin A1 (**75**)

Figure 5.22 Antiviral cyclic peptides.

B and E exhibited weak bacteriostatic activity against MRSA and MSSA (MIC 57 μM).

5.4.1.3 Antivirals

Mollamide F (**74**; Figure 5.22) (Alog$P$ = 2.44) was isolated from the marine invertebrate *Didemnum molle* [128]. This sequence was found to be ribosomally produced but posttranslationally modified to generate the thiazoline and D-Phe components. **74** was active in both an HIV integrase inhibition assay and a cytoprotective cell-based assay (IC$_{50}$ 39 and 78 μM, respectively).

Malformin A1 (**75**; Figure 5.22) (Alog$P$ = 0.67) was isolated from the endophytic fungus *Aspergillus tubingensis* FJBJ11 [129]. The Cys residues of the cyclic pentapeptide are linked through a disulfide bridge, forming a conformationally constrained bicycle. **75** has an inhibitory effect against infection by and replication of tobacco mosaic virus (IC$_{50}$ 37 and 85 μM, respectively), demonstrating promise as a lead for viricidal peptide development.

5.4.1.4 Antiparasitics

Ribifolin (**76**; Figure 5.23) (Alog$P$ = 1.40) is a ribosomally synthesized homodetic peptide isolated from the plant *Jatropha ribifolia* [130]. The proteinogenic cyclic octa-

peptide exhibits activity against *Plasmodium falciparum* (IC$_{50}$ 42 μM), while the linear analogue showed weaker activity (IC$_{50}$ 519 μM). Simulated annealing molecular dynamics simulations revealed that ribofolin adopted a low energy conformer in water displaying two γ-turns with IMHBs between Leu^{2}CO-Ser^{4}NH and Ile^{6}CO-Gly^{8}NH and transannular IMHBs between Ile^1 and Ile^5, resembling a β-strand.

Balgacyclamides A (**77**) and B (**78**) (Figure 5.23) (Alog$P$ = 2.33 and 1.50) were isolated from *Microcystis aeruginosa* EAWAG 251 [131]. The cyclic hexapeptides contain oxazolines and thiazoles generated by the post-translational condensation of consecutive residues. The presence of one oxazoline moiety is not necessary for antiparasitic activity against *P. falciparum* (IC$_{50}$ 9.0 and 8.2 μM for **77** and **78**, respectively). The macrocycles are also active against *T. brucei rhodesiense* (IC$_{50}$ 50 μM) and *Leishmania donovani* (IC$_{50}$ 30 μM), with no toxicity to rat myoblasts at 150 μM.

Companeramide A (**79**) and B (**80**) (Figure 5.23) (Alog$P$ = 4.14 and 3.98) were isolated from the cyanobacterium *Leptolyngbya* sp. [132]. The tetra-*N*-methylated cyclic depsipeptides contain 3-amino-2-methyl-octynoic acid (Amoya), hydroxy isovaleric acid (Hiva), and eight α-amino acids enriched in β-branching methyl groups. Both companeramides show strong antiparasitic activity against chloroquine-sensitive and chloroquine-insensitive strains of *P. falciparum* with little toxicity to human cancer cell lines at 1 μM. **79** is more active against the chloroquine-sensitive strain D6 (IC$_{50}$ 570 nM) than the chloroquine-insensitive strains Dd2 (IC$_{50}$ 1000 nM) and 7G8 (IC$_{50}$ 1100 nM), while **80** is more active against D6, Dd2, and 7G8 (IC$_{50}$ 220, 230, and 700 nM, respectively), demonstrating the importance of certain side chains.

Apicidin F (**81**; Figure 5.23) (Alog$P$ = 3.01) was synthesized via the overexpression of an apicidin-like gene cluster from *Fusarium fujikuroi* [133]. The cyclic tetrapeptide

Ribifolin (**76**)   Balgacyclamide A (**77**)   Balgacyclamide B (**78**)

Companeramide A (**79**)   Companeramide B (**80**)   Apicidin F (**81**)
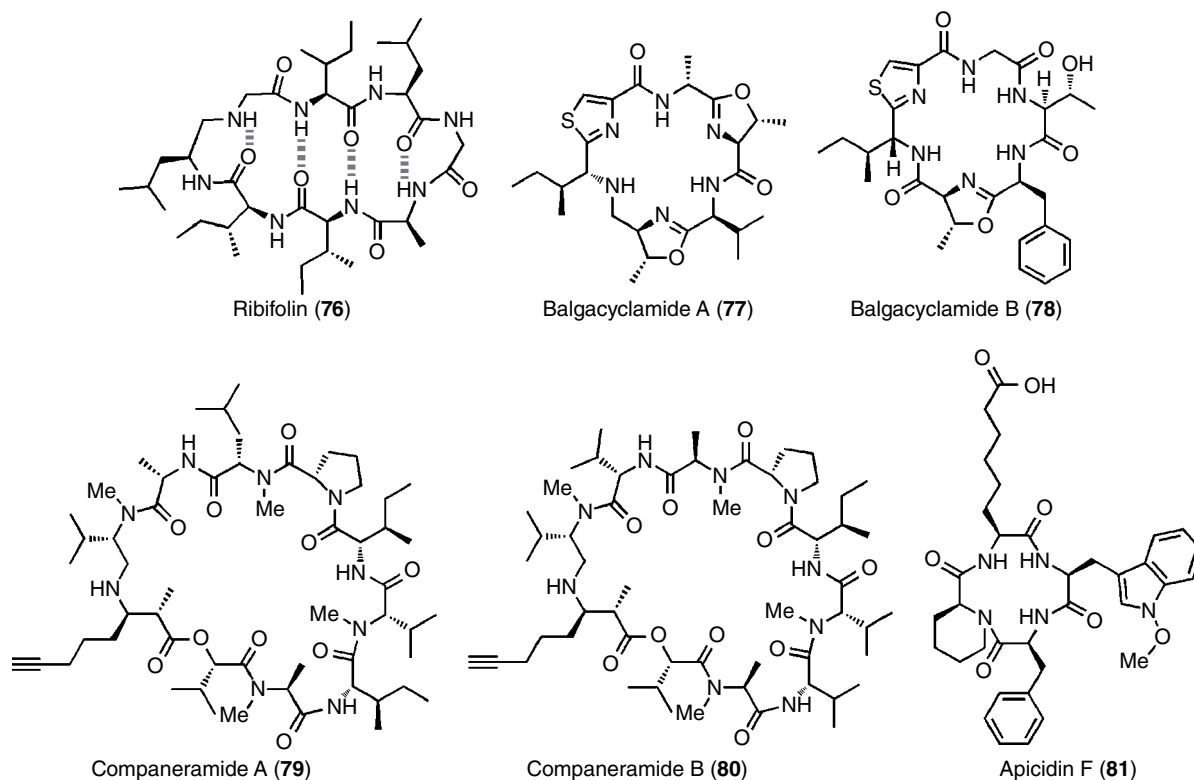
Figure 5.23 Antiparasitic cyclic peptides.

contains a pipecolic acid and an *N*-methoxytryptophan residue like other apicidins. However, the structure diverges from that of other apicidins with the presence of a free carboxylic acid at the terminus of the aliphatic tail and a phenylalanine in the macrocycle. Apicidin F (IC_{50} 0.67 μM) is threefold less active than apicidin (IC_{50} 0.2 μM) against *P. falciparum*.

5.4.1.5 Antifungals

Mohangamide A (**82**; Figure 5.24) was isolated from *Streptomyces* sp. [134]. This pseudodimeric dilactone-tethered cyclic peptide has aromatic polyketide-derived side chains. The compound showed activity as a *Candida albicans* isocitrate lyase inhibitor (IC_{50} 4.4 μM) and was active against *Candida* grown on acetate but not against *Candida* grown on glucose. **82** has an exceptionally high Alog*P* (3.24) for its size (MW = 2063) within the set of compounds reviewed here and may have the capacity to permeate membranes by passive diffusion.

The cyclic glycolipopeptides balticidins B (**83**) and D (**84**) (Figure 5.24) (Alog*P* = 0.87 and 0.75) were isolated along with linear analogues balticidins A and C from the cyanobacterium *Anabaena cylindrica* strain Bio33 [135]. The heavily hydroxylated lariat scaffolds of **83** and **84** are cyclized through a depsi-linkage and contain evidence of considerable posttranslational modifications, including N-methylation, unsaturation, and glycosylation.

Both cyclic peptides show strong specific antifungal activity with inhibition zones in agar diffusion assays of 21–32 mm against *C. albicans*, *krusei*, and *maltosa*.

5.4.1.6 Protease Inhibitors

Jatrophidin I (**85**; Figure 5.25) (Alog*P* = 0.94) was isolated from the latex of *Jatropha curcas* L. [136]. The cyclic octapeptide is composed completely of proteinogenic amino acids. **85** demonstrated selective pepsin inhibition (IC_{50} 0.88 μM). The backbone was found to adopt two conformations in d$_6$-DMSO, corresponding to Gly^7–Pro^8 cis–trans isomers.

New micropeptins (**86–90**; Figure 5.25) (Alog*P* = 0.62–1.72) were isolated from various *Microcystis* species [137, 138]. These lariat depsipeptides showed a variety of protease inhibitory activity. Specifically, HH978 (**86**) inhibited chymotrypsin (IC_{50} 4.3 μM) and elastase (IC_{50} 17.6 μM) but not trypsin or thrombin at 45 μM; HH960 (**87**) inhibited trypsin and elastase (IC_{50} 48.5 and 55.5 μM, respectively); HH992 (**88**) inhibited trypsin, chymotrypsin (IC_{50} 48.5 μM for both), and elastase (IC_{50} 16.9 μM). From the results for **86** and **88**, the 6-OH of 3-amino-6-hydroxy-2-piperidone (Ahp) is essential for inhibition of both chymotrypsin and elastase [137]. Sub-μM inhibition of chymotrypsin was achieved by KB928 (**89**) (IC_{50} 90 nM) but not KB992 (**90**) (IC_{50} > 45 μM) [138].

Mohangamide (**82**)

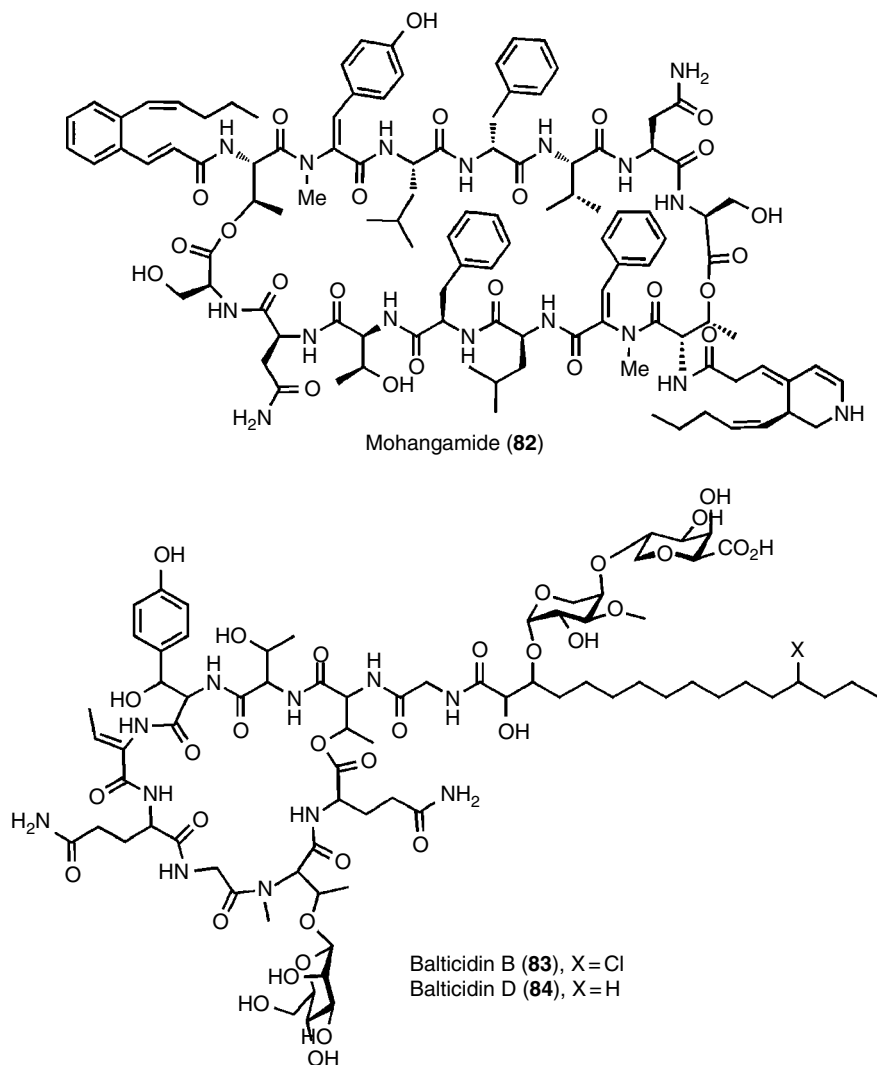Balticidin B (**83**), X = Cl
Balticidin D (**84**), X = H

Figure 5.24 Antifungal cyclic peptides.

Stigonemapeptin (**91**; Figure 5.25) (Alog$P$ = 1.26) was isolated from the cyanobacterium *Stigonema* sp. [139]. The lariat depsipeptide contains the uncommon amino acids Ahp, 2-amino-2-butenoic acid (Abu), and N-formylated proline. This cyclic peptide demonstrated notable selectivity for the inhibition of elastase (IC$_{50}$ 0.26 μM) over chymotrypsin (2.93 μM). The authors suggested that the positioning of Abu between Thr and Ahp could be responsible for this selectivity.

5.4.1.7 Other Bioactivities

Sungsanpin (**92**; Figure 5.25) (Alog$P$ = −1.57) is a lasso peptide from *Streptomyces* sp. [140]. This 15-amino acid structure contains an 8-membered N-terminal macrolactam formed through a Gly[1]–Asp[8] linkage and a 7-membered C-terminal tail, which threads through the loop. The peptide did not exhibit significant cytotoxicity

or antimicrobial activity but inhibited the migration of A-549 non-small-cell lung cancer *in vitro* by 25 and 47% at 5 and 50 μM, respectively. The compound also increased levels of tissue inhibitor metalloproteinase-1 (TIMP) mRNA levels in a concentration-dependent manner, suggesting that it could slow the degradation of extracellular matrices via inhibition of matrix metalloproteinases.

Coprisamides A (**93**) and B (**94**) (Figure 5.25) (Alog$P$ = −0.29) were isolated from a bacterium from the gut of the dung beetle *Copris tripartitus* [141]. These cyclic depsipeptides are highly modified and have two peptidic appendages. The structures contain β-methylaspartic acid, 2,3-diaminopropanoic acid, and 2-heptatrienyl cinnamic acid residues. Both **93** and **94** demonstrated dose-dependent activation of quinone reductase activity from 5 to 20 μM and may serve a role
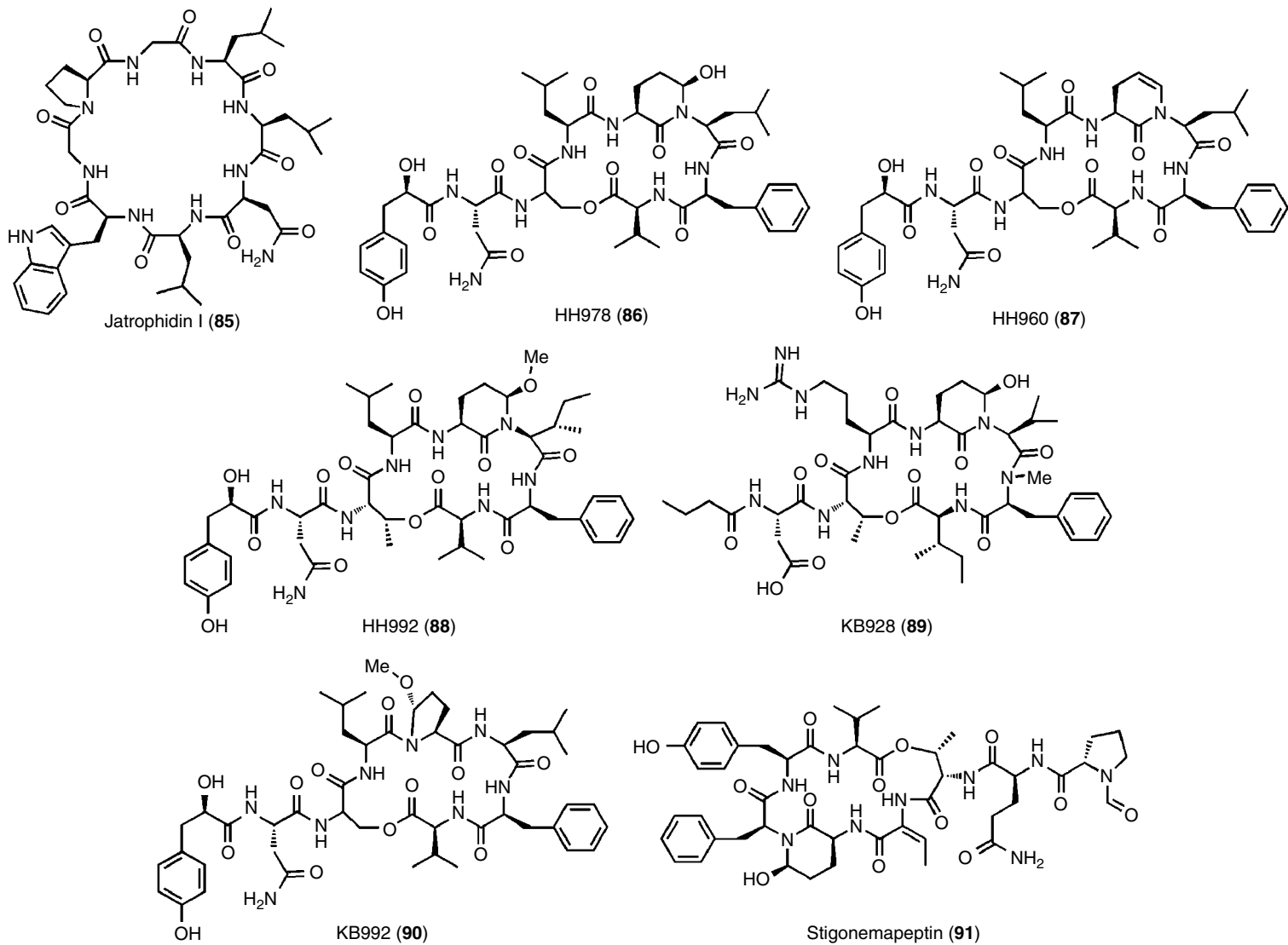
Figure 5.25 Protease-inhibiting cyclic peptides.

Jatrophidin I (**85**)

HH978 (**86**)

HH960 (**87**)

HH992 (**88**)

KB928 (**89**)

KB992 (**90**)

Stigonemapeptin (**91**)

in chemoprotective detoxification. Compounds **93** and **94** also inhibited the production of melanin content in mouse melana cells by 51 and 42%, respectively, at 20 μM.

Decatransin (**95**; Figure 5.26) (Alog$P$ = 4.17), a cyclic decadepsipeptide, was isolated from *Chaetosphaeria tulasneorum* [142]. The structure contains the non-proteinogenic amino acids pipecolic acid, *N*-methylhomoleucine, and the homoleucine-derived 2-hydroxy acid. It exhibits cytotoxic activity against HCT-116 and COS-1 (IC$_{50}$ 30–140 nM). It also inhibited *Saccharomyces cerevisiae* (IC$_{50}$ 2 μM). The compound has a chemogenomic profile comparable to those of HUN-7293 and cotransin, which inhibit co-translational translocation, and resistance mutants identified Sec61p, a gene involved in this process, as the target.

Psychrophilin G (**96**; Figure 5.26) (Alog$P$ = 2.30) was isolated from the marine-derived fungus *Aspergillus versicolor* ZLN-60 [143]. Showing no cytotoxicity, this small cyclic peptide exhibited lipid-lowering effects in HepG2 hepatocarcinoma cells at 10 μM. Intracellular lipid accumulation, similar to that of the cholesterol-lowering drug simvastatin, was observed.

Hikiamides A (**97**), B (**98**), and C (**99**) (Figure 5.26) (Alog$P$ = 3.75, 3.36, and 3.46, respectively) were isolated from *Fusarium* sp. TAMA 456 [144]. Although they differ in degree of N-methylation and aromatic residue identity, all three cyclic depsipeptides promoted adipocyte differentiation and activation of peroxisome proliferator-activated receptor γ (PPARγ) transcription in a concentration-dependent manner. The mRNA expression of adiponectin in adipocytes was enhanced with 2 μM **97** (13.3-fold), **98** (5.2-fold), and **99** (10-fold) relative to control. The N-methylated scaffolds, **97** and **99**, demonstrated increased potency over that of **98**. The hikiamides are the first set of cyclic peptides with adipogenic activity, with possible roles in the regulation of type 2 diabetes.

Autumnalide (**100**; Figure 5.27) (Alog$P$ = 1.51) was isolated from the cyanobacterium *Phormidium autumnale* [145]. The prenylated cyclic heptapeptide demonstrated activity as an indirect blocker of store-operated calcium channel influx to the endoplasmic reticulum.

Methylated cyclic tetrapeptides **101**, **102**, and **103** (Figure 5.27) (Alog$P$ = 3.04, 3.16, and 3.46) were isolated from *Onychocola sclerotica* [146]. In a calcium influx assay, **101** (IC$_{50}$ = 6.2 μM), **102** (IC$_{50}$ = 7.1 μM), and **103** (IC$_{50}$ = 5.0 μM) demonstrated inhibition on par with that of the benzothiazepine drug diltiazem.

Desmethylisaridins E (**104**), C2 (**105**), and C1 (**106**) (Figure 5.27) (Alog$P$ = 2.69, 2.94, and 2.95) were isolated from the filamentous fungus *Beauveria felina* spiked with the HDAC inhibitor suberoylanilide hydroxamic acid [147, 148]. The cyclic depsipeptides are composed of an *N*-methylvaline and a β-alanine residue in addition to proteinogenic amino acids and an isovaleric acid, which forms the ester linkage. Compound **105** has a β-methyl proline as well. They were found to exhibit a variety of moderate activities. Compound **106** was active against *E. coli* at 12 μM. Both **104** and **105** inhibited superoxide anion production in FMLP-induced human neutrophils, while **105** also inhibited elastase release from these cells (IC$_{50}$ 10 μM).

Cyclic depsipeptides turnagainolides A (**107**) and B (**108**) (Figure 5.27) (Alog$P$ = 2.51) were isolated from *Bacillus* sp. [149]. Compound **108** activates the inositol 5-phosphatase SHIP1, a negative regulator of the pathway found only in hematopoietic cells, *in vitro* (1.1-fold).

The dianthins G (**109**) and H (**110**) (Figure 5.28) (Alog$P$ = 0.89 and 0.79) were isolated from the medicinal plant *Dianthus superbus* [150]. These cyclic hexapeptides are composed of proteinogenic amino acids devoid of modification besides head-to-tail cyclization. The crystal structure of **109** adopts a conformation reminiscent of that of the N-methylated synthetic cyclic peptide of White *et al.* containing two IMHBs [14]. One IMHB (ThrNH-AlaCO) is a part of the β-turn and the other, between AlaNH and ThrOH, is noncanonical. The crystal structure of **110** is unavailable. **109** and **110** promoted rat osteoblast MC3T3-E1 cell proliferation at 10 nM by 38.2 and 33.9%, respectively.

Brachystemin F (**111**; Figure 5.28) (Alog$P$ = 0.39) was isolated from the herb *Brachystemma calycinum* [151]. The cyclic octapeptide showed significant inhibition of the secretion of monocyte chemokine ligand 2 (CCL-2), interleukin 6 (IL-6), and collagen IV from high-glucose-stimulated mesangial cells at concentrations of 10 μM like the previously reported brachystemidine A [152]. Other structural analogues obtained from the culture did not show this activity.

Stylissatin A (**112**; Figure 5.28) (Alog$P$ = 3.85) was isolated from the sponge *Stylissa massa* [153]. This proteinogenic cyclic heptapeptide was shown to inhibit NO production in LPS-stimulated murine macrophage RAW264.7 cells (IC$_{50}$ 87 μM).

5.4.2 Large/Complex Peptides

5.4.2.1 Cystine Knots

The conotoxin Lo1a (**113**; Figure 5.29) (Alog$P$ = −1.79) was isolated from the venom of the marine snail *Conus longurionis* [154]. The 18-amino acid α-conotoxin had disulfide bridges between Cys^3-Cys^9 and Cys^4-Cys^{17} that reinforced a W-shaped conformation containing two loops. Compound **113** was active against the α7 nicotinic acetylcholine receptor (α7 nAChR, IC$_{50}$ 3.24 μM). Lo1a mutant studies suggested that the C-terminus does not play a critical role in binding.
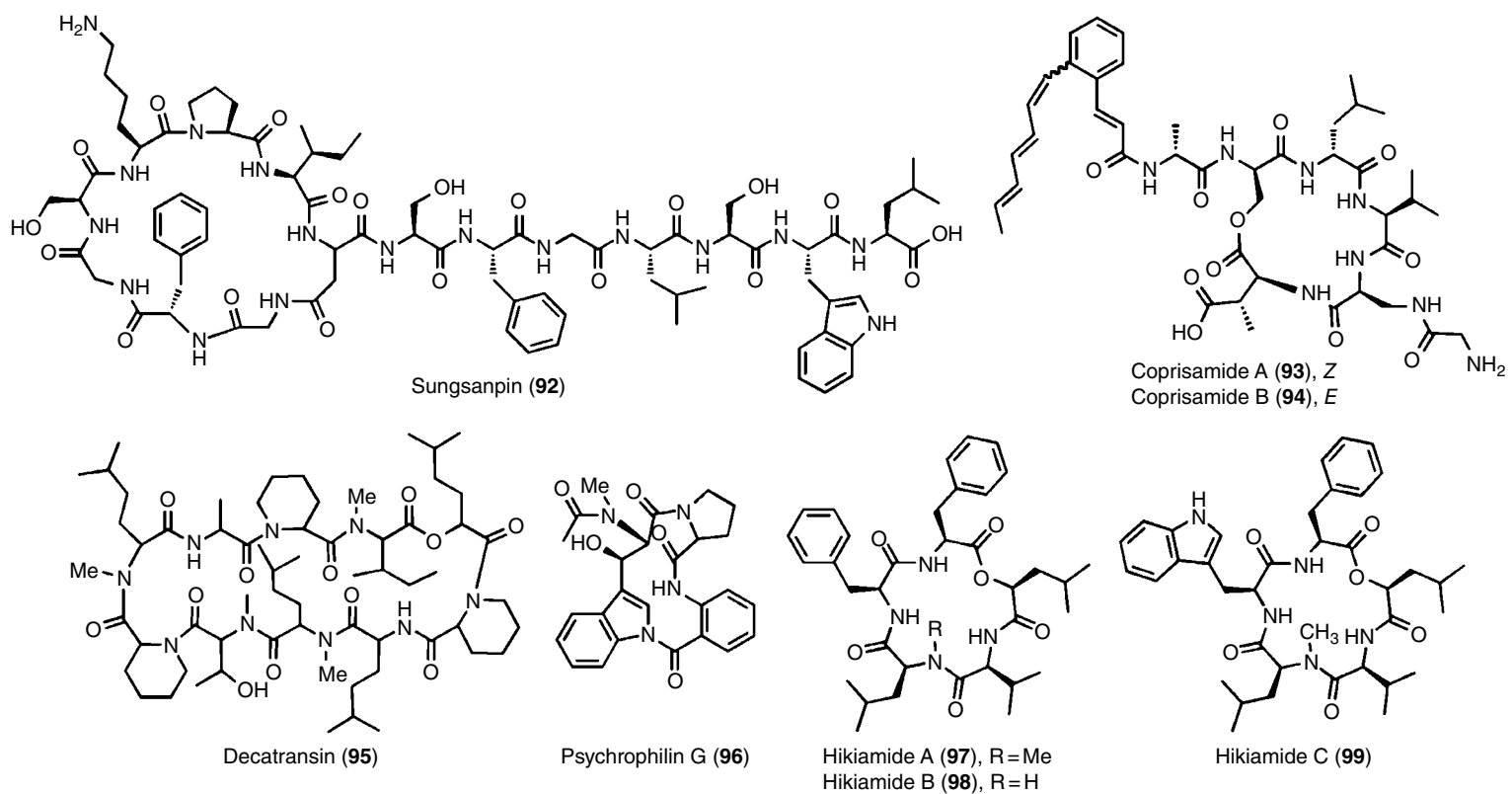
Sungsanpin (**92**)

Coprisamide A (**93**), *Z*
Coprisamide B (**94**), *E*

Decatransin (**95**)

Psychrophilin G (**96**)

Hikiamide A (**97**), R = Me
Hikiamide B (**98**), R = H

Hikiamide C (**99**)

Figure 5.26 Midsized cyclic peptides with various bioactivities I.

Autumnalide (**100**)

101

102

103

Desmethylisaridin E (**104**), R = H
Desmethylisaridin C2 (**105**), R = Me

Desmethylisaridin C1 (**106**)

Turnagainolide A (**107**), *R*
Turnagainolide B (**108**), *S*
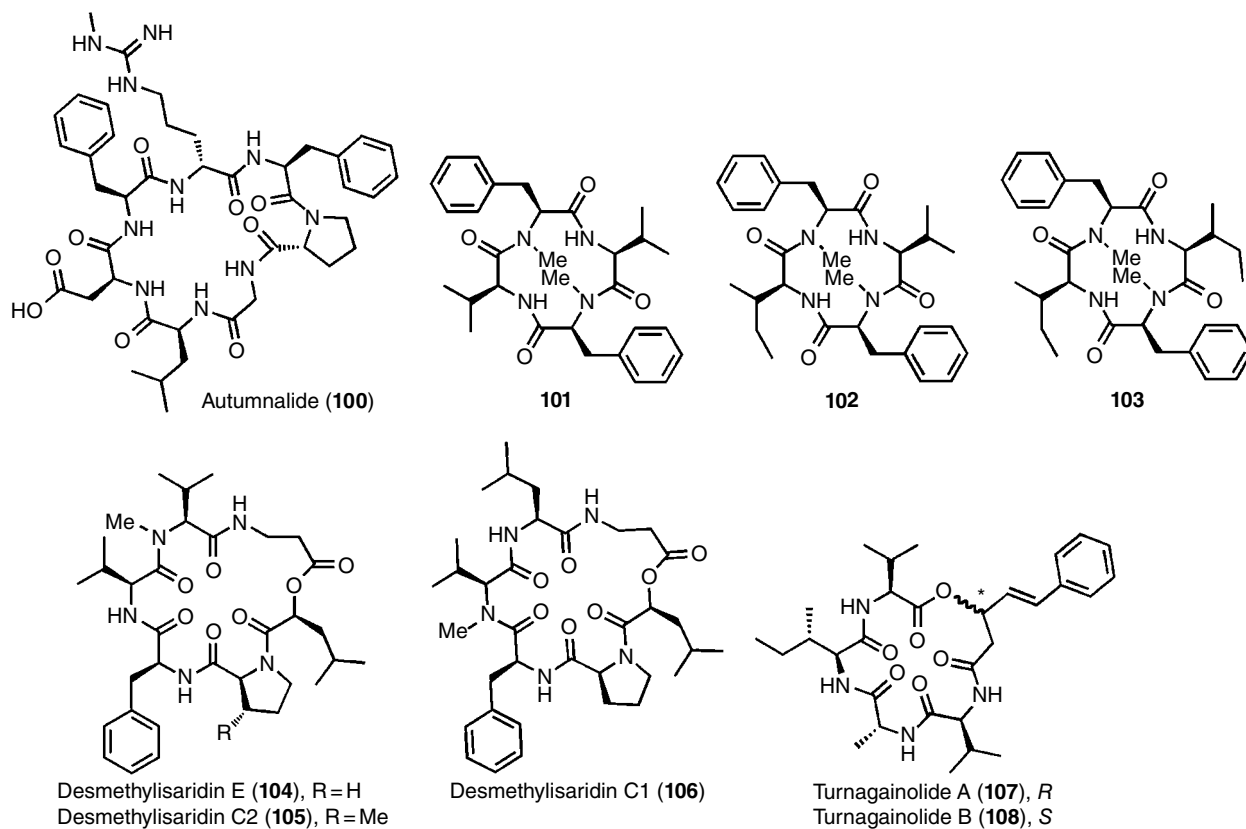
Figure 5.27 Midsized cyclic peptides with various bioactivities II.

Dianthin G (**109**)

Dianthin H (**110**)
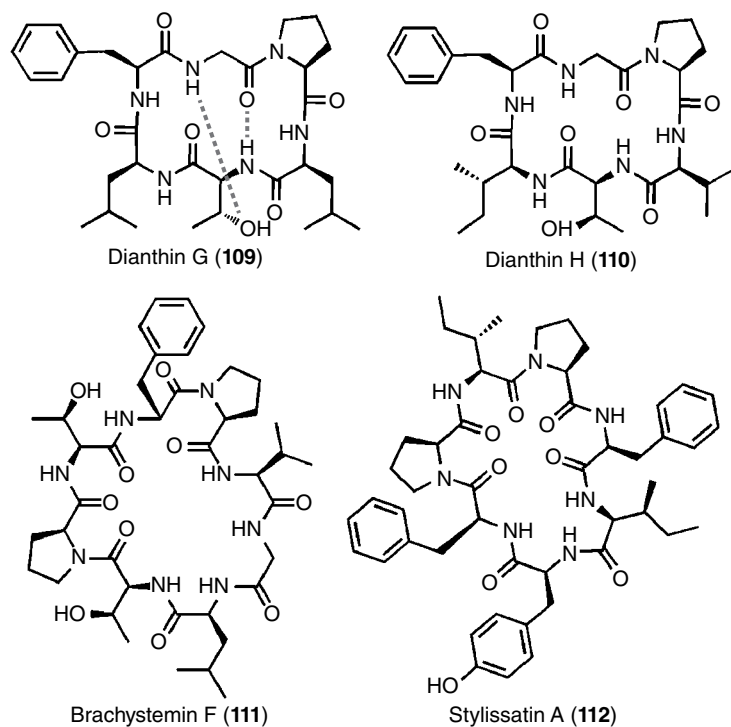
Figure 5.28 Midsized cyclic peptides with various bioactivities III.

Brachystemin F (**111**)

Stylissatin A (**112**)

Lo1a (**113**)

Glu-Gly-Cys-Cys-Ser-Asn-Pro-Ala-Cys-Arg-Thr-Asn-His-Pro-Glu-Val-Cys-Asp

Lv1a (**114**)

Gly-Cys-Cys-Ser-His-Pro-Ala-Cys-Asn-Val-Asp-His-Pro-Glu-Ile-Cys

Psysol 2 (**115**)

Leu-Pro-Ile-Cys-Gly-Glu-Ser-Cys-Val-Gly-Gly-Thr-Cys-Asn-Thr-Pro-Gly-Cys-Thr-Cys-Thr-Trp-Pro-Val-Cys-Thr-Arg-Asn-Gly
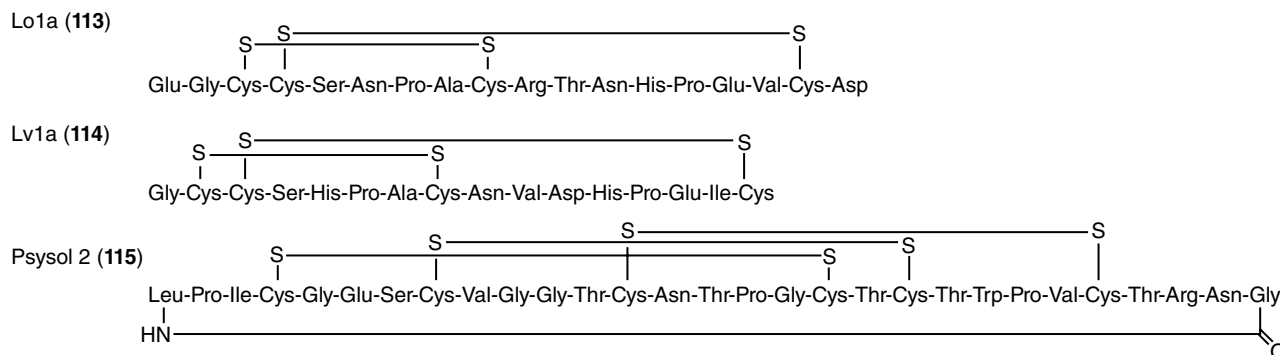
Figure 5.29 Cystine knot peptides.

DC1 (**116**)

Gly-Ala-Phe-Leu-Lys-Cys-Gly-Glu-Ser-Cys-Val-Tyr-Leu-Pro-Cys-Leu-Thr-Thr-Val-Val-Gly-Cys-Ser-Cys-Gln-Asn-Ser-Val-Cys-Tyr-Arg-Asp-CH$_2$COOH

DC2 (**117**)

Gly-Ala-Val-Pro-Cys-Gly-Glu-Thr-Cys-Val-Tyr-Leu-Pro-Cys-Ile-Thr-Pro-Asp-Ile-Gly-Cys-Ser-Cys-Gln-Asn-Lys-Val-Cys-Tyr-Arg-Asp-CH$_2$COOH

DC3 (**118**)

Gly-Thr-Ser-Cys-Gly-Glu-Thr-Cys-Val-Leu-Leu-Pro-Cys-Leu-Ser-Ser-Val-Leu-Gly-Cys-Thr-Cys-Gln-Asn-Lys-Arg-Cys-Tyr-Lys-Asp-CH$_2$COOH

Figure 5.30 Cyclotides from *Hedyotis diffusa*.

Lv1A (**114**; Figure 5.29) (Alog$P$ = −1.42) was isolated from *Conus lividus* [155]. The NMR solution structure was solved, and its selectivity for the nAChR $\alpha_3\beta_2$ subunit over $\alpha_6/\alpha_3\beta_2\beta_3$ was assessed *in silico* and *in vitro*. **114** adopts a random coil in water but is thought to become ordered upon binding. The peptide binds and blocks $\alpha_3\beta_2$ nAChR (IC$_{50}$ 8.7 nM) while inhibiting the competing receptor subunit (IC$_{50}$ > 100 nM).

Psysol 2 (**115**; Figure 5.29) (Alog$P$ = −0.39) is a cyclotide from the plant *Psychotria solitudinum* [156]. This ribosomally synthesized, posttranslationally modified peptide has high sequence homology with kalata B1 (Figure 5.2), containing the stabilizing cystine knot as well as three prolines that serve as likely substrates for prolyl enzymes. **115** displayed inhibitory activity against the serine-type protease human prolyl oligopeptidase (POP, IC$_{50}$ 25 μM) but did not inhibit trypsin or chymotrypsin at 25 or 75 μM, respectively. This cyclotide is the first example of a peptidic inhibitor of POP and could play a role in the treatment of neurodegenerative diseases.

The cyclotides **116**, **117**, and **118** (Figure 5.30) (Alog$P$ = −0.13, −0.18, and −2.27) were isolated from *Hedyotis diffusa* [157]. All three demonstrated cytotoxicity against prostate cancer cell lines in the micromolar to nanomolar range. Compound **118** was most active for LNCaP, PC3, and Du145 cell lines (IC$_{50}$ 210, 760, and 550 μM, respectively). **118** inhibited cell migration and invasion of LNCaP cells at 50 nM but not at 10 nM. It also inhibited growth (40% rate) of an LNCap xenograft in nude mice at 1 mg/kg, inoculated subcutaneously.

Three cyclotides I2 (**119**), O1 (**120**), and O3 (**121**) (Figure 5.31) (Alog$P$ = −0.68, −0.25, −0.72) were identified in the genome of *Violaceae* sp. and were semi-purified from *V. ignobilis* [158]. The peptides were found to inhibit the growth of *S. aureus* and *X. oryzae* in a halo growth inhibition assay.

Allotide C4 (**122**; Figure 5.32) (Alog$P$ = −1.16) is a knottin from the plant *Allamanda cathartica* [159]. **122** is a 30-amino acid peptide with two *cis*-prolines and one *trans*-proline that adopts two equally populated conformations in solution. The peptide has standard cystine

I2 (**119**)

Gly-Ile-Pro-Cys-Ser-Glu-Ser-Cys-Val-Phe-Ile-Gln-Cys-Phe-Thr-Ala-Ala-Ile-Gly-Cys-Ser-Cys-Asn-Ser-Lys-Val-Cys-tyr-Arg-Asn-Ser-Leu

O1 (**120**)

Gly-Ile-Pro-Cys-Gly-Glu-Ser-Cys-Val-Trp-Ile-Pro-Cys-Ile-Ser-Ala-Ala-Ile-Gly-Cys-Ser-Cys-Lys-Ser-Lys-Val-Cys-Tyr-Arg-Asn-Ser-Leu

O3 (**121**)

Ile-Pro-Cys-Gly-Glu-Ser-Cys-Val-Arg-Ile-Pro-Cys-Ile-Thr-Ala-Ala-Phe-Gly-Cys-Ser-Cys-Asn-Ser-Lys-Val-Cys-Tyr-Arg-Asn-Ser-Leu
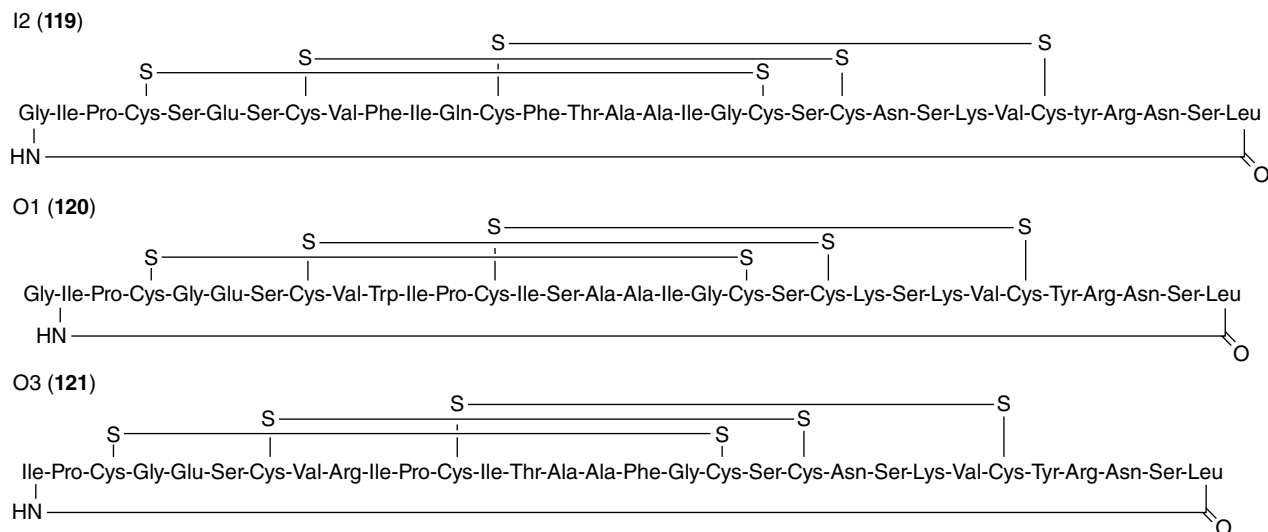
Figure 5.31 Cyclotides from *Violaceae ignobilis*.

Allotide C4 (**122**)

H₂N-Cys-Ile-Ala-His-Tyr-Gly-Lys-Cys-Asp-Gly-Ile-Ile-Asn-Gln-Cys-Cys-Asp-Pro-Trp-Leu-Cys-Thr-Pro-Pro-Ile-Ile-Gly-Phe-Cys-Leu-COOH

Asteropsin B (**123**)

Gly-Cys-Ala-Phe-Glu-Gly-Glu-Ser-Cys-Asn-Val-Glu-Phe-Tyr-Pro-Cys-Cys-Pro-Gly-Leu-Gly-Leu-Thr-Cys-Ile-Pro-Gly-Asn-Pro-Asp-Gly-Thr-Cys-Tyr-Tyr-Leu

Asteropsin C (**124**)

Asp-Cys-Pro-Gly-Glu-Gly-Glu-Gln-Cys-Asp-Val-Glu-Phe-Asn-Pro-Cys-Cys-Pro-Pro-Leu-Thr-Cys-Ile-Pro-Gly-Asp-Pro-Tyr-Gly-Ile-Cys-Tyr-Ile-Ile

Asteropsin D (**125**)

Gly-Cys-Ala-Gly-Pro-Gly-Glu-Glu-Cys-Ile-Val-Gly-Phe-Tyr-Asp-Cys-Cys-Pro-Gly-Tyr-Arg-Cys-Tyr-Pro-Gly-Asp-Pro-Gly-Gly-Ile-Cys-Tyr

Figure 5.32 Knottins.

knot topology as it contains the Cys(I–IV), (II–V), and (III–VI) disulfide pattern. NMR and computational modeling data suggest the two conformations differ based on disulfide bond rotation rather than proline amide isomerization. **122** demonstrated activity against mealworm *Tenebrio molitor* α-amylase in a dose-dependent manner (IC$_{50}$ 2.6 μM), but it did not inhibit mammalian or fungal α-amylases. The peptide did not exhibit cytotoxic or antibacterial activity up to 100 μM in a panel of cell lines.

Asteropsins B–D (**123–125**; Figure 5.32) (Alog*P* = 1.63, 2.33, and 0.56) are knottins isolated from *Asteropus* sp. [160]. Like other knottins, these structures adopt three intramolecular disulfide bridges between cysteines I–IV,

II–V, and III–VI and have protected N-termini. These peptides showed no cytotoxicity against a panel of human cell lines at 7 μM and were stable up to 4 h in the presence of chymotrypsin, elastase, and pepsin. Although biologically inactive, these natural peptides could serve as potentially orally bioavailable and inert drug carriers.

5.4.2.2 Lantibiotics

Suicin 3908 (**126**; Figure 5.33) (Alog*P* = −0.89) is a bacteriocin identified in a gene cluster of *Streptococcus suis* D12 [161].The ribosomally synthesized peptide was isolated and shown to inhibit the porcine pathogen *S. suis* MGGUS3 with an MIC of 140 nM. Although the post-translationally modified structure has not been solved,

Suicin 3908 (**126**)

> AGSGFVKTLTKDCPGFLSNVCNIGFISGCKNC

Pseudomycoicidin (**127**)

> GDCGGTCTWTKDCSICPSWSCWSWSC

Figure 5.33 Peptide sequences of ribosomally synthesized likely cyclic bioactives.

the authors propose the peptide could be used to prevent infection and reduce antibiotic use by the swine industry.

The gene cluster of pseudomycoicidin (**127**; Figure 5.33) was identified in *Bacillus pseudomycoides* [162]. This class II lantibiotic was heterologously expressed in *E. coli* with proteolytic cleavage of the GA leader sequence. The peptide has four dehydrations and at least one thioester, but the structure has not been fully elucidated. The lantibiotic was reported to inhibit Gram-negative bacteria in a halo assay.

5.5 Conclusions

Cyclic peptide natural products possess diverse structures and physicochemical properties. While some macrocycles are composed of hydrophobic proteinogenic amino acids, others contain extended amino acid units of polyketide origin, posttranslational modifications, and/or highly charged sequences. As a result of this compositional diversity, the range of shapes, sizes, lipophilicities, aqueous solubilities, and conformations of cyclic peptides are seemingly endless. This structural and physicochemical variance of cyclic peptides, in addition to their equally broad range of associated bioactivities, makes these scaffolds prime candidates as tunable templates for the further development of designed molecules.

Many cyclic peptide natural products are able to access and affect intracellular targets via passive membrane permeation or active cellular uptake mechanisms. The reported biological activities of many of these compounds are weak or moderate at best, suggesting that the native targets that drove the natural selection of these compounds in their producing organisms have yet to be discovered. It is doubtful, for example, that a compound with a reported EC_{50} of $20\,\mu M$ against a particular target could be successfully optimized against that target by extensive derivatization. Assay-guided purification techniques such as high-content image-based screening approaches that are less biased toward specific targets or phenotypes could, in principle, allow more obscure targets to be uncovered, especially for compounds that are only weakly toxic to cells. Nonetheless, many cyclic peptide natural products continue to yield potent biological activities in particular as antibiotics where the need for targeting drug-resistant strains continues to grow.

Bioactive cyclic peptide natural products, such as CsA, have inspired decades of peptide-based drug research. In more recent years, studies on synthetic peptides with natural product-like structures have coincided with resurgence of interest in the development of peptide-based pharmaceuticals. As natural products chemists continue to add to the ever-growing library of bioactive cyclic peptides, it is important for medicinal chemists to continue to probe the structures and physicochemical properties of these molecules. The move beyond "drug-like" chemical space raises numerous questions about what is possible in the interplay between ADME properties and the mass, polarity, and flexibility of complex macrocycles. The study of cyclic peptide natural products and their analogues will surely continue to further our understanding of the relationships between structure, pharmacokinetics, and pharmacodynamics.

References

1 Craik, D. J.; Fairlie, D. P.; Liras, S.; Price, D. The Future of Peptide-Based Drugs. *Chem. Biol. Drug Des.* **2013**, *81* (1), 136–147.

2 Joo, S. H. Cyclic Peptides as Therapeutic Agents and Biochemical Tools. *Biomol. Ther.* **2012**, *20* (1), 19–26.

3 Sun, L. Peptide-Based Drug Development. *Mod. Chem. Appl.* **2013**, *1* (1), e103.

4 Gavenonis, J.; Sheneman, B. A.; Siegert, T. R.; Eshelman, M. R.; Kritzer, J. A. Comprehensive Analysis of Loops at Protein-Protein Interfaces for Macrocycle Design. *Nat. Chem. Biol.* **2014**, *10* (9), 716–722.

5 Lipinski, C. A.; Lombardo, F.; Dominy, B. W.; Feeney, P. J. Experimental and Computational Approaches to Estimate Solubility and Permeability in Drug Discovery and Development Settings. *Adv. Drug Deliv. Rev.* **2012**, *64*, 4–17.

6 Veber, D. F.; Johnson, S. R.; Cheng, H.-Y.; Smith, B. R.; Ward, K. W.; Kopple, K. D. Molecular Properties that Influence the Oral Bioavailability of Drug Candidates. *J. Med. Chem.*. **2002**, *45* (12), 2615–2623.

7 Tedesco, D.; Haragsim, L. Cyclosporine: A Review. *J. Transplant.* **2012**, *2012*, 1–7.

8 Bhat, A.; Roberts, L. R.; Dwyer, J. J. Lead Discovery and Optimization Strategies for Peptide Macrocycles. *Eur. J. Med. Chem.* **2015**, *94*, 471–479.

9 Dandapani, S.; Marcaurelle, L. A. Grand Challenge Commentary: Accessing New Chemical Space for "Undruggable" Targets. *Nat. Chem. Biol.* **2010**, *6* (12), 861–863.

10 Giordanetto, F.; Kihlberg, J. Macrocyclic Drugs and Clinical Candidates: What Can Medicinal Chemists Learn from Their Properties? *J. Med. Chem..* **2013**, *57* (2), 278–295.

11 Villar, E. A.; Beglov, D.; Chennamadhavuni, S.; Porco, J. A.; Kozakov, D.; Vajda, S.; Whitty, A. How Proteins Bind Macrocycles. *Nat. Chem. Biol.* **2014**, *10* (9), 723–731.

12 Marsault, E.; Peterson, M. L. Macrocycles Are Great Cycles: Applications, Opportunities, and Challenges of Synthetic Macrocycles in Drug Discovery. *J. Med. Chem..* **2011**, *54* (7), 1961–2004.

13 Wessjohann, L. A.; Ruijter, E.; Garcia-Rivera, D.; Brandt, W. What Can a Chemist Learn from Nature's Macrocycles?—A Brief, Conceptual View. *Mol. Divers.* **2005**, *9* (1–3), 171–186.

14 White, T. R.; Renzelman, C. M.; Rand, A. C.; Rezai, T.; McEwen, C. M.; Gelev, V. M.; Turner, R. A.; Linington, R. G.; Leung, S. S. F.; Kalgutkar, A. S.; Bauman, J. N.; Zhang, Y.; Liras, S.; Price, D. A.; Mathiowetz, A. M.; Jacobson, M. P.; Lokey, R. S. On-Resin N-Methylation of Cyclic Peptides for Discovery of Orally Bioavailable Scaffolds. *Nat. Chem. Biol.* **2011**, *7* (11), 810–817.

15 Rezai, T.; Yu, B.; Millhauser, G. L.; Jacobson, M. P.; Lokey, R. S. Testing the Conformational Hypothesis of Passive Membrane Permeability Using Synthetic Cyclic Peptide Diastereomers. *J. Am. Chem. Soc.* **2006**, *128* (8), 2510–2511.

16 Niggemann, J.; Bozko, P.; Bruns, N.; Wodtke, A.; Gieseler, M. T.; Thomas, K.; Jahns, C.; Nimtz, M.; Reupke, I.; Brüser, T.; Auling, G.; Malek, N.; Kalesse, M. Baceridin, a Cyclic Hexapeptide from an Epiphytic Bacillus Strain, Inhibits the Proteasome. *ChemBioChem* **2014**, *15* (7), 1021–1029.

17 Zheng, M.-F.; Ren, H.; Luo, Y.; Dong, L.-M.; Wang, L.-Q.; Zhou, Z.-Y.; Tan, J.-W. A New Diantheramide and a New Cyclic Peptide from the Seeds of Vaccaria Hispanica. *Phytochem. Lett.* **2015**, *11*, 240–244.

18 Wu, Z.-C.; Li, S.; Nam, S.-J.; Liu, Z.; Zhang, C. Nocardiamides A and B, Two Cyclohexapeptides from the Marine-Derived Actinomycete *Nocardiopsis* sp. CNX037. *J. Nat. Prod..* **2013**, *76* (4), 694–701.

19 Hewitt, W. M.; Leung, S. S. F.; Pye, C. R.; Ponkey, A. R.; Bednarek, M.; Jacobson, M. P.; Lokey, R. S. Cell-Permeable Cyclic Peptides from Synthetic Libraries Inspired by Natural Products. *J. Am. Chem. Soc.* **2015**, *137* (2), 715–721.

20 Rezai, T.; Bock, J. E.; Zhou, M. V.; Kalyanaraman, C.; Lokey, R. S.; Jacobson, M. P. Conformational Flexibility, Internal Hydrogen Bonding, and Passive Membrane Permeability: Successful In Silico Prediction of the Relative Permeabilities of Cyclic Peptides. *J. Am. Chem. Soc.* **2006**, *128* (43), 14073–14080.

21 Ovadia, O.; Greenberg, S.; Chatterjee, J.; Laufer, B.; Opperer, F.; Kessler, H.; Gilon, C.; Hoffman, A. The Effect of Multiple N-Methylation on Intestinal Permeability of Cyclic Hexapeptides. *Mol. Pharmaceutics* **2011**, *8* (2), 479–487.

22 Marelli, U. K.; Bezençon, J.; Puig, E.; Ernst, B.; Kessler, H. Enantiomeric Cyclic Peptides with Different Caco-2 Permeability Suggest Carrier-Mediated Transport. *Chem. Eur. J.* **2015**, *21* (22), 8023–8027.

23 Ahlbach, C. L.; Lexa, K. W.; Bockus, A. T.; Chen, V.; Crews, P.; Jacobson, M. P.; Lokey, R. S. Beyond Cyclosporine A: Conformation-Dependent Passive Membrane Permeabilities of Cyclic Peptide Natural Products. *Future Med. Chem.* **2015**, *7* (16), 2121–2130.

24 Bockus, A. T.; Schwochert, J. A.; Pye, C. R.; Townsend, C. E.; Sok, V.; Bednarek, M. A.; Lokey, R. S. Going Out on a Limb: Delineating the Effects of B-Branching, N-Methylation, and Side Chain Size on the Passive Permeability, Solubility, and Flexibility of Sanguinamide a Analogues. *J. Med. Chem..* **2015**, *58* (18), 7409–7418.

25 Bockus, A. T.; Lexa, K. W.; Pye, C. R.; Kalgutkar, A. S.; Gardner, J. W.; Hund, K. C. R.; Hewitt, W. M.; Schwochert, J. A.; Glassey, E.; Price, D. A.; Mathiowetz, A. M.; Liras, S.; Jacobson, M. P.; Lokey, R. S. Probing the Physicochemical Boundaries of Cell Permeability and Oral Bioavailability in Lipophilic Macrocycles Inspired by Natural Products. *J. Med. Chem..* **2015**, *58* (11), 4581–4589.

26 Schwochert, J.; Turner, R.; Thang, M.; Berkeley, R. F.; Ponkey, A. R.; Rodriguez, K. M.; Leung, S. S. F.; Khunte, B.; Goetz, G.; Limberakis, C.; Kalgutkar, A. S.; Eng, H.; Shapiro, M. J.; Mathiowetz, A. M.; Price, D. A.; Liras, S.; Jacobson, M. P.; Lokey, R. S. Peptide to Peptoid Substitutions Increase Cell Permeability in Cyclic Hexapeptides. *Org. Lett.* **2015**, *17* (12), 2928–2931.

27 Schwochert, J.; Pye, C.; Ahlbach, C.; Abdollahian, Y.; Farley, K.; Khunte, B.; Limberakis, C.; Kalgutkar, A. S.; Eng, H.; Shapiro, M. J.; Mathiowetz, A. M.; Price, D. A.; Liras, S.; Lokey, R. S. Revisiting N-to-O Acyl Shift for Synthesis of Natural Product-Like Cyclic Depsipeptides. *Org. Lett.* **2014**, *16* (23), 6088–6091.

28 Nielsen, D. S.; Hoang, H. N.; Lohman, R. J.; Hill, T. A.; Lucke, A. J.; Craik, D. J.; Edmonds, D. J.; Griffith, D. A.; Rotter, C. J.; Ruggeri, R. B.; Price, D. A.; Liras, S.; Fairlie, D. P. Improving on Nature: Making a Cyclic Heptapeptide Orally Bioavailable. *Angew. Chem. Int. Ed.* **2014**, *53* (45), 12059–12063.

29 Nielsen, D. S.; Hoang, H. N.; Lohman, R. J.; Diness, F.; Fairlie, D. P. Total Synthesis, Structure, and Oral Absorption of a Thiazole Cyclic Peptide, Sanguinamide A. *Org. Lett.* **2012**, *14* (22), 5720–5723.

30 Wang, C. K.; Northfield, S. E.; Swedberg, J. E.; Colless, B.; Chaousis, S.; Price, D. A.; Liras, S.; Craik, D. J. Exploring Experimental and Computational Markers of Cyclic Peptides: Charting Islands of Permeability. *Eur. J. Med. Chem.* **2015**, *97*, 202–213.

31 Fouché, M.; Schäfer, M.; Blatter, M.; Berghausen, J.; Desrayaud, S.; Roth, H.-J. Pharmacokinetic Studies around the Mono- and Difunctionalization of a Bioavailable Cyclic Decapeptide Scaffold. *ChemMedChem* **2016**, *11* (10), 1060–1068.

32 Whitty, A.; Zhong, M.; Viarengo, L.; Beglov, D.; Hall, D. R.; Vajda, S. Quantifying the Chameleonic Properties of Macrocycles and Other High-Molecular-Weight Drugs. *Drug Discov. Today* **2016**, *21* (5), 712–717.

33 Bockus, A. T.; McEwen, C. M.; Lokey, R. S. Form and Function in Cyclic Peptide Natural Products: A Pharmacokinetic Perspective. *Future Med. Chem.* **2013**, *13* (7), 821–836.

34 Park, S.-C.; Park, Y.; Hahm, K.-S. The Role of Antimicrobial Peptides in Preventing Multidrug-Resistant Bacterial Infections and Biofilm Formation. *Int. J. Mol. Sci.* **2011**, *12* (9), 5971–5992.

35 Qian, Z.; Martyna, A.; Hard, R. L.; Wang, J.; Appiah-Kubi, G.; Coss, C.; Phelps, M. A.; Rossman, J. S.; Pei, D. Discovery and Mechanism of Highly Efficient Cyclic Cell-Penetrating Peptides. *Biochemistry* **2016**, *55* (18), 2601–2612.

36 Craik, D. J.; Daly, N. L.; Waine, C. The Cystine Knot Motif in Toxins and Implications for Drug Design. *Toxicon* **2001**, *39* (1), 43–60.

37 Kolmar, H. Alternative Binding Proteins: Biological Activity and Therapeutic Potential of Cystine-Knot Miniproteins. *FEBS J.*. **2008**, *275* (11), 2684–2690.

38 D'Souza, C.; Henriques, S. T.; Wang, C. K.; Craik, D. J. Structural Parameters Modulating the Cellular Uptake of Disulfide-Rich Cyclic Cell-Penetrating Peptides: MCoTI-II and SFTI-1. *Eur. J. Med. Chem.* **2014**, *88*, 10–18.

39 Henriques, S. T.; Huang, Y.-H.; Chaousis, S.; Sani, M.-A.; Poth, A. G.; Separovic, F.; Craik, D. J. The Prototypic Cyclotide Kalata B1 Has a Unique Mechanism of Entering Cells. *Chem. Biol.* **2015**, *22* (8), 1087–1097.

40 Traboulsi, H.; Larkin, H.; Bonin, M.-A.; Volkov, L.; Lavoie, C. L.; Marsault, E. Macrocyclic Cell Penetrating Peptides: A Study of Structure-Penetration Properties. *Bioconjugate Chem.* **2015**, *26* (3), 405–411.

41 Kaplan, I. M.; Wadia, J. S.; Dowdy, S. F. Cationic TAT Peptide Transduction Domain Enters Cells by Macropinocytosis. *J. Control. Release* **2005**, *102* (1), 247–253.

42 Kitagaki, J.; Shi, G.; Miyauchi, S.; Murakami, S.; Yang, Y. Cyclic Depsipeptides as Potential Cancer Therapeutics. *Anticancer Drugs* **2015**, *26* (3), 259–271.

43 Medina, R. A.; Goeger, D. E.; Hills, P.; Mooberry, S. L.; Huang, N.; Romero, L. I.; Ortega-Barría, E.; Gerwick, W. H.; McPhail, K. L. Coibamide A, a Potent Antiproliferative Cyclic Depsipeptide from the Panamanian Marine *Cyanobacterium leptolyngbya* sp. *J. Am. Chem. Soc.* **2008**, *130* (20), 6324–6325.

44 Maksimov, M. O.; Pan, S. J.; Link, A. J. Lasso Peptides: Structure, Function, Biosynthesis, and Engineering. *Nat. Prod. Rep.* **2012**, *29* (9), 996–1006.

45 Lee, J.-E.; Hitotsuyanagi, Y.; Kim, I.-H.; Hasuda, T.; Takeya, K. A Novel Bicyclic Hexapeptide, RA-XVIII, from Rubia Cordifolia: Structure, Semi-Synthesis, and Cytotoxicity. *Bioorg. Med. Chem. Lett.* **2008**, *18* (2), 808–811.

46 Ma, B.; Banerjee, B.; Litvinov, D. N.; He, L.; Castle, S. L. Total Synthesis of the Antimitotic Bicyclic Peptide Celogentin C. *J. Am. Soc. Mass Spectrom.* **2009**, *132* (3), 1159–1171.

47 Dobson, C. M. Chemical Space and Biology. *Nature* **2004**, *432* (7019), 824–828.

48 Wang, C. K.; Craik, D. J. Cyclic Peptide Oral Bioavailability: Lessons from the Past. *Biopolymers* **2016**, *106* (6), 901–909.

49 Matsson, P.; Doak, B. C.; Over, B.; Kihlberg, J. Cell Permeability beyond the Rule of 5. *Adv. Drug Deliv. Rev.* **2016**, *101*, 42–61.

50 Kobel, H.; Loosli, H. R.; Voges, R. Contribution to Knowledge of the Biosynthesis of Cyclosporin A. *Experientia* **1983**, *39* (8), 873–876.

51 Senn, H.; Weber, C.; Kobel, H.; Traber, R. Selective 13C-Labelling of Cyclosporin A. *Eur. J. Biochem.* **1991**, *199* (3), 653–658.

52 DrugBank, Cyclosporine, pharma knowledge base, **2016**. From http://www.pharmakb.com/cyclosporine/ (accessed March 25, 2017).

53 Jin, M.; Shimada, T.; Shintani, M.; Yokogawa, K.; Nomura, M.; Miyamoto, K.-I. Long-Term Levothyroxine Treatment Decreases the Oral Bioavailability of Cyclosporin A by Inducing P-Glycoprotein in Small Intestine. *Drug Metab. Pharmacokinet.* **2005**, *20* (5), 324–330.

54 Kessler, H.; Köck, M.; Wein, T.; Gehrke, M. Reinvestigation of the Conformation of Cyclosporin A in Chloroform. *Helv. Chim. Acta* **1990**, *73* (7), 1818–1832.

55 Alex, A.; Millan, D. S.; Perez, M.; Wakenhut, F.; Whitlock, G. A. Intramolecular Hydrogen Bonding to Improve Membrane Permeability and Absorption in Beyond Rule of Five Chemical Space. *Med. Chem. Commun.* **2011**, *2* (7), 669–674.

56 Lautz, J.; Kessler, H.; van Gunsteren, W. F.; Weber, H. P.; Wenger, R. M. On the Dependence of Molecular Conformation on the Type of Solvent Environment: A Molecular Dynamics Study of Cyclosporin A. *Biopolymers* **1990**, *29* (12), 1669–1687.

57 Huai, Q.; Kim, H. Y.; Liu, Y.; Zhao, Y.; Mondragon, A.; Liu, J. O.; Ke, H. Crystal Structure of Calcineurin–Cyclophilin–Cyclosporin Shows Common but Distinct Recognition of Immunophilin-Drug Complexes. *Proc. Natl. Acad. Sci. U. S. A.* **2002**, *99* (19), 12037–12042.

58 el Tayar, N.; Mark, A. E.; Vallat, P.; Brunne, R. M.; Testa, B.; van Gunsteren, W. F. Solvent-Dependent Conformation and Hydrogen-Bonding Capacity of Cyclosporin A: Evidence from Partition Coefficients and Molecular Dynamics Simulations. *J. Med. Chem.* **2002**, *36* (24), 3757–3764.

59 Altschuh, D. Cyclosporin A as a Model Antigen: Immunochemical and Structural Studies. *J. Mol. Recognit.* **2002**, *15* (5), 277–285.

60 Rosen, M. K.; Belshaw, P. J.; Alberg, D. G.; Schreiber, S. L. The Conformation of Cyclosporin A Bound to Cyclophilin Is Altered (Once Again) Following Binding to Calcineurin: An Analysis of Receptor-Ligand-Receptor Interactions. *Bioorg. Med. Chem. Lett.* **1992**, *2* (7), 747–753.

61 Ran, Y.; Zhao, L.; Xu, Q.; Yalkowsky, S. H. Solubilization of Cyclosporin A. *AAPS PharmSciTech* **2001**, *2* (1), 23–26.

62 Thansandote, P.; Harris, R. M.; Dexter, H. L.; Simpson, G. L.; Pal, S.; Upton, R. J.; Valko, K. Improving the Passive Permeability of Macrocyclic Peptides: Balancing Permeability with Other Physicochemical Properties. *Bioorg. Med. Chem.* **2015**, *23* (2), 322–327.

63 Tetko, I. V.; Gasteiger, J.; Todeschini, R.; Mauri, A.; Livingstone, D.; Ertl, P.; Palyulin, V. A.; Radchenko, E. V.; Zefirov, N. S.; Makarenko, A. S.; Tanchuk, V. Y.; Prokopenko, V. V. Virtual Computational Chemistry Laboratory—Design and Description. *J. Comput. Aided Mol. Des.* **2005**, *19* (6), 453–463.

64 VCCLAB, Virtual Computational Chemistry Laboratory. **2005**. From http://www.vcclab.org (accessed March 25, 2017).

65 Houssen, W. E.; Jaspars, M. Azole-Based Cyclic Peptides from the Sea Squirt Lissoclinum Patella: Old Scaffolds, New Avenues. *ChemBioChem* **2010**, *11* (13), 1803–1815.

66 Morris, L. A.; Milne, B. F.; Thompson, G. S.; Jaspars, M. Conformational Change in the Thiazole and Oxazoline Containing Cyclic Octapeptides, the Patellamides. Part 1. Cu2+ and Zn2+ Induced Conformational Change. *J. Chem. Soc., Perkin Trans. 2* **2002**, (6), 1072–1075.

67 Milne, B. F.; Morris, L. A.; Jaspars, M.; Thompson, G. S. Conformational Change in the Thiazole and Oxazoline Containing Cyclic Octapeptides, the Patellamides. Part 2. Solvent Dependent Conformational Change. *J. Chem. Soc., Perkin Trans. 2* **2002**, (6), 1076–1080.

68 van den Brenk, A. L.; Tyndall, J. D. A.; Cusack, R. M.; Jones, A.; Fairlie, D. P.; Gahan, L. R.; Hanson, G. R. Formation of Mononuclear and Chloro-Bridged Binuclear Copper(II) Complexes of Patellamide D, a Naturally Occurring Cyclic Peptide: Influence of Anion and Solvent. *J. Inorg. Biochem.* **2004**, *98* (11), 1857–1866.

69 Pressman, B. C. Biological Applications of Ionophores. *Annu. Rev. Biochem.* **1976**, *45* (1), 501–530.

70 Smith, T. C.; Levinson, C. Direct Measurement of the Membrane Potential of Ehrlich Ascites Tumor Cells: Lack of Effect of Valinomycin and Ouabain. *J. Membrane Biol.* **1975**, *23* (1), 349–365.

71 Smith, G. D.; Duax, W. L.; Langs, D. A.; DeTitta, G. T.; Edmonds, J. W.; Rohrer, D. C.; Weeks, C. M. Crystal and Molecular Structure of the Triclinic and Monoclinic Forms of Valinomycin, C54H90N6O18. *J. Am. Chem. Soc.* **1975**, *97* (25), 7242–7247.

72 Hamilton, J. A.; Sabesan, M. N.; Steinrauf, L. K. Crystal Structure of Valinomycin Potassium Picrate: Anion Effects on Valinomycin Cation Complexes. *J. Am. Chem. Soc.* **1981**, *103* (19), 5880–5885.

73 Rose, M. C.; Henkens, R. W. Stability of Sodium and Potassium Complexes of Valinomycin. *Biochim. Biophys.* **1974**, *372* (2), 426–435.

74 Tan, L. T.; Cheng, X. C.; Jensen, P. R.; Fenical, W. Scytalidamides A and B, New Cytotoxic Cyclic Heptapeptides from a Marine Fungus of the Genus Scytalidium. *J. Org. Chem.* **2003**, *68* (23), 8767–8773.

75 Amagata, T.; Morinaka, B. I.; Amagata, A.; Tenney, K.; Valeriote, F. A.; Lobkovsky, E.; Clardy, J.; Crews, P. A Chemical Study of Cyclic Depsipeptides Produced by a Sponge-Derived Fungus. *J. Nat. Prod.* **2006**, *69* (11), 1560–1565.

76 Sang, F.; Li, D.; Sun, X.; Cao, X.; Wang, L.; Sun, J.; Sun, B.; Wu, L.; Yang, G.; Chu, X.; Wang, J.; Dong, C.; Geng, Y.; Jiang, H.; Long, H.; Chen, S.; Wang, G.; Zhang, S.; Zhang, Q.; Chen, Y. Total Synthesis and Determination of the Absolute Configuration of Rakicidin A. *J. Am. Chem. Soc.* **2014**, *136* (44), 15787–15791.

77 Rinehart, K. L.; Gloer, J. B.; Hughes, R. G.; Renis, H. E.; McGovren, J. P.; Swynenberg, E. B.; Stringfellow, D. A.; Kuentzel, S. L.; Li, L. H. Didemnins: Antiviral and Antitumor Depsipeptides from a Caribbean Tunicate. *Science* **1981**, *212* (4497), 933–935.

78 Montgomery, D. W.; Zukoski, C. F. Didemnin B: A New Immunosuppressive Cyclic Peptide with Potent Activity In Vitro and In Vivo. *Transplantation* **1985**, *40* (1), 49.

79 Kucuk, O.; Young, M. L.; Habermann, T. M.; Wolf, B. C.; Jimeno, J.; Cassileth, P. A. Phase II Trial of Didemnin B in Previously Treated Non-Hodgkin's Lymphoma: an Eastern Cooperative Oncology Group (ECOG) Study. *Am. J. Clin. Oncol.* **2000**, *23* (3), 273.

80 Hossain, M. B.; Van der Helm, D.; Antel, J.; Sheldrick, G. M.; Sanduja, S. K.; Weinheimer, A. J. Crystal and Molecular Structure of Didemnin B, an Antiviral and Cytotoxic Depsipeptide. *Proc. Natl. Acad. Sci. U. S. A.* **1988**, *85* (12), 4118–4122.

81 Hossain, M. B.; Helm, D. V. D.; Antel, J.; Sheldrick, G. M.; Weinheimer, A. J.; Sanduja, S. K. Crystal and Molecular Structure of Didemnin A, an Antiviral Depsipeptide. *Int. J. Pept. Prot. Res.* **1996**, *47* (1), 20–27.

82 Searle, M. S.; Hall, J. G.; Kyratzis, I.; Wakelin, L. P. G. Didemnin B Conformation and Dynamics of an Antitumour and Antiviral Depsipeptide Studied in Solution by 1H and 13C. N.M.R. Spectroscopy. *Int. J. Pept. Prot. Res.* **1989**, *34* (6), 445–454.

83 Liu, B.-L.; Tzeng, Y.-M. Development and Applications of Destruxins: A Review. *Biotechnol. Adv.* **2012**, *30* (6), 1242–1254.

84 Steiner, J. R.; Barnes, C. L. Crystal and Molecular Structure of Destruxin B. *Int. J. Pept. Prot. Res.* **1988**, *31* (2), 212–219.

85 Yeh, S. F.; Pan, W.; Ong, G.-T.; Chiou, A.-J.; Chuang, C.-C.; Chiou, S.-H.; Wu, S.-H. Study of Structure–Activity Correlation in Destruxins, a Class of Cyclodepsipeptides Possessing Suppressive Effect on the Generation of Hepatitis B Virus Surface Antigen in Human Hepatoma Cells. *Biochem. Biophys. Res. Commun.* **1996**, *229* (1), 65–72.

86 Kling, A.; Lukat, P.; Almeida, D. V.; Bauer, A.; Fontaine, E.; Sordello, S.; Zaburannyi, N.; Herrmann, J.; Wenzel, S. C.; König, C.; Ammerman, N. C.; Barrio, M. B.; Borchers, K.; Bordon-Pallier, F.; Brönstrup, M.; Courtemanche, G.; Gerlitz, M.; Geslin, M.; Hammann, P.; Heinz, D. W.; Hoffmann, H.; Klieber, S.; Kohlmann, M.; Kurz, M.; Lair, C.; Matter, H.; Nuermberger, E.; Tyagi, S.; Fraisse, L.; Grosset, J. H.; Lagrange, S.; Müller, R. Targeting DnaN for Tuberculosis Therapy Using Novel Griselimycins. *Science* **2015**, *348* (6239), 1106–1112.

87 Rukachaisirikul, V.; Chantaruk, S.; Tansakul, C.; Saithong, S.; Chaicharernwimonkoon, L.; Pakawatchai, C.; Isaka, M.; Intereya, K. A Cyclopeptide from the Insect Pathogenic Fungus *Cordyceps* sp. BCC 1788. *J. Nat. Prod.* **2006**, *69* (2), 305–307.

88 Wang, X.; Morinaka, B. I.; Molinski, T. F. Structures and Solution Conformational Dynamics of Stylissamides G and H from the Bahamian Sponge Stylissa Caribica. *J. Nat. Prod.* **2014**, *77* (3), 625–630.

89 Weber, D.; Erosa, G.; Sterner, O.; Anke, T. Cylindrocyclin A, a New Cytotoxic Cyclopeptide from *Cylindrocarpon* sp. *J. Antibiot.* **2006**, *59* (8), 495–499.

90 Endo, M.; Takesako, K.; Kato, I.; Yamaguchi, H. Fungicidal Action of Aureobasidin a, a Cyclic Depsipeptide Antifungal Antibiotic, Against *Saccharomyces cerevisiae. Antimicrob. Agents Chemother.* **1997**, *41* (3), 672–676.

91 Sonda, S.; Sala, G.; Ghidoni, R.; Hemphill, A.; Pieters, J. Inhibitory Effect of Aureobasidin A on *Toxoplasma gondii. Antimicrob. Agents Chemother.* **2005**, *49* (5), 1794–1801.

92 Fujikawa, A.; In, Y.; Inoue, M.; Ishida, T.; Nemoto, N.; Kobayashi, Y.; Kataoka, R.; Ikai, K.; Takesako, K.; Kato, I. X-Ray and NMR Conformational Study of Aureobasidin E: A Cyclic Depsipeptide with Potent Antifungal Activity. *J. Org. Chem..* **1994**, *59* (3), 570–578.

93 In, Y.; Ishida, T.; Takesako, K. Unique Molecular Conformation of Aureobasidin A, a Highly Amide N-Methylated Cyclic Depsipeptide with Potent Antifungal Activity: X-Ray Crystal Structure and Molecular Modeling Studies. *Int. J. Pept. Prot. Res.* **1999**, *53* (5), 492–500.

94 Takesako, K.; Kuroda, H.; Inoue, T.; Haruna, F.; Yoshikawa, Y.; Kato, I.; Uchida, K.; Hiratani, T.; Yamaguchi, H. Biological Properties of Aureobasidin A, a Cyclic Depsipeptide Antifungal Antibiotic. *J. Antibiot.* **1993**, *46* (9), 1414–1420.

95 Ikai, K.; Shiomi, K.; Takesako, K.; Kato, I.; Naganawa, H. NMR Studies of Aureobasidins A and E. *J. Antibiot.* **1991**, *44* (11), 1199–1207.

96 Luesch, H.; Yoshida, W. Y.; Moore, R. E.; Paul, V. J.; Corbett, T. H. Total Structure Determination of Apratoxin a, a Potent Novel Cytotoxin from the Marine Cyanobacterium *Lyngbya majuscula. J. Am. Chem. Soc.* **2001**, *123* (23), 5418–5423.

97 Liu, Y.; Law, B. K.; Luesch, H. Apratoxin A Reversibly Inhibits the Secretory Pathway by Preventing Cotranslational Translocation. *Mol. Pharmacol.* **2009**, *76* (1), 91–104.

98 Shen, S.; Zhang, P.; Lovchik, M. A.; Li, Y.; Tang, L.; Chen, Z.; Zeng, R.; Ma, D.; Yuan, J.; Yu, Q. Cyclodepsipeptide Toxin Promotes the Degradation of Hsp90 Client Proteins Through Chaperone-Mediated Autophagy. *J. Cell Biol.* **2009**, *185* (4), 629–639.

99 Luesch, H.; Yoshida, W. Y.; Moore, R. E.; Paul, V. J. Structurally Diverse New Alkaloids from Palauan Collections of the Apratoxin-Producing Marine Cyanobacterium *Lyngbya* sp. *Tetrahedron* **2002**, *58* (39), 7959–7966.

100 Boudreau, P. D.; Byrum, T.; Liu, W.-T.; Dorrestein, P. C.; Gerwick, W. H. Viequeamide A, a Cytotoxic Member of the Kulolide Superfamily of Cyclic Depsipeptides from a Marine Button Cyanobacterium. *J. Nat. Prod..* **2012**, *75* (9), 1560–1570.

101 Chen, Z.; Song, Y.; Chen, Y.; Huang, H.; Zhang, W.; Ju, J. Cyclic Heptapeptides, Cordyheptapeptides C–E, from the Marine-Derived Fungus *Acremonium persicinum* SCSIO 115 and Their Cytotoxic Activities. *J. Nat. Prod..* **2012**, *75* (6), 1215–1219.

102 Fukuhara, K.; Takada, K.; Okada, S.; Matsunaga, S. Nazumazoles A–C, Cyclic Pentapeptides Dimerized Through a Disulfide Bond from the Marine Sponge *Theonella swinhoei. Org. Lett.* **2015**, *17* (11), 2646–2648.

103 Tan, K. C.; Wakimoto, T.; Takada, K.; Ohtsuki, T.; Uchiyama, N.; Goda, Y.; Abe, I. Cycloforskamide, a Cytotoxic Macrocyclic Peptide from the Sea Slug *Pleurobranchus forskalii*. *J. Nat. Prod.* **2013**, *76* (7), 1388–1391.

104 Coello, L.; Reyes, F.; Martín, M. J.; Cuevas, C.; Fernández, R. Isolation and Structures of Pipecolidepsins A and B, Cytotoxic Cyclic Depsipeptides from the Madagascan Sponge *Homophymia lamellosa*. *J. Nat. Prod.* **2014**, *77* (2), 298–303.

105 Huang, M.-B.; Zhao, S.-M.; Zeng, G.-Z.; Kuang, B.; Chen, X.-Q.; Tan, N.-H. Rubischumanins A–C, New Cytotoxic Cyclopeptides from Rubia Schumanniana. *Tetrahedron* **2014**, *70* (42), 7627–7631.

106 Kang, H.-S.; Krunic, A.; Shen, Q.; Swanson, S. M.; Orjala, J. Minutissamides A–D, Antiproliferative Cyclic Decapeptides from the Cultured Cyanobacterium *Anabaena minutissima*. *J. Nat. Prod.* **2011**, *74* (7), 1597–1605.

107 Iwasaki, A.; Ohno, O.; Sumimoto, S.; Matsubara, T.; Shimada, S.; Sato, T.; Suenaga, K. Mebamamides A and B, Cyclic Lipopeptides Isolated from the Green Alga *Derbesia marina*. *J. Nat. Prod.* **2015**, *78* (4), 901–908.

108 Kimura, M.; Wakimoto, T.; Egami, Y.; Tan, K. C.; Ise, Y.; Abe, I. Calyxamides A and B, Cytotoxic Cyclic Peptides from the Marine Sponge *Discodermia calyx*. *J. Nat. Prod.* **2012**, *75* (2), 290–294.

109 Luo, S.; Krunic, A.; Kang, H.-S.; Chen, W.-L.; Woodard, J. L.; Fuchs, J. R.; Swanson, S. M.; Orjala, J. Trichormamides A and B with Antiproliferative Activity from the Cultured Freshwater *Cyanobacterium trichormus* sp. UIC 10339. *J. Nat. Prod.* **2014**, *77* (8), 1871–1880.

110 Raju, R.; Gromyko, O.; Andriy, B.; Fedorenko, V. Oleamycins A and B: New Antibacterial Cyclic Hexadepsipeptides Isolated from a *Terrestrial streptomyces* sp. *J. Antibiot.* **2014**, *67* (4), 339–343.

111 Theodore, C. M.; Lorig-Roach, N.; Still, P. C.; Johnson, T. A.; Drašković, M.; Schwochert, J. A.; Naphen, C. N.; Crews, M. S.; Barker, S. A.; Valeriote, F. A.; Lokey, R. S.; Crews, P. Biosynthetic Products from a Nearshore-Derived Gram-Negative Bacterium Enable Reassessment of the Kailuin Depsipeptides. *J. Nat. Prod..* **2015**, *78* (3), 441–452.

112 Thornburg, C. C.; Cowley, E. S.; Sikorska, J.; Shaala, L. A.; Ishmael, J. E.; Youssef, D. T. A.; McPhail, K. L. Apratoxin H and Apratoxin A Sulfoxide from the Red Sea Cyanobacterium *Moorea producens*. *J. Nat. Prod.* **2013**, *76* (9), 1781–1788.

113 Popplewell, W. L.; Ratnayake, R.; Wilson, J. A.; Beutler, J. A.; Colburn, N. H.; Henrich, C. J.; McMahon, J. B.; McKee, T. C. Grassypeptolides F and G, Cyanobacterial Peptides from *Lyngbya majuscula*. *J. Nat. Prod.* **2011**, *74* (8), 1686–1691.

114 Thornburg, C. C.; Thimmaiah, M.; Shaala, L. A.; Hau, A. M.; Malmo, J. M.; Ishmael, J. E.; Youssef, D. T. A.; McPhail, K. L. Cyclic Depsipeptides, Grassypeptolides D and E and Ibu-Epidemethoxylyngbyastatin 3, from a Red Sea Leptolyngbya Cyanobacterium. *J. Nat. Prod.* **2011**, *74* (8), 1677–1685.

115 Woo, J.-K.; Jeon, J.-E.; Kim, C.-K.; Sim, C. J.; Oh, D.-C.; Oh, K.-B.; Shin, J. Gombamide a, a Cyclic Thiopeptide from the Sponge *Clathria gombawuiensis*. *J. Nat. Prod.* **2013**, *76* (7), 1380–1383.

116 Zhan, K.-X.; Jiao, W.-H.; Yang, F.; Li, J.; Wang, S.-P.; Li, Y.-S.; Han, B.-N.; Lin, H.-W. Reniochalistatins A–E, Cyclic Peptides from the Marine Sponge *Reniochalina stalagmitis*. *J. Nat. Prod.* **2014**, *77* (12), 2678–2684.

117 Krasnoff, S. B.; Englich, U.; Miller, P. G.; Shuler, M. L.; Glahn, R. P.; Donzelli, B. G. G.; Gibson, D. M. Metacridamides A and B, Macrocycles from Conidia of the Entomopathogenic Fungus *Metarhizium acridum*. *J. Nat. Prod.* **2012**, *75* (2), 175–180.

118 Gavrish, E.; Sit, C. S.; Cao, S.; Kandror, O.; Spoering, A.; Peoples, A.; Ling, L.; Fetterman, A.; Hughes, D.; Bissell, A.; Torrey, H.; Akopian, T.; Mueller, A.; Epstein, S.; Goldberg, A.; Clardy, J.; Lewis, K. Lassomycin, a Ribosomally Synthesized Cyclic Peptide, Kills *Mycobacterium tuberculosis* by Targeting the ATP-Dependent Protease ClpC1P1P2. *Chem. Biol.* **2014**, *21* (4), 509–518.

119 Metelev, M.; Tietz, J. I.; Melby, J. O.; Blair, P. M.; Zhu, L.; Livnat, I.; Severinov, K.; Mitchell, D. A. Structure, Bioactivity, and Resistance Mechanism of Streptomonomicin, an Unusual Lasso Peptide from an Understudied Halophilic Actinomycete. *Chem. Biol.* **2015**, *22* (2), 241–250.

120 Ling, L. L.; Schneider, T.; Peoples, A. J.; Spoering, A. L.; Engels, I.; Conlon, B. P.; Mueller, A.; Schäberle, T. F.; Hughes, D. E.; Epstein, S.; Jones, M.; Lazarides, L.; Steadman, V. A.; Cohen, D. R.; Felix, C. R.; Fetterman, K. A.; Millett, W. P.; Nitti, A. G.; Zullo, A. M.; Chen, C.; Lewis, K. A New Antibiotic Kills Pathogens without Detectable Resistance. *Nature* **2015**, *517* (7535), 455–459.

121 Ling, L. L.; Schneider, T.; Peoples, A. J.; Spoering, A. L.; Engels, I.; Conlon, B. P.; Mueller, A.; Schäberle, T. F.; Hughes, D. E.; Epstein, S.; Jones, M.; Lazarides, L.; Steadman, V. A.; Cohen, D. R.; Felix, C. R.; Fetterman, K. A.; Millett, W. P.; Nitti, A. G.; Zullo, A. M.; Chen, C.; Lewis, K. Erratum: A New Antibiotic Kills Pathogens without Detectable Resistance. *Nature* **2015**, *520* (7547), 388–388.

122 Fan, L.; Ji, Z.; Guo, Z.; Wu, W. NW-G12, a Novel Nonchlorinated Cyclohexapeptide from *Streptomyces alboflavus* 313. *Chem. Nat. Compd.* **2013**, *49* (5), 910–913.

123 Cai, G.; Napolitano, J. G.; McAlpine, J. B.; Wang, Y.; Jaki, B. U.; Suh, J.-W.; Yang, S. H.; Lee, I.-A.; Franzblau, S. G.; Pauli, G. F.; Cho, S. Hytramycins V and I, Anti-*Mycobacterium tuberculosis* Hexapeptides from a *Streptomyces hygroscopicus* Strain. *J. Nat. Prod.* **2013**, *76* (11), 2009–2018.

124 Song, Y.; Li, Q.; Liu, X.; Chen, Y.; Zhang, Y.; Sun, A.; Zhang, W.; Zhang, J.; Ju, J. Cyclic Hexapeptides from the Deep South China Sea-Derived *Streptomyces scopuliridis* SCSIO ZJ46 Active Against Pathogenic Gram-Positive Bacteria. *J. Nat. Prod.* **2014**, *77* (8), 1937–1941.

125 Miao, S.; Anstee, M. R.; LaMarco, K.; Matthew, J.; Huang, L. H. T.; Brasseur, M. M. Inhibition of Bacterial RNA Polymerases. Peptide Metabolites from the Cultures of *Streptomyces* sp. *J. Nat. Prod.* **1997**, *60* (8), 858–861.

126 Um, S.; Choi, T. J.; Kim, H.; Kim, B. Y.; Kim, S.-H.; Lee, S. K.; Oh, K.-B.; Shin, J.; Oh, D.-C. Ohmyungsamycins A and B: Cytotoxic and Antimicrobial Cyclic Peptides Produced by *Streptomyces* sp. from a Volcanic Island. *J. Org. Chem.* **2013**, *78* (24), 12321–12329.

127 Wyche, T. P.; Hou, Y.; Vazquez-Rivera, E.; Braun, D.; Bugni, T. S. Peptidolipins B–F, Antibacterial Lipopeptides from an Ascidian-Derived *Nocardia* sp. *J. Nat. Prod.* **2012**, *75* (4), 735–740.

128 Lu, Z.; Harper, M. K.; Pond, C. D.; Barrows, L. R.; Ireland, C. M.; Van Wagoner, R. M. Thiazoline Peptides and a Tris-Phenethyl Urea from *Didemnum molle* with Anti-HIV Activity. *J. Nat. Prod.* **2012**, *75* (8), 1436–1440.

129 Tan, Q.-W.; Gao, F.-L.; Wang, F.-R.; Chen, Q.-J. Anti-TMV Activity of Malformin A1, a Cyclic Penta-Peptide Produced by an Endophytic Fungus *Aspergillus tubingensis* FJBJ11. *Int. J. Mol. Sci.* **2015**, *16* (3), 5750–5761.

130 Pinto, M. E. F.; Batista, J. M., Jr.; Koehbach, J.; Gaur, P.; Sharma, A.; Nakabashi, M.; Cilli, E. M.; Giesel, G. M.; Verli, H.; Gruber, C. W.; Blanch, E. W.; Tavares, J. F.; da Silva, M. S.; Garcia, C. R. S.; Bolzani, V. S. Ribifolin, an Orbitide from *Jatropha ribifolia*, and Its Potential Antimalarial Activity. *J. Nat. Prod.* **2015**, *78* (3), 374–380.

131 Portmann, C.; Sieber, S.; Wirthensohn, S.; Blom, J. F.; Da Silva, L.; Baudat, E.; Kaiser, M.; Brun, R.; Gademann, K. Balgacyclamides, Antiplasmodial Heterocyclic Peptides from Microcystis Aeruginosa EAWAG 251. *J. Nat. Prod.* **2014**, *77* (3), 557–562.

132 Vining, O. B.; Medina, R. A.; Mitchell, E. A.; Videau, P.; Li, D.; Serrill, J. D.; Kelly, J. X.; Gerwick, W. H.; Proteau, P. J.; Ishmael, J. E.; McPhail, K. L. Depsipeptide Companeramides from a Panamanian Marine Cyanobacterium Associated with the Coibamide Producer. *J. Nat. Prod.* **2015**, *78* (3), 413–420.

133 Bargen, von, K. W.; Niehaus, E.-M.; Bergander, K.; Brun, R.; Tudzynski, B.; Humpf, H.-U. Structure Elucidation and Antimalarial Activity of Apicidin F: An Apicidin-Like Compound Produced by *Fusarium fujikuroi*. *J. Nat. Prod.* **2013**, *76* (11), 2136–2140.

134 Bae, M.; Kim, H.; Moon, K.; Nam, S.-J.; Shin, J.; Oh, K.-B.; Oh, D.-C. Mohangamides a and B, New Dilactone-Tethered Pseudo-Dimeric Peptides Inhibiting *Candida albicans* Isocitrate Lyase. *Org. Lett.* **2015**, *17* (3), 712–715.

135 Bui, T.-H.; Wray, V.; Nimtz, M.; Fossen, T.; Preisitsch, M.; Schröder, G.; Wende, K.; Heiden, S. E.; Mundt, S. Balticidins A–D, Antifungal Hassallidin-Like Lipopeptides from the Baltic Sea Cyanobacterium Anabaena Cylindrica Bio33. *J. Nat. Prod.* **2014**, *77* (6), 1287–1296.

136 Altei, W. F.; Picchi, D. G.; Abissi, B. M.; Giesel, G. M.; Flausino, O., Jr.; Reboud-Ravaux, M.; Verli, H.; Crusca, E., Jr.; Silveira, E. R.; Cilli, E. M.; Bolzani, V. S. Jatrophidin I, a Cyclic Peptide from Brazilian *Jatropha curcas* L.: Isolation, Characterization, Conformational Studies and Biological Activity. *Phytochemistry* **2014**, *107*, 91–96.

137 Lodin-Friedman, A.; Carmeli, S. Metabolites from *Microcystis aeruginosa* Bloom Material Collected at a Water Reservoir Near Kibbutz Hafetz Haim, Israel. *J. Nat. Prod.* **2013**, *76* (6), 1196–1200.

138 Elkobi-Peer, S.; Carmeli, S. New Prenylated Aeruginosin, Microphycin, Anabaenopeptin and Micropeptin Analogues from a Microcystis Bloom Material Collected in Kibbutz Kfar Blum, Israel. *Mar. Drugs* **2015**, *13* (4), 2347–2375.

139 Kang, H.-S.; Krunic, A.; Orjala, J. Stigonemapeptin, an Ahp-Containing Depsipeptide with Elastase Inhibitory Activity from the Bloom-Forming Freshwater Cyanobacterium *Stigonema* sp. *J. Nat. Prod.* **2012**, *75* (4), 807–811.

140 Um, S.; Kim, Y.-J.; Kwon, H.; Wen, H.; Kim, S.-H.; Kwon, H. C.; Park, S.; Shin, J.; Oh, D.-C. Sungsanpin, a Lasso Peptide from a Deep-Sea Streptomycete. *J. Nat. Prod.* **2013**, *76* (5), 873–879.

141 Um, S.; Park, S. H.; Kim, J.; Park, H. J.; Ko, K.; Bang, H.-S.; Lee, S. K.; Shin, J.; Oh, D.-C. Coprisamides A and B, New Branched Cyclic Peptides from a Gut Bacterium of the Dung Beetle *Copris tripartitus*. *Org. Lett.* **2015**, *17* (5), 1272–1275.

142 Junne, T.; Wong, J.; Studer, C.; Aust, T.; Bauer, B. W.; Beibel, M.; Bhullar, B.; Bruccoleri, R.; Eichenberger, J.; Estoppey, D.; Hartmann, N.; Knapp, B.; Krastel, P.; Melin, N.; Oakeley, E. J.; Oberer, L.; Riedl, R.; Roma, G.; Schuierer, S.; Petersen, F.; Tallarico, J. A.; Rapoport, T. A.; Spiess, M.; Hoepfner, D. Decatransin, a New Natural Product Inhibiting Protein Translocation at the Sec61/SecYEG Translocon. *J. Cell Sci.* **2015**, *128* (6), 1217–1229.

143 Peng, J.; Gao, H.; Zhang, X.; Wang, S.; Wu, C.; Gu, Q.; Guo, P.; Zhu, T.; Li, D. Psychrophilins E–H and Versicotide C, Cyclic Peptides from the Marine-Derived Fungus Aspergillus Versicolor ZLN-60. *J. Nat. Prod.* **2014**, *77* (10), 2218–2223.

144 Fukuda, T.; Sudoh, Y.; Tsuchiya, Y.; Okuda, T.; Matsuura, N.; Motojima, A.; Oikawa, T.; Igarashi, Y. Hikiamides A–C, Cyclic Pentadepsipeptides from *Fusarium* sp. TAMA 456. *J. Nat. Prod.* **2015**, *78* (4), 797–802.

145 Audoin, C.; Sánchez, J. A.; Genta-Jouve, G.; Alfonso, A.; Rios, L.; Vale, C.; Thomas, O. P.; Botana, L. M. Autumnalamide, a Prenylated Cyclic Peptide from the Cyanobacterium *Phormidium autumnale*, Acts on SH-SY5Y Cells at the Mitochondrial Level. *J. Nat. Prod.* **2014**, *77* (10), 2196–2205.

146 Pérez-Victoria, I.; Martín, J.; González-Menéndez, V.; de Pedro, N.; el Aouad, N.; Ortiz-López, F. J.; Tormo, J. R.; Platas, G.; Vicente, F.; Bills, G. F.; Genilloud, O.; Goetz, M. A.; Reyes, F. Isolation and Structural Elucidation of Cyclic Tetrapeptides from *Onychocola sclerotica*. *J. Nat. Prod.* **2012**, *75* (6), 1210–1214.

147 Chung, Y.-M.; El-Shazly, M.; Chuang, D.-W.; Hwang, T.-L.; Asai, T.; Oshima, Y.; Ashour, M. L.; Wu, Y.-C.; Chang, F.-R. Suberoylanilide Hydroxamic Acid, a Histone Deacetylase Inhibitor, Induces the Production of Anti-Inflammatory Cyclodepsipeptides from *Beauveria felina*. *J. Nat. Prod.* **2013**, *76* (7), 1260–1266.

148 Du, F.-Y.; Zhang, P.; Li, X.-M.; Li, C.-S.; Cui, C.-M.; Wang, B.-G. Cyclohexadepsipeptides of the Isaridin Class from the Marine-Derived Fungus *Beauveria felina* en-135. *J. Nat. Prod.* **2014**, *77* (5), 1164–1169.

149 Li, D.; Carr, G.; Zhang, Y.; Williams, D. E.; Amlani, A.; Bottriell, H.; Mui, A. L. F.; Andersen, R. J. Turnagainolides A and B, Cyclic Depsipeptides Produced in Culture by a *Bacillus* sp.: Isolation, Structure Elucidation, and Synthesis. *J. Nat. Prod.* **2011**, *74* (5), 1093–1099.

150 Tong, Y.; Luo, J.-G.; Wang, R.; Wang, X.-B.; Kong, L.-Y. New Cyclic Peptides with Osteoblastic Proliferative Activity from *Dianthus superbus*. *Bioorg. Med. Chem. Lett.* **2012**, *22* (5), 1908–1911.

151 Zhao, J.; Zhou, L.-L.; Li, X.; Xiao, H.-B.; Hou, F.-F.; Cheng, Y.-X. Bioactive Compounds from the Aerial Parts of *Brachystemma calycinum* and Structural Revision of an Octacyclopeptide. *J. Nat. Prod.* **2011**, *74* (6), 1392–1400.

152 Cheng, Y.-X.; Zhou, J.; Tan, N.-H.; Teng, R.-W.; Lu, Y.; Wang, C.; Zheng, Q.-T. Isolation and Characterization of Brachystemidines A–E, Novel Alkaloids from *Brachystemma calycinum*. *J. Nat. Prod.* **2002**, *65* (5), 750–752.

153 Kita, M.; Gise, B.; Kawamura, A.; Kigoshi, H. Stylissatin a, a Cyclic Peptide that Inhibits Nitric Oxide Production from the Marine Sponge *Stylissa massa*. *Tetrahedron Lett.*. **2013**, *54* (50), 6826–6828.

154 Lebbe, E. K. M.; Peigneur, S.; Maiti, M.; Devi, P.; Ravichandran, S.; Lescrinier, E.; Ulens, C.; Waelkens, E.; D'Souza, L.; Herdewijn, P.; Tytgat, J. Structure-Function Elucidation of a New A-Conotoxin, Lo1a, from *Conus longurionis*. *J. Biol. Chem.* **2014**, *289* (14), 9573–9583.

155 Luo, S.; Zhangsun, D.; Schroeder, C. I.; Zhu, X.; Hu, Y.; Wu, Y.; Weltzin, M. M.; Eberhard, S.; Kaas, Q.; Craik, D. J.; McIntosh, J. M.; Whiteaker, P. A Novel A4/7-Conotoxin LvIA from *Conus lividus* that Selectively Blocks A3β2 vs. A6/A3β2β3 Nicotinic Acetylcholine Receptors. *FASEB J.* **2014**, *28* (4), 1842–1853.

156 Hellinger, R.; Koehbach, J.; Puigpinós, A.; Clark, R. J.; Tarragó, T.; Giralt, E.; Gruber, C. W. Inhibition of Human Prolyl Oligopeptidase Activity by the Cyclotide Psysol 2 Isolated from *Psychotria solitudinum*. *J. Nat. Prod.* **2015**, *78* (5), 1073–1082.

157 Hu, E.; Wang, D.; Chen, J.; Tao, X. Novel Cyclotides from *Hedyotis diffusa* Induce Apoptosis and Inhibit Proliferation and Migration of Prostate Cancer Cells. *Int. J. Clin. Exp. Med.* **2015**, *8* (3), 4059–4065.

158 Roshan, A.; Zarrabi, M.; Asgarani, E.; Kanaani, M. R. Sequence Analysis of Gene Encoding Cyclotides in Three Species of Violaceae and Determination of Their Anti-Microbial Activities. *J. Biochem. Microbial Technol.* **2014**, *2* (1), 1–7.

159 Nguyen, P. Q. T.; Luu, T. T.; Bai, Y.; Nguyen, G. K. T.; Pervushin, K.; Tam, J. P. Allotides: Proline-Rich Cystine Knot A-Amylase Inhibitors from *Allamanda cathartica*. *J. Nat. Prod.* **2015**, *78* (4), 695–704.

160 Li, H.; Bowling, J. J.; Su, M.; Hong, J.; Lee, B.-J.; Hamann, M. T.; Jung, J. H. Asteropsins B–D, Sponge-Derived Knottins with Potential Utility as a Novel Scaffold for Oral Peptide Drugs. *Biochim. Biophys.* **2014**, *1840* (3), 977–984.

161 Vaillancourt, K.; LeBel, G.; Frenette, M.; Gottschalk, M.; Grenier, D. Suicin 3908, a New Lantibiotic Produced by a Strain of *Streptococcus suis* Serotype 2 Isolated From a Healthy Carrier Pig. *PLoS One* **2015**, *10* (2), e0117245.

162 Basi-Chipalu, S.; Dischinger, J.; Josten, M.; Szekat, C.; Zweynert, A.; Sahl, H.-G.; Bierbaum, G. Pseudomycoicidin, a Class II Lantibiotic from *Bacillus pseudomycoides*. *Appl. Environ. Microbiol.* **2015**, *81* (10), 3419–3429.

6

Chemical Approaches to Macrocycle Libraries

Ziqing Qian, Patrick G. Dougherty and Dehua Pei

Department of Chemistry and Biochemistry, The Ohio State University, Columbus, OH, USA

6.1 Introduction

Macrocycles are a rich source of biologically active compounds and are widely produced in nature by bacteria, fungi, plants, and so on. These naturally occurring chemical entities possess a broad range of biological activities, including antimicrobial, antifungal, immunosuppressant, antitumor, and hormonal activities [1, 2]. Indeed, several natural and synthetic macrocycles are already in clinical use (see Chapter 16) [2]. In recent years, there has been an increasing interest in macrocyclic structures as a third drug modality, in addition to small molecules and biologics, because neither of these have been particularly effective against one of the most exciting class of drug targets, that is, intracellular protein–protein interactions (PPIs) [2, 3]. It is estimated that PPIs represent ~80% of all disease-relevant targets [4], and yet they have remained largely undrugged to date, because small molecules generally do not bind to the large, flat PPI interfaces with high affinity or specificity, whereas biologics (e.g., monoclonal antibodies) can efficaciously disrupt PPI yet cannot enter the cell [5]. Macrocycles, on the other hand, are expected to capture the best of both worlds. First, with molecular weights typically in the range of 500–2000 Da, macrocycles are larger than conventional small-molecule drugs and can engage in a greater number of interactions with a binding site (even if the latter is a flat surface) to impart high affinity and specificity. Additionally, the more restricted conformational freedom of macrocycles (relative to their linear counterparts) can potentially improve both the binding affinity (due to lower entropic loss during target binding) and specificity toward a target of interest (due to reduced ability to adopt alternative conformations required to bind other targets). Indeed, there are now many examples of naturally occurring and synthetic macrocycles that bind to flat protein surfaces with antibody-like affinities and specificities [6]. Lastly, macrocycles retain many of the attractive drug-like properties of small molecules, including metabolic stability, membrane permeability, and even oral bioavailability [7–9].

Despite their enormous potential as therapeutic agents and chemical probes, macrocycles were historically underexploited, due to the lack of mature technologies to access this class of molecules. Compared to small-molecule drugs, rational design of macrocyclic drugs is very challenging in the absence of a prior structure of the target–ligand complex, precluding the application of structure-based drug discovery approaches for modeling macrocycles. Therefore, discovery of initial macrocyclic hit/lead compounds has frequently been accomplished by synthesizing and screening compound libraries. Over the past decade, several technologies have been developed to generate macrocyclic libraries of varying structures and diversities. Based on how much of the backbone contains the peptide bond linkage, macrocycles can be classified into cyclic peptides, semi-peptidic, and non-peptidic macrocycles. In general, non-peptidic and semi-peptidic macrocycles have been prepared by parallel synthesis, however their diversity is limited to ~10^4 compounds. On the other hand, cyclic peptide libraries can be synthesized in a combinatorial manner, on solid phase or in solution, to reach enormous compositional diversity—up to 10^{14} molecules. These cyclic peptide libraries can be further classified into biological versus chemical ones based on their method of synthesis, although certain hybrid methods introduce one or more chemical steps in conjunction with biological approaches. Both strategies still produce dominantly peptidic structures [10]. Biologically synthesized cyclic peptide library approaches include phage display [11], mRNA display [12], and peptide splicing using split inteins [13], all of which involve peptide synthesis by the ribosome. The main advantages of biologically prepared libraries include greater diversity, compatibility with library amplification techniques (e.g., polymerase chain

reaction), iterative screening, and straightforward hit identification (e.g., sequencing the encoding DNA/mRNA). However, ribosomal synthesis limits the library building blocks to the 20 proteinogenic amino acids and certain modified amino acids (e.g., N_α-methylated amino acids) [12, 14]. D-amino acids and non-peptidic building blocks are generally incompatible with these biological libraries, although recent efforts are making progress to change this [15, 16]. In contrast, both natural and unnatural building blocks can be readily incorporated into chemically derived synthetic libraries to generate more structurally diverse macrocycles.

In this chapter, we will provide an overview of the various methods developed for the chemical synthesis of libraries of cyclic peptides, peptidomimetics, and non-peptidic macrocycles. We will discuss the general features of these methods and their applications to the discovery of therapeutic agents and molecular probes, with a special emphasis on the combinatorial synthesis of relatively large libraries. For biologically synthesized macrocycle libraries and hybrid methods, readers are referred to Chapter 7 of this series and several excellent recent reviews [12, 17, 18]. Additionally, reviews on macrocyclization methodologies and the rational design of macrocyclic ligands against enzymes and protein receptors are also available [3, 19].

6.2 Challenges Associated with Macrocyclic One-Bead-One-Compound Libraries

Among the chemically synthesized compound libraries, the one-bead-one compound (OBOC) library has been the most widely practiced, as it offers several major advantages. First, because OBOC libraries are chemically synthesized, they are compatible with a wide variety of natural and unnatural building blocks. Second, very large numbers of compounds (up to 10^8) can be rapidly synthesized by the split-and-pool synthesis method [20–22]. Finally, each bead in an OBOC library displays roughly the same amount of a unique compound (e.g., ~100 pmol for a 90-µm TentaGel bead), allowing the entire library to be simultaneously screened against a target of interest with very high throughput. A common screening experiment involves incubating the library beads with a small amount of a fluorescently labeled protein (1 nM to 5 µM) in an appropriate plate (e.g., a Petri dish) and viewing the beads under a fluorescence microscope. Positive (fluorescent) beads can be isolated from the library either manually with a micropipette or by the COPAS instrument [23]. Another popular screening method involves labeling the target protein with biotin

and incubating the library beads with biotinylated protein in the presence of a small amount of streptavidin–alkaline phosphatase (SA–AP) [22]. Binding of the target protein to a positive bead recruits SA–AP to the bead surface that, upon the addition of 5-bromo-4-chloro-3-indolyl phosphate (BCIP), generates an indigo product and renders the bead turquoise colored. Kodadek and others also labeled target proteins with magnetic microparticles and employed magnetic sorting to isolate positive beads [24]. This method is operationally simple and can quickly reduce the number of library beads from millions to hundreds, although the relatively high false-positive and false-negative rates necessitate multiple rounds of sorting. In addition, the libraries can be screened for multiple rounds by employing a different screening assay in each round, maximizing the probability of isolating the most potent hits as well as eliminating false-positive beads [25].

Large libraries of macrocyclic compounds, such as cyclic peptides and peptidomimetics, can be readily prepared in the OBOC format and screened for binding to protein targets using the methods described earlier to produce *bona fide* hit compounds still covalently bound to individual beads. The challenge, however, lies in the structural identification of the hit compounds. With ~100 pmol (i.e., <1 µg) of compound derived from a single bead, structural determination by most conventional analytical techniques (e.g., NMR spectroscopy) is out of the question. Further, direct sequencing by Edman degradation is not possible because cyclic peptides lack the requisite free N-terminal amine, as opposed to linear peptides. Structural determination of cyclic peptides by tandem mass spectrometry (MS/MS) has also been difficult, because cyclic peptides have very complex fragmentation patterns, making spectral interpretation challenging with current data processing tools (see Chapter 1 for discussion) [26]. In addition, MS/MS methods cannot differentiate isobaric residues, for example, glutamine versus lysine, leucine versus isoleucine, or L- versus D-amino acids. These technical issues, in our knowledge, contributed significantly to the delayed progress in the area of combinatorial synthesis of cyclic peptides and peptidomimetics.

6.3 Deconvolution of Macrocyclic Libraries

In the absence of a robust technology to directly identify macrocyclic hits, early investigators employed two different deconvolution strategies, namely, iterative deconvolution and positional scanning [21], to discover cyclic peptidyl ligands against macromolecular targets. Iterative deconvolution involves preparing a series of

(a)

1st round:

Best pool

2nd round:

Best pool

3rd round:

Best pool

4th round:

Best pool

Best hit: **B-C-D-A**

(b)

1st round:

Best pool

2nd round:

Best pool

3rd round:

Best pool

4th round:

Best pool

Best hit: **B-C-D-A**

(c)

1
Endothelin receptor antagonist

2
μ-Opiod receptor ligand ($K_I = 39$ nM)
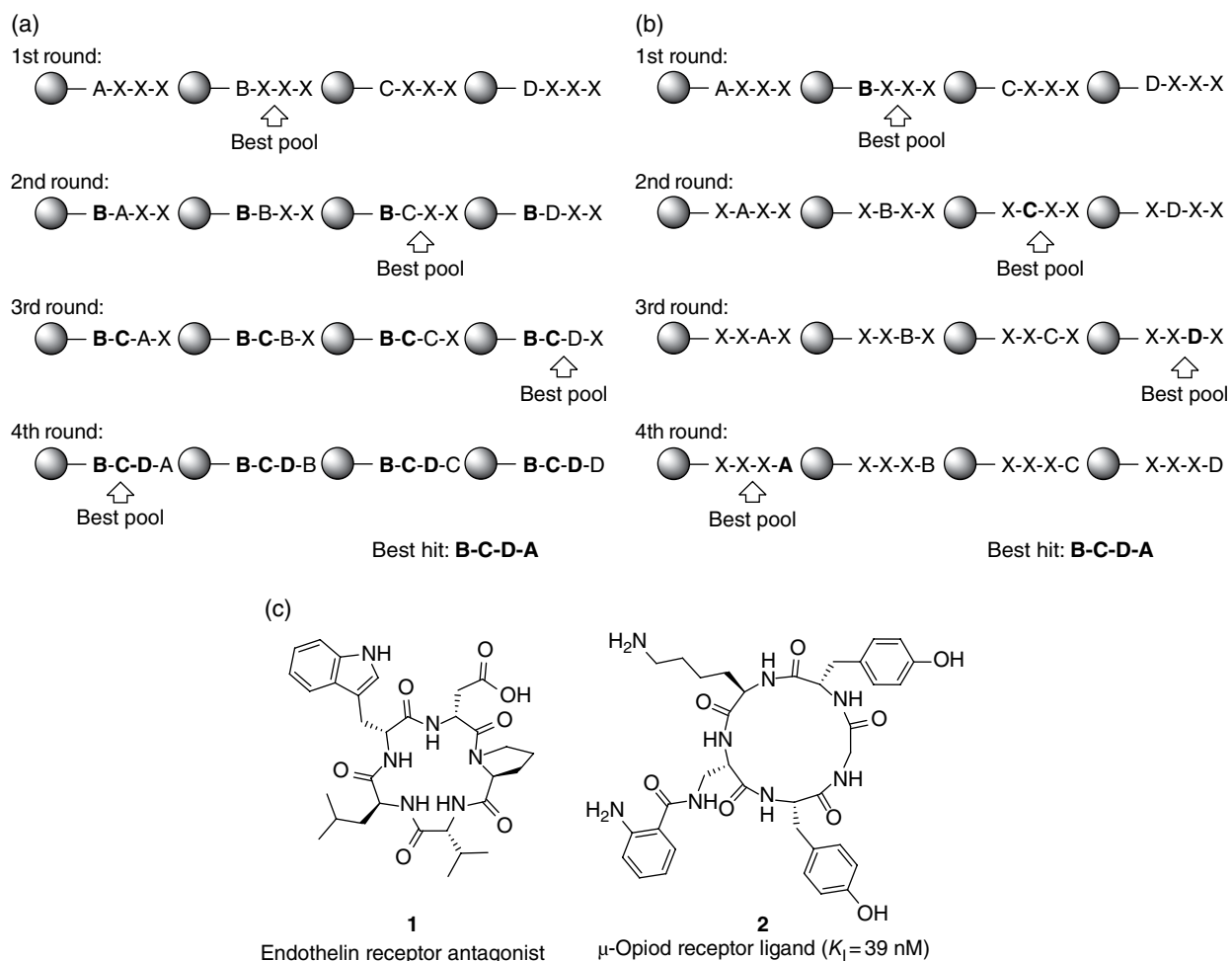
Figure 6.1 (a) Hit identification from a combinatorial library by iterative deconvolution; (b) hit identification from a combinatorial library by positional scanning; (c) two representative macrocyclic ligands discovered by the positional scanning method.

sub-libraries and multiple rounds of screening (Figure 6.1a). In the first round, multiple sub-libraries are synthesized with each sub-library containing a different residue at a single fixed position but randomized sequences at all other positions. Each sub-library is then separately subjected to an activity test against the target of interest (e.g., binding affinity). Comparison of the activities of all sub-libraries identifies the optimal residue(s) at the fixed position. During the next round, another series of sub-libraries are synthesized with all peptides containing the optimal residue identified from the first round. Again, each sub-library contains a different residue at a second fixed position and random sequences at all remaining variable positions. Activity tests of these sub-libraries in turn determine the most preferred residue at the second position. Repetition of the previously mentioned procedure for a total of n rounds (where n is the number of variable positions) in principle identifies the most active ligand against the target. This deconvolution process is very laborious and may fail to identify the most active ligand, or even any ligand at all, if, for example, sequence covariance is required for binding to the target. Nevertheless, Chu and coworkers were able to use this approach to identify a cyclic peptide ligand against streptavidin, which is bound with a 1000-fold higher affinity than the corresponding linear peptide, from a cyclic peptide library containing five random positions [27].

Deconvolution by positional scanning, in contrast, involves parallel synthesis of all sub-libraries at once (Figure 6.1b). For each variable position in this approach, a total of n sub-libraries (where n equals the number of building blocks used at that position) are synthesized, with each sub-library containing a different building block at the fixed position and random sequences at all other variable positions. Activity comparison of the n sub-libraries identifies the optimal building block at the fixed position. A total of $n \times m$ sub-libraries (where

m equals the number of variable positions in the peptide) are synthesized and assayed against the target. Combination of the optimal building blocks at all *m* positions in theory gives the most potent ligand against the target. Crozet *et al.* screened a homodetic cyclopentapeptide library against the endothelin receptor by positional scanning and rediscovered a previously reported antagonist, thus validating this approach (compound **1**, Figure 6.1c) [28]. Houghten and coworkers have extensively employed the positional scanning method to discover potent cyclic peptide ligands against protein targets, including α-glucosidase and the μ-opioid receptor (compound **2**, Figure 6.1c) [29, 30]. Positional scanning suffers from some of the same drawbacks as iterative deconvolution but is somewhat less labor intensive. Additionally, some targets may exhibit sequence covariance during ligand binding; in such cases, combination of optimal residues at all *m* positions may not produce a binding ligand.

6.4 Peptide-Encoded Macrocyclic Libraries

To provide a simpler, and yet robust, method for hit identification, Pei and coworkers designed one-bead-two-compound (OBTC) libraries in which each cyclic peptide is encoded on the same bead by the corresponding linear peptide [31]. Each library bead is spatially segregated into outer versus inner layers [32], with a unique cyclic peptide displayed on its surface and a linear peptide of identical sequence contained in its inner layer as an encoding tag (Figure 6.2). During library screening against protein targets, the proteins only have access to the cyclic peptides on the bead surface as the protein is too large to diffuse into the bead interior, and as a result the linear-encoding peptides do not interfere with the screening process. After an active bead/cyclic peptide is isolated from the library, its structure is readily determined by sequencing the linear-encoding peptide inside the bead. This can be accomplished by conventional Edman sequencing [33], partial Edman degradation–mass spectrometry (PED–MS) [34], or
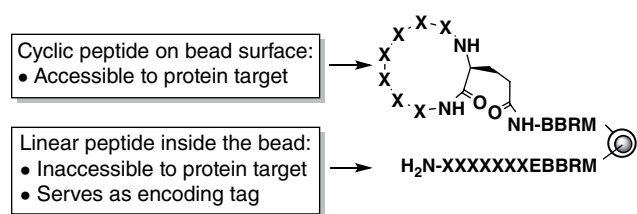
MS/MS methods [26, 35, 36]. PED–MS is a robust, high-throughput peptide sequencing technique previously developed by the Chait, Kent, and Pei laboratories [34, 37, 38]. It involves converting a resin-bound linear peptide into a family of N-terminally truncated fragments by subjecting the peptide to multiple rounds of Edman degradation in the presence of small amounts of a capping agent (e.g., Fmoc-OSu [34]). The resulting mixture of the peptide and its fragments is analyzed by MALDI-TOF MS to reveal the peptide sequence.

OBTC cyclic peptide libraries have been screened against a variety of protein targets, including many involved in PPIs. For example, screening of a naive cyclooctapeptide library against the extracellular domain of human prolactin receptor identified several moderately potent ligands against the receptor ($K_D = 2$–$3\,\mu M$ for compound **3**, Figure 6.3) [39]. A similar cyclic peptide library consisting of five random positions as well as variable ring sizes (cyclohepta- to cyclodecapeptides) was screened against the HIV-1 capsid protein to identify multiple cyclic peptide inhibitors that blocked the interaction between this protein and human lysyl-tRNA synthetase ($K_D = 0.4\,\mu M$) (compound **4**, Figure 6.3) [40]. Because OBTC libraries are chemically synthesized, known pharmacophores can be incorporated to generate biased/focused libraries with enhanced binding affinity and specificity to a target of interest. For example, incorporation of a phosphotyrosine (pY) residue into a cyclic peptide library and screening it against the Grb2 and tensin SH2 domains provided highly potent Grb2 and tensin inhibitors (lowest $K_D = 45\,nM$) [41]. Conjugation of a cell-penetrating peptide (CPP) (nona-arginine) to the glutamine side chain of a Grb2 inhibitor (compound **5**, Figure 6.3) resulted in a biologically active cyclic peptide that showed antiproliferative activity against cancer cells. Similarly, an OBTC cyclic peptide library was constructed with a D-phosphothreonyl residue as the embedded pharmacophore and screened against human peptidyl-prolyl isomerase Pin1 [42]. Many potent Pin1 inhibitors were discovered, with IC$_{50}$ values in the low nanomolar range (e.g., compound **6**, Figure 6.3). Further optimization of the library hits including attachment to CPPs resulted in cell-permeable monocyclic and bicyclic compounds that potently inhibited Pin1 function *ex vivo* [42, 43]. Finally, an OBTC cyclic peptide library was designed to have a degenerate peptide sequence containing difluorophosphonomethyl-phenylalanine (F$_2$Pmp, a non-hydrolyzable pY analogue) as the pharmacophore for target binding and a cell-penetrating hexapeptide for cell entry [43]. Screening of the library against protein–tyrosine phosphatase 1B (PTP1B) yielded competitive inhibitors with the most potent compound having a K_I value of ~30 nM. Further optimization of the hit

Figure 6.2 Design of a peptide-encoded OBTC cyclic peptide Library. B, β-alanine.

3
Prolactin receptor ligand ($K_D = 3.0\ \mu M$)

4
HIV capsid ligand ($K_D = 270\ nM$)

5
Grb2 SH2 ligand ($K_D = 45\ nM$)

6
Pin1 inhibitor ($K_D = 47\ nM$)

7
PTP1B inhibitor ($K_I = 37\ nM$)
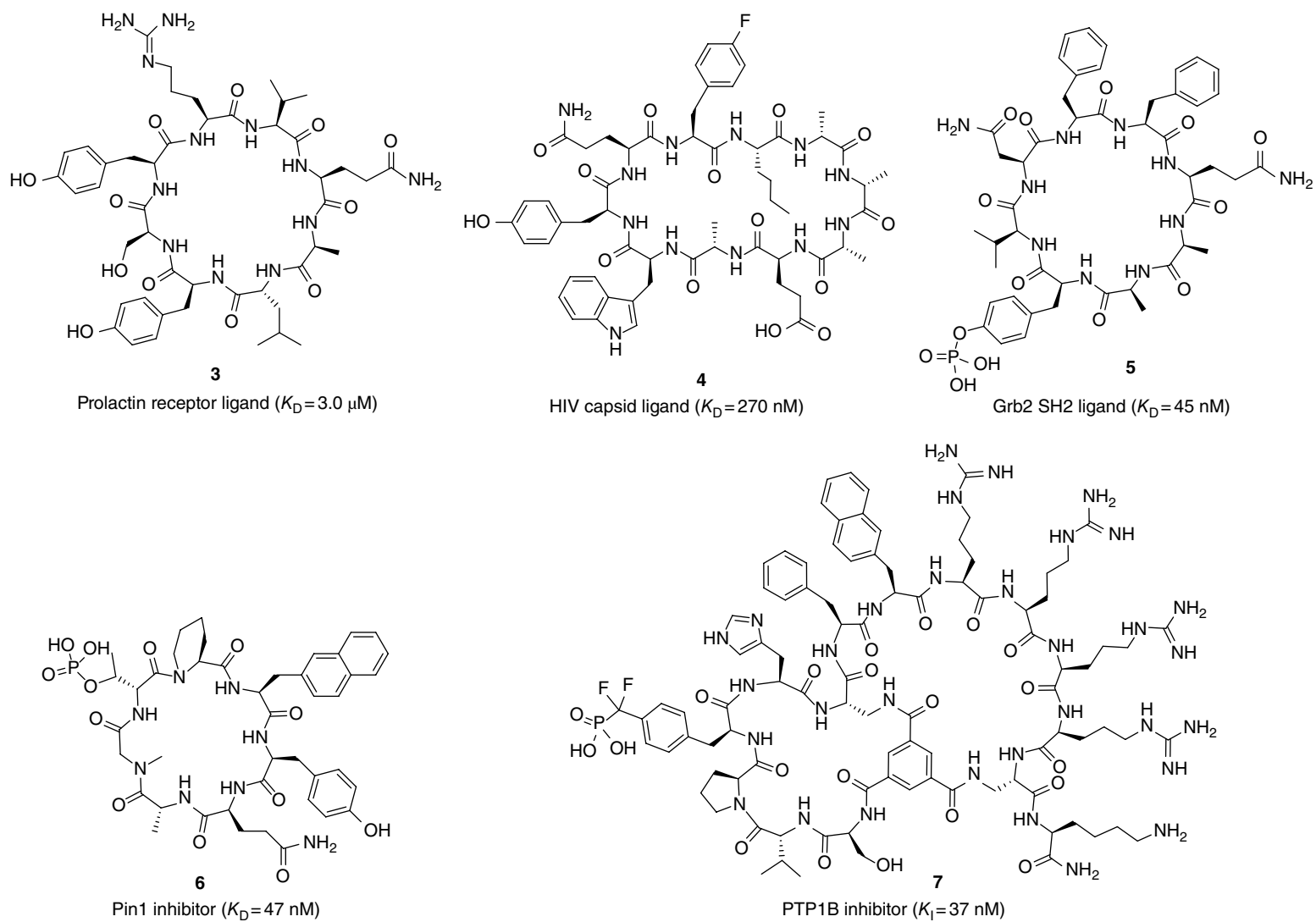
Figure 6.3 Structures of representative monocyclic and bicyclic peptide ligands discovered from peptide-encoded OBTC libraries.

compound yielded a cell-permeable and proteolytically stable bicyclic peptide that potently inhibited the intracellular PTP1B activity ($K_I = 37$ nM; compound **7**, Figure 6.3) and potentiated insulin receptor signaling at concentrations as low as 40 nM [43].

As mentioned previously, PPIs involving large, flat interfaces remain challenging targets for small molecules [5]. To test whether cyclic peptides are effective PPI inhibitors, Wu *et al.* [44] screened an OBTC library of ~3 million semi-peptidic macrocycles against K-Ras, one of the most important cancer drivers mutated in ~30% all human cancers [45]. One of the hit peptides bound to K-Ras with a K_D value of 0.83 μM and blocked Ras–Raf interaction *in vitro* with an IC50 value of 0.7 μM (compound **8**, Figure 6.4). Recognizing that the hit peptide contained a sequence motif rich in arginine and aromatic

hydrophobic residues, which are similar to CPPs, the investigators designed a second-generation OBTC library in which the CPP-like motif was retained, while the remaining sequence was replaced with a degenerate peptide sequence of one to five amino acids [46]. Screening of this second-generation library identified two cyclic peptides that inhibited Ras–Raf interaction with IC50 values of ~0.5 μM and showed modest antiproliferative activity against mutant K-Ras cancer cells (e.g., compound **9**, Figure 6.4). Further structure–activity relationship analysis and optimization resulted in a family of highly potent inhibitors against the Ras–Raf interaction *in vitro* (lowest IC50 = 14 nM) that have varying cell-penetrating capabilities. One of the compounds, cyclorasin 9A5 (compound **10**, Figure 6.4), is relatively potent against the Ras–Raf interaction (IC50 = 120 nM)

8
K-Ras ligand (IC50 = 0.7 μM)
impermeable

2nd-generation library

10
K-Ras ligand (IC50 = 0.12 μM)
high permeability

9
K-Ras ligand (IC50 = 0.6 μM)
low permeability
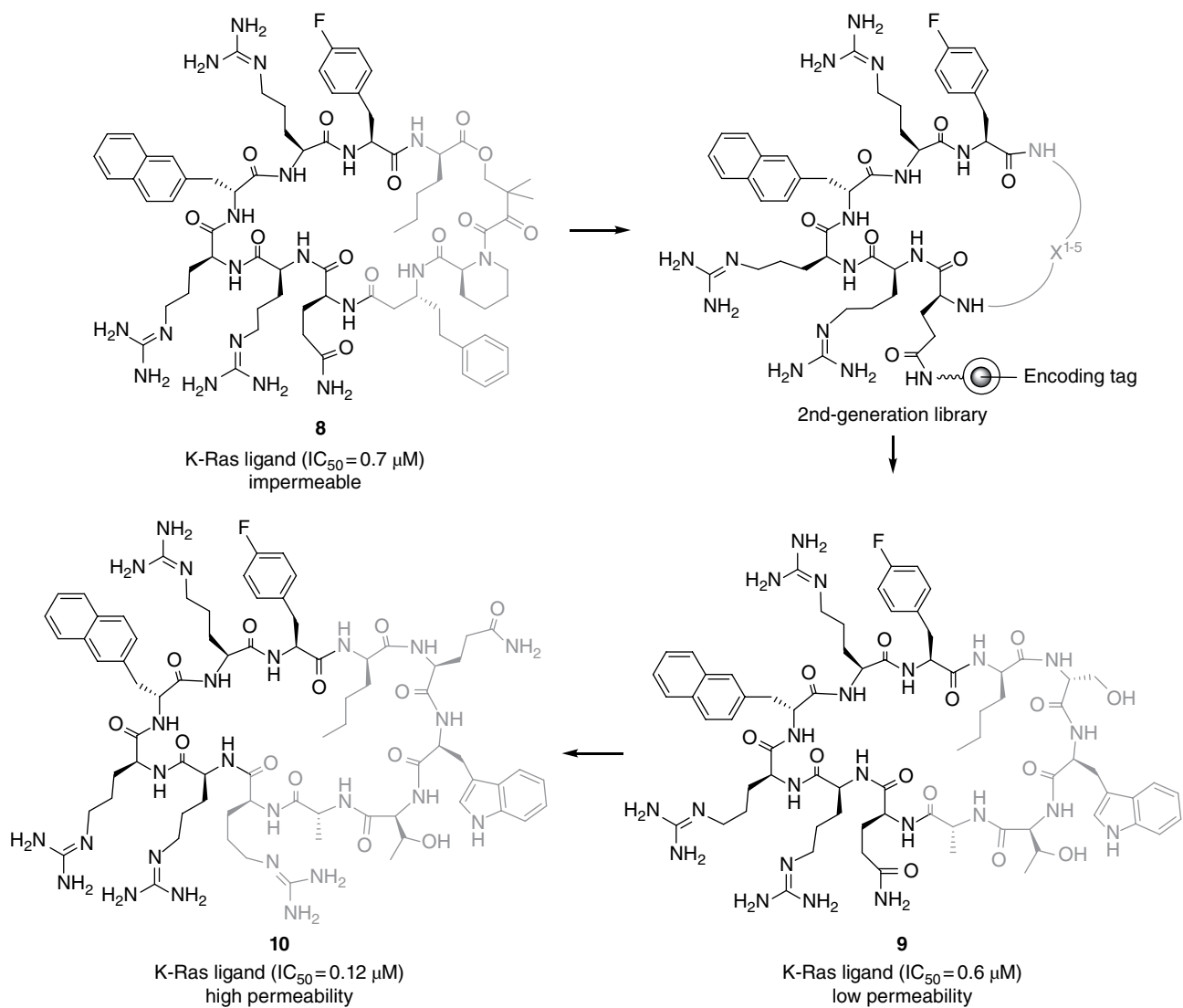
Figure 6.4 Design, synthesis, and screening a second-generation OBTC library against K-Ras G12V. The residues modified during library synthesis and optimization are colored in gray.

and has good cellular permeability. Cyclorasin 9A5 blocked Ras–Raf interaction inside cancer cells, inhibited the Ras signaling pathways, and induced apoptosis of the cancer cells with an EC_{50} of ~3 μM [46].

More recently, Lian *et al.* synthesized bicyclic libraries in the OBTC format by "wrapping" a peptide around a rigid trimesic acid scaffold (Figure 6.5) [47]. The increased rigidity of the bicyclic structure greatly enhances metabolic stability and target binding affinity. Indeed, the bicyclic peptide appears to be "privileged" for binding to flat surfaces at PPI interfaces. Screening of ~0.5 million of these bicyclic peptides against tumor necrosis factor-α (TNFα) identified a relatively potent TNFα antagonist ($K_D = 0.45$ μM), which protected cells from TNFα-induced cell death (compound **11**, Figure 6.5) [47]. The same library was also screened against K-Ras G12V, resulting in several K-Ras ligands with K_D values of 0.17–2.6 μM (e.g., compound **12**, Figure 6.5) [48]. Most of the ligands inhibited Ras–Raf interaction

in vitro, suggesting that they bind to a site at or near the effector-binding site. Unfortunately, these ligands showed little cellular activity likely due to poor cellular entry. To generate cell-permeable bicyclic peptides, Trinh *et al.* synthesized a 5.7 million-member library in which a CPP motif was incorporated into one ring, while the second ring contained a degenerate peptide sequence [49]. Screening of the bicyclic peptide library identified a cell-permeable K-Ras inhibitor that blocked the Ras–Raf interaction and induced apoptotic death of cancer cells.

OBTC libraries have been synthesized in which macrocycles were attached to the support via a cleavable linker, thus permitting selective release of the macrocycles for solution-phase screening. Xiao and Pei synthesized and screened 1716 tyrocidine A analogues for antibacterial activity in 96-well plate format [50]. In this case, the tyrocidine analogues were synthesized on TentaGel macrobeads (280–320 μm) by the split-and-pool method and attached to the solid phase via

(a)

m, n = 3–5

(b)

11
TNFα ligand ($K_D = 0.45$ μM)

(c)

12
K-Ras ligand ($K_D = 2.6$ μM)
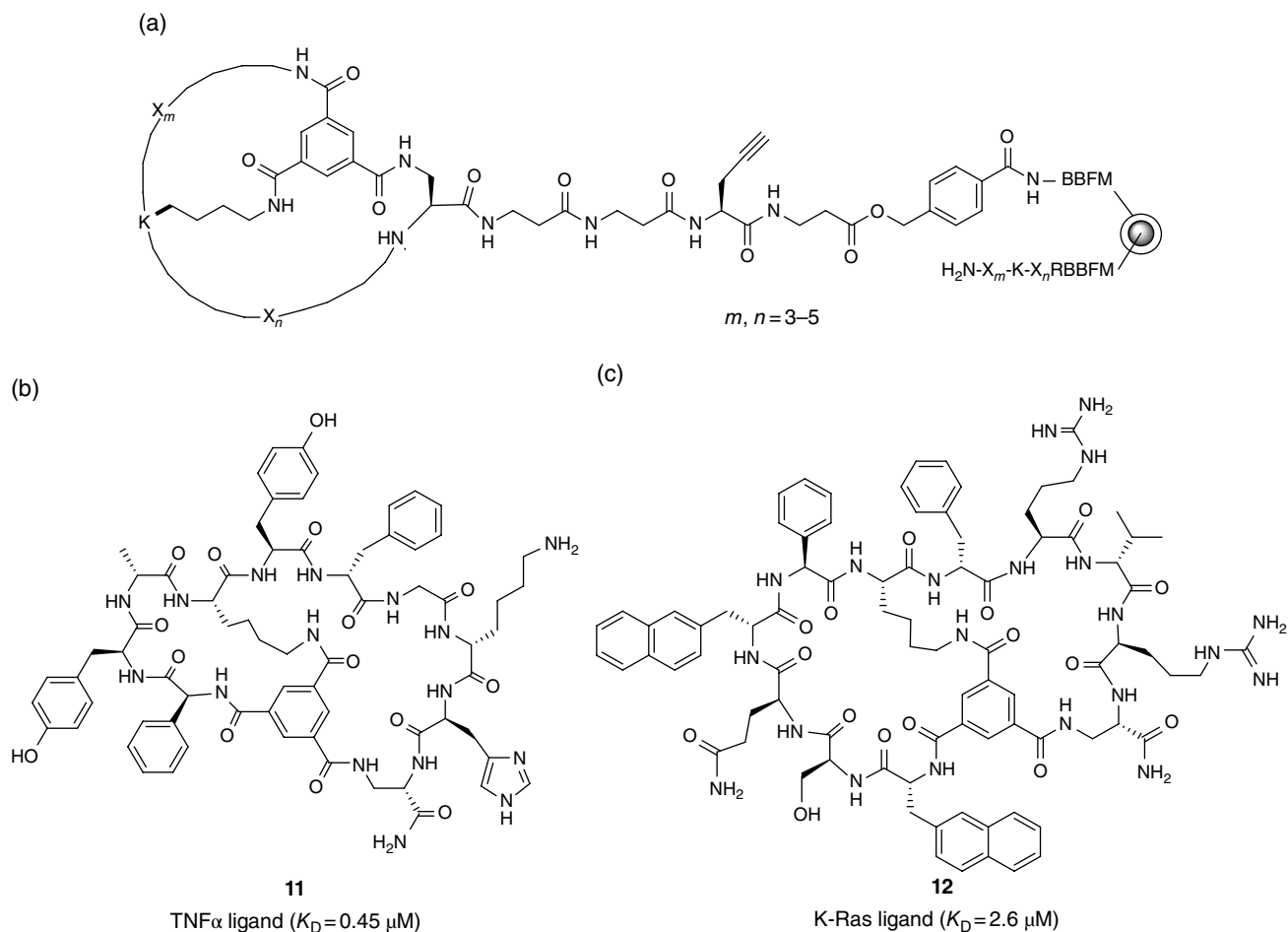
Figure 6.5 (a) Design of an OBTC bicyclic peptide library, in which the macrocycles are attached to the solid support through a releasable linker (e.g., ester, which can be cleaved by base hydrolysis), whereas the linear-encoding peptides are linked to the support through stable amide bonds. (b) TNFα antagonist identified from the bicyclic peptide library. (c) K-Ras inhibitor discovered from the bicyclic peptide library.

an ester linkage, whereas the encoding linear peptides were attached to the support via a more stable amide linkage. The library beads were manually distributed into 96-well plates and the tyrocidine analogues were selectively released from the beads by basic hydrolysis. The resulting cyclic peptide solutions, after neutralization, were tested for antibacterial activity in another set of 96-well plates containing bacterial cells. For cyclic peptides displaying desirable antibacterial activity, the corresponding beads containing the covalently attached linear-encoding peptides were retrieved and sequenced by PED–MS analysis. This study resulted in several tyrocidine analogues of improved therapeutic indices over the natural product [50]. The releasable OBTC libraries have also been screened against protein targets [25]. Typically, two to three rounds of on-bead screening reduced the number of positive beads to a few dozen or a few hundred, and the macrocycles on the positive beads were selectively labeled with a fluorophore via click chemistry and hydrolytically released into 96-well plates (Figure 6.6). The resulting dye-labeled macrocycles were then individually tested for binding to the protein target in solution by fluorescence anisotropy. Macrocycles with the highest binding affinities were finally identified by PED–MS analysis of the linear-encoding tags still covalently attached to the corresponding beads.

Another useful feature of the OBTC approach is that it allows the synthesis of libraries with reduced ligand density on the bead surface [51]. During on-bead library screening, high ligand density (estimated ~100 mM on typical TentaGel beads) causes high false-positive rates. Because high ligand density allows a macromolecule (e.g., a protein) to interact with multiple ligand molecules on a bead surface, a weak ligand may bind to the target with high avidity. In OBTC libraries, the surface ligand density can be reduced by any desired factor by simply mixing a library building block with an excess amount of a capping agent during library synthesis. The normal (high) density of the encoding tags inside the bead still provides sufficient quantity of peptides for sequencing. In an early demonstration of this strategy, Pei and coworkers showed that the *bona fide* ligands of certain SH2 domains could be identified only after a 10-fold reduction in surface ligand density [51]. They subsequently applied this strategy to improve the screening stringency of macrocycle libraries against PPI targets [45].

In addition to the OBTC/encoding method, other investigators explored alternative strategies to facilitate macrocyclic hit identification. Macrocycle libraries were usually designed to contain a chemical entity that permits selective ring opening of the macrocyclic hits prior to MS/MS analysis. Lim *et al.* utilized an alkyl triazine thioether moiety for both peptide cyclization and ring-opening purposes (Figure 6.7a) [52]. After positive hits were isolated from the library, the thioether linkage was oxidized into the corresponding sulfone and cleaved by
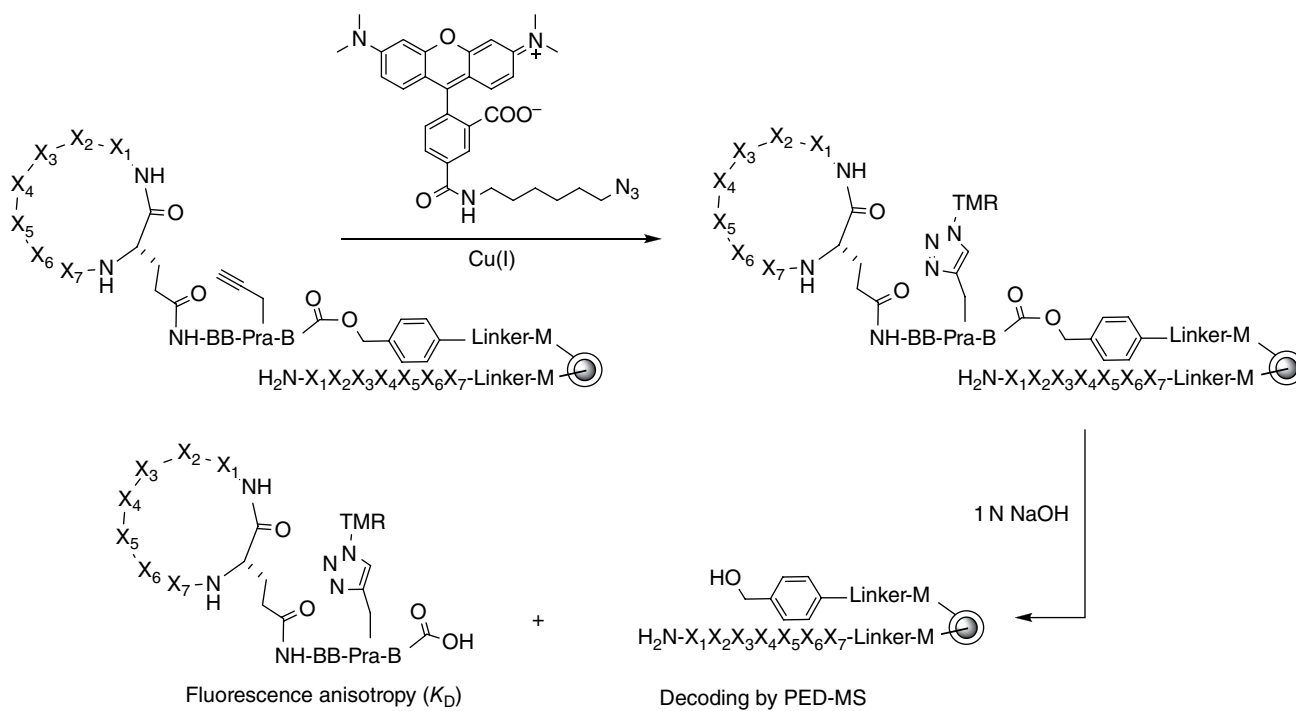
Figure 6.6 Selective on-bead labeling and release of a macrocyclic compound from a single bead, while the linear-encoding peptide is retained on the bead for later hit identification by PED–MS. TMR, tetramethyl rhodamine; Pra, L-propargylglycine.

(a)

(b)

(c)

(d)

(e)
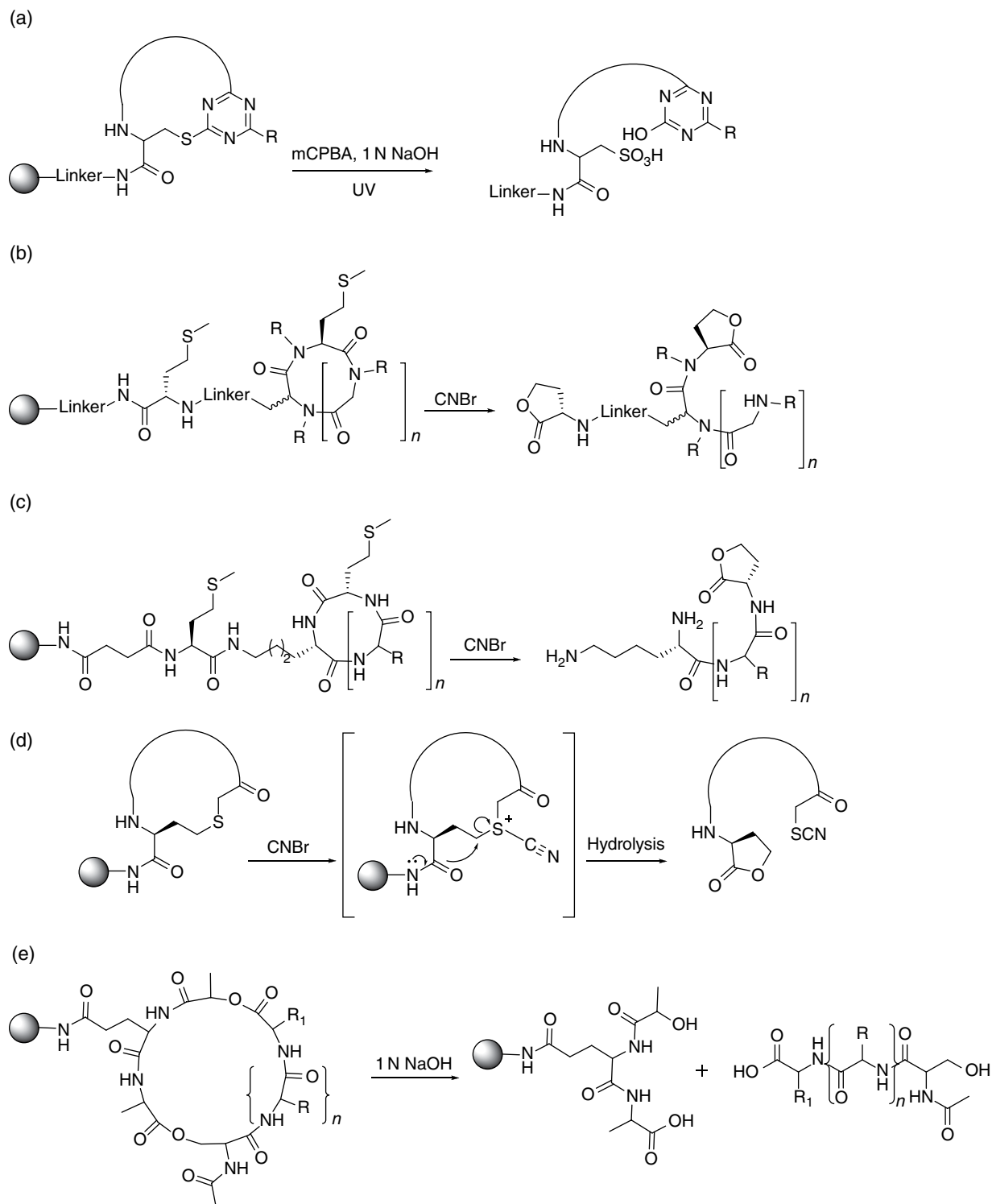
Figure 6.7 Various strategies for ring opening of macrocyclic compounds for MS/MS decoding. CNBr, cyanogen bromide; mCPBA, meta-chloroperoxybenzoic acid.

sodium hydroxide. The resulting linear peptides/peptoids were released from the resin by photolysis and analyzed by MS/MS. Kodadek and coworkers designed a cyclic peptoid library with two invariant methionine

residues, one within the macrocycle for ring opening and the other inside the linker to the solid support (Figure 6.7b) [53]. After library screening, the positive hits were treated with cyanogen bromide, resulting in

simultaneous linearization of the macrocycle and release from the solid support. The resulting linear peptide/peptoid was structurally identified by MS/MS analysis. Similarly, Biron and colleagues designed a linearizable cyclic peptide library with an inverted methionine residue as a tether to the resin. Cyanogen bromide treatment produces a linear peptide containing only one homoserine lactone moiety, simplifying the MS/MS analysis (Figure 6.7c) [54]. Lee and Lim designed a multifunctional thioether linker for the purpose of attachment to the solid support, peptide cyclization, and ring opening (Figure 6.7d) [55]. The thioether moiety is opened by treatment with CNBr and concomitant hydrolysis releases the linear oligomer from the resin for sequencing. This elegant design was applied to identify the hits derived from an OBOC library of cyclic peptide/peptoid hybrids. Finally, a cyclic depsipeptide library containing two ester bonds was generated for IgG binding. Upon treatment with alkaline conditions, the esters were hydrolyzed to produce and release linear peptides for MS/MS analysis (Figure 6.7e) [56].

6.5 DNA-Encoded Macrocyclic Libraries

The use of DNA as encoding tags was first proposed by Brenner and Lerner in 1992 [57]. Conceptually similar to other display technologies, the DNA-encoded chemical library can be screened against virtually any target for binding affinity by going through multiple rounds of library panning, selection, amplification, and decoding. Each member of the library contains the coding DNA and the displayed small molecule through a linker (e.g., on a bead). This concept was experimentally demonstrated a year later by Janda *et al.* using the split-and-pool synthesis and orthogonal chemistry to construct the peptides and their coding oligonucleotides [58]. While an important proof of concept, this first-generation DNA-encoded peptide library has not found broad application, presumably due to technical difficulties of synthesizing both oligomers on the same bead and potential interference of library screening by the encoding DNA.

DNA-encoded libraries were not fully implemented for biological applications until a decade later, when several DNA-encoding platforms were independently developed and applied for ligand discovery [59, 60]. While most of the DNA-encoded libraries were synthesized in the split-and-pool format, a unique, elegant system pioneered by Liu and coworkers took advantage of the hybridization ability of DNA strands to bring together reactants for enhanced reactivities [61]. In their DNA-templated synthesis (DTS) system, the proximity effect brought about by DNA stand annealing greatly increases the effective molarity and renders the transformations encoder dependent. Consequently, the sequence of the DNA template provides a record of the reaction steps and building blocks used to synthesize the functional molecule covalently linked to the DNA template and, as such, can be used to decode active components [61].

In their initial proof-of-concept study, Gartner *et al.* generated a 64-member macrocycle library containing three random positions by forming amide bonds between the building blocks with carbodiimides followed by macrocyclization via a Wittig olefination reaction (Figure 6.8) [62].

Screening of this small library against carbonic anhydrase greatly enriched ligands that contained a phenylsulfonamide pharmacophore (compound **13**, Figure 6.9). In a subsequent study, the investigators synthesized a DTS library of 13 824 macrocycles, which was screened for binding to 36 target proteins [63]. These efforts resulted in two compounds that selectively inhibited Src kinase, an oncogenic non-receptor tyrosine kinase, with submicromolar IC_{50} values (compound **14**, Figure 6.9). The initial hits were later further optimized through medicinal chemistry efforts, affording selective Src kinase inhibitors of low nanomolar IC_{50} values *in vitro* [64]. Unfortunately, the Src kinase inhibitors showed only weak activity in cellular assays, likely due to poor penetration of the cell membrane. The same library was also screened against insulin-degrading enzyme (IDE), a metalloprotease implicated in type 2 diabetes mellitus and Alzheimer's disease [65]. The most potent compound (**15**, Figure 6.9) isolated from the library inhibited IDE with an IC_{50} value of 50 nM and demonstrated antidiabetic activities *in vivo*.

The DTS platform has now been industrialized to aid hit discovery efforts. The DNA-programmed chemistry (DPC^{TM}) platform was greatly enhanced by the growing types of compatible chemical transformations (e.g., Diels–Alder, Suzuki coupling, reductive amination, and Mitsunobu reactions) [66, 67]. For example, an Ensemble Therapeutics group synthesized and screened a 160 000-member cyclopentapeptide library against X-chromosome-linked inhibitor of apoptosis protein (XIAP) and obtained potent ligands against the BIR2 and BIR3 domains of XIAP (e.g., $IC_{50} = 140$ nM for compound **16**, Figure 6.9. For a complete case study, see Chapter 17) [68].

6.6 Parallel Synthesis of Macrocyclic Libraries

One way to avoid deconvolution for hit identification is parallel synthesis of spatially addressable libraries, in which compound structures are encoded by their physical location on a surface. One platform that has
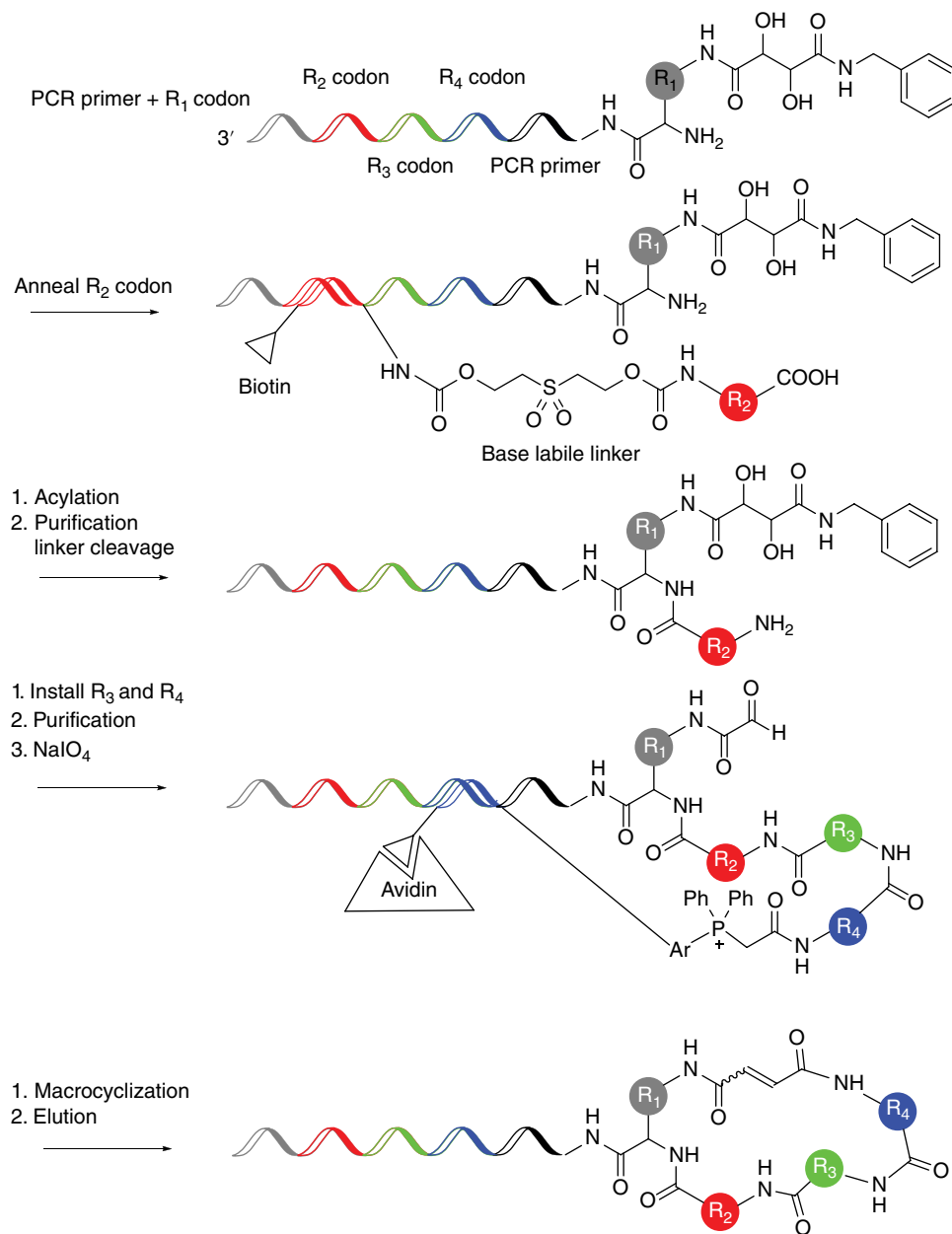
Figure 6.8 Steps involved in the synthesis of DNA-encoded macrocyclic libraries. (*See insert for color representation of the figure.*)

gained significant popularity is the SPOT synthesis method pioneered by Frank (Figure 6.10) [69]. Previous work had established that cellulose membranes enabled peptide synthesis to proceed to completion via the absorption of conventional SPPS reagents into the cellulose matrix [70]. SPOT synthesis exploits the absorptivity of the matrix, which limits the reagents to small, circular regions that can be spatially segregated and positionally addressed on a single continuous membrane. The identity of each peptide is inferred from the reagents dispensed to predefined spots on the membrane. Library sizes are constrained only by the size of the membrane

utilized or practical concerns for assaying (e.g., employing a conventional 96/384-well microtiter plate format). Binding assays, enzyme-linked assays, and cell adhesion assays can be carried out directly on the membranes [71]. The SPOT synthesis platform is readily amenable to the generation of peptidyl macrocycles as well. Peptide cyclization has been achieved through either disulfide bonds or amide bonds between the N-terminal amine and the side chain of the C-terminal glutamic acid. Hahn *et al*. utilized SPOT to generate an epitope-based array and identified epitope-homologous cyclic peptides that retained high affinity for anti-TGFα antibody [72].
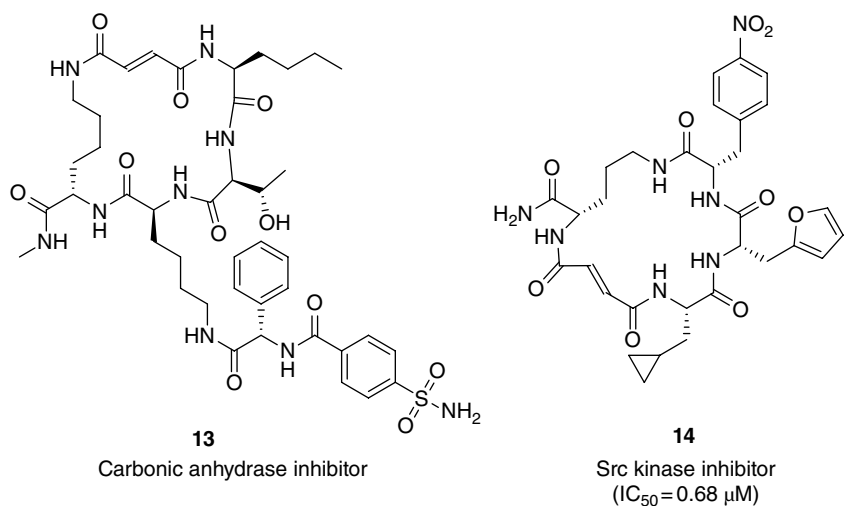
Figure 6.9 Structures of representative macrocyclic ligands discovered from DNA-encoded libraries.

13
Carbonic anhydrase inhibitor

14
Src kinase inhibitor
($IC_{50} = 0.68\ \mu M$)

15
IDE inhibitor
($IC_{50} = 50$ nM)

16
XIAP BIR domain ligand
($IC_{50} = 140$ nM)

Amino-functionalized membrane

Spatial segregation via pipetting reagents onto spots

Fmoc-R-COOH

a. DeFmoc
b. Fmoc-R-COOH

Hit identification
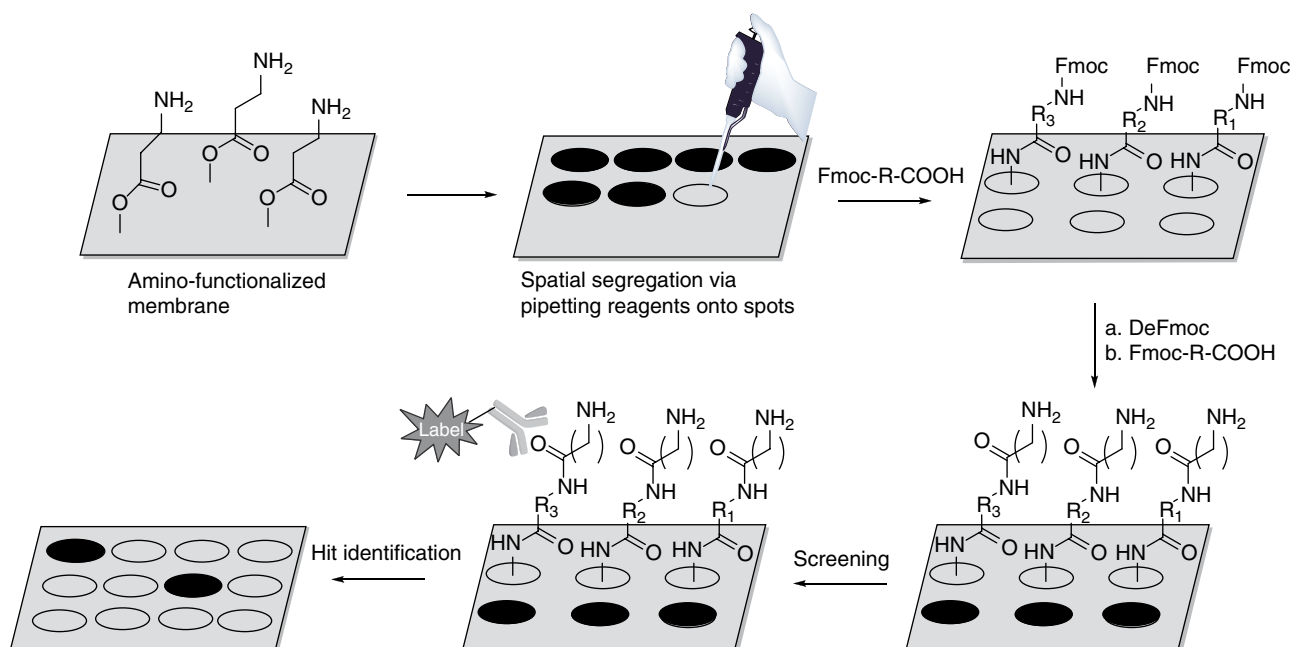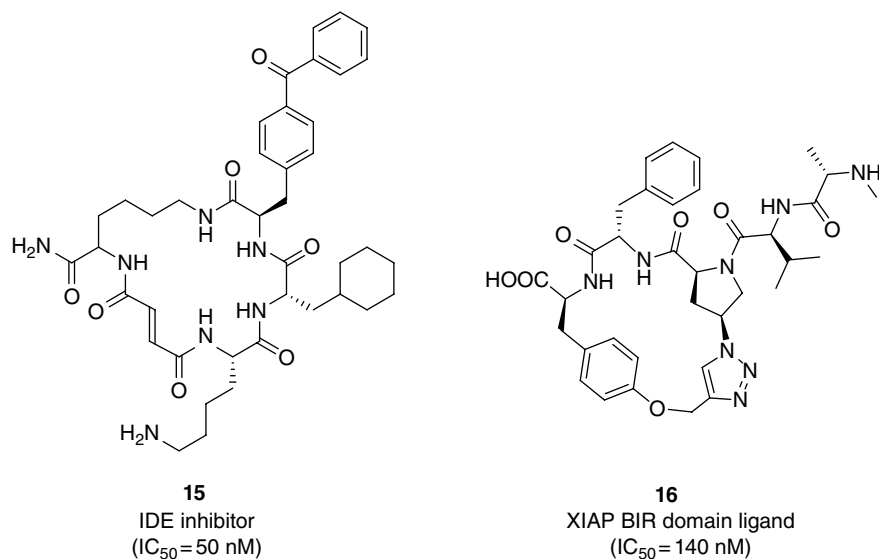
Screening

Figure 6.10 Synthesis and screening of peptide libraries by the SPOT method.
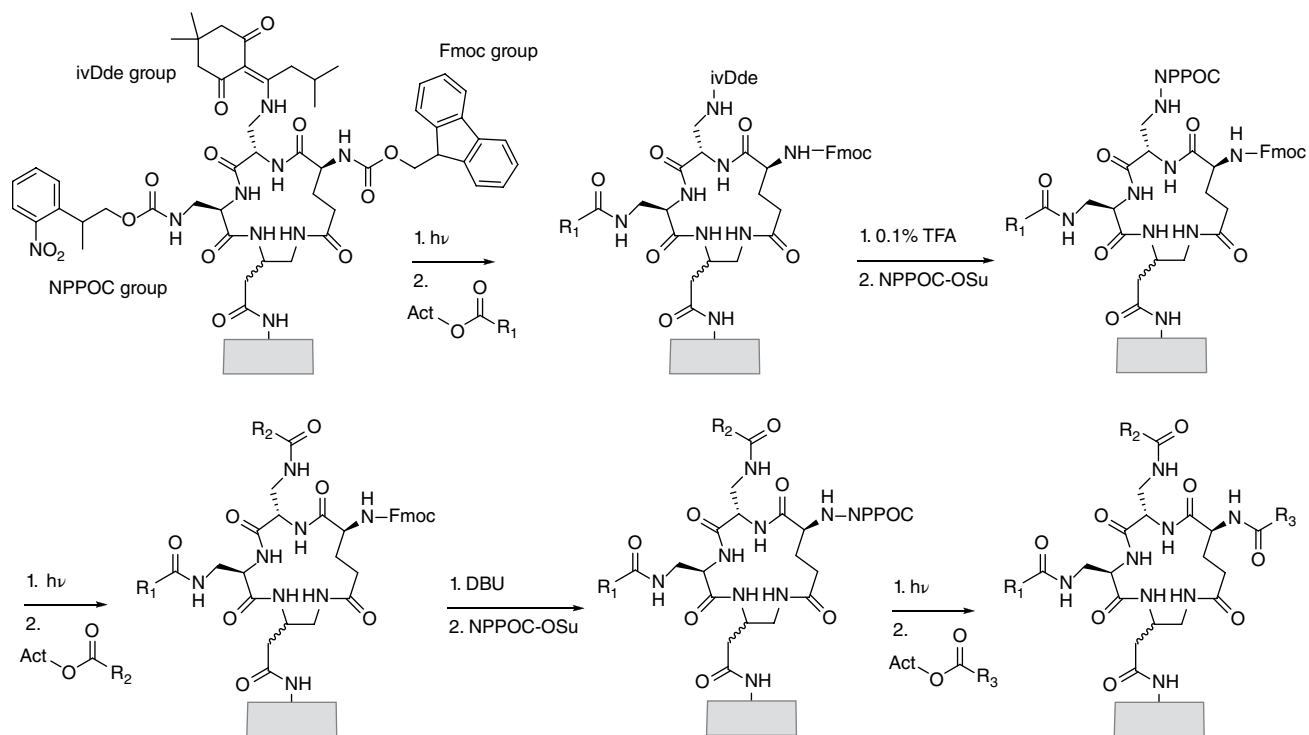
Figure 6.11 An example of photolithographic synthesis of macrocyclic peptide libraries using sequential NPPOC deprotection and coupling.

Photolithographic synthesis pioneered by Fodor *et al.* offers another option for synthesizing spatially addressable peptide libraries [73]. Spatially specific peptide synthesis is made possible by the use of a set of checkerboard-like photo masks, with a unique mask used for each coupling step. Gao *et al.* also developed an improved maskless approach for the synthesis of chip-based peptide arrays using digital photolithography [74], Boc-protected building blocks, and photolabile acid precursors for *in situ* deprotection [75]. In a proof-of-concept study, the investigators synthesized a peptide library on an ultrahigh-density microchip (up to 4000 peptides per $1.5\,cm^2$) with 281 unique sequences and identified linear peptide ligands that bound tightly to a human p53 antibody [75]. Kodadek *et al.* used this digital photolithographic, spatially addressable strategy to construct a microchip-based cyclic peptide library [76]. A cyclic tetrapeptidyl scaffold with three orthogonal protecting groups on three individual side chains was installed on the chip surface (Figure 6.11). Using computer-programmed photolysis and protecting group swapping, diversified amine reactive groups can be installed sequentially on desired side chains to produce decorated macrocycles. Unfortunately, significant improvement in the peptide array density using digital photolithography comes with major limitations, namely,

access to photolithography equipment and the handling of photolabile reagents.

6.7 Diversity-Oriented Synthesis

Originally proposed by Schreiber [77], diversity-oriented synthesis (DOS) aims to expand the accessible chemical space for drug discovery by generating diverse libraries around natural product-like scaffolds. Researchers at Tranzyme Pharma developed a parallel synthesis strategy for 14- to 18-atom macrocyclic peptidomimetics on the solid phase [78, 79]. The macrocycles were constructed by on-resin cyclization of a tripeptide sequence with a conformationally rigid organic tether. High-throughput fluorescence-based whole-cell screening of the macrocycle library (up to 10^4 unique members) yielded potent antagonists against the human motilin receptor (e.g., compound **17**, Figure 6.12). Further optimization through incorporation of unnatural amino acids produced potent, biologically active macrocycles in *ex vivo* assays [78, 80]. Screening of Tranzyme's proprietary libraries produced a clinical candidate that reached phase III development, TZP-101 (ulimorelin, compound **18**, Figure 6.12), a ghrelin receptor agonist, which is effective for treating postoperative ileus, a condition that

blocks the normal mechanical function of the gastrointestinal tract after surgery [81]. Multiple macrocyclic hits are shown to be orally bioavailable in both rats and monkeys. The scope of the strategy is quite broad, allowing for the incorporation of unnatural amino acids and derivatives, as well as a diverse array of potential tethers and generating potentially very large libraries. A detailed account of the identification of TZP-102, an oral ghrelin agonist that reached phase II clinical development, is given in Chapter 19. Jefferson *et al.* discovered antibiotic lead compounds by screening SNAr libraries of several thousand members [82, 83].

Meanwhile, researchers at the Broad Institute synthesized a 2070-member amino alcohol-based macrocycle library in the one macrobead–one stock solution format and used the compounds to generate a small-molecule microarray [84]. Screening of the microarray against sonic hedgehog N-terminal peptide (ShhN) produced a moderately potent hit ($K_D = 9\,\mu M$). Optimization of the initial hit gave robotnikinin (compound **19**, Figure 6.12, $K_D = 3.1\,\mu M$), which inhibited Shh signaling in a dose-dependent manner [85].

More recently, Schreiber and Nielsen devised a build/couple/pair (B/C/P) method to generate biologically active peptidomimetic macrocycles (Figure 6.13a) [86]. During the *build* step, a set of regiochemically and stereochemically diverse scaffolds, which also feature orthogonal protecting groups and handles for macrocyclization (e.g., alkynes for dipolar cycloadditions or thiols for thioether formation), are constructed through asymmetric synthesis. During the *couple* step, a series of individual building blocks (diversity elements) is coupled with the scaffold using conventional SPPS or chemical ligation methods. Finally, the *pair* step involves an intramolecular reaction to form the final macrocycle, with additional stereochemical diversity introduced depending on the cyclization strategy. A number of structurally diverse macrocyclic libraries possessing predetermined physiochemical properties have been prepared by this method [87–89]. Marcaurelle *et al.* generated several different macrolactam libraries from common linear precursors by employing nucleophilic aromatic substitution, Huisgen cycloaddition, or ring-closing metathesis (RCM) as the *pair* step (Figure 6.13b) [90–92]. Screening of DOS macrocyclic libraries has yielded useful therapeutic leads. For example, Heidebrecht *et al.* synthesized ~8000 structurally diverse macrocycles, starting from a single scaffold containing three positions for *coupling* with diversity elements. Screening of the library for *Plasmodium falciparum* growth inhibition yielded a family of compounds that not only showed good antimalarial activities but also provided a clear SAR for further
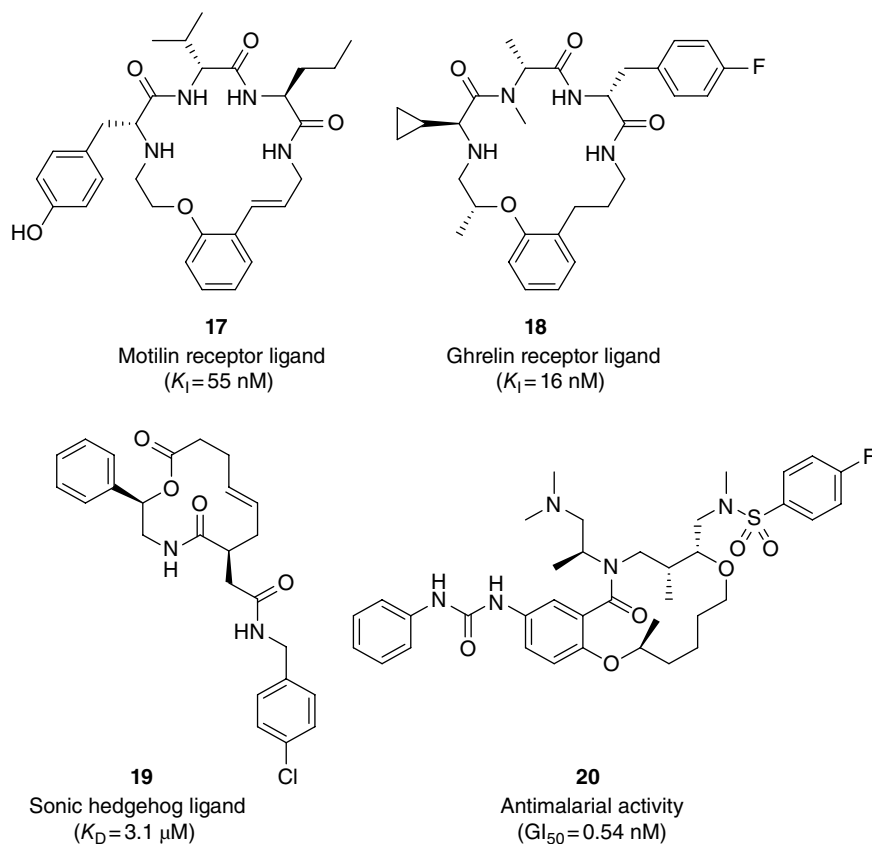
Figure 6.12 Structures of representative macrocyclic ligands discovered from DOS libraries.

17
Motilin receptor ligand
($K_I = 55$ nM)

18
Ghrelin receptor ligand
($K_I = 16$ nM)

19
Sonic hedgehog ligand
($K_D = 3.1\,\mu M$)

20
Antimalarial activity
($GI_{50} = 0.54$ nM)

(a)

Build
Synthesis of building blocks

Pair
Macrocyclization

(b)

Build
Synthesis of building blocks

Pair
S$_N$Ar

Pair
RCM

Pair
Cycloaddition
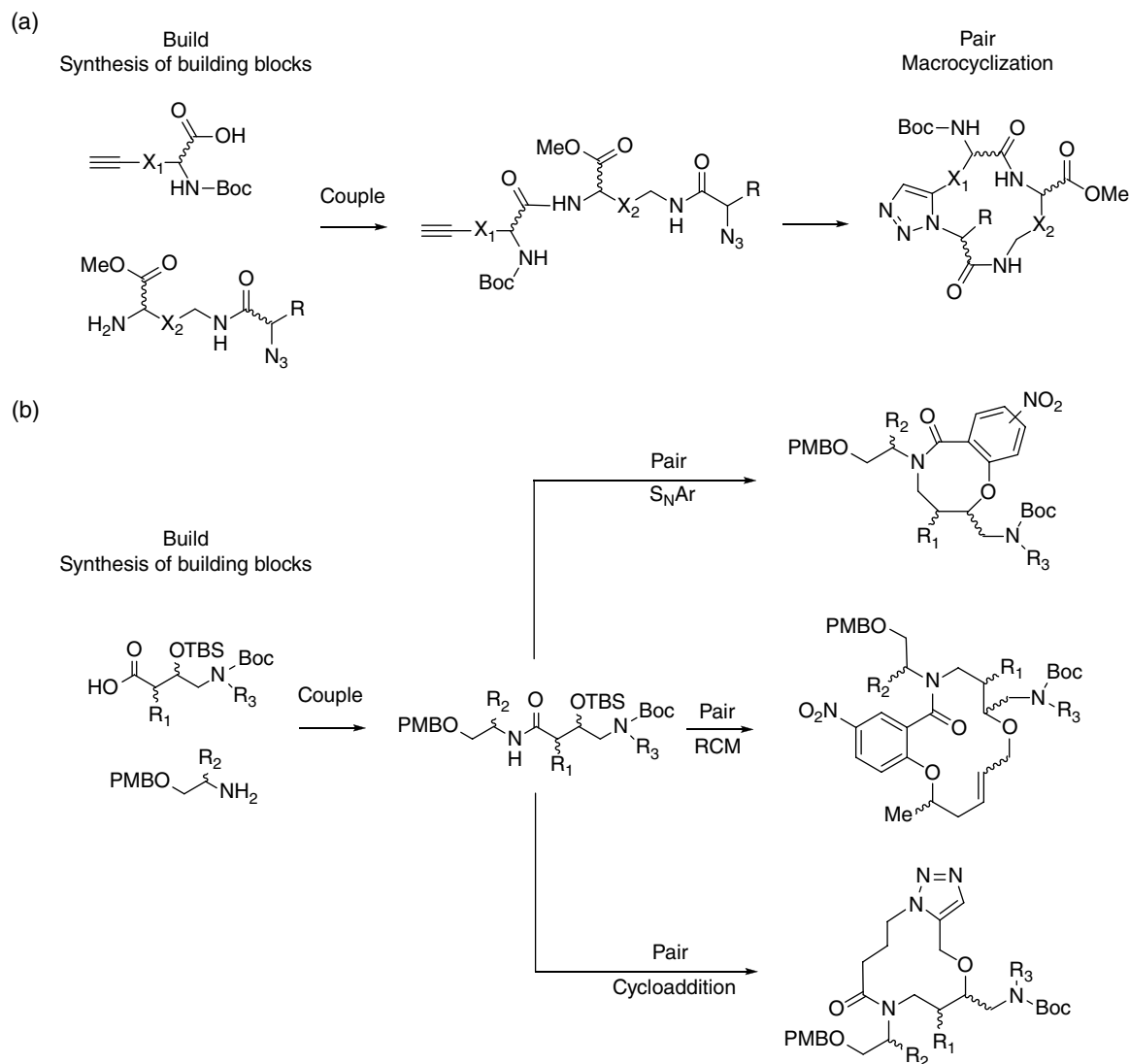
Figure 6.13 (a) Example of the build/couple/pair strategy using unique build fragments. (b) Build/couple/pair example using divergent pair steps to generate conformationally diverse macrocycles.

optimization [91]. These efforts led to a macrocyclic lead that exhibited pM GI$_{50}$ values against two malaria strains and adheres to Lipinski's Rule of Five (compound **20**, Figure 6.12).

The Harran group also utilized peptide-like scaffolds as the starting point to generate structurally divergent macrocycles by using palladium-catalyzed allylic substitution, Friedel–Crafts alkylation, or tyrosine O-alkylation for macrocyclization [92, 93]. The resulting macrocyclic peptidomimetics possess restricted conformational flexibility, enhanced proteolytic stability, and other useful pharmacological characteristics. The Spring group further extended the B/C/P method with multidimensional coupling to synthesize macrocyclic libraries [94]. They also expanded the method by employing iterative *couple* steps, which increase diversity by further

coupling reactions or, alternatively, terminating the coupling reaction after the initial round [95]. Most of these studies are currently at the stage of methodology development.

6.8 Perspective

The past decade has witnessed an explosive growth in research activities on macrocycles and the advent of multiple chemical technologies for macrocycle synthesis and screening. Table 6.1 summarizes the salient features and advantages of each of these methods. In contrast, cyclic and bicyclic peptide libraries synthesized by the ribosome can reach extremely high diversity (up to 10^{14}). In most cases, the libraries can be amplified and subjected

Table 6.1 Comparison of chemical approaches to macrocycle libraries.

Chemical approach for macrocycle libraries	Size	Type of chemical reactions	Synthesis infrastructure	Screening methods	Advantages	Molecular targets
Split-and-pool synthesis of OBOC and OBTC libraries	$<10^8$	Mostly amide bond formation	Solid-phase peptide synthesis	Solid- and solution-phase affinity selection, magnetic sorting, enzyme-linked assay, and cell-based screening	Easily adaptable, high-throughput screening, relatively high library size, and incorporation of cell-penetrating motifs	Pin1; [42, 96] Grb2 SH2; [41] HIV-1 capsid; [40] prolactin receptor; [39] PTP1B; [43] calcineurin; [25] K-Ras; [45, 46, 48] TNFα; [47] Histone deacetylase [97]
DNA-templated synthesis	$<10^6$	Amide bond formation, Wittig olefination, and cycloaddition	Preparation of orthogonal nucleotides–amino acid pairs	Affinity selection	Easy hit identification; solution-phase screening	Src, Akt3, MAPKAPK2, p38α, Pim1, VEGFR2 kinases; [63] insulin-degrading enzyme; [65] XIAP BIR domains [68]
Deconvolution (iterative deconvolution and positional scanning approach)	$<10^7$	Amide bond formation	Solid-phase peptide synthesis	Solid-phase affinity selection	Relatively high library size	Streptavidin; [27] endothelin receptor; [28] α-glucosidase; [29] μ-opioid receptor [30]
Diversity-oriented synthesis	$<10^5$	Amide bond, S_N2, $S_N Ar$, organometallic reactions, RCM, multicomponent reactions, cycloaddition, reductive amination, etc.	Organic synthesis and/or solid-phase synthesis	Solution-phase cell-based screening, solution-phase functional assay, microarrays	Ability to prepare non-peptidic, "drug-like" macrocycles; compatible with broad chemical reactions	Motilin receptor [78, 80], ghrelin receptor [81], Sonic Hedgehog [84, 85]

to iterative screening, resulting in hits with affinities and specificities rivaling those of monoclonal antibodies. On the other hand, these biological libraries are limited to building blocks that are recognizable by the ribosome, usually the 20 proteinogenic amino acids and a limited number of related derivatives. As such, peptide macrocycles isolated from biological libraries tend to be larger and frequently remain susceptible to proteolytic degradation. With the exception of the intein-based libraries, biological libraries have so far been screened almost exclusively for binding to targets *in vitro*. The resulting ligands are impermeable to the cell membrane and largely limited to extracellular targets.

The diversity of OBTC/peptide-encoded macrocycle libraries is limited by the amount of resin that can be conveniently handled in a research laboratory (~10 g), which corresponds to ≤10^8 beads/compounds. Screening naive OBTC libraries (no pharmacophore) against PPI targets typically produces hits with high nanomolar to low micromolar binding affinities, although potency can be greatly improved by incorporating appropriate pharmacophores into libraries or as part of subsequent optimization by conventional medicinal chemistry approaches. The availability of multiple moderately potent hits can actually be advantageous over a single, highly potent hit in a drug discovery project, because it offers an opportunity to select a hit(s) based on its overall properties including potency, selectivity, solubility, stability, and PK-ADME. As noted earlier, one of the most significant advantages of chemically synthesized libraries is their compatibility with unnatural building blocks, which can be employed to improve metabolic stability, as well as the structural diversity of the macrocycles. This feature allows the incorporation of pharmacophores and/or cell-penetrating motifs into the libraries. Indeed, highly potent, proteolytically stable, and cell-permeable macrocyclic inhibitors against intracellular targets have been discovered by the OBTC method [43, 96]. OBTC libraries can be screened either on-bead for target binding or in solution for biological activity against molecular targets or live cells. Diverse molecular targets including extracellular proteins [39], intracellular proteins/enzymes [46, 47, 97], and the cell membrane [31, 50] have successfully been screened against OBTC libraries. The OBTC platform does not require any special equipment and the libraries can be manually synthesized on a simple homemade peptide synthesis apparatus [98]. Most OBTC libraries have so far been prepared with amide bond-forming chemistry (e.g., peptides and peptoids); however, the platform is in principle compatible with a wide variety of other reaction types.

The diversity of DTS libraries is limited by the length of the coding DNA and the size of reported DTS macrocycle libraries has so far not exceeded 10^6 compounds. Other DNA-encoded chemical libraries have generated diversities comparable to that of phage- or mRNA-display libraries [67, 99]. However, to our knowledge, these other DNA-encoded methodologies have not yet been applied to construct macrocycle libraries. An advantage of DNA-encoded/templated libraries is that screening is carried out in solution and, therefore, avoids many of the problems associated with on-bead screening (e.g., high false-positive rates). As chemically synthesized libraries, they are not limited to amino acids as building blocks or amide formation for monomer coupling. In fact, a wide range of chemical reactions has been efficiently incorporated in DTS synthesis, including palladium-catalyzed cross coupling, click chemistry, and nucleophilic aromatic substitution [66, 67]. However, DTS libraries are limited to affinity-based screening and the reactions for library synthesis must be compatible with the DNA structure. Additionally, the larger size of the coding DNA can potentially interfere with target binding, and orthogonal DNA-building block conjugates need to be prepared and purified individually and are quite labor intensive.

Parallel synthesis including DOS is highly versatile with regard to the types of compatible building blocks and chemical reactions. The ability of DOS to generate natural product-like macrocycles rich in stereochemical diversity is highly attractive, as many of these macrocycles are "drug-like" and, therefore, expected to be biologically active against a wide variety of protein targets. In the case of DOS, macrocycles can be released in solution, making library screening very flexible (either for target binding or functional activity against molecular targets or live cells). The main drawback is that the library size is generally small, rarely exceeding 10^4, and the construction of such libraries can be quite labor intensive compared with on-resin split-pool or DNA-supported libraries. Despite their smaller size, such libraries have the advantage that compounds screened are not tethered to any support and SAR can be directly inferred from screening results. Further, the variety in building block components imbues them with a reasonably high diversity despite smaller numbers. Moreover, there is no need for a technology transfer step to move from hit generation to lead optimization, as opposed to the supported libraries. Finally, due to their labor-intensive nature, libraries requiring deconvolution are likely to have limited utility in the future, given the availability of the alternative macrocyclic library methods described earlier.

6.9 Conclusion

In summary, there is now a plethora of technological platforms available for synthesizing (both chemically and biologically) and screening macrocycle libraries

against disease-relevant targets. Nearly two dozen biopharmaceutical companies have been formed over the past decade with a focus on the development of macrocyclic therapeutics. In addition, large pharmaceutical companies are starting to embrace macrocycles as therapeutic options by in-licensing various macrocycle technologies and/or forming alliances with the specialty companies just described. Many academic groups are continuing to advance the various fundamental aspects of macrocyclic drug discovery and delivery technologies. It is thus highly probable that the next decade will see a significant number of macrocyclic drugs reaching the market, including some against the currently "undruggable" PPI targets.

References

1 Hamada, Y.; Shioiri, T. Recent Progress of the Synthetic Studies of Biologically Active Marine Cyclic Peptides and Depsipeptides. *Chem. Rev.* **2005**, *105*, 4441–4482.

2 Driggers, E. M.; Hale, S. P.; Lee, J.; Terrett, N. K. The Exploration of Macrocycles for Drug Discovery—An Underexploited Structural Class. *Nat. Rev. Drug Discov.* **2008**, *7*, 608–624.

3 Marsault, E.; Peterson, M. L. Macrocycles Are Great Cycles: Applications, Opportunities, and Challenges of Synthetic Macrocycles in Drug Discovery. *J. Med. Chem.* **2011**, *54*, 1961–2004.

4 Hopkins, A. L.; Groom, C. R. The Druggable Genome. *Nat. Rev. Drug Discov.* **2002**, *1*, 727–730.

5 Davies, D. R.; Cohen, G. H. Interactions of Protein Antigens with Antibodies. *Proc. Natl. Acad. Sci. U. S. A.* **1996**, *93*, 7–12.

6 Zinzalla, G.; Thurston, D. E. Targeting Protein-Protein Interactions for Therapeutic Intervention: A Challenge for the Future. *Future Med. Chem.* **2009**, *1*, 65–93.

7 Chatterjee, J.; Gilon, C.; Hoffman, A.; Kessler, H. N-Methylation of Peptides: A New Perspective in Medicinal Chemistry. *Acc. Chem. Res.* **2008**, *41*, 1331–1342.

8 White, T. R.; Renzelman, C. M.; Rand, A. C.; Rezai, T.; McEwen, C. M.; Gelev, V. M.; Turner, R. A.; Linington, R. G.; Leung, S. S. F.; Kalgutkar, A. S.; Bauman, J. N.; Zhang, Y.; Liras, S.; Price, D. A.; Mathiowetz, A. M.; Jacobson, M. P.; Lokey, R. S. On-Resin N-Methylation of Cyclic Peptides for Discovery of Orally Bioavailable Scaffolds. *Nat. Chem. Biol.* **2011**, *7*, 810–817.

9 Qian, Z.; Liu, T.; Liu, Y.-Y.; Briesewitz, R.; Barrios, A. M.; Jhiang, S. M.; Pei, D. Efficient Delivery of Cyclic Peptides into Mammalian Cells with Short Sequence Motifs. *ACS Chem. Biol.* **2013**, *8*, 423–431.

10 Frost, J. R.; Vitali, F.; Jacob, N. T.; Brown, M. D.; Fasan, R. Macrocyclization of Organo-Peptide Hybrids Through a Dual Bio-Orthogonal Ligation: Insights from Structure-Reactivity Studies. *ChemBioChem* **2013**, *14*, 147–160.

11 Molek, P.; Strukelj, B.; Bratkovic, T. Peptide Phage Display as a Tool for Drug Discovery: Targeting Membrane Receptors. *Molecules* **2011**, *16*, 857–887.

12 Josephson, K.; Ricardo, A.; Szostak, J. W. mRNA Display: From Basic Principles to Macrocycle Drug Discovery. *Drug Discov. Today* **2014**, *19*, 388–399.

13 Horswill, A. R.; Savinov, S. N.; Benkovic, S. J. A Systematic Method for Identifying Small-Molecule Modulators of Protein-Protein Interactions. *Proc. Natl. Acad. Sci. U. S. A.* **2004**, *101*, 15591–15596.

14 Hipolito, C. J.; Suga, H. Ribosomal Production and In Vitro Selection of Natural Product-Like Peptidomimetics: The FIT and RaPID Systems. *Curr. Opin. Chem. Biol.* **2012**, *16*, 196–203.

15 Kawakami, K.; Ohta, A.; Ohuchi, M.; Ashigai, H.; Murakami, H.; Suga, H. Diverse Backbone-Cyclized Peptides Via Codon Reprogramming. *Nat. Chem. Biol.* **2009**, *5*, 888–890.

16 Fujino, T.; Goto, Y.; Suga, H.; Murakami, H. Reevaluation of the d-Amino Acid Compatibility with the Elongation Event in Translation. *J. Am. Chem. Soc.* **2013**, *135*, 1830–1837.

17 Foster, A. D.; Ingram, J. D.; Leitch, E. K.; Lennard, K. R.; Osher, E. L.; Tavassoli, A. Methods for the Creation of Cyclic Peptide Libraries for Use in Lead Discovery. *J. Biomol. Screen.* **2015**, *20*, 563–576.

18 Heinis, C.; Winter, G. Encoded Libraries of Chemically Modified Peptides. *Curr. Opin. Chem. Biol.* **2015**, *26*, 89–98.

19 White, C. J.; Yudin, A. K. Contemporary Strategies for Peptide Macrocyclization. *Nat. Chem.* **2011**, *3*, 509–524.

20 Furka, A.; Sebestyén, F.; Asgedom, M.; Dibó, G. General Method for Rapid Synthesis of Multicomponent Peptide Mixtures. *Int. J. Pept. Protein Res.* **1991**, *37*, 487–493.

21 Houghten, R. A.; Pinilla, C.; Blondelle, S. E.; Appel, J. R.; Dooley, C. T.; Cuervo, J. H. Generation and Use of Synthetic Peptide Combinatorial Libraries for Basic Research and Drug Discovery. *Nature* **1991**, *354*, 84–86.

22 Lam, K. S.; Salmon, S. E.; Hersh, E. M.; Hruby, V. J.; Kazmierski, W. M.; Knapp, R. J. A New Type of Synthetic Peptide Library for Identifying Ligand-Binding Activity. *Nature* **1991**, *354*, 82–84.

23 Aina, O. H.; Liu, R.; Sutcliffe, J. L.; Marik, J.; Pan, C.-X.; Lam, K. S. From Combinatorial Chemistry to Cancer-Targeting Peptides. *Mol. Pharm.* **2007**, *4*, 631–651.

24 Mendes, K.; Ndungu, J. M.; Clark, L. F.; Kodadek, T. Optimization of the Magnetic Recovery of Hits from One-Bead-One-Compound Library Screens. *ACS Comb. Sci.* **2015**, *17*, 506–517.

25 Liu, T.; Qian, Z.; Xiao, Q.; Pei, D. High-Throughput Screening of One-Bead-One-Compound Libraries: Identification of Cyclic Peptidyl Inhibitors Against Calcineurin/NFAT Interaction. *ACS Comb. Sci.* **2011**, *13*, 537–546.

26 Redman, J. E.; Wilcoxen, K. M.; Ghadiri, M. R. Automated Mass Spectrometric Sequence Determination of Cyclic Peptide Library Members. *J. Comb. Chem.* **2003**, *5*, 33–40.

27 Zang, X.; Yu, Z.; Chu, Y. H. Tight-Binding Streptavidin Ligands from a Cyclic Peptide Library. *Bioorg. Med. Chem. Lett.* **1998**, *8*, 2327–2332.

28 Spatola, A. F.; Crozet, Y. Rediscovering an Endothelin Antagonist (BQ-123): A Self-Deconvoluting Cyclic Pentapeptide Library. *J. Med. Chem.* **1996**, *39*, 3842–3846.

29 Eichler, J.; Lucka, A. W.; Pinilla, C.; Houghten, R. A. Novel α-Glucosidase Inhibitors Identified Using Multiple Cyclic Peptide Combinatorial Libraries. *Mol. Divers.* **1996**, *1*, 233–240.

30 Li, Y.; Dooley, C. T.; Misler, J. A.; Debevec, G.; Giulianotti, M. A.; Cazares, M. E.; Maida, L.; Houghten, R. A. Fluorescent Mu Selective Opioid Ligands from a Mixture Based Cyclic Peptide Library. *ACS Comb. Sci.* **2012**, *14*, 673–679.

31 Joo, S. H.; Xiao, Q.; Ling, Y.; Gopishetty, B.; Pei, D. High-Throughput Sequence Determination of Cyclic Peptide Library Members by Partial Edman Degradation/Mass Spectrometry. *J. Am. Chem. Soc.* **2006**, *128*, 13000–13009.

32 Liu, R.; Marik, J.; Lam, K. S. A Novel Peptide-Based Encoding System for "One-Bead One-Compound" Peptidomimetic and Small Molecule Combinatorial Libraries. *J. Am. Chem. Soc.* **2002**, *124*, 7678–7680.

33 Wu, J.; Ma, Q. N.; Lam, K. S. Identifying Substrate Motifs of Protein Kinases by a Random Library Approach. *Biochemistry* **1994**, *33*, 14825–14833.

34 Thakkar, A.; Wavreille, A.-S.; Pei, D. Traceless Capping Agent for Peptide Sequencing by Partial Edman Degradation and Mass Spectrometry. *Anal. Chem.* **2006**, *78*, 5935–5939.

35 Biederman, K. J.; Lee, H.; Haney, C. A.; Kaczmarek, M.; Buettner, J. A. Combinatorial Peptide On-Resin Analysis: Optimization of Static Nanoelectrospray Ionization Technique for Sequence Determination. *J. Pept. Res.* **1999**, *53*, 234–243.

36 Lee, S. S.; Lim, J.; Tan, S.; Cha, J.; Yeo, S. Y.; Agnew, H. D.; Heath, J. R. Accurate MALDI-TOF/TOF Sequencing of One-Bead–One-Compound Peptide Libraries with Application to the Identification of Multiligand Protein Affinity Agents Using In Situ Click Chemistry Screening. *Anal. Chem.* **2010**, *82*, 672–679.

37 Chait, B. T.; Wang, R.; Beavis, R. C.; Kent, S. B. Protein Ladder Sequencing. *Science* **1993**, *262*, 89–92.

38 Wang, P.; Arabaci, G.; Pei, D. Rapid Sequencing of Library-Derived Peptides by Partial Edman Degradation and Mass Spectrometry. *J. Comb. Chem.* **2001**, *3*, 251–254.

39 Liu, T.; Joo, S. H.; Voorhees, J. L.; Brooks, C. L.; Pei, D. Synthesis and Screening of a Cyclic Peptide Library: Discovery of Small-Molecule Ligands against Human Prolactin Receptor. *Bioorg. Med. Chem.* **2009**, *17*, 1026–1033.

40 Dewan, V.; Liu, T.; Chen, K.-M.; Qian, Z.; Xiao, Y.; Kleiman, L.; Mahasenan, K. V.; Li, C.; Matsuo, H.; Pei, D.; Musier-Forsyth, K. Cyclic Peptide Inhibitors of HIV-1 Capsid-Human Lysyl-tRNA Synthetase Interaction. *ACS Chem. Biol.* **2012**, *7*, 761–769.

41 Zhang, Y.; Zhou, S.; Wavreille, A.-S.; DeWille, J.; Pei, D. Cyclic Peptidyl Inhibitors of Grb2 and Tensin SH2 Domains Identified from Combinatorial Libraries. *J. Comb. Chem.* **2008**, *10*, 247–255.

42 Liu, T.; Liu, Y.; Kao, H.-Y.; Pei, D. Membrane Permeable Cyclic Peptidyl Inhibitors against Human Peptidylprolyl Isomerase Pin1. *J. Med. Chem.* **2010**, *53*, 2494–2501.

43 Lian, W.; Jiang, B.; Qian, Z.; Pei, D. Cell-Permeable Bicyclic Peptide Inhibitors against Intracellular Proteins. *J. Am. Chem. Soc.* **2014**, *136*, 9830–9833.

44 Wu, X.; Upadhyaya, P.; Villalona-Calero, M. A.; Briesewitz, R.; Pei, D. Inhibition of Ras-Effector Interaction by Cyclic Peptides. *MedChemComm* **2013**, *4*, 378–382.

45 Prior, I. A.; Lewis, P. D.; Mattos, C. A Comprehensive Survey of Ras Mutations in Cancer. *Cancer Res.* **2012**, *72*, 2457–2467.

46 Upadhyaya, P.; Qian, Z.; Selner, N. G.; Clippinger, S. R.; Wu, Z.; Briesewitz, R.; Pei, D. Inhibition of Ras Signaling by Blocking Ras-Effector Interactions with Cyclic Peptides. *Angew. Chem. Int. Ed. Engl.* **2015**, *54*, 7602–7606.

47 Lian, W.; Upadhyaya, P.; Rhodes, C. A.; Liu, Y.; Pei, D. Screening Bicyclic Peptide Libraries for Protein-Protein Interaction Inhibitors: Discovery of a Tumor Necrosis Factor-α Antagonist. *J. Am. Chem. Soc.* **2013**, *135*, 11990–11995.

48 Upadhyaya, P.; Qian, Z.; Habir, N. A. A.; Pei, D. Direct Ras Inhibitors Identified from a Structurally Rigidified Bicyclic Peptide Library. *Tetrahedron* **2014**, *70*, 7714–7720.

49 Trinh, T. B., Upadhyaya, P., Qian, Z., Pei, D. Discovery of a Direct Ras Inhibitor by Screening a Combinatorial Library of Cell-Permeable Bicyclic Peptides. *ACS Comb Sci.* **2016**, *18*, 75–85.

50 Xiao, Q.; Pei, D. High-Throughput Synthesis and Screening of Cyclic Peptide Antibiotics. *J. Med. Chem.* **2007**, *50*, 3132–3137.

51 Chen, X.; Tan, P. H.; Zhang, Y.; Pei, D. On-Bead Screening of Combinatorial Libraries: Reduction of Nonspecific Binding by Decreasing Surface Ligand Density. *J. Comb. Chem.* **2009**, *11*, 604–611.

52 Lee, J. H.; Meyer, A. M.; Lim, H.-S. A Simple Strategy for the Construction of Combinatorial Cyclic Peptoid Libraries. *Chem. Commun.* **2010**, *46*, 8615–8617.

53 Simpson, L. S.; Kodadek, T. A Cleavable Scaffold Strategy for the Synthesis of One-Bead One-Compound Cyclic Peptoid Libraries That Can Be Sequenced by Tandem Mass Spectrometry. *Tetrahedron Lett.* **2012**, *53*, 2341–2344.

54 Liang, X.; Girard, A.; Biron, E. Practical Ring-Opening Strategy for the Sequence Determination of Cyclic Peptides from One-Bead-One-Compound Libraries. *ACS Comb. Sci.* **2013**, *15*, 535–540.

55 Lee, K. J.; Lim, H.-S. Facile Method to Sequence Cyclic Peptides/Peptoids Via One-Pot Ring-Opening/Cleavage Reaction. *Org. Lett.* **2014**, *16*, 5710–5713.

56 Menegatti, S.; Ward, K. L.; Naik, A. D.; Kish, W. S.; Blackburn, R. K.; Carbonell, R. G. Reversible Cyclic Peptide Libraries for the Discovery of Affinity Ligands. *Anal. Chem.* **2013**, *85*, 9229–9237.

57 Brenner, S.; Lerner, R. A. Encoded Combinatorial Chemistry. *Proc. Natl. Acad. Sci. U. S. A.* **1992**, *89*, 5381–5383.

58 Nielsen, J.; Brenner, S.; Janda, K. D. Synthetic Methods for the Implementation of Encoded Combinatorial Chemistry. *J. Am. Chem. Soc.* **1993**, *115*, 9812–9813.

59 Ottl, J. Reported Applications of DNA-Encoded Library Chemistry. In *A Handbook for DNA-Encoded Chemistry: Theory and Applications for Exploring Chemical Space and Drug Discovery*; Goodnow, R. A., Jr, Ed.; John Wiley & Sons, Inc., Hoboken, **2014**; pp 319–347.

60 Kleiner, R. E.; Dumelin, C. E.; Liu, D. R. Small-Molecule Discovery from DNA-Encoded Chemical Libraries. *Chem. Soc. Rev.* **2011**, *40*, 5707–5717.

61 Gartner, Z. J.; Liu, D. R. The Generality of DNA-Templated Synthesis as a Basis for Evolving Non-Natural Small Molecules. *J. Am. Chem. Soc.* **2001**, *123*, 6961–6963.

62 Gartner, Z. J.; Tse, B. N.; Grubina, R.; Doyon, J. B.; Snyder, T. M.; Liu, D. R. DNA-Templated Organic Synthesis and Selection of a Library of Macrocycles. *Science* **2004**, *305*, 1601–1605.

63 Kleiner, R. E.; Dumelin, C. E.; Tiu, G. C.; Sakurai, K.; Liu, D. R. In Vitro Selection of a DNA-Templated Small-Molecule Library Reveals a Class of Macrocyclic Kinase Inhibitors. *J. Am. Chem. Soc.* **2010**, *132*, 11779–11791.

64 Georghiou, G.; Kleiner, R. E.; Pulkoski-Gross, M.; Liu, D. R.; Seeliger, M. A. Highly Specific, Bisubstrate-Competitive Src Inhibitors from DNA-Templated Macrocycles. *Nat. Chem. Biol.* **2012**, *8*, 366–374.

65 Maianti, J. P.; McFedries, A.; Foda, Z. H.; Kleiner, R. E.; Du, X. Q.; Leissring, M. A.; Tang, W.-J.; Charron, M. J.; Seeliger, M. A.; Saghatelian, A.; Liu, D. R. Anti-Diabetic Activity of Insulin-Degrading Enzyme Inhibitors Mediated by Multiple Hormones. *Nature* **2014**, *511*, 94–98.

66 Kanan, M. W.; Rozenman, M. M.; Sakurai, K.; Snyder, T. M.; Liu, D. R. Reaction Discovery Enabled by DNA-Templated Synthesis and In Vitro Selection. *Nature* **2004**, *431*, 545–549.

67 Franzini, R. M.; Randolph, C. Chemical Space of DNA-Encoded Libraries. *J. Med. Chem.* **2016**, *59*, 6629–6644.

68 Seigal, B. A.; Connors, W. H.; Fraley, A.; Borzilleri, R. M.; Carter, P. H.; Emanuel, S. L.; Fargnoli, J.; Kim, K.; Lei, M.; Naglich, J. G.; Pokross, M. E.; Posy, S. L.; Shen, H.; Surti, N.; Talbott, R.; Zhang, Y.; Terrett, N. K. The Discovery of Macrocyclic XIAP Antagonists from a DNA-Programmed Chemistry Library, and Their Optimization to Give Lead Compounds with In Vivo Antitumor Activity. *J. Med. Chem.* **2015**, *58*, 2855–2861.

69 Frank, R. Spot-Synthesis: An Easy Technique for the Positionally Addressable, Parallel Chemical Synthesis on a Membrane Support. *Tetrahedron* **1992**, *48*, 9217–9232.

70 Frank, R. The SPOT-Synthesis Technique. Synthetic Peptide Arrays on Membrane Supports—Principles and Applications. *J. Immunol. Methods* **2002**, *267*, 13–26.

71 Reimer, U.; Reineke, U.; Schneider-Mergener, J. Peptide Arrays: From Macro to Micro. *Curr. Opin. Biotechnol.* **2002**, *13*, 315–320.

72 Hahn, M.; Winkler, D.; Welfle, K.; Misselwitz, R.; Welfle, H.; Wessner, H.; Zahn, G.; Scholz, C.; Seifert, M.; Harkins, R.; Schneider-Mergener, J.; Höhne, W. Cross-Reactive Binding of Cyclic Peptides to an Anti-TGFalpha Antibody Fab Fragment: An X-Ray Structural and Thermodynamic Analysis. *J. Mol. Biol.* **2001**, *314*, 293–309.

73 Fodor, S. P.; Read, J. L.; Pirrung, M. C.; Stryer, L.; Lu, A. T.; Solas, D. Light-Directed, Spatially Addressable Parallel Chemical Synthesis. *Science* **1991**, *251*, 767–773.

74 Singh-Gasson, S.; Green, R. D.; Yue, Y.; Nelson, C.; Blattner, F.; Sussman, M. R.; Cerrina, F. Maskless Fabrication of Light-Directed Oligonucleotide

Microarrays Using a Digital Micromirror Array. *Nat. Biotechnol.* **1999**, *17*, 974–978.

75 Pellois, J. P.; Zhou, X.; Srivannavit, O.; Zhou, T.; Gulari, E.; Gao, X. Individually Addressable Parallel Peptide Synthesis on Microchips. *Nat. Biotechnol.* **2002**, *20*, 922–926.

76 Li, S.; Marthandan, N.; Bowerman, D.; Garner, H. R.; Kodadek, T. Photolithographic Synthesis of Cyclic Peptide Arrays Using a Differential Deprotection Strategy. *Chem. Commun.* **2005**, *5*, 581–583.

77 Schreiber, S. L. Target-Oriented and Diversity-Oriented Organic Synthesis in Drug Discovery. *Science* **2000**, *287*, 1964–1969.

78 Marsault, E.; Hoveyda, H. R.; Peterson, M. L.; Saint-Louis, C.; Landry, A.; Vézina, M.; Ouellet, L.; Wang, Z.; Ramaseshan, M.; Beaubien, S.; Benakli, K.; Beauchemin, S.; Déziel, R.; Peeters, T.; Fraser, G. L. Discovery of a New Class of Macrocyclic Antagonists to the Human Motilin Receptor. *J. Med. Chem.* **2006**, *49*, 7190–7197.

79 Marsault, E.; Hoveyda, H. R.; Gagnon, R.; Peterson, M. L.; Vezina, M.; Saint-Louis, C.; Landry, A.; Pinault, J. F.; Ouellet, L.; Beauchemin, S.; Beaubien, S.; Mathieu, A.; Benakli, K.; Wang, Z.; Brassard, M.; Lonergan, D.; Bilodeau, F.; Ramaseshan, M.; Fortin, N.; Lan, R.; Li, S.; Galaud, F.; Plourde, V.; Champagne, M.; Doucet, A.; Bherer, P.; Gauthier, M.; Olsen, G.; Villeneuve, G.; Bhat, S.; Foucher, L.; Fortin, D.; Peng, X.; Bernard, S.; Drouin, A.; Deziel, R.; Berthiaume, G.; Dory, Y.; Fraser, G. L.; Deslongchamps, P. Efficient Parallel Synthesis of Macrocyclic Peptidomimetics. *Bioorg. Med. Chem. Lett.* **2008**, *18*, 4731–4735.

80 Marsault, E.; Benakli, K.; Beaubien, S.; Saint-Louis, C.; Déziel, R.; Fraser, G. Potent Macrocyclic Antagonists to the Motilin Receptor Presenting Novel Unnatural Amino Acids. *Bioorg. Med. Chem. Lett.* **2007**, *17*, 4187–4190.

81 Hoveyda, H. R.; Marsault, E.; Gagnon, R.; Mathieu, A. P.; Vézina, M.; Landry, A.; Wang, Z.; Benakli, K.; Beaubien, S.; Saint-Louis, C.; Brassard, M.; Pinault, J.-F.; Ouellet, L.; Bhat, S.; Ramaseshan, M.; Peng, X.; Foucher, L.; Beauchemin, S.; Bhérer, P.; Veber, D. F.; Peterson, M. L.; Fraser, G. L. Optimization of the Potency and Pharmacokinetic Properties of a Macrocyclic Ghrelin Receptor Agonist (Part I): Development of Ulimorelin (TZP-101) from Hit to Clinic. *J. Med. Chem.* **2011**, *54*, 8305–8320.

82 Jefferson, E. A.; Arakawa, S.; Blyn, L. B.; Miyaji, A.; Osgood, S. A.; Ranken, R.; Risen, L. M.; Swayze, E. E. New Inhibitors of Bacterial Protein Synthesis from a Combinatorial Library of Macrocycles. *J. Med. Chem.* **2002**, *45*, 3430–3439.

83 Jefferson, E. A.; Swayze, E. E.; Osgood, S. A.; Miyaji, A.; Risen, L. M.; Blyn, L. B. Antibacterial Activity of

Quinolone–Macrocycle Conjugates. *Bioorg. Med. Chem. Lett.* **2003**, *13*, 1635–1638.

84 Peng, L. F.; Stanton, B. Z.; Maloof, N.; Wang, X.; Schreiber, S. L. Syntheses of Aminoalcohol-Derived Macrocycles Leading to a Small-Molecule Binder to and Inhibitor of Sonic Hedgehog. *Bioorg. Med. Chem. Lett.* **2009**, *19*, 6319–6325.

85 Stanton, B. Z.; Peng, L. F.; Maloof, N.; Nakai, K.; Wang, X.; Duffner, J. L.; Taveras, K. M.; Hyman, J. M.; Lee, S. W.; Koehler, A. N.; Chen, J. K.; Fox, J. L.; Mandinova, A.; Schreiber, S. L. A Small Molecule That Binds Hedgehog and Blocks Its Signaling in Human Cells. *Nat. Chem. Biol.* **2009**, *5*, 154–156.

86 Nielsen, T. E.; Schreiber, S. L. Diversity-Oriented Syntheses Using the Build/Couple/Pair Strategy. *Angew. Chem. Int. Ed. Engl.* **2007**, *47*, 48–56.

87 Isidro-Llobet, A.; Murillo, T.; Bello, P.; Cilibrizzi, A.; Hodgkinson, J. T.; Galloway, W. R. J. D.; Bender, A.; Welch, M.; Spring, D. R. Diversity-Oriented Synthesis of Macrocyclic Peptidomimetics. *Proc. Natl. Acad. Sci. U. S. A.* **2011**, *108*, 6793–6798.

88 Comer, E.; Liu, H.; Joliton, A.; Clabaut, A.; Johnson, C.; Akella, L. B.; Marcaurelle, L. A. Fragment-Based Domain Shuffling Approach for the Synthesis of Pyran-Based Macrocycles. *Proc. Natl. Acad. Sci. U. S. A.* **2011**, *108*, 6751–6756.

89 Marcaurelle, L. A.; Comer, E.; Dandapani, S.; Duvall, J. R.; Gerard, B.; Kesavan, S.; Lee, M. D.; Liu, H.; Lowe, J. T.; Marie, J.-C.; Mulrooney, C. A.; Pandya, B. A.; Rowley, A.; Ryba, T. D.; Suh, B.-C.; Wei, J.; Young, D. W.; Akella, L. B.; Ross, N. T.; Zhang, Y.-L.; Fass, D. M.; Reis, S. A.; Zhao, W.-N.; Haggarty, S. J.; Palmer, M.; Foley, M. A. An Aldol-Based Build/Couple/Pair Strategy for the Synthesis of Medium- and Large-Sized Rings: Discovery of Macrocyclic Histone Deacetylase Inhibitors. *J. Am. Chem. Soc.* **2010**, *132*, 16962–16976.

90 Fitzgerald, M. E.; Mulrooney, C. A.; Duvall, J. R.; Wei, J.; Suh, B.-C.; Akella, L. B.; Vrcic, A.; Marcaurelle, L. A. Build/Couple/Pair Strategy for the Synthesis of Stereochemically Diverse Macrolactams Via Head-to-Tail Cyclization. *ACS Comb. Sci.* **2012**, *14*, 89–96.

91 Heidebrecht, R. W.; Mulrooney, C.; Austin, C. P.; Barker, R. H.; Beaudoin, J. A.; Cheng, K. C.-C.; Comer, E.; Dandapani, S.; Dick, J.; Duvall, J. R.; Ekland, E. H.; Fidock, D. A.; Fitzgerald, M. E.; Foley, M.; Guha, R.; Hinkson, P.; Kramer, M.; Lukens, A. K.; Masi, D.; Marcaurelle, L. A.; Su, X.-Z.; Thomas, C. J.; Weïwer, M.; Wiegand, R. C.; Wirth, D.; Xia, M.; Yuan, J.; Zhao, J.; Palmer, M.; Munoz, B.; Schreiber, S. Diversity-Oriented Synthesis Yields a Novel Lead for the Treatment of Malaria. *ACS Med. Chem. Lett.* **2012**, *3*, 112–117.

92 Lawson, K. V.; Rose, T. E.; Harran, P. G. Template-Constrained Macrocyclic Peptides Prepared from

Native, Unprotected Precursors. *Proc. Natl. Acad. Sci. U. S. A.* **2013**, *110*, E3753–E3760.

93 Rose, T. E.; Lawson, K. V.; Harran, P. G. Large Ring-Forming Alkylations Provide Facile Access to Composite Macrocycles. *Chem. Sci.* **2015**, *6*, 2219–2223.

94 Beckmann, H. S. G.; Nie, F.; Hagerman, C. E.; Johansson, H.; Tan, Y. S.; Wilcke, D.; Spring, D. R. A Strategy for the Diversity-Oriented Synthesis of Macrocyclic Scaffolds Using Multidimensional Coupling. *Nat. Chem.* **2013**, *5*, 861–867.

95 Isidro-Llobet, A.; Hadje Georgiou, K.; Galloway, W. R. J. D.; Giacomini, E.; Hansen, M. R.; Méndez-Abt, G.; Tan, Y. S.; Carro, L.; Sore, H. F.; Spring, D. R. A Diversity-Oriented Synthesis Strategy Enabling the Combinatorial-Type Variation of Macrocyclic Peptidomimetic Scaffolds. *Org Biomol Chem* **2015**, *13*, 4570–4580.

96 Jiang, B.; Pei, D. A Selective, Cell-Permeable Nonphosphorylated Bicyclic Peptidyl Inhibitor against Peptidyl-Prolyl Isomerase Pin1. *J. Med. Chem.* **2015**, *58*, 6306–6312.

97 Olsen, C. A.; Ghadiri, M. R. Discovery of Potent and Selective Histone Deacetylase Inhibitors Via Focused Combinatorial Libraries of Cyclic alpha3beta-Tetrapeptides. *J. Med. Chem.* **2009**, *52*, 7836–7846.

98 Qian, Z.; Upadhyaya, P.; Pei, D. Synthesis and Screening of One-Bead-One-Compound Cyclic Peptide Libraries. In *Peptide Libraries*; Derda, R., Ed.; Methods in Molecular Biology; Springer, New York, **2015**; pp 39–53.

99 Mannocci, L.; Leimbacher, M.; Wichert, M.; Scheuermann, J.; Neri, D. 20 Years of DNA-Encoded Chemical Libraries. *Chem. Commun.* **2011**, *47*, 12747–12753.

7

Biological and Hybrid Biological/Chemical Strategies in Diversity Generation of Peptidic Macrocycles

Francesca Vitali and Rudi Fasan

Department of Chemistry, University of Rochester, Rochester, NY, USA

7.1 Introduction

Macrocyclic peptides have attracted increasing attention as molecular scaffolds for the development of therapeutics and chemical probes to interrogate biological systems [1–4]. Interest in this structural class has been stimulated by the biomedical value and breadth of biological activities presented by macrocyclic peptides isolated from nature including cyclosporine A (immunosuppressant), caspofungin (antifungal), and polymyxin (antibiotic), among others [5]. Further, conformational restriction of peptidic structures via backbone/side-chain cyclization has often resulted in enhanced protein binding affinity [6, 7], selectivity [8], membrane permeability [9–11], and/or proteolytic stability [12, 13] over linear peptides, all of which are desirable features in the context of *in vivo* applications and therapeutic development.

Over the past decade, a number of enabling methodologies have been introduced to access peptide-based macrocycles via chemical modification and/or engineering of ribosomally produced polypeptides. Research in this area has been largely driven by the potential advantages these approaches can provide over purely synthetic methods. Among these, there is the high combinatorial potential inherent to the ribosomal synthesis of genetically encoded polypeptides, which enables the rapid generation of vast chemical libraries via genetic engineering. In addition, these methods may be coupled to powerful, high-throughput platforms (e.g., yeast, phage, mRNA display) or genetic selection systems for the rapid functional screening of these libraries. Finally, these libraries can be readily deconvoluted by DNA sequencing to elucidate the structures associated with the desired functional properties. At the same time, challenges in this area are concerned with (i) the need to orchestrate the desired macrocyclization in the presence of fully unprotected polypeptides (and other biomolecules) and (ii) the desire to overcome the limitations imposed by the restricted building block repertoire given by the twenty canonical amino acids. As discussed later, a number of creative approaches have been devised over the past few years to achieve this goal and tackle these challenges. These include the polypeptide-driven or chemically induced cyclization of linear precursor polypeptides, cyclopeptide synthesis through *in vitro* translation and genetic code reprogramming methods, and the creation of hybrid organo-peptide macrocycles via embedding of synthetic scaffolds into genetically encoded peptidic backbones. This chapter offers an overview of these strategies, as well as representative applications toward the discovery of bioactive compounds. A critical analysis of the relative advantages and limitations of these methodologies is also provided, along with an outlook on future directions of the field. To be noted, DNA-supported synthesis is not covered in this chapter; readers are directed to Chapter 6 for a description of the methodology and to Chapter 17 for a case study.

7.2 Cyclic Peptide Libraries on Phage Particles

Introduced by Smith and Devlin in 1990 [14, 15], phage display represents a powerful technique for the creation and screening of combinatorial libraries of genetically encoded peptides against a target protein of interest [16]. This methodology relies on the fusion of a genetically randomized polypeptide sequence to a coat protein of a bacteriophage (e.g., M13 phage), resulting in the display of the polypeptide on the surface of the phage particle, which also contains the DNA encoding for it. Upon "panning" of the phage display peptide library against a target protein immobilized on a plate or resin bead, library members capable of binding the target can be isolated, and their structure elucidated by DNA sequencing. Using this technique, vast peptide libraries comprising

up to 10^8–10^9 members can be generated and screened to identify peptides with the desired protein binding affinity and selectivity [16].

7.2.1 Disulfide-Bridged Cyclic Peptide Libraries

One of the earliest strategies for generating ribosomal libraries of conformationally constrained peptides entailed the use of phage display in combination with randomized peptide sequences flanked by two cysteine residues to form an intramolecular disulfide bridge (Figure 7.1).

This approach has been extensively investigated by industrial and academic groups to identify disulfide-bridged peptide inhibitors (or activators) for a variety of proteins and enzymes, as illustrated by the representative examples provided in Table 7.1.

One of the first key demonstrations of its potential utility for lead discovery was through the isolation of a cyclopeptide agonist for the erythropoietin (EPO) receptor [23]. Upon panning a "naïve" (i.e., fully randomized) 8-mer peptide library and further affinity maturation in a M13 pIII-fused format, a disulfide-bridged cyclic peptide (EMP1) was isolated that is capable of binding the EPO receptor *in vitro* and promoting the proliferation of EPO-responsive cells with sub-micromolar potency (IC_{50} and $EC_{50} \sim 200$ nM, respectively) [23]. Albeit much less potent than EPO ($EC_{50} \sim 20$ pM), the cyclic peptide nonetheless was found to be able to induce erythroid colony formation from human bone marrow cells while presenting reasonable stability in blood serum ($t_{1/2} \sim 8$ h). Another remarkable feature of this compound was its mode of action. X-ray crystallographic analysis of the peptide–EPO receptor complex indeed revealed that two molecules of the peptide stack against each other, each contacting both subunits of the EPO receptor [44]. This nearly symmetric molecular array mediates the dimerization and, thus, activation of the EPO receptor. Other successful applications of this strategy include the development of potent cyclic peptide inhibitors of integrins (IC_{50} 20–200 nM) [19, 20, 31] and various enzymes, including the angiotensin-converting enzyme 2 (ACE2) (K_i 2.8 nM) [18], factor VIIa (IC_{50} 1 nM) [24], urokinase-type plasminogen activator (uPA) (K_i 6.7 µM) [42], peptidylprolyl isomerase Pin1 (K_i 0.5 µM) [36], and Aurora A kinase (IC_{50} 6 µM) [21] (Table 7.1).

In addition to the aforementioned membrane receptors and enzymes, phage display libraries of disulfide-cyclized peptides have provided a source of compounds capable of interfering with protein–protein interactions (PPIs). Notable examples include the isolation of a 14-residue cyclic peptide inhibitor (p1-02) of the interaction between insulin-like growth factor 1 (IGF-1) and IGF-binding protein 1 (IGFBP-1) [33]. This compound was determined to block the IGF-1–IGFBP1 interaction *in vitro* (IC_{50} 50 nM) and to activate IGF-1-dependent kinase activity in cells (EC_{50} 190 nM) [33]. By screening a randomized 9-mer peptide library, Fairbrother *et al.* discovered a cyclic peptide capable of targeting the vascular epithelial growth factor (VEGF) by inhibiting its interaction with the KDR and Flt-1 receptors (IC_{50} 220 nM) and by suppressing VEGF-induced proliferation of human umbilical vascular endothelial cells (IC_{50} 9.6 µM) [43]. Upon screening a phage display library of randomized bicyclic peptides constrained by two disulfide bridges, Genentech scientists developed a potent antagonist (e131) of the high-affinity IgE receptor FcɛRI (IC_{50} 32 nM) [27]. This compound was reported to block IgE-induced histamine release from basophils with nano-molar activity (ED_{50} 30 nM) while remaining stable in biological matrices (i.e., lung homogenates) for over 24 h [27]. Structural studies by NMR showed that e131 adopts a stable and compact three-dimensional fold in solution, consisting of two "zeta"-shaped moieties [27]. Albeit with generally weaker affinity, disulfide-linked peptide inhibitors have been successfully developed for a number of other target proteins, including Grb2 and Grb7 SH2 domains (IC_{50} 1–25 µM) [29, 30], HIV gp41 protein (IC_{50} 3.6 µM) [28], IGF-1 (IC_{50} 1.4 µM) [17], and syntrophin PDZ domain (IC_{50} 360 nM) [39].

In general, a major advantage of this strategy based on the generation of conformationally constrained peptide libraries on phage resides in its technical simplicity, as the structural elements necessary for peptide cyclization are defined at the genetic level. Formation of the intramolecular disulfide bond is favored by the oxidizing environment provided by the periplasmic space of the bacterial host, to which the coat proteins are exposed during the assembly of the bacteriophage particles. Another attractive feature is the possibility to tune the "stringency" of the affinity selection step, thus facilitating the discovery of peptide ligands with the desired level of target affinity and selectivity. In addition, the valency of the displayed polypeptide can be varied depending on the choice of the coat protein to which the polypeptide is fused, ranging from hundreds (100–200) of copies (e.g., when fused to major coat protein pVIII in M13 bacteriophage) to a few (1–5) copies (e.g., when fused to minor coat protein pIII in M13) [16]. High-valency phage display peptide libraries typically yield moderate-affinity binders (K_D 10–100 µM), which can be subjected to further engineering and "affinity maturation" using a low-valency phage display format (Figure 7.1) [45]. This strategy has been applied by Genentech scientists in the context of various proteins (e.g., EPOR [23], factor VIIa [24], FcɛRIα [27], IGFBP-1 [33], IgG Fc; [34] Table 7.1), leading to the discovery of high-affinity binders and inhibitors for the corresponding target.
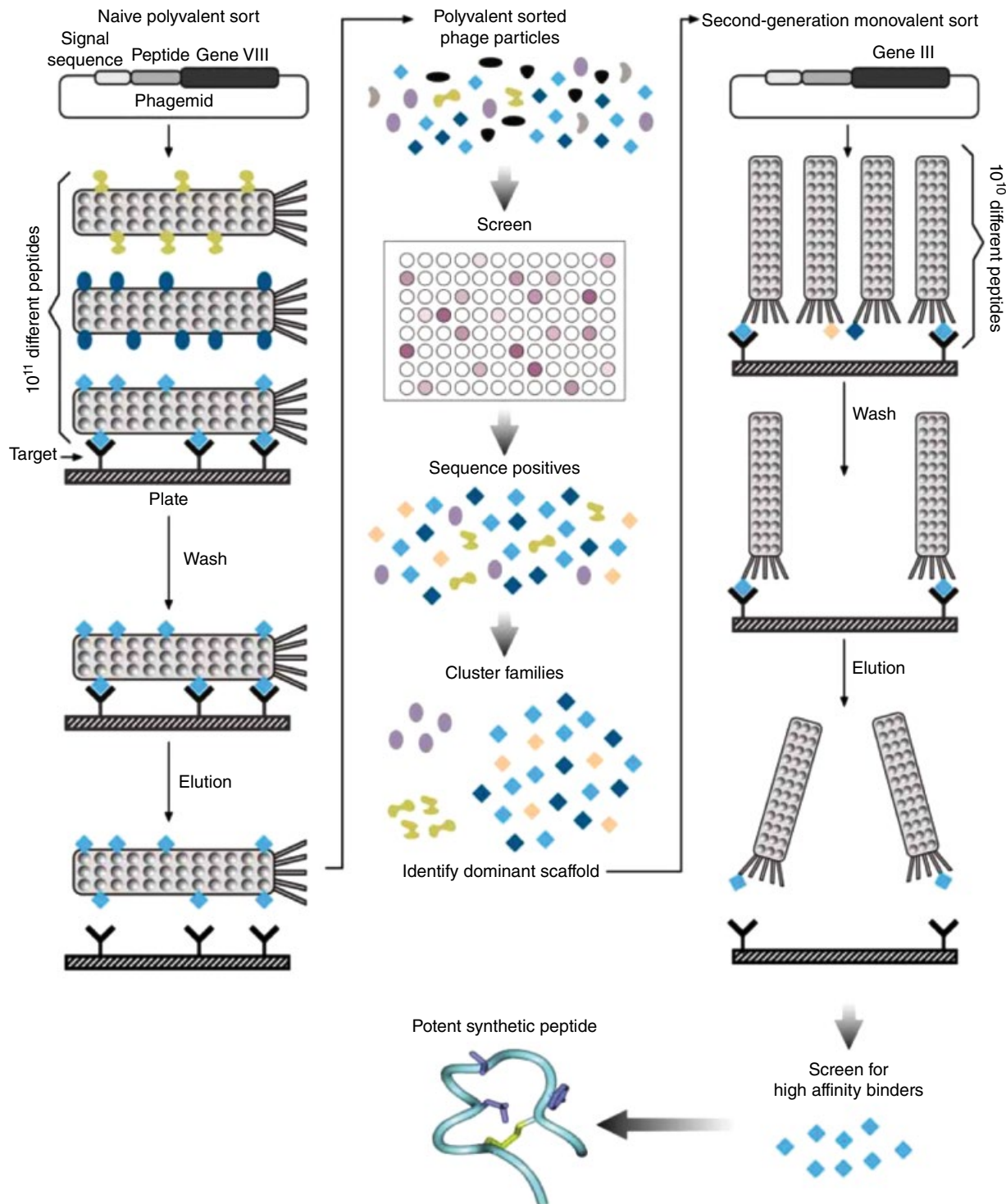
Figure 7.1 Schematic diagram for naïve selection and affinity maturation of disulfide-bridged cyclic peptide ligands via M13 phage display. A naïve library is first displayed on a high-valency format through fusion to the pVIII coat protein. Positive hits are validated via a phage ELISA assay and sequenced to identify consensus motifs. Affinity maturation of the ligand is achieved via a second-generation library designed based on the consensus motifs, followed by display on a low-valency format (pIII fusion) and affinity selection. Source: Adapted from Deshayes *et al*. [17]. Reproduced with permission of Elsevier. (*See insert for color representation of the figure.*)

Table 7.1 Representative examples of disulfide-bridged peptides isolated by M13 phage display against the indicated targets.

Target	Peptide sequence	Display	Activity	Reference
ACE-2	GDYSH**C**SPLRYYPWWK**C**TYPDPEGGG-NH$_2$ (DX600)	pIII	2.8 nM (K_i)	[18]
$\alpha_5\beta_1$ integrin	GA**C**RGD**C**LGA-NH$_2$	pIII	20 nM (IC$_{50}$) 100 nM (ED$_{50}$ cells)	[19]
$\alpha_v\beta_3$ integrin	A**C**D**C**RGD**C**F**C**G-NH$_2$ (RGD4C)	pIII	1 μM (IC$_{50}$) 0.2 μM (ED$_{50}$ cells)	[20]
Aurora A kinase	**C**PRFLPW**C**G-NH$_2$	pIII	6 μM (IC$_{50}$)	[21]
Human CXCR1/2	**C**LRSGRF**C**-NH$_2$	pIII	10 μM (IC$_{50}$)	[22]
EPOR	GGTYS**C**HFGPLTWV**C**KPQGG-NH$_2$ (EMP1)	pVIII/pIII	200 nM (IC$_{50}$)	[23]
Factor VIIa	AL**C**DDPRVDRWY**C**QFVEG-NH$_2$ (peptide E-76)	pVIII/pIII	8.5 nM (K_D) 1 nM (IC$_{50}$)	[24]
FcγRI	TDT**C**LMLPLLLG**C**DEE-NH$_2$	pIII	2 μM (IC$_{50}$)	[25]
FcεRIα	NLPR**C**TEGPWGWV**C**M-NH$_2$	pVIII / pIII	1.8 μM (IC$_{50}$) <10 μM (IC$_{50}$ cells)	[26]
FcεRI	VQ**C**PHF**C**YELDYEL**C**PDV**C**YV-NH$_2$ (e131)	pVIII / pIII	32 nM (IC$_{50}$) ~30 nM (ED$_{50}$ cells)	[27]
gp41	(D)-KKGA**C**ELLGWEWAWL**C**AA-NH$_2$ (D10-p5-2k)	pIII	3.6 μM (IC$_{50}$ cells)	[28]
Grb2 SH2 domain	**C**ELYENVGMY**C**-NH$_2$ (G1)	pIII	25 μM (IC$_{50}$)	[29]
Grb7 SH2 domain	**C**VWGYANDWL**C**-NH$_2$ (G7-8)	pIII	~1 μM (IC$_{50}$)	[30]
GP IIb/IIIa	**C**NWKRGD**C**-NH$_2$	pIII	150 nM (IC$_{50}$)	[31]
Hepatitis B core antigen	**C**WSFFSNI**C**-NH$_2$ (A1)	pIII	20 nM (K_D) 12 nM (IC$_{50}$)	[32]
IGF-1	RN**C**FESFVAALRR**C**MYG-NH$_2$	pVIII /pIII	1.4 μM (IC$_{50}$) ~5 μM (ED$_{50}$ cells)	[17]
IGFBP-1	SEVG**C**RAGPLQWL**C**EKYFG (p1-02)	pVIII	50 nM (IC$_{50}$) 190 nM (ED$_{50}$ cells)	[33]

Human IgG Fc domain	D**C**AWHLGELVW**C**T-NH$_2$ (Fc-III)	pVIII / pIII	25 nM (IC$_{50}$)	[34]
MMP-2	**C**TTHWGFTL**C**-NH$_2$	pIII	5 μM (IC$_{50}$)	[35]
PIN1	**C**RYPEVEI**C**-NH$_2$	pIII	0.5 μM (K_i)	[36]
Prostate-specific antigen	**C**VAY**C**IEHH**C**WT**C**-NH$_2$ (C-4)	pIII	2.9 μM (K_D)	[37]
Human serum albumin	RLIEDI**C**LPRWG**C**LWEDD-NH$_2$ (SA21)	pVIII/pIII	470 nM (K_D)	[38]
Syntrophin PDZ domain	AKET**C**LAGYY**C**-NH$_2$ (peptide F)	pIII	360 nM (K_D)	[39]
Src SH3 domain	(D)-DR**C**LSGLRLGLVP**C**A-OH (Pep-D1)	pIII	63 μM (K_D)	[40]
Streptavidin	AE**C**HPQF**C**IEGRK-NH$_2$	pIII	660 nM (K_D)	[41]
Urokinase-type plasminogen activator	**C**SWRGLENHRM**C**-NH$_2$ (upain-1)	pIII	6.7 μM (K_i)	[42]
VEGF	VEPN**C**DIHVMWEWE**C**FERL-NH$_2$ (v114)	pVIII/pIII	220 nM (IC$_{50}$) 9.6 μM (ED$_{50}$ cells)	[43]

The cysteines involved in the disulfide bond are highlighted. pVIII/pIII refers to the use of high-valency pVIII display followed by affinity maturation using a low-valency pIII system. (D) refers to peptides made solely of D-amino acids isolated using mirror image phage display.
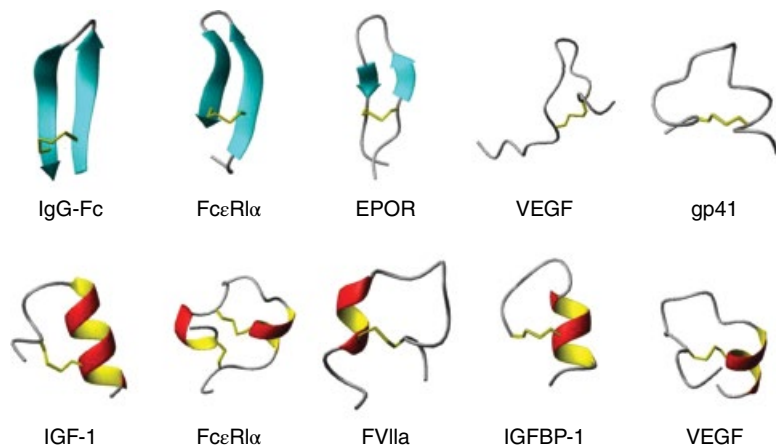
Figure 7.2 Three-dimensional structure representations of disulfide-bridged cyclic peptides isolated by phage display. The target proteins against which these peptides were selected are indicated: Fc region of human immunoglobulin G (IgG Fc; pdb 1DN2) [34]; FcεRIα (pdb 1JBF) [26]; erythropoietin hormone receptor (EPOR; pdb 1EBP) [44]; vascular epithelial growth factor (VEGF; v108 peptide, pdb 1VPP) [46]; glycoprotein 41 subunit of HIV-1 envelope (gp41, pdb 1CZQ) [28]; insulin-like growth factor 1 (IGF-1, pdb 1LB7) [17]; FcεRIα (pdb 1KCO) [27]; coagulation factor FVIIa (pdb 1DVA) [24]; insulin-like growth factor binding protein 1 (IGFBP-1, pdb 1GJE) [47]; VEGF (v107 peptide, pdb 1KAT) [46].

Another notable feature relates to the diversity of cyclic peptide topologies isolated through this method. Indeed, the screening of naïve peptide libraries constrained by disulfide bonds has frequently yielded peptides that are able to fold into a compact, stable structure, either free in solution or when bound to the respective receptor. As shown in Figure 7.2, these three-dimensional structures encompass supersecondary motifs commonly found in proteins, such as β-hairpins and α-helix-turn motifs, as well as less canonical folds [23, 34, 44, 47, 48]. These findings support the notion that structural pre-organization of the peptide molecules can facilitate high-affinity interactions with protein surfaces, as observed in the case of other biologically active peptides and peptidomimetics [49, 50]. The advantage of conformational restriction is also apparent from experiments in which libraries of linear peptides have been screened in parallel with libraries of disulfide-bridged peptides, with the latter typically being more efficient in yielding higher-affinity ligands for the protein of interest [22, 32, 51]. Almost invariably, removal of the disulfide bridge in the cyclic peptide ligands identified by phage display (e.g., via disulfide reduction or substitution of the cysteine residues with serine residues) led to a dramatic reduction (10- to 100-fold) of the desired activity [29, 36, 40], further supporting the critical importance of this structural constraint for the desired functional properties. In some cases, the selection of peptides capable of adopting a folded structure during the panning process was enforced through the incorporation of turn-inducing motifs (e.g., Gly-Pro) within randomized peptide sequences [26, 33, 38].

With respect to target selectivity, a viable strategy to favor the selection of peptide ligands directed toward a specific binding interface involves the use of competitive elution with the native binding partner or a known ligand for the protein of the interest. For example, this strategy was applied in the context of laminin-1 [52], *Escherichia*

coli H7 flagellin [53], and Aurora A kinase [21] to favor the enrichment and thus isolation of library members that specifically interact with the desired binding site. A number of other studies have demonstrated, however, that certain protein surfaces have an inherent propensity to interact with other biomolecules. For example, the "unbiased" screening of a naïve phage display cyclic peptide library against the Fc region of human IgG (hIgG) "converged" in the isolation of a β-hairpin peptide (Fc-III), which targets a consensus binding site recognized by several natural IgG Fc-binding proteins, such as bacterial protein A and protein G and an anti-IgG rheumatoid factor [34]. This example suggests that, at least for certain target proteins, the application of competitive elution strategies may not be necessary during the screening process in order to ensure the isolation of binders with high target selectivity.

Finally, an interesting variation of this technology is "mirror image phage display" [40], in which a (D)-enantiomeric form of the target protein is used during the affinity selection process. Upon identification of viable ligands, the corresponding (D)-peptide is produced to target the naturally occurring (L)-enantiomeric form of the protein. This approach was successfully applied to discover (D)-peptides with micromolar inhibitory activity against the Src SH3 domain [40], HIV gp41 protein [28], and the oncoprotein Hdm2 [54, 55].

7.2.2 From Phage Display to Peptide Macrocycle Design

Despite its successful application in a number of settings (Table 7.1), a major drawback of the methodology described earlier relates to the chemical instability of the disulfide bond in the resulting cyclic peptides. Although some of these peptides were found to exhibit good stability against proteolysis in biological matrices [27], in particular those isolated via mirror image phage display,

the disulfide linkage remains susceptible to thiol exchange and/or cleavage, especially under the reducing intracellular environment of cells. The latter restricts the utility of these peptide-based agents to only extracellular targets. To overcome this issue, phage display-derived peptides have been used as starting points for the development of more stable analogues via isosteric and/or functional replacement of the disulfide linkage or through stabilization by other means of cyclization. This approach is exemplified by the studies presented later.

A notable example concerns the development of a non-phosphorylated cyclic peptide inhibitor for the Grb2 Src homology 2 (SH2) domain [29]. SH2 domains play a key role in the regulation of intracellular signaling by mediating the recognition of tyrosine phosphorylation sites in proteins. Grb SH2 binds pTyr-containing sequences within several proteins including the adapter protein SHC, members of the ErbB receptor family, and oncoproteins, such as BCR-abl [29]. Screening of a 9-mer random peptide library flanked by cysteines (C-x_9-C) using phage display led to the initial identification of a cyclic peptide (**G1**; Figure 7.3) capable of inhibiting Grb2 SH2 *in vitro* with micromolar activity (IC$_{50}$ ~ 25 μM). Alanine scanning experiments showed that a Tyr-Glu-Asn motif within the peptide macrocycle is critical for interaction with the pTyr-binding site in Grb2 SH2, thus

providing an early example of a non-phosphorylated functional mimic of a pTyr-containing peptide. By modeling and NMR, this motif was determined to adopt a β-turn structure similar to that presented by the phosphopeptide substrate bound to Grb2 SH2 [56, 57]. In order to develop a more stable analogue of **G1**, the disulfide bridge was initially substituted with a head-to-side-chain thioether linkage obtained via cysteine alkylation of an α-chloroacetyl moiety appended to the N-terminus of the peptide [29]. This structural replacement led to an analogue equipotent to **G1** (**G1TE**, IC$_{50}$ 26 μM; Figure 7.3), which was slightly superior to an analogue containing an isosteric methylene-based linker (IC$_{50}$ 35 μM) [58]. Subsequent optimization of the molecule involved introduction of a 1-aminocyclohexanecarboxylic acid (Ach) residue to force the Tyr-Ach-Asn motif into the bioactive β-turn conformation, replacement of the solvent-exposed region of the peptide (when bound to Grb SH2) with a hydrocarbon linker, and substitution of the pharmacophoric Tyr with 3-amino-Tyr, resulting in a significantly (100-fold) more potent inhibitor of Grb SH2 (IC$_{50}$ 190 nM) [59, 60]. Notably, a further fourfold improvement in inhibitory potency (IC$_{50}$ = 58 nM) could be achieved by a subtle modification of the thioether linker (i.e., sulfoxidation), with the (*R*)- and (*S*)-configured sulfoxide analogues demonstrating drastically different
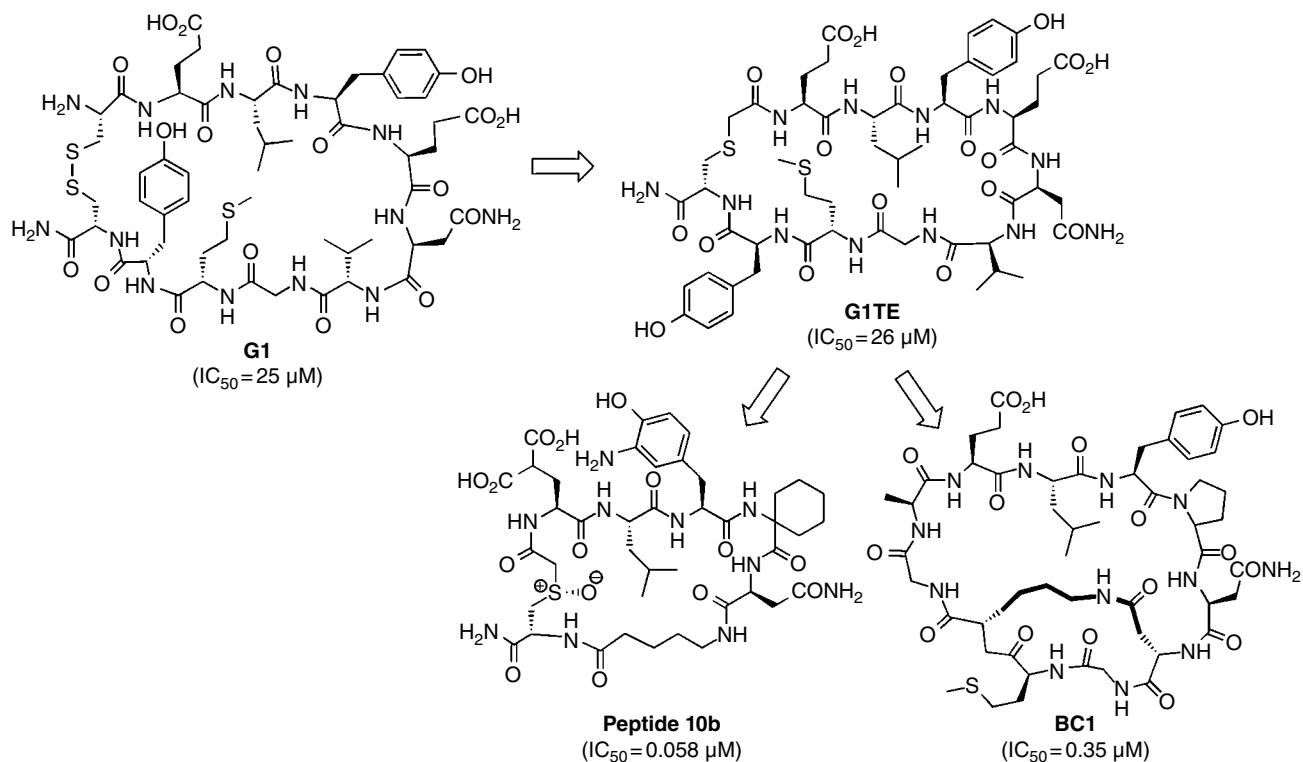
Figure 7.3 Non-phosphorylated cyclic peptide inhibitors of the Grb2 SH2 domain. Phage display-derived **G1** peptide and its non-reducible cyclic and bicyclic analogues.

activities (IC$_{50}$ 58 nM vs. 1500 nM, respectively) [59]. The optimized peptide (**10b**; Figure 7.3) was found to possess potent antimitogenic effects (ED$_{50}$ 19 nM) in erbB2-over-expressing breast cancer cells while having no effects on cancer cells that lack erbB2 growth dependence [59]. These results indicated that **10b** is able to interfere with Grb SH2-mediated stimulation of erbB2 signaling intra-cellularly and thus can penetrate cells despite its overall (−2) negative charge.

In more recent studies, the cyclic peptide **G1** served as the starting point for the preparation of cyclic and bicy-clic analogues in which the inter-side-chain disulfide linker was substituted by means of an Ala-Gly dipeptide linker connecting the N- and C-terminus of the peptide sequence [61]. This substitution led to a non-reducible **G1** analogue (called **HT1**) with approximately threefold higher *in vitro* binding affinity for Grb2 SH2 than G1 (IC$_{50}$ 6.0 μM vs. 20.5 μM). Interestingly, subtle variations of the linker moiety (e.g., D-Ala vs. L-Ala or β-Ala vs. Gly) resulted in complete loss of Grb2 SH2 binding. By fur-ther constraining **HT1** via an inter-side-chain lactam bridge, a bicyclic analogue (**BC1**; Figure 7.3) was obtained that exhibited significantly higher (17-fold) *in vitro* inhibitory activity toward Grb2 SH2 binding to a cognate phosphotyrosine-containing peptide substrate (IC$_{50}$ 0.35 μM) [61]. Furthermore, the bicyclic scaffold was found to increase the half-life of the peptide in blood serum (~50-fold) and enhance its selectivity toward the SH2 domain of Grb2 over that of tensin-1 (tensin-SH2). Upon amidation of the Glu^1 residue, the resulting charge-neutralized analogues of cyclic **HT1** and bicyclic **BC1** compounds were found to penetrate cells with compara-ble efficiency to a Tat peptide, with their cellular uptake relying on an energy-dependent endocytic mechanism [62]. In comparison, the parent, negatively (−1) charged **BC1** compound, showed significantly reduced cell per-meability, which was proposed to be the basis of its ina-bility to exhibit antiproliferative activity in cancer cells [62]. Interesting insights into the mode of binding of these compounds to Grb2 SH2 were gained from NMR and modeling studies, which suggested that the side chains of Glu^1 and Tyr^3 form a discontinuous epitope that mimics a phosphorylated tyrosine motif [62]. This rather unusual binding mode is consistent with the large effect of subtle structural variations within these [62] and previously investigated **G1** analogues [58–60, 63] on their ability to interact with Grb2 SH2 domain.

In addition to the aforementioned case, other strate-gies have been adopted to convert disulfide-bridged cyclic peptides into more chemically stable analogues. In a noteworthy example, Robinson and coworkers utilized the aforementioned phage display-derived Fc-III peptide [34] as a starting point to create a head-to-tail cyclic β-hairpin peptidomimetic with significantly enhanced

binding affinity for the Fc fragment of hIgG antibody [7]. The crystal structure of Fc-III in complex with the Fc fragment of hIgG showed that the peptide binds to the protein by adopting a β-hairpin conformation con-strained by the disulfide bridge (Figure 7.4a) [34]. By grafting the Fc-III peptide loop onto a hairpin-inducing D-Pro-L-Pro template [64], a backbone cyclic analogue (**FcBP2**; Figure 7.4b) was obtained that binds hIgG Fc with an 80-fold lower K_D (2.2 vs. 185 nM). In compari-son, a shorter analogue (**FcBP1**; Figure 7.4b) was found to bind hIgG Fc with much weaker affinity (K_i of 14.2 μM vs. 0.4 nM for FcBP2 in inhibition assay with protein A), a result that was attributed to a "wrong" orientation of a critical interfacial Trp residue on the opposite face of the hairpin compared with the corresponding Trp11 side chain in Fc-III (Figure 7.4a) as determined by NMR structural studies. Importantly, **FcBP2** was determined to maintain considerable Fc-binding properties under reducing conditions (IC$_{50}$ 550 nM), whereas reduction of the disulfide bridge in **Fc-III** completely abolishes its ability to interact with hIgG Fc (IC$_{50}$ ≫ 1 mM). The solu-tion structure of **FcBP2** revealed that the dipeptide tem-plate forces the peptide to adopt a stable β-hairpin conformation in solution that is highly superimposable with the protein-bound structure [7]. The benefit of this structural pre-organization in the bioactive form is nicely reflected by the 12-fold higher association rate constant measured for **FcBP2** compared with **Fc-III** using surface plasmon resonance (SPR) (k_{on} 4.83×10^6 M^{-1} s^{-1} vs. 3.75×10^5 M^{-1} s^{-1}). The more constrained structure of **FcBP2** also improved the stability of the peptide–Fc complex as evidenced by a slower dissociation rate as compared with **Fc-III** (k_{off} 1.07×10^{-2} s^{-1} vs. 6.96×10^{-2} s^{-1}). Since hairpin-shaped peptides are frequently identified from phage display libraries of disulfide-bridged pep-tides (Figure 7.2), the aforementioned strategy could be of general utility in converting these molecules into more potent and chemically robust protein-targeting agents.

7.2.3 Bicyclic Peptide Libraries on Phage

A different strategy for generating libraries of confor-mationally constrained peptides on phage particles has entailed the alkylation of cysteine residues by means of a chemical cross-linking agent. The methodological basis for this approach derives from studies by Timmerman and coworkers, who demonstrated the efficient cycliza-tion of synthetic peptides bearing two and three cysteine residues by means of 1,3-bis- and 1,3,5-tris-(bromome-thyl)aryl compounds to yield mono- or bicyclic peptides, respectively [65]. Using an analogous chemistry, Winter and Heinis developed a phage display-based methodol-ogy for creating and screening combinatorial libraries of bicyclic peptides (Figure 7.5a) [66]. In a first application
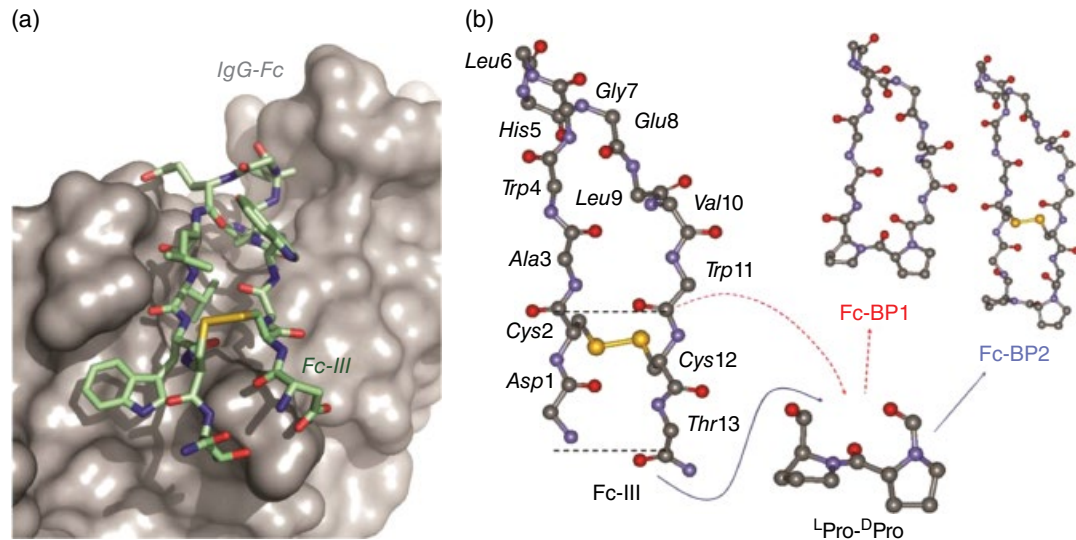
(a)

(b)

Figure 7.4 Macrocyclic peptide binders of human IgG Fc fragment. (a) View of **Fc-III** peptide (DCAWHLGELVWCT; green; stick models) bound to the surface of human IgG Fc domain (pdb 1DN2); (b) Computer models of **FcBP-1** and **FcBP-2** mimetics as prepared by transplanting 9 or 13 residues, respectively, from **Fc-III** onto the ^DPro-^LPro template. (*See insert for color representation of the figure.*)

(a)

(b)

(c)
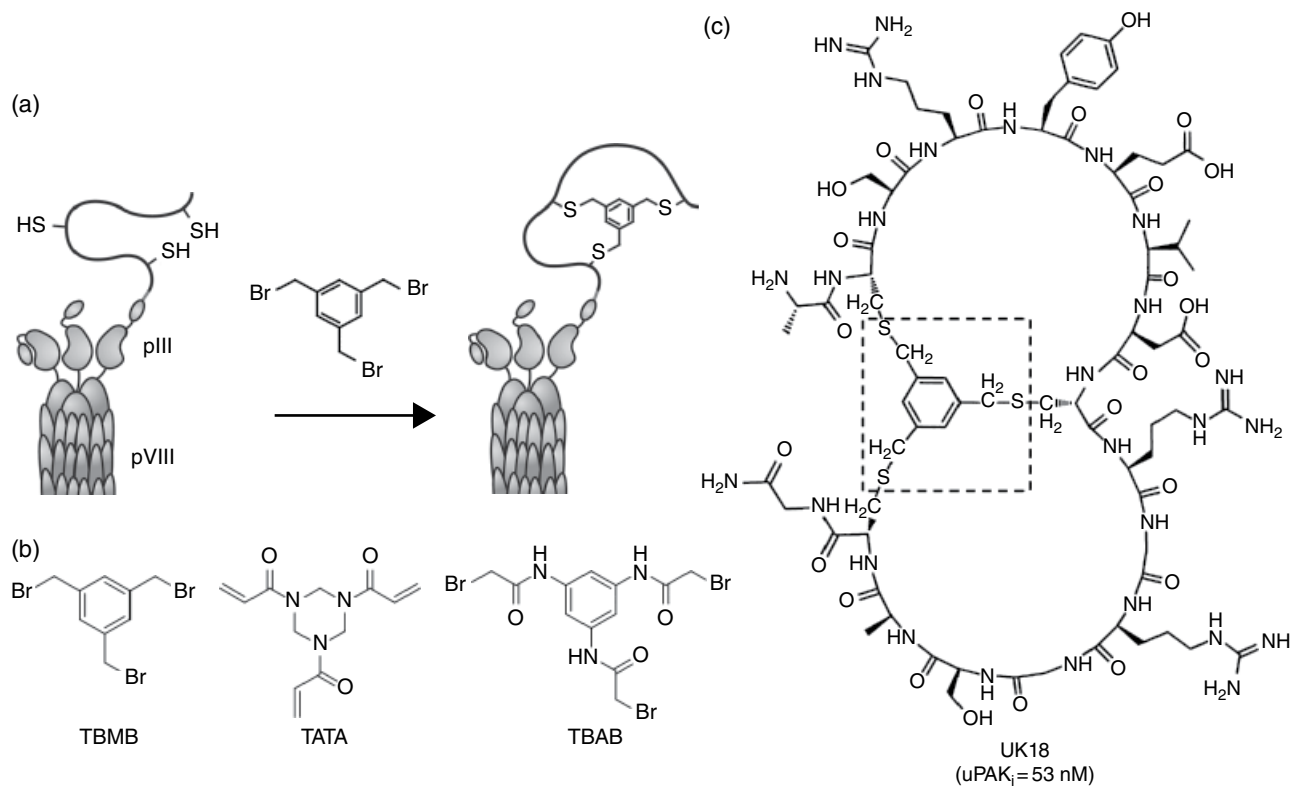
Figure 7.5 Bicyclic peptides on phages. (a) Overview of chemical cross-linking strategy for generating bicyclic peptides displayed on the surface of M13 phage particles. (b) Chemical structures of cysteine cross-linking agents. TATA, 1,3,5-triacryloyl-1,3,5-triazinane; TBAB, *N,N′,N″*-(benzene-1,3,5-triyl)tris(2-bromoacetamide); TBMB, 1,3,5-tris-(bromomethyl)benzene. (c) Structure of bicyclic peptide inhibitor (**UK18**) of human uPa isolated by phage display. The **TBMB**-derived linker is highlighted by the box. Source: Panels a and c are adapted from Heinis *et al.* [66]. Reproduced with permission of Nature Publishing Group.

of this strategy, a randomized polypeptide sequence with intercalating cysteine residues (Cys-X_6-Cys-X_6-Cys, where X is a randomized position) was fused to the minor coat protein pIII of M13 bacteriophage and subjected to cyclization upon reaction with the cross-linking reagent 1,3,5-tris-(bromomethyl)benzene (**TBMB**) (Figure 7.5b). The resulting library of phage-displayed "6 × 6" bicyclic peptides (10^9 members) was panned against two disease-related proteases, plasma kallikrein (PK) and cathepsin G, leading to the isolation of potent inhibitors for both targets (K_i of 1.7 nM and 100 nM, respectively) [66]. Although the bicyclic peptide PK inhibitor was found to lack a well-defined structure in solution by NMR, its acyclic counterpart showed a 6000-fold lower IC_{50}, which supports the critical role of the organic linker for the protease inhibitory activity of the bicyclic peptide. In another work [67], the same (6 × 6) bicyclic peptide library was panned against human uPA to yield a nanomolar inhibitor of this enzyme (**UK18**, K_i 53 nM; Figure 7.5c). Also in this case, the bicyclic structure was determined to be essential for the enzyme inhibitory activity, as indicated by the 7- and 320-fold higher K_i value displayed by monocyclic and linear variants of the peptide, respectively. To identify alternative bicyclic peptide inhibitors of uPA, a panel of 14 additional combinatorial libraries were generated via **TBMB**-mediated cyclization of Cys-X_m-Cys-X_n-Cys sequences (where m and n = 3, 4, 5, or 6) and panned against immobilized uPA [68]. Interestingly, the most potent inhibitors (K_i 0.7–0.9 μM) were obtained from the larger (6 × 6) bicyclic peptide library, whereas "hits" isolated from the smaller-sized bicyclic peptide libraries generally showed significantly lower inhibitory activity (K_i 5–50 μM).

Using a similar approach, a panel of structurally different bicyclic peptide libraries comprising more than 10 billion members were panned against the human coagulation factor FXIIa [69]. In this case, the most promising inhibitors were obtained from the libraries of the smaller-sized bicyclic peptides (4 × 4 compared with 6 × 6) cyclized with 1,3,5-triacryloyl-1,3,5-triazinane (**TATA**) (Figure 7.5b), instead of **TBMB**. The most potent peptide (FXII516) from this initial screening exhibited a K_i value of 0.16 μM in an *in vitro* FXIIa inhibition assay. FXII516 was then subjected to affinity maturation via randomization of amino acid positions outside the consensus region, which led to an eightfold more potent inhibitor (FXII618, K_i 22 nM). Despite its smaller size (1.8 kDa vs. 13.6 kDa, respectively), FXII618 compound possesses comparable FXIIa inhibitory activity to that of corn trypsin inhibitor (CTI), a protein-based coagulation inhibitor in use for suppressing contact activation of blood coagulation in diagnostic assays [69]. In addition, the bicyclic peptide showed high selectivity (>100–1000-fold) against FXIIa over several other proteases involved in coagulation pathways (e.g., plasmin, FXIa, PK, uPA, *t*PA, thrombin).

More recently, this technology based on phage-displayed bicyclic peptide libraries has been applied to identify binders and potential inhibitors for other target proteins besides enzymes. Bicyclic peptides with sub-micromolar binding affinity (150–300 nM) toward the human epidermal growth factor 2 (Her2) [70], the regulatory region of Notch1 [71], and the cytokine tumor necrosis factor alpha (TNF-α) [72] have been reported. Whereas the inhibitory activity of the Her2 binding peptides was not investigated, neither the Notch1 nor the TNF-α targeting bicyclic peptides were found to be effective in inhibiting the function of the respective target protein, indicating that their binding site is distinct from that involved in signaling.

The X-ray crystallographic analysis of human uPA in complex with different cyclic and bicyclic peptide inhibitors isolated from various studies provides an instructive example of how these different compounds interact with an identical binding pocket in the enzyme. Representative structures are presented in Figure 7.6 and include the complex of uPA with the disulfide-constrained monocyclic peptide upain-1 (K_i 6.7 μM) [42, 73], the **TBMB**-linked (6 × 6) bicyclic peptide UK18 (K_i 0.053 μM) [67], a **TBAB**-linked (5 × 5) bicyclic peptide (UK903, K_i 1.96 μM) [74], and a bicyclic disulfide-constrained peptide (UK504, K_i 8.0 μM) [75]. Interestingly, despite adopting generally different overall folds, all of the inhibitors, except UK903, were found to share some key interactions with the protein that is mediated by identical or structurally similar amino acid residues. These common features include an arginine residue that inserts into the S1 pocket of uPA and an aspartate or glutamate residue that blocks the oxyanion hole of the protease. At the same time, owing to its larger size and the presence of a second ring, **UK18** can establish a more extended network of non-covalent interactions with the protein binding cleft as compared with upain-1. This difference translates into a larger total buried surface area (700 $Å^2$ vs. 520 $Å^2$, respectively), as well as a higher number of hydrogen bond contacts with the protein surface (14 vs. 11, respectively) for **UK18** vs. upain-1, which provides a structural basis for the 200-fold greater inhibitory activity of the former compared with the disulfide-bridged peptide [67]. Another interesting comparison is between the binding mode of upain-1 and that of UK504. The C-terminal region of these compounds shares a nearly identical sequence, and the backbone of the two peptides in the uPA complex was found to overlap in a region spanning around five amino acids, yet the two backbones run in opposite directions (Figure 7.6).

Finally, UK903 provides an example of a bicyclic peptide that shares the same binding site as the other

Figure 7.6 Crystal structure of human uPA in complex with monocyclic and bicyclic peptide inhibitors. (a) Disulfide-bridged peptide upain-1 (pdb 2NWN); (b) TBMB-linked bicyclic peptide UK18 (pdb 3QN7); (c) TBAB-linked bicyclic peptide UK903 (pdb 4MNY); and (d) bicyclic disulfide-bridged peptide UK504 (pdb 4GLY). The TBMB and TBAB linkers are colored in magenta. Key amino acid residues involved in the interaction with uPA are showed as sphere models. For each complex, a schematic representation of the corresponding peptide ligand is provided. (*See insert for color representation of the figure.*)
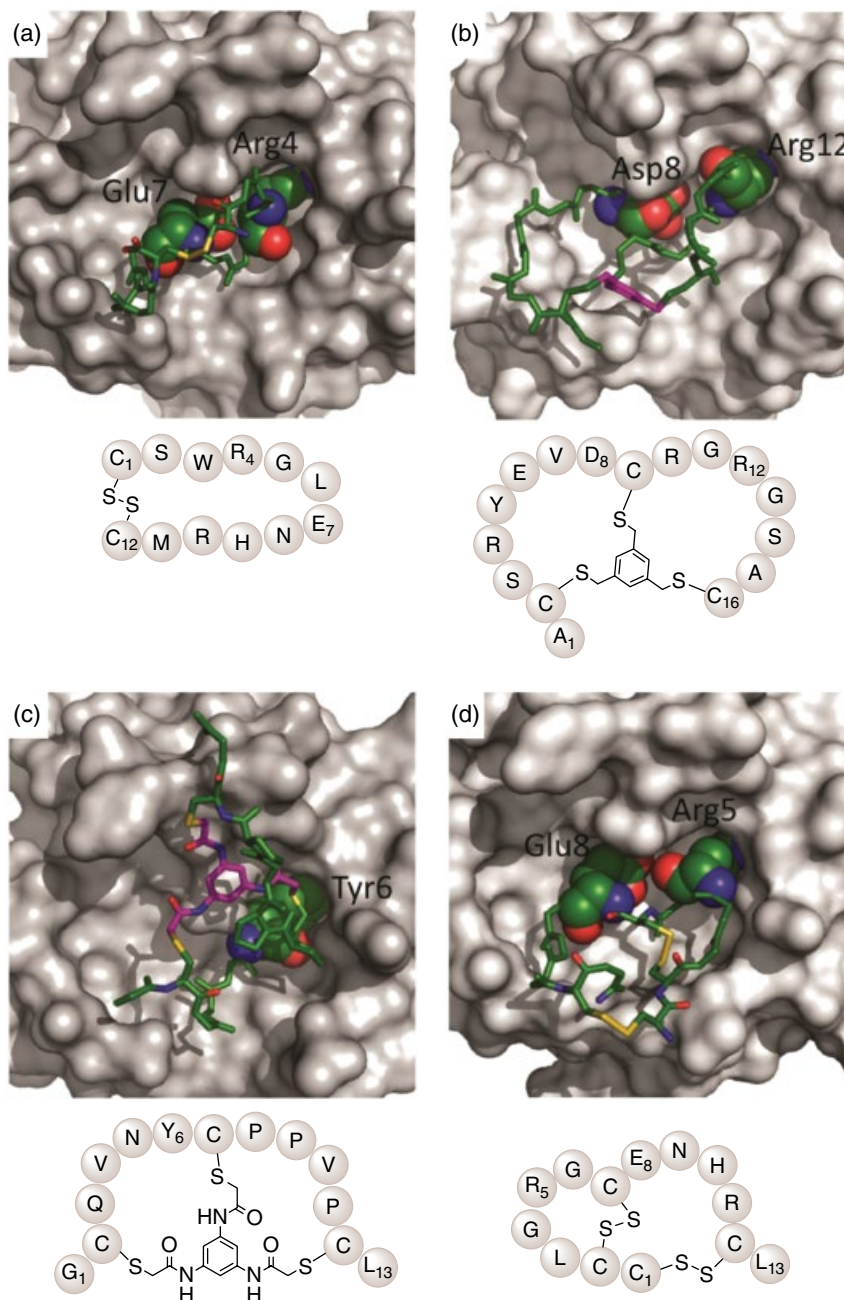
inhibitors but presents a completely unrelated amino acid sequence. Another peculiar feature of this compound is the involvement of the linker moiety in forming hydrogen bonds (3 each), both with the peptidic region of the inhibitor and with amino acids from the protein, which is made possible by the presence of polar acetamido groups in the **TBAB** scaffold. Although these interactions do not result in more potent inhibition of uPA as compared with the **TBMB**-linked UK18, it enables the molecule to adopt an overall more compact structure (Figure 7.6c). In the context of the same target enzyme,

the importance of structural pre-organization in the bioactive form is evidenced by another study, in which the upain-1 peptide was further constrained by means of N- to C-terminus cyclization [76]. The resulting bicyclic upain-1 analogue was found to exhibit a twofold lower K_D compared with the monocyclic counterpart, which could be attributed to a reduction of entropy loss upon binding by isothermal calorimetry analyses.

An anticipated beneficial effect of constraining a peptide sequence through a bicyclic scaffold is an increase in proteolytic stability. Stability studies showed

that the uPA inhibitor **UK18** exhibits an *in vitro* half-life ($t_{1/2}$) in serum of approximately 15 h [77]. In comparison, monocyclic analogues spanning either the entire sequence of the bicyclic peptide (i.e., the peptide cross-linked with only two cysteines) or part thereof (i.e., each of the individual rings) were found to be completely degraded within the same time frame. The judicious replacement of a glycine residue (Gly13) with a D-amino acid at one of the two proteolytically sensitive sites of the peptide sequence (ACSRYEVDCR↓GR↓GSACG) further enhanced the half-life of the bicyclic compound in blood serum ($t_{1/2} > 24$ h) [78]. Despite these promising stability properties, pharmacokinetic experiments indicated that **UK18** is rapidly cleared *in vivo* (mice) after intravenous bolus injection at 50 μM, showing a short elimination half-life ($t_{1/2}$ (β) 30 min) along with rapid clearance (Cl 8.78 ml/h) and reduced AUC (4.7 h μg/ml). In previous studies, the *in vivo* elimination half-life of peptide hormones (growth hormone, prolactin) and antibody Fab fragments could be effectively extended by 5- to 15-fold through conjugation with a disulfide-bridged albumin-binding peptide [38, 79, 80]. Using a similar approach, **UK18** was conjugated with a cyclic albumin-binding peptide, resulting in a compound with significantly improved pharmacokinetic properties ($t_{1/2}$ (β) 1440 min, Cl 0.009 ml/h, AUC 964 h μg/ml) [77]. In addition, the **UK18**/albumin-binding peptide conjugate showed no signs of proteolytic degradation after 48 h in mouse plasma, possibly due to shielding from plasma proteases as a result of its non-covalent association with albumin.

7.3 Macrocyclic Peptide Libraries via *In Vitro* Translation

The introduction of viable protocols for the cell-free translation of polypeptides has provided a basis for the implementation of enabling technologies for the creation of macrocycle peptide libraries produced *in vitro* [81]. A common feature of these methodologies is their compatibility with mRNA display (Figure 7.7), a powerful system for the functional screening and selection of large libraries of *in vitro* translated polypeptides [82]. In mRNA display, the translated polypeptide sequence is physically linked to its encoding mRNA molecule by means of a puromycin moiety chemically ligated to the 3′ end of the mRNA. Following translation, the appended puromycin moiety is ligated to the C-terminus of the peptide chain, thus creating a covalent link between the polypeptide and the mRNA molecule. Combinatorial libraries of peptide–RNA hybrids can be subjected to iterative cycles of affinity selection and amplification in order to isolate polypeptides that bind with high affinity to an immobilized target [83].

A second key advancement in this area involved the development of methods for "codon reprogramming," which has made possible the introduction of one or more unnatural amino acids (UAA) into *in vitro* translated polypeptides [84]. Instrumental to these advances was the development of a reconstituted *E. coli* translation system consisting of purified recombinant components of the ribosomal translational machinery (PURE system) [85, 86]. In the chemically defined medium of the PURE system, it has been possible to reassign specific codons of the genetic code to particular desired UAA, thus permitting their incorporation during ribosomal synthesis. Two major approaches have been pursued to achieve this goal. A first one, implemented by Szostak and coworkers, entails substituting one or more natural amino acids with structural analogues within the *in vitro* translation system [87, 88]. This strategy capitalizes on the ability of certain aminoacyl-tRNA synthetases (AARS) to mis-charge the cognate tRNA molecule with noncanonical amino acids that resemble the native substrate [89–91]. The second approach, introduced by Forster [92] and further developed by Suga and coworkers [81], involves the direct addition of *de novo* synthesized aminoacylated tRNAs to the PURE *in vitro* translation system. Although aminoacylated tRNAs can be produced chemically or chemoenzymatically, the accessibility of these molecules was facilitated by the evolution of a substrate-promiscuous ribozyme ("flexizyme") for coupling a given tRNA molecule to a pre-activated amino acid [93, 94]. As discussed later, combination of the aforementioned protocols with various cyclization strategies has permitted the creation and screening of very large macrocyclic peptide libraries, also incorporating a variety of non-proteinogenic amino acids, on an mRNA display format.

7.3.1 *In Vitro* Cyclic Peptide Libraries Via Chemical Cross-Linking

A first example of *in vitro* produced cyclic peptide libraries was reported by Roberts and coworkers, who generated head-to-side-chain cyclized peptides (Figure 7.8a) upon reaction of mRNA-linked randomized peptides (Met-(Xaa)$_n$-Lys-mRNA, with $n = 3$–11) with the bifunctional acylating reagent disuccinimidyl glutarate (DSG) [95]. DSG links the N-terminal amino group of the peptide with the side-chain amino group of a constant lysine residue with variable cyclization efficiency (30–55%) depending on the length of the intervening amino acid sequence [95]. Using mRNA display, the group constructed a very large (10^{12}-member) library of DSG-cross-linked peptide macrocycles (M(Xaa)$_{10}$K), from which a cyclic dodecamer peptide capable of binding the signaling protein Gα$_{i1}$ with high affinity (cycGiBP, K_D 2.1 nM) was successfully isolated [96]. Compared with its

Figure 7.7 Overview of mRNA display system for the selection of functional peptides. A template DNA library is first transcribed *in vitro* to generate a randomized mRNA library (i). After conjugation with puromycin (ii) and translation of the mRNA-encoded polypeptide (iii), a peptide–mRNA conjugate is formed. A double-stranded DNA/RNA hybrid is then generated via reverse transcription, followed by panning of the RNA/DNA-conjugated peptide library against an immobilized target protein. The protein-bound peptide–RNA/DNA molecules are then recovered and amplified by polymerase chain reaction (PCR), followed by transcription and translation. Iterative rounds of affinity selection and amplification enrich the library with peptide with high affinity for the target protein, whose sequence can be determined by DNA sequencing. (*See insert for color representation of the figure.*)

linear counterpart, cycGiBP exhibits a 15-fold higher affinity for $G\alpha_{i1}$ and a threefold longer half-life in the presence of proteases. To bias the selection process toward serum stable peptide ligands, the mRNA-displayed peptide library was later exposed to a protease prior to the affinity selection step. This process led to the identification of an equally potent cyclic peptide antagonist of $G\alpha_{i1}$ (cycPRP-3, K_D 9 nM; Table 7.2) with up to 85-fold longer half-life in human serum ($t_{1/2}$ 28 h vs. 0.33 h) [97].

Using a different approach [98], Szostak and coworkers constructed a 10^{10}-member mRNA display library of highly modified cyclopeptides based on the 12-mer sequence Met-Cys-(Xaa)$_{10}$-Cys-mRNA. In this case, the *in vitro* translated peptides were cyclized through alkylation of the cysteine residues flanking the randomized peptide sequence by means of 1,3-dibromomethylbenzene (Figure 7.8b). In addition, a variety of different noncanonical amino acids, including alkyne-, thiazolidine-,

and α,α-cyclopentyl-containing amino acids and halogenated Tyr and Phe derivatives, were introduced in the resulting cyclic peptides by substitution of 12 of the 20 natural amino acids with structural analogues. Screening of the peptide library against immobilized thrombin led to the isolation of potent inhibitors, one consisting of only natural amino acids (N1, K_i 1.5 nM; Table 7.2) and one comprising four noncanonical amino acids (U1, K_i 23 nM). Replacement of the latter with their naturally occurring analogues abolished enzyme binding, highlighting the critical importance of these unnatural components for thrombin inhibitory activity [98].

A different cyclization strategy was utilized to generate an mRNA-displayed library (10^{11} members) of cyclic peptides constrained by a lanthionine bond (Figure 7.8c) [99]. In this case, peptide cyclization was achieved through the incorporation of 4-selenalysine in the *in vitro* translated peptide, followed by its conversion to dehydroalanine (via oxidation with H_2O_2, then β-elimination).

(a)

(b)

(c)
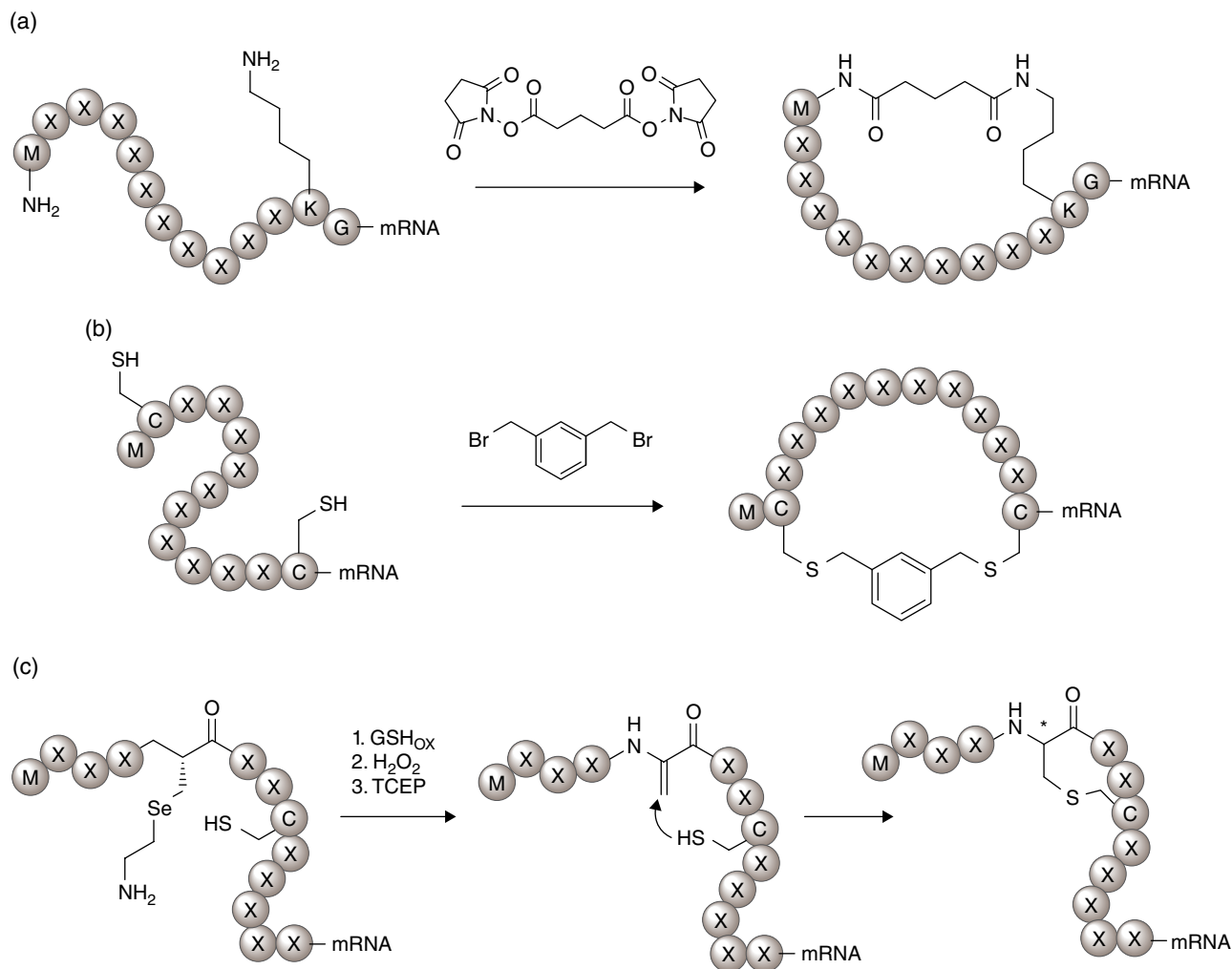
Figure 7.8 Strategies for macrocyclization of *in vitro* translated peptides. (a) DSG-mediated cyclization. (b) Cyclization via cysteine cross-linking with 1,3-dibromomethylbenzene. (c) Formation of lanthipeptide-like macrocycles via oxidation of 4-selenalysine to dehydroalanine, followed by cyclization via a Michael addition reaction.

The dehydroalanine residue is then attacked by a neighboring cysteine to give a thioether bridge [99]. Screening of the library led to a low micromolar binder for sortase A (K_D 3 µM; Table 7.2), although this compound was unable to inhibit the activity of the enzyme. Further investigation of the different isomers generated during the cyclization reaction revealed the critical importance of the stereochemical configuration of the lanthionine bridge for binding to sortase A.

7.3.2 *In Vitro* Macrocyclic Peptide Libraries Via the FIT and RaPID System

By utilizing a "flexible" *in vitro* translation (FIT) system supplemented with premade aminoacylated tRNAs, Suga and coworkers have demonstrated the successful incorporation of a large number of non-proteinogenic amino acids into *in vitro* translated peptide sequences, including N-methylated, α,α-disubstituted, β-, γ-, and D-amino acids [84, 109]. The combination of FIT, peptide cyclization, and mRNA display has provided a general platform for the screening of combinatorial libraries of cyclic peptides and peptidomimetics (referred to as Random nonstandard Peptide Integrated Discovery (RaPID) system) (Figure 7.9) [109].

Whereas various cyclization approaches have been investigated in the context of FIT-translated peptides [110–115], the main strategy adopted for generating cyclic peptide libraries has involved the formation of a thioether linkage between a 2-chloroacetyl group attached to the N-terminus of the peptide and a cysteine residue located downstream in the sequence (Figure 7.9c) [116]. This method allows for the formation of head-to-side-chain cyclopeptides of varying sizes (4–14 residues)

Table 7.2 Macrocyclic peptides isolated through the different cyclization and library screening strategies discussed in the text.

Target	Peptide sequence	Selection method	Posttranslational modification	Activity	Reference
Plasma kallikrein	A**C**SDRFRN**C**PADEAL**C**G (PK15)	Phage display	Bicyclization via TBMB cross-linking	1.7 nM (IC$_{50}$)	[66]
uPA	A**C**SRYEVD**C**RGRGSA**C**G (UK18)	Phage display	Bicyclization via TBMB cross-linking	53 nM (K_D)	[67]
uPA	G**C**QVNY**C**PPVP**C**L (UK903)	Phage display	Bicyclization via TBAB cross-linking	1.96 μM (K_i)	[74]
Notch1 regulatory region	A**C**ERYQG**C**FSVGGY**C**G (FL-NRR17)	Phage display	Bicyclization via TBMB cross-linking	150 nM (K_D)	[71]
TNFα	**C**PP**C**VWQVF**C** (M9)	Phage display	Bicyclization via TBMB(methyl) cross-linking	7.6 nM (K_D)	[72]
Factor XIIa	R**C**FRLP**C**RQLR**C**R (FXII618)	Phage display	Bicyclization via TATA cross-linking	22 nM (K_i)	[69]
Gαi1	*cyclo*(MTWFEFLSSTSK) (cycPRP-3)	mRNA display	DSG-mediated head-to-side chain cyclization	9 nM (K_i)	[97]
Thrombin	M**C**IIKKSRDPGR**C**VG (N1)	mRNA display	Dibromoxylene cross-linking; UAA incorporation with natural AARS	6.3 nM (K_i)	[98]
	M$_a$**C**L$_a$QNSY$_a$IAT$_a$K$_a$G**C**G (U1)			23 nM (K_i)	
Sortase	LWY**Lan**LS**Lan**WGRI (2$_{(2S,6R)}$)	mRNA display	Lanthionine bridge via 4-seleno-lysine oxidation	3 μM (K_D)	[99]
Akt2 kinase	*cyclo*(<u>**Y**</u>ILVRNRLLRVD<u>**C**</u>) (Pakti-L1)	mRNA display	*N*-α-Chloroacetyl-Tyr/Cys cyclization; FIT system	110 nM (IC$_{50}$)	[100]
E6AP ubiquitin ligase	*cyclo*(<u>**Ac^DW**</u>CDV^{Me}SGR^{Me}F^{Me}GY^{Me}FP<u>**C**</u>) (CM$_{11}$-1)	mRNA display	*N*-α-Chloroacetyl-^DTrp/Cys cyclization; multiple UAA incorporation via FIT system	0.6 nM (K_D)	[101]
SIRT2 deacetylase	*cyclo*(<u>**AcY**</u>SNFRIK^{Tfa}RYSNSS<u>**C**</u>) (S2iL8)	mRNA display	*N*-α-Chloroacetyl-^{L/D}Tyr/Cys cyclization; UAA incorporation via FIT system	3.2 nM (IC$_{50}$)	[102]
Met receptor	*cyclo*(<u>**AcY**</u>ISWNEFNSPNWRFIT<u>**C**</u>) (aML5)	mRNA display	*N*-α-Chloroacetyl-^{L/D}Tyr/Cys cyclization; FIT system	19 nM (K_D)	[103]
Human serum albumin	*cyclo*(<u>**ABPhe**</u>TYNERLFW<u>**C**</u>) (p1)	TRAP display	ClAB-Phe/Cys cyclization; FIT system	41 nM (K_D)	[104]
VEGFR2	*cyclo*(<u>**AcF**</u>VVVSTDPWVNGLYID<u>**C**</u>) (L1)	TRAP display	*N*-α-Chloroacetyl-^{L/D}Tyr/Cys cyclization; FIT system	50 nM (IC$_{50}$)	[105]
				~5 μM (IC$_{50}$ cells)	
HDM2/X	*cyclo* (<u>**pAcF**</u>SFAEYWNLLA)-SP8	N/A	MOrPH via oxime/AMA-mediated cyclization	110 nM (IC$_{50}$)	[106]
Streptavidin	*cyclo*(<u>**MeaF**</u>FTNYHPQDANA)	Multiwell plates	MeaF-mediated side chain-to-tail cyclization	1.1 μM (K_D)	[107]
Streptavidin	*cyclo*(S<u>**O2beY**</u>TNVHPQF<u>**C**</u>NA)	Multiwell plates	Bicyclic (head-to-tail cyclization + O2beY/Cys inter-side-chain linkage)	0.77 μM (IC$_{50}$)	[108]

The target proteins are indicated. The amino acid residues involved in the cyclization are highlighted. ClAB-Phe, *N*-[3-(2-chloroacetamido)benzoyl]phenylalanine; MeaF, 3-(2-mercapto-ethyl) amino-phenylalanine. Other abbreviations are the same as defined elsewhere in this chapter.

(a)

(b)

(c)

Cyclic N-methylated peptide library

Figure 7.9 Screening of *in vitro* translated cyclic peptide libraries via the FIT and RaPID system. (a) Flexizyme-catalyzed tRNA aminoacylation. Initiator tRNA_CAU is loaded with *N*-chloroacetyl-^DTrp, and other selected tRNAs are loaded with N-methylated amino acids (MeF, MeS, MeG, MeA). (b) Reprogrammed genetic code used for mRNA display peptide library against the HECT domain of ubiquitin ligase E6AP. Selected codons are made "vacant" via removal of the corresponding tRNA and AARS from the *in vitro* translation system. These codons are reprogrammed using the aminoacylated tRNAs prepared in (a). (c) Overview of the RaPID system for the selection of macrocyclic *N*-methylated peptides against E6AP. Messenger RNA libraries containing a randomized sequence, (NNU)$_{8-15}$, are transcribed from the corresponding cDNA library and conjugated with an oligonucleotide bearing a puromycin residue. The resulting mRNAs are translated by the FIT system in the presence of the appropriate aminoacylated tRNAs as in (a). The mRNA-displayed linear peptides are cyclized via a reaction between the cysteine residue and the N-terminal α-chloroacetyl group. After affinity selection against immobilized E6AP, the cDNAs of the protein-bound mRNA–peptide fusions are recovered and amplified by PCR. After multiple rounds of affinity selection/amplification (typically 6–10), the identity of the "hits" is determined by DNA sequencing. Source: Hipolito *et al.* [109] and Yamagishi *et al.* [101]. Reproduced with permission of Elsevier & American Chemical Society. (*See insert for color representation of the figure.*)

and is achieved by using an initiator tRNA pre-charged with an *N*-(2-chloroacetyl)-functionalized amino acid in a reconstituted translation system lacking methionine. Withdrawal of methionine is required for incorporation of the *N*-(2-chloroacetyl)-functionalized amino acid as the initial residue of the translated peptide. Using this peptide cyclization approach in conjunction with mRNA display, a macrocyclic inhibitor of E6AP was isolated (Figure 7.9) [101]. In this work, a 10^{12}-member library of 10-mer to 15-mer macrocyclic peptides containing an

N-terminal D-Trp residue and various *N*-methyl-amino acids was prepared by initiating the translated peptide sequence with *N*-(2-chloroacetyl)-D-Trp (ClAc^{D}W) and reassigning four codons to N-methylated Phe, Gly, Ser, and Ala, followed by cyclization via attack of a fixed C-terminal Cys residue onto ClAc^{D}W. Library screening led to the isolation of a potent binder of E6AP (CM$_{11}$-1, K_D 0.6 nM; Table 7.2), which contained four N-methylated amino acids in addition to D-Trp. Both the N-methylated backbone and cyclic structure of the peptide were found to be essential for E6AP binding [101]. *In vitro* assays using a reconstituted ubiquitinylation system showed that the best compound (CM$_{11}$-1) inhibited E6AP-mediated ubiquitinylation of p53 at low micromolar concentration (IC$_{50}$ ∼ 1 μM).

More recently, similar studies have been conducted in the context of other disease-related enzymes and receptors, resulting in the identification of potent inhibitors for Akt2 kinase (IC$_{50}$ 110 nM) [100], human deacetylase SIRT2 (IC$_{50}$ 3.2 nM) [102], and vascular endothelial growth factor receptor 2 (VEGFR2) [105] (Table 7.2). In the case of Akt2, multiple libraries of thioether-linked cyclic peptides produced via cysteine alkylation of an N-terminal *N*-(2-chloroacetyl)-L- or D-Tyr residue and comprising 4–12 amino acid-long sequences were used (∼10^{12} members). Upon library screening and deconvolution, the most potent Akt2 inhibitors were isolated from the ^{L}Tyr-cyclized 11-mer and 12-mer peptide libraries. These compounds were found to block Akt2-dependent kinase activity with *in vitro* IC$_{50}$'s of 90–110 nM while exhibiting 40- to 250-fold selectivity toward Akt2 over the homologous isoforms Akt1 and Akt3 (IC$_{50}$ 1–25 μM; Table 7.2) [100]. A similar approach was successfully applied to discover macrocyclic peptide inhibitors for SIRT2 [102]. N^{ε}-Trifluoroacetyl-Lys was incorporated within the cyclic peptide given the known ability of this modified residue to mimic acetylated Lys while being much less efficiently (10^5 slower rate) processed by the enzyme. The most promising hit was found to be a 14-mer cyclic peptide (S2iL8) capable of inhibiting SIRT2 with low nanomolar activity (IC$_{50}$ 3.2 nM; Table 7.2) while presenting a 10- to 100-fold lower inhibitory activity against SIRT1 and SIRT3 isoforms. In this case, however, the macrocyclic structure of the peptide was determined to be only partially important for the observed activity, as a linear analogue of S2iL8 as well as a truncated form thereof maintained high inhibitory activities (IC$_{50}$ 6–30 nM) [102]. A follow-up study provided insights into the binding mode of the macrocyclic peptides to SIRT2 and revealed a comparable functional role of the amino acids composing the macrocycle and its linear counterpart for interaction with the enzyme [117].

In another work, the RaPID system was applied to isolate a high-affinity macrocyclic binder (K_D 2–19 nM;

Table 7.2) for the hepatocyte growth factor (HGF) receptor (Met) [103]. Although unable to block binding of the HGF to Met, the compound could be used, in dimeric form, as a Met agonist by inducing dimerization of the Met receptor and consequent activation of the Met-dependent intracellular signaling pathway. The dimeric cyclic peptide was found to induce various HGF-like cellular responses, including cell proliferation and branching morphogenesis, in human cells with half-maximal effective doses in the low nanomolar range (ED$_{50}$ ∼ 2 nM) [103]. Finally, the RaPID system in combination with a modified and improved version of mRNA display (termed "TRAP display") [104] was recently applied to identify potent inhibitors of VEGFR2 [105]. In this case, a highly diverse library of mRNA-linked macrocyclic peptides (8–15 amino acids long) was generated using four different 2-chloro-acetamido-functionalized L- and D-Phe derivatives (mediating cyclization via Cys alkylation), 15 natural amino acids, and 4 non-proteinogenic amino acids (N-methylated Phe and His, cycloleucine, D-Tyr). A cyclic peptide library consisting of only natural amino acids was also tested. Library screening resulted in a number of macrocyclic ligands (10- to 17-mer) with nanomolar affinity (K_D 2–100 nM) for VEGFR2 (e.g., L1; Table 7.2). Among these, L1 and BL1, which comprise only natural amino acids, were most effective in inhibiting VEGFR2 activity in cell-based assays, suppressing VEGF-induced VEGFR2 autophosphorylation and proliferation of HUVEC cells with an IC$_{50}$ ∼ 50 nM and 5 μM, respectively [105].

7.4 Emerging Strategies for the Combinatorial Synthesis of Hybrid Macrocycles *In Vitro* and in Cells

7.4.1 Macrocyclic Organo-Peptide Hybrids (MOrPHs)

The strategies described in the previous sections have permitted the combinatorial synthesis of macrocyclic peptides incorporating various non-proteinogenic building blocks, but these structures have mainly consisted of UAAs or amino acid analogues. Methodologies developed by the Fasan group have recently enabled the synthesis of hybrid macrocycles in which a variety of synthetic amino acid-unrelated moieties are embedded within a ribosomally derived peptidic framework (Figure 7.10) [118–120]. These methodologies thus offer the capability of modulating the topology, ring size, and functionalization pattern of the macrocyclic products through variation of the synthetic moiety of these molecules in addition to variation of the genetically encoded peptide sequence.
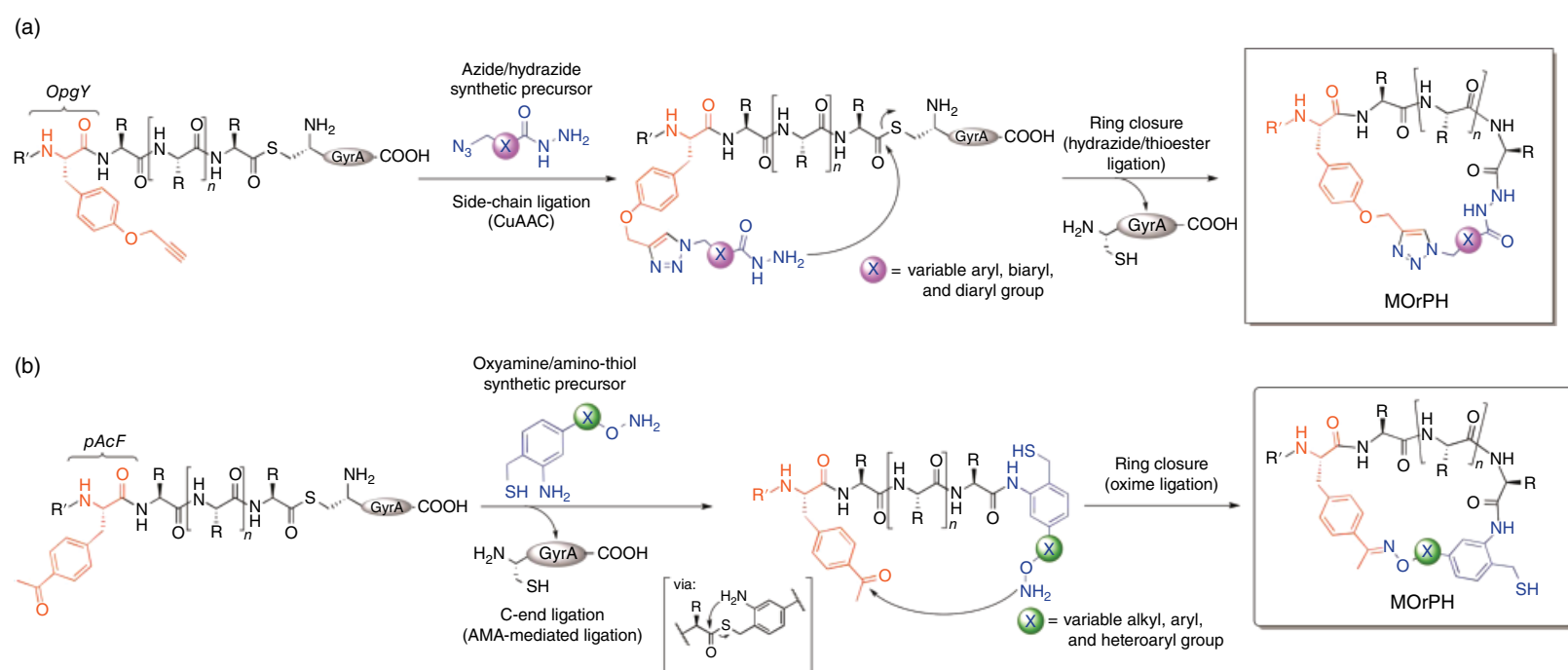
Figure 7.10 Strategies for the synthesis of macrocyclic organo-peptide hybrids (MOrPHs). (a) CuAAC/hydrazide-mediated ligation method. (b) Oxime/AMA-mediated ligation method. AMA, 2-amino-mercaptomethyl-aryl moiety; CuAAC, copper-catalyzed alkyne/azide cycloaddition.

These so-called macrocyclic organo-peptidic hybrids (MOrPHs) are produced via a dual bio-orthogonal ligation reaction between a bifunctional synthetic precursor and a recombinant protein precursor, in which a variable peptide target sequence is framed between a genetically encoded UAA and an engineered intein lacking C-terminal splicing ability. The UAA carries a judiciously chosen bio-orthogonal side-chain functional group (e.g., alkynyl, keto group) and is introduced in the precursor protein using amber stop codon suppression [121]. The bio-orthogonal side-chain functional group in the peptide provides a first ligation site to the synthetic molecule, whereas a second ligation reaction involving a nucleophilic group from the synthetic precursor and the intein-catalyzed thioester bond at the C-terminus of the peptide gives rise to a side chain-to-tail cyclic structure (Figure 7.10).

In a first implementation of this concept, azide/hydrazide-based synthetic precursors were used in combination with recombinant protein precursors equipped with an alkyne-containing Tyr derivative (OpgY) to generate macrocycles via a side-chain Cu(I)-catalyzed azide–alkyne cycloaddition followed by ring closure via hydrazide attack onto the intein thioester (Figure 7.10a) [118]. This cyclization strategy proved viable across variable target sequence lengths (4-mer to 12-mer) and structurally different phenyl/biphenyl-based synthetic precursors. In a subsequent study, a different class of MOrPH structures were obtained through a dual oxime/intein-mediated ligation using an oxyamino/1,3-aminothiol-aryl reagent and a biosynthetic precursor bearing a side-chain keto group provided by the UAA *p*-acetyl-Phe (pAcF; Figure 7.10b) [119]. This strategy permits the efficient and clean synthesis of organo-peptide macrocycles of varying size and composition, that is, encompassing 4–12 amino acid residues and structurally diverse non-peptidic moieties [120], and could be readily applied to produce MOrPH libraries with randomized peptide sequences [119]. The method was later further expanded to give access to structurally diverse hybrid molecules with a bicyclic backbone [122]. Using this methodology, MOrPH structures can be assembled as fused to the C-terminus of an arbitrary protein or peptide sequence, thus enabling the introduction of affinity tags for immobilization/detection of the macrocycles, as well as the integration of this cyclization strategy with display systems compatible with C-terminal fusion (e.g., yeast, bacterial, and T7 phage display) [123, 124].

The utility of MOrPHs as molecular scaffolds for the development of macrocyclic inhibitors of PPI was recently investigated by targeting the cancer-relevant interaction between tumor suppressor p53 and oncoproteins HDM2 and HDMX [106]. A small set of MOrPH-based mimics of p53 were prepared by constraining a linear HDM2-binding peptide by means of different non-peptidic linkers that would match the distance between the side chain of a solvent-exposed residue (i) and the C-terminal carboxy group of a residue at the $i + 6$ or $i + 10$ position [106]. The most potent compound was found to act as a dual inhibitor of HDM2 and HDMX oncoproteins with an IC_{50} of 110 nM and 340 nM, respectively. In addition, this macrocyclic peptide showed significantly enhanced (10-fold) half-life in the presence of proteases as compared with its acyclic counterpart. Interestingly, the non-peptidic moiety was found to have a significant influence in modulating the conformational properties of the macrocycles, as well as their HDM2/X isoform selectivity [106].

7.4.2 Synthesis of Macrocyclic Peptides in Living Cells

The methodologies discussed in the aforementioned sections all rely on the cyclization of peptide sequences by virtue of chemical modifications performed *in vitro* and/or through cyclization of *in vitro* translated peptide sequences. The capability of producing cyclic peptides directly in living cells offers unique advantages with respect to coupling library production with an intracellular reporter system [125, 126], a phenotypic screen [127], or a selection system [128–131], in which a desired activity is linked to survival of the cell. Accordingly, a number of strategies have been developed over the past few years for enabling the spontaneous posttranslational formation of cyclic peptide in cells.

A first enabling methodology useful for the production of cyclic peptides of arbitrary sequences in living cells is the split-intein circular ligation of peptides and proteins (SICLOPPS) method developed by Benkovic and coworkers [132]. Briefly, this method involves the insertion of a target peptide sequence between the C-terminal (In_C) and N-terminal (In_N) domain of a split intein (e.g., *Ssp* DnaE). Upon expression, the split-intein N- and C-terminal domain In_C and In_N domains undergo a transsplicing reaction, resulting in the release of a head-to-tail cyclic peptide encompassing the target sequence (Figure 7.11a) [132]. This method has been applied to the creation of cyclic peptide libraries in *E. coli* [132], yeast [127], or human cells [133] and coupled to genetic selection [128, 129, 131] or intracellular reporter systems [125, 126] to enable the discovery of cyclopeptide-based inhibitors for various protein and enzyme targets [134]. The scope and applications of this methodology are discussed in a more comprehensive manner in Chapter 8.

Fasan and coworkers recently introduced two alternative and complementary methods to direct the biosynthesis of macrocyclic peptides of arbitrary sequence in living cells [107, 135]. The first approach, which permits
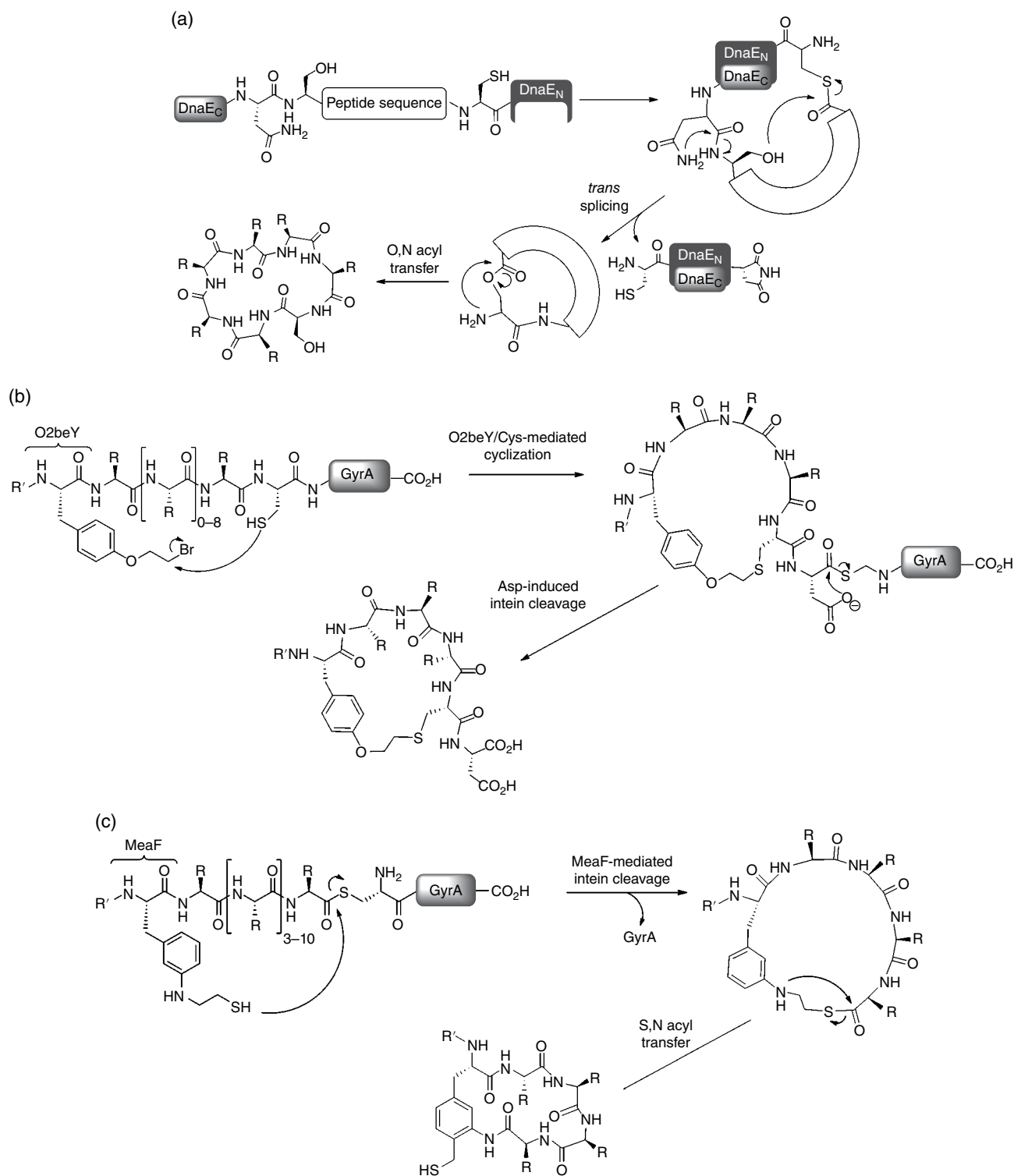
Figure 7.11 Strategies for the production of macrocyclic peptide libraries in living cells. (a) Overview of SICLOPPS method for production of head-to-tail cyclic peptides (see Chapter 8 for further details). (b) Overview of biomimetic method for intracellular synthesis of cyclic peptides constrained by an inter-side-chain thioether linkage. O2beY is incorporated into the precursor polypeptide via amber stop codon suppression using an engineered aminoacyl-tRNA synthetase and a cognate TAG suppressor tRNA. Upon expression of the polypeptide, spontaneous peptide cyclization occurs via reaction of O2beY with a neighboring cysteine (2–10 residues apart). Aspartate-mediated hydrolysis of the peptide–intein thioester linkage releases the cyclic peptide from the intein moiety. (c) Overview of MeaF-based method for directing the intracellular synthesis of side chain-to-tail cyclic peptides. The unnatural amino acid MeaF is incorporated into the precursor polypeptide via amber stop codon suppression. After ribosomal synthesis of the polypeptide, the macrocyclic peptide is formed via an intramolecular transthioesterification reaction involving MeaF side-chain aminothiol group and the C-terminal intein moiety, followed by an S,N-acyl rearrangement.

the creation of side chain-to-side chain cyclized peptides, hinges upon the use of an intein-fused precursor protein containing a genetically encoded UAA (*O*-2-bromoethyltyrosine (O2beY)) equipped with a cysteine-reactive electrophilic side-chain group (Figure 7.11b) [135]. Upon translation of the precursor protein in the cell, a spontaneous reaction between O2beY and a cysteine residue located upstream or downstream of an arbitrary target sequence gives rise to a macrocyclic structure constrained by an inter-side-chain thioether linkage. Concomitantly, aspartate-induced cleavage releases the macrocyclic peptide from the C-terminal intein moiety, whose function is to stabilize and facilitate the expression of the precursor protein. This strategy proved useful in mediating the efficient intracellular formation of cyclic peptides comprising 3–12 amino acids [135]. Furthermore, the efficiency of the cyclization reaction was found to be predictably dependent only upon the length of the intervening peptide sequence while being unaffected by its amino acid composition or by the relative orientation of the O2beY/Cys pair. Since the O2beY/Cys-mediated cyclization involves two side-chain functional groups, both the N-terminal and the C-terminal tail of the resulting macrocyclic peptide can be readily modified for the purpose of creating lariat-shaped peptides, fusing the cyclic peptide to an affinity tag peptide/protein, or integrating this cyclization strategy with any display system. In another application, O2beY/Cys-mediated peptide cyclization strategy was coupled to split-intein-catalyzed peptide circularization to enable the production of natural product-like bicyclic peptides featuring a head-to-tail cyclic backbone and an intramolecular thioether bond [108]. Upon incorporation of a streptavidin-binding motif (His-Pro-Gln) within the target peptide sequence, a bicyclic peptide with sub-micromolar affinity for streptavidin was obtained (IC$_{50}$ 0.77 μM; Table 7.2). The monocyclic head-to-tail cyclized counterpart showed a 2.5-fold reduced affinity for the protein, illustrating the beneficial effect of the additional conformational constraint provided by the intramolecular thioether bond [108].

A complementary methodology was recently developed to direct the intracellular synthesis of macrocyclic peptides featuring a side chain-to-tail cyclic backbone [107]. In this case, a genetically encodable Phe derivative equipped with a side-chain 1,2-aminothiol moiety (MeaF) was exploited to induce peptide cyclization (Figure 7.11c). Specifically, the MeaF residue promotes side chain-to-tail cyclization of the target peptide sequence via a trans-thioesterification reaction between the MeaF side-chain thiol group and the C-terminal intein thioester, a process accompanied by cleavage of the intein moiety. This step is followed by an irreversible intramolecular S-to-N acyl transfer, which results in a ring contraction and formation of a hydrolytically stable macrocyclic lactam. This approach proved effective in mediating the formation of medium to large peptide macrocycles (i.e., spanning 6–12 amino acid-long target sequences) in bacterial cells. Using MeaF-mediated cyclization, a library of cyclic 11-mer peptides comprising an HPQ streptavidin-binding motif and a partially randomized peptide sequence was generated in *E. coli*. Upon screening of the library using an ELISA-like functional assay and deconvolution of "hits" by DNA sequencing of the gene encoding for the corresponding precursor protein, a low micromolar binder (K_D 1.1 μM; Table 7.2) for the model target protein streptavidin was successfully isolated [107]. These results illustrate the utility of this approach toward the discovery of functional peptide macrocycles.

7.5 Comparative Analysis of Technologies

As discussed earlier, a number of complementary technologies have emerged over the course of the past 10–15 years to enable the combinatorial synthesis of conformationally constrained macrocyclic peptides derived from ribosomally produced polypeptides. Evolving (and departing) from the initial simplest concept of disulfide-bridged peptide libraries displayed on phage, these technologies have created new opportunities toward accessing different ring topologies (i.e., side chain-to-side chain, side chain-to-tail, side chain-to-tail, head-to-tail cyclic structures, bicyclic structures) and incorporating noncanonical amino acids, as well as non-peptidic elements, into the resulting macrocycles. With a growing number of applications of these methodologies appearing in the literature, it is possible and instructive to advance some general considerations regarding the relative advantages and shortcomings of these strategies as molecular discovery tools. It is clear that this picture is bound to evolve with time as knowledge is gained in this field, for example, as the newer strategies begin to be applied toward protein targets other than model systems and as more established technologies are tested in the context of a larger and more diverse panel of protein targets.

In terms of technical accessibility, the phage display disulfide-bridged peptide libraries and SICLOPPS libraries are undoubtedly the easiest to access and produce, since they rely on purely genetic methods. Commercial kits containing premade phage display libraries of disulfide-bridged peptides with fully randomized sequences are also available (e.g., New England Biolabs Ph.D.™-C7C library). Heinis and Winter's bicyclic peptide technology and Fasan's methodologies based on UAA-mediated peptide cyclization are also technically straightforward, as they require simple reagents that are

either commercially available or can be synthesized in few steps. The bifunctional reagents useful for the MOrPH cyclization methods typically require longer syntheses, but scalable and divergent routes for their preparation can be devised [120]. A technical challenge associated with the production of bicyclic peptide libraries on phage is the potential risk of reducing or abrogating the infectivity of the M13 phage particles during the cysteine alkylation process with the cross-linking reagent. The use of an M13 variant bearing a cysteine-free pIII coat protein was found to alleviate this problem [66], but the reaction conditions must be tightly controlled to avoid undesirable side reactions that lead to inactivation of the phage particles and, thus, their inability to be propagated during the biopanning process [75]. A potential approach to overcome this limitation involves the use of more chemoselective cysteine cross-linking agents such as 1,3-dichloroacetone [136], which was recently applied to assemble cyclic glycopeptides fused to the pIII protein of M13 bacteriophage [137].

Compared with the aforementioned strategies, the *in vitro* translation methods are more laborious, in part due to the requirement for reconstituting a translation system that typically consists of >30 proteins, enzymes, and nucleic acid components (e.g., AARS, translation factors, ribosome, etc.) [85], most of which must be expressed and purified individually. Compared with Suga's method, Szostak's approach is technically more facile in that the amino acid analogues that serve as the building blocks for the macrocyclic peptide library can be simply added to the reconstituted *in vitro* translation system without chemical modification. Drawbacks of this approach, however, are the potential cross-reactivity of the AARS toward the same amino acid analogue (i.e., different AARS mischarging the same UAA onto their cognate tRNA) [88] and/or competition from contaminant natural amino acids (e.g., in the translation system and/or commercial amino acids), both of which can lead to multiple undesired products during translation. These potential problems are largely addressed in Suga's FIT system, in which preformed aminoacylated tRNAs are added to an *in vitro* translation system lacking selected AARS enzymes. This method, on the other hand, requires the synthesis and isolation of each individual noncanonical amino acid building block used during library generation, first in the form of an activated ester for tRNA aminoacylation and then in the form conjugated to the tRNA molecule (Figure 7.9a). Although the development of broad specificity ribozymes (flexizymes) has facilitated the preparation of the desired aminoacylated tRNAs, the nature and quantity of the reagents involved in the FIT system make this approach significantly more demanding and laborious than any of the other methodologies.

The chemical space accessible through these technologies is another important aspect to consider, as structurally and functionally more diverse libraries of macrocycles are generally expected to bear a higher potential to yield promising hits for a given target protein or enzyme. In general, *in vitro* translation methods have enabled the creation and, in combination with mRNA display, the screening of molecular libraries of the largest size, typically comprising 10^{12}–10^{13} members. In the context of macrocyclic peptide libraries displayed on phage (e.g., disulfide-bridged and cysteine-cross-linked peptides) or produced via SICLOPPS and UAA-mediated cyclizations, factors related to the transformation efficiency of DNA material into bacterial cells limit the maximal achievable size of these libraries to about 10^9 members.

In terms of functional diversity, *in vitro* translation methods currently allow for the use of a broader range of UAA building blocks for library construction compared with other methods. Recent studies showed that approximately 100 amino acid analogues could be mischarged onto tRNAs using native AARS and that more than half of these structures could be incorporated into the translated peptide by the ribosomal machinery [88, 138]. In comparison, about 300 noncanonical amino acid structures have been introduced into polypeptides using the FIT system [81, 84]. Challenges facing both these methods include the decreasing yield of the desired peptide product as more noncanonical amino acids are incorporated into the translated peptide [88, 139]. Other problems relate to the incompatibility of certain types of noncanonical amino acids (e.g., D-, β-, and γ-amino acids) with peptide chain elongation at the ribosomal level [88, 140]. Strategies directed at addressing these issues have begun to emerge, for example, via codon optimization of the mRNA template [141] or using modified initiator tRNA^{Met} [140].

In addition to sequence diversity, an equally and perhaps even more important element of diversification relates to the possibility to generate diverse macrocyclic architectures as dictated by the cyclization strategy (i.e., head-to-tail vs. side chain-to-side chain cyclization) and/or the nature of the non-peptidic linkers involved in peptide cyclization (e.g., synthetic precursors in MOrPHs). Although different strategies have been reported for the cyclization of *in vitro* translated peptides produced through the FIT system [110–115], thus far, only the one involving cysteine alkylation via an N-terminal α-chloroacetamido group (Figure 7.9c) has been utilized for the construction and screening of combinatorial macrocycle libraries, possibly due to its higher reliability and/or compatibility with the *in vitro* translation system. The split-intein-mediated mechanism of peptide cyclization exploited in SICLOPPS gives access to macrocyclic peptides with a head-to-tail cyclized backbone [132].

In comparison, a broader range of macrocyclic structures including cyclic, lariat, and bicyclic topologies are accessible through peptide cyclization strategies involving genetically encodable UAA [107, 108, 135].

For methods that rely on chemical cross-linking of the peptide sequence (e.g., via Cys alkylation or amine coupling), an element of structural diversification derives from the specific reagent used for mediating the cross-linking process. For example, in addition to the originally introduced reagent TMTB [66], other cysteine-alkylating reagents, such as TATA and TBAB [142], have been successfully utilized for diversifying bicyclic peptide libraries displayed on phage. A factor limiting the choice of cross-linking reagents within these methodologies is the requirement that compounds possess either a two- or threefold rotational symmetry in order to avoid the formation of multiple regioisomers upon cyclization, which would complicate hit deconvolution, as well as post-screening synthesis of these hits for downstream analyses. In addition, certain cross-linking reagents simply do not exhibit sufficient levels of reactivity and/or chemoselectivity for use in the context of these methodologies [142]. In comparison, the use of two orthogonal bond-forming reactions during MOrPH synthesis allows for the application of a virtually unlimited range of linker structures to diversify the size and structure of the resulting hybrid macrocycles.

Finally, some general considerations can be made with respect to the relative success of the different methodologies in yielding binders and/or inhibitors for a given molecular target. It should be noted that these analyses are inherently influenced by several factors, including the time that these technologies have been available for, the differential efforts invested in each project, the modalities in which the screening processes are carried out, and, last but not least, an incomplete knowledge about failed experiments that typically remain unreported. Phage display libraries of disulfide-bridged peptide have generally provided a source of high- to moderate-affinity binders ($K_D \sim 0.1$–$10\,\mu$M; Table 7.1) for a broad range of targets including enzymes, protein hormones, and membrane receptors. Although low micromolar binders have been typically isolated from peptide libraries displayed on M13 pVIII coat protein, 10- to 100-fold improvements in binding affinity for the target receptor have been achieved through subsequent affinity maturation using a low-valency format, such as fusion to the pIII coat protein. Interestingly, cyclic peptides isolated through this method have exhibited a broad range of three-dimensional folds in their protein-bound form or free in solution (Figure 7.2), supporting the versatility of a simple disulfide linkage in stabilizing these structures. As noted earlier, however, an important shortcoming of these ligands lies in the chemical instability of the disulfide bond, which limits the utility of the compounds as probes and potential therapeutic agents. Isosteric or functional substitution of the disulfide linkage has provided a means to obtain nonreducible analogues of these compounds, although the peculiar conformational properties of the disulfide bond have imposed that this replacement strategy be optimized on a case-by-case basis [7, 58, 143, 144].

The screening of *in vitro* translated cyclic peptide libraries on mRNA display formats has often yielded ligands with very high affinity for the target receptor, typically exhibiting K_D values in the mid-low to low nanomolar range (1–100 nM; Table 7.2) [81]. This outcome has been attributed to the very large size of the molecular libraries that can be explored using these platforms. It should be noted, however, that the size of these ligands (10- to 15-mers; Table 7.2) is typically larger than those explored in the context of other systems, for example, phage display disulfide-bridged peptides (6- to 9-mers; Table 7.1). Whereas the larger size of the former ligands is likely to provide advantages in terms of target affinity (e.g., by facilitating more extensive ligand–receptor interactions), it could potentially complicate optimization of their drug-like properties for therapeutic applications. *In vitro* methodologies have permitted the creation of macrocyclic peptide libraries containing multiple noncanonical amino acids, although it is currently unclear whether this capability provided any distinct advantage during the hit identification process. Indeed, whenever libraries of cyclic peptides containing multiple UAA have been screened in parallel with those consisting of all natural amino acids, the latter have yielded equally or more efficient binders and inhibitors than the former [98, 100, 102, 103, 105]. Backbone modifications, in particular N-methylation and D-amino acid substitution, are, however, likely to confer macrocyclic peptides with enhanced resistance against proteolysis, as well as improve other desirable pharmacological properties. In this regard, proteolytically stable cyclic peptide ligands composed of all (D)-amino acids are accessible through mirror image phage display of disulfide-bridged peptide libraries [28, 40], and a similar strategy could be reasonably extended to other types of cyclization strategies and/or display system. A factor limiting the scope of this approach is related to the synthetic accessibility of the target protein in its D-enantiomeric form.

Heinis and Winter's technology based on bicyclic peptide libraries displayed on phage has enabled the discovery of potent ($K_i \sim 1$–100 nM) and selective inhibitors for a number of target enzymes. In this regard, it is interesting to note how certain enzymes (e.g., FXIIa) have posed a significantly greater barrier for the identification of high-affinity ($K_i < 100$ nM) bicyclic peptide inhibitors compared with other targets, such as uPA. Indeed, the

development of FXIIa inhibitors [69, 145] required the screening of a comparatively larger panel of bicyclic peptide libraries along with multiple rounds of affinity maturation as compared with uPA [67]. These results suggest that certain protein binding sites may be more amenable than others to recognition by these bicyclic peptide scaffolds. Initial attempts directed at extending the scope of this approach to nonenzymatic targets (e.g., Her2, Notch1, TNFα) have so far met with only partial success [70–72]. Despite the successful isolation of sub-micromolar binders for these proteins upon affinity maturation ($K_D \sim 100$–$300\,$nM), these compounds have failed to block the signaling function of the proteins. These results notwithstanding, it is reasonable to expect that upon modification of the selection conditions and/or optimization of currently identified ligands, compounds exhibiting also inhibitory activity may be found. The problem of identifying tight binders that are yet unable to inhibit the function of the enzyme or protein used as bait during the affinity selection process is actually quite common and often encountered also upon the screening of mRNA display cyclic peptide libraries [100, 105, 146]. In that regard, the ability of coupling the functional selection process with inhibition of the target enzyme [129, 131] or PPI [130, 147] provides a definitive advantage toward the identification of true inhibitors during the library screening process. This capability is offered, for example, by methodologies that allow for the creation of macrocyclic peptide libraries directly in cells, thus linking library screening with cell survival or a phenotypic readout as a result of the compound inhibitory activity on a target enzyme or biomolecular interaction. A potential challenge related to these systems though, in particular those based on selection, is that false positives can emerge as a result of the selective pressure, for example, through random genetic mutations within the host cell [126].

7.6 Conclusions

In conclusion, this chapter illustrates the significant progress made toward the development and application of platforms for the creation and screening of peptide-based macrocycles using purely biological or hybrid chemical/biological strategies. As discussed earlier, these methodologies offer several complementary advantages, which include the ability to access diverse macrocyclic structures and topologies, also incorporating non-proteinogenic or non-peptidic elements. Among others, this capability is expected to aid the discovery of potent and selective inhibitors (or activators) for a broad range of proteins and PPIs, which are inherently diverse in nature. Looking forward, a key outstanding challenge concerns the ability of these methodologies to deliver agents that can penetrate cells and access intracellular targets. Screening efforts involving phage display libraries of disulfide-bridged peptides and bicyclic peptides have mostly focused on extracellular targets. Potent inhibitors of intracellular enzymes have been isolated from mRNA-displayed macrocyclic peptide libraries, but the cell permeability properties of these molecules have not been investigated, at least in the published literature. Addressing this challenge, along with continuing to develop efficient and versatile platforms for macrocyclic ligand discovery, is anticipated to significantly aid the discovery and development of new classes of therapeutic agents for a variety of human diseases.

References

1 Driggers, E. M.; Hale, S. P.; Lee, J.; Terrett, N. K. The exploration of macrocycles for drug discovery—an underexploited structural class. *Nat. Rev. Drug Discov.* **2008**, *7*, 608–624.

2 Obrecht, D.; Robinson, J. A.; Bernardini, F.; Bisang, C.; DeMarco, S. J.; Moehle, K.; Gombert, F. O. Recent progress in the discovery of macrocyclic compounds as potential anti-infective therapeutics. *Curr. Med. Chem.* **2009**, *16*, 42–65.

3 Marsault, E.; Peterson, M. L. Macrocycles are great cycles: applications, opportunities, and challenges of synthetic macrocycles in drug discovery. *J. Med. Chem.* **2011**, *54*, 1961–2004.

4 Katsara, M.; Tselios, T.; Deraos, S.; Deraos, G.; Matsoukas, M. T.; Lazoura, E.; Matsoukas, J.; Apostolopoulos, V. Round and round we go: cyclic peptides in disease. *Curr. Med. Chem.* **2006**, *13*, 2221–2232.

5 Nolan, E. M.; Walsh, C. T. How nature morphs peptide scaffolds into antibiotics. *ChemBioChem* **2009**, *10*, 34–53.

6 Tang, Y. Q.; Yuan, J.; Osapay, G.; Osapay, K.; Tran, D.; Miller, C. J.; Ouellette, A. J.; Selsted, M. E. A cyclic antimicrobial peptide produced in primate leukocytes by the ligation of two truncated alpha-defensins. *Science* **1999**, *286*, 498–502.

7 Dias, R. L. A.; Fasan, R.; Moehle, K.; Renard, A.; Obrecht, D.; Robinson, J. A. Protein ligand design: from phage display to synthetic protein epitope mimetics in human antibody Fc-binding peptidomimetics. *J. Am. Chem. Soc.* **2006**, *128*, 2726–2732.

8 Henchey, L. K.; Porter, J. R.; Ghosh, I.; Arora, P. S. High specificity in protein recognition by hydrogen-bond-

surrogate alpha-helices: selective inhibition of the p53/MDM2 complex. *ChemBioChem* **2010**, *11*, 2104–2107.

9 Walensky, L. D.; Kung, A. L.; Escher, I.; Malia, T. J.; Barbuto, S.; Wright, R. D.; Wagner, G.; Verdine, G. L.; Korsmeyer, S. J. Activation of apoptosis in vivo by a hydrocarbon-stapled BH3 helix. *Science* **2004**, *305*, 1466–1470.

10 Rezai, T.; Bock, J. E.; Zhou, M. V.; Kalyanaraman, C.; Lokey, R. S.; Jacobson, M. P. Conformational flexibility, internal hydrogen bonding, and passive membrane permeability: successful in silico prediction of the relative permeabilities of cyclic peptides. *J. Am. Chem. Soc.* **2006**, *128*, 14073–14080.

11 Rezai, T.; Yu, B.; Millhauser, G. L.; Jacobson, M. P.; Lokey, R. S. Testing the conformational hypothesis of passive membrane permeability using synthetic cyclic peptide diastereomers. *J. Am. Chem. Soc.* **2006**, *128*, 2510–2511.

12 Fairlie, D. P.; Tyndall, J. D. A.; Reid, R. C.; Wong, A. K.; Abbenante, G.; Scanlon, M. J.; March, D. R.; Bergman, D. A.; Chai, C. L. L.; Burkett, B. A. Conformational selection of inhibitors and substrates by proteolytic enzymes: implications for drug design and polypeptide processing. *J. Med. Chem.* **2000**, *43*, 1271–1281.

13 Wang, D.; Liao, W.; Arora, P. S. Enhanced metabolic stability and protein-binding properties of artificial alpha helices derived from a hydrogen-bond surrogate: application to Bcl-xL. *Angew. Chem. Int. Ed. Engl.* **2005**, *44*, 6525–6529.

14 Scott, J. K.; Smith, G. P. Searching for peptide ligands with an epitope library. *Science* **1990**, *249*, 386–390.

15 Devlin, J. J.; Panganiban, L. C.; Devlin, P. E. Random peptide libraries: a source of specific protein binding molecules. *Science* **1990**, *249*, 404–406.

16 Smith, G. P.; Petrenko, V. A. Phage display. *Chem. Rev.* **1997**, *97*, 391–410.

17 Deshayes, K.; Schaffer, M. L.; Skelton, N. J.; Nakamura, G. R.; Kadkhodayan, S.; Sidhu, S. S. Rapid identification of small binding motifs with high-throughput phage display: discovery of peptidic antagonists of IGF-1 function. *Chem. Biol.* **2002**, *9*, 495–505.

18 Huang, L. L.; Sexton, D. J.; Skogerson, K.; Devlin, M.; Smith, R.; Sanyal, I.; Parry, T.; Kent, R.; Enright, J.; Wu, Q. L.; Conley, G.; DeOliveira, D.; Morganelli, L.; Ducar, M.; Wescott, C. R.; Ladner, R. C. Novel peptide inhibitors of angiotensin-converting enzyme 2. *J. Biol. Chem.* **2003**, *278*, 15532–15540.

19 Koivunen, E.; Gay, D. A.; Ruoslahti, E. Selection of peptides binding to the alpha-5-beta-1 integrin from phage display library. *J. Biol. Chem.* **1993**, *268*, 20205–20210.

20 Koivunen, E.; Wang, B.; Ruoslahti, E. Phage libraries displaying cyclic peptides with different ring sizes: ligand specificities of the RGD-directed integrins. *Biotechnology (NY)* **1995**, *13*, 265–270.

21 Shomin, C. D.; Restituyo, E.; Cox, K. J.; Ghosh, I. Selection of cyclic-peptide inhibitors targeting Aurora kinase A: problems and solutions. *Bioorg. Med. Chem.* **2011**, *19*, 6743–6749.

22 Houimel, M.; Mazzucchelli, L. hCXCR1 and hCXCR2 antagonists derived from combinatorial peptide libraries. *Cytokine* **2012**, *57*, 322–331.

23 Wrighton, N. C.; Farrell, F. X.; Chang, R.; Kashyap, A. K.; Barbone, F. P.; Mulcahy, L. S.; Johnson, D. L.; Barrett, R. W.; Jolliffe, L. K.; Dower, W. J. Small peptides as potent mimics of the protein hormone erythropoietin. *Science* **1996**, *458–463*.

24 Dennis, M. S.; Eigenbrot, C.; Skelton, N. J.; Ultsch, M. H.; Santell, L.; Dwyer, M. A.; O'Connell, M. P.; Lazarus, R. A. Peptide exosite inhibitors of factor VIIa as anticoagulants. *Nature* **2000**, *404*, 465–470.

25 Bonetto, S.; Spadola, L.; Buchanan, A. G.; Jermutus, L.; Lund, J. Identification of cyclic peptides able to mimic the functional epitope of IgG1-Fc for human Fc gammaRI. *FASEB J.* **2009**, *23*, 575–585.

26 Nakamura, G. R.; Starovasnik, M. A.; Reynolds, M. E.; Lowman, H. B. A novel family of hairpin peptides that inhibit IgE activity by binding to the high-affinity IgE receptor. *Biochemistry* **2001**, *40*, 9828–9835.

27 Nakamura, G. R.; Reynolds, M. E.; Chen, Y. M.; Starovasnik, M. A.; Lowman, H. B. Stable "zeta" peptides that act as potent antagonists of the high-affinity IgE receptor. *Proc. Natl. Acad. Sci. U. S. A* **2002**, *99*, 1303–1308.

28 Eckert, D. M.; Malashkevich, V. N.; Hong, L. H.; Carr, P. A.; Kim, P. S. Inhibiting HIV-1 entry: discovery of D-peptide inhibitors that target the gp41 coiled-coil pocket. *Cell* **1999**, *99*, 103–115.

29 Oligino, L.; Lung, F. D.; Sastry, L.; Bigelow, J.; Cao, T.; Curran, M.; Burke, T. R., Jr.; Wang, S.; Krag, D.; Roller, P. P.; King, C. R. Nonphosphorylated peptide ligands for the Grb2 Src homology 2 domain. *J. Biol. Chem.* **1997**, *272*, 29046–29052.

30 Pero, S. C.; Oligino, L.; Daly, R. J.; Soden, A. L.; Liu, C.; Roller, P. P.; Li, P.; Krag, D. N. Identification of novel non-phosphorylated ligands, which bind selectively to the SH2 domain of Grb7. *J. Biol. Chem.* **2002**, *277*, 11918–11926.

31 O'Neil, K. T.; Hoess, R. H.; Jackson, S. A.; Ramachandran, N. S.; Mousa, S. A.; Degrado, W. F. Identification of novel peptide antagonists for GpIIb/IIIa from a conformationally constrained phage peptide library. *Proteins* **1992**, *14*, 509–515.

32 Ho, K. L.; Yusoff, K.; Seow, H. F.; Tan, W. S. Selection of high affinity ligands to hepatitis B core antigen from a phage-displayed cyclic peptide library. *J. Med. Virol.* **2003**, *69*, 27–32.

33 Lowman, H. B.; Chen, Y. M.; Skelton, N. J.; Mortensen, D. L.; Tomlinson, E. E.; Sadick, M. D.; Robinson, I. C.;

Clark, R. G. Molecular mimics of insulin-like growth factor 1 (IGF-1) for inhibiting IGF-1: IGF-binding protein interactions. *Biochemistry* **1998**, *37*, 8870–8878.

34 DeLano, W. L.; Ultsch, M. H.; de Vos, A. M.; Wells, J. A. Convergent solutions to binding at a protein-protein interface. *Science* **2000**, *287*, 1279–1283.

35 Koivunen, E.; Arap, W.; Valtanen, H.; Rainisalo, A.; Medina, O. P.; Heikkila, P.; Kantor, C.; Gahmberg, C. G.; Salo, T.; Konttinen, Y. T.; Sorsa, T.; Ruoslahti, E.; Pasqualini, R. Tumor targeting with a selective gelatinase inhibitor. *Nat. Biotechnol.* **1999**, *17*, 768–774.

36 Duncan, K. E.; Dempsey, B. R.; Killip, L. E.; Adams, J.; Bailey, M. L.; Lajoie, G. A.; Litchfield, D. W.; Brandl, C. J.; Shaw, G. S.; Shilton, B. H. Discovery and characterization of a nonphosphorylated cyclic peptide inhibitor of the peptidylprolyl isomerase, Pin1. *J. Med. Chem.* **2011**, *54*, 3854–3865.

37 Wu, P.; Leinonen, J.; Koivunen, E.; Lankinen, H.; Stenman, U. H. Identification of novel prostate-specific antigen-binding peptides modulating its enzyme activity. *Eur. J. Biochem.* **2000**, *267*, 6212–6220.

38 Dennis, M. S.; Zhang, M.; Meng, Y. G.; Kadkhodayan, M.; Kirchhofer, D.; Combs, D.; Damico, L. A. Albumin binding as a general strategy for improving the pharmacokinetics of proteins. *J. Biol. Chem.* **2002**, *277*, 35035–35043.

39 Gee, S. H.; Sekely, S. A.; Lombardo, C.; Kurakin, A.; Froehner, S. C.; Kay, B. K. Cyclic peptides as non-carboxyl-terminal ligands of syntrophin PDZ domains. *J. Biol. Chem.* **1998**, *273*, 21980–21987.

40 Schumacher, T. N.; Mayr, L. M.; Minor, D. L., Jr.; Milhollen, M. A.; Burgess, M. W.; Kim, P. S. Identification of D-peptide ligands through mirror-image phage display. *Science* **1996**, *271*, 1854–1857.

41 Giebel, L. B.; Cass, R. T.; Milligan, D. L.; Young, D. C.; Arze, R.; Johnson, C. R. Screening of cyclic peptide phage libraries identifies ligands that bind streptavidin with high affinities. *Biochemistry* **1995**, *34*, 15430–15435.

42 Hansen, M.; Wind, T.; Blouse, G. E.; Christensen, A.; Petersen, H. H.; Kjelgaard, S.; Mathiasen, L.; Holtet, T. L.; Andreasen, P. A. A urokinase-type plasminogen activator-inhibiting cyclic peptide with an unusual P2 residue and an extended protease binding surface demonstrates new modalities for enzyme inhibition. *J. Biol. Chem.* **2005**, *280*, 38424–38437.

43 Fairbrother, W. J.; Christinger, H. W.; Cochran, A. G.; Fuh, G.; Keenan, C. J.; Quan, C.; Shriver, S. K.; Tom, J. Y.; Wells, J. A.; Cunningham, B. C. Novel peptides selected to bind vascular endothelial growth factor target the receptor-binding site. *Biochemistry* **1998**, *37*, 17754–17764.

44 Livnah, O.; Stura, E. A.; Johnson, D. L.; Middleton, S. A.; Mulcahy, L. S.; Wrighton, N. C.; Dower, W. J.; Jolliffe, L. K.; Wilson, I. A. Functional mimicry of a protein hormone by a peptide agonist: the EPO receptor complex at 2.8 Å. *Science* **1996**, 464–471.

45 Sidhu, S. S.; Lowman, H. B.; Cunningham, B. C.; Wells, J. A. Phage display for selection of novel binding peptides. *Methods Enzymol.* **2000**, *328*, 333–363.

46 Wiesmann, C.; Christinger, H. W.; Cochran, A. G.; Cunningham, B. C.; Fairbrother, W. J.; Keenan, C. J.; Meng, G.; de Vos, A. M. Crystal structure of the complex between VEGF and a receptor-blocking peptide. *Biochemistry* **1998**, *37*, 17765–17772.

47 Skelton, N. J.; Chen, Y. M.; Dubree, N.; Quan, C.; Jackson, D. Y.; Cochran, A.; Zobel, K.; Deshayes, K.; Baca, M.; Pisabarro, M. T.; Lowman, H. B. Structure-function analysis of a phage display-derived peptide that binds to insulin-like growth factor binding protein I. *Biochemistry* **2001**, *40*, 8487–8498.

48 Pan, B.; Li, B.; Russell, S. J.; Tom, J. Y.; Cochran, A. G.; Fairbrother, W. J. Solution structure of a phage-derived peptide antagonist in complex with vascular endothelial growth factor. *J. Mol. Biol.* **2002**, *316*, 769–787.

49 Hruby, V. J.; Li, G. G.; HaskellLuevano, C.; Shenderovich, M. Design of peptides, proteins, and peptidomimetics in chi space. *Biopolymers* **1997**, *43*, 219–266.

50 Hruby, V. J.; Balse, P. M. Conformational and topographical considerations in designing agonist peptidomimetics from peptide leads. *Curr. Med. Chem.* **2000**, *7*, 945–970.

51 Rudolf, M. P.; Vogel, M.; Kricek, F.; Ruf, C.; Zurcher, A. W.; Reuschel, R.; Auer, M.; Miescher, S.; Stadler, B. M. Epitope-specific antibody response to IgE by mimotope immunization. *J. Immunol.* **1998**, *160*, 3315–3321.

52 Kazmin, D. A.; Hoyt, T. R.; Taubner, L.; Teintze, M.; Starkey, J. R. Phage display mapping for peptide 11 sensitive sequences binding to laminin-1. *J. Mol. Biol.* **2000**, *298*, 431–445.

53 Ide, T.; Baik, S. H.; Matsuba, T.; Harayama, S. Identification by the phage-display technique of peptides that bind to H7 flagellin of *Escherichia coli*. *Biosci. Biotechnol. Biochem.* **2003**, *67*, 1335–1341.

54 Liu, M.; Li, C.; Pazgier, M.; Li, C. Q.; Mao, Y. B.; Lv, Y. F.; Gu, B.; Wei, G.; Yuan, W. R.; Zhan, C. Y.; Lu, W. Y.; Lu, W. Y. D-peptide inhibitors of the p53-MDM2 interaction for targeted molecular therapy of malignant neoplasms. *Proc. Natl. Acad. Sci. U. S. A* **2010**, *107*, 14321–14326.

55 Liu, M.; Pazgier, M.; Li, C. Q.; Yuan, W. R.; Li, C.; Lu, W. Y. A left-handed solution to peptide inhibition of the p53-MDM2 interaction. *Angew. Chem. Int. Ed. Engl.* **2010**, *49*, 3649–3652.

56 Lou, Y. C.; Lung, F. D.; Pai, M. T.; Tzeng, S. R.; Wei, S. Y.; Roller, P. P.; Cheng, J. W. Solution structure and

dynamics of G1TE, a nonphosphorylated cyclic peptide inhibitor for the Grb2 SH2 domain. *Arch. Biochem. Biophys.* **1999**, *372*, 309–314.

57 Rahuel, J.; Gay, B.; Erdmann, D.; Strauss, A.; GarciaEcheverria, C.; Furet, P.; Caravatti, G.; Fretz, H.; Schoepfer, J.; Grutter, M. G. Structural basis for specificity of GRB2-SH2 revealed by a novel ligand binding mode. *Nat. Struct. Biol.* **1996**, *3*, 586–589.

58 Long, Y. Q.; Lung, F. D.; Roller, P. P. Global optimization of conformational constraint on non-phosphorylated cyclic peptide antagonists of the Grb2-SH2 domain. *Bioorg. Med. Chem.* **2003**, *11*, 3929–3936.

59 Song, Y. L.; Peach, M. L.; Roller, P. P.; Qiu, S.; Wang, S.; Long, Y. Q. Discovery of a novel nonphosphorylated pentapeptide motif displaying high affinity for Grb2-SH2 domain by the utilization of 3'-substituted tyrosine derivatives. *J. Med. Chem.* **2006**, *49*, 1585–1596.

60 Jiang, S.; Li, P.; Peach, M. L.; Bindu, L.; Worthy, K. W.; Fisher, R. J.; Burke, T. R., Jr.; Nicklaus, M.; Roller, P. P. Structure-based design of potent Grb2-SH2 domain antagonists not relying on phosphotyrosine mimics. *Biochem. Biophys. Res. Commun.* **2006**, *349*, 497–503.

61 Quartararo, J. S.; Wu, P.; Kritzer, J. A. Peptide bicycles that inhibit the Grb2 SH2 domain. *ChemBioChem* **2012**, *13*, 1490–1496.

62 Quartararo, J. S.; Eshelman, M. R.; Peraro, L.; Yu, H.; Baleja, J. D.; Lin, Y. S.; Kritzer, J. A. A bicyclic peptide scaffold promotes phosphotyrosine mimicry and cellular uptake. *Bioorg. Med. Chem.* **2014**, *22*, 6387–6391.

63 Jiang, S.; Liao, C.; Bindu, L.; Yin, B.; Worthy, K. W.; Fisher, R. J.; Burke, T. R., Jr.; Nicklaus, M. C.; Roller, P. P. Discovery of thioether-bridged cyclic pentapeptides binding to Grb2-SH2 domain with high affinity. *Bioorg. Med. Chem. Lett.* **2009**, *19*, 2693–2698.

64 Obrecht, D.; Chevalier, E.; Moehle, K.; Robinson, J. A. β-Hairpin protein epitope mimetic technology in drug discovery. *Drug Discov. Today* **2012**, *9*, e63–e69.

65 Timmerman, P.; Beld, J.; Puijk, W. C.; Meloen, R. H. Rapid and quantitative cyclization of multiple peptide loops onto synthetic scaffolds for structural mimicry of protein surfaces. *ChemBioChem* **2005**, *6*, 821–824.

66 Heinis, C.; Rutherford, T.; Freund, S.; Winter, G. Phage-encoded combinatorial chemical libraries based on bicyclic peptides. *Nat. Chem. Biol.* **2009**, *5*, 502–507.

67 Angelini, A.; Cendron, L.; Chen, S. Y.; Touati, J.; Winter, G.; Zanotti, G.; Heinis, C. Bicyclic peptide inhibitor reveals large contact interface with a protease target. *ACS Chem. Biol.* **2012**, *7*, 817–821.

68 Rebollo, I. R.; Angelini, A.; Heinis, C. Phage display libraries of differently sized bicyclic peptides. *MedChemComm* **2013**, *4*, 145–150.

69 Baeriswyl, V.; Calzavarini, S.; Chen, S. Y.; Zorzi, A.; Bologna, L.; Angelillo-Scherrer, A.; Heinis, C. A synthetic factor XIIa inhibitor blocks selectively intrinsic coagulation initiation. *ACS Chem. Biol.* **2015**, *10*, 1861–1870.

70 Diderich, P.; Heinis, C. Phage selection of bicyclic peptides binding Her2. *Tetrahedron* **2014**, *70*, 7733–7739.

71 Urech-Varenne, C.; Radtke, F.; Heinis, C. Phage selection of bicyclic peptide ligands of the Notch1 receptor. *ChemMedChem* **2015**, *10*, 1754–1761.

72 Luzi, S.; Kondo, Y.; Bernard, E.; Stadler, L. K. J.; Vaysburd, M.; Winter, G.; Holliger, P. Subunit disassembly and inhibition of TNF alpha by a semi-synthetic bicyclic peptide. *Protein Eng. Des. Sel.* **2015**, *28*, 45–52.

73 Zhao, G.; Yuan, C.; Wind, T.; Huang, Z.; Andreasen, P. A.; Huang, M. Structural basis of specificity of a peptidyl urokinase inhibitor, upain-1. *J. Struct. Biol.* **2007**, *160*, 1–10.

74 Chen, S. Y.; Bertoldo, D.; Angelini, A.; Pojer, F.; Heinis, C. Peptide ligands stabilized by small molecules. *Angew. Chem. Int. Ed. Engl.* **2014**, *53*, 1602–1606.

75 Chen, S. Y.; Rebollo, I. R.; Buth, S. A.; Morales-Sanfrutos, J.; Touati, J.; Leiman, P. G.; Heinis, C. Bicyclic peptide ligands pulled out of cysteine-rich peptide libraries. *J. Am. Chem. Soc.* **2013**, *135*, 6562–6569.

76 Roodbeen, R.; Paaske, B.; Jiang, L. G.; Jensen, J. K.; Christensen, A.; Nielsen, J. T.; Huang, M. D.; Mulder, F. A. A.; Nielsen, N. C.; Andreasen, P. A.; Jensen, K. J. Bicyclic peptide inhibitor of urokinase-type plasminogen activator: mode of action. *ChemBioChem* **2013**, *14*, 2179–2188.

77 Angelini, A.; Morales-Sanfrutos, J.; Diderich, P.; Chen, S. Y.; Heinis, C. Bicyclization and tethering to albumin yields long-acting peptide antagonists. *J. Med. Chem.* **2012**, *55*, 10187–10197.

78 Chen, S. Y.; Gfeller, D.; Buth, S. A.; Michielin, O.; Leiman, P. G.; Heinis, C. Improving binding affinity and stability of peptide ligands by substituting glycines with D-amino acids. *ChemBioChem* **2013**, *14*, 1316–1322.

79 Nguyen, A.; Reyes, A. E.; Zhang, M.; McDonald, P.; Wong, W. L. T.; Damico, L. A.; Dennis, M. S. The pharmacokinetics of an albumin-binding Fab (AB.Fab) can be modulated as a function of affinity for albumin. *Protein Eng. Des. Sel.* **2006**, *19*, 291–297.

80 Langenheim, J. F.; Chen, W. Y. Improving the pharmacokinetics/pharmacodynamics of prolactin, GH, and their antagonists by fusion to a synthetic albumin-binding peptide. *J. Endocrinol.* **2009**, *203*, 375–387.

81 Passioura, T.; Katoh, T.; Goto, Y.; Suga, H. Selection-based discovery of drug-like macrocyclic peptides. *Ann. Rev. Biochem.* **2014**, *83*, 727–752.

82 Roberts, R. W.; Szostak, J. W. RNA-peptide fusions for the in vitro selection of peptides and proteins. *Proc. Natl. Acad. Sci. U. S. A* **1997**, *94*, 12297–12302.

83 Takahashi, T. T.; Austin, R. J.; Roberts, R. W. mRNA display: ligand discovery, interaction analysis and beyond. *Trends Biochem. Sci.* **2003**, *28*, 159–165.

84 Rogers, J. M.; Suga, H. Discovering functional, non-proteinogenic amino acid containing, peptides using genetic code reprogramming. *Org. Biomol. Chem.* **2015**, *13*, 9353–9363.

85 Shimizu, Y.; Inoue, A.; Tomari, Y.; Suzuki, T.; Yokogawa, T.; Nishikawa, K.; Ueda, T. Cell-free translation reconstituted with purified components. *Nat. Biotechnol.* **2001**, *19*, 751–755.

86 Forster, A. C.; Weissbach, H.; Blacklow, S. C. A simplified reconstitution of mRNA-directed peptide synthesis: activity of the epsilon enhancer and an unnatural amino acid. *Anal. Biochem.* **2001**, *297*, 60–70.

87 Josephson, K.; Hartman, M. C.; Szostak, J. W. Ribosomal synthesis of unnatural peptides. *J. Am. Chem. Soc.* **2005**, *127*, 11727–11735.

88 Hartman, M. C.; Josephson, K.; Lin, C. W.; Szostak, J. W. An expanded set of amino acid analogs for the ribosomal translation of unnatural peptides. *PLoS One* **2007**, *2*, e972.

89 Hortin, G.; Boime, I. Applications of amino-acid-analogs for studying co-translational and posttranslational modifications of proteins. *Methods Enzymol.* **1983**, *96*, 777–784.

90 Wilson, M. J.; Hatfield, D. L. Incorporation of modified amino-acids into proteins in vivo. *Biochim. Biophys. Acta* **1984**, *781*, 205–215.

91 Budisa, N.; Minks, C.; Alefelder, S.; Wenger, W.; Dong, F. M.; Moroder, L.; Huber, R. Toward the experimental codon reassignment in vivo: protein building with an expanded amino acid repertoire. *FASEB J.* **1999**, *13*, 41–51.

92 Forster, A. C.; Tan, Z.; Nalam, M. N.; Lin, H.; Qu, H.; Cornish, V. W.; Blacklow, S. C. Programming peptidomimetic syntheses by translating genetic codes designed de novo. *Proc. Natl. Acad. Sci. U. S. A* **2003**, *100*, 6353–6357.

93 Murakami, H.; Saito, H.; Suga, H. A versatile tRNA aminoacylation catalyst based on RNA. *Chem. Biol.* **2003**, *10*, 655–662.

94 Murakami, H.; Ohta, A.; Ashigai, H.; Suga, H. A highly flexible tRNA acylation method for non-natural polypeptide synthesis. *Nat. Methods* **2006**, *3*, 357–359.

95 Millward, S. W.; Takahashi, T. T.; Roberts, R. W. A general route for post-translational cyclization of mRNA display libraries. *J. Am. Chem. Soc.* **2005**, *127*, 14142–14143.

96 Millward, S. W.; Fiacco, S.; Austin, R. J.; Roberts, R. W. Design of cyclic peptides that bind protein surfaces with antibody-like affinity. *ACS Chem. Biol.* **2007**, *2*, 625–634.

97 Howell, S. M.; Fiacco, S. V.; Takahashi, T. T.; Jalali-Yazdi, F.; Millward, S. W.; Hu, B. L.; Wang, P.; Roberts, R. W. Serum stable natural peptides designed by mRNA display. *Sci. Rep.* **2014**, *4*, 6008.

98 Schlippe, Y. V.; Hartman, M. C.; Josephson, K.; Szostak, J. W. In vitro selection of highly modified cyclic peptides that act as tight binding inhibitors. *J. Am. Chem. Soc.* **2012**, *134*, 10469–10477.

99 Seebeck, F. P.; Ricardo, A.; Szostak, J. W. Artificial lantipeptides from in vitro translations. *Chem. Commun. (Camb.)* **2011**, *47*, 6141–6143.

100 Hayashi, Y.; Morimoto, J.; Suga, H. In vitro selection of anti-Akt2 thioether-macrocyclic peptides leading to isoform-selective inhibitors. *ACS Chem. Biol.* **2012**, *7*, 607–613.

101 Yamagishi, Y.; Shoji, I.; Miyagawa, S.; Kawakami, T.; Katoh, T.; Goto, Y.; Suga, H. Natural product-like macrocyclic N-methyl-peptide inhibitors against a ubiquitin ligase uncovered from a ribosome-expressed de novo library. *Chem. Biol.* **2011**, *18*, 1562–1570.

102 Morimoto, J.; Hayashi, Y.; Suga, H. Discovery of macrocyclic peptides armed with a mechanism-based warhead: isoform-selective inhibition of human deacetylase SIRT2. *Angew. Chem. Int. Ed. Engl.* **2012**, *51*, 3423–3427.

103 Ito, K.; Sakai, K.; Suzuki, Y.; Ozawa, N.; Hatta, T.; Natsume, T.; Matsumoto, K.; Suga, H. Artificial human Met agonists based on macrocycle scaffolds. *Nat. Commun.* **2015**, *6*, 6373–6376.

104 Ishizawa, T.; Kawakami, T.; Reid, P. C.; Murakami, H. TRAP display: a high-speed selection method for the generation of functional polypeptides. *J. Am. Chem. Soc.* **2013**, *135*, 5433–5440.

105 Kawakami, T.; Ishizawa, T.; Fujino, T.; Reid, P. C.; Suga, H.; Murakami, H. In vitro selection of multiple libraries created by genetic code reprogramming to discover macrocyclic peptides that antagonize VEGFR2 activity in living cells. *ACS Chem. Biol.* **2013**, *8*, 1205–1214.

106 Smith, J. M.; Frost, J. R.; Fasan, R. Designer macrocyclic organo-peptide hybrids inhibit the interaction between p53 and HDM2/X by accommodating a functional α-helix. *Chem. Commun. (Camb.)* **2014**, *50*, 5027–5030.

107 Frost, J. R.; Jacob, N. T.; Papa, L. J.; Owens, A. E.; Fasan, R. Ribosomal synthesis of macrocyclic peptides in vitro and in vivo mediated by genetically encoded aminothiol unnatural amino acids. *ACS Chem. Biol.* **2015**, *10*, 1805–1816.

108 Bionda, N.; Fasan, R. Ribosomal synthesis of natural-product-like bicyclic peptides in *Escherichia coli*. *ChemBioChem* **2015**, *16*, 2011–2016.

109 Hipolito, C. J.; Suga, H. Ribosomal production and in vitro selection of natural product-like peptidomimetics: the FIT and RaPID systems. *Curr. Opin. Chem. Biol.* **2012**, *16*, 196–203.

110 Sako, Y.; Goto, Y.; Murakami, H.; Suga, H. Ribosomal synthesis of peptidase-resistant peptides closed by a nonreducible inter-side-chain bond. *ACS Chem. Biol.* **2008**, *3*, 241–249.

111 Sako, Y.; Morimoto, J.; Murakami, H.; Suga, H. Ribosomal synthesis of bicyclic peptides via two orthogonal inter-side-chain reactions. *J. Am. Chem. Soc.* **2008**, *130*, 7232–7234.

112 Kawakami, T.; Ohta, A.; Ohuchi, M.; Ashigai, H.; Murakami, H.; Suga, H. Diverse backbone-cyclized peptides via codon reprogramming. *Nat. Chem. Biol.* **2009**, *5*, 888–890.

113 Yamagishi, Y.; Ashigai, H.; Goto, Y.; Murakami, H.; Suga, H. Ribosomal synthesis of cyclic peptides with a fluorogenic oxidative coupling reaction. *ChemBioChem* **2009**, *10*, 1469–1472.

114 Goto, Y.; Iwasaki, K.; Torikai, K.; Murakami, H.; Suga, H. Ribosomal synthesis of dehydrobutyrine- and methyllanthionine-containing peptides. *Chem. Commun. (Camb.)* **2009**, 3419–3421.

115 Kang, T. J.; Hayashi, Y.; Suga, H. Synthesis of the backbone cyclic peptide sunflower trypsin inhibitor-1 promoted by the induced peptidyl-tRNA drop-off. *Angew. Chem. Int. Ed. Engl.* **2011**, *50*, 2159–2161.

116 Goto, Y.; Ohta, A.; Sako, Y.; Yamagishi, Y.; Murakami, H.; Suga, H. Reprogramming the translation initiation for the synthesis of physiologically stable cyclic peptides. *ACS Chem. Biol.* **2008**, *3*, 120–129.

117 Yamagata, K.; Goto, Y.; Nishimasu, H.; Morimoto, J.; Ishitani, R.; Dohmae, N.; Takeda, N.; Nagai, R.; Komuro, I.; Suga, H.; Nureki, O. Structural basis for potent inhibition of SIRT2 deacetylase by a macrocyclic peptide inducing dynamic structural change. *Structure* **2014**, *22*, 345–352.

118 Smith, J. M.; Vitali, F.; Archer, S. A.; Fasan, R. Modular assembly of macrocyclic organo-peptide hybrids using synthetic and genetically encoded precursors. *Angew. Chem. Int. Ed. Engl.* **2011**, *50*, 5075–5080.

119 Satyanarayana, M.; Vitali, F.; Frost, J. R.; Fasan, R. Diverse organo-peptide macrocycles via a fast and catalyst-free oxime/intein-mediated dual ligation. *Chem. Commun. (Camb.)* **2012**, *48*, 1461–1463.

120 Frost, J. R.; Vitali, F.; Jacob, N. T.; Brown, M. D.; Fasan, R. Macrocyclization of organo-peptide hybrids through a dual bio-orthogonal ligation: insights from structure-reactivity studies. *ChemBioChem* **2013**, *14*, 147–160.

121 Liu, C. C.; Schultz, P. G. Adding new chemistries to the genetic code. *Annu. Rev. Biochem.* **2010**, *79*, 413–444.

122 Smith, J. M.; Hill, N. C.; Krasniak, P. J.; Fasan, R. Synthesis of bicyclic organo-peptide hybrids via oxime/intein-mediated macrocyclization followed by disulfide bond formation. *Org. Biomol. Chem.* **2014**, *12*, 1135–1142.

123 Sergeeva, A.; Kolonin, M. G.; Molldrem, J. J.; Pasqualini, R.; Arap, W. Display technologies: application for the discovery of drug and gene delivery agents. *Adv. Drug Deliv. Rev.* **2006**, *58*, 1622–1654.

124 Lofblom, J. Bacterial display in combinatorial protein engineering. *Biotechnol. J.* **2011**, *6*, 1115–1129.

125 Cheng, L.; Naumann, T. A.; Horswill, A. R.; Hong, S. J.; Venters, B. J.; Tomsho, J. W.; Benkovic, S. J.; Keiler, K. C. Discovery of antibacterial cyclic peptides that inhibit the ClpXP protease. *Protein Sci.* **2007**, *16*, 1535–1542.

126 Nordgren, I. K.; Tavassoli, A. A bidirectional fluorescent two-hybrid system for monitoring protein-protein interactions. *Mol. Biosyst.* **2014**, *10*, 485–490.

127 Kritzer, J. A.; Hamamichi, S.; McCaffery, J. M.; Santagata, S.; Naumann, T. A.; Caldwell, K. A.; Caldwell, G. A.; Lindquist, S. Rapid selection of cyclic peptides that reduce alpha-synuclein toxicity in yeast and animal models. *Nat. Chem. Biol.* **2009**, *5*, 655–663.

128 Horswill, A. R.; Savinov, S. N.; Benkovic, S. J. A systematic method for identifying small-molecule modulators of protein-protein interactions. *Proc. Natl. Acad. Sci. U. S. A* **2004**, *101*, 15591–15596.

129 Naumann, T. A.; Tavassoli, A.; Benkovic, S. J. Genetic selection of cyclic peptide Dam methyltransferase inhibitors. *ChemBioChem* **2008**, *9*, 194–197.

130 Tavassoli, A.; Lu, Q.; Gam, J.; Pan, H.; Benkovic, S. J.; Cohen, S. N. Inhibition of HIV budding by a genetically selected cyclic peptide targeting the Gag-TSG101 interaction. *ACS Chem. Biol.* **2008**, *3*, 757–764.

131 Young, T. S.; Young, D. D.; Ahmad, I.; Louis, J. M.; Benkovic, S. J.; Schultz, P. G. Evolution of cyclic peptide protease inhibitors. *Proc. Natl. Acad. Sci. U. S. A* **2011**, *108*, 11052–11056.

132 Scott, C. P.; Abel-Santos, E.; Wall, M.; Wahnon, D. C.; Benkovic, S. J. Production of cyclic peptides and proteins in vivo. *Proc. Natl. Acad. Sci. U. S. A* **1999**, *96*, 13638–13643.

133 Kinsella, T. M.; Ohashi, C. T.; Harder, A. G.; Yam, G. C.; Li, W.; Peelle, B.; Pali, E. S.; Bennett, M. K.; Molineaux, S. M.; Anderson, D. A.; Masuda, E. S.; Payan, D. G. Retrovirally delivered random cyclic peptide libraries yield inhibitors of interleukin-4 signaling in human B cells. *J. Biol. Chem.* **2002**, *277*, 37512–37518.

134 Lennard, K. R.; Tavassoli, A. Peptides come round: using SICLOPPS libraries for early stage drug discovery. *Chem. Eur. J.* **2014**, *20*, 10608–10614.

135 Bionda, N.; Cryan, A. L.; Fasan, R. Bioinspired strategy for the ribosomal synthesis of thioether-bridged macrocyclic peptides in bacteria. *ACS Chem. Biol.* **2014**, *9*, 2008–2013.

136 Assem, N.; Ferreira, D. J.; Wolan, D. W.; Dawson, P. E. Acetone-linked peptides: a convergent approach for peptide macrocyclization and labeling. *Angew. Chem. Int. Ed. Engl.* **2015**, *54*, 8665–8668.

137 Ng, S.; Lin, E.; Kitov, P. I.; Tjhung, K. F.; Gerlits, O. O.; Deng, L.; Kasper, B.; Sood, A.; Paschal, B. M.; Zhang, P.; Ling, C. C.; Klassen, J. S.; Noren, C. J.; Mahal, L. K.; Woods, R. J.; Coates, L.; Derda, R. Genetically encoded fragment-based discovery of glycopeptide ligands for carbohydrate-binding proteins. *J. Am. Chem. Soc.* **2015**, *137*, 5248–5251.

138 Hartman, M. C.; Josephson, K.; Szostak, J. W. Enzymatic aminoacylation of tRNA with unnatural amino acids. *Proc. Natl. Acad. Sci. U. S. A* **2006**, *103*, 4356–4361.

139 Kawakami, T.; Murakami, H.; Suga, H. Ribosomal synthesis of polypeptoids and peptoid-peptide hybrids. *J. Am. Chem. Soc.* **2008**, *130*, 16861–16863.

140 Ohshiro, Y.; Nakajima, E.; Goto, Y.; Fuse, S.; Takahashi, T.; Doi, T.; Suga, H. Ribosomal synthesis of backbone-macrocyclic peptides containing gamma-amino acids. *ChemBioChem* **2011**, *12*, 1183–1187.

141 Subtelny, A. O.; Hartman, M. C.; Szostak, J. W. Optimal codon choice can improve the efficiency and fidelity of N-methyl amino acid incorporation into peptides by in-vitro translation. *Angew. Chem. Int. Ed. Engl.* **2011**, *50*, 3164–3167.

142 Chen, S.; Morales-Sanfrutos, J.; Angelini, A.; Cutting, B.; Heinis, C. Structurally diverse cyclisation linkers impose different backbone conformations in bicyclic peptides. *ChemBioChem* **2012**, *13*, 1032–1038.

143 Foister, S.; Taylor, L. L.; Feng, J. J.; Chen, W. L.; Lin, A.; Cheng, F. C.; Smith, A. B.; Hirschmann, R. Design and synthesis of potent cystine-free cyclic hexapeptide agonists at the human urotensin receptor. *Org. Lett.* **2006**, *8*, 1799–1802.

144 Empting, M.; Avrutina, O.; Meusinger, R.; Fabritz, S.; Reinwarth, M.; Biesalski, M.; Voigt, S.; Buntkowsky, G.; Kolmar, H. "Triazole Bridge": disulfide-bond replacement by ruthenium-catalyzed formation of 1,5-disubstituted 1,2,3-triazoles. *Angew. Chem. Int. Ed. Engl.* **2011**, *50*, 5207–5211.

145 Baeriswyl, V.; Calzavarini, S.; Gerschheimer, C.; Diderich, P.; Angelillo-Scherrer, A.; Heinis, C. Development of a selective peptide macrocycle inhibitor of coagulation factor XII toward the generation of a safe antithrombotic therapy. *J. Med. Chem.* **2013**, *56*, 3742–3746.

146 Hofmann, F. T.; Szostak, J. W.; Seebeck, F. P. In vitro selection of functional lantipeptides. *J. Am. Chem. Soc.* **2012**, *134*, 8038–8041.

147 Miranda, E.; Nordgren, I. K.; Male, A. L.; Lawrence, C. E.; Hoakwie, F.; Cuda, F.; Court, W.; Fox, K. R.; Townsend, P. A.; Packham, G. K.; Eccles, S. A.; Tavassoli, A. A cyclic peptide inhibitor of HIF-1 heterodimerization that inhibits hypoxia signaling in cancer cells. *J. Am. Chem. Soc.* **2013**, *135*, 10418–10425.

8

Macrocycles for Protein–Protein Interactions

Eilidh Leitch and Ali Tavassoli

Department of Chemistry, University of Southampton, Southampton, UK

8.1 Introduction

Over the past two decades, significant advances in understanding the nature and significance of protein–protein interactions (PPIs) have been made. The diverse and complex network of PPIs is integral to all biological processes, with an extraordinary physiological regulatory impact [1–3]. As a result, PPIs are an important class of pharmacological targets that have proven challenging to successfully modulate therapeutically. Targeting PPIs using traditional approaches has proven unsuccessful; indeed, traditional drug discovery tends to focus on uncovering small molecules that target binding grooves and pockets, for example, those present on targets with naturally occurring small molecule-like binding partners (G protein-coupled receptors (GPCRs), enzymes, hormone receptors, ion channels, etc.). The presence of a natural binding site and small molecule-like binding partner provides an excellent scaffold from which a traditional small molecule modulator can be developed. The therapeutic modulation of PPIs poses an altogether different challenge, mainly due to the large interaction interfaces of PPIs, typically approximately 1500–3000 Å^2 [4, 5]. Many PPI interfaces also tend to be flat and featureless, lacking obvious binding pockets and grooves that are present on target surfaces that bind small molecules [6]. Additionally, the amino acid residues that form the protein dimer interface can present distant epitopes, that is, be noncontiguous in the polypeptide sequence, making it difficult for small polypeptides consisting of these residues to provide a chemical starting point for development. An exception to the previously mentioned statement is the growing class of stapled peptides and structural mimetics [7]. Here, the aim is to mimic the structure of the binding partner with the hope of also mirroring the biological activity.

Alanine scanning mutagenesis is a widely used technique whereby residues of a target protein are systematically substituted for alanine; the use of alanine in this manner eliminates side chain interactions while maintaining stereochemistry and backbone conformation of the protein. With the application of this technique at the protein interaction interface, it has been revealed that there is an uneven distribution of individual residues contributing to the free energy of binding [8]. A few key residues were found to contribute the majority of free energy to the interface; these residues are known as "hot spots." Hot spots are defined as sites where alanine replacement causes an increase in binding free energy by at least 2.0 kcal mol^{-1}. A statistical analysis of the Thorn and Bogan database of the calculated effects of alanine mutations on the free energy of binding in protein interactions [9] has determined that an average of 9.5% of interfacial residues of the total protein surface may be characterized as hot spots [10]. A hot spot can be specific or promiscuous, allowing the protein to bind to multiple protein partners. Theoretically, one may inhibit a given PPI using molecules that specifically bind to a hot spot, competing with its natural binding partner.

Due to the inherently difficult nature of PPI interfaces as targets, increasing attention has been paid to the investigation of compounds that fall outside the normal definition of "drug-likeness." Providing general guidelines for this definition, Christopher Lipinski laid down what is known as the rule of five, after having analyzed over 2000 drugs and candidates in clinical trials [11]. Turning to nature however, there are several examples of naturally occurring compounds that break this rule of five, showing that drug-likeness, that is, solubility, lipophilicity, metabolic stability, and oral bioavailability, can be achieved outside of these guidelines. These are increasingly termed the beyond rule of 5 (Bro5) compounds [12] (see Chapter 3 for a discussion on permeability).

Many natural products that have evolved to interact with proteins are macrocycles, fitting a chemical space

that spans the region between small molecules and biologics (see also Chapter 4) [13]. Macrocyclization provides several potential advantages: for example, introduction of a ring structure restricts conformational freedom of a molecule compared with its linear counterpart, potentially increasing affinity for a target. In addition to the enforced rigidity in a structure [14], cyclization of peptides, in particular, provides protection against proteolytic degradation, enabling longer half-lives in comparison with linear peptides [15]. Due to these attributes, macrocycles are increasingly considered the ideal scaffold with which to target PPIs, potentially providing an optimal backbone from which novel therapeutics can be developed and built. As a result, there have been several methodological advances for the preparation of large libraries of macrocyclic molecules (see Chapters 6 and 7).

8.2 Library Approaches to Macrocyclic PPI Inhibitors

Chemical and biological methods have been developed for the preparation of cyclic peptide libraries, with several used for the specific purpose of targeting PPIs [16] (see Chapter 7 for a review of biological and chemi-biological methods for macrocycle library synthesis). Taking a genetically encoded approach to the production of cyclic peptide libraries, the Tavassoli group has been successful in generating libraries of approximately 100 million members utilizing a method termed split-intein circular ligation of peptides and proteins (SICLOPPS) [17]. The generation of SICLOPPS libraries relies solely on standard molecular biology techniques and is therefore relatively straightforward. As a result, SICLOPPS has been utilized by a number of groups for the identification of PPI inhibitors [18]. A second method for the generation of macrocyclic peptide libraries involves the utilization of a promiscuous transfer ribonucleic acid (tRNA) acylation ribozyme, known as a flexizyme. Flexizymes hold the capacity to charge noncanonical amino acids onto tRNAs, which are then used in the production of polypeptides in a manually reconstituted *in vitro* transcription/translation system. The genetic reprogramming system is integrated with an messenger RNA (mRNA) display method allowing for selection of ligands that specifically bind target proteins. This process is termed random nonstandard peptide integrated discovery (RaPID) and has been successfully utilized by the Suga group to identify inhibitors against disease-related proteins such as the well-characterized AKT2. Here, we will explore and discuss these methods for the generation of cyclic peptide libraries aimed at the inhibition of PPIs.

8.2.1 SICLOPPS

SICLOPPS is a method for the generation of large libraries of randomized macrocyclic peptides that utilizes split inteins for head-to-tail cyclization of peptides. Inteins are fully functional stand-alone domains, which retain functionality when inserted into a polypeptide sequence. SICLOPPS utilizes DnaE split inteins, first identified in the gene encoding the catalytic subunit of deoxyribonucleic acid (DNA) polymerase III in *Synechocystis* sp. PCC6803 [19]. The open reading frame (ORF) for the N-terminal portion of the DnaE split intein is followed by the 123 residue N-intein and is 745 kilobase (kb) away from the ORF that encodes the 36 residue C-terminal intein. In SICLOPPS, the order of the inteins has been rearranged such that the C-intein precedes the N-intein, and both inteins flank an internal peptide of protein sequence (extein). When the inteins come together to form an active *cis*-intein, splicing occurs, liberating the internal peptide sequence as a macrocycle (Figure 8.1a) [20].

SICLOPPS plasmid libraries are constructed by incorporating a set number of codons for all 20 amino acids into the extein, using degenerate oligonucleotides and polymerase chain reaction (PCR) [17]. This approach allows for full control over both the size of the macrocycle library and the number and position of randomized residues. The degenerate oligonucleotide contains a predetermined number of NNS repeats, where N represents any of the four DNA bases (A, G, C, or T) with S representing C or G. By constraining the third position within the codons, two out of the three stop codons are eliminated (ochre, UAA, and opal, UGA) while still covering all 20 peptidogenic amino acids with 32 codons. The intein chemistry requires the first extein residue to be a cysteine or serine in order to initiate splicing. However, there are no limits to the size of the target peptide. Most commonly, five or six variable amino acids are incorporated at the DNA level, generating libraries of 3.2×10^6 or 6.4×10^7 members, respectively.

SICLOPPS was first reported in 1999 [20]; however, its full potential was not realized until 2004 when it was combined with a bacterial reverse two-hybrid system (RTHS) [21] to enable the screening of cyclic peptide libraries of around a hundred million members against a given PPI. The RTHS is based on the bacteriophage regulatory system and links the disruption of either the homo- or heterodimerization of target proteins to the expression of a downstream reporter cassette, consisting of the *His3* (imidazole glycerol phosphate dehydratase), *Kan^R* (kanamycin resistance), and *LacZ* (β-galactosidase) genes. *His3* and *Kan^R* are both chemically tunable and conditionally selective genes that are required for host cell survival on selective media. The latter, *LacZ*, is used for quantitative analysis of the targeted PPI via β-galactosidase assays (Figure 8.1b).

Figure 8.1 Split-intein circular ligation of peptides and proteins (SICLOPPS) and the reverse two-hybrid system (RTHS). (a) The expressed SICLOPPS intein (I_C : target peptide : I_N) folds to form an active intein. An *N*-to-*S* acyl shift occurs at the target N-terminal intein junction to produce a thioester, which upon transesterification with a side chain nucleophile (serine or cysteine, $X = O$ or S, respectively) at the C-terminal intein junction forms a lariat intermediate. An asparagine side chain liberates the cyclic peptide as a lactone, which then undergoes rearrangement to generate the desired cyclic peptide as a lactam. (b) RTHS: Interacting proteins X and Y are expressed as N-terminal fusions with the 434 and p22 repressor proteins, respectively, under the control of the IPTG promoter. Dimerization of X and Y forms an active repressor construct, with 434 and p22 binding to their respective deoxyribonucleic acid (DNA) response elements and inhibiting downstream expression of the reporter cassette. When a cyclic peptide inhibits the interaction between X and Y, the repressor construct is not formed, therefore allowing for cell survival on selective media. For identification of inhibitors of homodimeric PPIs, a homodimeric system composed of only the 434 repressors can be used. (*See insert for color representation of the figure.*)

SICLOPPS library screening was first used to identify inhibitors of the heterodimeric interaction of ribonucleotide reductase (RR) using a *cyclo*-CX$_5$ library [21]. RR is an enzyme that catalyzes the reduction of ribonucleotides to 2′-deoxyribonucleotides, which is the rate limiting step in *de novo* DNA synthesis [22], and has been proposed to be a therapeutic target with both antiviral and anticancer potential. Mammalian RR is comprised of two subunits, mR1 and mR2; both the active and the allosteric regulatory sites are found in the mR1 subunit;

however, the tyrosyl radical required for efficient substrate turnover is found in the mR2 subunit [23]. The enzymatic activity of RR is therefore entirely dependent upon the interaction between the two subunits. SICLOPPS screening identified 24 potential inhibitors from a total of 10^8 library transformants. These 24 candidates were ranked for their PPI inhibitory activity based on their ability to restore growth of the RTHS strain (by drop spotting), leading to just eight that displayed a high level of selectivity for RR. This final 1 in 10 million hit rate clearly demonstrates the necessity for a high throughput approach for the identification of PPI modulators. It was found that the lead candidates of this screen could be generally classed into two groups: neutral and charged sequences. Interestingly, those sequences present in the neutral group resembled the Ar–X–F motif (Ar = aromatic, X = any amino acid) previously identified in linear peptidic dissociative inhibitors of RR [24].

From these eight compounds, the four with the highest RR specificity and activity (**1–4**, Figure 8.2), as well as containing residues more lenient toward synthesis, were subjected to quantitative analysis of PPI inhibitory effect through the utilization of the *LacZ* reporter gene present in the RTHS used for the RR inhibitor screening. All four cyclic peptides showed noticeable restoration of *LacZ* activity above background levels of expression, with three showing enhanced activity upon induction. The activity of these molecules was next analyzed by enzyme-linked immunosorbent assay (ELISA), but none of the peptides were able to demonstrate superior potency to that of a control peptide containing the N-acetylated sequence AcF[1]TLDADF[7] (known as P7). P7 corresponds to the C-terminal of the mR2 subunit and competes for binding to mR1 with a K_d of 9 μM. Despite this, all peptides displayed the ability to disrupt the association between mR1 and mR2, hence, successfully demonstrating the ability for genetic selection as a solution to the inherent issue of targeting large protein interfaces.

The first example of the use of SICLOPPS to identify a cyclic peptide inhibitor of a homodimeric interaction was directed toward the enzyme that catalyzes the final two stages in *de novo* purine biosynthesis, 5-aminoimidazole-4-carboxamide ribonucleotide (AICAR) transformylase/IMP cyclohydrolase (ATIC) [25]. The AICAR transformylase activity of ATIC is dependent upon the formation of a homodimer, whose interface spans approximately 5000 $Å^2$ [26]. An RTHS was constructed to monitor for homodimerization of ATIC and used to screen a 3.2×10^6 member *cyclo*-CX5 library. The most potent molecule identified from this library was *cyclo*-CRYFNV (**5**, Figure 8.2). This compound was verified to inhibit ATIC homodimerization and AICAR transformylase activity with a K_i of 17 ± 4 μM. The mechanism of

action of this molecule was determined to be inhibition of ATIC dimerization through progress rate kinetics. The potential of SICLOPPS-derived cyclic peptides has been demonstrated by the development of a small molecule ATIC inhibitor (K_i of 685 ± 35 nM) from the active motif of the cyclic peptide identified by alanine scanning [27]. This compound was further used to identify the role of intracellular AICAR as an activator of AMPK and the potential of using ATIC inhibition for therapeutic activation of AMPK [28]. The previously mentioned examples demonstrate the power and utility of molecules identified from SICLOPPS libraries not only as starting points for the development of potential therapeutics but also as tools to uncover the role of PPIs in cells.

SICLOPPS libraries have also been used for the identification of isoform-specific inhibitors of transcription factor (TF) PPIs. This is an area of significant biological interest as the ability to selectively target TF enables the ability to modulate signaling pathways at the earliest stage. In a recent example, a SICLOPPS library of 6.4×10^7 members encoding *cyclo*-SGWX$_6$ was screened for inhibitors of C-terminal binding protein (CtBP) homodimerization [29]. CtBP is a transcriptional corepressor that dimerizes in response to elevation in intracellular nicotinamide adenine dinucleotide (NADH) to form the core of a transcription repressor complex that targets a broad network of tumor suppressor genes. This screen identified *cyclo*-SGWTVVRMY (CP61) (**6**, Figure 8.2) whose CtBP inhibitory activity was measured *in vitro*, yielding an IC$_{50}$ value of 19 ± 4 μM, with binding demonstrated to be biphasic (dependent upon the oligomeric state of CtBP) with affinities of 3 and 11 μM. The CtBP inhibitory activity of CP61 was also demonstrated in cells; this molecule was used as a tool to gain new insight into the role of NADH-dependent CtBP dimerization in breast cancer cells.

In another example, a *cyclo*-CX$_5$ library was screened for inhibitors of the HIF-1α/HIF-1β (hypoxia inducible factor) PPI [30]. HIF-1 is the master regulator of cellular hypoxia response, altering the transcription of over 300 genes to allow cells to survive and grow in a low oxygen environment [31]. Due to their rapid growth, tumors constantly outstrip the supply of oxygen and nutrients provided by the existing vasculature and therefore, need to adapt to a hypoxic microenvironment. This response is mediated through HIF-1, and inhibition of this TF has long been proposed as a possible cancer therapeutic strategy. SICLOPPS screening identified *cyclo*-CLLFVY (**7**, Figure 8.2) as an isoform-specific inhibitor of HIF-1, without affecting the closely related HIF-2 TF, *in vitro* (K_d 124 nM) and in cells [30]. This compound was further used as a tool to demonstrate the presence of a transactivation loop by which HIF-1 upregulates the transcription of its own α subunit in response to hypoxia [32].
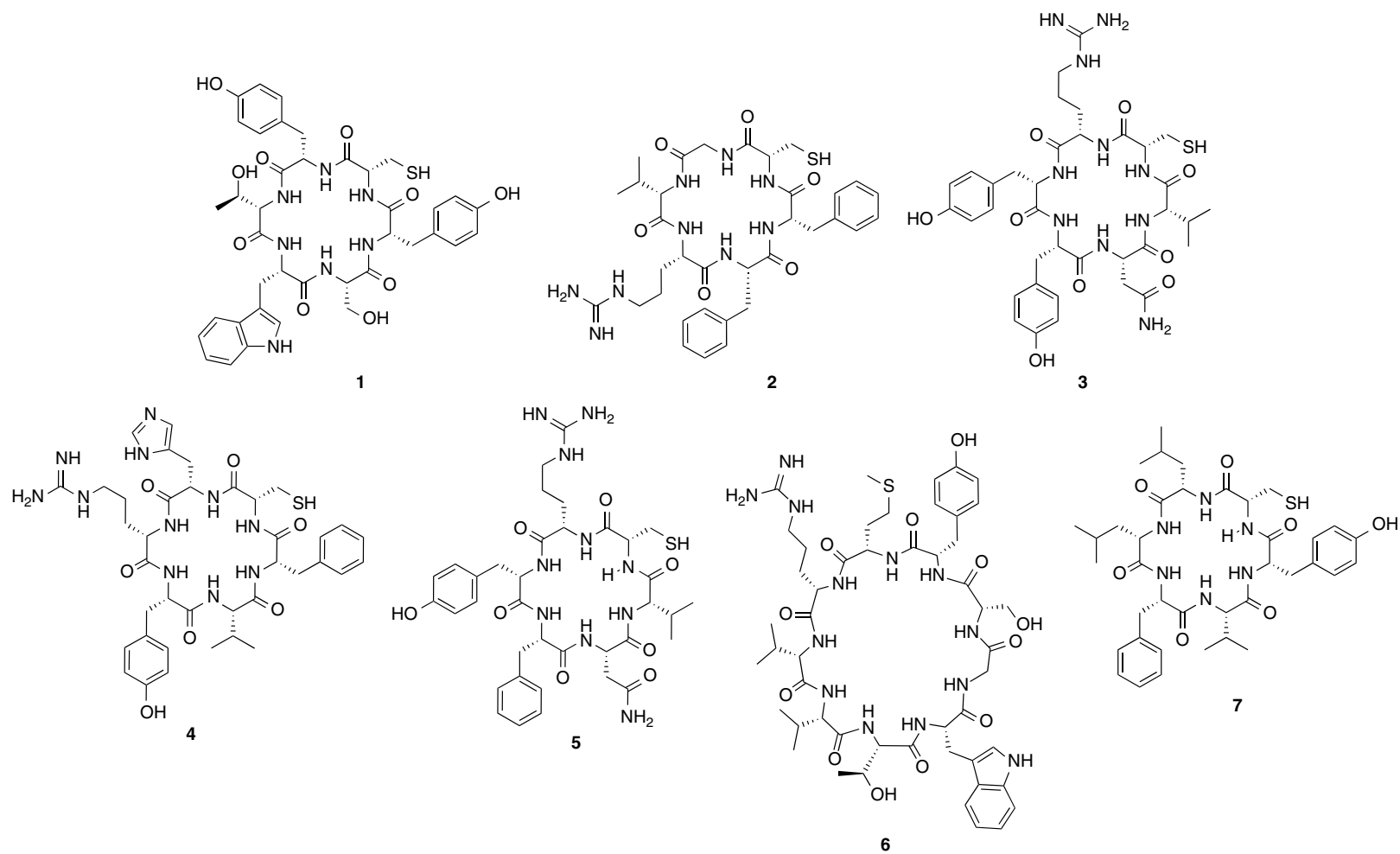
Figure 8.2 Cyclic peptide inhibitors of PPIs identified through SICLOPPS. (**1–4**) Ribonucleotide reductase inhibitors. (**5**) *Cyclo*-CRYFNV, ATIC homodimerization inhibitor. (**6**) Cyclo-SGWTVVRMY, C-terminal binding protein (CtBP) inhibitor. (**7**) *Cyclo*-CLLFVY, HIF-1 inhibitor.

8.2.2 FIT and RaPID

Several techniques have been introduced over the last decade that use genetic code reassignment to enable the incorporation of noncanonical amino acids through sense codon suppression [33, 34] and are generally coupled with a modified *in vitro* translation system, as demonstrated by Forster in 2003 [33]. Since this initial example, two further methods have also been developed based on the principle of genetic code reprogramming. One approach uses a recombinant *Escherichia coli* translation system called protein synthesis using recombinant elements (PURE). This process involves the depletion of certain amino acids to generate vacant codon boxes, relying upon the ability of certain aminoacyl-tRNA synthetases to mischarge nonnatural amino acids assigned to the vacant codon boxes. This allows for the expression of peptides containing these nonnatural amino acids [35, 36]. The second method also takes advantage of a recombinant *E. coli* translation system; however, in this case, the genetic code reassignment is achieved through the utilization of flexizymes. Flexizymes are short ribonucleotides (45–46 nucleotides in length), which recognize the specific leaving groups of amino esters rather than the side chains or amino groups of amino acids. Therefore, flexizymes are able to charge a vast range of nonstandard amino acids onto tRNAs. Additionally, the interaction between the 3′-end motif of the flexizyme and the 3′-end sequence of the tRNA is used for tRNA recognition; as the anticodon sequence is not involved, flexizymes can promiscuously charge any tRNA. Through the integration of an *in vitro* translation system such as PURE, flexizymes have been utilized as part of an extremely versatile peptide expression system termed flexible *in vitro* translation (FIT) [37].

The FIT system has been coupled with an *in vitro* display method to enable the identification of peptides capable of binding a target protein of interest. Deconvolution of hits is achieved via mRNA display during which each peptide is covalently conjugated to its encoding mRNA [38], allowing for sequence identification via the amplification and reading of the cognate mRNA sequence. This system of combining FIT with mRNA display is termed RaPID [39].

RaPID (Figure 8.3) involves the creation of a DNA library consisting of the following elements: T7 promoter, 5′-UTR (untranslated region), an ORF incorporating a random sequence between 5 and 15 NNK codons (N = G, A, T, C; K = T, G), a linker sequence (typically a Gly-Ser triple repeat), and a 3′-UTR. The DNA library in turn is transcribed to mRNA (Figure 8.3, step 1). A DNA sequence complementary to the 3′-UTR region conjugated to a CC-puromycin-PEG is then ligated to the 3′-end of the mRNA by T4 RNA ligase (Figure 8.3, step 2).

The mRNA template is then translated into a nonstandard peptide using the FIT system (Figure 8.3, step 3). During translation, the ribosome stalls at the UAG stop codon, allowing for the puromycin to enter the ribosomal A site to generate an amide bond between the peptide and the puromycin linker. This yields a peptide–linker–mRNA construct. In order to prevent nonspecific binding of the random mRNA to the target protein during the selection process, reverse transcription is performed to form an mRNA-complementary deoxyribonucleic acid (cDNA) duplex (Figure 8.3, step 4). During selection, the target protein is immobilized onto magnetic beads, mixed with the previously mentioned library, and peptides that bind the target protein are isolated (Figure 8.3, step 5). PCR amplification of the DNA sequences encoding these peptides is then used for enrichment of the library (Figure 8.3, step 6). This process is repeated through several rounds, resulting in a library enriched with the active species. The sequences of the active peptides are deconvoluted via the conjugated oligonucleotide tag, and hit peptides chemically synthesized for further analysis. This method allows for an initial library of greater than 10^{12} nonstandard peptides.

The inherent versatility of the FIT system has allowed for the incorporation of a variety of nonstandard amino acids for the purpose of generating libraries of genetically encoded macrocycles. There are several reactions that lend themselves to macrocyclization in this manner. One example is the incorporation of glycolic acid after a cysteine–proline dipeptide sequence, which has been demonstrated to result in self-rearrangement to form a diketopiperidine thioester, leading to the release of the glycolytic acid residue and self head-to-tail cyclization of the peptide backbone (Figure 8.4a) [40]. The insertion of other nonnatural amino acids at the initiation position or internal elongation positions also allows for macrocyclization to occur via assisted oxidative coupling and Michael addition [41]. The FIT system is not limited to the generation of monocyclic molecules; bicyclic macrocycles have also been shown to be accessible by this method and are formed through thioether formation coupled with Huisgen 1,3-dipolar cycloaddition [42].

One of the first examples for the use of this type of library technology was directed toward the inhibition of E6AP [43], the founding member of the HECT (homologous to E6AP C-terminal) domain family of E3 ubiquitin ligases. The binding partner of E6AP is the human papillomavirus (HPV) E6 protein, with the resulting complex conferring the E3 ligase activity, specific for the transfer of polyubiquitin chains onto p53 [44]. This event targets p53 for degradation, thus preventing the p53-dependent apoptosis pathways. E6AP also behaves in an E6-independent nature, targeting the promyelocytic leukemia

Figure 8.3 Random nonstandard peptide integrated discovery (RaPID) system. A complementary deoxyribonucleic acid (cDNA) library is generated via polymerase chain reaction (PCR), containing random sequences, which is transcribed to form an mRNA library (1). A puromycin linker is ligated to the 3′-end of each mRNA species (2). The mRNA is translated to a nonstandard peptide using the flexible *in vitro* translation (FIT) system, (3) forming a library of peptide–puromycin linker–mRNA species. These undergo reverse transcription (4) to prevent nonspecific binding during selection. The target protein is immobilized with a magnetic bead and the resultant peptide–mRNA–cDNA library is then screened for target binding (5). Library enrichment is performed through PCR amplification of those sequences found to contain target binders (6). (*See insert for color representation of the figure.*)

(PML) tumor suppressor [45] and a human analogue of the yeast DNA repair protein Rad23 (HHR23A) [46]. The lead macrocycle identified during the RaPID selection process was CM$_{11}$-1 (Figure 8.4b). This compound contains four *N*-methyl residues within a consensus sequence (^{Me}Ser^4, Gly^5, ^{Me}Phe^7, ^{Me}Phe^{10}, Pro^{11}) common to other sequences isolated in the screen and is cyclized between ClAc^{D}W and a Cys residue through a nonreducible thioether bond. The binding ability of CM$_{11}$-1

was determined via surface plasmon resonance (SPR) against the E6AP HECT domain. Rate kinetics were determined giving k_{on} and k_{off} values of $2.66 \times 10^6 \, \text{M}^{-1} \, \text{s}^{-1}$ and $1.60 \times 10^{-3} \, \text{M}^{-1} \, \text{s}^{-1}$, respectively, leading to a dissociation constant in the sub-nanomolar range (K_d 0.6 nM). CM$_{11}$-1 was also shown to inhibit the biological activity of E6AP through the prevention of poly-ubiquitination of targets Prx1 and p53 [47]. Prior to these studies, there was no known inhibitor for E6AP, with the targeting of
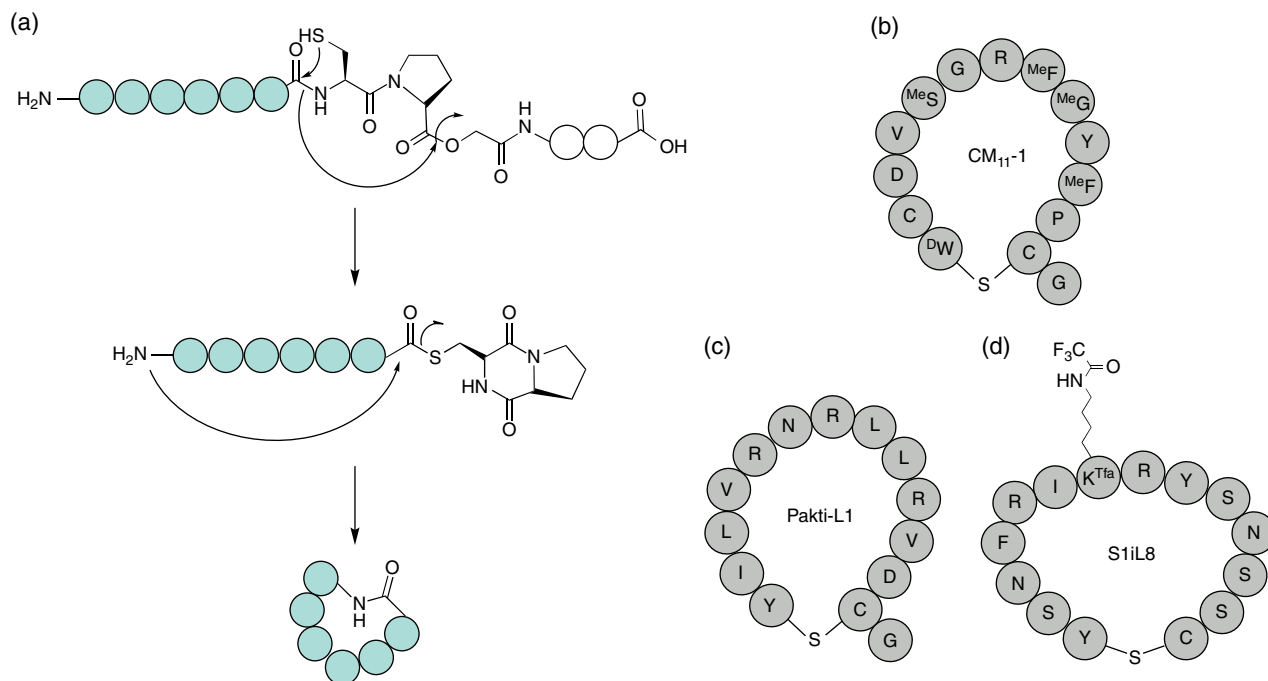
Figure 8.4 (a) Macrocyclization utilizing glycolic acid. Diketopiperazine-thioester formation facilitates macrocyclization through the free amino group at the N-terminus of the peptide construct. (b) Structure of CM_{11}-1, the E6AP inhibitor identified from a library of N-methylated thioether macrocyclic peptides. CM_{11}-1 exhibits an IC_{50} of 3.2 nM against E6AP. (c) Pakti-L1, an AKT2-selective inhibitor with an IC_{50} of 110 nM. (d) S1iL8, a SIRT-2 selective inhibitory cyclic peptide armed with the warhead trifluoroacetyl lysine (K^{Tfa}). S1iL8 has an IC_{50} of 3.2 nM.

HECT-type E3 ligases deemed an arduous challenge. The identification of the N-methylated macrocyclic CM_{11}-1 further demonstrates the potential for using macrocycles for the inhibition of previously deemed "undruggable" targets such as PPIs. This methodology (for the identification of thioether macrocyclic peptides) has also identified selective inhibitors of the AKT2-isoform (Pakti-L1, Figure 8.4c), a key component of insulin receptor signal transduction, and SIRT2-isoform selective inhibitors (S1iL8, Figure 8.4d), targeting cell cycle dysregulation [48].

8.3 Structural Mimicry

There are several advantages to the head-to-tail cyclization of peptides; it not only restricts conformational flexibility but also increases resistance to proteolytic degradation. In particular, head-to-tail cyclization eliminates the free N- and C-termini, degraded by aminopeptidases and carboxypeptidases, respectively. Building upon this rationale, it has become commonplace to also structurally constrained cyclic peptides to more closely mimic protein secondary structures, forming strand, sheet, turn, and loop conformations.

8.3.1 β-Strands

Approximately 30% of protein secondary structure consists of β-strands, which are linear peptide sequences arranged in parallel, antiparallel, or barrel β-sheets, stabilized by interstrand hydrogen bonds [49]. Strands are considered highly significant recognition motifs in PPIs such as those involved in protease interactions, the most studied target for β-strand mimicry. A key feature common across hundreds of proteases is the recognition of a peptide β-strand in both natural substrates and inhibitors, demonstrated in the crystal structures of over 100 aspartic, serine, cysteine, metalloproteases, and threonine proteases bound to substrates and inhibitors [50–52]. In one example, small cyclic peptides constrained to β-strand conformations have been shown to successfully and selectively inhibit the human immunodeficiency virus (HIV) protease. These peptides were cyclized via side chain-to-side chain or side chain-to-main chain linkages, hence, locking the peptides in a β-strand backbone conformation, with the conformation being retained within the active site of the protease enzymes [7]. Three exemplary macrocycles (Figure 8.5, a–c) displayed K_i values of 1.7, 0.6 and 0.3 nM, respectively, against HIV protease. However when investigated *in vitro*, there was a decrease in potency between 1 and 2 orders of

Figure 8.5 β-strand mimetic cyclic peptide inhibitors of human immunodeficiency virus (HIV) protease.

(a)

K_i 1.7 nM

(b)

K_i 0.6 nM

(c)

K_i 0.3 nM
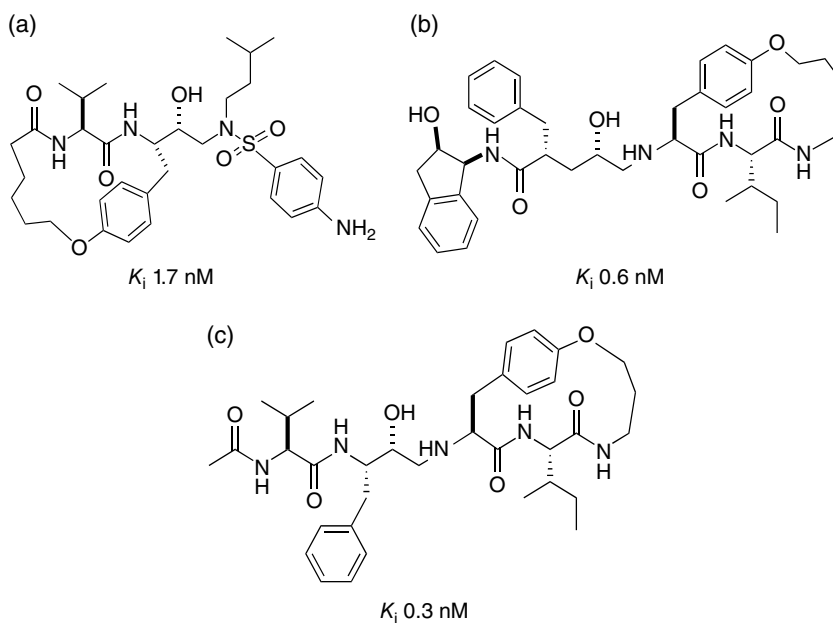
magnitude, displaying antiviral activity against HIV-1-infected primary peripheral blood mononuclear cells with IC_{50} values of 45, 56, and 95 nM, respectively. Although this pointed toward suboptimal cellular uptake, the activity of the β-strand cyclic peptides was in line with both indinavir and amprenavir [53], marketed HIV protease inhibitor antiretrovirals. Furthermore, it was demonstrated that by locking these peptides in the β-strand conformation, the affinity of the inhibitors for the HIV protease active site was enhanced by 10^1–10^4-fold, in comparison with their unconstrained counterparts.

Recently, a series of macrocyclic β-strand inhibitors of the immunomodulatory CD2 : CD58 PPI have been identified [54–56]. CD2 and CD58 are integral membrane glycoproteins found on the surface of T-cells and epithelial cells, respectively [57, 58]. CD2 expression on the surface of CD4+ and CD8+ T-cells is upregulated upon T-cell activation, and CD58 is implicated in autoimmune diseases, being overexpressed in antigen presenting cells [59, 60]. It is known that by inhibiting the interaction between CD2 and CD58 T-cell activation can be suppressed [61], making this particular PPI an interesting target against autoimmune diseases, such as rheumatoid arthritis. The interface of CD58 binding on CD2 comprises a flat β-sheet consisting of multiple charged residues, which in turn bind in a face-to-face manner with a second β-sheet on the CD58 surface [62]. The β-sheet at the CD2 surface consists of two antiparallel β-strands (F- and C-strands) consisting of 8–9 residues, which are noncontiguous in the protein sequence. The initial approach to the development of a CD2 : CD58 inhibitor was to develop a macrocyclic β-strand hairpin peptide containing the two strands found at the CD2 interface.

The first generation of such inhibitors was constrained through the introduction of a Pro-Gly sequence and cyclized via disulfide bridges and a peptide bond at each end [54]. Although these molecules could successfully inhibit the interaction between T-cells and epithelial cells, a second generation of macrocycles was developed through the introduction of a more rigid structure to enhance β-hairpin structures [55]. To achieve this, a (D)-Pro-Pro sequence or a dibenzofuran moiety was used to link the F- and C-strands between D31 and D87, while the opposite end of the sheet was cyclized by a main chain peptide bond, forming a more stable peptide structure. The insertion of (D)-Pro at the $i+1$ position of the β-turn lends itself to the formation of Type II′ or I′ turns. Additionally the inclusion of both the (D)-Pro-Pro sequence and the dibenzofuran moiety is known to nucleate the β-hairpin structure [63, 64]. From this series, two lead peptides (Lead 1 and Lead 2, Table 8.1) were shown to adopt a stable β-hairpin structure in solution by NMR and were shown to inhibit cell adhesion activity with IC_{50} values of 9.4 ± 0.3 nM and 25.7 ± 1.5 nM, respectively. Additionally, Lead 1 was also shown to suppress antigen-specific immune responses *in vitro* at nanomolar concentrations [55].

Following this success, Lead 1 was further optimized to achieve enhanced *in vivo* stability [65] through the use of naturally occurring head-to-tail cyclic peptides that are resistant to enzymatic, chemical, and thermal degradation. These peptides have previously been explored for pharmaceutical applications [66] and include examples such as the plant-derived cyclotides (consisting of ~30 AA, three disulfide bridges) [67], sunflower trypsin inhibitor (SFTI, ~14 AA, one disulfide bridge) [68], and

Table 8.1 Sequences of Lead 1 and 2 and novel grafted cyclic β-sheet peptides.

Name	Sequence	Cell adhesion inhibition IC$_{50}$ (μM)
Lead 1	Cyclo (1,10) SITDpPDDIK	0.0094 ± 0.0003
Lead 2	Cyclo (1,6) KDD-DBF-DYI	0.025 ± 0.0015
STFI-a	C**K**ASAPP**S**C**YDGDD**	0.043 ± 0.025
STFI-b	C**K**AEAK**PS**C**YDGDD**	>50
RTD-a	GAC**D**C**D**C**K**AGSC**Y**C**D**CTA	>50
RTD-b	**DD**CKCECAAGSC**K**C**S**C**Y**G	>50
RTD-c	G**D**CDCKCEAGKCSCYC**D**A	0.027 ± 0.015

Residues grafted from CD2 epitope in Lead 1 are in bold, and residues present in β-strands are underlined. Lower case letters refer to D-amino acids, and upper case letters refer to L-amino acids.
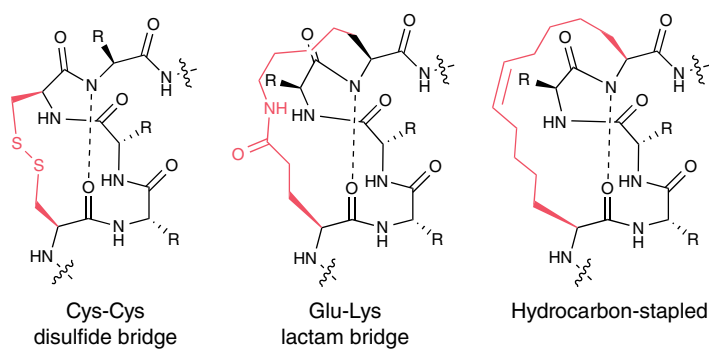
Figure 8.6 Examples of covalent macrocyclization techniques for α-helix stabilization.

the mammalian rhesus theta defensins (RTD, ~20 AA, three disulfide bridges) [69]. In this case, SFTI and RTD were chosen, since structurally they both consist of antiparallel β-strands, stabilized by disulfide bridges. The CD2 epitope from Lead 1 was grafted on to either SFTI or RTD, adopting the design strategy of maintaining the core structure of SFTI and RTD while focusing on adapting one face of the β-strand. As the side chains of alternating residues of a β-strand are on the same face, residues of SFTI and RTD were mutated in this manner, to binding residues from Lead 1, while maintaining the disulfide pattern and minimizing mutations within the turn regions. In this way two SFTI-1 (SFTI-a and SFTI-b), and three RTD-1 analogues (RTD-a, RTD-b, and RTD-c) were evaluated for pharmacological activity (Table 8.1). SFTI-a displayed inhibition of cell adhesion with an IC$_{50}$ value of 43 ± 25 nM, and RTD-c showed an IC$_{50}$ of 27 ± 15 nM, with the remaining analogues displaying weak inhibitory activity with IC$_{50}$ values above 50 μM. The cell adhesion inhibitory activity of SFTI-a and RTD-c was attributed to inhibition of the PPI and not cellular cytotoxicity through a cell viability assay and was shown not to be toxic at 100 μM. Furthermore, binding of SFTI-a to CD58 was demonstrated by SPR, with association and dissociation kinetics revealing a K_D of 14.6 μM. It was also shown that

SFTI-a was stable at increased temperatures and in serum, pointing toward increased *in vivo* stability [56].

These examples have provided evidence that constraining a macrocycle in a β-sheet/strand manner leads to enhanced target selectivity, cell permeability and bioavailability, showing that these structures are a sought after approach to targeting PPIs.

8.3.2 α-Helices

Type I mimetics are short peptides that aim to reproduce the topography of a naturally occurring α-helical motif, which are found in a large number of PPI interfaces. From a survey of the Protein Data Bank (PDB), 62% of protein complexes feature helical surfaces [70]. Common techniques for the stabilization of the helical structure include covalent cyclization through the introduction of disulfide and lactam bridges (Figure 8.6) [71]. Due to the inherent topology of the helical structure, the i, $i+4$, $i+7$, and $i+11$ residues are situated on the same face; the covalent linkage of these pairs of residues in a synthetic peptide can therefore artificially promote the formation of a helical structure [72].

An interesting example of α-helix mimicry comes from a disulfide-bridged nonapeptide shown to inhibit the
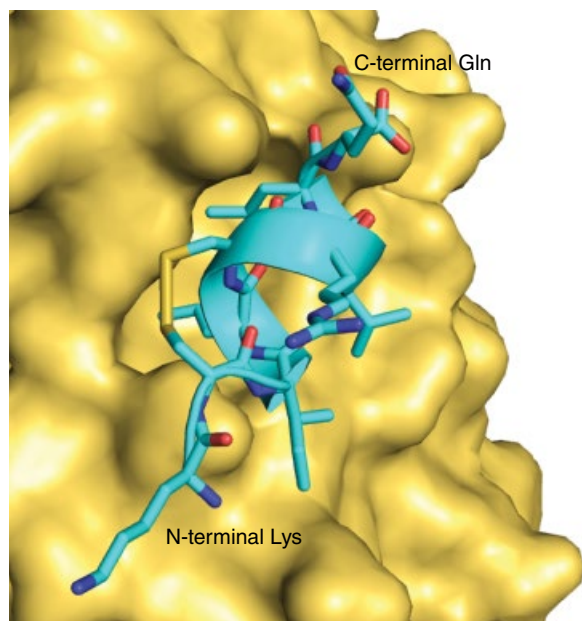
Figure 8.7 Interaction of PERM-1 with the surface of ERα. The surface of ERα (yellow) provides a good fit for the residues of PERM-1 (cyan). The N-terminal Lys and C-terminal Gln residues of PERM-1 are labeled. Protein data bank (PDB) code: 1PCG. (*See insert for color representation of the figure.*)

interaction between the estrogen receptor (ER) and its co-activator [73]. This particular macrocycle (PERM-1) demonstrated a K_i of 25 nM, which was an order of magnitude greater than that of a lactam-bridged analogue (K_i 220 nM). It is interesting to note that the circular dichroism spectra of the disulfide-bridged peptide in an aqueous environment shows a distinct lack of helical structure, whereas the X-ray crystal structure of the peptide bound to its target shows that the expected helical structure is induced upon binding (Figure 8.7) [73].

Lactam bridges have been successfully used for the formation of macrocycles adopting helical structures aimed at PPIs. In one example, a 14-residue macrocyclic peptide corresponding to the C-terminal heptad repeat of HIV1 gp41 (C-peptide) was developed; [74] C-peptides are able to inhibit HIV-1 entry into cells by binding to a trimeric coiled coil structure of HIV1 gp41, hence preventing binding of the endogenous C-terminal heptad repeat of gp41. The constrained macrocycle (C14linkmid) was shown by X-ray crystallography to bind with an almost identical helical structure as the native C-terminal peptide-binding partner. This peptide was crosslinked between positions i and $i+7$, both glutamic acid residues, with an α,ω-diaminoalkane group. The resultant macrocycle displayed an IC_{50} value of 35 μM, with a K_d of 1.2 μM. In comparison with its linear counterpart, C14linkmid bound the hydrophobic pocket of HIV gp41 approximately 7 times more tightly and also was

approximately 15 times more effective at inhibiting cell–cell fusion, therefore providing evidence that macrocyclization through the introduction of a lactam crossbridge has the potential to confer increased biological activity of such compounds.

Arguably, the most successful method for constraining macrocycles to an α-helical structure is hydrocarbon stapling of the peptide backbone (Figure 8.6) [75, 76]. This approach involves introducing nonnative carbon–carbon bond constraints through ring-closing metathesis with *O*-allyl serine or $C_α$-alkenyl residues using synthetic methodology pioneered by Grubbs and Blackwell in 1998 [77]. This chemical strategy cross-links two amino acid side chains with an all-hydrocarbon bridge and has been demonstrated to confer protease resistance while promoting cellular uptake. Several examples of hydrocarbon-stapled macrocycles have been used to probe and modulate PPIs, providing insight into mechanisms and potential therapeutic advantages [76, 78]. This technique has successfully been used to target several PPIs, an example of which is the development of a p53/human double minute 2 homolog (HDM2) interaction inhibitor. HDM2 is an E3 ubiquitin ligase that binds p53, leading to its ubiquitination and ultimate degradation via the proteasome. Loss of activity of p53 through mutation, deletion, or HDM2 overexpression is the most reported defect in human cancer. A series of hydrocarbon stapled peptides fashioned upon the transactivation helix of p53, SAH-p53 (stabilized alpha helix of p53), were synthesized through the incorporation of olefinic amino acid derivatives and cross-linked in the i, $i+7$ positions by ruthenium catalyzed ring closure to produce stapled helices (Figure 8.8). The lead candidate (SAH-p53-8) was shown to successfully target HDM2 [75], leading to the inhibition of p53 ubiquitination and therefore restoration of the p53 pathway.

Another successful example of a stapled α-helical peptide PPI inhibitor is the MDM2/MDMX inhibitor ATSP-7041 (Figure 8.9) [80]. MDM2 and MDMX, like HDM2, are binders and regulators of p53. MDM2 directly binds to the p53 transactivation domain, which blocks the nuclear import of p53 and also possesses E3 ubiquitin ligase activity, allowing for ubiquitination and proteasomal degradation of p53 [81, 82]. MDMX binds p53 and inhibits its transcriptional activity [81]. It has been shown that heterodimerization of MDM2 and MDMX allows for increased E3 ligase activity of MDM2. Overexpression of both MDM and MDMX are observed in several cancer types [83], and bivalent targeting is seen as a desirable approach as they regulate distinct functions of p53. ATSP-7041 is derived from the native p53 α-helix involved in the MDM2/MDMX interaction and successfully antagonizes both p53 negative regulators and was shown to suppress the growth of human tumor

(a)

(b)

Compound	Sequence $* = R_8 * = S_5$	Charge at pH 7.4	α helicity (%)	K_d (nM)	Cell permeable	Cell death
WT	Ac-LSQETFSDLWKLLPEN-NH$_2$	−2	11	410 ± 19	No	−
SAH-p53-1	Ac-LSQETFSD*WKLLPE*-NH$_2$	−2	25	100 ± 8	No	−
SAH-p53-2	Ac-LSQE*FSDLWK*LPEN-NH$_2$	−2	10	400 ± 50	No	−
SAH-p53-3	Ac-LSQ*TFSDLW*LLPEN-NH$_2$	−2	12	1200 ± 89	No	−
SAH-p53-4	Ac-LSQETF*DLWKLL*EN-NH$_2$	−2	59	0.92 ± 0.11	No	−
SAH-p53-5	Ac-LSQETF*NLWKLL*QN-NH$_2$	0	20	0.80 ± 0.05	Yes	−
SAH-p53-6	Ac-LSQQTE*NLWRLL*QN-NH$_2$	+1	14	56 ± 11	Yes	−
SAH-p53-7	Ac-QSQQTF*NLWKLL*QN-NH$_2$	+1	36	50 ± 10	Yes	−
SAH-p53-8	Ac-QSQQTF*NLWRLL*QN-NH$_2$	+1	85	55 ± 11	Yes	+
SAH-p53-8$_{F19A}$	Ac-QSQQTA*NLWRLL*QN-NH$_2$	+1	39	>4000	Yes	−
UAH-p53-8	Ac-QSQQTF*NLWRKK*QN-NH$_2$	+1	36	100 ± 10	Yes	−

Figure 8.8 Synthesis and sequences of SAH-p53 peptides. (a) Nonnatural olefinic amino acid derivatives were incorporated into the sequence at positions avoiding critical HDM2-binding residues and cross-linked at the *i*, *i* + 7 positions by ruthenium catalyzed ring-closing olefin metathesis. (b) The series of SAH-p53 peptides were generated by stapling the p53$_{14-29}$ sequence at the indicated positions within the sequences shown. Charge, α-helicity, HDM2 binding affinity, cell permeability, and impact on cell viability are all indicated. Source: Reprinted with permission from Bernal et al. [75]. © 2007 American Chemical Society. (*See insert for color representation of the figure.*)

Figure 8.9 Structure of ATSP-7041, a potent stapled inhibitor of the p53–MDM2/MDMX interaction, derived from the native p53 α-helix. Source: Reprinted with permission from Gavenonis *et al*. [79]. © 2014 Macmillan Publishers Ltd.

xenografts overexpressing MDM2/MDMX. Additionally, ATSP-7041 was able to maintain the biologically active α-helix conformation found within the p53 protein as well as displaying desirable drug-like properties, including efficient cell penetration, specific, high-affinity binding to both targets, and stability *in vivo* [80].

A more recent strategy for the production of macrocycles has been applied to the generation of a constrained α-helical macrocycle also directed toward p53-mediated processes and involves the generation of macrocyclic

organo-peptide hybrids (MOrPHs; see Chapter 7). These hybrid molecules are formed from both bifunctional synthetic and genetically encoded polypeptide precursors through chemo- and regioselective ligation, occurring in the presence of either a copper catalyst or catalyst-free through an *N–S* acyl shift reaction [84, 85]. This time however, looking to target the interaction between p53 and both oncoprotein targets HDM2 and human double minute X homolog (HDMX). It had previously been difficult to identify dual inhibitors of

p53–HDM2/X interactions, with compounds active against HDM2 failing when tested against HDMX. This is due to the very subtle differences in the p53 binding cleft present on both targets. Both HDM homologues bind to the p53 N-terminal transactivation domain, which forms a well-defined α-helix upon dimerization. A series of MOrPHs were generated, based upon a linear 12-mer peptide, identified during phage display library screening (PMI: T^{1}SFAEYWNLLSP^{12}) [86], which effectively accommodated and stabilized the α-helical protein binding motif of p53. The most active of these displayed IC$_{50}$ values against HDM2 and HDMX of 110 ± 15 and 340 ± 44 nM, respectively, and provide the first example of the use of side chain-to-tail cyclization for the mimicry of the α-helix structure [87].

Finally, DNA-supported synthesis has also generated several macrocyclic PPI inhibitors, as exemplified in Chapter 17.

8.4 Multi-Cycles for PPIs

There is significant interest in expanding the complexity and rigidity of cyclic peptides from monocyclic to bicyclic peptides and beyond. There are several examples of bicyclic peptides in nature (see also Chapter 5), including α-amanitin. This toxin, extracted from mushrooms [88], is a *cyclo*-octamer formed through side chain-to-side chain transannular Trp–Cys cross-linkage, hence forming two conjoined rings via a sulfoxide linker, and is a potent inhibitor of RNA polymerase II [89]. This, among other similar structures, has inspired the development of synthetic bicyclic peptides. One successful approach has been the development of a phage-encoded library of peptides containing three cysteine residues that, upon the addition of tris-(bromomethyl)benzene (TBMB), generates a repertoire of macrocycles containing two peptide loops anchored to the mesitylene core (Figure 8.10a; for further details on phage-encoded libraries, see Chapter 7) [90]. The first inhibitor identified in this manner was PK15 (Figure 8.10b), a specific inhibitor of the protease human plasma kallikrein, displaying a K_i value of 1.5 nM. Interestingly, it was found that the N-terminal loop of PK15 contained a tight turn structure, which has been found in other peptidic macrocycles, including the hormone oxytocin [91, 92]. Additionally, the mesitylene conjugates display properties similar to those found in zinc finger proteins, for example, both contain polypeptide chains coordinated by cysteine residues to a core molecule to yield a tertiary structure. The difference is apparent in that zinc fingers form non-covalent bonds to the core zinc ion, whereas the cysteine residues in molecules such as PK15 covalently interact with the mesitylene [90].

Since the discovery of PK15, several other bicyclic PPI inhibitors have been identified in the same way, for example, an inhibitor of urokinase-type plasminogen activator (uPA), a trypsin-like serine protease, involved in the turnover of the extracellular matrix. This inhibitor (UK18) is selective (K_i 53 nM) and forms an extended structure, with both loops interacting with the target site, hence forming a large interaction surface of 701 Å^2 [93]. This type of extended interaction is reflective of those formed at PPI interfaces, therefore providing evidence for the constraining of peptides in this manner to behave as small protein mimics, an approach needed for the targeting of the huge interfaces of PPIs.

8.5 The Future for Targeting PPIs with Macrocycles

The approaches described earlier for the production of macrocycles demonstrate the high interest in their therapeutic potential against previously undruggable targets such as PPIs. The future holds much promise for these molecules. An example of recent advances in the field is the synthesis of a fused tricyclic peptide, compatible with the aforementioned FIT RaPID system. The linear peptide was translated *in vitro*, containing an N-terminal chloroacetyl group, hence, providing a mechanism for cyclization through formation of a disulfide bond with the sulfhydryl group of a downstream cysteine [94] and four cysteine residues. Upon addition of TBMB, a tricyclic peptide is formed. Various loop lengths between Cys^2, Cys^3, and Cys^4 residues were investigated, and each successfully formed the tricyclic structure, as indicated by an increase of 114 Da during matrix-assisted laser desorption/ionization-time of flight-mass spectrometry (MALDI-TOF-MS) analysis [95]. Despite the lack of reported inhibitors of this type, the demonstration that these multi-cyclic macrocycles can be formed provides potential for the development of compounds that display a higher order of tertiary structure, providing bioactive species that could potentially tightly bind to targets.

While there has been a significant effort in targeting both α-helix- and β-strand-mediated PPIs, as much as 50% of all PPIs have a non-regular secondary structure [96], that is, loop structures. A recent effort to identify protein complexes in the PDB mediated by short peptide loops led to the successful development of LoopFinder, a program developed to search all structural databases for loop mediated PPIs [79]. LoopFinder aims to provide a platform upon which loop mediated PPIs can be explored, identifying "hot loops," (Figure 8.11) analogous to hot spots, providing novel targets from which macrocyclic inhibitors can be designed. During the development of LoopFinder, loops were limited to segments of
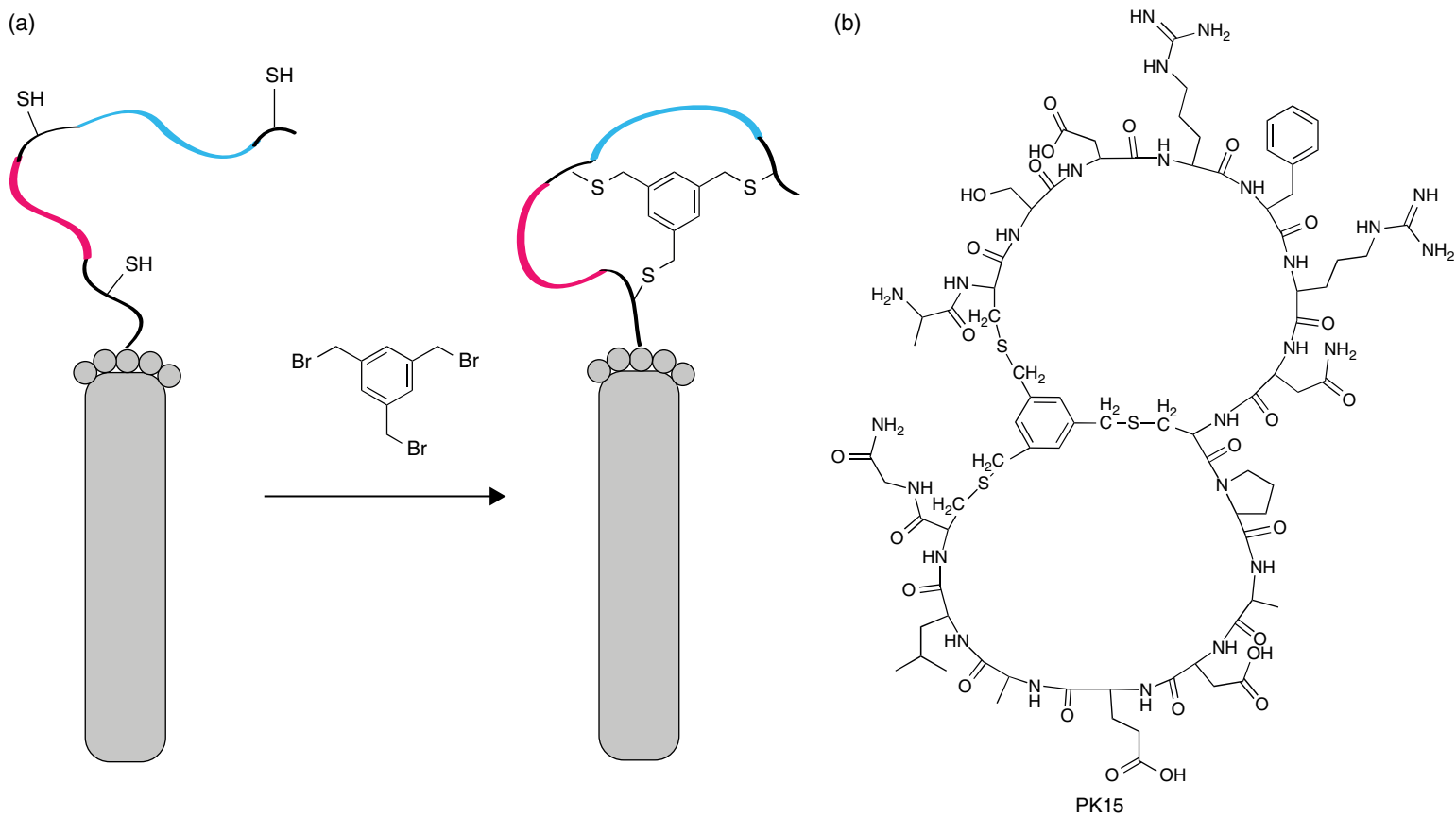
Figure 8.10 Generation of phage-encoded library of bicyclic peptides and an isolated active example. (a) A phage-encoded peptide, containing three cysteine residues is scaffolded by the trifunctional mesitylene TBMB. The library is screened for selectivity against the target protein. (b) Structure of PK15, a bicyclic inhibitor of plasma kallikrein ($K_i = 1.5$ nM), isolated through phage display.

Figure 8.11 Hot loops are defined by meeting one or more of the following three criteria: (i) the average $\Delta\Delta G_{residue}$ over the entire loop must be greater than 1 kcal mol^{-1}, (ii) the loop contains greater than or equal to three hot spot residues ($\Delta\Delta G_{residue} > 1$ kcal mol^{-1}), and (iii) the loop contains greater than or equal to two consecutive hot spot residues. Loops representing each category are represented in the yellow, blue, and red circles. Some hot loops satisfy two of these criteria, and representative loops in green, purple, and boxes. There are 67 hot loops that fulfill all three criteria with one example depicted in the gray box. All structures, rendered in PyMOL (PDB codes depicted in boxes), show the interfacial chain in blue, binding partner in gray, hot loop in green, and hot spot residues in orange ($\Delta\Delta G_{residue} > 1$ kcal mol^{-1}) and yellow ($\Delta\Delta G_{residue} > 2$ kcal mol^{-1}). Source: Reprinted with permission from Gavenonis *et al.* [79]. © 2014 Macmillan Publishers Ltd. (*See insert for color representation of the figure.*)

four to eight consecutive amino acids, conforming to the molecular weight range desirable for peptide and macrocyclic ligands. In addition to this, greater than or equal to 80% of residues had to be present near the PPI interface, and a cutoff distance between α-carbons of the loop termini was introduced to exclude repeating secondary structures. This cutoff had a value of 4.7 Å for loops of four amino acids and 5.83 Å for loops of five amino acids in length. These specific constraints were written into the program to be able to identify loop structures that would be amenable to mimicry by small macrocycles. Using these parameters, greater than 120 000 loops from greater than 9 000 structures were identified.

These structures were then stringently analyzed for the presence and location of hot spot residues, defined as $\Delta\Delta G_{residue} \geq 1$ kcal mol^{-1}, through alanine scanning. Any loop containing two or more consecutive hot

spots and those with an average $\Delta\Delta G_{residue}$ value of greater than 1 kcal mol^{-1} were defined as hot loops. This identified that only 5.6% of the total interface loops were classified as hot loops and, therefore, provided evidence that a small subset of loops are critical for the mediation of PPIs, with 67% of these hot loops contributing over a quarter of the predicted binding energy at PPI interfaces.

Through the use of LoopFinder, several well-characterized PPIs have been identified that contain hot loops of nonconsecutive hotspot residues, which display a wide range of loop architectures, and would, therefore, lend themselves to the development of designed constrained macrocyclic inhibitors. Examples of these hot loop-containing PPIs include the interaction between the human growth hormone and its binding partner (hGH-hGHbp), for which two hot loops were identified:

P61-E66 of hGH and I165-M170 of hGHbp. Similarly, a single 6-residue loop (D77-E82) was identified from the crystal structure of Keap1 bound to Nrf2, an interaction key to the monitoring of levels of Nrf2, a TF activated in response to oxidative stress [79]. Both are therapeutically relevant targets that benefit from loop identification in this way. The utilization of software such as LoopFinder can potentially deliver a plethora of therapeutically relevant starting points from which any number of constrained peptides and macrocycles can be developed.

There have also been recent advances in computational methods that analyze macrocycle binding to proteins and provide the basis of *de novo* molecule design. One example is the first systematic survey of macrocycle binding modes [97]. It was through such analysis that a new set of guidelines have tentatively been laid out for the design and synthesis of macrocycles targeted to PPIs, containing five key structural features a macrocycle should contain to achieve pharmacological activity at PPI interfaces:

1) **The macrocycle should typically contain one to two large substituents**. These should provide around 20–30 heavy atoms. Smaller substituents such as acetyl, methoxy, or isobutyl groups should also be included, with all regions of the macrocycle considered potentially critical for interaction with the target. It has been shown that typically one in three ring atoms bind to their target protein; these interactions account for almost 25% of the interaction surface, with ring, peripheral, and substituent atoms being equally likely to bind to a hot spot.

2) **The correct balance of heavy atoms and peripheral substituents is key for achieving good protein binding activity.** This is due to the disproportionate role in binding played by heavy atoms. One can utilize naturally occurring macrocycles as a template in this respect by introducing polar atoms in these peripheral positions, ensuring adequate polar surface area required for aqueous solubility.

3) **The macrocycle should contain one polar (O or N) atom for every two to three nonpolar (C, S, Cl) atoms**. This is to ensure the maintenance of a drug-like physiochemical balance. This leads to oral macrocycles retaining *c*Log*P* values that are in line with conventional drugs.

4) **Developing macrocycles with a large range of substituents dispersed around the ring is beneficial to the targeting of a wide range of protein binding sites**. Macrocycles bind to protein surfaces in either a face-on or a side-on fashion, dictated by the topology of the protein surface. Face-on binders interact with the target such that the large side chain substituents can access large, hydrophobic pockets or clefts. In contrast, the side-on binders do so in a flattened and elongated manner, allowing for even the solvent-exposed substituents to make contact with the target protein. Therefore, including a variety of substituents in both types of binders is important, as binding substituents are not restricted to one face of the macrocycle.

5) **The macrocycle should be unsaturated, providing ring constraint(s)**. This is a common feature across many pharmaceutically active macrocycles, potentially providing oral bioavailability.

Through combinatorial approaches that include expansion into larger chemical space (multi-cycles, αβα, βαβ structure mimicry, etc.), computationally focused design, and the incorporation of the previously mentioned set of "rules," the field of macrocycle therapeutics for PPIs holds significant promise. Not only have these types of structures been shown to increase affinity and efficacy in comparison with their linear counterparts, but also they can provide a more desirable adsorption, distribution, metabolism, and excretion (ADME) profile compared to linear peptides due to their inherent resistance to degradation by proteases and improved bioavailability.

References

1 LaCount, D. J.; Vignali, M.; Chettier, R.; Phansalkar, A.; Bell, R.; Hesselberth, J. R.; Schoenfeld, L. W.; Ota, I.; Sahasrabudhe, S.; Kurschner, C.; Fields, S.; Hughes, R. E. A protein interaction network of the malaria parasite *Plasmodium falciparum*. *Nature* **2005**, *438*, 103–107.

2 Pu, S. Y.; Vlasblom, J.; Emili, A.; Greenblatt, J.; Wodak, S. J. Identifying functional modules in the physical interactome of *Saccharomyces cerevisiae*. *Proteomics* **2007**, *7*, 944–960.

3 Komurov, K.; White, M. Revealing static and dynamic modular architecture of the eukaryotic protein interaction network. *Mol. Syst. Biol.* **2007**, *3*, 110.

4 Jones, S.; Thornton, J. M. Principles of protein–protein interactions. *Proc. Natl. Acad. Sci. U. S. A.* **1996**, *93*, 13–20.

5 Lo Conte, L.; Chothia, C.; Janin, J. The atomic structure of protein–protein recognition sites. *J. Mol. Biol.* **1999**, *285*, 2177–2198.

6 Hopkins, A. L.; Groom, C. R. The druggable genome. *Nat. Rev. Drug Discov.* **2002**, *1*, 727–730.

7 Hill, T. A.; Shepherd, N. E.; Diness, F.; Fairlie, D. P. Constraining cyclic peptides to mimic protein structure motifs. *Angew. Chem. Int. Ed. Engl.* **2014**, *53*, 13020–13041.

8 Bogan, A. A.; Thorn, K. S. Anatomy of hot spots in protein interfaces. *J. Mol. Biol.* **1998**, *280*, 1–9.

9 Thorn, K. S.; Bogan, A. A. ASEdb: A database of alanine mutations and their effects on the free energy of binding in protein interactions. *Bioinformatics* **2001**, *17*, 284–285.

10 Moreira, I. S.; Fernandes, P. A.; Ramos, M. J. Hot spots: A review of the protein–protein interface determinant amino-acid residues. *Proteins* **2007**, *68*, 803–812.

11 Lipinski, C. A.; Lombardo, F.; Dominy, B. W.; Feeney, P. J. Experimental and computational approaches to estimate solubility and permeability in drug discovery and development settings. *Adv. Drug Deliv. Rev.* **1997**, *23*, 3–25.

12 Doak, B. C.; Over, B.; Giordanetto, F.; Kihlberg, J. Oral druggable space beyond the rule of 5: Insights from drugs and clinical candidates. *Chem. Biol.* **2014**, *21*, 1115–1142.

13 Mullard, A. Protein–protein interaction inhibitors get into the groove. *Nat. Rev. Drug Discov.* **2012**, *11*, 172–174.

14 Gilon, C.; Halle, D.; Chorev, M.; Selinger, Z.; Byk, G. Backbone cyclization: A new method for conferring conformational constraint on peptides. *Biopolymers* **1991**, *31*, 745–750.

15 Adessi, C.; Soto, C. Converting a peptide into a drug: Strategies to improve stability and bioavailability. *Curr. Med. Chem.* **2002**, *9*, 963–978.

16 Passioura, T.; Katoh, T.; Goto, Y.; Suga, H. Selection-based discovery of druglike macrocyclic peptides. *Annu. Rev. Biochem.* **2014**, *83*, 727–752.

17 Tavassoli, A.; Benkovic, S. J. Split-intein mediated circular ligation used in the synthesis of cyclic peptide libraries in *E. coli*. *Nat. Protoc.* **2007**, *2*, 1126–1133.

18 Lennard, K. R.; Tavassoli, A. Peptides come round: Using SICLOPPS libraries for early stage drug discovery. *Chemistry* **2014**, *20*, 10608–10614.

19 Wu, H.; Hu, Z.; Liu, X. Q. Protein trans-splicing by a split intein encoded in a split DnaE gene of *Synechocystis* sp. PCC6803. *Proc. Natl. Acad. Sci. U. S. A.* **1998**, *95*, 9226–9231.

20 Abel-Santos, E.; Scott, C. P.; Benkovic, S. J. Use of inteins for the in vivo production of stable cyclic peptide libraries in *E. coli*. *Methods Mol. Biol.* **2003**, *205*, 281–294.

21 Horswill, A. R.; Savinov, S. N.; Benkovic, S. J. A systematic method for identifying small-molecule modulators of protein–protein interactions. *Proc. Natl. Acad. Sci. U. S. A.* **2004**, *101*, 15591–15596.

22 Jordan, A.; Reichard, P. Ribonucleotide reductases. *Annu. Rev. Biochem.* **1998**, *67*, 71–98.

23 Stubbe, J.; van der Donk, W. A. Ribonucleotide reductases: Radical enzymes with suicidal tendencies. *Chem. Biol.* **1995**, *2*, 793–801.

24 Gao, Y.; Liehr, S.; Cooperman, B. S. Affinity-driven selection of tripeptide inhibitors of ribonucleotide reductase. *Bioorg. Med. Chem. Lett.* **2002**, *12*, 513–515.

25 Tavassoli, A.; Benkovic, S. J. Genetically selected cyclic-peptide inhibitors of AICAR transformylase homodimerization. *Angew. Chem. Int. Ed.* **2005**, *44*, 2760–2763.

26 Greasley, S. E.; Horton, P.; Ramcharan, J.; Beardsley, G. P.; Benkovic, S. J.; Wilson, I. A. Crystal structure of a bifunctional transformylase and cyclohydrolase enzyme in purine biosynthesis. *Nat. Struct. Biol.* **2001**, *8*, 402–406.

27 Spurr, I. B.; Birts, C. N.; Cuda, F.; Benkovic, S. J.; Blaydes, J. P.; Tavassoli, A. Targeting tumour proliferation with a small-molecule inhibitor of AICAR transformylase homodimerization. *Chembiochem* **2012**, *13*, 1628–1634.

28 Asby, D. J.; Cuda, F.; Beyaert, M.; Houghton, F. D.; Cagampang, F. R.; Tavassoli, A. AMPK activation via modulation of *de novo* purine biosynthesis with an inhibitor of ATIC homodimerization. *Chem. Biol.* **2015**, *22*, 838–848.

29 Birts, C. N.; Nijjar, S. K.; Mardle, C. A.; Hoakwie, F.; Duriez, P. J.; Blaydes, J. P.; Tavassoli, A. A cyclic peptide inhibitor of C-terminal binding protein dimerization links metabolism with mitotic fidelity in breast cancer cells. *Chem. Sci.* **2013**, *4*, 3046–3057.

30 Miranda, E.; Nordgren, I. K.; Male, A. L.; Lawrence, C. E.; Hoakwie, F.; Cuda, F.; Court, W.; Fox, K. R.; Townsend, P. A.; Packham, G. K.; Eccles, S. A.; Tavassoli, A. A cyclic peptide inhibitor of HIF-1 heterodimerization that inhibits hypoxia signaling in cancer cells. *J. Am. Chem. Soc.* **2013**, *135*, 10418–10425.

31 Nordgren, I. K.; Tavassoli, A. Targeting tumour angiogenesis with small molecule inhibitors of hypoxia inducible factor. *Chem. Soc. Rev.* **2011**, *40*, 4307–4317.

32 Asby, D. J.; Cuda, F.; Hoakwie, F.; Miranda, E.; Tavassoli, A. HIF-1 promotes the expression of its alpha-subunit via an epigenetically regulated transactivation loop. *Mol. Biosyst.* **2014**, *10*, 2505–2508.

33 Forster, A. C.; Tan, Z.; Nalam, M. N.; Lin, H.; Qu, H.; Cornish, V. W.; Blacklow, S. C. Programming peptidomimetic syntheses by translating genetic codes designed de novo. *Proc. Natl. Acad. Sci. U. S. A.* **2003**, *100*, 6353–6357.

34 Frankel, A.; Roberts, R. W. *In vitro* selection for sense codon suppression. *RNA* **2003**, *9*, 780–786.

35 Hartman, M. C.; Josephson, K.; Lin, C. W.; Szostak, J. W. An expanded set of amino acid analogs for the ribosomal translation of unnatural peptides. *PLoS One* **2007**, *2*, e972.

36 Josephson, K.; Hartman, M. C.; Szostak, J. W. Ribosomal synthesis of unnatural peptides. *J. Am. Chem. Soc.* **2005**, *127*, 11727–11735.

37 Goto, Y.; Katoh, T.; Suga, H. Flexizymes for genetic code reprogramming. *Nat. Protoc.* **2011**, *6*, 779–790.

38 Nemoto, N.; Miyamoto-Sato, E.; Husimi, Y.; Yanagawa, H. *In vitro* virus: Bonding of mRNA bearing puromycin at the 3′-terminal end to the C-terminal end of its encoded protein on the ribosome *in vitro*. *FEBS Lett.* **1997**, *414*, 405–408.

39 Passioura, T.; Suga, H. Flexizymes, their evolutionary history and diverse utilities. *Top. Curr. Chem.* **2014**, *344*, 331–345.

40 Kawakami, T.; Ohta, A.; Ohuchi, M.; Ashigai, H.; Murakami, H.; Suga, H. Diverse backbone-cyclized peptides via codon reprogramming. *Nat. Chem. Biol.* **2009**, *5*, 888–890.

41 Hipolito, C. J.; Suga, H. Ribosomal production and *in vitro* selection of natural product-like peptidomimetics: The FIT and RaPID systems. *Curr. Opin. Chem. Biol.* **2012**, *16*, 196–203.

42 Sako, Y.; Morimoto, J.; Murakami, H.; Suga, H. Ribosomal synthesis of bicyclic peptides via two orthogonal inter-side-chain reactions. *J. Am. Chem. Soc.* **2008**, *130*, 7232–7234.

43 Huibregtse, J. M.; Scheffner, M.; Beaudenon, S.; Howley, P. M. A family of proteins structurally and functionally related to the E6-Ap ubiquitin-protein ligase (Vol 92, Pg 2563, 1995). *Proc. Natl. Acad. Sci. U. S. A.* **1995**, *92*, 5249.

44 Talis, A. L.; Huibregtse, J. M.; Howley, P. M. The role of E6AP in the regulation of p53 protein levels in human papillomavirus (HPV)-positive and HPV-negative cells. *J. Biol. Chem.* **1998**, *273*, 6439–6445.

45 Louria-Hayon, I.; Alsheich-Bartok, O.; Levav-Cohen, Y.; Silberman, I.; Berger, M.; Grossman, T.; Matentzoglu, K.; Jiang, Y. H.; Muller, S.; Scheffner, M.; Haupt, S.; Haupt, Y. E6AP promotes the degradation of the PML tumor suppressor. *Cell Death Differ.* **2009**, *16*, 1156–1166.

46 Kumar, S.; Talis, A. L.; Howley, P. M. Identification of HHR23A as a substrate for E6-associated protein-mediated ubiquitination. *J. Biol. Chem.* **1999**, *274*, 18785–18792.

47 Yamagishi, Y.; Shoji, I.; Miyagawa, S.; Kawakami, T.; Katoh, T.; Goto, Y.; Suga, H. Natural product-like macrocyclic *N*-methyl-peptide inhibitors against a ubiquitin ligase uncovered from a ribosome-expressed *de novo* library. *Chem. Biol.* **2011**, *18*, 1562–1570.

48 Ito, K.; Passioura, T.; Suga, H. Technologies for the synthesis of mRNA-encoding libraries and discovery of bioactive natural product-inspired non-traditional macrocyclic peptides. *Molecules* **2013**, *18*, 3502–3528.

49 Nowick, J. S. Chemical models of protein beta-sheets. *Acc. Chem. Res.* **1999**, *32*, 287–296.

50 Tyndall, J. D. A.; Fairlie, D. P. Conformational homogeneity in molecular recognition by proteolytic enzymes. *J. Mol. Recognit.* **1999**, *12*, 363–370.

51 Fairlie, D. P.; Tyndall, J. D. A.; Reid, R. C.; Wong, A. K.; Abbenante, G.; Scanlon, M. J.; March, D. R.; Bergman, D. A.; Chai, C. L. L.; Burkett, B. A. Conformational selection of inhibitors and substrates by proteolytic enzymes: Implications for drug design and polypeptide processing. *J. Med. Chem.* **2000**, *43*, 1271–1281.

52 Tyndall, J. D. A.; Nall, T.; Fairlie, D. P. Proteases universally recognize beta strands in their active sites. *Chem. Rev.* **2005**, *105*, 973–999.

53 Tyndall, J. D.; Reid, R. C.; Tyssen, D. P.; Jardine, D. K.; Todd, B.; Passmore, M.; March, D. R.; Pattenden, L. K.; Bergman, D. A.; Alewood, D.; Hu, S. H.; Alewood, P. F.; Birch, C. J.; Martin, J. L.; Fairlie, D. P. Synthesis, stability, antiviral activity, and protease-bound structures of substrate-mimicking constrained macrocyclic inhibitors of HIV-1 protease. *J. Med. Chem.* **2000**, *43*, 3495–3504.

54 Liu, J. N.; Li, C.; Ke, S.; Satyanarayanajois, S. D. Structure-based rational design of beta-hairpin peptides from discontinuous epitopes of cluster of differentiation 2 (CD2) protein to modulate cell adhesion interaction. *J. Med. Chem.* **2007**, *50*, 4038–4047.

55 Gokhale, A.; Weldeghiorghis, T. K.; Taneja, V.; Satyanarayanajois, S. D. Conformationally constrained peptides from CD2 to modulate protein–protein interactions between CD2 and CD58. *J. Med. Chem.* **2011**, *54*, 5307–5319.

56 Sable, R.; Durek, T.; Taneja, V.; Craik, D. J.; Pallerla, S.; Gauthier, T.; Jois, S. Constrained cyclic peptides as immunomodulatory inhibitors of the CD2:CD58 protein–protein interaction. *ACS Chem. Biol.* **2016**, *11*, 2366–2374.

57 Chen, L. P.; Flies, D. B. Molecular mechanisms of T cell co-stimulation and co-inhibition. *Nat. Rev. Immunol.* **2013**, *13*, 227–242.

58 Davis, S. J.; Ikemizu, S.; Wild, M. K.; van der Merwe, P. A. CD2 and the nature of protein interactions mediating cell–cell recognition. *Immunol. Rev.* **1998**, *163*, 217–236.

59 Webber, A.; Hirose, R.; Vincenti, F. Novel strategies in immunosuppression: Issues in perspective. *Transplantation* **2011**, *91*, 1057–1064.

60 Wakisaka, S.; Suzuki, N.; Nagafuchi, H.; Takeba, Y.; Kaneko, A.; Asai, T.; Sakane, T. Characterization of tissue outgrowth developed *in vitro* in patients with rheumatoid arthritis: Involvement of T cells in the development of tissue outgrowth. *Int. Arch. Allergy Immunol.* **2000**, *121*, 68–79.

61 Mrowietz, U. Treatment targeted to cell surface epitopes. *Clin. Exp. Dermatol.* **2002**, *27*, 591–596.

62 Wang, J.; Smolyar, A.; Tan, K. M.; Liu, J.; Kim, M. Y.; Sun, Z. J.; Wagner, G.; Reinherz, E. L. Structure of a heterophilic adhesion complex between the human CD2 and CD58 (LFA-3) counterreceptors. *Cell* **1999**, *97*, 791–803.

63 Mayo, K. H.; Dings, R. P. M.; Flader, C.; Nesmelova, I.; Hargittai, B.; van der Schaft, D. W. J.; van Eijk, L. I.; Walek, D.; Haseman, J.; Hoye, T. R.; Griffioen, A. W. Design of a partial peptide mimetic of anginex with antiangiogenic and anticancer activity. *J. Biol. Chem.* **2003**, *278*, 45746–45752.

64 Saha, I.; Chatterjee, B.; Shamala, N.; Balaram, P. Crystal structures of peptide enantiomers and race mates: Probing conformational diversity in heterochiral Pro-Pro sequences. *Biopolymers* **2008**, *90*, 537–543.

65 Vlieghe, P.; Lisowski, V.; Martinez, J.; Khrestchatisky, M. Synthetic therapeutic peptides: Science and market. *Drug Discov. Today* **2010**, *15*, 40–56.

66 Poth, A. G.; Chan, L. Y.; Craik, D. J. Cyclotides as grafting frameworks for protein engineering and drug design applications. *Biopolymers* **2013**, *100*, 480–491.

67 Craik, D. J.; Daly, N. L.; Bond, T.; Waine, C. Plant cyclotides: A unique family of cyclic and knotted proteins that defines the cyclic cystine knot structural motif. *J. Mol. Biol.* **1999**, *294*, 1327–1336.

68 Luckett, S.; Garcia, R. S.; Barker, J. J.; Konarev, A. V.; Shewry, P. R.; Clarke, A. R.; Brady, R. L. High-resolution structure of a potent, cyclic proteinase inhibitor from sunflower seeds. *J. Mol. Biol.* **1999**, *290*, 525–533.

69 Daly, N. L.; Chen, Y. K.; Rosengren, K. J.; Marx, U. C.; Phillips, M. L.; Waring, A. J.; Wang, W.; Lehrer, R. I.; Craik, D. J. Retrocyclin-2: Structural analysis of a potent anti-HIV theta-defensin. *Biochemistry* **2007**, *46*, 9920–9928.

70 Jochim, A. L.; Arora, P. S. Systematic analysis of helical protein interfaces reveals targets for synthetic inhibitors. *ACS Chem. Biol.* **2010**, *5*, 919–923.

71 Garner, J.; Harding, M. M. Design and synthesis of alpha-helical peptides and mimetics. *Org. Biomol. Chem.* **2007**, *5*, 3577–3585.

72 Azzarito, V.; Long, K.; Murphy, N. S.; Wilson, A. J. Inhibition of alpha-helix-mediated protein-protein interactions using designed molecules. *Nat. Chem.* **2013**, *5*, 161–173.

73 Leduc, A. M.; Trent, J. O.; Wittliff, J. L.; Bramlett, K. S.; Briggs, S. L.; Chirgadze, N. Y.; Wang, Y.; Burris, T. P.; Spatola, A. F. Helix-stabilized cyclic peptides as selective inhibitors of steroid receptor-coactivator interactions. *Proc. Natl. Acad. Sci. U. S. A.* **2003**, *100*, 11273–11278.

74 Sia, S. K.; Carr, P. A.; Cochran, A. G.; Malashkevich, V. N.; Kim, P. S. Short constrained peptides that inhibit HIV-1 entry. *Proc. Natl. Acad. Sci. U. S. A.* **2002**, *99*, 14664–14669.

75 Bernal, F.; Tyler, A. F.; Korsmeyer, S. J.; Walensky, L. D.; Verdine, G. L. Reactivation of the p53 tumor suppressor pathway by a stapled p53 peptide. *J. Am. Chem. Soc.* **2007**, *129*, 2456–2457.

76 Braun, C. R.; Mintseris, J.; Gavathiotis, E.; Bird, G. H.; Gygi, S. P.; Walensky, L. D. Photoreactive stapled BH3 peptides to dissect the BCL-2 family interactome. *Chem. Biol.* **2010**, *17*, 1325–1333.

77 Blackwell, H. E.; Grubbs, R. H. Highly efficient synthesis of covalently cross-linked peptide helices by ring-closing metathesis. *Angew. Chem. Int. Ed.* **1998**, *37*, 3281–3284.

78 Walensky, L. D.; Kung, A. L.; Escher, I.; Malia, T. J.; Barbuto, S.; Wright, R. D.; Wagner, G.; Verdine, G. L.; Korsmeyer, S. J. Activation of apoptosis *in vivo* by a hydrocarbon-stapled BH3 helix. *Science* **2004**, *305*, 1466–1470.

79 Gavenonis, J.; Sheneman, B. A.; Siegert, T. R.; Eshelman, M. R.; Kritzer, J. A. Comprehensive analysis of loops at protein–protein interfaces for macrocycle design. *Nat. Chem. Biol.* **2014**, *10*, 716–722.

80 Chang, Y. S.; Graves, B.; Guerlavais, V.; Tovar, C.; Packman, K.; To, K. H.; Olson, K. A.; Kesavan, K.; Gangurde, P.; Mukherjee, A.; Baker, T.; Darlak, K.; Elkin, C.; Filipovic, Z.; Qureshi, F. Z.; Cai, H. L.; Berry, P.; Feyfant, E.; Shi, X. G. E.; Horstick, J.; Annis, D. A.; Manning, A. M.; Fotouhi, N.; Nash, H.; Vassilev, L. T.; Sawyer, T. K. Stapled alpha-helical peptide drug development: A potent dual inhibitor of MDM2 and MDMX for p53-dependent cancer therapy. *Proc. Natl. Acad. Sci. U. S. A.* **2013**, *110*, E3445–E3454.

81 Wade, M.; Wahl, G. M. Targeting Mdm2 and Mdmx in cancer therapy: Better living through medicinal chemistry? *Mol. Cancer Res.* **2009**, *7*, 1–11.

82 Haupt, Y.; Maya, R.; Kazaz, A.; Oren, M. Mdm2 promotes the rapid degradation of p53. *Nature* **1997**, *387*, 296–299.

83 Marine, J. C. Mdm2 and Mdmx in cancer and development. *Curr. Top. Dev. Biol.* **2011**, *94*, 45–75.

84 Fasan, R.; Smith, J. M.; Vitali, F. Assembly of macrocyclic organo-peptide hybrids (MOrPHs) from genetically encoded precursors. *Abstr. Pap. Am. Chem. Soc.* **2011**, 241.

85 Smith, J. M.; Vitali, F.; Archer, S. A.; Fasan, R. Modular assembly of macrocyclic organo-peptide hybrids using synthetic and genetically encoded precursors. *Angew. Chem. Int. Ed.* **2011**, *50*, 5075–5080.

86 Pazgiera, M.; Liu, M.; Zou, G. Z.; Yuan, W. R.; Li, C. Q.; Li, C.; Li, J.; Monbo, J.; Zella, D.; Tarasov, S. G.; Lu, W. Structural basis for high-affinity peptide inhibition of p53 interactions with MDM2 and MDMX. *Proc. Natl. Acad. Sci. U. S. A.* **2009**, *106*, 4665–4670.

87 Smith, J. M.; Frost, J. R.; Fasan, R. Designer macrocyclic organo-peptide hybrids inhibit the interaction between p53 and HDM2/X by accommodating a functional alpha-helix. *Chem. Commun.* **2014**, *50*, 5027–5030.

88 Wieland, T. *Peptides of poisonous Amanita mushrooms*. Springer-Verlag: New York, **1986**; p xiv, 256 p.

89 Bushnell, D. A.; Cramer, P.; Kornberg, R. D. Structural basis of transcription: Alpha-amanitin-RNA polymerase II cocrystal at 2.8 A resolution. *Proc. Natl. Acad. Sci. U. S. A.* **2002**, *99*, 1218–1222.

90 Heinis, C.; Rutherford, T.; Freund, S.; Winter, G. Phage-encoded combinatorial chemical libraries based on bicyclic peptides. *Nat. Chem. Biol.* **2009**, *5*, 502–507.

91 Wood, S. P.; Tickle, I. J.; Treharne, A. M.; Pitts, J. E.; Mascarenhas, Y.; Li, J. Y.; Husain, J.; Cooper, S.; Blundell, T. L.; Hruby, V. J.; Buku, A.; Fischman, A. J.; Wyssbrod, H. R. Crystal-structure analysis of deamino-oxytocin: Conformational flexibility and receptor-binding. *Science* **1986**, *232*, 633–636.

92 Bhaskaran, R.; Chuang, L. C.; Yu, C. Conformational properties of oxytocin in dimethyl-sulfoxide solution: NMR and restrained molecular-dynamics studies. *Biopolymers* **1992**, *32*, 1599–1608.

93 Angelini, A.; Cendron, L.; Chen, S. Y.; Touati, J.; Winter, G.; Zanotti, G.; Heinis, C. Bicyclic peptide inhibitor reveals large contact interface with a protease target. *ACS Chem. Biol.* **2012**, *7*, 817–821.

94 Goto, Y.; Ohta, A.; Sako, Y.; Yamagishi, Y.; Murakami, H.; Suga, H. Reprogramming the translation initiation for the synthesis of physiologically stable cyclic peptides. *ACS Chem. Biol.* **2008**, *3*, 120–129.

95 Bashiruddin, N. K.; Nagano, M.; Suga, H. Synthesis of fused tricyclic peptides using a reprogrammed translation system and chemical modification. *Bioorg. Chem.* **2015**, *61*, 45–50.

96 Wells, J. A.; McClendon, C. L. Reaching for high-hanging fruit in drug discovery at protein–protein interfaces. *Nature* **2007**, *450*, 1001–1009.

97 Villar, E. A.; Beglov, D.; Chennamadhavuni, S.; Porco, J. A.; Kozakov, D.; Vajda, S.; Whitty, A. How proteins bind macrocycles. *Nat. Chem. Biol.* **2014**, *10*, 723–731.

Part III

The Synthetic Toolbox for Macrocycles

9

Synthetic Strategies for Macrocyclic Peptides

Éric Biron, Simon Vézina-Dawod and François Bédard

Faculty of Pharmacy, Université Laval, Quebec City, Quebec, Canada

9.1 Introduction to Peptide Macrocyclization

Peptide macrocycles form an outstanding class of natural and synthetic bioactive compounds. Showing an important molecular diversity and displaying a wide spectrum of biological activities via a great variety of modes of action, they have recently gained significant interest in drug discovery [1–5]. Compared with their linear counterparts, cyclic peptides are more resistant to proteases [6, 7], and their conformational rigidity lowers the entropic cost of binding, making them tighter—binding to a given target macromolecule [2]. Moreover, their ability to mimic protein secondary structures has been demonstrated, and they offer the opportunity to perform functional and conformational fine-tuning [2, 8–10]. Therefore, peptide macrocycles are very useful scaffolds in structure–activity relationship studies and valuable lead compounds in drug development [1, 4, 11–13].

Even though biological methods such as phage display can produce cyclic peptides in very large numbers, chemical synthesis remains the method of choice to generate structural diversity, optimize pharmacological properties, and obtain sufficient quantities for biological investigations. In some cases, the synthesis of peptide macrocycles is straightforward, but many are notoriously difficult to prepare. Many factors such as ring size, cyclization topology, amino acid configuration, presence of turn-inducing residues, and C-terminal epimerization need to be considered before selecting the appropriate synthetic strategy. Over the years, a wide variety of synthetic methodologies have been developed to overcome major challenges in peptide macrocyclization, and several review articles on the synthesis of cyclic peptides have been published [2, 13–18]. In this chapter, synthetic strategies for the final ring-closing reaction by the widely employed and versatile processes of lactamization, lactonization, and disulfide bridge formation will

be discussed. Other strategies including ring-closing metathesis, cycloadditions, palladium-catalyzed multi-component reactions, and many others will be covered in Chapters 10–14.

9.1.1 Cyclic Peptide Topologies

According to the nature of the chemical bond found in the backbone, cyclic peptides can be classified in two major categories: *homodetic* peptides that contain exclusively amide bonds and *heterodetic* peptides that may also contain ester, ether, disulfide, thioether, or thioester bonds. Depending on the functional groups involved in ring closure, peptide macrocyclization can be performed in four different ways: head-to-tail (C-terminus to N-terminus), side chain-to-tail, head-to-side chain, and side chain-to-side chain (Figure 9.1). In addition to these conventional approaches, macrocyclization can also be achieved via the backbone amide nitrogen to yield amide-to-amide, head-to-amide, amide-to-tail, and side chain-to-amide cyclic peptides [7, 19, 20].

Among the different ring-closing strategies, reactions involving lactamization, lactonization, or disulfide bridge formation are the most commonly used [16, 21]. Typically, a linear sequence is first assembled on a polymeric support, although for smaller peptides this could also be done in solution, and cyclization is either performed in solution after cleavage from the resin or directly on solid support after selective side chain deprotection (Figure 9.2). In both approaches, the side chain protecting groups are removed in the final step.

For both solution- and solid-phase macrocyclization methods, the solid support plays a critical role in the linear precursor assembly and should be mechanically stable, show good swelling properties in common organic solvents, and be compatible with the selected synthetic methodology. The Boc/Bzl and Fmoc/tBu synthetic methodologies are the two most common solid-phase peptide synthesis (SPPS) strategies, and the strategy
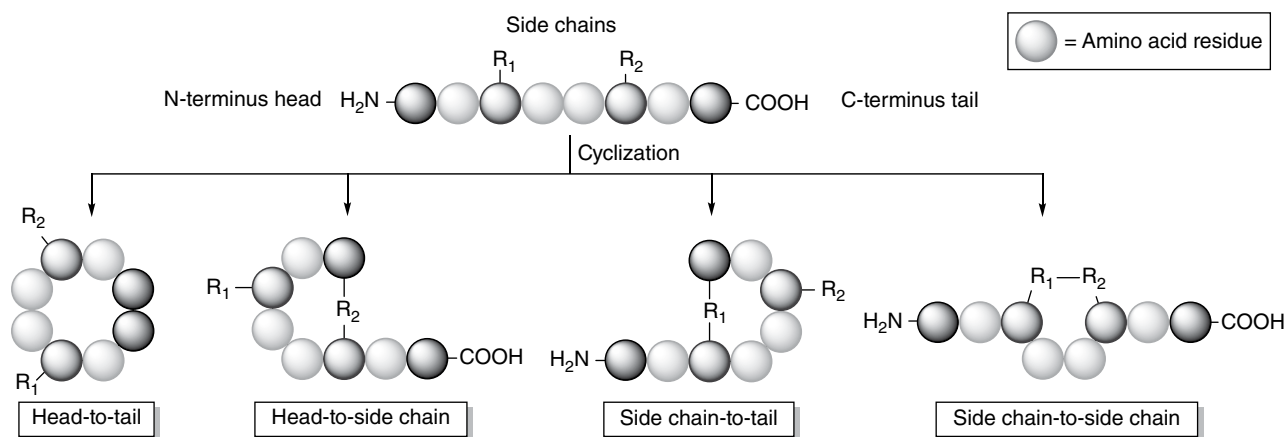
Figure 9.1 Four possibilities for peptide macrocyclization.

utilized should be considered when choosing the appropriate type of resin linker [22]. Based on the mild acidic conditions for final deprotection and the commercial availability of a wide variety of orthogonally protected amino acids, the Fmoc/tBu approach is probably the most efficient and attractive strategy to prepare cyclic peptides.

9.1.2 Solution-Phase Versus Solid-Supported Macrocyclization

Compared with normal peptide bond formation, ring-closing reactions usually proceed much more slowly, and side reactions, such as unwanted intermolecular bond formation leading to oligomerization and cyclodimerization of linear peptide precursors, may even predominate [23–25]. Indeed, macrocyclization is a unimolecular reaction in which transannular interactions may either help or hamper proper folding of the chain prior to ring closure. These intermolecular processes can be minimized by performing cyclization under high dilution conditions, typically sub-millimolar concentrations (10^{-4} to 10^{-3} M) [16]. Such conditions necessitate large amounts of solvent and become problematic when large quantities of peptides need to be prepared. The volume of solvent needed for cyclization can be reduced by performing the reaction under "pseudo-high" dilution conditions, whereby the linear precursor and coupling reagent are added simultaneously, using a dual syringe pump at a very slow rate, to a small volume of solvent and base [26]. Another efficient approach is to perform the macrocyclization step while the peptide is still bound to the solid support (Figure 9.2). Owing to the physical distance imposed by the resin, peptides attached to an insoluble polymer are less mobile and less prone to encounter one another compared with molecules in solution that can freely diffuse. If resin loading is not too high, this pseudo-dilution phenomenon favors intramolecular reactions of resin-bound peptides over intermolecular side reactions [27–29]. Moreover, another advantage of solid-supported macrocyclization is that, as the desired product is bound to the resin, simple washing and filtration steps facilitate the whole procedure and allow the use of a larger excess of coupling reagent to increase cyclization efficiency. This approach requires at least three dimensions of orthogonal protecting groups (for instance, Fmoc/tBu/allyl) to allow the synthesis of the linear peptide, selective deprotection of the reactive ends (N- or C-terminus or side chain), macrocyclization, and then final cleavage from the solid support (Figure 9.2) [30–35]. In the case of head-to-tail cyclic peptides, the linear precursor is most commonly anchored to the support via the side chain of a C-terminal trifunctional amino acid such as Asp, Glu, Lys, Ser, or Tyr (Section 9.4.1). Alternatively, the linear precursor may also be anchored to the solid support via a backbone amide (Section 9.4.2) [36–38]. In this case, special care should be taken when choosing the C-terminal amino acid and the carboxylic acid protecting group to minimize diketopiperazine (DKP) formation [37, 38]. For example, C-terminal allyl and methyl esters combined with unhindered amino acids such as glycine should be avoided as they have been shown to promote DKP formation at the dipeptide stage [38].

The selection of a suitable strategy to achieve macrocyclization will depend greatly on the peptide sequence, and different factors, such as ring size, conformational preferences of the linear precursor, steric hindrance of the reactive ends, and the propensity of the C-terminal residue for racemization, also should be considered. Whether a solution- or solid-phase approach is used for the macrocyclization step, the linker will play a critical role to successfully obtain cyclic peptides, and special attention should be paid when choosing a suitable linker for the selected strategy.
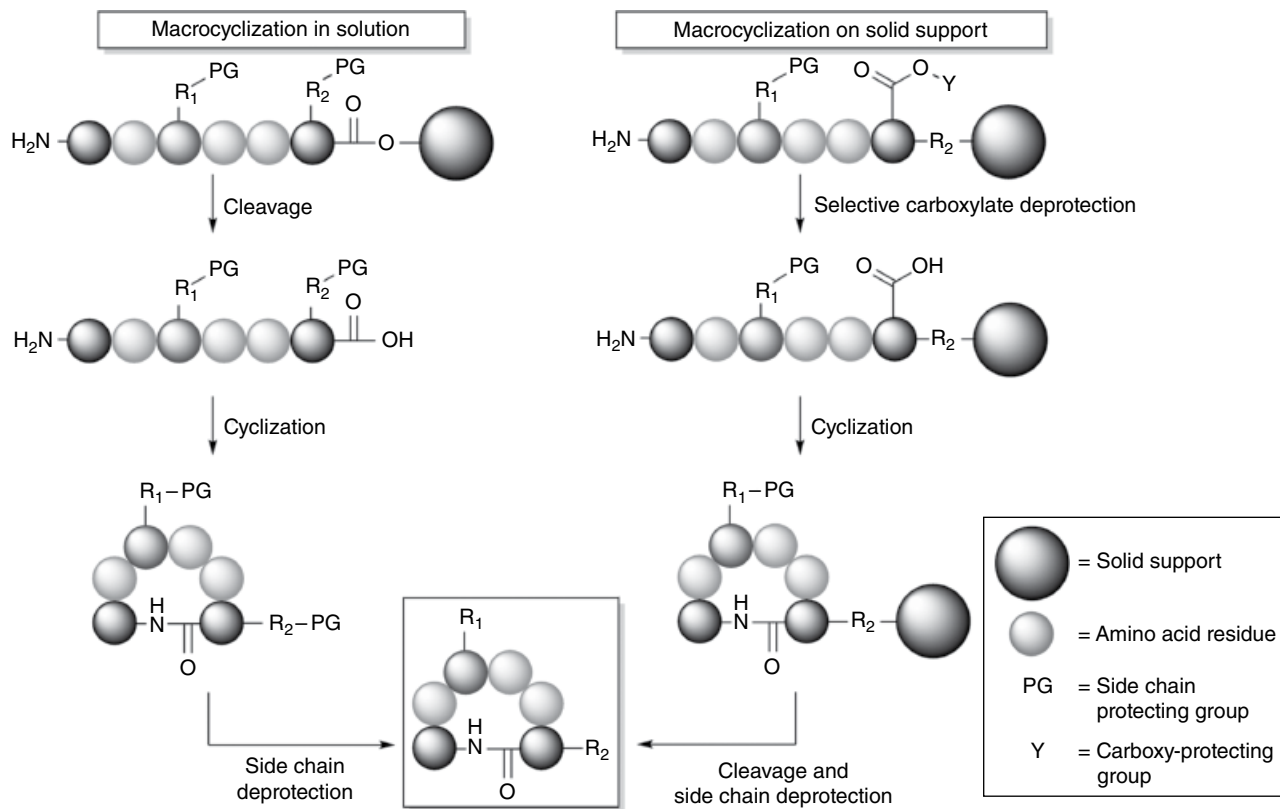
Figure 9.2 Solution- versus solid-phase macrocyclization for head-to-tail cyclic peptides.

9.2 One Size Does Not Fit All: Factors to Consider During Synthesis Design

In principle, all methods suitable for peptide bond formation can be applied for head-to-tail macrocyclization of linear peptides; however the reaction usually proceeds more slowly than the corresponding bimolecular version. The main challenge in peptide macrocyclization is to overcome the ring–chain equilibrium to minimize the probability of oligomerization and improve cyclization efficiency (see Chapter 1). Besides the use of high or pseudo-high dilution conditions to favor intramolecular reactivity, different strategies have been developed to promote folding of the linear precursor into ringlike conformations that are conducive to cyclization [39].

9.2.1 Ring Size

The ability of a linear precursor to bring reactive ends in close spatial proximity dramatically influences the chances of success of macrocyclization [39]. Therefore, ring size is the most important factor to consider when choosing a suitable strategy for peptide macrocyclization, especially for the head-to-tail configuration.

The formation of small- to medium-sized cyclic peptides, especially those containing three, four, or five amino acid residues, can often be troublesome, if not impossible. In this case, the ground-state *trans*-peptide bonds typically prevent ringlike folding of the linear precursor and reactive ends from coming in close proximity [40–42]. Moreover, ecliptic and transannular interactions may energetically disfavor the conformational pre-organization of the linear precursor [23, 43–45]. On the other hand, head-to-tail cyclization of peptides containing more than seven amino acid residues is generally straightforward and usually not hampered by sequence-specific problems since the ring size of 21 atoms or more can accommodate *trans*-peptide bonds and unfavorable interactions. In order to overcome the drawbacks associated with the synthesis of small- and medium-sized cyclic peptides, specific strategies to direct ringlike conformations of linear precursor have been developed over the years [2, 39, 46].

9.2.2 Incorporation of Turn-Inducing Elements

Short peptides composed exclusively of L-amino acid residues are usually very difficult to cyclize [23, 44, 45]. An efficient strategy to help bring the reactive ends of a

peptide together is to induce a β-turn-like conformation in the linear precursor by introducing a *cis*-amide bond in the middle of the peptide chain (Figure 9.3). In this case, the presence of turn-inducing elements that favor *cis*-peptide bonds, such as proline or *N*-methyl amino acids, can significantly increase the macrocyclization rate of small- to medium-sized peptide sequences [47–51]. This strategy has been successfully used for the synthesis of a wide variety of cyclic peptides including tri-, tetra-, and pentapeptides as well as larger macrocyclic β-hairpin mimetics based on the heterochiral D-Pro-L-Pro template [50–54].

Considering the *cis*-inducing effect of *N*-methyl amino acids, backbone amide protecting groups can also be used as reversible turn inducers during cyclic peptide synthesis (Figure 9.3) [55]. Initially developed to prevent aspartimide formation and intra- or interchain aggregation of the resin-bound peptides [56–59], these protecting groups alter the backbone conformation by the tertiary amide bond that is formed and facilitate macrocyclization. Similarly, the synthesis of small-sized cyclic N-substituted glycines (peptoids) was reported to occur in excellent yields [60–62]. Almost all backbone protecting groups are based on a substituted benzyl group structure [63], and the most commonly used for the Fmoc/tBu strategy are 2-hydroxy-4-methoxybenzyl (Hmb, **1**) [64, 65], 2,4-dimethoxybenzyl (Dmb, **2**) [66–68], and 2,4,6-trimethoxybenzyl (Tmob, **3**) (Figure 9.3) [57]. These groups can be readily removed with the standard trifluoroacetic acid (TFA) cocktails used in

Fmoc/tBu SPPS. Otherwise, photolabile protecting groups such as 4-methoxy-2-nitrobenzyl (Mnb, **4**) and 2-hydroxy-6-nitrobenzyl (Hnb, **5**) can also be utilized (Figure 9.3) [69, 70]. In this case, protecting group removal is performed under UV irradiation. Most backbone protecting groups are introduced by reductive amination of the protecting group's corresponding aldehyde with the amine moiety of the amino acid, followed by either α-amino protection or dipeptide formation [55, 66, 67, 71, 72]. Moreover, as described later in this chapter, hydroxyl-containing groups such as Hmb and Hnb can be exploited for *O*-to-*N* acyl transfer and ring contraction strategies (RCS) to generate cyclic peptides [73–75].

In cases where a serine, threonine, or cysteine residue is found in the sequence, a pseudoproline residue can be used as a turn-inducing element (Figure 9.3) [76–80]. Pseudoprolines are modified heterocyclic amino acids derived from serine **6** and threonine **7** ((4*S*)-oxazolidine-4-carboxylic acid) or cysteine **8** ((4*R*)-thiazolidine-4-carboxylic acid), and their incorporation into a peptide chain predominantly induces a *cis*-conformation of the preceding amide bond [79, 81, 82]. Oxa- and thiazolidine moieties in pseudoprolines are employed also for side chain hydroxyl or thiol protection during peptide elongation. Hence, a major advantage of using pseudoprolines as turn inducers is that they can be cleaved post-cyclization under acidic conditions to free the respective Ser, Thr, or Cys residue and thereby yield cyclic peptides devoid of turn-inducing elements.
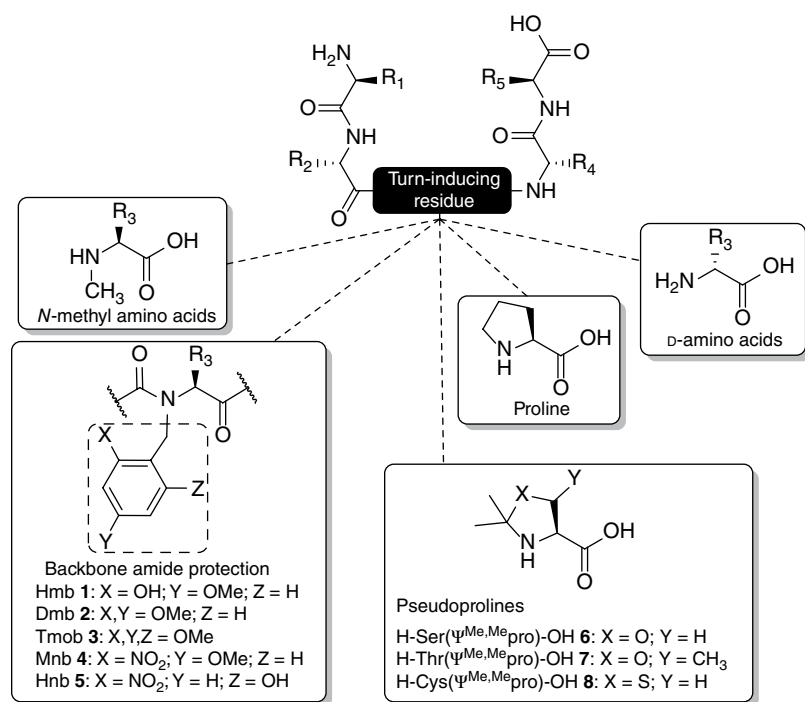
Figure 9.3 Turn-inducing residues to promote *cis*-amide bond and folded conformations.

Pseudoprolines from serine or threonine are commercially available as dipeptides (Fmoc-Xaa-Ser($\Psi^{Me,Me}$pro)-OH or Fmoc-Xaa-Thr($\Psi^{Me,Me}$pro)-OH) and can be incorporated in standard Fmoc-strategy SPPS. These powerful and traceless turn-inducing elements have even shown better turn-inducing capabilities than proline when used in the synthesis of various small and constrained macrocycles that could not be conventionally cyclized in a head-to-tail fashion [76, 78–80, 83].

It has been shown that peptides, exclusively composed of L-residues and lacking turn-inducing structures, would often cyclize only once the C-terminal α-carbon has epimerized to the D-configuration [84, 85]. Another study on peptide diastereomers showed that cyclization is favored between two residues of opposite stereochemical configuration, that is, a peptide containing both a D- and an L-residue at its termini [86, 87]. Therefore, the incorporation of D-amino acids into all-L peptides can also be considered as a turn-inducing strategy and has been used to improve the yields of various peptide macrocyclizations [84, 88, 89].

Other potential strategies involving external templates to facilitate macrocyclization of peptides have been developed and include metal ion-assisted [90–95], chemoenzymatic [96, 97], and polymeric scaffold [43, 98] approaches.

9.2.3 C-Terminal Epimerization

During synthesis design, the C-terminal amino acid of the linear precursor and the coupling reagent should be carefully chosen to minimize epimerization at the C-terminal residue during cyclization. Because of prolonged reaction times, macrocyclization reactions involving carboxy activation of chiral amino acids can sometimes lead to undesired high level of epimerization at the C-terminal amino acid [99]. Therefore, as observed in peptide fragment ligation, a C-terminal residue that is less prone to racemization such as glycine or proline should be chosen whenever possible. If not possible, it has been suggested to use amino acids lacking β-substitution as they should be more resistant to epimerization [100]. Otherwise, side reactions can be minimized by using a coupling reagent combining important properties such as high reactivity for rapid cyclization, low epimerization potential, and improved stability of the activated species to avoid acyl hydrolysis.

In principle, all coupling reagents suitable for amide bond formation can be used for backbone cyclization, but it has been shown that reagents based on 7-aza-1-hydroxybenzotriazole (HOAt, **9**) (Figure 9.4) gave high cyclization yields with low racemization rates [84]. It is also recommended to avoid uronium/aminium derivatives commonly used in standard SPPS, such as 2-(1*H*-benzo-

triazole-1-yl)-1,1,3,3-tetramethylaminium hexafluorophosphate (HBTU, **11**) or its tetrafluoroborate derivative (TBTU, **12**), 2-(6-chloro-1*H*-benzotriazole-1-yl)- and 1-[bis(dimethylamino)methylen]-1*H*-1,2,3-triazolo[4,5-*b*] pyridinium 3-oxide hexafluorophosphate (HATU, **13**), as they can form undesired N-terminal guanylated side product and are prone to hydrolysis of the activated acyl species if the macrocyclization reaction is too slow [101–104]. However, this N-capping problem may be overcome by the addition of 1-hydroxybenzotriazole (HOBt, **10**) and HOAt **9** or via the use of phosphonium derivatives such as benzotriazol-1-yloxy-tris(dimethylamino) phosphonium hexafluorophosphate (BOP, **14**), benzotriazol-1-yloxy-tris-pyrrolidinophosphonium hexafluorophosphate (PyBOP, **15**), or its HOAt analogue 7-azabenzotriazol-l-yloxy-tris-pyrrolidinophosphonium hexafluorophosphate (PyAOP, **16**) (Figure 9.4) [104, 105].

Epimerization of the C-terminal residue usually occurs through the formation of a 5(4*H*)-oxazolone intermediate and can take place with most of the standard carboxylic acid activating reagents used in peptide synthesis [106]. Formation of oxazolone intermediates has not been detected with acyl azides, and the use of azide derivatives such as diphenylphosphoryl azide (DPPA, **17**) can be considered when the C-terminus contains an amino acid prone to epimerization [101, 107]. However, compared to other activated acyl derivatives, the aminolysis of acyl azides is significantly slower, and prolonged reaction times are required [25, 85].

Anyone planning a macrocyclization from a linear peptide will face a tremendous choice of coupling reagents. The application and efficiency of coupling reagents have been extensively studied and reported in several reviews [101, 103, 108]. Besides the most commonly used coupling reagents including the HOAt derivatives, PyBOP, BOP, and DPPA, successful macrocyclization of linear peptides has been reported when using the corresponding pentafluorophenyl (Pfp) esters [109, 110], 1-ethyl-3-(3′-dimethylaminopropyl)carbodiimide hydrochloride (EDC, **18**) [111, 112], pentafluorophenyl diphenylphosphinate (FDPP, **19**) [76, 78, 113, 114], 3-(diethoxyphosphoryloxy)-1,2,3-benzotriazin-4(3*H*)-one (DEPBT, **20**) [91, 115], 4-(4,6-dimethoxy-1,3,5-triazin-2-yl)-4-methylmorpholinium tetrafluoroborate (DMTMM·BF$_4$, **21**) (Figure 9.4) [78, 116], and others.

9.2.4 Choosing the Right Macrocyclization Site

The synthesis of cyclic peptides generally involves an entropically disfavored head-to-tail cyclization. Therefore, the ring disconnection site must be chosen carefully during the design of a strategy as it can make the difference between success and failure. This difference has been clearly illustrated by investigating all ring disconnection
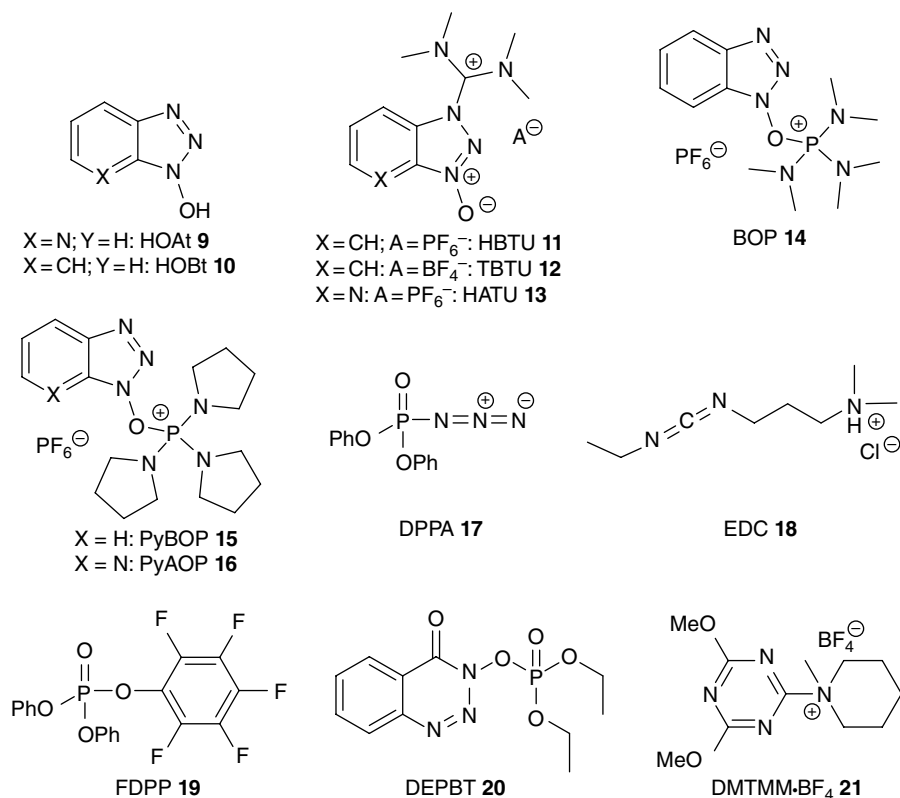
Figure 9.4 Structure of different coupling reagents used for peptide synthesis and macrolactamization.
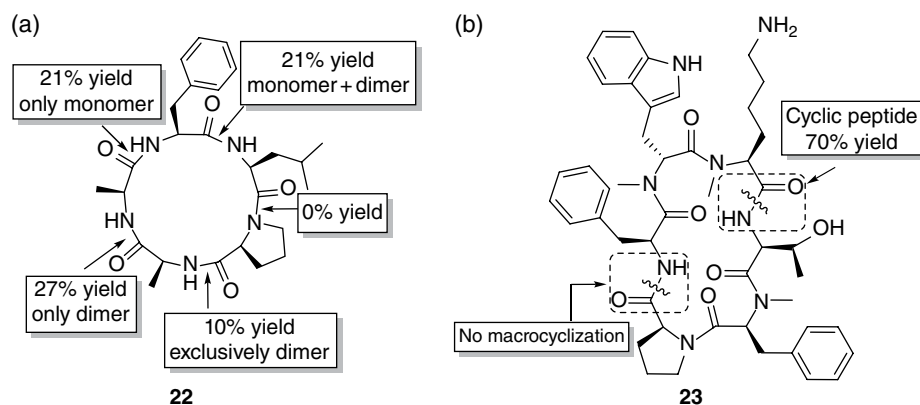
Figure 9.5 Ring disconnection sites and yields obtained in the synthesis of (a) cyclo[Pro-Ala-Ala-Phe-Leu] **22** and (b) cyclo[NMe-Phe-Pro-Phe-NMe-D-Trp-NMe-Lys-Thr] **23**.

possibilities on a representative cyclic peptide (cyclo[Pro-Ala-Ala-Phe-Leu], **22**) [23]. Important disparities were observed in the macrocyclization yields obtained, and, indeed, only the linear precursor H-Phe-Leu-Pro-Ala-Ala-OH was successfully cyclized exclusively as the desired monomer, albeit in 21% yield (Figure 9.5a). It was proposed that the turn-inducing effect of the Pro residue and the formation of a strong intramolecular hydrogen bond were required to enforce proper folding of the precursor to enable cyclization. Another example has been

described by Kessler and coworkers where an inappropriate ring disconnection on the N-methylated cyclic peptide **23** led to no cyclization at all (Figure 9.5b) [117]. It was observed that the turn-inducing Pro residue in the central part of the linear precursor was critical for efficient cyclization and the desired cyclic peptide was then obtained in 70% yield. On the other hand, this turn is not present when the Pro residue is located at the C-terminus, and, in this instance, the linear peptide failed to cyclize.

As the cyclization position can dictate the level of success in cyclic peptide synthesis, simple guidelines have been proposed to assist in choosing the disconnection site [118]. For example, the macrocyclization yield can be optimized: (i) if macrocyclization occurs between two residues of opposite stereochemical configuration (D- and L-residue) [84], (ii) if the cyclization site is not sterically encumbered by *N*-alkyl, α,α-substituted, or β-branched amino acids, (iii) if turn-inducing elements such as Gly or Pro are present in the sequence [23, 117], and (iv) if intra-chain hydrogen bonds can be formed to facilitate folding [39, 119]. However, adhering to these simple guidelines does not guarantee that any cyclic product will be obtained and the opposite can also be true. For example, Kirchenbaum and coworkers have shown that peptoid hexamers with sterically encumbered N-terminal and no possible intra-chain hydrogen bond can be cyclized in 5 min with PyBOP as coupling reagent in 97% yields [62].

To overcome the challenges associated with peptide macrocyclization, a wide variety of synthetic strategies has been developed over the last years. The following sections will describe different solution- and solid-phase approaches that have been recently reported to prepare cyclic peptides by amide bond and disulfide bridge formation.

9.3 Peptide Macrocyclization in Solution

In many cases, the solution-phase strategy is the best choice for performing the macrocyclization step, especially when larger quantities of cyclic peptide are required (for scale-up examples and issues with macrocycles; see Chapter 15). Compared with solid-phase cyclization, the solution-phase approach is often faster, and the final products are frequently recovered in higher yields. The use of this strategy greatly depends on the ability to prepare orthogonally protected bifunctional linear

precursors with free terminal groups and intact side chain protection. Solid-phase synthesis is the most convenient and efficient method to generate such linear precursors, and a wide variety of acid-labile linkers allowing the release of the linear peptide from the polymer without sacrificing side chain protection has been developed [120, 121]. Handles for standard Fmoc/tBu-based SPPS of protected peptides and the conditions used for cleavage have been recently reviewed [120]. Two of the best examples in Fmoc-SPPS to release side chain protected peptide acids under mild acidic conditions are 2-chlorotrityl chloride resin [122–124] and 4-hydroxymethyl-3-methoxyphenoxybutyric acid (HMPB) linker [125, 126].

In classical solution-phase macrolactamization methods, the linear side chain protected peptide obtained after cleavage from the resin is cyclized using a coupling reagent in the presence of a base under high dilution conditions (Figure 9.6). Typically, the reaction is performed in DMF at concentrations from 0.1 to 1 mM, but if the linear precursor readily pre-organizes itself into a ringlike conformation, the concentration can be significantly increased. Other solvents such as DCM, THF, or CH_3CN and their combination with DMF have also been reported for the cyclization step. After macrocyclization, side chains are deprotected, and the product purified by HPLC, or the opposite (HPLC purification followed by deprotection), can also be performed to yield the desired cyclic peptide.

This classical approach is straightforward and often works well with less constrained medium- and large-sized peptides, especially when turn-inducing elements are present in the linear precursor. Otherwise, a great number of synthetic strategies have also been developed to give access to more strained and complex cyclic peptides.

9.3.1 Ring Contraction Strategies

The RCS is based on the formation of a larger, more flexible macrocycle followed by an intramolecular ring contraction to generate the desired peptide. Over the last

Figure 9.6 General synthetic route for head-to-tail macrocyclization in solution through activated ester formation (PG, side chain protecting group).
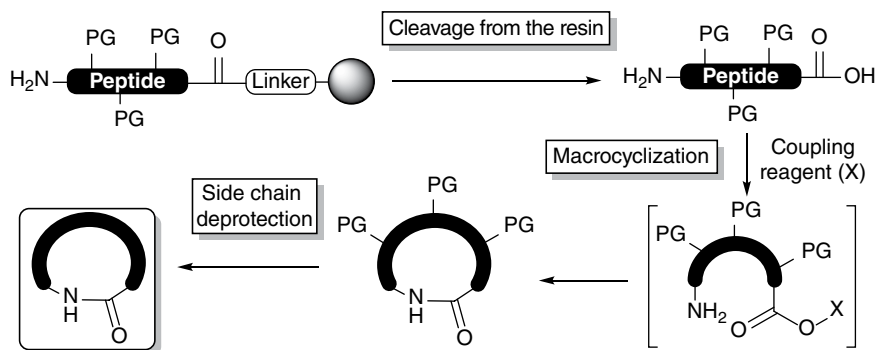
decade, this strategy has emerged as an efficient method to prepare constrained cyclic tetra- and pentapeptides. It generally involves the formation of an ester or thioester bond between a C-terminal carboxyl or ester and an N-terminal amine, a side chain, or a protecting group to allow the transfer of the acyl chain to the amino function (*O*-to-*N* or *S*-to-*N* acyl migration), and the formation of a homodetic cyclic peptide.

Earlier examples of intramolecular *O*-to-*N* acyl transfer in cyclic peptide synthesis involved the formation of a cyclodepsipeptide via a Ser residue side chain followed by ring contraction through migration of the acyl from the hydroxyl group to the N-terminal amine (Figure 9.7) [127]. In this study, the C-terminus of an *N*-Boc-protected serine was anchored to the resin and the linear peptide assembled by Fmoc-SPPS via its side chain. After cleavage from the solid support, the depsipeptide was cyclized under high dilution using BOP as coupling reagent and the *N*-Boc group removed to allow the *O*-to-*N*

acyl transfer under basic conditions. This strategy proved effective to prepare cyclic penta-, hexa-, and heptapeptides, while no product was observed for the tetrapeptide derivative [127].

Another strategy involving macrolactones uses an N-terminal backbone amide protecting group to help form the less constrained ring and allow a ring contraction by *O*-to-*N* acyl migration [73–75, 128, 129]. In this case, the turn-inducing element participates in macrolactonization and ring contraction but is removed thereafter. In one approach, the photolabile protecting group Hnb **5** is attached to the N-terminus of a peptide chain by reductive amination (Figure 9.8). After cleavage from the resin, a macrolactonization is performed in solution between the C-terminal carboxyl and the hydroxyl function of the Hnb group using BOP or HATU as coupling reagent to form a cyclic nitrophenyl ester intermediate. The close proximity of the N-terminal amino group in the cyclic depsipeptide facilitates *O*-to-*N* acyl transfer to yield the

Figure 9.7 Synthesis of head-to-tail cyclic peptides via *O*-to-*N* acyl migration.
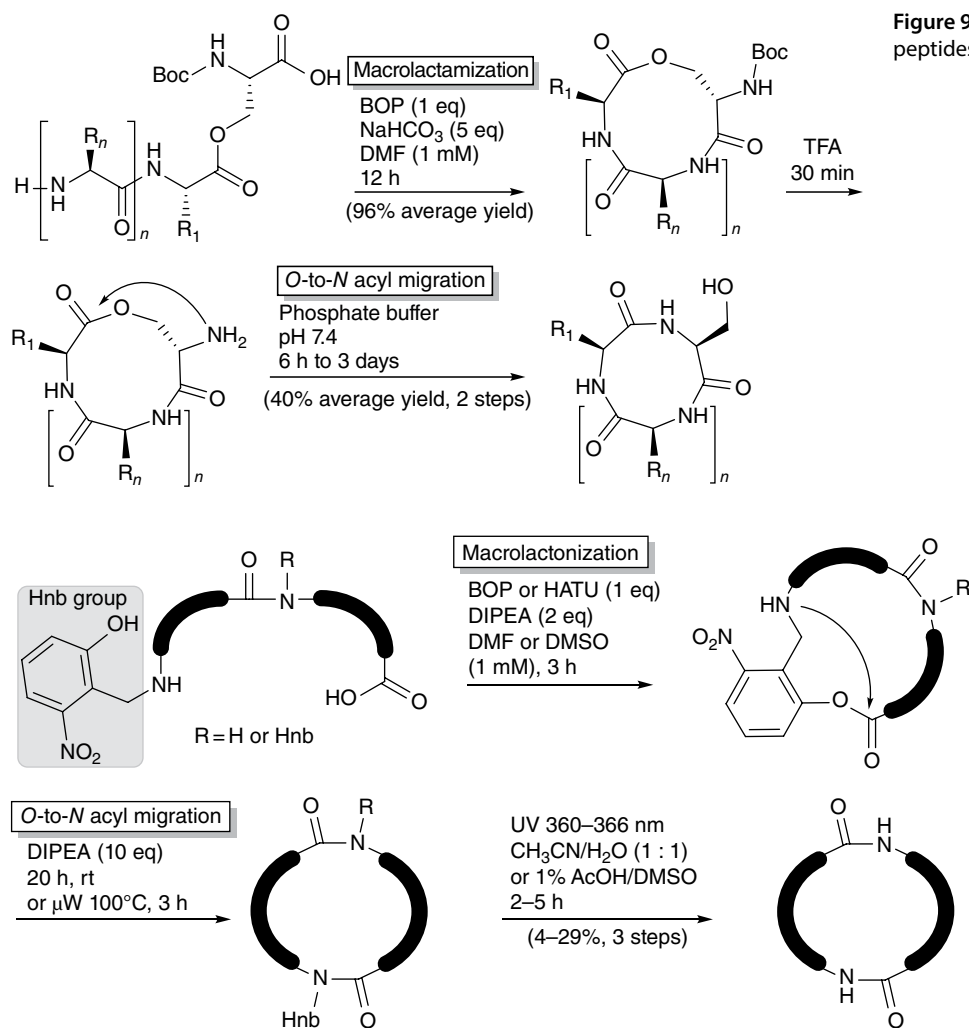
Figure 9.8 Head-to-tail macrocyclization through a ring contraction strategy using a hydroxylated photolabile auxiliary.

corresponding *N*-Hnb cyclic peptide. Finally the Hnb group is removed by photolysis. As a proof of concept, a linear peptide Ala-Phe-Leu-Pro-Ala, which cannot be converted into monocyclic product under conventional cyclization conditions, was successfully cyclized in 42% yield when the aforementioned N-terminal Hnb method was applied [73]. Later, the same approach was applied to tetrapeptides, and it was demonstrated that even highly constrained all L-cyclotetrapeptides could be efficiently obtained when an additional Hnb group was incorporated within the sequence [74, 75]. In this way the N-terminal Hnb group acts as the cyclization auxiliary for ring closure and ring contraction, while the second Hnb group acts as a *cis*-amide bond promoter to conformationally favor macrocyclization. Surprisingly, in the case of all-L cyclotetrapeptides, Hnb removal yielded linearized products from a ring expansion/opening reaction. To avoid this side reaction, the hydroxyl groups of Hnb had to be methylated prior to photolysis [75].

In another approach, (*E*)-2-(2-nitrovinyl)phenol **24** was used as a C-terminal auxiliary in the synthesis of cyclotetrapeptides by RCS (Figure 9.9) [130]. After cleavage from the resin, an *N*-Boc-protected peptide was esterified with (*E*)-2-(2-nitrovinyl)phenol, followed by deprotection of the N-terminal amino group. Upon basification, the N-terminus attacks the alkene moiety of the auxiliary via an intramolecular Michael addition reaction, giving a cyclic depsipeptide intermediate that allows *O*-to-*N* acyl transfer along with simultaneous release of the auxiliary to yield the desired cyclic peptide. The all-L tetrapeptide cyclo[Phe-Tyr-Ala-Gly] was prepared in 28% yield with this method, which is an improvement compared with the 11% yield reported for the same peptide using the Hnb auxiliary [74].

Recently, Li and coworkers developed an efficient imine-induced RCS based on an intramolecular Ser/Thr ligation approach [131–134]. This RCS requires a Ser or Thr residue at the N-terminus and a 2-phenylcarboxaldehyde ester at the C-terminus. Peptide salicylaldehyde esters then can be prepared without racemization by

both Boc-SPPS [131–133] and Fmoc-SPPS [134, 135] in moderate yields (Figure 9.10a and b). Cyclization of the linear precursor proceeds through intramolecular head-to-tail imine formation, and subsequent ring contraction by an *O*-to-*N* acyl transfer gives an *N*,*O*-benzylidene acetal, which is removed upon acidic treatment to afford the desired cyclic peptide (Figure 9.10c). While this method was successfully applied to the synthesis of natural bioactive cyclic peptides such as daptomycin [136], cyclomontanin B [137], mahafacyclin [133], and yunnanin C [131], a series of cyclotetrapeptides containing all L-amino acids was obtained in low overall yields [132]. In this instance, cyclic dimers were often formed in high proportions when the reaction was performed in pyridine/acetic acid (1:2) at 1 mM peptide concentration at room temperature for 4 h [132]. For larger ring sizes, the reaction could be performed at 5–10 mM precursor concentration [131, 133].

Overall, the RCS presented previously involve the formation of a cyclodepsipeptide intermediate prior to *O*-to-*N* acyl migration and generation of the final cyclic peptide. Some of these approaches have been used to prepare highly constrained cyclic peptides that failed with classical macrocyclization methods. Therefore, the development of new RCS is a very promising approach to access complex and otherwise difficult-to-construct peptide macrocycles.

9.3.2 Sulfur-Mediated Macrocyclizations

Most natural macrocyclic peptides are produced by nonribosomal biosynthesis using synthetases that activate the C-terminal carboxyl of linear precursors through thioester linkages to perform the macrocyclization [138]. Considering the high macrocyclization efficiency observed in biosynthetic pathways, many biomimetic approaches employing thioester activation of the C-terminal carbonyl have been developed.

Inspired by the important role of histidine in catalytic reactions such as proteolysis and transfer of activated

Figure 9.9 Head-to-tail macrocyclization via a ring contraction strategy using the (*E*)-2-(2-nitrovinyl)phenol auxiliary **24**.
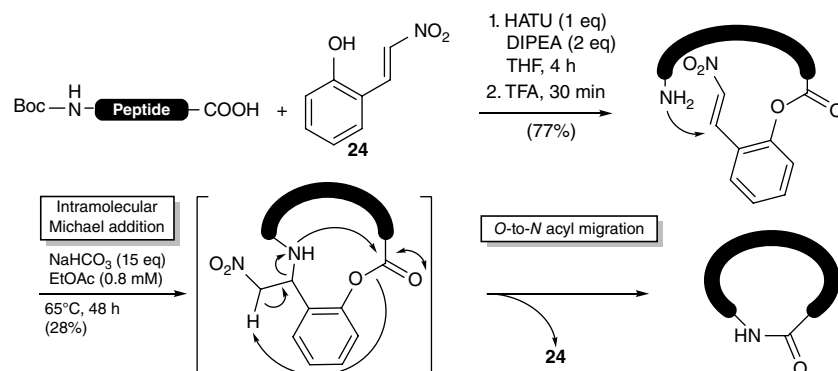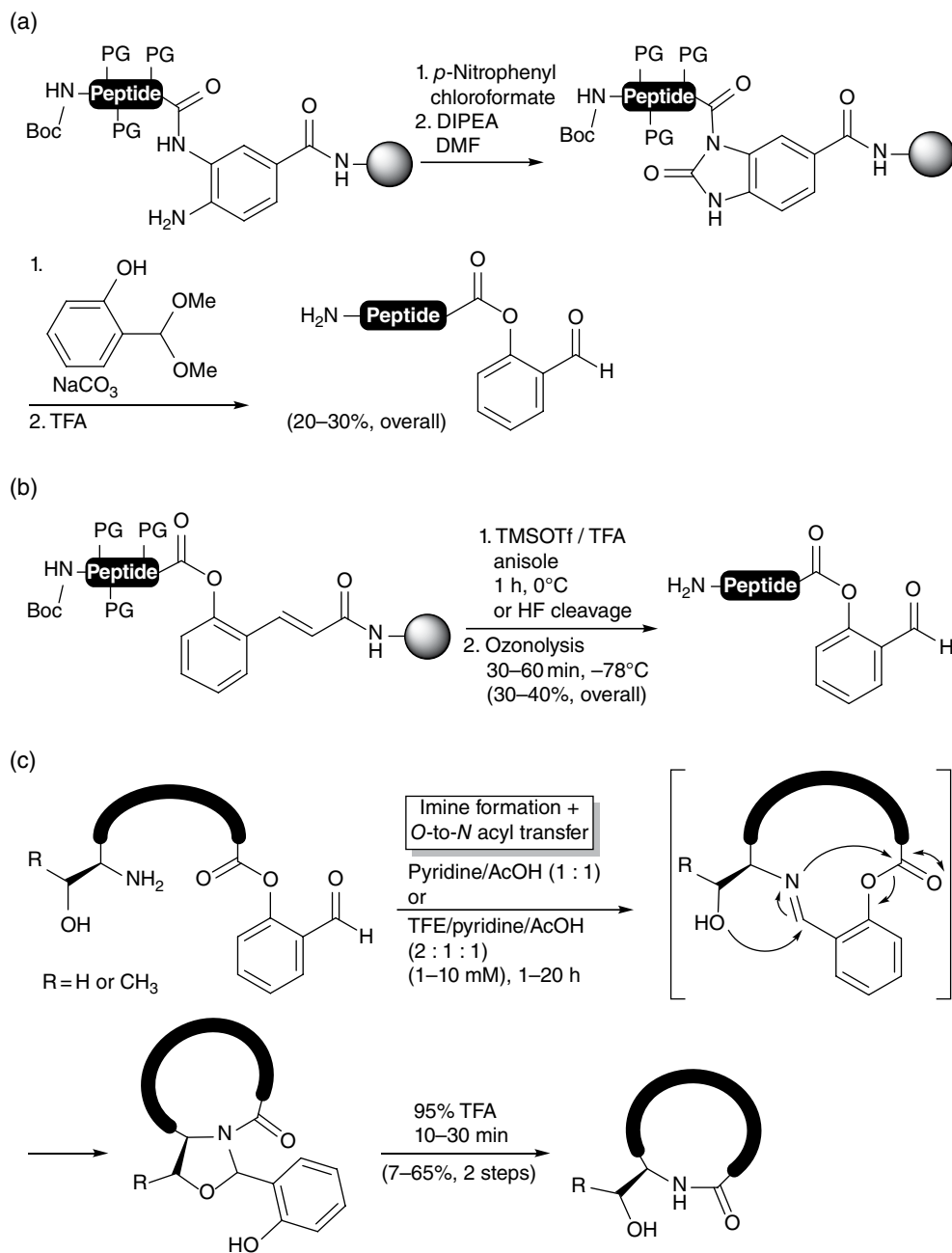
Figure 9.10 Ring contraction strategy by Ser/Thr ligation. Preparation of peptide salicylaldehyde esters by (a) Fmoc-SPPS and (b) Boc-SPPS. (c) Macrocyclization by intramolecular imine-induced *O*-to-*N* acyl migration (PG, side chain protecting group).

acyl groups, Houghten and coworkers developed a method to prepare head-to-tail cyclic peptides by the direct aminolysis of peptide thioesters in the presence of imidazole (Figure 9.11) [139]. Imidazole is proposed to act as a nucleophilic catalyst that attacks the carbonyl group of the thioester to form a reactive acyl imidazolyl intermediate, which subsequently reacts with the N-terminal amino group. Five to eleven residue peptides were cyclized in yields ranging from 15 to 51%, and the macrocyclization rate was found to be dependent on ring size. It was also shown that imidazole plays a critical role in macrocyclization by suppressing thioester hydrolysis, as only hydrolyzed linear precursor was observed when imidazole was not used. This approach was also employed in the synthesis of the cyclodepsipeptide kahalalide B and its analogues through a macrolactonization between a C-terminal thioester and the side chain hydroxyl group of a Ser residue in good yields [140].
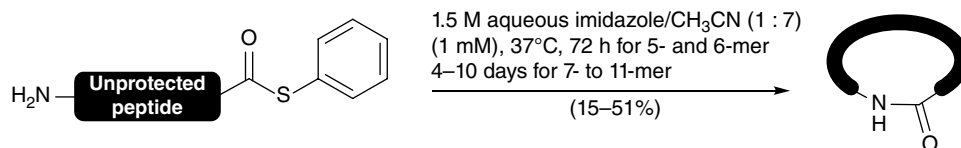
Figure 9.11 Head-to-tail cyclization of peptide thioesters catalyzed by imidazole.

Figure 9.12 Head-to-tail macrocyclization of peptide thioacids using Sanger's reagent.
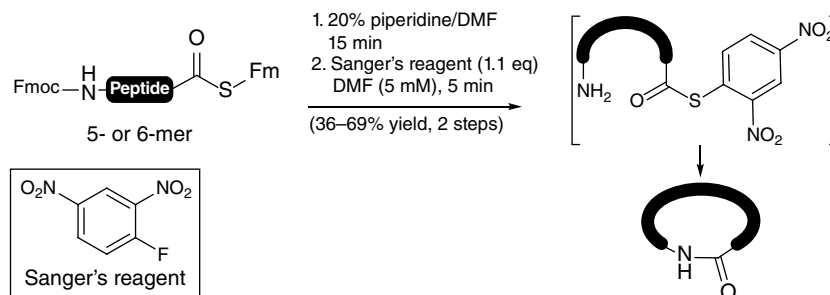
Figure 9.13 Head-to-tail macrocyclization of peptide thioesters by native chemical ligation.
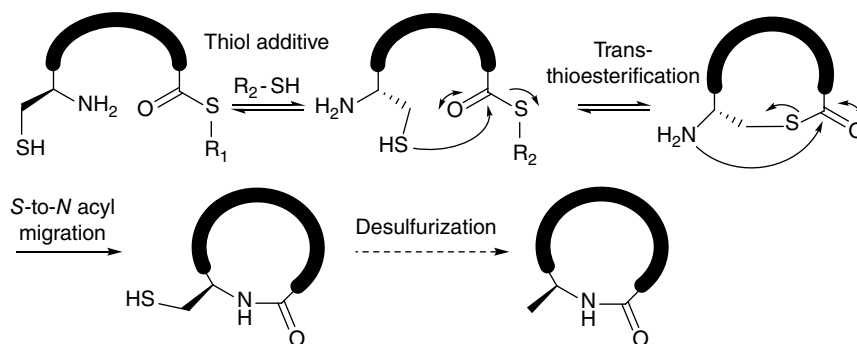
In another approach developed by Crich and Sasaki, 1-fluoro-2,4-dinitrobenzene (also known as Sanger's reagent) was used with peptide thioacids to generate activated thioesters and allow macrocyclization (Figure 9.12) [141]. In this case, an *N*-Fmoc-protected and C-terminal 9-fluorenylmethyl thioester (SFm) peptide is treated with piperidine to release the peptide thioacid. Macrocyclization is performed at a concentration of 5 mM in the presence of Sanger's reagent and proceeds through an initial aromatic substitution on the reagent to generate a reactive thioester that is subsequently attacked by the N-terminal amino group. This method was used to prepare cyclic penta- and hexapeptides in 44–69% yields and was shown to be compatible with free carboxylic acids and hydroxyl groups. Another advantage of this method is the short reaction time required for macrocyclization. For example, the peptide cyclo(D-Glu-Ala-D-Val-Leu-D-Trp) was obtained in only 5 min from the unprotected linear precursor. Cyclotetrapeptides could not be prepared by this approach, yielding only cyclodimerization products.

Among the different acyl transfer strategies, native chemical ligation (NCL) is probably the most successful and popular [142–145]. Originally described by Kent and coworkers to link peptide fragments together [146], this powerful method has been exploited to generate homodetic cyclic peptides [147]. The reported RCS and sulfur-mediated cyclization strategies generally involve the use of an N-terminal 1,2-aminothiol group to form a thioester bond between a C-terminal carbonyl and an N-terminal thiol side chain to allow transfer of the acyl chain to the amino function (*S*-to-*N* acyl migration) and the formation of a peptide bond (Figure 9.13). This reaction is mainly driven by the higher thermodynamic stability of the amide over the thioester bond and the proximity of the functional groups involved in the *S*-to-*N* acyl migration. It was demonstrated that the reaction can be performed in the presence of unprotected functionalized side chains with no evidence of racemization.

After cleavage from the resin, cyclization of the peptide thioester precursor is performed, in most cases, under high dilution (5 mM) in aqueous buffer around

neutral pH, in the presence of a thiol derivative such as mercaptophenylacetic acid (MPAA), thiophenol, or mercaptopropionic acid. Generally used in excess, these reagents reduce intermolecular disulfides and serve as nucleophilic catalysts to generate a more electrophilic C-terminal active thioester and a better leaving group after attack on the carbonyl by the Cys thiol. The NCL cyclization strategy has been successfully used to prepare a wide variety of peptide macrocycles ranging from small-sized cyclotetrapeptides [148] to more complex cyclic peptides such as cyclotides [149–151], conotoxins [152, 153], sunflower trypsin inhibitor (SFTI-1) [154], and protein catenane (two interlocked cyclic peptides) [155]. The NCL method has also been applied to macrocyclization on solid support.

As effective as NCL may be, the strategy is limited to peptides containing an N-terminal Cys residue. To circumvent this cumbersome structural requirement, Kent and coworkers described the use of an oxyethanethiol moiety as a removable auxiliary group attached to the amino group of an N-terminal glycine to mimic the N-terminal cysteine (Figure 9.14) [156]. Macrocyclization was performed on the unprotected N-terminally modified peptide thioester precursor via a thiolactone intermediate, which then underwent *S*-to-*N* rearrangement to yield the desired macrolactams. After NCL macrocyclization, the *N*-oxyethanethiol group was removed with zinc dust in dilute acetic acid to yield the desired cyclic 19-mer peptides in 18–41% yields for two steps. In an effort to extend the NCL method to other amino acids, Dawson and Yan used a desulfurization reaction with Raney nickel after the NCL macrocyclization to generate an Ala residue from the Cys (see Figure 9.13) [157]. This practical approach fueled the emergence of mild and metal-free radical desulfurization protocols [158–160] and the development of β- or γ-thiol amino acids to expand the ligation–desulfurization method to

other amino acid residues such as Phe, Val, Arg, Leu, Asp, Lys, Thr, Gln, Glu, and Pro [161–163].

While Boc-SPPS can be used to prepare peptide thioesters [164], several methods compatible with Fmoc-SPPS have been developed to facilitate the construction of C-terminal thioesters or their latent surrogates (Figure 9.15) [165–170]. Dawson and coworkers reported an efficient Fmoc-SPPS approach to peptide *N*-acyl-benzimidazolinones (Nbz), which can be readily converted to peptide thioesters upon treatment with an exogenous aryl thiol [170]. In this strategy, an *o*-aminoanilide linker is used on an acid-labile handle to perform peptide elongation by standard Fmoc-SPPS and allow the formation of a resin-bound benzamidazolinone upon treatment with *p*-nitrophenyl chloroformate and a hindered base (Figure 9.15a). After cleavage from the resin with standard TFA cocktails, the unprotected peptide Nbz can be converted to the corresponding thioester through addition of a suitable thiol. In another innovative approach, a hydrazine 2-chlorotrityl resin is used to prepare hydrazine peptides by Fmoc-SPPS (Figure 9.15b) [148, 168]. After cleavage from the resin, the unprotected peptide hydrazide is activated by treatment with $NaNO_2$, while subsequent addition of an aryl thiol promotes the conversion of the acyl azide intermediate into the desired reactive C-terminal thioester for NCL. The use of *in situ* *N*-to-*S* acyl transfer has also emerged as promising approach to prepare peptide thioester precursors for NCL [171]. One of the best example is the development of the bis(2-sulfanylethyl)amino (SEA) group that has been employed as a linker (SEA–Trt resin) and an on/off redox switch, enabling one-pot macrocyclization and iterative NCL (Figure 9.15c) [166, 167, 172, 173].

Another thioester-based RCS based on the traceless Staudinger ligation has been applied to the synthesis of cyclic peptides [174, 175]. Developed by Hackenberger and Kleineweischede, the method involves an intramolecular
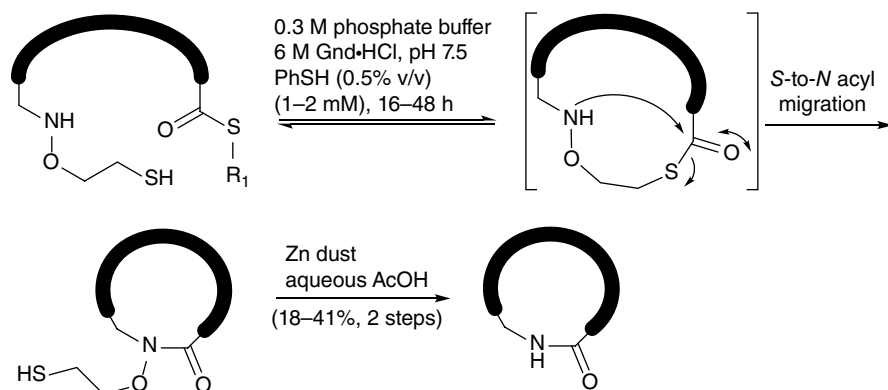
Figure 9.14 Head-to-tail macrocyclization of unprotected peptide thioesters with removable N-terminal oxyethanethiol by native chemical ligation (Gnd, guanidine).
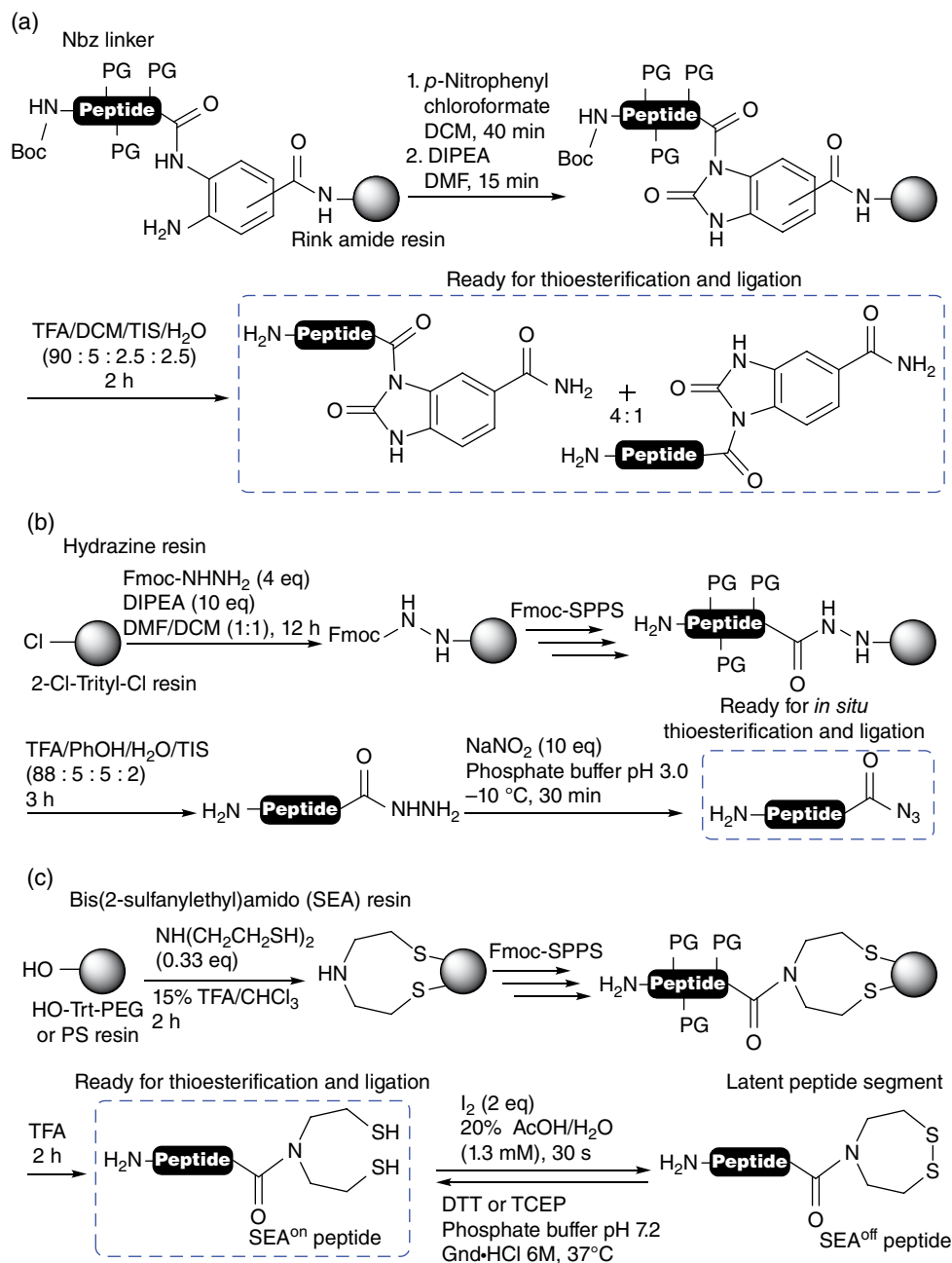
Figure 9.15 Solid supports for the synthesis of peptide thioesters by Fmoc-SPPS. (a) Dbz linker on Rink amide resin to prepare peptide *N*-acyl-benzimidazolinones; (b) hydrazine resin for the synthesis of peptide hydrazides as thioester surrogates; (c) SEA–Trt resin for the synthesis of SEA^on/off peptide precursors.

reaction between a C-terminal phosphine-tethered thioester and an N-terminal azide, yielding a cyclic iminophosphorane, which contracts to form a native amide bond as the nitrogen of the aza-ylide attacks the thioester (Figure 9.16). In the original study, the Staudinger RCS was applied to three globally deprotected undecapeptides and the cyclization conducted in DMF at a concentration of 6 mM for 12 h to afford the corresponding cyclic peptides in overall yields ranging from 20 to 36% [174]. More recently, a variant of this approach employing a tributylphosphine-activated *N*-azide peptide thioester was used to prepare a small cyclotripeptide in 48% yield [175].

9.3.3 Cyclic Depsipeptides and Peptoids

Cyclic depsipeptides are macrocyclic lactones containing one or several ester bonds in the backbone and are,
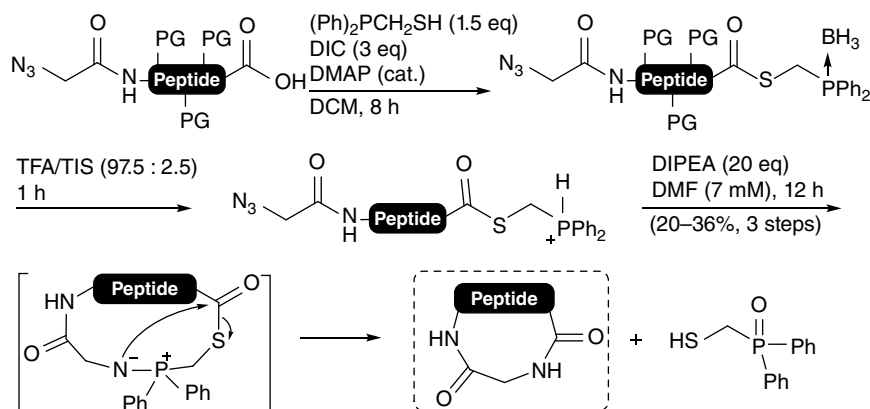
Figure 9.16 Head-to-tail macrocyclization by traceless Staudinger ligation.

therefore, heterodetic cyclic peptides. In these peptides, the ester bond can be formed between an α-hydroxy acid or the side chain of a Ser or Thr residue and a backbone C-terminal or side chain carboxyl. A great number of cyclodepsipeptides with important biological activities produced by a wide variety of organisms and have been recently reviewed [176, 177]. The significance of incorporating an ester bond in the macrocycle is not clear, but appears to be essential for biological activity, since the corresponding all-amide analogues are often inactive. Both solution- and solid-phase methods for the synthesis of cyclodepsipeptides have been reported [176, 177]. In most cases, since the ester bond is recognized as being more difficult to incorporate into the backbone than amides, macrolactamization has been the method of choice for depsipeptide ring closure. Therefore, the ester bond is most often preformed in the linear precursor prior to cyclization by using carbodiimide reagents in the presence of catalytic amounts of DMAP or another efficient coupling reagent for esterification [178]. Macrocyclization is then performed using the same conditions as developed for homodetic macrocycles. Nevertheless, a few successful examples of macrolactonization have been reported, such as the synthesis of jasplakinolide using DCC/DMAP and A54556 acyldepsipeptides with 2-methyl-6-nitrobenzoic anhydride (MNBA), DMAP, and a lanthanide triflate [177, 179, 180].

Peptoids are oligomers of N-substituted glycines (with the N-substituent duplicating an amino acid side chain) possessing very attractive peptidomimetic capabilities and biological properties for the development of therapeutic candidates and molecular tools [181–185]. Despite their inability to donate hydrogen bonds and the presence of a hindered N-terminal N-substituted amino group, the cyclization of peptoids is effective. This efficiency has been attributed to the lower *cis/trans* interconversion energy barrier that facilitates chain folding required for macrocyclization. In the case of cyclic peptoids, macrocycle size is also critical. Kirschenbaum

and coworkers cyclized a broad range of peptoid sizes from 5- to 20-mers with PyBOP in 71–97% yields in only 5 min at a concentration of 2.3 mM in DMF [62]. However, cyclic tetrapeptoids were generated in only 12% yield under these conditions. In a more recent study, Culf and coworkers evaluated different conditions to prepare cyclic tri-, tetra-, and pentapeptoids [60]. They also observed no macrocycle formation with PyBOP and identified EDC/HOAt in the presence of triethylamine in DMF at a concentration around 5 mM as the best conditions to prepare cyclic tri- and pentapeptoids with 90 and 97% yields, respectively. For cyclic tetrapeptoids, the best results were obtained with HATU/HOAt in the presence of DIPEA at 50°C, which gave 80% yield.

9.4 Peptide Macrocyclization on Solid Support

As described previously, most macrocyclizations in solution require high dilution to limit competing intermolecular reactions. In an effort to decrease the volume of solvent used in the cyclization step and facilitate the process, a wide range of solid-phase macrocyclization strategies have been developed. With the linear precursor immobilized on the solid support, this approach creates "pseudo-dilution" conditions that favor intramolecular reactions over undesired intermolecular side reactions. As the cyclized product is bound to the solid support, the possibility to use reagents in high molar excess followed by simple washings to remove them makes this method a powerful tool to produce and diversify complex macrocyclic scaffolds [186–190].

Most solid-phase macrocyclization strategies require a third dimension of orthogonality versus backbone/side chain protection and the linker to allow the synthesis of the linear precursor, selective deprotection of the reactive ends (N- or C-terminus or side chain),

macrocyclization, and final cleavage from the solid support [30–35]. Palladium-labile moieties, such as allyl esters (OAll) or allylcarbamates (Alloc), have been widely used as orthogonal protection in Fmoc/tBu SPPS, and their cleavage was found to be nearly quantitative [191–196]. Highly acid-labile protecting groups such as trityl (Trt) or phenylisopropyl (PhiPr) esters have also been used, as long as their removal can be performed in mild acidic conditions to remain orthogonal to the other side chain protecting groups and the linker. While the chemical strategy is somewhat straightforward, regiochemistry must be meticulously considered. Solid-phase head-to-tail macrocyclization implies anchoring of the linear peptide precursor via (i) a side chain functional group, (ii) a backbone amide, or (iii) C-terminal bonding on latent inducible linkers (safety catch) for cyclative cleavage. Other cyclic peptide topologies can also be accessed through these strategies, but this section will focus on backbone-cyclized peptides [197].

9.4.1 Side Chain Anchoring

A great number of side chain anchoring strategies have been developed over the last decades, making this one of the most common approaches to prepare cyclic peptides on solid support; as a result, it has been applied to a wide range of amino acids and linkers. With their great range of sensitivity and the availability of many orthogonal protecting groups, acid-labile linkers are those most commonly used to anchor an amino acid by its side chain (Table 9.1).

The first step of this strategy is the anchoring of the amino acid to the solid support via its side chain functional group while the C-terminal carboxyl is orthogonally protected. After peptide assembly, protecting groups at the C- and N-terminus are sequentially removed, and the peptide is cyclized with selected coupling reagents in order to minimize the epimerization at the C-terminal residue. Many amino acids have been successfully anchored via their side chain to various linkers (Table 9.2). Depending on the linker, it is possible to release a side chain bearing a carboxylic acid (Trt, Wang, PAM, HMPA, and HMPB resins), an amide (Rink and PAL resins), a hydroxyl (HMPB, Wang, Trt, DHP, and active carbonate resins), or an amine (Trt, Met handle, active carbonate, and DHP resins). Among the trifunctional amino acids available for side chain anchoring, the most widely used functional group is the carboxyl of aspartic or glutamic acid [30, 186, 187, 195, 198–203, 205–207, 213, 214, 216–219]. Different orthogonal C-terminal protecting groups have been studied, including the Pd^0 labile allyl ester, the acid super-labile dimethoxybenzyl ester (ODmb), the hydrazine labile 4-[*N*-[1-(4,4′-dimethyl-2,6-dioxocyclohexylidene)-3-methylbutyl]

amino]benzyl ester (ODmab), or the base labile fluorenylmethyl ester (OFm) used in Boc chemistry. Even the NCL has been used in solid-supported macrocyclization through the thioesterification of a C-terminal carboxyl after allyl ester removal [203].

Amines found on the side chains of lysine, ornithine, and 2,4-diaminobutyric (Dab) acid have also been reported as efficient anchoring moieties [31, 220–222]. The amino group can react with Trt chloride resins, as well as active carbonate resin. The reverse Met handle has also been reported for side chain anchoring of lysine by reverse coupling and allows a selective cleavage from the resin with CNBr [220, 222]. More recently, Subra *et al.* reported the coupling of an amino group on a pipecolic linker that enabled the release of the primary amine under acidic condition [221]. Histidine has been successfully anchored by the imidazole nitrogen on Trt resin, but DKP formation was observed [209–211]. The use of fast Fmoc deprotection and neutralization procedure limited the formation of this undesired product to less than 20% [211]. Tryptophan and hydroxyproline have been successfully anchored via the indole nitrogen and the hydroxyl, respectively, on a DHP resin in the presence of pyridinium 4-toluenesulfonate [188, 215]. Hydroxyl-functionalized serine, threonine, and tyrosine have been anchored on active carbonate resins, trichloroacetimidate-activated Wang resin, and trityl chloride resins [208, 212, 223]. Fmoc-Tyr-OMe has also been immobilized on Wang resin through a Mitsunobu reaction, and after peptide assembly, selective C-terminal hydrolysis with LiOH or NaOH allowed head-to-tail cyclization [204]. Finally, an interesting approach involving the anchoring of Fmoc-Phe(*p*NH$_2$)-OAll through a triazene linkage has been recently described. After cyclization, this approach allowed the release of cyclic peptides containing an unsubstituted Phe residue upon acidic treatment followed by diazonium salt reduction with iron(II) sulfate [224].

Several problems might occur during the synthesis with side chain anchored, and care must be taken to choose adequate anchoring and cyclization strategies. Remacle and coworkers reported the formation of aspartimide with side chain-anchored aspartic acid via an amide bond, which precluded macrocyclization and favored N-terminal capping by uronium/aminium coupling reagent through the formation of *N*-tetramethylguanidinium [214]. DKP formation was also reported by Papini and coworkers at the dipeptide stage of the synthesis. It was suggested that this side reaction was caused by unhindered glycine at the C-terminal position and the leaving capabilities of the OAll group and could be avoided or minimized using fast Fmoc deprotection procedure [209]. Additional by-products were reported by Kates and coworkers while attempting to perform

Table 9.1 Linkers and resins used for side chain anchoring in the solid-phase macrocyclization strategy.

Name	Structure	Cleavage condition	References
PAM 4-(Hydroxymethyl)phenylacetic acid		HF	[186, 198, 199]
HMPA (PAC) 4-(Hydroxymethyl)phenoxyacetic acid		90–95% TFA	[30, 200–203]
HMPB 4-(4-Hydroxymethyl-3-methoxyphenoxy)butyric acid		96% TFA	[204]
Wang 4-(Hydroxymethyl)phenoxymethyl polystyrene or acetic acid		92–95% TFA	[205–208]
Trt, **CTC** Trityl or 2-chlorotrityl resins		83–95% TFA	[189, 209–212]
Rink amide 4-[(2,4-Dimethoxyphenyl)(amino)methyl]phenoxyacetic acid		82–95% TFA	[187, 213]
PAL 5-(4-(Aminomethyl)-3,5-dimethoxyphenoxy)valeric acid		90% TFA	[30, 214]
DHP 3,4-Dihydro-2H-pyran-2-methyloxymethyl polystyrene		5–40% TFA	[188, 215]

macrocyclization on solid support using the Dmab protecting group. In addition to the previously described N-terminal tetramethylguanidinium formation, they observed C-terminal piperidyl amide formation that could be avoided or minimized by a brief acidic treatment prior to cyclization. Elimination of 4,4′-dimethyl-2,6-dioxocyclohexylidene was also observed during the synthesis, leading to 4-aminobenzyl ester. Finally, premature cleavage of the peptide was also reported during allyl ester cleavage when the peptide was anchored to a trityl linker via a glutamic acid side chain [206].

9.4.2 Backbone Amide Anchoring

An alternative strategy to perform on-resin macrocyclization is to anchor the C-terminal amino acid on the solid support via its amino group, which then becomes a backbone amide during peptide synthesis. Known as the backbone amide linker (BAL) strategy, this strategy allows the release of cyclic peptides under acidic conditions, and the N-alkylated amide anchor can facilitate macrocyclization through a turn-inducing effect as observed with N-methyl amino acid residues (Section 9.2.2). Typically,

Table 9.2 Side chain anchoring strategies for peptide cyclization.

Amino acid				
Xaa	**Nα-protection (PG)**	**Orthogonal carboxyl protection (Y)**	**Linker**	**References**
Asp/Glu	Boc	OFm	PAM	[186, 198]
	Fmoc	ODmb	HMPA	[200]
	Fmoc	OAll	HMPA	[216]
	Fmoc	OAll	HMPA/PAL	[30, 214]
	Fmoc	ODmb	Wang	[205]
	Fmoc	OAll	Rink	[187, 213]
	Fmoc	OAll	PEG-PS	[217]
	Fmoc/Boc	OAl/OFm	PAM	[199]
	Fmoc	ODmab	HMPA	[201]
	Fmoc	ODmab	Rink	[218]
	Fmoc	ODmb/ODmab/OAll	Rink	[202]
	Fmoc	OAll	Trt/Wang	[206]
	N-term Trt-Cys(Xan)-OH	OAll, then SBzl	HMPA	[203]
	Fmoc	OAll	Wang	[207]
	Fmoc	OAll	TentaGel®-NH$_2$	[219]
	Fmoc	OAll	Met	[195]
Dab	Fmoc	OAll	Trt	[189]
His	Fmoc	OAll	Trt	[209–211]
Hyp	Fmoc	OAll	DHP	[188]
Lys	Fmoc	OAll	Active carbonate	[31]
	Fmoc	OAll	Met handle	[220]
	Fmoc	OAll	Pip	[221]
	Fmoc	OAll	Met handle/Rink	[222]
Ser/Tyr/Thr	Boc	OAll	Active carbonate	[223]
	Fmoc	OMe	HMPB-MBHA	[204]
	Fmoc	OAll	Wang	[208]
	Fmoc	OAll	Trt	[212]
Trp	Fmoc	OAll	DHP	[215]
Phe	Fmoc	OAll	Triazene	[224]

the first residue is coupled as an amino ester (H-Xaa-OPG) to an aromatic aldehyde linker via reductive amination to generate a supported benzylic secondary amine (Figure 9.17). Acylation can then be performed with the next amino acid under standard coupling conditions to obtain supported *N*-benzylamides, and the oligomerization can proceed. As seen in the side chain anchoring strategy, the carboxyl of the first amino acid must be orthogonally protected to allow cyclization upon selective N- and C-terminus deprotection.

After peptide assembly, selective C- and N-terminus deprotection, and macrocyclization under standard
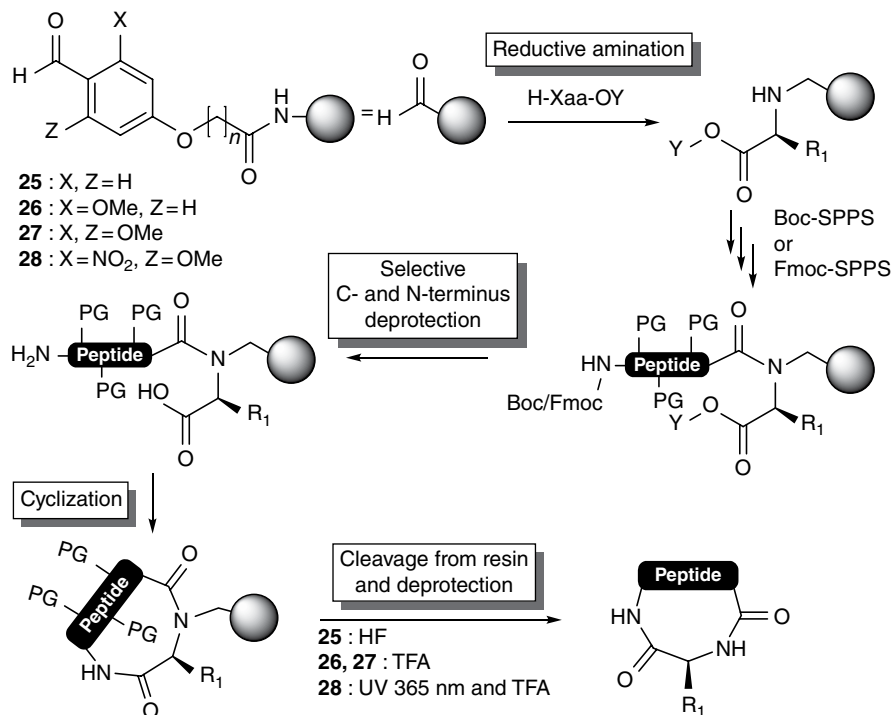
Figure 9.17 Solid-phase peptide macrocyclization via backbone anchoring strategy (PG, side chain protecting group; Y, carboxyl protecting group).

conditions via peptide coupling, the cyclic peptide is finally released from the resin. The BAL strategy has been extensively reviewed and several linker cores can be used [121]. Because it allows a great range of cleavage conditions depending on the electron-donating group substitution pattern, the most attractive and widely used is the benzyl core (Figure 9.17) [36, 38, 225–235]. Alkoxybenzylamide moieties **25** are prone to cleavage under very strong acidic conditions such as HF as used in Boc-SPPS [36, 225]. One major advantage of Boc-SPPS is the substantially reduced risk of DKP formation at the dipeptide stage because the amine is protonated until the neutralization/coupling step. Cleavage with refluxing TFA [231] and HBr : AcOH : TFA 1 : 3 : 40 for extended times has also been reported [228]. The 2,4-dialkoxybenzylamide **26** allows the release of cyclic peptides under somewhat milder acidic conditions, and cleavage with 92% TFA solutions has been reported, consistent with the electron-donating effect of the additional methoxy group that stabilizes the carbonium ion during acidolysis [229]. Microwaves can be used to considerably accelerate the cleavage of those linkers [235]. This report showed complete acidolysis of alkoxy- and *m*-dialkoxy-benzylamides with a 95% TFA cocktail at 80–100°C for 30–40 min under microwave irradiation, while no acidolysis was observed at room temperature. The use of microwave irradiation for cleavage could be very useful to expand

the selectivity and orthogonality in the synthesis of complex cyclic peptides. The trialkoxybenzylamide core **27** is the most widely used BAL linker and allows cleavage in very mild acidic conditions such as 1–5% TFA solutions [236, 237], as well as stronger media like 90–100% TFA [38, 226, 227, 230, 232–234, 238].

In such anchoring systems, since N-alkylated peptide bonds are *cis*-bond inducers (Section 9.2.2), special care should be taken to avoid DKP formation at the dipeptide stage [38, 239]. It has been demonstrated that the leaving group capability of the C-terminal carboxyl protecting group, stereochemistry, and steric hindrance play a pivotal role in that process [37, 233, 239]. For example, an allyl ester as carboxyl protecting group combined with unhindered amino acids such as glycine has been shown to be very prone to DKP formation [38]. In another approach, acid-sensitive Nα-protecting groups have been used on the second residue to allow N-deprotection under very mild acidic conditions and the generation of an N-terminal ammonium, which is unable to attack the C-terminal ester. For example, selective removal of Nα-Trt or Nα-(α,α-dimethyl-3,5-dimethoxy-benzyloxycarbonyl) (Ddz) protecting groups with 2–3% TFA for 5 min was reported to avoid DKP formation at the dipeptide stage when C-terminal allyl esters were used [38, 234]. C-terminal orthogonally protected β-amino acids have also been anchored to eliminate DKP

Figure 9.18 Different backbone amide linker derivatives.
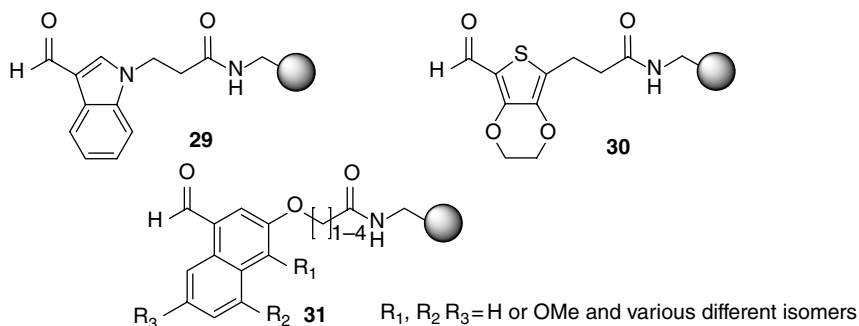
formation [230, 232]. In another study, Guichard and coworkers prevented the formation of DKP by removing the C-terminal allyl ester at the dipeptide stage to couple an allyl amino ester residue to the C-terminus prior to Fmoc removal, thereby forming a supported tripeptide unable to form DKP [233]. Overall, the most commonly used orthogonal C-terminal carboxyl protecting groups that allow solid-phase macrocyclization on BAL resins include allyl ester (OAll) [38, 227, 233], *p*-nitrobenzyl ester (O*p*Nb) [230], and phenylisopropyl ester (OPhiPr) [232].

Coupling of the second amino acid residue on the supported N-substituted bi- and tri-alkoxybenzylamines requires longer reaction times and stronger coupling reagents, such as HATU, symmetrical anhydrides, and carbodiimides because of the increased steric hindrance caused by the *o*-methoxy groups and the supported

amino ester residue [38, 240]. This led to the development of heteroaryl linker cores like the indole derivative **29** and several thiophene derivatives **30** (Figure 9.18) [236, 241]. Cleavage conditions for these linkers have been reported to be as mild as 2–5% TFA in DCM for 4 h for the indolyl linker and 1% TFA in DCM for 2 h for the thiophene derivatives. In addition, an *o*-nitrobenzyl core **28** was used as a photolabile BAL [242] (Figure 9.17), and naphthyl cores **31** were also described for fine-tuning of the acid lability [243].

9.4.3 Safety-Catch Resin Anchoring and Cyclative Cleavage

The use of safety-catch resins allows head-to-tail cyclization by intramolecular aminolysis (Figure 9.19). Head-to-side chain and side chain-to-side chain macrocyclization

Figure 9.19 Safety-catch linkers for cyclative cleavage strategy; (a) sulfonamide safety-catch linker and (b) *O-tert*-butyl-protected catechol safety-catch linker.
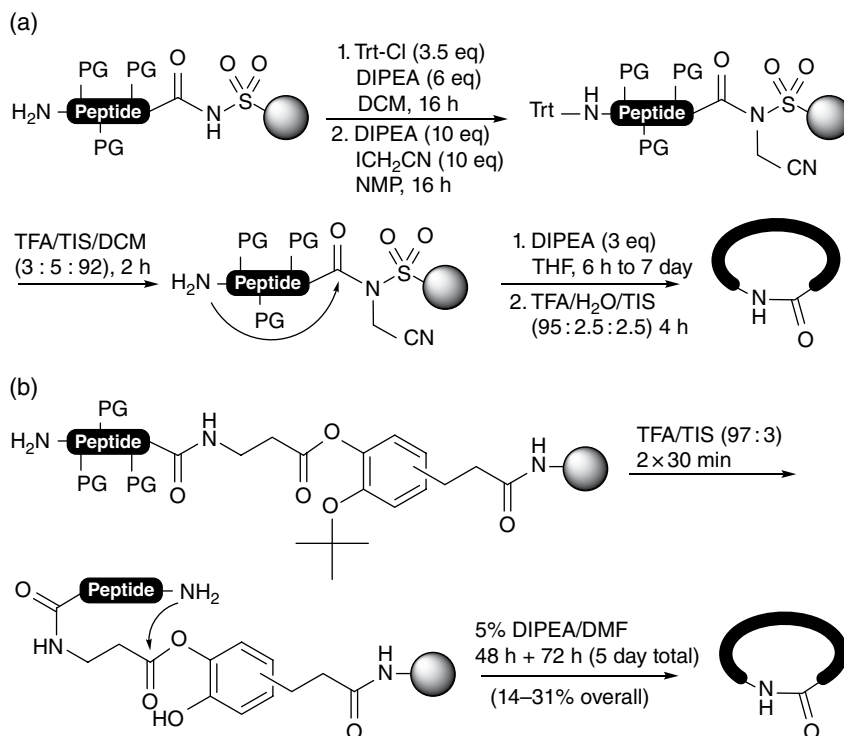
may also be performed with appropriate anchoring and suitable orthogonal side chain protection. In this strategy, the peptide is attached to the resin by its C-terminus and the linear precursor sequentially assembled by standard SPPS. The linker moiety is stable during the coupling and deprotection reactions, yet can be selectively activated after peptide synthesis, so that the bound linear precursor can undergo intramolecular aminolysis. The latter, called cyclative cleavage or cyclative release, allows simultaneous macrocyclization and release from the resin of the desired cyclic peptide. An example of a "safety-catch"-type linker for this process is the use of sulfonamide anchoring [244]. Initially reported by Moriello and coworkers for peptide macrocyclization, the sulfonamide linker allows intramolecular aminolysis upon N-alkylation of the sulfonamide with iodoacetonitrile followed by basic conditions (Figure 9.19a) [245–250]. Removal of the N-terminal protection, followed by base-induced ring closure on the newly activated linker and final deprotection, provides the cyclized product. This approach generally involves replacing the N-terminal Fmoc protecting group by an acid-labile alternative such as trityl prior to linker activation [245–249]. The additional step was performed because the Fmoc group was believed to be unstable upon cyanomethylation during linker activation. However, Kumarn and coworkers were able to avoid this step by using iodoacetonitrile freshly filtered through a plug of basic alumina and triethylamine as base for a final dual Fmoc removal and cyclization step [250]. The sulfonamide safety-catch linker was successfully applied to prepare bioactive cyclic homodetic peptides such as the decapeptides phakellistatin 12 and streptocidins A–D [247, 249], heptapeptides integerrimide A and B [250], hexapeptide cherimolacyclopeptide E [251], and tetrapeptide cyclo (GSPE) [252]. For this strategy, ring size plays a very important role and the reported overall yields generally vary from 5 to 21%. In another study, Smythe and coworkers used a mono-*O-tert*-butyl-protected catechol linker to perform a cyclative cleavage after activation of the linker with TFA to remove the *t*-butyl ether (Figure 9.19b). After neutralization and intramolecular aminolysis, cyclic pentapeptides have been obtained in 10–31% overall yields [253].

9.5 Peptide Macrocyclization by Disulfide Bond Formation

Disulfide bonds, which are formed by oxidative cross-linking of two thiol groups from Cys residues, play a key role in the folding and structural stability of a wide variety of bioactive peptides [254–256] and clinically important cyclic peptides such as oxytocin [257], vasopressin [258], and calcitonin [259]. The addition of a disulfide bond can also enhance the biological activity of a peptidic compound [260]. Cells utilize several strategies to form disulfides, most often catalyzed by an enzyme family called thiol-disulfide oxidoreductases, which contain a Cys-X-X-Cys motif. In its reduced form, this motif promotes disulfide exchange, leading to disulfide bond formation of a targeted protein [261–263].

A major advantage of disulfide bond formation is the wide range of ring sizes accessible for cyclization. For example, disulfide bonds can be formed between two adjacent Cys residues or between two Cys residues 80 amino acids away from each other in the primary sequence [264–267]. As observed with head-to-tail cyclic peptides, turn-inducing elements can facilitate macrocyclization [268–270]. Peptide macrocyclization by disulfide bond formation can be performed by both solution- and solid-phase methods (Figure 9.20). This section focuses on the synthesis of monocyclic disulfide-bridged peptides. Strategies to perform multiple disulfide bond formation with orthogonal Cys protections have been recently reviewed [21, 63, 271, 272].

9.5.1 Disulfide Bond Formation in Solution

The synthesis of monocyclic disulfide bridges is usually straightforward and disulfide bond formation in solution is often preferred to solid-phase strategies. Solution-phase approaches increase the scalability of macrocyclization, accelerate reaction kinetics, and, despite the pseudo-dilution phenomenon on solid phase, limit intermolecular side reactions compared with on-resin disulfide formation, especially for larger macrocycles [273]. In most solution-phase methods, a linear peptide sequence containing two identically side chain protected Cys residues is assembled on solid support. Following cleavage from the resin and removal of either all side chain protecting groups or selectively thiol protecting groups, macrocyclization is performed under high dilution conditions (~1 mM). A wide variety of methodologies have been developed to perform the oxidative linkage and achieve the macrocyclization. Among the different oxidants used to prepare disulfide bond-containing cyclic peptides, air oxygen, iodine, 2,2′-dithiodipyridine derivatives, and DMSO are the most commonly used for monocyclic peptides, while other reagents such as azodicarboxylates, pyridylsulfenyl chlorides, alkyloxycarbonylsulfenyl chlorides, alkyltrichlorosilane/sulfoxide, or thallium(III) trifluoroacetate are applied more frequently in stepwise formation of multiple disulfide bonds [272, 274]. Besides the oxidizing agent used for disulfide bond formation, experimental parameters such as pH, ionic strength, solvent, temperature, and time can also greatly influence the success of cyclization. Moreover, since some amino acid side
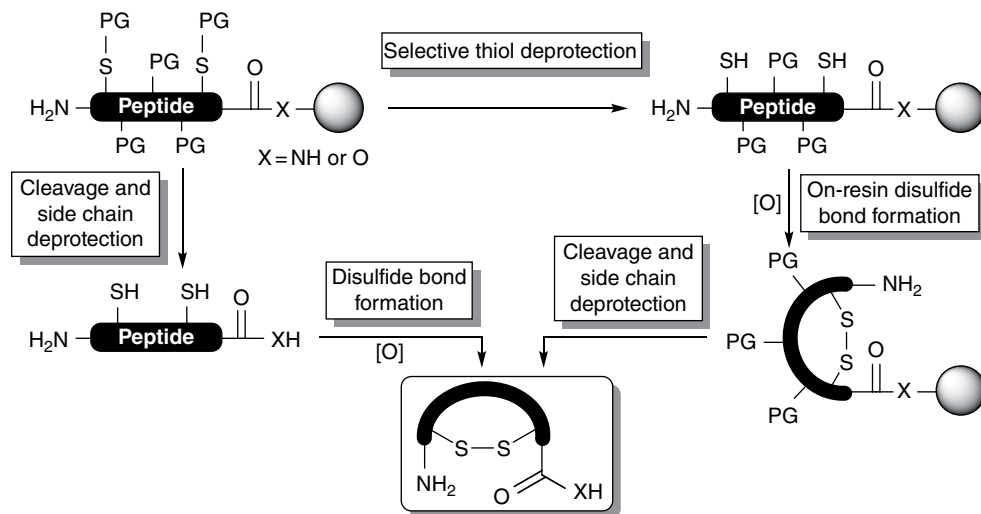
Figure 9.20 General synthetic solution- and solid-phase approaches for macrocyclization by disulfide bond formation.

chains, particularly His, Met, Trp, and Tyr, are susceptible to strong oxidants, the disulfide bond formation method should be carefully chosen to avoid oxidation of these residues.

In the air oxidation method, the disulfide bond is typically formed in water adjusted to pH 7.5–8.5 with a basic solution such as dilute ammonia, and the reaction is monitored by HPLC. After complete cyclization, the mixture is acidified with TFA to pH 2.5, and the peptide purified [275]. Ellman's reagent can also be used to monitor and quantify thiol oxidation after disulfide bond formation [276, 277]. Highly hydrophobic peptides can aggregate and precipitate in aqueous buffers. To overcome this problem during the reaction, 6 M urea or guanidine hydrochloride can be added [278]. Another method to prevent this situation is to employ DMSO as a mild oxidizing agent. In this case, the linear precursor is typically dissolved in aqueous acetic acid (up to 25% AcOH) containing 20% DMSO and the pH adjusted with $(NH_4)_2CO_3$. The conditions used for this method were found to be accommodating, and pH ranges from 3 to 8 have been reported. After cyclization, the reaction

mixture is directly loaded onto a preparative HPLC for purification [279]. In another convenient method, the purified linear peptide was dissolved in 5% DMSO in H_2O/ACN (3:1) and the pH adjusted with dilute NH_4OH to pH 8. After 24 h at room temperature, the oxidized cyclic peptide was directly lyophilized without HPLC purification [280].

In an effort to reduce reaction time and increase selectivity to avoid side reactions on amino acids such as Met and Trp, other oxidizing reagents like *trans*-3,4-dihydroxyselenolane oxide (DHS) [281, 282] and *N*-chlorosuccinimide (NCS) have been developed. For example, Postma and Albericio reported disulfide bond formation in only 15 min when the reaction was performed in H_2O/ACN (1:1) with 2 equivalents of NCS, and they obtained 84 and 94% yields for the cyclization to form octreotide and oxytocin, respectively [273].

Considering the success obtained with certain reagents and to facilitate purification, several oxidizing reagents have been attached to a solid support (Figure 9.21). A major advantage of this strategy is that only peptidic products are recovered after the

Figure 9.21 Solid-supported oxidizing reagents for disulfide bond formation.

Supported NCS **32**

Supported Npys **33**

Oxyfold resin **34**

Clear-Ox resin **35**
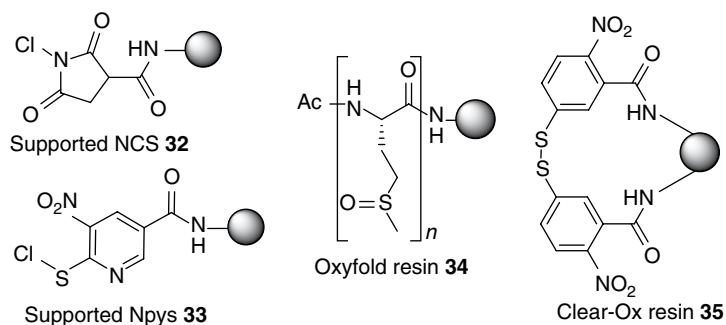
Table 9.3 Conditions for disulfide bond formation in solution with solid-supported oxidizing agents.

Resin	Peptide conc. (mg/ml)	Oxidizing agent (eq)	Solvent	Time (h)	Cyclization yield (%)	References
NCS **32**	2.8–4.5	2	H_2O/ACN (1:1)	0.5–1	90–91	[283]
Npys **33**	3.5–6.2	5	(a) 90% formic acid	1	71	[284]
			(b) DMF/H_2O (2:1)	0.5		
Oxyfold **34**	2	5	Phosphate buffer pH 7.5	4–24	80–100	[285, 286]
Clear-Ox™ **35**	5–7	3	0.1 M NH_4OAc pH 6.8 in ACN (1:1)	2	28–51	[286, 287]

procedure and no reagent residues are present. Among the available solid-supported oxidizing reagents, NCS **32** [283], 3-nitro-2-pyridinesulfenyl (Npys) **33** [284], Oxyfold **34** (Met sulfoxide oligomers) [285, 286], and Ellman's reagent **35** (commercially available Clear-Ox™ resin) [286, 287] are the most commonly used (Table 9.3).

9.5.2 Disulfide Bond Formation on Solid Support

The solid-phase strategy is usually not recommended for larger peptides as intermolecular disulfide can be formed, especially with high loading resins. However this strategy is more suitable for smaller peptides as the pseudo-dilution conditions favor intramolecular disulfide bond formation. As described previously with homodetic cyclic peptides, this strategy allows simple washing and filtration steps to eliminate reagents in excess and can be very convenient, particularly when metals are used as oxidative regents. A wide variety of orthogonal protective groups for both Boc- and Fmoc-SPPS have been developed to perform selective deprotection of the thiol groups prior to cyclization [63]. Among the commercially available orthogonally side chain protected cysteine derivatives, the acetamidomethyl (Acm), *tert*-butylsulfanyl (S*t*Bu), monomethoxytrityl (Mmt), and Trt side chain protecting groups are the most commonly used when the formation of the disulfide is planned on the solid support (Table 9.4).

The Acm protecting group can be utilized for both Boc- and Fmoc-SPPS. When Cys(Acm) is used in a peptide sequence, it is possible to simultaneously remove the Acm group and perform the disulfide formation. This one-step deprotection/cyclization can be achieved with reagents such as thallium(III) trifluoroacetate, I_2, or alkyltrichlorosiloxane. Disulfide bond formation with thallium(III) trifluoroacetate is generally performed in TFA with the presence of anisole or in DMF [288]. While the toxicity of thallium is a drawback, Acm adducts on Ser and Thr residues also have been observed [294]. The use of glycerol was proposed to prevent such side reaction [294]. Iodine has been widely applied for the Acm deprotection/disulfide formation reaction. In this case, side reactions have also been observed, but the use of organic acids such as ascorbic or acetic acid has been proposed to prevent these adducts [289]. The alkyltrichlorosiloxane method involves the reaction of DMSO with $MeSiCl_3$ for 30 min at 4 °C prior to cyclization. However, this method is not compatible with Trp residues as they become fully chlorinated in these conditions unless the indole is protected with a formyl group [290].

S*t*Bu is also a very useful group compatible with Boc- and Fmoc-SPPS protocols. The side chain S–S bond can be selectively reduced with a solution of 20% β-mercaptoethanol (BME) and *N*-methylmorpholine (NMM) (0.1 M) in DMF for 8 h or for 2 h by increasing the ratio of β-mercaptoethanol in the solution to 50% [295]. Recently, the trimethoxyphenylthio (STmp) protective group has been described for cysteine thiol protection. This protecting group is more labile than S*t*Bu and allows complete side chain deprotection in a few minutes [280]. After cysteine side chain thiol deprotection, the disulfide bond can be formed with any suitable oxidizing agent. For example, NCS can also be used for on-resin disulfide macrocyclization. In this case, Postma and Albericio obtained oxytocin in 75% yield after on-resin cyclization with 5 equivalents of NCS in H_2O/ACN or in DMF for only 30–60 min [296].

Acid-labile protecting groups have also been used to selectively generate free thiols on solid support. The best example is the Mmt group that can be removed in mild acidic conditions such as 1% TFA in DCM for 30–40 min [291]. These conditions allow on-resin cyclization as they are compatible with linkers requiring stronger acidic conditions to release the peptide such as Rink and Wang resins. For example, disulfide bond-containing

Table 9.4 Commonly used cysteine thiol protecting groups for disulfide bond formation on solid support.

Protecting group	Structure	Removal and/or oxidants	References
Acm (acetamidomethyl)		(1) Tl(CF$_3$CO$_2$)$_3$	[288]
		(2) I$_2$	[289]
		(3) MeSiCl$_3$, DMSO/TFA	[290]
S*t*Bu (*tert*-butylsulfanyl)		(4) 0.1 M NMM, 20% BME/DMF	[280]
S-Tmp (2,4,6-trimethoxyphenylsulfanyl)		0.1 M NMM, 5% DTT/DMF (DTT = 1,4-dithiothreitol)	[280]
Mmt (monomethoxytrityl)		1% TFA in DCM + scavengers	[291–293]
Trt (trityl)		3% TFA in DCM + scavengers	[63]

cyclic peptides have been prepared from Mmt-protected cysteine upon treatment with a 1% TFA/DCM solution including 5% TIS followed by 2–10 equivalent of trimethylamine in NMP for 5–36 h with air agitation [292]. In another study, the Mmt protecting group was used as orthogonal protection with the S*t*Bu group to form a disulfide bond on solid support and prevent side reactions and Met oxidation. In this case, the S*t*Bu was first removed with a β-mercaptoethanol solution as described previously and the free thiol treated with 2,2′-dithiobis(5-nitropyridine) (DTNP) in DCM to form the 5-Npys group. The cyclization then occurred spontaneously upon Mmt removal with 1% TFA in DCM [293].

9.6 Conclusion

Macrocyclic peptides are a very promising class of bioactive molecules for the development of new pharmaceuticals. With high molecular diversity, easy accessibility, and the possibility to fine-tune the structure, macrocyclic peptides are attractive scaffolds in medicinal chemistry for lead discovery and optimization. Also, with the increasing number of protein–protein interactions validated as therapeutic targets, the demand for molecules that can engage in extended interactions such as macrocyclic peptides is rapidly growing. In many cases, the efficient synthesis of macrocyclic peptides remains an important chemical challenge. The ring disconnection site must be chosen carefully during the design of a synthetic strategy, and a number of factors, such as ring size, amino acid stereochemistry, and the presence of *cis*-bond-inducing residues, must be considered. To address this difficulty, a variety of approaches including the introduction of turn-inducing elements and RCS have been developed to facilitate macrocyclization. Strategies based on *O-* or *S-*to-*N* acyl migration offer a very attractive alternative method to overcome many synthetic challenges and prepare difficult macrocyclic peptides, which are inaccessible with classical approaches. The recent progress in both solution- and solid-phase synthesis of peptide macrocycles is very promising, and the application of these new methodologies will provide access to even wider molecular diversity and more complex structures.

References

1 Driggers, E. M.; Hale, S. P.; Lee, J.; Terrett, N. K. The Exploration of Macrocycles for Drug Discovery—An Underexploited Structural Class. *Nat. Rev. Drug Discov.* **2008**, *7*, 608–624.

2 Yudin, A. K. Macrocycles: Lessons from the Distant Past, Recent Developments, and Future Directions. *Chem. Sci.* **2015**, *6*, 30–49.

3 Fosgerau, K.; Hoffmann, T. Peptide Therapeutics: Current Status and Future Directions. *Drug Discov. Today* **2015**, *20*, 122–128.

4 Thapa, P.; Espiritu, M.; Cabalteja, C.; Bingham, J.-P. The Emergence of Cyclic Peptides: The Potential of Bioengineered Peptide Drugs. *Int. J. Pept. Res. Ther.* **2014**, *20*, 545–551.

5 Che, Y.; Marshall, G. R. Privileged Scaffolds Targeting Reverse-Turn and Helix Recognition. *Expert Opin. Ther. Targets* **2008**, *12*, 101–114.

6 Tyndall, J. D. A.; Nall, T.; Fairlie, D. P. Proteases Universally Recognize Beta Strands in Their Active Sites. *Chem. Rev.* **2005**, *105*, 973–999.

7 Hess, S.; Ovadia, O.; Shalev, D. E.; Senderovich, H.; Qadri, B.; Yehezkel, T.; Salitra, Y.; Sheynis, T.; Jelinek, R.; Gilon, C.; Hoffman, A. Effect of Structural and Conformation Modifications, Including Backbone Cyclization, of Hydrophilic Hexapeptides on Their Intestinal Permeability and Enzymatic Stability. *J. Med. Chem.* **2007**, *50*, 6201–6211.

8 Weide, T.; Modlinger, A.; Kessler, H. Spatial Screening for the Identification of the Bioactive Conformation of Integrin Ligands. In *Bioactive Conformation I*, Peters, T., Ed. Springer-Verlag Berlin: Berlin, **2007**; Vol. *272*, pp 1–50.

9 Heckmann, D.; Kessler, H. Design and Chemical Synthesis of Integrin Ligands. In *Integrins*, Cheresh, D. A., Ed. Elsevier Academic Press Inc.: San Diego, **2007**; Vol. *426*, pp 463–503.

10 Hill, T. A.; Shepherd, N. E.; Diness, F.; Fairlie, D. P. Constraining Cyclic Peptides to Mimic Protein Structure Motifs. *Angew. Chem. Int. Ed.* **2014**, *53*, 13020–13041.

11 Tapeinou, A.; Matsoukas, M.-T.; Simal, C.; Tselios, T. Cyclic Peptides on a Merry-Go-Round; Towards Drug Design. *Biopolymers (Pept. Sci.)* **2015**, *104*, 453–461.

12 Mallinson, J.; Collins, I. Macrocycles in New Drug Discovery. *Future Med. Chem.* **2012**, *4*, 1409–1438.

13 Marsault, E.; Peterson, M. L. Macrocycles Are Great Cycles: Applications, Opportunities, and Challenges of Synthetic Macrocycles in Drug Discovery. *J. Med. Chem.* **2011**, *54*, 1961–2004.

14 De Leon Rodriguez, L. M.; Weidkamp, A. J.; Brimble, M. A. An Update on New Methods to Synthesize Cyclotetrapeptides. *Org. Biomol. Chem.* **2015**, *13*, 6906–6921.

15 White, C. J.; Yudin, A. K. Contemporary Strategies for Peptide Macrocyclization. *Nat. Chem.* **2011**, *3*, 509–524.

16 Davies, J. S. The Cyclization of Peptides and Depsipeptides. *J. Pept. Sci.* **2003**, *9*, 471–501.

17 Lambert, J. N.; Mitchell, J. P.; Roberts, K. D. The Synthesis of Cyclic Peptides. *J. Chem. Soc., Perkin Trans. 1* **2001**, 471–484.

18 Jiang, S.; Li, Z.; Ding, K.; Roller, P. P. Recent Progress of Synthetic Studies to Peptide and Peptidomimetic Cyclization. *Curr. Org. Chem.* **2008**, *12*, 1502–1542.

19 Gellerman, G.; Elgavi, A.; Salitra, Y.; Kramer, M. Facile Synthesis of Orthogonally Protected Amino Acid Building Blocks for Combinatorial N-Backbone Cyclic Peptide Chemistry. *J. Pept. Res.* **2001**, *57*, 277–291.

20 Qvit, N.; Reuveni, H.; Gazal, S.; Zundelevich, A.; Blum, G.; Niv, M. Y.; Feldstein, A.; Meushar, S.; Shalev, D. E.; Friedler, A.; Gilon, C. Synthesis of a Novel Macrocyclic Library: Discovery of an IGF-IR Inhibitor. *J. Comb. Chem.* **2008**, *10*, 256–266.

21 Góngora-Benítez, M.; Tulla-Puche, J.; Albericio, F. Multifaceted Roles of Disulfide Bonds. Peptides as Therapeutics. *Chem. Rev.* **2014**, *114*, 901–926.

22 Sewald, N.; Jakubke, H.-D. Peptide Synthesis. In *Peptides: Chemistry and Biology*, Wiley-VCH Verlag GmbH & Co. KGaA: Weinheim, **2009**; pp 175–315.

23 Schmidt, U.; Langner, J. Cyclotetrapeptides and Cyclopentapeptides: Occurrence and Synthesis. *J. Pept. Res.* **1997**, *49*, 67–73.

24 Izumiya, N.; Kato, T.; Waki, M. Synthesis of Biologically Active Cyclic Peptides. *Biopolymers* **1981**, *20*, 1785–1791.

25 Schmidt, R.; Neubert, K. Cyclization Studies with Tetra- and Pentapeptide Sequences Corresponding to β-Casomorphins. *Int. J. Pept. Protein Res.* **1991**, *37*, 502–507.

26 Malesevic, M.; Strijowski, U.; Bächle, D.; Sewald, N. An Improved Method for the Solution Cyclization of Peptides under Pseudo-High Dilution Conditions. *J. Biotechnol.* **2004**, *112*, 73–77.

27 Mazur, S.; Jayalekshmy, P. Chemistry of Polymer-Bound O-Benzyne. Frequency of Encounter between Substituents on Crosslinked Polystyrenes. *J. Am. Chem. Soc.* **1979**, *101*, 677–683.

28 Scott, L. T.; Rebek, J.; Ovsyanko, L.; Sims, C. L. Organic Chemistry on the Solid Phase. Site-Site Interactions on Functionalized Polystyrene. *J. Am. Chem. Soc.* **1977**, *99*, 625–626.

29 Barany, G.; Merrifield, R. B. Special Methods in Peptide Synthesis. In *The Peptides: Analysis, Synthesis, Biology*,

Gross, E.; Meienhofer, J., Eds. Academic Press: New York, **1980**; Vol. *2*, pp 1–255.

30 Kates, S. A.; Solé, N. A.; Johnson, C. R.; Hudson, D.; Barany, G.; Albericio, F. A Novel, Convenient, Three-Dimensional Orthogonal Strategy for Solid-Phase Synthesis of Cyclic Peptides. *Tetrahedron Lett.* **1993**, *34*, 1549–1552.

31 Alsina, J.; Rabanal, F.; Giralt, E.; Albericio, F. Solid-Phase Synthesis of "Head-to-Tail" Cyclic Peptides Via Lysine Side-Chain Anchoring. *Tetrahedron Lett.* **1994**, *35*, 9633–9636.

32 Spatola, A. F.; Darlak, K.; Romanovskis, P. An Approach to Cyclic Peptide Libraries: Reducing Epimerization in Medium Sized Rings During Solid Phase Synthesis. *Tetrahedron Lett.* **1996**, *37*, 591–594.

33 Romanovskis, P.; Spatola, A. F. Preparation of Head-to-Tail Cyclic Peptides Via Side-Chain Attachment: Implications for Library Synthesis. *J. Pept. Res.* **1998**, *52*, 356–374.

34 Grieco, P.; Gitu, P. M.; Hruby, V. J. Preparation of 'Side-Chain-to-Side-Chain' Cyclic Peptides by Allyl and Alloc Strategy: Potential for Library Synthesis. *J. Pept. Res.* **2001**, *57*, 250–256.

35 Blackburn, C.; Kates, S. A. Solid-Phase Synthesis of Cyclic Homodetic Peptides. In *Methods in Enzymology*, Academic Press: New York, **1997**; Vol. *289*, pp 175–198.

36 Bourne, G.; Golding, S.; Meutermans, W. F.; Smythe, M. Synthesis of a Cyclic Peptide Library Based on the Somatostatin Sequence Using the Backbone Amide Linker Approach. *Lett. Pept. Sci.* **2000**, *7*, 311–316.

37 Alsina, J.; Jensen, K. J.; Albericio, F.; Barany, G. Solid-Phase Synthesis with Tris(Alkoxy)Benzyl Backbone Amide Linkage (BAL). *Chem. Eur. J.* **1999**, *5*, 2787–2795.

38 Jensen, K. J.; Alsina, J.; Songster, M. F.; Vágner, J.; Albericio, F.; Barany, G. Backbone Amide Linker (BAL) Strategy for Solid-Phase Synthesis of C-Terminal-Modified and Cyclic Peptides. *J. Am. Chem. Soc.* **1998**, *120*, 5441–5452.

39 Martí-Centelles, V.; Pandey, M. D.; Burguete, M. I.; Luis, S. V. Macrocyclization Reactions: The Importance of Conformational, Configurational, and Template-Induced Preorganization. *Chem. Rev.* **2015**, *115*, 8736–8834.

40 Poteau, R.; Trinquier, G. All-*cis* Cyclic Peptides. *J. Am. Chem. Soc.* **2005**, *127*, 13875–13889.

41 Oakley, M. T.; Oheix, E.; Peacock, A. F. A.; Johnston, R. L. Computational and Experimental Investigations into the Conformations of Cyclic Tetra-α/β-Peptides. *J. Phys. Chem. B* **2013**, *117*, 8122–8134.

42 Cavelier-Frontin, F.; Pepe, G.; Verducci, J.; Siri, D.; Jacquier, R. Prediction of the Best Linear Precursor in the Synthesis of Cyclotetrapeptides by Molecular Mechanic Calculations. *J. Am. Chem. Soc.* **1992**, *114*, 8885–8890.

43 Tai, D.-F.; Lin, Y.-F. Molecularly Imprinted Cavities Template the Macrocyclization of Tetrapeptides. *Chem. Commun.* **2008**, 5598–5600.

44 El Haddadi, M.; Cavelier, F.; Vives, E.; Azmani, A.; Verducci, J.; Martinez, J. All-L-Leu-Pro-Leu-Pro: A Challenging Cyclization. *J. Pept. Sci.* **2000**, *6*, 560–570.

45 Hoffmann, R. W. Flexible Molecules with Defined Shape—Conformational Design. *Angew. Chem. Int. Ed.* **1992**, *31*, 1124–1134.

46 Blankenstein, J.; Zhu, J. Conformation-Directed Macrocyclization Reactions. *Eur. J. Org. Chem.* **2005**, *2005*, 1949–1964.

47 Chalmers, D. K.; Marshall, G. R. Pro-D-NMe-Amino Acid and D-Pro-NMe-Amino Acid: Simple, Efficient Reverse-Turn Constraints. *J. Am. Chem. Soc.* **1995**, *117*, 5927–5937.

48 Takeuchi, Y.; Marshall, G. R. Conformational Analysis of Reverse-Turn Constraints by N-Methylation and N-Hydroxylation of Amide Bonds in Peptides and Non-Peptide Mimetics. *J. Am. Chem. Soc.* **1998**, *120*, 5363–5372.

49 Laufer, B.; Chatterjee, J.; Frank, A. O.; Kessler, H. Can N-Methylated Amino Acids Serve as Substitutes for Prolines in Conformational Design of Cyclic Pentapeptides? *J. Pept. Sci.* **2009**, *15*, 141–146.

50 Chatterjee, J.; Mierke, D.; Kessler, H. N-Methylated Cyclic Pentaalanine Peptides as Template Structures. *J. Am. Chem. Soc.* **2006**, *128*, 15164–15172.

51 Chatterjee, J.; Mierke, D. F.; Kessler, H. Conformational Preference and Potential Templates of N-Methylated Cyclic Pentaalanine Peptides. *Chem. Eur. J.* **2008**, *14*, 1508–1517.

52 Rothe, M.; Steffen, K. D.; Rothe, I. Synthesis of Cyclotri-L-Prolyl, a Cyclotripeptide Having a Nine-Membered Ring. *Angew. Chem. Int. Ed.* **1965**, *4*, 356.

53 Favre, M.; Moehle, K.; Jiang, L.; Pfeiffer, B.; Robinson, J. A. Structural Mimicry of Canonical Conformations in Antibody Hypervariable Loops Using Cyclic Peptides Containing a Heterochiral Diproline Template. *J. Am. Chem. Soc.* **1999**, *121*, 2679–2685.

54 Robinson, J. A. B-Hairpin Peptidomimetics: Design, Structures and Biological Activities. *Acc. Chem. Res.* **2008**, *41*, 1278–1288.

55 Fujita, Y.; Fujita, S.; Okada, Y.; Chiba, K. Soluble Tag-Assisted Peptide Head-to-Tail Cyclization: Total Synthesis of Mahafacyclin B. *Org. Lett.* **2013**, *15*, 1155–1157.

56 Narayan, R. S.; VanNieuwenhze, M. S. Versatile and Stereoselective Syntheses of Orthogonally Protected β-Methylcysteine and β-Methyllanthionine. *Org. Lett.* **2005**, *7*, 2655–2658.

57 Johnson, T.; Quibell, M.; Owen, D.; Sheppard, R. C. A Reversible Protecting Group for the Amide Bond in Peptides. Use in the Synthesis of 'Difficult Sequences'. *Chem. Commun.* **1993**, 369–372.

58 Cebrián, J.; Domingo, V.; Reig, F. Synthesis of Peptide Sequences Related to Thrombospondin: Factors Affecting Aspartimide By-Product Formation. *J. Pept. Res.* **2003**, *62*, 238–244.

59 Hyde, C.; Johnson, T.; Owen, D.; Quibell, M.; Sheppard, R. C. Some 'Difficult Sequences' Made Easy. *Int. J. Pept. Protein Res.* **1994**, *43*, 431–440.

60 Culf, A. S.; Čuperlović-Culf, M.; Léger, D. A.; Decken, A. Small Head-to-Tail Macrocyclic α-Peptoids. *Org. Lett.* **2014**, *16*, 2780–2783.

61 Park, S.; Kwon, Y.-U. Facile Solid-Phase Parallel Synthesis of Linear and Cyclic Peptoids for Comparative Studies of Biological Activity. *ACS Comb. Sci.* **2015**, *17*, 196–201.

62 Shin, S. B. Y.; Yoo, B.; Todaro, L. J.; Kirshenbaum, K. Cyclic Peptoids. *J. Am. Chem. Soc.* **2007**, *129*, 3218–3225.

63 Isidro-Llobet, A.; Álvarez, M.; Albericio, F. Amino Acid-Protecting Groups. *Chem. Rev.* **2009**, *109*, 2455–2504.

64 Zeng, W.; Regamey, P.-O.; Rose, K.; Wang, Y.; Bayer, E. Use of Fmoc-N-(2-Hydroxy-4-Methoxybenzyl) Amino Acids in Peptide Synthesis. *J. Pept. Res.* **1997**, *49*, 273–279.

65 Johnson, T.; Quibell, M.; Sheppard, R. C. *N,O-bis*Fmoc Derivatives of N-(2-Hydroxy-4-Methoxybenzyl)-Amino Acids: Useful Intermediates in Peptide Synthesis. *J. Pept. Sci.* **1995**, *1*, 11–25.

66 Zahariev, S.; Guarnaccia, C.; Pongor, C. I.; Quaroni, L.; Čemažar, M.; Pongor, S. Synthesis of 'Difficult' Peptides Free of Aspartimide and Related Products, Using Peptoid Methodology. *Tetrahedron Lett.* **2006**, *47*, 4121–4124.

67 Zahariev, S.; Guarnaccia, C.; Zanuttin, F.; Pintar, A.; Esposito, G.; Maravić, G.; Krust, B.; Hovanessian, A. G.; Pongor, S. Efficient Synthesis and Comparative Studies of the Arginine and Nω,Nω-Dimethylarginine Forms of the Human Nucleolin Glycine/Arginine Rich Domain. *J. Pept. Sci.* **2005**, *11*, 17–28.

68 Weygand, F.; Steglich, W.; Bjarnason, J.; Akhtar, R.; Khan, N. M. Leicht Abspaltbare Schutzgruppen Für Säureamidfunktionen 1. Mitteilung. *Tetrahedron Lett.* **1966**, *7*, 3483–3487.

69 Johnson, E. C. B.; Kent, S. B. H. Synthesis, Stability and Optimized Photolytic Cleavage of 4-Methoxy-2-Nitrobenzyl Backbone-Protected Peptides. *Chem. Commun.* **2006**, 1557–1559.

70 Miranda, L. P.; Meutermans, W. D. F.; Smythe, M. L.; Alewood, P. F. An Activated $O \rightarrow N$ Acyl Transfer Auxiliary: Efficient Amide-Backbone Substitution of Hindered "Difficult" Peptides. *J. Org. Chem.* **2000**, *65*, 5460–5468.

71 Nicolás, E.; Pujades, M.; Bacardit, J.; Giralt, E.; Albericio, F. A New Approach to Hmb-Backbone Protection of Peptides: Synthesis and Reactivity of Nα-Fmoc-Nα-(Hmb)amino Acids. *Tetrahedron Lett.* **1997**, *38*, 2317–2320.

72 Isidro-Llobet, A.; Just-Baringo, X.; Álvarez, M.; Albericio, F. EDOTn and MIM, New Peptide Backbone Protecting Groups. *Biopolymers (Pept. Sci.)* **2008**, *90*, 444–449.

73 Meutermans, W. D. F.; Golding, S. W.; Bourne, G. T.; Miranda, L. P.; Dooley, M. J.; Alewood, P. F.; Smythe, M. L. Synthesis of Difficult Cyclic Peptides by Inclusion of a Novel Photolabile Auxiliary in a Ring Contraction Strategy. *J. Am. Chem. Soc.* **1999**, *121*, 9790–9796.

74 Horton, D. A.; Bourne, G. T.; Coughlan, J.; Kaiser, S. M.; Jacobs, C. M.; Jones, A.; Ruhmann, A.; Turner, J. Y.; Smythe, M. L. Cyclic Tetrapeptides via the Ring Contraction Strategy: Chemical Techniques Useful for Their Identification. *Org. Biomol. Chem.* **2008**, *6*, 1386–1395.

75 Meutermans, W. D. F.; Bourne, G. T.; Golding, S. W.; Horton, D. A.; Campitelli, M. R.; Craik, D.; Scanlon, M.; Smythe, M. L. Difficult Macrocyclizations: New Strategies for Synthesizing Highly Strained Cyclic Tetrapeptides. *Org. Lett.* **2003**, *5*, 2711–2714.

76 Skropeta, D.; Jolliffe, K. A.; Turner, P. Pseudoprolines as Removable Turn Inducers: Tools for the Cyclization of Small Peptides. *J. Org. Chem.* **2004**, *69*, 8804–8809.

77 Postma, T. M.; Albericio, F. Cysteine Pseudoprolines for Thiol Protection and Peptide Macrocyclization Enhancement in Fmoc-Based Solid-Phase Peptide Synthesis. *Org. Lett.* **2014**, *16*, 1772–1775.

78 Fairweather, K. A.; Sayyadi, N.; Luck, I. J.; Clegg, J. K.; Jolliffe, K. A. Synthesis of All-L Cyclic Tetrapeptides Using Pseudoprolines as Removable Turn Inducers. *Org. Lett.* **2010**, *12*, 3136–3139.

79 Rückle, T.; de Lavallaz, P.; Keller, M.; Dumy, P.; Mutter, M. Pseudo-Prolines in Cyclic Peptides: Conformational Stabilisation of Cyclo[Pro-Thr(ΨMe,Mepro)-Pro]. *Tetrahedron* **1999**, *55*, 11281–11288.

80 Sayyadi, N.; Taleski, D.; Leesch, S.; Jolliffe, K. A. Investigating the Scope of Pseudoproline Assisted Peptide Cyclization. *Tetrahedron* **2014**, *70*, 7700–7706.

81 Wöhr, T.; Wahl, F.; Nefzi, A.; Rohwedder, B.; Sato, T.; Sun, X.; Mutter, M. Pseudo-Prolines as a Solubilizing, Structure-Disrupting Protection Technique in Peptide Synthesis. *J. Am. Chem. Soc.* **1996**, *118*, 9218–9227.

82 Dumy, P.; Keller, M.; Ryan, D. E.; Rohwedder, B.; Wöhr, T.; Mutter, M. Pseudo-Prolines as a Molecular Hinge: Reversible Induction of *cis* Amide Bonds into Peptide Backbones. *J. Am. Chem. Soc.* **1997**, *119*, 918–925.

83 Keller, M.; Sager, C.; Dumy, P.; Schutkowski, M.; Fischer, G. S.; Mutter, M. Enhancing the Proline Effect: Pseudo-Prolines for Tailoring Cis/Trans Isomerization. *J. Am. Chem. Soc.* **1998**, *120*, 2714–2720.

84 Ehrlich, A.; Heyne, H.-U.; Winter, R.; Beyermann, M.; Haber, H.; Carpino, L. A.; Bienert, M. Cyclization of All-L-Pentapeptides by Means of 1-Hydroxy-7-Azabenzotriazole-Derived Uronium and Phosphonium Reagents. *J. Org. Chem.* **1996**, *61*, 8831–8838.

85 Mästle, W.; Link, U.; Witschel, W.; Thewalt, U.; Weber, T.; Rothe, M. Conformation and Formation Tendency of the Cyclotetrapeptide Cyclo(D-Pro-D-Pro-L-Pro-L-Pro): Experimental Results and Molecular Modeling Studies. *Biopolymers* **1991**, *31*, 735–744.

86 Brady, S. F.; Varga, S. L.; Freidinger, R. M.; Schwenk, D. A.; Mendlowski, M.; Holly, F. W.; Veber, D. F. Practical Synthesis of Cyclic Peptides, with an Example of Dependence of Cyclization Yield Upon Linear Sequence. *J. Org. Chem.* **1979**, *44*, 3101–3105.

87 Yongye, A.; Li, Y.; Giulianotti, M.; Yu, Y.; Houghten, R.; Martínez-Mayorga, K. Modeling of Peptides Containing D-Amino Acids: Implications on Cyclization. *J. Comput. Aided Mol. Des.* **2009**, *23*, 677–689.

88 Kessler, H.; Haase, B. Cyclic Hexapeptides Derived from the Human Thymopoietin III. *Int. J. Pept. Protein Res.* **1992**, *39*, 36–40.

89 Tamaki, M.; Akabori, S.; Muramatsu, I. Biomimetic Synthesis of Gramicidin S. Direct Formation of the Antibiotic from Pentapeptide Active Esters Having No Protecting Group on the Side Chain of the Orn Residue. *J. Am. Chem. Soc.* **1993**, *115*, 10492–10496.

90 Haas, K.; Ponikwar, W.; Nöth, H.; Beck, W. Facile Synthesis of Cyclic Tetrapeptides from Nonactivated Peptide Esters on Metal Centers. *Angew. Chem. Int. Ed.* **1998**, *37*, 1086–1089.

91 Ye, Y.-H.; Gao, X.-M.; Liu, M.; Tang, Y.-C.; Tian, G.-L. Studies on the Synthetic Methodology of Head to Tail Cyclization of Linear Peptides. *Lett. Pept. Sci.* **2003**, *10*, 571–579.

92 Liu, M.; Tang, Y. C.; Fan, K. Q.; Jiang, X.; Lai, L. H.; Ye, Y. H. Cyclization of Several Linear Penta- and Heptapeptides with Different Metal Ions Studied by CD Spectroscopy. *J. Pept. Res.* **2005**, *65*, 55–64.

93 Zhang, L.; Tam, J. P. Metal Ion-Assisted Peptide Cyclization. *Tetrahedron Lett.* **1997**, *38*, 4375–4378.

94 Zhang, L.; Tam, J. P. Lactone and Lactam Library Synthesis by Silver Ion-Assisted Orthogonal Cyclization of Unprotected Peptides. *J. Am. Chem. Soc.* **1999**, *121*, 3311–3320.

95 Ha, K.; Lebedyeva, I.; Hamedzadeh, S.; Li, Z.; Quiñones, R.; Pillai, G. G.; Williams, B.; Nasajpour, A.; Martin, K.; Asiri, A. M.; Katritzky, A. R. Tandem Deprotection–Dimerization–Macrocyclization Route to C2 Symmetric Cyclo-Tetrapeptides. *Chem. Eur. J.* **2014**, *20*, 4874–4879.

96 Kohli, R. M.; Walsh, C. T.; Burkart, M. D. Biomimetic Synthesis and Optimization of Cyclic Peptide Antibiotics. *Nature* **2002**, *418*, 658–661.

97 Goto, Y.; Ohta, A.; Sako, Y.; Yamagishi, Y.; Murakami, H.; Suga, H. Reprogramming the Translation Initiation for the Synthesis of Physiologically Stable Cyclic Peptides. *ACS Chem. Biol.* **2008**, *3*, 120–129.

98 Amore, A.; van Heerbeek, R.; Zeep, N.; van Esch, J.; Reek, J. N. H.; Hiemstra, H.; van Maarseveen, J. H. Carbosilane Dendrimeric Carbodiimides: Site Isolation as a Lactamization Tool. *J. Org. Chem.* **2006**, *71*, 1851–1860.

99 Benoiton, N. L.; Lee, Y. C.; Steinaur, R.; Chen, F. M. F. Studies on Sensitivity to Racemization of Activated Residues in Couplings of N-Benzyloxycarbonyldipeptides. *Int. J. Pept. Protein Res.* **1992**, *40*, 559–566.

100 Albericio, F.; Lloyd-Williams, P.; Giralt, E. Convergent Solid-Phase Peptide Synthesis. In *Methods in Enzymology*, Academic Press: New York, **1997**; Vol. *289*, pp 313–336.

101 El-Faham, A.; Albericio, F. Peptide Coupling Reagents, More Than a Letter Soup. *Chem. Rev.* **2011**, *111*, 6557–6602.

102 El-Faham, A.; Funosas, R. S.; Prohens, R.; Albericio, F. COMU: A Safer and More Effective Replacement for Benzotriazole-Based Uronium Coupling Reagents. *Chem. Eur. J.* **2009**, *15*, 9404–9416.

103 Valeur, E.; Bradley, M. Amide Bond Formation: Beyond the Myth of Coupling Reagents. *Chem. Soc. Rev.* **2009**, *38*, 606–31.

104 Albericio, F.; Bofill, J. M.; El-Faham, A.; Kates, S. A. Use of Onium Salt-Based Coupling Reagents in Peptide Synthesis. *J. Org. Chem.* **1998**, *63*, 9678–9683.

105 Klose, J.; El-Faham, A.; Henklein, P.; Carpino, L. A.; Bienert, M. Addition of HOAt Dramatically Improves the Effectiveness of Pentafluorophenyl-Based Coupling Reagents. *Tetrahedron Lett.* **1999**, *40*, 2045–2048.

106 Antonovics, I.; Young, G. T. Amino-Acids and Peptides. Part XXV. The Mechanism of the Base-Catalysed Racemisation of the p-Nitrophenyl Esters of Acylpeptides. *J. Chem. Soc. C* **1967**, 595–601.

107 Shioiri, T.; Ninomiya, K.; Yamada, S. Diphenylphosphoryl Azide. New Convenient Reagent for a Modified Curtius Reaction and for Peptide Synthesis. *J. Am. Chem. Soc.* **1972**, *94*, 6203–6205.

108 Montalbetti, C. A. G. N.; Falque, V. Amide Bond Formation and Peptide Coupling. *Tetrahedron* **2005**, *61*, 10827–10852.

109 Dahiya, R.; Gautam, H. Toward the Synthesis and Biological Screening of a Cyclotetrapeptide from Marine Bacteria. *Mar. Drugs* **2010**, *9*, 71.

110 Dahiya, R.; Maheshwari, M.; Kumar, A. Toward the Synthesis and Biological Evaluation of Hirsutide. *Monatsh. Chem.* **2009**, *140*, 121–127.

111 Shreder, K.; Zhang, L.; Dang, T.; Yaksh, T. L.; Umeno, H.; DeHaven, R.; Daubert, J.; Goodman, M. Synthesis

and Biological Activity of a Novel Methylamine-Bridged Enkephalin Analogue (MABE): A New Route to Cyclic Peptides and Peptidomimetics. *J. Med. Chem.* **1998**, *41*, 2631–2635.

112 Davies, J. S.; Enjalbal, C.; Nguyen, C.; Al-Jamri, L.; Naumer, C. The Synthesis and Properties of Gla- and Phe-Containing Analogues of Cyclic RGD Pentapeptides. *J. Chem. Soc., Perkin Trans. 1* **2000**, 2907–2915.

113 Samy, R.; Kim, H. Y.; Brady, M.; Toogood, P. L. Total Synthesis of Motuporin and 5-[L-Ala]-Motuporin. *J. Org. Chem.* **1999**, *64*, 2711–2728.

114 Pfizenmayer, A. J.; Ramanjulu, J. M.; Vera, M. D.; Ding, X.; Xiao, D.; Wei-Chuan, C.; Joullié, M. M. Synthesis and Biological Activities of [N-MeLeu5]- and [N-MePhe5]-Didemnin B. *Tetrahedron* **1999**, *55*, 313–334.

115 Tang, Y.-C.; Xie, H.-B.; Tian, G.-L.; Ye, Y.-H. Synthesis of Cyclopentapeptides and Cycloheptapeptides by DEPBT and the Influence of Some Factors on Cyclization. *J. Pept. Res.* **2002**, *60*, 95–103.

116 Kamiński, Z. J.; Kolesińska, B.; Kolesińska, J.; Sabatino, G.; Chelli, M.; Rovero, P.; Błaszczyk, M.; Główka, M. L.; Papini, A. M. N-Triazinylammonium Tetrafluoroborates. A New Generation of Efficient Coupling Reagents Useful for Peptide Synthesis. *J. Am. Chem. Soc.* **2005**, *127*, 16912–16920.

117 Biron, E.; Chatterjee, J.; Ovadia, O.; Langenegger, D.; Brueggen, J.; Hoyer, D.; Schmid, H. A.; Jelinek, R.; Gilon, C.; Hoffman, A.; Kessler, H. Improving Oral Bioavailability of Peptides by Multiple N-Methylation: Somatostatin Analogues. *Angew. Chem. Int. Ed.* **2008**, *47*, 2595–2599.

118 Humphrey, J. M.; Chamberlin, A. R. Chemical Synthesis of Natural Product Peptides: Coupling Methods for the Incorporation of Noncoded Amino Acids into Peptides. *Chem. Rev.* **1997**, *97*, 2243–2266.

119 Wenger, R. M. Synthesis of Cyclosporine. Total Syntheses of 'Cyclosporin A' and 'Cyclosporin H', Two Fungal Metabolites Isolated from the Species *Tolypocladium inflatum* GAMS. *Helv. Chim. Acta* **1984**, *67*, 502–525.

120 Góngora-Benítez, M.; Tulla-Puche, J.; Albericio, F. Handles for Fmoc Solid-Phase Synthesis of Protected Peptides. *ACS Comb. Sci.* **2013**, *15*, 217–228.

121 Boas, U.; Brask, J.; Jensen, K. J. Backbone Amide Linker in Solid-Phase Synthesis. *Chem. Rev.* **2009**, *109*, 2092–2118.

122 Chatzi, K. B. O.; Gatos, D.; Stavropoulos, G. 2-Chlorotrityl Chloride Resin. *Int. J. Pept. Protein Res.* **1991**, *37*, 513–520.

123 Athanassopoulos, P.; Barlos, K.; Gatos, D.; Hatzi, O.; Tzavara, C. Application of 2-Chlorotrityl Chloride in

Convergent Peptide Synthesis. *Tetrahedron Lett.* **1995**, *36*, 5645–5648.

124 Barlos, K.; Gatos, D. 9-Fluorenylmethyloxycarbonyl/*t*-Butyl-Based Convergent Protein Synthesis. *Biopolymers (Pept. Sci.)* **1999**, *51*, 266–278.

125 Riniker, B.; Flörsheimer, A.; Fretz, H.; Sieber, P.; Kamber, B. A General Strategy for the Synthesis of Large Peptides: The Combined Solid-Phase and Solution Approach. *Tetrahedron* **1993**, *49*, 9307–9320.

126 McMurray, J. S.; Lewis, C. A. The Synthesis of Cyclic Peptides Using Fmoc Solid-Phase Chemistry and the Linkage Agent 4-(4-Hydroxymethyl-3-Methoxyphenoxy)-Butyric Acid. *Tetrahedron Lett.* **1993**, *34*, 8059–8062.

127 Lécaillon, J.; Gilles, P.; Subra, G.; Martinez, J.; Amblard, M. Synthesis of Cyclic Peptides Via *O–N*-Acyl Migration. *Tetrahedron Lett.* **2008**, *49*, 4674–4676.

128 Bieraugel, H.; Schoemaker, H. E.; Hiemstra, H.; van Maarseveen, J. H. A Pincer Auxiliary to Force Difficult Lactamisations. *Org. Biomol. Chem.* **2003**, *1*, 1830–1832.

129 Springer, J.; Jansen, T. P.; Ingemann, S.; Hiemstra, H.; van Maarseveen, J. H. Improved Auxiliary for the Synthesis of Medium-Sized Bis(lactams). *Eur. J. Org. Chem.* **2008**, *2008*, 361–367.

130 Rutters, J. P. A.; Verdonk, Y.; de Vries, R.; Ingemann, S.; Hiemstra, H.; Levacher, V.; van Maarseveen, J. H. Synthesis of Strained Cyclic Peptides Via an Aza-Michael-Acyl-Transfer Reaction Cascade. *Chem. Commun.* **2012**, *48*, 8084–8086.

131 Wong, C. T. T.; Lam, H. Y.; Li, X. Effective Synthesis of Cyclic Peptide Yunnanin C and Analogues Via Ser/Thr Ligation (STL)-Mediated Peptide Cyclization. *Tetrahedron* **2014**, *70*, 7770–7773.

132 Wong, C. T. T.; Lam, H. Y.; Song, T.; Chen, G.; Li, X. Synthesis of Constrained Head-to-Tail Cyclic Tetrapeptides by an Imine-Induced Ring-Closing/Contraction Strategy. *Angew. Chem. Int. Ed.* **2013**, *52*, 10212–10215.

133 Zhao, J.-F.; Zhang, X.-H.; Ding, Y.-J.; Yang, Y.-S.; Bi, X.-B.; Liu, C.-F. Facile Synthesis of Peptidyl Salicylaldehyde Esters and Its Use in Cyclic Peptide Synthesis. *Org. Lett.* **2013**, *15*, 5182–5185.

134 Lee, C. L.; Li, X. Serine/Threonine Ligation for the Chemical Synthesis of Proteins. *Curr. Opin. Chem. Biol.* **2014**, *22*, 108–114.

135 Zhang, Y.; Xu, C.; Lam, H. Y.; Lee, C. L.; Li, X. Protein Chemical Synthesis by Serine and Threonine Ligation. *Proc. Natl. Acad. Sci. U. S. A* **2013**, *110*, 6657–6662.

136 Lam, H. Y.; Zhang, Y.; Liu, H.; Xu, J.; Wong, C. T. T.; Xu, C.; Li, X. Total Synthesis of Daptomycin by Cyclization Via a Chemoselective Serine Ligation. *J. Am. Chem. Soc.* **2013**, *135*, 6272–6279.

137 Wong, C. T. T.; Lam, H. Y.; Li, X. Effective Synthesis of Kynurenine-Containing Peptides Via On-Resin Ozonolysis of Tryptophan Residues: Synthesis of Cyclomontanin B. *Org. Biomol. Chem.* **2013**, *11*, 7616–7620.

138 Felnagle, E. A.; Jackson, E. E.; Chan, Y. A.; Podevels, A. M.; Berti, A. D.; McMahon, M. D.; Thomas, M. G. Nonribosomal Peptide Synthetases Involved in the Production of Medically Relevant Natural Products. *Mol. Pharm.* **2008**, *5*, 191–211.

139 Li, Y.; Yongye, A.; Giulianotti, M.; Martinez-Mayorga, K.; Yu, Y.; Houghten, R. A. Synthesis of Cyclic Peptides through Direct Aminolysis of Peptide Thioesters Catalyzed by Imidazole in Aqueous Organic Solutions. *J. Comb. Chem.* **2009**, *11*, 1066–1072.

140 Li, Y.; Giulionatti, M.; Houghten, R. A. Macrolactonization of Peptide Thioesters Catalyzed by Imidazole and Its Application in the Synthesis of Kahalalide B and Analogues. *Org. Lett.* **2010**, *12*, 2250–2253.

141 Sasaki, K.; Crich, D. Cyclic Peptide Synthesis with Thioacids. *Org. Lett.* **2010**, *12*, 3254–3257.

142 Tam, J. P.; Wong, C. T. T. Chemical Synthesis of Circular Proteins. *J. Biol. Chem.* **2012**, *287*, 27020–27025.

143 Clark, R. J.; Craik, D. J. Native Chemical Ligation Applied to the Synthesis and Bioengineering of Circular Peptides and Proteins. *Biopolymers (Pept. Sci.)* **2010**, *94*, 414–422.

144 Panda, S. S.; Hall, C. D.; Oliferenko, A. A.; Katritzky, A. R. Traceless Chemical Ligation from *S*-, *O*-, and *N*-Acyl Isopeptides. *Acc. Chem. Res.* **2014**, *47*, 1076–1087.

145 Tailhades, J.; Patil, N. A.; Hossain, M. A.; Wade, J. D. Intramolecular Acyl Transfer in Peptide and Protein Ligation and Synthesis. *J. Pept. Sci.* **2015**, *21*, 139–147.

146 Dawson, P.; Muir, T.; Clark-Lewis, I.; Kent, S. Synthesis of Proteins by Native Chemical Ligation. *Science* **1994**, *266*, 776–779.

147 Zhang, L.; Tam, J. P. Synthesis and Application of Unprotected Cyclic Peptides as Building Blocks for Peptide Dendrimers. *J. Am. Chem. Soc.* **1997**, *119*, 2363–2370.

148 Zheng, J.-S.; Tang, S.; Guo, Y.; Chang, H.-N.; Liu, L. Synthesis of Cyclic Peptides and Cyclic Proteins Via Ligation of Peptide Hydrazides. *ChemBioChem* **2012**, *13*, 542–546.

149 Thongyoo, P.; Tate, E. W.; Leatherbarrow, R. J. Total Synthesis of the Macrocyclic Cysteine Knot Microprotein MCoTI-II. *Chem. Commun.* **2006**, 2848–2850.

150 Leta Aboye, T.; Clark, R. J.; Craik, D. J.; Göransson, U. Ultra-Stable Peptide Scaffolds for Protein Engineering—Synthesis and Folding of the Circular Cystine Knotted Cyclotide Cycloviolacin O2. *ChemBioChem* **2008**, *9*, 103–113.

151 Daly, N. L.; Clark, R. J.; Craik, D. J. Disulfide Folding Pathways of Cystine Knot Proteins: Tying the Knot within the Circular Backbone of the Cyclotides. *J. Biol. Chem.* **2003**, *278*, 6314–6322.

152 Clark, R. J.; Fischer, H.; Dempster, L.; Daly, N. L.; Rosengren, K. J.; Nevin, S. T.; Meunier, F. A.; Adams, D. J.; Craik, D. J. Engineering Stable Peptide Toxins by Means of Backbone Cyclization: Stabilization of the A-Conotoxin Mii. *Proc. Natl. Acad. Sci. U. S. A* **2005**, *102*, 13767–13772.

153 Lovelace, E. S.; Armishaw, C. J.; Colgrave, M. L.; Wahlstrom, M. E.; Alewood, P. F.; Daly, N. L.; Craik, D. J. Cyclic Mria: A Stable and Potent Cyclic Conotoxin with a Novel Topological Fold that Targets the Norepinephrine Transporter. *J. Med. Chem.* **2006**, *49*, 6561–6568.

154 Chen, Y.-Q.; Chen, C.-C.; He, Y.; Yu, M.; Xu, L.; Tian, C.-L.; Guo, Q.-X.; Shi, J.; Zhang, M.; Li, Y.-M. Efficient Synthesis of Trypsin Inhibitor SFTI-1 Via Intramolecular Ligation of Peptide Hydrazide. *Tetrahedron Lett.* **2014**, *55*, 2883–2886.

155 Yan, L. Z.; Dawson, P. E. Design and Synthesis of a Protein Catenane. *Angew. Chem. Int. Ed.* **2001**, *40*, 3625–3627.

156 Shao, Y.; Lu, W.; Kent, S. B. H. A Novel Method to Synthesize Cyclic Peptides. *Tetrahedron Lett.* **1998**, *39*, 3911–3914.

157 Yan, L. Z.; Dawson, P. E. Synthesis of Peptides and Proteins without Cysteine Residues by Native Chemical Ligation Combined with Desulfurization. *J. Am. Chem. Soc.* **2001**, *123*, 526–533.

158 Rohde, H.; Seitz, O. Ligation—Desulfurization: A Powerful Combination in the Synthesis of Peptides and Glycopeptides. *Biopolymers (Pept. Sci.)* **2010**, *94*, 551–559.

159 Dawson, P. E. Native Chemical Ligation Combined with Desulfurization and Deselenization: A General Strategy for Chemical Protein Synthesis. *Isr. J. Chem.* **2011**, *51*, 862–867.

160 Wan, Q.; Danishefsky, S. J. Free-Radical-Based, Specific Desulfurization of Cysteine: A Powerful Advance in the Synthesis of Polypeptides and Glycopolypeptides. *Angew. Chem. Int. Ed.* **2007**, *46*, 9248–9252.

161 Hackenberger, C. P. R.; Schwarzer, D. Chemoselective Ligation and Modification Strategies for Peptides and Proteins. *Angew. Chem. Int. Ed.* **2008**, *47*, 10030–10074.

162 Thompson, R. E.; Chan, B.; Radom, L.; Jolliffe, K. A.; Payne, R. J. Chemoselective Peptide Ligation–Desulfurization at Aspartate. *Angew. Chem. Int. Ed.* **2013**, *52*, 9723–9727.

163 Malins, L. R.; Payne, R. J. Recent Extensions to Native Chemical Ligation for the Chemical Synthesis of Peptides and Proteins. *Curr. Opin. Chem. Biol.* **2014**, *22*, 70–78.

164 Camarero, J. A.; Muir, T. W. Chemoselective Backbone Cyclization of Unprotected Peptides. *Chem. Commun.* **1997**, 1369–1370.

165 Mende, F.; Seitz, O. 9-Fluorenylmethoxycarbonyl-Based Solid-Phase Synthesis of Peptide α-Thioesters. *Angew. Chem. Int. Ed.* **2011**, *50*, 1232–1240.

166 Raibaut, L.; Drobecq, H.; Melnyk, O. Selectively Activatable Latent Thiol and Selenoesters Simplify the Access to Cyclic or Branched Peptide Scaffolds. *Org. Lett.* **2015**, *17*, 3636–3639.

167 Boll, E.; Drobecq, H.; Ollivier, N.; Blanpain, A.; Raibaut, L.; Desmet, R.; Vicogne, J.; Melnyk, O. One-Pot Chemical Synthesis of Small Ubiquitin-Like Modifier Protein–Peptide Conjugates Using *bis*(2-Sulfanylethyl)Amido Peptide Latent Thioester Surrogates. *Nat. Protoc.* **2015**, *10*, 269–292.

168 Zheng, J.-S.; Tang, S.; Qi, Y.-K.; Wang, Z.-P.; Liu, L. Chemical Synthesis of Proteins Using Peptide Hydrazides as Thioester Surrogates. *Nat. Protoc.* **2013**, *8*, 2483–2495.

169 Huang, Y.-C.; Chen, C.-C.; Li, S.-J.; Gao, S.; Shi, J.; Li, Y.-M. Facile Synthesis of C-Terminal Peptide Hydrazide and Thioester of NY-ESO-1 (A39-A68) from an Fmoc-Hydrazine 2-Chlorotrityl Chloride Resin. *Tetrahedron* **2014**, *70*, 2951–2955.

170 Blanco-Canosa, J. B.; Dawson, P. E. An Efficient Fmoc-SPPS Approach for the Generation of Thioester Peptide Precursors for Use in Native Chemical Ligation. *Angew. Chem. Int. Ed.* **2008**, *47*, 6851–6855.

171 Macmillan, D.; Adams, A.; Premdjee, B. Shifting Native Chemical Ligation into Reverse through N → S Acyl Transfer. *Isr. J. Chem.* **2011**, *51*, 885–899.

172 Ollivier, N.; Vicogne, J.; Vallin, A.; Drobecq, H.; Desmet, R.; El Mahdi, O.; Leclercq, B.; Goormachtigh, G.; Fafeur, V.; Melnyk, O. A One-Pot Three-Segment Ligation Strategy for Protein Chemical Synthesis. *Angew. Chem. Int. Ed.* **2012**, *51*, 209–213.

173 Boll, E.; Drobecq, H.; Ollivier, N.; Raibaut, L.; Desmet, R.; Vicogne, J.; Melnyk, O. A Novel Peg-Based Solid Support Enables the Synthesis of >50 Amino-Acid Peptide Thioesters and the Total Synthesis of a Functional SUMO-1 Peptide Conjugate. *Chem. Sci.* **2014**, *5*, 2017–2022.

174 Kleineweischede, R.; Hackenberger, C. P. R. Chemoselective Peptide Cyclization by Traceless Staudinger Ligation. *Angew. Chem. Int. Ed.* **2008**, *47*, 5984–5988.

175 Ha, K.; Monbaliu, J.-C. M.; Williams, B. C.; Pillai, G. G.; Ocampo, C. E.; Zeller, M.; Stevens, C. V.; Katritzky, A. R. A Convenient Synthesis of Difficult Medium-Sized Cyclic Peptides by Staudinger Mediated Ring-Closure. *Org. Biomol. Chem.* **2012**, *10*, 8055–8058.

176 Sivanathan, S.; Scherkenbeck, J. Cyclodepsipeptides: A Rich Source of Biologically Active Compounds for Drug Research. *Molecules* **2014**, *19*, 12368.

177 Li, W.; Schlecker, A.; Ma, D. Total Synthesis of Antimicrobial and Antitumor Cyclic Depsipeptides. *Chem. Commun.* **2010**, *46*, 5403–5420.

178 Murai, M.; Kaji, T.; Kuranaga, T.; Hamamoto, H.; Sekimizu, K.; Inoue, M. Total Synthesis and Biological Evaluation of the Antibiotic Lysocin E and Its Enantiomeric, Epimeric, and N-Demethylated Analogues. *Angew. Chem. Int. Ed.* **2015**, *54*, 1556–1560.

179 Goodreid, J. D.; da Silveira dos Santos, E.; Batey, R. A. A Lanthanide(III) Triflate Mediated Macrolactonization/Solid-Phase Synthesis Approach for Depsipeptide Synthesis. *Org. Lett.* **2015**, *17*, 2182–2185.

180 Grieco, P. A.; Hon, Y. S.; Perez-Medrano, A. Convergent, Enantiospecific Total Synthesis of the Novel Cyclodepsipeptide (+)-Jasplakinolide (Jaspamide). *J. Am. Chem. Soc.* **1988**, *110*, 1630–1631.

181 Simon, R. J.; Kania, R. S.; Zuckermann, R. N.; Huebner, V. D.; Jewell, D. A.; Banville, S.; Simon, N.; Wang, L.; Rosenberg, S.; Marlowe, C. K.; Spellmeyer, D. C.; Tan, R.; Frankel, A. D.; Santi, D. V.; Cohen, F. E.; Bartlett, P. A. Peptoids: A Modular Approach to Drug Discovery. *Proc. Natl. Acad. Sci. U. S. A* **1992**, *89*, 9367–9371.

182 Culf, A. S.; Ouellette, R. J. Solid-Phase Synthesis of N-Substituted Glycine Oligomers (α-Peptoids) and Derivatives. *Molecules* **2010**, *15*, 5282–5335.

183 Fowler, S. A.; Blackwell, H. E. Structure-Function Relationships in Peptoids: Recent Advances toward Deciphering the Structural Requirements for Biological Function. *Org. Biomol. Chem.* **2009**, *7*, 1508–1524.

184 Dohm, M. T.; Kapoor, R.; Barron, A. E. Peptoids: Bio-Inspired Polymers as Potential Pharmaceuticals. *Curr. Pharm. Des.* **2011**, *17*, 2732–2747.

185 Yoo, B.; Kirshenbaum, K. Peptoid Architectures: Elaboration, Actuation, and Application. *Curr. Opin. Chem. Biol.* **2008**, *12*, 714–721.

186 Tromelin, A.; Fulachier, M.-H.; Mourier, G.; Ménez, A. Solid Phase Synthesis of a Cyclic Peptide Derived from a Curaremimetic Toxin. *Tetrahedron Lett.* **1992**, *33*, 5197–5200.

187 Franzyk, H.; Christensen, M. K.; Jørgensen, R. M.; Meldal, M.; Cordes, H.; Mouritsen, S.; Bock, K. Constrained Glycopeptide Ligands for MPRs. Limitations of Unprotected Phosphorylated Building Blocks. *Biorg. Med. Chem.* **1997**, *5*, 21–40.

188 Anderson, M. O.; Shelat, A. A.; Guy, R. K. A Solid-Phase Approach to the Phallotoxins: Total Synthesis of [Ala7]-Phalloidin. *J. Org. Chem.* **2005**, *70*, 4578–4584.

189 Xu, W.-L.; Cui, A. L.; Hu, X.-X.; You, X.-F.; Li, Z.-R.; Zheng, J.-S. A New Strategy for Total Solid-Phase Synthesis of Polymyxins. *Tetrahedron Lett.* **2015**, *56*, 4796–4799.

190 Lian, W.; Upadhyaya, P.; Rhodes, C. A.; Liu, Y.; Pei, D. Screening Bicyclic Peptide Libraries for Protein–Protein Interaction Inhibitors: Discovery of a Tumor Necrosis Factor-α Antagonist. *J. Am. Chem. Soc.* **2013**, *135*, 11990–11995.

191 Simpson, L. S.; Kodadek, T. A Cleavable Scaffold Strategy for the Synthesis of One-Bead One-Compound Cyclic Peptoid Libraries that Can Be Sequenced by Tandem Mass Spectrometry. *Tetrahedron Lett.* **2012**, *53*, 2341–2344.

192 Lian, W.; Jiang, B.; Qian, Z.; Pei, D. Cell-Permeable Bicyclic Peptide Inhibitors against Intracellular Proteins. *J. Am. Chem. Soc.* **2014**, *136*, 9830–9833.

193 Gao, Y.; Kodadek, T. Direct Comparison of Linear and Macrocyclic Compound Libraries as a Source of Protein Ligands. *ACS Comb. Sci.* **2015**, *17*, 190–195.

194 Menegatti, S.; Ward, K. L.; Naik, A. D.; Kish, W. S.; Blackburn, R. K.; Carbonell, R. G. Reversible Cyclic Peptide Libraries for the Discovery of Affinity Ligands. *Anal. Chem.* **2013**, *85*, 9229–9237.

195 Thakkar, A.; Trinh, T. B.; Pei, D. Global Analysis of Peptide Cyclization Efficiency. *ACS Comb. Sci.* **2013**, *15*, 120–129.

196 Morimoto, J.; Kodadek, T. Synthesis of a Large Library of Macrocyclic Peptides Containing Multiple and Diverse N-Alkylated Residues. *Mol. Biosyst.* **2015**, *11*, 2770–2779.

197 Vig, B. S.; Murray, T. F.; Aldrich, J. V. Synthesis and Opioid Activity of Side-Chain-to-Side-Chain Cyclic Dynorphin A-(1–11) Amide Analogues Cyclized between Positions 2 and 5. 1. Substitutions in Position 3. *J. Med. Chem.* **2004**, *47*, 446–455.

198 Rovero, P.; Quartara, L.; Fabbri, G. Synthesis of Cyclic Peptides on Solid Support. *Tetrahedron Lett.* **1991**, *32*, 2639–2642.

199 Valero, M. L.; Giralt, E.; Andreu, D. A Comparative Study of Cyclization Strategies Applied to the Synthesis of Head-to-Tail Cyclic Analogs of a Viral Epitope. *J. Pept. Res.* **1999**, *53*, 56–67.

200 McMurray, J. S. Solid Phase Synthesis of a Cyclic Peptide Using Fmoc Chemistry. *Tetrahedron Lett.* **1991**, *32*, 7679–7682.

201 Cudic, M.; Wade, J. D.; Otvos, J. L. Convenient Synthesis of a Head-to-Tail Cyclic Peptide Containing an Expanded Ring. *Tetrahedron Lett.* **2000**, *41*, 4527–4531.

202 Teixido, M.; Altamura, M.; Quartara, L.; Giolitti, A.; Maggi, C. A.; Giralt, E.; Albericio, F. Bicyclic Homodetic Peptide Libraries: Comparison of Synthetic Strategies for Their Solid-Phase Synthesis. *J. Comb. Chem.* **2003**, *5*, 760–768.

203 Tulla-Puche, J.; Barany, G. On-Resin Native Chemical Ligation for Cyclic Peptide Synthesis1,2. *J. Org. Chem.* **2004**, *69*, 4101–4107.

204 Cabrele, C.; Langer, M.; Beck-Sickinger, A. G. Amino Acid Side Chain Attachment Approach and Its Application to the Synthesis of Tyrosine-Containing Cyclic Peptides. *J. Org. Chem.* **1999**, *64*, 4353–4361.

205 Müller, A.; Schumann, F.; Koksch, M.; Sewald, N. Synthesis of Cyclic RGD-Peptides Containing β-Amino Acids. *Lett. Pept. Sci.* **1997**, *4*, 275–281.

206 Alcaro, M. C.; Sabatino, G.; Uziel, J.; Chelli, M.; Ginanneschi, M.; Rovero, P.; Papini, A. M. On-Resin Head-to-Tail Cyclization of Cyclotetrapeptides: Optimization of Crucial Parameters. *J. Pept. Sci.* **2004**, *10*, 218–228.

207 Salvati, M.; Cordero, F. M.; Pisaneschi, F.; Cini, N.; Bottoncetti, A.; Brandi, A. New Cyclic Arg-Gly-Asp Pseudopentapeptide Containing the β-Turn Mimetic GPTM. *Synlett* **2006**, *2006*, 2067–2070.

208 Yan, L. Z.; Edwards, P.; Flora, D.; Mayer, J. P. Synthesis of Cyclic Peptides through Hydroxyl Side-Chain Anchoring. *Tetrahedron Lett.* **2004**, *45*, 923–925.

209 Sabatino, G.; Chelli, M.; Mazzucco, S.; Ginanneschi, M.; Papini, A. M. Cyclisation of Histidine Containing Peptides in the Solid-Phase by Anchoring the Imidazole Ring to Trityl Resins. *Tetrahedron Lett.* **1999**, *40*, 809–812.

210 Alcaro, M. C.; Orfei, M.; Chelli, M.; Ginanneschi, M.; Papini, A. M. Solid-Phase Approach to the Synthesis of Cyclen Scaffolds from Cyclotetrapeptides. *Tetrahedron Lett.* **2003**, *44*, 5217–5219.

211 Ngyen, H.; Orlamuender, M.; Pretzel, D.; Agricola, I.; Sternberg, U.; Reissmann, S. Transition Metal Complexes of a Cyclic Pseudo Hexapeptide: Synthesis, Complex Formation and Catalytic Activities. *J. Pept. Sci.* **2008**, *14*, 1010–1021.

212 Rizzi, L.; Cendic, K.; Vaiana, N.; Romeo, S. Alcohols Immobilization onto 2-Chlorotritylchloride Resin under Microwave Irradiation. *Tetrahedron Lett.* **2011**, *52*, 2808–2811.

213 Qian, Z.; Liu, T.; Liu, Y. Y.; Briesewitz, R.; Barrios, A. M.; Jhiang, S. M.; Pei, D. Efficient Delivery of Cyclic Peptides into Mammalian Cells with Short Sequence Motifs. *ACS Chem. Biol.* **2013**, *8*, 423–431.

214 Delforge, D.; Dieu, M.; Delaive, E.; Art, M.; Gillon, B.; Devreese, B.; Raes, M.; Van Beeumen, J.; Remacle, J. Solid-Phase Synthesis of Tailed Cyclic Peptides: The Use of α-Allyl-Protected Aspartic Acid Leads to

Aspartimide and Tetramethylguanidinium Formation. *Lett. Pept. Sci.* **1996**, *3*, 89–97.

215 Torres-García, C.; Díaz, M.; Blasi, D.; Farràs, I.; Fernández, I.; Ariza, X.; Farràs, J.; Lloyd-Williams, P.; Royo, M.; Nicolás, E. Side Chain Anchoring of Tryptophan to Solid Supports Using a Dihydropyranyl Handle: Synthesis of Brevianamide F. *Int. J. Pept. Res. Ther.* **2012**, *18*, 7–19.

216 Trzeciak, A.; Bannwarth, W. Synthesis of 'Head-to-Tail' Cyclized Peptides on Solid Support by Fmoc Chemistry. *Tetrahedron Lett.* **1992**, *33*, 4557–4560.

217 Patel, G.; Husman, W.; Jehanli, A. M.; Deadman, J. J.; Green, D.; Kakkar, V. V.; Brennand, D. M. A Cyclic Peptide Analogue of the Loop III Region of Platelet-Derived Growth Factor-BB Is a Synthetic Antigen for the Native Protein. *J. Pept. Res.* **1999**, *53*, 68–74.

218 Medzihradszky, K.; Ambulos, N.; Khatri, A.; Osapay, G.; Remmer, H.; Somogyi, A.; Kates, S. Mass Spectrometry Analysis for the Determination of Side Reactions for Cyclic Peptides Prepared from an Fmoc/tBu/Dmab Protecting Group Strategy. *Lett. Pept. Sci.* **2001**, *8*, 1–12.

219 Fluxa, V. S.; Reymond, J.-L. On-Bead Cyclization in a Combinatorial Library of 15,625 Octapeptides. *Biorg. Med. Chem.* **2009**, *17*, 1018–1025.

220 Kappel, J.; Barany, G. Methionine Anchoring Applied to the Solid-Phase Synthesis of Lysine-Containing 'Head-to-Tail' Cyclic Peptides. *Lett. Pept. Sci.* **2003**, *10*, 119–125.

221 Masurier, N.; Zajdel, P.; Verdié, P.; Pawłowski, M.; Amblard, M.; Martinez, J.; Subra, G. A New Highly Versatile Handle for Chemistry on a Solid Support: The Pipecolic Linker. *Chem. Eur. J.* **2012**, *18*, 11536–11540.

222 Liang, X.; Girard, A.; Biron, E. Practical Ring-Opening Strategy for the Sequence Determination of Cyclic Peptides from One-Bead-One-Compound Libraries. *ACS Comb. Sci.* **2013**, *15*, 535–540.

223 Alsina, J.; Chiva, C.; Ortiz, M.; Rabanal, F.; Giralt, E.; Albericio, F. Active Carbonate Resins for Solid-Phase Synthesis through the Anchoring of a Hydroxyl Function. Synthesis of Cyclic and Alcohol Peptides. *Tetrahedron Lett.* **1997**, *38*, 883–886.

224 Torres-García, C.; Pulido, D.; Carceller, M.; Ramos, I.; Royo, M.; Nicolás, E. Solid-Phase Synthesis of Phenylalanine Containing Peptides Using a Traceless Triazene Linker. *J. Org. Chem.* **2012**, *77*, 9852–9858.

225 Bourne, G. T.; Meutermans, W. D. F.; Alewood, P. F.; McGeary, R. P.; Scanlon, M.; Watson, A. A.; Smythe, M. L. A Backbone Linker for Boc-Based Peptide Synthesis and On-Resin Cyclization: Synthesis of Stylostatin 1. *J. Org. Chem.* **1999**, *64*, 3095–3101.

226 Giovannoni, J.; Subra, G.; Amblard, M.; Martinez, J. Solid-Phase Synthesis of 3,7-Disubstituted

Perhydro-1,4-Diazepine-2,5-Diones from Amino Acids and β-Amino Acids. *Tetrahedron Lett.* **2001**, *42*, 5389–5392.

227 Royo, M.; Van Den Nest, W.; del Fresno, M.; Frieden, A.; Yahalom, D.; Rosenblatt, M.; Chorev, M.; Albericio, F. Solid-Phase Syntheses of Constrained RGD Scaffolds and Their Binding to the αvβ3 Integrin Receptor. *Tetrahedron Lett.* **2001**, *42*, 7387–7391.

228 Virta, P.; Sinkkonen, J.; Lönnberg, H. Synthesis of Spirobicyclic Peptides on a Solid Support. *Eur. J. Org. Chem.* **2002**, *2002*, 3616–3621.

229 Rew, Y.; Goodman, M. Solid-Phase Synthesis of Amine-Bridged Cyclic Enkephalin Analogues via On-Resin Cyclization Utilizing the Fukuyama—Mitsunobu Reaction. *J. Org. Chem.* **2002**, *67*, 8820–8826.

230 Royo, M.; Farrera-Sinfreu, J.; Solé, L.; Albericio, F. Four-Dimensional Orthogonal Solid-Phase Synthesis of New Scaffolds Based on Cyclic Tetra-β-Peptides. *Tetrahedron Lett.* **2002**, *43*, 2029–2032.

231 Gu, W.; Silverman, R. B. Solid-Phase Total Synthesis of Scytalidamide A. *J. Org. Chem.* **2003**, *68*, 8774–8779.

232 Virta, P.; Karskela, M.; Lönnberg, H. Orthogonally Protected Cyclo-β-Tetrapeptides as Solid-Supported Scaffolds for the Synthesis of Glycoclusters. *J. Org. Chem.* **2006**, *71*, 1989–1999.

233 Bianco, A.; Fournel, S.; Wieckowski, S.; Hoebeke, J.; Guichard, G. Solid-Phase Synthesis of CD40L Mimetics. *Org. Biomol. Chem.* **2006**, *4*, 1461–1463.

234 Tulla-Puche, J.; Getun, I.; Angell, Y.; Alsina, J.; Albericio, F.; Woodward, C.; Barany, G. Synthetic Approaches to Disulfide-Free Circular Bovine Pancreatic Trypsin Inhibitor (c-BPTI) Analogues. *Int. J. Pept. Res. Ther.* **2006**, *12*, 93–104.

235 Claerhout, S.; Duchene, T.; Tourwe, D.; Van der Eycken, E. V. Development of a New Microwave-Assisted Cleavable Backbone Amide Linker (BAL): A Comparative Study. *Org. Biomol. Chem.* **2010**, *8*, 60–65.

236 Jessing, M.; Brandt, M.; Jensen, K. J.; Christensen, J. B.; Boas, U. Thiophene Backbone Amide Linkers, a New Class of Easily Prepared and Highly Acid-Labile Linkers for Solid-Phase Synthesis. *J. Org. Chem.* **2006**, *71*, 6734–6741.

237 Boas, U.; Brask, J.; Christensen, J. B.; Jensen, K. J. The Ortho Backbone Amide Linker (O-BAL) Is an Easily Prepared and Highly Acid-Labile Handle for Solid-Phase Synthesis. *J. Comb. Chem.* **2002**, *4*, 223–228.

238 Müller-Hartwieg, J. C. D.; Akyel, K. G.; Zimmermann, J. Synthesis and Conformational Investigation of Cyclic Dipeptides: 7-Membered Rings Containing α- and β-Amino Acids. *J. Pept. Sci.* **2003**, *9*, 187–199.

239 del Fresno, M.; Alsina, J.; Royo, M.; Barany, G.; Albericio, F. Solid-Phase Synthesis of

Diketopiperazines, Useful Scaffolds for Combinatorial Chemistry. *Tetrahedron Lett.* **1998**, *39*, 2639–2642.

240 Boojamra, C. G.; Burow, K. M.; Thompson, L. A.; Ellman, J. A. Solid-Phase Synthesis of 1,4-Benzodiazepine-2,5-Diones. Library Preparation and Demonstration of Synthesis Generality. *J. Org. Chem.* **1997**, *62*, 1240–1256.

241 Estep, K. G.; Neipp, C. E.; Stephens Stramiello, L. M.; Adam, M. D.; Allen, M. P.; Robinson, S.; Roskamp, E. J. Indole Resin: A Versatile New Support for the Solid-Phase Synthesis of Organic Molecules. *J. Org. Chem.* **1998**, *63*, 5300–5301.

242 Minkwitz, R.; Meldal, M. Application of a Photolabile Backbone Amide Linker for Cleavage of Internal Amides in the Synthesis Towards Melanocortin Subtype-4 Agonists. *QSAR Comb. Sci.* **2005**, *24*, 343–353.

243 Boas, U.; Christensen, J. B.; Jensen, K. J. Two Dialkoxynaphthalene Aldehydes as Backbone Amide Linkers for Solid-Phase Synthesis. *J. Comb. Chem.* **2004**, *6*, 497–503.

244 Backes, B. J.; Ellman, J. A. An Alkanesulfonamide "Safety-Catch" Linker for Solid-Phase Synthesis. *J. Org. Chem.* **1999**, *64*, 2322–2330.

245 Yang, L.; Morriello, G. Solid Phase Synthesis of 'Head-to-Tail' Cyclic Peptides Using a Sulfonamide 'Safety-Catch' Linker: The Cleavage by Cyclization Approach. *Tetrahedron Lett.* **1999**, *40*, 8197–8200.

246 Andrews, M. J. I.; McInnes, C.; Kontopidis, G.; Innes, L.; Cowan, A.; Plater, A.; Fischer, P. M. Design, Synthesis, Biological Activity and Structural Analysis of Cyclic Peptide Inhibitors Targeting the Substrate Recruitment Site of Cyclin-Dependent Kinase Complexes. *Org. Biomol. Chem.* **2004**, *2*, 2735–2741.

247 Qin, C.; Zhong, X.; Ng, N. L.; Bu, X.; Chan, W. S.; Guo, Z. Facile Solid-Phase Synthesis of Cyclic Decapeptide Antibiotic Streptocidins A–D. *Tetrahedron Lett.* **2004**, *45*, 217–220.

248 Qin, C.; Bu, X.; Zhong, X.; Joyce Ng, N. L.; Guo, Z. Optimization of Antibacterial Cyclic Decapeptides. *J. Comb. Chem.* **2004**, *6*, 398–406.

249 Ali, L.; Musharraf, S. G.; Shaheen, F. Solid-Phase Total Synthesis of Cyclic Decapeptide Phakellistatin 12. *J. Nat. Prod.* **2008**, *71*, 1059–1062.

250 Kumarn, S.; Chimnoi, N.; Ruchirawat, S. Synthesis of Integerrimide a by an On-Resin Tandem Fmoc-Deprotection Macrocyclisation Approach. *Org. Biomol. Chem.* **2013**, *11*, 7760–7767.

251 Shaheen, F.; Rizvi, T. S.; Musharraf, S. G.; Ganesan, A.; Xiao, K.; Townsend, J. B.; Lam, K. S.; Choudhary, M. I. Solid-Phase Total Synthesis of Cherimolacyclopeptide E and Discovery of More Potent Analogues by Alanine Screening. *J. Nat. Prod.* **2012**, *75*, 1882–1887.

252 Lim, H.; Tan, L.; Chia, C. S. B. Exploring Solution-Phase Cyclization and Sulfamyl Safety-Catch Resin

253 Strategies for the Total Synthesis of the Marine Antimicrobial Cyclic Tetrapeptide Cyclo(GSPE). *Int. J. Pept. Res. Ther.* **2013**, *19*, 25–31.

253 Ravn, J.; Bourne, G. T.; Smythe, M. L. A Safety Catch Linker for Fmoc-Based Assembly of Constrained Cyclic Peptides. *J. Pept. Sci.* **2005**, *11*, 572–578.

254 Rizo, J.; Gierasch, L. M. Constrained Peptides: Models of Bioactive Peptides and Protein Substructures. *Annu. Rev. Biochem.* **1992**, *61*, 387–416.

255 Hogg, P. J. Disulfide Bonds as Switches for Protein Function. *Trends Biochem. Sci.* **2003**, *28*, 210–214.

256 Werle, M.; Bernkop-Schnurch, A. Strategies to Improve Plasma Half Life Time of Peptide and Protein Drugs. *Amino Acids* **2006**, *30*, 351–367.

257 du Vigneaud, V.; Ressler, C.; Swan, C. J. M.; Roberts, C. W.; Katsoyannis, P. G.; Gordon, S. The Synthesis of an Octapeptide Amide with the Hormonal Activity of Oxytocin. *J. Am. Chem. Soc.* **1953**, *75*, 4879–4880.

258 Live, D. H.; Agosta, W. C.; Cowburn, D. A Rapid, Efficient Synthesis of Oxytocin and [8-Arginine]-Vasopressin. Comparison of Benzyl, p-Methoxybenzyl, and p-Methylbenzyl as Protecting Groups for Cysteine. *J. Org. Chem.* **1977**, *42*, 3556–3561.

259 Sieber, P.; Brugger, M.; Kamber, B.; Riniker, B.; Rittel, W. Human Calcitonin. IV. Synthesis of Calcitonin M. *Helv. Chim. Acta* **1968**, *51*, 2057–2061.

260 Yokoyama, F.; Suzuki, N.; Haruki, M.; Nishi, N.; Oishi, S.; Fujii, N.; Utani, A.; Kleinman, H. K.; Nomizu, M. Cyclic Peptides from the Loop Region of the Laminin Alpha 4 Chain Lg4 Module Show Enhanced Biological Activity Over Linear Peptides. *Biochemistry* **2004**, *43*, 13590–13597.

261 Bulleid, N. J.; Ellgaard, L. Multiple Ways to Make Disulfides. *Trends Biochem. Sci.* **2011**, *36*, 485–492.

262 Sevier, C. S.; Kaiser, C. A. Formation and Transfer of Disulphide Bonds in Living Cells. *Nat. Rev. Mol. Cell Biol.* **2002**, *3*, 836–847.

263 Gilbert, H. F. Molecular and Cellular Aspects of Thiol–Disulfide Exchange. In *Advances in Enzymology and Related Areas of Molecular Biology*, John Wiley & Sons, Inc.: Hoboken, **1990**; pp 69–172.

264 Xiao-Yan, W.; Qin, W.; Xiao-Yi, H.; Tao, W.; Xiao-Qi, Y. Synthesis of Small Cyclic Peptides Containing Disulfide Bonds. *ARKIVOC* **2006**, *2006*, 148.

265 Ranganathan, D.; Lakshmi, C.; Karle, I. L. Hydrogen-Bonded Self-Assembled Peptide Nanotubes from Cystine-Based Macrocyclic Bisureas. *J. Am. Chem. Soc.* **1999**, *121*, 6103–6107.

266 Hartig, G. R.; Tran, T. T.; Smythe, M. L. Intramolecular Disulphide Bond Arrangements in Nonhomologous Proteins. *Protein Sci.* **2005**, *14*, 474–482.

267 Zhu, Q.; Kao, L.; Azimov, R.; Abuladze, N.; Newman, D.; Kurtz, I. Interplay between Disulfide Bonding and

N-Glycosylation Defines SLC4 Na$^+$-Coupled Transporter Extracellular Topography. *J. Biol. Chem.* **2015**, *290*, 5391–5404.

268 Zhang, R. M.; Snyder, G. H. Factors Governing Selective Formation of Specific Disulfides in Synthetic Variants of Alpha-Conotoxin. *Biochemistry* **1991**, *30*, 11343–11348.

269 Zhang, R. M.; Snyder, G. H. Dependence of Formation of Small Disulfide Loops in Two-Cysteine Peptides on the Number and Types of Intervening Amino Acids. *J. Biol. Chem.* **1989**, *264*, 18472–18479.

270 Falcomer, C. M.; Meinwald, Y. C.; Choudhary, I.; Talluri, S.; Milburn, P. J.; Clardy, J.; Scheraga, H. A. Chain Reversals in Model Peptides: Studies of Cystine-Containing Cyclic Peptides. 3. Conformational Free Energies of Cyclization of Tetrapeptides of Sequence Ac-Cys-Pro-X-Cys-NHMe. *J. Am. Chem. Soc.* **1992**, *114*, 4036–4042.

271 Andreu, D.; Albericio, F.; Solé, N.; Munson, M.; Ferrer, M.; Barany, G. Formation of Disulfide Bonds in Synthetic Peptides and Proteins. In *Peptide Synthesis Protocols*, Pennington, M.; Dunn, B., Eds. Humana Press: Totowa, **1995**; Vol. *35*, pp 91–169.

272 Postma, T. M.; Albericio, F. Disulfide Formation Strategies in Peptide Synthesis. *Eur. J. Org. Chem.* **2014**, *2014*, 3519–3530.

273 Postma, T. M.; Albericio, F. N-Chlorosuccinimide, an Efficient Peptide Disulfide Bond-Forming Reagent in Aqueous Solution. *RSC Adv.* **2013**, *3*, 14277–14280.

274 Szabo, I.; Schlosser, G.; Hudecz, F.; Mezo, G. Disulfide Bond Rearrangement During Regioselective Oxidation in PhS(O)Ph/CH$_3$SiCl$_3$ Mixture for the Synthesis of α-Conotoxin GI. *Biopolymers* **2007**, *88*, 20–28.

275 Klodt, J.; Kuhn, M.; Marx, U. C.; Martin, S.; Rosch, P.; Forssmann, W. G.; Adermann, K. Synthesis, Biological Activity and Isomerism of Guanylate Cyclase C-Activating Peptides Guanylin and Uroguanylin. *J. Pept. Res.* **1997**, *50*, 222–230.

276 Hansen, R. E.; Østergaard, H.; Nørgaard, P.; Winther, J. R. Quantification of Protein Thiols and Dithiols in the Picomolar Range Using Sodium Borohydride and 4,4′-Dithiodipyridine. *Anal. Biochem.* **2007**, *363*, 77–82.

277 Riener, C. K.; Kada, G.; Gruber, H. J. Quick Measurement of Protein Sulfhydryls with Ellman's Reagent and with 4,4′-Dithiodipyridine. *Anal. Bioanal. Chem.* **2002**, *373*, 266–276.

278 Morjana, N. A.; McKeone, B. J.; Gilbert, H. F. Guanidine Hydrochloride Stabilization of a Partially Unfolded Intermediate During the Reversible Denaturation of Protein Disulfide Isomerase. *Proc. Natl. Acad. Sci. U. S. A* **1993**, *90*, 2107–2111.

279 Tam, J. P.; Wu, C. R.; Liu, W.; Zhang, J. W. Disulfide Bond Formation in Peptides by Dimethyl Sulfoxide. Scope and Applications. *J. Am. Chem. Soc.* **1991**, *113*, 6657–6662.

280 Postma, T. M.; Giraud, M.; Albericio, F. Trimethoxyphenylthio as a Highly Labile Replacement for tert-Butylthio Cysteine Protection in Fmoc Solid Phase Synthesis. *Org. Lett.* **2012**, *14*, 5468–5471.

281 Iwaoka, M.; Kumakura, F.; Yoneda, M.; Nakahara, T.; Henmi, K.; Aonuma, H.; Nakatani, H.; Tomoda, S. Direct Observation of Conformational Folding Coupled with Disulphide Rearrangement by Using a Water-Soluble Selenoxide Reagent—A Case of Oxidative Regeneration of Ribonuclease A under Weakly Basic Conditions. *J. Biochem.* **2008**, *144*, 121–130.

282 Arai, K.; Noguchi, M.; Singh, B. G.; Priyadarsini, K. I.; Fujio, K.; Kubo, Y.; Takayama, K.; Ando, S.; Iwaoka, M. A Water-Soluble Selenoxide Reagent as a Useful Probe for the Reactivity and Folding of Polythiol Peptides. *FEBS Open Bio.* **2013**, *3*, 55–64.

283 Postma, T. M.; Albericio, F. Immobilized N-Chlorosuccinimide as a Friendly Peptide Disulfide-Forming Reagent. *ACS Comb. Sci.* **2014**, *16*, 160–163.

284 Taguchi, A.; Fukumoto, K.; Asahina, Y.; Kajiyama, A.; Shimura, S.; Hamada, K.; Takayama, K.; Yakushiji, F.; Hojo, H.; Hayashi, Y. 3-Nitro-2-Pyridinesulfenyl-Mediated Solid-Phase Disulfide Ligation in the Synthesis of Disulfide Bond-Containing Cyclic Peptides. *Org. Biomol. Chem.* **2015**, *13*, 3186–3189.

285 Verdie, P.; Ronga, L.; Cristau, M.; Amblard, M.; Cantel, S.; Enjalbal, C.; Puget, K.; Martinez, J.; Subra, G. Oxyfold: A Simple and Efficient Solid-Supported Reagent for Disulfide Bond Formation. *Chem. Asian J.* **2011**, *6*, 2382–2389.

286 Ronga, L.; Verdie, P.; Sanchez, P.; Enjabal, C.; Maurras, A.; Jullian, M.; Puget, K.; Martinez, J.; Subra, G. Supported Oligomethionine Sulfoxide and Ellman's Reagent for Cysteine Bridges Formation. *Amino Acids* **2013**, *44*, 733–742.

287 Darlak, K.; Wiegandt Long, D.; Czerwinski, A.; Darlak, M.; Valenzuela, F.; Spatola, A. F.; Barany, G. Facile Preparation of Disulfide-Bridged Peptides Using the Polymer-Supported Oxidant Clear-OX^{TM}. *J. Pept. Res.* **2004**, *63*, 303–312.

288 Albericio, F.; Hammer, R. P.; Garcia-Echeverria, C.; Molins, M. A.; Chang, J. L.; Munson, M. C.; Pons, M.; Giralt, E.; Barany, G. Cyclization of Disulfide-Containing Peptides in Solid-Phase Synthesis. *Int. J. Pept. Protein Res.* **1991**, *37*, 402–413.

289 Zhang, S.; Lin, F.; Hossain, M.; Shabanpoor, F.; Tregear, G.; Wade, J. Simultaneous Post-Cysteine(S-Acm) Group Removal Quenching of Iodine and

Isolation of Peptide by One Step Ether Precipitation. *Int. J. Pept. Res. Ther.* **2008**, *14*, 301–305.

290 Akaji, K.; Tatsumi, T.; Yoshida, M.; Kimura, T.; Fujiwara, Y.; Kiso, Y. Disulfide Bond Formation Using the Silyl Chloride-Sulfoxide System for the Synthesis of a Cystine Peptide. *J. Am. Chem. Soc.* **1992**, *114*, 4137–4143.

291 Barlos, K.; Gatos, D.; Hatzi, O.; Koch, N.; Koutsogianni, S. Synthesis of the Very Acid-Sensitive Fmoc-Cys(Mmt)-OH and Its Application in Solid-Phase Peptide Synthesis. *Int. J. Pept. Protein Res.* **1996**, *47*, 148–153.

292 Galanis, A. S.; Albericio, F.; Grotli, M. Enhanced Microwave-Assisted Method for on-Bead Disulfide Bond Formation: Synthesis of α-Conotoxin MII. *Biopolymers* **2009**, *92*, 23–34.

293 Galande, A. K.; Weissleder, R.; Tung, C. H. An Effective Method of On-Resin Disulfide Bond Formation in Peptides. *J. Comb. Chem.* **2005**, *7*, 174–177.

294 Lamthanh, H.; Roumestand, C.; Deprun, C.; Menez, A. Side Reaction During the Deprotection of (S-Acetamidomethyl)Cysteine in a Peptide with a High Serine and Threonine Content. *Int. J. Pept. Protein Res.* **1993**, *41*, 85–95.

295 Kwon, Y.; Coleman, M. A.; Camarero, J. A. Selective Immobilization of Proteins onto Solid Supports Through Split-Intein-Mediated Protein Trans-Splicing. *Angew. Chem. Int. Ed.* **2006**, *45*, 1726–1729.

296 Postma, T. M.; Albericio, F. N-Chlorosuccinimide, an Efficient Reagent for On-Resin Disulfide Formation in Solid-Phase Peptide Synthesis. *Org. Lett.* **2013**, *15*, 616–619.

10

Ring-Closing Metathesis-Based Methods in Chemical Biology

Building a Natural Product-Inspired Macrocyclic Toolbox to Tackle Protein–Protein Interactions

Jagan Gaddam, Naveen Kumar Mallurwar, Saidulu Konda, Mahender Khatravath,
Madhu Aeluri, Prasenjit Mitra and Prabhat Arya

Dr. Reddy's Institute of Life Sciences (DRILS), University of Hyderabad, Gachibowli, Hyderabad, India

10.1   Introduction

The post-genomics chemical biology age has brought challenges to the biomedical research community trying to develop a better understanding of protein–protein interaction (PPI)-based signaling networks [1–4]. It is becoming clear that signaling networks are central to both normal and dysfunctional cellular processes [5–9]. In most cases, these networks involve multiple, dynamic, highly complex PPIs. These confounding features have resulted in the lack of a thorough understanding of normal and disease-related cellular signaling networks, which has severely limited our ability to develop therapeutic approaches that exploit these networks. It is hoped that having a wide arsenal of *relevant* small-molecule chemical modulators of PPI will result in a more informative probing of such dynamic processes, both in normal and dysregulated cellular processes. In the long run, it will allow the biomedical researchers to better explore the biological space of proteins, something that has not currently been considered highly attractive. Thus, tremendous opportunities exist within the challenges of developing new therapeutic approaches, if one includes PPI as the biological targets [10, 11].

10.2   Protein–Protein Interactions: Challenges and Opportunities

Several factors have contributed to the limited success of small molecules as modulators of PPIs [1]. In general, PPIs involve shallow surfaces and cover relatively large surface areas (see Figure 10.1). Proteins also have regions known as "hot spots" [10]. Indeed, in several cases, it has been observed that these "hot spots" contribute significantly to overall binding, and the targeting of these "focused surface areas" has successfully led to the design of small-molecule modulators. There are a few examples in the literature where the structural information of a protein–protein complex has led to the design of small molecules that exploit these "hot spots" [4]. One such example of a rationally designed molecule involved the synthesis of small-molecule modulators capable of interfering with caspase 9–IAP BIR 3 domain interactions [12–18].

However, despite available structural information on the protein surface(s), there are very few cases where this information has successfully led to the rational design of small-molecule modulators of PPI. Thus, developing organic synthesis methods to build the chemical toolboxes containing natural product-inspired compounds or even hybrid natural products is an attractive strategy for the identification of such modulators [4, 19, 20]. This leads to two important queries: (i) in the absence of any structural information, what types of small molecules are likely to be successful for disrupting signaling networks based on dynamic PPI, and (ii) does nature already have an answer to this question?

10.3   Natural Products as Modulators of Protein–Protein Interactions

Over the years, architecturally complex natural products have been used as small-molecule probes to understand protein function(s). The search for novel natural products with interesting biological properties is still ongoing [21–23]. Embedded in these natural products are a number of highly diverse chiral functional groups, which represent potential sites for protein binding. One of the structural features commonly found in the many natural products is macrocyclic ring skeleton. Macrocyclic natural products have evolved to fulfill numerous
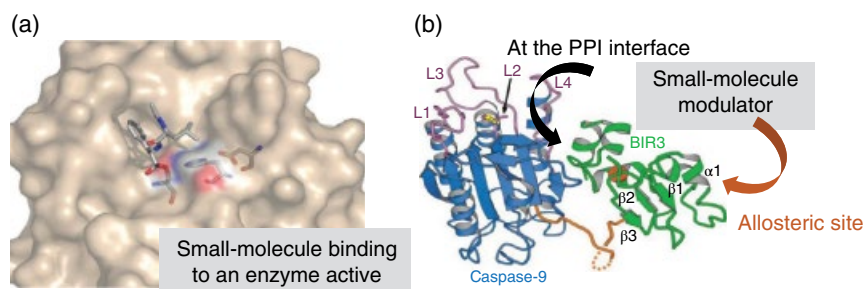
(a)

(b)

Figure 10.1 (a) An illustration of a small-molecule binding to an enzyme active site. (b) Small-molecule modulators of protein–protein interactions via interface or an allosteric site. (*See insert for color representation of the figure.*)

Radicicol **(1)**

Cryptophycin 1 **(2)**
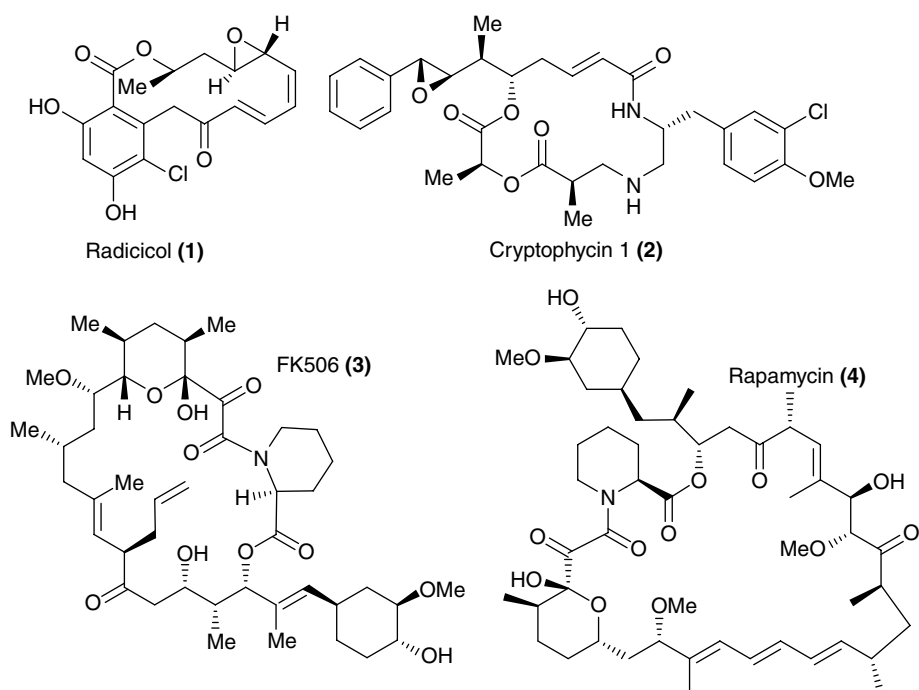
Figure 10.2 Examples of bioactive macrocyclic natural products as modulators of protein–protein interactions.

FK506 **(3)**

Rapamycin **(4)**

biochemical functions, and their profound pharmacological properties have led to their development as drugs [24]. A macrocycle provides diverse functionality and stereochemical complexity in a conformationally pre-organized ring structure. This can result in a high affinity and selectivity for protein targets while preserving sufficient bioavailability, reaching the intracellular locations [24]. In Figure 10.2, some examples of bioactive natural products that are obtained from different sources and function as PPI modulators are shown. Radicicol (**1**) is a potent and specific inhibitor of the ATPase activity of Hsp90 with a K_d of 19.0 nM [25]. Cryptophycin (**2**) is a well-known highly potent cytotoxin that acts as a tubulin modulator to inhibit cell division [26–29]. FK506 (**3**) [30–35] and rapamycin (**4**) [36–41] are two immunosuppressive agents known for their abilities to function as chemical inducers of protein dimerization.

However, a high complexity of macrocycles in most bioactive natural products hampers their synthetic

modification(s) and pharmacokinetic (PK) optimization. Thus, synthetic macrocycles possessing sufficient complexity has gained serious attention in the drug discovery arena in recent years. This has led to the discovery of many synthetic macrocyclic small molecules as modulators with appropriate PK properties for the challenging new targets related to PPIs.

In this chapter, we will focus mainly on synthetic macrocyclic probe compounds obtained using the ring-closing metathesis (RCM) strategy.

10.4 Introduction to Ring-Closing Metathesis

In the past two decades, RCM evolved as a powerful tool for the synthesis of carbocyclic and heterocyclic compounds [42], especially for the synthesis of macrocyclic compounds. Mainly, there are three types of metathesis

1. Alkene metathesis

2. Enyne metathesis

3. Alkyne metathesis
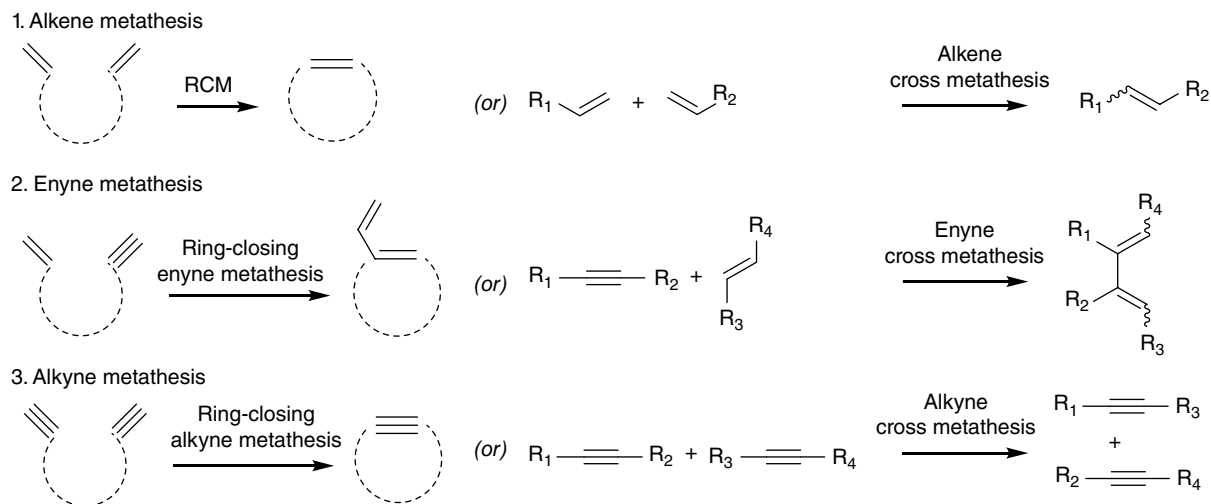
Figure 10.3 Different types of metathesis reactions.

reactions, and these are known as alkene [43, 44], enyne [45, 46], and alkyne metathesis [47], respectively (Figure 10.3). Among these, alkene metathesis gained a lot of attention in organic synthesis because of the presence of alkene functionalities in many biologically and medically important molecules as well as natural products. Moreover, RCM catalysts are readily available commercially, which can be used for the synthesis of milligram- to kilogram-scale reactions (see also Chapter 15).

10.4.1 Ring-Closing Olefin Metathesis

Although alkene metathesis was known since the 1970s, it was widely used until the molybdenum-based carbene complex **5** was reported by Schrock in the 1990s [48]. Catalyst **5** showed very good metathesis reactivity with different olefin substrates, including sterically hindered olefins. However, the applications were limited because of its high sensitivity to oxygen, moisture (extreme dry conditions required), and low functional group tolerance. Shortly thereafter, Grubbs and coworkers introduced ruthenium-based complex **6** [49, 50] (now known as Grubbs first-generation catalyst). Though this catalyst showed less activity than Schrock catalyst **5**, it showed very good tolerance to many functional groups [42]. Later, several research groups worked on the optimization of catalyst **6** and reported the replacement of the phosphine ligand with *N*-heterocyclic carbenes (NHC), resulting in catalyst **7** [51–54], known as Grubbs second-generation catalyst. Catalyst **7** showed very good reactivity compared with catalyst **5** and is also tolerable to a wide variety of functional groups. Following this elegant work, Hoveyda and coworkers reported the synthesis of two catalysts, **8** and **9**, now known as Hoveyda–Grubbs

catalysts [55, 56]. All these catalysts are now commercially available and successfully used for olefin cross metathesis and RCM in natural product and natural product-like molecule synthesis [44]. Some representative examples are shown in Figure 10.4.

10.4.2 *Z*-Selective Ring-Closing Metathesis

Ru-based catalysts generally possess good reactivity for RCM and good stability toward oxygen and moisture and are tolerant to various functional groups. A major drawback of these catalysts is the lack of control of the geometry (*E/Z*) of the newly formed olefin in the product. Predicting olefin geometry has been a long-standing challenge in RCM. Some of the Ru catalysts are known to provide predominantly the *E*-isomer [57]; however this observation is not applicable to all cases.

It is challenging to achieve the synthesis of *Z*-alkenes (kinetic product) over *E*-alkene (thermodynamic product) in RCM. The first *Z*-selective RCM using Mo- and W-based mono-aryloxy pyrrolidine complexes **14–16** (Figure 10.5) was reported by Schrock, Hoveyda, and coworkers [58, 59]. In parallel work, Grubbs reported Ru-based carbene complex **17** [60] for *Z*-selective RCM. Catalysts **14–17** were successfully employed for *Z*-selective cross metathesis and RCM of several macrocyclic natural products [60–62], as shown in Figure 10.5.

An alternate approach to obtain *Z*-olefin in RCM was reported by Young and coworkers using vinyl siloxanes [63], which give *E*-olefin, which upon desilylation leads to *Z*-olefin, as shown in Figure 10.6a. Another way to synthesize *Z*- or *E*-olefin is through ring-closing alkyne metathesis followed by reduction of alkyne to alkene selectively (Figure 10.6b) [47].

(a)

(b)

(c)
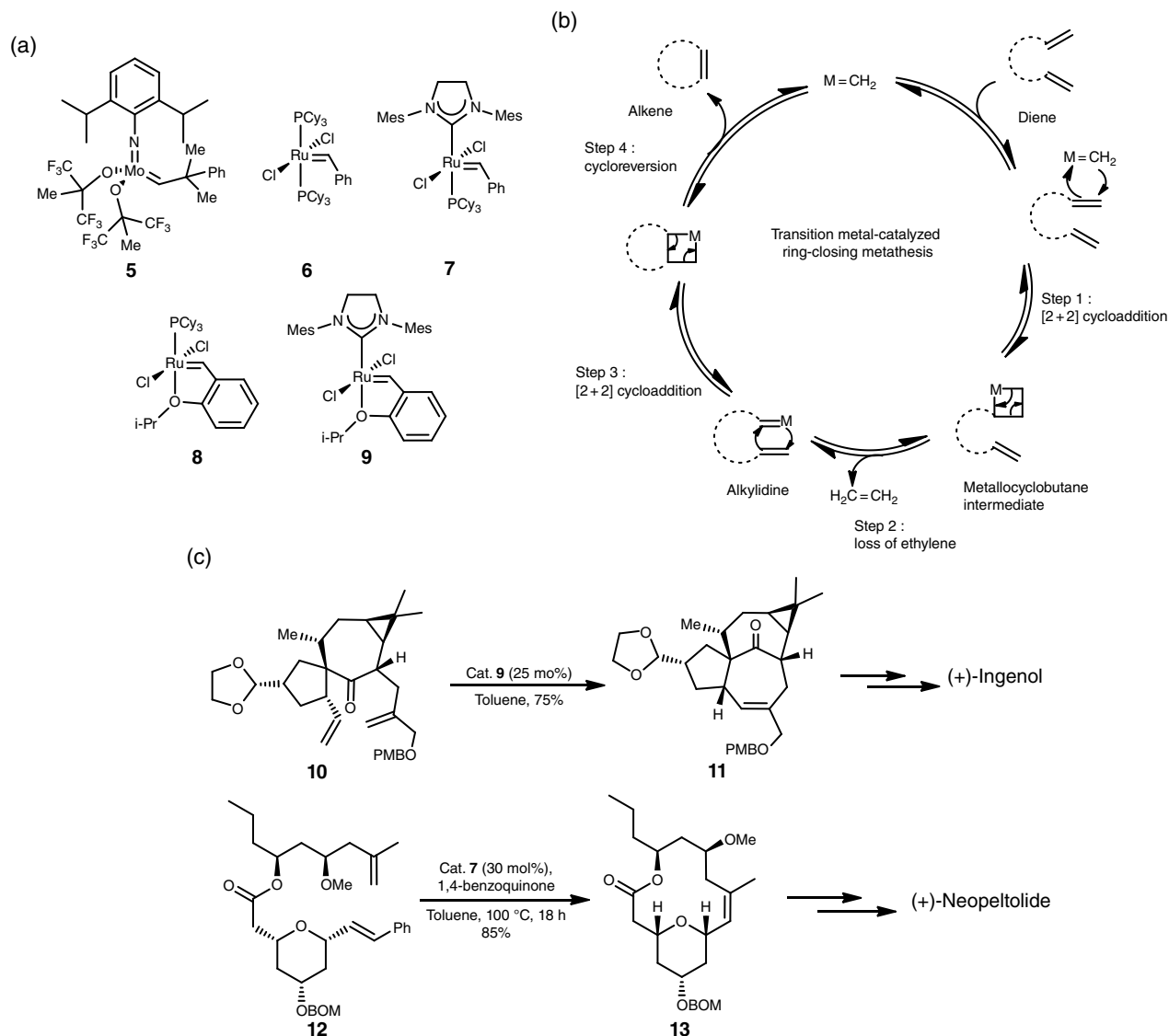
Figure 10.4 (a) Commonly employed catalyst for RCM. (b) General mechanism for RCM. (c) Examples for RCM in total synthesis.

10.5 Selected Examples of Synthetic Macrocyclic Probes Using RCM-Based Approaches

There are several reports of synthetic macrocyclic probes obtained using RCM as a key step for macrocyclization. In this section, a few selected examples are discussed.

10.5.1 Identification of Sonic Hedgehog Inhibitor from the RCM Library

Schreiber and coworkers screened 10 000 compounds derived from diversity-oriented synthesis (DOS) using sonic hedgehog N-terminal peptide (ShhN) small-molecule microarray [64–67], and this study yielded several related macrocyclic hits. Systematic SAR studies on one of the hits, 13-membered macrocyclic compound (**39**) [68, 69], resulted in a highly potent 12-membered macrocyclic compound (**42**) [68, 69], also known as robotnikinin.

Two key reactions were utilized in the synthesis of 12-, 13-, and 14-membered ring macrocyclic compounds (**38**, **40**, and **41**): (i) asymmetric alkylation using Evans' auxiliary (**35**) and (ii) RCM for closing the ring as shown in Figure 10.7. In this synthetic pathway, an asymmetric alkyl product was converted to linear precursor **37** in five steps. This was then subjected to RCM using Grubbs second-generation catalyst (**7**), providing macrocyclic products. The diversity sites introduced in the macrocycles were from the 1,2-amino alcohols and unsaturated carboxylic acids having different chain lengths.

(a)

(b)

Entry	Ring size	Catalyst	m	n	Yield (%)	Z:E
1	13	7	1	3	46	15:85
2	13	14	1	3	49	69:31
3	13	15	1	3	46	73:27
4	13	17	1	3	40	86:14
5	14	7	1	4	74	7:93
6	14	14	1	4	46	80:20
7	14	15	1	4	46	82:18
8	14	17	1	4	46	85:15
9	17	7	7	1	46	23:77
10	17	14	7	1	46	91:9
11	17	15	7	1	46	88:12
12	17	17	7	1	46	89:11

Entry	Catalyst	Yield (%)	Z:E
1	9	nd	34:66
2	14	nd	85:15
3	15	nd	79:21
4	16	86	96:4

1. RCM
2. HF.Py

Epothilone C, 21

(c)

M = Mo or W

Favored TS, 22   Disfavored TS, 23   Favored TS, 24   Disfavored TS, 25

Figure 10.5 (a) Z-selective catalyst for RCM. (b) Examples for Z-selective RCM. (c) Favored and disfavored transition states for Mo- and Ru-based Z-selective catalysis.

(a)

(b)
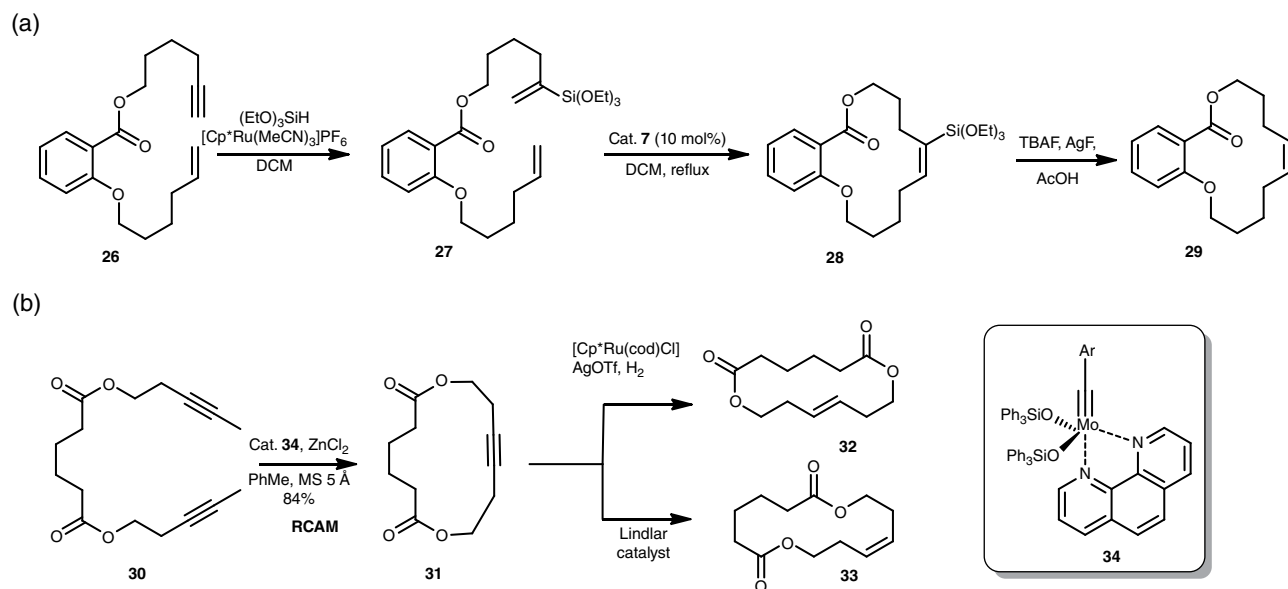
Figure 10.6 (a) Vinyl siloxane-based RCM for Z-olefin synthesis. (b) Selective synthesis of E and Z macrocycles using RCM.
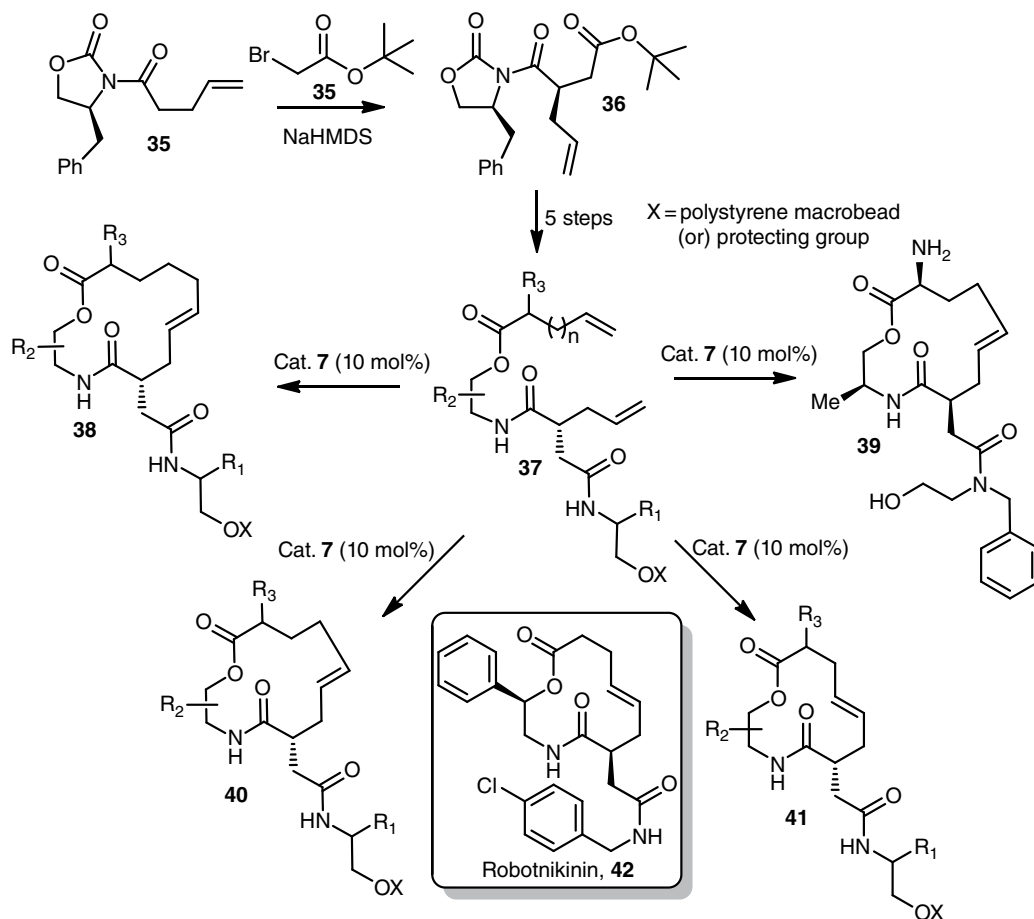
Figure 10.7 Synthesis of macrocyclic library using RCM-based approach.
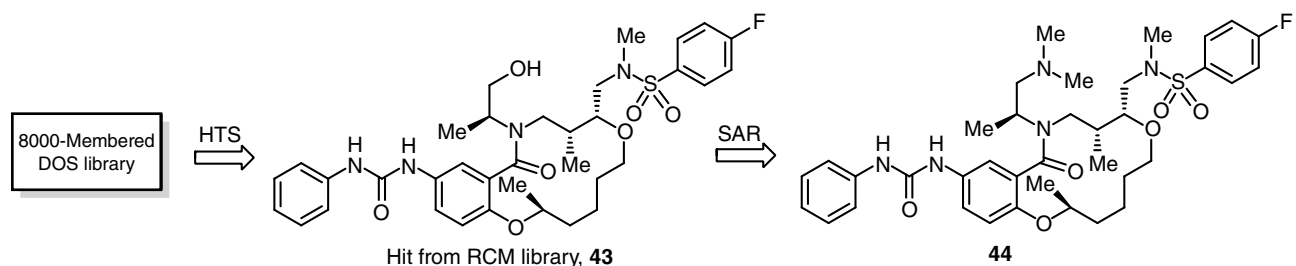
Figure 10.8 Hit from the RCM library of compounds and optimized SAR compound.

10.5.2 Identification of Antimalarial Compounds from the RCM Library

Heidebrecht and coworkers screened 8000-membered small-molecule library generated using a DOS approach in growth inhibition assay (72 h, DAPI) with multidrug-resistant Dd2 *P. falciparum* parasites at 5.0 μM concentration. This study identified 590 small molecules possessing >90% inhibition [70, 71]. Further, experiments at four different concentrations yielded 26 distinct

possessing >50% inhibition at 280 nM. From these 26 compounds, 20 compounds were synthesized using RCM [70], and compound **43** (Figure 10.8) was identified as the most active compound from this library [70]. Further optimization efforts led to compound **44**.

The synthetic scheme utilized in RCM library generation is shown in Figure 10.9. Secondary amine **45** was coupled with the benzoic acid derivative **46** using PyBOP coupling reagent, giving an amide **47**. Removal of TBS group with TBAF followed by the allylation of secondary
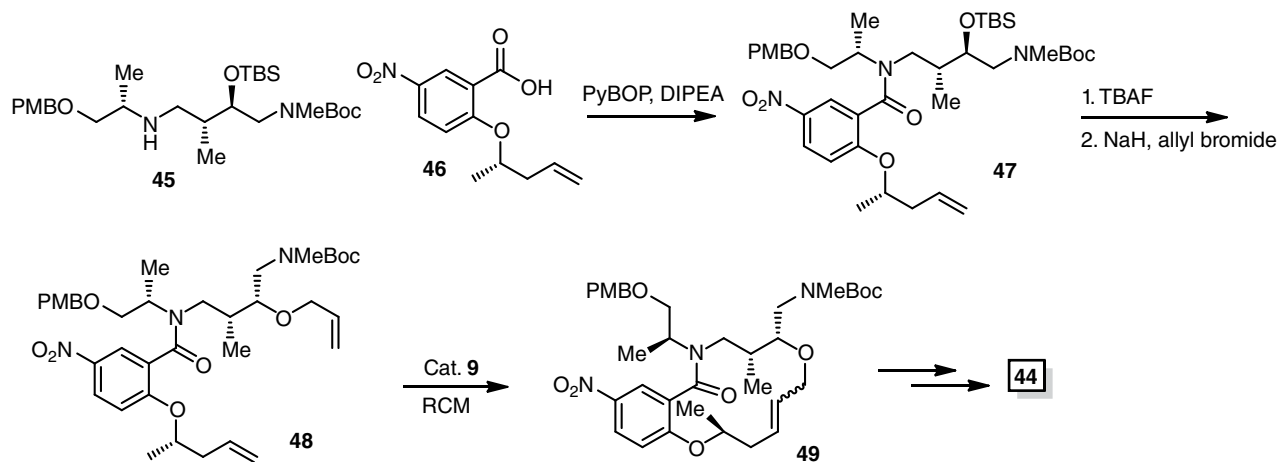
Figure 10.9 Synthesis of compound **44** using RCM approach.

hydroxyl group with allyl bromide/NaH gave the bis-allyl product **48**. This compound was subjected to RCM using Hoveyda–Grubbs second-generation catalyst to obtain 14-membered macrocyclic compound, which was subsequently converted to **44** [70].

10.5.3 Synthesis of Natural Product-Like Molecules Using RCM as the Key Strategy

Spring and coworkers synthesized 51 distinct natural product-like macrocycles using build/couple/pair strategy (Figure 10.10), and out of them 48 scaffolds are unique scaffolds [72]. The rare one-pot organocatalysis and metal catalysis (RCM) approach was utilized in the synthesis. They used NHC for organocatalysis because NHC ligands possess unique characteristics; they enable "umpolung" of functional groups, for example, alpha or gamma position of an aldehyde into a nucleophile [73–75]. Finally, Grubbs catalyst was used for the synthesis of macrocycles (Figure 10.11).

The macrocyclic library obtained was visualized in the form of a principal moment of inertia (PMI) plot and principal component analysis (PCA) featuring 15 calculated physicochemical properties. The macrocyclic library was compared with a set of 40 top-selling drugs and 60 natural products [72]. This analysis showed that the macrocyclic library exhibited broad shape diversity and more prominent spherical characteristics compared with natural product library than the drug reference set; the PCA illustrated more drug-like properties of the macrocyclic library [72].

10.5.4 Alkaloid Natural Product-Inspired Macrocyclic Chemical Probes

Several alkaloid natural products are known to function as PPI modulators. Given their biological importance,

the Arya group initiated a synthesis program to build a chemical toolbox based on the derivatives of indoline and tetrahydroquinoline core scaffolds found in these natural products. Toward this objective, shown in Figures 10.12, 10.13, 10.14, and 10.15 are various chemical approaches that our team has developed. A brief description of each of them is presented in the following section.

10.5.5 Indoline Alkaloid-Inspired Macrocyclic Chemical Probes

The indoline substructure is considered a privileged scaffold and is found in a wide variety of common alkaloid natural products. Based on this precedence, we launched a synthesis program that was aimed at designing functionalized indoline derivatives that could further be used for building different natural product-inspired polycyclic and macrocyclic architectures. Our first- and second-generation synthetic targets, **73** (racemic) and **74** (enantio-enriched), are shown in Figure 10.12. Our second-generation indoline scaffold, **74**, is densely functionalized and can be easily obtained in an enantio-enriched manner. In addition to having the functional groups that were present in the first-generation design, **74** also contains an amino group that is orthogonally protected from the indoline secondary amine. The presence of multiple functional groups on this scaffold makes it highly attractive for developing modular approaches to obtain three-dimensionally diverse macrocyclic architectures.

With the goal of producing different indoline-based, functionalized, macrocyclic architectures and using such architectures in library generation, we developed a practical enantio-controlled synthesis of an aminoindoline scaffold, **75** (Figure 10.13) [76].
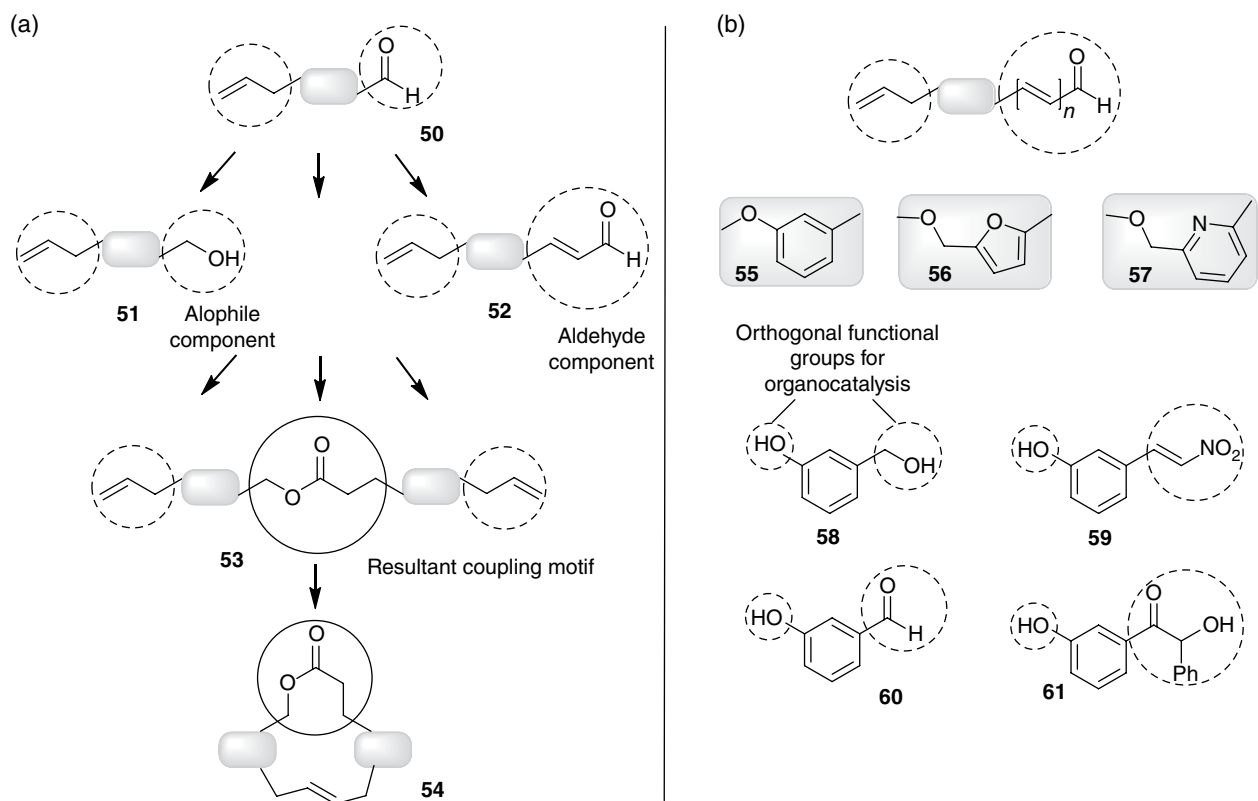
Figure 10.10 General approach for building the DOS library; (a) proposed B/C/P strategy and (b) building blocks with pluripotent and orthogonal functional group.
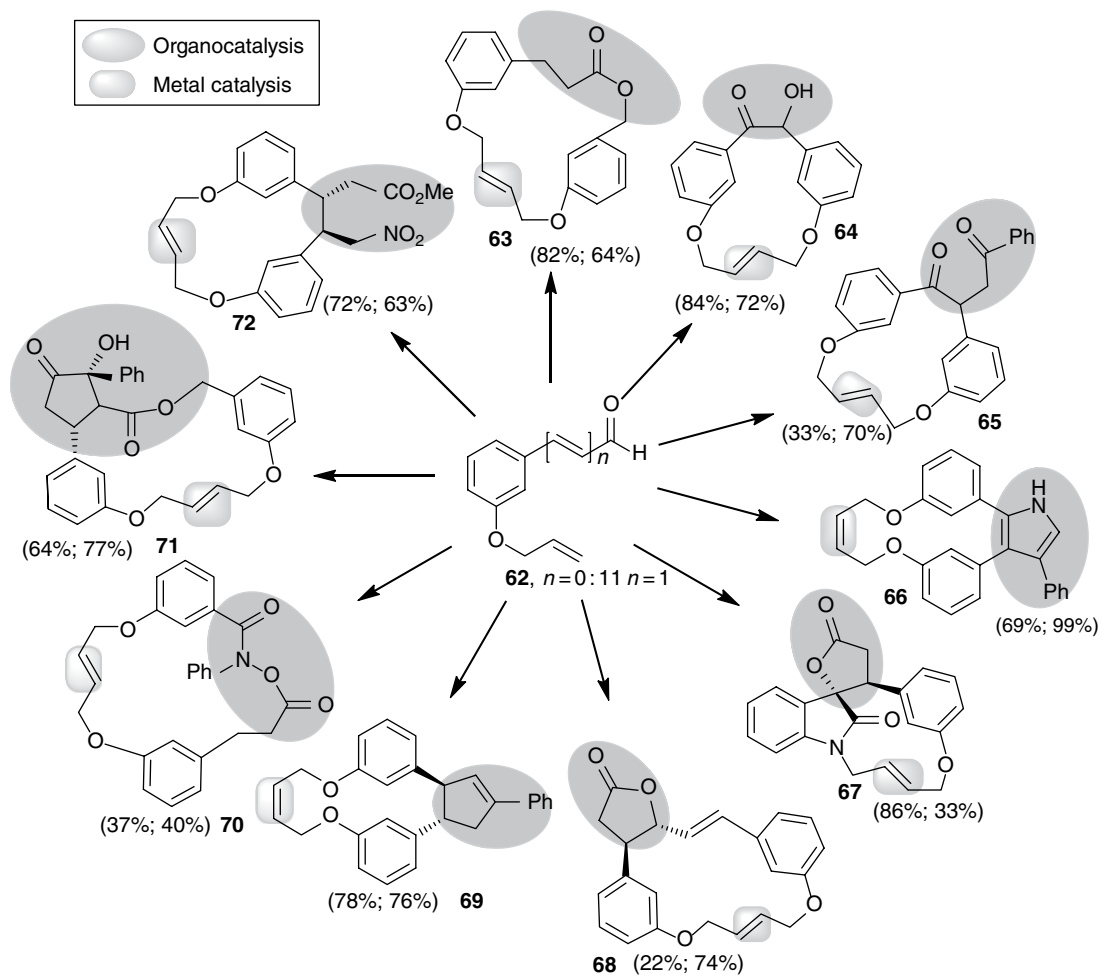
Figure 10.11 Few examples of macrocycles from DOS library by David Spring.

Figure 10.12 First- and second-generation functionalized indoline scaffolds.

73 (Racemic)
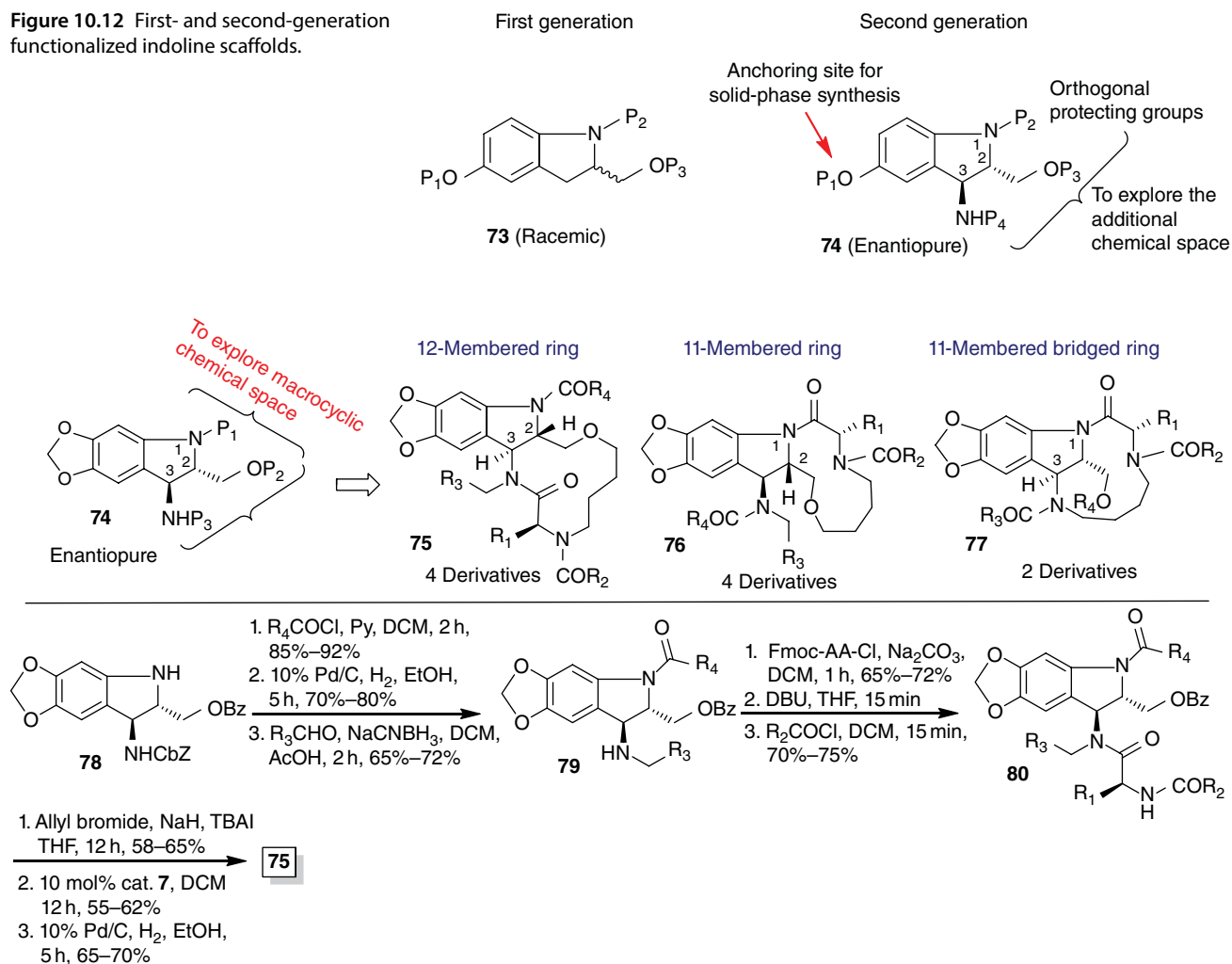
74 (Enantiopure)

Figure 10.13 Building a diverse set of macrocyclic toolbox from enantiopure scaffold **5.1**.

Our aim was to utilize the 1,2-*trans* amino alcohol functionality to obtain the additional 12-membered ring on aminoindole scaffold. This was achieved via key reactions: (i) amide bond formation to incorporate the amino acid bearing an allyl group, (ii) −O-allylation, and (iii) subsequent RCM. This approach was successfully developed and led to the completion of the synthesis of **75** possessing four diversity sites, that is, R_1, R_2, R_3, and R_4. As a proof of concept, we synthesized four derivatives that further utilized these diversity points. On a similar line, we were also able to accomplish the synthesis of two more types of macrocyclic compounds, **76** (four derivatives) and **77** (2 derivatives), having 11-membered rings. It is interesting to note that **77** possesses a *branched* 11-membered bridge macrocycle, achieved by utilizing both amino groups of the scaffold. Our plans to enter into the macrocyclic arena were based on the following attractive features that, in general, functionalized large ring compounds offer [24, 77]: (i) such compounds can

span a large surface area, which can be of prime importance to modulate PPIs; (ii) pre-organized dynamic structures can be highly attractive for binding to protein surfaces; and (iii) in general, it is also believed that these cyclic compounds have the potential to exhibit enhanced cell permeation behavior over linear structures. Combining all these features, the development of synthetic methods to build chemical toolboxes having compounds closer to bioactive natural products and also containing different types of large-sized rings is an emerging area within the drug discovery community.

10.5.6 Tetrahydroquinoline Alkaloid-Like Macrocyclic Chemical Probes

Tetrahydroquinoline and tetrahydroisoquinoline are two privileged substructures commonly found in a wide variety of alkaloid natural products. With the objective of exploring the chemical space around the tetrahydroquinoline
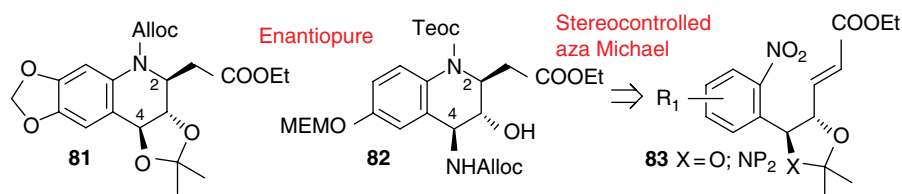
Figure 10.14 A stereocontrolled aza-Michael approach to obtain enantiopure tetrahydroquinoline-based scaffolds **81** and **82**.
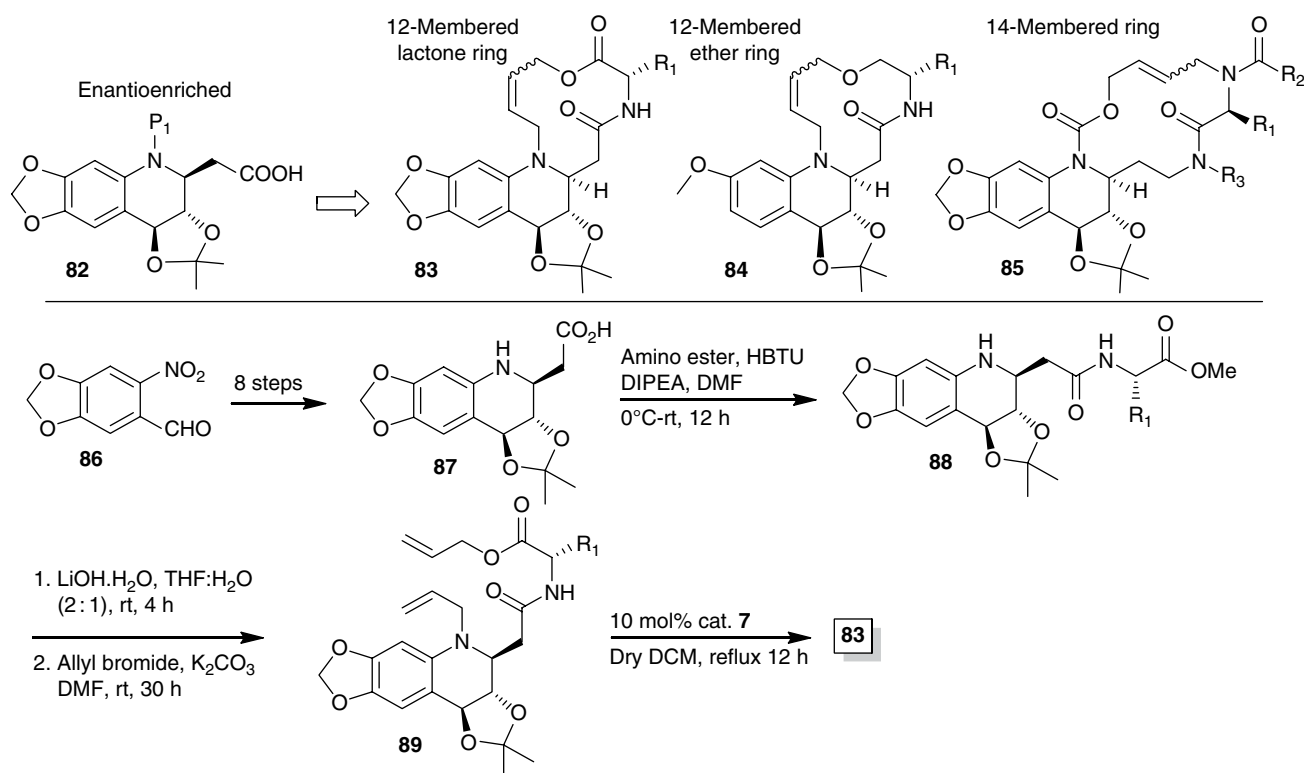
Figure 10.15 A diverse set of tetrahydroquinoline-based macrocyclic derivatives.

substructure, we developed a highly practical enantiose-lective synthesis of functionalized tetrahydroaminoqui-noline scaffolds **81** and **82** based on an intramolecular aza-Michael reaction (Figure 10.14) [78]. Several features of these scaffolds make them quite versatile and amenable to the production of a wide variety of very different poly-cyclic architectures. These key features include the pres-ence of (i) the β-amino acid moiety, (ii) the ε-amino/hydroxy moiety, (iii) the γ-hydroxy carboxyl ester func-tionality, and (iv) the phenolic hydroxyl group that could be used as an anchoring site during solid-phase synthesis.

Having the successful route for an enantioselective synthesis of **82** on a large scale, using the β-amino acid functionality from this scaffold in conjunction with the previously described macrocyclic strategy, compounds **83** (4 derivatives), **84** (4 derivatives), and **85** (4 derivatives) were then obtained (Figure 10.15). Various diversity sites

incorporated in these macrocyclic compounds also allowed us in obtaining sufficient analogues to validate the synthetic methodology.

10.5.7 Enantio-enriched Benzofuran-Based Macrocyclic Toolbox

With an objective to build a benzofuran-based chemical toolbox, in 2008 [79] we reported a practical enantiose-lective synthesis of **90** (Figure 10.16) that possesses sev-eral attractive features: (i) the presence of a privileged scaffold as the benzofuran substructure, (ii) a *trans*-β-amino acid functionality, and (iii) an additional func-tional group on the aromatic rings that can be further modified. Using this scaffold as the starting material, we decided to develop a divergent approach to obtain two different sets of macrocyclic architectures, **91/92** and
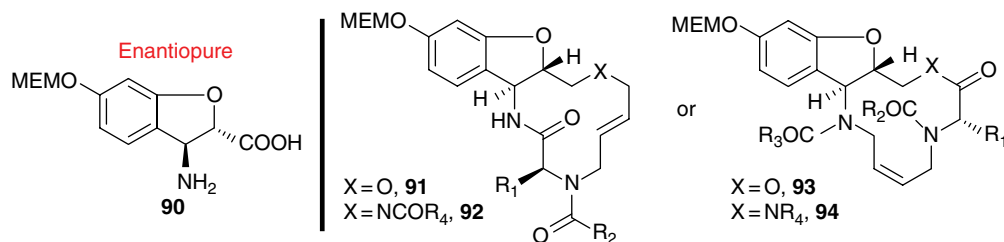
Figure 10.16 Building a diverse set of macrocyclic toolbox from an enantiopure benzofuran-based *trans*-β-amino acid.
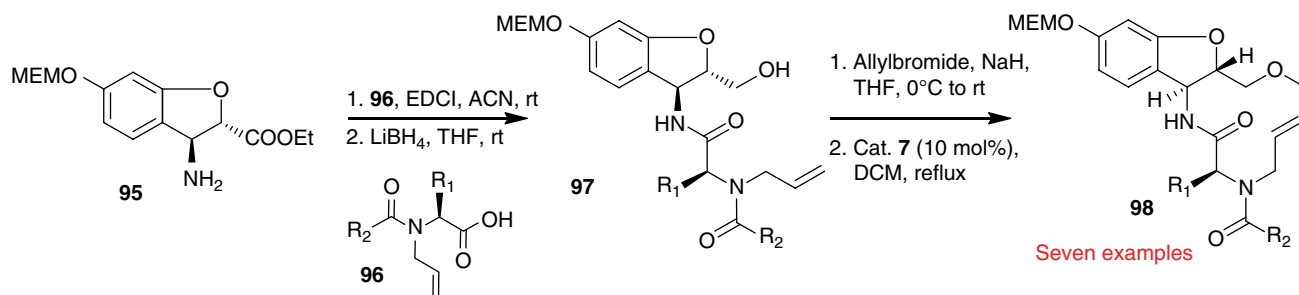
Figure 10.17 An example of the synthesis of a tricyclic derivative, **98**, from the bicyclic scaffold **95**.

93/94 [80]. In the **91/92** series, the amino acid functionality is coupled starting from the benzylic amine site, and the RCM-based macrocyclization gives the 12-membered macrocyclic ring. In the other approach, using the primary amine group to couple the amino acid moiety, we can obtain a totally different set of 12-membered compounds (**93/94**).

Our synthesis plan to accessing these two macrocyclic sets is shown in Figure 10.17. As a start, we developed an enantioselective synthesis of benzofuran-based *trans*-β-amino ester, **95**. This was then coupled with a modified amino acid derivative, **96**, bearing an *N*-allyl moiety followed by reduction of ester to obtain alcohol **97**. Following hydroxyl allylation of **97**, RCM-based macrocyclization using 10 mol% Grubbs second-generation catalyst worked very well, giving only the *trans* geometry across the double bond within the 12-membered macrocycle product, **98**. Several examples were synthesized as a validation of this methodology. These are highly attractive structures possessing several unique features, including (i) a benzofuran moiety with a fused *trans*-12-membered macrocycle containing a *trans*-alkene, (ii) substitution on the aromatic moiety, and (iii) macrocycle having embedded amino acid functionality. Overall, the presence of two diversity sites (R₁, R₂) further allows access to several analogues to explore the chemical space around this macrocyclic architecture.

10.5.8 Building a Diverse 14-Membered Ring-Based Chemical Toolbox

There are several examples of bioactive natural products possessing either a 14-membered macrocyclic ring alone, such as erythromycin A (**102**) and oleandomycin (**103**) [81–84], or having the macrocycle fused with an aromatic moiety, for example, radicicol (**1** [85–87]; Figure 10.2), pochonin [88–90] (**99**; Figure 10.18), aigialomycin D (**100**), and hypothemycin [85, 91–93] (**101**). Keeping in mind the importance of the 14-membered ring in the disease biology arena, we decided to develop modular synthesis methods to allow us to build a diverse chemical toolbox having two different types of 14-membered rings fused to an aromatic moiety (Figure 10.19).

With this objective, we were interested in developing a modular synthesis method to accessing natural product-inspired 14-membered ring-derived macrocyclic toolbox [94]. Natural product-inspired macrocycles are closer to natural products than traditional small molecules in terms of three-dimensional (3D) shapes and dense display of chiral functional groups. In our modular design strategy, we had an option to incorporate the amino acid functionality either through the aromatic amine or from the aliphatic side chain (see macrocyclic targets **104**, **105**, **106**, and **107**; Figure 10.19). Further, variation in the side chain, that is, R₂, R₃, and R₄, on the macrocyclic skeleton can be achieved through selective
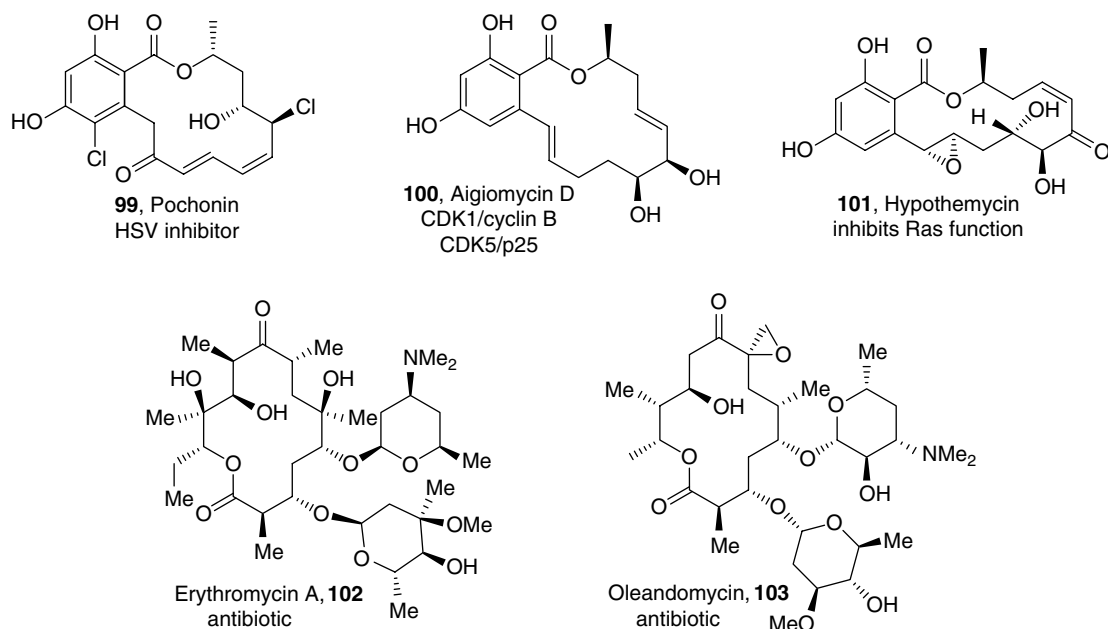
Figure 10.18 Examples of bioactive natural products having a 14-membered ring.
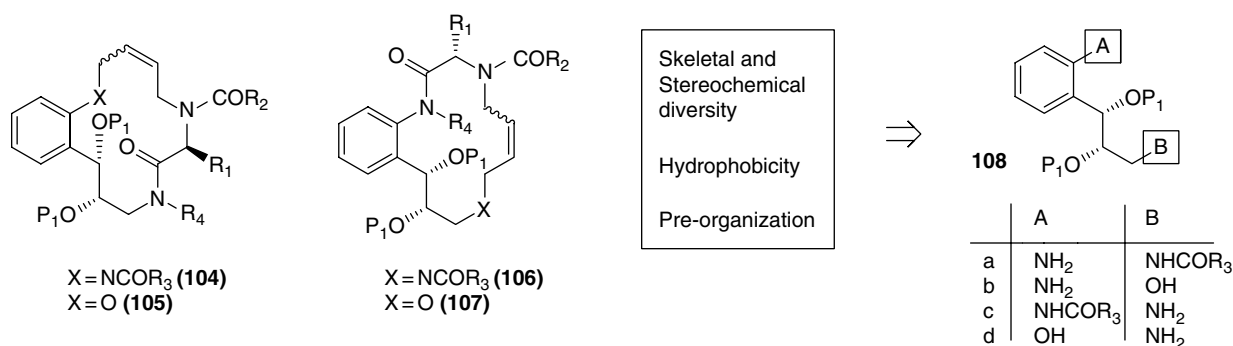
Figure 10.19 A strategy to build a diverse 14-membered ring-derived small-molecule toolbox.

acylation, acylation, and alkylation, respectively. We successfully developed the synthesis routes necessary to access a small library of 14-membered macrocycles and then tested them in a zebrafish-based assay to search for anti-angiogenesis agents and inhibitors of early embryonic development.

One of our synthetic plans to obtain a 14-membered ring-based macrocycle is shown in Figure 10.20 [94]. It starts with enantio-enriched fragment **109**, easily prepared using Sharpless enantioselective dihydroxylation. Having a free amino group, this was alkylated and then coupled with the required amino acid functionality to obtain **110**, which was then converted to **111** in four steps. Using **111** as the starting material, we obtained the *bis*-allyl derivative **112**, a key precursor for the crucial RCM-based macrocyclization using Grubbs second-generation catalyst. We were delighted to note that the macrocyclization strategy worked well (obtained 80–90%

RCM yields) with this series and eight compounds were obtained using three diversity sites. In one example (**113**), we also succeeded in obtaining the X-ray structure (**114**), and this further confirmed assignment of the *trans*-olefin geometry within the macrocycle.

By simply extending this approach to carbohydrates, we also succeeded in obtaining totally different sets of 14-membered ring-based macrocyclic compounds (Figure 10.21) [95]. This methodology can be further applied to a wide variety of carbohydrates to obtain a highly diverse set of macrocyclic compounds. This approach is quite unique and provides an excellent opportunity to exploit the chirality from different carbohydrates in obtaining amphiphilic 14-membered glycohybrids.

Outlined in Figure 10.22 is one of the key approaches utilized in building these glyco-based 14-membered macrocyclic compounds [95]. For example, **123** was
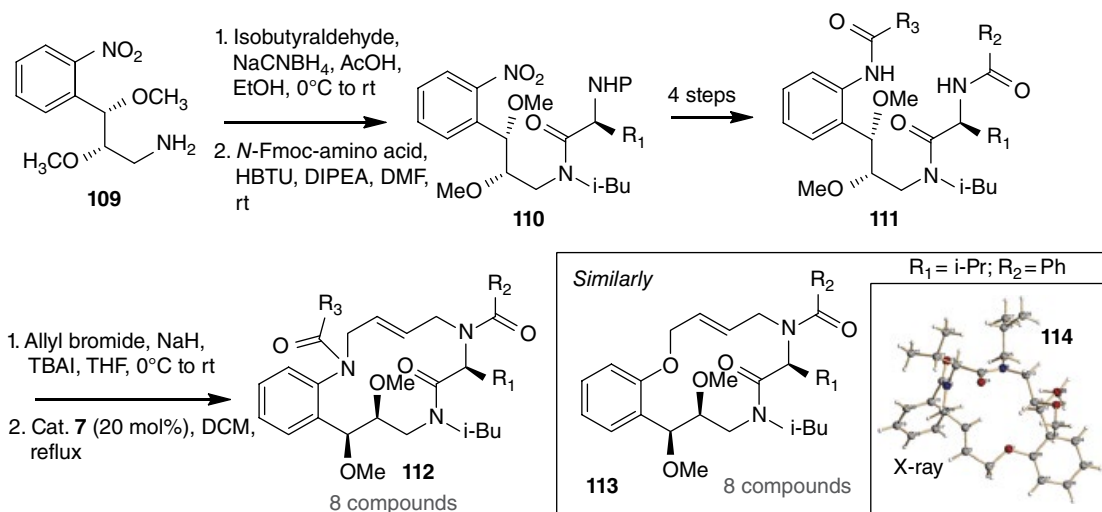
Figure 10.20 Our approach to obtain two different sets of 14-membered ring macrocyclic scaffolds for a diversity-based small-molecule toolbox.
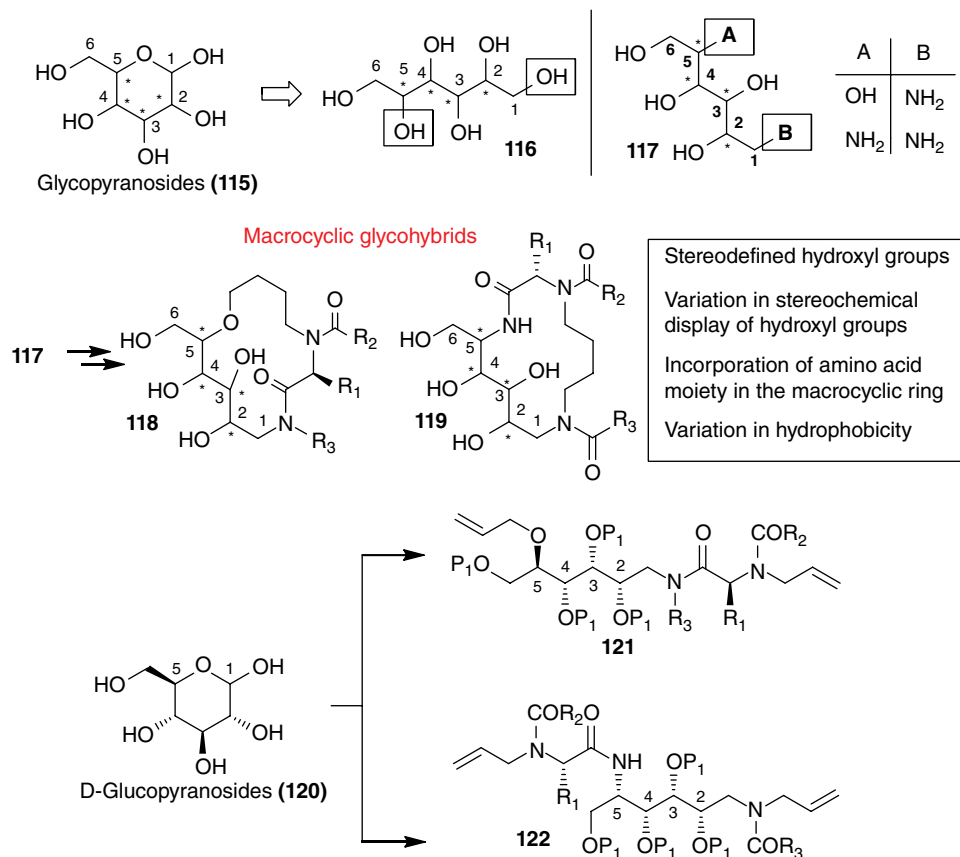
Figure 10.21 A general approach to building 14-membered glycohybrids from carbohydrates.

converted to an open structure possessing a secondary amine on C-1, **124**. This was then coupled with an amino acid moiety, giving **125**. Allylation of the amide nitrogen on the N-terminal amino acid functionality and the C–5–

OH then gave the precursor required on which to apply the RCM technology. As observed in the previous case, RCM with 10 mol% Grubbs second-generation catalyst worked quite well, and the approach delivered
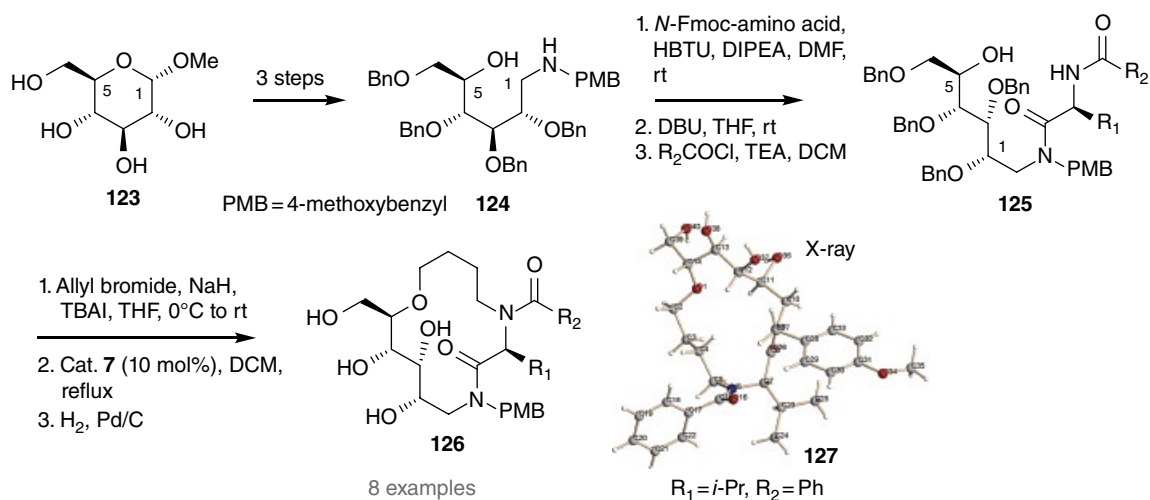
Figure 10.22 Our synthetic pathway to building 14-membered glycohybrid-based macrocyclic toolbox.
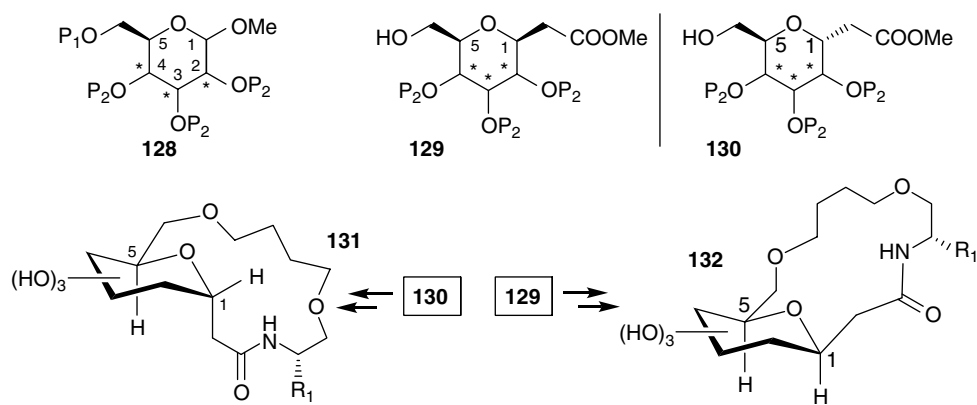
Figure 10.23 A general approach to building macrocyclic diversity from C-linked carbohydrates.

14-membered ring hybrid compounds having both a carbohydrate fragment and an amino acid moiety embedded in the macrocycle with two diversity sites, as exemplified by **126**. In one case (**127**), X-ray structure confirmed the formation of the 14-membered macrocycle.

10.5.9 Building a Diverse C-Linked Glyco-Based Macrocyclic Toolbox

In another effort using carbohydrates as the starting materials, we embarked on a program that utilizes C-linked glycosides [96–99] at the anomeric position. As shown in Figure 10.23, the first level targets were two α- and β-C-linked glycosides, **129** and **130**. It is well known that C-linked glycosides provide anomeric stability and are easy to handle under various reaction conditions. In general, their expected increased stability was highly attractive, and we were interested in utilizing both α- and β-positions to obtain macrocyclic diversity (**131** and **132**).

In one approach, we obtained compound **133** (Figure 10.24) as a mixture of diastereomers at the C-1

anomeric position [100]. This mixture, in three steps, led to the synthesis of **134**, which was then coupled with the amino alcohol-based moiety **135** to provide the key intermediate for RCM macrocyclization. The successful implementation of RCM with 10 mol% of Grubbs second-generation catalyst allowed us to obtain two different macrocyclic compounds, **136** and **137**. Following macrocyclization, the diastereomeric mixture was easily separated, and both pure products were thoroughly characterized.

10.5.10 Evaluation of the Chemical Toolbox in Search for Anti-angiogenesis Agents

The development of biological assays in the zebrafish system is constantly growing in the literature. The use of zebrafish offers several advantages:

i) A transparent higher vertebrate animal model.
ii) Embryonic zebrafish can be utilized in the study.
iii) The small-molecule effect(s) can be easily visualized.
iv) It is possible to execute studies in a high-throughput manner [101–109].

Figure 10.24 An example of the synthesis of two different macrocycles from *C*-linked carbohydrates.
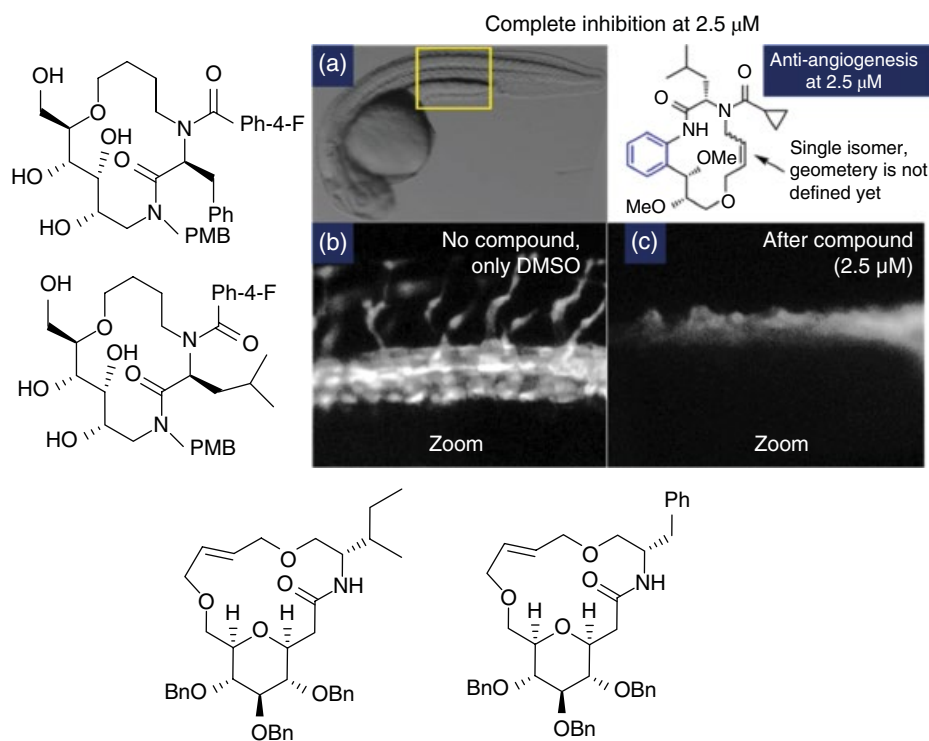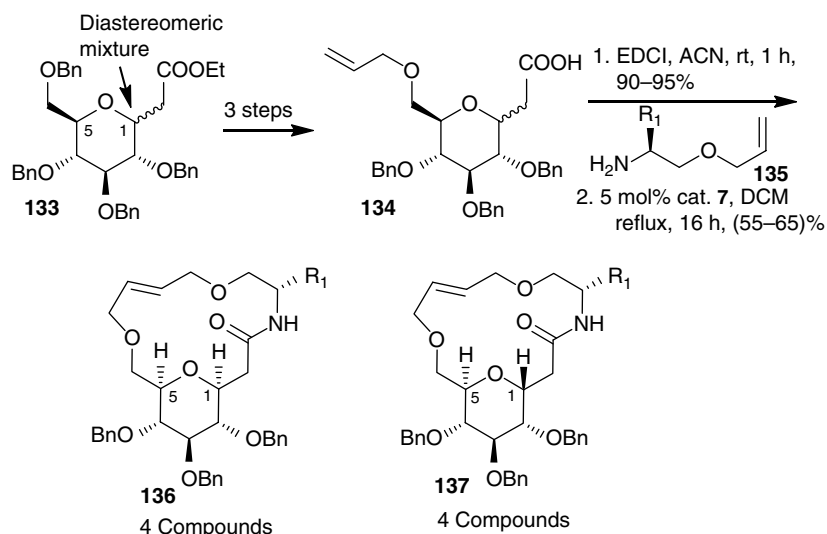
Figure 10.25 The discovery of several macrocyclic compounds functioning as anti-angiogenesis agents in an embryonic zebrafish study; (a) zoom section; (b) with DMSO as a control; and (c) the effect of a small molecule. (*See insert for color representation of the figure.*)

With the objective to search for small-molecule modulators of angiogenesis in an embryonic zebrafish study, we established a collaboration with the Kitambi team at the Karolinska Institutet, Sweden, and thoroughly tested our chemical toolbox containing a wide set of small molecules. Interestingly, novel compounds from several of the aforementioned scaffolds were identified as potent inhibitors of angiogenesis as shown in Figure 10.25 [94, 95, 100, 110–112]. Further work is needed to understand the precise mechanism(s) of these small molecules, as it is important to find out how specifically these functional compounds are playing a key role in modulating some of the signaling pathways or PPIs.
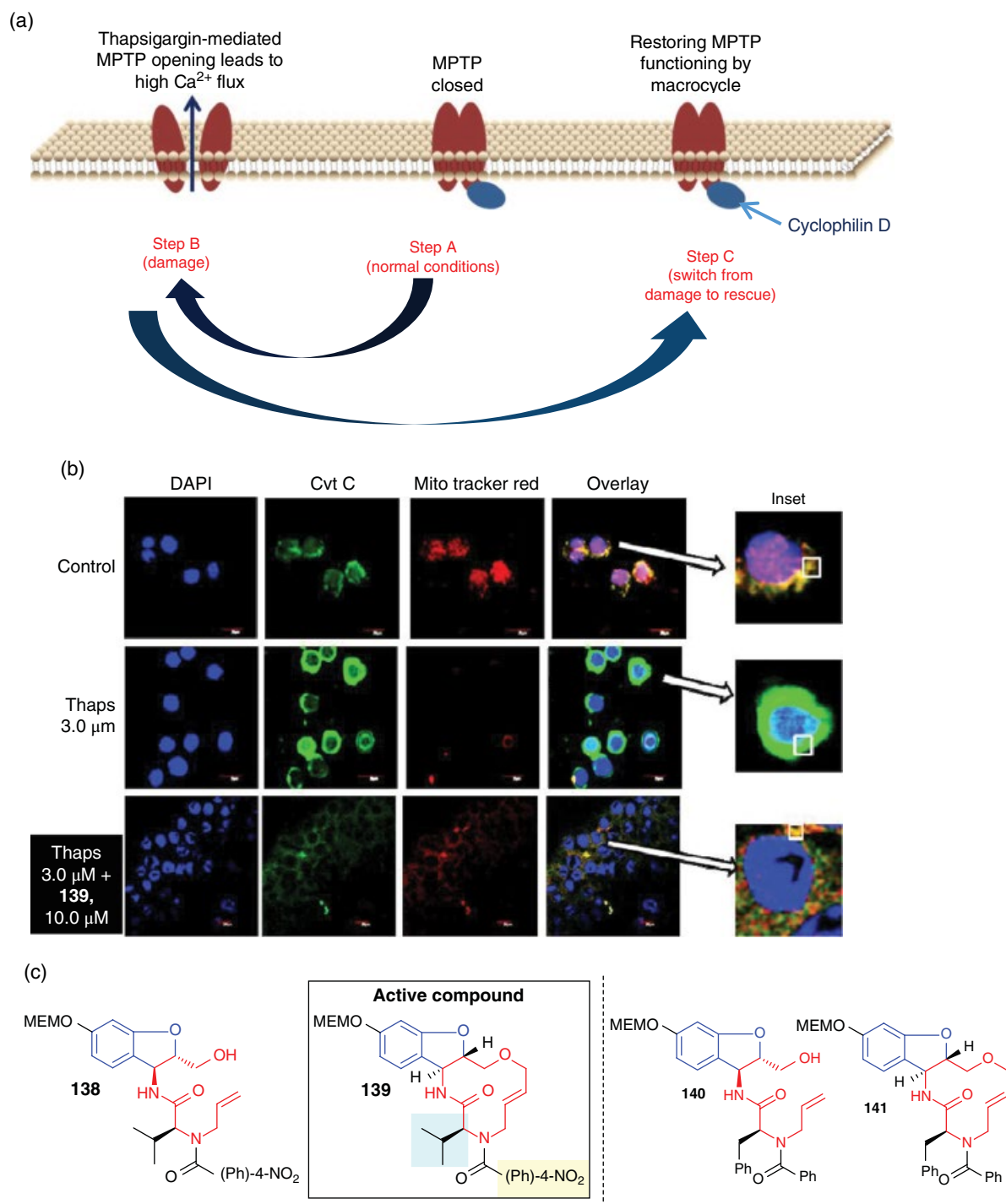
(a)

(b)

(c)

Figure 10.26 The discovery of macrocyclic small molecules functioning as correctors of the damage induced in the pore formation caused by thapsigargin, resulting in the rescue of cell death in pancreatic β-cells: (a) our proposed working model for the dynamic regulation of protein–protein interactions; (b) mitochondrial images with thapsigargin-induced damage and subsequent reorganization of mitochondria in the presence of **139**; (c) two sets of macrocyclic compounds and their acyclic precursors. (*See insert for color representation of the figure.*)

In another collaborative study [80], we examined a small-molecule toolbox to identify novel compounds that could rescue the damage caused by thapsigargin to the mitochondrial machinery in pancreatic β-cells. There are several dynamic PPI-based complexes in the mitochondrial membrane, commonly known as the mitochondrial permeability transition pore (MPTP). Its tightly controlled regulation instructs the flow of ions and other biomacromolecules, such as cytochrome *c*, across mitochondria. *In a healthy environment, this process is tightly regulated. In the disease state (e.g., in metabolic disorders), dysregulation leads to an improper flow of ions, which then leads to cell death.* Our study was aimed at identifying novel small molecules with the ability to correct this damage, presumably through modulation of dysregulated PPIs. We were delighted to identify a set of novel benzofuran-based 12-membered ring macrocyclic compounds (e.g., **139** in Figure 10.26) able to correct the damage caused by thapsigargin and further rescued cell death in pancreatic β-cells. This was presumably achieved through the reorganization of the mitochondrial machinery. Another interesting observation was that this corrector effect was seen only by a specific macrocyclic compound (**139**) and not by its acyclic precursor. This led to the hypothesis that the precise orientation of several functional moieties in the macrocycle seems to play a key role in the activity. To our knowledge, this is the first discovery of a novel set of natural product-inspired 12-membered macrocyclic compounds that seem to function through the modulation of a PPI to exhibit their biological response. However, the exact mechanism of action is not available at this stage.

10.6 Summary

A rise in the interest in modulating biological targets emerging from the dysregulation of signaling pathways and PPI necessitates novel sets of small molecules that are closer in structure to bioactive natural products. This shift toward PPI targets or phenotypic screens requires compounds that are rich in sp^3 character, in contrast with traditional small-molecule compounds typically dominated by heterocyclic compounds with enriched sp^2 character. Additionally, these new structures must be more complex stereochemically and able to display 3D diversity. Thus, several directions emerge, such as DOS and biology-oriented synthesis (BIOS). All of these will allow the community to embrace the complexity of cell biology and tackle PPI/pathways-based targets. In this chapter, we summarized several years of work dedicated to going beyond classical heterocyclic chemical space and developed new diversity-based synthetic methods that allowed the elaboration of a chemical toolbox replenished with macrocyclic compounds that can be classified with "natural product-like or product-inspired" character. In addition to highlighting our chemistry efforts, we also outlined two collaborative biological case studies, namely, (i) angiogenesis in zebrafish and (ii) mitochondrial machinery in pancreatic β-cells, and further showed several functional chemical probes identified from these two programs. In both cases, our findings are at a preliminary stage, and more work is required to obtain a deeper knowledge to define the precise roles of these novel functional probes.

References

1 Wells, J. A.; McClendon, C. L.: Reaching for high-hanging fruit in drug discovery at protein–protein interfaces. *Nature* **2007**, *450*, 1001–1009.

2 Fishman, M. C.; Porter, J. A.: Pharmaceuticals: a new grammar for drug discovery. *Nature* **2005**, *437*, 491–493.

3 Tate, E. W.: Chemical intervention in signalling networks: recent advances and applications. *Signal Transduct.* **2006**, *6*, 144–159.

4 Aeluri, M.; Chamakuri, S.; Dasari, B.; Guduru, S. K.; Jimmidi, R.; Jogula, S.; Arya, P.: Small molecule modulators of protein–protein interactions: selected case studies. *Chem. Rev.* **2014**, *114*, 4640–4694.

5 Pawson, T.; Nash, P.: Assembly of cell regulatory systems through protein interaction domains. *Science* **2003**, *300*, 445–452.

6 Pawson, T.; Scott, J. D.: Protein phosphorylation in signaling: 50 years and counting. *Trends Biochem. Sci.* **2005**, *30*, 286–290.

7 Scott, J. D.; Pawson, T.: Cell signaling in space and time: where proteins come together and when they're apart. *Science* **2009**, *326*, 1220–1224.

8 Pawson, T.; Warner, N.: Oncogenic re-wiring of cellular signaling pathways. *Oncogene* **2007**, *26*, 1268–1275.

9 Pawson, T.: Dynamic control of signaling by modular adaptor proteins. *Curr. Opin. Cell Biol.* **2007**, *19*, 112–116.

10 Arkin, M. R.; Wells, J. A.: Small-molecule inhibitors of protein–protein interactions: progressing towards the dream. *Nat. Rev. Drug Discov.* **2004**, *3*, 301–317.

11 Arkin, M.: Protein–protein interactions and cancer: small molecules going in for the kill. *Curr. Opin. Chem. Biol.* **2005**, *9*, 317–324.

12 LaCasse, E. C.; Baird, S.; Korneluk, R. G.; MacKenzie, A. E.: The inhibitors of apoptosis (IAPs) and their emerging role in cancer. *Oncogene* **1998**, *17*, 3247–3259.

13 Riedl, S. J.; Renatus, M.; Schwarzenbacher, R.; Zhou, Q.; Sun, C.; Fesik, S. W.; Liddington, R. C.; Salvesen, G. S.: Structural basis for the inhibition of caspase-3 by XIAP. *Cell* **2001**, *104*, 791–800.

14 Fesik, S. W.; Shi, Y.: Structural biology: controlling the caspases. *Science* **2001**, *294*, 1477–1478.

15 Schimmer, A. D.; Dalili, S.; Batey, R. A.; Riedl, S. J.: Targeting XIAP for the treatment of malignancy. *Cell Death Differ.* **2006**, *13*, 179–188.

16 Schimmer, A. D.; Dalili, S.: Targeting the IAP family of caspase inhibitors as an emerging therapeutic strategy. *Hematol. Am. Soc. Hematol. Educ. Program* **2005**, 215–219.

17 Reed, J. C.: Apoptosis-based therapies. *Nat. Rev. Drug. Discov.* **2002**, *1*, 111–121.

18 Huang, Z.: The chemical biology of apoptosis: exploring protein–protein interactions and the life and death of cells with small molecules. *Chem. Biol.* **2002**, *9*, 1059–1072.

19 Dandapani, S.; Marcaurelle, L. A.: Grand challenge commentary: accessing new chemical space for 'undruggable' targets. *Nat. Chem. Biol.* **2010**, *6*, 861–863.

20 Marcaurelle, L. A.; Foley, M. A.: The evolving role of molecular diversity in drug discovery. *Curr. Opin. Chem. Biol.* **2010**, *14*, 285–288.

21 Cragg, G. M.; Grothaus, P. G.; Newman, D. J.: Impact of natural products on developing new anti-cancer agents. *Chem. Rev.* **2009**, *109*, 3012–3043.

22 Newman, D. J.; Cragg, G. M.: Natural products from marine invertebrates and microbes as modulators of antitumor targets. *Curr. Drug Targets* **2006**, *7*, 279–304.

23 Newman, D. J.; Cragg, G. M.; Snader, K. M.: The influence of natural products upon drug discovery. *Nat. Prod. Rep.* **2000**, *17*, 215–234.

24 Driggers, E. M.; Hale, S. P.; Lee, J.; Terrett, N. K.: The exploration of macrocycles for drug discovery: an underexploited structural class. *Nat. Rev. Drug Discov.* **2008**, *7*, 608–624.

25 Moulin, E.; Zoete, V.; Barluenga, S.; Karplus, M.; Winssinger, N.: Design, synthesis, and biological evaluation of HSP90 inhibitors based on conformational analysis of radicicol and its analogues. *J. Am. Chem. Soc.* **2005**, *127*, 6999–7004.

26 Rohr, J.: Cryptophycin anticancer drugs revisited. *ACS Chem. Biol.* **2006**, *1*, 747–750.

27 Liang, J.; Moore, R. E.; Moher, E. D.; Munroe, J. E.; Al-awar, R. S.; Hay, D. A.; Varie, D. L.; Zhang, T. Y.; Aikins, J. A.; Martinelli, M. J.; Shih, C.; Ray, J. E.; Gibson, L. L.; Vasudevan, V.; Polin, L.; White, K.; Kushner, J.; Simpson, C.; Pugh, S.; Corbett, T. H.: Cryptophycins-309, 249 and other cryptophycin analogs: preclinical efficacy studies with mouse and human tumors. *Invest. New Drugs* **2005**, *23*, 213–224.

28 Eggen, M.; Georg, G. I.: The cryptophycins: their synthesis and anticancer activity. *Med. Res. Rev.* **2002**, *22*, 85–101.

29 Correia, J. J.; Lobert, S.: Physiochemical aspects of tubulin-interacting antimitotic drugs. *Curr. Pharm. Des.* **2001**, *7*, 1213–1228.

30 Schreiber, S. L.; Crabtree, G. R.: The mechanism of action of cyclosporin A and FK506. *Immunol. Today* **1992**, *13*, 136–142.

31 Spencer, D. M.; Wandless, T. J.; Schreiber, S. L.; Crabtree, G. R.: Controlling signal transduction with synthetic ligands. *Science* **1993**, *262*, 1019–1024.

32 Schreiber, S. L.; Crabtree, G. R.: Immunophilins, ligands, and the control of signal transduction. *Harvey Lect.* **1995**, *91*, 99–114.

33 Crabtree, G. R.; Schreiber, S. L.: Three-part inventions: intracellular signaling and induced proximity. *Trends Biochem. Sci.* **1996**, *21*, 418–422.

34 Belshaw, P. J.; Ho, S. N.; Crabtree, G. R.; Schreiber, S. L.: Controlling protein association and subcellular localization with a synthetic ligand that induces heterodimerization of proteins. *Proc. Natl. Acad. Sci. U. S. A.* **1996**, *93*, 4604–4607.

35 Klemm, J. D.; Schreiber, S. L.; Crabtree, G. R.: Dimerization as a regulatory mechanism in signal transduction. *Annu. Rev. Immunol.* **1998**, *16*, 569–592.

36 LoRusso, P. M.: Mammalian target of rapamycin as a rational therapeutic target for breast cancer treatment. *Oncology* **2013**, *84*, 43–56.

37 Choi, J.; Chen, J.; Schreiber, S. L.; Clardy, J.: Structure of FKBP12-rapamycin complex interacting with the binding domain of human FRAP. *Science* **1996**, *273*, 239–242.

38 Chakraborty, T. K.; Weber, H. P.; Nicolaou, K. C.: Design and synthesis of a rapamycin-based high affinity binding FKBP12 ligand. *Chem. Biol.* **1995**, *2*, 157–161.

39 Brown, E. J.; Albers, M. W.; Shin, T. B.; Ichikawa, K.; Keith, C. T.; Lane, W. S.; Schreiber, S. L.: A mammalian protein targeted by G1-arresting rapamycin-receptor complex. *Nature* **1994**, *369*, 756–758.

40 Kunz, J.; Henriquez, R.; Schneider, U.; Deuter-Reinhard, M.; Movva, N. R.; Hall, M. N.: Target of rapamycin in yeast, TOR2, is an essential phosphatidylinositol kinase homolog required for G1 progression. *Cell* **1993**, *73*, 585–596.

41 Heitman, J.; Movva, N. R.; Hall, M. N.: Targets for cell cycle arrest by the immunosuppressant rapamycin in yeast. *Science* **1991**, *253*, 905–909.

42 Grubbs, R. H.; Chang, S.: Recent advances in olefin metathesis and its application in organic synthesis. *Tetrahedron* **1998**, *54*, 4413–4450.

43 Fürstner, A.: Teaching metathesis "simple" stereochemistry. *Science* **2013**, *341*, 1229713.

44 Nicolaou, K.; Bulger, P. G.; Sarlah, D.: Metathesis reactions in total synthesis. *Angew. Chem. Int. Ed.* **2005**, *44*, 4490–4527.

45 Villar, H.; Frings, M.; Bolm, C.: Ring closing enyne metathesis: a powerful tool for the synthesis of heterocycles. *Chem. Soc. Rev.* **2007**, *36*, 55–66.

46 Diver, S. T.; Giessert, A. J.: Enyne metathesis (enyne bond reorganization). *Chem. Rev.* **2004**, *104*, 1317–1382.

47 Fürstner, A.: Alkyne metathesis on the rise. *Angew. Chem. Int. Ed.* **2013**, *52*, 2794–2819.

48 Schrock, R. R.; Murdzek, J. S.; Bazan, G. C.; Robbins, J.; DiMare, M.; O'Regan, M.: Synthesis of molybdenum imido alkylidene complexes and some reactions involving acyclic olefins. *J. Am. Chem. Soc.* **1990**, *112*, 3875–3886.

49 Nguyen, S. T.; Johnson, L. K.; Grubbs, R. H.; Ziller, J. W.: Ring-opening metathesis polymerization (ROMP) of norbornene by a group VIII carbene complex in protic media. *J. Am. Chem. Soc.* **1992**, *114*, 3974–3975.

50 Grubbs, R. H.; Miller, S. J.; Fu, G. C.: Ring-closing metathesis and related processes in organic synthesis. *Acc. Chem. Res.* **1995**, *28*, 446–452.

51 Weskamp, T.; Kohl, F. J.; Hieringer, W.; Gleich, D.; Herrmann, W. A.: Highly active ruthenium catalysts for olefin metathesis: the synergy of N-heterocyclic carbenes and coordinatively labile ligands. *Angew. Chem. Int. Ed.* **1999**, *38*, 2416–2419.

52 Scholl, M.; Trnka, T. M.; Morgan, J. P.; Grubbs, R. H.: Increased ring closing metathesis activity of ruthenium-based olefin metathesis catalysts coordinated with imidazolin-2-ylidene ligands. *Tetrahedron Lett.* **1999**, *40*, 2247–2250.

53 Huang, J.; Stevens, E. D.; Nolan, S. P.; Petersen, J. L.: Olefin metathesis-active ruthenium complexes bearing a nucleophilic carbene ligand. *J. Am. Chem. Soc.* **1999**, *121*, 2674–2678.

54 Furstner, A.; Thiel, O. R.; Ackermann, L.; Schanz, H.-J.; Nolan, S. P.: Ruthenium carbene complexes with N,N'-bis(mesityl)imidazol-2-ylidene ligands: RCM catalysts of extended scope. *J. Org. Chem.* **2000**, *65*, 2204–2207.

55 Kingsbury, J. S.; Harrity, J. P.; Bonitatebus, P. J.; Hoveyda, A. H.: A recyclable Ru-based metathesis catalyst. *J. Am. Chem. Soc.* **1999**, *121*, 791–799.

56 Garber, S. B.; Kingsbury, J. S.; Gray, B. L.; Hoveyda, A. H.: Efficient and recyclable monomeric and dendritic Ru-based metathesis catalysts. *J. Am. Chem. Soc.* **2000**, *122*, 8168–8179.

57 Lee, C. W.; Grubbs, R. H.: Stereoselectivity of macrocyclic ring-closing olefin metathesis. *Org. Lett.* **2000**, *2*, 2145–2147.

58 Jiang, A. J.; Zhao, Y.; Schrock, R. R.; Hoveyda, A. H.: Highly Z-selective metathesis homocoupling of terminal olefins. *J. Am. Chem. Soc.* **2009**, *131*, 16630–16631.

59 Meek, S. J.; O'Brien, R. V.; Llaveria, J.; Schrock, R. R.; Hoveyda, A. H.: Catalytic Z-selective olefin cross-metathesis for natural product synthesis. *Nature* **2011**, *471*, 461–466.

60 Rosebrugh, L. E.; Herbert, M. B.; Marx, V. M.; Keitz, B. K.; Grubbs, R. H.: Highly active ruthenium metathesis catalysts exhibiting unprecedented activity and Z-selectivity. *J. Am. Chem. Soc.* **2013**, *135*, 1276–1279.

61 Yu, M.; Wang, C.; Kyle, A. F.; Jakubec, P.; Dixon, D. J.; Schrock, R. R.; Hoveyda, A. H.: Synthesis of macrocyclic natural products by catalyst-controlled stereoselective ring-closing metathesis. *Nature* **2011**, *479*, 88–93.

62 Wang, C.; Yu, M.; Kyle, A. F.; Jakubec, P.; Dixon, D. J.; Schrock, R. R.; Hoveyda, A. H.: Efficient and selective formation of macrocyclic disubstituted Z alkenes by ring-closing metathesis (RCM) reactions catalyzed by Mo-or W-based monoaryloxide pyrrolide (MAP) complexes: applications to total syntheses of epilachnene, yuzu lactone, ambrettolide, epothilone C, and nakadomarin A. *Chem. Eur. J.* **2013**, *19*, 2726–2740.

63 Wang, Y.; Jimenez, M.; Hansen, A. S.; Raiber, E.-A.; Schreiber, S. L.; Young, D. W.: Control of olefin geometry in macrocyclic ring-closing metathesis using a removable silyl group. *J. Am. Chem. Soc.* **2011**, *133*, 9196–9199.

64 Bradner, J. E.; McPherson, O. M.; Mazitschek, R.; Barnes-Seeman, D.; Shen, J. P.; Dhaliwal, J.; Stevenson, K. E.; Duffner, J. L.; Park, S. B.; Neuberg, D. S.: A robust small-molecule microarray platform for screening cell lysates. *Chem. Biol.* **2006**, *13*, 493–504.

65 MacBeath, G.; Koehler, A. N.; Schreiber, S. L.: Printing small molecules as microarrays and detecting protein-ligand interactions en masse. *J. Am. Chem. Soc.* **1999**, *121*, 7967–7968.

66 Barnes-Seeman, D.; Park, S. B.; Koehler, A. N.; Schreiber, S. L.: Expanding the functional group compatibility of small-molecule microarrays: discovery of novel calmodulin ligands. *Angew. Chem. Int. Ed. Engl.* **2003**, *42*, 2376–2379.

67 Koehler, A. N.; Shamji, A. F.; Schreiber, S. L.: Discovery of an inhibitor of a transcription factor using small molecule microarrays and diversity-oriented synthesis. *J. Am. Chem. Soc.* **2003**, *125*, 8420–8421.

68 Stanton, B. Z.; Peng, L. F.; Maloof, N.; Nakai, K.; Wang, X.; Duffner, J. L.; Taveras, K. M.; Hyman, J. M.; Lee, S. W.; Koehler, A. N.; Chen, J. K.; Fox, J. L.; Mandinova, A.; Schreiber, S. L.: A small molecule that binds Hedgehog and blocks its signaling in human cells. *Nat. Chem. Biol.* **2009**, *5*, 154–156.

69 Peng, L. F.; Stanton, B. Z.; Maloof, N.; Wang, X.; Schreiber, S. L.: Syntheses of aminoalcohol-derived macrocycles leading to a small-molecule binder to and

inhibitor of Sonic Hedgehog. *Bioorg. Med. Chem. Lett.* **2009**, *19*, 6319–6325.

70 Heidebrecht, R. W., Jr.; Mulrooney, C.; Austin, C. P.; Barker, R. H., Jr.; Beaudoin, J. A.; Cheng, K. C.; Comer, E.; Dandapani, S.; Dick, J.; Duvall, J. R.; Ekland, E. H.; Fidock, D. A.; Fitzgerald, M. E.; Foley, M.; Guha, R.; Hinkson, P.; Kramer, M.; Lukens, A. K.; Masi, D.; Marcaurelle, L. A.; Su, X. Z.; Thomas, C. J.; Weiwer, M.; Wiegand, R. C.; Wirth, D.; Xia, M.; Yuan, J.; Zhao, J.; Palmer, M.; Munoz, B.; Schreiber, S.: Diversity-oriented synthesis yields a novel lead for the treatment of malaria. *ACS Med. Chem. Lett.* **2012**, *3*, 112–117.

71 Comer, E.; Beaudoin, J. A.; Kato, N.; Fitzgerald, M. E.; Heidebrecht, R. W.; Lee IV, M. D.; Masi, D.; Mercier, M.; Mulrooney, C.; Muncipinto, G.: Diversity-oriented synthesis-facilitated medicinal chemistry: toward the development of novel antimalarial agents. *J. Med. Chem.* **2014**, *57*, 8496–8502.

72 Grossmann, A.; Bartlett, S.; Janecek, M.; Hodgkinson, J. T.; Spring, D. R.: Diversity-oriented synthesis of drug-like macrocyclic scaffolds using an orthogonal organo-and metal catalysis strategy. *Angew. Chem. Int. Ed.* **2014**, *53*, 13093–13097.

73 Enders, D.; Niemeier, O.; Henseler, A.: Organocatalysis by N-heterocyclic carbenes. *Chem. Rev.* **2007**, *107*, 5606–5655.

74 Nair, V.; Menon, R. S.; Biju, A. T.; Sinu, C.; Paul, R. R.; Jose, A.; Sreekumar, V.: Employing homoenolates generated by NHC catalysis in carbon–carbon bond-forming reactions: state of the art. *Chem. Soc. Rev.* **2011**, *40*, 5336–5346.

75 Vora, H. U.; Wheeler, P.; Rovis, T.: Exploiting acyl and enol azolium intermediates via N-hetero cyclic carbene-catalyzed reactions of α-reducible aldehydes. *Adv. Synth. Catal.* **2012**, *354*, 1617–1639.

76 Gan, Z.; Reddy, P. T.; Quevillon, S.; Couve-Bonnaire, S.; Arya, P.: Stereocontrolled solid-phase synthesis of a 90-member library of indoline-alkaloid-like polycyclics from an enantioenriched aminoindoline scaffold. *Angew. Chem. Int. Ed.* **2005**, *44*, 1366–1368.

77 Terrett, N.: Making it big. *NewScientist* **2002**, 1–4.

78 Prakesch, M.; Sharma, U.; Sharma, M.; Khadem, S.; Leek, D. M.; Arya, P.: Part 1. Modular approach to obtaining diverse tetrahydroquinoline-derived polycyclic skeletons for use in high-throughput generation of natural-product-like chemical probes. *J. Comb. Chem.* **2006**, *8*, 715–734.

79 Nandy, J. P.; Rakic, B.; Sarma, B. V. N. B.; Babu, N.; Lefrance, M.; Enright, G. D.; Leek, D. M.; Daniel, K.; Sabourin, L. A.; Arya, P.: Benzofuran-derived cyclic β-amino acid scaffold for building a diverse set of flavonoid-like probes and the discovery of a cell motility inhibitor. *Org. Lett.* **2008**, *10*, 1143–1146.

80 Jimmidi, R.; Shroff, G. K.; Satyanarayana, M.; Reddy, B. R.; Reddy, J.; Sawant, M. A.; Sitaswad, S. L.; Arya, P.; Mitra, P.: The prevention of mitochondrial membrane permeabilization and pancreatic b-cell death by an enantioenriched, macrocyclic small molecule. *Eur. J. Org. Chem.* **2014**, *20*, 1151–1156.

81 Goldman, R. C.; Scaglione, F.: The macrolide-bacterium interaction and its biological basis. *Curr. Drug Targets Infect. Disord.* **2004**, *4*, 241–260.

82 Hu, T.; Takenaka, N.; Panek, J. S.: Total synthesis of oleandolide. *J. Am. Chem. Soc.* **1999**, *121*, 9229–9230.

83 Paterson, I.; Arya, P.: Degradation of oleandomycin: controlled removal of sugars to give oleandolide C3, C5-acetonide. *Tetrahedron* **1988**, *44*, 253–260.

84 Paterson, I.; Ward, R. A.; Romea, P.; Norcross, R. D.: Substrate-controlled aldol reactions of chiral ethyl ketones: application of the total synthesis of oleandomycin. *J. Am. Chem. Soc.* **1994**, *116*, 3623–3624.

85 Winssinger, N.; Barluenga, S.: Chemistry and biology of resorcylic acid lactones. *Chem. Commun. (Camb)* **2007**, 22–36.

86 Turbyville, T. J.; Wijeratne, E. M.; Liu, M. X.; Burns, A. M.; Seliga, C. J.; Luevano, L. A.; David, C. L.; Faeth, S. H.; Whitesell, L.; Gunatilaka, A. A.: Search for Hsp90 inhibitors with potential anticancer activity: isolation and SAR studies of radicicol and monocillin I from two plant-associated fungi of the Sonoran desert. *J. Nat. Prod.* **2006**, *69*, 178–184.

87 Barluenga, S.; Moulin, E.; Lopez, P.; Winssinger, N.: Solution-and solid-phase synthesis of radicicol (monorden) and pochonin C. *Chem. Eur. J.* **2005**, *11*, 4935–4952.

88 Dakas, P. Y.; Jogireddy, R.; Valot, G.; Barluenga, S.; Winssinger, N.: Divergent syntheses of resorcylic acid lactones: L-783277, LL-Z1640-2, and hypothemycin. *Chemistry* **2009**, *15*, 11490–11497.

89 Barluenga, S.; Wang, C.; Fontaine, J. G.; Aouadi, K.; Beebe, K.; Tsutsumi, S.; Neckers, L.; Winssinger, N.: Divergent synthesis of a pochonin library targeting HSP90 and in vivo efficacy of an identified inhibitor. *Angew. Chem. Int. Ed. Engl.* **2008**, *47*, 4432–4435.

90 Hellwig, V.; Mayer-Bartschmid, A.; Muller, H.; Greif, G.; Kleymann, G.; Zitzmann, W.; Tichy, H. V.; Stadler, M.: Pochonins A-F, new antiviral and antiparasitic resorcylic acid lactones from Pochonia chlamydosporia var. catenulata. *J. Nat. Prod.* **2003**, *66*, 829–837.

91 Zhou, H.; Gao, Z.; Qiao, K.; Wang, J.; Vederas, J. C.; Tang, Y.: A fungal ketoreductase domain that displays substrate-dependent stereospecificity. *Nat. Chem. Biol.* **2012**, *8*, 331–333.

92 Saruwatari, T.; Praseuth, A. P.; Sato, M.; Torikai, K.; Noguchi, H.; Watanabe, K.: A comprehensive overview on genomically directed assembly of aromatic polyketides and macrolide lactones using fungal megasynthases. *J. Antibiot. (Tokyo)* **2011**, *64*, 9–17.

93 Hearn, B. R.; Sundermann, K.; Cannoy, J.; Santi, D. V.: Semisynthesis and cytotoxicity of hypothemycin analogues. *ChemMedChem* **2007**, *2*, 1598–1600.

94 Aeluri, M.; Pramanik, C.; Chetia, L.; Mallurwar, N. K.; Balasubramanian, S.; Chandrasekar, G.; Kitambi, S. S.; Arya, P.: 14-Membered macrocyclic ring-derived toolbox: the identification of small molecule inhibitors of angiogenesis and early embryo development in zebrafish assay. *Org. Lett.* **2013**, *15*, 436–439.

95 Dasari, B.; Jogula, S.; Borhade, R.; Balasubramanian, S.; Chandrasekar, G.; Kitambi, S. S.; Arya, P.: Macrocyclic glycohybrid toolbox identifies novel antiangiogenesis agents from zebrafish assay. *Org. Lett.* **2013**, *15*, 432–435.

96 Palomo, C.; Oiarbide, M.; Landa, A.; Gonzalez-Rego, M. C.; Garcia, J. M.; Gonzalez, A.; Odriozola, J. M.; Martin-Pastor, M.; Linden, A.: Design and synthesis of a novel class of sugar-peptide hybrids: C-linked glyco β-amino acids through a stereoselective "acetate" Mannich reaction as the key strategic element. *J. Am. Chem. Soc.* **2002**, *124*, 8637–8643.

97 Griffin, F. K.; Paterson, D. E.; Taylor, R. J. K.: Ramberg-Backlund approaches to the synthesis of C-linked disaccharides. *Angew. Chem. Int. Ed. Engl.* **1999**, *38*, 2939–2942.

98 Arya, P.; Ben, R. N.; Qin, H.: Remote asymmetric induction: synthesis of C-linked α-galactoserine and homoserine derivatives by electrophilic amination. *Tetrahedron Lett.* **1998**, *39*, 6131–6134.

99 Lowary, T.; Meldal, M.; Helmboldt, A.; Vasella, A.; Bock, K.: Novel type of rigid C-linked glycosylacetylene-phenylalanine building blocks for combinatorial synthesis of C-linked glycopeptides. *J. Org. Chem.* **1998**, *63*, 9657–9668.

100 Jogula, S.; Bhanudas Dasari, B.; Khatravath, M.; Chandrasekar, G.; Kitambi, S. S.; Arya, P.: Building a macrocyclic toolbox from C-linked carbohydrates identifies novel anti angiogenesis agents from zebrafish assay. *Eur. J. Org. Chem.* **2013**, *19*, 5036–5040.

101 Kaufman, C. K.; White, R. M.; Zon, L.: Chemical genetic screening in the zebrafish embryo. *Nat. Protoc.* **2009**, *4*, 1422–1432.

102 Stoletov, K.; Klemke, R.: Catch of the day: zebrafish as a human cancer model. *Oncogene* **2008**, *27*, 4509–4520.

103 Canaple, L.; Beuf, O.; Armenean, M.; Hasserodt, J.; Samarut, J.; Janier, M.: Fast screening of paramagnetic molecules in zebrafish embryos by MRI. *NMR Biomed.* **2008**, *21*, 129–137.

104 Murphey, R. D.; Zon, L. I.: Small molecule screening in the zebrafish. *Methods* **2006**, *39*, 255–261.

105 Peterson, R. T.; Shaw, S. Y.; Peterson, T. A.; Milan, D. J.; Zhong, T. P.; Schreiber, S. L.; MacRae, C. A.; Fishman, M. C.: Chemical suppression of a genetic mutation in a zebrafish model of aortic coarctation. *Nat. Biotechnol.* **2004**, *22*, 595–599.

106 Peterson, R. T.; Fishman, M. C.: Discovery and use of small molecules for probing biological processes in zebrafish. *Methods Cell Biol.* **2004**, *76*, 569–591.

107 Pichler, F. B.; Laurenson, S.; Williams, L. C.; Dodd, A.; Copp, B. R.; Love, D. R.: Chemical discovery and global gene expression analysis in zebrafish. *Nat. Biotechnol.* **2003**, *21*, 879–883.

108 Serbedzija, G. N.; Flynn, E.; Willett, C. E.: Zebrafish angiogenesis: a new model for drug screening. *Angiogenesis* **1999**, *3*, 353–359.

109 Kimmel, C. B.; Ballard, W. W.; Kimmel, S. R.; Ullmann, B.; Schilling, T. F.: Stages of embryonic development of the zebrafish. *Dev. Dyn.* **1995**, *203*, 253–310.

110 Guduru, S. K. R.; Chamakuri, S.; Chandrasekar, G.; Kitambi, S. S.; Arya, P.: Tetrahydroquinoline-derived macrocyclic toolbox identifies novel anti-angiogenesis agents and inhibitors of an early embryo development in zebrafish assays. *ACS Med. Chem. Lett.* **2013**, *4*, 666–670.

111 Chamakuri, S.; Guduru, S. K. R.; Pamu, S.; Chandrasekar, G.; Kitambi, S. S.; Arya, P.: A modular approach to build the macrocyclic diversity on aminoindoline scaffold identifies novel anti-angiogenesis agents from zebrafish assay. *Eur. J. Org. Chem.* **2013**, *19*, 3959–3964.

112 Aeluri, M.; Gaddam, J.; Davarakonda, V. K. S. T.; Chandrasekar, G.; Kitambi, S. S.; Arya, P.: An intramolecular heck approach to obtain 17-membered macrocyclic diversity and the identification of anti-angiogenesis agent from zebrafish study. *Eur. J. Org. Chem.* **2013**, *19*, 3955–3958.

11

The Synthesis of Peptide-Based Macrocycles by Huisgen Cycloaddition

Ashok D. Pehere[1] and Andrew D. Abell[2]

[1] *University of Texas M.D. Anderson Cancer Center, Houston, TX, USA*
[2] *Department of Chemistry and ARC Centre of Excellence for Nanoscale BioPhotonics, The University of Adelaide, Adelaide, South Australia, Australia*

11.1   Introduction

Synthetic macrocycles are receiving ever-increasing attention as important and versatile scaffolds for the development of small-molecule therapeutics to target a range of diseases [1–9]. These structures provide a number of tangible benefits as templates for drug discovery. Specifically, they provide access to a novel and varied chemical space to give compounds with enhanced bio-stability, bioavailability, potency, and receptor selectivity [1, 3, 5, 10, 11]. Macrocycles are also widespread in nature, with approximately 3% of natural products belonging to this class [3, 5, 6]. Natural macrocycles are often involved in key biological functions, such as the stimulation of growth, formation of mycelia and spores, and cell–cell communication via autocrine hormones and mediators [3]. Small-molecule therapeutics based on such macrocycles have been well known for more than 60 years, for example, the macrolide antibiotic erythromycin (**1**, Figure 11.1) was launched commercially in 1952 [11], with many other macrocyclic drugs (e.g., vancomycin (**2**) [3, 5, 12], simeprevir (Olysio®) (**3**) [13]) discovered thereafter (Figure 11.1). The biological targets for macrocycles have expanded significantly in recent times to include a range of proteins, such as kinases, ATPases, proteases, GPCRs, and many other key enzymes [1, 3, 5, 12, 14–17].

This expansion of activity has been somewhat driven by advances in methods for the synthesis of larger rings, with an improved ability to produce libraries of such molecules in a parallel or combinatorial fashion. A number of general approaches are now available for their construction based on ring-closing metathesis (RCM) [18–24], alkylation [25, 26], macrolactonization [27] and macrolactamization [28, 29], Suzuki reaction [30], Heck reaction [31, 32], Sonogashira [33, 34] reaction, and,

recently, Huisgen cycloaddition [35, 36]. Some of these approaches have even been successfully applied to the construction of libraries of macrocyclic molecules suitable for use in high-throughput screening (HTS) programs. This versatility of synthesis is particularly apparent with peptidomimetic macrocycles used to constrain a peptide backbone into a specific geometry, for example, by side chain-to-side chain cyclization (principally P_1 to P_3, Figure 11.2a) [21, 25, 36], N-terminus to C-terminus cyclization (Figure 11.2b) [37, 38], and, less commonly, side chain-to-N-terminus cyclization (Figure 11.2c) [39, 40].

The choice of ring size in these structures is particularly important for biological activity, and while small rings significantly reduce conformational flexibility, they do not generally define a biologically significant geometry, such as a β-strand or α-helix [41, 42]. In comparison, larger rings are generally too conformationally mobile to be of general use. The chemical makeup of the macrocycle is also critical to define its conformation and, hence, potential biological target. This is particularly apparent in peptidomimetic macrocycles that inhibit proteases where the known recognition sequences of natural substrates must be incorporated into the design. Some of this functionality, such as an aryl group, has the added advantage of further reducing conformational mobility and thereby helping to define overall geometry.

This chapter discusses one relatively new approach to the preparation of biologically active macrocycles based on azide–alkyne cycloaddition, a reaction known as the Huisgen cycloaddition [43, 44]. This methodology is gaining increasing importance in the macrocycle field, and the time is right for a review in the area [45, 46]. Other cycloaddition reactions have been employed for macrocyclization, and these include thiol-ene cycloaddition [47], Pd-catalyzed [3 + 2] cycloaddition [48], and

(a) (b) (c)
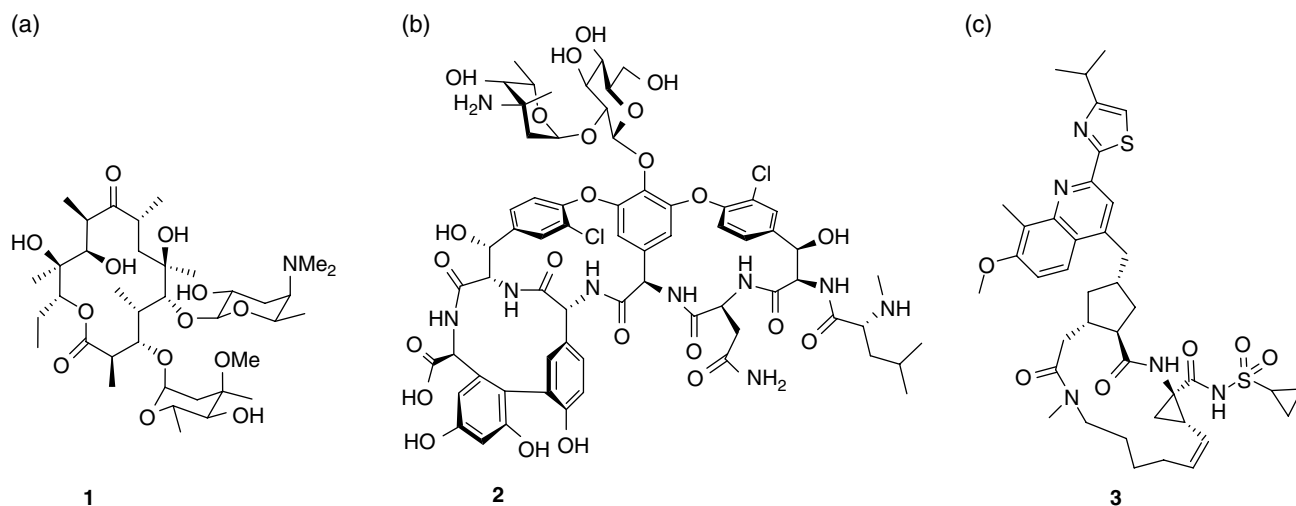
Figure 11.1 Representative macrocycles: (a) erythromycin, (b) vancomycin, and (c) simeprevir.

(a) (b) (c)
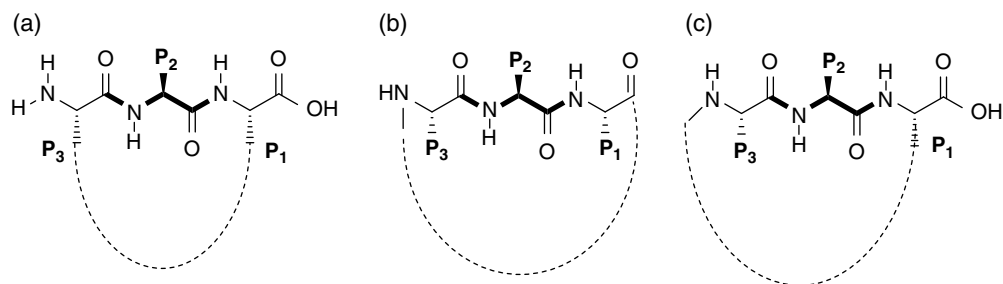
Figure 11.2 Different examples of peptide cyclization. (a) Side chain-to-side chain cyclization, (b) "head-to-tail" cyclization, and (c) side chain-to-N-terminus cyclization.

gold-catalyzed [2 + 2] cycloaddition [5]. Other synthetic methods to build macrocycles are reviewed in Part III of this book.

11.2 Dipolar Cycloaddition Reactions

The [3 + 2] azide–alkyne cycloaddition (Huisgen cycloaddition, an example of "click" chemistry) [49] is now an established tool in modern medicinal chemistry [26]. The broad chemical orthogonality and versatility of this chemistry presents a range of opportunities in drug discovery, pharmacology, materials science, and nanotechnology. The first reports on this cycloaddition involved reaction of an azide with an alkyne at elevated temperatures to give a mixture of both the 1,4- and 1,5-triazole regioisomers as shown in Scheme 11.1 [3, 4, 50, 51].

A real advance to this methodology came through the independent work of Meldal [52] and Sharpless [53], who found that copper (I) catalysis of this reaction results in high regioselectivity for the 1,4-isomer (reaction 2 in Scheme 11.1). This transformation has the added advantage of high chemoselectivity, since few other functional groups react with azides or alkynes in the absence of other reagents. It is also important to note that the triazole functionality is a useful isostere of the peptide bond, making this approach particularly suited for the synthesis of macrocyclic peptidomimetics [54–56]. The reaction also has high atom economy and biocompatibility.

The mechanism of the copper-catalyzed azide–alkyne Huisgen cycloaddition reaction, although not fully elucidated, is as proposed in Figure 11.3 [57–59]. Step one involves coordination of the alkyne **a** to the Cu(I) species, resulting in the displacement of a ligand (L_n). The azide replaces another ligand as it binds to copper on intermediate **b**, forming intermediate **c**. The terminal nitrogen then interacts with the C-2 carbon of the acetylide, forming a six-membered copper (III) metallocycle **d**. This structure has a low energy barrier for ring contraction; hence, the triazolyl-copper derivative readily forms **e**. In the final step, protolysis releases the free 1,4-disubstituted triazole **f** and the copper catalyst $[L_nCu]^+$. Ascorbate has been used as a mild reductant to keep the metal in +1 oxidation state. In addition, Bertozzi *et al.* have

(Reaction 1)

(Reaction 2)
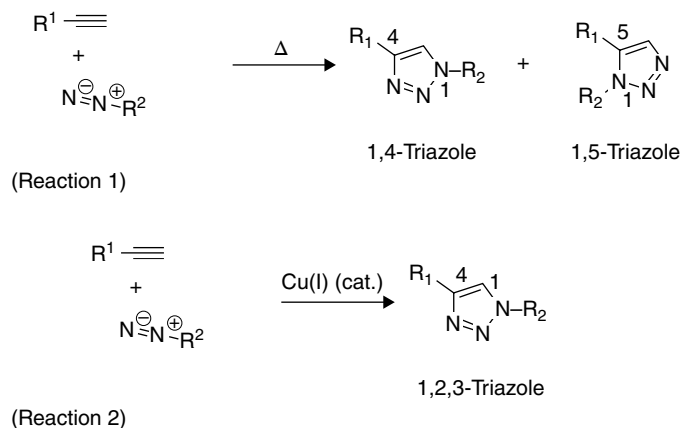
Scheme 11.1 [3+2] Azide–alkyne cycloaddition [50].
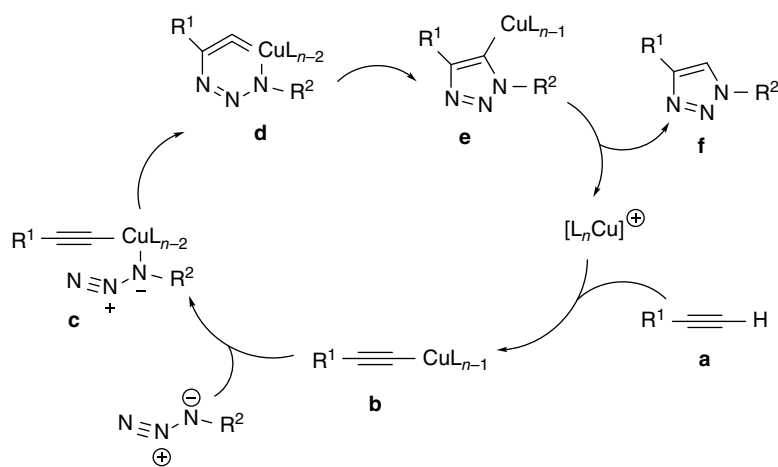
Figure 11.3 Putative mechanism of the Cu-mediated azide–alkyne Huisgen cycloaddition.

developed Cu-free click chemistry taking advantage of strained alkynes; however to date this methodology has not been used in the synthesis of macrocycles. This methodology offers advantages of bioorthogonality compatible with cultured cells [60–63]. The outcome of CuAAC-mediated macrocyclization reactions is known to be dependent on the ring size formed and other factors such as conformation and ring constraints [64, 65].

11.3 Macrocyclic Peptidomimetics

Click chemistry has been used in the synthesis of macrocycles of varying sizes for a broad range of target classes and therapeutic indications. In the following text are some representative examples.

11.3.1 Macrocyclic Antagonists for the Treatment of Cancer

Terrett and coworkers recently reported the synthesis and biological evaluation of macrocyclic XIAP BIR2 and BIR3 domain inhibitors [66]. X chromosome-linked inhibitor of apoptosis protein (XIAP) is an endogenous protein that binds and inhibits the activation of caspases responsible for programmed cell death or apoptosis. It is thus an important medicinal target for cancer, neurodegenerative disorders, and autoimmunity [16].

A DNA-programmed library [67] of 160 000 cyclic peptidomimetics was produced, leading to the general structure shown in Figure 11.4. This library was constructed using 20 different amino acid building blocks for incorporation at each of the P_1, P_3, and P_4 positions and five azido-substituted amino acids at position P_5, to allow covalent attachment to the DNA-encoding template. The macrocycle ring was then formed using azide–alkyne cycloaddition of a P_5 azide onto the alkyne side chain of the P_2 amino acid to give macrocycles containing a 1,4 disubstituted triazole. This library was used to identify a potent antagonist (**4**) (BIR2 $IC_{50} = 4.9\,\mu M$, BIR3 $IC_{50} = 0.39\,\mu M$) [66]. Co-crystal structures of compound **4** bound to the isolated XIAP-BIR2 domain revealed the conformation of the bound macrocycle to be as shown in Figure 11.5. This structure reveals that the peptide backbone of **4** makes a series of hydrogen-bonding interactions with the BIR2 protein, most importantly from the P_1, P_3, and P_4 side chains.
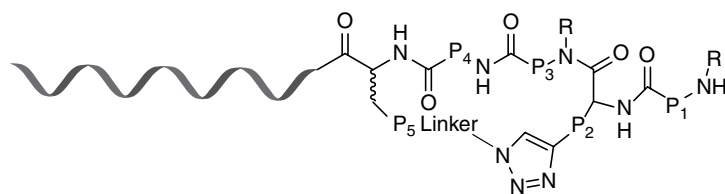
Figure 11.4 Generic structure of macrocycles used in the DPC-generated ELC library.
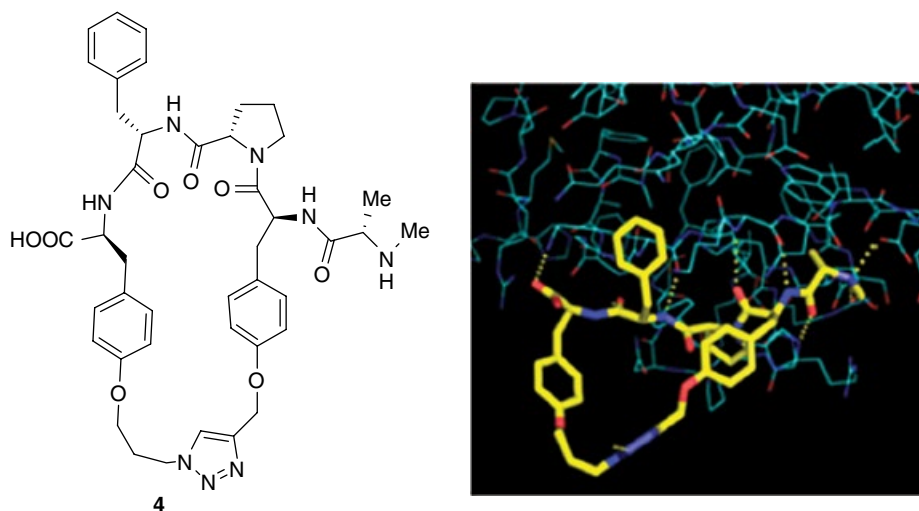
Figure 11.5 Macrocyclic XIAP antagonists with X-ray structure bound to the isolated XIAP-BIR2 domain depicted right. (*See insert for color representation of the figure.*)

Furthermore, optimization of compounds through medicinal chemistry identified XIAP antagonists in which the peptide sequence was cyclized from the P_3 proline group to the P_5 position (see macrocycle **6** in Scheme 11.2). All these macrocycles were synthesized from a linear precursor, where the component P_3–P_5 azido alkyne was cyclized on treatment with Cu(II) in the presence of ascorbic acid and DIPEA. For example, the linear peptidomimetic **5** gave a mixture of macrocycle **6** and dimeric macrocycle **7**, which were separated by HPLC [66]. Screening of a range of such dimeric macrocycles against XIAP BIR2 and BIR3 domains identified **7** as an active with IC_{50} values of 0.097 and 0.036 μM against BIR2 and BIR3, respectively. The monomeric macrocycle **6** was less active, with corresponding IC_{50} values of 0.827 and 0.214 μM. Compound **7**, therefore, represents a novel macrocyclic ligand with unprecedented affinity for each of these domains [66]. A detailed case study of this work is presented in Chapter 17.

11.3.2 Dimeric Macrocyclic Antagonists of Apoptosis Proteins

The same team reported another series of dimeric macrocycles as inhibitors of apoptosis proteins (IAPs) that displayed superior potency and pharmacokinetic properties compared with dimeric macrocycle **7** [68]. The most potent compound (**10**) was synthesized by an azide–alkyne cycloaddition reaction in tandem with RCM of the resulting diene, as exemplified in Scheme 11.3. Dimer **10** was shown to bind both XIAP and cIAP with high affinity. Analysis of binding data showed that compound **10** binds to XIAP BIR3 proteins with an IC_{50} value of 0.8 nM. It also has highly potent antitumor activity (IC_{50} 19 nM) in the A875 human melanoma xenograft model.

11.3.3 Macrocyclic Grb2 SH2 Domain Inhibitor

The growth factor receptor-bound protein 2 (Grb2) is a ubiquitous adapter module comprising one SH2 domain and two SH3 domains that provide a critical link between cell surface growth factor receptors and the Ras signaling pathway [69]. Works with kinase inhibitors [70] highlight the potential therapeutic utility of downregulating signaling pathways that include Grb2-dependent processes involved with diseases such as breast and kidney cancers [71]. This functional profile makes Grb2 a high priority target for anticancer drug development. Burke and coworkers [72] employed click chemistry for the synthesis of triazole-containing macrocycles based on the Grb2 SH2 domain-binding motif, "Pmp-Ac6c-Asn," where Pmp
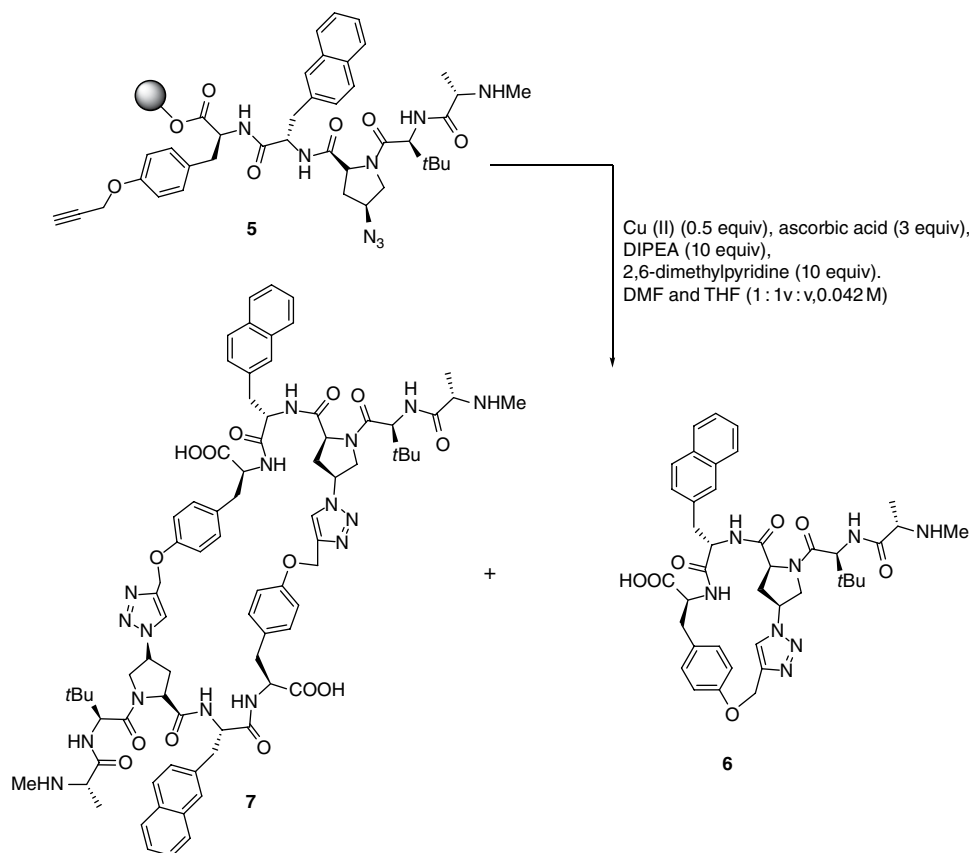
Scheme 11.2 Macrocycle antagonists of XIAP BIR2 and BIR3 domains.

and Ac6c refer to 4-phosphonomethyl-phenylalanine and α-aminocyclohexane carboxylic acid, respectively. Reaction of key intermediate azido alkyne **11** with CuI, L-ascorbate, DIPEA, and CH_3CN/tBuOH/H_2O gave the 14-membered constrained macrocycle **12** in mixture with the dimeric macrocycles **13** (Scheme 11.4). The monomeric (S)-Pmp-containing macrocycle exhibited a K_d value of 0.23 μM against Grb2 SH2 domain in binding assays, while the corresponding dimeric macrocycle was even more potent (50-fold) with $K_{d1} = 1.8$ nM and $K_{d2} = 4.0$ nM.

11.3.4 STAT3 Inhibitors

Signal transducer and activator of transcription (STAT) proteins are a family of cytoplasmic transcription factors. STAT proteins are thought to be ideal targets for anticancer therapy since cancer cells are more dependent on STAT activity than their normal counterparts. Wang and colleagues reported macrocyclic peptidomimetics that directly target STAT signaling [73]. The macrocycle **15** was prepared by azide–alkyne cycloaddition of **14** on treatment with $CuSO_4 \cdot 5H_2O$/sodium ascorbate in H_2O/tBuOH as shown in Scheme 11.5. Further elaboration at the N-terminus gave STAT3 inhibitor **16** [71].

This conformationally constrained peptidomimetic displayed a K_i of 7.3 μM, which is threefold more potent than the linear peptide **17** in blocking STAT3 dimerization [73].

11.3.5 Histone Deacetylase Inhibitors

Histone deacetylase (HDAC) inhibitors are an emerging class of anticancer drugs [74]. This large family of inhibitors includes a range of naturally occurring and synthetic compounds. Two HDAC inhibitors have received approval from the US FDA for the treatment of cutaneous T-cell lymphoma: romidepsin (Istodax®, a depsipeptide) and vorinostat (Zolinza®, suberoylanilide hydroxamic acid) [74]. Ghadiri and coworkers [75] reported an azide–alkyne cycloaddition synthesis of cyclic pseudotetrapeptide **19** as an analogue of apicidin, a naturally occurring cyclic tetrapeptide inhibitor of HDACs (Scheme 11.6). This study demonstrated the utility of the triazole unit as both a pharmacophore and a "locked" amide surrogate. Macrocycle **19** proved useful for identifying the most bioactive conformation (*trans–trans–trans–trans*) of the original cyclic tetrapeptide HDAC inhibitor (apicidin, shown in Scheme 11.6), with IC_{50} values of 25 nM.
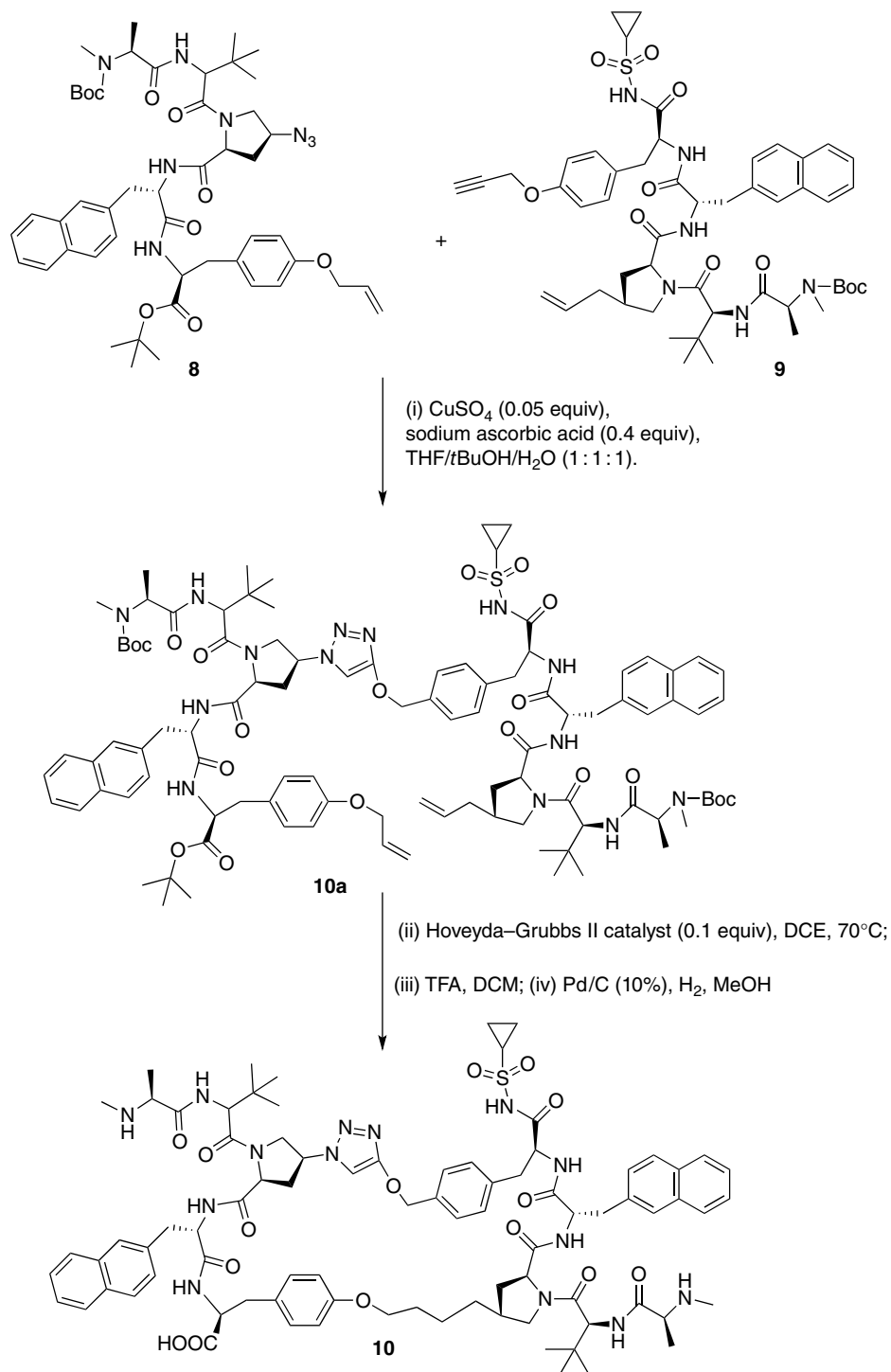
Scheme 11.3 Macrocyclic IAP antagonists.
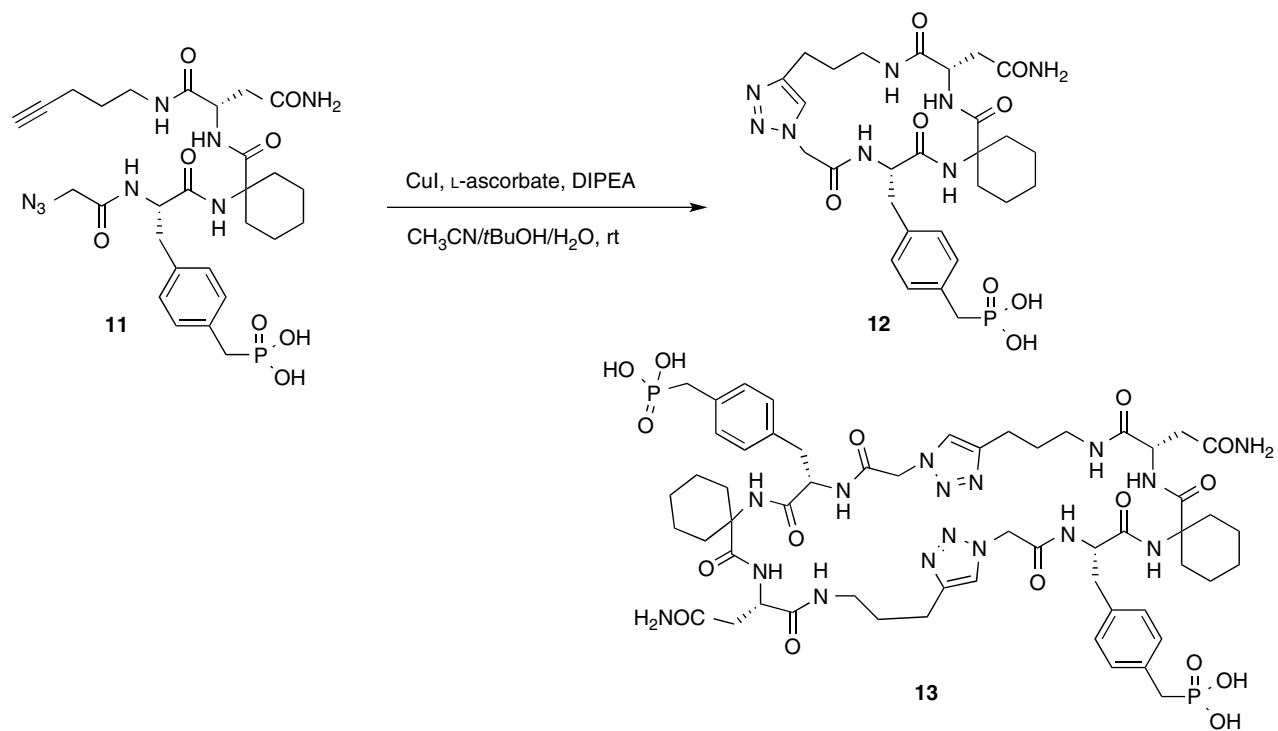
Scheme 11.4 Macrocyclic Grb2 SH2 domain inhibitors.
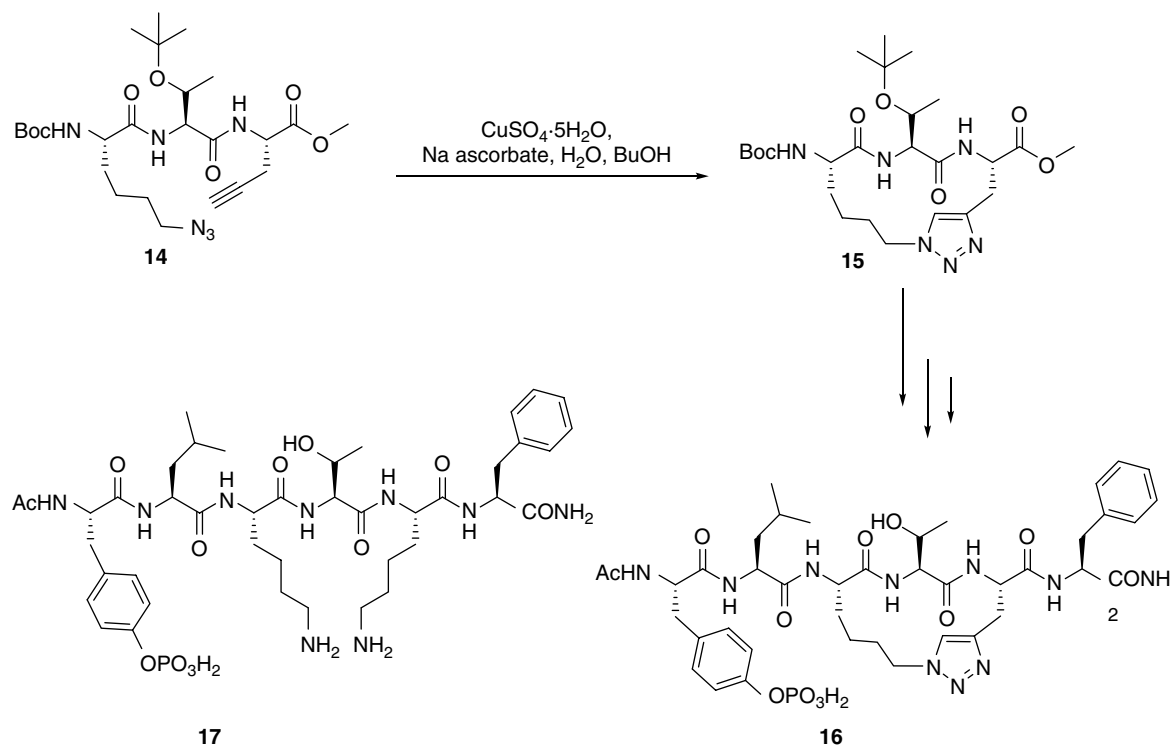
Scheme 11.5 Macrocyclic STAT3 inhibitors.
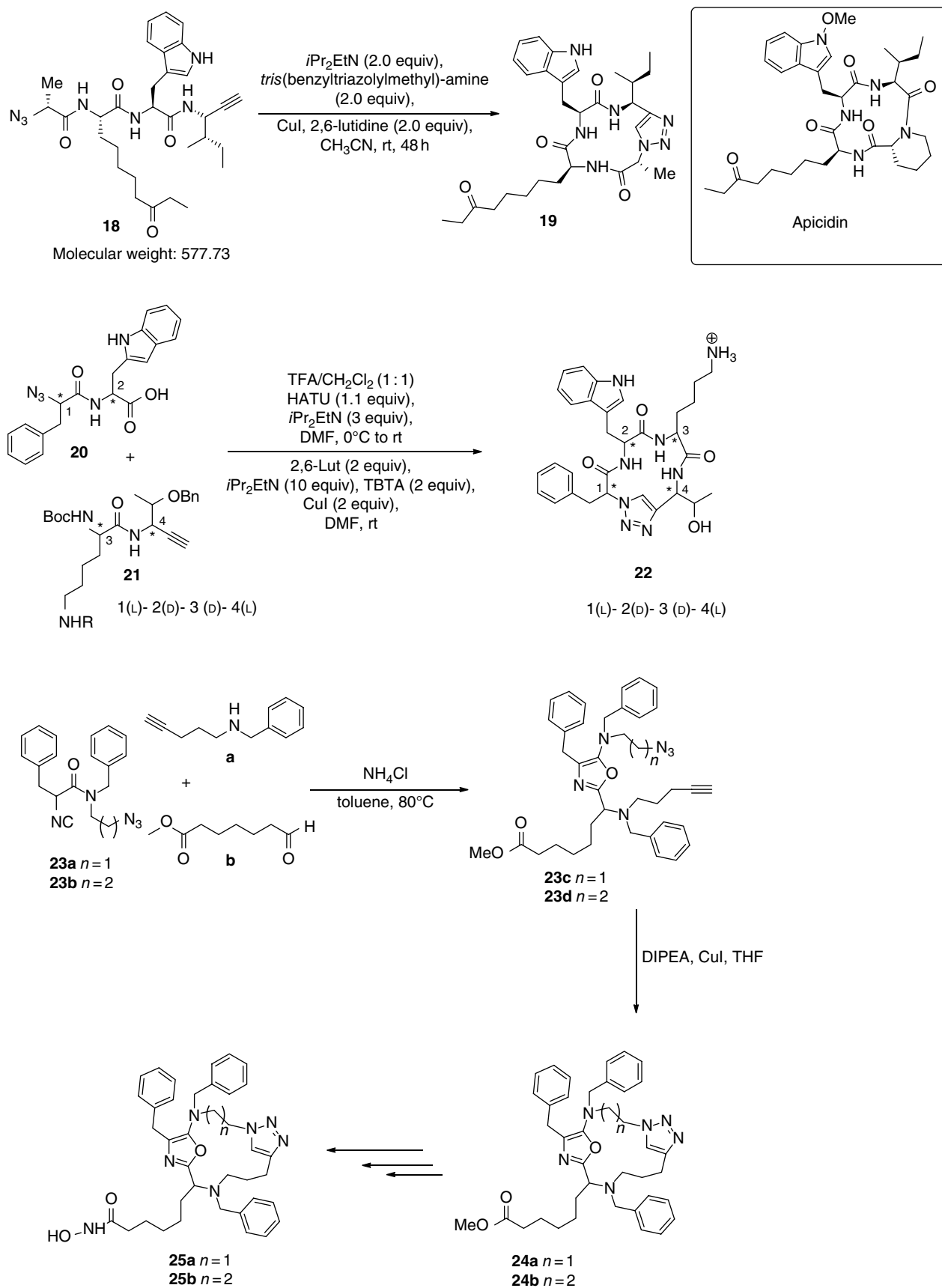
Scheme 11.6 Macrocyclic HDAC inhibitors and somatostatin modulators.

Tron and coworkers reported a multicomponent azide–alkyne cycloaddition [76] synthesis of macrocycle peptide mimetics that display inhibitory potential against HDACs, enzymes involved in transcription of genes associated with cell cycle progression and carcinogenesis. A three-component reaction gave substituted oxazoles **23c** and **23d**, the azide, and terminal alkyne of which were cyclized with CuI to give macrocycles **24a** and **24b** (Scheme 11.6). Saponification of the methyl esters and subsequent conversion to hydroxamic acids afforded the desired compounds **25a** and **25b**. These macrocycles showed IC_{50} values of 6.2 and 6.6 μM in a cytotoxicity assay, respectively. The mechanism of action was confirmed by a cellular fluorometric HDAC activity assay and HDAC inhibition assay, which showed IC_{50} values of 4.3 and 6.1 μM, respectively [76].

11.3.6 Somatostatin Modulators

Somatostatins are peptide hormones that regulate diverse cellular functions, such as neurotransmission, cell proliferation, and endocrine signaling, as well as inhibiting the release of many hormones and other secretory proteins. Ghadiri and coworkers [77] reported 1,4-substituted triazole-based peptidomimetics, such as **22** (Scheme 11.6), as ligands for the somatostatin receptor (SSTR). Here, the triazole was used to mimic a *trans*-peptide bond within a tetrapeptide. These macrocycles were similarly synthesized by azide–alkyne cycloaddition, using the ligand TBTA and CuI catalyst to catalyze formation of the triazole. NMR analysis revealed that **22** exists in a single preferred conformation. Macrocycle **22** showed an IC_{50} value of 67 nM toward *h*SSTR3 (human SSTR subtype 3) twofold selective compared to *h*SSTRS1, *h*SSTRS2, *h*SSTRS4, and *h*SSTRS5.

11.4 Macrocyclic β-Strand Mimetics as Cysteine Protease Inhibitors

An analysis of more than 1500 three-dimensional X-ray structures of proteases in the Protein Data Bank concluded that proteases almost universally bind their ligands in a β-strand conformation [17], a motif defined by optimum ϕ, Ψ, and τ angles of –139°, 135°, and –177.2°, respectively, and $d = 8.0$ Å (Figure 11.6a) [78]. A β-strand conformation allows the side chain residues of protease substrates and peptide-based inhibitors to adopt optimal interactions with respective subsites in protease active site as depicted in Figure 11.6b [79]. This mode of binding is effectively defined by the relative chemical makeup and location of the complementary S and S′ sites in the protease active site that accommodate the respective amino acid side chain group (designated P) within a substrate or inhibitor (Figure 11.6b). Subsites are numbered depending on their position relative to the scissile bond as shown in Figure 11.6b [79].

The introduction of an appropriate macrocycle into the backbone of an inhibitor can effectively pre-organize the molecule into a β-strand geometry to reduce the entropy of binding to the target protease. A macrocycle can also lead to enhanced stability toward proteolytic cleavage and an opportunity for the rational design of inhibitors with improved potency, selectivity, and, hence, therapeutic potential. Peptide-based macrocycles **32–36** were prepared with this in mind [35, 36]. The synthesis of **32** involves treatment of the key intermediate azido alkyne **30** with CuBr in CH_2Cl_2 to give triazole-containing macrocycle **31**, the primary alcohol of which was then oxidized to give the active inhibitor (Scheme 11.7)
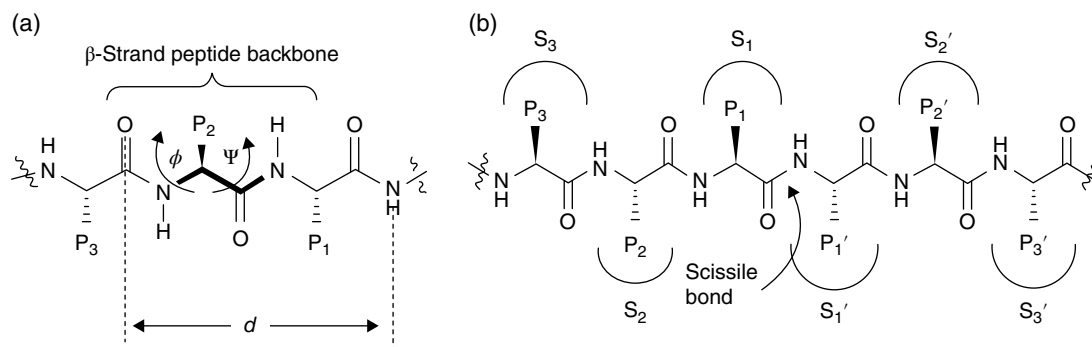
Figure 11.6 (a) Peptide β-strand backbone with torsional angles ϕ, Ψ, and ω; (b) Interactions between a peptide substrate (with residues Px) and a protease (binding subsites Sx) using the nomenclature of Schechter and Berger.
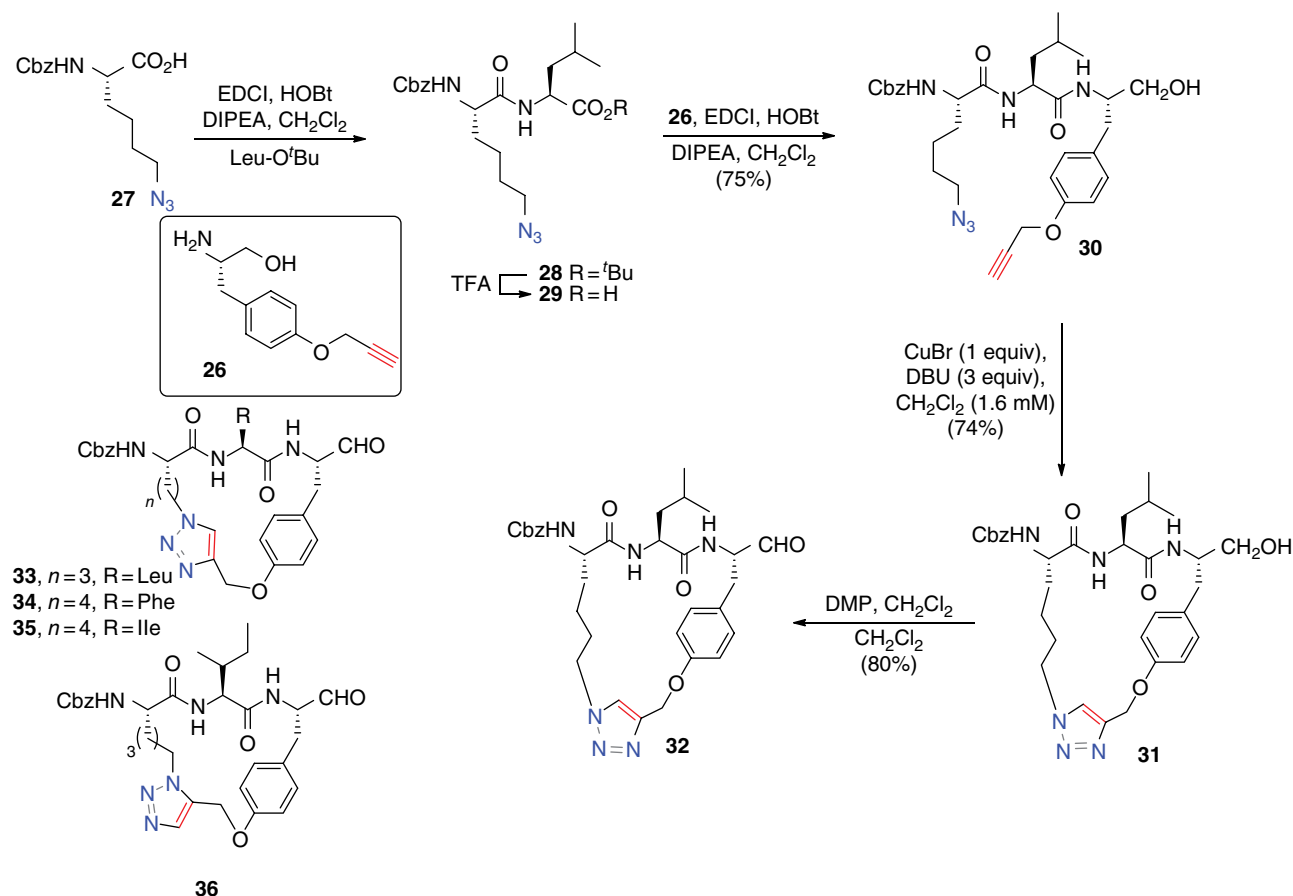
Scheme 11.7 Macrocyclic protease inhibitors.

[35, 36, 80, 81]. Here again, the macrocyclic precursor (**30**) was readily prepared by standard peptide synthesis. A range of macrocyclic protease inhibitors (e.g., **32–36**, Scheme 11.7) [35, 36, 82] were prepared using this approach, where backbone geometries were determined and defined by detailed NMR analysis. Macrocycles **32–36** all displayed $^3J_{\text{NHC}}\alpha_{\text{H}}$ coupling constants >8 Hz, which suggests a ϕ torsion angle of $\approx -120°$ and hence a β-strand geometry for the associated backbone [35, 36].

The macrocyclic aldehydes **32–36** proved to be particularly potent against cathepsin S (IC$_{50}$ < 5 nM), while **32**, **33**, and **34** were also highly active against calpain II (IC$_{50}$ values of 137, 97, and 89 nM, respectively) [35, 36, 82]. In addition, **32–35** were weakly potent against the chymotrypsin-like activity of the proteasome (IC$_{50}$ < 1 μM), while being essentially inactive against trypsin-like and caspase-like proteasome activities. Cathepsin S and related cysteine proteases are known to be important therapeutic targets for arthritis, cancer, and cardiovascular diseases while the inhibition of the proteasome has attracted considerable interest for the treatment of cancer [83].

Macrocycles **32–34** with IC$_{50}$ value 137, 97, and 89 nM were significantly more active (6–11-fold) than their

acyclic analogues against calpain II [36], a cysteine protease known to play a key role in several medical conditions associated with cellular damage, including traumatic brain injury, stroke, and cataract [84]. This difference in potency presumably reflects the fact that the constraint effectively defines the β-strand geometry required for active site binding. The acyclic analogues proved to be more active against the chymotrypsin-like activity of the proteasome [82, 85]. This is consistent with reports [86, 87] that the proteasome does not favor binding of inhibitors in a classic β-strand geometry: unlike other proteases, the P2 group does not seem to form important contacts with the active site. Interestingly, 1,5-disubstituted triazole **36** retains potency against calpain II IC$_{50}$ value 390 nM, cathepsin S IC$_{50}$ value 3.9 nM, and the 26S proteasome IC$_{50}$ value 250 nM but has reduced activity against cathepsin L (fourfold) compared to cathepsin S[36]. This suggests a possible way forward for fine-tuning selectivity for one protease over another.

A related set of triazole-tethered macrocycles, lacking a phenyl ether bridge, were also shown to template the formation of extended parallel β-sheet rod-like structures. The synthesis here involved a series of peptide
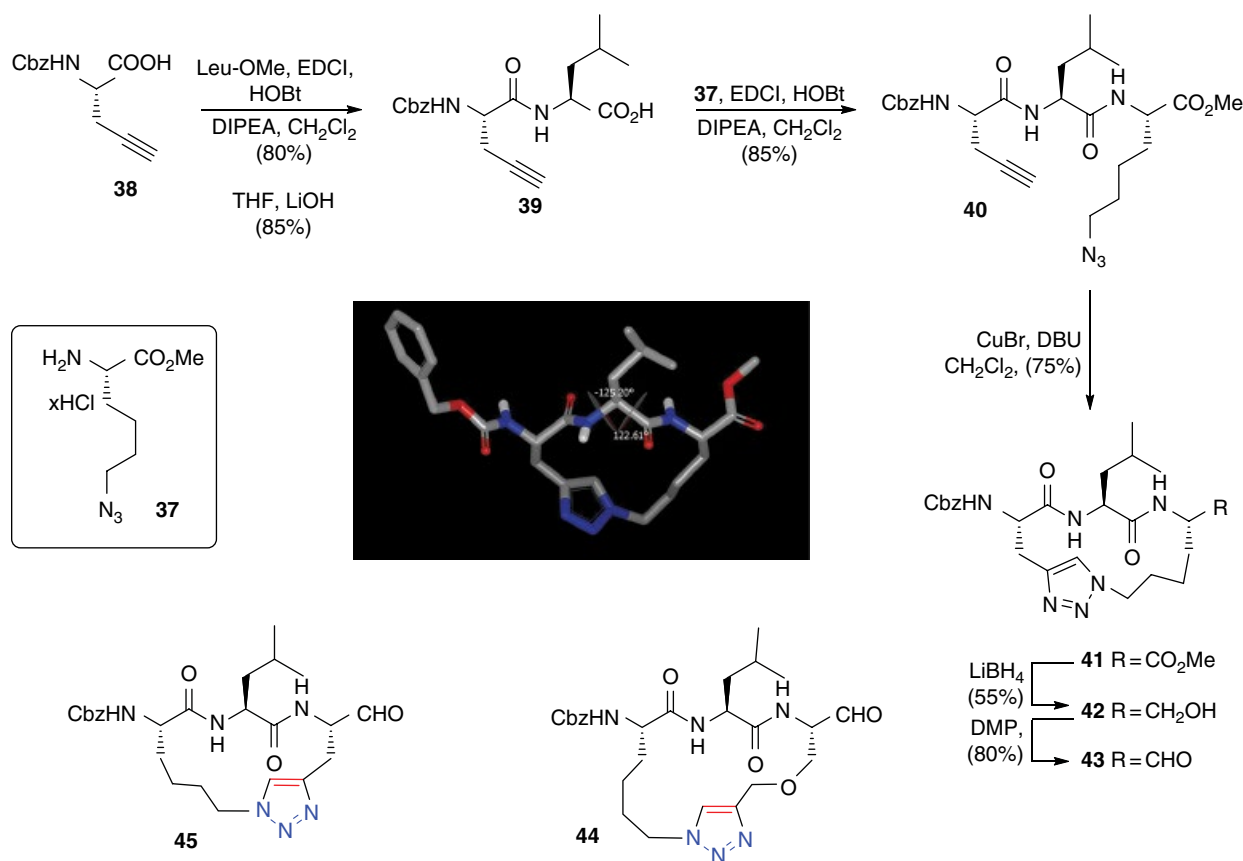
Scheme 11.8 Additional macrocyclic protease inhibitors. (*See insert for color representation of the figure.*)

coupling steps with a final copper-catalyzed azide–alkyne cycloaddition to give the desired triazole **41** (Scheme 11.8). The methyl ester was reduced with lithium borohydride to give the macrocyclic alcohol **42**, which was oxidized with Dess–Martin periodinane (DMP) to give the macrocyclic aldehyde **43**. Macrocycles **44** and **45** were similarly prepared [88].

The triazole macrocycles **41–45** displayed large $^3J_{\text{NHC}\alpha\text{H}}$ coupling constants >8 Hz and strong $\text{CH}_{\alpha i}$–NH_{i+1} ROESY correlations, indicative of a β-strand conformation similar to macrocycles **32–36**. This suggests a Φ torsion angle of ≈−120° and, hence, a β-strand geometry [78]. Molecular docking and X-ray crystallographic studies were consistent with this geometry assignment. Crystallographic analysis of triazole **41** also revealed that it stacks to form an extended nanotubular parallel structure as shown in (Figure 11.7b) [88]. The tripeptide sequence in the macrocycle presents a planar β-strand backbone, with the carbonyl and NH groups alternating up and down to allow intermolecular hydrogen bonding (Figure 11.7a). The macrocyclic ϕ and ψ dihedral angles in the solid-state structure of triazole **41** were in excellent agreement with docked structures to calpain II and cathepsin S, as shown in Figure 11.7d. An ESI mass spectrum

and an SEM image of **41** also were consistent with these extended β-sheet-like nanotubular structures (Figure 11.7c) [88]. Macrocycles **43–45** proved to be moderate inhibitors of calpain II (IC$_{50}$ = 355, 582, and 697 nM, respectively) but highly potent inhibitors of cathepsin S (IC$_{50}$ = 10, 27, and 20 nM, respectively) [36, 88].

11.5 Conclusion

In this review, we present representative examples of macrocyclic inhibitors that target important therapeutic conditions such as cancer and cataract. The component macrocycles were introduced by azide–alkyne cycloaddition using a Cu(I) catalyst to give the triazole-containing macrocycle, which links either P$_1$ and P$_3$ amino acid R groups, or an amino acid R group to the N-terminus, or, less commonly, an amino acid R group to the C-terminus. Examples of monomeric and dimeric macrocyclic IAP and XIAP antagonists and macrocyclic Grb2 SH2, STAT3, and HDAC inhibitors are discussed as potential anticancer agents. The final part of the review discusses macrocyclic protease inhibitors that are constrained into a β-strand that is known to favor

Figure 11.7 (a) A view of the intermolecular hydrogen bonding observed between two macrocycles of **41** with the hydrogen atoms of the side chains omitted for clarity. Peptide backbone hydrogen bonds are shown as yellow dashed bonds and the triazole hydrogen bonds as dashed red lines. (b) A representation of the structure of **41** showing the nanotubular structure. The structure of **41** showing extended β-sheet conformation, with the triazole-containing macrocyclic linkage omitted for clarity. Side view of the dimerization of the nanotubular structures in the crystal. Top view of the dimerized nanotubes in a space-filling representation. (c) ESI spectrum of compound **41** showing the formation of oligomeric assemblies in the gas phase [M+Na] and an SEM image of the rod-like assemblies of **41**. (d) Superimposition of the crystallographic structure of **41** (green) with **43** (black) docked into cathepsin S. (*See insert for color representation of the figure.*)

active site binding. The azide–alkyne Huisgen cycloaddition reaction is particularly efficient for the synthesis of macrocyclic peptidomimetics, with an ability to produce libraries of macrocyclic molecules in a parallel or combinatorial fashion. This synthetic methodology is an example of a click reaction, with an ability to be conducted in an aqueous environment over a range of pH values. In addition, it is compatible with a range of functional groups commonly found in biomolecules such as peptides and proteins. However, its extended use has been somewhat limited by the need for copper catalysis. However, recent advances have delivered copper-free click chemistry circumvent this limitation [60–63]. This offers much promise for the further advancement of the use of this methodology within a biological setting.

References

1 Giordanetto, F.; Kihlberg, J. Macrocyclic Drugs and Clinical Candidates: What Can Medicinal Chemists Learn from Their Properties? *J. Med. Chem.* **2014**, *57*, 278–295.

2 Mallinson, J.; Collins, I. Macrocycles in New Drug Discovery. *Future Med. Chem.* **2012**, *4*, 1409–1438.

3 Driggers, E. M.; Hale, S. P.; Lee, J.; Terrett, N. K. The Exploration of Macrocycles for Drug Discovery: An Underexploited Structural Class. *Nat. Rev. Drug Discov.* **2008**, *7*, 608–624.

4 Yu, X. F.; Sun, D. Q. Macrocyclic Drugs and Synthetic Methodologies Toward Macrocycles. *Molecules* **2013**, *18*, 6230–6268.

5 Marsault, E.; Peterson, M. L. Macrocycles Are Great Cycles: Applications, Opportunities, and Challenges of Synthetic Macrocycles in Drug Discovery. *J. Med. Chem.* **2011**, *54*, 1961–2004.

6 Clardy, J.; Walsh, C. Lessons from Natural Molecules. *Nature* **2004**, *432*, 829–837.

7 Yudin, A. K. Macrocycles: Lessons from the Distant Past, Recent Developments, and Future Directions. *Chem. Sci.* **2015**, *6*, 30–49.

8 Marti-Centelles, V.; Pandey, M. D.; Burguete, M. I.; Luis, S. V. Macrocyclization Reactions: The Importance of Conformational, Configurational, and Template-Induced Preorganization. *Chem. Rev.* **2015**, *115*, 8736–8834.

9 White, C. J.; Yudin, A. K. Contemporary Strategies for Peptide Macrocyclization. *Nat. Chem.* **2011**, *3*, 509–524.

10 Villar, E. A.; Beglov, D.; Chennamadhavuni, S.; Porco, J. A.; Kozakov, D.; Vajda, S.; Whitty, A. How Proteins Bind Macrocycles. *Nat. Chem. Biol.* **2014**, *10*, 723–731.

11 Washington II, J. A., Wilson, W. R. Erythromycin: A Microbial and Clinical Perspective after 30 Years of Clinical Use. (Second of Two Parts). *Mayo Clin. Proc.* **1985**, *60*(4), 271–278.

12 Wessjohann, L.; Ruijter, E.; Garcia-Rivera, D.; Brandt, W. What Can a Chemist Learn from Nature's Macrocycles? A Brief, Conceptual View. *Mol. Divers.* **2005**, *9*, 171–186.

13 Lin, T. I.; Lenz, O.; Fanning, G.; Verbinnen, T.; Delouvroy, F.; Scholliers, A.; Vermeiren, K.; Rosenquist, A.; Edlund, M.; Samuelsson, B.; Vrang, L.; de Kock, H.; Wigerinck, P.; Raboisson, P.; Simmen, K. In Vitro Activity and Preclinical Profile of TMC435350, a Potent Hepatitis C Virus Protease Inhibitor. *Antimicrob. Agents Chemother.* **2009**, *53*, 1377–1385.

14 Hill, T. A.; Shepherd, N. E.; Diness, F.; Fairlie, D. P. Constraining Cyclic Peptides to Mimic Protein Structure Motifs. *Angew. Chem. Int. Ed. Engl.* **2014**, *53*, 13020–13041.

15 Jones, R. M.; Boatman, P. D.; Semple, G.; Shin, Y. J.; Tamura, S. Y. Clinically Validated Peptides as Templates for De Novo Peptidomimetic Drug Design at G-Protein-Coupled Receptors. *Curr. Opin. Pharmacol.* **2003**, *3*, 530–543.

16 Wilkinson, J. C.; Cepero, E.; Boise, L. H.; Duckett, C. S. Upstream Regulatory Role for XIAP in Receptor-Mediated Apoptosis. *Mol. Cell. Biol.* **2004**, *24*, 7003–7014.

17 Tyndall, J. D. A.; Nall, T.; Fairlie, D. P. Proteases Universally Recognize β Strands in Their Active Sites. *Chem. Rev.* **2005**, *105*, 973–1000.

18 Jones, M. A.; Coxon, J. M.; McNabb, S. B.; Mehrtens, J. M.; Alexander, N. A.; Jones, S.; Chen, H. Y.; Buisan, C.; Abell, A. D. Efficient Large-Scale Synthesis of CAT811, a Potent Calpain Inhibitor of Interest in the Treatment of Cataracts. *Aust. J. Chem.* **2009**, *62*, 671–675.

19 Hanessian, S.; Yang, G. Q.; Rondeau, J. M.; Neumann, U.; Betschart, C.; Tintelnot-Blomley, M. Structure-Based Design and Synthesis of Macroheterocyclic Peptidomimetic Inhibitors of the Aspartic Protease β-Site Amyloid Precursor Protein Cleaving Enzyme (BACE). *J. Med. Chem.* **2006**, *49*, 4544–4567.

20 Tsantrizos, Y. S.; Bolger, G.; Bonneau, P.; Cameron, D. R.; Goudreau, N.; Kukolj, G.; LaPlante, S. R.; Llinas-Brunet, M.; Nar, H.; Lamarre, D. Macrocyclic Inhibitors of the NS3 Protease as Potential Therapeutic Agents of Hepatitis C Virus Infection. *Angew. Chem. Int. Ed.* **2003**, *42*, 1355–1360.

21 Abell, A. D.; Jones, M. A.; Coxon, J. M.; Morton, J. D.; Aitken, S. G.; McNabb, S. B.; Lee, H. Y. Y.; Mehrtens, J. M.; Alexander, N. A.; Stuart, B. G.; Neffe, A. T.; Bickerstaff, R. Molecular Modeling, Synthesis, and Biological Evaluation of Macrocyclic Calpain Inhibitors. *Angew. Chem. Int. Ed.* **2009**, *48*, 1455–1458.

22 Miller, S. J.; Blackwell, H. E.; Grubbs, R. H. Application of Ring-Closing Metathesis to the Synthesis of Rigidified Amino Acids and Peptides. *J. Am. Chem. Soc.* **1996**, *118*, 9606–9614.

23 Gradillas, A.; Pérez-Castells, J. Macrocyclization by Ring-Closing Metathesis in the Total Synthesis of Natural Products: Reaction Conditions and Limitations. *Angew. Chem. Int. Ed.* **2006**, *45*, 6086–6101.

24 Abell, A. D.; Alexander, N. A.; Aitken, S. G.; Chen, H.; Coxon, J. M.; Jones, M. A.; McNabb, S. B.; Muscroft-Taylor, A. Synthesis of Macrocyclic β-Strand Templates by Ring Closing Metathesis. *J. Org. Chem.* **2009**, *74*, 4354–4356.

25 Chen, H.; Jiao, W.; Jones, M. A.; Coxon, J. M.; Morton, J. D.; Bickerstaffe, R.; Pehere, A. D.; Zvarec, O.; Abell, A. D. New Tripeptide-Based Macrocyclic Calpain Inhibitors Formed by N-Alkylation of Histidine. *Chem. Biodivers.* **2012**, *9*, 2473–2484.

26 Martin, J. L.; Begun, J.; Schindeler, A.; Wickramasinghe, W. A.; Alewood, D.; Alewood, P. F.; Bergman, D. A.; Brinkworth, R. I.; Abbenante, G.; March, D. R.; Reid, R. C.; Fairlie, D. P. Molecular Recognition of Macrocyclic Peptidomimetic Inhibitors by HIV-1 Protease. *Biochemistry* **1999**, *38*, 7978–7988.

27 Parenty, A.; Moreau, X.; Niel, G.; Campagne, J. M. Update 1 of: Macrolactonizations in the Total Synthesis of Natural Products. *Chem. Rev.* **2013**, *113*, PR1–PR40.

28 Xue, C.-B.; He, X.; Roderick, J.; DeGrado, W. F.; Cherney, R. J.; Hardman, K. D.; Nelson, D. J.; Copeland, R. A.; Jaffee, B. D.; Decicco, C. P. Design and Synthesis of Cyclic Inhibitors of Matrix Metalloproteinases and TNF-α Production. *J. Med. Chem.* **1998**, *41*, 1745–1748.

29 Singh, Y.; Stoermer, M. J.; Lucke, A. J.; Guthrie, T.; Fairlie, D. P. Structural Mimicry of Two Cytochrome b562 Interhelical Loops Using Macrocycles Constrained by Oxazoles and Thiazoles. *J. Am. Chem. Soc.* **2005**, *127*, 6563–6572.

30 Dufour, J.; Neuville, L.; Zhu, J. Intramolecular Suzuki–Miyaura Reaction for the Total Synthesis of Signal Peptidase Inhibitors, Arylomycins A2 and B2. *Chem. Eur. J.* **2010**, *16*, 10523–10534.

31 Hiroshige, M.; Hauske, J. R.; Zhou, P. Palladium-Mediated Macrocyclization on Solid Support and Its Applications to Combinatorial Synthesis. *J. Am. Chem. Soc.* **1995**, *117*, 11590–11591.

32 Aeluri, M.; Gaddam, J.; Trinath, D. V. K. S.; Chandrasekar, G.; Kitambi, S. S.; Arya, P. An Intramolecular Heck Approach to Obtain 17-Membered Macrocyclic Diversity and the Identification of an Antiangiogenesis Agent from a Zebrafish Assay. *Eur. J. Org. Chem.* **2013**, *19*, 3955–3958.

33 Spivey, A. C.; McKendrick, J.; Srikaran, R.; Helm, B. A. Solid-Phase Synthesis of an A-B Loop Mimetic of the Cε3 Domain of Human IgE: Macrocyclization by Sonogashira Coupling. *J. Org. Chem.* **2003**, *68*, 1843–1851.

34 ten Brink, H. T.; Rijkers, D. T. S.; Liskamp, R. M. J. Synthesis of Alkyne-Bridged Cyclic Tripeptides toward Constrained Mimics of Vancomycin. *J. Org. Chem.* **2006**, *71*, 1817–1824.

35 Pehere, A. D.; Abell, A. D. New β-Strand Templates Constrained by Huisgen Cycloaddition. *Org. Lett.* **2012**, *14*, 1330–1333.

36 Pehere, A. D.; Pietsch, M.; Gutschow, M.; Neilsen, P. M.; Pedersen, D. S.; Nguyen, S.; Zvarec, O.; Sykes, M. J.; Callen, D. F.; Abell, A. D. Synthesis and Extended Activity of Triazole-Containing Macrocyclic Protease Inhibitors. *Chem. Eur. J.* **2013**, *19*, 7975–7981.

37 Punna, S.; Kuzelka, J.; Wang, Q.; Finn, M. G. Head-to-Tail Peptide Cyclodimerization by Copper-Catalyzed Azide-Alkyne Cycloaddition. *Angew. Chem. Int. Ed.* **2005**, *44*, 2215–2220.

38 Alcaro, M. C.; Sabatino, G.; Uziel, J.; Chelli, M.; Ginanneschi, M.; Rovero, P.; Papini, A. M. On-Resin Head-to-Tail Cyclization of Cyclotetrapeptides: Optimization of Crucial Parameters. *J. Pept. Sci.* **2004**, *10*, 218–228.

39 Aimetti, A. A.; Shoemaker, R. K.; Lin, C.-C.; Anseth, K. S. On-Resin Peptide Macrocyclization Using Thiol-Ene Click Chemistry. *Chem. Commun.* **2010**, *46*, 4061–4063.

40 Botti, P.; Pallin, T. D.; Tam, J. P. Cyclic Peptides from Linear Unprotected Peptide Precursors through Thiazolidine Formation. *J. Am. Chem. Soc.* **1996**, *118*, 10018–10024.

41 Shepherd, N. E.; Hoang, H. N.; Abbenante, G.; Fairlie, D. P. Single Turn Peptide Alpha Helices with Exceptional Stability in Water. *J. Am. Chem. Soc.* **2005**, *127*, 2974.

42 Loughlin, W. A.; Tyndall, J. D. A.; Glenn, M. P.; Hill, T. A.; Fairlie, D. P. Update 1 of: Beta-Strand Mimetics. *Chem. Rev.* **2010**, *110*, PR32.

43 Huisgen, R. Kinetics and Mechanism of 1,3-Dipolar Cycloadditions. *Angew. Chem. Int. Ed. Engl.* **1963**, *2*, 633–645.

44 Huisgen, R.; Szeimies, G.; Möbius, L. 1.3-Dipolare Cycloadditionen, XXXII. Kinetik der Additionen organischer Azide an CC-Mehrfachbindungen. *Chem. Ber.* **1967**, *100*, 2494–2507.

45 Pedersen, D. S.; Abell, A. 1,2,3-Triazoles in Peptidomimetic Chemistry. *Eur. J. Org. Chem.* **2011**, *13*, 2399–2411.

46 Thirumurugan, P.; Matosiuk, D.; Jozwiak, K. Click Chemistry for Drug Development and Diverse Chemical-Biology Applications. *Chem. Rev.* **2013**, *113*, 4905–4979.

47 Elduque, X.; Pedroso, E.; Grandas, A. Orthogonal Protection of Peptides and Peptoids for Cyclization by the Thiol–Ene Reaction and Conjugation. *J. Org. Chem.* **2014**, *79*, 2843–2853.

48 Balraju, V.; Dev, R. V.; Reddy, D. S.; Iqbal, J. Synthesis of Cyclic Peptides Using a Palladium-Catalyzed Enyne Cycloisomerization. *Tetrahedron Lett.* **2006**, *47*, 3569–3571.

49 Kolb, H. C.; Finn, M. G.; Sharpless, K. B. Click Chemistry: Diverse Chemical Function from a Few Good Reactions. *Angew. Chem. Int. Ed.* **2001**, *40*, 2004–2021.

50 Huisgen, R. 1,3-Dipolar Cycloaddition: Introduction, Survey, Mechanism. In *1,3-Dipolar Cycloaddition Chemistry*, Padwa, A. ed., John Wiley & Sons, Inc., New York, **1984**.

51 Huisgen, R. 1,3-Dipolar Cycloadditions. *Proc. Chem. Soc.* **1961**, 357–396.

52 Tornøe, C. W.; Christensen, C.; Meldal, M. Peptidotriazoles on Solid Phase: [1,2,3]-Triazoles by Regiospecific Copper(I)-Catalyzed 1,3-Dipolar Cycloadditions of Terminal Alkynes to Azides. *J. Org. Chem.* **2002**, *67*, 3057–3064.

53 Rostovtsev, V. V.; Green, L. G.; Fokin, V. V.; Sharpless, K. B. A Stepwise Huisgen Cycloaddition Process: Copper(I)-Catalyzed Regioselective "Ligation" of Azides and Terminal Alkynes. *Angew. Chem. Int. Ed.* **2002**, *41*, 2596–2599.

54 Angell, Y. L.; Burgess, K. Peptidomimetics via Copper-Catalyzed Azide-Alkyne Cycloadditions. *Chem. Soc. Rev.* **2007**, *36*, 1674–1689.

55 Tron, G. C.; Pirali, T.; Billington, R. A.; Canonico, P. L.; Sorba, G.; Genazzani, A. A. Click Click Chemistry for Dynamic In Vivo Imaging Applications of the 1,3-Dipolar Cycloaddition between Azides and Alkynes. *Med. Res. Rev.* **2008**, *28*, 278–308.

56 Bock, V. D.; Speijer, D.; Hiemstra, H.; van Maarseveen, J. H. 1,2,3-Triazoles as Peptide Bond Isosteres: Synthesis and Biological Evaluation of Cyclotetrapeptide Mimics. *Org. Biomol. Chem.* **2007**, *5*, 971–975.

57 Makarem, A.; Berg, R.; Rominger, F.; Straub, B. F. A Fluxional Copper Acetylide Cluster in CuAAC Catalysis. *Angew. Chem. Int. Ed. Engl.* **2015**, *54*, 7431–7435.

58 Iacobucci, C.; Reale, S.; Gal, J.-F.; De Angelis, F. Dinuclear Copper Intermediates in Copper(I)-Catalyzed Azide-Alkyne Cycloaddition Directly Observed by Electrospray Ionization Mass Spectrometry. *Angew. Chem. Int. Ed.* **2015**, *54*, 3065–3068.

59 Himo, F.; Lovell, T.; Hilgraf, R.; Rostovtsev, V. V.; Noodleman, L.; Sharpless, K. B.; Fokin, V. V. Copper(I)-Catalyzed Synthesis of Azoles. DFT Study Predicts Unprecedented Reactivity and Intermediates. *J. Am. Chem. Soc.* **2005**, *127*, 210–216.

60 Sletten, E. M.; Bertozzi, C. R. From Mechanism to Mouse: A Tale of Two Bioorthogonal Reactions. *Acc. Chem. Res.* **2011**, *44*, 666–676.

61 Baskin, J. M.; Prescher, J. A.; Laughlin, S. T.; Agard, N. J.; Chang, P. V.; Miller, I. A.; Lo, A.; Codelli, J. A.; Bertozzi, C. R. Copper-Free Click Chemistry for Dynamic In Vivo Imaging. *Proc. Natl. Acad. Sci. U. S. A.* **2007**, *104*, 16793–16797.

62 Schoenebeck, F.; Ess, D. H.; Jones, G. O.; Houk, K. N. Reactivity and Regioselectivity in 1,3-Dipolar Cycloadditions of Azides to Strained Alkynes and Alkenes: A Computational Study. *J. Am. Chem. Soc.* **2009**, *131*, 8121–8133.

63 Schultz, M. K.; Parameswarappa, S. G.; Pigge, F. C. Synthesis of a DOTA-Biotin Conjugate for Radionuclide Chelation via Cu-Free Click Chemistry. *Org. Lett.* **2010**, *12*, 2398–2401.

64 Bogdan, A. R.; James, K. Synthesis of 5-Iodo-1,2,3-triazole-Containing Macrocycles Using Copper Flow Reactor Technology. *Org. Lett.* **2011**, *13*, 4060–4063.

65 Bogdan, A. R.; Jerome, S. V.; Houk, K. N.; James, K. Strained Cyclophane Macrocycles: Impact of Progressive Ring Size Reduction on Synthesis and Structure. *J. Am. Chem. Soc.* **2012**, *134*, 2127–2138.

66 Seigal, B. A.; Connors, W. H.; Fraley, A.; Borzilleri, R. M.; Carter, P. H.; Emanuel, S. L.; Fargnoli, J.; Kim, K.; Lei, M.; Naglich, J. G.; Pokross, M. E.; Posy, S. L.; Shen, H.; Surti, N.; Talbott, R.; Zhang, Y.; Terrett, N. K. The Discovery of Macrocyclic XIAP Antagonists from a DNA-Programmed Chemistry Library, and Their Optimization to Give Lead Compounds with In Vivo Antitumor Activity. *J. Med. Chem.* **2015**, *58*, 2855–2861.

67 Gartner, Z. J.; Tse, B. N.; Grubina, R.; Doyon, J. B.; Snyder, T. M.; Liu, D. R.; DNA-Templated Organic Synthesis and Selection of a Library of Macrocycles. *Science* **2004**, *305*, 1601–1605.

68 Zhang, Y.; Seigal, B. A.; Terrett, N. K.; Talbott, R. L.; Fargnoli, J.; Naglich, J. G.; Chaudhry, C.; Posy, S. L.; Vuppugalla, R.; Cornelius, G.; Lei, M.; Wang, C.; Zhang, Y.; Schmidt, R. J.; Wei, D. D.; Miller, M. M.; Allen, M. P.; Li, L.; Carter, P. H.; Vite, G. D.; Borzilleri, R. M. Dimeric Macrocyclic Antagonists of Inhibitor of Apoptosis Proteins for the Treatment of Cancer. *ACS Med. Chem. Lett.* **2015**, *6*, 770–775.

69 Tari, A. M.; Lopez-Berestein, G. GRB2: A Pivotal Protein in Signal Transduction. *Semin. Oncol.* **2001**, *28*, 142–147.

70 Traxler, P.; Bold, G.; Buchdunger, E.; Caravatti, G.; Furet, P.; Manley, P.; O'Reilly, T.; Wood, J.; Zimmermann, J. Tyrosine Kinase Inhibitors: From Rational Design to Clinical Trials. *Med. Res. Rev.* **2001**, *21*, 499–512.

71 Garbay, C.; Liu, W. Q.; Vidal, M.; Rogues, B. P. Inhibitors of RAS Signal Transduction as Antitumor Agents. *Biochem. Pharmacol.* **2000**, *60*, 1165–1169.

72 Choi, W. J.; Shi, Z.-D.; Worthy, K. M.; Bindu, L.; Karki, R. G.; Nicklaus, M. C.; Fisher, R. J.; Burke Jr., T. R. Application of Azide-Alkyne Cycloaddition 'Click Chemistry' for the Synthesis of Grb2 SH2 Domain-Binding Macrocycles. *Bioorg. Med. Chem. Lett.* **2006**, *16*, 5265–5269.

73 Chen, J.; Nikolovska-Coleska, Z.; Yang, C.-Y.; Gomez, C.; Gao, W.; Krajewski, K.; Jiang, S.; Roller, P.; Wang, S. Design and Synthesis of a New, Conformationally Constrained, Macrocyclic Small-Molecule Inhibitor of STAT3 via 'Click Chemistry'. *Bioorg. Med. Chem. Lett.* **2007**, *17*, 3939–3942.

74 Ververis, K.; Hiong, A.; Karagiannis, T. C.; Licciardi, P. V. Histone Deacetylase Inhibitors (HDACIs): Multitargeted Anticancer Agents. *Biologics* **2013**, *7*, 47–60.

75 Horne, W. S.; Olsen, C. A.; Beierle, J. M.; Montero, A.; Ghadiri, M. R. Probing the Bioactive Conformation of an Archetypal Natural Product HDAC Inhibitor with Conformationally Homogeneous Triazole-Modified Cyclic Tetrapeptides. *Angew. Chem. Int. Ed. Engl.* **2009**, *48*, 4718–4724.

76 Pirali, T.; Faccio, V.; Mossetti, R.; Grolla, A. A.; Di Micco, S.; Bifulco, G.; Genazzani, A. A.; Tron, G. C. Synthesis, Molecular Docking and Biological Evaluation as HDAC Inhibitors of Cyclopeptide Mimetics by a Tandem Three-Component Reaction and Intramolecular [3+2] Cycloaddition. *Mol. Divers.* **2010**, *14*, 109–121.

77 Beierle, J. M.; Horne, W. S.; van Maarseveen, J. H.; Waser, B.; Reubi, J. C.; Ghadiri, M. R. Conformationally Homogeneous Heterocyclic Pseudotetrapeptides as Three-Dimensional Scaffolds for Rational Drug Design: Receptor-Selective Somatostatin Analogues. *Angew. Chem. Int. Ed. Engl.* **2009**, *48*, 4725–4729.

78 Loughlin, W. A.; Tyndall, J. D. A.; Glenn, M. P.; Hill, T. A.; Fairlie, D. P. Update 1 of: β-Strand Mimetics. *Chem. Rev.* **2010**, *110*, PR32–PR69.

79 Schechter, I.; Berger, A. On the Size of the Active Site in Proteases. I. Papain. *Biochem. Biophys. Res. Commun.* **1967**, *27*, 157–162.

80 Pehere, A.; Abell, A. Macrocyclic Protease Inhibitors Constrained into a β-Strand Geometry. In *Proteases in Health and Disease*, Chakraborti, S.; Dhalla, N. S. eds., Springer: New York, **2013**; Vol. *7*, pp 181–192.

81 Pehere, A. D.; Abell, A. D. An Improved Large Scale Procedure for the Preparation of N-Cbz Amino Acids. *Tetrahedron Lett.* **2011**, *52*, 1493–1494.

82 Neilsen, P. M.; Pehere, A. D.; Pishas, K. I.; Callen, D. F.; Abell, A. D. New 26S Proteasome Inhibitors with High Selectivity for Chymotrypsin-Like Activity and p53-Dependent Cytotoxicity. *ACS Chem. Biol.* **2013**, *8*, 353–359.

83 Wilkinson, R. D.; Williams, R.; Scott, C. J.; Burden, R. E. Cathepsin S: Therapeutic, Diagnostic, and Prognostic Potential. *Biol. Chem.* **2015**, *396*, 867–882.

84 Pietsch, M.; Chua, K. C.; Abell, A. D. Calpains: Attractive Targets for the Development of Synthetic Inhibitors. *Curr. Top. Med. Chem.* **2010**, *10*, 270–293.

85 Borissenko, L.; Groll, M. 20S Proteasome and Its Inhibitors: Crystallographic Knowledge for Drug Development. *Chem. Rev.* **2007**, *107*, 687–717.

86 Loidl, G.; Groll, M.; Musiol, H.-J.; Huber, R.; Moroder, L. Bivalency as a Principle for Proteasome Inhibition. *Proc. Natl. Acad. Sci. U. S. A.* **1999**, *96*, 5418–5422.

87 Huber, E. M.; de Bruin, G.; Heinemeyer, W.; Paniagua Soriano, G.; Overkleeft, H. S.; Groll, M. Systematic Analyses of Substrate Preferences of 20S Proteasomes Using Peptidic Epoxyketone Inhibitors. *J. Am. Chem. Soc.* **2015**, *137*, 7835–7842.

88 Pehere, A. D.; Sumby, C. J.; Abell, A. D. New Cylindrical Peptide Assemblies Defined by Extended Parallel β-Sheets. *Org. Biomol. Chem.* **2013**, *11*, 425–429.

12

Palladium-Catalyzed Synthesis of Macrocycles

Thomas O. Ronson, William P. Unsworth and Ian J. S. Fairlamb

Department of Chemistry, University of York, York, UK

12.1　Introduction

Pd-catalyzed transformations have proven to be invaluable to modern synthetic chemistry over the past two decades, with a huge number of efficient and selective carbon–carbon and carbon–heteroatom bond-forming reactions reported. It is no surprise, therefore, that Pd-mediated cross-coupling reactions have been applied with great success to the synthesis of a wide variety of macrocyclic structures: they have found long-standing use in the construction of macrocyclic natural products [1] and shape-persistent macrocycles (SPMs) [2]. They are also increasingly being used in medicinally oriented research, for example, in the synthesis of macrocyclic peptides [3].

Promoting macrocyclization over competing intermolecular reactions is a key challenge in any large ring-forming cyclization method, and Pd-catalyzed macrocyclization reactions are no different. In common with other ring-closing methods, the most common strategy used to minimize unwanted intermolecular side reactions is to perform the reaction at high dilution [4]. Inevitably, this leads to a reduction in reaction rate, impacts the practicality and scalability of the macrocyclization reaction, and also introduces a number of other difficulties more specific to Pd catalysis. Firstly, while the literature precedent for carbon–carbon and carbon–heteroatom bond-forming reactions involving Pd catalysts is vast, the majority of these have been developed for intermolecular reactions or for smaller ring synthesis; hence, they are typically optimized for much higher reaction concentrations (*ca*. 0.1 M) than what is normally used in macrocyclization reactions (*ca*. 0.001 M). The increase in reaction vessel volume and amount of solvent used also makes it more likely that impurities detrimental to the performance of the catalytic system (e.g., adventitious air or water) are introduced into the reaction, and this, along with the decreased reaction rate

caused by the high dilution, often necessitates an increase in catalyst loading (and quantities of associated ligands/additives). Of course, high catalyst loadings bring their own problems, in particular, the cost of catalyst itself, purification difficulties, environmental impact, and toxicity concerns. These factors are particularly important in medicinal chemistry research, where overall process costs are crucial and there is a requirement to produce products without significant metal contaminants. It is, therefore, unsurprising that Pd-catalyzed macrocyclization reactions have found greater utility in natural product synthesis (where such factors are generally considered secondary to the overriding goal of generating the target molecule) than in medicinal chemistry, although, as this account will show, there are notable exceptions (see also Chapter 15).

With the aforementioned in mind, the examples selected for discussion in this review have been chosen to highlight some of the key strengths and weaknesses of Pd-catalyzed methods to perform the key macrocyclization step. In particular, the reaction concentration and catalyst loading of the methods will be emphasized, as these two factors are arguably the most important challenges to overcome in this field. The five Pd-catalyzed macrocyclization reactions that have proven to be the most useful to date are the Stille, Suzuki–Miyaura, Heck, Sonogashira, and Tsuji–Trost reactions, and this chapter is accordingly divided by reaction type. The final section deals with miscellaneous Pd-catalyzed macrocyclization reactions, which leads to the conclusions and a discussion of the future directions of this field.

12.2　Stille Reaction

The Stille reaction is the name given to the Pd-catalyzed coupling of an organostannane with an organic electrophile to form a new carbon–carbon bond. The reaction

was pioneered by John K. Stille at the end of the 1970s [5, 6] and has since been developed to become one of the most versatile and useful cross-coupling reactions available to the organic chemist [7]. A large part of the appeal of the Stille reaction is the ease of handling of the required organotin reagents and the mildness of the conditions under which it can be carried out. The most commonly employed organostannanes contain a tributyltin group, although the more reactive (and more hazardous) trimethyltin analogues can also be used, with the three alkyl moieties acting as spectator groups in the transmetallation step of the mechanism. The electrophilic coupling partner is normally an organohalide or -triflate and can be alkenyl, aryl, acyl, benzylic, or allylic. The carbonylative Stille reaction is a variant conducted by carrying out the reaction under an atmosphere of carbon monoxide and results in a carbonyl group being inserted between the two coupling partners, giving a ketone. A number of key discoveries that have led to improvements in the effectiveness of the Stille protocol have been made since its original inception; in particular, in the early 1990s, it was discovered that large rate accelerations could be observed in the Stille reaction by both the use of weakly coordinating $AsPh_3$ and $P(2\text{-furyl})_3$ ligands [8] and the addition of copper(I) salts [9, 10]. Both of these modifications have since become widespread, especially in the context of macrocyclization reactions where a fast reaction is often critical due to the high dilution employed.

While the stability of trialkyltin groups allows them to be carried through multiple synthetic steps, the tin residues that are produced as by-products of the Stille reaction are oftentimes difficult to separate from the desired product and have somewhat limited the use of the Stille reaction in medicinal or large-scale industrial applications [11]. Poor atom economy associated with the use of the high molecular weight tributyltin group represents another limitation of this method.

The utility of the Stille reaction as a macrocyclization protocol was first demonstrated by Stille in 1987 [12], and subsequent use of this strategy is found almost exclusively in the field of total synthesis, where it has been employed as the macrocyclization step in the synthesis of more than 35 separate large-ring natural products and associated model systems to date [1, 13, 14]. Representative examples from the past several decades include (±)-jatrophone [15], rapamycin [16, 17], 14,15-anhydropristinamycin II_B [18, 19], (+)-mycotrienin [20, 21], sanglifehrin A [22], rhizoxin D [23, 24], (−)-sarain A [25, 26], vicenistatin [27], chivosazole F [28], and amythiamicin C [29], among others [30–43] and are illustrated in Figure 12.1 (**1–10**), with the C–C bond(s) formed during the macrocyclization step highlighted in grey. Further key examples are discussed in more detail in the following text.

Since it was first discovered in the early 1990s [8], the combination of Pd_2dba_3 (dba = *E,E*-dibenzylideneacetone) with $AsPh_3$ has become the most common catalytic system with which to conduct a Stille macrocyclization reaction. Recent successful examples of the application of these conditions include the work of Taylor and coworkers during studies toward the first total synthesis of 'upenamide (**12**), a macrocyclic marine alkaloid isolated from the Indonesian sponge *Echinochalina* sp. (Equation 1, Scheme 12.1) [45, 46]. These conditions were employed, along with i-Pr_2NEt and LiCl in THF, to generate the desired macrocycle in an excellent 74% yield. While the catalyst loading (10 mol%) would be considered high for a standard intermolecular cross-coupling reaction, it is typical of what is required for an efficient Pd-catalyzed macrocyclization, as can be seen in many of the following examples.

The use of the Stille reaction in the synthesis of macrocyclic peptides has been elegantly demonstrated by Bach and coworkers in their synthesis of the thiazolyl peptide GE2270 A (**15**), one of a family of antibiotics produced by *Planobispora rosea* (Equation 2, Scheme 12.1) [47, 48]. They achieved the macrocyclization of an extremely complex and multifunctional system in an impressive 75% yield employing $Pd(PPh_3)_4$ as the catalyst (note: although we refer to $Pd(PPh_3)_4$ as a catalyst, it is important to recognize that the real catalyst is likely to be $Pd^0(PPh_3)_n$, where $n = 1$ or 2). This example is also a convincing demonstration that the intramolecular Stille reaction is highly tolerant of a diversity of functional groups, some of which may have been otherwise anticipated to interfere with a metal-mediated reaction (pyridine, thiazole, amide bonds, etc.). An alternative macrolactonization approach to this molecule examined by the same authors [29] and others [49] was found to be considerably lower yielding. The same Stille macrocyclization approach was subsequently used in the synthesis of the related natural products, amythiamicins C and D [29].

Some of the most dramatic examples of ring-forming Stille reactions are "stitching cyclizations," wherein a small, bifunctional reagent is inserted into an appropriately functionalized precursor, and following both inter- and intramolecular Stille reactions gives rise to a cyclic product. An example of this strategy is found in Danishefsky and coworkers' synthesis of dynemicin A (**19**), whereby slow addition of a dilute solution of bis-stannane **17** to bisiodide **16** in DMF in the presence of 10 mol% $Pd(PPh_3)_4$ led to the smooth formation of **18** in a remarkable 80% yield (Equation 3, Scheme 12.1) [50, 51]. This reaction also serves as an unusual example of an sp^2–sp Stille coupling.

The immobilization of a cyclization precursor onto a solid support can be an effective way to improve the efficiency of a cyclization reaction by affording a "pseudo-dilution" environment, thus reducing the chances
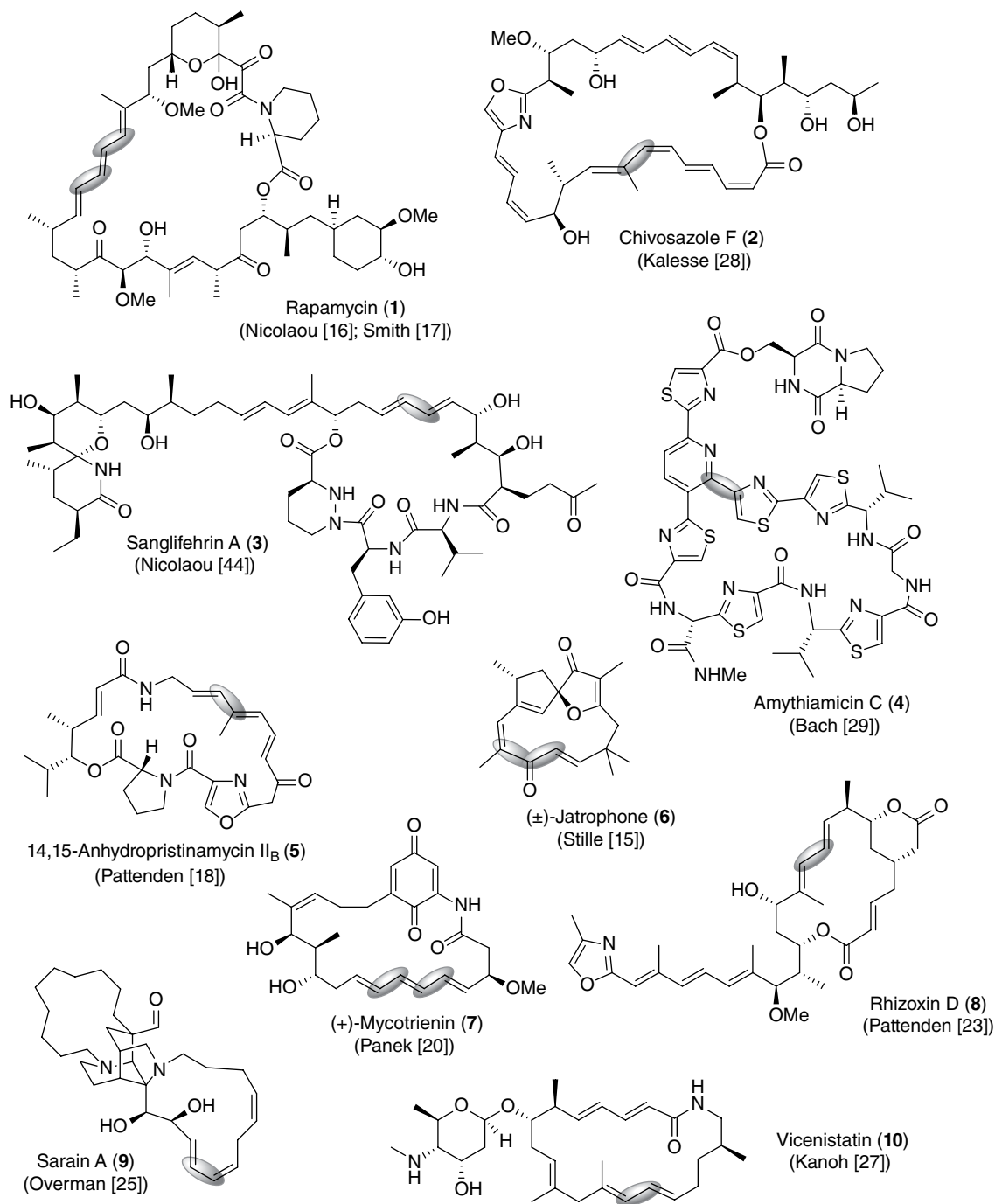
Figure 12.1 Representative examples of natural products synthesized using a Stille macrocyclization step (bond(s) formed in this step shaded in grey).

of intermolecular coupling [52]. An early demonstration of this principle was reported by Nicolaou and coworkers in their application of a "Stille coupling/cyclorelease" strategy to the total synthesis of (*S*)-zearalenone (**22**) (Equation 4, Scheme 12.1) [53]. Adapting a previous synthesis of the same natural product [54], the authors constructed their cyclization precursor **20** attached, via

the stannyl group, to a polystyrene (PS) resin. Upon exposure to Pd(PPh$_3$)$_4$ (10 mol%) in toluene at 100 °C for 48 h, the substrate simultaneously underwent both cyclization and cleavage from the resin, giving the desired macrocycle **21** in 54% yield.

A novel Pd pre-catalyst, Pd(*N*-succ)(Br)(AsPh$_3$)$_2$, named AsCat for simplicity [55], has been shown to be
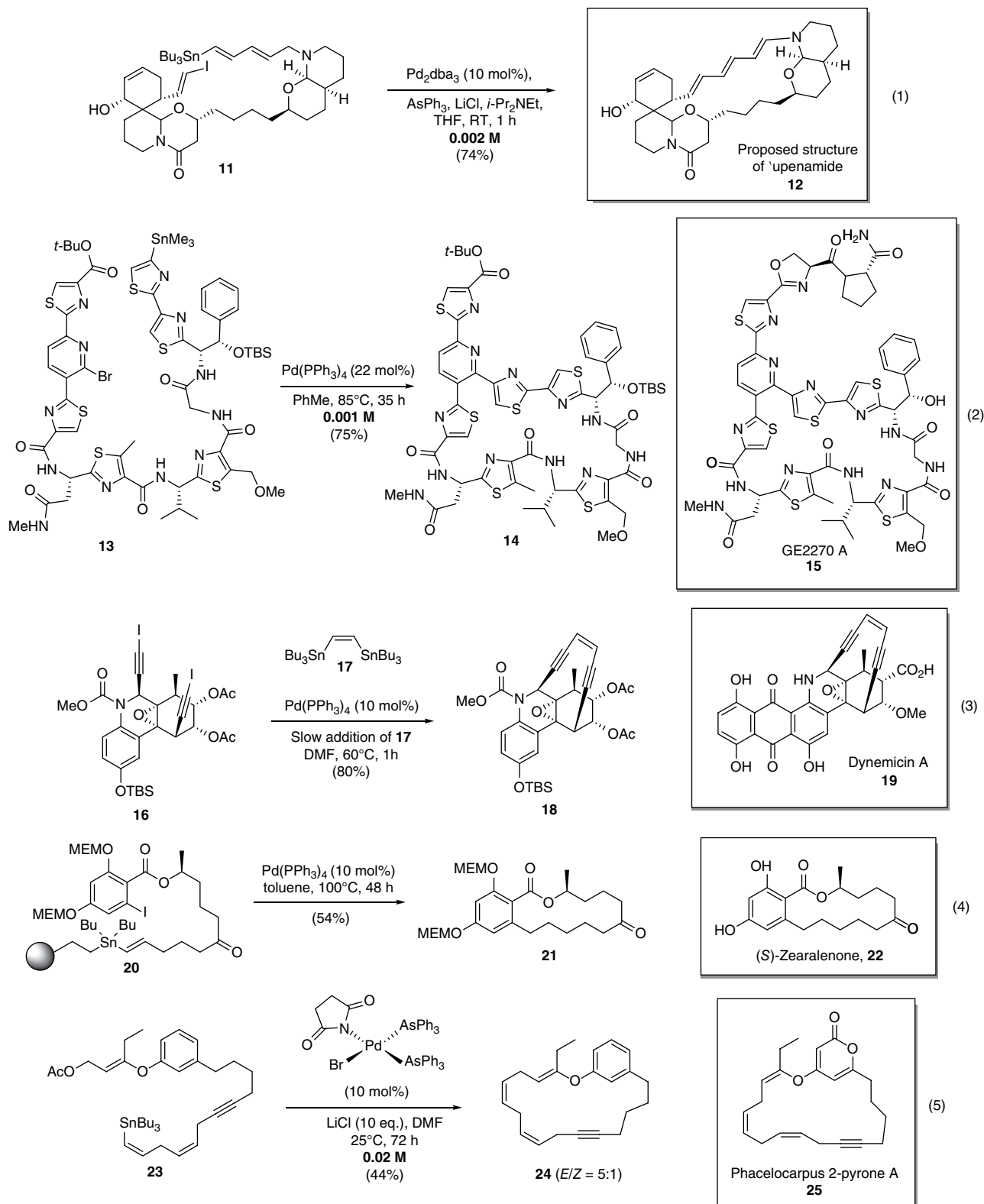
Scheme 12.1 Examples of the Stille macrocyclization reaction in natural product total synthesis.

effective for macrocyclization processes using the π-allyl Stille coupling (equation 5, Scheme 12.1). In studies toward a model system (**24**) of the natural product phacelocarpus 2-pyrone A (**25**), the catalyst was shown to be more efficient at mediating the coupling of a stannane with an allylic acetate than the standard Pd$_2$dba$_3$/AsPh$_3$ system, achieving the macrocyclization step in 44% yield (vs. 28% using the standard conditions) [56]. The natural product (**25**) was subsequently synthesized by the same strategy [57]. This final example serves as a reminder that, although the Stille methodology has been employed with huge success over the past several decades, there is much scope for improving efficiency, in particular by using more effective and selective Pd catalysts for these more complex transformations, for example, beyond simple benchmark substrates.

This section has offered an insight into the different conditions and techniques that can be used to construct a structurally diverse range of macrocycles using the Stille reaction. It can be seen that this is a highly effective strategy, which has become the favored cross-coupling macrocyclization reaction in the challenging context of natural product total synthesis. In contrast, as discussed previously, the relatively high catalyst loadings and unavoidable tin by-products have made it somewhat less applicable in other areas, where alternative cross-coupling reactions have often been preferred.

12.3 Suzuki–Miyaura Reaction

The cross-coupling of an organoborane with an electrophile, resulting in the formation of a C–C bond, is known as the Suzuki–Miyaura reaction. The boron-containing substrate is typically a borane (RBR′$_2$), boronic acid (RB(OH)$_2$), boronic ester (RB(OR′)$_2$), or potassium trifluoroborate salt (RBF$_3$K). A base is required for reaction, the transmetalation step of which proceeds via a negatively charged boron "ate" species. The use of thallium bases has been reported to offer large rate enhancements in Suzuki couplings [58–60], and, for this reason, they are often used in Suzuki macrocyclizations, especially in the context of natural product synthesis, when sensitive cyclization precursors can be prone to degradation at long reaction times. The Suzuki–Miyaura reaction is a particularly effective way to form aryl–aryl bonds and has numerous attractive features, which have led it to be widely adopted across organic synthesis, as well as in industrial and large-scale applications: it is operationally simple and relatively insensitive to air, can be carried out under biphasic conditions using an aqueous base, and the boron residues produced in the reaction are easily removed from the product and normally nontoxic.

The Suzuki–Miyaura reaction has been well used as a macrocyclization tool in the total synthesis of natural products. Following early studies by Miyaura [61], several impressive natural targets have been completed using this strategy. One such example is the synthesis of marinomycin A (**27**) by Nicoloau and coworkers (Equation 1, Scheme 12.2); [62] in this case, the organoboron group was generated *in situ* by hydroboronation of a terminal alkyne, followed by quenching with water and direct addition of Pd(PPh$_3$)$_4$ and TlOEt to the solution. This strategy afforded the desired target **27** in 23% yield following silyl deprotection with TBAF. Examination of various bases confirmed TlOEt as the optimal choice (caution: thallium and its salts are highly toxic). Given Jutand's recent findings, n-Bu$_4$NX bases may find application here as a substitute for thallium bases [60].

Another elegant example is found in the synthesis of rhizopodin (**30**) by Menche and coworkers (Equation 2, Scheme 12.2) [63, 64]. They employed 50 mol% PdCl$_2$(dppf) with Ba(OH)$_2$·8H$_2$O in DMF and were able to conduct the macrocyclization at ambient temperature, rapidly and in 68% yield (dppf = 1,1′-bis(diphenylphosphino)ferrocene). Although the catalyst loading used here is rather high, it was found that either increasing (100 mol%) or decreasing (30 mol%) the amount of catalyst resulted in a lower yield of the desired compound.

The use of trifluoroborate salts in these macrocyclizations has been demonstrated by Molander and coworkers (Equation 3, Scheme 12.2) [65]. During synthetic efforts toward oximidine II (**33**), they were able to effect the cyclization of compound **31** by treatment with 10 mol% Pd(PPh$_3$)$_4$ and Cs$_2$CO$_3$ in a biphasic THF/H$_2$O reaction solvent, isolating the target compound **32** in 42% yield. The success of this reaction was found to be highly dependent on concentration, catalyst, and solvent, with several attempts at a higher molarity (0.002 or 0.005 M), employing PdCl$_2$(dppf) as pre-catalyst, or DMF as solvent, giving lower yields.

Other examples of successful Suzuki macrocyclizations in natural product total synthesis that are not discussed here include synthetic studies toward rutamycin B [66, 67], apoptolidinones A and D [68, 69], complestatin [70–73], epothilone 490 [74], phomactin A [75–78], rimocidinolide [79], arylomycins A$_2$ [80–82] and B$_2$ [81], xestocyclamine A [83], mycocyclosin A [84], isoplagiochin D [85], riccardin C [86], biphenomycin B [87], and RP-66453 [88].

Given the low toxicity of the reagents employed, and the reliability of the Suzuki reaction for the construction of aryl–aryl bonds, it is not surprising that it has found some utility in the synthesis of macrocyclic peptides. Cyclic peptides and peptidomimetics have been shown to exhibit increased bioavailability, enhanced

i. Cy₂BH, catecholborane; H₂O
ii. TlOEt, Pd(PPh₃)₄ (10 mol%), THF/H₂O, RT, 4 h, **0.006 M**
iii. TBAF, THF, RT, 18 h

(23% over three steps)

Marinomycin A (**27**)

PdCl₂(dppf) (50 mol%), Ba(OH)₂•8H₂O, DMF, RT, 3 h
0.009 M

(68%)

Pd(PPh₃)₄ (10 mol%), Cs₂CO₃, THF/H₂O (10:1) reflux, 20 h, **0.001 M**

(42%)

Oximidine II (**33**)

Rhizopodin (**30**)
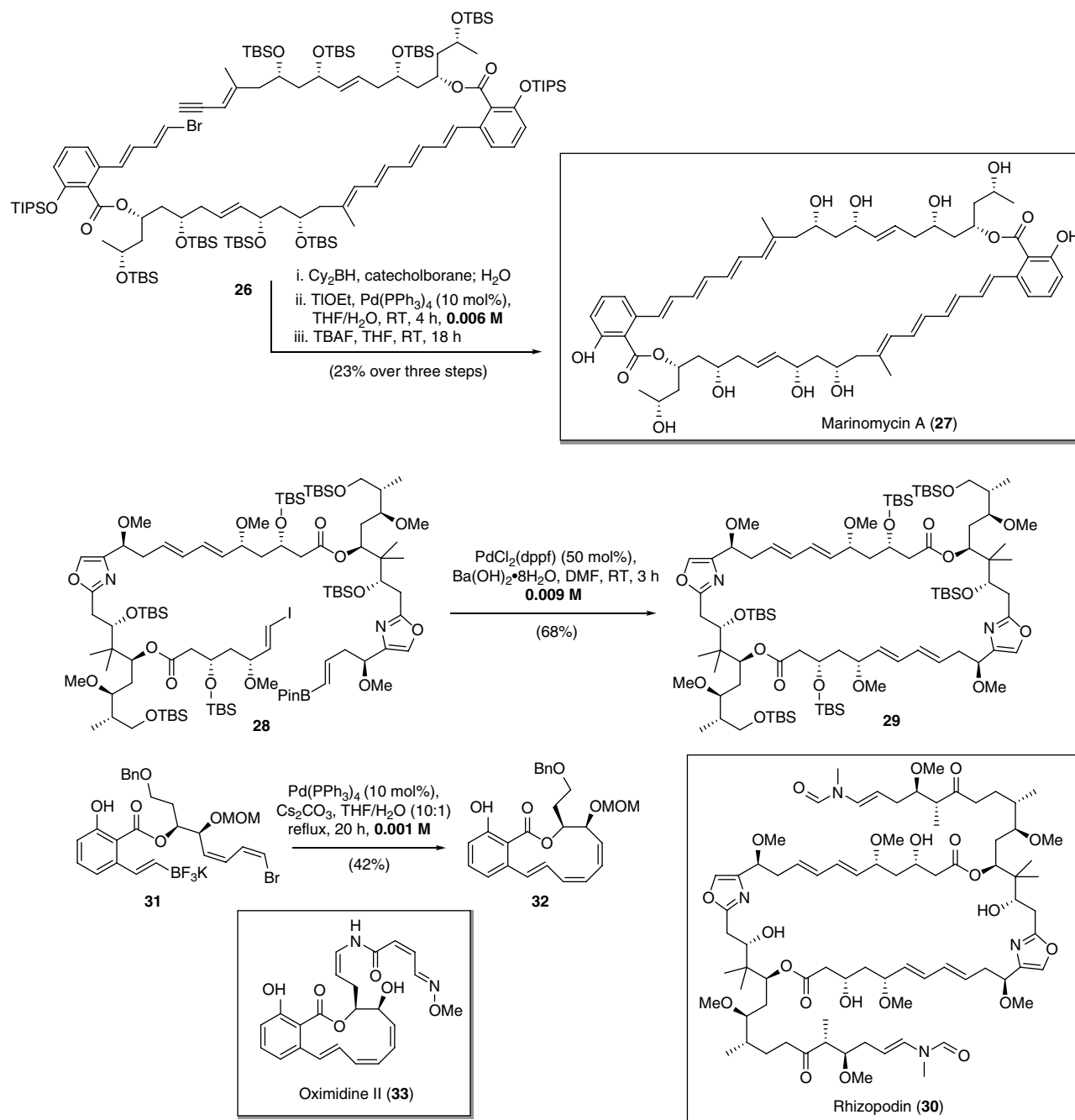
Scheme 12.2 Examples of Suzuki–Miyaura macrocyclizations in natural product total synthesis.

cell permeability, and greater metabolic stability than linear analogues in many cases [89, 90]. They also have less conformational flexibility than linear molecules, hence, are able to bind to biological targets without major entropic penalties but are more flexible than smaller cyclic compounds, allowing them to "mold" to target receptors. In particular, this has brought success when addressing targets such as protein–protein interactions that are highly challenging to modulate using

traditional small molecule drugs; therefore, much effort has gone into developing methods for their synthesis (for more detail see Chapters 3 and 5). Early work by Burgess [91], Vaultier, and Alcaraz [92] established that immobilization of an appropriately functionalized peptide substrate on a solid support followed by exposure to Suzuki–Miyaura conditions could be an effective way to achieve macrocyclization. A recent example reported by James and coworkers shows how the peptide (**34**) can
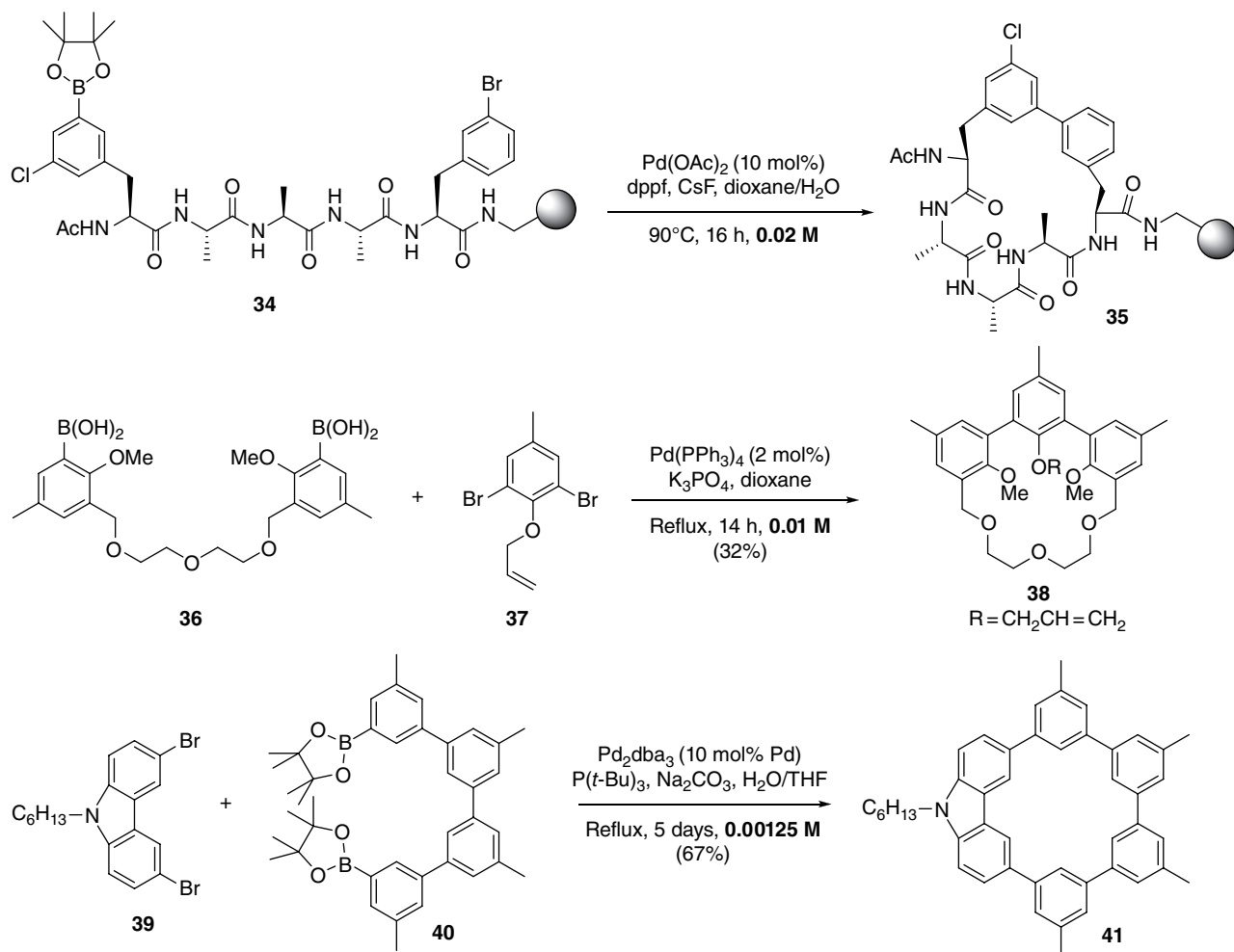
Scheme 12.3 Examples of Suzuki–Miyaura macrocyclizations for peptidomimetics, hemispherands, and SPMs.

be constructed stepwise directly on the solid support, incorporating the suitably derivatized amino acids, and then cyclized under standard conditions, before being cleaved from the resin under acidic conditions (Equation 1, Scheme 12.3) [93]. This overall process is remarkably high yielding, giving, for example, 12.5% yield over 14 steps (average 86% yield per step) for a five-residue peptide containing two *meta*-functionalized phenylalanine derivatives (**35**). It is worth noting that the macrocyclization step is also conducted under much more concentrated conditions than normally used for these reactions (0.02 M). The chloride substituent in compound **35** could be removed by hydrogenolysis or, in theory, employed as a point of further diversification. Similar results could be obtained in solution-phase synthesis, but with somewhat lower overall yields, and requiring chromatographic purification. An analogous approach has also been reported by Planas and coworkers, allowing cyclization of peptides containing up to eight residues in a similar manner [94]. These examples clearly demonstrate the

potential value of solid-supported synthesis in Pd-catalyzed macrocyclization, although advantages should be balanced against the fact that larger excesses of reagents are typically required for transformations performed on solid supports.

Another strategy to improve the efficiency of macrocyclization reactions is by templating the cyclization precursor around a metal ion in order to "pre-organize" it into a favorable conformation to undergo cyclization. This method has been demonstrated for Pd-catalyzed processes by Reinhoudt and coworkers in their synthesis of a series of hemispherand ligands (e.g., **38**, Equation 2, Scheme 12.3) [95]. They found that in their two-component macrocyclization reaction employing **36** and **37**, the choice of alkali metal salt as base could have a marked impact on the yield of the cyclization reaction. The combination of $Pd(PPh_3)_4$ with Na_2CO_3, K_2CO_3, or K_3PO_4 was found to be superior to other alkali metal carbonates, and this was attributed to a templating effect of the K^+ or Na^+ ions prior to macrocyclization. While the use

of alkali metal cation templates in Pd-catalyzed macro-cyclization reactions has not been widely explored since, it is worth noting that Pd itself could feasibly play a similar role in situations where the cyclization precursor is suitably functionalized and that this could account for the favorable results observed in many of the examples detailed here.

A final area where the Suzuki reaction has proved useful is the synthesis of SPMs. Following from the early work in the area [96, 97], Bo and coworkers have achieved excellent yields in the synthesis of a variety of SPMs using a biphasic catalyst-transfer system (Equation 3, Scheme 12.3) [98]. They proposed that this approach maintains a low concentration of the reactive species and results in pseudo-high dilution conditions that favor macrocyclization, although their cyclization substrates **39** and **40** appear to have a high degree of pre-organization, which can also facilitate macrocyclization considerably. The best yield of 67% was obtained in the synthesis of compound **41** using a 10 mol% catalyst loading; however, this could be lowered without a dramatic drop in yield (e.g., 55% at 0.5 mol% Pd).

These final examples illustrate key methods that can be used to improve efficiency more broadly in Pd-catalyzed macrocyclization reactions: immobilization of the substrate on a solid support or "pre-organization," either by templating or by using a cyclization precursor, which adopts a conformation favorable for cyclization. These strategies have been utilized in a range of contexts, as can be seen from many of the other examples detailed throughout this account.

12.4 Heck Reaction

The Heck reaction, which is the coupling of an alkene with a halide or pseudo-halide, can be thought of in similar terms to the Stille or Suzuki–Miyaura reactions, but with the C–H bond of the alkene taking the place of the organometallic group. This approach offers clear advantages in terms of atom economy and fewer requirements for pre-functionalization, although these advantages should be balanced against potential problems concerning regioselectivity and stereochemistry associated with the reaction taking place on an unfunctionalized alkene. Fortunately, the nature of a cyclization reaction imparts a degree of selectivity. In practice, mixtures of regioisomers are rarely a problem in Heck macrocyclizations; in general macrocyclizations of this type are *endo* selective, meaning that the reactive alkene becomes part of the resulting ring, while cyclizations forming smaller rings often exhibit the opposite *exo*-selectivity. Practically, the reaction usually takes place under mild conditions in the presence of a weak base and a Pd

source and is relatively insensitive to the presence of air or moisture.

The ubiquity of alkenes and the simplicity of the transformation have led the Heck macrocyclization to be widely applied in the syntheses of numerous macrocycles across natural product and medicinal chemistry [99]. The field of total synthesis offers many elegant examples of the use of the Heck reaction to form macrocyclic scaffolds, where it often compares favorably to alternative approaches. For example, during their formal total synthesis of palmerolide A (**44**), Maier and Jägel found that Heck macrocyclization of **42** using Pd(OAc)$_2$, Cs$_2$CO$_3$, and Et$_3$N proceeded in high yield (Equation 1, Scheme 12.4), giving a single isomer of the product **43**, while the analogous Stille reaction, although giving comparable yields, afforded unwanted *E/Z* mixtures [100]. The somewhat high Pd loading used (130 mol%) is not uncommon, and when performing the macrocyclization step on a very small scale (0.01 mmol in this case), as is typical in the final stages of a total synthesis, this is not particularly problematic, especially when the scale of reaction renders any meaningful optimization impractical. The intramolecular Heck approach has since been used in a number of other formal syntheses of the same natural product [101–103].

Another example can be found in the total synthesis of etnangien (**47**) and its methyl ester by Menche and coworkers, who found the Heck macrocyclization to be superior to both macrolactonization and ring-closing metathesis (Equation 2, Scheme 12.4). Using 100 mol% Pd(OAc)$_2$, K$_2$CO$_3$, and Bu$_4$NCl in DMF, they achieved a 70% yield of the desired product **46** with a reaction time of just 1 h [104, 105]. They later used the same synthetic sequence to produce four simplified analogues of etnangien for structure–activity relationship studies [106]. Other natural products synthesized using the Heck macrocyclization include rhizopodin [107], archazolid B [108], isoplagiochin [85], kulkenon [109], aspercyclide A [110, 111], and the proposed structure of diazonamide A [112–114].

Arya, Kitambi, and coworkers have used the intramolecular Heck reaction to build a series of ten natural product-inspired synthetic macrocycles (e.g., **49a–e**), which were then tested for anti-angiogenesis activity (Equation 3, Scheme 12.4) [115]. They used a modular approach, incorporating amino acids into the macrocyclic skeleton to allow a straightforward variation of the structure. By employing Pd(OAc)$_2$, P(*o*-tol)$_3$, and *i*-Pr$_2$NEt for the Heck macrocyclization of substrates **48a–e**, they isolated all of the desired macrocycles in 55–60% yields (corrected for recovered starting material). Other natural product analogues, for example, of paclitaxel [116, 117] and FK-506 [118], have also been constructed using a Heck macrocyclization as the key transformation.
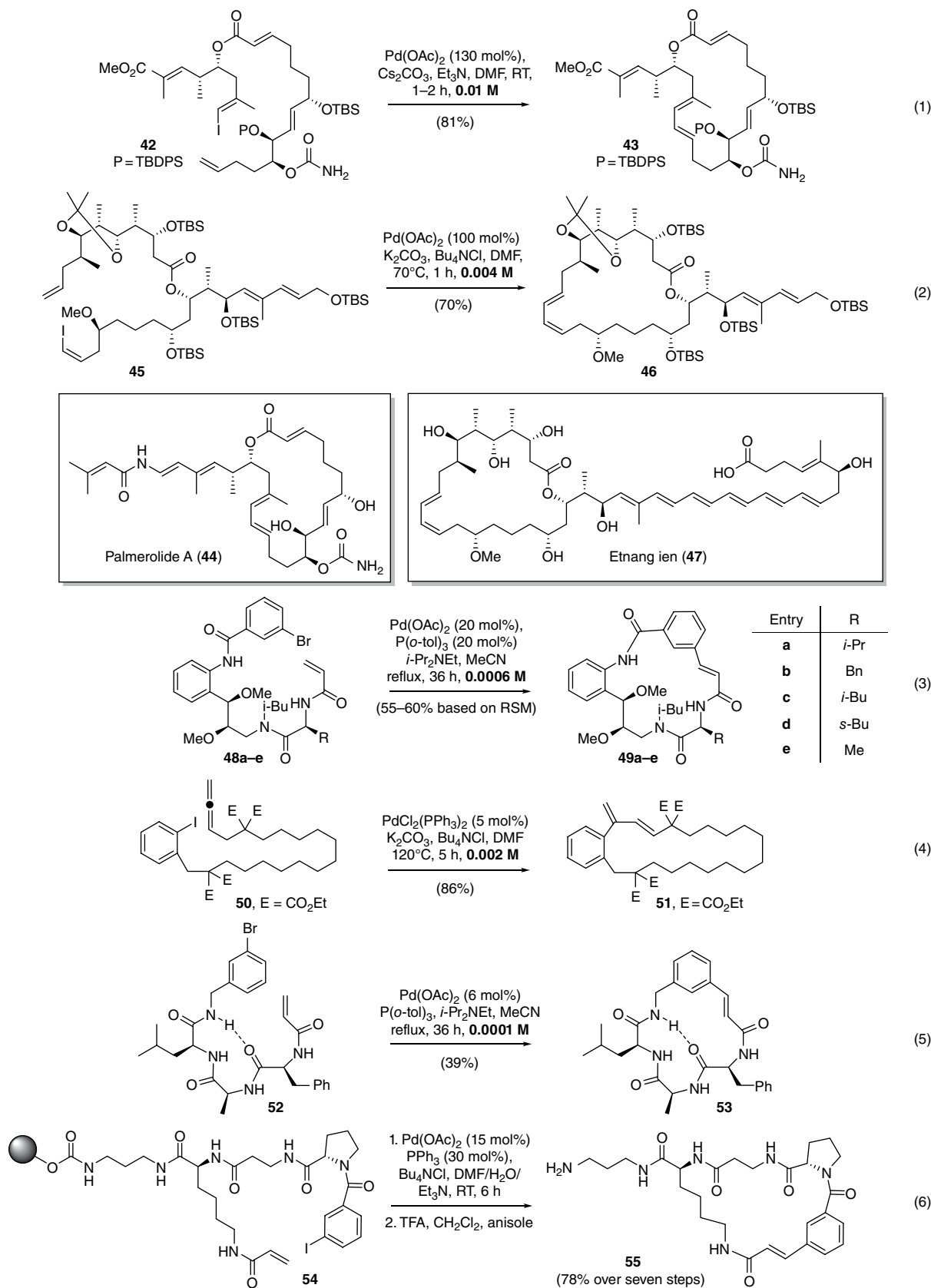
Scheme 12.4 Examples of the use of the Heck macrocyclization in various applications.

Negishi and Ma carried out an early study demonstrating the utility of allenes in intramolecular Heck-type reactions, in which the new carbon–carbon bond is formed to the central allene carbon atom resulting in a 1,3-diene with an *exo*-methylene group not forming part of the ring (Equation 4, Scheme 12.4) [119]. As part of a wider investigation considering a range of ring sizes, they effected the macrocyclization of a number of ω-haloallenes (e.g., **50**) in yields of up to 86% using 5 mol% $PdCl_2(PPh_3)_2$ along with K_2CO_3 and Bu_4NCl in DMF. By comparison, employing the corresponding alkenes in a standard Heck cyclization gave considerably lower yields and in some cases (i.e., eight- and nine-membered rings) failed altogether. The authors suggest that the greater reactivity of an allene compared to an alkene gives rise to an increased rate of cyclization, thus minimizing undesired side reactions and leading to higher yields.

Macrocyclic peptides have also been synthesized using the Heck reaction. Iqbal and coworkers have demonstrated the solution-phase cyclization of two different tripeptides using a Heck reaction with $Pd(OAc)_2$, P(*o*-tol)$_3$, and *i*-PrNEt in MeCN at 80°C for 36 h (Equation 5, Scheme 12.4) [120]. Despite the very dilute conditions (0.0001 M) and relatively low Pd loading (6 mol%), they isolated the two macrocycles in respectable 39 and 49% yields. They further noted the presence of a hydrogen bond in both the precursors (e.g., **52**) and the products (e.g., **53**) and suggested that this could give rise to a degree of pre-organization leading to a facile ring-closure.

In a powerful early demonstration of macrocyclization on a solid support, Hauske and coworkers synthesized a library of 15 different peptide-based macrocycles using the Heck reaction (Equation 6, Scheme 12.4) [121]. The cyclization step (e.g., **54→55**) took place in only 6 h at RT using $Pd(OAc)_2$ (15 mol%), PPh$_3$ (30 mol%), and Bu_4NCl (30 mol%) in a mixture of DMF, H_2O, and Et$_3$N (9:1:1). Substrate **55**, for example, when cleaved from the resin, was isolated in a remarkable 78% yield over seven steps. An analogous and similarly successful solid-phase Heck protocol was subsequently reported by Akaji and coworkers [122, 123].

The examples in this section exhibit the power of the Heck reaction as a macrocyclization technique and hint at its future potential for the synthesis of medicinally relevant large-ring compounds, in particular, macrocyclic peptides and peptidomimetics. Variants of this reaction, such as the use of an allene in place of an alkene (e.g., Equation 3, Scheme 12.4), also hold great promise for application in more complex systems.

12.5 Sonogashira Reaction

The Sonogashira reaction involves the coupling of a terminal alkyne with a vinyl or aryl halide upon treatment with a Pd catalyst, along with a copper salt and/or base, and is a mainstay of synthetic chemistry [124]. Particular advantages of this coupling method are its high functional group tolerance, the fact that the alkyne moiety does not need to be pre-functionalized with a metal component, and its relative insensitivity to water, making it arguably one of the simplest Pd-catalyzed couplings to perform experimentally, which is important when considering the added practical complications associated with macrocyclization reactions. Trace air can cause issues with Pd(0) oxidation, promoting alkyne homocoupling to give Glaser-type 1,4-diyne products, although this seems particularly prevalent when using polar solvents with Et$_3$N base [125].

Compared with the methods described previously, the Sonogashira reaction has been used only infrequently in the synthesis of macrocyclic natural product synthesis, presumably due to the relative rarity of natural ring systems containing conjugated alkynes. There are a few notable examples, however, the earliest being a report by Schreiber and coworkers, who used an intramolecular Sonogashira reaction in their synthesis of analogues of the antitumor natural product dynemicin (**59**); [126] thus, the treatment of alkyne **56** with Pd(PPh$_3$)$_4$ and CuI in toluene led to the formation of 15-membered macrocycle **57**, which subsequently underwent transannular Diels–Alder reaction *in situ*, furnishing compound **58** in 25% yield (Equation 1, Scheme 12.5). The loading of the Pd(PPh$_3$)$_4$ catalyst is low (2 mol%) for a macrocyclization reaction, although a relatively high amount of CuI was also included in the reaction, while the reaction concentration was not reported.

Hirama and coworkers later reported the synthesis of macrocycle **61** using a Pd$_2$dba$_3$·CHCl$_3$/CuI catalyst system in their synthesis of kedarcidin chromophore (**62**) (Equation 2, Scheme 12.5) [127]. The macrocyclization yield was a remarkable 88–90%, although a high loading of Pd$_2$dba$_3$ (55 mol%) was required to achieve this under the dilute reaction conditions.

Arguably the most successful use of Sonogashira macrocyclization in natural product synthesis was reported by Mohapatra and coworkers in their total synthesis of penarolide sulfate A$_1$ (**65**), an α-glucosidase inhibitor isolated from the marine sponge *Penares* sp. (Equation 3, Scheme 12.5) [128]. While the natural product contains no alkyne or even alkene functionalities, the Sonogashira reaction was used to construct a 30-membered macrocyclic precursor **64** using catalytic Pd(PPh$_3$)$_4$ and CuI in Et$_2$NH, in just 30 min at room temperature. The most noteworthy aspect of the macrocyclization step is that a reasonable yield (35%) was achieved at an unusually high reaction concentration (0.22 M); the authors did not speculate on why this particular cyclization proceeded so efficiently, although one could reasonably propose that the proline derivative in the backbone may be important, as this could lead to the molecule adopting a
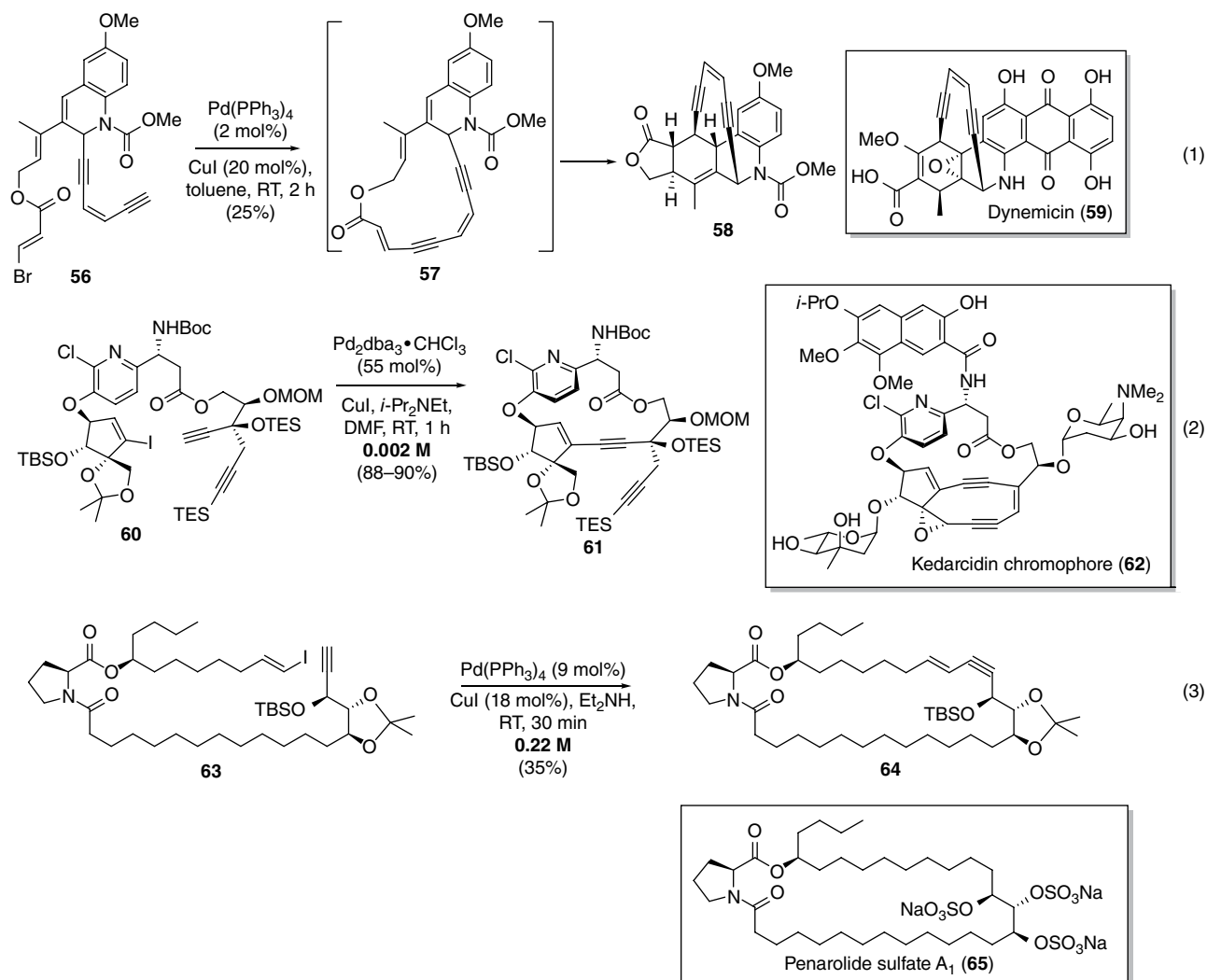
Scheme 12.5 Sonogashira reactions in the synthesis of macrocyclic natural products.

low energy conformation in which the reactive components are held close in space and hence are well suited to undergo macrocyclization.

The Sonogashira reaction has found considerably wider use in the synthesis of nonnatural macrocycles [129–136], and, most notably, in the synthesis of biologically active conformationally constrained cyclic peptides [130, 131]. An early Sonogashira macrocyclization in this area was reported by Spivey and coworkers; [130] linear precursor **66** was assembled on a Rink amide PS resin using standard solid-phase peptide synthesis, before macrocyclization was performed "on resin" using a catalyst system of PdCl$_2$(PPh$_3$)$_2$, CuI, and PPh$_3$ in THF, followed by cleavage from the support and global deprotection under acidic conditions to afford macrocycle **67** in around 15% yield (Equation 1, Scheme 12.6). The catalyst loading for the macrocyclization is particularly high in this example, but the reaction is impressive nonetheless, given that a highly complex 65-membered

peptidomimetic is formed. It is noted that the high catalyst loading may partly be a consequence of the very small scale of the reaction (2.5 μmol).

A homogeneous Sonogashira macrocyclization protocol was described soon afterward by Iqbal and coworkers, who reported the synthesis of six di-, tri-, and tetra-peptidomimetics, exemplified by the synthesis of macrocycle **69** (Equation 2, Scheme 12.6) [131]. In this Cu-free "Heck-alkynylation" method, the linear precursor **68** was heated at 110°C in acetonitrile with Pd(OAc)$_2$ and P(*o*-tol)$_3$, with the reported examples proceeding in 12–36% yield. Again, high catalyst loadings and dilute conditions were used in this protocol. A related method, from Liskamp and coworkers, is exemplified by the Sonogashira macrocyclization of linear precursor **70** to generate product **71**, using a catalyst system of Pd(PPh$_3$)$_4$, CuI, and Et$_2$NH in acetonitrile (Equation 3, Scheme 12.6) [137]. Improved catalyst loadings and reaction concentrations are described compared with the earlier
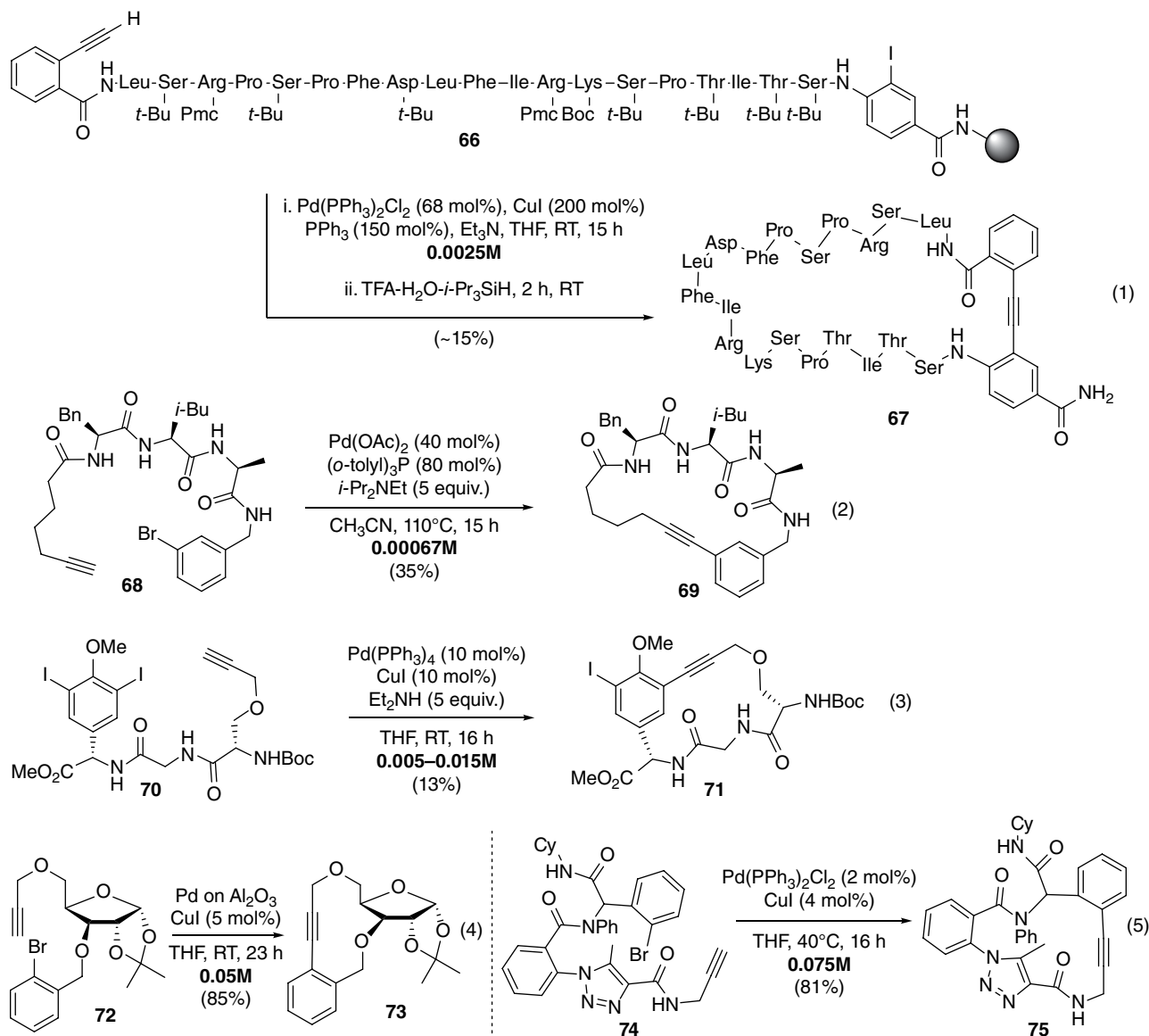
Scheme 12.6 Examples of the Sonogashira macrocyclization in the synthesis of cyclic peptides and other systems.

examples, although the macrocyclization yields are relatively low (6–23%), and it should also be noted that the same products could be obtained more efficiently via an analogous macrolactamization reaction.

Using substrate control to circumvent problems associated with dilution is a common strategy in a number of macrocyclization reactions, an effect that can be seen in the work of Mukherjee and coworkers, who reported the synthesis of a series of carbohydrate-containing 10–13-membered benzannulated ring systems using a heterogeneous Pd catalyst [138, 139]. The catalyst was made by immobilizing Pd(II)Cl$_2$ onto an alumina support, which, in combination with CuI, promoted Sonogashira macrocyclization in very good yields (e.g., **72→73**, Equation 4,

Scheme 12.6). The reactions are performed at much higher concentrations (0.05 M) than those typically used in macrocyclization reactions. This could be a consequence of the embedded carbohydrate group, which likely plays a key role in rigidifying the structure, imparting a reactive conformation well disposed to undergo cyclization. Cai and coworkers describe a similar method, in which *ortho*-substituted aromatics are proposed to facilitate macrocyclization [140]. In this work, low catalyst loadings of PdCl$_2$(PPh$_3$)$_2$ and CuI promote effective macrocyclization at 40°C (e.g., **74→75**, Equation 5, Scheme 12.6). The exemplary reaction was performed at a concentration of 0.075 M and afforded macrocycle **75** in 81% yield and could even be conducted at higher

concentration, albeit with a drop in yield (the same reaction at 0.5 M furnished **75** in 51% yield).

The final two examples in this section (Equations 4 and 5, Scheme 12.6) highlight the fact that high yielding Sonogashira macrocyclization reactions are realistic on substrates bearing substituents able to bias the conformation of the linear precursor toward cyclization. However, in general, high dilution and high catalyst loadings are usually required, which is a problem given the relatively high cost and toxicity of Pd catalysts. A potential solution, at least to some of these problems, was first proposed by Collins and coworkers [141] and later studied by Georg [142], who both reported Pd-free variants of Sonogashira macrocyclization reactions. The only metal catalysts in either system are copper based, hence, toxicity and cost concerns are reduced, and competing alkyne dimerization (homocoupling) reactions are also said to be diminished under these reaction conditions. Of course, there is still a need to perform the reactions at high dilution, but, nonetheless, these systems certainly warrant further investigation in the context of macrocyclizations in the future.

12.6 Tsuji–Trost Reaction

Pd-catalyzed allylations of nucleophiles, most commonly active methylenes, enolates, amines, and phenols, with π-allyl complexed electrophiles, derived *in situ* from compounds such as allyl acetates, allyl carbonates, and allyl halides, are commonly referred to as Tsuji–Trost reactions. As with the Heck cyclization just described, intramolecular Tsuji–Trost reactions present the possibility of forming two isomeric rings, depending on the site of attack on the π-allyl complex. [143] The ratio of these two products depends on a variety of factors, but while smaller ring systems (4–9-membered) often afford mixtures of products, in larger systems (>10-membered), terminal substitution products usually predominate, leading to the formation of the larger possible ring size, and this high regioselectivity has led to Tsuji–Trost reactions being widely used to construct complex macrocycles.

The Tsuji–Trost reaction was one of the first Pd-catalyzed coupling reactions to be discovered, in the late 1960s, and was also the earliest to be used as a macrocyclization reaction. The first examples were reported by the groups of Yamamoto [144] and Trost [145], who utilized this method as a key step in the synthesis of natural product targets. Similar reaction conditions were described in both reports (each used Pd(PPh$_3$)$_4$ and NaH, with the Yamamoto report employing additional additives and heating) to deliver humulene (**78**) and exaltolide (**81**), respectively (Equations 1 and 2, Scheme 12.7).

Yamamoto and coworkers used a β-ketoester (**76**) as the nucleophilic component, while Trost used β-ketosulfonyl compound **82** and achieved a higher yield.

The use of 1,3-bis(diphenylphosphino)propane (dppp) in the previous Yamamoto example is the first example of many in which a bidentate phosphine ligand has been used to tune the reactivity of a Tsuji–Trost macrocyclization. This is exemplified by another reaction reported by Trost and coworkers [146], in their synthesis of the antibiotic natural product A26771B (**84**, Equation 3, Scheme 12.7). In this work, it was shown that the nature and stoichiometry of the bidentate phosphine ligand can have a profound impact on macrocyclization; for example, while it was found that dppp or 1,4-bis(diphenylphosphino) butane (dppb, see Equation 3, Scheme 12.7) worked similarly well, it was also found that two equivalents of 1,2-bis(diphenylphosphino)ethane (dppe) relative to the Pd(PPh$_3$)$_4$ catalyst resulted in no cyclization. This was attributed to the formation of a catalytically inactive "Pd(dppe)$_2$" species, which has high stability with respect to ligand dissociation, and is supported by the fact that reducing the number of equivalents of dppe to 1.05 led to the cyclized product being isolated in 59% yield. In all of these cases, the need to exclude oxygen in order to achieve a successful reaction was noted.

Tsuji–Trost macrocyclization reactions have subsequently been used in increasingly complex systems. Sorensen and coworkers reported the syntheses of the polyketide-derived natural product (+)-macquarimicin A (**87**), while Tadano and coworkers described the synthesis of (−)-FR182877 (**90**) [147–150], both using similar synthetic approaches, with a Tsuji–Trost reaction as a key step (Equations 4 and 5, Scheme 12.7). In each report, a β-ketoester was coupled with an allylic carbonate in high yield, at reaction concentrations (0.0027 and 0.005 M, respectively) that compare favorably with related macrocyclizations. In the case of (−)-FR182877, multigram quantities (5.4 g) of a direct precursor to the natural product were accessible via this route.

The popularity of the Tsuji–Trost macrocyclization reaction in natural product synthesis is highlighted by the fact that it has also been used in several other total syntheses not presented in this account [151–158]. High dilution is a common theme in all of the reactions described previously; however, a recent report by Breinbauer and coworkers highlights a potentially useful solution to this problem by using immobilized Pd catalysts [52]. In this work, vinyl epoxide **91** was shown to undergo Tsuji–Trost macrocyclization at a concentration of 0.2 M using Pd on PS resin (1% DVB, 200–400 mesh), to form macrocycle **92** in 45% yield (Equation 1, Scheme 12.8). Attaching reaction substrates onto solid supports is well known to improve the efficiency of macrocyclization by imparting a pseudo-high
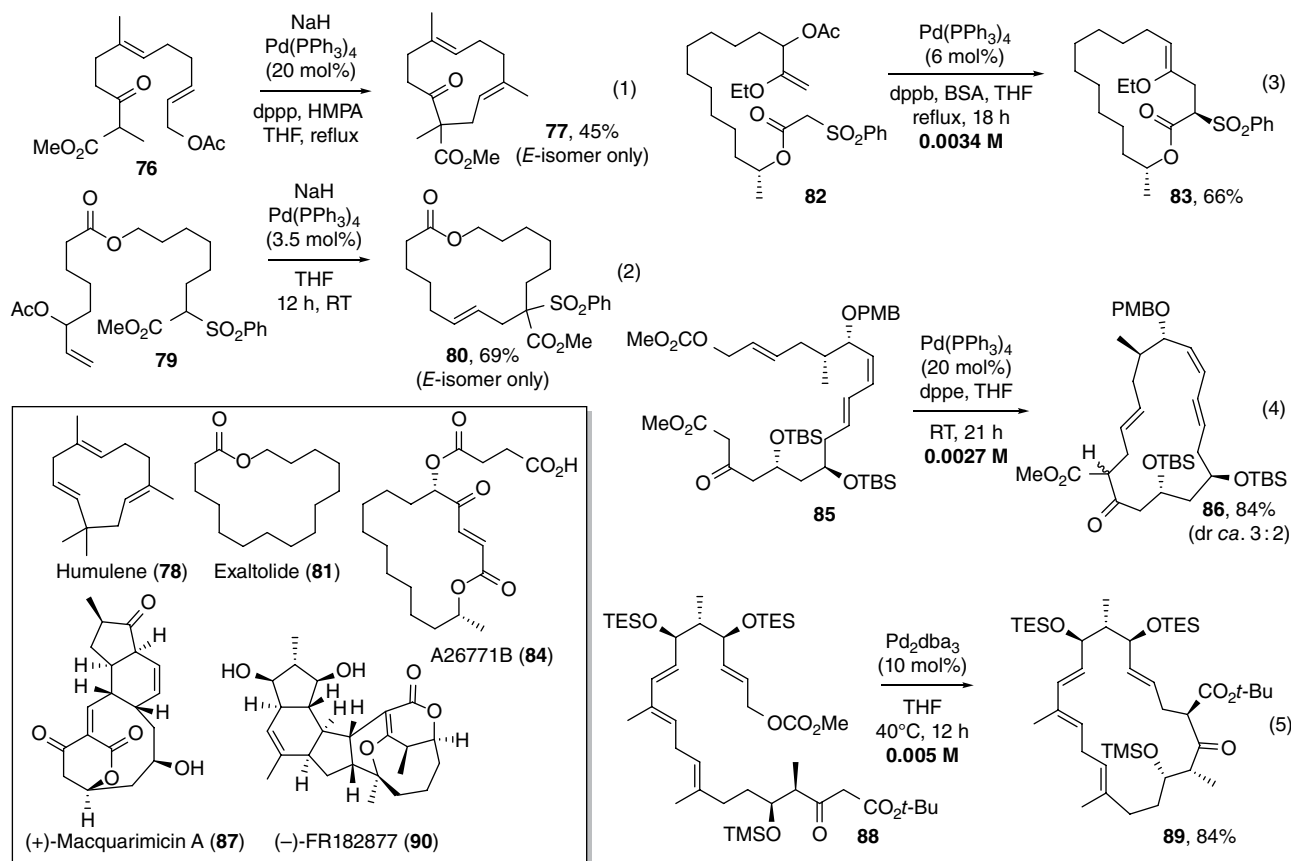
Scheme 12.7 Examples of Tsuji–Trost macrocyclizations in natural product total synthesis.

dilution effect through site isolation [3, 159–161], and there are also examples in which immobilization of the catalyst imparts a similar effect [162, 163]. In this case, a pseudo-dilution effect is proposed to result from intermittent immobilization of the substrate as a Pd-allyl complex within a polymeric bead, which then restricts the conformational reach of the linear precursor and promotes macrocyclization. It is also suggested that intramolecular deprotonation of the carbon pro-nucleophile is assisted by the conformational restrictions imposed by the polymeric bead (depicted in **93**). This is not the first reported example of a Tsuji–Trost cyclization of this type, however, with a similar transformation described by Trost and Warner as early as 1982 [143, 164, 165]. In this work, it was found that by immobilizing Pd onto a PS support, cyclization reactions of vinyl epoxides could be achieved at 0.1–0.5 M concentrations, in cases where the analogous homogeneous reactions were ineffective (e.g., **94 → 95**, Equation 2, Scheme 12.8).

Finally, in a recent publication by Harran and coworkers, a series of impressive macrocyclic etherification reactions between a Pd-allyl complex and a phenol are described [166]. The key design feature of this work is the incorporation of cinnamyl-containing fragment **96**

into the macrocycle precursor (**97**), which is thought to provide a "template" for macrocyclization, effectively by forcing the linear precursor to adopt a conformation that is well disposed to undergo macrocyclization. The relatively ordered nature of the templated compound also means that there is less of an entropic penalty upon macrocyclization than in more conformationally flexible systems. Other examples in which the facility of macrocyclization is promoted by internal structural elements have also been reported [167–170]. The need to include the template in the final product is a limitation of this method, but the broad substrate scope demonstrated, both in terms of compatible functionality and the various ring sizes accessible, that this method has great potential for the synthesis of medicinally important macrocycles. Furthermore, high yields of macrocyclic ethers (**98**) can be formed using comparatively low catalyst loadings (Pd(PPh$_3$)$_4$, 5 mol%) at practical reaction concentrations (up to 0.1 M) using this method (Equation 3, Scheme 12.8).

The catalyst loadings in many of the Tsuji–Trost macrocyclization reactions described in this section compare favorably with other Pd-catalyzed macrocyclization reactions. Furthermore, they typically proceed with high regioselectivity, resulting from nucleophilic attack at the
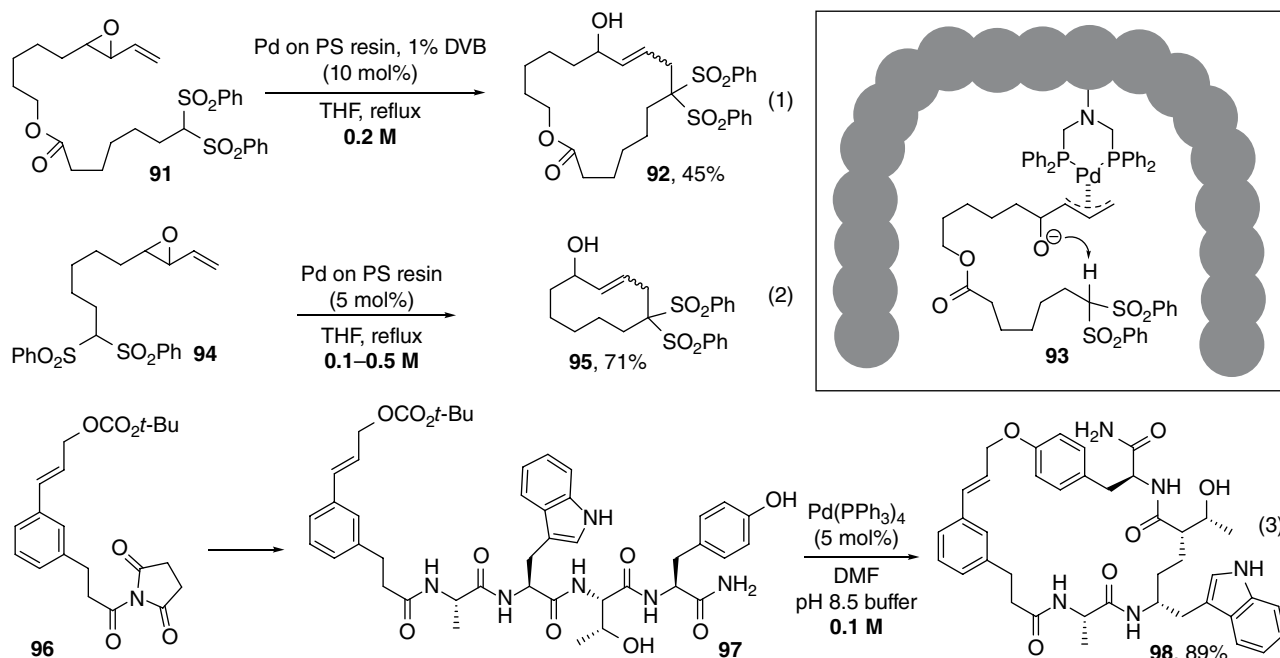
Scheme 12.8 Examples of the use of solid-supported Pd catalysts in Tsuji–Trost macrocyclizations.

terminal site of the intermediate π-allyl complex, which is another key feature of these reactions. The solid supported variants initiated by Trost and coworkers, and expanded upon more recently by Breinbauer and coworkers, are intriguing and certainly warrant further investigation. In particular, extending this immobilized method to other Pd-catalyzed macrocyclization processes would be of interest, although it should be noted that a pseudo-dilution effect was not observed for analogous Sonogashira and Suzuki reactions, so more work will be required before this strategy can be considered to be general. Nonetheless, the resulting benefits in terms of the relatively low catalyst loadings and high reaction concentrations are clear.

12.7 Other Reactions

A number of Pd-catalyzed macrocyclization methods have been developed, which do not fit into any of the previous sections; selected examples of such reactions are detailed in the following, starting with those from natural product synthesis. Denmark and coworkers reported a silicon-assisted Pd-catalyzed macrocyclization during the total synthesis of 12-membered macrocycle oximidine II (**33**) using a modified Hiyama coupling (Equation 1, Scheme 12.9) [171]. The method involves the silicon-assisted cross-coupling reaction of the siloxane ring and an alkenyl iodide moiety of linear precursor **99**, using [Pd(allyl)Cl]$_2$ and TBAF·6H$_2$O in DMF, to form

macrocycle **100** in 74% yield. This method has also been used for the synthesis of medium ring compounds [172] and in the total synthesis of the nine-membered cyclic ether (+)-brasilenyne [173, 174]. Hiyama coupling reactions, and related Hiyama–Denmark coupling reactions, are interesting alternatives to Stille and Suzuki–Miyaura reactions, with the ease of handling and low toxicity of the requisite silane/silanol groups being key features.

Hoye and Wang applied a rarely used Pd-catalyzed allylation reaction, first reported by Kaneda and coworkers [175], to close the macrocyclic ring in their total synthesis of (−)-haterumalide NA (**103**, also known as (−)-oocydin A) [176], a cytotoxic 14-membered macrolactone (Equation 2, Scheme 12.9). In this process, tertiary allylic chloride **101** was found to cyclize onto a terminal alkyne in the presence of PdCl$_2$(PhCN)$_2$, furnishing macrocycle **102**. The overall yield (91%) is excellent, with the product isolated being as a 1 : 1.4 Z : E ratio across the Δ [4,5]-alkene, although, in order to achieve this impressive yield, particularly dilute reaction conditions (0.00035 M) and the slow addition of reagents were both required.

An interesting example of macrocyclization in which the ring-closure is performed via heterocycle synthesis was reported by Boger and coworkers, who employed a Larock indole synthesis as a macrocyclization step in the total synthesis of complestatin (**106**) [177, 178] and also later generalized the method for the synthesis of indole-containing macrocycles [179]. The Larock indole synthesis involves the Pd-catalyzed reaction between a 2-halo-aniline and an
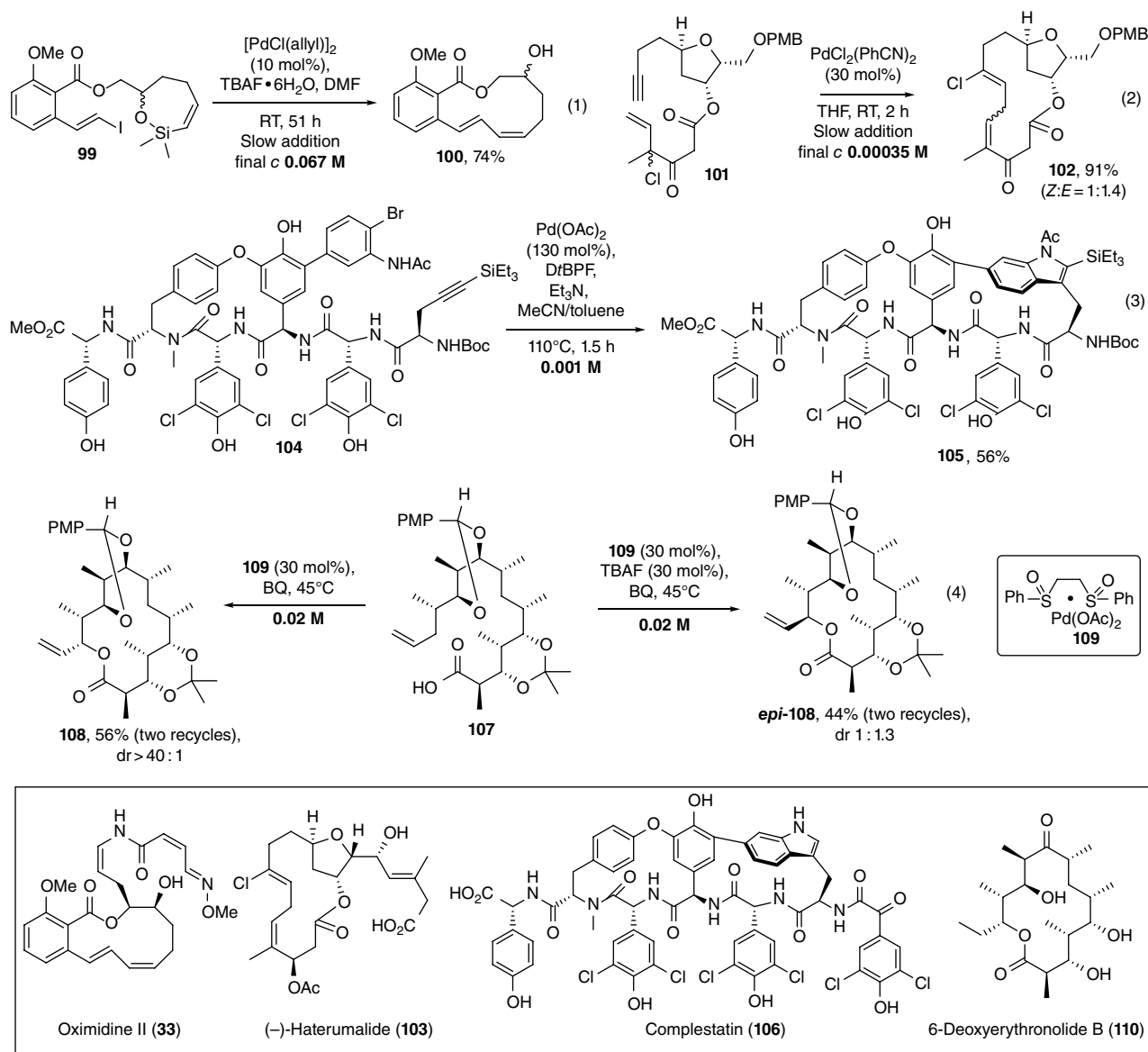
Scheme 12.9 Miscellaneous Pd-catalyzed macrocyclizations in natural product synthesis.

internal alkyne. Optimized reaction conditions were developed (Pd(OAc)$_2$, 1,1′-bis(di-*tert*-butylphosphino)ferrocene (DtBPF), Et$_3$N in toluene/MeCN (1:1) at 110°C, under high dilution conditions, 0.001 M), which were able to promote the conversion of compound **104** into macrocycle **105** at a late stage in the synthesis, with complete *atropo*-diastereoselectivity and in good yield (Equation 3, Scheme 12.9). At the time this work was published, intermolecular variants of the reaction were known [180–182], but this appears to represent the first use of the Larock indole procedure in a macrocyclization.

Selective C–H insertion reactions are of great importance in modern synthetic chemistry as they typically allow complex frameworks to be assembled from simpler

precursors without the need to install additional reactive functionality, improving both the atom economy and step economy of synthetic processes. An impressive demonstration of C–H insertion in a Pd-catalyzed macrocyclization was reported recently by White and coworkers, who employed a late-stage oxidative C–H functionalization in their total synthesis of 6-deoxyerythronolide B **110** (Equation 4, Scheme 12.9) [183, 184]. It was found that precursor **107** reacts to form a single diastereoisomer of the macrolide **108** in 56% yield (after two recycles), upon treatment with catalyst **109** in 1,4-benzoquninone (BQ), at 45°C, at a concentration of 0.02 M, which is relatively high for a macrocyclization reaction [183]. Furthermore, epimeric compound ***epi*-108** could also be formed with
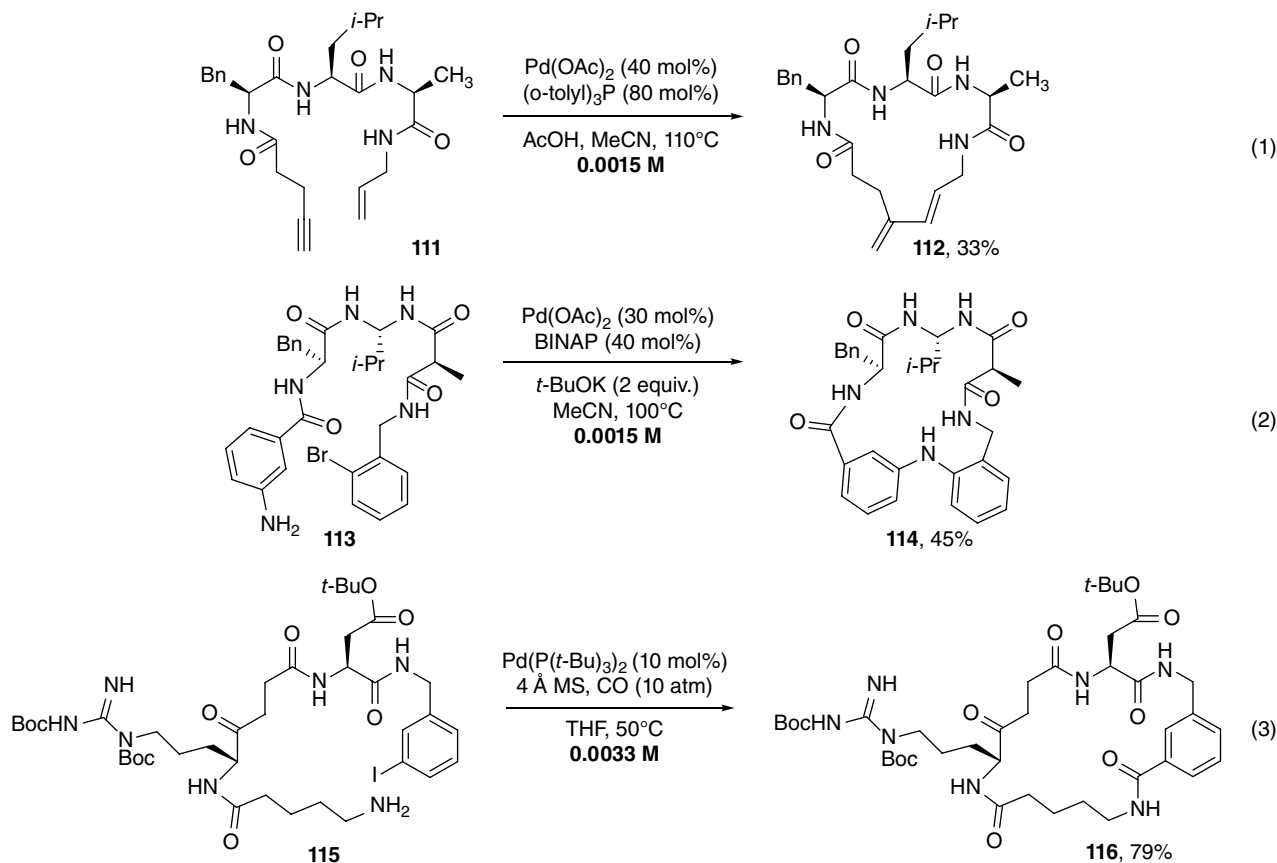
Scheme 12.10 Other Pd-catalyzed reactions in the formation of macrocyclic peptides and peptidomimetic compounds.

high selectivity, although in lower yield and with poorer diastereoselectivity, simply by adding a fluoride source into the reaction, with the switch being attributed to disruption of chelation control in the macrocyclization step. This approach is a clear demonstration of the power of Pd-catalyzed C–H bond activation chemistry in target synthesis, and it is highly likely that much effort will go into the development of related processes in the future.

Iqbal and coworkers reported the use of a Pd-catalyzed enyne cycloisomerization protocol in the synthesis of six 16–19-membered macrocyclic peptidomimetics [185]. Reaction conditions were developed in which Pd(OAc)$_2$ and P(*o*-tol)$_3$ were employed at a relatively high catalyst loading, under typical high dilution conditions in a mixture of acetic acid and acetonitrile at 110°C. Yields ranged from 28 to 54%, with the reaction exemplified in Scheme 12.10. The same group also has reported a strategy for macrocyclic peptidomimetic synthesis using Buchwald–Hartwig C–N coupling [186]. In this work, standard Buchwald–Hartwig coupling conditions are applied using similar catalyst loadings and the same reaction concentration as for the cycloisomerization procedure to form biarylamine-linked peptidomimetics. This is exemplified by the conversion of substrate **113**

into macrocycle **114** (Equation 2, Scheme 12.10), with further 11 examples also being reported (yields 20–65%). An analogous approach has been used by others to access additional medicinally relevant macrocyclic frameworks [187–190].

Finally, Takahashi and coworkers described a single example of a carbonylative macrolactamization from a similar starting material (**115**, Equation 3, Scheme 12.10) to those used by Iqbal and coworkers [191]. In this work, compound **115** was treated with Pd(P(*t*-Bu)$_3$)$_2$, 4 Å molecular sieves, and carbon monoxide (10 atm) to furnish macrocycle **116** in good yield. Significant optimization was performed to achieve this yield, with the choice of THF as solvent proving to be a key factor. The authors subsequently expanded upon this work, using solid-phase peptide synthesis in conjunction with the carbonylative macrocyclization to create a combinatorial library of 24 different macrocyclic peptides [192]. In subsequent work by Alper and Lu, a similar process was reported utilizing Pd-complexed dendrimers on silica gel as the catalyst, which has the added advantage that the catalyst can be recycled [193]. Previous to this work, Takahashi and coworkers reported a conceptually similar carbonylative macrolactonization protocol,

in this case performing the transformation on a polymer support to facilitate macrocyclization [194]. This was employed to successfully construct a small library of 122 macrosphelides.

12.8 Conclusion

This chapter has provided us with a wonderful opportunity to showcase the diverse application of Pd-mediated cross-coupling, as well as related processes, in the synthesis of macrocyclic natural products and nonnatural macrocyclic derivatives. Classical cross-coupling processes, including Heck, Stille, Suzuki–Miyaura, and Sonogashira reactions, have been widely applied. The Tsuji–Trost reaction has emerged as a complementary tool for accessing macrocyclic compounds in an exquisite manner. We are beginning to see the first shoots derived from the seeds spread from the C–H bond activation/functionalization field, promising synthetic methodologies that have been widely developed over the past 10 years or so, with much potential in the field of macrocyclic synthesis. Templating macrocyclization reactions is an intriguing concept and one that can be done in a number of ways, for example, using cations such as Na, K, or Cs derived from a mandatory base, or indeed the Pd catalyst itself, to both template and promote macrocyclization, using the condition deemed most suitable.

It is clear from our survey of this area that there is a definite need for new Pd catalysts (and pre-catalysts) specifically sharpened against macrocyclization synthetic targets. Testing new catalysts/pre-catalysts against substrates beyond the simple benchmark examples is imperative for the field, generally, in our view. It presents a tougher challenge for the catalysis field, but the rewards in terms of application and the resulting accessible molecules are high. A wider exchange of Pd catalysts from laboratory to laboratory, across the globe, could perhaps aid this endeavor. There are clearly hundreds of Pd complexes reported as catalysts/pre-catalysts for cross-coupling of simple substrates, but hardly any of these are applied in more complex synthesis. A good starting place would be their adoption in macrocyclic target-oriented synthesis.

References

1 Ronson, T. O.; Taylor, R. J. K.; Fairlamb, I. J. S. Palladium-Catalysed Macrocyclisations in the Total Synthesis of Natural Products. *Tetrahedron* **2015**, *71*, 989–1009.

2 Zhang, W.; Moore, J. S. Shape-Persistent Macrocycles: Structures and Synthetic Approaches from Arylene and Ethynylene Building Blocks. *Angew. Chem. Int. Ed.* **2006**, *45*, 4416–4439.

3 Marsault, E.; Peterson, M. L. Macrocycles Are Great Cycles: Applications, Opportunities, and Challenges of Synthetic Macrocycles in Drug Discovery. *J. Med. Chem.* **2011**, *54*, 1961–2004.

4 Kitsiou, C.; Hindes, J. J.; I'Anson, P.; Jackson, P.; Wilson, T. C.; Daly, E. K.; Felstead, H. R.; Hearnshaw, P.; Unsworth, W. P. The Synthesis of Structurally Diverse Macrocycles by Successive Ring Expansion. *Angew. Chem. Int. Ed.* **2015**, *54*, 15794–15798.

5 Milstein, D.; Stille, J. K. A General, Selective, and Facile Method for Ketone Synthesis from Acid Chlorides and Organotin Compounds Catalyzed by Palladium. *J. Am. Chem. Soc.* **1978**, *100*, 3636–3638.

6 Milstein, D.; Stille, J. K. Palladium-Catalyzed Coupling of Tetraorganotin Compounds with Aryl and Benzyl Halides. Synthetic Utility and Mechanism. *J. Am. Chem. Soc.* **1979**, *101*, 4992–4998.

7 Farina, V.; Krishnamurthy, V.; Scott, W. J. The Stille Reaction. *Org. React.* **1997**, *50*, 1–652.

8 Farina, V.; Krishnan, B. Large Rate Accelerations in the Stille Reaction with Tri-2-furylphosphine and Triphenylarsine as Palladium Ligands: Mechanistic and Synthetic Implications. *J. Am. Chem. Soc.* **1991**, *113*, 9585–9595.

9 Liebeskind, L. S.; Fengl, R. W. 3-Stannylcyclobutenediones as Nucleophilic Cyclobutenedione Equivalents. Synthesis of Substituted Cyclobutenediones and Cyclobutenedione Monoacetals and the Beneficial Effect of Catalytic Copper Iodide on the Stille Reaction. *J. Org. Chem.* **1990**, *55*, 5359–5364.

10 Farina, V.; Kapadia, S.; Krishnan, B.; Wang, C.; Liebeskind, L. S. On the Nature of the "Copper Effect" in the Stille Cross-Coupling. *J. Org. Chem.* **1994**, *59*, 5905–5911.

11 Harrowven, D. C.; Curran, D. P.; Kostiuk, S. L.; Wallis-Guy, I. L.; Whiting, S.; Stenning, K. J.; Tang, B.; Packard, E.; Nanson, L. Potassium Carbonate-silica: A Highly Effective Stationary Phase for the Chromatographic Removal of Organotin Impurities. *Chem. Commun.* **2010**, *46*, 6335–6337.

12 Stille, J. K.; Tanaka, M. Intramolecular Palladium-Catalyzed Cyclizations of Esters Containing Vinyl Triflate and Vinylstannane Groups at the Termini. Synthesis of Large Ring Lactones. *J. Am. Chem. Soc.* **1987**, *109*, 3785–3786.

13 Duncton, M. A. J.; Pattenden, G. The Intramolecular Stille Reaction. *J. Chem. Soc., Perkin Trans. 1* **1999**, 1235–1246.

14 Pattenden, G.; Sinclair, D. J. The Intramolecular Stille Reaction in Some Target Natural Product Syntheses. *J. Organomet. Chem.* **2002**, *653*, 261–268.

15 Gyorkos, A. C.; Stille, J. K.; Hegedus, L. S. The Total Synthesis of (±)-Epi-jatrophone and (±)-Jatrophone Using Palladium-Catalyzed Carbonylative Coupling of Vinyl Triflates with Vinyl Stannanes as the Macrocycle-Forming Step. *J. Am. Chem. Soc.* **1990**, *112*, 8465–8472.

16 Nicolaou, K. C.; Chakraborty, T. K.; Piscopio, A. D.; Minowa, N.; Bertinato, P. Total Synthesis of Rapamycin. *J. Am. Chem. Soc.* **1993**, *115*, 4419–4420.

17 Smith, A. B.; Condon, S. M.; McCauley, J. A.; Leazer, J. L.; Leahy, J. W.; Maleczka, R. E. Total Synthesis of Rapamycin and Demethoxyrapamycin. *J. Am. Chem. Soc.* **1995**, *117*, 5407–5408.

18 Entwistle, D. A.; Jordan, S. I.; Montgomery, J.; Pattenden, G. Total Synthesis of the Virginiamycin Antibiotic 14,15-Anhydropristinamycin IIB. *J. Chem. Soc., Perkin Trans. 1* **1996**, 1315–1317.

19 Entwistle, D. A.; Jordan, S. I.; Montgomery, J.; Pattenden, G. Total Synthesis of Oxazole-Based Virginiamycin Antibiotics: 14,15-Anhydropristinamycin IIB. *Synthesis* **1998**, 603–612.

20 Panek, J. S.; Masse, C. E. Total Synthesis of (+)-Mycotrienol and (+)-Mycotrienin I. *J. Org. Chem.* **1997**, *62*, 8290–8291.

21 Masse, C. E.; Yang, M.; Solomon, J.; Panek, J. S. Total Synthesis of (+)-Mycotrienol and (+)-Mycotrienin I: Application of Asymmetric Crotylsilane Bond Constructions. *J. Am. Chem. Soc.* **1998**, *120*, 4123–4134.

22 Nicolaou, K. C.; Murphy, F.; Barluenga, S.; Ohshima, T.; Wei, H.; Xu, J.; Gray, D. L. F.; Baudoin, O. Total Synthesis of the Novel Immunosuppressant Sanglifehrin A. *J. Am. Chem. Soc.* **2000**, *122*, 3830–3838.

23 Mitchell, I. S.; Pattenden, G.; Stonehouse, J. P. A Concise Enantioselective Total Synthesis of Rhizoxin D. *Tetrahedron Lett.* **2002**, *43*, 493–497.

24 Mitchell, I. S.; Pattenden, G.; Stonehouse, J. A Total Synthesis of the Antitumour Macrolide Rhizoxin D. *Org. Biomol. Chem.* **2005**, *3*, 4412–4431.

25 Garg, N. K.; Hiebert, S.; Overman, L. E. Total Synthesis of (–)-Sarain A. *Angew. Chem. Int. Ed.* **2006**, *45*, 2912–2915.

26 Becker, M. H.; Chua, P.; Downham, R.; Douglas, C. J.; Garg, N. K.; Hiebert, S.; Jaroch, S.; Matsuoka, R. T.; Middleton, J. A.; Ng, F. W.; Overman, L. E. Total Synthesis of (–)-Sarain A. *J. Am. Chem. Soc.* **2007**, *129*, 11987–12002.

27 Fukuda, H.; Nakamura, S.; Eguchi, T.; Iwabuchi, Y.; Kanoh, N. Concise Total Synthesis of Vicenistatin. *Synlett* **2010**, 2589–2592.

28 Brodmann, T.; Janssen, D.; Kalesse, M. Total Synthesis of Chivosazole F. *J. Am. Chem. Soc.* **2010**, *132*, 13610–13611.

29 Ammer, C.; Bach, T. Total Syntheses of the Thiopeptides Amythiamicin C and D. *Chem. Eur. J.* **2010**, *16*, 14083–14093.

30 Pattenden, G.; Thom, S. M. Polyene Macrolactam Construction Using a Stille Vinyl-Vinyl Coupling Protocol: An Approach to the Antitumour Antibiotic Substance Leinamycin. *Synlett* **1993**, 215–216.

31 Troast, D. M.; Yuan, J.; Porco, J. A. Studies Toward the Synthesis of (–)-Zampanolide: Preparation of the Macrocyclic Core. *Adv. Synth. Catal.* **2008**, *350*, 1701–1711.

32 Boyce, R. J.; Pattenden, G. Sequential sp^2-sp^2 Coupling Reactions in Polyene Macrolide Synthesis. A Novel Approach to Macrolactin A. *Tetrahedron Lett.* **1996**, *37*, 3501–3504.

33 Smith, A. B.; Ott, G. R. Total Syntheses of (–)-Macrolactin A, (+)-Macrolactin E, and (–)-Macrolactinic Acid: An Exercise in Stille Cross-Coupling Chemistry. *J. Am. Chem. Soc.* **1998**, *120*, 3935–3948.

34 Kim, Y.; Singer, R. A.; Carreira, E. M. Total Synthesis of Macrolactin A with Versatile Catalytic, Enantioselective Dienolate Aldol Addition Reactions. *Angew. Chem. Int. Ed.* **1998**, *37*, 1261–1263.

35 Paterson, I.; Brown, R. E.; Urch, C. J. Studies Towards the Synthesis of Lophotoxin and Pukalide: Synthesis of the 14-membered Macrocyclic Core and Some Acyclic Structural Analogues. *Tetrahedron Lett.* **1999**, *40*, 5807–5810.

36 Cases, M.; González-López de Turiso, F.; Pattenden, G. Total Synthesis of the Furanocembrane bis-Deoxylophotoxin. *Synlett* **2001**, 1869–1872.

37 Cases, M.; González-López de Turiso, F.; Hadjisoteriou, M. S.; Pattenden, G. Synthetic Studies Towards Furanocembrane Diterpenes. A Total Synthesis of bis-Deoxylophotoxin. *Org. Biomol. Chem.* **2005**, *3*, 2786–2804.

38 Chen, Q.; Schweitzer, D.; Kane, J.; Davisson, V. J.; Helquist, P. Total Synthesis of Iejimalide B. *J. Org. Chem.* **2011**, *76*, 5157–5169.

39 Deng, H.; Jung, J.-K.; Liu, T.; Kuntz, K. W.; Snapper, M. L.; Hoveyda, A. H. Total Synthesis of Anti-HIV Agent Chloropeptin I. *J. Am. Chem. Soc.* **2003**, *125*, 9032–9034.

40 Fukuyama, Y.; Yaso, H.; Nakamura, K.; Kodama, M. Total Synthesis of Plagiochin D, A Nacrocyclic bis(Bibenzyl) from Liverworts by Intramolecular Still-Kelly Reaction. *Tetrahedron Lett.* **1999**, *40*, 105–108.

41 Fukuyama, Y.; Yaso, H.; Mori, T.; Takahashi, H.; Minami, H.; Kodama, M. Total Syntheses of Plagiochins A and D, Macrocyclic bis(Bibenzyls), by Pd(0) Catalyzed Intramolecular Stille-Kelly Reaction. *Heterocycles* **2001**, *54*, 259–274.

42 Boden, C.; Pattenden, G. Alkenyl Stannane-Allylic Halide Macrocyclisations. An Approach to Amphidinolide A and Related Polyolefin Macrolide Systems. *Synlett* **1994**, 181–182.

43 Lam, H. W.; Pattenden, G. Total Synthesis of the Presumed Amphidinolide A. *Angew. Chem. Int. Ed.* **2002**, *41*, 508–511.

44 Nicolaou, K. C.; Xu, J.; Murphy, F.; Barluenga, S.; Baudoin, O.; Wei, H.; Gray, D. L. Ohshima, T. Total Synthesis of Sanglifehrin A. *Angew. Chem. Int. Ed.* **1999**, *38*, 2447–2451.

45 Unsworth, W. P.; Gallagher, K. A.; Jean, M.; Schmidt, J. P.; Diorazio, L. J.; Taylor, R. J. K. Direct Imine Acylation: Synthesis of the Proposed Structures of 'Upenamide. *Org. Lett.* **2013**, *15*, 262–265.

46 Unsworth, W. P.; Taylor, R. J. K. 'Upenamide: Trials and Tribulations. *Org. Biomol. Chem.* **2013**, *11*, 7250–7261.

47 Müller, H. M.; Delgado, O.; Bach, T. Total Synthesis of the Thiazolyl Peptide GE2270 A. *Angew. Chem. Int. Ed.* **2007**, *46*, 4771–4774.

48 Delgado, O.; Müller, H. M.; Bach, T. Concise Total Synthesis of the Thiazolyl Peptide Antibiotic GE2270 A. *Chem. Eur. J.* **2008**, *14*, 2322–2339.

49 Nicolaou, K. C.; Zou, B.; Dethe, D. H.; Li, D. B.; Chen, D. Y. K. Total Synthesis of Antibiotics GE2270A and GE2270T. *Angew. Chem.* **2006**, *118*, 7950–7956.

50 Shair, M. D.; Yoon, T.; Danishefsky, S. J. A Remarkable Cross Coupling Reaction to Construct the Enediyne Linkage Relevant to Dynemicin A: Synthesis of the Deprotected ABC System. *J. Org. Chem.* **1994**, *59*, 3755–3757.

51 Shair, M. D.; Yoon, T.-Y.; Danishefsky, S. J. Total Synthesis of (±)-Dynemicin A. *Angew. Chem. Int. Ed.* **1995**, *34*, 1721–1723.

52 Brehm, E.; Breinbauer, R. Investigation of the Origin and Synthetic Application of the Pseudodilution Effect for Pd-catalyzed Macrocyclisations in Concentrated Solutions with Immobilized Catalysts. *Org. Biomol. Chem.* **2013**, *11*, 4750–4756.

53 Nicolaou, K. C.; Winssinger, N.; Pastor, J.; Murphy, F. Solid-Phase Synthesis of Macrocyclic Systems by a Cyclorelease Strategy: Application of the Stille Coupling to a Synthesis of (S)-Zearalenone. *Angew. Chem. Int. Ed.* **1998**, *37*, 2534–2537.

54 Kalivretenos, A.; Stille, J. K.; Hegedus, L. S. Synthesis of β-Resorcylic Macrolides Via Organopalladium Chemistry. Application to the Total Synthesis of (S)-Zearalenone. *J. Org. Chem.* **1991**, *56*, 2883–2894.

55 Ronson, T. O.; Carney, J. R.; Whitwood, A. C.; Taylor, R. J. K.; Fairlamb, I. J. S. AsCat and FurCat: New Pd Catalysts for Selective Room-temperature Stille Cross-couplings of Benzyl Chlorides with Organostannanes. *Chem. Commun.* **2015**, *51*, 3466–3469.

56 Ronson, T. O.; Voelkel, M. H. H.; Taylor, R. J. K.; Fairlamb, I. J. S. Macrocyclic Polyenynes: A Stereoselective Route to Vinyl-ether-containing Skipped Diene Systems. *Chem. Commun.* **2015**, *51*, 8034–8036.

57 Ronson, T. O.; Burns, M. J.; Voelkel, M. H. H.; Evans, K. J.; Lynam, J. M.; Taylor, R. J. K.; Fairlamb, I. J. S. Total Synthesis and Stereochemical Revision of Phacelocarpus 2-Pyrone A. *Chem. Eur. J.* **2015**, *21*, 18905–18909.

58 Uenishi, J.; Beau, J. M.; Armstrong, R. W.; Kishi, Y. Dramatic Rate Enhancement of Suzuki Diene Synthesis. Its Application to Palytoxin Synthesis. *J. Am. Chem. Soc.* **1987**, *109*, 4756–4758.

59 Frank, S. A.; Chen, H.; Kunz, R. K.; Schnaderbeck, M. J.; Roush, W. R. Use of Thallium(I) Ethoxide in Suzuki Cross Coupling Reactions. *Org. Lett.* **2000**, *2*, 2691–2694.

60 Amatore, C.; Jutand, A.; Le Duc, G. Mechanistic Origin of Antagonist Effects of Usual Anionic Bases (OH−, CO32−) as Modulated by Their Countercations (Na+, Cs+, K+) in Palladium-Catalyzed Suzuki–Miyaura Reactions. *Chem. Eur. J.* **2012**, *18*, 6616–6625.

61 Miyaura, N.; Suginome, H.; Suzuki, A. New Stereo- and Regiospecific Synthesis of Humulene by Means of the Palladium-Catalyzed Cyclization of Haloalkenylboranes. *Tetrahedron Lett.* **1984**, *25*, 761–764.

62 Nicolaou, K. C.; Nold, A. L.; Milburn, R. R.; Schindler, C. S.; Cole, K. P.; Yamaguchi, J. Total Synthesis of Marinomycins A–C and of Their Monomeric Counterparts Monomarinomycin A and iso-Monomarinomycin A. *J. Am. Chem. Soc.* **2007**, *129*, 1760–1768.

63 Dieckmann, M.; Kretschmer, M.; Li, P.; Rudolph, S.; Herkommer, D.; Menche, D. Total Synthesis of Rhizopodin. *Angew. Chem. Int. Ed.* **2012**, *51*, 5667–5670.

64 Kretschmer, M.; Dieckmann, M.; Li, P.; Rudolph, S.; Herkommer, D.; Troendlin, J.; Menche, D. Modular Total Synthesis of Rhizopodin: A Highly Potent G-Actin Dimerizing Macrolide. *Chem. Eur. J.* **2013**, *19*, 15993–16018.

65 Molander, G. A.; Dehmel, F. Formal Total Synthesis of Oximidine II via a Suzuki-Type Cross-Coupling Macrocyclization Employing Potassium Organotrifluoroborates. *J. Am. Chem. Soc.* **2004**, *126*, 10313–10318.

66 White, J. D.; Jackson, R. W.; Hanselmann, R. Total Synthesis of Rutamycin B via Suzuki Macrocyclization. *Chem. Commun.* **1998**, 79–80.

67 White, J. D.; Hanselmann, R.; Jackson, R. W.; Porter, W. J.; Ohba, Y.; Tiller, T.; Wang, S. Total Synthesis of Rutamycin B, a Macrolide Antibiotic from

Streptomyces Aureofaciens. *J. Org. Chem.* **2001**, *66*, 5217–5231.

68 Wu, B.; Liu, Q.; Sulikowski, G. A. Total Synthesis of Apoptolidinone. *Angew. Chem. Int. Ed.* **2004**, *43*, 6673–6675.

69 Ghidu, V. P.; Wang, J.; Wu, B.; Liu, Q.; Jacobs, A.; Marnett, L. J.; Sulikowski, G. A. Synthesis and Evaluation of the Cytotoxicity of Apoptolidinones A and D. *J. Org. Chem.* **2008**, *73*, 4949–4955.

70 Elder, A. M.; Rich, D. H. Two Syntheses of the 16- and 17-Membered DEF Ring Systems of Chloropeptin and Complestatin. *Org. Lett.* **1999**, *1*, 1443–1446.

71 Shinohara, T.; Deng, H.; Snapper, M. L.; Hoveyda, A. H. Isocomplestatin: Total Synthesis and Stereochemical Revision. *J. Am. Chem. Soc.* **2005**, *127*, 7334–7336.

72 Jia, Y.; Bois-Choussy, M.; Zhu, J. Synthesis of DEFG Ring of Complestatin and Chloropeptin I: Highly Atropdiastereoselective Macrocyclization by Intramolecular Suzuki-Miyaura Reaction. *Org. Lett.* **2007**, *9*, 2401–2404.

73 Wang, Z.; Bois-Choussy, M.; Jia, Y.; Zhu, J. Total Synthesis of Complestatin (Chloropeptin II). *Angew. Chem. Int. Ed.* **2010**, *49*, 2018–2022.

74 Njardarson, J. T.; Biswas, K.; Danishefsky, S. J. Application of Hitherto Unexplored Macrocyclization Strategies in the Epothilone Series: Novel Epothilone Analogs by Total Synthesis. *Chem. Commun.* **2002**, *92*, 2759–2761.

75 Chemler, S. R.; Danishefsky, S. J. Transannular Macrocyclization via Intramolecular B-Alkyl Suzuki Reaction. *Org. Lett.* **2000**, *2*, 2695–2698.

76 Mohr, P. J.; Halcomb, R. L. Total Synthesis of (+)-Phomactin A Using a B-Alkyl Suzuki Macrocyclization. *J. Am. Chem. Soc.* **2003**, *125*, 1712–1713.

77 Kallan, N. C.; Halcomb, R. L. Synthesis of the Ring System of Phomactin D Using a Suzuki Macrocyclization. *Org. Lett.* **2000**, *2*, 2687–2690.

78 Teng, D.; Wang, B.; Augatis, A. J.; Totah, N. I. Studies Toward the Synthesis of Phomactin A. An Approach to the Macrocyclic Core. *Tetrahedron Lett.* **2007**, *48*, 4605–4607.

79 Smith, A. B.; Foley, M. A.; Dong, S.; Orbin, A. (+)-Rimocidin Synthetic Studies: Construction of the C(1–27) Aglycone Skeleton. *J. Org. Chem.* **2009**, *74*, 5987–6001.

80 Roberts, T. C.; Smith, P. A.; Cirz, R. T.; Romesberg, F. E. Structural and Initial Biological Analysis of Synthetic Arylomycin A2. *J. Am. Chem. Soc.* **2007**, *129*, 15830–15838.

81 Dufour, J.; Neuville, L.; Zhu, J. Intramolecular Suzuki–Miyaura Reaction for the Total Synthesis of Signal Peptidase Inhibitors, Arylomycins A2 and B2. *Chem. Eur. J.* **2010**, *16*, 10523–10534.

82 Dufour, J.; Neuville, L.; Zhu, J. Total Synthesis of Arylomycin A2, a Signal Peptidase I (SPase I) Inhibitor. *Synlett* **2008**, *2008*, 2355–2359.

83 Gagnon, A.; Danishefsky, S. J. Evaluation of Diene Hierarchies for Diels–Alder Reactions En Route to Xestocyclamine A: Elaboration of an Ansa Bridge by B-Alkyl Suzuki Macrocyclization. *Angew. Chem. Int. Ed.* **2002**, *41*, 1581–1584.

84 Cochrane, J. R.; White, J. M.; Wille, U.; Hutton, C. A. Total Synthesis of Mycocyclosin. *Org. Lett.* **2012**, *14*, 2402–2405.

85 Esumi, T.; Wada, M.; Mizushima, E.; Sato, N.; Kodama, M.; Asakawa, Y.; Fukuyama, Y. Efficient Synthesis of Isoplagiochin D, A Macrocyclic bis(bibenzyls), by Utilizing an Intramolecular Suzuki–Miyaura Reaction. *Tetrahedron Lett.* **2004**, *45*, 6941–6945.

86 Hioki, H.; Shima, N.; Kawaguchi, K.; Harada, K.; Kubo, M.; Esumi, T.; Nishimaki-Mogami, T.; Sawada, J.-i.; Hashimoto, T.; Asakawa, Y.; Fukuyama, Y. Synthesis of Riccardin C and Its Seven Analogues. Part 1: The Role of Their Phenolic Hydroxy Groups as LXRα Agonists. *Bioorg. Med. Chem. Lett.* **2009**, *19*, 738–741.

87 Lépine, R.; Zhu, J. Microwave-Assisted Intramolecular Suzuki – Miyaura Reaction to Macrocycle, a Concise Asymmetric Total Synthesis of Biphenomycin B. *Org. Lett.* **2005**, *7*, 2981–2984.

88 Bois-Choussy, M.; Cristau, P.; Zhu, J. Total Synthesis of an Atropdiastereomer of RP-66453 and Determination of Its Absolute Configuration. *Angew. Chem. Int. Ed.* **2003**, *42*, 4238–4241.

89 Joo, S.-H. Cyclic Peptides as Therapeutic Agents and Biochemical Tools. *Biomol. Ther.* **2012**, *20*, 19–26.

90 Tapeinou, A.; Matsoukas, M.-T.; Simal, C.; Tselios, T. Review Cyclic Peptides on a Merry-go-round; Towards Drug Design. *Pept. Sci.* **2015**, *104*, 453–461.

91 Li, W.; Burgess, K. A New Solid-phase Linker for Suzuki Coupling with Concomitant Macrocyclization: Synthesis of β-Turn Mimics. *Tetrahedron Lett.* **1999**, *40*, 6527–6530.

92 Lobregat, V.; Alcaraz, G.; Bienayme, H.; Vaultier, M. Application of the "Resin-Capture-Release" Methodology to Macrocyclisation Intramolecular Suzuki-Miyaura Coupling. *Chem. Commun.* **2001**, 817–818.

93 Meyer, F.-M.; Collins, J. C.; Borin, B.; Bradow, J.; Liras, S.; Limberakis, C.; Mathiowetz, A. M.; Philippe, L.; Price, D.; Song, K.; James, K. Biaryl-Bridged Macrocyclic Peptides: Conformational Constraint via Carbogenic Fusion of Natural Amino Acid Side Chains. *J. Org. Chem.* **2012**, *77*, 3099–3114.

94 Afonso, A.; Feliu, L.; Planas, M. Solid-phase Synthesis of Biaryl Cyclic Peptides by Borylation and Microwave-Assisted Intramolecular Suzuki–Miyaura Reaction. *Tetrahedron* **2011**, *67*, 2238–2245.

95 Ostaszewski, R.; Verboom, W.; Reinhoudt, D. N. A Novel Synthesis of Hemispherands. *Synlett* **1992**, *1992*, 354–356.

96 Hensel, V.; Lützow, K.; Schlüter, A.-D.; Jacob, J.; Gessler, K.; Saenger, W. Repetitive Construction of Macrocyclic Oligophenylenes. *Angew. Chem. Int. Ed.* **1997**, *36*, 2654–2656.

97 Hensel, V.; Schlüter, A. D. A Cyclotetraicosaphenylene. *Chem. Eur. J.* **1999**, *5*, 421–429.

98 Huang, W.; Wang, M.; Du, C.; Chen, Y.; Qin, R.; Su, L.; Zhang, C.; Liu, Z.; Li, C.; Bo, Z. Synthesis of Shape-Persistent Macrocycles by a One-Pot Suzuki–Miyaura Cross-Coupling Reaction. *Chem. Eur. J.* **2011**, *17*, 440–444.

99 Link, J. T. The Intramolecular Heck Reaction. *Org. React.* **2004**, *60*, 157–561.

100 Jägel, J.; Maier, M. E. Formal Total Synthesis of Palmerolide A. *Synthesis* **2009**, *17*, 2881–2892.

101 Prasad, K. R.; Pawar, A. B. Enantioselective Formal Synthesis of Palmerolide A. *Org. Lett.* **2011**, *13*, 4252–4255.

102 Lisboa, M. P.; Jones, D. M.; Dudley, G. B. Formal Synthesis of Palmerolide A, Featuring Alkynogenic Fragmentation and syn-Selective Vinylogous Aldol Chemistry. *Org. Lett.* **2013**, *15*, 886–889.

103 Jena, B. K.; Mohapatra, D. K. Formal Total Synthesis of Palmerolide A. *Tetrahedron* **2015**, *71*, 5678–5692.

104 Li, P.; Li, J.; Arikan, F.; Ahlbrecht, W.; Dieckmann, M.; Menche, D. Total Synthesis of Etnangien. *J. Am. Chem. Soc.* **2009**, *131*, 11678–11679.

105 Li, P.; Li, J.; Arikan, F.; Ahlbrecht, W.; Dieckmann, M.; Menche, D. Stereoselective Total Synthesis of Etnangien and Etnangien Methyl Ester. *J. Org. Chem.* **2010**, *75*, 2429–2444.

106 Menche, D.; Li, P.; Irschik, H. Design, Synthesis and Biological Evaluation of Simplified Analogues of the RNA Polymerase Inhibitor Etnangien. *Bioorg. Med. Chem. Lett.* **2010**, *20*, 939–941.

107 Dieckmann, M.; Rudolph, S.; Dreisigacker, S.; Menche, D. Concise Synthesis of the Macrocyclic Core of Rhizopodin by a Heck Macrocyclization Strategy. *J. Org. Chem.* **2012**, *77*, 10782–10788.

108 Menche, D.; Hassfeld, J.; Li, J.; Mayer, K.; Rudolph, S. Modular Total Synthesis of Archazolid A and B. *J. Org. Chem.* **2009**, *74*, 7220–7229.

109 Symkenberg, G.; Kalesse, M. Structure Elucidation and Total Synthesis of Kulkenon. *Angew. Chem. Int. Ed.* **2014**, *53*, 1795–1798.

110 Carr, J. L.; Offermann, D. A.; Holdom, M. D.; Dusart, P.; White, A. J. P.; Beavil, A. J.; Leatherbarrow, R. J.; Lindell, S. D.; Sutton, B. J.; Spivey, A. C. Total Synthesis of (±)-Aspercyclide A and its C19 Methyl Ether. *Chem. Commun.* **2010**, *46*, 1824–1826.

111 Sejberg, J. J. P.; Smith, L. D.; Leatherbarrow, R. J.; Beavil, A. J.; Spivey, A. C. Enantioselective Synthesis of (+)-Aspercyclide A. *Tetrahedron Lett.* **2013**, *54*, 4970–4972.

112 Jeong, S.; Chen, X.; Harran, P. G. Macrocyclic Triarylethylenes via Heck Endocyclization: A System Relevant to Diazonamide Synthesis. *J. Org. Chem.* **1998**, *63*, 8640–8641.

113 Chen, X.; Esser, L.; Harran, P. G. Stereocontrol in Pinacol Ring-Contraction of Cyclopeptidyl Glycols: The Diazonamide C10 Problem. *Angew. Chem. Int. Ed.* **2000**, *39*, 937–940.

114 Li, J.; Jeong, S.; Esser, L.; Harran, P. G. Total Synthesis of Nominal Diazonamides—Part 1: Convergent Preparation of the Structure Proposed for (−)-Diazonamide A. *Angew. Chem. Int. Ed.* **2001**, *40*, 4765–4769.

115 Aeluri, M.; Gaddam, J.; Trinath, D. V. K. S.; Chandrasekar, G.; Kitambi, S. S.; Arya, P. An Intramolecular Heck Approach to Obtain 17-Membered Macrocyclic Diversity and the Identification of an Antiangiogenesis Agent from a Zebrafish Assay. *Eur. J. Org. Chem.* **2013**, *2013*, 3955–3958.

116 Boge, T. C.; Wu, Z.-J.; Himes, R. H.; Vander Velde, D. G.; Georg, G. I. Conformationally Restricted Paclitaxel Analogues: Macrocyclic Mimics of the "Hydrophobic Collapse" Conformation. *Bioorg. Med. Chem. Lett.* **1999**, *9*, 3047–3052.

117 Geng, X.; Miller, M. L.; Lin, S.; Ojima, I. Synthesis of Novel C2–C3 'N-Linked Macrocyclic Taxoids by Means of Highly Regioselective Heck Macrocyclization. *Org. Lett.* **2003**, *5*, 3733–3736.

118 Stocks, M. J.; Harrison, R. P.; Teague, S. J. Macrocyclic Ring Closures Employing the Intramolecular Heck Reaction. *Tetrahedron Lett.* **1995**, *36*, 6555–6558.

119 Ma, S.; Negishi, E.-i. Palladium-Catalyzed Cyclization of ω-Haloallenes. A New General Route to Common, Medium, and Large Ring Compounds via Cyclic Carbopalladation. *J. Am. Chem. Soc.* **1995**, *117*, 6345–6357.

120 Rajamohan Reddy, P.; Balraju, V.; Madhavan, G. R.; Banerji, B.; Iqbal, J. Synthesis of Small Cyclic Peptides via Intramolecular Heck Reactions. *Tetrahedron Lett.* **2003**, *44*, 353–356.

121 Hiroshige, M.; Hauske, J. R.; Zhou, P. Palladium-Mediated Macrocyclization on Solid Support and Its Applications to Combinatorial Synthesis. *J. Am. Chem. Soc.* **1995**, *117*, 11590–11591.

122 Akaji, K.; Kiso, Y. Macrocyclization on Solid Support Using Heck Reaction. *Tetrahedron Lett.* **1997**, *38*, 5185–5188.

123 Akaji, K.; Teruya, K.; Akaji, M.; Aimoto, S. Synthesis of Cyclic RGD Derivatives via Solid Phase

Macrocyclization Using the Heck Reaction. *Tetrahedron* **2001**, *57*, 2293–2303.

124 Chinchilla, R.; Nájera, C. The Sonogashira Reaction: A Booming Methodology in Synthetic Organic Chemistry. *Chem. Rev.* **2007**, *107*, 874–922.

125 Batsanov, A. S.; Collings, J. C.; Fairlamb, I. J. S.; Holland, J. P.; Howard, J. A. K.; Lin, Z.; Marder, T. B.; Parsons, A. C.; Ward, R. M.; Zhu, J. Requirement for an Oxidant in Pd/Cu Co-Catalyzed Terminal Alkyne Homocoupling to Give Symmetrical 1,4-Disubstituted 1,3-Diynes. *J. Org. Chem.* **2005**, *70*, 703–706.

126 Porco, J. A.; Schoenen, F. J.; Stout, T. J.; Clardy, J.; Schreiber, S. L. Transannular Diels–Alder Route to Systems Related to Dynemicin A. *J. Am. Chem. Soc.* **1990**, *112*, 7410–7411.

127 Koyama, Y.; Lear, M. J.; Yoshimura, F.; Ohashi, I.; Mashimo, T.; Hirama, M. Efficient Construction of the Kedarcidin Chromophore Ansamacrolide. *Org. Lett.* **2005**, *7*, 267–270.

128 Mohapatra, D. K.; Bhattasali, D.; Gurjar, M. K.; Khan, M. I.; Shashidhara, K. S. First Asymmetric Total Synthesis of Penarolide Sulfate A1. *Eur. J. Org. Chem.* **2008**, *2008*, 6213–6224.

129 Krauss, J.; Unterreitmeier, D.; Neudert, C.; Bracher, F. Short and Efficient Approach Towards Macrocyclic Lactones Based on a Sonogashira Reaction. *Arch. Pharm.* **2005**, *338*, 605–608.

130 Spivey, A. C.; McKendrick, J.; Srikaran, R.; Helm, B. A. Solid-Phase Synthesis of an A–B Loop Mimetic of the Cε3 Domain of Human IgE: Macrocyclization by Sonogashira Coupling. *J. Org. Chem.* **2003**, *68*, 1843–1851.

131 Balraju, V.; Reddy, D. S.; Periasamy, M.; Iqbal, J. Synthesis of Conformationally Constrained Cyclic Peptides Using an Intramolecular Sonogashira Coupling. *J. Org. Chem.* **2005**, *70*, 9626–9628.

132 Schmittel, M.; Ammon, H. Preparation of a Rigid Macrocycle with Two Exotopic Phenanthroline Binding Sites. *Synlett* **1999**, *6*, 750–752.

133 Yamasaki, R.; Shigeto, A.; Saito, S. Preparation of Shape-Persistent Macrocycles with a Single Pyridine Unit by Double Cross-Coupling Reactions of Aryl Bromides and Alkynes. *J. Org. Chem.* **2011**, *76*, 10299–10305.

134 Miki, K.; Fujita, M.; Inoue, Y.; Senda, Y.; Kowada, T.; Ohe, K. Synthesis of Strained Pyridine-Containing Cyclyne via Reductive Aromatization. *J. Org. Chem.* **2010**, *75*, 3537–3540.

135 Odermatt, S.; Alonso-Gómez, J. L.; Seiler, P.; Cid, M. M.; Diederich, F. Shape-Persistent Chiral Alleno-Acetylenic Macrocycles and Cyclophanes by Acetylenic Scaffolding with 1,3-Diethynylallenes. *Angew. Chem. Int. Ed.* **2005**, *44*, 5074–5078.

136 Chen, G.; Wang, L.; Thompson, D. W.; Zhao, Y. Highly π-Extended TTF Analogues with a Conjugated Macrocyclic Enyne Core. *Org. Lett.* **2008**, *10*, 657–660.

137 ten Brink, H. T.; Rijkers, D. T. S.; Liskamp, R. M. J. Synthesis of Alkyne-Bridged Cyclic Tripeptides Toward Constrained Mimics of Vancomycin. *J. Org. Chem.* **2006**, *71*, 1817–1824.

138 Hussain, A.; Yousuf, S. K.; Kumar, D.; Lambu, M.; Singh, B.; Maity, S.; Mukherjee, D. Intramolecular Base-Free Sonogashira Reaction for the Synthesis of Benzannulated Chiral Macrocycles Embedded in Carbohydrate Templates. *Adv. Synth. Catal.* **2012**, *354*, 1933–1940.

139 Hussain, A.; Yousuf, S. K.; Sharma, D. K.; Mallikharjuna Rao, L.; Singh, B.; Mukherjee, D. Design and Synthesis of Carbohydrate Based Medium Sized Sulfur Containing Benzannulated Macrocycles: Applications of Sonogashira and Heck Coupling. *Tetrahedron* **2013**, *69*, 5517–5524.

140 Niu, T.-F.; Sun, M.; Lv, M.-F.; Yi, W.-B.; Cai, C. Synthesis of Highly Functionalized Macrocycles by Tandem Multicomponent Reactions and Intramolecular Sonogashira Cross-Coupling. *Org. Biomol. Chem.* **2013**, *11*, 7232–7238.

141 Santandrea, J.; Bédard, A.-C.; Collins, S. K. Cu(I)-Catalyzed Macrocyclic Sonogashira-Type Cross-Coupling. *Org. Lett.* **2014**, *16*, 3892–3895.

142 Li, W.; Schneider, C. M.; Georg, G. I. Synthesis of Strained 1,3-Diene Macrocycles via Copper-Mediated Castro–Stephens Coupling/Alkyne Reduction Tandem Reactions. *Org. Lett.* **2015**, *17*, 3902–3905.

143 Trost, B. M. Cyclizations via Palladium-Catalyzed Allylic Alkylations [New Synthetic Methods (79)]. *Angew. Chem. Int. Ed.* **1989**, *28*, 1173–1192.

144 Kitagawa, Y.; Itoh, A.; Hashimoto, S.; Yamamoto, H.; Nozaki, H. Total Synthesis of Humulene. A Stereoselective Approach. *J. Am. Chem. Soc..* **1977**, *99*, 3864–3867.

145 Trost, B. M.; Verhoeven, T. R. Cyclizations via Organopalladium Intermediates. Macrolide formation. *J. Am. Chem. Soc.* **1977**, *99*, 3867–3868.

146 Trost, B. M.; Brickner, S. J. Palladium-Assisted Macrocyclization Approach to Cytochalasins: A Synthesis of Antibiotic A26771B. *J. Am. Chem. Soc.* **1983**, *105*, 568–575.

147 Vosburg, D. A.; Vanderwal, C. D.; Sorensen, E. J. A Synthesis of (+)-FR182877, Featuring Tandem Transannular Diels–Alder Reactions Inspired by a Postulated Biogenesis. *J. Am. Chem. Soc.* **2002**, *124*, 4552–4553.

148 Vanderwal, C. D.; Vosburg, D. A.; Weiler, S.; Sorensen, E. J. An Enantioselective Synthesis of FR182877 Provides a Chemical Rationalization of Its Structure

and Affords Multigram Quantities of Its Direct Precursor. *J. Am. Chem. Soc.* **2003**, *125*, 5393–5407.

149 Munakata, R.; Katakai, H.; Ueki, T.; Kurosaka, J.; Takao, K.-I.; Tadano, K.-I. Total Synthesis of (+)-Macquarimicin A. *J. Am. Chem. Soc.* **2003**, *125*, 14722–14723.

150 Munakata, R.; Katakai, H.; Ueki, T.; Kurosaka, J.; Takao, K.-i.; Tadano, K.-i. Total Synthesis of Macquarimicins Using an Intramolecular Diels–Alder Approach Inspired by a Biosynthetic Pathway. *J. Am. Chem. Soc.* **2004**, *126*, 11254–11267.

151 Trost, B. M.; Verhoeven, T. R. Stereocontrolled Synthesis of (±)-Recifeiolide via Organopalladium Chemistry. *Tetrahedron Lett.* **1978**, *19*, 2275–2278.

152 Trost, B. M.; Cossy, J. Palladium-Mediated Macroheterocyclization. A Synthesis of Inandenin-12-one. *J. Am. Chem. Soc.* **1982**, *104*, 6881–6882.

153 Trost, B. M.; Ohmori, M.; Boyd, S. A.; Okawara, H.; Brickner, S. J. Palladium-Catalyzed Synthesis of Macrocycles. A Total Synthesis of (−)-Aspochalasin B. *J. Am. Chem. Soc.* **1989**, *111*, 8281–8284.

154 Marshall, J. A.; Andrews, R. C.; Lebioda, L. Synthetic Studies on Cembranolides. Stereoselective Total Synthesis of Isolobophytolide. *J. Org. Chem.* **1987**, *52*, 2378–2388.

155 Fürstner, A.; Weintritt, H. Total Synthesis of Roseophilin. *J. Am. Chem. Soc.* **1998**, *120*, 2817–2825.

156 Bitar, A. Y.; Frontier, A. J. Formal Synthesis of (±)-Roseophilin. *Org. Lett.* **2008**, *11*, 49–52.

157 Hu, T.; Corey, E. J. Short Syntheses of (±)-δ-Araneosene and Humulene Utilizing a Combination of Four-Component Assembly and Palladium-Mediated Cyclization. *Org. Lett.* **2002**, *4*, 2441–2443.

158 Sengoku, T.; Xu, S.; Ogura, K.; Emori, Y.; Kitada, K.; Uemura, D.; Arimoto, H. Total Synthesis of the Antibiotic Kendomycin: A Macrocyclization Using the Tsuji–Trost Etherification. *Angew. Chem. Int. Ed.* **2014**, *53*, 4213–4216.

159 Franzyk, H.; Christensen, M. K.; Jørgensen, R. M.; Meldal, M.; Cordes, H.; Mouritsen, S.; Bock, K. Constrained Glycopeptide Ligands for MPRs. Limitations of Unprotected Phosphorylated Building Blocks. *Bioorg. Med. Chem.* **1997**, *5*, 21–40.

160 Herb, C.; Maier, M. E. A Formal Total Synthesis of the Salicylihalamides. *J. Org. Chem.* **2003**, *68*, 8129–8135.

161 Gonthier, E.; Breinbauer, R. Solid-Supported Reagents and Catalysts for the Preparation of Large Ring Compounds. *Mol. Divers.* **2005**, *9*, 51–62.

162 Stille, J. K.; Su, H.; Hill, D. H.; Schneider, P.; Tanaka, M.; Morrison, D. L.; Hegedus, L. S. Synthesis of Large-Ring Keto Lactones by the Homogeneous and Polymer-Supported Palladium-Catalyzed Carbonylative Coupling of Esters Having Vinyl Triflate and Vinylstannane Termini. *Organometallics* **1991**, *10*, 1993–2000.

163 Kelly, A. R.; Wei, J.; Kesavan, S.; Marié, J.-C.; Windmon, N.; Young, D. W.; Marcaurelle, L. A. Accessing Skeletal Diversity Using Catalyst Control: Formation of n and n + 1 Macrocyclic Triazole Rings. *Org. Lett.* **2009**, *11*, 2257–2260.

164 Trost, B. M.; Warner, R. W. Macrocyclization via an Isomerization Reaction at High Concentrations Promoted by Palladium Templates. *J. Am. Chem. Soc.* **1982**, *104*, 6112–6114.

165 Trost, B. M.; Warner, R. W. Macrolide Formation via an Isomerization Reaction. An Unusual Dependence on Nucleophile. *J. Am. Chem. Soc.* **1983**, *105*, 5940–5942.

166 Lawson, K. V.; Rose, T. E.; Harran, P. G. Template-Constrained Macrocyclic Peptides Prepared from Native, Unprotected Precursors. *Proc. Natl. Acad. Sci. U. S. A.* **2013**, *110*, E3753–E3760.

167 Hili, R.; Rai, V.; Yudin, A. K. Macrocyclization of Linear Peptides Enabled by Amphoteric Molecules. *J. Am. Chem. Soc.* **2010**, *132*, 2889–2891.

168 Fu, H.; Chang, H.; Shen, J.; Yu, L.; Qin, B.; Zhang, K.; Zeng, H. An Unusual Macrocyclization Reagent for Highly Selective One-Pot Synthesis of Strained Macrocyclic Aromatic Hexamers. *Chem. Commun.* **2014**, *50*, 3582–3584.

169 White, C. J.; Hickey, J. L.; Scully, C. C. G.; Yudin, A. K. Site-Specific Integration of Amino Acid Fragments into Cyclic Peptides. *J. Am. Chem. Soc.* **2014**, *136*, 3728–3731.

170 Zaretsky, S.; Hickey, J. L.; Tan, J.; Pichugin, D.; St. Denis, M. A.; Ler, S.; Chung, B. K. W.; Scully, C. C. G.; Yudin, A. K. Mechanistic Investigation of Aziridine Aldehyde-driven Peptide Macrocyclization: The Imidoanhydride Pathway. *Chem. Sci.* **2015**, *6*, 5446–5455.

171 Denmark, S. E.; Muhuhi, J. M. Development of a General, Sequential, Ring-Closing Metathesis/Intramolecular Cross-Coupling Reaction for the Synthesis of Polyunsaturated Macrolactones. *J. Am. Chem. Soc.* **2010**, *132*, 11768–11778.

172 Denmark, S. E.; Yang, S.-M. Intramolecular Silicon-Assisted Cross-Coupling Reactions: General Synthesis of Medium-Sized Rings Containing a 1,3-cis-cis Diene Unit. *J. Am. Chem. Soc.* **2002**, *124*, 2102–2103.

173 Denmark, S. E.; Yang, S.-M. Intramolecular Silicon-Assisted Cross-Coupling: Total Synthesis of (+)-Brasilenyne. *J. Am. Chem. Soc.* **2002**, *124*, 15196–15197.

174 Denmark, S. E.; Yang, S.-M. Total Synthesis of (+)-Brasilenyne. Application of an Intramolecular Silicon-Assisted Cross-Coupling Reaction. *J. Am. Chem. Soc.* **2004**, *126*, 12432–12440.

175 Kaneda, K.; Uchiyama, T.; Fujiwara, Y.; Imanaka, T.; Teranishi, S. Selective Codimerization of Acetylenes and Allyl Halides Catalyzed by Palladium Complexes. *J. Org. Chem.* **1979**, *44*, 55–63.

176 Hoye, T. R.; Wang, J. Alkyne Haloallylation [with Pd(II)] as a Core Strategy for Macrocycle Synthesis: A Total Synthesis of (−)-Haterumalide NA/(−)-Oocydin A. *J. Am. Chem. Soc.* **2005**, *127*, 6950–6951.

177 Garfunkle, J.; Kimball, F. S.; Trzupek, J. D.; Takizawa, S.; Shimamura, H.; Tomishima, M.; Boger, D. L. Total Synthesis of Chloropeptin II (Complestatin) and Chloropeptin I. *J. Am. Chem. Soc.* **2009**, *131*, 16036–16038.

178 Shimamura, H.; Breazzano, S. P.; Garfunkle, J.; Kimball, F. S.; Trzupek, J. D.; Boger, D. L. Total Synthesis of Complestatin: Development of a Pd(0)-Mediated Indole Annulation for Macrocyclization. *J. Am. Chem. Soc.* **2010**, *132*, 7776–7783.

179 Breazzano, S. P.; Poudel, Y. B.; Boger, D. L. A Pd(0)-Mediated Indole (Macro)cyclization Reaction. *J. Am. Chem. Soc.* **2013**, *135*, 1600–1606.

180 Larock, R. C.; Yum, E. K. Synthesis of Indoles via Palladium-Catalyzed Heteroannulation of Internal Alkynes. *J. Am. Chem. Soc.* **1991**, *113*, 6689–6690.

181 Larock, R. C.; Yum, E. K.; Refvik, M. D. Synthesis of 2,3-Disubstituted Indoles via Palladium-Catalyzed Annulation of Internal Alkynes. *J. Org. Chem.* **1998**, *63*, 7652–7662.

182 Shen, M.; Li, G.; Lu, B. Z.; Hossain, A.; Roschangar, F.; Farina, V.; Senanayake, C. H. The First Regioselective Palladium-Catalyzed Indolization of 2-Bromo- or 2-Chloroanilines with Internal Alkynes: A New Approach to 2,3-Disubstituted Indoles. *Org. Lett.* **2004**, *6*, 4129–4132.

183 Fraunhoffer, K. J.; Prabagaran, N.; Sirois, L. E.; White, M. C. Macrolactonization via Hydrocarbon Oxidation. *J. Am. Chem. Soc.* **2006**, *128*, 9032–9033.

184 Stang, E. M.; Christina White, M. Total Synthesis and Study of 6-Deoxyerythronolide B by Late-Stage C–H Oxidation. *Nat. Chem.* **2009**, *1*, 547–551.

185 Balraju, V.; Dev, R. V.; Reddy, D. S.; Iqbal, J. Synthesis of Cyclic Peptides Using a Palladium-Catalyzed Enyne Cycloisomerization. *Tetrahedron Lett.* **2006**, *47*, 3569–3571.

186 Balraju, V.; Iqbal, J. Synthesis of Cyclic Peptides Constrained with Biarylamine Linkers Using Buchwald–Hartwig C–N Coupling. *J. Org. Chem.* **2006**, *71*, 8954–8956.

187 Zapf, C. W.; Bloom, J. D.; McBean, J. L.; Dushin, R. G.; Nittoli, T.; Ingalls, C.; Sutherland, A. G.; Sonye, J. P.; Eid, C. N.; Golas, J.; Liu, H.; Boschelli, F.; Hu, Y.; Vogan, E.; Levin, J. I. Design and SAR of Macrocyclic Hsp90 Inhibitors with Increased Metabolic Stability and Potent Cell-Proliferation Activity. *Bioorg. Med. Chem. Lett.* **2011**, *21*, 2278–2282.

188 Zapf, C. W.; Bloom, J. D.; Li, Z.; Dushin, R. G.; Nittoli, T.; Otteng, M.; Nikitenko, A.; Golas, J. M.; Liu, H.; Lucas, J.; Boschelli, F.; Vogan, E.; Olland, A.; Johnson, M.; Levin, J. I. Discovery of a Stable Macrocyclic o-Aminobenzamide Hsp90 Inhibitor which Significantly Decreases Tumor Volume in a Mouse Xenograft Model. *Bioorg. Med. Chem. Lett.* **2011**, *21*, 4602–4607.

189 Zapf, C. W.; Bloom, J. D.; McBean, J. L.; Dushin, R. G.; Golas, J. M.; Liu, H.; Lucas, J.; Boschelli, F.; Vogan, E.; Levin, J. I. Discovery of a Macrocyclic o-aminobenzamide Hsp90 Inhibitor with Heterocyclic Tether that Shows Extended Biomarker Activity and In Vivo Efficacy in a Mouse Xenograft Model. *Bioorg. Med. Chem. Lett.* **2011**, *21*, 3627–3631.

190 Zapf, C. W.; Bloom, J. D.; McBean, J. L.; Dushin, R. G.; Nittoli, T.; Otteng, M.; Ingalls, C.; Golas, J. M.; Liu, H.; Lucas, J.; Boschelli, F.; Hu, Y.; Vogan, E.; Levin, J. I. Macrocyclic Lactams as Potent Hsp90 Inhibitors with Excellent Tumor Exposure and Extended Biomarker Activity. *Bioorg. Med. Chem. Lett.* **2011**, *21*, 3411–3416.

191 Doi, T.; Kamioka, S.; Shimazu, S.; Takahashi, T. A Synthesis of RGD Model Cyclic Peptide by Palladium-Catalyzed Carbonylative Macrolactamization. *Org. Lett.* **2008**, *10*, 817–819.

192 Kamioka, S.; Shimazu, S.; Doi, T.; Takahashi, T. Combinatorial Synthesis of RGD Model Cyclic Peptides Utilizing a Palladium-Catalyzed Carbonylative Macrolactamization on a Polymer Support. *J. Comb. Chem.* **2008**, *10*, 681–690.

193 Lu, S.-M.; Alper, H. Synthesis of Large Ring Macrocycles (12–18) by Recyclable Palladium-Complexed Dendrimers on Silica Gel Catalyzed Intramolecular Cyclocarbonylation Reactions. *Chem. Eur. J.* **2007**, *13*, 5908–5916.

194 Takahashi, T.; Kusaka, S.-I.; Doi, T.; Sunazuka, T.; Ōmura, S. A Combinatorial Synthesis of a Macrosphelide Library Utilizing a Palladium-Catalyzed Carbonylation on a Polymer Support. *Angew. Chem. Int. Ed.* **2003**, *42*, 5230–5234.

13

Alternative Strategies for the Construction of Macrocycles

Jeffrey Santandrea, Anne-Catherine Bédard, Mylène de Léséleuc, Michaël Raymond and Shawn K. Collins

Department of Chemistry and Centre for Green Chemistry and Catalysis, Université de Montréal, Montréal, Québec, Canada

13.1   Introduction

Macrocyclization is recognized as an inherently challenging chemical transformation that in most cases suffers from slow rates of ring closure and subsequent undesirable intermolecular reactions (Chapter 1). Nonetheless, chemists can open the "synthetic toolbox" and exploit various methods for the synthesis of large ring compounds. In a medicinal chemistry context, there are a number of macrocyclization tools that have become commonplace among synthetic practitioners. When common functional groups like esters and amides are found embedded within a macrocyclic framework, chemists can use well-known tools such as activated anhydride reagents for macrolactonizations [1] and peptide coupling reagents for macrolactamizations (Chapter 9) [2]. The construction of an all-carbon tether in a macrocycle is often recognized as arising from another synthetic tool, the olefin metathesis reaction (Chapter 10) [3]. The aforementioned transformations are immensely useful and are the analogous "hammers" and "screwdrivers" of macrocyclization tools. Consequently, these methods traditionally garner much of the focus in published reviews on macrocycle synthesis. However, there are a number of more specialized transformations or tools that can greatly aid in the synthesis of medicinally relevant motifs within macrocyclic skeletons. Often one can rummage to the bottom of the toolbox to find a less common tool, which ends up being ideally suited to the problem at hand. The analogy is no less valid for practitioners of medicinal chemistry. As such, the present chapter aims to provide background into some of the less practiced tools for macrocycle synthesis and highlight how they may be alternatives when some of the "hammers" and "screwdrivers" of macrocycle construction are not the best tools to handle the challenge. To aid the reader, the following chapter is divided into four main subsections, each dealing with a particular bond construction. The subsections include carbon–carbon bond-forming strategies, as well as tools for forming heteroatom-containing motifs such as carbon–oxygen, carbon–nitrogen, and carbon–sulfur bonds. To be noted, this chapter is not an extensive review of all the examples from the literature, and we chose to focus largely on examples drawn from the total synthesis of complex natural products.

13.2   Alternative Methods for Macrocyclization Involving Carbon–Carbon Bond Formation

Carbon–carbon (C–C) bond-forming reactions are traditionally viewed as the most challenging bond construction in organic chemistry. In the past decade, the development of palladium-catalyzed cross-coupling reactions and ruthenium-catalyzed olefin metathesis reactions has provided important tools for medicinal chemists to exploit in the construction of macrocycles via C–C bonds (Chapters 12 and 10, respectively) [3, 4]. The following subsection not only provides some alternative catalytic cross-coupling methods for the synthesis of large ring compounds but also sheds light on other stoichiometric reagent-based methods including enolate and Mitsunobu-based alkylations.

13.2.1   Alkylation

Enolate chemistry is a reliable macrocyclization strategy, which allows the synthesis of macrocycles via C–C bond formation. The total synthesis of biologically active natural products can exploit aldol and Dieckmann reactions [5]. An example of such a strategy was used in the synthesis of the heteroaromatic atropisomeric core of the cytotoxic marine metabolite diazonamide A (Scheme 13.1) [6]. The LDA-promoted macrocyclization
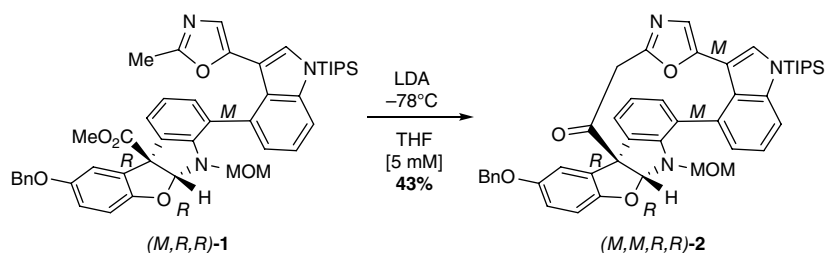
Scheme 13.1 LDA-promoted Dieckmann condensation in the synthesis of diazonamide A.
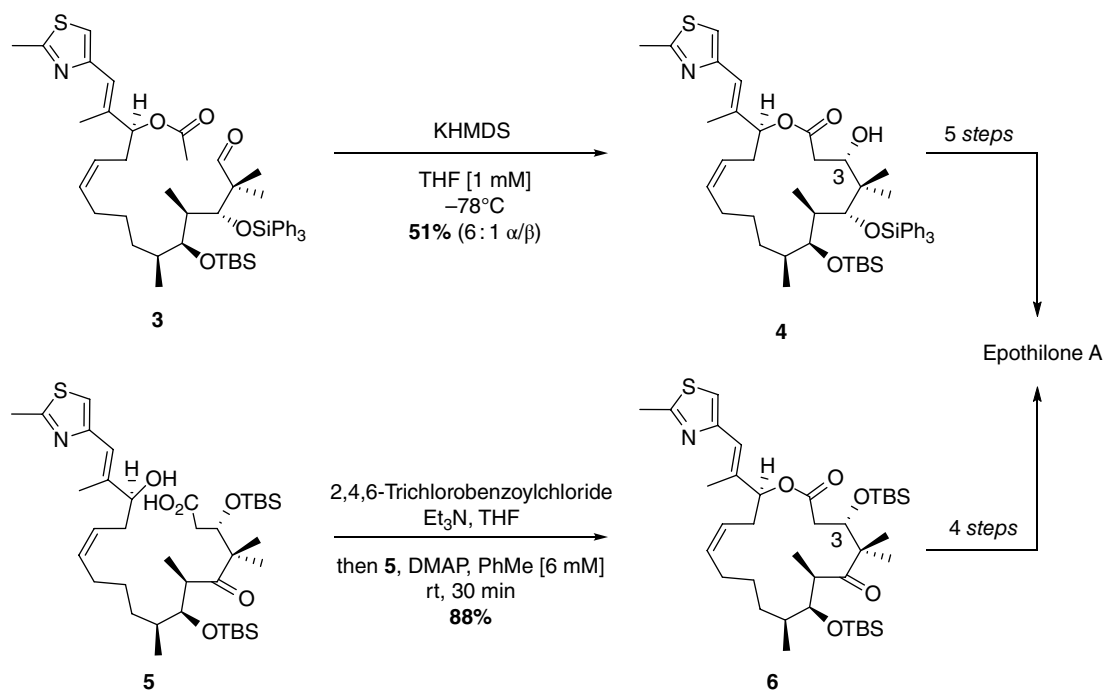
Scheme 13.2 Macroaldolization *versus* macrolactonization in the total synthesis of epothilone A.

was sensitive to temperature, and −78°C was found to be optimal. The reaction proceeded below the threshold required for atropisomer interconversion, and the major atropisomer (**2**) was isolated in 43% yield.

In the total synthesis of epothilones A and B, a macroaldolization reaction was used to prepare the 16-membered macrolide core **4** (Scheme 13.2, *top*) [7]. The aldol reaction was used as an alternative to the macrolactonization strategy (Scheme 13.2, *bottom*). This aldol-based strategy is noteworthy as it allows for installation of the chirality at the C-3 carbon in the ring-closing event, and such chirality-inducing macrocyclization reactions are rare. It is also worth noting that Danishefsky and coworkers accessed the 31-membered ring of the immunosuppressive agent rapamycin via a novel titanium-mediated aldol macrocyclization, where more common lithium- or cerium-based enolates failed [8].

While these enolate-based chemistries focused on anionic intermediates, the generation of radical-based enolate species has also shown synthetic utility in

macrocyclization. For example, macrocycles can be formed via heterodimerization employing a manganese(III)-enolate complex as a carbon radical promoter of β-ketoester enolates. The reaction between oligomethylene-tethered dienes, as well as oxamethylene-tethered dienes [9], and bis(3-oxobutanoate)s in the presence of Mn(OAc)$_3$ at elevated temperature yields macrocycles such as **9** with varying ring sizes (11–32-membered rings) (Scheme 13.3).

Another example of radical-based enolate chemistry for the synthesis of macrocycles was reported by Nicolaou and coworkers, who accessed *exo*-enol ether/cyclic acetal motifs within macrocyclic frameworks from linear precursors containing furanoid β-ketoesters (Scheme 13.4). The macrocyclizations allowed for the synthesis of furanocembranoids, a class of marine diterpenoids that exhibit cytotoxic and antimalarial properties [10]. The authors developed specific conditions to selectively obtain either the monomer **11** (9- to 20-membered rings) or the dimer products **12** (18- to 40-membered rings).

Scheme 13.3 Manganese-catalyzed macrocyclization of oligomethylene-tethered diene **7** and bis(3-oxobutanoate) **8**.
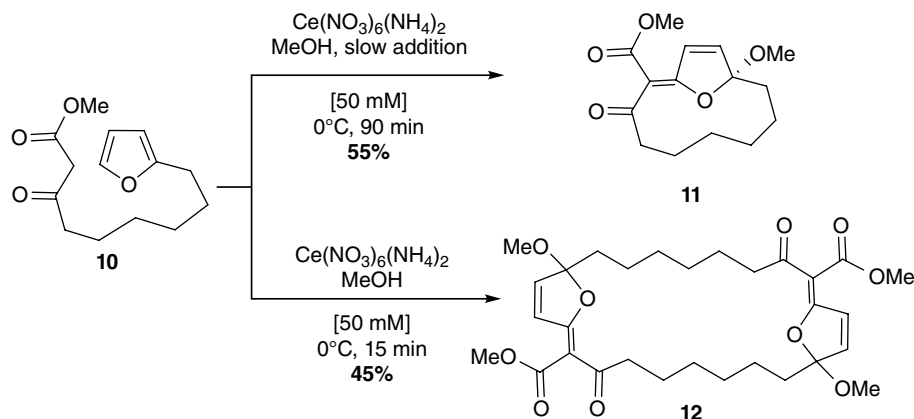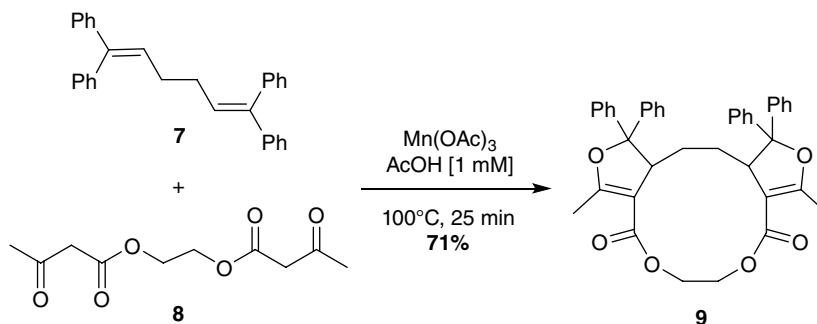
Scheme 13.4 Macrocyclization of β-ketoesters onto furans.

Another type of alkylation useful for macrocycle synthesis is metal-free Friedel–Crafts-type alkylations. Methanesulfonic acid has shown its proficiency to promote macrocyclic alkylations from mixed carbonate-containing peptides. The method efficiently forms large rings without the need of protecting groups in highly functionalized precursors. When the tripeptide Orn-Hyp-Tyr was functionalized with a cinnamyl *t*-butyl carbonate [11], a Brønsted acid was used to decompose the carbonate, forming CO_2, *t*-butanol, and an allyl cation that selectively underwent arylation *ortho* to the tyrosyl phenol (Scheme 13.5). Remarkably, neither the protonated primary amine, the carboxylic acid, nor the secondary alcohol produced any notable side reactions, and the 24-membered ring macrocycle **14** was formed in 70% yield. Subsequently, other substituted phenol analogues, as well as nitrogen-containing heterocycles, were synthesized in order to probe the selectivity of the alkylation site.

13.2.2 Glaser–Hay Coupling

The terminal alkyne is a versatile functionality for use in cross-coupling chemistry, most notably in the Sonogashira cross-coupling. However, the Glaser–Hay oxidative coupling of alkynes is a versatile alternative

for the construction of C–C bonds and macrocycles. The resulting 1,3-dienes can impart geometrically well-defined structures to the corresponding macrocycles, while global hydrogenation provides more flexible saturated alkyl motifs within the macrocycles.

In supramolecular chemistry, crown ether-type macrocycles are highly sought after, most notably for their incorporation into catenanes and rotaxanes [12]. An example of a synthesis of crown ethers was reported by Babu and coworkers, where rigidified polyether macrocycles (**16**) possessing a 1,3-diyne unit were synthesized under oxidative copper catalysis (Scheme 13.6). The procedure gives rise to 18- to 27-membered macrocycles containing various alkyl- and aryl-based linkers despite the presence of the diyne, which imposes certain geometrical restraints. Single crystal X-ray analyses of selected macrocycles illustrated that the 1,3-diyne unit is not linear and may bend up to 18°. Furthermore, the synthetic utility of the diyne moiety was demonstrated by its derivatization to the corresponding thiophene and isoxazole [13].

Other rigidified cyclophane structures could be prepared via Glaser–Hay coupling when employing a conformational control element (CCE). Collins and coworkers reported the cyclization of dialkynes (**17**) using a quinolinium-based additive that affords
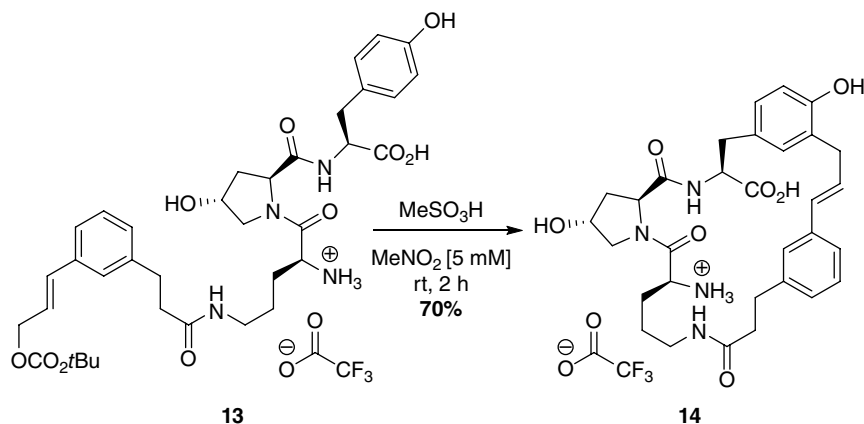
Scheme 13.5 Metal-free Friedel–Crafts-type alkylations on functionalized peptides.
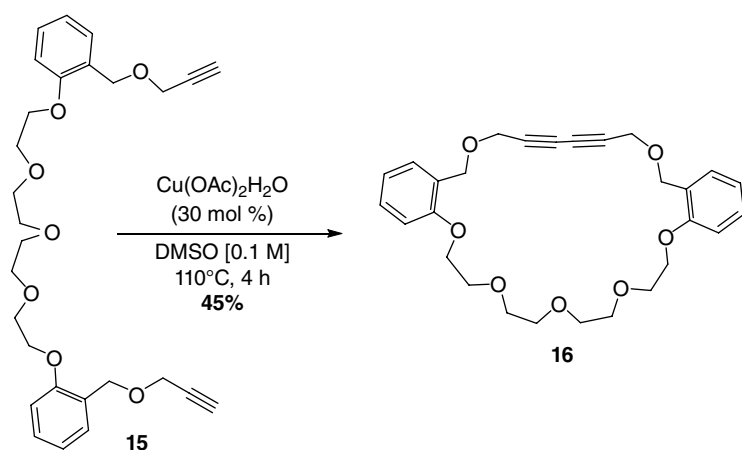
Scheme 13.6 Synthesis of a rigidified polyether macrocycle under oxidative copper catalysis.
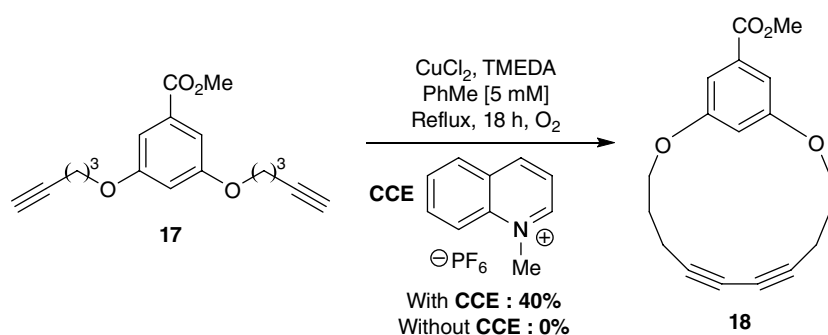
Scheme 13.7 Efficient synthesis of a rigidified cyclophane structure.

cyclophanes (**18**) that are not synthetically accessible by other methods (Scheme 13.7) [14]. The electron-deficient CCE is thought to improve the dialkyne macrocyclization through cation–arene interactions. The interactions are believed to sterically block one face of the arene, influencing the orientation of the side chains to favor the desired macrocyclization.

Additionally, oxidative coupling of alkynes has been used to synthesize a family of optically active cyclophanes capable of carbohydrate recognition. Trimer **20** is obtained in low yield, and after deprotection, the hydroxyl groups of the internal cavity are aligned to coordinate with monosaccharides (Scheme 13.8) [15].

Further, the Glaser–Hay coupling could be successfully applied toward the synthesis of chiral glycophanes. Depending on the linker, 22- or 23-membered rings could be obtained. The authors described the synthesis of the cyclic disaccharide and its dimer, a cyclic tetrasaccharide [16]. Oxidative coupling of acetylenes has also been used to prepare extended alkynyl networks for materials science applications [17, 18]. Industrially relevant macrocycles such as musk-type macrolactones (**22**;
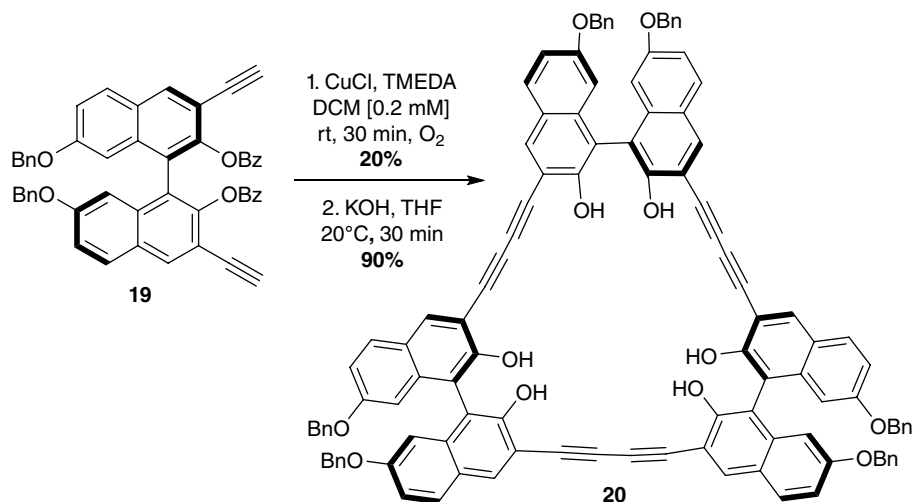
Scheme 13.8 Synthesis of a macrocycle capable of carbohydrate recognition.
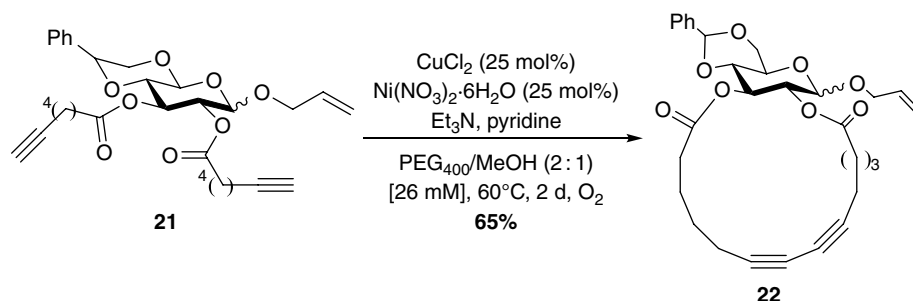
Scheme 13.9 Synthesis of a macrocycle at high concentration using Glaser–Hay coupling.

Scheme 13.10 Glaser–Hay macrocyclization of a macrocyclic lipid under continuous flow conditions.
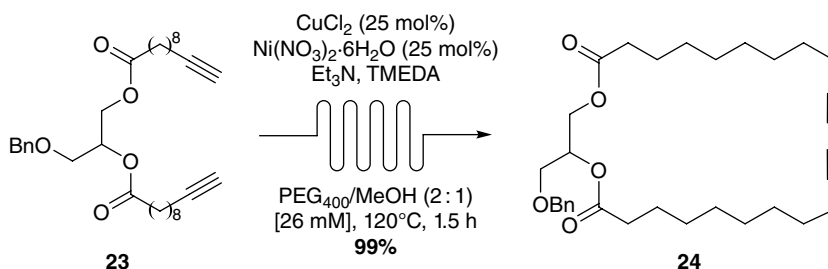
Scheme 13.9) could be efficiently synthesized at high concentration using a phase separation strategy. Of note, the methodology [19] allows for macrocyclization to be conducted at up to 500 times higher concentrations and has been adapted to continuous flow chemistry [20]. The scope of this transformation includes ring sizes ranging from 14- to 28-membered rings and is tolerant to various functional groups (Scheme 13.9).

Similarly, rigidified macrocyclic lipids (**24**) that mimic those found in *archaeal* membranes were synthesized

via Glaser–Hay coupling [20], and the synthesis was amenable to continuous flow conditions (Scheme 13.10).

13.2.3 Nickel/Ruthenium/ Copper-Catalyzed Couplings

Transition metal-catalyzed cross-coupling is a well-established method for forming macrocycles. Palladium-catalyzed transformations such as Suzuki coupling for the formation of C_{sp2}–C_{sp2} bonds or the boro-alkyl

Suzuki coupling for the formation of C_{sp2}–C_{sp3} bonds have been demonstrated for macrocyclization in complex natural product systems (Chapter 12). However, a number of other transition metal-catalyzed reactions can be used to promote the efficient synthesis of macrocycles as well. Nickel catalysis has been widely used in macrocyclization reactions between alkynes and aldehydes (ynals) to achieve structurally diverse connectivity depending on the catalyst system. The preparation of macrocyclic allylic alcohols by the nickel-catalyzed reductive exocyclization of ynals with internal alkynes was initially reported by Jamison and coworkers for the syntheses of amphidinolides T1 and T4 (Scheme 13.11) [21]. It was found that treatment with Ni(COD)$_2$ and basic phosphines, such as PBu$_3$, in the presence of triethylborane could afford the desired 19-membered ring **26** with excellent diastereoselectivity.

Montgomery and coworkers subsequently reported the synthesis of macrocyclic allylic alcohols through the reductive cyclization of ynals in the presence of Ni(COD)$_2$ and *N*-heterocyclic carbenes (NHC) as ligands (Scheme 13.12) [22]. Modification of the catalyst system demonstrated utility toward either endocyclic or exocyclic ligand-controlled reductive cyclizations of ynals. Macrocycles varying in size from 14- to 22-membered rings were generated under optimized conditions when using triethylsilane as the reducing agent. It was shown that terminal alkynes and aryl alkynes display substrate control in regioselection that overrides ligand influences. In contrast, when using aliphatic internal alkynes, it was found that the addition of the most hindered alkyne

terminus (R$_L$) is favored when using bulky ligands, whereas the addition of the least hindered alkyne terminus (R$_S$) is favored by the use of small ligands. The nickel-catalyzed ynal macrocyclization methodology was later applied to the total synthesis of aigialomycin D [23].

Montgomery and coworkers also reported a strategy for regiochemical reversal of late-stage reductive
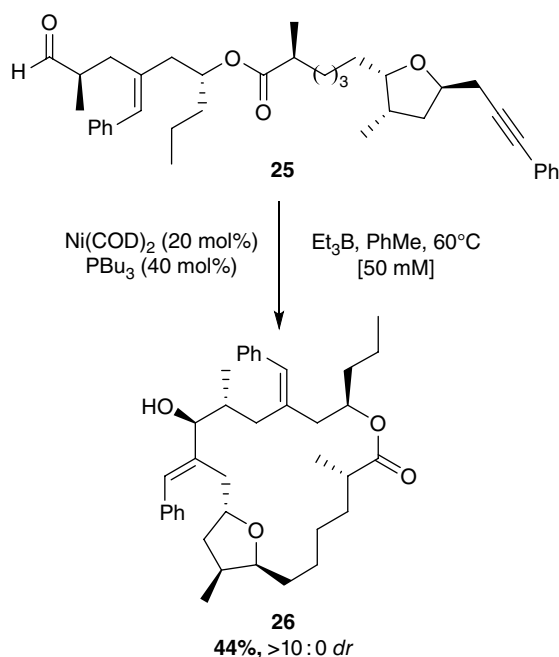
Scheme 13.11 Nickel-catalyzed macrocyclization of an aldehyde and internal alkyne.
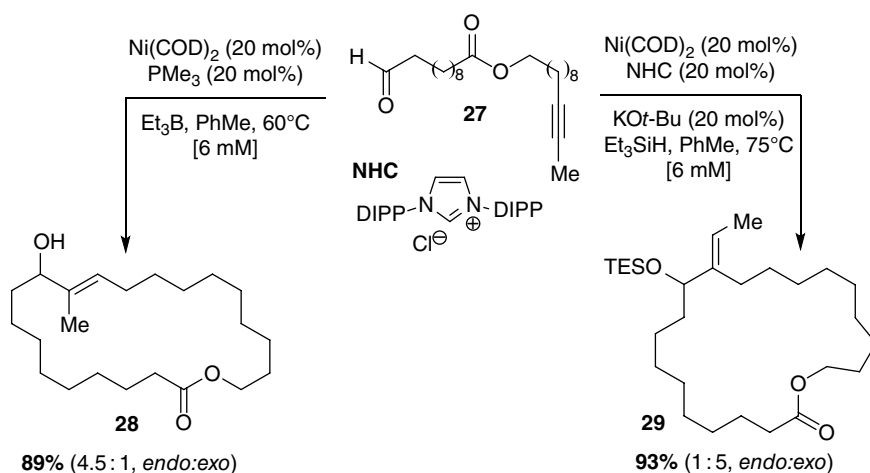
Scheme 13.12 Ligand control in nickel-catalyzed macrocyclizations.
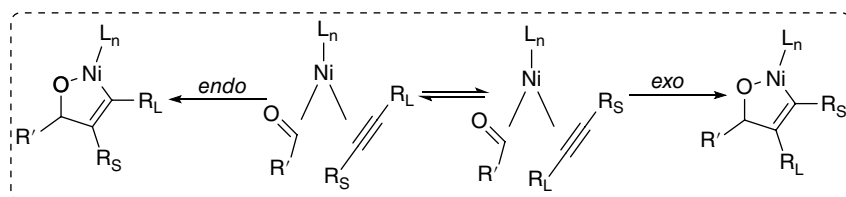
Scheme 13.13 Influence of NHC structure on nickel-catalyzed macrocyclizations.
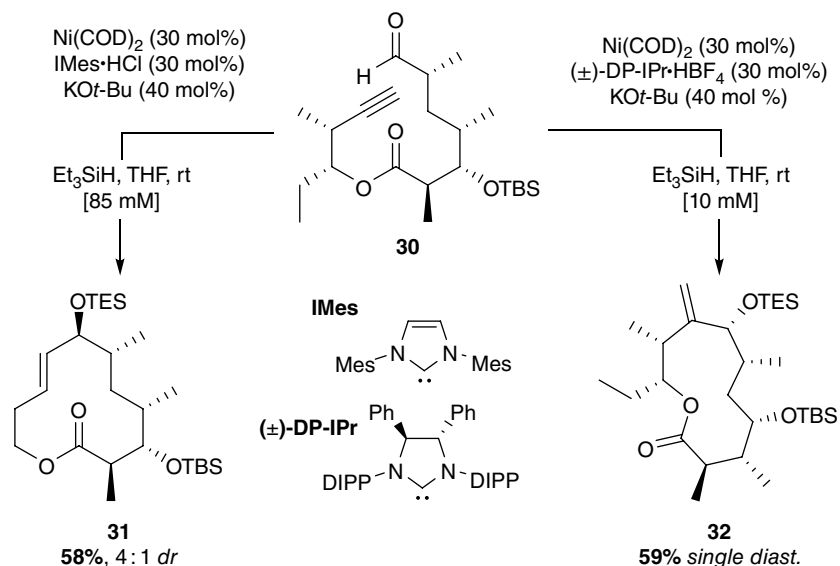
Scheme 13.14 Nickel-catalyzed exo-selective macrocyclization.
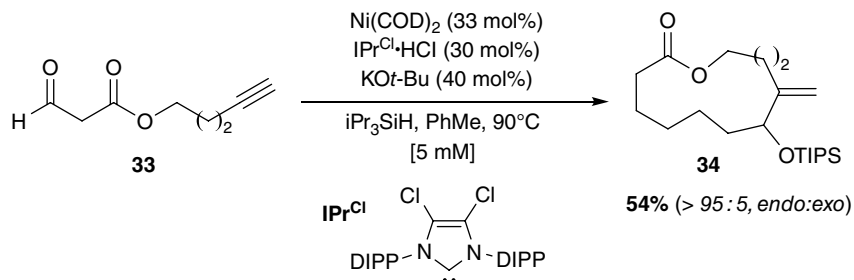
macrocyclizations of aldehydes and terminal alkynes toward the synthesis of macrolides (Scheme 13.13) [24]. It was found that the choice of NHC ligand was crucial for favoring either exo- or endocyclizations from a common intermediate, as only the latter were previously observed for terminal alkyne reductive macrocyclizations. The cyclization of the acyclic ynal precursor was first examined using IMes as ligand, since it is well established for favoring endo-selective macrocyclizations of terminal alkynes. Treatment of the acyclic ynal precursor **30** with Ni(COD)$_2$ and IMes allowed clean production of the 12-membered ring adduct **31** from reductive endocyclization in 58% yield. The macrocycle was then converted to 10-deoxymethynolide to complete an efficient synthesis of the natural product. When modifying the ligand to (±)-DP-IPr under the same reaction conditions, it was found that the acyclic ynal precursor converted into a single regio- and stereoisomer to provide the unnatural 11-membered ring **32** in 59% yield upon exocyclization.

The same group later developed a general exo-selective macrocyclization protocol of terminal alkynes and aldehydes using a slightly modified nickel–NHC complex (Scheme 13.14) [25]. The use of Ni(COD)$_2$ and IPr^{Cl} in the presence of triisopropylsilane offered excellent regioselec-

tivity (exo/endo >95:5) for a series of 10- to 21-membered macrocycles such as **34** bearing an exomethylene substituent in moderate to good yields (45–75%).

Montgomery and coworkers also reported an intramolecular nickel-catalyzed ynal reductive coupling performed asymmetrically when using a chiral NHC complex (Scheme 13.15) [26]. A survey of various C_2-symmetric chiral NHC ligands, readily synthesized from commercially available starting materials, displayed modest to good catalytic activity (40–98%) and enantioselectivity (27–78% *ee*) for the intermolecular system. The optimal reaction conditions could be applied to a broad range of substrates, including a macrocyclic ynal precursor. Upon cyclization, a 14-membered macrocycle (**36**) and 13-membered macrocycle (**37**) were generated in 65% and 11% yields, respectively.

Although ruthenium catalysis for the synthesis of macrocycles has been dominated by olefin metathesis, it can also be used for macrocyclic cycloisomerization reactions from alkenes and alkynes [27]. Trost and coworkers initially reported the use of Cp(COD)RuCl as catalyst to promote a selective and atom economical cyclization. The methodology was applied toward the synthesis of amphidinolide A [28], where the active cationic ruthenium catalyst [CpRu(MeCN)$_3$]PF$_6$ allowed

Scheme 13.15 Enantioselective nickel-catalyzed macrocyclization of an aldehyde and internal alkyne.
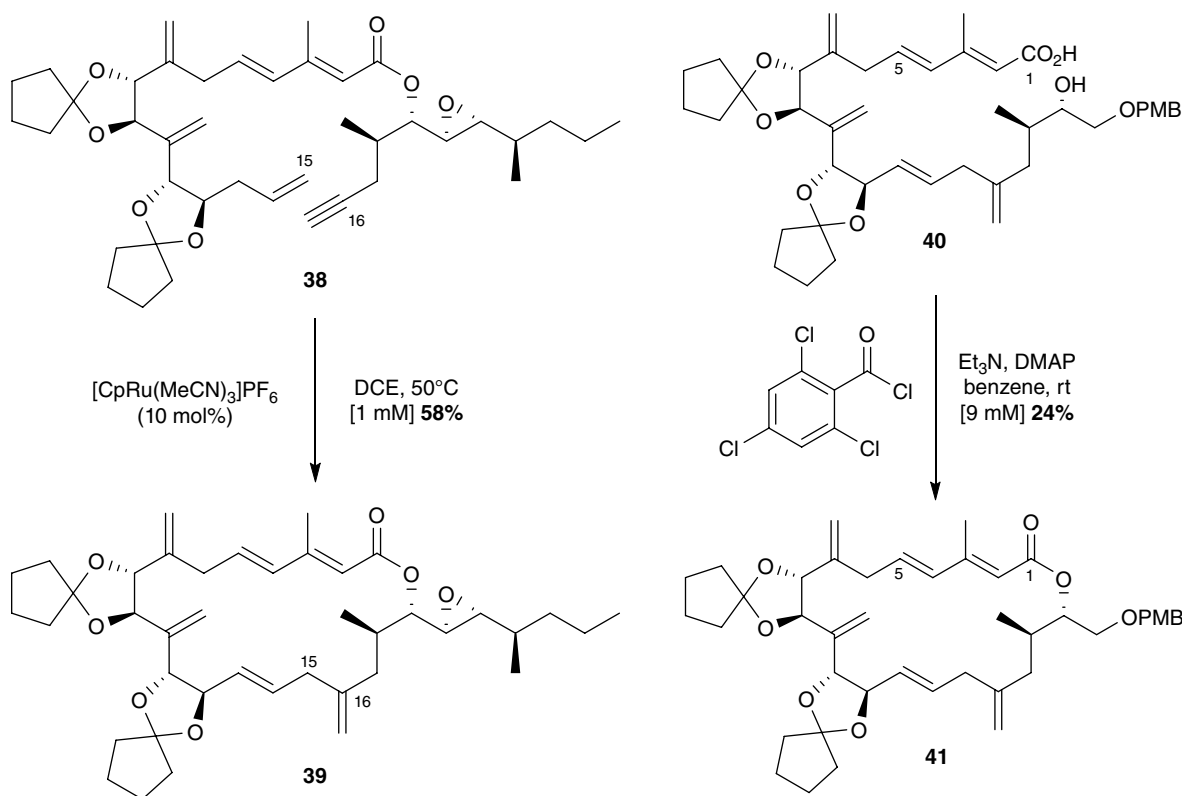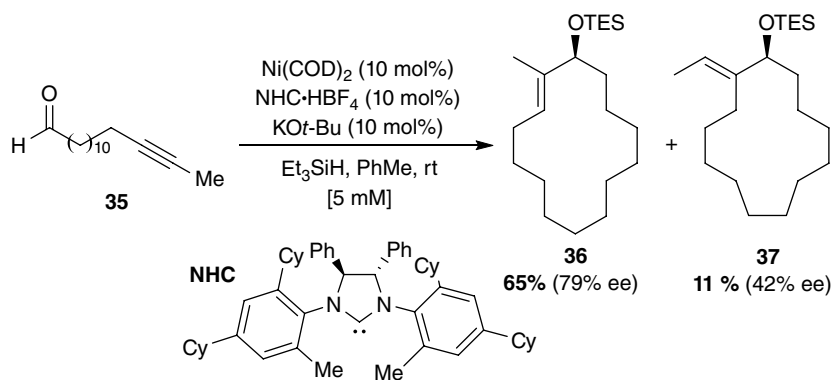
Scheme 13.16 Macrocyclic cycloisomerization toward amphidinolide A.

Scheme 13.17 Macrolactonization toward amphidinolide A.

for intramolecular cycloisomerization of ene–yne **38** to form the C15–C16 bond in 58% yield (Scheme 13.16).

The ruthenium-catalyzed macrocyclization step was actually found to be the most effective route toward the synthesis of amphidinolide A [29]. When macrocyclization was attempted via macrolactonization of seco-acid **40** under standard Yamaguchi conditions, extensive isomerization of the unsaturated C1–C5 portion occurred, providing a number of by-products, and only afforded the desired macrocycle **41** in 24% yield (Scheme 13.17).

The tremendous success of palladium catalysis in cross-coupling reactions is in part due to the high selectivity for predictable bond formation between coupling partners, the generally mild reaction conditions, and wide functional group tolerance. Recently, there has been much interest in alternative metal sources for cross-coupling because of the high cost and low abundance of palladium. A resurgence of first row transition metal catalysis has thus been observed over the past decade in an effort to develop more environmentally benign inter- and intramolecular cross-coupling reactions. Collins and coworkers reported the first macrocyclic

Scheme 13.18 Copper-catalyzed Sonogashira-type cross-coupling toward (S)-zearalane.
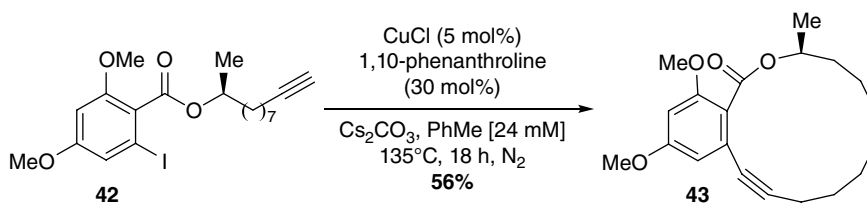
Scheme 13.19 Copper-catalyzed Sonogashira-type cross-coupling with *in situ* reduction to form 1,3-dienes.
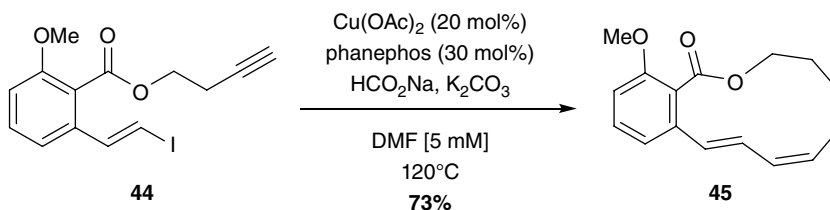
Scheme 13.20 Macrocyclization toward the trienomycins.
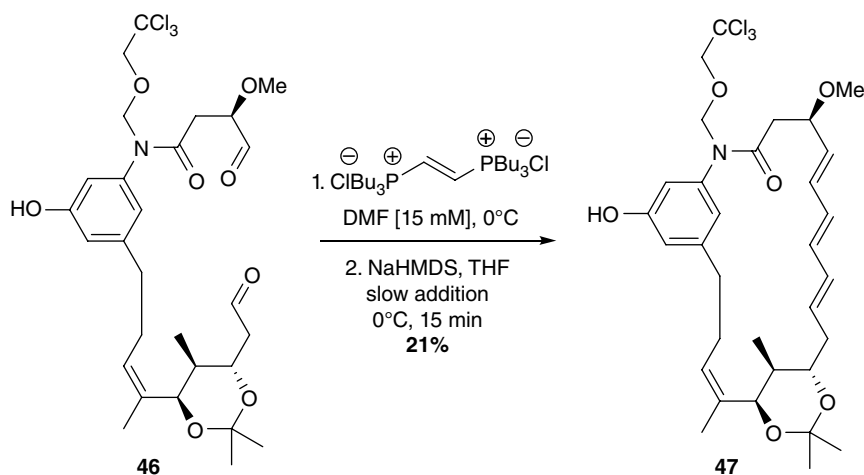
copper-catalyzed Sonogashira-type cross-coupling reaction, which can be used to access 10- to 25-membered macrocycles in modest to good yields (38–83%) (Scheme 13.18) [30]. The CuCl/1,10-phenanthroline catalyst system was found to be more efficient than Pd-catalyzed protocols for the coupling between aryl iodides and aliphatic alkynes. The methodology can be performed at relatively high concentration (24 mM) without the need of slow addition techniques. The optimized protocol was also employed in the synthesis of (S)-zearalane, a member of the resorcyclic acid lactone family.

Georg and coworkers later reported a similar copper-catalyzed Sonogashira-type cross-coupling, followed by a tandem alkyne reduction reaction, to access macrocyclic 1,3-dienes (Scheme 13.19) [31]. The initial ene–yne macrocyclization step with vinyl iodides can be achieved using Cu(OAc)$_2$ with a phosphine-based ligand. It was found that the subsequent alkyne reduction step can occur in the presence of sodium formate as the reducing agent. The methodology can be applied to the synthesis of strained 8- to 13-membered macrocycles in poor to good yield (12–82%) using variable reaction conditions.

A complementary stepwise procedure was also developed for less strained 14- and 17-membered ring systems. The authors utilized the tandem protocol for the syntheses of lactimidomycin [32] and oximidine II, as an alternative to ring-closing metathesis (RCM) reactions, to obtain the desired *E,Z*-configuration of the 1,3-dienes.

13.2.4 Wittig and Other Olefinations

Although the synthesis of macrocyclic olefins is now dominated by catalytic olefin metathesis reactions, the Wittig reaction, including its variants, remains a very popular method for macrocyclic ring closure. With respect to applications in the total synthesis of complex biologically active compounds, a very wide variety of reaction conditions have been reported, which may be in part due to the complexity of the compounds and the necessity to find reaction conditions that tolerate the functionality present in the respective linear precursors [33]. Macrolactams (+)-trienomycins A and F were both synthesized via double Wittig olefination reactions (Scheme 13.20). A diphosphonium salt was coupled with
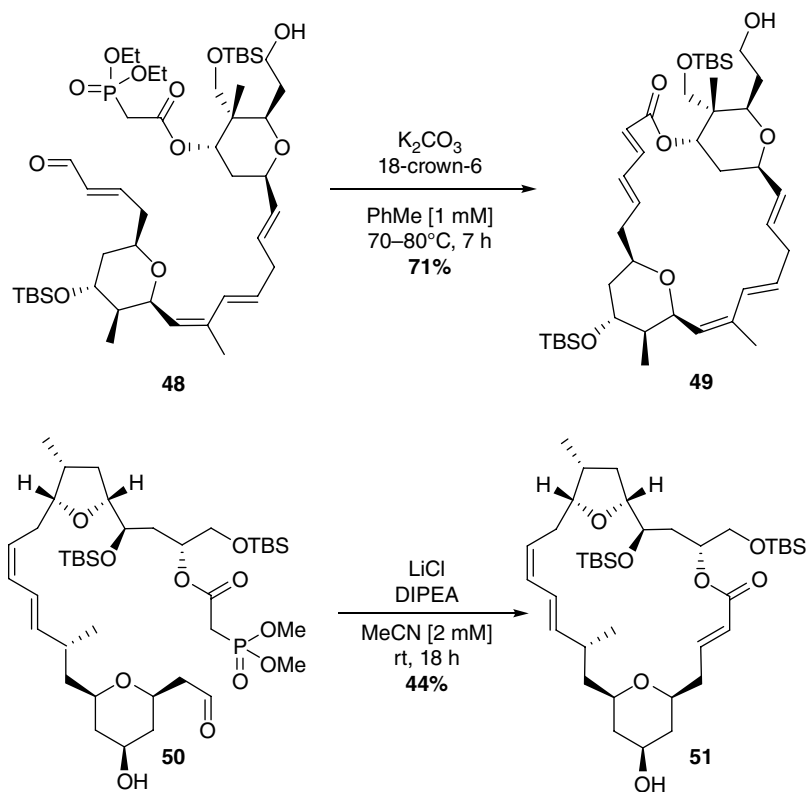
Scheme 13.21 Macrocyclization via Horner–Wadsworth–Emmons or Masamune–Roush reactions.

a bis-aldehyde linear precursor **46** to afford (*E,E,E*)-triene **47** in 21% yield [34]. The Horner–Wadsworth–Emmons modification was employed for the total synthesis of rhizoxin D using Ba(OH)$_2$·H$_2$O as the optimal base for ylide formation, yielding an 18-membered ring in a modest 49% yield [35]. The same reagent was utilized to promote the rapid cyclization of amphidinolide B [36]. Interestingly, in this case, the TPAP oxidation conditions used to form the aldehyde also activated the cyclization. Barium hydroxide was only added to accelerate the rate of the reaction to achieve completion in 4 h.

The Horner–Wadsworth–Emmons method was also used in the synthesis of (+)-lasonolide A (Scheme 13.21, *top*). When linear precursor **48** was exposed to K$_2$CO$_3$/18-crown-6, a 71% yield was achieved as a single diastereoisomer for the newly formed conjugate diene **49** [37]. A variation, using Masamune–Roush conditions (LiCl, DIPEA), was employed to prepare macrocycle **51** in the total synthesis of mandelalide A, which led to structural revision of the natural product (Scheme 13.21, *bottom*) [38].

(+)-Dactylolide was prepared by a Horner–Wadsworth–Emmons macrocyclization after macrolactonization failed using NaHMDS at low temperature to afford the desired macrocycle in 60% yield (Scheme 13.22, *top*) [39]. The synthesis of the macrocyclic portion of

lactimidomycin through olefination was challenging due to competing dimerization under different sets of reaction conditions (e.g., conventional reaction conditions (K$_2$CO$_3$/18-crown-6, LiHMDS, DBU/LiCl) afforded up to 65% of dimer). The solution was the use of an added Lewis acid (Zn(OTf)$_2$) in the presence of both TMEDA and Et$_3$N, providing 12-membered ring **55** in 93% yield [40].

The Still–Gennari olefination has also been employed in the macrocyclization step of the total synthesis of (+)-phorboxazole A (Scheme 13.23). Selectivity issues were observed in the initial attempts at cyclization, where only a 3:2 ratio (*Z*:*E*) was obtained with a 77% yield under K$_2$CO$_3$/18-crown-6 conditions. However, when an adequately protected compound (**56**) was used, the olefination proceeded in good yield (82%) and better *Z*:*E* ratio (3:1) [41].

13.2.5 Cyclopropanation

Macrocyclization reactions via cyclopropanation are rare among catalytic ring-closing reactions, as problematic reactivity is often observed with kinetically accessible functionality to form 5- or 6-membered rings. However, in appropriately functionalized or protected precursors, macrocyclic cyclopropanation can afford efficient cyclization. For example, a catalytic intramolecular

Scheme 13.22 Macrocyclization toward (+)-dactylolide and lactimidomycin.
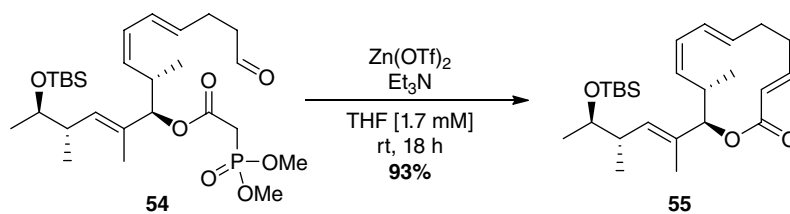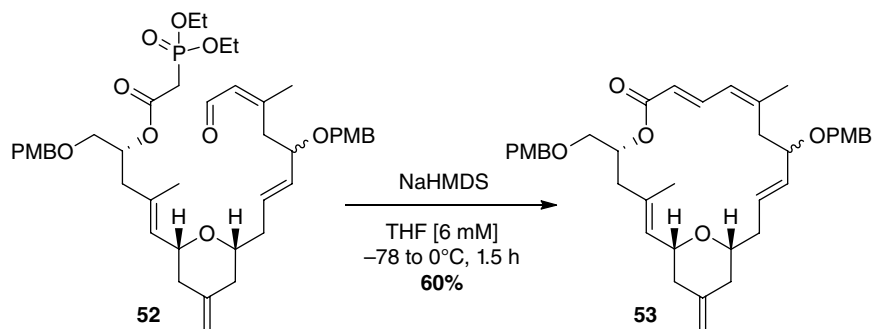
Scheme 13.23 Macrocyclization toward (+)-phorboxazole A.
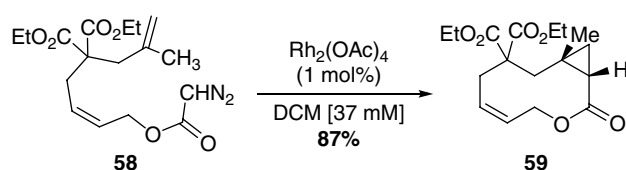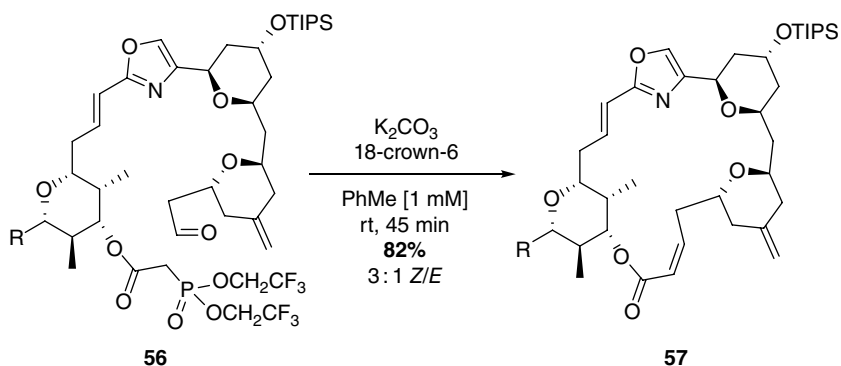
Scheme 13.24 Rhodium-catalyzed intramolecular cyclopropanation by diazoacetates to form macrolactones.

cyclopropanation via diazoacetates to form macrolactones was reported by Doyle and coworkers [42]. High diastereoselectivity can be obtained and is dependent on the ligand used with the transition metal catalyst. Interestingly, when proximal allylic cyclopropanation can be a competing pathway, increasing catalyst electrophilicity actually favors the remote cyclopropanation that leads to the desired macrocyclization product (**59**) in 87% yield (Scheme 13.24) [43].

Doyle and coworkers also demonstrated that the presence of a chiral linker between the reactive functionalities induces diastereoselectivity in the cyclopropanation reaction to be either under substrate or catalyst control (Scheme 13.25). When diazoacetates prepared from the butane-2,3-diacetal of (D)- and (L)-threitol were submitted to a chiral dirhodium(II) carboxamidate-catalyzed ring closure, selectivities up to 91:9 were obtained due to matched pairs between diazoacetate and catalyst. In contrast, the conformational bias inherent in the reactant diazoacetate appears to have minimal influence on diastereoselectivity when using $Cu(MeCN)_4PF_6/(S,S)$-*t*-Bu-BOX [44].

13.2.6 Oxidative Coupling of Arenes

Biaryls are a prevalent structural motif in nature. The oxidative coupling of various arenes has been widely investigated to access biologically relevant macrocycles
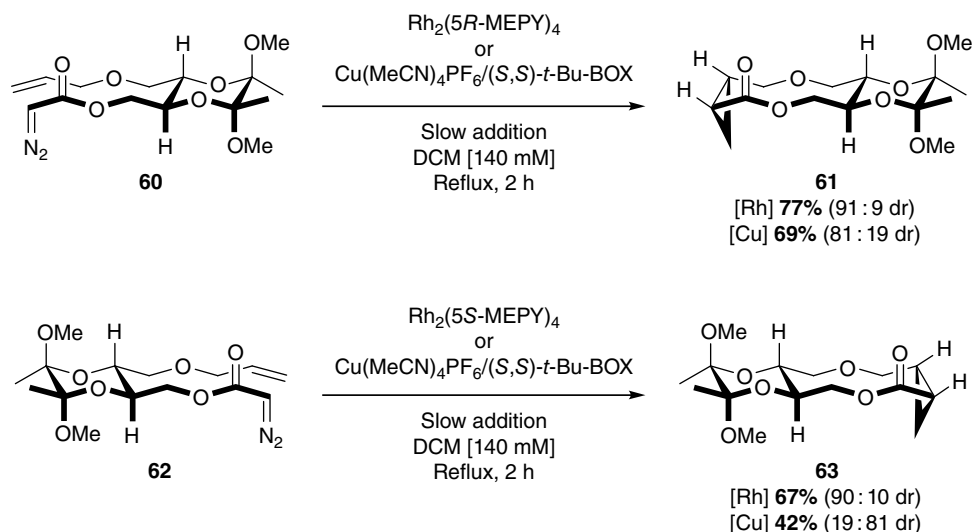
Scheme 13.25 Chiral linkers in rhodium- and copper-catalyzed intramolecular cyclopropanation.
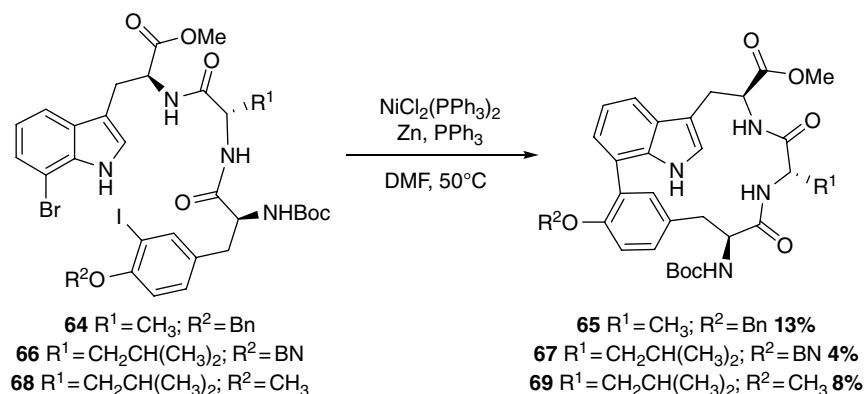
Scheme 13.26 Nickel-mediated oxidative coupling macrocyclization.
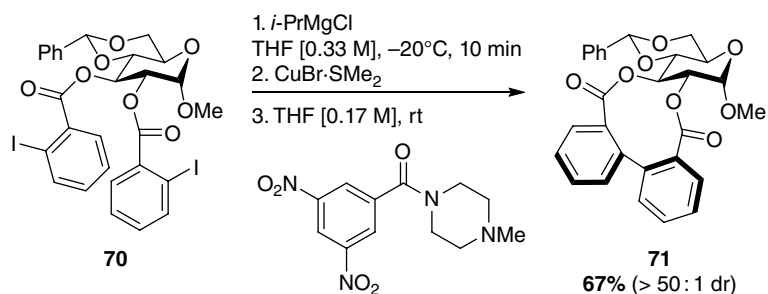
Scheme 13.27 Macrocyclization by organocuprate oxidation.

and is often an alternative to cross-coupling strategies. The most common arenes exploited in oxidative couplings are electron-rich benzene rings such as phenols and heteroarenes such as pyrroles and thiophenes. An example of oxidative coupling of haloarenes is provided in the synthesis of constrained macrocyclic peptide analogues of TMC-95A, a potential proteasome inhibitor. Using a nickel-mediated macrocyclization, various products (**65**, **67**, and **69**) could be formed without the need to protect the indole nitrogen, albeit in very low yields

(Scheme 13.26) [45]. It should be noted that indoles can also be oxidatively coupled using *p*-benzoquinone as a stoichiometric reagent [46].

As well, the oxidative coupling of haloarenes can be accomplished via organocuprate oxidation such as in the macrocyclization toward the synthesis of sanguiin H-5, a member of the ellagitannin family of natural products (Scheme 13.27) [47].

Alternatively, enzyme catalysis can be used to perform macrocyclic oxidative biaryl formation. For example,

Scheme 13.28 Horseradish peroxidase (HRP)-catalyzed macrocyclization toward dihydrolyfoline.
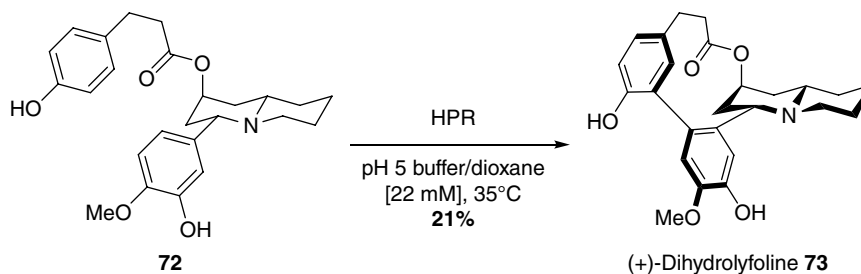
Scheme 13.29 Oxidative macrocyclization of a pentapyrrane bearing two terminal β-linked pyrroles.
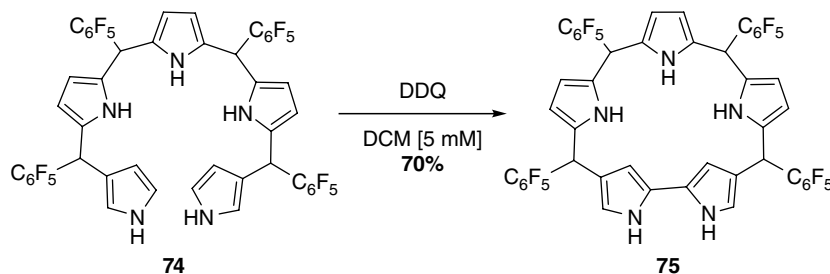
Scheme 13.30 Gold-catalyzed macrocyclization to form cyclobutenes.
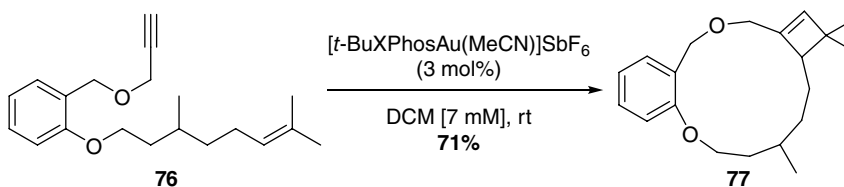
horseradish peroxidase (HRP) was utilized to execute the key macrocyclization step in the synthesis of (+)-dihydrolyfoline **73** and (−)-5-epi-dihydrolyfoline by She and coworkers (Scheme 13.28) [48]. The use of an enzyme allowed for high regioselectivity and diastereoselectivity in the phenolic oxidative coupling. Notably, the reaction conditions provided each macrocycle as a single coupling product.

Porphyrins have found use in medicinal chemistry in photodynamic therapy. Oxidative macrocyclization using DDQ of a pentapyrrane bearing two terminal β-linked pyrroles (**74**) afforded dihydrosapphyrin isomer **75** (Scheme 13.29). The pyrroles are linked in a rare β,α-α,β mode that make it rather reactive toward ring contraction and expansion [49]. A similar 2,2′-bipyrrole oxidative cyclization was used in the synthesis of a cyclo[8]pyrrole with eight 9,10-dihydroanthracene wings [50].

13.2.7 Gold Catalysis

Gold catalysis has emerged as a powerful tool for the creation of new carbon–carbon bonds with unsaturated functionalities such as alkenes, alkynes, and allenes due to the carbophilic properties of gold. Echavarren and coworkers have reported multiple intermolecular and intramolecular gold(I)-catalyzed [2+2] cycloadditions

between terminal alkynes and alkenes, leading to the construction of various cyclobutene-containing small molecules [51]. The methodology was further extended to the formation of 9- to 15-membered macrocycles such as **77** (Scheme 13.30) incorporating a cyclobutene moiety from larger 1,n-enynes ($n = 10$–16) in moderate to good yield (20–71%) [52]. The reaction requires the use of a gold(I) catalyst bearing a sterically hindered biphenylphosphine ligand under mild conditions. It was found that a phenyl ring in the spacer of the acyclic precursor was necessary to favor reactivity, as aliphatic precursors did not react under the optimized reaction conditions. The protocol can also be applied to access *m*-cyclophanes in good yield (70–71%).

Sun and coworkers reported the use of *t*-BuXPhosAuCl in the presence of NaBARF for the intramolecular coupling of diazo compounds to produce cyclic olefins (Scheme 13.31) [53]. It was shown that the *Z*/*E* selectivity of the generated olefins highly depends on the ring size of the product macrocycles. The optimized conditions offer olefins with high *Z* selectivity (up to >20:1) when forming 12- to 18-membered rings from acyclic bis-diazoacetate precursors. As an illustration, the diazo precursor **78** is cyclized in 54% yield to the macrocyclic olefin **79**. However, the selectivity is reversed when generating 19- to 24-membered macrocycles within the same class of compounds. A similar trend was observed when using
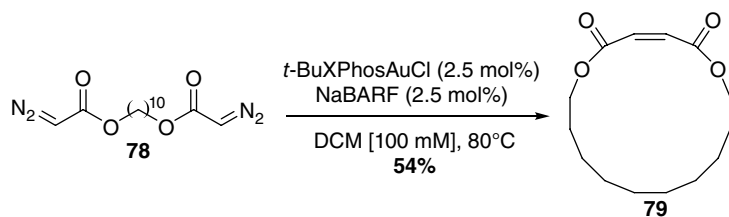
Scheme 13.31 Gold-catalyzed olefination.
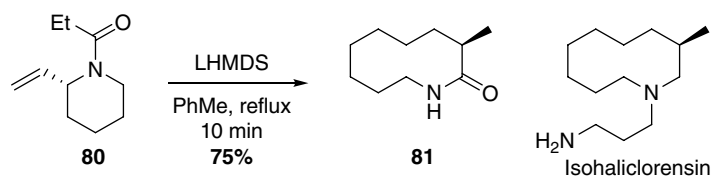
Scheme 13.32 Aza-Claisen ring expansion in the total synthesis of isohaliclorensin.
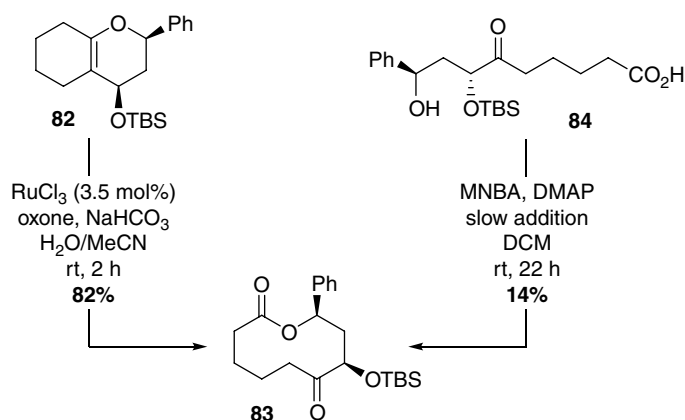
Scheme 13.33 Comparison between ring expansion and lactonization routes for the synthesis of macrolactones.

bis-diazocarbonyl substrates. In that series, smaller 8-membered rings tended to favor olefins with high *Z* selectivity, whereas larger 12- to 18-membered rings favored olefins with high *E* selectivity.

13.3 Alternative Methods for Macrocyclization Involving Carbon–Carbon Bond Formation: Ring Expansion and Photochemical Methods

Ring expansion techniques have been recognized for over 50 years as one of the most efficient ways to prepare large ring compounds [54]. The following section presents a few of the more recent developments for the synthesis of macrocycles via such techniques, as well as photochemical methods.

13.3.1 Ring Expansion

A ring expansion strategy, often involving fragmentation of a bicyclic system to form a monocyclic compound possessing a larger ring, is a useful synthetic alternative

to the cyclization of a linear precursor to form a macro-cycle. Ten-membered rings are among the most difficult to form via macrocyclization [55]. Huang and coworkers used an aza-Claisen ring expansion strategy in the total synthesis of the 10-membered marine alkaloid isohali-clorensin (Scheme 13.32) [56].

Similarly, oxidative cleavage of a bridging double bond in polycyclic enol ether **82** was used by Tan to afford macrolactones such as **83** [57]. Interestingly, the authors compared the lactonization reaction of the corresponding seco-acid **84** to the ring expansion strategy, and the latter afforded superior yields (Scheme 13.33). While the just-described methods involve ring expansions of up to 4 atoms, the most common is of a single atom. Examples successfully applied to macrocycles include the Baeyer–Villiger oxidation [58] and the Stevens rearrangement [59].

Ring expansion has been extensively exploited in the synthesis of macrocyclic musks, an important family of industrially relevant macrocycles. Exaltolide®, a 16-membered example of this compound class, can be formed using the Story ring expansion. The macrocycle can be formed by condensation of peroxides with ketones, such as **85**, which can then decompose either

thermally or photochemically to afford macrolactone **86** (Scheme 13.34) [60]. It should be noted that this strategy can be used to form various ring sizes depending on the number of carbons in the peroxide precursor.

Another example of musk synthesis via ring expansion was reported by Rüedi, involving a thermal three-carbon ring expansion from cyclopropane-bearing precursor **87** to obtain the corresponding enone **88** by means of flash vacuum pyrolysis (FVP), which, following hydrolysis, yields macrocyclic musk **89** (Scheme 13.35) [61]. A ring expansion was also used to obtain the 10-membered macrolactam in the synthesis of an NEP inhibitor by MacPherson [62].

Trans-lactonization is also a commonly employed ring expansion strategy. When the 12-membered lactone **90** was submitted to acidic conditions, trans-lactonization to the thermodynamically more stable 15-membered macrolactone **91** was observed (Scheme 13.36) [63]. Similarly, an unexpected ring expansion of the bryolactone core to generate the corresponding 21-membered ring analogue was reported by Keck [64].

Tan and coworkers reported that macrocyclic ketones can also be obtained by Grob fragmentation of a tricyclic system under acidic conditions [65]. The authors were able to synthesize a library of medium-sized macrocycles such as **93** by acid-mediated ring expansion substrates such as **92** (Scheme 13.37).

Grubbs and coworkers have used a ring expansion strategy relying on olefin metathesis to access a wide variety of macrocyclic structures. The process involves expansion of a small ring such as cyclopentene **95** onto a linear diene such as **94** in the presence of a Ru catalyst to afford the corresponding macrocycle **96** in 52% yield (Scheme 13.38). As such, the expansion exploits three types of olefin metathesis processes (ring opening, cross, and ring closing) and can form macrocycles ranging from 19- to 28-membered rings [66].

Scheme 13.34 Story's synthesis of Exaltolide®.
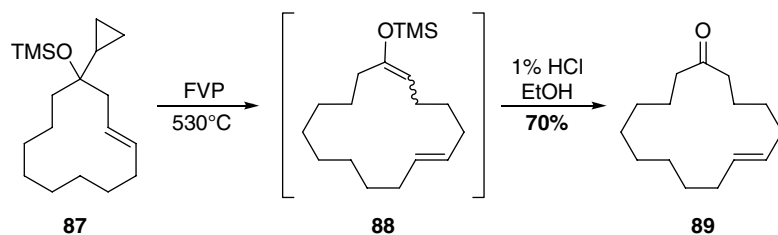
Scheme 13.35 Ring expansion via opening of cyclopropane moiety.
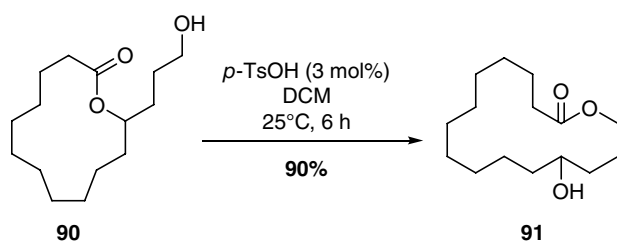
Scheme 13.36 Trans-lactonization ring expansion reaction.
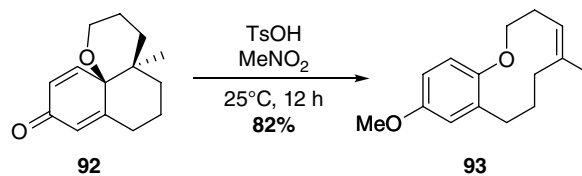
Scheme 13.37 Ring expansion via Grob fragmentation.
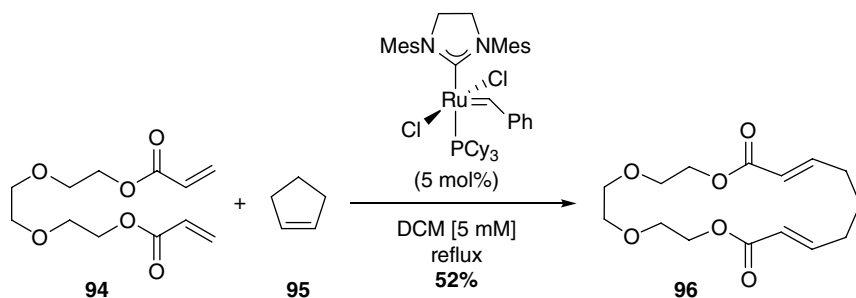
Scheme 13.38 Ring expansion via olefin metathesis.

13.3.2 Photochemical Methods

Photochemical methods have been exploited for the synthesis of macrocycles but are typically involved in rearrangements or fragmentations. The methods described herein involve photochemical syntheses utilized for the cyclization of linear precursors. A pertinent example, the macrocyclic thiol–ene reaction, will be described later in this chapter (Section 13.6.2). Photochemistry can be used to promote radical additions to alkenes to generate carbon–carbon bonds and, in some instances, can be exploited in macrocyclization reactions. Most strategies involve a decarboxylation sequence as a source of alkyl-free radicals. For example, Yoshimi and coworkers exploited the generation of alkyl radicals from carboxylic acids to form a variety of macrocyclic lactones, lactams, and ketones photochemically [67]. Their protocol involves the use of phenanthrene and 1,4-dicyanobenzene in the presence of carboxylic acids tethered to α,β-unsaturated carbonyl moieties (Scheme 13.39). The decarboxylative intramolecular radical cyclization can be performed to generate 16- to 20-membered macrocycles **98** in moderate to very good yield (51–84%).

Other functionalities such as alkenes, arenes, amines, and thioethers also have been exploited as electron donors in intramolecular photoinitiated electron transfer cyclizations onto tethered phthalimido groups [68]. The transformations give access to various chromophore-containing tricyclic compounds in a single step. For example, Maruyama and coworkers reported the synthesis of macrolactones from *N*-alkenylphthalimides (**99**) under light irradiation (Scheme 13.40) [69]. It was shown that styrene radical cations were trapped by methanol with anti-Markovnikov selectivity when the reactions were performed in methanol as solvent.
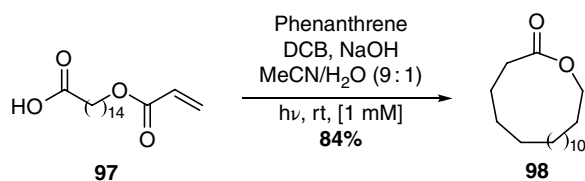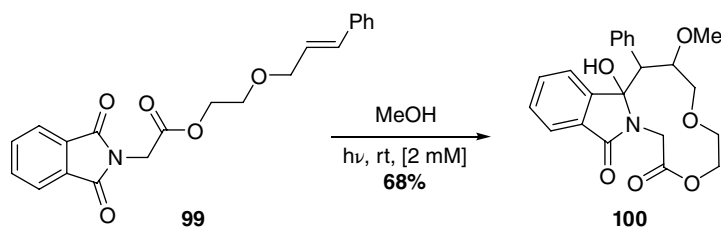
The resulting biradical intermediate would subsequently combine intramolecularly to generate 11- to 15-membered macrolactones (**100**) in moderate to good yield (35–68%).

Photochemical inter- and intramolecular aromatic substitutions have also demonstrated utility in macrocycle synthesis as alternatives to traditional thermal aromatic substitution or coupling reactions. Some examples showcase the use of either α-chloroacetamides or aryl halides with activated aryl coupling partners to generate structurally diverse macrocycles. As reported by Hoshino and coworkers, *meta*-bridged aromatic lactams can be synthesized photochemically when both aromatic rings contain electron-donating substituents (Scheme 13.41) [70]. Under optimized conditions, various 11-membered lactams (**102**) can be synthesized in generally low to moderate yield (22–46%).

13.4 Alternative Methods for Macrocyclization Involving Carbon–Oxygen Bond Formation

Carbon–oxygen bonds are commonly found in important functional groups, notably carbonyl compounds and ethers. As such, a variety of methods exist for the formation of these functional groups in a macrocyclic template.

13.4.1 Chan–Lam–Evans Coupling

The Chan [71]–Lam [72]–Evans [73] cross-coupling reaction has been developed as an alternative to the Ullmann coupling (Section 13.4.4) to form C–O and C–N bonds between arylboronic acids and aromatic phenols and amines, normally via copper catalysis. In contrast to the Ullmann cross-coupling, the Chan–Lam–Evans variation can be conducted at lower temperatures. Evans and coworkers utilized this coupling for the synthesis of derivatives of SE205, a macrocyclic matrix metalloproteinase (MMP) inhibitor bioavailable in rats and dogs (Scheme 13.42) [74,75]. Macrocyclization conditions were sufficiently mild to tolerate esters and amides. When using copper(II) acetate in the presence of triethylamine, macrocyclization can occur

Scheme 13.39 Photochemical decarboxylation and subsequent macrocyclization.

Scheme 13.40 Photochemical synthesis of a macrolactone from *N*-alkenylphthalimide.

Scheme 13.41 Photochemical reaction of an aryl halide to form a macrocyclic biaryl.
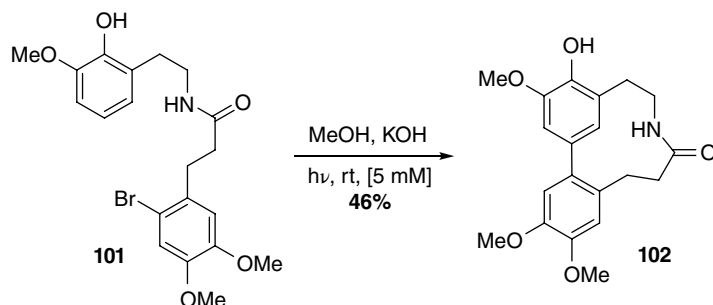
Scheme 13.42 Chan–Lam–Evans coupling to MMP derivatives.
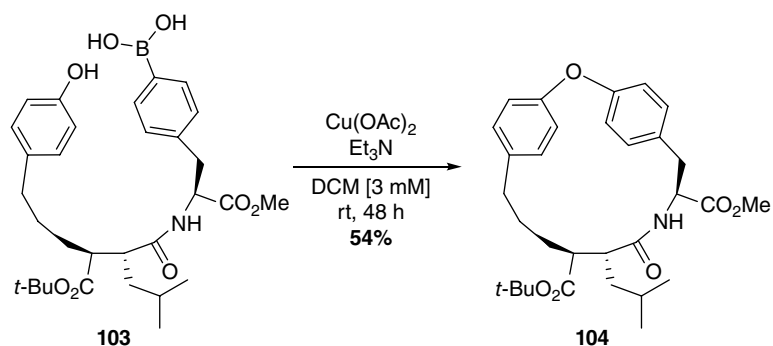
Scheme 13.43 Chan–Lam–Evans macrocyclization in the synthesis of chloropeptin I.
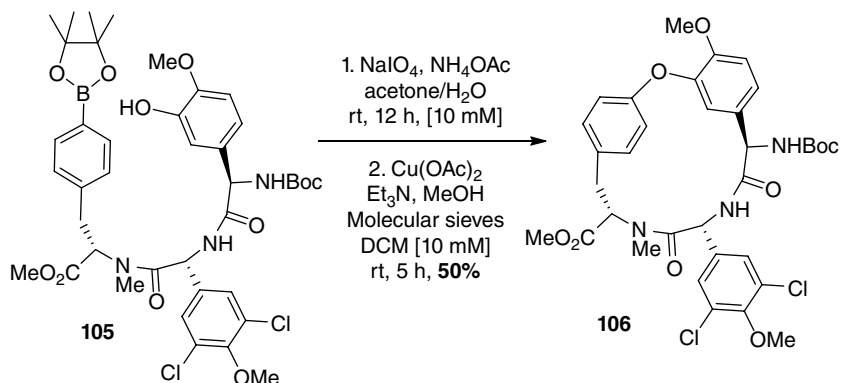
at room temperature with yields varying from 43 to 54%. A similar protocol was used by Takeya and coworkers for the synthesis of two L,L-cycloisodityrosines [76], where they demonstrated the importance of 4-(dimethylamino)-pyridine (DMAP) as the base for the cross-coupling.

Hoveyda and coworkers utilized the Chan–Lam–Evans reaction for the synthesis of the anti-HIV agent chloropeptin I (Scheme 13.43) [77]. They demonstrated that the addition of 10 equivalents of methanol to the standard reaction conditions helped to obtain higher yields of the desired macrocycle. They suggested that the influence of methanol might be linked to *in situ* formation of the boron dimethyl ester or to the increased solubility of the copper catalyst.

13.4.2 Alkylation

Alkylation reactions involving the synthesis of C–O bonds can be performed under a variety of reaction conditions. An example of alkylative C–O bond formation was demonstrated by Barnickel and Schobert using a macrocyclic Williamson etherification. In the synthesis of nor-macrocidin A [78], a ω-bromophenolate was generated *in situ* by Pd-mediated *ortho*-deallylation of **107** and subsequent alkylation to provide macrocycle **108** in 25% yield (Scheme 13.44).

The Mitsunobu reaction allows for the substitution of primary or secondary alcohols with various nucleophiles in the presence of a trialkylphosphine or triarylphosphine and a dialkyl azodicarboxylate [79]. Many variations of the transformation have been developed over the years
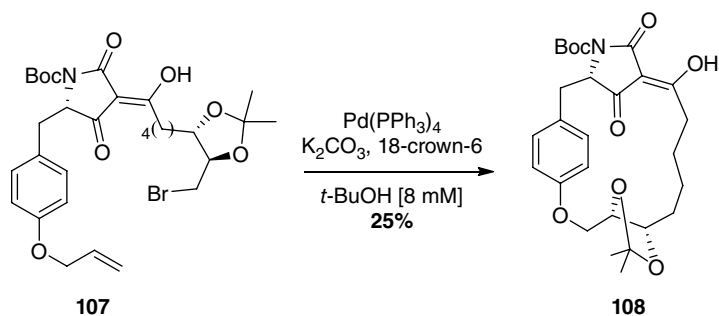
Scheme 13.44 Macrocyclic Williamson etherification of an ω-bromophenolate.
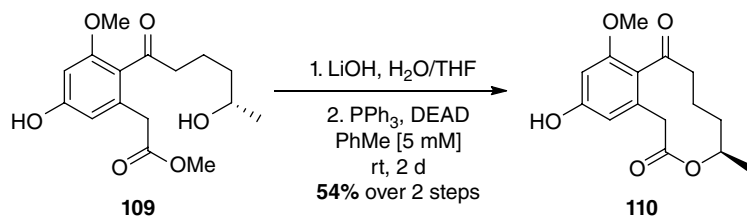
Scheme 13.45 Mitsunobu reaction in the total synthesis of xestodecalactone A.
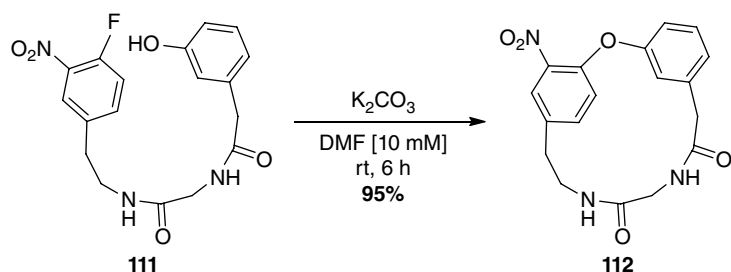
Scheme 13.46 Macrocyclization via S_NAr for the synthesis of models of vancomycin.

[80], and the Mitsunobu reaction is often used as a key step in natural product synthesis for the formation of different carbon–heteroatom (O, N, S) bonds [81, 82]. In the total synthesis of xestodecalactone A [83], Danishefsky and coworkers coupled the seco-acid of ester **109** under Mitsunobu conditions (PPh₃/DEAD), and the chiral secondary alcohol underwent complete inversion of configuration to afford macrocycle **110** (Scheme 13.45).

13.4.3 Nucleophilic Aromatic Substitution

The aromatic nucleophilic substitution (S_NAr) reaction involves a nucleophilic partner and an electrophilic aromatic ring. In macrocyclization, S_NAr reactions are most often used to form biaryl ethers. For example, Zhu and coworkers used S_NAr reactions for the synthesis of vancomycin derivatives (Scheme 13.46) [84]. Upon treating phenol **111** with potassium carbonate in dimethylformamide (DMF) at room temperature, they obtained a 95% yield of 16-membered macrocycle **112**. They were able to prepare other analogues of the ring systems present in vancomycin [85] and demonstrated the use of cesium fluoride as a base [86], as well as the benefits of

18-crown-6 as an additive [87]. The S_NAr strategy has been used by Boger [88] and Zhu [89] to synthesize cycloisodityrosines (62–78% yield) and by González-Zamora and coworkers for the synthesis of plagiochin D [90]. It should be noted that other solvents, such as THF (for the synthesis of models of chloropeptins I and II) [91] or DMSO (total synthesis of chloropeptin II) [92, 93], can also be used for S_NAr reactions.

In order to promote macrocyclization, ruthenium π-complexes can be exploited to facilitate S_NAr processes. Pearson and coworkers reported the formation of a cyclic peptide model for teicoplanin [94]. When the ruthenium complexes are treated with sodium 2,6-di-*t*-butylphenoxide in acetone at −30°C, it is possible to obtain 29% of the desired macrocycle **114** after photolytic removal of the ruthenium complex from the molecule (Scheme 13.47). Later, Pearson and coworkers showed that cesium carbonate in DMF could also promote the macrocyclization of amino acid-containing precursors [95, 96] and the reaction conditions are mild enough to prevent epimerization in some cases [97].

Sammakia and coworkers used a S_NAr reaction for the total synthesis of diazonamide A, a marine natural
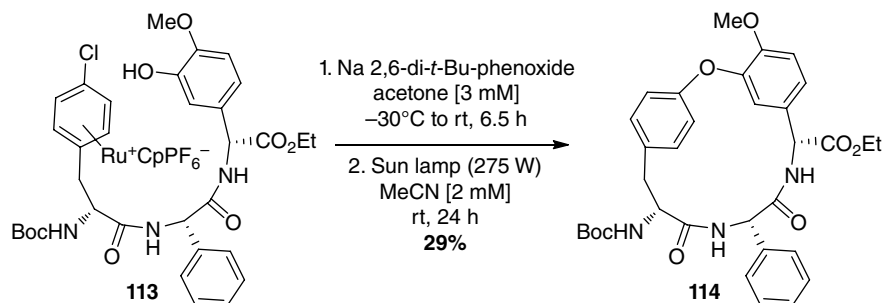
Scheme 13.47 S_NAr macrocyclization facilitated by Ru-π complexes.

Scheme 13.48 S_NAr macrocyclization forming a quaternary stereocenter.
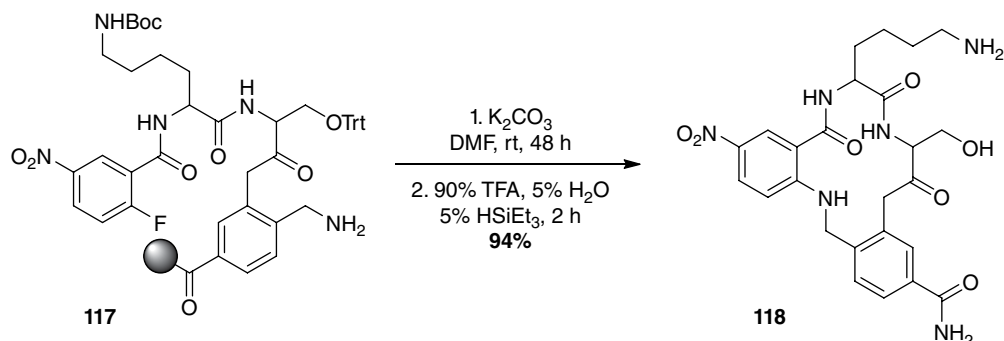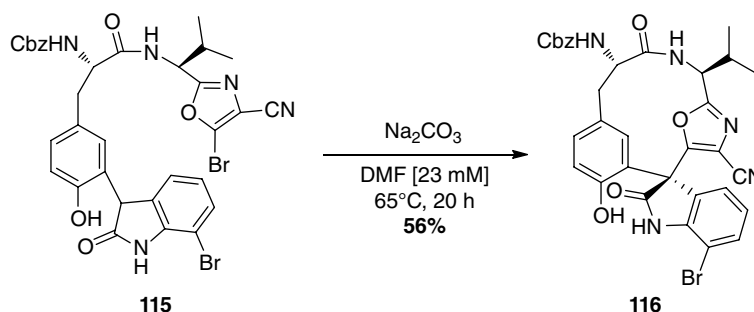
Scheme 13.49 On-resin S_NAr macrocyclization toward peptidomimetics.

product with potent antimitotic activity [98]. The authors coupled an oxindole and a bromooxazole using sodium carbonate to form macrocycle **116** bearing a hindered quaternary stereocenter in 56% yield, with no need of protecting groups on the phenol or oxindole nitrogen group (Scheme 13.48).

On-resin macrocyclic S_NAr processes have also been utilized toward the synthesis of C^{10} β-turn peptidomimetics as demonstrated by Burgess and coworkers [99]. The solid-phase procedure gave access to a library of compounds designed to mimic or disrupt specific protein–protein interactions. Following deprotection of the benzylic heteroatom (O, S, N), acyclic precursors such as **117** underwent a base-mediated ring closure after 48 h at room temperature (Scheme 13.49). A simultaneous removal of the side-chain protecting groups and cleavage

of the macrocycle (**118**) from the resin can then be attained in generally good yield.

13.4.4 Ullmann Coupling

The Ullmann coupling is a useful reaction to form biaryl ethers but typically requires strongly basic conditions and high reaction temperatures, which reduces its applications in complex synthesis. Nevertheless, Boger and coworkers applied the Ullmann coupling to the synthesis of a model of deoxybouvardin [100]. When macrocyclic precursor **119** was submitted to sodium hydride and CuBr·SMe$_2$, 58% yield of the desired macrocyclic biaryl ether **120** was obtained (Scheme 13.50). An Ullmann coupling was also applied to the total synthesis of deoxybouvardin and RA-VII,

with 2,4,6-collidine used as solvent to avoid racemization of the natural product [101].

A variety of reaction conditions can be used for Ullmann coupling. In the case of the total synthesis of (+)-piperazinomycin, only the use of CuBr·SMe$_2$ in DMF afforded macrocyclic products [102], while in the total synthesis of combretastatin D2 [103], CuMe was required as a reagent to help form cuprous phenoxide in solution. Zhou and coworkers reported Ullmann couplings using a copper–iron catalyst system [104]. Among bases, 2,6-lutidine can be used as solvent to help solubilize the cuprous phenoxides formed at the beginning of the reaction [105]. Ma and coworkers have shown that a mixture of copper(I) iodide, *N,N*-dimethylglycine, and cesium carbonate in 1,4-dioxane, along with the aid of *ortho* activating groups such as amides, can help promote macrocyclic Ullmann couplings at room temperature in good yields [106]. Uchiro and coworkers have shown the first example of a macrocyclic Ullmann coupling using an aliphatic secondary alcohol (Scheme 13.51) [107]. Cyclization of alcohol **121** with an excess of CuI and 1,10-phenanthroline afforded a 42% yield of 13-membered macrocycle **122**, which could be further transformed for the total synthesis of hirsutellone B.

Sun and coworkers have shown that it is possible to accelerate Ullmann couplings by using microwave irradiation [108]. They were able to synthesize macrocyclic ethers in 15 min when superheating in pyridine (Scheme 13.52). In comparison, the reaction requires greater than 17 h to reach completion using standard oil bath heating [109].

13.4.5 C–H Activation

Traditional macrolactonization reactions require stoichiometric activating reagents and high dilution techniques. However, macrolactones can also be obtained by C–H activation of ω-alkenoic acids via palladium catalysis [110, 111]. The key bond formation occurs between an oxygen of the carboxylic acid unit and an allylic carbon. The resulting macrocycles contain an exocyclic alkene, which could be useful for further functionalization. When acid **125** was treated with a palladium-bound disulfone ligand and benzoquinone (BQ), ligand exchange and an inner-sphere reductive elimination gave the corresponding macrolactone **126** in 63% yield (Scheme 13.53). Macrocycles ranging from 14- to 19-membered rings could be produced with this method in good yields (52–63%), and the reaction tolerated a wide variety of alcohol protecting groups, including acetonide, methoxy, methoxymethyl, and benzyl. Chiral centers, even when remote from the reaction site, affected the diastereoselectivity of the macrolactone formation. The protocol was also used for the cyclization step in the total synthesis of 6-deoxyerythronolide B [112].

In a similar fashion, ω-alkynoic acids can be cyclized using rhodium catalysis where the resulting macrolactones contain an exocyclic alkene (Scheme 13.54) [113]. A formal C–H propargylic activation together with a formal hydride shift produces a globally redox-neutral reaction as the alkyne is reduced to the alkene when the C–H

Scheme 13.50 Ullmann coupling applied to the synthesis of a model of deoxybouvardin.
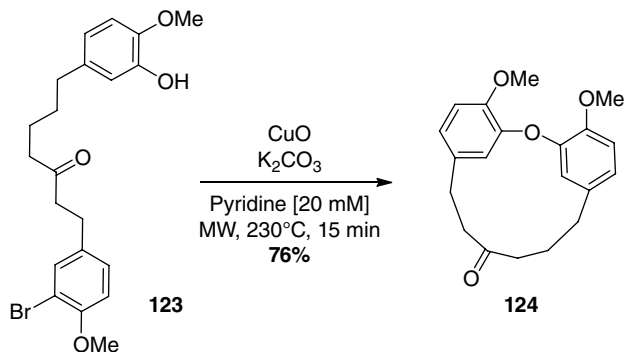
Scheme 13.52 Macrocyclic Ullmann coupling using microwave irradiation.
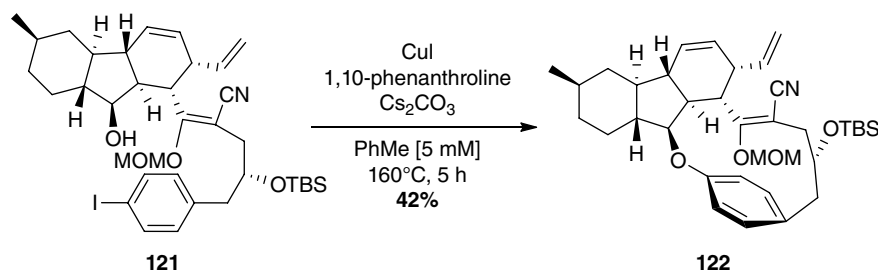
Scheme 13.51 Macrocyclic Ullmann coupling using an aliphatic secondary alcohol.

Scheme 13.53 Macrocyclization via allylic C–H activation.

125 → **126**
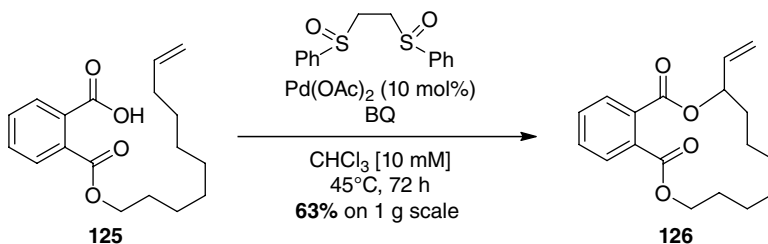
Scheme 13.54 Macrocyclization via propargylic C–H activation.

127 → **128**
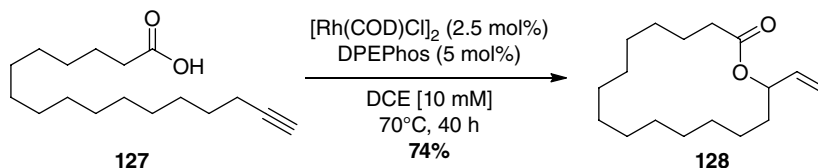
Scheme 13.55 Macrocyclization via alkylation of 2-nitrobenzenesulfonamide.

129 → **130**
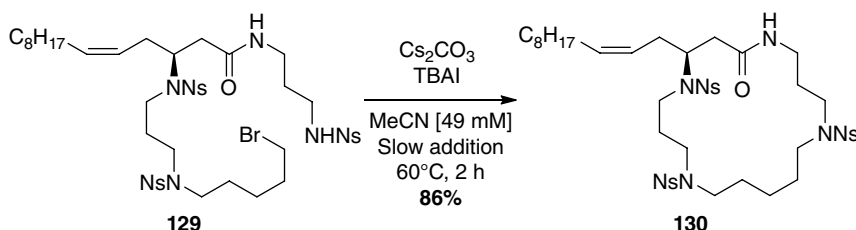
oxidation occurs. As opposed to the C–H allylic activation, an external oxidant is therefore not needed. Hence, in the cyclization of the alkynyl acid **127**, the pre-catalyst ([Rh(COD)Cl]$_2$) and the ligand (DPEPhos) are all that is needed to afford macrocycle **128** in 74% yield.

13.5 Alternative Methods for Macrocyclization Involving Carbon–Nitrogen Bond Formation

Most of the alternative methods used for forming macrocycles via carbon–nitrogen (C–N) bonds are analogous to those used for C–O bonds.

13.5.1 Alkylation

Fukuyama and coworkers reported macrocyclization conditions based on the alkylation of a 2-nitrobenzenesulfonamide [114]. The authors were able to access medium- and large-sized cyclic amines and demonstrated the applicability in the alkylation of bromide **129** to macrocycle **130** in the total synthesis of lipogrammistin A (Scheme 13.55).

Meyers and coworkers reported the synthesis of chiral diazamacrocycles [115]. The key cyclization step was a double alkylation of bis-1,3(1-tetrahydroisoquinolinyl) propane **131** to afford a mixture of the monomer **132**

and dimer **133** in varying yields. Interestingly, the concentration of the reaction had little effect on yield and product distribution (Scheme 13.56).

Macrocyclization via C–N bond formation was used by Fukuyama and coworkers in the total synthesis of (−)-ephedradine A (Scheme 13.57) [116]. Treatment of acyclic amino alcohol **134** under Mitsunobu conditions (PPh$_3$/DEAD) promoted the desired macrocyclization reaction to afford polyamine **135** in 77% yield. Similar conditions (PPh$_3$/DIAD) were also utilized by Hovinen and coworkers toward the synthesis of 10- and 12-membered azamacrocycles [117].

13.5.2 Nucleophilic Aromatic Substitution

Nucleophilic aromatic substitution reactions can also be used to form macrocycles via C–N bond formation. Zhu and coworkers synthesized a variety of macrocyclic *para*-cyclophanes, with yields ranging from 23 to 98%, using potassium carbonate in DMF [118]. Analogous to macrocyclic C–O bond-forming S$_N$Ar reactions, ruthenium π-complexes can be exploited to facilitate S$_N$Ar processes for the formation of C–N bonds as well. Rich and coworkers have shown that it is possible to synthesize tripeptides via a Ru-π complex (Scheme 13.58). The imidazole ring in precursor **136** could be employed for cyclization upon treatment with potassium *t*-butoxide. Subsequent photo-deruthenation afforded the macrocyclic tripeptide **137** in 24% yield [119].
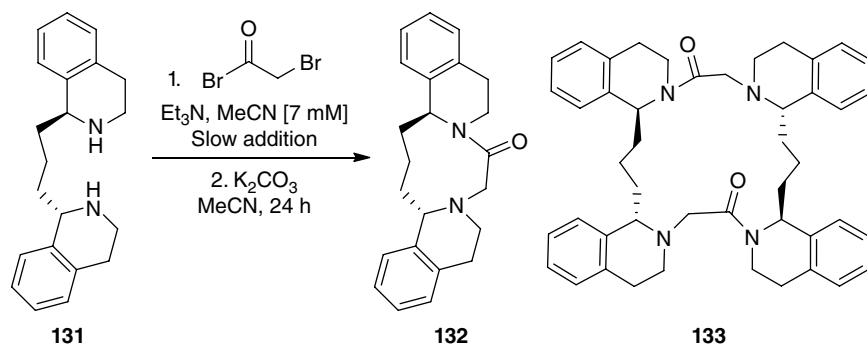
Scheme 13.56 Macrocyclization via double alkylation.
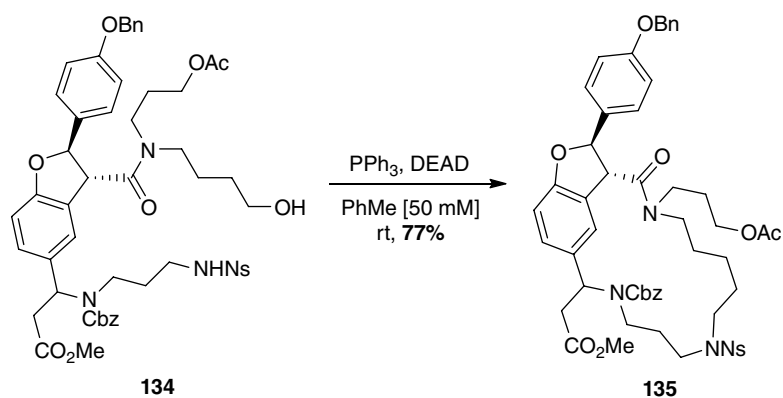
Scheme 13.57 Macrocyclic Mitsunobu reaction for the formation of a C–N bond.
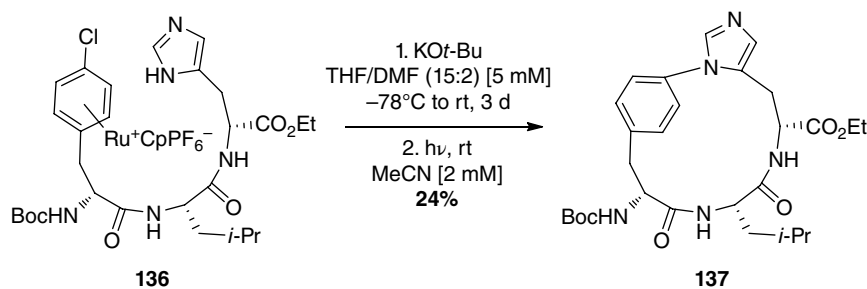
Scheme 13.58 Macrocyclic S$_N$Ar reaction for the formation of a C–N bond.

13.5.3 Ullmann Coupling

Macrocyclic Ullmann couplings also can be used to form C–N bonds using amides and heterocycles as substrates, often under catalytic conditions. Evano and coworkers have shown that it is possible to prepare macrocyclic enamides from the coupling between an iodoalkene and an amine using CuI as catalyst and *N,N*-dimethylethylene-1,2-diamine (DMEDA) as ligand. Cyclization of iodoalkene **138** under catalytic conditions afforded the macrocyclic enamide **139**, a precursor of abyssenine A, in 83% yield after 3 days (Scheme 13.59) [120].

In another example, James and coworkers used 8-hydroxyquinoline (8-HQ) as a ligand in DMSO to catalyze macrocyclic Ullmann couplings. Intramolecular cyclization between the iodoarene and the imidazole of

precursor **140** afforded the 22- and 23-membered macrocycles **141** and **142** as a 1:5 mixture in high yield (97%) (Scheme 13.60) [121].

13.6 Alternative Methods for Macrocyclization Involving Carbon–Sulfur Bond Formation

While a number of chemical reactions for forming macrocycles via C–O and C–N bonds have been developed, there also exist a number of important strategies for forming large ring compounds based upon carbon–sulfur (C–S) bonds. Macrocyclizations involving sulfur-based functional groups are important given the

Scheme 13.59 Macrocyclic enamide via Ullmann coupling.
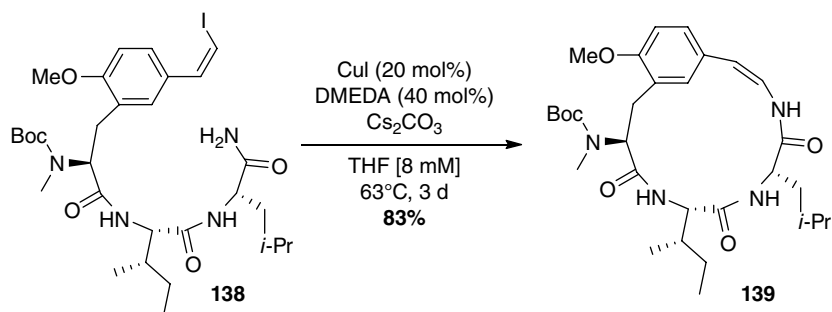
Scheme 13.60 Macrocyclic Ullmann coupling.
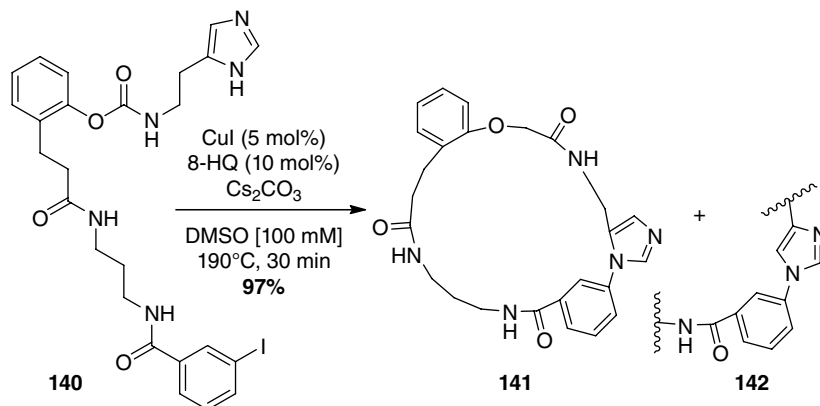
abundance of sulfur in amino acids and heterocycles that are commonly exploited in medicinal chemistry.

13.6.1 Ramberg–Bäcklund Reaction

The Ramberg–Bäcklund reaction is a multistep transformation involving the formation of a carbon–sulfur bond, oxidation of the sulfur atom, and subsequent extrusion of SO_2 with concomitant formation of a carbon–carbon bond as an alkene. As such, this reaction represents an interesting alternative to the olefin metathesis reaction for the formation of macrocyclic alkenes. During the total synthesis of manzamine C [122], the cyclization step involved a double S_N2 reaction to displace two bromides of **143** with sulfur. In order to avoid the formation of dimers, high dilution conditions (0.2 mM) were necessary (Scheme 13.61). It was also observed that dimers were formed when the corresponding bis-iodo starting material was used. The α-sulfone **145** was obtained by a NCS-promoted chlorination followed by a peroxide oxidation. The extrusion of SO_2 occurred at room temperature in the presence of potassium t-butoxide in DMSO with an excellent yield and high selectivity for the E-alkene **146**.

It should be noted that the thioalkylation used in the Ramberg–Bäcklund reaction is also a popular method for forming macrocycles. For example, 4-chloromethyl-thiazole **147** was utilized in a protocol directed toward the synthesis of macrocyclic peptides and afforded

macrocycle **148** in 45% yield (Scheme 13.62) [123]. The scope of macrocyclization allowed for the formation of cyclic tri-, tetra-, penta-, and hexapeptides in high purity and good yields. A similar thioalkylation strategy was used in the synthesis of a 12-membered *meta*-heterophane [124].

The Ramberg–Bäcklund rearrangement can also be used to unmask an alkene in a macrocyclic compound. In the total synthesis of aigialomycin D, the presence of a vinylic alkene was problematic under olefin metathesis conditions as it could rapidly react to form a six-membered ring [125]. As a chemical subterfuge, a sulfone moiety was first introduced, and then RCM induced to provide the desired macrocycle. Benzylic chlorination using CCl_4 followed by *in situ* deprotonation and ring contraction rearrangement produced macrocycle **151** exclusively as the E olefin in very good yield (Scheme 13.63).

13.6.2 Thiol–Ene Reaction

The thiol–ene reaction allows for the formation of a C–S bond, typically between alkenes and primary thiols, under ultraviolet or visible light irradiation. This free-radical-mediated coupling is considered a "click" process due to its high efficiency and chemoselectivity. It is a favored reaction in biofunctionalization and materials science because of the formation of robust thioether linkages. The utility of the thiol–ene process has been
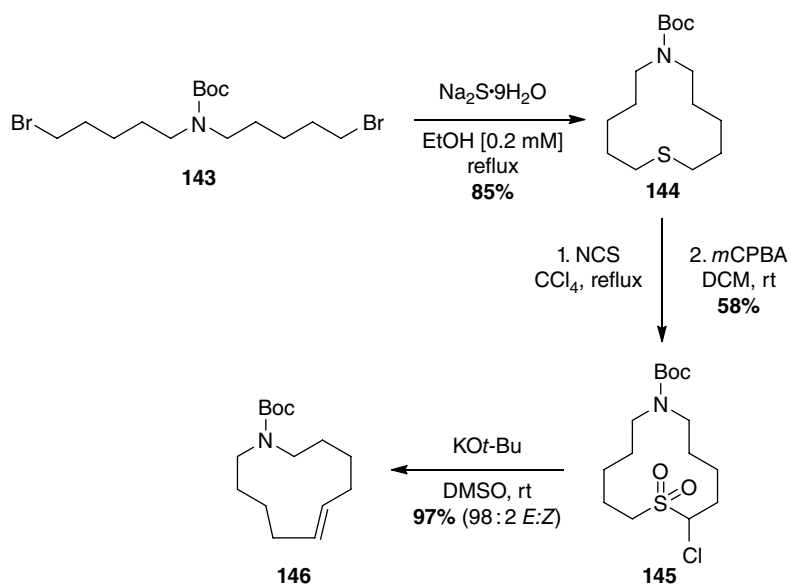
Scheme 13.61 Ramberg–Bäcklund approach to a macrocyclic amine.
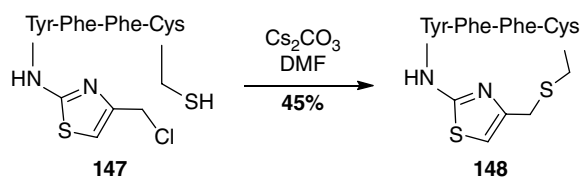
Scheme 13.62 Synthesis of a macrocyclic peptide via thioalkylation.
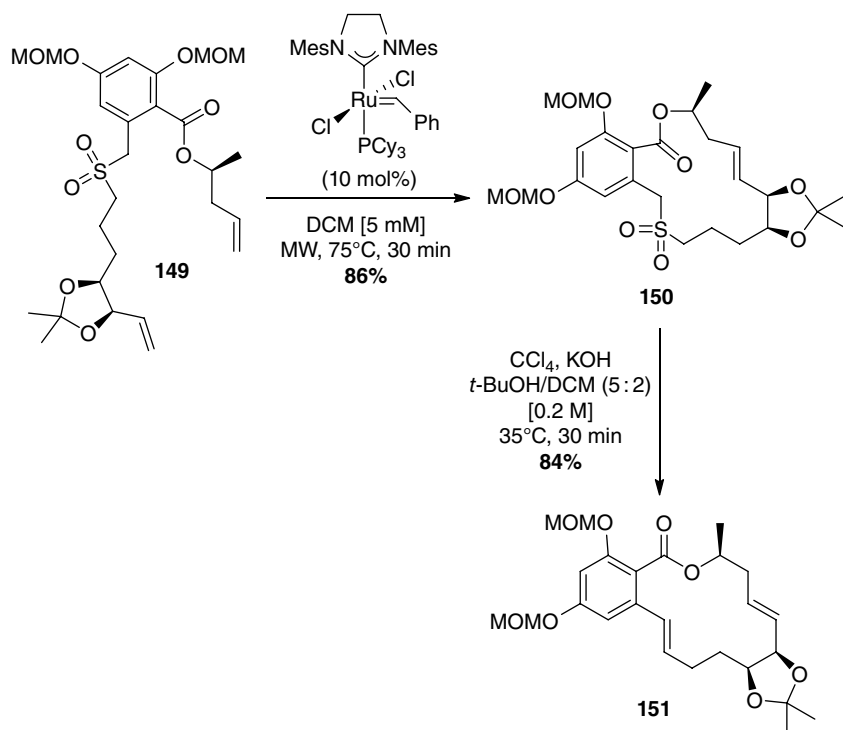
Scheme 13.63 Ramberg–Bäcklund reaction within a macrocyclic framework.

Scheme 13.64 Thiol–ene macrocyclization of a peptide on solid support.
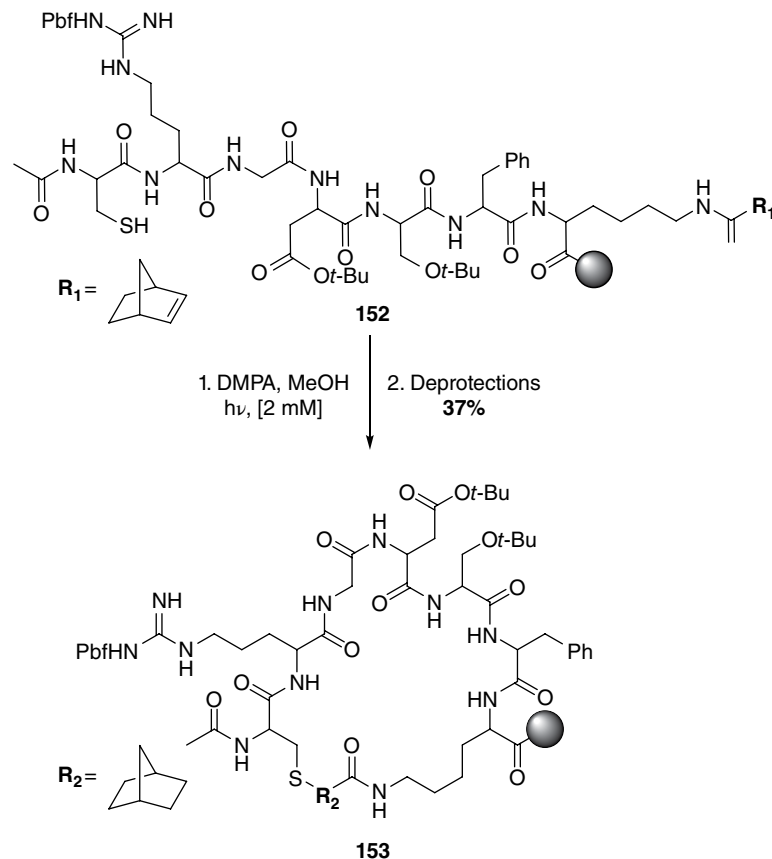
demonstrated by Anseth and coworkers, who utilized an on-resin macrocyclization strategy between cysteine amino acid residues and various peptide-bound alkenes to generate cyclized peptides such as **153** in 37% yield (Scheme 13.64) [126].

Chou and coworkers reported an approach to macrocycles employing the thiol–ene coupling between two cysteine residues of native unprotected peptides and α,ω-dienes (Scheme 13.65) [127]. The reaction conditions tolerate the presence of sensitive functional groups and enable the synthesis of macrocycles such as **155** containing five to nine amino acids and a linker in high yield (76–92%). The authors also demonstrated the use of the two-component thiol–ene method for stapling peptides with *i*, *i*+4 or *i*, *i*+7 linkages as an alternative to more conventional RCM methods.

13.7 Conclusion and Summary

As challenging a process as macrocyclization may be, chemists have succeeded in opening the "synthetic

toolbox" for methods to access small to large ring compounds. Given the current emphasis placed upon catalysis, green chemical approaches, and sustainable synthesis, it is safe to say that we have only seen the top of the toolbox, and more tools still wait to be discovered. Indeed, the aforementioned chapter has shown that a number of more specialized transformations or tools can greatly aid in the synthesis of medicinally relevant macrocycles. In fact, virtually any chemical reaction can potentially be applied to macrocyclization. This chapter has discussed various methods to build carbon–carbon and carbon–heteroatom bonds within macrocycles, but tools for forming increasingly complex motifs are still under development. For example, other carbon–heteroatom bonds such as carbon–phosphorus and carbon–boron are of interest to medicinal chemists, but respective macrocyclization methods are rare. In addition, various heteroatom motifs found in nature like nitrogen–nitrogen bonds and sulfur–sulfur bonds are scarcely seen in the literature. It seems that macrocyclization chemistry will continue to grow and develop as we rummage through the "synthetic toolbox."
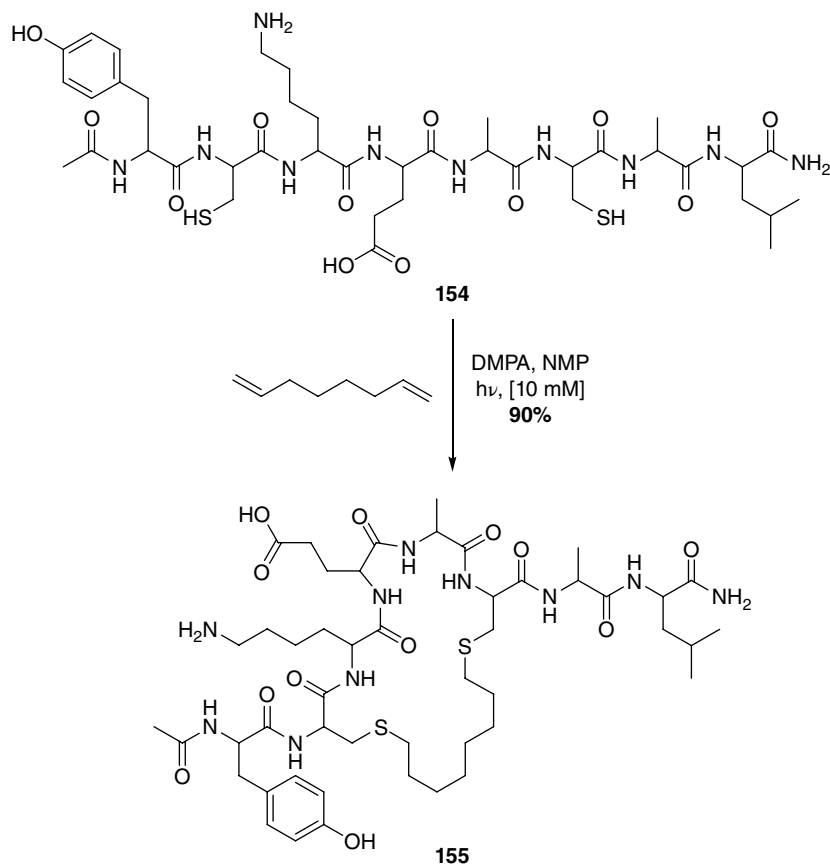
References

1 Parenty, A.; Moreau, X.; Niel, G.; Campagne, J.-M. Update 1 of: Macrolactonizations in the Total Synthesis of Natural Products. *Chem. Rev.* **2013**, *113*, PR1–PR40.

2 Davies, J. S. The Cyclization of Peptides and Depsipeptides. *J. Peptide Sci.* **2003**, *9*, 471–501.

3 Nicolaou, K. C.; Bulger, P. G.; Sarlah, D. Metathesis Reactions in Total Synthesis. *Angew. Chem., Int. Ed.* **2005**, *44*, 4490–4527.

4 Nicolaou, K. C.; Bulger, P. G.; Sarlah, D. Palladium-Catalyzed Cross-Coupling Reactions in Total Synthesis. *Angew. Chem., Int. Ed.* **2005**, *44*, 4442–4489.

5 Marsault, E.; Toró, A.; Nowak, P.; Deslongchamps, P. The Transannular Diels-Alder Strategy: Applications to Total Synthesis. *Tetrahedron* **2001**, *57*, 4243–4260.

6 Mutule, I.; Joo, B.; Medne, Z.; Kalnins, T.; Vedejs, E.; Suna, E. Stereoselective Synthesis of the Diazonamide A Macrocyclic Core. *J. Org. Chem.* **2015**, *80*, 3058–3066.

7 Meng, D.; Bertinato, P.; Balog, A.; Su, D.-S.; Kamenecka, T.; Sorensen, E. J.; Danishefsky, S. J. Total Syntheses of Epothilones A and B. *J. Am. Chem. Soc.* **1997**, *119*, 10073–10092.

8 Hayward, C. M.; Yohannes, D.; Danishefsky, S. J. Total Synthesis of Rapamycin via a Novel Titanium-Mediated Aldol Macrocyclization Reaction. *J. Am. Chem. Soc.* **1993**, *115*, 9345–9346.

9 Ito, Y.; Yoshinaga, T.; Nishino, T. Efficient Macrocyclization Using Methylene-Tethered Terminal Dienes and Bis(manganese(III)-enolate)s. *Tetrahedron* **2010**, *66*, 2683–2694.

10 Nicolaou, K. C.; Hale, C. R. H.; Ebned, C.; Nilewski, C.; Ahles, C. F.; Rhoades, D. Synthesis of Macroheterocycles through Intramolecular Oxidative Coupling of Furanoid β-Ketoesters. *Angew. Chem., Int. Ed.* **2012**, *51*, 4726–4730.

11 Rose, T. E.; Lawson, K. V.; Harran, P. G. Large Ring-Forming Alkylations Provide Facile Access to Composite Macrocycles. *Chem. Sci.* **2015**, *6*, 2219–2223.

12 Hansen, J. G.; Feeder, N.; Hamilton, D. G.; Gunter, M. J.; Becher, J.; Sanders, J. K. M. Macrocyclization and Molecular Interlocking via Mitsunobu Alkylation: Highlighting the Role of C−H⋯O Interactions in Templating. *Org. Lett.* **2000**, *2*, 449–452.

13 Babu, N. S. A.; Kaur, G.; Aslam, N. A.; Karanam, M. Glaser–Eglinton–Hay sp–sp Coupling and Macrocyclization: Construction of a New Class

of Polyether Macrocycles Having a 1,3-Diyne Unit. *RSC Adv.* **2014**, *4*, 18904–18916.

14 Bolduc, P.; Jacques, A.; Collins, S. K. Efficient Macrocyclization Achieved via Conformational Control Using Intermolecular Noncovalent π-Cation/Arene Interactions. *J. Am. Chem. Soc.* **2010**, *132*, 12790–12791.

15 Bähr, A.; Droz, A. S.; Püntener, M.; Neidlein, U.; Anderson, S.; Seiler, P.; Diederich, F. Molecular Recognition of Pyranosides by a Family of Trimeric, 1,1′-Binaphthalene-Derived Cyclophane Receptors. *Helv. Chim. Acta* **1998**, *81*, 1931–1963.

16 Belghiti, T.; Joly, J.-P.; Alem, H.; Chapleur, H. Synthèse de Macroglycophanes par Couplage d'Acétyléniques Vrais. *C. R. Chimie* **2003**, *6*, 553–564.

17 Ohkita, M.; Ando, K.; Suzuki, T.; Tsuji, T. Syntheses of Acetylenic Oligophenylene Macrocycles Based on a Novel Dewar Benzene Building Block Approach. *J. Org. Chem.* **2000**, *65*, 4385–4390.

18 Marsden, J. A.; Haley, M. M. Carbon Networks Based on Dehydrobenzoannulenes. 5. Extension of Two-Dimensional Conjugation in Graphdiyne Nanoarchitectures. *J. Org. Chem.* **2005**, *70*, 10213–10226.

19 Bédard, A.-C.; Collins, S. K. Phase Separation as a Strategy Toward Controlling Dilution Effects in Macrocyclic Glaser-Hay Couplings. *J. Am. Chem. Soc.* **2011**, *133*, 19976–19981.

20 Bédard, A.-C.; Régnier, S. Collins, S. K. Continuous Flow Macrocyclization at High Concentrations: Synthesis of Macrocyclic Lipids. *Green. Chem.* **2013**, *15*, 1962–1966.

21 Colby, E. A.; O'Brien, K. C.; Jamison, T. F. Total Syntheses of Amphidinolides T1 and T4 via Catalytic, Stereoselective, Reductive Macrocyclizations. *J. Am. Chem. Soc.* **2005**, *127*, 4297–4307.

22 Knapp-Reed, B.; Mahandru, G. M.; Montgomery, J. Access to Macrocyclic Endocyclic and Exocyclic Allylic Alcohols by Nickel-Catalyzed Reductive Cyclization of Ynals. *J. Am. Chem. Soc.* **2005**, *127*, 13156–13157.

23 Chrovian, C. C.; Knapp-Reed, B.; Montgomery, J. Total Synthesis of Aigialomycin D: Surprising Chemoselectivity Dependence on Alkyne Structure in Nickel-Catalyzed Cyclizations. *Org. Lett.* **2008**, *10*, 811–814.

24 Shareef, A.-R.; Sherman, D. H.; Montgomery, J. Nickel-Catalyzed Regiodivergent Approach to Macrolide Motifs. *Chem. Sci.* **2012**, *3*, 892–895.

25 Wang, H.; Negretti, S.; Knauff, A. R.; Montgomery, J. Exo-Selective Reductive Macrocyclization of Ynals. *Org. Lett.* **2015**, *17*, 1493–1496.

26 Chaulagain, M. R.; Sormunen, G. J.; Montgomery, J. New *N*-Heterocyclic Carbene Ligand and Its Application in Asymmetric Nickel-Catalyzed Aldehyde/Alkyne Reductive Couplings. *J. Am. Chem. Soc.* **2007**, *129*, 9568–9569.

27 Trost, B. M.; Indolese, A. F.; Mueller, T. J. J.; Treptow, B. A Ru Catalyzed Addition of Alkenes to Alkynes. *J. Am. Chem. Soc.* **1995**, *117*, 615–623.

28 Trost, B. M.; Chisholm, J. D.; Wrobleski, S. T.; Jung, M. Ruthenium-Catalyzed Alkene-Alkyne Coupling: Synthesis of the Proposed Structure of Amphidinolide A. *J. Am. Chem. Soc.* **2002**, *124*, 12420–12421.

29 Trost, B. M.; Harrington, P. E.; Chisholm, J. D.; Wrobleski, S. T. Total Synthesis of (+)-Amphidinolide A. Structure Elucidation and Completion of the Synthesis. *J. Am. Chem. Soc.* **2005**, *127*, 13598–13610.

30 Santandrea, J.; Bédard, A.-C.; Collins, S. K. Cu(I)-Catalyzed Macrocyclic Sonogashira-Type Cross-Coupling. *Org. Lett.* **2014**, *16*, 3892–3895.

31 Li, W.; Schneider, C. M.; Georg, G. I. Synthesis of Strained 1,3-Diene Macrocycles via Copper-Mediated Castro–Stephens Coupling/Alkyne Reduction Tandem Reactions. *Org. Lett.* **2015**, *17*, 3902–3905.

32 Li, W.; Georg, G. I. A Concise Formal Total Synthesis of Lactimidomycin. *Chem. Commun.* **2015**, *51*, 8634–8636.

33 Gartner, Z. J.; Tse, B. N.; Grubina, R.; Doyon, J. B.; Snyder, T. M.; Liu, D. R. DNA-Templated Organic Synthesis and Selection of a Library of Macrocycles. *Science* **2004**, *305*, 1601–1605.

34 Smith, A. B.; Barbosa, J.; Wong, W.; Wood, J. L. Total Syntheses of (+)-Trienomycins A and F via a Unified Strategy. *J. Am. Chem. Soc.* **1996**, *118*, 8316–8328.

35 Lafontaine, J. A.; Provencal, D. P.; Gardelli, C.; Leahy, J. W. The Enantioselective Total Synthesis of the Antitumor Macrolide Natural Product Rhizoxin D. *Tetrahedron Lett.* **1999**, *40*, 4145–4148.

36 Lu, L.; Zhang, W.; Nam, S.; Horne, D. A.; Jove, R.; Carter, R. G. Amphidinolide B: Total Synthesis, Structural Investigation, and Biological Evaluation. *J. Org. Chem.* **2013**, *78*, 2213–2247.

37 Kang, S. H.; Kang, S. Y.; Kim, C. M.; Choi, H.-W.; Jun, H.-S.; Lee, B. M.; Park, C. M.; Jeong, J. W. Total Synthesis of Natural (+)-Lasonolide A. *Angew. Chem., Int. Ed.* **2003**, *42*, 4779–4782.

38 Lei, H.; Yan, J.; Yu, J.; Liu, Y.; Wang, Z.; Xu, Z.; Ye, T. Total Synthesis and Stereochemical Reassignment of Mandelalide A. *Angew. Chem., Int. Ed.* **2014**, *53*, 6533–6537.

39 Sanchez, C. C.; Keck, G. E. Total Synthesis of (+)-Dactylolide. *Org. Lett.* **2005**, *7*, 3053–3056.

40 Larsen, B. J.; Sun, Z.; Nagorny, P. Synthesis of Eukaryotic Translation Elongation Inhibitor Lactimidomycin via Zn(II)-Mediated Horner–Wadsworth–Emmons Macrocyclization. *Org. Lett.* **2013**, *15*, 2998–3001.

41 Pattenden, G.; Gonzalez, M. A.; Little, P. B.; Millan, D. S.; Plowright, A. T.; Tornos, J. A.; Ye, T. Total Synthesis of (+)-Phorboxazole A, a Potent Cytostatic Agent from the Sponge Phorbas sp. *Org. Biomol. Chem.* **2003**, *1*, 4173–4208.

42 Doyle, M. P.; Protopopova, M. N.; Poulter, C. D.; Rogers, D. H. Macrocyclic Lactones from Dirhodium(II)-Catalyzed Intramolecular Cyclopropanation and Carbon-Hydrogen Insertion. *J. Am. Chem. Soc.* **1995**, *117*, 7281–7282.

43 Doyle, M. P.; Peterson, C. S.; Protopopova, M. N.; Marnett, A. B.; Parker Jr., D. L.; Ene, D. L.; Lynch, V. Macrocycle Formation by Catalytic Intramolecular Cyclopropanation. A New General Methodology for the Synthesis of Macrolides. *J. Am. Chem. Soc.* **1997**, *119*, 8826–8837.

44 Weathers Jr., T. M.; Doyle, M. P.; Carducci, M. D. Substrate versus Catalyst Control of Stereoselectivity in the Cyclopropanation of a Carbon-Carbon Double Bond Linked to the Reactant Diazoacetate through a Chiral Linker. *Adv. Synth. Catal.* **2006**, *348*, 449–455.

45 Berthelot, A.; Piguel, S.; Le Dour, G.; Vidal, J. Synthesis of Macrocyclic Peptide Analogues of Proteasome Inhibitor TMC-95A. *J. Org. Chem.* **2003**, *68*, 9835–9838.

46 Chen, R.; Bhadbhade, M.; Kumar, N.; St Clair Black, D. Synthesis of Macrocyclic Tetraindolyls via Oxidative Coupling Reactions. *Tetrahedron Lett.* **2012**, *53*, 3337–3341.

47 Surry, D. S.; Su, X.; Fox, D. J.; Franckevicius, V.; Macdonald, S. J. F.; Spring, D. R. Synthesis of Medium-Ring and Iodinated Biaryl Compounds by Organocuprate Oxidation. *Angew. Chem., Int. Ed.* **2005**, *44*, 1870–1873.

48 Mei, R.; Xu, D.; Hu, H.; Song, D.; Zhang, H.; Ma, D.; Xie, X.; She, X. Biomimetic Total Syntheses of (+)-Dihydrolyfoline and (−)-5-epi-Dihydrolyfoline. *Org. Lett.* **2015**, *17*, 2230–2233.

49 Xie, Y.; Wei, P.; Li, X.; Hong, T.; Zhang, K.; Furuta, H. Macrocycle Contraction and Expansion of a Dihydrosapphyrin Isomer. *J. Am. Chem. Soc.* **2013**, *135*, 19119–19122.

50 Okujima, T.; Ando, C.; Mori, S.; Nakae, T.; Yamada, H.; Uno, H. Synthesis and Molecular Structure of Cyclo[8](9,10-dihydro-9,10-anthraceno)pyrrole. *Heterocycles* **2014**, *88*, 417–424.

51 Dorel, R.; Echavarren, A. M. Gold(I)-Catalyzed Activation of Alkynes for the Construction of Molecular Complexity. *Chem. Rev.* **2015**, *115*, 9028–9072.

52 Obradors, C.; Leboeuf, D.; Aydin, J.; Echavarren, A. M. Gold(I)-Catalyzed Macrocyclization of 1,*n*-Enynes. *Org. Lett.* **2013**, *15*, 1576–1579.

53 Zhu, C.; Xu, G.; Liu, K.; Qiu, L.; Peng, S.; Sun, J. Gold-Catalyzed Intramolecular Diazo Coupling: An

54 Stach, H.; Hesse, M. Synthesis of Macrocyclic Compounds by Ring Enlargement. *Tetrahedron* **1988**, *44*, 1573–1590.

55 Illuminati, G.; Luigi Mandolini, L. Ring Closure Reactions of Bifunctional Chain Molecules. *Acc. Chem. Res.* **1981**, *14*, 95–102.

56 Zheng, J.-F.; Jin, L.-R.; Huang, P.-Q. Enantiodivergent Synthesis of Both Enantiomers of Marine Alkaloids Haliclorensin and Isohaliclorensin, a Constituent of Halitulin. *Org. Lett.* **2004**, *6*, 1139–1142.

57 Kopp, F.; Stratton, C. F.; Akella, L. B.; Tan, D. S. A Diversity-Oriented Synthesis Approach to Macrocycles via Oxidative Ring Expansion. *Nat. Chem. Biol.* **2012**, *8*, 358–365.

58 Rivera, D. G.; Pando, O.; Bosch, R.; Wessjohann, L. A. A Biomimetic Approach for Polyfunctional Secocholanes: Tuning Flexibility and Functionality on Peptidic and Macrocyclic Scaffolds Derived from Bile Acids. *J. Org. Chem.* **2008**, *73*, 6229–6238.

59 Ellis-Holder, K. K.; Peppers, B. P.; Kovalevsky, A. Y.; Diver, S. T. Macrocycle Ring Expansion by Double Stevens Rearrangement. *Org. Lett.* **2006**, *8*, 2511–2514.

60 Story, P. R.; Denson, D. D.; Bishop, C. E.; Clark, B. C.; Farine, J. C. A New General Synthesis of Macrocyclic Compounds. *J. Am. Chem. Soc.* **1968**, *90*, 817–818.

61 Rüedi, G.; Nagel, M.; Hansen, H.-J. Three-Carbon Ring Expansion by Cyclopropane Insertion: Macrocyclic Musks from Readily Available C-12 Starting Materials. *Org. Lett.* **2004**, *6*, 2989–2991.

62 MacPherson, L. J.; Bayburt, E. K.; Capparelli, M. P.; Bohacek, R. S.; Clarke, F. H.; Ghai, R. D.; Sakane, Y.; Berry, C. J.; Peppard, J. V.; Trapani, A. J. Design and Synthesis of an Orally Active Macrocyclic Neutral Endopeptidase 24.11 Inhibitor. *J. Med. Chem.* **1993**, *36*, 3821–3828.

63 Corey, E. J.; Brunelle, D. J.; Nicolaou, K. C. A Translactonization Route to Macrocyclic Lactones. *J. Am. Chem. Soc.* **1977**, *99*, 7359–7360.

64 Kraft, M. B.; Poudel, Y. B.; Kedei, N.; Lewin, N. E.; Peach, M. L.; Blumberg, P. M.; Keck, G. E. Synthesis of a des-B-Ring Bryostatin Analogue Leads to an Unexpected Ring Expansion of the Bryolactone Core. *J. Am. Chem. Soc.* **2014**, *136*, 13202–13208.

65 Bauer, R. A.; Wenderski, T. A.; Tan, D. S. Biomimetic Diversity-Oriented Synthesis of Benzannulated Medium Rings via Ring Expansion. *Nat. Chem. Biol.* **2013**, *9*, 21–29.

66 Lee, C. W.; Choi, T.-L.; Grubbs, R. H. Ring Expansion via Olefin Metathesis. *J. Am. Chem. Soc.* **2002**, *124*, 3224–3225.

67 Nishikawa, K.; Yoshimi, Y.; Maeda, K.; Morita, T.; Takahashi, I.; Itou, T.; Inagaki, S.; Hatanaka, M. Radical

Efficient Macrocyclization Towards Cyclic Olefins. *Chem. Commun.* **2015**, *51*, 12768–12770.

Photocyclization Route for Macrocyclic Lactone Ring Expansion and Conversion to Macrocyclic Lactams and Ketones. *J. Org. Chem.* **2013**, *78*, 582–589.

68 Griesbeck, A. G.; Henz, A.; Hirt, J. Photochemical Synthesis of Macrocycles. *Synthesis* **1996**, *1996*, 1261–1276.

69 Maruyama, K.; Kubo, Y. Solvent-Incorporated Medium to Macrocyclic Compounds by the Photochemical Cyclization of *N*-Alkenylphthalimides. *J. Am. Chem. Soc.* **1978**, *100*, 7772–7773.

70 Hoshino, O.; Ogasawara, H.; Takahashi, A.; Umezawa, B. Photo-Induced Formation of *meta*-Bridged Aromatic Lactams Having Eleven Membered Ring. *Heterocycles* **1985**, *23*, 1943–1946.

71 Chan, D. M. T.; Monaco, K. L.; Wang, R. P.; Winters, M. P. New N- and O-Arylations with Phenylboronic Acids and Cupric Acetate. *Tetrahedron Lett.* **1998**, *39*, 2933–2936.

72 Lam, P. Y. S.; Clark, C. G.; Saubern, S.; Adams, J.; Winters, M. P.; Chan, D. M. T.; Combs, A. New Aryl/ heteroaryl C-N Bond Cross-Coupling Reactions via Arylboronic Acid/Cupric Acetate Arylation. *Tetrahedron Lett.* **1998**, *39*, 2941–2944.

73 Evans, D. A.; Katz, J. L.; West, T. R. Synthesis of Diaryl Ethers through the Copper-Promoted Arylation of Phenols with Arylboronic Acids. An Expedient Synthesis of Thyroxine. *Tetrahedron Lett.* **1998**, *39*, 2937–2940.

74 Xue, C. B.; He, X.; Roderick, J.; DeGrado, W. F.; Cherney, R. J.; Hardman, K. D.; Nelson, D. J.; Copeland, R. A.; Jaffee, B. D.; Decicco, C. P. Design and Synthesis of Cyclic Inhibitors of Matrix Metalloproteinases and TNF-Alpha Production. *J. Med. Chem.* **1998**, *41*, 1745–1748.

75 Decicco, C. P.; Evans, D. A. Intramolecular O-Arylation of Phenols with Phenyl Boronic Acids: Application to the Synthesis of Macrocyclic Metalloproteinase Inhibitors. *Org. Lett.* **2001**, *3*, 1029–1032.

76 Hitotsuyanagi, Y.; Ishikawa, H.; Naito, S.; Takeya, K. Synthesis of L,L-Cycloisodityrosines by Copper(II) Acetate-DMAP-Mediated Intramolecular O-Arylation of Phenols with Phenylboronic Acids. *Tetrahedron Lett.* **2003**, *44*, 5901–5903.

77 Deng, H.; Jung, J. K.; Liu, T.; Kuntz, K. W.; Snapper, M. L.; Hoveyda, A. H. Total Synthesis of Anti-HIV Agent Chloropeptin I. *J. Am. Chem. Soc.* **2003**, *125*, 9032–9034.

78 Barnickel, B.; Schobert, R. Toward the Macrocidins: Macrocyclization via Williamson Etherification of a Phenolate. *J. Org. Chem.* **2010**, *75*, 6716–6719.

79 Mitsunobu, O.; Yamada, Y. Preparation of Esters of Carboxylic and Phosphoric Acid via Quaternary Phosphonium Salts. *Bull. Chem. Soc. Japan* **1967**, *40*, 2380–2382.

80 Kumara Swarny, K. C.; Bhuvan Kumar, N. N.; Balaraman, E.; Pavan Kumar, K. V. P. Mitsunobu and Related Reactions: Advances and Applications. *Chem. Rev.* **2009**, *109*, 2551–2651.

81 Mitsunobu, O. The Use of Diethyl Azodicarboxylate and Triphenylphosphine in Synthesis and Transformation of Natural Products. *Synthesis* **1981**, *1*, 1–28.

82 Fletcher, S. The Mitsunobu Reaction in the 21st Century. *Org. Chem. Front.* **2015**, *2*, 739–752.

83 Yoshino, T.; Ng, F.; Danishefsky, S. J. A Total Synthesis of Xestodecalactone A and Proof of Its Absolute Stereochemistry: Interesting Observations on Dienophilic Control with 1,3-Disubstituted Nonequivalent Allenes. *J. Am. Chem. Soc.* **2006**, *128*, 14185–14191.

84 Beugelmans, R.; Zhu, J.; Husson, N.; Bois-Choussy, M.; Singh, G. P. The First Examples of SNAr-Based Macrocyclisation: Synthesis of Model Carboxylate-Binding Pockets of Vancomycin. *J. Chem. Soc., Chem. Commun.* **1994**, 439–440.

85 Beugelmans, R.; Singh, G. P.; Bois-choussy, M.; Chastanet, J. SNAr-Based Macrocyclization: An Application to the Synthesis of Vancomycin Family Models. *J. Org. Chem.* **1994**, *59*, 5535–5542.

86 Beugelmans, R.; Bois-Choussy, M.; Vergne, C.; Bouillon, J.-P.; Zhu, J. Synthesis of a Model Bicyclic C-O-D-O-E Ring of Vancomycin by a One-Pot, Double S$_N$Ar Based Macrocyclization. *Chem. Commun.* **1996**, *9*, 1029–1030.

87 Beugelmans, R.; Bourdet, S.; Zhu, J. A New Access to 14-Membered Macrocycle: Synthesis of Model F-O-G Ring of Teicoplanin. *Tetrahedron Lett.* **1995**, *36*, 1279–1282.

88 Boger, D. L.; Borzilleri, R. M. An Unusually Facile SNAr 14-Membered Biaryl Ether Macrocyclization Reaction Suitable for Preparation of the Cycloisodityrosine Subunit of Bouvardin, Deoxybouvardin and Related Agents. *Bioorg. Med. Chem. Lett.* **1995**, *5*, 1187–1190.

89 Beugelmans, R.; Bigot, A.; Bois-Choussy, M.; Zhu, J. A New Approach to the Synthesis of Piperazinomycin and Bouvardin: Facile Access to Cycloisodityrosine via an Intramolecular S$_N$Ar Reaction. *J. Org. Chem.* **1996**, *61*, 771–774.

90 Cortes Morales, J. C.; Guillen Torres, A.; González-Zamora, E. Total Synthesis of Plagiochin D by an Intramolecular S$_N$Ar Reaction. *Eur. J. Org. Chem.* **2011**, *17*, 3165–3170.

91 Roussi, G.; Zamora, E. G.; Carbonnelle, A. C.; Beugelmans, R. Synthesis of a Model of Chloropeptins I, II Western Subunit by the Intramolecular S$_N$Ar Based Methodology. *Tetrahedron Lett.* **1997**, *38*, 4401–4404.

92 Wang, Z.; Bois-Choussy, M.; Jia, Y.; Zhu, J. Total Synthesis of Complestatin (Chloropeptin II). *Angew. Chem., Int. Ed.* **2010**, *49*, 2018–2022.

93 Taoues, L.; Zhu, J. An Asymmetric Total Synthesis of Sanjoinine G1. *Tetrahedron Lett.* **1999**, *40*, 83–86.

94 Pearson, A. J.; Bignan, G.; Zhang, P.; Chelliah, M. Cycloetherification Reactions of Areneruthenium Complexes: Construction of a 16-Membered Cyclic Peptide Model for Teicoplanin. *J. Org. Chem.* **1996**, *61*, 3940–3941.

95 Pearson, A. J.; Heo, J.-N. Synthetic Studies on the DEF Ring System of Ristocetin A via Ruthenium-Promoted S_NAr Reaction: Problems and Solutions Using Arylserine–Ru Complexes. *Tetrahedron Lett.* **2000**, *41*, 5991–5996.

96 Pearson, A. J.; Heo, J.-N. Approaches to the Fully Functionalized DEF Ring System of Ristocetin A via Highly Selective Ruthenium-Promoted S_NAr Reaction. *Org. Lett.* **2000**, *2*, 2987–2990.

97 Pearson, A. J.; Zigmantas, S. Synthetic Studies on the BCDF Ring System of Ristocetin A via Ruthenium-Promoted S_NAr Reaction. *Tetrahedron Lett.* **2001**, *42*, 8765–8768.

98 Mai, C.-K.; Sammons, M. F.; Sammakia, T. A Concise Formal Synthesis of Diazonamide A by the Stereoselective Construction of the C10 Quaternary Center. *Angew. Chem., Int. Ed.* **2010**, *49*, 2397–2400.

99 Lee, H. B.; Zaccaro, M. C.; Pattarawarapan, M.; Roy, S.; Saragovi, H. U.; Burgess, K. Syntheses and Activities of New C10 β-Turn Peptidomimetics. *J. Org. Chem.* **2004**, *69*, 701–713.

100 Boger, D. L.; Yohannes, D. Intramolecular Ullmann Condensation Reaction: An Effective Approach to Macrocyclic Diaryl Ethers. *J. Org. Chem.* **1991**, *4*, 1763–1767.

101 Boger, D. L.; Yohannes, D. Total Synthesis of Deoxybouvardin and RA-VII: Macrocyclization via an Intramolecular Ullmann Reaction. *J. Am. Chem. Soc.* **1991**, *113*, 1427–1429.

102 Boger, D. L.; Zhou, J. Total Synthesis of (+)-Piperazinomycin. *J. Am. Chem. Soc.* **1993**, *115*, 11426–11433.

103 Boger, D. L.; Sakya, S. M.; Yohannes, D. Total Synthesis of Combretastatin D-2: Intramolecular Ullmann Macrocyclization Reaction. *J. Org. Chem.* **1991**, *56*, 4204–4207.

104 Zhou, Q.; Su, L.; Jiang, T.; Zhang, B.; Chen, R.; Jiang, H.; Ye, Y.; Zhu, M.; Han, D.; Shen, J.; Dai, G.; Li, Z. Copper/Iron-Catalyzed Ullmann Coupling of Diiodo- and Dibromoarenes and Diphenols for the Synthesis of Aryl Ether Macrocycles. *Tetrahedron* **2014**, *70*, 1125–1132.

105 Boger, D. L.; Patane, M. A.; Zhou, J. C. Total Synthesis of Bouvardin, O-Methylbouvardin, and O-Methyl-N-9-Desmethylbouvardin. *J. Am. Chem. Soc.* **1994**, *116*, 8544–8556.

106 Cai, Q.; Zou, B.; Ma, D. Mild Ullmann-Type Biaryl Ether Formation Reaction by Combination of Ortho-Substituent and Ligand Effects. *Angew. Chem., Int. Ed.* **2006**, *45*, 1276–1279.

107 Uchiro, H.; Kato, R.; Arai, Y.; Hasegawa, M.; Kobayakawa, Y. Total Synthesis of Hirsutellone B via Ullmann-Type Direct 13-Membered Macrocyclization. *Org. Lett.* **2011**, *13*, 6268–6271.

108 Shen, L.; Simmons, C. J.; Sun, D. Microwave-Assisted Synthesis of Macrocycles via Intramolecular and/or Bimolecular Ullmann Coupling. *Tetrahedron Lett.* **2012**, *53*, 4173–4178.

109 Shen, L.; Maddox, M. M.; Adhikari, S.; Bruhn, D. F.; Kumar, M.; Lee, R. E.; Hurdle, J. G.; Lee, R. E.; Sun, D. Syntheses and Evaluation of Macrocyclic Engelhardione Analogs as Antitubercular and Antibacterial Agents. *J. Antibiot.* **2013**, *66*, 319–325.

110 Fraunhoffer, K. J.; Prabagaran, N.; Sirois, L. E.; White, M. C. Macrolactonization via Hydrocarbon Oxidation. *J. Am. Chem. Soc.* **2006**, *128*, 9032–9033.

111 Stang, E. M.; White, M. C. Total Synthesis and Study of 6-Deoxyerythronolide B by Late-Stage C–H Oxidation. *Nat. Chem.* **2009**, *1*, 547–551.

112 Stang, E. M.; White, M. C. On the Macrocyclization of the Erythromycin Core: Preorganization Is Not Required. *Angew. Chem., Int. Ed.* **2011**, *50*, 2094–2097.

113 Lumbroso, A.; Abermil, N.; Breit, B. Atom Economic Macrolactonization and Lactonization via Redox-Neutral Rhodium-Catalyzed Coupling of Terminal Alkynes with Carboxylic Acids. *Chem. Sci.* **2012**, *3*, 789–793.

114 Kan, T.; Fujiwara, A.; Kobayashi, H. Efficient Macrocyclization by Means of 2-Nitrobenzenesulfonamide and Total Synthesis of Lipogrammistin-A. *Tetrahedron* **2002**, *58*, 6267–6276.

115 Hughes, R.; Meyers A. I. A Route to Chiral, Non-Racemic Macroheterocycles. *Tetrahedron* **1998**, *54*, 9895–9902.

116 Kurosawa, W.; Kan, T.; Fukuyama, T. Stereocontrolled Total Synthesis of (−)-Ephedradine A (Orantine). *J. Am. Chem. Soc.* **2003**, *125*, 8112–8113.

117 Hovinen, J.; Sillanpää, R. Synthesis of Azamacrocycles via a Mitsunobu Reaction. *Tetrahedron Lett.* **2005**, *46*, 4387–4389.

118 Cristau, P.; Vors, J.-P.; Zhu, J. Rapid Synthesis of Cyclopeptide Alkaloid-Likepara-Cyclophanes by Combined Use of Ugi-4CR and Intramolecular SNAr Reaction. *QSAR Comb. Sci.* **2006**, *25*, 519–526.

119 West, C. W.; Rich, D. H. Novel Cyclic Tripeptides and Substituted Aromatic Amino Acids via Ruthenium-Activated S_NAr Reactions. *Org. Lett.* **1999**, *1*, 1819–1822.

120 Toumi, M.; Couty, F.; Evano, G. Total Synthesis of the Cyclopeptide Alkaloid Abyssenine A. Application of

Inter- and Intramolecular Copper-Mediated Coupling Reactions in Organic Synthesis. *J. Org. Chem.* **2007**, *72*, 9003–9009.

121 Collins, J. C.; Farley, K. A.; Limberakis, C.; Liras, S.; Price, D.; James, K. Macrocyclizations for Medicinal Chemistry: Synthesis of Druglike Macrocycles by High-Concentration Ullmann Coupling. *J. Org. Chem.* **2012**, *77*, 11079–11090.

122 MaGee, D. I.; Beck, E. J. The Use of the Ramberg-Bäcklund Rearrangement for the Formation of Aza-Macrocycles: A Total Synthesis of Manzamine C, *Can. J. Chem.* **2000**, *78*, 1060–1066.

123 Nefzi, A.; Arutyunyan, S.; Fenwick, J. E. Two-Step Hantzsch Based Macrocyclization Approach for the Synthesis of Thiazole-Containing Cyclopeptides. *J. Org. Chem.* **2010**, *75*, 7939–7941.

124 Baird, L. J.; Timmer, M. S.; Teesdale-Spittle, P. H.; Harvey, J. E. Total Synthesis of Aigialomycin D using a Ramberg-Bäcklund/RCM Strategy. *J. Org. Chem.* **2009**, *74*, 2271–2277.

125 Zhang, J.; Niu, Y.; Cao, X.; Ye, X.-S. Convenient One-Pot Synthesis of Thiosugars and Their Efficient Conversion to Polyoxygenated Cycloalkenes. *Tetrahedron* **2012**, *68*, 4242–4247.

126 Aimetti, A. A.; Shoemaker, R. K.; Lin, C.-C.; Anseth, K. S. Synthesis of Cyclic, Multivalent Arg-Gly-Asp using Sequential Thiol-Ene/Thiol-Yne Photoreactions. *Chem. Commun.* **2010**, *46*, 5781–5783.

127 Wang, Y.; Chou, D. H.-C. A Thiol-Ene Coupling Approach to Native Peptide Stapling and Macrocyclization. *Angew. Chem., Int. Ed.* **2015**, *54*, 10931–10934.

14

Macrocycles from Multicomponent Reactions

Ludger A. Wessjohann, Ricardo A. W. Neves Filho, Alfredo R. Puentes and Micjel Chávez Morejón

Leibniz Institute of Plant Biochemistry, Halle (Saale), Germany

14.1 Introduction

Macrocycles are designated as molecules that bear a ring architecture composed of 12 or more atoms. Although there is some agreement around this informal definition, some authors also refer to medium-sized cycles (9–12 atoms) as macrocycles [1]. Currently, more than 100 000 natural products are known, and within this group, at least 3% possess a macrocyclic ring (Figure 14.1) [2]. Notwithstanding the relatively small (but compared to macrocycles in synthetic molecules still over-proportional) rate of occurrence, these compounds have delighted scientists around the world due to their special physicochemical properties, their roles in biological systems, and the associated synthetic challenges [3–5].

Despite the rapid advancement of molecular modeling, synthetic, and combinatorial techniques, which constantly improve the performance of rational drug design, some 40% of the currently marketed drugs are natural products or synthetic compounds derived from them [6]. This trend is even more pronounced when analyzing the restricted space of marketed macrocyclic drugs [7]. Although some purely synthetic macrocycles are currently in clinical phase development, so far mostly natural compounds or derived compounds have been approved as marketable drugs. In fact, while most of drug discovery research has been performed within the limits of the Lipinski's rule of five and other guidelines for oral availability [8], most of the marketed naturally occurring macrocycle pharmaceuticals violate these rules. A good example is the case of the cyclosporine A, an orally available cyclo-undecapeptide used since many years as an immunosuppressant agent in organ transplantation [9]. This compound possesses 5 hydrogen bond donors, 11 hydrogen bond receptors, 6.92 cLog$P$ value, and 1202 Da molecular weight and, accordingly, clearly violates Lipinski's rule of five in all aspects. The secret behind the bioavailability and high binding power

of cyclosporine A and other macrocycles is their inherent conformational mobility, which allows them to reduce conformational flexibility via transannular interactions or enables them to show Janus-like behavior. In other words, these compounds are able to turn inside out and back to present either hydrophilic or lipophilic groups on the outside, allowing them to modulate their externally evident physicochemical characteristics according to the environment. Making use of this property, the macrocyclic framework of cyclosporine A can "hide" its excessive hydrogen bonds donors and acceptors when exposed to a hydrophobic environment (Figure 14.2) [10, 11]. These changes reduce the total polar surface area, and the compound becomes membrane permeable (see also Chapter 3) [12].

In peptidic natural macrocycles like cyclosporine, lipophilicity, conformation—including *s-cis/s-trans* isomerism of the peptide bonds—and the hydrogen donor and internal hydrogen bridges are commonly controlled by N-methylation (in addition to proline and pipecolic acid units). Indeed, proper positioning of amide N-alkylation can be considered a crucial step in controlling conformation, physicochemical properties, and biodegradation inertia in such macrocycles and will have to be addressed by any synthetic access to such compounds.

For the same reasons, that is, conformational bias paired with conformational mobility, macrocycles can bind to their enzymatic receptors with a reduced entropic penalty [1, 10, 13]. Moreover, macrocycles can display their surface area in a different way than their acyclic analogues that makes them especially suited for binding flat, extended protein surfaces [13]. Because of these features, it is widely accepted that macrocyclization can lead to improved binding and pharmacokinetics compared to many similar linear drug candidates [14]. Table 14.1 highlights some examples of this trend. To summarize, the fact of being conformationally constrained, but not
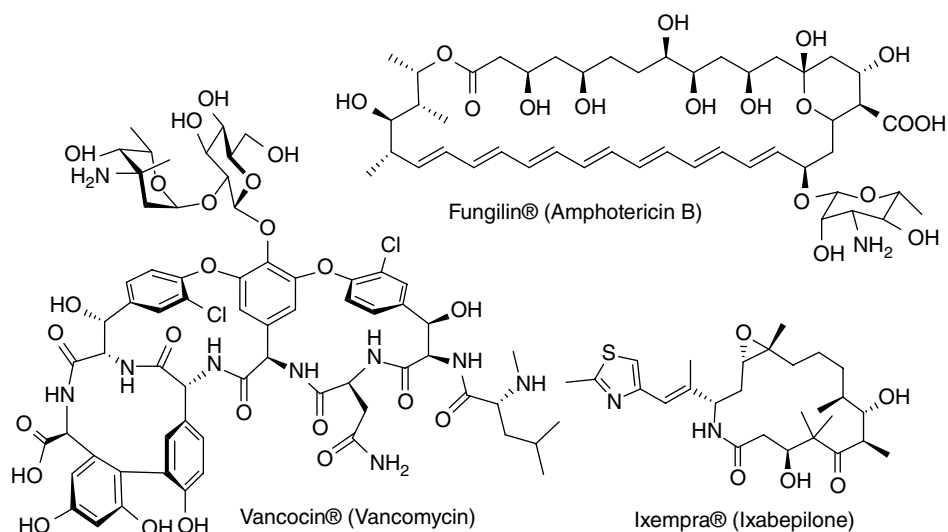
Figure 14.1 Selected naturally occurring macrocyclic drugs or simple derivatives derived from a natural product lead.
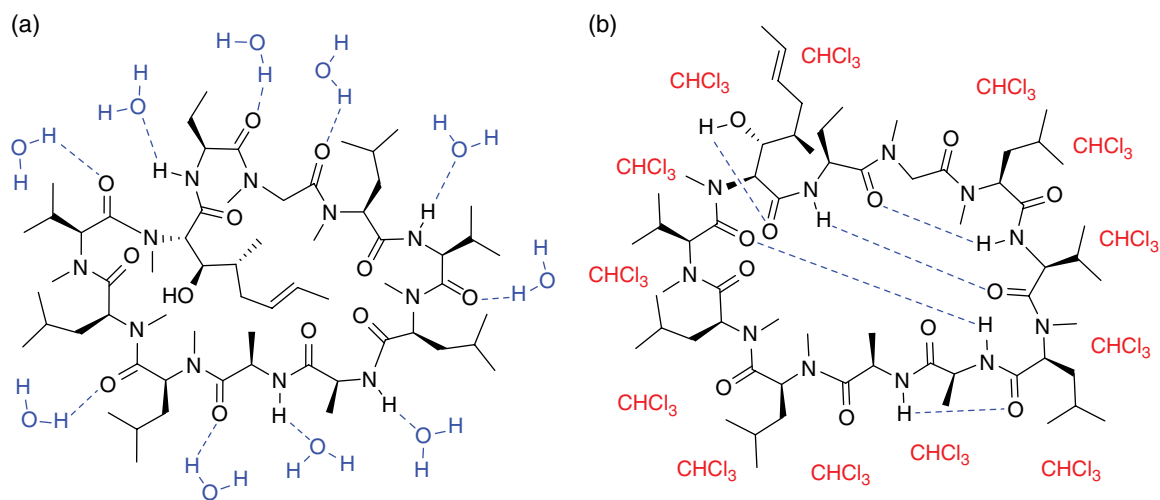
Figure 14.2 (a) Schematic sketch of solvated cyclosporine A conformation in polar medium (water), highlighting possible hydrogen interactions with the solvent. (b) Schematic sketch of cyclosporine A conformation in nonpolar medium (chloroform), showing the macrocycle "hiding" some of its hydrogen donors and acceptors through intramolecular interactions. (*See insert for color representation of the figure.*)

entirely rigid, places macrocycles in a privileged intermediate position within bioactive compound space, exhibiting the binding power of biologics while retaining the bioavailability and other favorable development characteristics of small ligands at the same time [20]. Moreover, macrocyclic drug hits have also been found in fields where rational design is difficult, for example, antibiotic research [21].

The applications of macrocycles in medicinal chemistry seem limitless, and, most likely, unprecedented uses for these compounds are still hidden in the unique properties they may exhibit. Nevertheless, the exploration of this chemical space depends on the constant development of synthetic methods to enable the efficient preparation of these compounds with a reasonable level of structural control and functional diversity [22, 23]. Although the difficulties associated with the synthesis of macrocycles have hampered the exploration of this class of compound within the pharmaceutical industry in the past years, thanks to the recent advances in synthetic approaches, this picture is changing and a number of purely synthetic macrocycles are already in clinical development (Figure 14.3) [7, 24]. For example, the dual JAK2/FLT3 inhibitor, pacritinib, advanced to phase II

Table 14.1 Effect of macrocyclization on the biological activity of linear molecules.
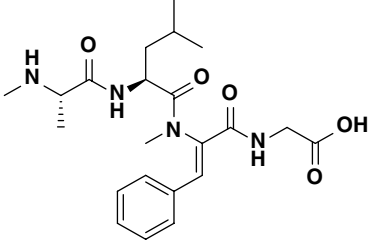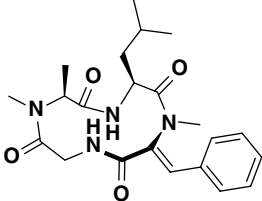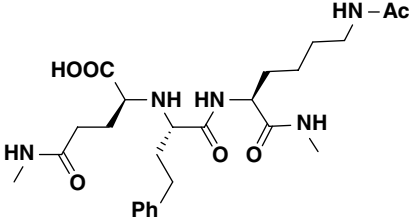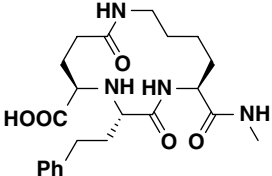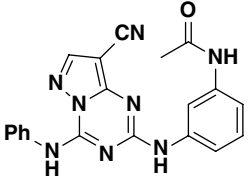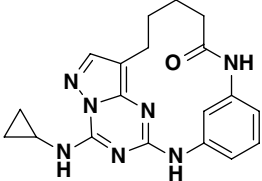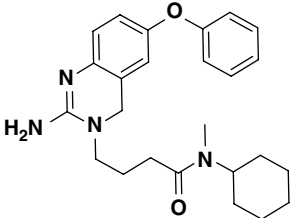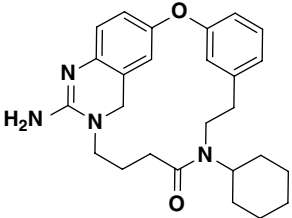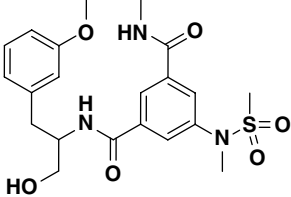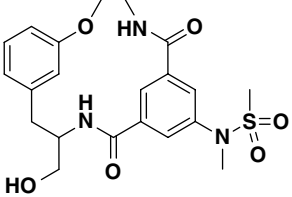
Compound		Property	Gain in activity (fold)
Linear	Cyclic		
		Phytotoxicity toward lettuce seedlings	1.31 [Ref. 15]
		Metalloproteinase MMP-8 inhibitor	17 [Ref. 16]
		Checkpoint kinase 1 (CK1) inhibitor	1.2 [Ref. 17]
		Beta secretase (BACE) inhibitor	180 [Ref. 18]
		Beta secretase 1 (BACE-1) inhibitor	>35 [Ref. 19]

Figure 14.3 Synthetic macrocyclic drug candidates. (a) JAK2/FLT3 inhibitor pacritinib (Phase II). (b) Anti-angiogenic RGD-cyclopeptide (v.i.) cilengitide (Phase III).

(a)

Pacritinib (SB1518)
JAK2/FLT3 kinase inhibitor

(b)

Cilengitide
Anti-angiogenic compound
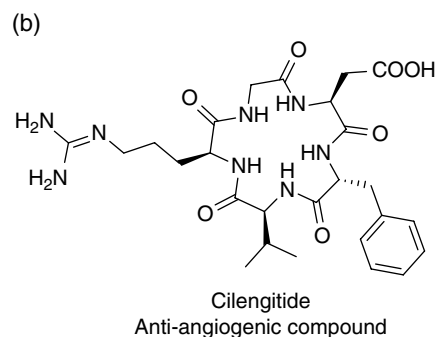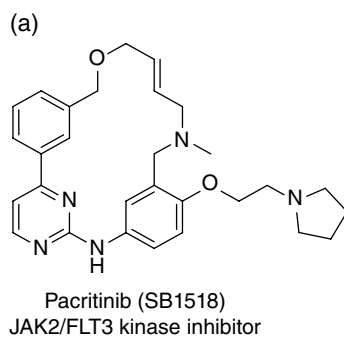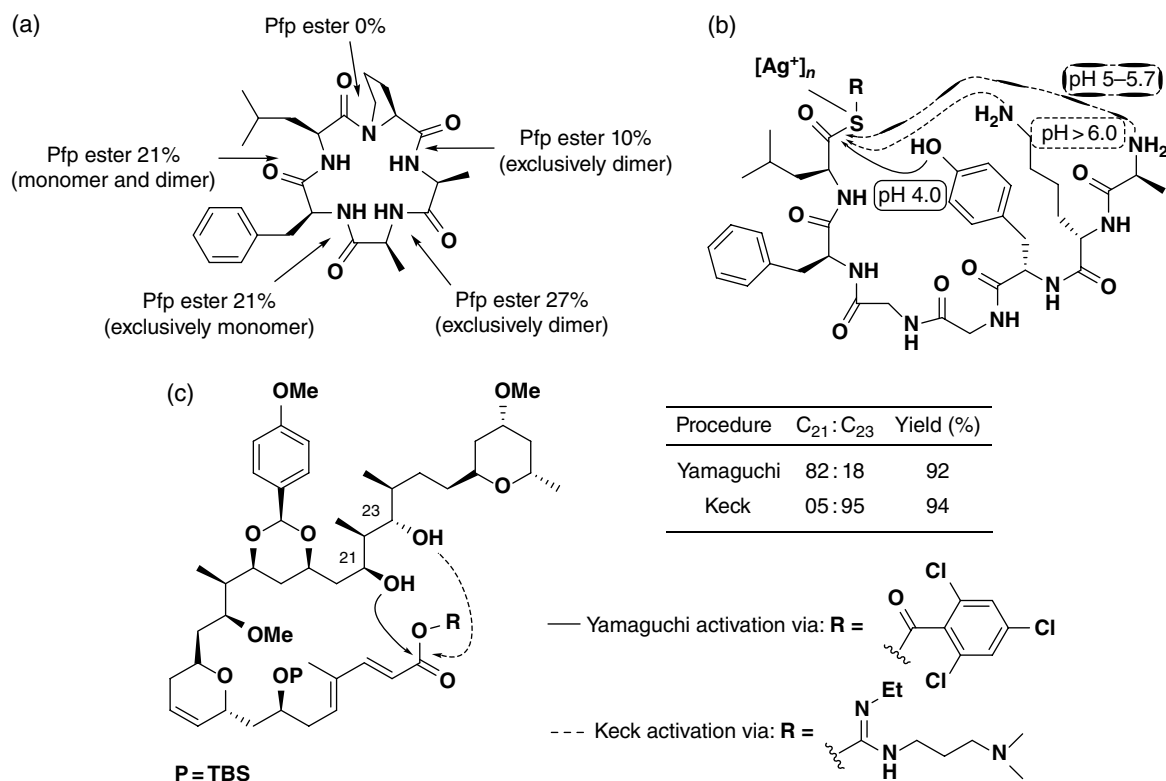
Figure 14.4 Some significant parameters in macrocyclization [29]. (a) All possible macrocyclization sites toward *cyclo*-[Pro-Ala-Ala-Phe-Leu] and associated yields. (b) pH-dependent Ag-ion-catalyzed macrocyclization of heptapeptide thioester. (c) Influence of coupling reagent on the macrolactonization of hemiswinholide A precursor. Source: Wessjohann *et al.* [1, 29]. Reproduced with permission of John Wiley & Sons.

trials, while the synthetic cyclic RGD-family peptide cilengitide is currently under phase III evaluation and is a promise for the treatment of glioblastoma [25, 26].

The most challenging step in the synthesis of a macrocycle is the macrocyclization reaction itself. The main drawbacks, associated with this transformation, are the occurrence of side reactions, mainly oligomerization, that is, linear or cyclic polymerization of the linear precursor to be (mono-) cyclized. In order to overcome this problem, macrocyclizations are usually performed under high- or pseudo-high-dilution conditions. In the latter case, the concentration of the cyclizing species is kept very low by adding it slowly to the reaction mixture [27]. Besides the reaction concentration, the outcome of a macrocyclization may also be influenced by other constraints, like structural features (prefolding) or pH and activation protocols, to mention a few [23, 28]. For example, in the synthesis of the *cyclo*[Pro-Ala-Ala-Phe-Leu], the choice of the position of the macrocyclization has a strong influence on the product formation (Figure 14.4a) [30]. In the silver-mediated cyclization of a heptapeptide thioester (Figure 14.4b) [31], it was observed that, at pH 4.0, macrolactonization involving the phenolic group of the tyrosine residue took place exclusively, since the amino functionalities were protonated and therefore unable to perform a nucleophilic attack on the activated C-terminus. In contrast, raising the pH to 5–5.7 range favored the head-to-tail cyclization, while more alkaline conditions (pH > 6.0) triggered the lactamization with the nucleophilic side chain (ε-amine of the lysine residue). In peptide cyclizations, the partial or total epimerization of the C-terminal residue is also often observed. Another interesting precedent is found in the end game of Peterson's total synthesis of hemiswinholide A [32] where macrolactonization of the linear precursor, under different activation conditions (Yamaguchi or Keck protocols; Figure 14.4c) [33, 34], leads to the formation of the natural product or its regioisomer, selectively.

In spite of the difficulties, a good level of understanding about macrocyclization processes has been achieved, and this knowledge has been used in the design and synthesis of macrocycles for a specific aim (see also Chapter 1). Macrocyclizations may be performed through two main processes: single-component (two center) reactions and multicomponent reactions (MCRs). Most of the single-component reaction-based macrocyclizations begin with the synthesis of a linear precursor carrying two tethered joinable functional
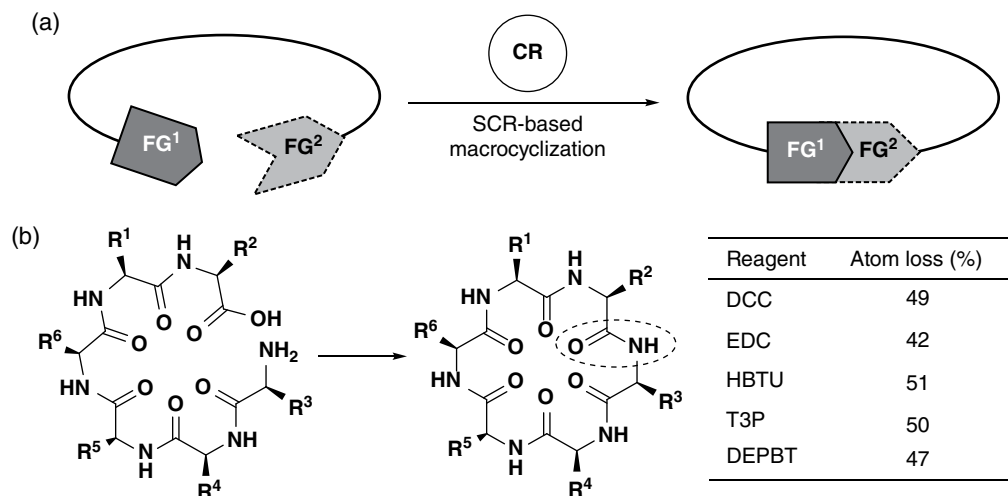
Scheme 14.1 (a) General scheme of a single-component macrocyclization approach (SCR). (b) SCR-macrolactamization of a hypothetical peptide and the effect of different coupling reagents on the atom economy of the entire process.

groups (FG). The ring-closure step is then triggered by the addition of a coupling partner, which may be a coupling reagent or a catalyst (Scheme 14.1a). This concept comprises many reactions like macrolactamizations, macrolactonizations, olefin metathesis, cycloadditions, and cross-couplings, which have been employed with remarkable results to cyclize long linear molecules [35]. In single-component reaction-based macrocyclizations, the role of the coupling partner is merely to activate the joinable FG and perform the ring-closing step; therefore, it does not offer any further possibility to add diversity into the final macrocyclic framework. Moreover, in some single-component macrocyclizations, many atoms are lost during the activation stage, which decreases considerably the atom efficiency of the entire process. As an example, Scheme 14.1b illustrates the macrolactamization of a hypothetical peptide and the effect of different coupling partners on the atom economy of the entire process.

An MCR is a process wherein three or more reagents condense to generate a product that contains most of the atoms involved in the operation. Each additional reagent delivers a diversity input into the final product, and, thus, with an *n*-component reaction, *n* variables of diversity are introduced per reaction, or, if two reaction centers are combined in one building block, for example, as in some in cyclization precursors (*vide infra*), *n* – 1 variables for diversity are possible. With the advent of green chemistry and the increasing pursuit for chemical processes endowed with high atom economy, MCRs stand out as a promise of sustainable development in organic synthesis. Among the known MCRs, the ones involving an isonitrile (isocyanide) [36] have experienced a tremendous boost since the discovery of the Passerini

three-component reaction (P-3CR) (Scheme 14.2a) and Ugi four-component reaction (Ugi-4CR) (Scheme 14.2b) [37–39]. A special beauty of these reactions is not only their diversity generating power and the excellent atom economy but also, foremost, the ease of application. They are mostly performed in alcohols, but they work in almost all kinds of solvents, even in water or without solvent, usually under normal humid oxidative atmosphere—as long as the building blocks themselves permit the conditions chosen. Although isonitrile-based multicomponent reactions (IMCRs), in particular the Ugi-4CR, have been employed in the synthesis of linear precursors of macrocycles toward diverse applications [40], their systematic use to accomplish the macrocyclization step itself remained overlooked until the last decade.

In contrast to classical SCR macrocyclizations, the MCR-based ones have a different working principle. In MCR macrocyclizations, the linear precursor carrying two tethered joinable FG is not activated by a transient reagent, but rather by a building block itself, which fulfills the macrocyclization step and installs new endo- or exocyclic functionalities with a minimum atom loss (Scheme 14.2c). In other words, IMCR-based protocols not only mediate the ring-closure step but also allow the atom economical incorporation of one or more components as additional diversity elements into the final product in one single transformation without demanding additional activation or purification of intermediates (Scheme 14.2d) [22, 41].

This chapter will survey approaches where IMCRs were applied to accomplish the macrocyclization of long linear molecules. The first part will introduce some insights about general aspects, concepts, and classifications of IMCR-based macrocyclizations.
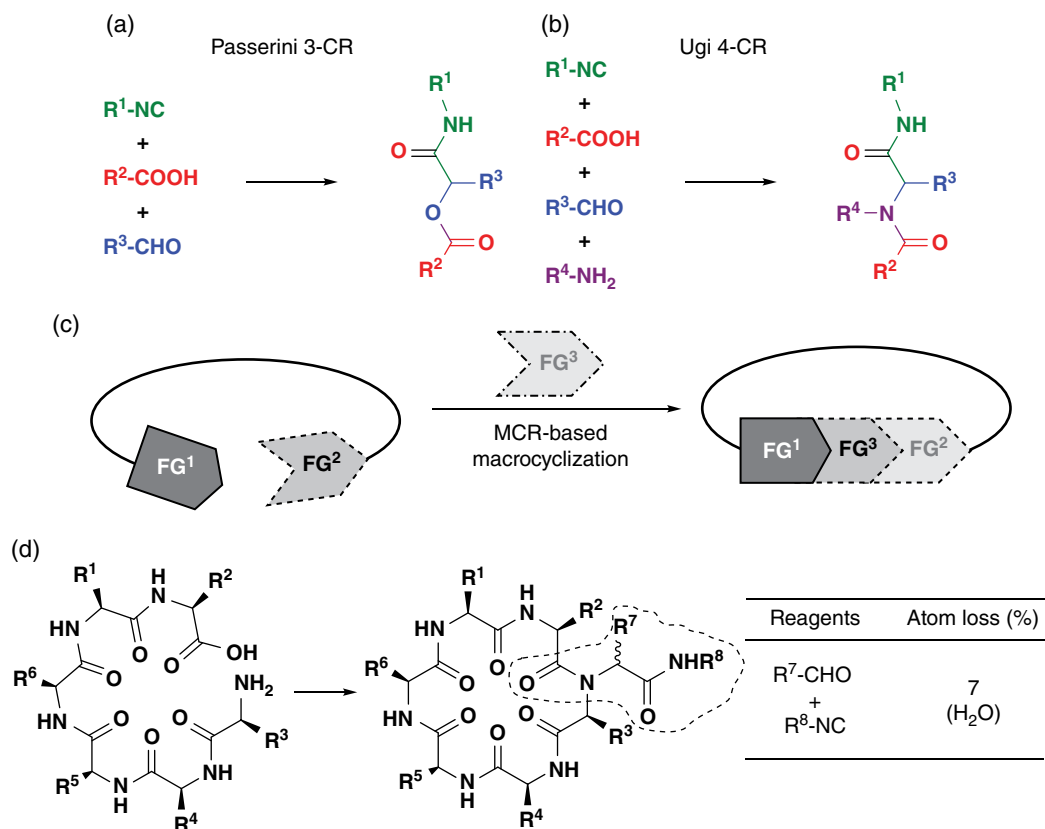
Scheme 14.2 (a) The Passerini three-component reaction (P3CR). (b) The Ugi four-component reaction (U4CR). (c) General scheme of a multicomponent macrocyclization approach (MiB). The macrocycle carries the diversity delivered by the additional component FG³ [22]. (d) Multicomponent reaction-based macrocyclization of a hypothetical peptide highlighting the atom economy of the entire process. (*See insert for color representation of the figure.*)

The second part will focus on the early development of this method and case studies, where it was applied to the synthesis of rationally designed macrocyclic molecules. Finally, a special topic on the use of multiple IMCR-based macrocyclizations for synthesizing three-dimensional structures will also be covered.

14.2 General Aspects of Multicomponent Reactions (MCRs) in Macrocycle Syntheses

14.2.1 The MiB Concept

In the context of macrocyclization, the term "MiB" stands for *multiple multicomponent macrocyclization including bifunctional building blocks* [22]. According to this general concept, one, two, or many bi- or polyfunctional building blocks carrying reactive functionalities are simultaneously submitted to an IMCR to build up a macrocyclic framework. Most typically, a Ugi reaction is involved as this provides peptide-like structures, with predominantly N-alkylated amide/lactam bonds, or a Passerini reaction for depsipeptide moieties. Both elements are commonly found in natural product drugs (see preceding text). The MiB strategy may be further classified as unidirectional (as in nature) or bidirectional depending on the amino(*N*)-to-carboxylate(*C*)-termini directionality of the peptide units formed (Scheme 14.3). MiBs involving one bifunctional building block can only be unidirectional (Scheme 14.3a). On the other hand, MiBs involving bifunctional building blocks may be unidirectional or bidirectional (Scheme 14.3b vs. c). For example, MiBs involving bifunctional building blocks of two different Ugi-reactive groups result in macrocycles containing dipeptide moieties (from the Ugi-4CR) running in the same direction (N- to C-terminal direction) and are, therefore, classified as unidirectional (Scheme 14.3b). Likewise, MiBs involving symmetrically bifunctionalized building blocks lead to the formation of dipeptide moieties running in counter directions from N- to C-terminus and are termed bidirectional (Scheme 14.3c). Although uncommon in nature, the bidirectional arrangement is easier with respect to building block synthesis and stability
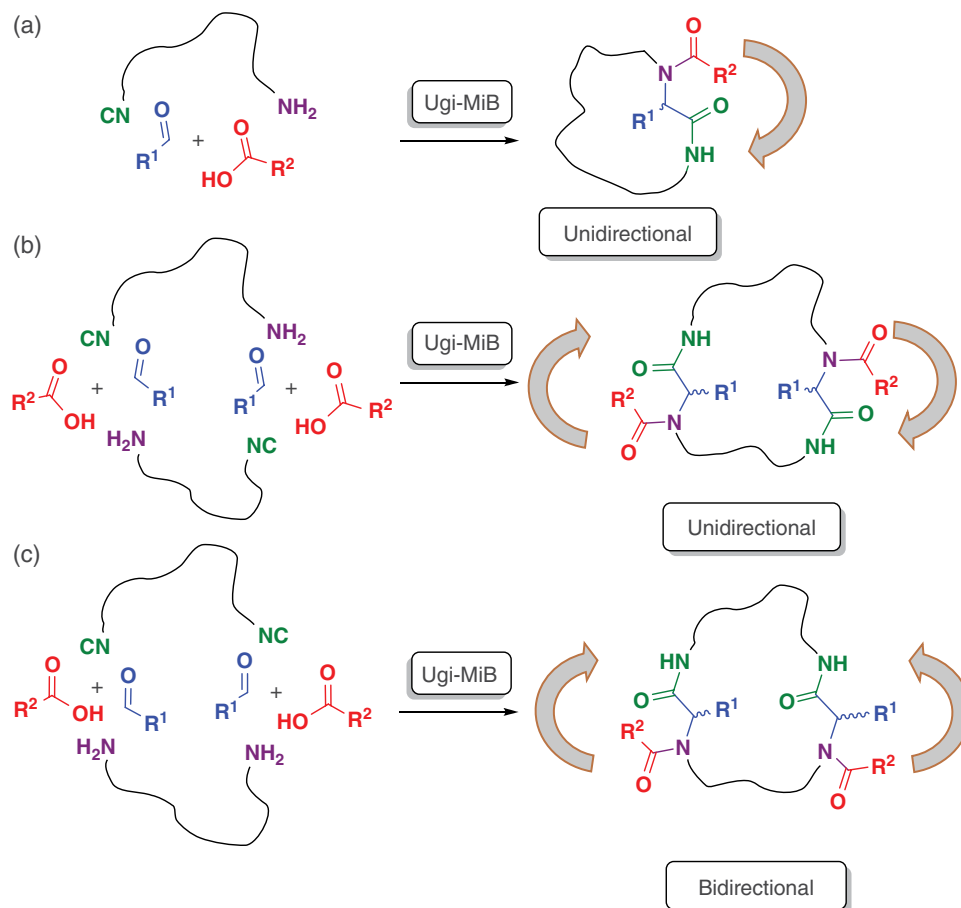
Scheme 14.3 Peptide N → C directionality in Ugi-MiB reactions. (a) MiBs involving one bifunctional building block. (b) Unidirectional Ugi-MiB involving two bifunctional building blocks. (c) Bidirectional Ugi-MiB with equally bifunctionalized building blocks lead to bidirectional products (N → C-terminus directions of peptide moieties run in counter-orientation) [22].
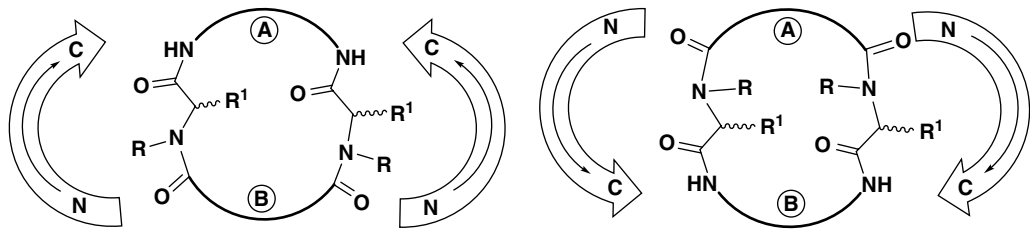
and also provides more elements of diversity, providing equally valuable scaffolds to those with the natural orientation.

The unidirectional MiBs are exposed to all limitations of the IMCR-based macrocyclization of a single bifunctional building block, for example, restricted compatibility of some functionalities if placed in the same building block. Meanwhile, the bidirectional approach has fewer restrictions since more building blocks are easily synthesized, interconvertible, or commercially available [22]. As stated previously, the bidirectional approach furnishes one extra element of diversity per moiety produced for each MCR. For instance, of the twelve possible bifunctional building block combinations [42], up to 64 possible isomers exist without even varying substituents within the building blocks (Table 14.2) [22]. It is important to note that, in the MiB lexicon, the term "symmetrically bifunctionalized" denotes a bifunctional building block with the same two FG (e.g., two isonitrile groups) on both ends of the molecule, which are important for MCR reactivity. The central part of the bifunctional building block

itself may be symmetric or asymmetric, independent of this. Similarly, "unsymmetrically bifunctionalized" building blocks have two different MCR-reactive FGs on either side (e.g., isonitrile and amino group). This terminology is independent of structural symmetry or asymmetry of the core of the building block, which attributes to the symmetry of the molecule as a whole and relates solely to the chemical equivalence of the reactive FGs (i.e., a (C_2)-symmetric bifunctional building block like $C{\equiv}N{-}CH_2{-}CH_2{-}N{\equiv}C$ is to be distinguished from a symmetrically bifunctionalized (unsymmetrical) building block like $C{\equiv}N{-}CH_2{-}C(CH_3)_2{-}N{\equiv}C$ or a symmetrically bifunctionalized (asymmetric) building block like $C{\equiv}N{-}CH_2{-}CH(CH_3){-}N{\equiv}C$).

14.2.2 Unidirectional Multicomponent Macrocyclizations/Cyclooligomerizations

One of the essential conditions for the cyclization reaction to take place is that at least one of the molecular building blocks must possess two reacting functionalities.

Table 14.2 Number of library members available for the two diacid/diisocyanide combinations in bidirectional Ugi-MiBs, excluding higher cyclic oligomers.

Diversity elements

Bifunctional building block	Oxo-cpd	Constitut. isomers	Diastereomers	All isoforms
sym. A = sym. B	$R^1 = H$	1	1	1
sym. A = sym. B	$R^1 \neq H$	1	2	3*
sym. A ≠ sym. B	$R^1 = H$	2 (C↔N)	2	2
sym. A ≠ sym. B	$R^1 \neq H$	2 (C↔N)	4	6*
C_2-unsym. A ≠ sym. B	$R^1 = H$	2 (C↔N)	2	2
C_2-unsym. A ≠ sym. B	$R^1 \neq H$	2 (C↔N)	4	8
C_2-unsym. A ≠ C_2-unsym. B	$R^1 = H$	4 (C↔N + regio)	4	4
C_2-unsym. A ≠ C_2-unsym. B	$R^1 \neq H$	4 (C↔N + regio)	8	16
asym. A ≠ sym. B	$R^1 \neq H$	2 (C↔N)	8	16
asym. A ≠ asym. B	$R^1 \neq H$	4 (C↔N + regio)	16	32

Σ 32 variations for C → N + Σ 32 variations for N → C

Shown are selected combinations of only some of the overall 64 tunable diversity elements: combinations of oxo- and bifunctional groups of varying symmetry (R not varied).

C↔N, both directionalities of the peptoid boxes appear (C→N + N→C); Regio, mixture of head-to-head (H–H), and head-to-tail (H–T) isomers; Diastereomers, Σ of all diastereomers of all constitutional isomers; Isoforms, Σ of all constitutional and stereoisomers; *, Meso + D/L-form(s); Asym., chiral bifunctional building block; C_2-unsym., achiral bifunctional building block without C_2-axis halfway between the two Ugi-reactive groups, for example, $CN–CH_2–CH_2–C(CH_3)_2–NC$.

If the size of the ring formed during the closing step of these two groups is of at least 12 atoms, the obtained product can be classified as a macrocycle based on the accepted definition. Among all the reactions comprising IMCRs, the Ugi-4CR allows, theoretically, the achievement of at least six different building block combinations based upon the components of this process (Scheme 14.4): (a) amino–carboxylic acid (peptide), (b) carboxylic acid–isonitrile, (c) carboxylic acid–aldehyde, (d) amine–aldehyde, (e) aldehyde–isonitrile, and (f) amine–isonitrile. For every combination, the atoms belonging to the bifunctional building blocks remain endocyclic, while those from the additional monofunctional Ugi-components appear totally, or to some extent, exocyclic, that is, they define the side chain functionality [42].

Out of these six combinations, the most widely explored and successful unidirectional approach is using the amino–carboxylic acid bifunctional building block, that is, ω-amino acids or peptides. Several efforts have been done to perform macrocyclizations involving the

other combinations. All combinations work but some drawbacks have been found for some. For example, an MiB involving a carboxylic acid–isonitrile bifunctional building block (Scheme 14.4b) gave only traces of the desired product [1b, 22, 29]. The authors suggested the incompatibility of carboxylic acid and isonitrile functionalities as the cause for the unsatisfying reaction outcome. However, this obstacle has been recently overcome by replacing the carboxylic acid moiety for its related carboxylate in a combined carboxylate—isonitrile bifunctional building block. The authors use α-isocyano-ω-carboxylates of different lengths ($n = 9–15$) to assembly scaffolds in which all Ugi-components get in an endocyclical functionalized macrocycle, topologically similar as appears in Scheme 14.4b [41].

In 1979, Failli and coworkers reported the first macrocyclization protocol based on IMCR [43]. The investigation began with the reaction of benzaldehyde, cyclohexyl isonitrile, and the tripeptide **1**, trying to generate the monomeric macrocycle **2** (Scheme 14.5a). The formation
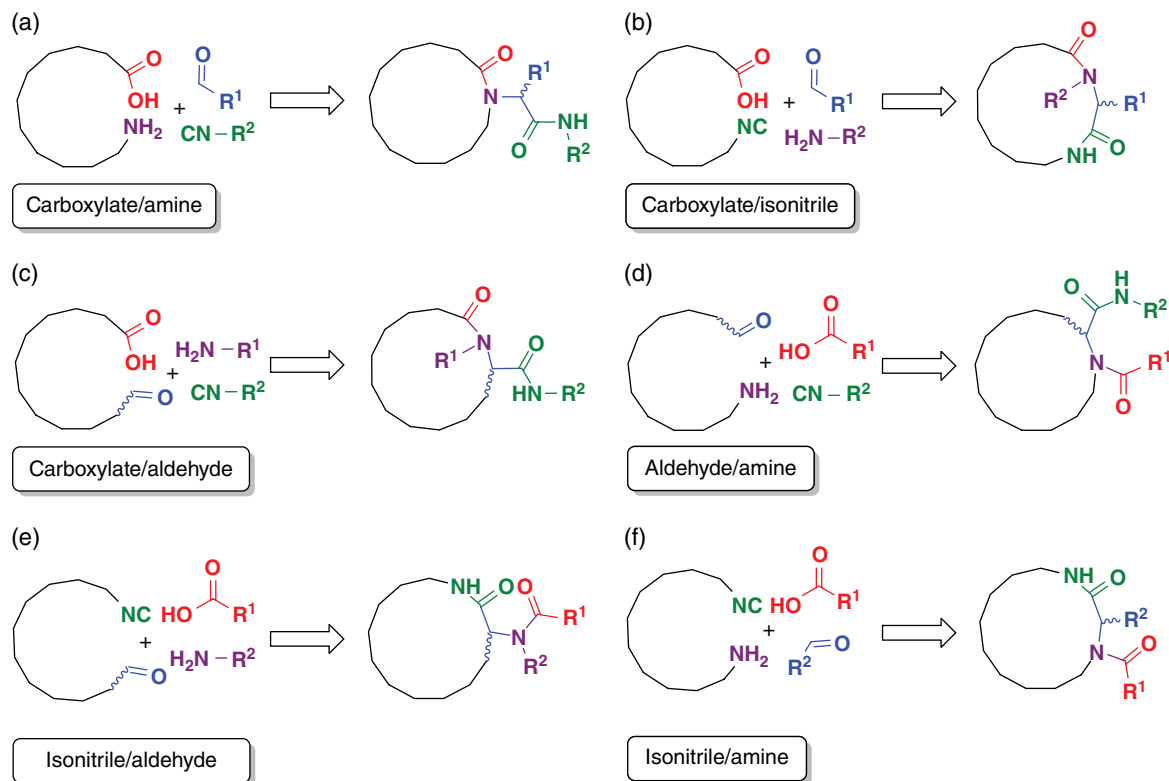
Scheme 14.4 Ugi-4CR-based macrocyclizations of single bifunctional building blocks. The monofunctional building blocks define the side chain functionality. (*See insert for color representation of the figure.*)

of the expected product was not observed; instead, dimeric macrocycle **3** was obtained in low yield. Apparently the high strain required for the formation of a 9-membered ring directed the reaction into a cyclodimeric pathway. In order to verify this hypothesis, a second experiment using the hexapeptide **4** was performed. In this example, the expected macrocycle **5** was formed, and no trace of cyclooligomerization was detected (Scheme 14.5b). Lately, this reaction was used to synthesize a cyclic analogue (**6**) of eledoisin, a neural peptide of mollusk origin (Scheme 14.5c) [44].

After almost 30 years since the publication of Failli's first exploratory research, the inactivity in linking MCRs and macrocycles was broken by Wessjohann and coworkers [1b, 42]. They synthesized a series of cyclopentapeptoids containing the bioactive Arg–Gly–Asp (RGD) sequence [45]. The relevance of the RGD sequence lays in its universal recognition role in cell–cell and cell–matrix interactions [46]. This recognition function is involved in countless important pathological processes, including tumor metastasis, angiogenesis, osteoporosis, and thrombosis [26, 47]. It is also known that binding of extracellular proteins to cellular receptors is inhibited when the RGD sequence has a defined conformation, which may be achieved by macrocyclization (cf. also Fig 14.3b).

Instead of cyclizing natural RGDx-peptides by MCR, the RGD moiety itself can also be mimicked and substituted by Ugi-MCR-dipept(o)ids [45]. The designed peptidomimetics are built on a peptoidic framework in which the side chain is bonded to the amide nitrogen instead of the alpha carbon. This structural modification not only alters the hydrogen-bonding pattern of the backbone in this kind of peptide surrogate but also changes the conformational space it occupies and increases its metabolic stability in biological systems [48]. The synthesis of the different linear precursors was developed through a sequence of systematic Ugi-4CRs as depicted in Scheme 14.6. The macrocyclization step of pentapeptoid **7** was accomplished in the presence of *tert*-butyl isonitrile and paraformaldehyde by slowly adding the bifunctional pept(o)id component under pseudo-high-dilution conditions in order to avoid undesirable oligomerization. This protocol provided the RGD-cyclopeptoid **7** in 21% yield (four steps), after removal of the protecting groups (Scheme 14.6a). Recently, a similar procedure was employed in the synthesis of cyclodepsipeptoid analogues of Sansalvamide A (Scheme 14.6b), a natural pentacyclodepsipeptide that exhibits cytotoxicity against multiple cancer cell lines [49].

A comparison of the reaction conditions employed in Failli's and Wessjohann's work shows that Ugi-4CR-based

(a)

Ethylene glycol
(0.6 M) r.t., 9 days

Cyclomonomer (**2**)
(not observed)

Cyclodimer (**3**)
Yield: 5%

(b)

DMSO
(0.3 M) r.t., 5 days

Cyclomonomer (**5**)
Yield: 19%

Cyclodimer
(not observed)

(c)

DMF
(0.4 M), r.t. 65 h

Eledoisin analog (**6**)
33%
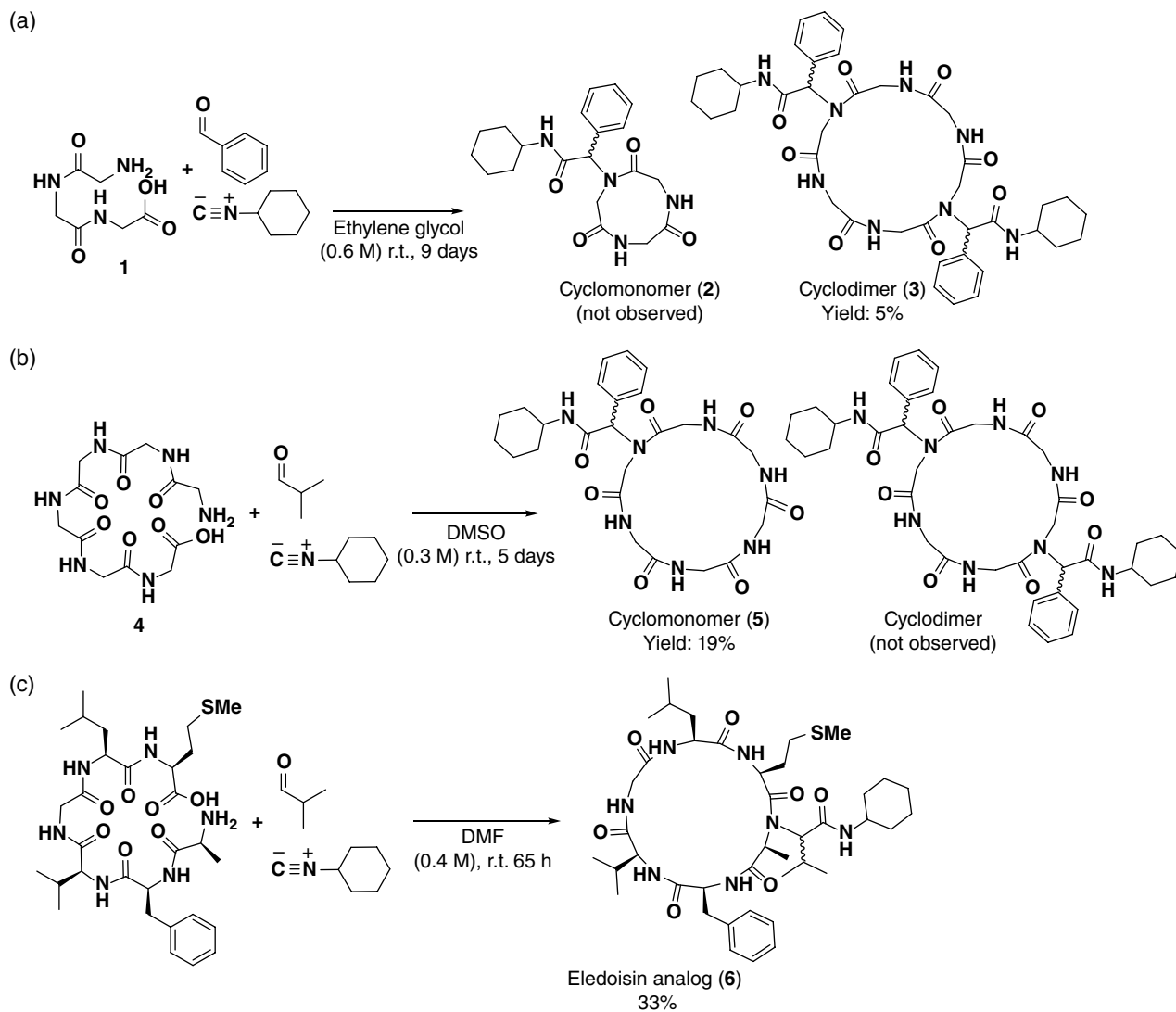
Scheme 14.5 The first Ugi-4CR macrocyclizations reported utilized linear oligoglycines. (a) Unidirectional MiB reaction involving triglycine; (b) Unidirectional MiB reaction involving hexaglycine; (c) Synthesis of an eledoisin cyclic analogue (**6**).

(a)

Dmb = dimethoxybenzyl
Pmc = 2,2,5,7,8-pentamethyl-6-sulfonyl

1. *t*-BuNC, (CH₂O)ₙ, MeOH
   2 mM (0.6 ml h⁻¹), 24 h.
2. TFA, CH₂Cl₂

21%
7

(b)

(CH₂O)ₙ + R-NC

Na₂SO₄, MeOH
0.6 ml h⁻¹(0.8 mM)
r.t. 4.5 days

6 examples
33–49% yield
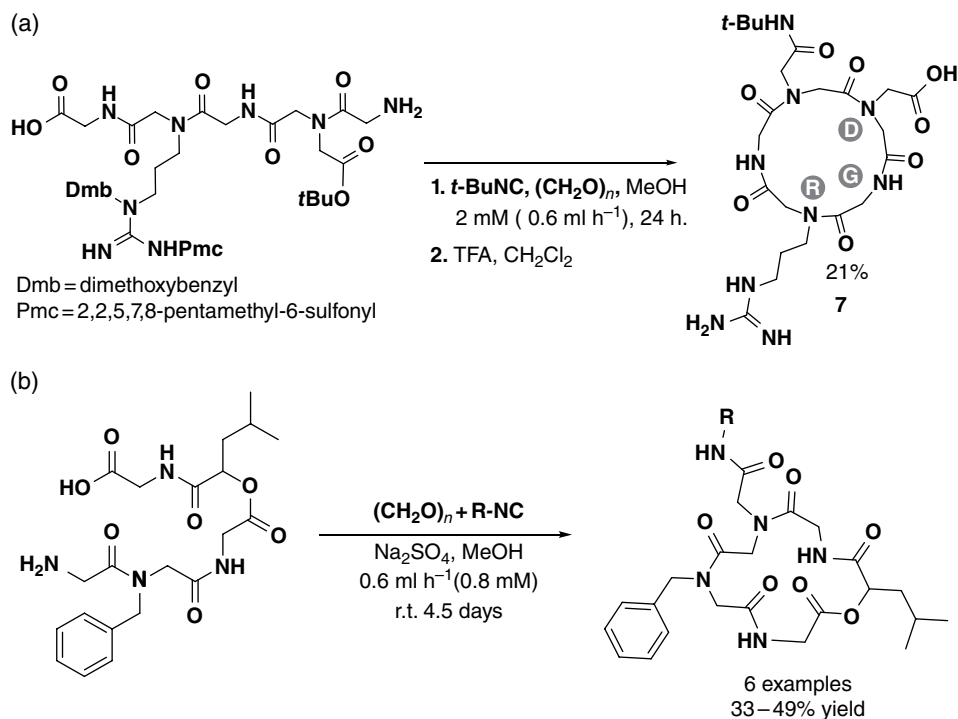
Scheme 14.6 (a) MiB approach to RGD mimetic cyclopeptoid **7**. (b) MiB approach to cyclodepsipeptoid analogues of Sansalvamide A.

macrocyclizations can be successfully achieved in both concentrated and pseudo-dilution conditions. This raises the question whether the bifunctional precursor concentration plays the same critical role in the Ugi-4CR-based macrocyclization of peptides compared to conventional peptide couplings (where it is crucial if no suitable prefolding is present). Recently, Yudin's group provided proof that Ugi-4CR-based macrocyclization may be run under higher concentration conditions than comparable standard macrocyclizations (Scheme 14.7a) [50, 51]. They proposed that in particular organic solvents, short linear peptides may adopt circular conformations as a result of the electrostatic interactions between the C- and N-termini. In conventional peptide macrocyclizations, the carboxylic acid group is converted into an activated, uncharged intermediate, which then undergoes a nucleophilic attack by the tethered amino group, giving rise to a macrocycle. During this process, the interaction between the ion pairs belonging to the structure of the zwitterionic free peptide is lost, and with it the preassembled conformation. These macrocyclization procedures are usually developed under high- or pseudo-dilution conditions, in order to compensate for the entropic gain. On the other hand, Ugi-4CR-based activation starts with iminium-ion formation, which does not affect ion-pairing interaction and, hence, the pre-cyclization conformation (Scheme 14.7a, see also Chapter 1). The macrocyclization reaction is then initiated by the approach of an isonitrile molecule. As a result, it was expected that Ugi-4CR-based macrocyclizations of peptides might be carried out to completion without high dilution. In order to evaluate this hypothesis, Yudin's group implemented several Ugi-4CR-based macrocyclizations of peptides containing a proline residue at the N-terminus, as well as pivotal amphoteric aziridine carboxaldehydes and isonitriles. The integration of the electrophilic aziridine ring inside the macrocyclic framework occurs, likely via an Ugi–Split reaction mechanism, adding a new position for further functionalization [52], as well as inducing good diastereoselectivity. By using this approach, a set of di- to pentapeptides was cyclized at 0.2 M concentration to give macrocycles **8–10** in relatively short times, with high diastereoselectivity (>20 : 1), and with good yields (Scheme 14.7b) [50]. Later, they focused on more challenging applications. The homochiral oligoproline systems are known as "molecular rulers," since these polypeptides possess higher rigidity [53]. They assumed that electrostatic interactions between the C- and N-termini might be able to break the helical structure of these peptides and generate a loop, which would allow macrocyclization. L-Oligoprolines containing 2, 3, 4, 6, 8, 10, and 12 residues were submitted to an Ugi-4CR macrocyclization with *tert*-butyl isocyanide and aziridine carboxaldehyde in TFE at 0.2 M for 4 h [54]. For

comparison, a series of controlled macrocyclizations of (Pro)$_6$, using different coupling reagents and concentrations, was also attempted. The Ugi-4CR-based macrocyclizations worked with remarkable results, giving the desired macrocycles (**11**) in good yields, while standard coupling protocols resulted in undesired cyclooligomerization or recovery of starting material. These enlightening results underline the helpfulness of IMCR-based macrocyclizations even using very rigid frameworks (Scheme 14.7c). Recently, Marsault, Yudin, and coworkers explored this concept further by developing Ugi-4CR-based macrocyclizations of peptides on solid phase (Scheme 14.7d). This new work combines all the advantages of the MiB approach with the versatility of solid phase synthesis and is very effective for generating libraries of highly functionalized cyclic peptidomimetics [55].

In order to automate the new macrocyclization process toward high-throughput preparation of macrocycles in parallel, Yudin's group developed a synchronized synthesis of macrocycles by a new microfluidic technique [56]. In this approach, discrete nanoliter to microliter droplets of sample and reagents are placed on an electronic chip. By applying a series of electrical potentials to an array of electrodes coated with a hydrophobic insulator, it is possible to move the drops in parallel in a predetermined order. The technique has been successfully employed in the synthesis of small cyclic peptides and diketopiperazines (Scheme 14.8).

After Yudin's group explored the Ugi-4CR based macrocyclizations of peptides involving amphoteric aziridine aldehydes, they turned their attention toward applications in the synthesis of medicinally relevant macrocycles. In 2012 a series of cell-penetrating cyclopeptides (**12**) using Ugi-4CR-based macrocyclizations was reported [57]. In addition to the aziridine aldehyde, a fluorescent isonitrile was employed in order to label the macrocycles for cellular uptake studies. In these experiments, it was observed that cyclic probes presented higher cell penetrability than their linear analogues (Scheme 14.9a). Shortly after, the same macrocyclization protocol was employed in the synthesis of various fluorescein-labeled RGD-containing $\alpha_V\beta_3$ integrin receptor targeting macrocycles (**13**). In contrast to the earlier example, in this case, the fluorescent tag was installed subsequent to the macrocyclization step by a series of aziridine ring opening and addition of the reporter tag (Scheme 14.9b). An analogous approach has also proven to be effective toward the synthesis of cyclo-tail peptide **14** [58]. A representative example is illustrated in Scheme 14.9c. The cyclopeptide **15** was obtained in 52% yield, after an Ugi-4CR involving the dipeptide H-Pro-Leu-OH, aziridine aldehyde, and thioester isonitrile. The "tail" peptide H-Cys-Asn-Trp-Val-OH was installed via a native chemical ligation
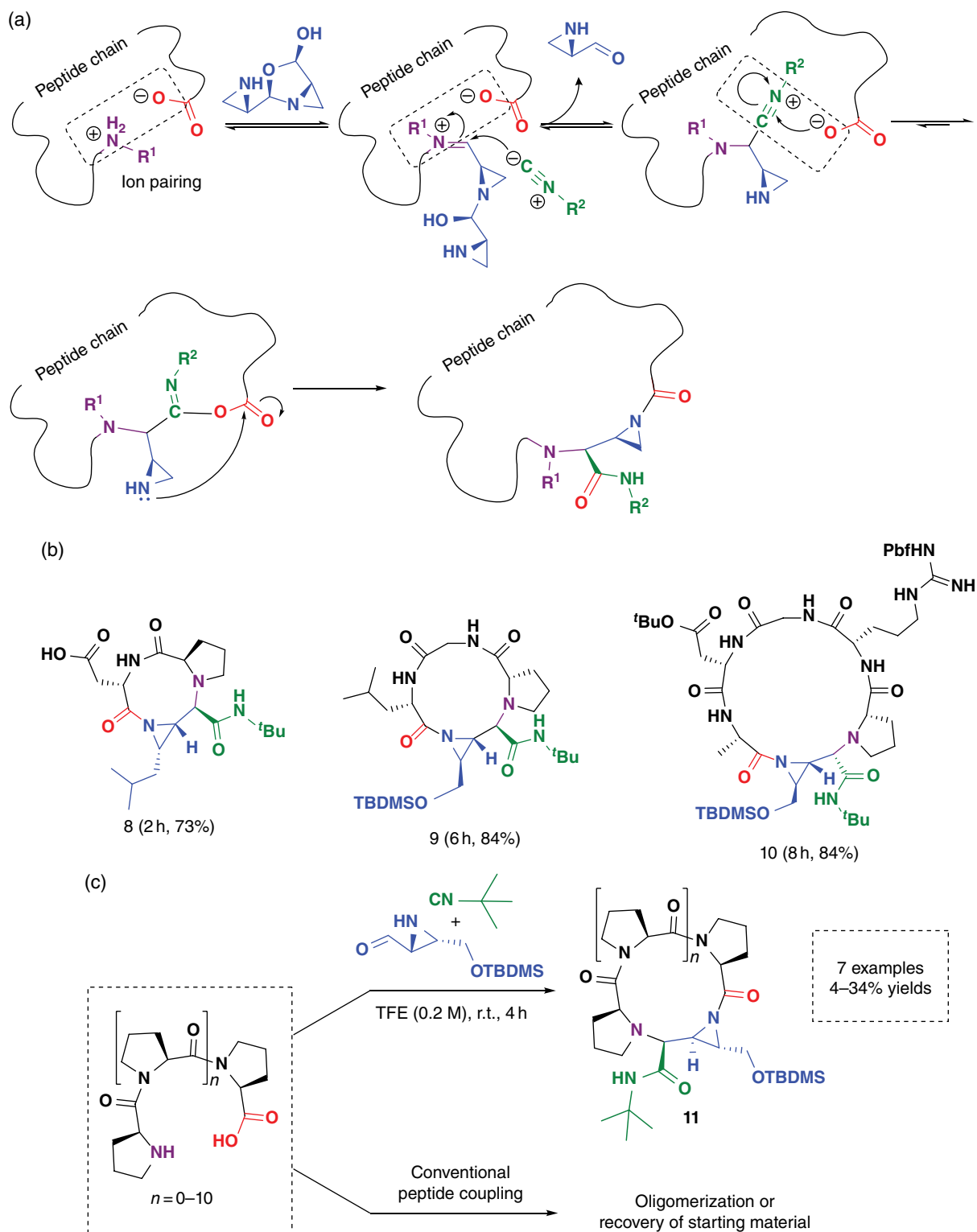
(a)

(b)

8 (2 h, 73%)

9 (6 h, 84%)

10 (8 h, 84%)

(c)

TFE (0.2 M), r.t., 4 h

7 examples
4–34% yields

11

n = 0–10

Conventional
peptide coupling

Oligomerization or
recovery of starting material

Scheme 14.7 Ugi-4CR-based macrocyclizations of peptides involving amphoteric aziridine carboxaldehydes (a) Proposed mechanism. (b) Examples of synthesized macrocycles **8–10**. (c) Application in the macrocyclization of rigid homochiral oligoprolines and comparison with standard procedures. (d) On-resin Ugi-4CR macrocyclization of peptides with aziridine carboxaldehyde and *tert*-butyl isonitrile. (*See insert for color representation of the figure.*)

(d)
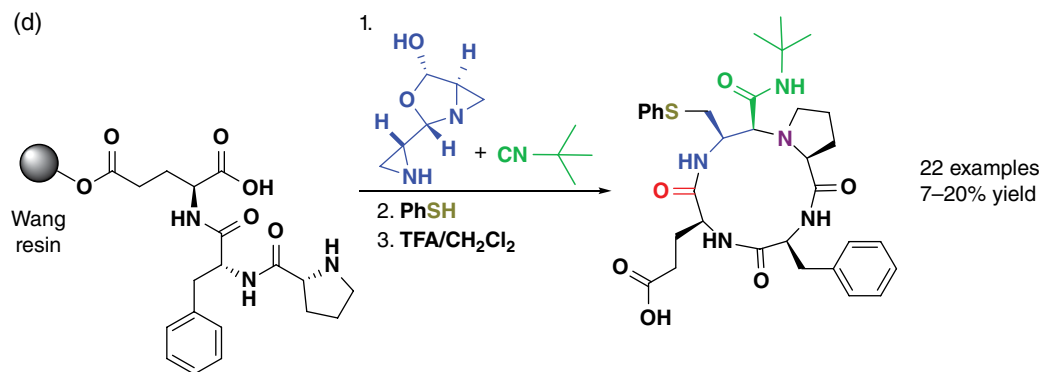
Scheme 14.7 (Continued)
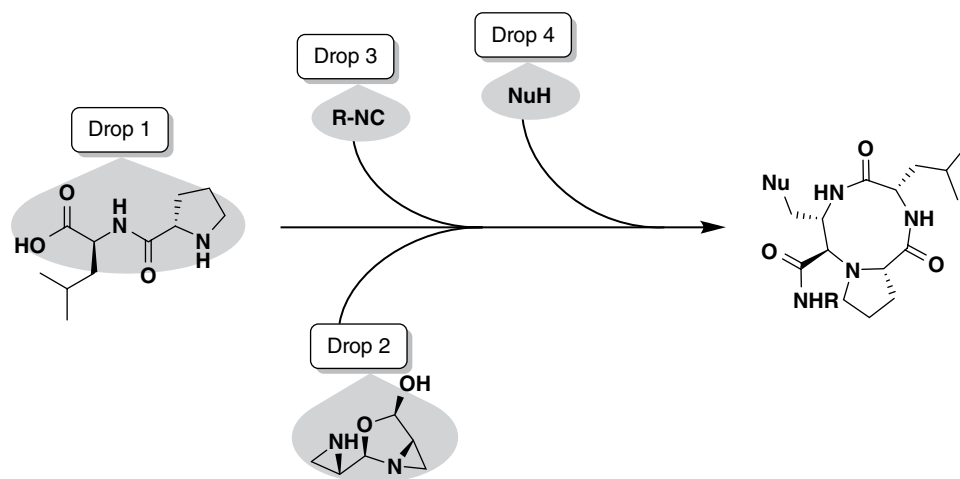
Scheme 14.8 Synchronized synthesis of macrocycles with a droplet-based microfluidic technique.

procedure to afford the desired cyclo-tail peptide **14** in 73% yield.

The incorporation of constraint-generating elements in the macrocyclic backbone increases rigidity, and if this restriction favors the bioactive conformation, it may enhance their ability to interfere in protein–protein interactions. The additional constraint can be achieved via post-cyclization functionalization (e.g., bridge formation). In a first attempt to synthesize a cyclic peptide bearing a disulfide bridge, an Ugi-4CR with the peptide **16**, aziridine carboxaldehyde, and *tert*-butyl isonitrile was performed. Nevertheless, this reaction afforded an imidazolidinone product (**17**) along with just traces of the desired macrocycle (Scheme 14.10a) [59]. Probably, the disulfide bridge forced the linear precursor in a conformation where the carboxylic acid could not easily approach the iminium ion, precluding the cyclization process. In order to overcome this problem, peptide **18** containing Acm-*S*-protected cysteines was submitted to Ugi-4CR. A succession of aziridine ring opening, deprotection, and eventually thiol deprotection/oxidation

resulted in the disulfide-bridged peptidomimetic macrocycle **19** (Scheme 14.10b) [59].

Although many efforts have been directed toward the development of Ugi-4CR macrocyclizations of peptides, these works focused solely on macrocyclizations involving the N- and C-termini, which are usually referred to as head-to-tail cyclizations. Nevertheless, peptides containing Ugi-reactive functionalities as their side chains, for example, Lys, Asp, Glu, and so on, offer other possibilities like head-to-side chain, side chain-to-head, side chain-to-side chain, and side chain-to-tail macrocyclizations (Scheme 14.11a). Recently, the Rivera and Wessjohann groups jointly investigated the latter two possibilities in order to access different folded peptide conformations. It was found that side chain-to-side chain macrocyclizations performed better than the head-to-side chain ones (Scheme 14.11b), but there were no great differences compared with the side chain-to-tail procedure (Scheme 14.11c), presumably due to the higher flexibility of the Lys side chain amino group. Furthermore, NMR and MD analyses of the products revealed the

(a)

(Xaa)$_n$ — Xab

$n = 0-9$

(Xaa)$_n$ = Xab = α–amino acid

Fluorescent isonitrile

TFE (0.2 M), r.t., 1–6 h

12

(b)

OtBu

A

A

D

G

P

R

Pbf

+

NC

1. TFE (0.2 M), r.t., 17–19 h
2. H$_2$N—SH
3. Fluorescein-NHS
4. TFA

HO

COOH

A

A

D

G

P

R

13
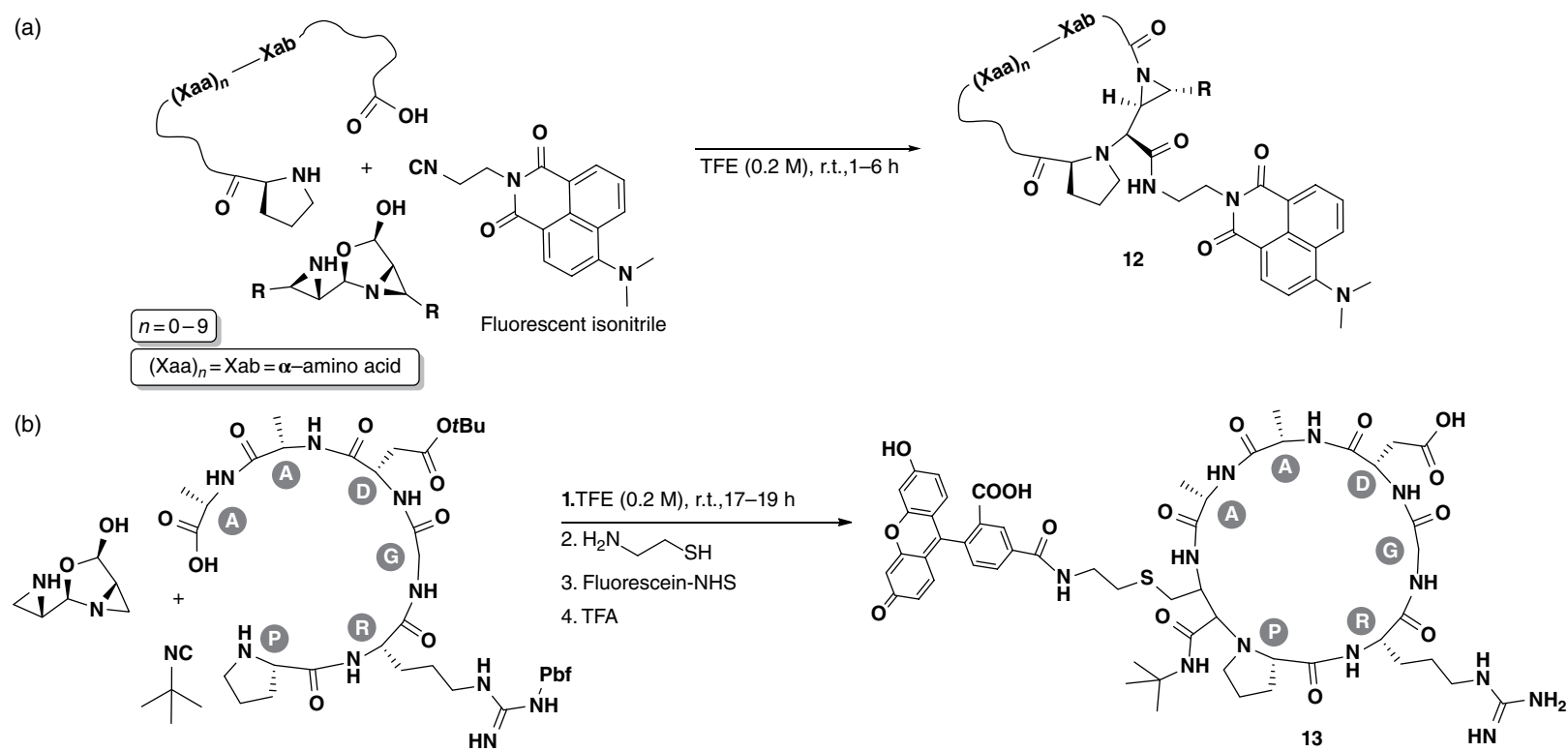
Scheme 14.9 Application of Ugi-4CR-based macrocyclizations in the synthesis of medicinally significant macrocycles. (a) Synthesis of cell-penetrating fluorescently labeled macrocycle **12**. (b) Fluorescein-labeled RGD-containing α$_V$β$_3$ integrin receptor targeting macrocycle **13**. (c) Ugi-4CR/peptide native ligation toward synthesis of cyclo-tail peptides **14**.

(c)

MPAA (4-mercaptophenylacetic acid)
HFIP (hexafluoroisopropanol)
TCEP(tris(2-carboxyethyl)phosphine)
DPBS (Dulbecco's phosphate buffered saline)

HFIP (0.05 M), 3 h

15
52%

MPAA (40 mM), TCEP·HCl
(80 mM), DPBS, pH = 7.5.

14
73%
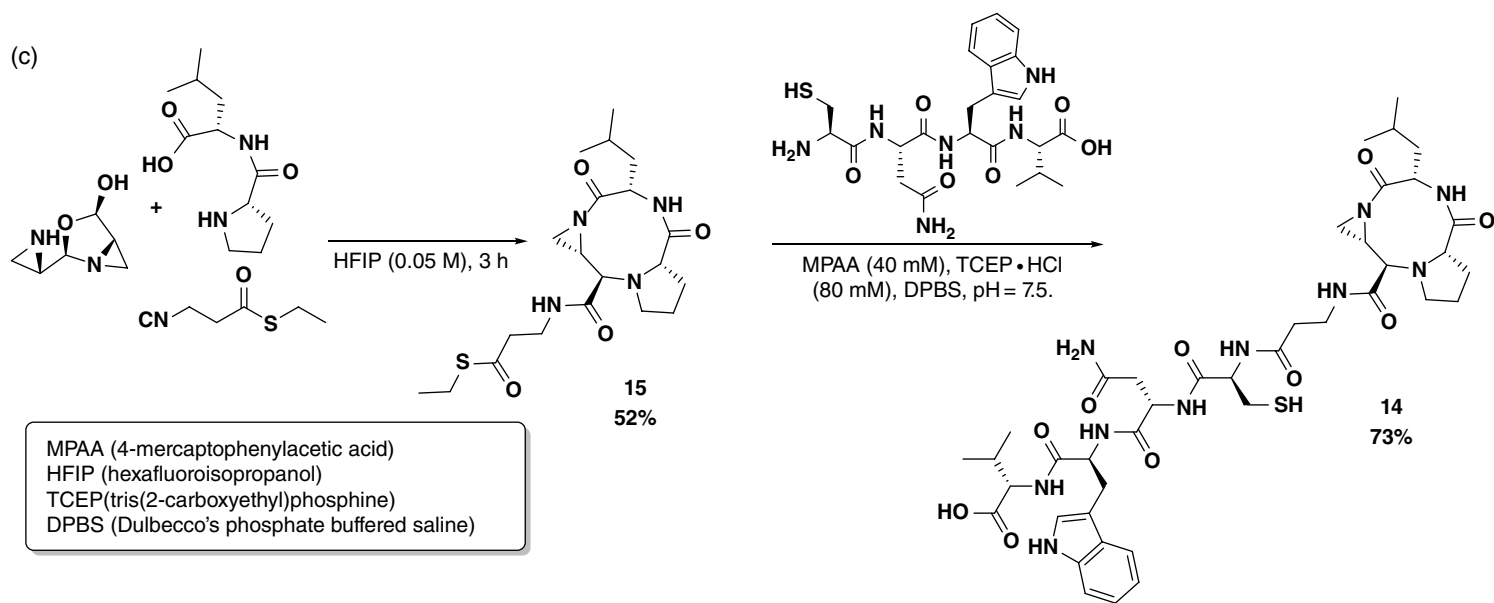
Scheme 14.9 (Continued)
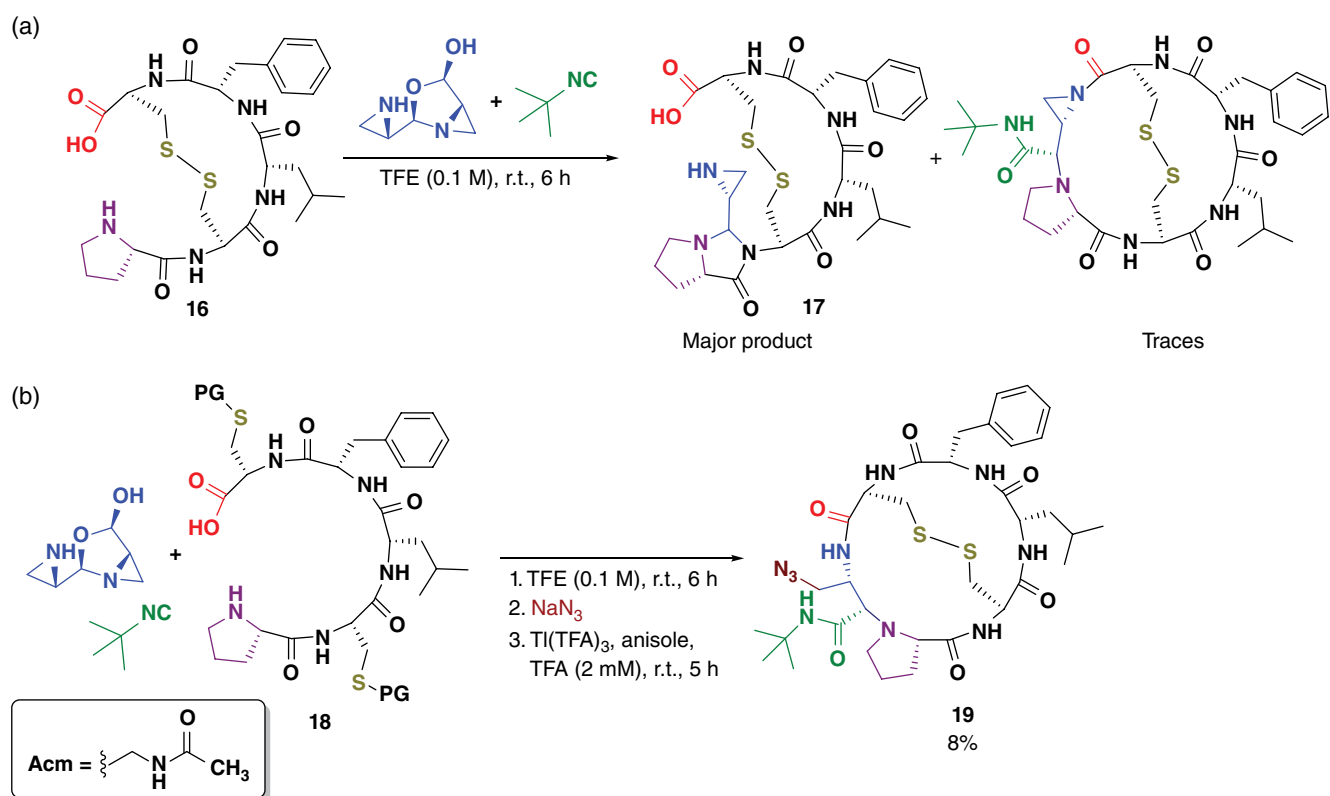
Scheme 14.10 Synthesis of the disulfide-bridged peptidomimetic macrocycle **19**.

(a)

Head to tail

Glu · aa · aa · Lys · aa · aa · aa · aa · aa · N · R¹ · O · HN · R²

Ugi-4CR

R¹ ⟨⟩ O   R² — NC

A

Side chain to side chain

R²—NH · O · O · Glu · Lys · N · R¹

H₂N · aa · aa · aa · aa · aa · aa · aa · CO₂H

B

CO₂H · Glu · aa · aa · H₂N · Lys · aa · aa · CO₂H
H₂N · aa · aa · aa

C

Head to side chain

aa · aa · aa · Glu · N · R¹ · O · HN · R² · aa · aa · Lys · aa · aa · CO₂H

D

Side chain to tail

R²—HN · O · R¹ · N · O · aa · Lys · aa
H₂N · aa · aa · aa · Glu · aa · aa
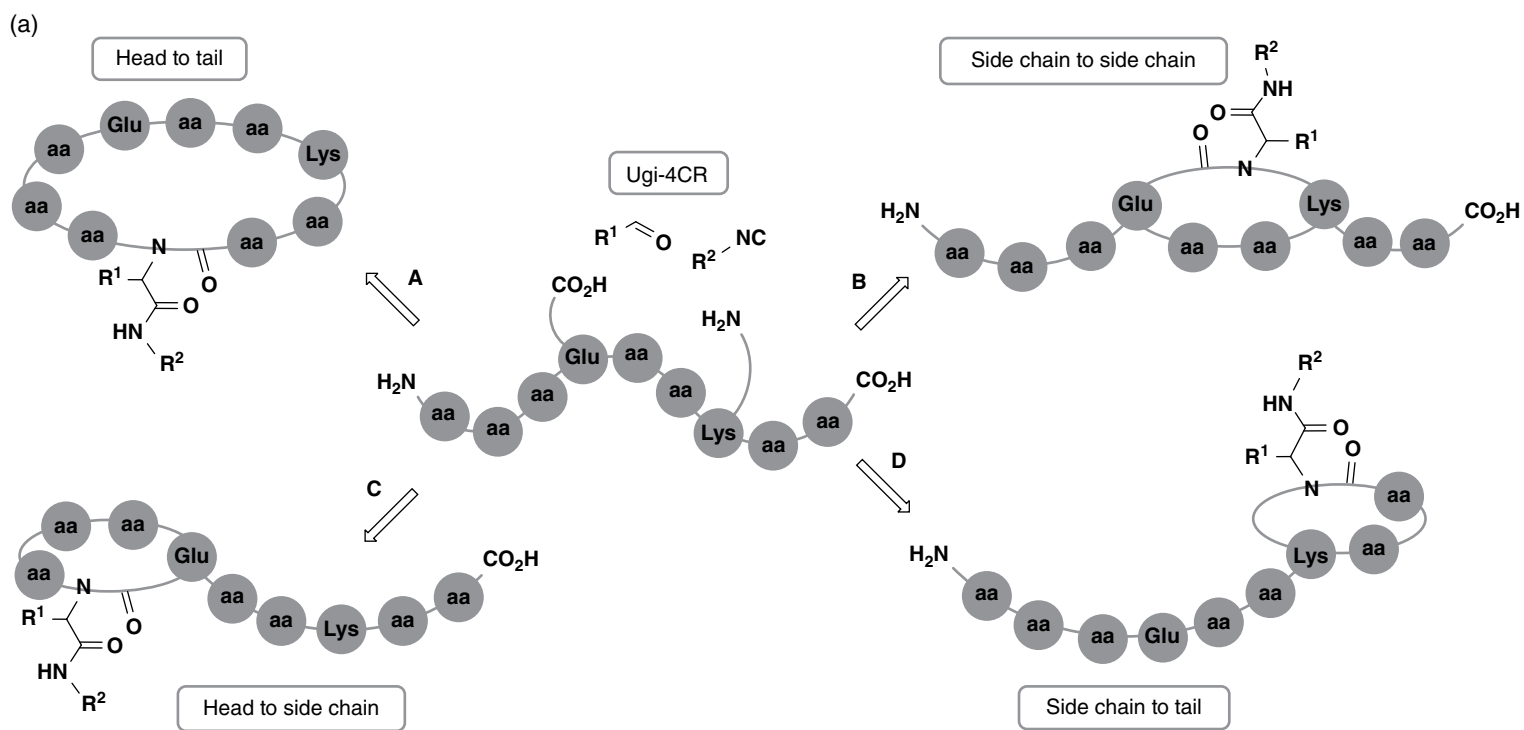
Scheme 14.11 (a) Extended possibilities for Ugi-4CR macrocyclizations of peptides (b) Side chain-to-side chain MiB. (c) Side chain-to-head MiB.

(b)

$$NC + (CH_2O)_n$$

MeOH (2 mM), 72 h

59%

(c)

$$NC + (CH_2O)_n$$

MeOH (2 mM), 72 h

60%
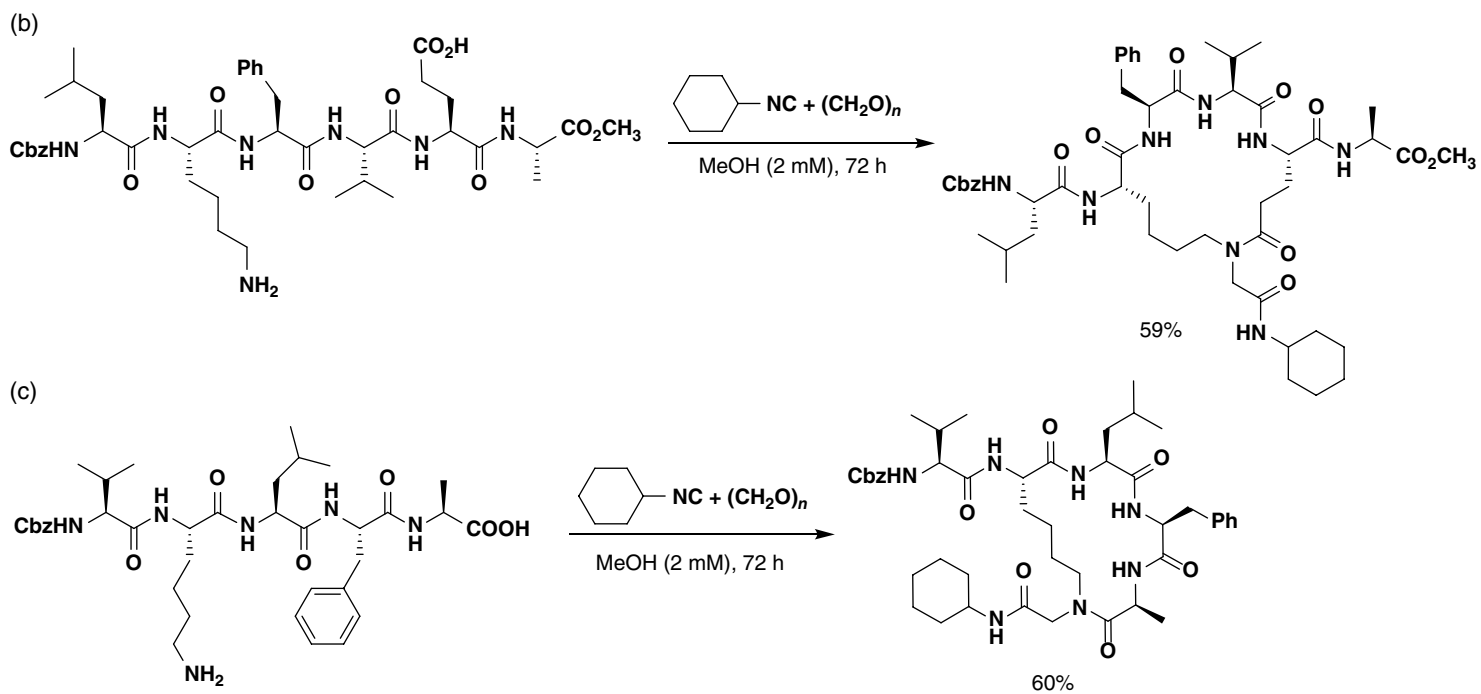
Scheme 14.11 (Continued)
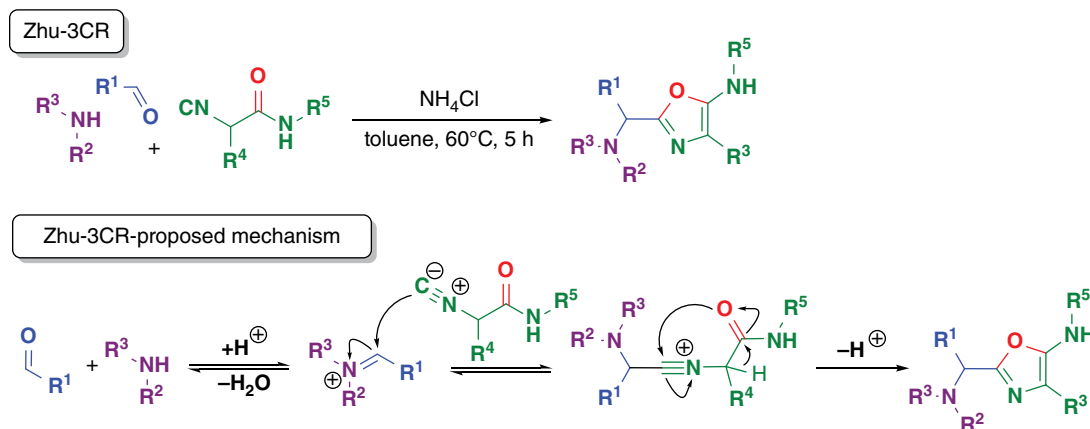
Scheme 14.12 Formation of 5-aminooxazoles by MCR between aldehydes, amines, and α-isocyanoacetamides (Zhu-3CR).

stabilization of folded structures like helical, alpha, and beta turns [60].

Although most of IMCR-based macrocyclizations involving a single bifunctional building block rely on the use of Ugi-4CRs, other IMCRs have also been employed with remarkable results. The condensation between aldehydes, amines, and α-isocyanoacetamides reported by Zhu and coworkers in 2001 is a highly versatile method to obtain 5-aminooxazoles, and its huge potential has been employed in the preparation of heterocyclic compound libraries reminiscent of the many bioactive oxazole- and thiazole-containing natural macrocycles (Scheme 14.12) [61, 62].

The same group hypothesized that a bifunctional building block carrying a nucleophilic moiety attached at the head and a carboxylic acid at the tail could be cyclized [63], if a 5-aminooxazole moiety was conveniently placed between them (Scheme 14.13a) [64–66]. Mechanistically, the cascade process starts with the protonation of the oxazole ring in **20** to spring an electrophilic iminium ion **21**. The nucleophilic attack of the carboxylate on the iminium ion, favored by a 5-membered ring transition state, leads to spirolactone **22**. This latter constrained intermediate undergoes a nucleophilic attack by the tethered nucleophile to afford a macrocyclic structure **23**. Although the Zhu-3CR is not responsible for the ring-closure step itself, it generates the 5-aminooxazole moiety that acts at the same time as building block and carboxylic acid traceless activator. In order to demonstrate this concept, amino alcohols **24** reacted with aldehydes and α-isocyanoacetamides **25** to afford, after saponification, the suitable bifunctional building block (**20**-like product). The cascade process is then triggered by a few equivalents of TFA to afford a macrocyclic depsipeptide (**26**) in good overall yields (Scheme 14.13b) [64]. The same approach was later employed in the

synthesis of glycocyclodepsipeptide **27** with striking results (Scheme 14.13c) [67].

Beyond the extended use of IMCRs to target macrocyclic structures, some new multicomponent processes, in which the isocyanide lacks as a component, have been explored in this endeavor. A multicomponent condensation of substituted anilines with formaldehyde and hydrogen sulfide is attributed to cascade "domino" reaction and leads to formation of thioaza macrocycles [68]. The relative position of the substituents in the aromatic ring plays a key role in the architecture of the output products. Whereas *o*- and *p*-isomers give small heteroatom rings, *m*-isomers undergo intermolecular condensation to form thioaza macroheterocycles (Scheme 14.14). It is supposed that the regioselectivity of the isomeric anilines in the interaction with CH_2O and H_2S is caused by the change in NH_2 group basicity according to its arrangement in the aromatic ring [68].

Consecutive MCRs have also been used toward post-MCR macrocyclization. Cai's group made use of the combination of two MCRs and an intramolecular Sonogashira cross-coupling reaction to synthesize triazole-containing macrocycle compounds (Scheme 14.15) [69]. In the example, aniline, 2-bromobenzaldehyde, *ortho*-azido-benzoic acid, and cyclohexyl isocyanide condense to give intermediate Ugi-product, used without isolation in the next MCR reaction [70]. The sequential one-pot reaction with 2-propynylamine, diketene, and DBU allows to install the alkyne moiety necessary to prompt post-MCR macrocyclization by an intramolecular Sonogashira cross-coupling reaction. Notably, no cyclic or acyclic dimers were found, and macrocycle **30** was reached in good yield. However, to enhance the ratio **28**:**29**, optimization of the one-pot MCR condition was required. The optimal result for the MCR tandem was obtained using MeOH as a solvent and 1.5 equiv. of diketene, 1.5 equiv.

(a)

(b)

26a R = CH₂CH₂OH, n = 1, 40%
26b R = H, n = 2, 59%
26c R = H, n = 3, 57%
26d R = H, n = 4, 61%
26e R = Bn, n = 4, 75%

4 examples
55–84% yields

n = 2–5

26a–e

26f 40%

(c)

27
49% (over 2 steps)
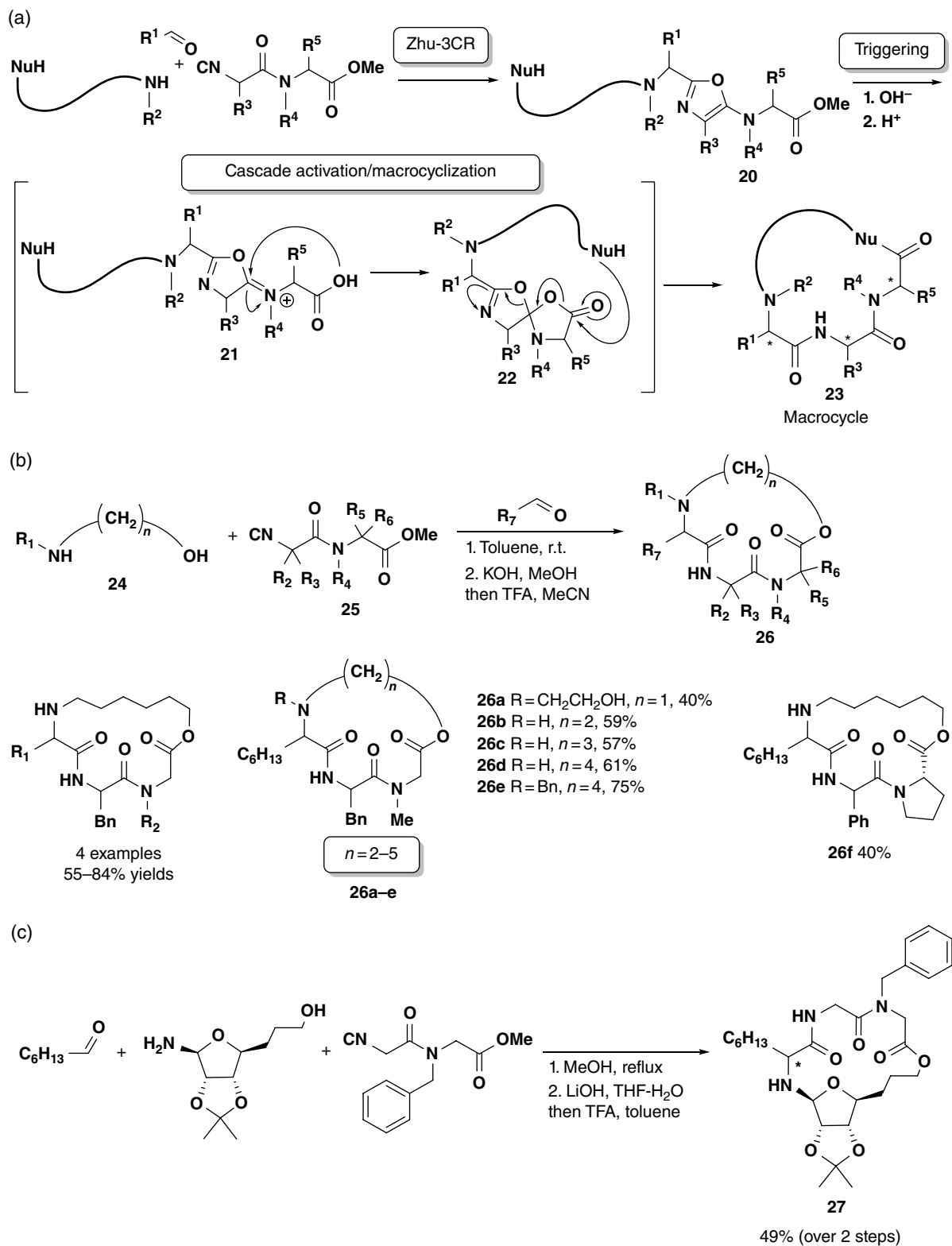
Scheme 14.13 Zhu-3CR/traceless activation/macrocyclization cascade. (a) Proposed mechanism. (b) Examples of synthesized depsicyclopeptides **26a–f**. (c) Application in the synthesis of endoglycodepsipeptides **27**.

(a) Heterocycles

OH
a,c (58–86%)

SH
a–c (~70%)

c (18%)

a (80%)

a (50%) + a (16%)

20°C
0°C
20°C
20–80°C
20°C

R = –OH
R = –SH
R = –NH₂

NH₂
R + CH₂O – H₂S
(a–c)

R = –OH, –SH, –NH₂

a,b,c: correspond with
o-, *m*-, *p*-isomers,
respectively.

(b) Thioaza macrocycles

40°C
20°C
20°C

R = –OH
R = –SH
R = –NH₂

b (9–39%)   n = 1–7

b (17%)

b (~90%)
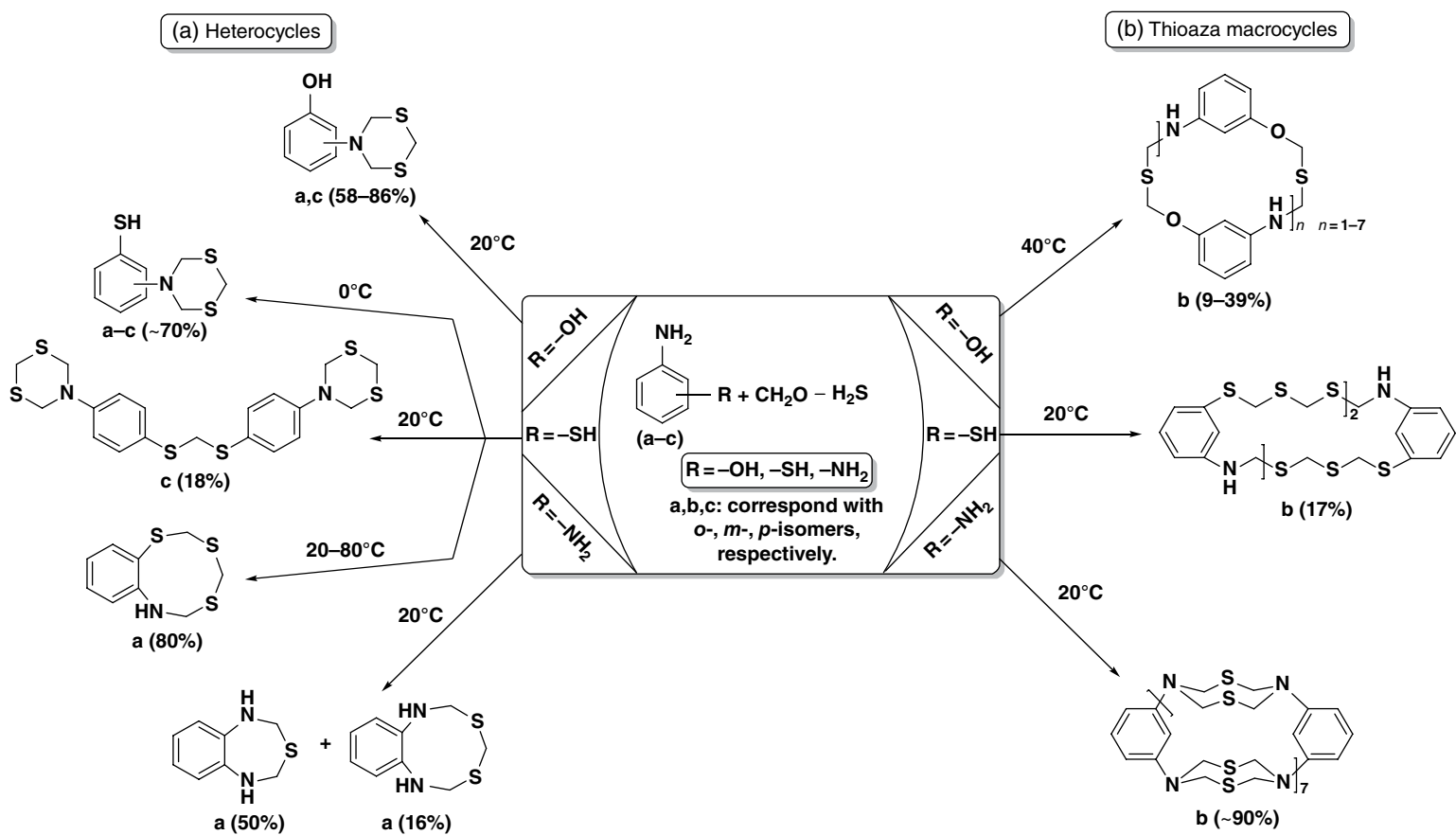
Scheme 14.14 Synthesis of heterocycles (a) and thioaza macrocycles (b).
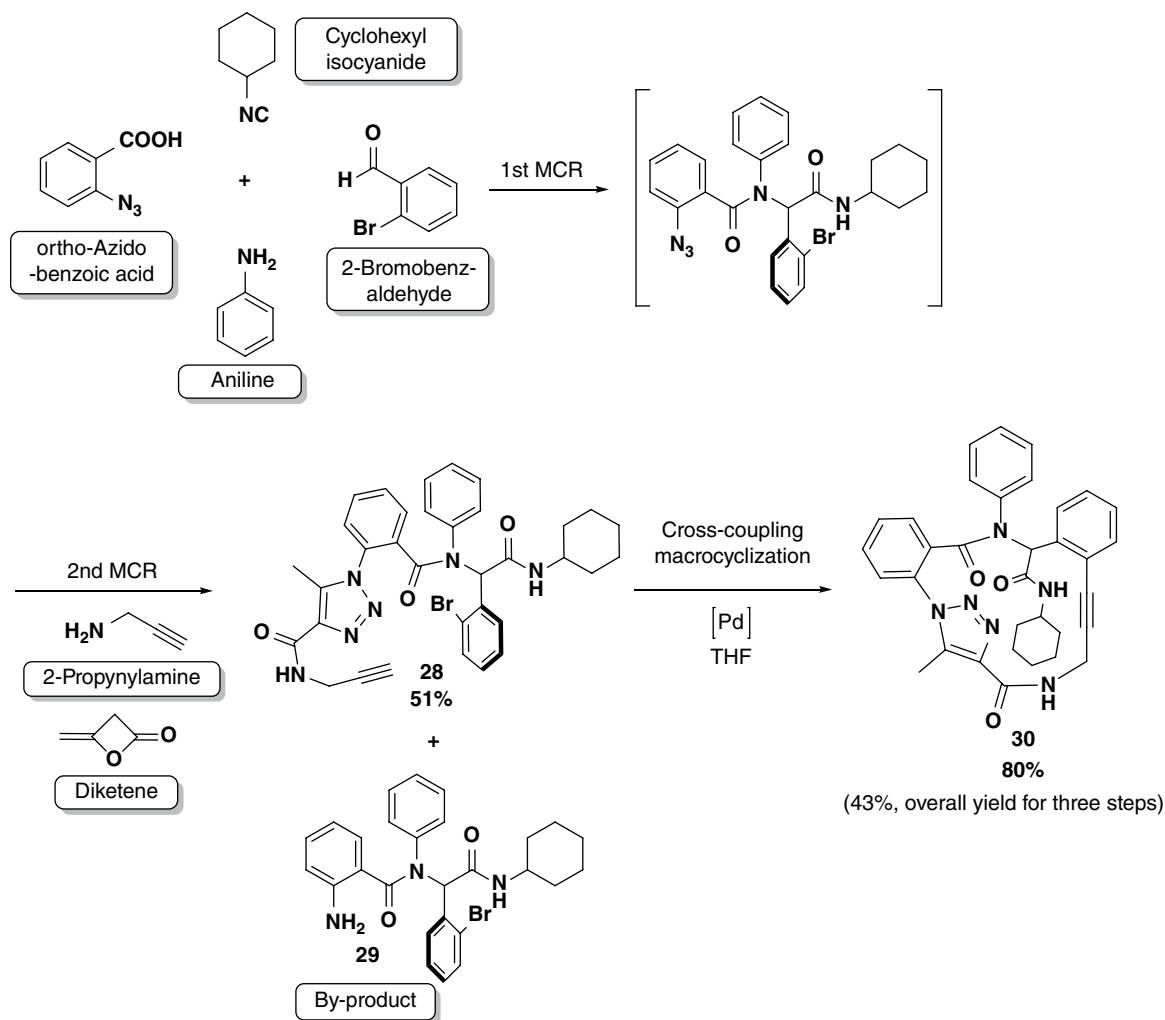
Scheme 14.15 Synthesis of triazole-containing macrocycle compounds by tandem MCRs and intramolecular Sonogashira cross-coupling.

of 2-propynylamine, and 1.5 equiv. of DBU as catalyst. Intermediate **28** was obtained in over 50% total yield, and the by-product **29** was less than 10% yield (Scheme 14.15) [69].

14.2.3 Bidirectional Multicomponent Macrocyclizations

During the synthesis of *m*-cyclophanes (**33**), Zhu and coworkers reported the first planned synthetic strategy toward macrocycles by an MiB bidirectional approach (Scheme 14.16a) [71]. By using bifunctional diamines (**31**) and diisocyanides (**32**), this one-pot multicomponent process generates at least three elements of diversity in the final symmetric macrocycles, including the creation of six chemical bonds with the associated formation of two oxazole groups as part of a new structure. Interestingly, the macrocyclization reaction performed better at high concentration (0.1 M) affording a set of

macrocycles (**33a–e**) in 42–52% yields (Scheme 14.16b). Since no template effect was employed, the key to success of this process likely is based on the rigidifying effect of the formed oxazole ring, which could prompt a pre-organized conformation prone to cyclization. Probably, the ring-closure step does not take place simultaneously with oxazole formation; rather, the formation of the small ring should proceed first, followed by the macrocyclizing Zhu-3CR between the tethered amino and isonitrile groups. Based upon this hypothesis, one can speculate that the concentration of the *in situ* generated pre-organized precursor, in the cascade process, might be much lower than the concentration of the starting reagents, causing an intrinsic pseudo-dilution effect.

In parallel to Zhu's pioneering work, Wessjohann and coworkers developed a straightforward approach toward the synthesis of steroid–peptoid hybrid macrocycles [42]. The bidirectional MiB begins by employing the diisonitrile **34** as a common counterpart of diamine **35** and

(a)

(b)

33a
52%

33b, R = H, 45%
33c, R = Et, 42%

33d
43%

33e
47%
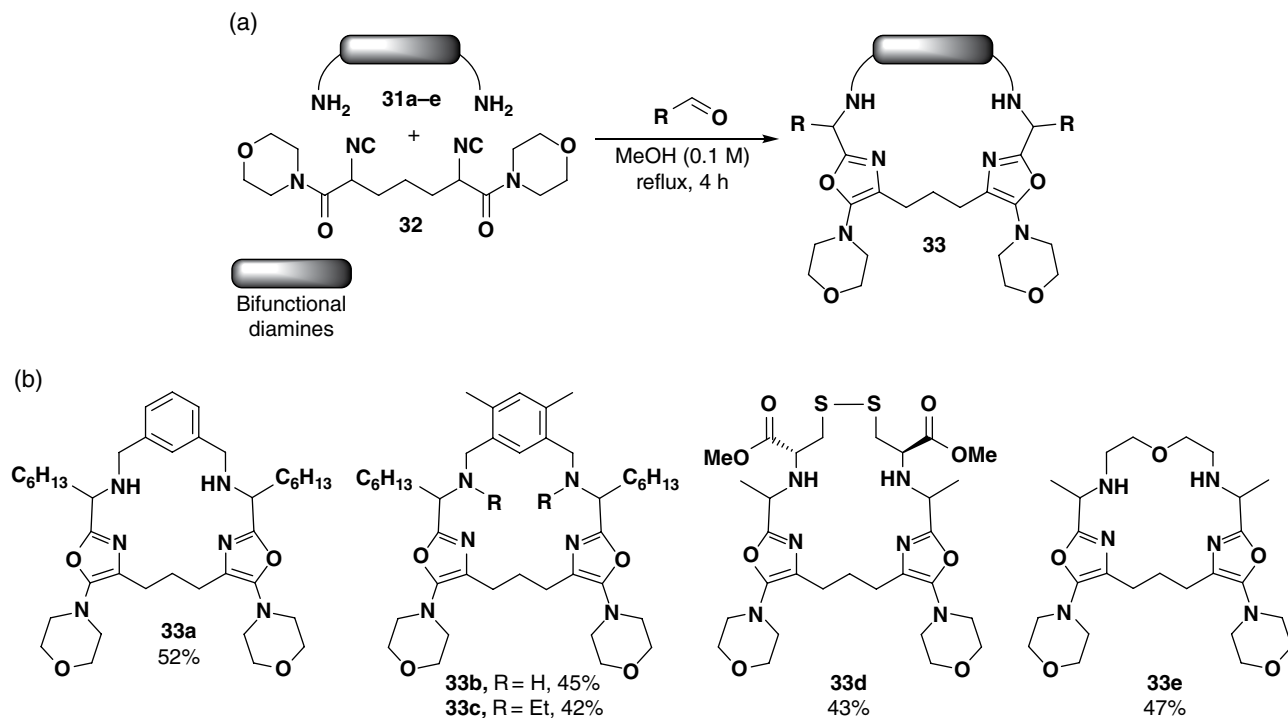
Scheme 14.16 Zhu-3CR-based approach for the synthesis of *m*-cyclophanes. (a) Reaction conditions. (b) Examples and yields of synthesized macrocycles.

37a R = H, 58%
37b R = *i*Pr, 28%

38a R = H, 50%
38b R = *i*Pr, 14%
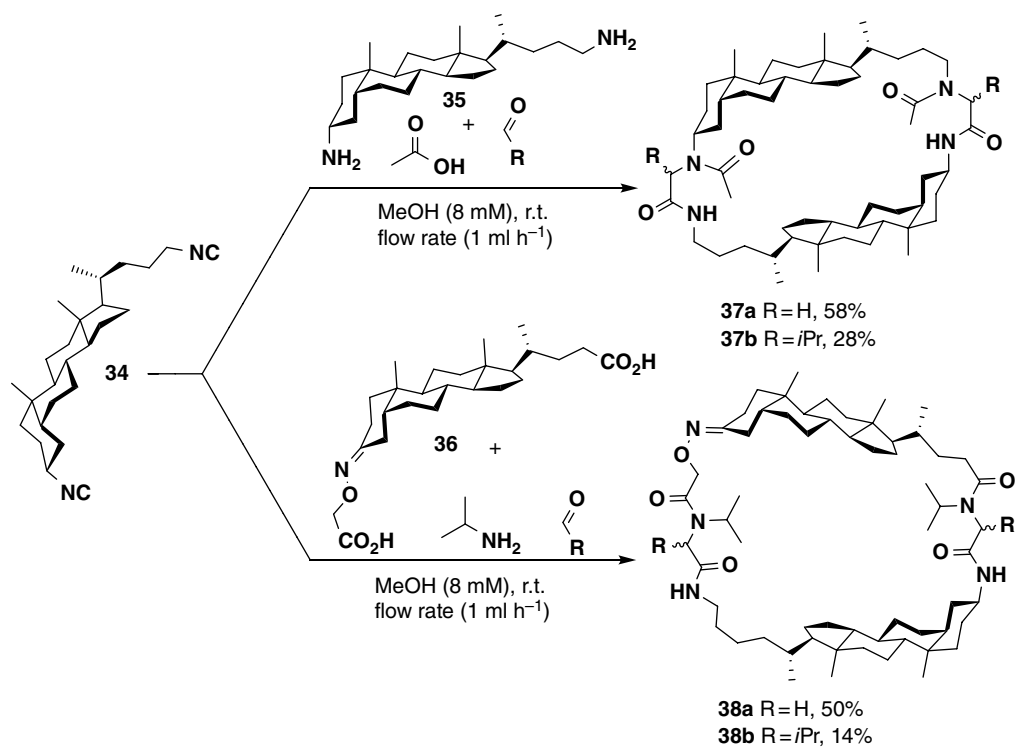
Scheme 14.17 Synthesis of steroid–peptoid hybrid macrocycles by bidirectional Ugi-4CRs involving two bifunctional building blocks. Head-to-head (H–H) and head-to-tail (H–T) regioisomers are formed in almost equal amounts. Yields refer to the mixture, but, for clarity, only the H–T isomers are shown.

(a)

(b)

TBDMSO = *tert*-butyldimethylsilyl ether
TBAF = tetra-*n*-butylammonium fluoride
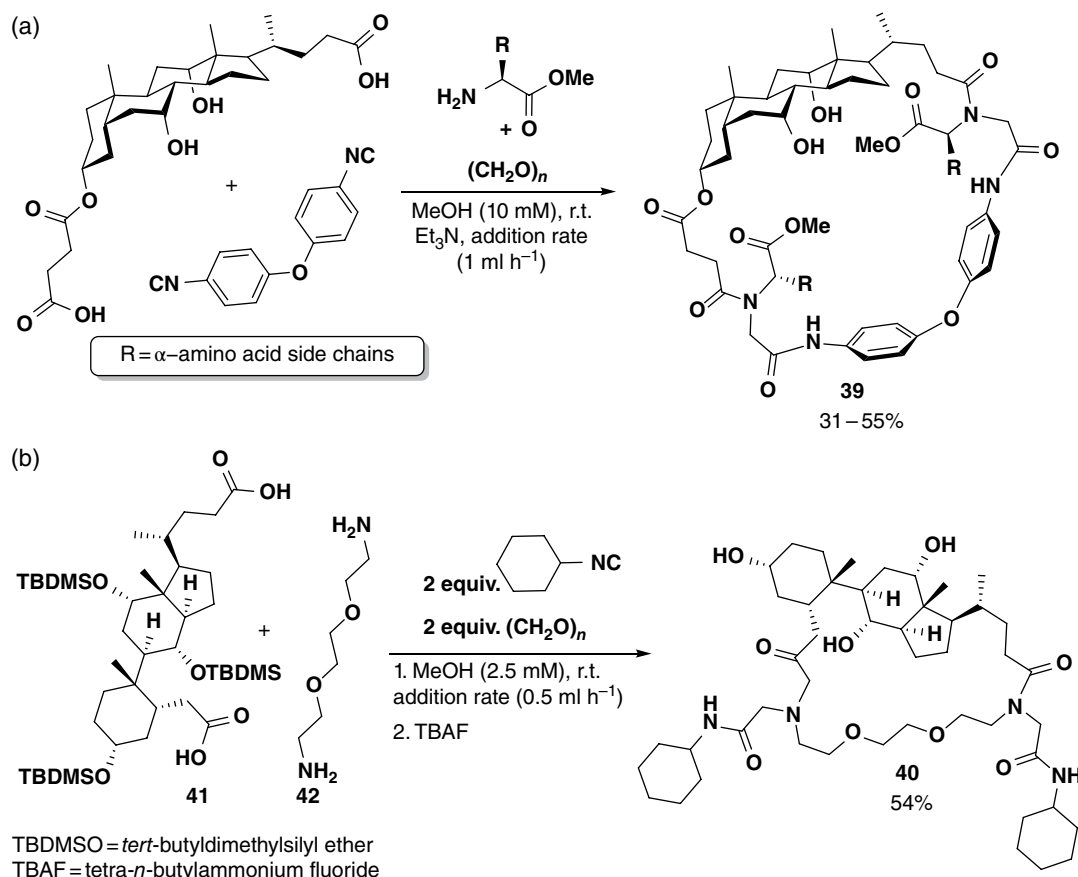
Scheme 14.18 Steroid–peptoid hybrid macrocycles enhanced with higher hydrophilicity or lipophilicity. (a) Installation of the lipophilic diphenyl ether moiety common in natural antibiotics in syntheses of steroid–peptoid macrocyclic hybrids **39**. (b) Installation of hydrophilic motifs toward the synthesis of secocholane hybrid macrocycle **40**.

dicarboxylic acid **36** in the Ugi-4CR. Through this procedure, two different types of peptoid backbones are produced (**37** and **38**, Scheme 14.17). To minimize the competing (cyclo)oligomerization, the reactions were performed under pseudo-dilution conditions by adding the diisonitrile building block slowly as a solution via syringe pump. Both macrocycles **37a,b** and **38a,b** were isolated as almost equally distributed mixtures of diastereomers of head-to-tail and head-to-head cyclic dimers (Scheme 14.17; for clarity reasons, only the head-to-tail regioisomer is shown). It is noteworthy that the diamine/diisocyanide combination generates a macrocycle with an exocyclic amide bond, which increases the flexibility of the peptoid portion even though shortening the tethered chain. On the other hand, the diacid/diisocyanide combination affords a macrocycle with endocyclic amide bonds [72].

Further exploring the synthesis of peptoid macrocyclic hybrids, Wessjohann and coworkers focused on the synthesis of more complex structures. The designed compounds featured the presence of a biaryl ether moiety to enhance lipophilicity and elements of importance in natural recognition processes, that is, amino acid resi-

dues (e.g., Cys, Arg, His, Trp) and carbohydrates (Scheme 14.18a). The MiB strategy enables not only the generation of appendage diversity but also of the macrocyclic cavity in one pot [72]. The process worked smoothly and afforded steroid–peptoid macrocyclic hybrids (**39**) in good yields. The MiB approach may also be applied to the synthesis of steroid–peptoid macrocyclic hybrids endowed with enhanced hydrophilicity. By employing this principle, the synthesis of the PEG-containing secocholane hybrid macrocycle **40** was accomplished, in 54% yield, by employing the bile diacid derivative **41**, PEGylated diamine **42**, formaldehyde, and cyclohexylisonitrile (Scheme 14.18b).

The presence of biaryl ether moieties is common in many biologically active natural products, including antibiotics and antitumor agents [73, 74], which makes it an attractive moiety for target-oriented synthesis. On peptidic scaffolds, cyclization is among the most effective synthetic tools to reduce the intrinsic flexibility of both the peptide backbone and the side chains [75]. This results in an increased ligand binding affinity to the biological target directly related with improvement in the

pharmacological properties when compared to the acyclic precursor [1a, 76]. Encouraged by these facts, bis-isonitrile-functionalized biaryl ether **43** and its relative aryl–alkyl diisocyanides have been employed by Wessjohann and coworkers as key building blocks for the efficient one-step assembly of natural product-inspired macrocycles [77, 78]. The reaction of bis-isonitrile **43** with diacids (**44**), isopropylamine, and formaldehyde afforded the desired macrocycles (**45a–c**) in 8–30% yields (Scheme 14.19a). It was found that the size of the diacid building block has a clear influence on macrocyclization reaction performance. In this reaction model, dicarboxylic acids containing longer chains gave higher yields than those with short ones. It is likely that product or intermediate strain disfavor short bifunctional counterparts to give good yields. Moreover, in a controlled experiment, the hemialkyl bis-isonitrile **46** displayed higher reactivity in comparison to the fully aromatic bis-isonitrile **43** (Scheme 14.19b). The reason behind this difference in reactivity lays probably in the greater flexibility of compound **46** originating from the presence of the saturated alkyl chain and *meta*-connectivity.

The next focus was the installation of exocyclic elements of high relevancy in recognition processes, for example, amino acid residues or sugars. Thus, bis-isonitrile **43** was submitted to an Ugi-MiB reaction with the diamine **48**, formaldehyde, and carboxylic acid **47** to afford the integrated synthesis of glycosylated macrocycle **50** in 35% yield (Scheme 14.19c) [79]. This process was also effective when using peptides as the dicarboxylic acid component (Scheme 14.19d) [80]. Later, the bis-aryl isonitrile **43** was also employed in the synthesis of macrocycle **53**, which is endowed with a photoreactive unit, which can be used to switch conformation and thus physicochemical properties like color (Scheme 14.19e) [81].

Although bidirectional MiB approaches employing multiple Zhu-3CR and, especially, Ugi-4CR is dominating the current macrocycle syntheses, other MCRs are available for the same purpose. The Wessjohann group investigated the applicability of Passerini-3CRs involving multiple bifunctional building blocks toward the synthesis of macrolactones and cyclic depsipeptides [49, 82, 83]. In a similar way to Ugi-MiBs, Passerini-MiBs are able to generate a high level of skeletal diversity based on the variation of the corresponding building blocks (and its intrinsic functionalities). Taking into consideration the three-component aspect of this reaction, it is possible to devise three different combinations of bifunctional building blocks for the bidirectional MiB approach, that is, diacid/diisocyanide, diacid/dialdehyde, and dialdehyde/diisocyanide. **Scheme** 14.20 illustrates the synthesis of depsipeptide-like macrocycles using each of these combinations. As a specific example, Boc-glutamic acid

(Boc-Glu-OH) and isobutyraldehyde reacted with the diisocyanide **54** to afford the macrolactone **55** in 37% yield (**Scheme** 14.20a). The diacid/dialdehyde combination appeared to be more challenging due to the more difficult access to the dialdehyde component. Dialdehydes are commercially unavailable and can be very unstable, being sensitive to aldol self-condensation for instance. On the other hand, diols as potential precursors are cheap and abundant. Using an elegant modification of the Passerini-3CR based on alcohols reported by Zhu, the dialdehydes are available *in situ* to afford the representative macrolactone **57** in 59% yield (Scheme 14.20b) [84]. This procedure also worked very well for the dialdehyde/diisocyanide combination, employing diisocyanide **54**, diol **56**, and carboxylic acid Boc-Gly-OH (Scheme 14.20c).

More than any other macrocyclization method, the MiB concept lends itself to combinatorial chemistry [85]. In this endeavor, the synthesis of small combinatorial libraries of peptoid-based macro(multi)cycles was demonstrated. While the parallel assembly grants access only to equally functionalized peptoid backbones from each Ugi-4CR process, the combinatorial one also allows the inclusion of different functionalities attached to each peptoid moiety [85]. Scheme 14.21a illustrates an example of the combinatorial MiB approach toward the synthesis of a small combinatorial library of functionalized peptoid-based macrocycles. The same approach was also employed in the combinatorial synthesis of cholane–peptoid hybrid macrocycles (Scheme 14.21b) [86].

Oligomeric mixtures of cyclic imines are often very difficult to isolate because of the instability of the Schiff bases. In order to tackle this problem, a well-established strategy is to freeze the imine formation equilibrium, with the aim of generating compounds stable enough for isolation. Commonly, these imine mixtures are converted, via reductive amination, into their respective amines, which are more stable. Although very effective, this approach can also just "quench" the imine mixture but does not offer any possibility for further addition of side chain diversity. Aiming to develop a new protocol, which would allow a tandem quench and functionalization of oligomeric mixtures of cyclic imines, Wessjohann and coworkers proposed that an Ugi-MiB reaction should be able to accomplish this transformation, turning a mixture of cyclic oligoimines into stable macrocycles containing peptoid backbones and appendage diversity [87]. Thus, dialdehyde **61** and diamine **62** were reacted to give rise to a dynamic mixture of cyclic imine oligomers (dimer, trimer, etc.) as confirmed by ESI-MS analysis (Scheme 14.22). To this mixture were then added acetic acid and *tert*-butylisonitrile to afford macrocycles **63** and **64** in 21 and 14% yield, respectively. In order to know whether the ratio of the formed macrocycles could be changed, the dynamic mixture was re-equilibrated by

(a)

45a, *n* = 4 (8%)
45b, *n* = 6 (16%)
45c, *n* = 10 (30%)

(b)

n = 0, oxalic acid
n = 6, sebacic acid

47a, *n* = 0 (2.5%)
47b, *n* = 6 (46%)

(c)

50
35%

(d)

52
Yield: 39%
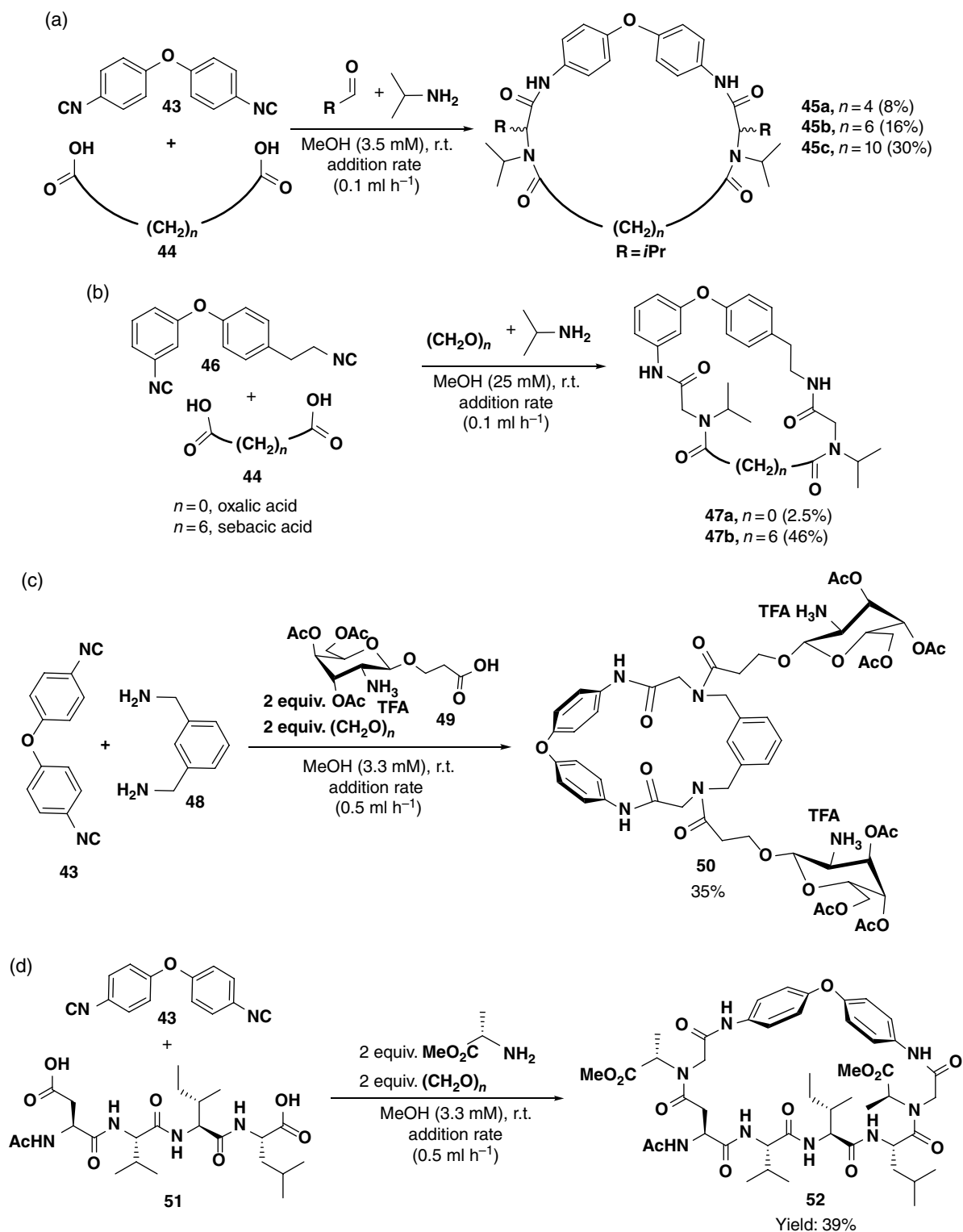
Scheme 14.19 Application of biaryl ether bis-isonitriles in Ugi-MiBs. (a) and (b) Synthesis of natural product-inspired biaryl ether-cyclopeptoid macrocycles **45** and **47** (note: these reactions were run without using (pseudo)dilution). (c) Synthesis of glycosylated macrocycle **50** (protected form) integrating macrocyclization and introduction of the glycosyl building block. (d) Side chain-to-backbone and backbone-to-backbone bidirectional macrocyclizations of peptides by double Ugi-4CR. (e) Synthesis of cyclopeptid **53** containing a photoswitchable unit. Note: Macrocyclization is usually performed using pseudo-dilution by slow addition of diisocyanide and acid/diacid building blocks to the preformed imines.

(e)
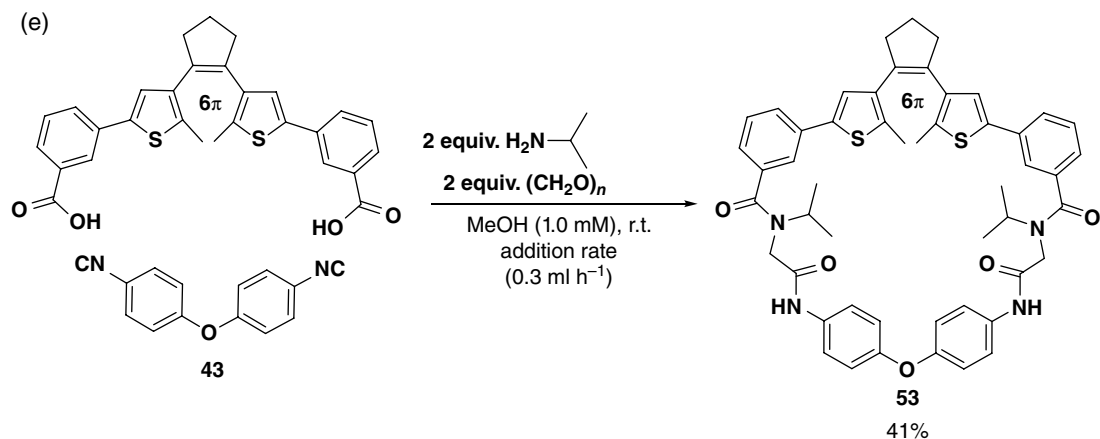
Scheme 14.19 (Continued)
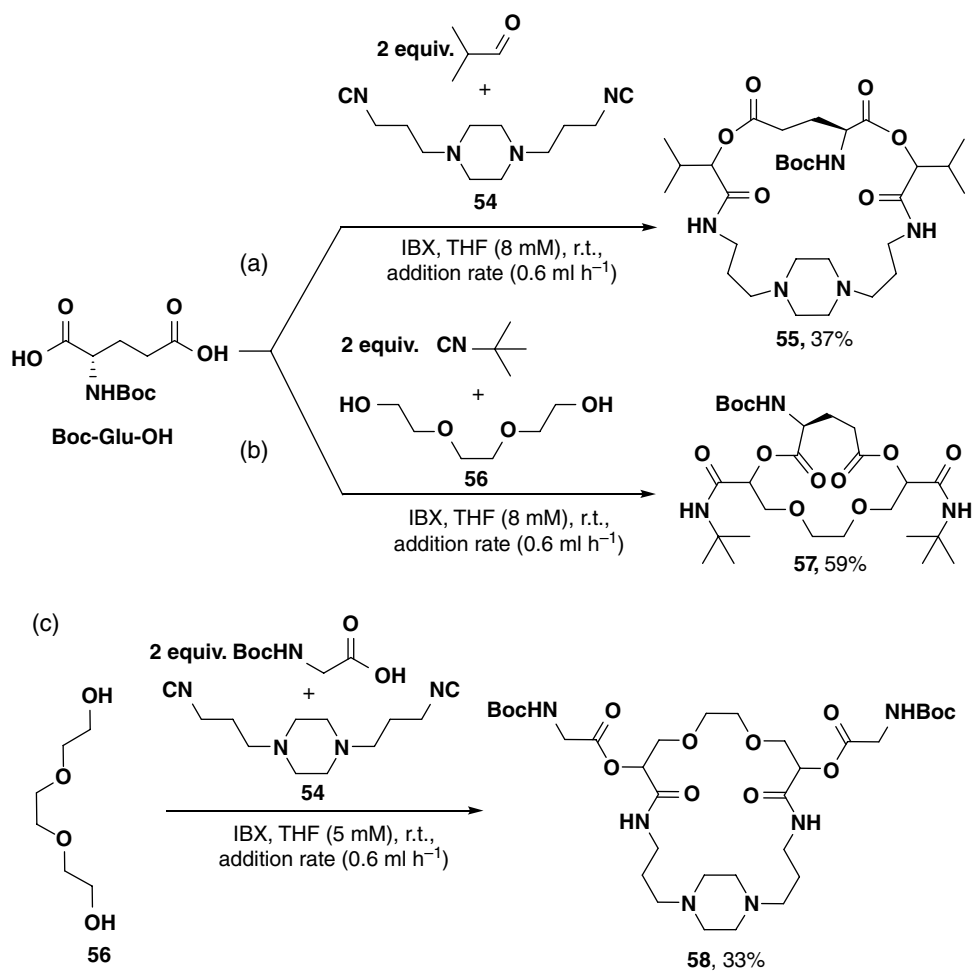
Scheme 14.20 Passerini-3CR-MiB approach toward macrolactones. (a) Diacid/diisocyanide combination. (b) Diacid/diol combination. (c) Diisonitrile/diol combination with exocyclic ester formation.
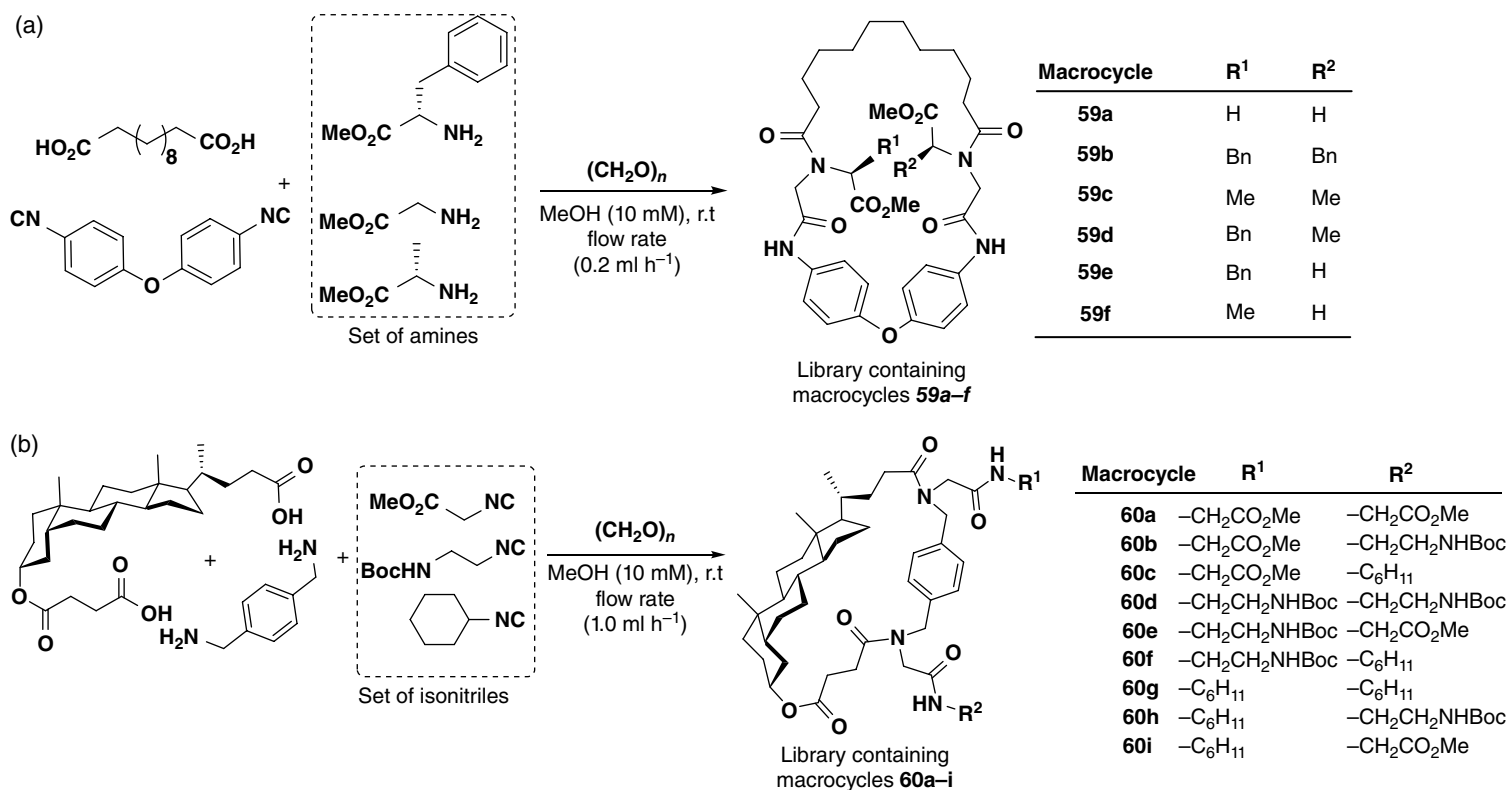
Scheme 14.21 (a) Combinatorial library of macrocycles by MiB approach. (b) MiB-combinatorial synthesis of cholane–peptoid hybrid macrocycles.
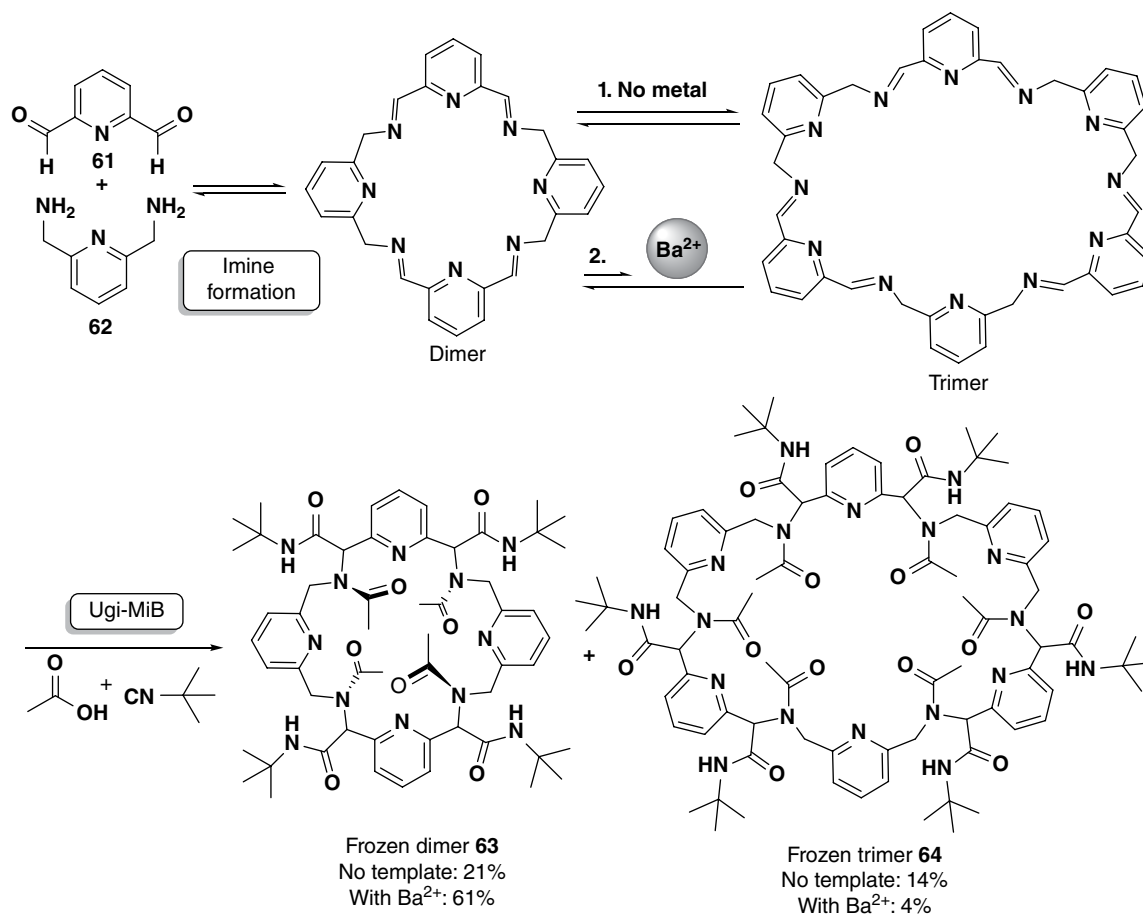
Scheme 14.22 Ugi-MiB-based quenching approach of macrocyclic oligoimine-based DCLs generated from **61** and **62**.

addition of barium (II) cations (templating effect), which, after adding the missing Ugi-4CR components, led to the selective formation of macrocycles **63** in higher yield. This underlines the usefulness of the MiB approach to freeze the imine exchange process in dynamic combinatorial libraries (DCLs) and is quite well suited for designing diversity-oriented libraries of macrocycles.

The MiB principle can be extended to trifunctional building blocks in order to construct three-dimensional molecular frameworks. Although such macrocyclic networks so far are only used as hosts in coordination chemistry, they offer a new (third) dimension for future drug development or other purposes too. The first approaches focused on the use of threefold Ugi-4CR macrocyclizations to obtain tris(2-aminoethyl)amine (TREN)-based receptors in the form of cryptands, cryptophanes, and steroid-based molecular cages. TREN-based receptors present potential for the chelation of main group and transition metal ions (as required for detoxification or imaging compounds in medicine) due to their favorable arrangement of multiple amides and the presence of the central tertiary amine in the coordination process.

Some examples of this accomplishment are presented in Scheme 14.23.

The reaction of TREN-isonitrile **65** with tricarboxylic acid **66**, glycine methyl ester, and formaldehyde leads to the cryptand **67** in 47% yield, and with TREN itself as second trifunctional building block and Cbz-Gly-OH as the carboxylic acid gave cryptand **68** in 41% yield. Please note that this yield is exceptional given that 12 new bonds are formed from 8 components, including two macrocyclizations. Other architectures, such as cryptophanes (**69**) and steroid-based molecular cages (**70**), can be devised too, as depicted in Scheme 14.23 [88].

A key feature of this one-pot assembly of eight components is the rapid variation of molecular topologies achievable by employing constitutionally different building blocks. Although reaction yields did not decrease compared with the 2D-MiBs, much care has to be taken in the selection of building blocks that have to match in size as well as complementarity and in terms of conformational flexibility. Considering this, the low synthetic cost, rapid diversity generation, and easy operation renders the MiB-3D approach particularly suitable for
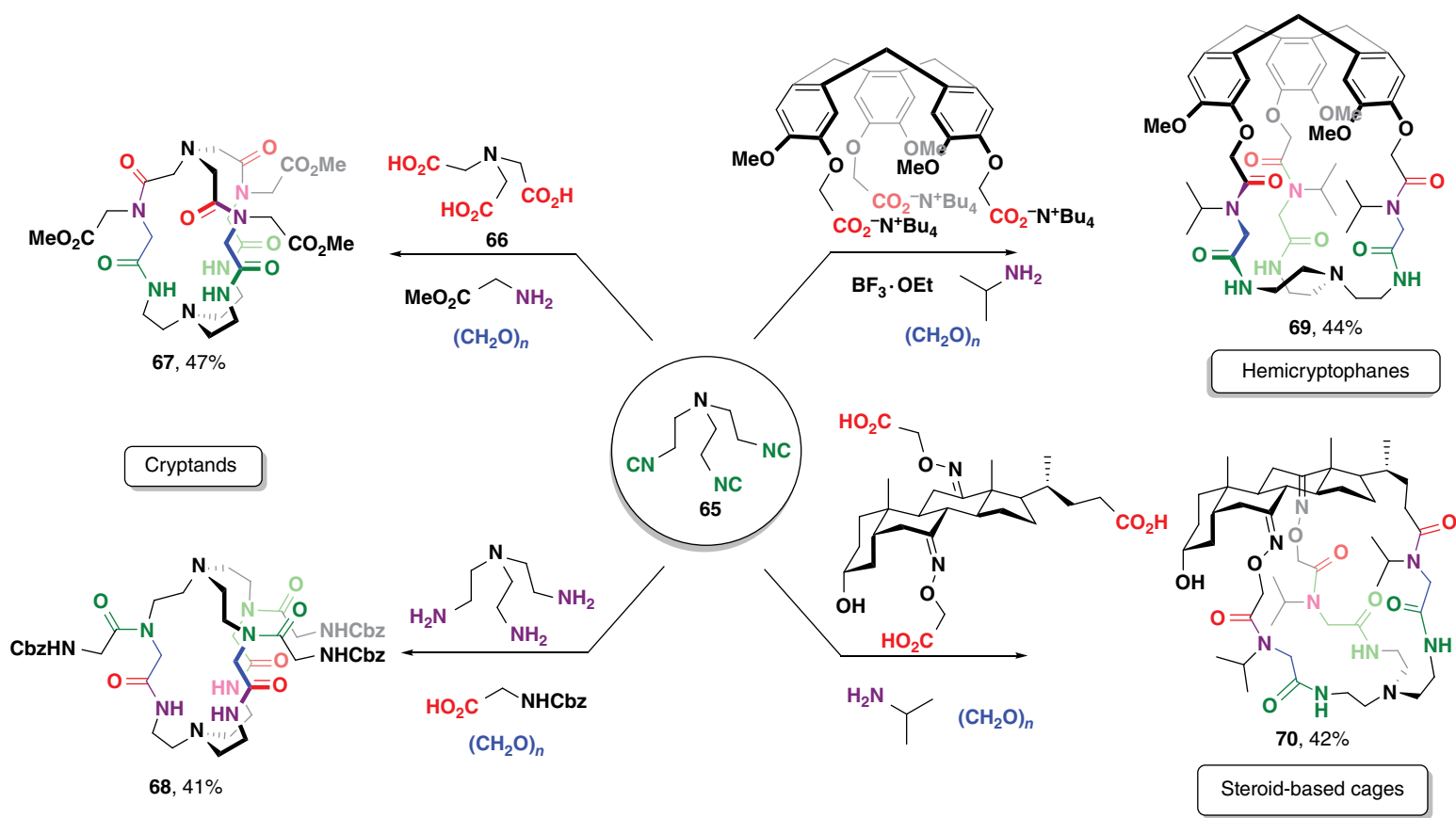
Scheme 14.23 Synthesis of three-dimensional multi-macrocycles by threefold Ugi-4CR-based macrocyclizations, including trifunctional building blocks. (*See insert for color representation of the figure.*)

Scheme 14.24 Synthesis of a mixed library of cryptands by a threefold combinatorial MiB. (*See insert for color representation of the figure.*)

Cryptand	R^1	R^2	R^3
71a	Bn	Bn	Bn
71b	Bn	Bn	*i*-Pr
71c	Bn	Bn	CH$_2$CO$_2$Me
71d	Bn	*i*-Pr	CH$_2$CO$_2$Me
71e	Bn	CH$_2$CO$_2$Me	CH$_2$CO$_2$Me
71f	Bn	*i*-Pr	*i*-Pr
71g	*i*-Pr	*i*-Pr	*i*-Pr
71h	*i*-Pr	*i*-Pr	CH$_2$CO$_2$Me
71i	*i*-Pr	CH$_2$CO$_2$Me	CH$_2$CO$_2$Me
71j	CH$_2$CO$_2$Me	CH$_2$CO$_2$Me	CH$_2$CO$_2$Me

applications in the search of supramolecular receptors requiring combinatorial generation. By using the same combination highlighted in Scheme 14.21a (i.e., diacid–diisocyanide), but this time with equally functionalized trifunctional building blocks, it is possible to accomplish a threefold Ugi-4CR-based combinatorial macrocyclization to give a mixed library of cryptands [85]. As presented in Scheme 14.24, by employing three different amines as a source of variation in the triacid–triisocyanide combination, it is possible to synthesize a library of compounds composed of 10 constitutionally different macrobicycles.

14.2.4 Iterative IMCR-Based Macrocyclizations with Multiple Bifunctional Building Blocks

Macrocycles and cages from non-combinatorial MiB approaches involving two or more MCRs possess identical moieties (tethers) as the same monofunctional building blocks are attached. In order to increase access to more complex (multi)macrocycles and generate different moieties on every tether between knots of cryptands in a defined way, sequential IMCR-based macrocyclizations of multiple bifunctional building blocks are required. This approach has been named sequential MiB. It consists of an MCR reaction with a bifunctional building block containing a third, protected Ugi-reactive group. After cleavage of the protecting group, a second MCR reaction may take place on the previously synthesized macrocycle, now acting as a bi- or polyfunctional building block itself. By using this strategy, it is possible to synthesize topologically very complex structures like nonsymmetric cryptands, steroid-based clams, or igloo-shaped molecules, depending on the designed building blocks and their frameworks (Scheme 14.25) [89]. The ability to achieve such intriguing molecules in only a few steps, often even performed in a tandem fashion, avoids exhaustive step-by-step protocols and constitutes a new approach for the synthesis of complex molecules. The concept was termed architectural chemistry [89]. If consequently applied and developed, in the future, this concept may lead to (biostable) mimics of larger protein patches or even macrocyclic compounds endowed with enzyme-like recognition and functional abilities.

14.3 Concluding Remarks and Future Perspectives

MCRs have revolutionized access to diverse libraries of macrocycles in both major parts of their assembly: the synthesis of linear precursors, as well as the macrocyclization step itself. So far, they have been especially successful for the syntheses of macrocycles with pseudopeptidic, peptoid, and some heterocyclic elements.
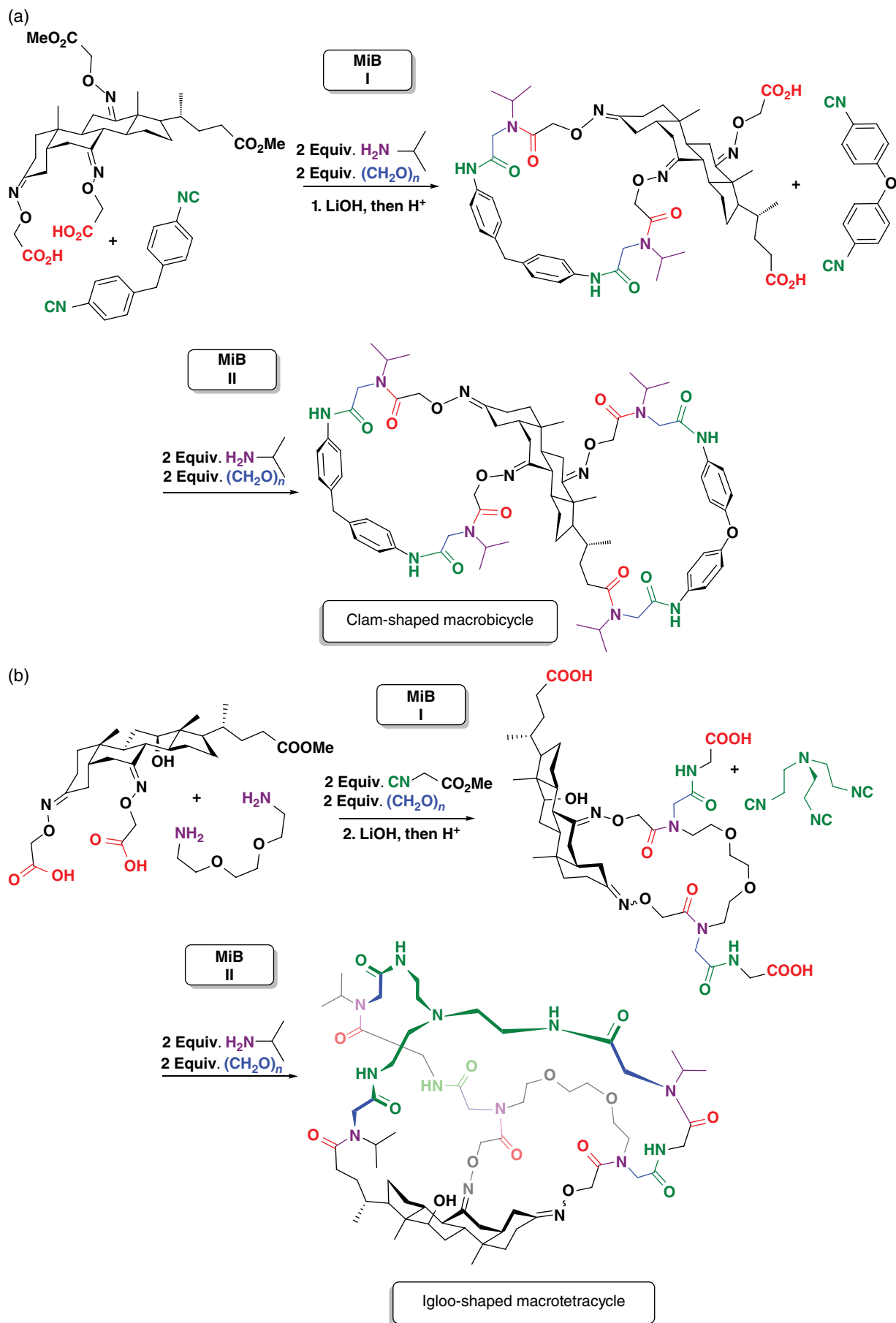
Scheme 14.25 Sequential MiBs applied to the synthesis of multi-macrocycles. (a) Clam-shaped macrobicycles and (b) igloo-shaped macrotetracycles. (*See insert for color representation of the figure.*)

The following advantages are general for most MCRs so far utilized in macrocycle syntheses:

- High input of diversity
- High atom and step economy
- Usually simple and efficient reaction conditions
- No condensing reagent required
- Macrocyclizations with simultaneous introduction of functional elements

Specifically for isonitrile MCRs like Ugi-4CR or Passerini-3CR, further advantages and some disadvantages apply:

- High macrocyclization yield through persistent ion pairing in amino–carboxylic acid linear precursors, sometimes to the extent that (pseudo-)dilution is not required.
- Natural product-like and drug-like moieties generated (e.g., depsi- or *N*-alkyl peptide moieties).
- No special inert atmosphere or solvent required (reaction in water and with unprotected hydroxyls possible).
- Steric bulk usually tolerated.
- Most components are abundant and commercially available or easily synthesized (e.g., di-isonitriles from diamines).

- IMCRs usually allow access to all stereoisomers without a relevant bias for one isomer, that is, the reactions will not select out potentially active stereoisomers in library syntheses.
- Good control of stereoselectivity is not easily possible; usually separation of isomers is easier.

In the past, most studies were directed toward understanding the principles of using MCRs in macrocyclizations and to explore the scope of these reactions, especially of the valuable IMCRs. In the future, this will be extended to even more and different MCRs, which in themselves are only at the advent of being explored. More importantly, with the groundwork laid on how to efficiently use this methodology in macrocycle syntheses, near future work will concentrate on two topics of this yet underused concept: on the one hand, the generation of functional libraries for certain purposes, in medicinal chemistry or other, where rapid, easy variation is required; and, on the other hand, for the efficient synthesis of defined molecules with specific biological or other function. The architectural chemistry design of one-pot-generated multi-macrocycles paves the way to more advanced constructs that mimic larger 3-dimensional folded peptides, address large area protein–protein interactions, or produce nano-containers (for drug delivery) and more.

References

1 (a) Wessjohann, L. A.; Ruijter, E.; Garcia-Rivera, D.; Brandt, W. What Can a Chemist Learn from Nature's Macrocycles? A Brief, Conceptual View. *Mol. Divers.* **2005**, *9*, 171–186. (b) Wessjohann, L. A.; Ruijter, E. Macrocycles rapidly produced by multiple multicomponent reactions including bifunctional building blocks (MiBs). *Mol. Diversity* **2005**, *9*, 159–169.

2 Heinis, C. Drug Discovery: Tools and Rules for Macrocycles. *Nat. Chem. Biol.* **2014**, *10*, 696–698.

3 (a) Blunt, J. W.; Copp, B. R.; Keyzers, R. A.; Munro, M. H.; Prinsep, M. R. Marine Natural Products. *Nat. Prod. Rep.* **2013**, *30*, 237–323. (b) Schwarzer, D.; Finking, R.; Marahiel, M. A. Nonribosomal Peptides: From Genes to Products. *Nat. Prod. Rep.* **2003**, *20*, 275–287. (c) Maksimov, M. O.; Pan, S. J.; James Link, A. Lasso Peptides: Structure, Function, Biosynthesis, and Engineering. *Nat. Prod. Rep.* **2012**, *29*, 996–1006. (d) Blunt, J. W.; Copp, B. R.; Keyzers, R. A.; Munro, M. H. G.; Prinsep, M. R. Marine Natural Products. *Nat. Prod. Rep.* **2012**, *29*, 144–222. (e) Blunt, J. W.; Copp, B. R.; Munro, M. H. G.; Northcote, P. T.; Prinsep, M. R. Marine Natural Products. *Nat. Prod. Rep.* **2011**, *28*, 196–268.

4 Wessjohann, L. A., Ruijter, E., Strategies for Total and Diversity-Oriented Synthesis of Natural Product(-Like) Macrocycles In *Topics in Current Chemistry*; Mulzer, J. H., Ed.; Springer: Heidelberg, **2005**; *243*, 137–184.

5 Newman, D. J.; Cragg, G. M.; Snader, K. M. The Influence of Natural Products upon Drug Discovery. *Nat. Prod. Rep.* **2000**, *17*, 215–234.

6 Newman, D. J.; Cragg, G. M. Natural Products as Sources of New Drugs over the 30 Years from 1981 to 2010. *J. Nat. Prod.* **2012**, *75*, 311–335.

7 Driggers, E. M.; Hale, S. P.; Lee, J.; Terrett, N. K. The Exploration of Macrocycles for Drug Discovery: An Underexploited Structural Class. *Nat. Rev. Drug Discov.* **2008**, *7*, 608–624.

8 Lipinski, C. A.; Lombardo, F.; Dominy, B. W.; Feeney, P. J. Experimental and Computational Approaches to Estimate Solubility and Permeability in Drug Discovery and Development Settings. *Adv. Drug Deliv. Rev.* **2001**, *46*, 3–26.

9 Rüegger, V. A.; Kuhn, M.; Lichti, H.; Loosli, H.; Huguenin, R.; Quiquerez, C.; von Wartburg, A. Cyclosporin A, Ein Immunsuppressiv Wirksamer Peptidmetabolit Aus *Trichoderma polysporum* (Link ex Pers.) Rifai. *Helv. Chim. Acta* **1976**, *59*, 1075–1092.

10 Brandt, W.; Haupt, V. J.; Wessjohann, L. A. Chemoinformatic Analysis of Biologically Active Macrocycles. *Curr. Top. Med. Chem.* **2010**, *10*, 1361–1379.

11 Hyung, S. J.; Feng, X.; Che, Y.; Stroh, J. G.; Shapiro, M. Detection of Conformation Types of Cyclosporin Retaining Intramolecular Hydrogen Bonds by Mass Spectrometry. *Anal. Bioanal. Chem.* **2014**, *406*, 5785–5794.

12 Whitty, A.; Zhong, M.; Viarengo, L.; Beglov, D.; Hall, D. R.; Vajda, S. Quantifying the Chameleonic Properties of Macrocycles and Other High-Molecular-Weight Drugs. *Drug Discov. Today* **2016**, *21*, 712–717.

13 Marsault, E.; Peterson, M. L. Macrocycles Are Great Cycles: Applications, Opportunities, and Challenges of Synthetic Macrocycles in Drug Discovery. *J. Med. Chem.* **2011**, *54*, 1961–2004.

14 (a)Adessi, C.; Soto, C. Converting a Peptide into a Drug: Strategies to Improve Stability and Bioavailability. *Curr. Med. Chem.* **2002**, *9*, 963–978. (b)Pauletti, G. M.; Gangwar, S.; Siahaan, T. J.; Aubé, J.; Borchardt, R. T. Improvement of Oral Peptide Bioavailability: Peptidomimetics and Prodrug Strategies. *Adv. Drug Deliv. Rev.* **1997**, *27*, 235–256. (c)McGeary, R. P.; Fairlie, D. P. Macrocyclic Peptidomimetics: Potential for Drug Development. *Curr. Opin. Drug Discov. Dev.* **1998**, *1*, 208–217.

15 Edwards, J. V.; Lax, A. R.; Lillehoj, E. B.; Boudreaux, G. J. Structure-Activity Relationships of Cyclic and Acyclic Analogues of the Phytotoxic Peptide Tentoxin. *J. Agric. Food Chem.* **1987**, *35*, 451–456.

16 Cherney, R. J.; Wang, L.; Meyer, D. T.; Xue, C.-B.; Wasserman, Z. R.; Hardman, K. D.; Welch, P. K.; Covington, M. B.; Copeland, R. A.; Arner, E. C.; DeGrado, W. F.; Decicco, C. P. Macrocyclic Amino Carboxylates as Selective MMP-8 Inhibitors. *J. Med. Chem.* **1998**, *41*, 1749–1751.

17 Nie, Z.; Perretta, C.; Erickson, P.; Margosiak, S.; Lu, J.; Averill, A.; Almassy, R.; Chu, S. Structure-Based Design and Synthesis of Novel Macrocyclic Pyrazolo[1,5-a][1,3,5]triazine Compounds as Potent Inhibitors of Protein Kinase CK2 and Their Anticancer Activities. *Bioorg. Med. Chem. Lett.* **2008**, *18*, 619–623.

18 Huang, Y.; Strobel, E. D.; Ho, C. Y.; Reynolds, C. H.; Conway, K. A.; Piesvaux, J. A.; Brenneman, D. E.; Yohrling, G. J.; Arnold, H. M.; Rosenthal, D.; Alexander, R. S.; Tounge, B. A.; Mercken, M.; Vandermeeren, M.; Parker, M. H.; Reitz, A. B.; Baxter, E. W. Macrocyclic BACE Inhibitors: Optimization of a Micromolar Hit to Nanomolar Leads. *Bioorg. Med. Chem. Lett.* **2010**, *20*, 3158–3160.

19 Stachel, S. J.; Coburn, C. A.; Sankaranarayanan, S.; Price, E. A.; Pietrak, B. L.; Huang, Q.; Lineberger, J.; Espeseth, A. S.; Jin, L.; Ellis, J.; Holloway, M. K.; Munshi, S.; Allison, T.; Hazuda, D.; Simon, A. J.; Graham, S. L.; Vacca, J. P. Macrocyclic Inhibitors of β-Secretase: Functional Activity in an Animal Model. *J. Med. Chem.* **2006**, *49*, 6147–6150.

20 Veber, D. F.; Johnson, S. R.; Cheng, H. Y.; Smith, B. R.; Ward, K. W.; Kopple, K. D. Molecular Properties that Influence the Oral Bioavailability of Drug Candidates. *J. Med. Chem.* **2002**, *45*, 2615–2623.

21 von Nussbaum, F.; Brands, M.; Hinzen, B.; Weigand, S.; Häbich, D. Antibacterial Natural Products in Medicinal Chemistry-Exodus or Revival? *Angew. Chem. Int. Ed. Engl.* **2006**, *45*, 5072–5129.

22 Wessjohann, L. A.; Rivera, D. G.; Vercillo, O. E. Multiple Multicomponent Macrocyclizations (MiBs): A Strategic Development Toward Macrocycle Diversity. *Chem. Rev.* **2009**, *109*, 796–814.

23 White, C. J.; Yudin, A. K. Contemporary Strategies for Peptide Macrocyclization. *Nat. Chem.* **2011**, *3*, 509–524.

24 Zhu, J. Recent Developments in Reversing Glycopeptide-Resistant Pathogens. *Expert Opin. Ther. Pat.* **1999**, *9*, 1005–1019.

25 William, A. D.; Lee, A. C.-H.; Blanchard, S.; Poulsen, A.; Teo, E. L.; Nagaraj, H.; Tan, E.; Chen, D.; Williams, M.; Sun, E. T.; Goh, K. C.; Ong, W. C.; Goh, S. K.; Hart, S.; Jayaraman, R.; Pasha, M. K.; Ethirajulu, K.; Wood, J. M.; Dymock, B. W. Discovery of the Macrocycle 11-(2-Pyrrolidin-1-Yl-Ethoxy)-14,19-Dioxa-5,7,26-Triaza-tetracyclo[19.3.1.1(2,6).1(8,12)]heptacosa-1(25),2(26),3,5,8,10,12(27),16,21,23-Decaene (SB1518), a Potent Janus Kinase 2/Fms-Like Tyrosine Kinase-3 (JAK2/FLT3) Inhibitor. *J. Med. Chem.* **2011**, *54*, 4638–4658.

26 Burke, P. A.; DeNardo, S. J.; Miers, L. A.; Lamborn, K. R.; Matzku, S.; DeNardo, G. L. Cilengitide Targeting of αvβ3 Integrin Receptor Synergizes with Radioimmunotherapy to Increase Efficacy and Apoptosis in Breast Cancer Xenografts. *Cancer Res.* **2002**, *62*, 4263–4272.

27 Masson, G.; Neuville, L.; Bughin, C.; Fayol, A.; Zhu, J. *Topics in Heterocyclic Chemistry*; Springer-Verlag: Berlin, Heidelberg, **2010**.

28 Yudin, A. K. Macrocycles: Lessons from the Distant Past, Recent Developments, and Future Directions. *Chem. Sci.* **2015**, *6*, 30–49.

29 Wessjohann, L. A., Neves Filho, R. A. W., Puentes, A. R., Morejon, M. C. Macrocycles from Multicomponent Reactions. In *Multicomponent Reactions*; Zhu, J. Ed.; Wiley-VCH: Weinheim, **2015**; *2*, 231–261.

30 Schmidt, U.; Langner, J. Cyclotetrapeptides and Cyclopentapeptides: Occurrence and Synthesis. *J. Pept. Res.* **1997**, *49*, 67–73.

31 Zhang, L.; Tam, J. P. Lactone and Lactam Library Synthesis by Silver Ion-Assisted Orthogonal

Cyclization of Unprotected Peptides. *J. Am. Chem. Soc.* **1999**, *121*, 3311–3320.

32 Paterson, I.; Yeung, K.-S.; Ward, R. A.; Cumming, J. G.; Smith, J. D. Total Synthesis of Swinholide A and Hemiswinholide A. *J. Am. Chem. Soc.* **1994**, *116*, 9391–9392.

33 Inanaga, J.; Hirata, K.; Saeki, H.; Katsuki, T.; Yamaguchi, M. A Rapid Esterification by Means of Mixed Anhydride and Its Application to Large-Ring Lactonization. *Bull. Chem. Soc. Jpn.* **1979**, *52*, 1989–1993.

34 Boden, E. P.; Keck, G. E. Proton-Transfer Steps in Steglich Esterification: A Very Practical New Method for Macrolactonization. *J. Org. Chem.* **1985**, *50*, 2394–2395.

35 Wipf, P. Synthetic Studies of Biologically Active Marine Cyclopeptides. *Chem. Rev.* **1995**, *95*, 2115–2134.

36 (a) Sunderhaus, J. D.; Martin, S. F. Applications of Multicomponent Reactions to the Synthesis of Diverse Heterocyclic Scaffolds. *Chem. Eur. J.* **2009**, *15*, 1300–1308. (b) Isambert, N.; Lavilla, R. Heterocycles as Key Substrates in Multicomponent Reactions: The Fast Lane towards Molecular Complexity. *Chem. Eur. J.* **2008**, *14*, 8444–8454.

37 Kazemizadeh, A. R.; Ramazani, A. Synthetic Applications of Passerini Reaction. *Curr. Org. Chem.* **2012**, *16*, 418–450.

38 Ugi, I.; Meyr, R.; Fetzer, U.; Steinbrückner, C. Versuche mit Isonitrilen. *Angew. Chem. Int. Ed.* **1959**, *71*, 386–386.

39 Selected reviews:(a) Bienaymé, H.; Hulme, C.; Oddon, G.; Schmitt, P. Maximizing Synthetic Efficiency: Multi-Component Transformations Lead the Way. *Chem. Eur. J.* **2000**, *6*, 3321–3329. (b) Zhu, J. Recent Developments in the Isonitrile-Based Multicomponent Synthesis of Heterocycles. *Eur. J. Org. Chem.* **2003**, *7*, 1133–1144. (c) Dömling, A. Recent Developments in Isocyanide Based Multicomponent Reactions in Applied Chemistry. *Chem. Rev.* **2006**, *106*, 17–89. (d) Hulme, C.; Gore, V. Multi-Component Reactions: Emerging Chemistry in Drug Discovery from Xylocain to Crixivan. *Curr. Med. Chem.* **2003**, *10*, 51–80.

40 (a) Cristau, P.; Vors, J.-P.; Zhu, J. A Rapid Access to Biaryl Ether Containing Macrocycles by Pairwise Use of Ugi 4CR and Intramolecular SNAr-Based Cycloetherification. *Org. Lett.* **2001**, *3*, 4079–4082. (b) Cristau, P.; Vors, J.-P.; Zhu, J. Rapid and Diverse Route to Natural Product-like Biaryl Ether Containing Macrocycles. *Tetrahedron* **2003**, *59*, 7859–7870. (c) Cristau, P.; Vors, J.-P.; Zhu, J. Rapid Synthesis of Cyclopeptide Alkaloid-Like Para-Cyclophanes by Combined Use of Ugi-4CR and Intramolecular SNAr Reaction. *QSAR Comb. Sci.* **2006**, *25*, 519–526. (d) de Greef, M.; Abeln, S.; Belkasmi, K.; Dömling, A.; Orru,

R. V. A.; Wessjohann, L. A. Rapid Combinatorial Access to Macrocyclic Ansapeptoids and Ansapeptides with Natural-Product-like Core Structures. *Synthesis (Stuttg)* **2006**, *23*, 3997–4004. (e) For further examples of MCRs + ring closure see: Wessjohann, L. A.; Rhoden, C. R. B.; Rivera, D. G.; Vercillo, O. E. Cyclic Peptidomimetics and Pseudopeptides from Multicomponent Reactions. In *Synthesis of Heterocycles via Multicomponent Reactions I*; Orru, A. R. V., Ruijter, E., Eds.; Springer: Berlin, Heidelberg, **2010**; 199–226.

41 Liao, G. P.; Abdelraheem, E. M. M.; Neochoritis, C. G.; Kurpiewska, K.; Kalinowska-Tłuścik, J.; McGowan, D. C.; Dömling, A. Versatile Multicomponent Reaction Macrocycle Synthesis Using α-Isocyano-ω-Carboxylic Acids. *Org. Lett.* **2015**, *17*, 4980–4983.

42 Wessjohann, L. A.; Voigt, B.; Rivera, D. G. Diversity Oriented One-Pot Synthesis of Complex Macrocycles: Very Large Steroid-Peptoid Hybrids from Multiple Multicomponent Reactions Including Bifunctional Building Blocks. *Angew. Chem. Int. Ed.* **2005**, *44*, 4785–4790.

43 Failli, A.; Immer, H.; Götz, M. The Synthesis of Cyclic Peptides by the Four Component Condensation (4 CC). *Can. J. Chem.* **1979**, *57*, 3257–3261.

44 De Marco, A.; Gatti, G. 1H and 13C NMR of Eledoisin and Intermediate Oligopeptides. *Int. J. Pept. Protein Res.* **1975**, *7*, 437–444.

45 Vercillo, O. E.; Andrade, C. K.; Wessjohann, L. A. Design and Synthesis of Cyclic RGD Pentapeptoids by Consecutive Ugi Reactions. *Org. Lett.* **2008**, *10*, 205–208.

46 (a)Ruoslahti, E.; Pierschbacher, M. D. New Perspectives in Cell Adhesion: RGD and Integrins. *Science* **1987**, *238*, 491–497. (b)Banfi, L.; Basso, A.; Damonte, G.; De Pellegrini, F.; Galatini, A.; Guanti, G.; Monfardini, I.; Riva, R.; Scapolla, C. Synthesis and Biological Evaluation of New Conformationally Biased Integrin Ligands Based on a Tetrahydroazoninone Scaffold. *Bioorg. Med. Chem. Lett.* **2007**, *17*, 1341–1345.

47 Haubner, R.; Schmitt, W.; Hölzemann, G.; Goodman, S. L.; Jonczyk, A.; Kessler, H. Cyclic RGD Peptides Containing β-Turn Mimetics. *J. Am. Chem. Soc.* **1996**, *118*, 7881–7891.

48 Miller, S. M.; Simon, R. J.; Ng, S.; Zuckermann, R. N.; Kerr, J. M.; Moos, W. H. Comparison of the Proteolytic Susceptibilities of Homologous L-Amino Acid, D-Amino Acid, and N-Substituted Glycine Peptide and Peptoid Oligomers. *Drug Dev. Res.* **1995**, *35*, 20–32.

49 Barreto, A. F.; Vercillo, O. E., Wessjohann, L. A., Andrade, C. K. Z. Consecutive Isocyanide-Based Multicomponent Reactions: Synthesis of Cyclic Pentadepsipeptoids. *Beilstein J. Org. Chem.* **2014**, *10*, 1017–1022.

50 Hili, R.; Rai, V.; Yudin, A. K. Macrocyclization of Linear Peptides Enabled by Amphoteric Molecules. *J. Am. Chem. Soc.* **2010**, *132*, 2889–2891.

51 Rotstein, B. H.; Rai, V.; Hili, R.; Yudin, A. K. Synthesis of Peptide Macrocycles Using Unprotected Amino Aldehydes. *Nat. Protoc.* **2010**, *5*, 1813–1822.

52 Giovenzana, G. B.; Tron, G. C.; Di Paola, S.; Menegotto, I. G.; Pirali, T. A Mimicry of Primary Amines by Bis-Secondary Diamines as Components in the Ugi Four-Component Reaction. *Angew. Chem. Int. Ed. Engl.* **2006**, *45*, 1099–1102.

53 Sahoo, H.; Roccatano, D.; Hennig, A.; Nau, W. M. A 10-Å Spectroscopic Ruler Applied to Short Polyprolines. *J. Am. Chem. Soc.* **2007**, *129*, 9762–9772.

54 Scully, C. C. G.; Rai, V.; Poda, G.; Zaretsky, S.; Burns, D. C.; Houliston, R. S.; Lou, T.; Yudin, A. K. Bending Rigid Molecular Rods: Formation of Oligoproline Macrocycles. *Chem. Eur. J.* **2012**, *18*, 15612–15617.

55 Treder, A. P.; Hickey, J. L.; Tremblay, M. C. J.; Zaretsky, S.; Scully, C. C. G.; Mancuso, J.; Doucet, A.; Yudin, A. K.; Marsault, E. Solid-Phase Parallel Synthesis of Functionalised Medium-to-Large Cyclic Peptidomimetics through Three-Component Coupling Driven by Aziridine Aldehyde Dimers. *Chem. Eur. J.* **2015**, *21*, 9249–9255.

56 (a) Jebrail, M. J.; Ng, A. H. C.; Rai, V.; Hili, R.; Yudin, A. K.; Wheeler, A. R. Synchronized Synthesis of Peptide-Based Macrocycles by Digital Microfluidics. *Angew. Chem. Int. Ed. Engl.* **2010**, *49*, 8625–8629. (b) Jebrail, M. J.; Assem, N.; Mudrik, J. M.; Dryden, M. D.; Lin, K.; Yudin, A. K.; Wheeler, A. R. Combinatorial Synthesis of Peptidomimetics Using Digital Microfluidics. *J. Flow Chem.* **2012**, *2*, 103–107.

57 Rotstein, B. H.; Mourtada, R.; Kelley, S. O.; Yudin, A. K. Solvatochromic Reagents for Multicomponent Reactions and Their Utility in the Development of Cell-Permeable Macrocyclic Peptide Vectors. *Chem. Eur. J.* **2011**, *17*, 12257–12261.

58 Rotstein, B. H.; Winternheimer, D. J.; Yin, L. M.; Deber, C. M.; Yudin, A. K. Thioester-Isocyanides: Versatile Reagents for the Synthesis of Cycle–tail Peptides. *Chem. Commun.* **2012**, *48*, 3775–3777.

59 Chung, B. K. W.; Hickey, J. L.; Scully, C. C. G.; Zaretsky, S.; Yudin, A. K. Bicycle Synthesis through Peptide Macrocyclization Using Aziridine Aldehydes Followed by Late Stage Disulfide Bond Installation. *Med. Chem. Commun.* **2013**, *4*, 1124–1128.

60 Vasco, A. V.; Pérez, C. S.; Morales, F. E.; Garay, H. E.; Vasilev, D.; Gavín, J. A.; Wessjohann, L. A.; Rivera, D. G. Macrocyclization of Peptide Side Chains by the Ugi Reaction: Achieving Peptide Folding and Exocyclic N-Functionalization in One Shot. *J. Org. Chem.* **2015**, *80*, 6697–6707.

61 Sun, X.; Janvier, P.; Zhao, G.; Bienaymé, H.; Zhu, J. A Novel Multicomponent Synthesis of Polysubstituted 5-Aminooxazole and Its New Scaffold-Generating Reaction to Pyrrolo[3,4-b]pyridine. *Org. Lett.* **2001**, *3*, 877–880.

62 (a) Montano, R. G.; Zhu, J. Rapid Access to Tetracyclic Ring System of Lennoxamine Type Natural Product by Combined Use of a Novel Three-Component Reaction and Pummerer Cyclization. *Chem. Commun.* **2002**, *20*, 2448–2449. (b) Fayol, A.; Zhu, J. Synthesis of Furoquinolines by a Multicomponent Domino Process. *Angew. Chem. Int. Ed. Engl.* **2002**, *41*, 3633–3635. (c) Janvier, P.; Bienaymé, H.; Zhu, J. A Five-Component Synthesis of Hexasubstituted Benzene. *Angew. Chem. Int. Ed. Engl.* **2002**, *41*, 4291–4294. (d) Gámez-Montaño, R.; González-Zamora, E.; Potier, P.; Zhu, J. Multicomponent Domino Process to Oxa-Bridged Polyheterocycles and Pyrrolopyridines, Structural Diversity Derived from Work-up Procedure. *Tetrahedron* **2002**, *58*, 6351–6358. (e) Fayol, A.; Zhu, J. Three-Component Synthesis of Polysubstituted 6-Azaindolines and Its Tricyclic Derivatives. *Org. Lett.* **2005**, *7*, 239–242.

63 Zhu, J. Built-in 5-Aminooxazole as an Internal Activator of the Terminal Carboxylic Acid: An Alternative Access to Macrocyclodepsipeptides. *Chim. Int. J. Chem.* **2011**, *65*, 710–714.

64 Zhao, G.; Sun, X. W.; Bienayme, H.; Zhu, J. P. Activation of a Terminal Carboxylic Acid by an Internal Oxazole: A Novel Synthesis of Macrocyclodepsipeptide. *J. Am. Chem. Soc.* **2001**, *123*, 6700–6701.

65 Pirali, T.; Tron, G. C.; Masson, G.; Zhu, J. Ammonium Chloride Promoted Three-Component Synthesis of 5-Iminooxazoline and Its Subsequent Transformation to Macrocyclodepsipeptide. *Org. Lett.* **2007**, *9*, 5275–5278.

66 Bughin, C.; Zhao, G.; Bienayme, H.; Zhu, J. P. 5-Aminooxazole as an Internal Traceless Activator of C-Terminal Carboxylic Acid: Rapid Access to Diversely Functionalized Cyclodepsipeptides. *Chem. Eur. J.* **2006**, *12*, 1174–1184.

67 Bughin, C.; Masson, G.; Zhu, J. Rapid Synthesis of Cyclodepsipeptides Containing a Sugar Amino Acid or a Sugar Amino Alcohol by a Sequence of a Multicomponent Reaction and Acid-Mediated Macrocyclization. *J. Org. Chem.* **2007**, *72*, 1826–1829.

68 Akhmetova, V. R.; Khabibullina, G. R.; Rakhimova, E. B.; Vagapov, R. A.; Khairullina, R. R.; Niatshina, Z. T.; Murzakova, N. N. Multicomponent Reactions of Amines with Aldehydes and H_2S as Efficient Route to Heterocycles and Thioaza Macrocycles. *Mol. Divers.* **2010**, *14*, 463–471.

69 Niu, T.; Sun, M.; Lv, M.; Yi, W.; Cai, C. Synthesis of Highly Functionalized Macrocycles by Tandem

Multicomponent Reactions and Intramolecular Sonogashira Cross-Coupling. *Org. Biomol. Chem.* **2013**, *11*, 7232–7238.

70 Pokhodylo, N. T.; Matiychuk, V. S.; Obushak, M. D. One-Pot Multicomponent Synthesis of 1-Aryl-5-Methyl-N-R2-1H-1,2,3-Triazole-4-Carboxamides: An Easy Procedure for Combinatorial Chemistry. *J. Comb. Chem.* **2009**, *11*, 481–485.

71 (a) Janvier, P.; Bois-Choussy, M.; Bienaymé, H.; Zhu, J. A One-Pot Four-Component (ABC2) Synthesis of Macrocycles. *Angew. Chem. Int. Ed. Engl.* **2003**, *42*, 811–814. (b) Sun, X.; Janvier, P.; Zhao, G.; Bienaymé, H.; Zhu, J. A Novel Multicomponent Synthesis of Polysubstituted 5-Aminooxazole and Its New Scaffold-Generating Reaction to Pyrrolo[3,4-b]pyridine. *Org. Lett.* **2001**, *3*, 877–880. (c) Janvier, P.; Sun, X.; Bienaymé, H.; Zhu, J. Ammonium Chloride-Promoted Four-Component Synthesis of Pyrrolo[3,4-b]pyridin-5-one. *J. Am. Chem. Soc.* **2002**, *124*, 2560–2567.

72 Wessjohann, L. A.; Rivera, D. G.; Coll, F. Synthesis of Steroid-Biaryl Ether Hybrid Macrocycles with High Skeletal and Side Chain Variability by Multiple Multicomponent Macrocyclization Including Bifunctional Building Blocks. *J. Org. Chem.* **2006**, *71*, 7521–7526.

73 (a) Nubbemeyer, U. Synthesis of Medium-Sized Ring Lactams. In *Stereoselective Heterocyclic Synthesis III*; Metz, P., Ed.; Springer: Berlin, Heidelberg, **2001**; *216*, 125–196. (b) Shu, Y.-Z. Recent Natural Products Based Drug Development: A Pharmaceutical Industry Perspective. *J. Nat. Prod.* **1998**, *61*, 1053–1071. (c) Newman, D. J.; Cragg, G. M.; Snader, K. M. The Influence of Natural Products upon Drug Discovery. *Nat. Prod. Rep.* **2000**, *17*, 215–234.

74 For synthetic approaches of the naturally occurring cyclic peptides containing biaryl or biaryl ether linkages, see the review: Feliu, L.; Planas, M. Cyclic Peptides Containing Biaryl and Biaryl Ether Linkages. *Int. J. Pept. Res. Ther.* **2005**, *11*, 53–97.

75 (a) Kessler, H. Conformation and Biological Activity of Cyclic Peptides. *Angew. Chem. Int. Ed. Engl.* **1982**, *21*, 512–523. (b) Hruby, V. J. Conformational Restrictions of Biologically Active Peptides via Amino Acid Side Chain Groups. *Life Sci.* **1982**, *31*, 189–199. (c) Jiang, S.; Li, Z.; Ding, K.; Roller, P. P. Recent Progress of Synthetic Studies to Peptide and Peptidomimetic Cyclization. *Curr. Org. Chem.* **2008**, *12*, 1502–1542. (d) Craik, D. J.; Fairlie, D. P.; Liras, S.; Price, D. The Future of Peptide-Based Drugs. *Chem. Biol. Drug Des.* **2013**, *81*, 136–147.

76 (a) Driggers, E. M.; Hale, S. P.; Lee, J.; Terrett, N. K. The Exploration of Macrocycles for Drug Discovery: An Underexploited Structural Class. *Nat. Rev. Drug Discov.* **2008**, *7*, 608–624. (b) Giordanetto, F.; Kihlberg,

J. Macrocyclic Drugs and Clinical Candidates: What Can Medicinal Chemists Learn from Their Properties? *J. Med. Chem.* **2014**, *57*, 278–295.

77 Michalik, D.; Schaks, A.; Wessjohann, L. A. One-Step Synthesis of Natural Product-Inspired Biaryl Ether-Cyclopeptoid Macrocycles by Double Ugi Multiple-Component Reactions of Bifunctional Building Blocks. *Eur. J. Org. Chem.* **2007**, *1*, 149–157.

78 Westermann, B.; Michalik, D.; Schaks, A.; Kreye, O.; Wagner, C.; Merzweiler, K.; Wessjohann, L. A. Natural Product Inspired meta/para-Biaryl Ether Lactam Macrocycles by Double Ugi Multicomponent Reactions. *Heterocycles* **2007**, *73*, 863–872.

79 Rivera, D. G.; Vercillo, O. E.; Wessjohann, L. A. Rapid Generation of Macrocycles with Natural-Product-like Side Chains by Multiple Multicomponent Macrocyclizations (MiBs). *Org. Biomol. Chem.* **2008**, *6*, 1787–1795.

80 Ricardo, M. G.; Morales, F. E.; Garay, H.; Reyes, O.; Vasilev, D.; Wessjohann, L. A.; Rivera, D. G. Bidirectional Macrocyclization of Peptides by Double Multicomponent Reactions. *Org. Biomol. Chem.* **2015**, *13*, 438–446.

81 Kreye, O.; Westermann, B.; Rivera, D. G.; Johnson, D. V.; Orru, R. V. A.; Wessjohann, L. A. Dye-Modified and Photoswitchable Macrocycles by Multiple Multicomponent Macrocyclizations Including Bifunctional Building Blocks (MiBs). *QSAR Comb. Sci.* **2006**, *25*, 461–464.

82 Leon, F.; Rivera, D. G.; Wessjohann, L. A. Multiple Multicomponent Macrocyclizations Including Bifunctional Building Blocks (MiBs) Based on Staudinger and Passerini Three-Component Reactions. *J. Org. Chem.* **2008**, *73*, 1762–1767.

83 Wessjohann, L. A.; Morejón, M. C.; Ojeda, G. M.; Rhoden, C. R. B.; Rivera, D. G. Applications of Convertible Isonitriles in the Ligation and Macrocyclization of Multicomponent Reaction-Derived Peptides and Depsipeptides. *J. Org. Chem.* **2016**, *81*, 6535–6545.

84 Ngouansavanh, T.; Zhu, J. Alcohols in Isonitrile-Based Multicomponent Reaction: Passerini Reaction of Alcohols in the Presence of *O*-Iodoxybenzoic Acid. *Angew. Chem. Int. Ed. Engl.* **2006**, *45*, 3495–3497.

85 Rivera, D. G.; Vercillo, O. E.; Wessjohann, L. A. Combinatorial Synthesis of Macrocycles by Multiple Multicomponent Macrocyclization Including Bifunctional Building Blocks (MiB). *Synlett* **2007**, *2*, 308–312.

86 Rivera, D. G.; Wessjohann, L. A. Synthesis of Novel Steroid-Peptoid Hybrid Macrocycles by Multiple Multicomponent Macrocyclizations Including Bifunctional Building Blocks (MiBs). *Molecules* **2007**, *12*, 1890–1899.

87 Wessjohann, L. A.; Rivera, D. G.; León, F. Freezing Imine Exchange in Dynamic Combinatorial Libraries with Ugi Reactions: Versatile Access to Templated Macrocycles. *Org. Lett.* **2007**, *9*, 4733–4736.

88 Rivera, D. G.; Wessjohann, L. A. Supramolecular Compounds from Multiple Ugi Multicomponent Macrocyclizations: Peptoid-Based Cryptands, Cages,

and Cryptophanes. *J. Am. Chem. Soc.* **2006**, *128*, 7122–7123.

89 Rivera, D. G.; Wessjohann, L. A. Architectural Chemistry: Synthesis of Topologically Diverse Macromulticycles by Sequential Multiple Multicomponent Macrocyclizations. *J. Am. Chem. Soc.* **2009**, *131*, 3721–3732.

15

Synthetic Approaches Used in the Scale-Up of Macrocyclic Clinical Candidates

Jongrock Kong

Department of Process Research & Development, Merck Research Laboratories, Merck & Co., Inc., Rahway, NJ, USA

15.1 Introduction

Macrocyclic motifs are commonly found in bioactive natural products and pharmaceutical molecules, and these macromolecules have received intense recent interest from the pharmaceutical industry due to the potential opportunity they afford to open up vast new therapeutic area [1]. According to the recent review by Giordanetto and Kihlberg [2], 68 registered macrocyclic drugs are approved for human use along with 35 macrocyclic drug candidates in late-stage clinical development. The majority of these registered drugs are natural products or directly derived from natural products. Over the last decades, great progress has been made to advance the synthesis of complex natural product macrocycles [3–5]. Relative to total syntheses of natural product macrocycles in academic laboratories, industrial applications of macrocyclization reactions have historically been more limited. Recently, however, synthetic macrocyclic compounds have received intense attention from pharmaceutical companies, and a number of these macrocycles have been identified as preclinical or clinical candidates (see Chapter 16). As a result of the increasing interest of synthetic macrocycles in drug discovery, there has been significant progress on large-scale synthesis of macrocyclic compounds to enable their clinical development. Efficient and cost-effective scale-up of a clinical candidate is one of the key steps required for its subsequent development and commercialization. Accordingly, the goal of this chapter is to exemplify the synthetic strategies for macrocyclization on large scales within the pharmaceutical industry. In this chapter, a macrocycle is defined as a molecule that contains a cyclic framework of at least 12 atoms [1a] and "large scale" refers to the reaction scale having been demonstrated for the intent of clinical supply. Discussion of general aspects of macrocyclization from an industrial perspective is given in the background (Section 15.2), followed by a survey of

literature examples in Section 15.3. The main focus is to highlight the synthetic strategies used so far for large-scale production of macrocycles and provide potential future directions of macrocyclization in a commercial setting.

15.2 Background

It is generally considered that construction of the macrocyclic core structure is a critical and challenging step in the synthesis of macrocyclic molecules, regardless of scale (see also Chapter 1). The traditional macrocyclization methodologies such as macrolactonization [3] and macrolactamization [6] are among the most standard approaches. Recently, ring-closing metathesis (RCM) has become another reliable method for this transformation [4]. Macrocyclization methods used in industrial-scale production are not different from those of the small-scale total synthesis of natural products in academic settings and the synthesis of bioactive molecules in medicinal chemistry. However, for the large-scale synthesis of macrocyclic compounds, selection of macrocyclization methodology is more complicated, and the synthetic route is determined by multiple process factors: (i) development timeline, (ii) availability of raw materials, (iii) robustness of the reaction, (iv) cost efficiency, and (v) intellectual property (IP) issues. Thus, the development of a robust process takes a significant amount of time and resources for successful translation from lab scale to production scale.

Compared to the number of publications from academia for total synthesis of macrocyclic molecules, the number of publications from pharmaceutical R&D departments for large-scale production of macrocyclic active pharmaceutical ingredients (API) is much lower. One reason could be the fact that the majority of macrocyclic drugs are natural products, or directly derived

from natural products, and isolation of the natural products or macrocyclic cores from natural sources for subsequent semisynthesis of the natural product derivatives is still more cost effective than total chemical synthesis [7]. Table 15.1 summarizes macrocyclic drugs launched on the market and the corresponding manufacturing process for the macrocyclization step since 1960. Fully synthetic process was limited to the production of peptide-based macrocyclic drugs until eribulin mesylate (Halaven®) was commercialized in 2010. Following the breakthrough of the eribulin process, several fully synthetic HCV drugs such as simeprevir, paritaprevir, and vaniprevir were launched.

15.3 Literature Examples

In this section, examples of industrial applications of macrocyclization reactions that have either been commercialized or have noteworthy commercialization potential are discussed.

15.3.1 Macrolactonization

Macrolactones constitute a major type of naturally occurring macrocycles, and over 16 macrolactone-containing drugs have been commercialized since 1960 (Table 15.1). However, presently, all commercial macrolactone-containing drugs are produced by fermentation or semisynthesis. One exceptional example of full synthetic macrolactones in clinical trials is sagopilone (ZK-EOP) [8]. Sagopilone (Scheme 15.1), under development by Bayer Schering Pharma AG, is a 16-membered novel epothilone B analogue that is representative of a new class of microtubule-stabilizing agents having a similar mechanism of action to taxanes [9]. Structurally, sagopilone (**1**) is very similar to natural epothilone B. The methyl group at C-6 and the vinyl thiazole group at C-15 in the natural epothilone B (**2**) were replaced by an allyl group and a benzothiazole in sagopilone, respectively.

In 2012, the Bayer process team reported an asymmetric synthesis of sagopilone in multi-kilogram scale using macrolactonization as a key transformation to build the 16-membered ring (Scheme 15.2) [10]. The linear precursor (**5**) was prepared from two key intermediates (**3** and **4**) in seven steps with 50% overall yield. For macrolactonization, a modified Yamaguchi protocol [11] was developed. Firstly, the linear precursor **5** was activated with 2,4,6-trichlorobenzoyl chloride to form the intermediate mixed anhydride **6**. Then, macrocyclization was carried out employing a reverse addition technique to minimize intermolecular oligomerization side reactions [12]. It was found that longer addition time was also important to achieve a high yield. Therefore, the solution

of **6** in a mixture of THF and DCM was slowly added to a solution of DMAP in DCM at room temperature over 14h. This reverse addition technique substantially reduced the reaction volume to approximately 100 volume at 10 kg scale. After chromatographic purification, the desired macrolactone (**7**) was obtained in 75–85% yield. After TBDMS deprotection followed by dimethyldioxirane (DMDO) epoxidation, approximately 8 kg of API was isolated via crystallization from a toluene–hexane mixture in 94% yield and greater than 99.7% purity.

15.3.2 Macrolactamization

Along with macrolactones, macrolactams constitute a major proportion of macrocyclic molecules, and over 20 macrolactam-containing drugs have been commercialized between 1960 and 2015 (Table 15.1). Most of those drugs have been produced by fermentation or semisynthesis (for the semisynthetic process toward the phase III clinical antibiotic solithromycin; see Chapter 20). Recently, the increasing interest in synthetic macrocyclic peptides in the field of discovery chemistry has driven the progress of chemical process development of macrolactam-containing drugs and clinical candidates.

The Bayer process team used macrolactamization for the synthesis of desoxy-biphenomycin B core. Desoxy-biphenomycin B (**9**, Scheme 15.3) is a synthetic analogue of the natural product biphenomycin B (**10**) that exhibits good antibacterial activities against Gram-positive and β-lactamase resistance bacteria. Structurally, **9** is almost identical to its parent natural product. The hydroxy group at C-24 in **10** is the only missing functionality in **9**. Since kilogram quantities of desoxy-biphenomycin B core (**8**) were required to support the internal research and development program, a scalable process for its synthesis needed to be developed.

Unlike macrolactonization, weak activation of the carboxylic acid is often sufficient for effective macrolactamization, owing to the strong nucleophilicity of the amine coupling partner. Therefore, the Bayer process team chose a pentafluorophenyl ester as the activating method [13]. Firstly (Scheme 15.4), the carboxylic acid **11** was converted to mixed anhydride **12** with isobutyl chloroformate *in situ*, then **12** was transformed into pentafluorophenyl ester **13** by reaction with the corresponding phenol at room temperature overnight. In general, for process development, having a crystalline intermediate right before a key step is a huge advantage because it allows control of purity required for the critical reaction. Bayer's process team took advantage of the high crystallinity of the pentafluorophenyl ester intermediate and efficiently isolated **13** in 98% yield over two steps through crystallization from water. The final macrolactamization was a two-step process involving Boc deprotection

Table 15.1 List of macrocyclic drugs launched between 1960 and 2015.

	Generic name	Launched year	Trade name	Manufacturer	Manufacturing process
1	Actinomycin D	1963	Cosmegen	Merck	Fermentation
2	Rifampicin	1967	Rifadin	Sanofi	Semisynthesis
3	Desmopressin acetate	1973	DDAVP	Ferring	Full chemical synthesis
4	Cyclosporin A	1983	Sanimmune	Novartis	Fermentation
5	Midecamycin acetate	1985	Medemycin	Meiji Seika	Fermentation
6	Rokitamycin	1986	Ricamycin	Asahi Kasei	Fermentation
7	Erythromycin acistrate	1987	Erasis	Orion	Fermentation
8	Roxithromycin	1987	Rulid	Sanofi	Semisynthesis
9	Teicoplanin	1988	Targocid	Sanofi	Fermentation
10	Azithromycin	1988	Zmax	Pfizer	Semisynthesis
11	Octreotide acetate	1988	Sandostatain	Novartis	Full chemical synthesis
12	Rifaximin	1988	Xifaxan	Salix	Semisynthesis
13	Erythromycin stinoprate	1989	Eritrocist	Edmond	Fermentation
14	Clarithromycin	1990	Biaxi	Abbott	Semisynthesis
15	Rifabutin	1992	Mycobutin	Pfizer	Semisynthesis
16	Dirithromycin	1993	Dynabac	Eli Lilly	Semisynthesis
17	Tacrolimus	1993	Prograf	Astellas	Fermentation
18	Indium In 111 Pentetreotide	1994	OctreoScan	Mallinckrodt	Semisynthesis
19	Lanreotide acetate	1994	Somatuline	Ipsen	Full chemical synthesis
20	Carbetocin	1996	Duratocin	Ferring	Full chemical synthesis
21	Flurithromycin	1997	Flurizic	Pantafarm	Semisynthesis
22	Eptifibatide	1998	Integrilin	Genentech	Full chemical synthesis
23	Rifapentine	1998	Priftin	Sanofi	Semisynthesis
24	Quinupristin mesilate	1999	Synercid	Sanofi	Semisynthesis
25	Dalfopristin mesilate	1999	Synercid	Sanofi	Semisynthesis
26	Sirolimus (Rapamycin)	1999	Rapamune	Pfizer	Fermentation
27	Atosiban	2000	Tractocile	Ferring	Full chemical synthesis
28	Telithromycin	2001	Ketek	Sanofi	Semisynthesis
29	Caspofungin acetate	2001	Cancidas	Merck	Semisynthesis
30	Pimecrolimus	2002	Elidel	Novartis	Semisynthesis
31	Micafungin sodium	2002	Mycamine	Astellas	Fermentation
32	Daptomycin	2003	Cubicin	Cubist	Fermentation
33	Everolimus	2004	Zortress	Novartis	Semisynthesis
34	Zotarolimus	2005	Endeavor	Avott	Semisynthesis
35	Anidulafungin	2006	Eraxis	Pfizer	Semisynthesis
36	Temsirolimus	2007	Torisel	Pfizer	Semisynthesis
37	Ixabepilone (azaepothilone B)	2007	Ixempra	BMS	Semisynthesis
38	Sugammadex sodium	2008	Bridion	Merck	Semisynthesis
39	Telavancin hydrochloride	2009	Vibative	Theravance	Semisynthesis
40	Eribulin mesylate	2010	Halaven	Eisai	Full chemical synthesis
41	Romidepsin	2010	Istodax	Celgene	Fermentation
42	Icotinib-HCl	2011	Conmana	Zhejiang	Full chemical synthesis
43	Pasireotide	2012	Signifor	Novartis	Full chemical synthesis
44	Simeprevir	2013	Olysio	J & J	Full chemical synthesis
45	Paritaprevir	2014	Viekira Pak	Abbvie	Full chemical synthesis
46	Oritavancin	2014	Orbactiv	Eli Lilly	Semisynthesis
47	Vaniprevir	2015	Vanihep	Merck	Full chemical synthesis
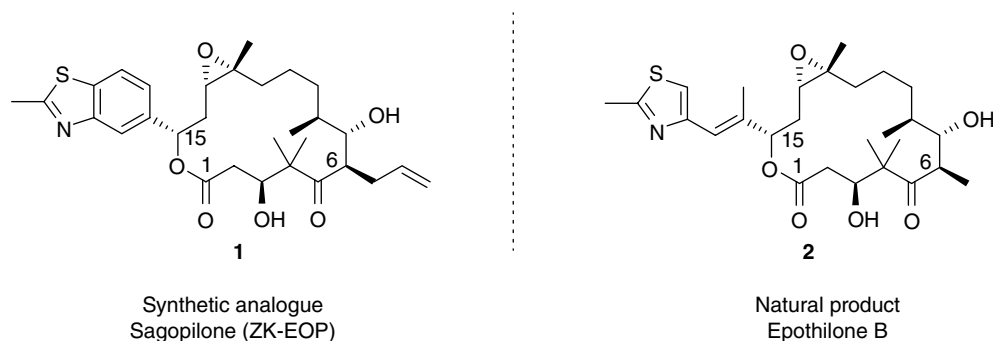
Scheme 15.1 Structures of sagopilone and epothilone B.

followed by ring closure. Since the cyclization reaction was relatively fast, a reverse addition method was successfully applied to minimize intermolecular oligomerization side products (concentration 57 mM). The resulting HCl salt (**14**) in THF, obtained after Boc deprotection with HCl in dioxane, was slowly added to a solution of excess triethylamine in THF over 70 min. Since the protected desoxy-biphenomycin B core (**8**) was poorly soluble in organic solvent, the desired product was effectively isolated through direct crystallization from the reaction solution by adding more THF as well as acetonitrile. After extensive washing, 1.37 kg of high quality **8** was obtained in 73% yield with 97% purity (Scheme 15.4). Although the Bayer process team presented an efficient kilogram synthesis of desoxy-biphenomycin B core [13], its usage, unfortunately, has not been reported in the literature.

Another example for macrolactamization is the Novartis pasireotide synthesis [14]. Pasireotide (**15**) is a hexameric peptide macrolactam and a synthetic analogue of the 38-membered natural macrocyclic peptide somatostatin **16** (Scheme 15.5). Pasireotide was granted marketing authorization by the European Commission for the treatment of Cushing's disease in 2009 and the US FDA in 2012.

Structurally, pasireotide is much simpler than natural somatostatin because it includes fewer residues (6 vs. 14 amino acids), a smaller ring (18- vs. 38-membered), and no disulfide bond in the macrocyclic core. This makes the synthesis of **15** more straightforward. For large-scale production (Scheme 15.6) [15], solid-phase peptide synthesis (SPPS) [16] was used as the approach, and macrolactamization was applied for the construction of the macrocyclic structure. Firstly, the linear peptide **19** was synthesized from commercially available Fmoc-Lys(Boc)-*O*-resin (**17**) through standard stepwise SPPS procedures. After cleavage of the peptide fragment from solid support, cyclization of the resulting linear peptide (**19**) was accomplished by adaptation of the diphenylphosphoryl azide (DPPA)-mediated cyclization previously reported by Merck for the large-scale synthesis of

a cyclic hexapeptide analogue of somatostatin [17]. Mechanistically, DPPA converts the carboxylic acid group to an acyl azide intermediate (**20**) under mild conditions. This acyl azide is then coupled with the free amine to form the macrocycle. One significant advantage with such DPPA-mediated macrocyclizations is that mild reaction conditions can minimize potential racemization risk at tyrosine. Global Boc deprotection under aqueous TFA conditions at 0°C followed by precipitation into a mixture of MTBE, and heptane at room temperature provided 53 wt% of crude API (**21**). It should be noted that this process is an excellent example for contemporary large-scale manufacture of cyclic peptide therapeutics by fully chemical synthesis.

Another example of large-scale macrolactamization was reported by a group from Tranzyme Pharma in the synthesis of the ghrelin receptor agonist, ulimorelin (TZP-101, **24**, Scheme 15.7) [18], which advanced through phase III clinical trials. The ghrelin receptor is a GPCR implicated in a number of physiological functions, including stimulation of gastrointestinal motility, which was the intended use for **24**. Ulimorelin is a synthetic peptidomimetic having an 18-membered macrolactam ring. In the early discovery stage, both solid-phase and solution-phase synthetic methodologies were used for rapid preparation of analogues. Then, solution-phase strategies were selected for late-stage program support. For kilogram cGMP scale-up of TZP-101, the solution-phase discovery chemistry route was used with minor modifications (Scheme 15.7) [19]. The linear precursor **23** was efficiently synthesized from chiral tosylate **22** in five steps with 68% overall yield. For the key macrolactamization step, 3-(diethoxyphosphoryloxy)-1,2,3-benzotriazin-4(3*H*)-one (DEPBT) was selected as the coupling agent based on high macrolactamization yield and excellent diastereomeric purity (less racemization on peptide chiral centers). At kilogram scale, the DEPBT-mediated process produced the desired macrolactam **24** in high yield (>80%) with high diastereomeric purity (<0.1% diastereomeric impurity on any of the stereogenic centers) after recrystallization of the HCl salt. It is

3

+

4

7 steps →

5

Linear precursor

→

6

↓

2 steps ←

7

2

Sagopilone (ZK-EOP)
8 kg (>99.7% purity)
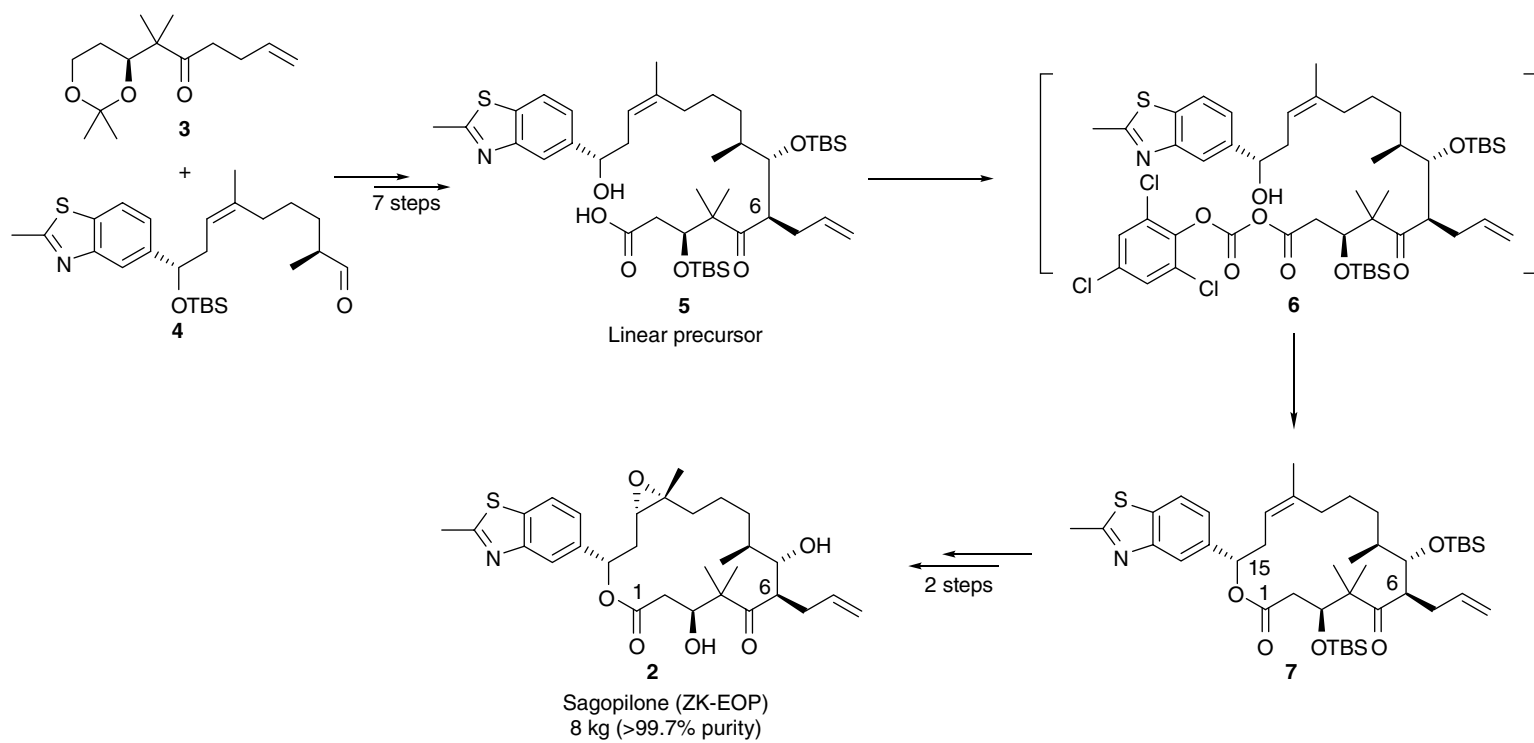
Scheme 15.2 Synthesis of sagopilone (ZK-EOP).
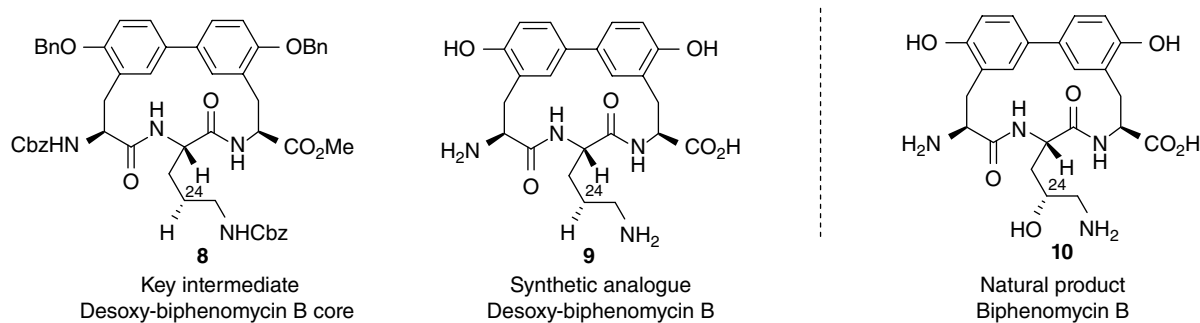
Scheme 15.3 Structures of desoxy-biphenomycin B and biphenomycin B.

noteworthy that the macrolactamization step did not require high-dilution conditions or reverse addition techniques and was executed at a concentration as high as 0.2 M in THF at room temperature (Scheme 15.7).

Recently, the Merck process team reported macrolactamization approaches for the large-scale production of HCV protease inhibitor compounds vaniprevir (MK-7009) [20] and grazoprevir (MK-5172) [21] (Scheme 15.8).

The 20-membered macrocycle vaniprevir (**25**) [22] is an HCV protease inhibitor developed by Merck and was approved for treating hepatitis C in 2014 in Japan. The Merck process team investigated several synthetic routes such as intramolecular Heck, Suzuki and Sonogashira couplings, RCM, and macrolactamization to find the most efficient way to build a macrocyclic core structure for late-stage clinical supplies and commercial production. Among those methods, EDC-mediated macrolactamization was selected based on good chemical yield and reaction profile. Initial proof of concept of the macrolactamization approach prompted the development of a robust synthesis of linear precursor **31** (Scheme 15.9). The synthesis of **31** started with intermolecular Heck coupling between bromide **27** and alkene **28**. The major issue in the Heck coupling was moderate regioselectivity between the desired linear product (**29**) and the undesired branched product (**30**). This issue was considered as a critical factor for process development because poor selectivity substantially decreased chemical yield and also significantly increased purification risk downstream. Despite exhaustive ligand and solvent screening, the ratio of regioisomers did not change. More interestingly, it was found that the regioselectivity of intermolecular Heck coupling was not dependent upon the ligand and consistently produced 10–12% of **30** regardless of ligand identity. Based on high-throughput experimentation (HTE) data and careful data analysis, the Merck process team developed a robust Heck coupling process with only 0.75 mol% of Pd(OAc)$_2$ in NMP without necessity of any costly ligand. Subsequent hydrogenation of the Heck products was next investigated. Although high conversion (~95%) was obtained utilizing only the residual Pd

from the Heck coupling under 60 psi H$_2$ pressure, additional charge of Pd/C (5 wt%) was required to achieve more than 99% conversion, which was the level required to de-risk any purity control issue caused by unreacted Heck coupling products. Since the purification option through crystallization of the hydrogenated linear precursor **31** did not appear feasible, the crude reaction mixture in DMF/NMP was directly carried on to the subsequent macrolactamization step (Scheme 15.10).

For macrolactamization, a variety of amidation reagents was investigated. Although complete conversion was observed in nearly all cases, the corresponding yields and reaction rates were significantly impacted by the identity of the coupling agent. From systematic screening work, HATU was identified as the reagent of choice. However, the high cost and potential IP issues with HATU led to the development of an alternative macrolactamization process. Gratifyingly, it was quickly identified that an EDC–HOPO system was an effective surrogate for the HATU system. High dilution (100× volume; 10 g/l) was required for both systems in order to maximize chemical yield. A reverse addition technique with the EDC–HOPO system [23] was attempted to reduce reaction volume, but a significantly lower yield was obtained due to the relatively slower reaction rate. The resulting macrolactam (**33**) was efficiently isolated by crystallization from DMF/water. In order to upgrade purity, a recrystallization protocol was added after isolation. After recrystallization, the high-purity macrocyclic ester (macester) **33** was obtained as a crystalline monohydrate from isopropyl acetate (IPAc) with 5 equiv. of water. It is noteworthy that over 10% macrocyclic impurities derived from branched Heck product **30** was efficiently removed at this crystallization stage. Hydrolysis of **33** followed by EDC-mediated coupling with amine **34** to install the side chain afforded vaniprevir (MK-7009, **25**) in 89% yield over the final two steps (Scheme 15.10).

The Merck process team also demonstrated HATU-mediated macrolactamization for grazoprevir (MK-5192, **26**) [24] clinical supplies in pilot scale (Scheme 15.11). The formation of the 18-membered macrocyclic inter-
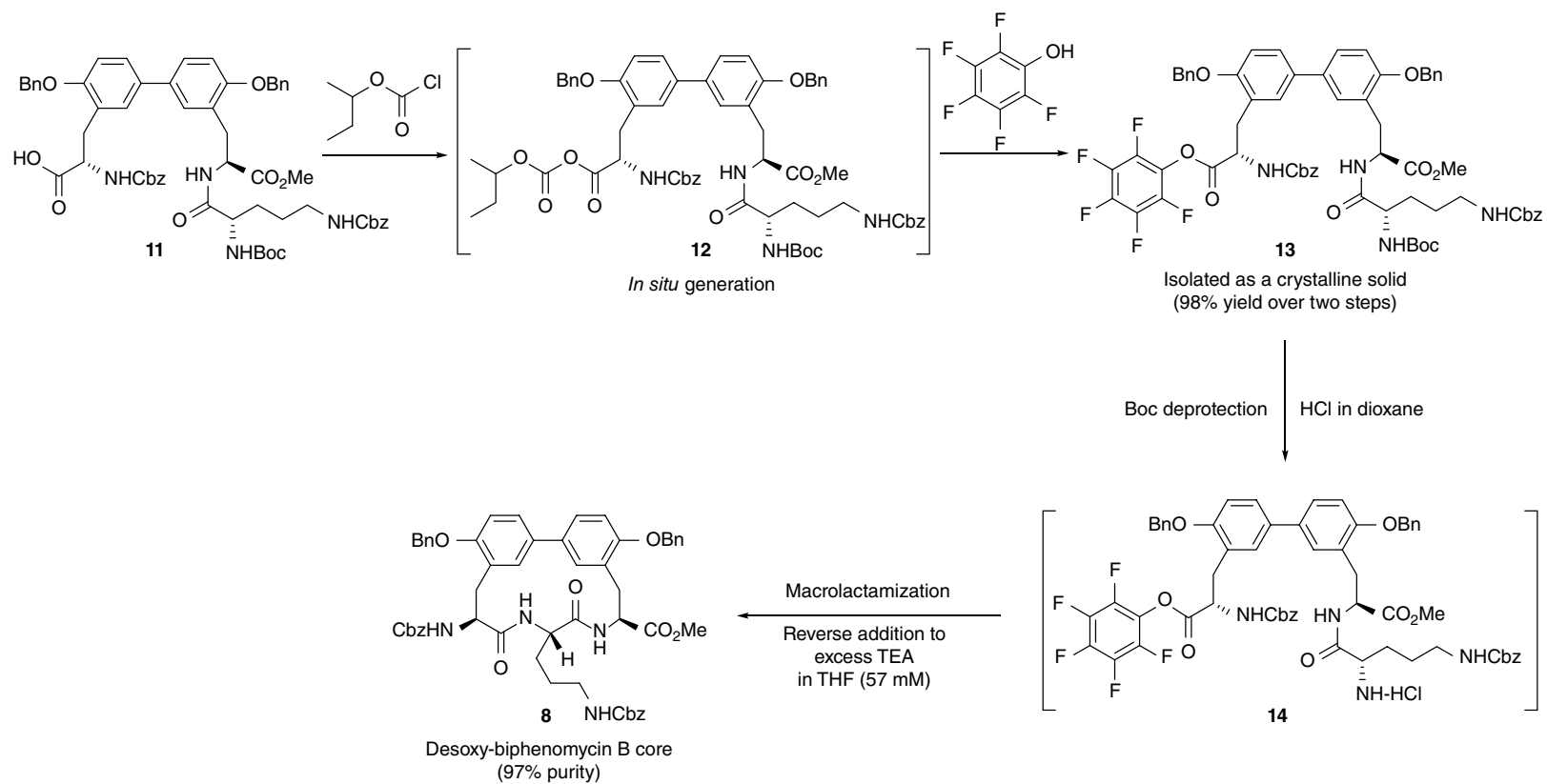
Scheme 15.4 Scalable synthesis of desoxy-biphenomycin B Core.
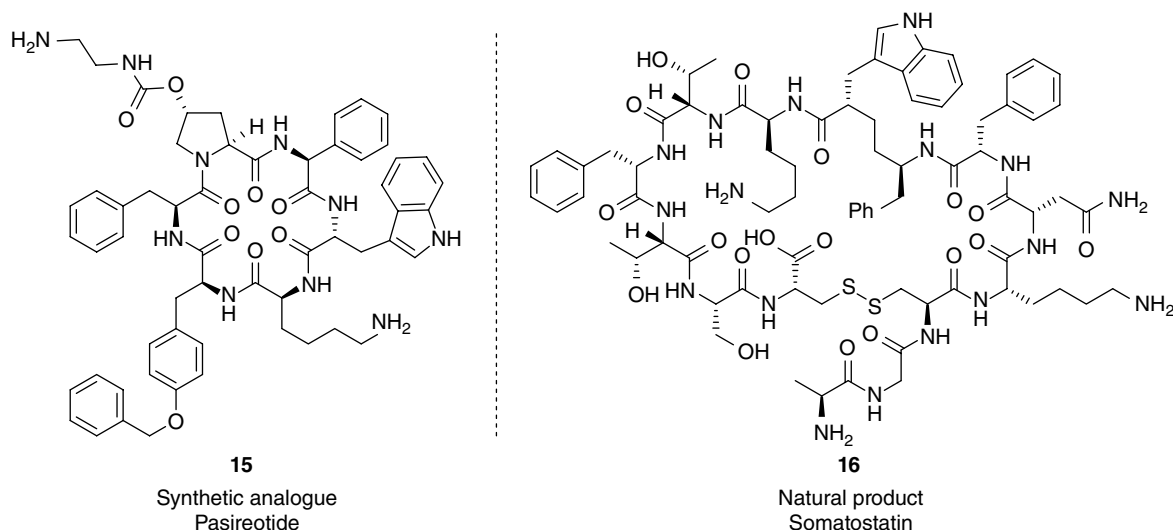
Scheme 15.5 Structures of pasireotide and somatostatin.

mediate was considered the most challenging aspect of the synthesis regarding isolation yield, purity control, and volume productivity. The linear intermediate **36** was produced through hydrogenation of alkyne **35** followed by Boc deprotection. Since crystallization of the benzenesulfonic acid (BSA) salt **36** was not feasible, the crude BSA salt in MeCN was directly carried on to the next, the macrocyclization step. For macrolactamization, the reverse addition technique was applied to minimize intermolecular dimerization/oligomerization and maintain high productivity. After the addition of diisopropylethylamine (DIPEA) to adjust pH to 8–9, the crude stock solution of **36** in MeCN was slowly added to the HATU solution in MeCN over 8 h at room temperature. High purity product (**26**) was obtained from direct crystallization of the reaction mixture after concentration of the batch in 65% overall yield from intermediate **35**.

15.3.3 Ring-Closing Metathesis

In recent years, RCM has emerged as a new and powerful technology for the construction of macrocyclic compounds [4]. Not only has this technology been widely used in academic research but also it has shown great promise for large-scale synthesis of macrocyclic clinical candidates in pharmaceutical settings. Boehringer Ingelheim (BI) pioneered the use of the RCM reaction in their large-scale synthesis of HCV protease inhibitor ciluprevir (BILN-2061), a 15-membered macrocyclic compound containing a (*Z*)-olefin (Scheme 15.12) [25].

Initially, Grubbs' 1G catalyst was used to cyclize linear diene **42** (Scheme 15.13). However, RCM of **42** with 5 mol% catalyst in refluxing dichloromethane for 24 h produced up to 50% of the undesired **epi-43**. Control

experiments suggested that free PCy_3 liberated by the catalyst during metathesis was responsible for epimerization. Further investigation identified that the epimerization was also promoted by secondary amine impurities carried over from the previous step [25c]. The greatest concern in terms of process robustness was that the extent of epimerization varied from batch to batch and reaction scale.

To resolve this issue, additional catalysts were screened. *N*-Heterocyclic carbene (NHC)-containing catalysts such as Grubbs 2G and Hoveyda–Grubbs 2G significantly reduced the content of epimerization but generated up to 10 mol% of a new impurity, a cyclic dimer, which lowered yield and increased purification risk. After extensive process development work, the Ru-based first-generation Hoveyda's catalyst was chosen as an appropriate catalyst for a viable process of BILN-2016 regarding high yield, a much cleaner reaction profile and operational benefit from air stability of the catalyst. This first-generation RCM process was scaled to produce more than 100 kg of the API [25b]. During the first production campaign, however, a serious issue arose. The scale-up reaction, under conditions identical to that in lab scale, produced 10–15 mol% of epimerized side product **epi-43**, extended reaction time from 8 to over 12 h, and required increased catalyst loading from 3 to 5.3 mol% to achieve complete conversion. After another thorough investigation, it was found that traces of morpholine (<20 ppm) in the technical-grade toluene was the main root cause, and the issue was quickly resolved by removing morpholine and other unknown basic nucleophiles from bulk toluene through simple aqueous HCl washing of the solvent prior to use. Finally, with 3–5 mol% catalyst at 0.01 M diene concentration, macrocycle **45**
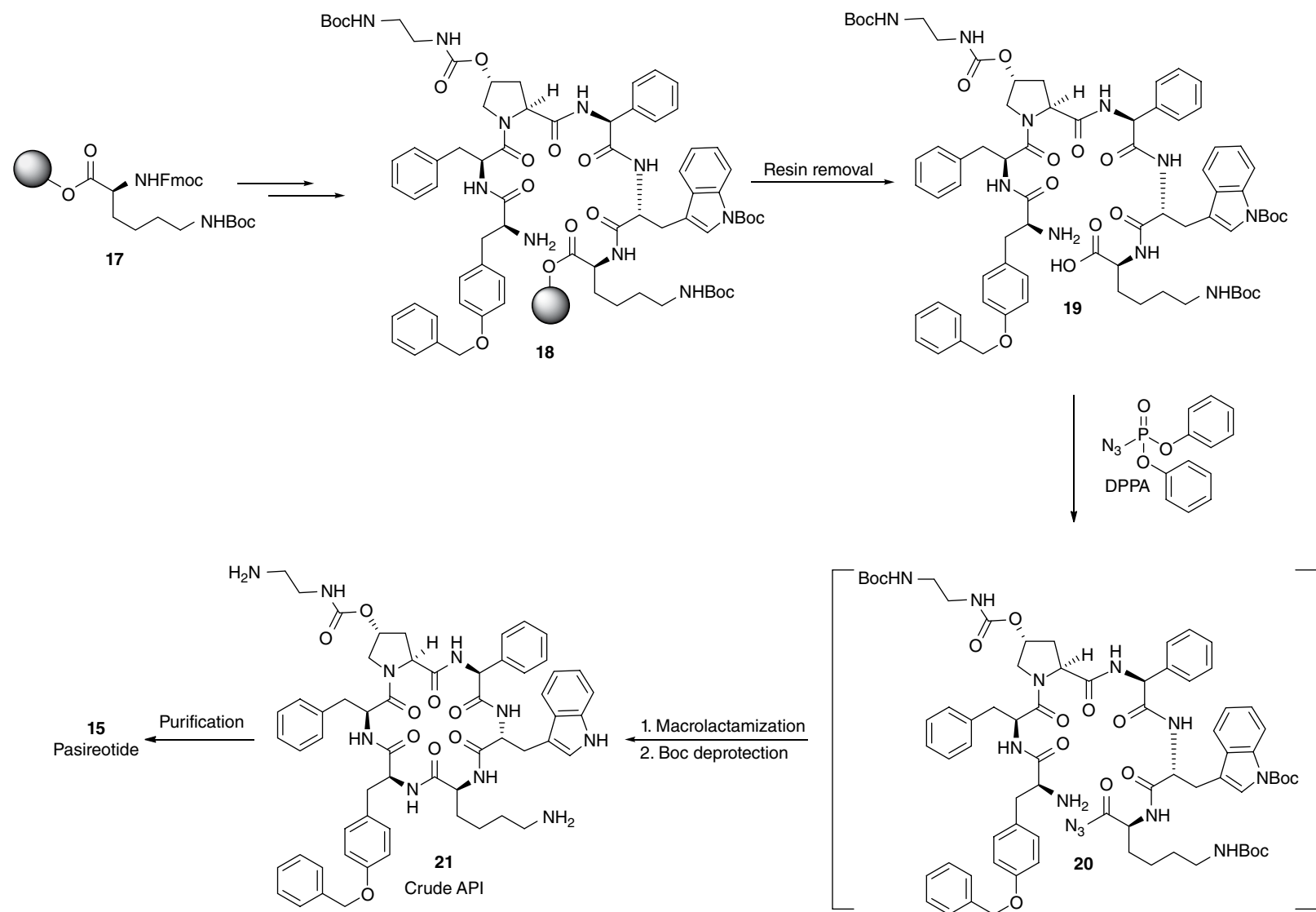
Scheme 15.6 Scalable synthesis of pasireotide.
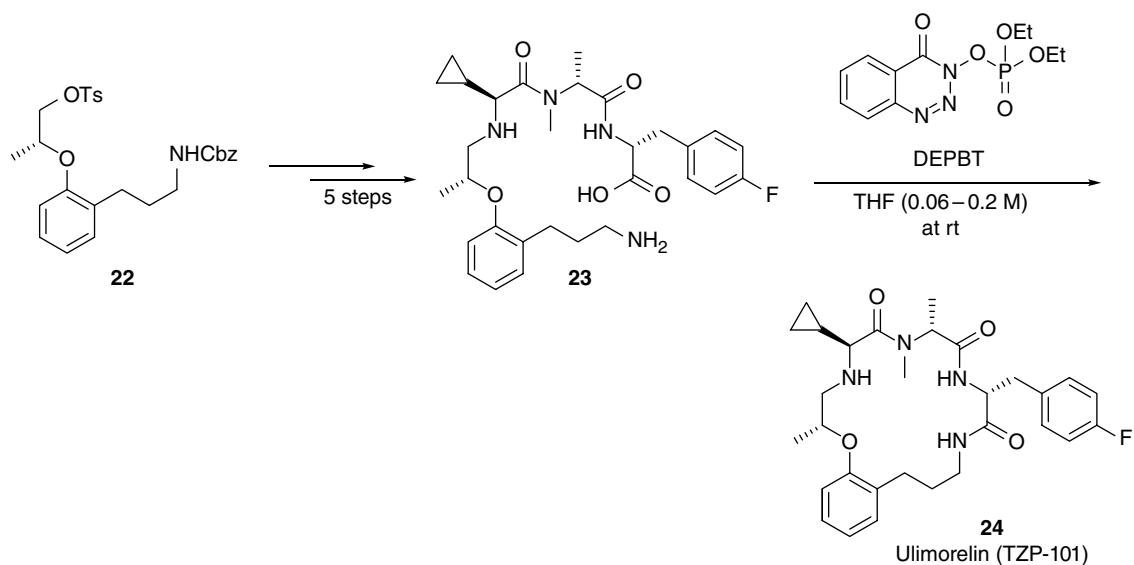
Scheme 15.7 Synthesis of ulimorelin (TZP-101).
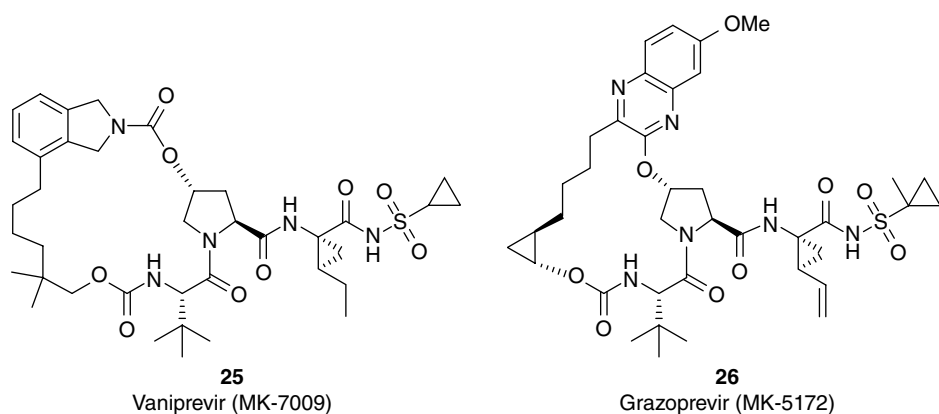
Scheme 15.8 Structures of vaniprevir and grazoprevir.
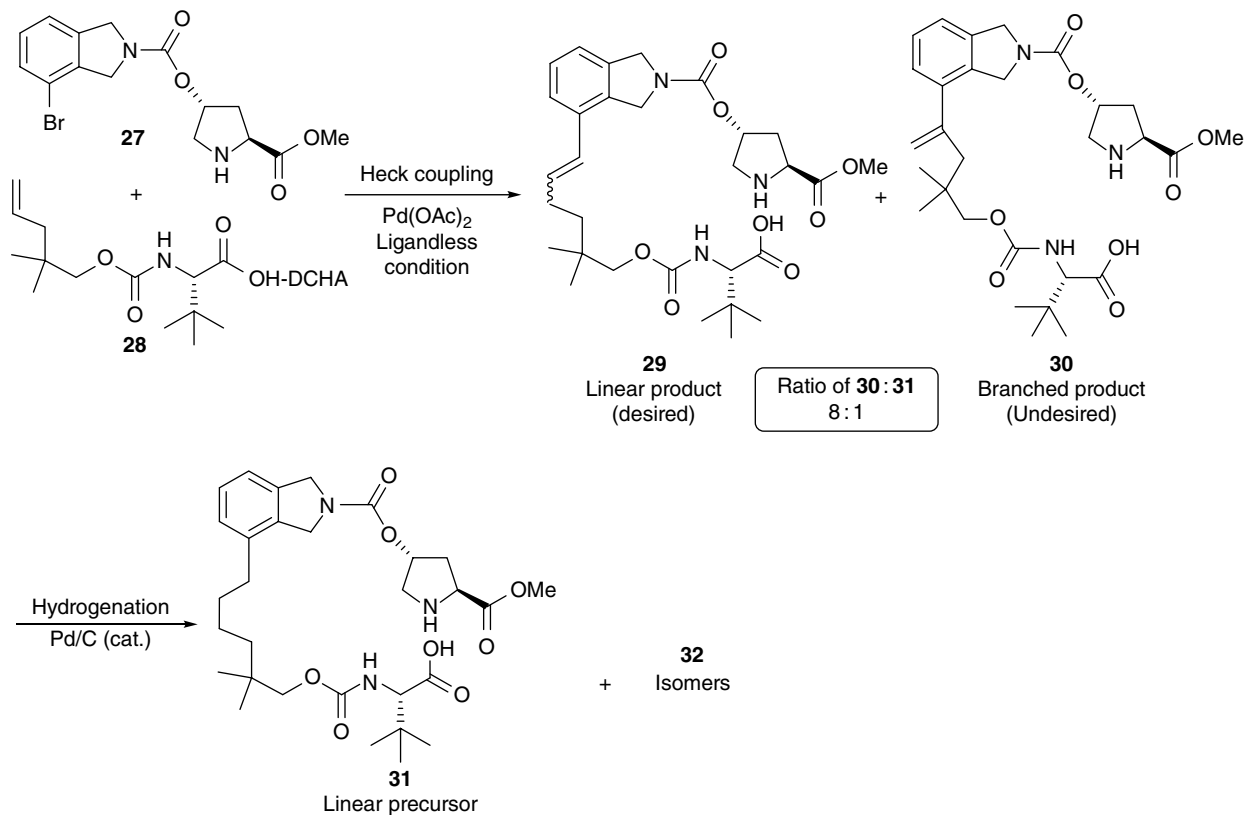
Scheme 15.9 Synthesis of the linear precursor **31** for vaniprevir.
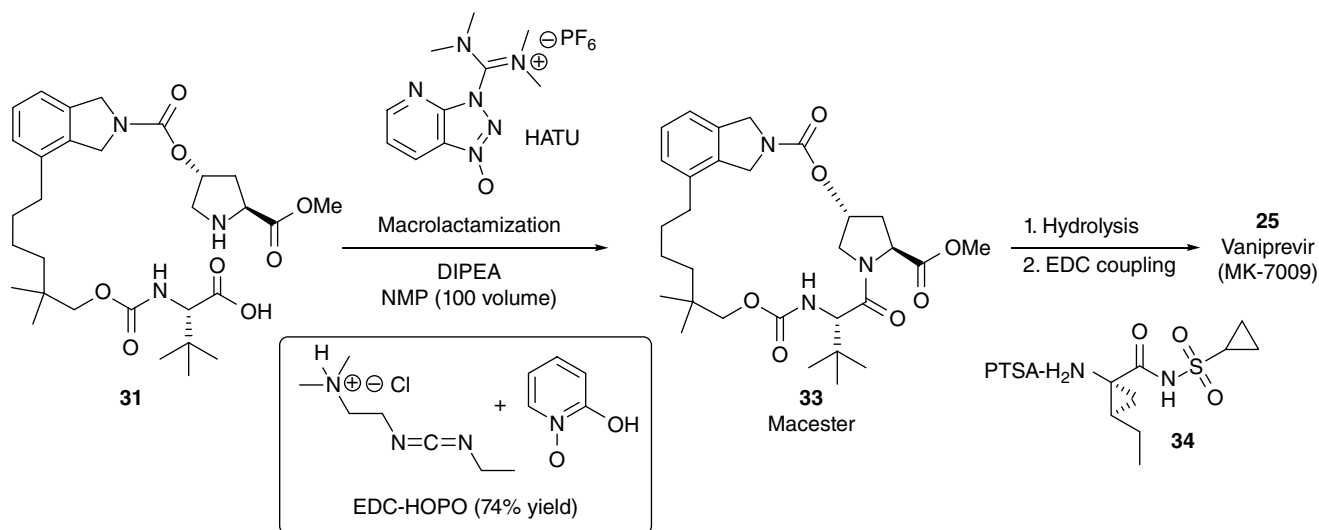
Scheme 15.10 Scalable synthesis of vaniprevir.

was obtained in 90–95% yield after 24 h in refluxing toluene. Almost 400 kg of macrocycle **45** was manufactured through this modified first-generation RCM process, and more than 100 kg API was manufactured from macrocycle **45** (Scheme 15.14).

Although the first-generation RCM process was proven to be suitable for the preparation of API supplies for pivotal clinical trials, several critical scale-up concerns still remained, such as (i) poor volume productivity due to high dilution and (ii) high catalyst cost due to large catalyst loading. Based on the early observation of a remote substituent effect at the C-4 position on RCM performance, a series of diene precursors with different substituents on the C-4 amide nitrogen were synthesized and evaluated in the RCM reaction. Surprisingly, RCM reaction of the diene containing a Boc protecting group on the C-4 amide nitrogen using Grela catalyst dramatically improved yield and reaction profile [25e]. With this breakthrough, called the "*N*-Boc-effect," the RCM reaction could be conducted at standard concentrations (>0.2 M) with extremely low catalyst loadings (<0.1 mol%). This second-generation RCM process stands as a real-world example of green chemistry and a good illustration of the expedient implementation of lab-scale catalysis in an industrial setting (Scheme 15.15).

An RCM approach was also used for the production of simeprevir (TMC435, **52**) [26], a 14-membered macrocyle that is a very potent HCV protease inhibitor developed by Medivir and marketed by Janssen (Johnson & Johnson's pharmaceutical division). Structurally, simeprevir is similar to ciluprevir except possessing a trans-cyclopentane unit instead of the hydroxyproline unit in ciluprevir and a cyclopropylsulfonamide side chain

instead of the carboxylic acid group in ciluprevir (Scheme 15.16). Obviously, RCM was used for the construction of the 14-membered macrocyclic core in the early discovery stage and accepted as a potential route for large-scale synthesis. Process development of the RCM route focused on safety, robustness, quality control, environmental impact, and cost efficiency. Initial RCM reaction of the diene **48**, having no Boc-protecting group on the amide, in refluxing dichloroethane using 2.5 mol% Hoveyda–Grubbs 1G catalyst provided the desired *cis*-macrocyclic ester (**50**) in 47% yield at 0.01 M concentration. The Janssen process team found that the *N*-Boc-effect discovered by BI during development of the ciluprevir process was also applicable to the RCM reaction of the diene **49** [25e]. In addition, the use of a simulated high-dilution (SHD) technique proved to be another critical process factor for the improvement of RCM performance because it could minimize generation of major side products such as dimers and oligomers. With several process improvements, including the introduction of the Boc group onto the corresponding amide NH and the use of the SDH technique, RCM of **49** with 0.3 mol% M2 catalyst in refluxing toluene (0.05 M) produced the desired macrocycle (**51**) in 82% yield (Scheme 15.16).

Another RCM approach used for large-scale API synthesis is Idenix's processes for HCV protease inhibitor clinical candidates IDX316 and IDX320 (Scheme 15.17) [27].

The original discovery route of IDX316 [28] used RCM as the key transformation to build a macrocyclic ring (Scheme 15.18). The small-scale RCM of TBDMS-protected diene **57** with Hoveyda–Grubbs 2G catalyst could prepare the 14-membered macrocycle **58** with the requisite
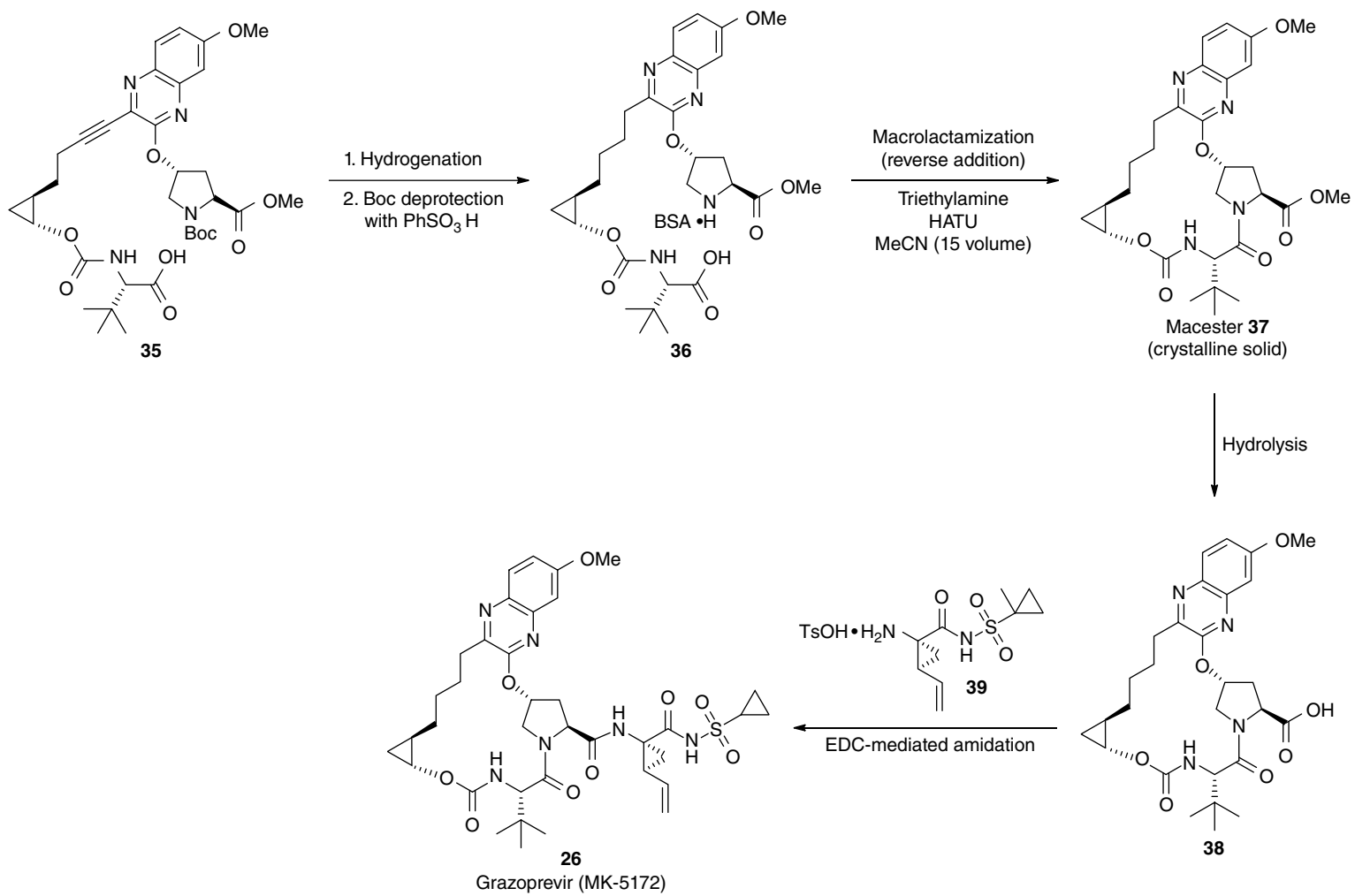
Scheme 15.11 Scalable synthesis of grazoprevir.
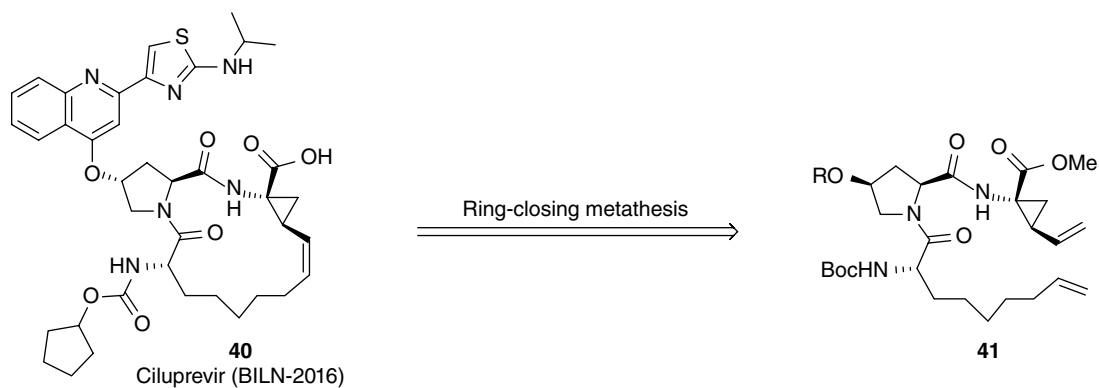
Scheme 15.12 Retrosynthetic analysis of ciluprevir.

Initial RCM results
- High catalyst loading
- Epimerization at C-6
- Batch-to-batch variability
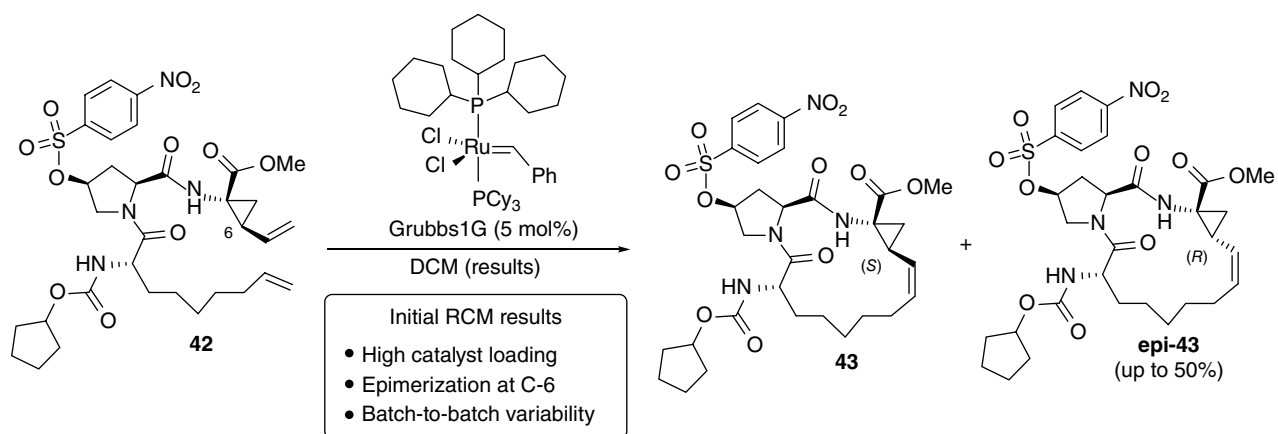
Scheme 15.13 Initial RCM of linear diene **42** toward ciluprevir.

Issues with first generation process
- High catalyst loading (3–5 mol%)
- High dilution (0.01 M) and low productivity
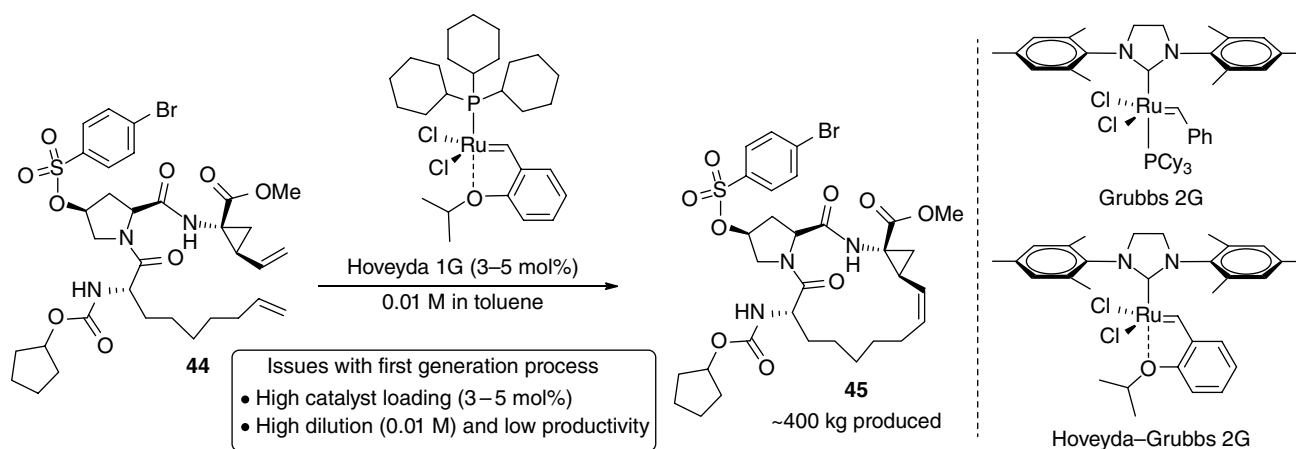
Scheme 15.14 First-generation RCM process for ciluprevir.
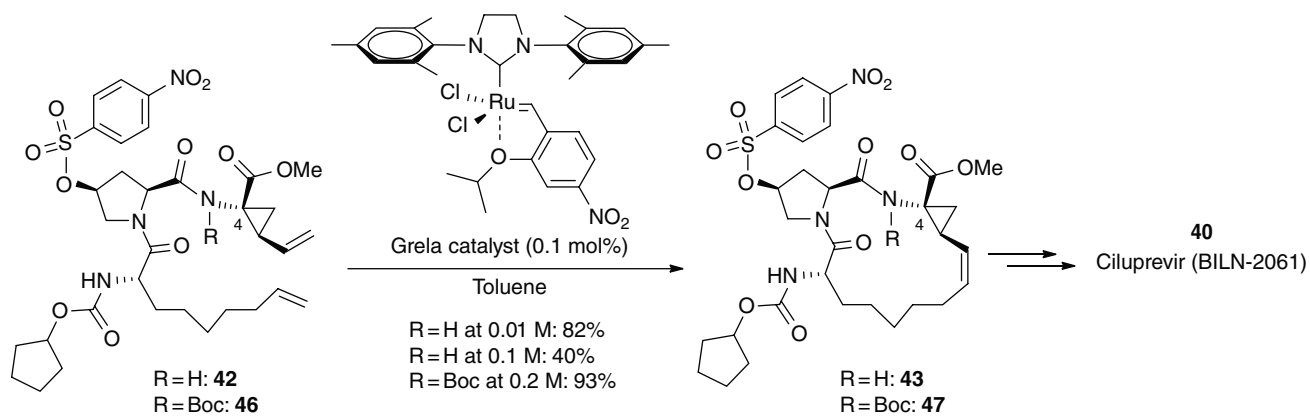
Scheme 15.15 Second-generation RCM process for ciluprevir.
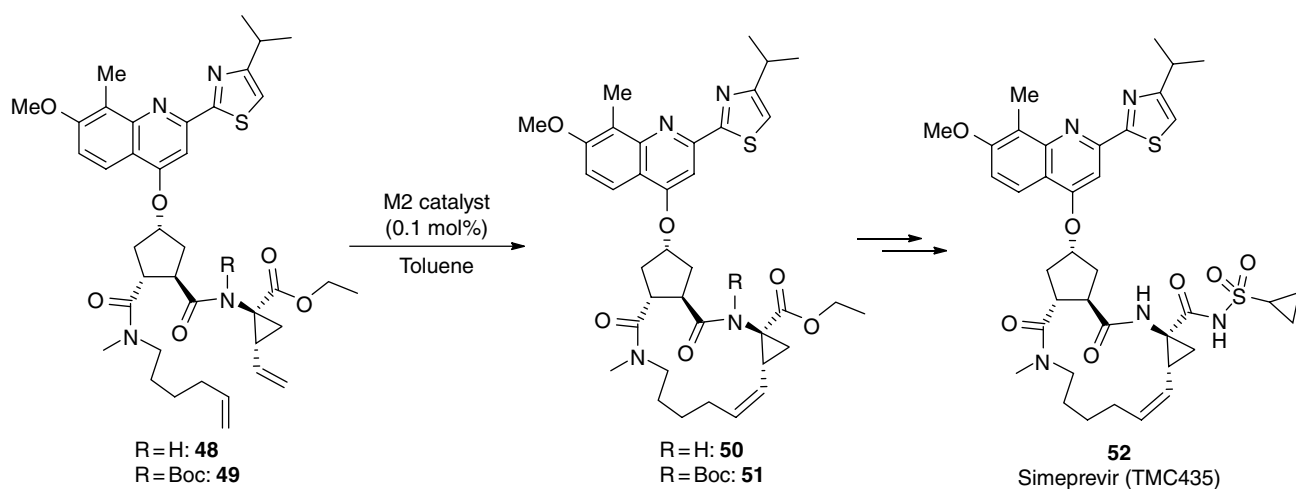
Scheme 15.16 RCM process for simeprevir.
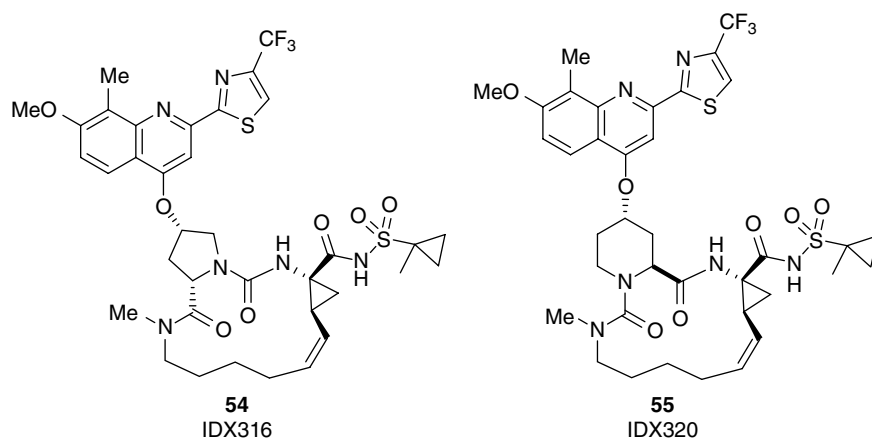
Scheme 15.17 Structures of IDX316 and IDX320.
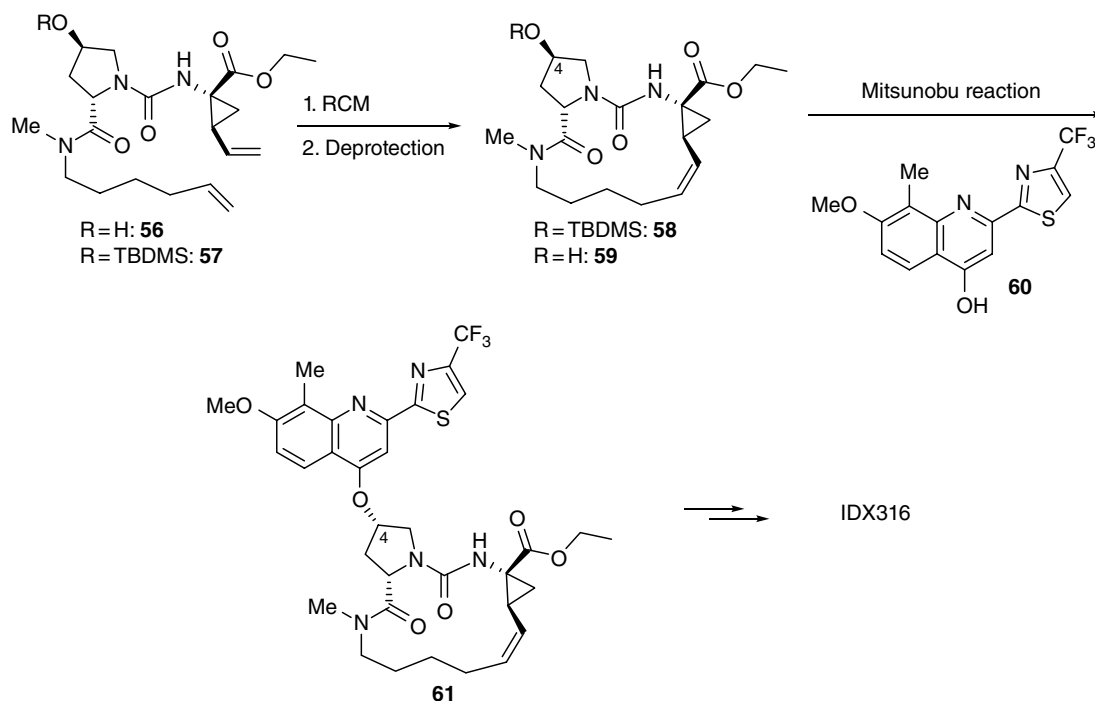
Scheme 15.18 Discovery route to IDX316.

cis-alkene bond in 51% yield. Subsequent TBDPS deprotection followed by Mitsunobu reaction with quinolinol **60** produced macrocyclic ester **61** with inversion of stereochemistry at C-4 of the hydroxyproline. Hydrolysis followed by the introduction of the cyclopropylsulfonamide side chain produced IDX316 on milligram scale.

On assessment of the feasibility of the discovery route for production of multigram and potentially multi-kilogram quantities of IDX316, several issues were identified. The most critical challenge was the scale-up of the RCM step due to the requirement of extremely high dilution (1242 g of solvent per gram of diene **56**, 0.0019 M) and high catalyst loading. The initial calculations indicated that the discovery route had a process mass intensity (PMI) over 59 000. PMI was introduced by the Environmental Protection Agency (EPA) and the American Chemical Society Green Chemistry Institute (ACS GCI) in 2006 to assess the efficiency of chemical processes by considering all materials used in a step or process [29]. Therefore, low PMI is highly recommended for late-stage processes for cost-effectiveness as well as environmental protection. It was envisioned that RCM reaction on a substrate with the quinolinol unit already installed could reduce reaction steps by avoiding a protection–deprotection sequence. In the meantime, the first example of a highly efficient RCM approach on production scale was reported, with the synthesis of ciluprevir discussed earlier. The Idenix team decided to develop an independent scalable process instead of

following BI's process, which utilized the *N*-Boc effect to improve RCM performance. The RCM reaction with advanced diene **62** gave a significantly better reaction profile than TBDMS-protected diene **57** or unprotected diene **56**. The RCM at a concentration of 250 ml/g of diene **62** (0.0049 M) with 1.4 mol% Zhan catalyst-IB produced the final API (**63**) in 88% yield with less than 1% of the total of all cyclic and linear oligomeric side products. Since the improved RCM route included a transition metal catalysis (Ru-based RCM) in the final API step, it was recognized that the removal of Ru metal could be very challenging. After extensive investigation on possible resin treatments to effect removal, it was found that the combination of triphenylphosphine oxide (TPPO) and Siliabond-DMT[1] treatments could efficiently reduce Ru content below 10 ppm, which was the typical regulatory requirement (Scheme 15.19) [30].

During the process development of IDX316, the more potent HCV protease inhibitor IDX320 was selected as a clinical candidate. On the basis of the successful proof of concept achieved for IDX316, the RCM reaction conditions defined for IDX316 were directly applied to IDX320. However, the RCM reaction of diene **64** with Zhan catalyst-IB at 0.005 M concentration gave the

---

1 Siliabond-DMT is the silica-bound equivalent of 2,4,6-trimercaptotriazine (trithiocyanuric acid, TMT). It is a versatile metal scavenger for a variety of metals and the preferred metal scavenger for ruthenium catalysts and hindered Pd complexes.
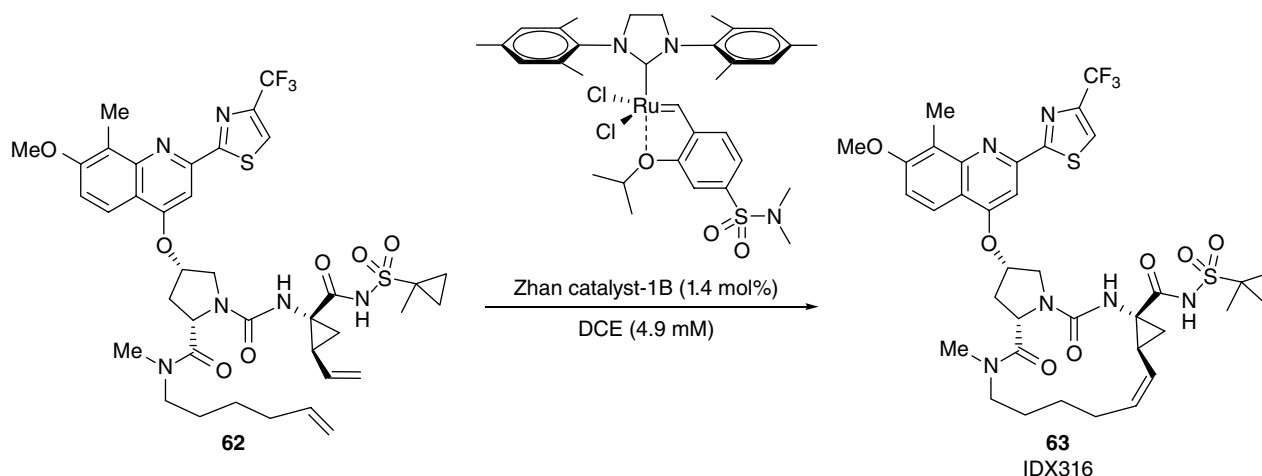
Scheme 15.19 RCM approach to IDX316.

desired product **65** in 34% yield along with 10% cyclodimerization as a major side product. Although increasing dilution by a factor of two improved the isolated yield to the 60–65% range, the use of a large quantity of ICH class 1 solvent DCE was considered as a critical environmental issue. After a brief survey of solvent effects on this RCM, more promising results were obtained from the use of EtOAc solvent (ICH class 3). Hence, RCM of diene **64** at 0.005 M in EtOAc with 3 mol% Zhan catalyst-1B produced the desired product (**65**) in 63% yield. The yield was further increased when the RCM was run more dilute at 0.003 M in EtOAc. The reaction was immediately scaled up to 1.5 kg of diene **64** at 0.0024 M EtOAc with 3.3 mol% Zhan catalyst-1B to produce 1 kg of the desired product IDX320 (**65**) in 66% yield with 98.4% HPLC purity. Unlike the IDX316 process, simple crystallization of the RCM product from IPA effectively removed Ru metal below 10 ppm without the necessity of using the Siliabond-DMT metal scavenger (Scheme 15.20).

Recently, the Merck process team reported full details of the RCM process toward the HCV protease inhibitor vaniprevir (MK-7009) [31]. As shown in Scheme 15.21, there are three possible RCM options for the construction of the macrocycle based on different positions of olefin metathesis: styryl–homoallyl (RCM-1), allyl–allyl (RCM-2), and homoallyl–vinyl diene (RCM-3). Process development of RCM-1 as used in the lead optimization stage by medicinal chemists [22] was discontinued due to its high catalyst loading requirement and low volume productivity. It was envisioned that RCM-2 would be synthetically more straightforward and more cost effective compared with RCM-3.

Process development of RCM-2 mainly focused on resolution of two critical issues: (i) relatively high expense of RCM catalysts due to high catalyst loading and (ii) high-dilution conditions typically employed for RCM, which

presented a severe limitation for material throughput/volume productivity when operating at manufacturing scale. Profiling of the RCM reaction during process development showed that the catalytic activity was very high in the beginning of the reaction but quickly diminished as the reaction proceeded. To resolve what appeared to be a catalyst stability issue, slow addition of Hoveyda–Grubbs 2G in toluene over 1 h was attempted, and this simple operational change significantly reduced catalyst loading from 5 to 1 mol% and increased yield from 67 to 82% under medium-dilution conditions (0.035 M). Direct implementation of slow addition of the catalyst at higher reaction concentration (0.058 M) afforded the desired 20-membered product **67** in only 61% yield along with 9% of the 19-membered macester **71**. It was postulated that **71** was derived from allyl group isomerization and subsequent RCM of the styryl isomer **70**. This double-bond migration presumably occurs through catalysis of Ru–H species, which have been known to be formed as a decomposition product of Ru carbene (Scheme 15.22) [32].

Gratifyingly, isomerization was suppressed by addition of 10 mol% 2,6-dichloroquinone additive, which either inhibited the decomposition of the catalyst or suppressed Ru–H catalyzed olefin isomerization. More importantly, addition of 2,6-dichloroquinone to the reaction enabled an increase of the reaction temperature to 100°C and a reduction of catalyst loading to 0.2 mol% due to the higher performance of the catalyst at 100°C. However, high dilution (0.086 M) was still required to achieve optimal yields. Otherwise, the yield of the RCM product significantly dropped due to the formation of high levels of dimers and oligomers. Through extensive process development work, the Merck team found that simultaneous slow addition of both catalyst and diene substrate **69** efficiently suppressed the formation of dimers and oligomers. With the use of this simultaneous
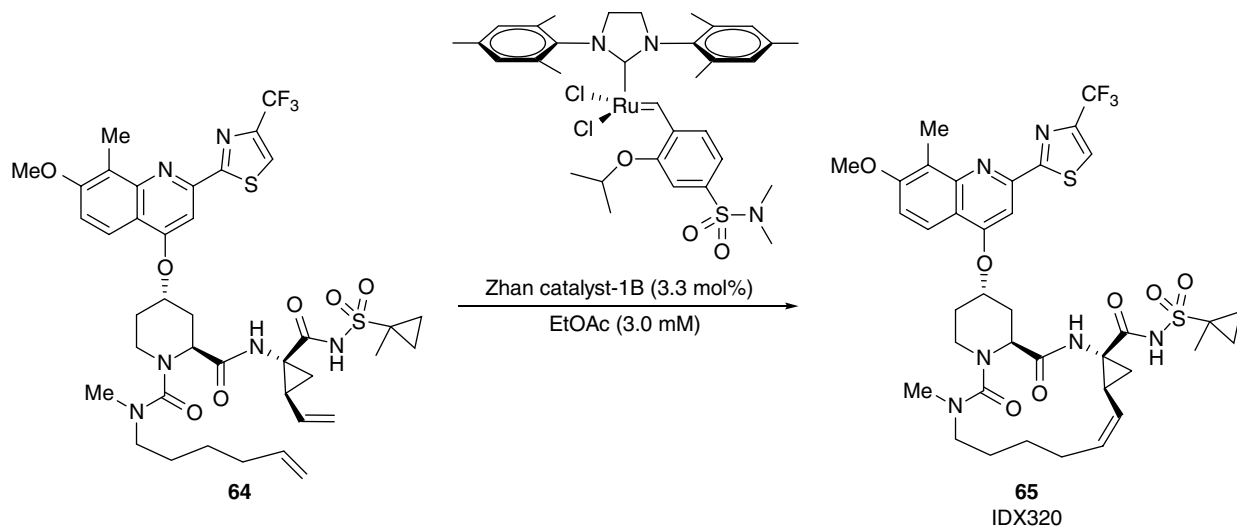
Scheme 15.20 RCM approach of IDX320.
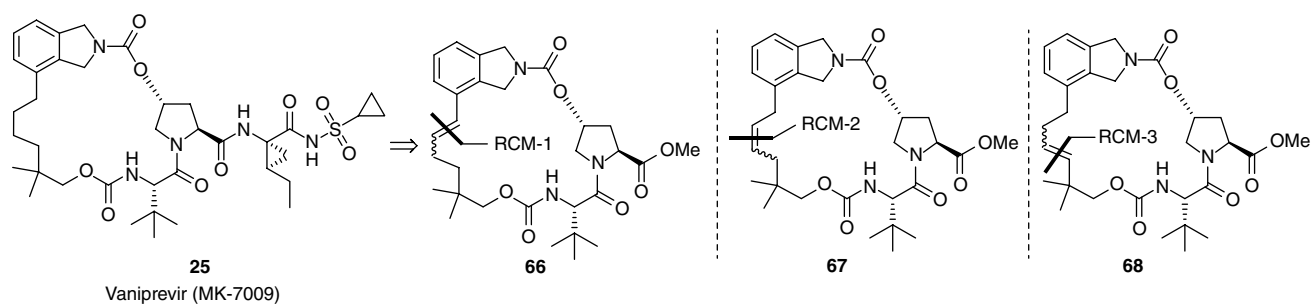
Scheme 15.21 Potential RCM options for vaniprevir.
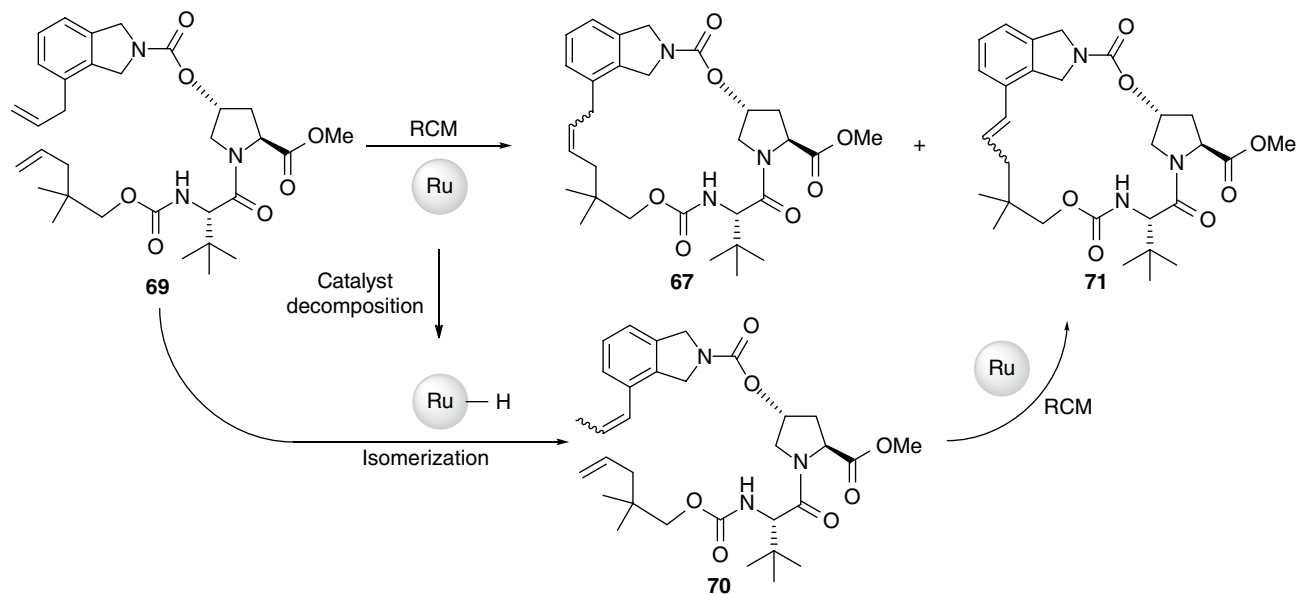
Reaction conditions	Volume ratio (ml/g diene)	20-Macester **67**	19-Macester **71**
1 mol% GH-2G Slow addition of catalyst over 1 h toluene, 60°C	50	82%	<1%
	30	61%	9%

Scheme 15.22 RCM-2 option toward vaniprevir.
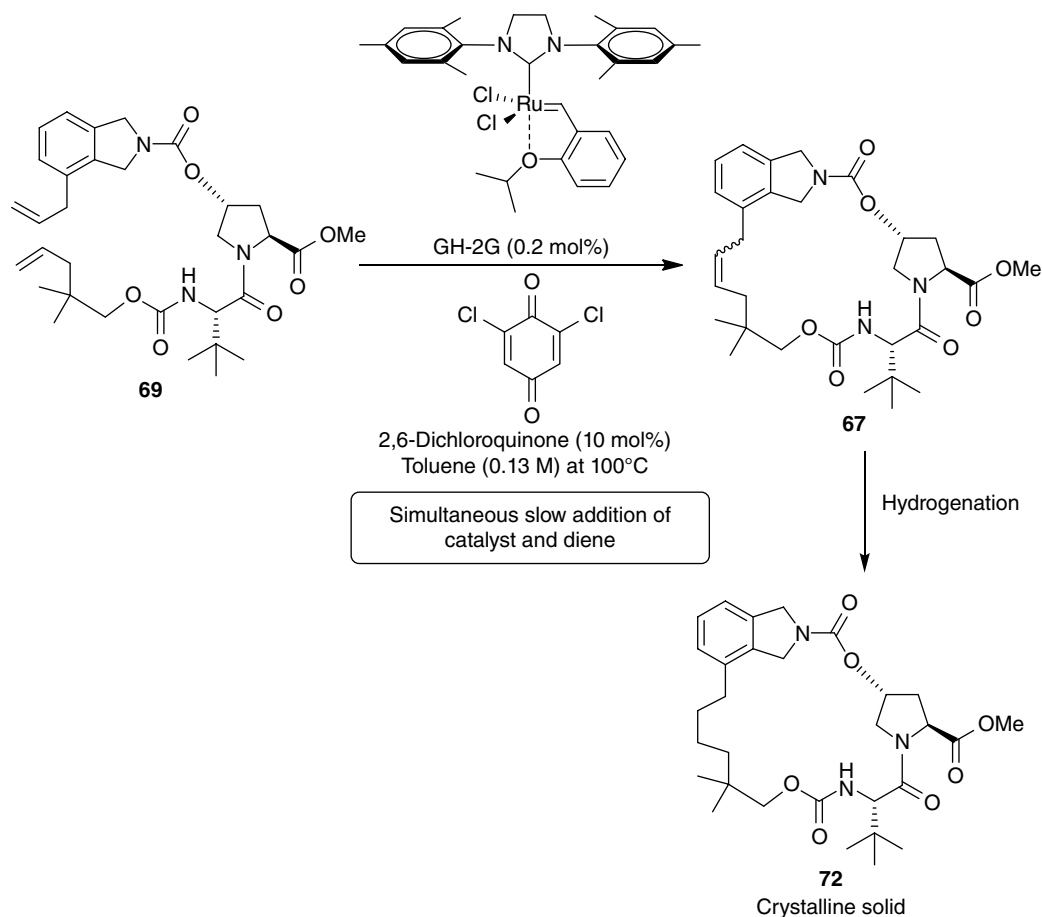
Scheme 15.23 First-generation RCM route toward vaniprevir.

slow addition technique, RCM of diene **69** with 0.2 mol% Hoveyda–Grubbs 2G at a higher concentration (0.13 M) produced the desired product **67** in 91% yield (Scheme 15.23).

The first-generation RCM process of MK-7009 demonstrated well the feasibility of this technology for the synthesis of MK-7009. However, in general, the sensitivity of RCM to impurities is a key challenge for developing a robust manufacturing process. The success of RCM under low catalyst loading (below 0.2 mol%) will be highly dependent on the purity of the starting material. The diene-ester **69**, on the other hand, was an oil, which limited purity control prior to RCM reaction. To reinforce the robustness of the RCM route, the Merck team developed a second-generation RCM process for MK-7009. In this strategy, it was found that potassium salt **73** was a nice crystalline solid and could be isolated consistently in high purity. The direct use of **73** for RCM was not suitable due to its poor solubility in representative RCM solvents such as toluene or IPAc. Fortunately, **73** was readily converted to diene acid, and the resulting diene acid stock solution in IPAc was directly used for the next RCM reaction. RCM of the diene acid followed

by hydrogenation produced mac-acid **74** in 83% yield. It is noteworthy that a three-step through process was possible because all three reactions (salt breaking, RCM, and hydrogenation) could be run in IPAc (Scheme 15.24) [31].

RCM technology has been also used outside of HCV protease inhibitors. For instance, synthesis of a kinase inhibitor, SB1317, an 18-membered macrocycle, used RCM as a key step [33]. Surprisingly, typical RCM conditions employing Grubbs 1G catalyst (G1) or Grubbs 2G catalyst (G2) failed to afford any desired product. It was hypothesized that the basic functionality on diene **75** (Scheme 15.25, particularly the tertiary amine functional group) might coordinate the metal center of the catalyst and deactivate its RCM activity. Fortunately, neutralization of the basic functionality with HCl could reactivate the RCM catalyst to form the desired macrocycle **76** along with undesired regioisomer **77**. However, the RCM reaction using G1 with such an HCl additive resulted in moderate *trans:cis* selectivity and low yield. Simple replacement of catalyst to G2 improved both reaction yield and regioselectivity. Finally, RCM with G2 and TFA as additive instead of HCl produced a mixture of **76** and **77** in 89% yield with 94 : 6 *trans:cis* ratio. The *trans*
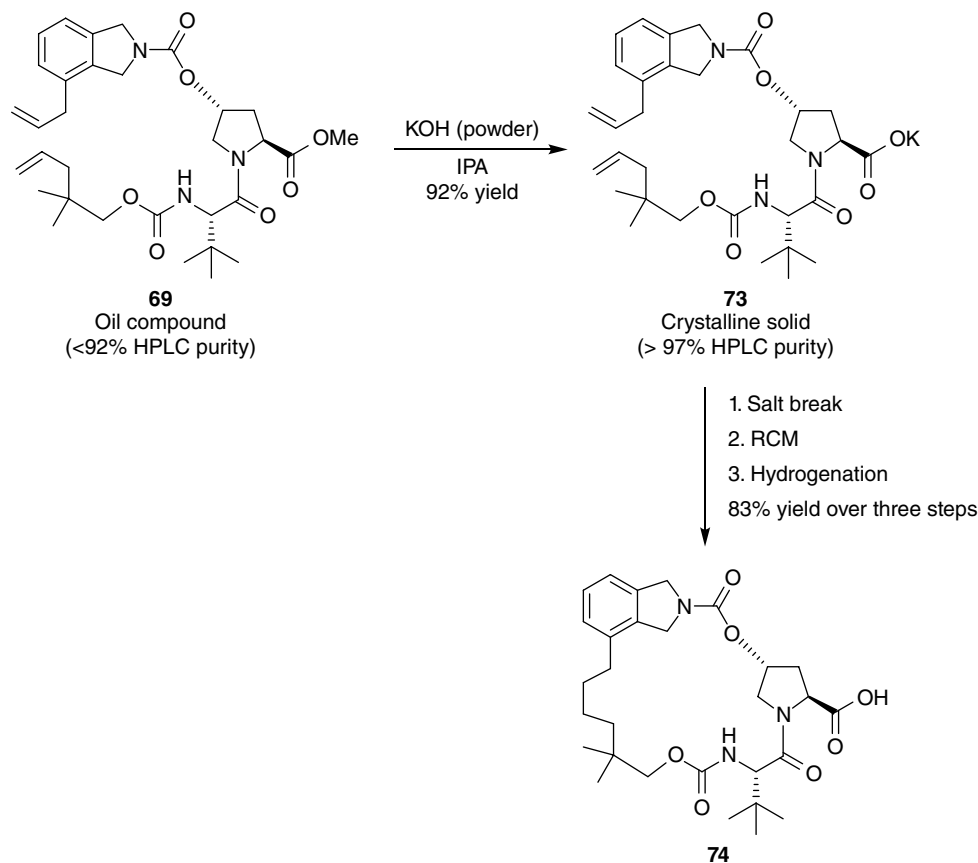
Scheme 15.24 Second-generation RCM route toward vaniprevir.

isomer purity was increased to more than 98% by simple crystallization followed by washing the wet cake product with cold EtOAc. Recently, SB1317 was licensed by Tragara Pharmaceuticals, Inc., and entered the clinic in mid-2010 as TG02. The RCM approach was proven to be atom efficient without the use of protecting groups and scalable for the supply of larger quantities of API for clinical trials (Scheme 15.25).

15.3.4 Metal-Catalyzed Cross-Coupling

In addition to the examples described in the previous sections, other interesting methods have been developed for large-scale synthesis of macrocyclic drugs and clinical candidates. Recently, the Eisai process team reported a commercial manufacturing process of eribulin (**79**, Scheme 15.26) [34], in which a Nozaki–Hiyama–Kishi (NHK) reaction [35] was highlighted as a key macrocyclization method. Eribulin is a highly potent cytotoxic agent approved in the United States for treatment of certain patients with metastatic breast cancer. Eribulin is structurally similar to the marine natural product halichondrin B (**80**). One key structural difference between **80** and **79** is that the former is a macrolide having a

macrolactone core, while the latter is a macrocyclic ketone. Although the macrocyclic core of **80** can be constructed by well-established macrolactonization methodologies, **79** required the formation of a carbon–carbon bond in the macrocyclization step.

The synthetic strategy to prepare eribulin (Scheme 15.27) employed a convergent synthesis featuring the late-stage coupling of the known C1–C13 fragment **82** [36] and C14–C35 fragment **81** [37] to construct the macrocyclic ring. Disconnection to **82** was well suited for the establishment of both C0–C1 and C13–C14 carbon–carbon bonds. The coupling partner, C14–C35 sulfone alcohol **81**, was a new fragment designed specifically for eribulin.

With the coupling product **83** secured (Scheme 15.28), selective removal of the sulfone moiety in **83** was accomplished via SmI_2-mediated reductive desulfonylation [38] in THF-MeOH solution at –78°C to afford ketoaldehyde **84** in 85% yield. Investigation of solvent effect on desulfonylation revealed that MeOH was optimal for the process due to higher chemoselectivity. It was hypothesized that the more nucleophilic MeOH might be involved in a samarium-mediated temporary protection of the aldehyde group as a hemiacetal. Macrocyclic carbon–carbon bond formation relied on the application

Catalyst	Additive	*trans* : *cis*	Yield (%)
G1	none	NA	0
G2	none	NA	0
G1	HCl	84 : 14	10
G2	HCl	94 : 6	70
G2	TFA	94 : 6	89
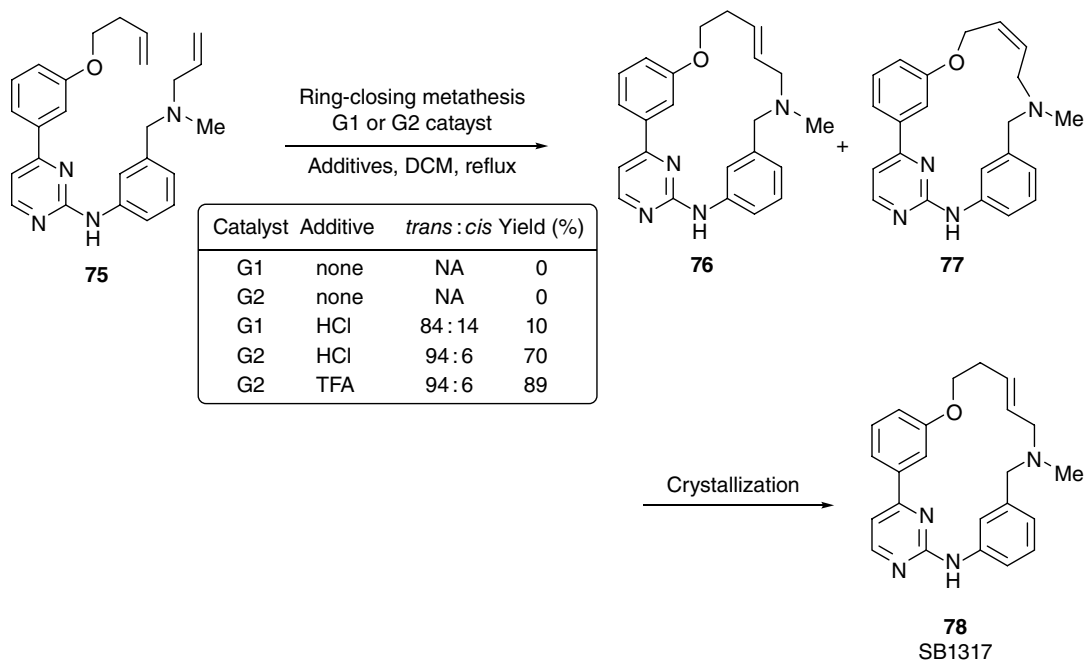
Scheme 15.25 RCM route toward SB1317.
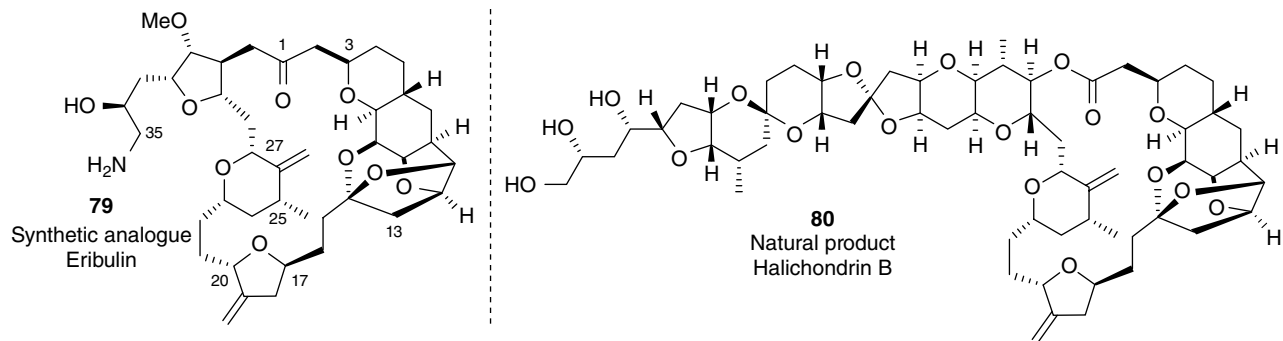
Scheme 15.26 Structures of eribulin and halichondrin B.
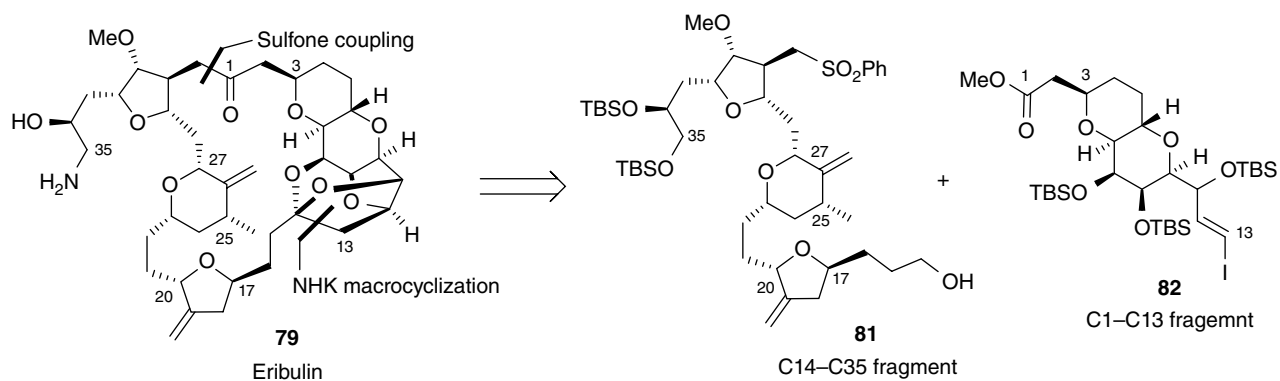
Scheme 15.27 Retrosynthetic analysis of eribulin.
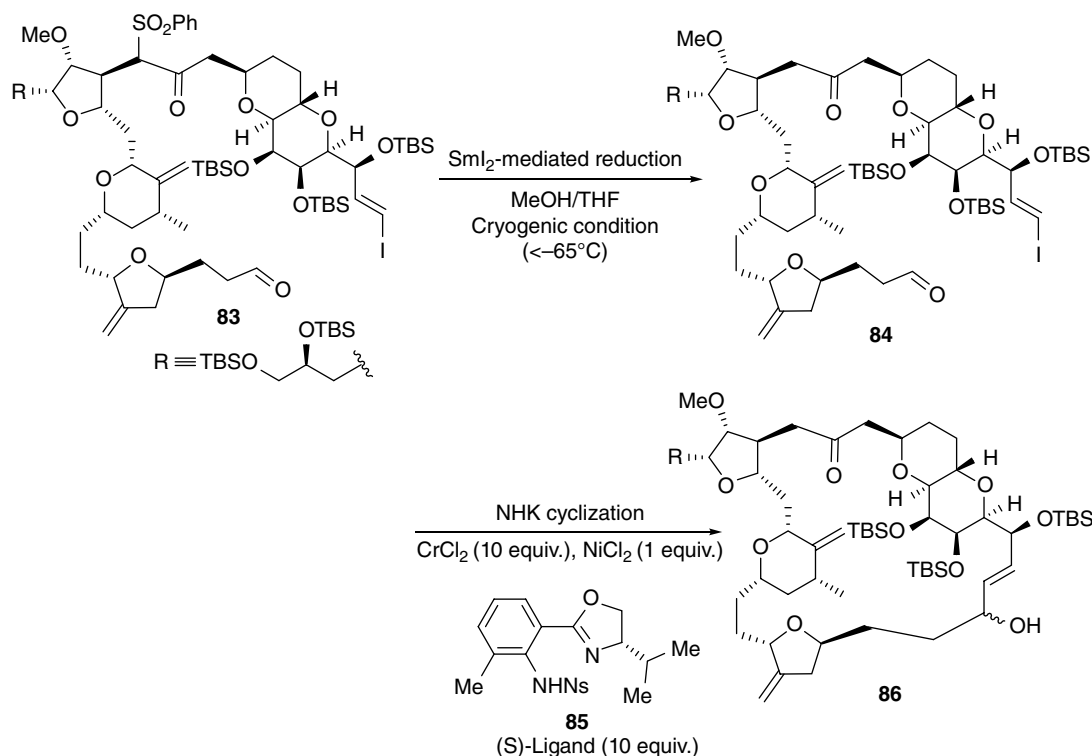
Scheme 15.28 First-generation eribulin process.

of Ni(II)/Cr(II)-mediated NHK reaction [39]. Although stereoselective construction of the secondary alcohol in **86** was not necessary, asymmetric NHK was used for macrocyclization because the asymmetric variant NHK utilizing (*S*)-ligand **85** proceeded more efficiently in terms of reaction time and yield than the ligand-free process. After achieving proof of concept of asymmetric NHK for macrocyclization in 200 g scale, the process was subsequently scaled up to provide kilogram quantities for clinical supplies (Scheme 15.28).

Although the first-generation process could be carried out on manufacturing scale, a few issues were identified for further scale-up: (i) the use of cryogenic conditions for the desulfonylation step and (ii) the use of an excess amount of air- or moisture-sensitive and expensive reagents (SmI_2 and $CrCl_2$). To address these issues, the Eisai team developed an alternative synthetic route to compound **86**, which included a catalytic NHK reaction followed by reductive desulfonylation with the Cr–ligand–Mn system (Scheme 15.29). During process development of the reactions, activation of the Mn surface was found to be the most important factor for success of the reaction. When the reactions were scaled up with an impeller agitation system instead of a stir bar agitation system, which was limited to use in pilot scale, the conversion rates were substantially decreased because of inefficient activation of Mn by the impeller

system. To overcome the issue, several activation methods were investigated, including chemical activation with I_2, the use of micronized Mn, the use of ultrasonic waves, and the physical activation with batch-type rotor–stator high-shear systems. The use of the latter with IKA T65 gave the best results in terms of yields and process robustness [40]. Finally, the scale-up demonstration at 300 g provided comparable reaction yields to the small-scale reaction with stir bar agitation. Such an approach might be expected to solve problems with scale-up of similar types of metal-mediated heterogeneous reactions.

Pd-catalyzed cross-coupling is yet another important tool for accessing macrocyclic framework. Recently, the Merck process team reported a practical asymmetric synthesis of the complex fused bis-macrocyclic HCV protease inhibitor MK-6325 (**88**, Scheme 15.30) [41]. Structurally, MK-6325 has a substantial difference from other macrocyclic HCV-targeted compounds, such as ciluprevir, simeprevir, or vaniprevir, because it includes two fused rings (15- and 18-membered rings). Therefore, an efficient construction of the unique bis-macrocycle was identified as a key synthetic strategy feature. Unfortunately, the RCM–RCM strategy used by discovery chemistry turned out to be infeasible for multi-kilogram scale due to several scale-up issues including (i) synthetic challenge for preparation of vinyl quinoxaline
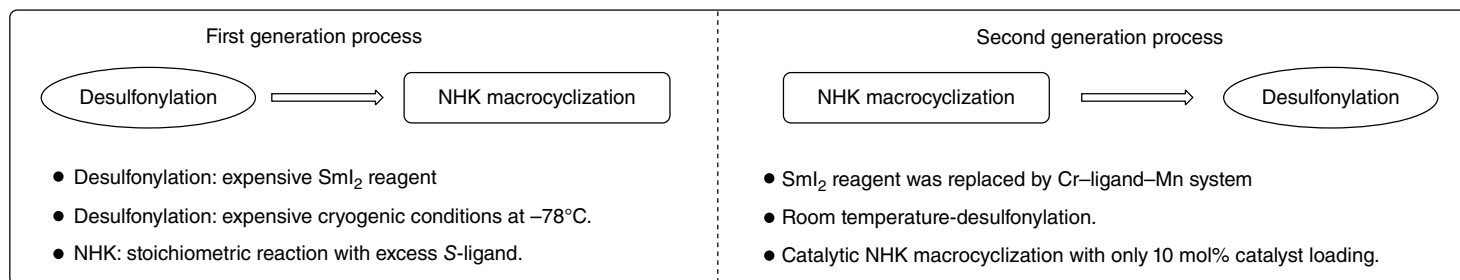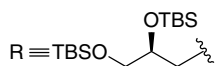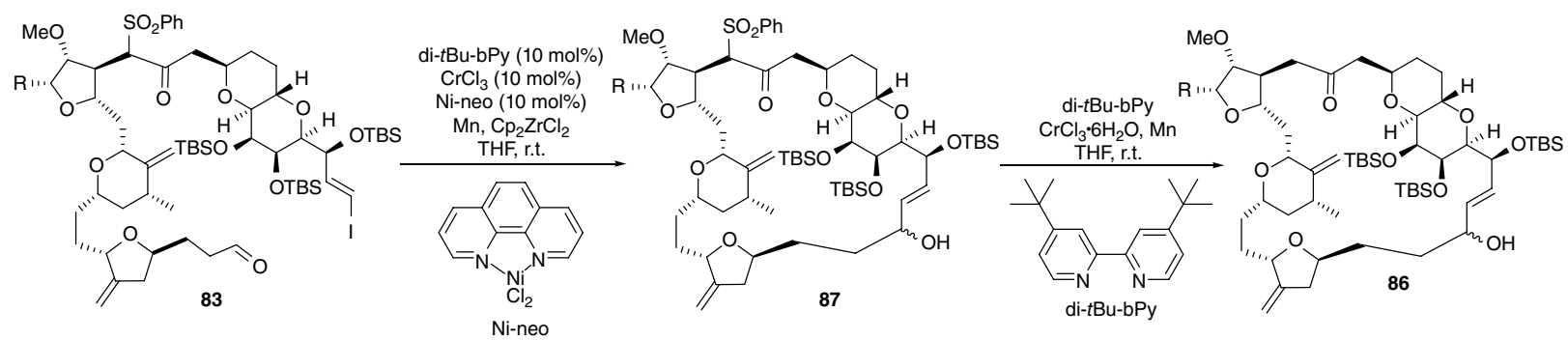
Scheme 15.29 Second-generation eribulin process.
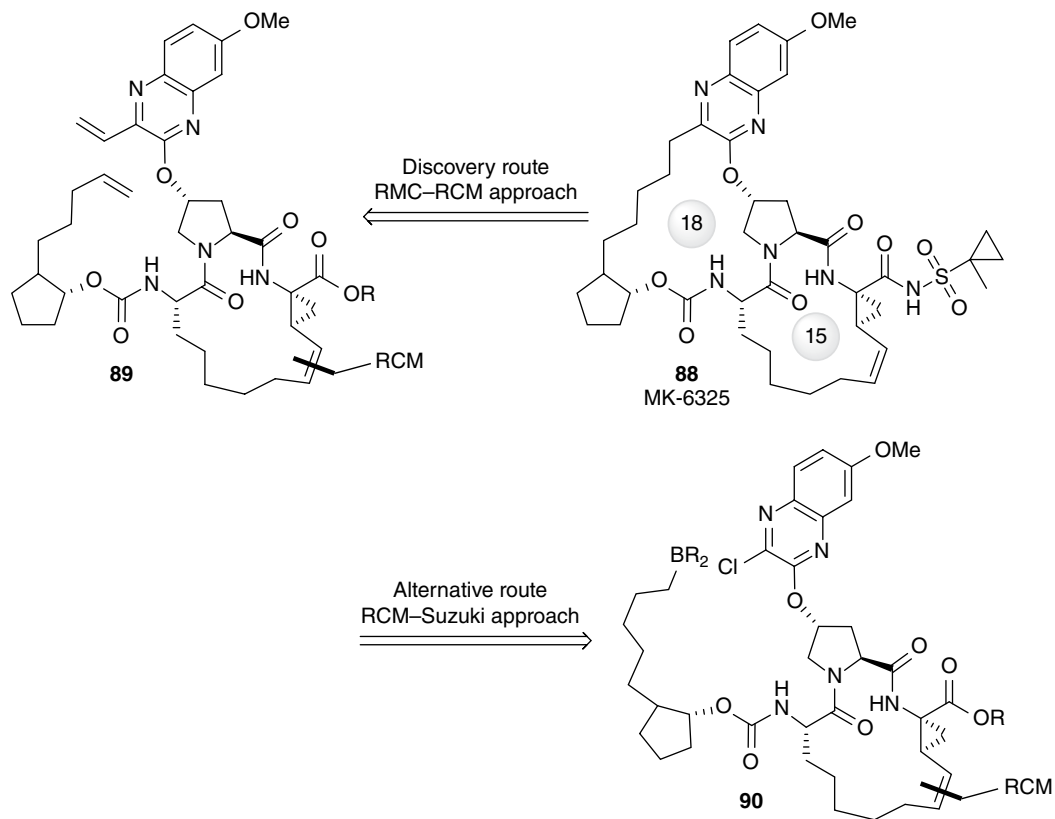
Scheme 15.30 Retrosynthetic analysis of MK-6325.

moiety, (ii) instability of vinyl quinoxaline RCM precursor **89**, and (iii) selective reduction of the alkene on the 18-membered ring in the presence of the other alkene on 15-membered ring at scale. It was envisioned that an alternative approach to construct the 18-membered ring through Pd-catalyzed intramolecular Suzuki–Miyaura coupling of substrate **90** could resolve these issues because the use of such an sp^2–sp^3 coupling would directly establish the required oxidation state and does not require a selective alkene reduction step (Scheme 15.30).

Process development started with the synthesis of compound **92** containing a 15-membered macrocyclic ring (Scheme 15.31). It was found that the *N*-Boc effect discovered by BI [25e] for the BILN-2061 process was also applicable to RCM of diene **91**. Under optimized conditions, RCM of **91** with 0.45 mol% Zhan-1B catalyst at a concentration of 20 ml/g of **91** at 80°C produced the desired macrocycle **92** in 91% yield. Subsequent TFA-mediated Boc deprotection followed by carbamate formation with **93** in a basic biphasic system afforded Suzuki–Miyaura substrate **94** in 77% yield. With **94** secured, Pd-catalyzed intramolecular Suzuki–Miyaura coupling was investigated for the installation of the second macrocycle. Reaction development within the Merck catalysis facility identified cataCXium A (Ad₂PBu)

as a superior ligand for use with **94**. Hence, Suzuki–Miyaura macrocyclization of **94** under pressure (ca. 50 psi) in cyclopentyl methyl ether (CPME)/water (0.04 M) at 100°C gave more than 98% conversion with only 5% proto-deborylation product. The macrocyclization product (**95**) was efficiently isolated as its p-TSA salt from CPME in 70% yield. The use of DMA as a cosolvent was found critical to suppress dimer formation. The intramolecular sp^2–sp^3 Suzuki–Miyaura macrocyclization with **94** was successfully demonstrated on multi-kilogram scale for clinical supply of MK-6325. This process showcased the feasibility of Suzuki–Miyaura macrocyclizations at scale and represented the largest such macrocyclization disclosed to date.

15.3.5 Oxidative Disulfide Formation

The total chemical synthesis of peptides is a very well-developed area [16b]. In particular, the introduction of a solid-phase peptide synthesis by Merrifield [16a] in the 1960s and the development of orthogonal Fmoc protection strategy by Carpino [42] in 1970s enabled the rapid production of large quantities of peptides. Moreover, newer advances in synthetic technology could expedite peptide-based drug discovery (see also Chapter 9). Along
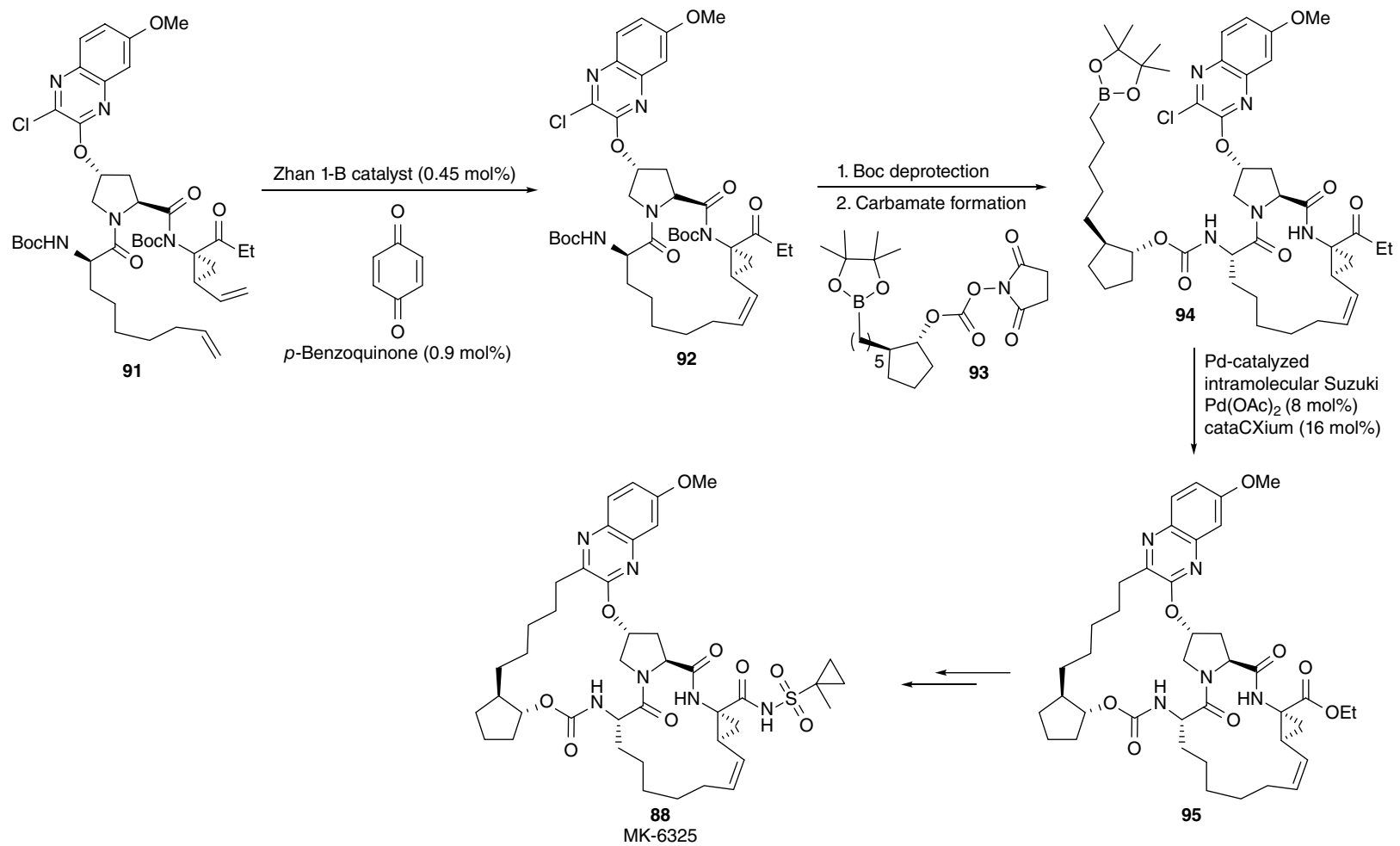
Scheme 15.31 Scalable synthesis of MK-6325.
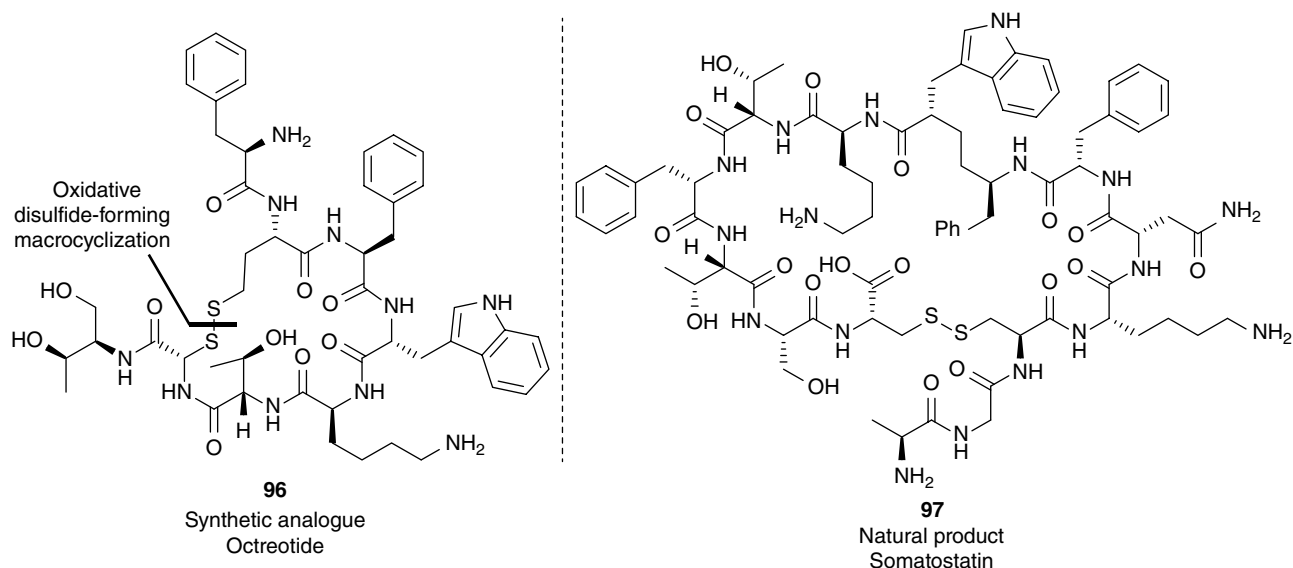
Scheme 15.32 Structures of octreotide and somatostatin.

with linear peptide therapeutics, a significant number of marketed cyclic peptide therapeutics are produced through total chemical synthesis, including desmopressin and octreotide (**96**, Scheme 15.32), lanreotide, eptifibatide, and atosiban (Table 15.1). Since these therapeutics all possess a disulfide bond in the macrocyclic skeleton, oxidative disulfide-forming cyclization was commonly used for the construction of the macrocyclic core structure on scale. In 1983, Sandoz published an air-induced disulfide-forming cyclization for the preparation of octreotide. Octreotide, a cyclic octapeptide [43], is a highly potent and pharmacologically selective analogue of somatostatin (**97**) and was approved by the FDA in 1998 as Sandostatin LAR® Depot (octreotide acetate for injectable suspension, Sandoz) for the treatment of acromegaly. Strategically, disulfide bond formation was selected as the final synthetic step in the process to avoid potential scale-up issues caused by the substantial thermal and chemical liability of the disulfide linkage.

For octreotide, the protected linear peptide **99** was efficiently prepared from **98** through a solution-phase peptide synthesis protocol using orthogonally protected amino acid synthons (Scheme 15.33). Then, removal of the *p*-methoxybenzyl protecting group under BTFA–TFA conditions followed by Boc deprotection under acidic conditions (5 N HCl) afforded the unprotected linear precursor **100** containing free thiols. With the precursor secured, air-induced disulfide bond formation with atmospheric O_2 was performed under extremely high-dilution conditions (0.27 mM in dioxane/water) to minimize intermolecular oligomerization reactions. The transformation was carefully monitored for complete consumption of –SH groups using the Ellmann test [44].

After pH adjustment to 3–4 by addition of HCl, the crude material was purified through gel chromatography (Bio-Rad P4) to yield the desired cyclic peptide.

Since it was expected that patent protection of octreotide would reach expiry in key markets other than the United States in July 2010, several CMO companies developed SPPS approaches to the molecule as well as a few solution-phase peptide syntheses. Among the patented processes [45], Wockhardt's solution-phase synthesis revealed a substantial improvement by utilizing an I_2-mediated disulfide-forming macrocyclization as the key step (Scheme 15.34). The patent claimed that most solid-phase syntheses were limited to the production of small quantities of octreotide (100–300 mg) because they needed to use expensive resins and Fmoc-*t*-butyl protected amino acids in two to four times excess at every step. On the other hand, the solution-phase synthesis could substantially reduce production cost by efficiently preparing the linear octapeptide **102** without using resin or excess amounts of protected amino acids. It should be noted that acetamidomethyl (Acm) was used as the thiol protecting group instead of *p*-methoxybenzyl (PMB) to avoid a potential tryptophan stability issue under the strong acidic deprotection conditions, such as BTFA–TFA, required for PMB deprotection. Actually, I_2 in MeOH played dual roles: (i) for the removal of the Acm-protecting group to liberate free thiol and (ii) as an oxidizing agent for subsequent disulfide-forming cyclization. The use of a reverse addition technique was also found critical to minimize intermolecular oligomerization and reduce the quantity of solvent (5.4 mM vs. 0.24 mM for the Sandoz process). A solution of **102** in 90% MeOH was slowly added into a solution of 90%
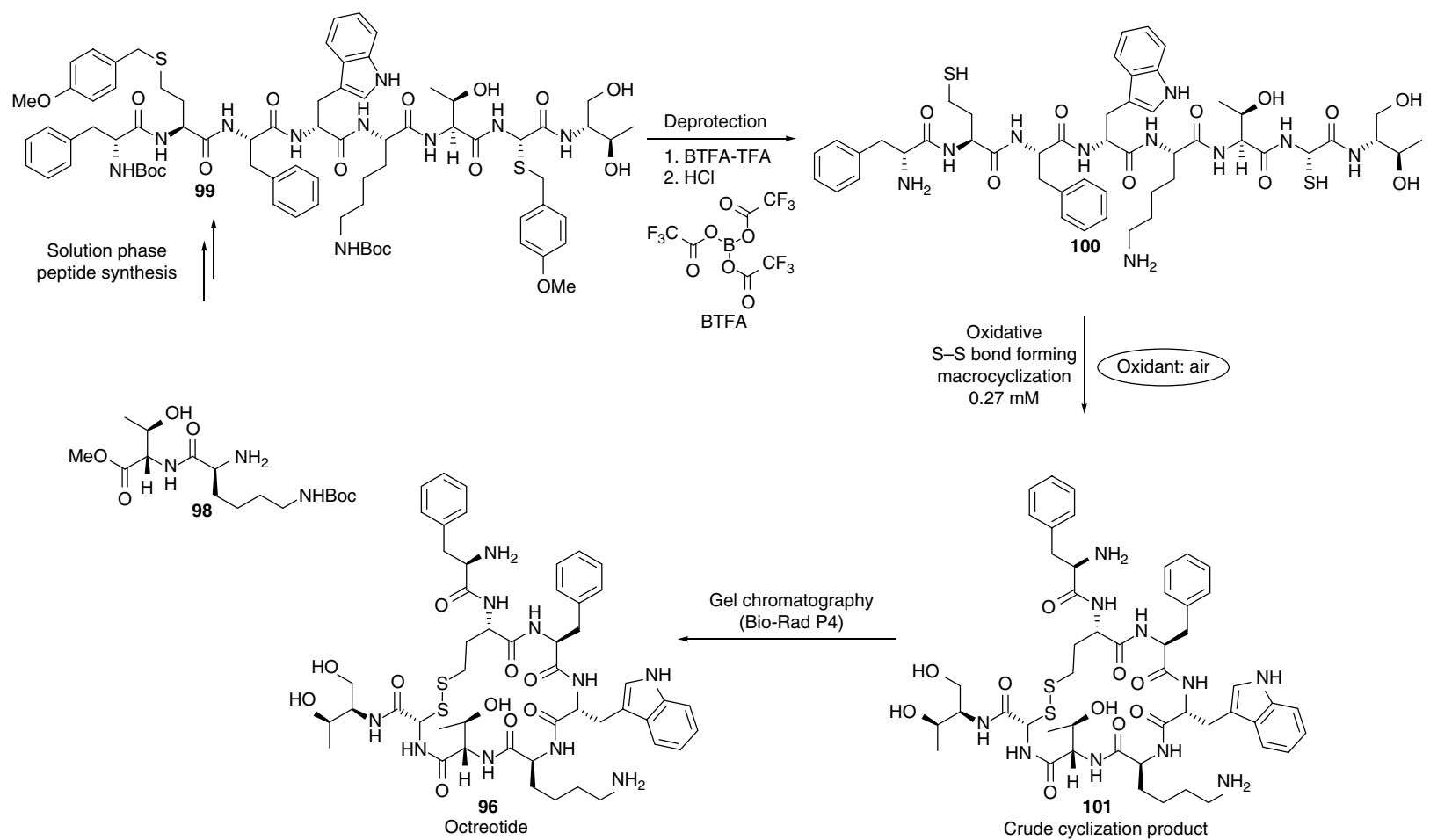
Scheme 15.33 Sandoz process for octreotide.
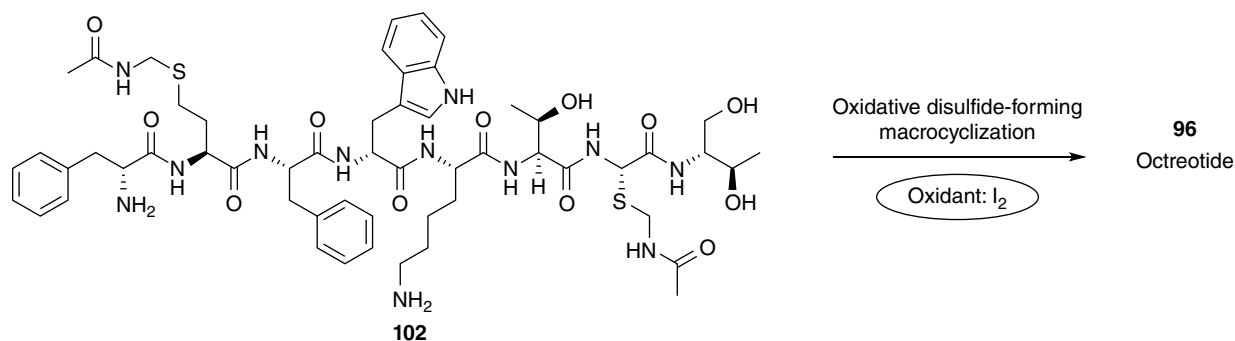
Scheme 15.34 Wockhardt process for octreotide.

Generic name	Desmopressin	Eptifibatide
Peptide length	Nonapeptide	Heptapeptide
Ring size	20	23
Oxidizing agent	Iodine	Iodine
Concentration	0.94 mM	0.5 mM

105

Atosiban
Nonapeptide
20
Iodine
1.0 mM
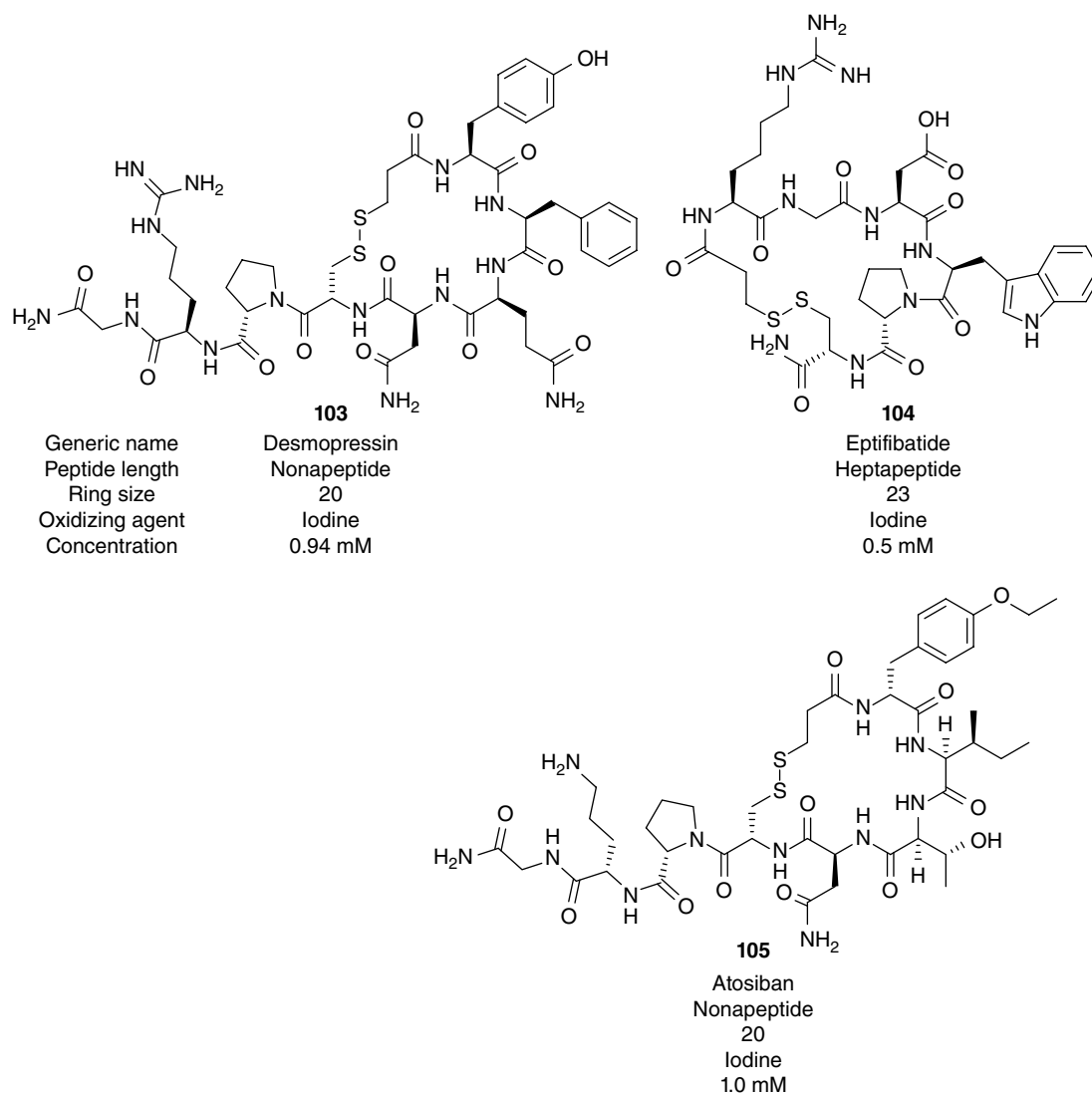
Scheme 15.35 Other examples of macrocyclic peptides constructed by disulfide bond formation.

MeOH containing iodine (5 equiv.) over a period of 1 h at 30 °C. After quenching the reaction with sodium bisulfite at 5 °C, the crude material was purified by column chromatography to afford high-quality octreotide in 84% yield (Scheme 15.34). Along with octreotide, several other macrocyclic peptide drugs have been prepared by the use of oxidative disulfide-forming macrocyclization as a key step (Scheme 15.35).

15.3.6 Other Approaches

Electrolytic macrocyclization technology is a new and attractive approach possessing excellent atom economy as well as sustainable green chemistry prospects [29]. Indeed, industrial-scale electrochemical processing of organic chemicals has a long history with use for the production of numerous chemicals such as benzidine, sorbitol, mannitol, pinacol, vanillin, and anthraquinone [46]. However, the application of electrolytic reactions in the pharmaceutical setting for the production of API is very rare and has remained less explored. In 2015, an exceptional example was reported by the Haran group with Paraza Pharma and Joyant Pharmaceuticals. A novel electrolytic macrocyclization technology was successfully utilized as a key transformation for the synthesis of the potential clinical candidate DZ-2384 (**106**) [47], a simplified analogue of the natural product (–)-diazonamide A (**107**, Scheme 15.36). Since **106** showed full retention of the antimitotic characteristics of **106** but was 10–50-fold more efficacious as a cancer therapeutic *in vivo*, it was selected as a development candidate in 2012 [48].

The key challenge in the synthesis of DZ-2384 was building the core triarylacetaldehyde in proper diarylaminal form. Although PhI(OAc)$_2$-mediated Kita oxidation was proven to be an efficient method for direct construction of 12-membered rings in small-scale reactions, it became a bottleneck for expeditive supply of the key intermediate **109** due to complications in its purification and low isolated yield (Scheme 15.37). Alongside the desired product **109**, PhI(OAc)$_2$ oxidation of **108** invariably produced comparable amount of undesired **110** and spirocyclohexadienone **111**. Development of a scalable synthetic route was critical to support the development program.

Through extensive investigations aimed at finding an alternative approach, the Haran group discovered that an electrochemical reaction could selectively oxidize the indole nucleus rather than the phenol and circumvent side product formations inherent to the Kita protocol (Scheme 15.38). At a controlled potential of +1.6 V, electrochemical reaction of **108** afforded **109** and **110** in a 3 : 1 ratio without producing any **111**. To further improve efficiency of the route to DZ-2384, the key electrochemical reaction step was moved to the end from the middle of the synthetic sequence. To effect this, substrate **113** was readily synthesized from hydrobromide **112** in 63% yield with 87% purity without applying chromatographic purification. Anodic oxidation of crude **113** at a controlled potential of +1.6 V afforded the desired DZ-2384 in 35% yield with more than 98% purity and 2.3 : 1 dr along with unreacted **113** (16%) (Scheme 15.38). This route successfully demonstrated the feasibility of electrochemical reaction for relatively large-scale macrocycle synthesis and prepared sufficient API (over 280 g of DZ-2384) for preclinical studies. DZ-2384 is currently in preclinical development targeting an IND submission in Q4 2016.

S$_N$2-based macrocyclization was reported by Beta Pharma as a route to a kinase inhibitor. Icotinib (**114**), a macrocyclic version of Roche's erlotinib (**115**, $1.2 billion sales in 2015), is a highly selective epidermal growth factor receptor tyrosine kinase inhibitor (EGFR-TKI) and was launched in China in 2011 as Conmana™ (Scheme 15.39) [49].

The process started with tosylation of triethylene glycol ether **116** in aqueous THF using KOH as a base, followed by direct crystallization to produce 59 kg of intermediate **117** as a white crystalline power in 91.4% yield with 97% HPLC purity (Scheme 15.40). Subsequent macrocyclization by double S$_N$2 reaction between bisphenol **118** and bis-tosylate **117** utilizing a reverse addition technique produced 1.65 kg of benzocrown ether **119** in 28% yield. No further improvement on the macrocyclization step has yet been reported [50].
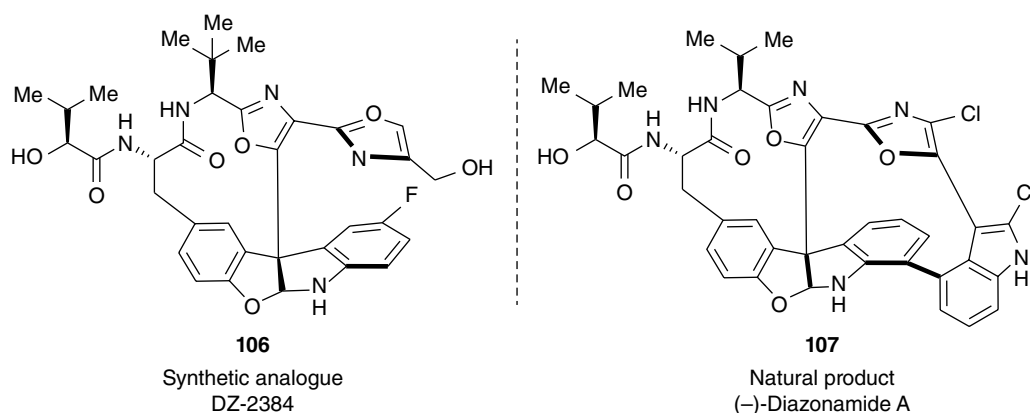
Scheme 15.36 Structures of DZ-2384 and (–)-diazonamide A.
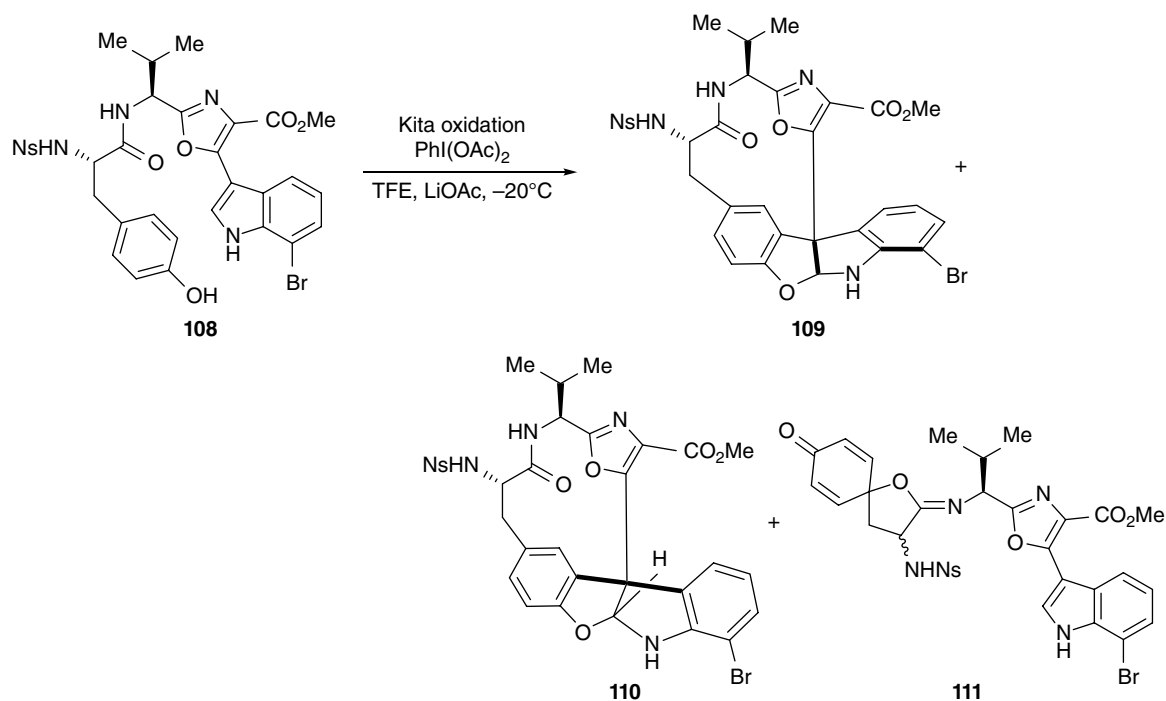
Scheme 15.37 Macrocyclization via Kita oxidation.
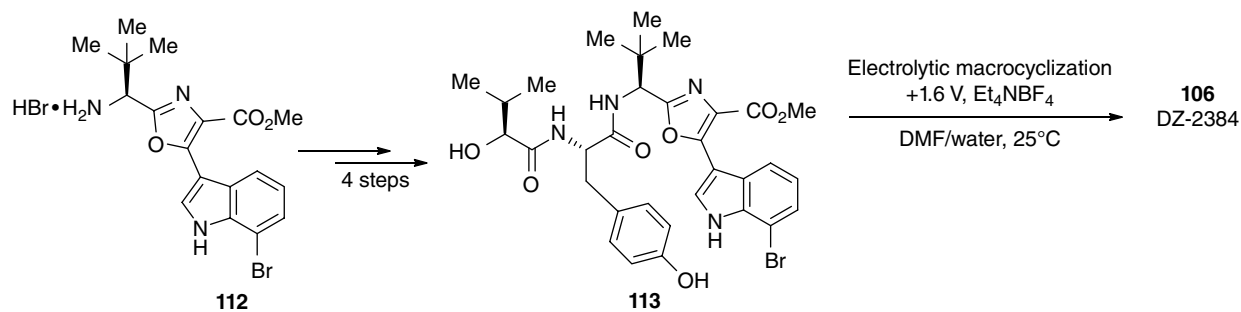
Scheme 15.38 Electrolytic macrocyclization.

114
Macrocycle version
Icotinib

115
Roche's drug
Erlotinib
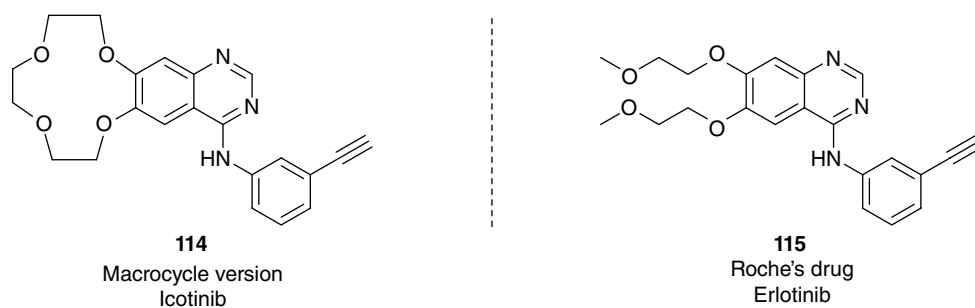
Scheme 15.39 Structures of icotinib and erlotinib.
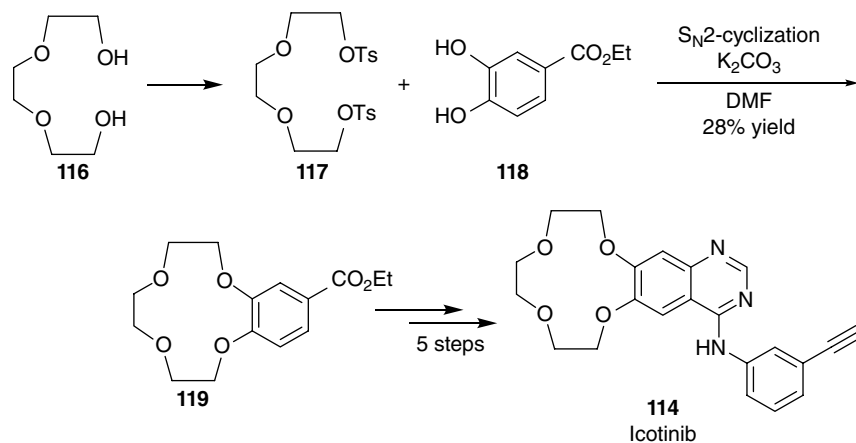
Scheme 15.40 Scalable synthesis of icotinib.

15.4   Conclusions

The aim of this chapter was to provide the reader with a realistic overview of the current state of the art of large-scale macrocycle production in the pharmaceutical industry. The highlighted examples illustrate that advancements in macrocyclization technologies and their diversity have enabled accelerated drug discovery and development. Traditional macrocyclization approaches such as macrolactonization and macrolactamization will remain an important method for large-scale synthesis of unnatural macrolide drug candidates and cyclic peptides. However, given several successful examples of RCM manufacturing processes demonstrated for late-stage clinical candidates, RCM is poised to be one of the most effective technologies available for macrocyclic core construction on an industrial scale. With respect to new macrocyclization methods, metal-catalyzed cross-coupling strategies and electrolytic macrocyclizations have emerged as elegant and environmentally friendly methods and redefined the limits of what may be synthesized on large scale today.

Future research on large-scale macrocyclization will undoubtedly bring about novel applicable chemistries and allow the pharmaceutical industry to further maximize the speed of drug development. Enabling new macrocyclizaton methods will not only accelerate process chemistry groups in the rapid delivery of clinical candidates but also provide practical and efficient synthetic tools for medicinal chemists to design novel macrocyclic motifs and expedite structure–activity relation (SAR).

References

1 (a) Driggers, E. M.; Hale, S. P.; Lee, J.; Terrett, N. K. The exploration of macrocycles for drug discovery: an underexploited structural class. *Nat. Rev. Drug Discov.* **2008**, *7*, 608–624. (b) Yu X.; Sun D. Macrocyclic drugs and synthetic methodologies toward macrocycles. *Molecules* **2013**, *18*, 6230–6268. (c) Doak, B. C.; Zheng J.; Dobritzsch D.; Kihlberg, J. How beyond rule of 5 drugs and clinical candidates bind to their targets. *J. Med. Chem.* **2016**, *59*, 2312–2327. (d) Mallinson, J.; Collins, I. Macrocycles in new drug discovery. *Future Med. Chem.* **2012**, *4*, 1409–1438.

2 Giordanetto, F.; Kihlberg J. Macrocyclic drugs and clinical candidates: what can medicinal chemists learn from their properties? *J. Med. Chem.* **2014**, *57*, 278–295.

3 (a) Partenty, A.; Moreau, X.; Campagne, J.-M. Macrolactonizations in the total synthesis of natural products. *Chem. Rev.* **2006**, *106*, 911–939. (b) Parteny, A.; Moreau, X.; Niel, G.; Campagne, J.-M. Update 1 of: macrolactonizations in the total synthesis of natural products. *Chem. Rev.* **2013**, *1113*, PR1–PR40.

4 (a) Gradillas, A; Pérez-Castells, J. Macrocyclization by ring-closing metathesis in total synthesis of natural products: reaction conditions and limitations. *Angew. Chem. Int. Ed. Engl.* **2006**, *45*, 6086–6101. (b) Nicolaou, K. C.; Bulger, P. G.; Sarlah, D. Metathesis reactions in total synthesis. *Angew. Chem. Int. Ed. Engl.* **2005**, *44*, 4490–4527.

5 Kang, E.; Lee, E. Total synthesis of oxacyclic macrodiolide natural products. *Chem. Rev.* **2005**, *105*, 4348–4378.

6 Hamada, Y.; Shioiri, T. Recent progress of the synthetic studies of biologically active marine cyclic peptides and depsipeptides. *Chem. Rev.* **2005**, *105*, 4441–4482.

7 Kasun, Z. A.; Gao, X.; Lipinski, R. M.; Krische, M. J. Direct generation of triketide stereopolyads via merged redox-construction events: total synthesis of (+)-zincophorin methyl ester. *J. Am. Chem. Soc.* **2015**, *137*, 8900–8903.

8 Klar, U.; Buchmann, G.; Schwede, W.; Skuballa, W.; Hoffmann, J.; Lichtner, R. B. Total synthesis and antitumor activity of ZK-EPO: the first fully synthetic epothilone in clinical development. *Angew. Chem. Int. Ed. Engl.* **2006**, *45*, 7942–7948.

9 Harris, C. R.; Danishefsky, S. J. Complex target-oriented synthesis in the drug discovery process: a case history in the dEpoB series. *J. Org. Chem.* **1999**, *64*, 8434–8456.

10 (a) Klar, U.; Platzek, J.; Zorn, L. (Schering AG). Optically active, heteroaromatic β-hydroxy esters, processes for their preparation from β-keto esters and processes for the preparation of these β-keto esters. PCT Int. Appl. WO 200564006, July 14, **2005**. (b) Klar, U.; Platzek, J. Asymmetric total synthesis of the epothilone sagopilone-from research to development. *Synlett* **2012**, *23*, 1291–1299. (c) Gottfried, K. Klar, U.; Platxek, J.; Zorn, L. Biocatalysis at work: applications in the development of sagopilone. *ChemMedChem* **2015**, *10*, 1240–1248.

11 Kawanami, Y.; Dainobu, Y.; Inanaga, J. Katsuki, T.; Yamaguchi, M. Synthesis of thiol esters by carboxylic trichlorobenzoic anhydrides. *Bull. Chem. Soc. Jpn.* **1981**, *54*, 943–944.

12 Illuninati G.; Mandolini, L. Ring closure reactions of bifunctional chain molecules. *Acc. Chem. Res.* **1981**, *14*, 95–102.

13 Merwe, M.; Jöntgen, W.; Krüger, J.; Cancho-Grande, Y.; Lampe, T.; Michels, M.; Paulscen, H.; Raddatz, S.; Weigand, S. Scalable synthesis of the desoxy-biphenomycin B core. *Org. Process Res. Dev.* **2011**, *15*, 1348–1357.

14 Lewis, I.; Bauer, W.; Albert, R.; Chandramouli, N.; Pless, J.; Weckbecker, G.; Bruns, C. A novel somatostatin mimic with broad somatotropin release inhibitory factor receptor binding and superior therapeutic potential. *J. Med. Chem.* **2003**, *46*, 2334–2344.

15 Hellstern, H.; Pachinger, W.; Prikoszovich, W.; Wietfeld, B. (Novartis Pharma Gmbh). Preparation of somatostatin peptides. PCT Int. Appl. WO 2005014624, February 17, **2005**.

16 (a) Merrifield, R. B. Solid phase peptide synthesis. I. The synthesis of a tetrapeptide. *J. Am. Chem. Soc..* **1963**, *85*, 2149–2154. (b) Brady, B. L. Large-scale manufacture of peptide therapeutics by chemical synthesis. *Nat. Rev. Drug Discov.* **2003**, *2*, 587–593.

17 Brady, S. F.; Freidinger, R. M.; Paleveda, W. J.; Colton, C. D.; Homnick, C. F.; Whitter, W. L.; Curley, P.; Nutt, R. F.; Veber, D. F. Large-scale synthesis of a cyclic hexapeptide analogue of somatostatin. *J. Org. Chem.* **1987**, *52*, 764–769.

18 Hoveyda, H. R.; Marsault, E.; Gagnon, R.; Mathieu, A. P.; Vézina, M.; Landry, A.; Wang, Z.; Benakli, K.; Beaubien, S.; Saint-Louis, C.; Brassard, M.; Pinault, J.; Ouellet, L.; Bhat, S.; Ramaseshan, M.; Peng, X.; Foucher, L.; Beauchemin, S.; Bhérer, P.; Veber, D. F.; Peterson, M. L.; Fraser, G. L. Optimization of the potency and pharmacokinetic properties of a macrocyclic ghrelin receptor agonist (part I): development of ulimorelin (TZP-101) from hit to clinic. *J. Med. Chem.* **2011**, *54*, 8305–8320.

19 Marsault, E. ;Ouellet, L.; St-Louis, C.; Beaubien, S.; Benakli, K.; Hoveyda, H. R.; Peterson, M. L. Bhat, S. (Tranzyme Pharma Inc.). Marcrocyclic modulators of the ghrelin receptor. U.S. Patent US 20090198050, August 6, **2009**.

20 Song, Z. J.; Tellers, D. M.; Journet, M.; Kuethe, J. T.; Lieberman, D.; Humphrey, G.; Zhang, F.; Peng, Z.; Waters, M. S.; Zewge, D.; Nolting, A.; Zhao, D.; Reamer, R. A.; Dormer, P. G.; Belyk, K. M.; Davies, I. W.; Devine, P. N.; Tschaen, D. M. Synthesis of vanipreir (MK-7009): lactamization to prepare a 20-membered macrocycle. *J. Org. Chem.* **2011**, *76*, 7804.

21 Kuethe, J.; Zhong, Y.-L.; Yasuda, N.; Beutner, G.; Linn, K.; Kim, M.; Marcune, B.; Dreher, S. D.; Humphrey, G.; Pei, T. Development of a practical, asymmetric synthesis of the hepatitis C virus protease inhibitor MK-5172. *Org. Lett.* **2013**, *15*, 4174–4177.

22 McCauley, J. A.; McIntyre, C. J.; Rudd, M. T.; Nguyen, K. T.; Romano, J. J.; Butcher, J. W.; Gilbert, K. F.; Bush, K. J.; Holloway, M. K.; Swestock, J.; Wan, B.-L.; Carroll, S. S.; DiMuzio, J. M.; Graham, D. J.; Ludmerer, S. W.; Mao, S.-S.; Stahlhut, M. W.; Fandozzi, C. M.; Trainor, N.; Olsen, D. B.; Vacca, J. P.; Liverton, N. J. Discovery of vaniprevir (MK-7009), a macrocyclic hepatitis C virus NS3/4a protease inhibitor. *J. Med. Chem.* **2010**, *53*, 2443–2463.

23 Ho, G.-J.; Mather, D. A.; Song, Z.; Emerson, K. (Merck & Co., Inc.). Process for peptide segment condensation. PCT Int. Appl. WO 1995027727, October 19, **1995**.

24 Harper, S.; McCauley, J. A.; Rudd, M. T.; Ferrara, M.; DiFilippo, M.; Crescenzi, B.; Koch, U.; Petrocchi, A.; Holloway, M. K.; Butcher, J. W.; Romano, J. J.; Bush, K. J.; Gilbert, K. F.; McIntyre, C. J.; Nguyen, K. T.; Nizi, E.; Carrol, S. S.; Ludmerer, S. W.; Burlein, C.; DiMuzio, J. M.; Graham, D. J.; Mchale, C. M.; Stahlhut, M. W.; Olsen, D. B.; Monteagudo, E.; Cianetti, S.; Giuliano, C.; Pucci, V.; Trainor, N.; Fandozzi, C. M.; Rowley, M.; Coleman, P. J.; Vacca, J. P.; Summa, V.; Liverton, N. J. Discovery of MK-5172, a macrocyclic hepatitis C virus NS3/4a protease inhibitor. *Bioorg. Med. Chem. Lett.* **2012**, *3*, 332–336.

25 (a) Poirier, M.; Aubry, N.; Boucher, C.; Ferland, J.-M.; LaPlante, S.; Tsantrizos, Y. S. RCM of tripeptide dienes containing a chiral vinylcyclopropane moiety: impact of different Ru-based catalysts on the stereochemical integrity of the macrocyclic products. *J. Org. Chem.* **2005**, *70*, 10765–10773. (b) Nicola, T.; Brenner, M.; Donsbach, K.; Kreye, P. First scale-up to production scale of a ring closing metathesis reaction forming a 15-membered macrocycle as a precursor of an active pharmaceutical ingredient. *Org. Process Res. Dev.* **2005**, *9*, 513–515. (c) Yee, N. K.; Farina, V.; Houpis, I. N.; Haddad, N.; Frutos, R. P.; Gallou, F.; Wang, X.; Wei, X.; Skimpson, R. D.; Feng, X.; Fuch, V.; Xu, Y.; Tan, J.; Zhang, L.; Xu, J.; Smith-Keenan, L. L.; Vitous, J.; Ridges, M. D.; Spinelli, E. M.; Johnson, M. Efficient large-scale synthesis of BILN 2061, a potent HCV protease inhibitor, by a convergent approach based on ring-closing metathesis. *J. Org. Chem.* **2006**, *71*, 7133–7145. (d) Gallou, F.; Saim, S.; Koenig, K. J.; Bochniak, D.; Horhota, S. T.; Yee, N. K.; Senanayake, C. H. A practical method for the removal of ruthenium byproducts by supercritical fluid extraction. *Org. Process Res. Dev.* **2006**, *10*, 937–940. (e) Shu, C.; Zeng, X.; Hao, M.-H.; Wei, X.; Yee, N. K.; Busacca, C. A.; Han, Z.; Farina, V.; Senanayake, C. H. RCM macrocyclization made practical: an efficient synthesis of HCV protease inhibitor BILN 2061. *Org. Lett.* **2008**, *6*, 1303–1306. (f) Farina, V.; Shu, C.; Zeng, X.; Wei, X.; Han, Z.; Yee, N. K.; Senanayake, C. H. Second-generation process for the HCV protease inhibitor BILN 2061: a greener approach to Ru-catalyzed ring-closing metathesis. *Org. Process Res. Dev.* **2009**, *13*, 250–254.

26 (a) Rosenquist, Å.; Samuelsson, B.; Johansson, P.-O.; Cummings, M. D.; Lenz, O.; Raboisson, P.; Simmen, K.; Vendeville, S.; de Kock, H.; Nilsson, M.; Horvath, A.; Kalmeijer, R.; de la Ros, G.; Meumont-Mauviel, M. Discovery and development of simeprevir (TMC435), a HCV NS3/4A protease inhibitor. *J. Med. Chem.* **2014**, *57*, 1673–1693. (b) Horvath, A.; Wuyts, S.; Depré, D. P. M.; Couck, W. L. J.; Cuypers, J. L. J.; Harutyunyan, S.; Binot, G. F. S. Improved process for preparing an intermediate of the macrocyclic protease inhibitor tmc 435. PCT Int. Appl. WO 2013061285, May 2, **2013**.

27 Arumugasamy, J.; Arunachalam, K.; Bauer, D.; Becker, A.; Caillet, C. A.; Glynn, R.; Latham, G. M.; Kim, J.; Liu, J.; Mayes, B. A.; Moussa, A.; Rosinovsky, E.; Salanson, A. E.; Soret, A. F.; Stewart, A.; Wang, J.; Wu, X. Development of related HCV protease inhibitor: macrocyclization of two highly functionalized dienyl-urea via ring-closing metathesis. *Org. Process Res. Dev.* **2013**, *17*, 811–828.

28 Parsy, C. C.; Alexandre, F.-R.; Surleraux, D.; Derock, M. Leroy F. (Idenix Pharma-ceuticals, Inc.). Macrocyclic serine protease inhibitors. PCT Int. Appl. WO 2009099596, February 4, **2010**.

29 Roschangar, F.; Sheldon, R. A.; Senanayake, C. H. Overcoming barriers to green chemistry in the pharmaceutical industry: the Green Aspiration Level^{TM} concept. *Green Chem.* **2015**, *17*, 752–768.

30 FDA ICH Q3D Elemental Impurities in Drug Products Guidance for Industry, June, **2016**.

31 Kong, J.; Chen, C.; Balsells-Padros, J.; Cao, Y.; Dunn, R. F.; Dolman, S. J.; Janey, J.; Li, H.; Zacuto, M. J. Synthesis of the HCV protease inhibitor vaniprevir (MK-7009) using ring-closing metathesis strategy. *J. Org. Chem.* **2012**, *77*, 3820–3828.

32 Hong, S. H.; Sanders, D. P.; Lee, C. W.; Grubbs, R. H. Prevention of undesirable isomerization during olefin metathesis. *J. Am. Chem. Soc.* **2005**, *127*, 17160–17161.

33 William, A. D.; Lee, A. C.-H.; Poulsen, A.; Goh, K. C.; Madan, B.; Hart, S.; Tan, E.; Wang, H.; Nagaraj, H.; Chen, D.; Lee, C. P.; Su, E. T. Jayaraman, R.; Pasha, M. K.; Ethirajulu, K.; Wood, J. M.; Dymock, B. W. Discovery of the macrocycle (9E)-15-(2-(pyrrolidin-1-yl)ethoxy)-7,12,25-trioxa-19,21,24-triaza-tetracyclo[18.3.1.1(2,5).1(14,18)] hexacosa-1(24),2,4,9,14(26),15,17,20,22-nonaene (SB1578), a potent inhibitor of Janus kinase 2/Fms-like tyrosine kinase-3 (JAK2/FLT3) for the treatment of rheumatoid arthritis. *J. Med. Chem.* **2012**, *55*, 2623–2640.

34 (a) Austad, B. C.; Calkins, T. L.; Chase, C. E.; Fang, F. G.; Horstmann, T. E.; Hu, Y.; Lewis, B. M.; Niu, X.; Noland, T. A.; Orr, J. D.; Schnaderbeck, M. J.; Zhang, H.; Asakawa, N.; Asai, N.; Chiba, H.; Hasebe, T.; Hoshino, Y.; Ishizuka, H.; Kajima, T.; Kayano, A.; Komatsu, Y.; Kuroda, H.; Kajima, T.; Watanabe, T. Commercial manufacture of Halaven®: chemoselective transformations en route to structurally complex macrocyclic ketones. *Synlett* **2013**, *24*, 333–337. (b) Fukuyama, T.; Chiba, H.; Takigawa, T.; Komatsu, Y.; Kayano, A.; Tagami, K. Application of a roto-stator high-shear system for Cr/Mn-mediated reactions in eribulin mesylate synthesis. *Org. Process Res. Dev.* **2016**, *20*, 100–104. (c) Inanaga, K.; Fukuyama, T.; Kubota, M.; Komatsu, Y.; Chiba, H.; Kayano, A.; Tagami, K. Novel and efficient chromium(II)-mediated desulfonylation of α-sulfonyl ketone. *Org. Lett.* **2015**, *17*, 3158–3161.

35 Hargaden, G. C.; Guiry, P. J. The development of the asymmetric Nozaki–Hiyama–Kishi reaction. *Adv. Synth. Catal.* **2007**, *349*, 2407–2424.

36 Chase, C. E.; Fang, F. G.; Lewis, B. M.; Wilkie, G. D.; Xchnaderbeck, M. J.; Zhu, X. Process development of Halaven®: synthesis of the C1-C13 fragment from d-(−)-gulono-1,4-lactone. *Synlett* **2013**, *24*, 323–326.

37 Austad B. C.; Benayoud, F.; Calkins, T. L.; Campagna, S.; Chase, C. E.; Choi, H.-W.; Christ, W.; Costanzo, R.; Cutter, J.; Endo, A.; Fang, F. G.; Hu, Y.; Lewis, B. M.; Lewis, M. D.; McKenna, S.; Noland, T. A.; Orr, J. D.; Pesant, M.; Schnaderbeck, M. J.; Wilkie, G. D.; Abe, T.; Asai, N.; Asai, Y.; Kayano, A.; Kimoto, Y.; Komatsu, Y.; Kubota, M.; Kuroda, H.; Mizuno, M.; Nakamura, T.; Omae, T.; Ozeki, N.; Suzuki, T.; Kakigawa, T.; Watanabe, T.; Yshizawa, K. Process development of Halaven®: synthesis of the C14-C35 fragment via iterative Nozaki–Hiyama–Kishi reaction-Williamson ether cyclization. *Synlett* **2013**, *24*, 327–332.

38 Molander, G. A.; Hahn, G. Lanthanides in organic synthesis. 2. Reduction of α-hetero-substituted ketones. *J. Org. Chem.* **1986**, *51*, 1135–1138.

39 Namba, K.; Kishi, Y. Catalytic Ni/Cr-mediated macrocyclization without use of high-dilution techniques. *J. Am. Chem. Soc.* **2005**, *127*, 15382–15383.

40 Fufuyama, T.; Chiba, H.; Kuroda, H.; Takigawa, T.; Kayano, A.; Tagami, K. Application of continuous flow for Dibal-H reduction and n-BuLi mediated coupling reaction in the synthesis of eribulin mesylate. *Org. Process Res. Dev.* **2016**, *20*, 503–509.

41 Li, H.; Scott, J. P.; Chen, C.; Jornet, M.; Belyk, K.; Balsells, J.; Kosjek, B.; Baxter, C. A.; Stewart, G. W.; Alam, M.; Song, Z. J.; Tan, L. Synthesis of bis-macrocyclic HCV protease inhibitor MK-6325 via intramolecular sp2–sp3 Suzuki–Miyaura coupling and ring closing metathesis. *Org. Lett.* **2015**, *17*, 1533–1536.

42 Carpino, L. A.; Han, G. Y. The 9-fluorenylmethoxycarbonyl function, a new base-sensitive amino-protecting group. *J. Am. Chem. Soc.* **1970**, *92*, 5748–5749.

43 Bauer, W.; Pless, J. (Sandoz Ltd.). Novel polypeptides, processes for their production, pharmaceutical compositions comprising said polypeptides and their use. U.S. Patent US 4395403, July 26, **1983**.

44 (a) Ellman, G. L. Tissue sulfhyldryl groups. *Arch. Biochem. Biophys.* **1959**, *82*, 70–77. (b) Bulaj, G.; Kortemme, T.; Goldenberg, D. P. Ionization-reactivity relationships for cysteine thiols in polypeptides. *Biochemistry* **1998**, *37*, 8965–8972.

45 (a) Sabatino, G.; Guryanov, I.; Rombecchi, A.; Zanon, J.; Ricci, A.; Cabri, W.; Papini, A. M.; Rovero, P. Production of peptides as generic drugs: a patent landscape of octreotide. *Expert Opin. Ther. Pat.* **2016**, *26*, 485–495. (b) Chaturvedi, N. C.; Beri, S.; Yeole, R. D.; De Souza, N. J. Process for production of the somatostatin analog, octreotide. U.S. Patent US 6987167, January 17, **2006**. (c) Kota, S.; Tallapaneni, V.; Adibhatla, K. S. B. R.; Nannapaneni, V. C. (Natco Pharma Limited). Improved process for preparation of octreotide by solution phase peptide synthesis. PCT Int. Appl. WO 2013132505, September 12, **2013**.

46 Sequeira, C. A. C.; Santos, D. M. F. Electrochemical routes for industrial synthesis. *J. Braz. Chem. Soc.* **2009**, *20*, 389–406.

47 Ding, H.; DeRoy, P. L.; Perreault, C.; Larivée, A.; Siddiqui, A.; Galdwell, C. G.; Harran, S.; Harran, P. G. Electrolytic macrocyclizations: scalable synthesis of a diazonamide-based drug development candidate. *Angew. Chem. Int. Ed.* **2015**, *54*, 4818–4822.

48 Wei, Q.; Zhou, M.; Xu, X.; Caldwell, C.; Harran, S.; Wang, L. Diazonamide analogs. U.S. Patent US 8592469, November 26, **2013**.

49 Tan, F.; Shen, X.; Wang, D.; Xie, G.; Zhang, X.; Ding, L.; Hu, Y.; He, W.; Wang, Y.; Wang, Y. Icotinib (BPI-2009H), a novel EGFR tyrosine kinase inhibitor, displays potent efficacy in preclinical studies. *Lung Cancer* **2012**, *76*, 177–182.

50 Wang, Y.; Ding, L.; Tan, F.; Hu, Y.; He, W.; Han, B.; Long, W.; Liu, Y. Icotinib hydrochloride, synthesis, crystallographic form, medical combination, and uses thereof. PCT Int. Appl. WO 2010003313, April 22, **2010**.

Part IV

Macrocycles in Drug Development: Case Studies

16

Overview of Macrocycles in Clinical Development and Clinically Used

Silvia Stotani[1] and Fabrizio Giordanetto[2]

[1] *Medicinal Chemistry, Taros Chemicals GmbH & Co. KG, Dortmund, Germany*
[2] *D.E. Shaw Research LLC, New York, NY, USA*

16.1 Introduction

When designing new drugs, small molecules are often the preferred choice because of their demonstrated potential for favorable pharmacokinetic and physicochemical properties. These properties enable oral administration and increased patient compliance, as well as the possibility to manufacture them at reduced cost compared with, for example, biological drugs [1–4]. However, small molecules have limitations when targeting extended binding sites (e.g., class B G protein–coupled receptors (GPCRs), protein–protein interactions (PPIs)), thus preventing their more widespread use. When compared with small molecules, macrocyclic compounds' larger size and structural complexity allow for many and diffuse interactions with a given target, which could confer higher affinity and selectivity, thus making them suitable to tackle these "challenging" targets [5–7]. Furthermore, macrocyclization could reduce the entropic loss upon binding with the receptor (when compared with linear analogues) and could improve permeability, metabolic stability, and pharmacokinetics [8–13]. Despite these potential advantages, complex synthetic routes and high scale-up costs have limited the interest of pharmaceutical companies in investing in macrocycle drug discovery. Furthermore, our knowledge about their absorption, distribution, metabolism, excretion, and toxicity (ADMET) is in its infancy and constitutes one of the barriers restricting the broader development of new macrocyclic compounds [14–20]. However, recent improvements in synthetic methodologies and a renewed interest in the high biological relevance of natural products (many of them being macrocyclic) have triggered a substantial reinvestigation of this compound class for drug discovery applications [21–24].

In the following, we present a survey of the several macrocycles that have already been approved and used successfully as drugs and of the many macrocyclic compounds currently in clinical development (phases I–III). Their molecular properties, structural classes, and associated pharmacokinetic profiles are discussed, with a view to learn from these successful examples, and set the basis for the future investigation and exploitation of this exciting compound class.

16.2 Datasets Generation

Macrocyclic drugs on the market and in clinical trials form the basis for the present study. The GVK BIO online-structure–activity relationship (GOSTAR) [25] database was mined to collect information about marketed macrocycles, resulting in a dataset of 74 macrocyclic drugs. Contrast agents, veterinary drugs, polypeptides with >30 amino acids, and rings with <12 atoms were excluded from our analysis. Physicochemical properties, pharmacokinetics, pharmacology, bioavailability, route of administration, and dose in humans were extracted accordingly from the scientific literature (see Appendix 16.A, Table A.16.1 for more information). In a similar manner, a dataset of 53 macrocycles in clinical trials was generated using Adis R&D Insight [26] and the relevant literature. Most likely, this dataset is an underestimation of the true volume of clinical stage macrocycles, as compounds that have been discontinued (e.g., INO 4885, friulimicin, tanespimycin), compounds that did not progress to later clinical trial phases in the last 5 years (e.g., lotilibcin) or with no disclosed chemical structure (e.g., POL6326, POL7080, CYT1010) [27] were excluded from this analysis (see Appendix 16.A, Tables A.16.2 and A.16.3 for more information).

16.3 Marketed Macrocyclic Drugs

16.3.1 General Characteristics

From a therapeutic point of view, >50% of the 74 marketed macrocyclic drugs are used for the treatment of infections, mostly of bacterial origin (Figure 16.1a). Ten out of seventy-four macrocycles are used in oncology to treat different kinds of cancer (e.g., renal, breast, T-cell lymphoma), and the remaining 24 compounds have found use in different applications, especially in the cure of cardiovascular disease (i.e., hypertension, heart failure, thrombosis), in gynecology (i.e., inhibition/induction of labor, fertility), and in immunology (i.e., immunosuppressant).

Most of the marketed macrocycles ($N = 70$, 95%) are derived from natural products. Here, two main chemical classes can be identified: macrolides and cyclic peptides, consisting of 25 and 32 drugs, respectively. The ansamycin and porphyrin classes account for a total of 10 compounds, and the remaining four classes (alkaloid, bicyclam, cyclodextrin, and epothilone) account for just one drug each (Figure 16.1b). Three recently marketed macrocyclic drugs (grazoprevir, paritaprevir, and simeprevir) cannot be ascribed to any specific natural product class but are rather the result of intense chemical modification and optimization. Accordingly, they have been assigned to a "*de novo* designed" chemical class (Figure 16.1b), and this will be discussed separately (Section 16.5). Thirty percent of the marketed macrocyclic drugs ($N = 22$) are administered orally, and 82% of these oral drugs ($N = 18$) are used to treat infectious diseases, as shown in Figure 16.1a. While only 1 out of the 32 cyclic peptides, cyclosporine A (CsA), is delivered orally, the majority of the macrolide drugs (15 out of 25) is administered orally. Macrocyclic

drugs belonging to the other chemical classes are administered parenterally, except for the ansamycins, and the "*de novo* designed" classes, where 75 and 100%, respectively, of the macrocycles are dosed orally. Parenteral macrocycles belong to all of the nine chemical classes analyzed, and they are used for different therapeutic applications (see Appendix 16.A, Table A.16.1 for a complete overview of chemical classes and indications for marketed macrocycles).

Comparing calculated physicochemical properties for the macrocyclic drugs with their route of administration reveals that orally administered macrocycles are smaller in size and more lipophilic than parenteral macrocycles, as further indicated by their lower polar surface area (PSA) and fewer hydrogen bond donors (HBDs) (Table 16.1). Interestingly, oral marketed macrocycles display similar lipophilicity to a set ($N = 89$) of oral small molecule drugs with molecular weight (MW) of >500, lacking a macrocyclic structure (calculated partition coefficient for *n*-octanol/water (cLogP) mean value 4.4 and 4.2, respectively), thus emphasizing the importance of lipophilicity to cellular absorption processes. While parenteral macrolides have MW, PSA, and number of HBD very similar to oral macrocycles, their cLogP values are significantly lower (mean value 2.1 and 4.4, respectively).

16.3.2 Cyclic Peptides

Almost half of the macrocyclic compounds on the market ($N = 32$, 43%) belong to the cyclic peptide class (Figure 16.1b). This class can be further divided into 10 different subclasses according to distinguishing
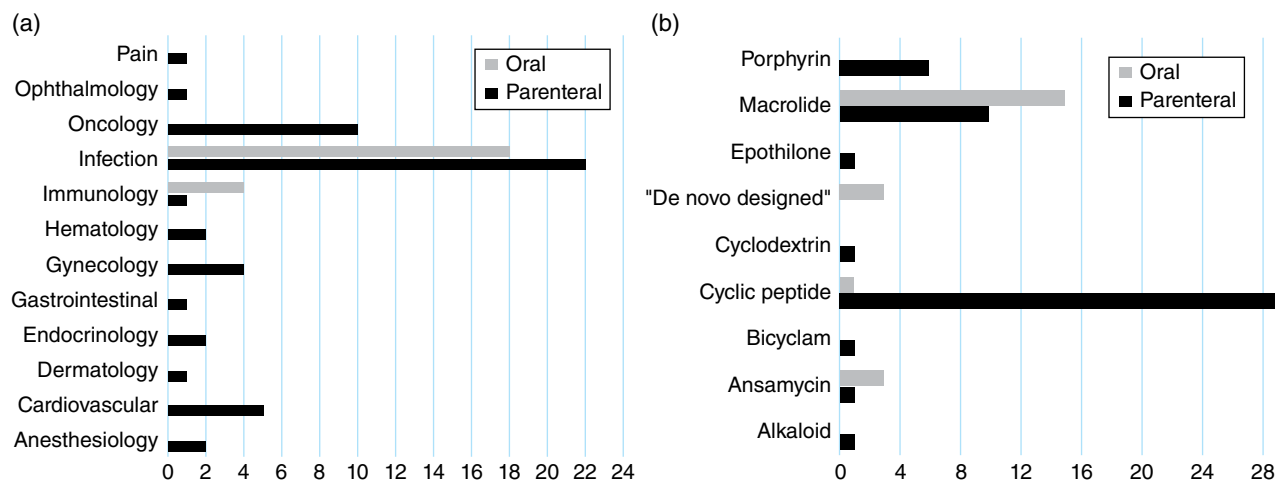
Figure 16.1 (a) Therapeutic indications and (b) chemical classes for oral (gray bars, $N = 22$) and parenteral (black bars, $N = 52$) approved macrocycles.

Table 16.1 Calculated physicochemical properties for oral small molecule drugs, different classes of registered macrocycle drugs, and macrocycles in clinical development.

Status	Class	Route of administration	N	HBD[a]	PSA[a]	MW[a]	cLogP[a]
Registered	Small molecule	Oral	1589	2 (2–2)	74 (71–76)	322 (317–328)	2.2 (2.1–2.4)
		Oral, MW > 500	89	2 (2–3)	139 (127–152)	602 (582–624)	4.2 (3.7–4.9)
	Macrocycle	Oral	21	4 (3–4)	208 (195–221)	840 (794–886)	4.4 (3.2–5.7)
		Parenteral	47	14 (11–17)	424 (354–494)	1155 (1020–1290)	0.5 (–1.2 to 2.2)
	Cyclic peptide	Oral	1	5	290	1203	14.4
		Parenteral	28	19 (15–22)	531 (449–614)	1331 (1161–1501)	–0.8 (–2.9 to 1.3)
	Macrolide	Oral	14	4 (3–4)	205 (193–216)	831 (795–867)	3.7 (2.6–4.7)
		Parenteral	9	6 (3–9)	240 (185–295)	867 (754–980)	2.1 (–1.7 to 6.0)
	"*De novo* designed"	Oral	3	3 (1–4)	183 (124–242)	761 (737–785)	4.8 (0.2–9.4)
Clinical development	Macrocycle	Oral	21	9 (6–11)	286 (229–343)	958 (843–1074)	5.4 (3.1–7.7)
		Parenteral	31	9 (6–11)	289 (229–350)	963 (839–1087)	0.2 (–2.0 to 2.4)
	Cyclic peptide	Oral	5	16 (12–20)	444 (356–533)	1269 (1091–1446)	5.0 (–7.3 to 17.4)
		Parenteral	17	16 (12–21)	472 (388–557)	1283 (1089–1477)	–3.0 (–5.8 to –0.1)
	Macrolide	Oral	2	3 (2–3)	203 (190–215)	911 (755–1067)	5.2 (1.2–9.1)
		Parenteral	3	3 (2–4)	173 (87–260)	733 (402–1064)	4.8 (0.9–8.8)
	"*De novo* designed"	Oral	12	2 (1–3)	135 (94–177)	648 (516–781)	5.4 (4.3–6.5)
		Parenteral	1	4	173	937	6.1

[a] Mean value (lower and upper margins of 95% confidence interval).

Figure 16.2 Subclass distribution of oral (gray bar, N = 1) and parenteral (black bars, N = 31) macrocyclic peptide drugs.
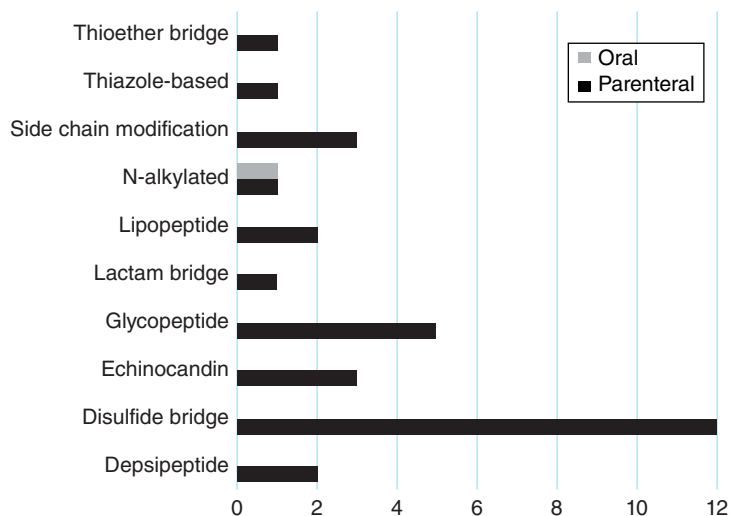
structural features (Figure 16.2). Disulfide-based cyclic peptides are the most frequently occurring macrocyclic peptide subclass (N = 12, 38%), and most of them (9 out of 12) represent chemical modifications of natural hormones or hormones themselves. Drugs belonging to this subclass find application in different therapeutic areas: cardiovascular (e.g., eptifibatide), endocrinology (e.g., lanreotide), gastroenterology (e.g., linaclotide),

gynecology (e.g., atosiban), oncology (e.g., octreotide), and pain (e.g., ziconotide). The recent approval of new vancomycin derivatives has increased the number of drugs in the glycopeptides subclass to five. The two subclasses of the echinocandins and the cyclic peptides with side chain modifications count three members each, while the remaining nine cyclic peptides are spread into six different subclasses.

All but one of the macrocyclic peptide drugs ($N = 31$) are administered parentally. This set of compounds displays high MW, large PSA, numerous HBD, and low *c*Log*P*, providing a clear rationale for why parenteral administration is required (Table 16.1).

CsA is the only marketed cyclic peptide administered orally. The conformational flexibility of the molecule allows the formation of intramolecular hydrogen bonds in nonpolar media, thus resulting in high cell permeability and oral bioavailability (*F*) (see Chapter 3 for further discussion) [28–31]. CsA bioavailability is nevertheless variable (5–60%) due to competition between passive diffusion absorption in the gastrointestinal tract and active secretion by P-glycoprotein (P-gp). Suspensions, microemulsions, and lipid-based formulations for oral administration have thus been developed in order to improve its bioavailability [32–35].

Macrocycles belonging to the glycopeptide subclass are extremely polar, as suggested by their large PSA, numerous HBD, and low *c*Log*P* (Table 16.2). All of them are parenterally administered, due to their poor gastrointestinal absorption. Two vancomycin analogues, dalbavancin and oritavancin, have been recently approved by the Food and Drug Administration (FDA) for the treatment of acute bacterial skin and skin structure infections (ABSSSI). Both of them bear a peripheral hydrophobic group attached to a carbohydrate, reminiscent of naturally occurring lipidated sugars (Table 16.2). The long alkyl chains in dalbavancin and telavancin are thought to enhance membrane anchoring and thus their antibiotic activity [36]. Dalbavancin also has a free and flexible C-terminal dimethylaminopropyl group available for binding with the negative phospholipid head of the bacterial membrane. The hydrophobic group of oritavancin is an *N*-(4-chlorobiphenyl)methyl moiety, which introduces a second mechanism by which the compound exhibits its antimicrobial activity. The modified carbohydrate is in fact thought to directly inhibit transglycosylases, thereby increasing its antibiotic potency [37–39]. The two highly lipophilic groups of dalbavancin and oritavancin are responsible for hydrophobic interactions with serum proteins (binding = 93 and 85%, respectively), thus contributing to their enhanced half-life ($t_{1/2}$). While vancomycin and telavancin have a $t_{1/2}$ of 4–6 and 8 h, respectively, dalbavancin's $t_{1/2}$ is >14 days, allowing for once weekly dosing, contrary to the at least 2–3 doses per day required for vancomycin and telavancin (Table 16.3) [40–45].

16.3.3 Macrolides and Ansamycins

Approximately one-third of the macrocyclic drugs on the market ($N = 25$, 34%) belong to the macrolide class, and 60% of them ($N = 15$) are administered orally.

Macrolides can be further classified into several subclasses according to their structural features (Figure 16.3).
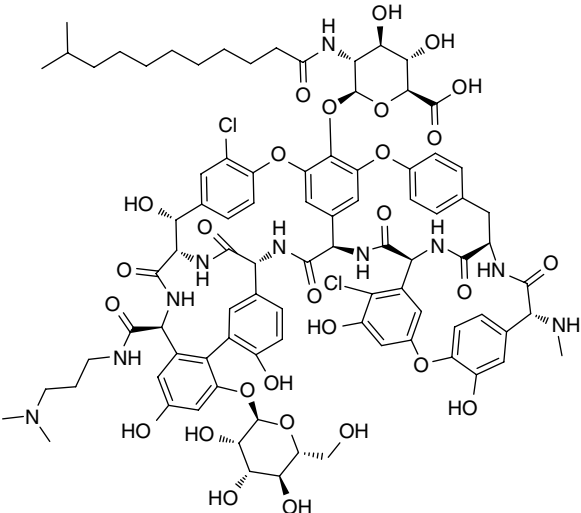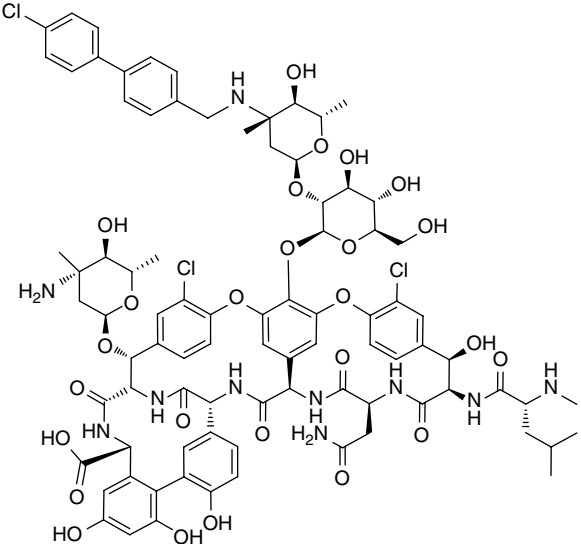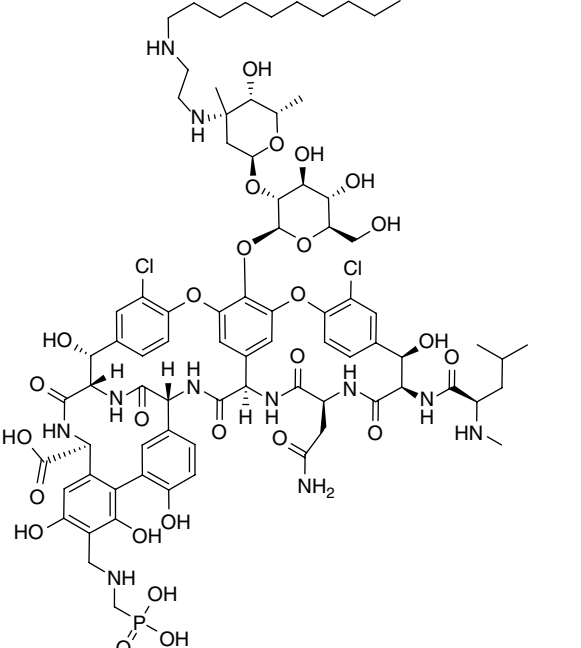
The most populated subclass ($N = 8$) is the erythronolides (e.g., azithromycin, clarithromycin, erythromycin), which are all delivered orally and used for the treatment of a wide range of infections (e.g., respiratory tract, urinary, soft tissue). The leucomycin subclass counts three members (i.e., josamycin, rokitamycin, spiramycin), which are also administered orally and used to treat infections (e.g., respiratory, stomatological, and urogenital). Conversely, the three polyene macrolides, amphotericin b, natamycin, and nystatin, are used parenterally as antifungal agents.

The subclasses of ascomycins, naphthoquinone-based ansamycins and rapamycins, have members administered both orally and parenterally. Tacrolimus was approved in 1994 as an oral immunosuppressant for use after allogeneic organ transplant and in 2000 as an ointment (0.1 and 0.03%) for the treatment of atopic eczema. Pimecrolimus has a structure very similar to tacrolimus and was approved in 2001 as a cream (1%). It has been proven effective in various inflammatory skin diseases, such as vitiligo [46], psoriasis [47, 48], and seborrheic dermatitis [49]. Tacrolimus possesses a propenyl group in position 8 of the macrolactam and a hydroxyl substituent attached to position 4 of the cyclohexyl moiety, while pimecrolimus possesses, respectively, an ethyl substituent and a chlorine atom (Table 16.4). Despite these similar structures, the two drugs are administered through different routes. In phase I and II clinical trials, both of them displayed rapid absorption after oral administration [50].

In their topical form, pimecrolimus cream showed higher affinity to skin proteins [51], resulting in lower permeation through the skin [52] when compared with tacrolimus ointment in the treatment of atopic eczema [53, 54].

The naphthoquinone-based ansamycin subclass includes three orally administered (rifabutin, rifampicin, rifapentine) and one parenterally delivered (rifaximin) drugs (Table 16.5). Rifaximin, due to its poor oral bioavailability, is used to treat traveler's diarrhea caused by *Escherichia coli*. Its crystal structure [55] shows coplanarity of the naphthoquinone nucleus and the pyrido-imidazolic ring. This results in a mesomeric betaine structure with a formal positive charge on N_1 and a negative charge on N_7. This zwitterionic character and the presence of anionic phenolic hydroxyl groups are responsible for its constant ionization throughout the intestine, minimizing its systemic absorption [56]. Rifaximin received orphan drug status from FDA in 1998 for the treatment of hepatic encephalopathy. The disease is caused by accumulation of toxic substances (normally removed by the liver) in the bloodstream.

Table 16.2 Macrocyclic drugs of the glycopeptide subclass.

Drug name	Structure	Therapeutic area	Oral	HBD	PSA	MW	cLogP
Dalbavancin		Infection	No	21	564	1817	−1.5
Oritavancin		Infection	No	20	561	1793	−0.7
Telavancin		Infection	No	24	665	1756	1.9

(*Continued*)

Table 16.2 (Continued)
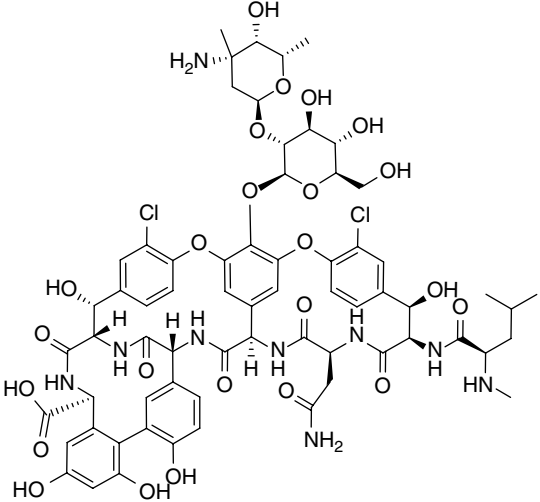
Drug name	Structure	Therapeutic area	Oral	HBD	PSA	MW	cLogP
Vancomycin		Infection	No	21	585	1449	−1.1

Table 16.3 Pharmacokinetic parameters of glycopeptide macrocycles.

	Dalbavancin	Oritavancin	Telavancin	Vancomycin
C_{max} (mg/l)	287	138	93.6	63
Clearance (l/h)	0.0513	0.445	0.0139	0.048
$t_{1/2}$ (h)	346	245	8	4–6
Metabolism	No apparent metabolism; hydroxyl-dalbavancin is a minor metabolite found in the urine but not in plasma of healthy subjects	Not metabolized	Not metabolized	Not metabolized
Elimination	Feces (20%) and urine (33% unchanged dalbavancin, 12% hydroxyl-dalbavancin)	Feces (<1%) and urine (5% unchanged oritavancin)	Feces (<1%) and urine (76%)	Urine (75%)
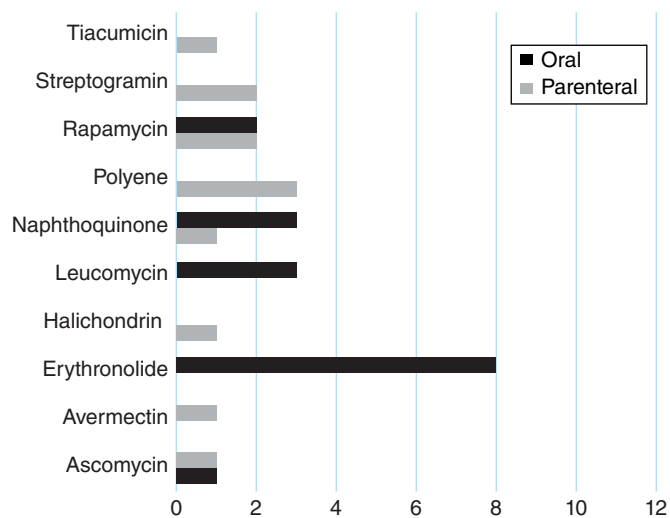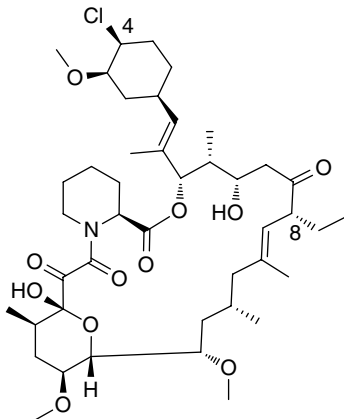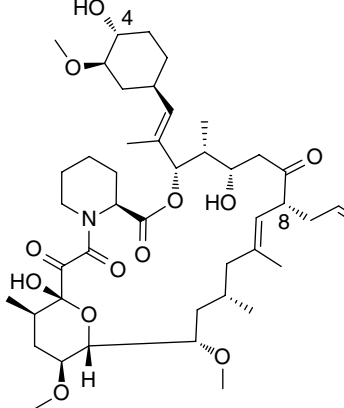
Figure 16.3 Subclass distribution of oral (black bars, $N=18$) and parenteral (gray bars, $N=11$) ansamycin and macrolide drugs.

Table 16.4 Macrocyclic drugs of the ascomycin subclass.

Drug name	Structure	Therapeutic area	Oral	Human, *F* (%)	HBD	PSA	MW	*c*Log*P*
Pimecrolimus		Dermatology	No		2	158	811	6.0
Tacrolimus		Immunology	Yes	15	3	186	804	5.8

Treatment relies on suppressing the production of the toxic substances in the intestine using the laxative lactulose or nonabsorbable antibiotics, such as rifaximin [57].
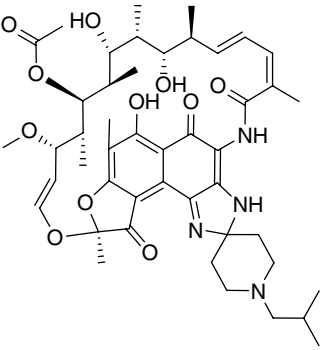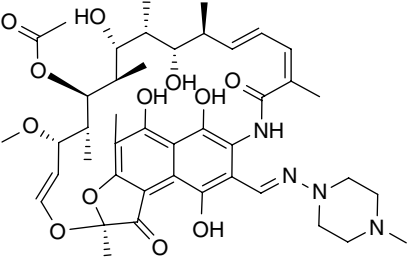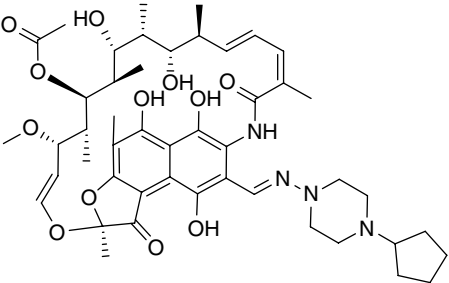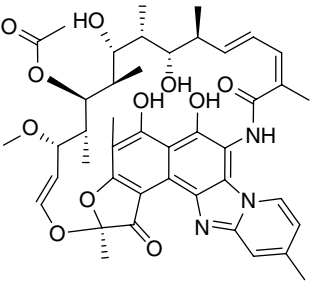
The rapamycin subclass includes four drugs, two of which are orally administered (Table 16.6). Sirolimus was the first rapamycin macrolide approved by the FDA (1999). Originally developed as an antifungal agent, it is now used to prevent organ rejection in transplants (especially the kidney), due to its potent immunosuppressive and antiproliferative properties. In 2015, it also received FDA approval for the treatment of lymphangioleiomyomatosis (LAM) [58]. Temsirolimus, the 2,2-bis(hydroxymethyl)propanoic ester of sirolimus, is administered parenterally to treat renal cell carcinoma [59–61]. It was developed to reduce sirolimus' immunosuppressive properties, and, despite showing minimal oral bioavailability (1.5–2.5%) in cancer patients, it displays higher solubility and shorter $t_{1/2}$ than sirolimus [62, 63]. Everolimus, the 40-*O*-(2-hydroxyethyl) ether of sirolimus, is administered orally, once daily, to prevent organ transplant rejection and to treat renal cancer and other tumors [64, 65]. Its $t_{1/2}$ is shorter than that of sirolimus (28 and 62 h, respectively) because it is extensively metabolized *in vivo* [66]. The replacement of the hydroxyl group of sirolimus with a 1*H*-tetrazol-1-yl substituent led to zotarolimus, an immunosuppressant used to reduce coronary artery restenosis. The compound is extremely lipophilic and has limited water solubility. These features allow its use in a drug-loaded stent to guarantee a slow, extended release directly into the wall of coronary vessels [67].

16.3.4 Bioavailability and Doses of Macrocyclic Drugs

The analysis of the daily dosages of macrocyclic drugs (macrolides, ansamycins, and CsA) revealed significantly higher values for orally administered drugs, compared with the ones delivered through the parenteral route (mean/median: 633/500 mg vs. 199/20 mg, respectively,

Table 16.5 Macrocyclic drugs of the ansamycin subclass.
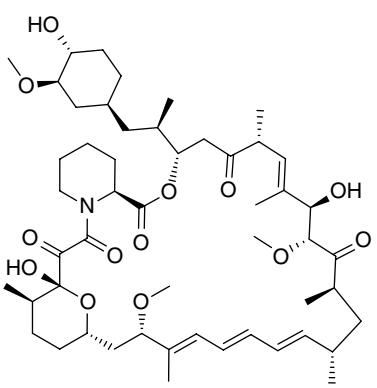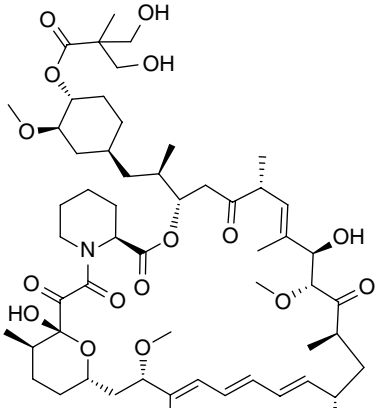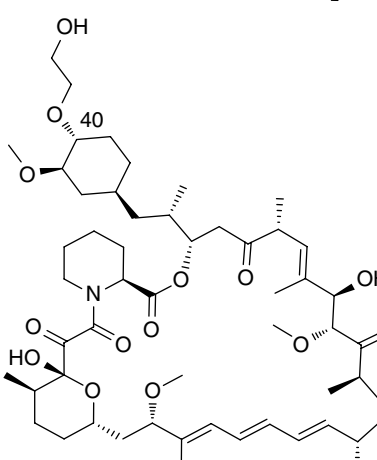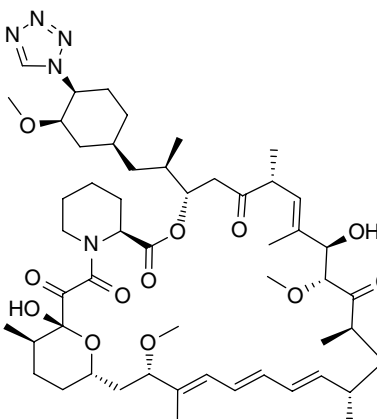
Drug name	Structure	Therapeutic area	Oral	Human, *F* (%)	HBD	PSA	MW	*c*Log*P*
Rifabutin		Infection	Yes	53	5	217	847	4.7
Rifampicin		Infection	Yes	50	6	234	823	3.7
Rifapentine		Infection	Yes	70	5	211	847	5.1
Rifaximin		Infection	No		5	206	786	7.2

$p < 0.05$). A plausible explanation is the fact that oral macrocycles are mostly used to treat infections where high doses might be required to maximize their bacteriostatic and/or bactericidal actions.

Unsurprisingly, seven parenteral macrocycles (e.g., dalfopristin, ramoplanin, vancomycin) having daily doses of ≥500 mg (~1300, 500, and 2000 mg, respectively) are anti-infective drugs. Formulation also plays a key role in influencing daily dosages, as shown by the case of ivermectin. The potent broad-spectrum antiparasitic agent, approved in 2014 as a cream (1%) for the treatment of rosacea [68], is dosed in the 3–15 mg/day range. As an ethanolic solution, it displays bioavailability twice as high when compared with the tablet and capsule pharmaceutical forms showing, nevertheless, the same rate of absorption in all three cases [69, 70].

Table 16.6 Macrocyclic drugs of the rapamycin subclass.

Drug name	Structure	Therapeutic area	Oral	Human, F (%)	HBD	PSA	MW	cLogP
Sirolimus		Immunology	Yes	14	3	204	914	7.0
Temsirolimus		Oncology	No		4	254	1030	7.5
Everolimus		Immunology	Yes	20	3	213	958	7.1
Zotarolimus		Immunology	No		2	222	966	7.5

16.4 Macrocycles in Clinical Studies

16.4.1 General Characteristics

Fifty-three macrocycles are now in different stages of clinical trials. Similarly to marketed products, most of the macrocyclic clinical candidates ($N = 35$, 66%) are used for the treatment of infections and in oncology. The remaining compounds find different applications ranging from cardiology to ophthalmology (Figure 16.4a). From a chemical point of view, while the percentage of drugs belonging to the class of cyclic peptides stays constant across marketed and developmental macrocycles (i.e., 43%), the number of compounds ascribable to the macrolide class is much lower for those in clinical trials than for marketed drugs ($N = 5$, 9% and $N = 25$, 34%, respectively, cf. Figures 16.1b and 16.4b). This could be the result of decades of intense exploitation of macrolides as a source of new drugs, which has been nowadays partly replaced by the rational design of new chemical entities, thus resulting in a sixfold higher number of clinical candidates belonging to the "*de novo* designed" class when compared with marketed drugs ($N = 13$, 24% and $N = 3$, 4%, respectively). Almost half ($N = 22$, 41%) of the macrocyclic compounds in clinical trials are delivered orally, showing a significantly increased interest in the development of macrocycles that could be suitable for oral administration. Similarly to approved macrocycles, clinical macrocycles administered orally have higher lipophilicity, as assessed by cLog$P$, than their parenteral counterparts. Nevertheless, no significant differences in HBDs, PSA, and MW emerged when comparing clinical macrocycles that differ in their mode of administration (Table 16.1).

16.4.2 Cyclic Peptides

The majority of macrocyclic clinical candidates ($N = 23$, 43%) belong to the cyclic peptide class. These can be organized according to their structural features into seven different subclasses (Figure 16.5). The two most populated are cyclic peptides displaying (a) at least one N-alkylated peptide bond and (b) a lactam bridge ($N = 5$, 21% and $N = 6$, 26%, respectively). All the six lactam bridge-containing cyclic peptides are administered parenterally, and half of them are hormone derivatives. An interesting example of how the route of administration can influence the ADMET properties of a potential drug is offered by bremelanotide (PT-141). Structurally related to the α-melanocyte-stimulating hormone (α-MSH), PT-141 is an active metabolite of the discontinued drug melanotan II (MT2), a skin melanin-pigmentation enhancer. During phase I clinical trials of MT2, its beneficial effects on both female and male sexual arousal were accidentally discovered. Originally administered intranasally, it was temporarily discontinued in 2008 due to the increased blood pressure observed in some patients. It is now in phase III clinical trials for female sexual dysfunction using a subcutaneous administration formulation, and, to date, no significant variations in blood pressure have been registered in treated patients when compared with placebo (Table 16.7) [71–73].

Four out of five N-alkylated cyclic peptides in clinical trials are orally administered CsA analogues. All four compounds maintain the undecapeptide core structure of CsA but have been differentially modified at position 1, 3, and 4. Modifications at residues 3 and 4 drastically reduce the immunosuppressive properties of CsA while increasing its antiviral activity. This feature has been used to develop three novel compounds with potent
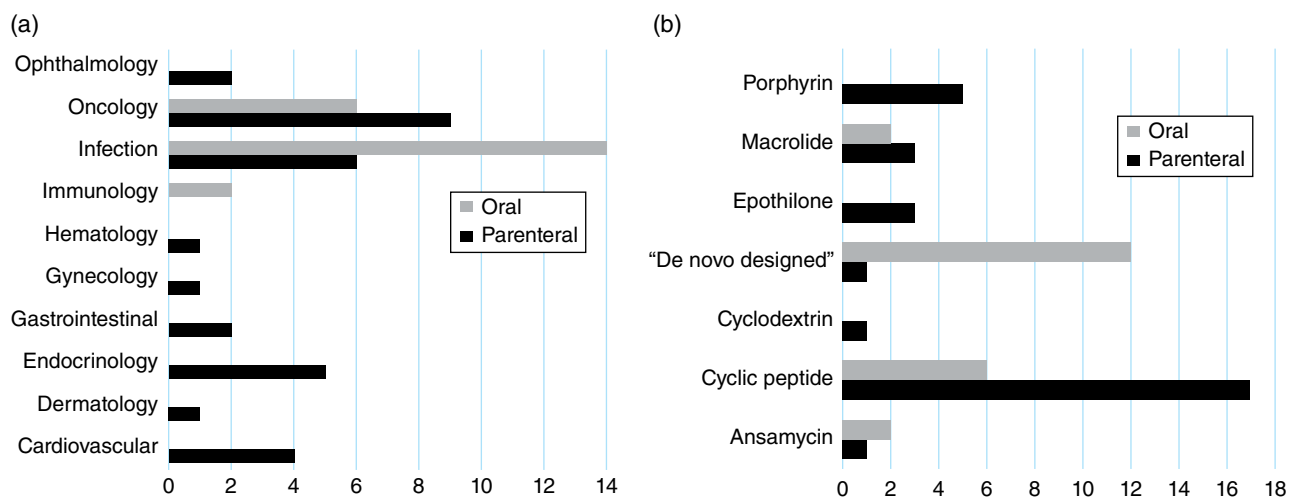
Figure 16.4 (a) Therapeutic indications and (b) chemical classes for oral (gray bars, $N = 22$) and parenteral (black bars, $N = 31$) macrocycles in clinical trials.

Figure 16.5 Subclass distribution of oral (gray bars, $N=6$) and parenteral (black bars, $N=17$) macrocyclic peptides drugs.
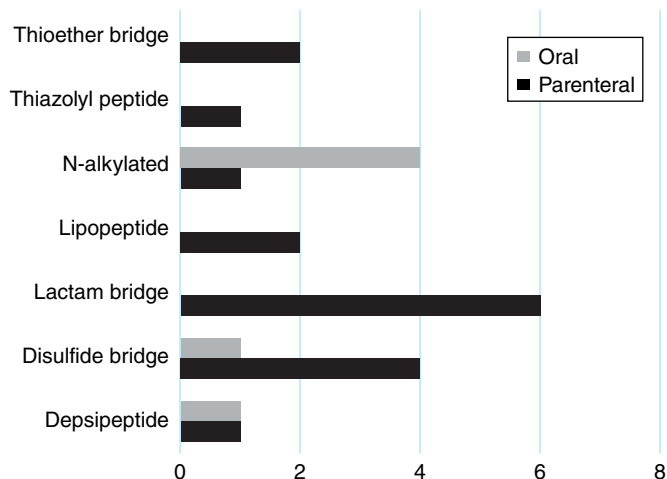
anti-hepatitis C virus (HCV) activity: NIM811 **1**, SCY-635 **2**, and alisporivir (DEB025) (Table 16.8) [74–76].

Cyclic peptide **1** was obtained by substitution of the methyl leucine at position 4 of CsA with a methyl isoleucine. This CsA analogue binds to cyclophilins with higher affinity than CsA itself, but the resulting complex does not interact with calcineurin, which suppresses immunosuppressant activity. *In vitro* studies proved its significant antiviral activity alone or in combination with pegylated interferon (PEG-IFN) [77, 78].

The introduction of a dimethylamino-ethylthio substituent on the α-carbon of the *N*-methylglycine at position 3 of CsA and of a hydroxyl group on the γ-carbon of the *N*-methyl-leucine at position 4 yielded the non-immunosuppressive cyclophilin inhibitor **2**. The macrocyclic compound **2** prevents the interaction of NS5A (HCV nonstructural 5A protein) with cyclophilin A (CypA), thus blocking HCV replication. Cyclic peptide **2** is a weak inhibitor and a poor substrate for P-gp, showing rapid absorption and sufficient oral bioavailability, ranging from 18.9 to 23.1% in rats and from 11.1 to 17.7% in monkeys [79, 80].
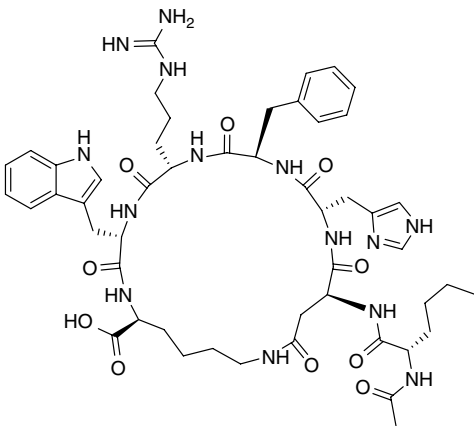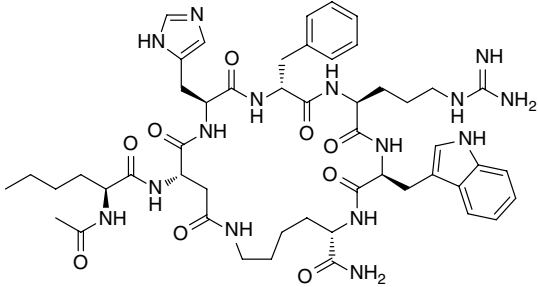
Alisporivir differs from the parent molecule CsA through the substitution of *N*-methylglycine at position 3 and *N*-methyl-leucine at position 4 with D-alanine and *N*-ethyl-valine, respectively [81, 82]. Alisporivir is administered orally as soft gel capsules and displays good passive permeability properties (Caco-2 $P_{app} = 8.46 \times 10^{-6}$ cm/s),[1] resulting in rapid absorption after oral administration [83–86]. The immunosuppressant clinical candidate voclosporin is the result of the elongation of the residue at position 1 of CsA by a single carbon to yield a *trans*-terminal diene. Modification at position 1 instead of positions 3 and/or 4 of CsA allows for the maintenance

of immunosuppressive properties, making voclosporin a potent calcineurin inhibitor that is now in clinical trials for preventing organ rejection in transplants. Similar to other CsA analogues, voclosporin is well absorbed after oral administration. Based on the manifest structural similarities between CsA and its analogues, it can be assumed that the adequate cell permeability and oral absorption demonstrated for CsA, due to the formation of intramolecular hydrogen bonds, could be enabled for the earlier analogues as well [87, 88].

Three natural product-based cyclic peptides are now in different stages of clinical trials for the treatment of *Clostridium difficile* infections. *C. difficile* causes severe gut inflammation and diarrhea in infected patients. Although several drugs are available as first-line treatment (e.g., metronidazole, vancomycin, fidaxomicin), they are inadequate to prevent infection recurrences [89]. The new thiazolyl peptide LFF571 (**3**; Table 16.9), derived from the natural antibiotic GE2270, is now in phase II clinical trials for the treatment of *C. difficile*–associated diarrhea (CDAD). Compound **3** is the result of structure–activity relationship (SAR) studies performed on a series of 4-aminothyazolyl analogues of GE2270 in order to improve antibacterial activity and enhance aqueous solubility with respect to the parent natural product. The cyclohexylurethane-containing diacid derivative **3** displays antibacterial activity *in vitro* across a panel of Gram-positive bacteria and shows *in vitro* and *in vivo* potency. The diacid moiety proved to be essential to increase aqueous solubility (12 mg/ml at pH = 7.4) and reduce oral absorption, thus resulting in minimal oral bioavailability ($F < 0.1\%$ in rats) [90]. Compound **3** was also evaluated in infected hamsters, displaying limited systemic exposure (due to poor absorption) but high intestinal exposure, essential for treating infections involving the intestine [91].

---
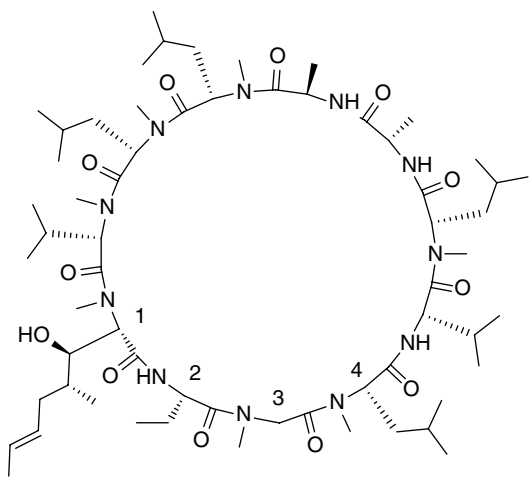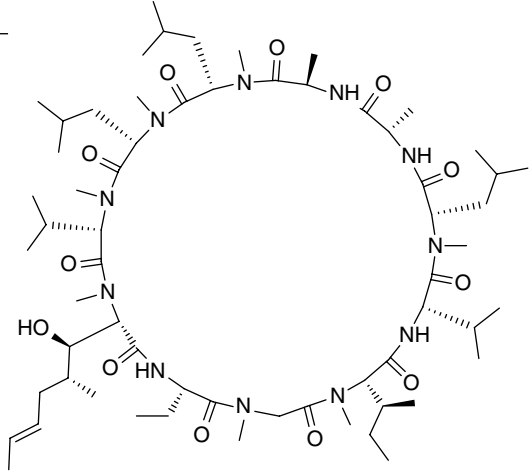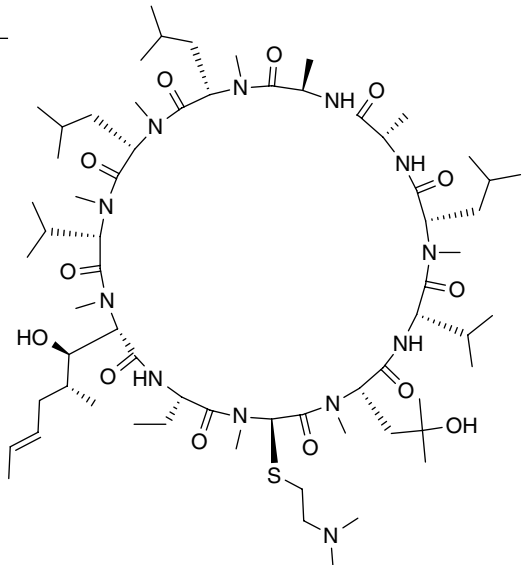
1 P_{app} refers to apparent permeability.

Table 16.7 Macrocyclic drugs of the lactam bridge cyclic peptide subclass.

Compound name	Structure	Therapeutic area	Oral	Clinical phase	HBD	PSA	MW	cLog$P$
Bremelanotide (PT-141)		Endocrinology	No	III	15	407	1025	−1.8
Melanotan II[a] (MT2)		Dermatology	No	Discontinued	16	385	1024	−2.7
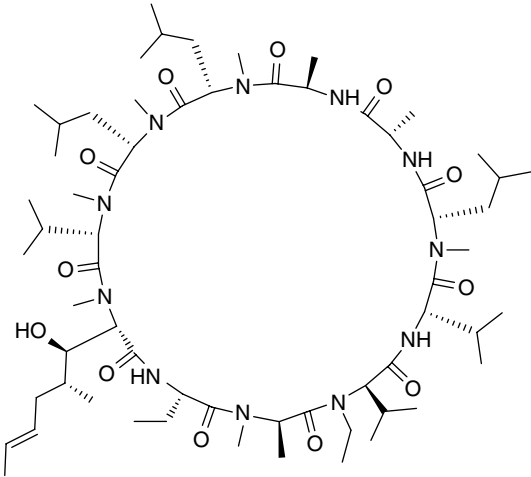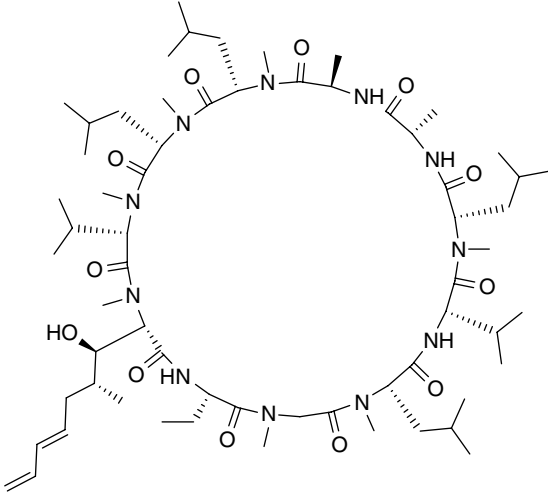
[a] The discontinued cyclic peptide MT2 is included for comparison to its analogue.

Table 16.8 Orally administered CsA analogues in clinical development.

Compound name	Structure	Therapeutic area	Oral	Clinical phase	HBD	PSA	MW	*cLogP*
Cyclosporine A (CsA)[a]		Immunology	Yes	Approved	5	290	1203	14.4
NIM811 **1**		Infection	Yes	II	5	279	1203	3.7
SCY-635 **2**		Infection	Yes	II	6	314	1322	13.1

(*Continued*)

Table 16.8 (Continued)

Compound name	Structure	Therapeutic area	Oral	Clinical phase	HBD	PSA	MW	cLogP
Alisporivir (UNIL025, DEB025)		Infection	Yes	III	5	279	1217	4.2
Voclosporin (ISA 247)		Immunology	Yes	III	5	290	1215	14.5

a The approved cyclic peptide cyclosporine A is included for comparison to its analogues.

NVB302 (**4**; Table 16.9) is a semisynthetic derivative of deoxyactagardine B (DAB), a type B lantibiotic. Compound **4** proved to be stable in the gastrointestinal tract and efficacious in a hamster caecitis model [92]. The thioether-bridged macrocycle is poorly absorbed following oral administration, thus resulting in optimal concentration at the site of infection. **4** was shown to be selective against *C. difficile* over the predominantly Gram-negative normal gut flora, potentially diminishing the chance for recurrent infections [92].

Surotomycin (CB-183, 315; Table 16.9) is a novel oral cyclic lipopeptide now in phase III clinical trials for the treatment of CDAD. Surotomycin works by disrupting the bacterial membrane potential, and *in vitro* data indi-

cate that it is less toxic to gastrointestinal flora than vancomycin. In December 2012, the macrocyclic compound received "qualified infectious disease product" (QIDP) status from the FDA, making it eligible for priority review, fast-track status, and a 5-year post-approval exclusivity. Surotomycin displays good selectivity *in vitro*, low resistance development, *in vivo* efficacy in the hamster infection model, and low oral bioavailability ($F < 1\%$) [93–96].

16.4.3 Macrolides and Ansamycins
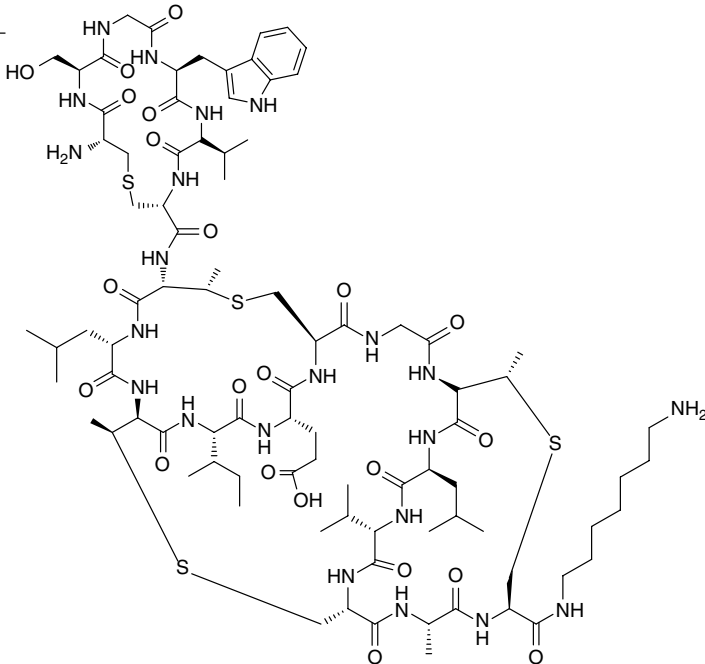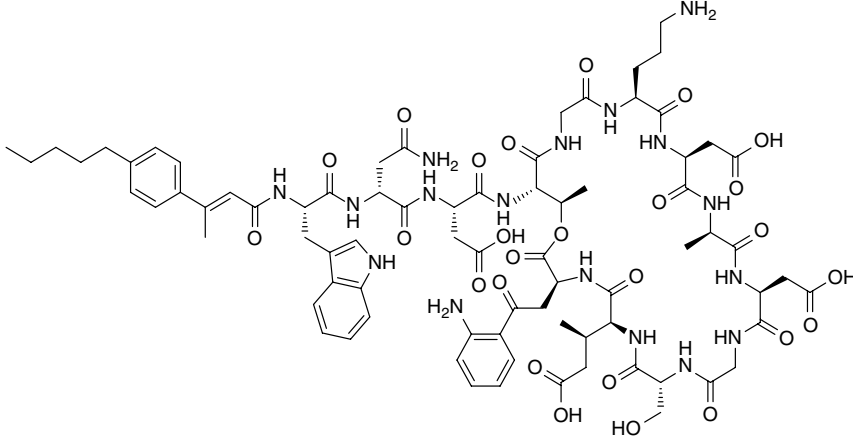
Only eight macrocycles currently in clinical trials belong to the macrolide and ansamycin chemical classes

Table 16.9 Macrocycles in the *Clostridium difficile* drug pipeline.

Compound name	Structure	Therapeutic area	Oral	Clinical phase	HBD	PSA	MW	cLogP
LFF571 **3**		Infection	No	II	8	539	1366	3.5

(*Continued*)

Table 16.9 (Continued)

Compound name	Structure	Therapeutic area	Oral	Clinical phase	HBD	PSA	MW	cLogP
NVB302 **4**		Infection	No	I	24	678	1987	−5.1
Surotomycin (CB-183,315)		Infection	No	III	22	702	1681	−5.7

($N = 5$ and $N = 3$, respectively) and are equally distributed between oral and parenteral administration (Figure 16.4b). Due to their structural similarity to other marketed macrocycles, ridaforolimus, solithromycin, rifalazil, rifamycin SV, and retaspimycin represent interesting case studies for a better understanding of the influence of structural features on pharmacokinetics (Table 16.10). Ridaforolimus, the dimethylphosphinate analogue of sirolimus (Table 16.6), is undergoing clinical development as an anticancer macrolide, belonging to the subclass of rapamycins. The dimethylphosphinate group increases its solubility and allows for both oral and intravenous administration [97, 98]. Solithromycin is a member of the ketolide subclass of macrolides. It is an acid-stable erythronolide antibiotic, which is orally administered and rapidly absorbed [99] and has been demonstrated to be safer than the first approved ketolide (telithromycin) due to the presence of a substituted 1,2,3-triazol-1-yl side chain [100].

On the other hand, telithromycin displays a 4-pyridin-3-imidazol-1-yl group, which is thought to be responsible for its antagonist action on nicotinic acetylcholine receptors at the neuromuscular junction ($\alpha_3\beta_2$ and NMJ), the ciliary ganglion of the eye ($\alpha_3\beta_4$ and α_7), and the vagus nerve (α_7). As a result, treatment with telithromycin causes myasthenia gravis, visual disturbance, and liver failure [101].

Rifamycin SV is a semisynthetic ansamycin antibiotic that is poorly absorbed in the intestine and thus suitable for the treatment of traveler's diarrhea caused by *E. coli.* Rifamycin SV, already approved for parenteral use, is now in phase III clinical trials as a controlled-release oral tablet pharmaceutical form using a multimatrix (MMX) structure. The pH-resistant coating allows the release of the active pharmaceutical ingredients only when the tablets have reached the cecum, avoiding unwanted effects on the saprophytic beneficial bacterial flora living in the upper portions of the gastrointestinal tract. As a result, this pharmaceutical form increases rifamycin SV's efficacy due to direct topical release [102].

Rifalazil is also an oral ansamycin antibiotic, derived from rifamycin SV, which is being developed for the treatment of chlamydia, diarrhea, and tuberculosis. The presence of a benzoxazine ring makes rifalazil more lipophilic than the other orally administered ansamycin drugs (Table 16.5). The high lipophilicity provides good penetration across lipid barriers, thus resulting in high distribution into blood cells, tissues, and organs as proven in both preclinical (rats and dogs) and human studies [103]. Rifalazil's lipophilic nature can also explain the extensive level of plasma lipoprotein binding, resulting in a very long $t_{1/2}$ (~100 h) allowing once weekly dosing [104].

16.5 *De Novo* Designed Macrocycles
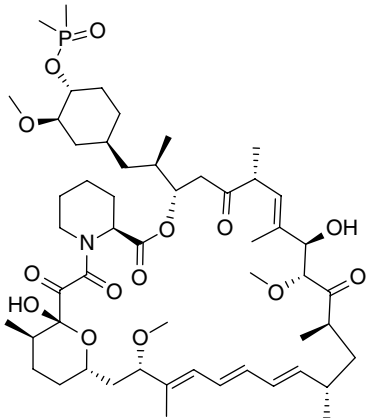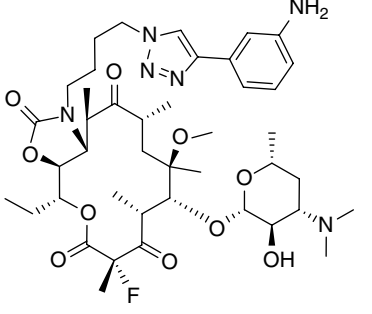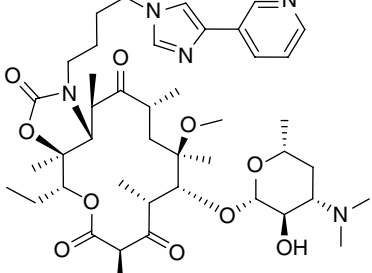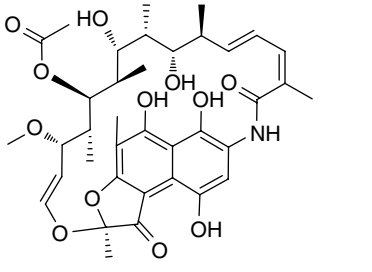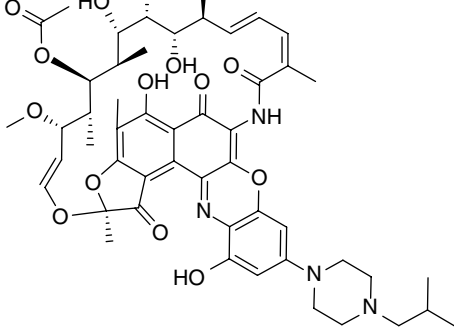
16.5.1 Protease and Polymerase Inhibitors

Boceprevir [105, 106] and telaprevir [107–109] are first-generation covalent inhibitors of the viral HCV nonstructural 3/4a serine protease (NS3/4a) protease. The two drugs are administered orally in combination with ribavirin and PEG-IFN for the treatment of chronic genotype 1 HCV infections. Severe side effects (e.g., neutropenia, thrombocytopenia, depression) [110] and the rapid emergence of resistant mutants with this triple combination therapy have inspired the development of a second generation of linear (asunaprevir [111], faldaprevir [112]) and macrocyclic (grazoprevir [113], simeprevir [114], paritaprevir [115], GS-9256 [116], vaniprevir [117], danoprevir [118], furaprevir [119] MK-2748, MK-6325 [120]) non-covalent inhibitors, now in different stages of clinical trials.

The structures of the new compounds were inspired by the NS3 macrocyclic inhibitor ciluprevir (BILN 2061; Table 16.11), which was halted in clinical development due to cardiac toxicity at high doses in Rhesus monkeys [121–130]. Macrocyclic HCV inhibitors have proven more potent than their linear analogues due to the reduction of conformational entropic loss upon binding to the protease. All but one (GS-9256) NS3/4a protease inhibitor display an acylsulfonamide-linked P1 moiety and differ in terms of hydrophobic P3 side chain, P4 capping group, and P2 heterocyclic substituents. Three of the second-generation inhibitors (grazoprevir [131], simeprevir [132], and paritaprevir [133]) recently received FDA approval for the treatment of chronic genotype 1 HCV infections (Table 16.11). Simeprevir is the only compound of the series bearing a trisubstituted cyclopentane instead of a substituted hydroxyproline as a P2 structural element. It has good passive diffusion in Caco-2 monolayer ($P_{app} = 8 \times 10^{-6}$ cm/s) and variable oral bioavailability among species, ranging from 2.5% in rabbits to 88% in monkeys. *In vitro* studies indicate that simeprevir is a substrate for P-gp, efflux (i.e., MRP2, BRCP1), and uptake (i.e., OATP1B1, OATP1B3, NTCP) pumps and is extensively bound to plasma proteins (>99.9%) [134].

Paritaprevir displays good passive permeability properties (Caco-2 P_{app} ranges from 6.7 to 9.8×10^{-6} cm/s) and high protein binding (>97%) [135]. It is also a substrate for efflux (i.e., MDR-1, BCRP) and uptake (i.e., OATP1B1, OATP1B3) transporters and shows moderate permeability *in vitro*, resulting in low bioavailability. Oral absorption can be increased (from 15 to 51% in rats) by coadministration with ritonavir due to inhibition of both cytochrome P450 (CYP450)-mediated first-pass metabolism and efflux transporters [135]. Oral bioavailability

Table 16.10 Macrolides and ansamycins in clinical development.

Compound name	Structure	Therapeutic area	Oral	Clinical phase	HBD	PSA	MW	*cLogP*
Ridaforolimus (AP23573, deforolimus, MK 8669)		Oncology	Yes	Preregistration	2	209	990	7.2
Solithromycin (CEM 101, OP-1068)		Infection	Yes	Preregistration	3	197	831	3.2
Telithromycin[a]		Infection	Yes	Approved	1	163	812	3.8
Rifamycin SV		Infection	Yes	III[b]	6	201	698	4.2
Rifalazil (ABI 1648, KRM 1648, PA 1648, AMI-1648)		Infection	Yes	III	5	235	941	8.2

[a] The approved ketolide telithromycin is included for comparison to solithromycin.
[b] Phase III clinical trial is referred to the controlled-released oral tablet pharmaceutical form.

Table 16.11 Macrocyclic NS3/4a and NS5B inhibitors in clinical development.

Compound name	Structure	Therapeutic area	Oral	Clinical phase	HBD	PSA	MW	*cLogP*
Ciluprevir (BILN2061)								
Grazoprevir[a]		Infection	Yes	Approved	3	203	767	6.3
Simeprevir[a]		Infection	Yes	Approved	2	157	750	5.3
Paritaprevir[a]		Infection	Yes	Approved	3	190	766	2.7

(*Continued*)

Table 16.11 (Continued)
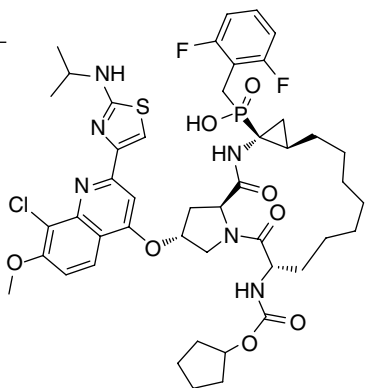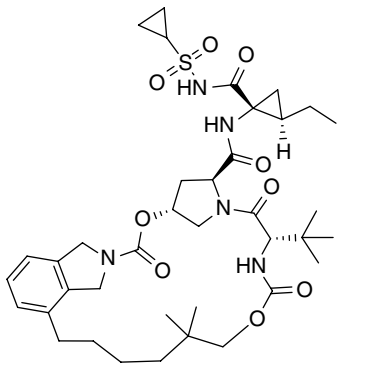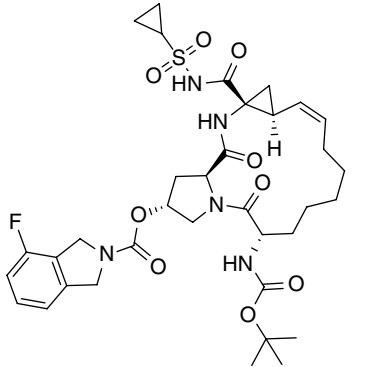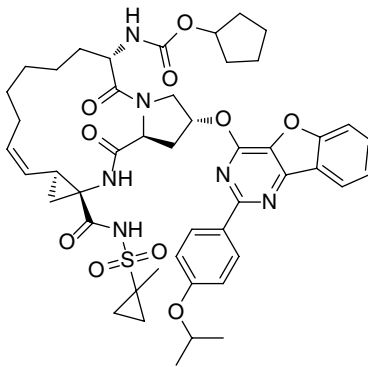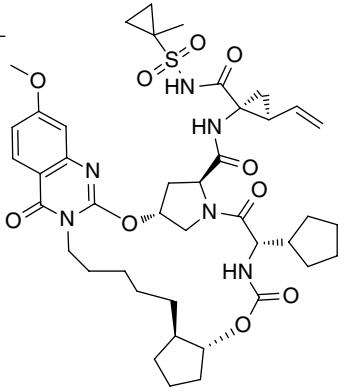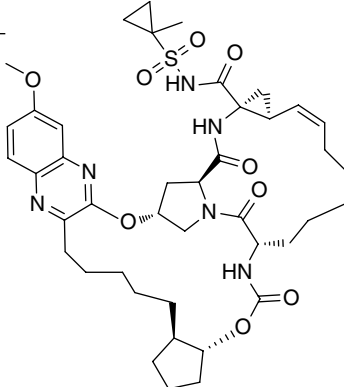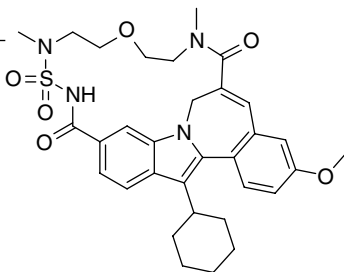
Compound name	Structure	Therapeutic area	Oral	Clinical phase	HBD	PSA	MW	cLogP
GS-9256 **5**		Infection	Yes	II b	4	181	958	8.1
Vaniprevir (MK 7009)		Infection	Yes	III	3	193	758	7.2
Danoprevir (R7227, ITMN-191)		Infection	Yes	III	3	193	732	5.6
Furaprevir (TG-2349)		Infection	Yes	II	3	208	897	6.5

Table 16.11 (Continued)

Compound name	Structure	Therapeutic area	Oral	Clinical phase	HBD	PSA	MW	*cLogP*
MK-2748 **6**		Infection	Yes	I	3	202	837	4.3
MK-6325 **7**		Infection	Yes	I	3	195	821	4.8
TMC647055 **8**		Infection	Yes	II	1	110	607	6.5

[a] The approved drugs grazoprevir, simeprevir, and paritaprevir are included for comparison with the other NS3/4a HCV inhibitors.

of paritaprevir can be enhanced by food consumption: relative to fasting conditions, administration of the drug with a moderate-fat meal (approximately 600 kcal; 20–30% calories from fat) or with a high-fat meal (~900 kcal, 60% calories from fat) increases the mean systemic exposure by 211 and 180%, respectively [136, 137].

While paritaprevir and simeprevir contain an olefin tether connecting the P1 and P3 moieties, grazoprevir (Table 16.11) is a P2–P4 macrocycle bearing an ether-linked quinoxaline P2 moiety and showing potent activity against several HCV genotypes and resistant mutants. Following oral administration, grazoprevir demonstrated moderate bioavailability in rats and dogs (12 and 13%, respectively) but, when tested in HCV-infected chimpanzees, displayed excellent 24 h liver concentration, resulting in good *in vivo* efficacy [138, 139].

GS-9256 (**5**; Table 16.11) is the only NS3/4A protease inhibitor containing a benzyl phosphinic acid moiety at P1 instead of the typical acylsulfonamide group. Compound **5** is the result of SAR studies performed on a series of benzyl phosphinic acid derivatives of ciluprevir in order to increase its permeability and bioavailability. The 2,6-difluoro benzyl substitution proved effective to enhance Caco-2 permeability, and the addition of a chlorine atom at position 8 of the quinoline ring at P2 resulted in an 18-fold increase of oral bioavailability ($F = 21\%$) in dogs with respect to the unsubstituted ring [140, 141].

Danoprevir and vaniprevir (Table 16.11) both display a carbamate-linked isoindoline moiety at P2, but the macrocyclization topology is different: danoprevir possesses a P1–P3 macrocyclization, whereas vaniprevir contains a P2–P4 macrocycle and a saturated P1 side chain. Danoprevir possesses good oral absorption, and, similarly to paritaprevir, its bioavailability can be increased by food consumption. Danoprevir is metabolized by cytochrome P450-3A4 subtype (CYP3A4), therefore, coadministration with CYP3A4 inhibitors such as ritonavir can greatly improve its pharmacokinetic profile [142–144]. The pharmacokinetic profile of vaniprevir was measured in four different preclinical species: rats, dogs, rhesus monkeys, and chimpanzees, following both oral and intravenous administration. Plasma exposure and bioavailability proved to be, in both cases, poor for rats, dogs, and rhesus monkeys but excellent for chimpanzees, probably suggesting species differences in active transport of the compound. For all four species, the significant liver concentrations observed at 24 h post-dosing were determinant in the selection of vaniprevir for clinical development [145, 146].

Furaprevir (TG-2349; Table 16.11) is a novel, potent, and selective pan-genotypic HCV inhibitor now in phase II clinical trials. Similarly to danoprevir, paritaprevir, and simeprevir, it possesses a P1–P3 macrocycle and is substi-

tuted at P2 with a 2-(4-isopropoxyphenyl)[1]benzofuro[3,2-*d*]pyrimidin-4-yl- moiety. To date, furaprevir proved to be well tolerated without affecting ECG or other vital parameters after dosing. It is slowly absorbed ($T_{max} \sim 6$ h), but, analogously to danoprevir and paritaprevir, fed conditions increases its AUC and maximum (serum) concentration (C_{max}). Three days of treatment reduce to $10^{-3}/10^{-4}$ the viral load in patient blood, and furaprevir is active also against many different drug resistance mutations (e.g., D168V, D168Q, R155K) [147, 148].
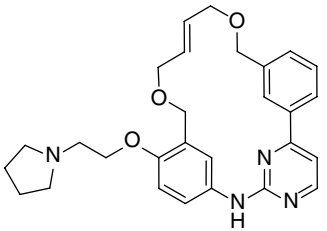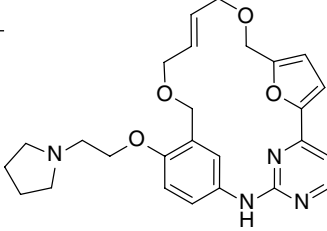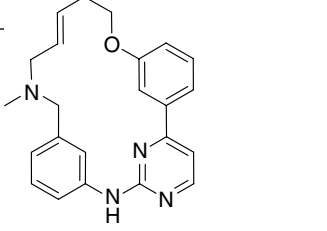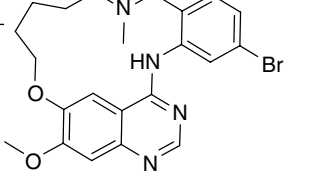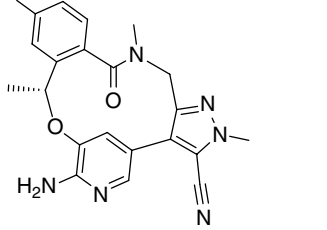
Scientists at Merck, Sharp, and Dohme laboratories recently reported the discovery of the two new NS3/4A protease inhibitors MK-2748 **6** and MK-6325 **7**, which both possess broad genotype (i.e., gt1b, gt3a, gt1b) and mutant (i.e., R155K, A156T, A156V, D168Y) spectrum as well as favorable pharmacokinetic properties (Table 16.11). Compounds **6** and **7** both contain a cyclopentanol carbamate P2–P4 linker and a methylcyclopropyl acylsulfonamide at P1. The P2-quinazolinone macrocycle **6** showed moderate oral bioavailability in preclinical species (27% in dog, ~40% in rat at 3 and 5 mg/kg, respectively) and short $t_{1/2}$ (1.9–2.5 h), while the 18-/15-membered-bis-macrocyle **7** displayed low bioavailability (~8% in rat and 12% in dog at 5 mg/kg) but higher $t_{1/2}$ (2.3–3.8 h).

TMC647055 (**8**; Table 16.11) is a macrocyclic indole inhibitor of the HCV NS5B polymerase in multiple phase II clinical trials in combination with simeprevir. TMC647055 was obtained by lead optimization of a 6-carboxylic acid indole via a macrocyclization strategy in order to (i) improve permeability, (ii) increase metabolic stability, and (iii) provide inhibitors with superior potency and pharmacokinetic profiles due to the effect of conformational restriction. Indeed, **8** displayed high distribution to the liver, moderate clearance, and very good bioavailability in rats and dogs (66 and 87%, respectively) [149, 150].

16.5.2 Kinase Inhibitors

Five macrocyclic kinase inhibitors, each displaying physicochemical properties very similar to oral small molecules (e.g., MW < 500, PSA < 140 Å and HBD < 2), are now in different stages of clinical trials (Table 16.12). Pacritinib is a novel selective Janus-associated kinase 2 (JAK2) and FMS-like tyrosine kinase 3 (FLT3) inhibitor now in phase III clinical trials for the treatment of myelofibrosis, acute myeloid leukemia (AML), and lymphoma [151, 152]. Preclinical studies revealed high permeability (Caco-2 $P_{app} = 16 \times 10^{-6}$ cm/s), rapid to moderate absorption ($t_{max} = 1$, 4, and 2 h, in mice, rats, and dogs, respectively) and variable bioavailability (39, 24, and 10%, in mice, rats, and dogs, respectively). Pacritinib is not a P-gp substrate and is >99% bound to plasma proteins both in preclinical

Table 16.12 Macrocyclic kinase inhibitors in clinical development.

Compound name	Structure	Therapeutic area	Oral	Clinical phase	HBD	PSA	MW	*cLogP*
Pacritinib (ONX 0803, SB1518)		Oncology	Yes	III	1	62	473	4.3
SB1578/CT1578 9		Immunology	Yes	I	1	72	463	3.7
SB1317/TG02 10		Oncology	Yes	I	1	45	373	5.4
JNJ 26483327 11		Oncology	Yes	I	1	54	457	6.6
Lorlatinib (PF-06463922)		Oncology	Yes	I/II	1	110	406	1.6

species and humans [153–155]. The recent patient deaths due to cardiac arrest, cardiac failure, and intracranial hemorrhage observed in the patient group exposed to a pacritinib dosing algorithm, induced FDA to place a clinical hold on the drug for myelofibrosis trials [156]. The JAK2, FLT3, and M-CSF (macrophage colony-stimulating factor) kinase inhibitor SB 1578 (**9**; Table 16.12) is the result of an isosteric replacement of one of the phenyl rings of pacritinib with a furan. *In vitro* studies showed **9** had high solubility, permeability (Caco-2 $P_{app} = 24.8 \times 10^{-6}$ cm/s), and plasma protein binding (~99% in humans and monkeys, 87.3–87.5% in mice, rats and dogs). Further, **9** is not a substrate for P-gp, thus showing rapid to moderately fast absorption (t_{max} 0.5–3 h) in preclinical species. The oral bioavailability that resulted was moderate in mice and monkeys (32 and 34%, respectively) and poor in rats and dogs (6%) [157–159]. The JAK2, FLT3, cyclin-dependent kinase (CDK) inhibitor SB1317/TG02 (**10**; Table 16.12) has completed phase I clinical trials for the treatment of hematological malignancies. Compound **10**, due to its basic and hydrophobic nature, displays very high permeability *in vitro* (Caco-2 $P_{app} = 28 \times 10^{-6}$ cm/s) but low to moderate bioavailability *in vivo* (3.8, 24, and 37%, respectively, in rats, mice, and dogs) [159, 160].

JNJ26483327 (**11**; Table 16.12) is an oral, potent, multitargeted tyrosine kinase inhibitor in phase I clinical trials in patients with advanced solid tumors. In preclinical studies, a twice daily oral administration resulted in a bioavailability of ~80% in mice. In humans, **11** is rapidly absorbed after oral administration but not in a dose–proportional relationship [161]. Lorlatinib (PF-06463922) (Table 16.12) is a macrocyclic anaplastic lymphoma kinase (ALK) and c-ros oncogene 1 (ROS1) inhibitor in phase I/II clinical trial for non-small cell lung carcinoma (NSCLC) and associated brain metastasis. It displays broad-spectrum potency, including against resistant mutants, high selectivity and high distribution to the central nervous system (AUC CSF/plasma and AUC brain/plasma 0.31 and 0.21, respectively). Preclinical studies performed in rat showed an outstanding pharmacokinetic profile: lorlatinib displayed low plasma clearance, P-gp efflux, and protein binding as well as 100% bioavailability after oral administration (see Chapter 18 for a complete case study) [162].

16.6 Overview and Conclusions

The number (127), chemical diversity (9 structural classes), and widespread disease applications (12 disease areas) of the marketed and clinical stage macrocycles analyzed here greatly exemplify their therapeutic importance.

Infection and oncology are dominant indications for macrocycles, due to the historical focus on typical natural product classes (e.g., macrolides and ansamycins). Nevertheless, virtually all other major therapeutic areas feature at least one macrocyclic drug and clinical compound, thus adding to their overall therapeutic versatility.

Macrocycles can be orally administered, as demonstrated by 30% of marketed macrocycles and 41% of clinical candidates. While the orally administered macrocycles tend to be more lipophilic than their parenterally administered counterparts, a better understanding of the properties and structural features that confer oral bioavailability, tissue penetration, and cell permeability is required (see Chapter 3). This picture is further blurred by confounding effects on cellular membrane transporters and metabolic pathways, since the majority of macrocycles are reported substrates for these systems. This, in turn, increases the difficulties in discerning pharmacokinetic *in vitro–in vivo* relationships and understanding preclinical species variability, thus posing an additional hurdle to development.

Natural products, bacterial metabolites, and endogenous hormones still represent the major (87%) sources of macrocyclic drugs and clinical compounds. Here, the macrocyclic elements are typically already present in the chemical starting points and the macrocyclic skeleton, and its side chains are normally modified during optimization. It is, however, intriguing to witness the more recent use of macrocyclization strategies on "linear" small molecule classes. This has yielded a large number of macrocyclic protease, polymerase and kinase inhibitors, of which 3 are approved drugs and 13 are in different stages of clinical development. Here, it is interesting to note the substantial use of structural information on the bioactive conformation of the linear starting point, derived from co-crystallized ligand–protein complexes, to inspire and inform the rational design and synthesis of possible macrocycles.

The macrocyclic drugs and clinical candidates discussed herein represent an incredible source of inspiration to medicinal chemists. They have revealed that even minute chemical changes can drastically influence their overall pharmacokinetic profile and route of administration, all the way to therapeutic application, thus making it challenging to derive generalized principles for their design and optimization outside the confines of a specific compound class.

Nevertheless, more widespread use of *de novo* designed macrocycles as a complement to a more systematic exploration of natural macrocycles and the future availability of biologically relevant macrocyclic compound libraries (see Chapters 6 and 7) are expected to result in a further expansion of the available macrocyclic chemical

space. This, fueled by the renewed interest in macrocycles [14–20] and recent improvements in synthetic macrocyclization methodologies (see Part III) [21–24], will enable the practical investigation of macrocycles' advantages and limitations.

Appendix   16.A

16.A.1   Methods

Informations about macrocyclic drugs (macrocycle's size ≥ 12 atoms) were collected using the GOSTAR [163]. Contrast agents, polypeptides with >30 amino acids, drugs for veterinary use, discontinued or not yet on the market, were excluded from the analysis.

The 74 members collected were classified according to the nature of their chemical structure (e.g., being a cyclic peptide, an alkaloid, etc.); the two largest classes (i.e., cyclic peptides and macrolides) were further subclassified according to distinguishing structural features (e.g., glycopeptides, rapamycins, etc.).

MW, PSA, number of HBDs and cLog$P$ were calculated using ChemAxon (Marvin sketch version 15.3.2.0) [164]. Physicochemical properties were not calculated for those drugs consisting of a mixture of different chemical entities, that is, capreomycin, ivermectin, polymyxin B, porfimer, quinupristin/dalfopristin, teicoplanin for the approved drugs, and linopristin/flopristin for macrocycles in clinical trials.
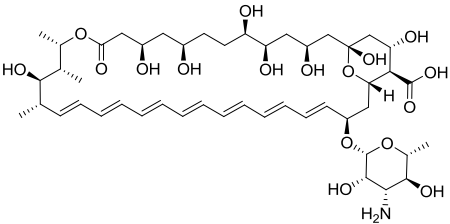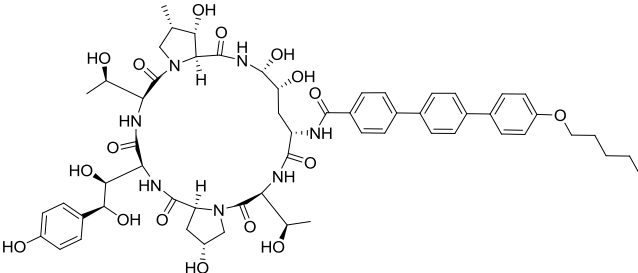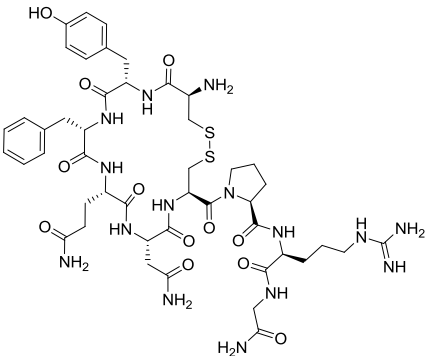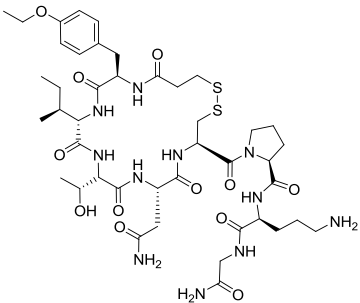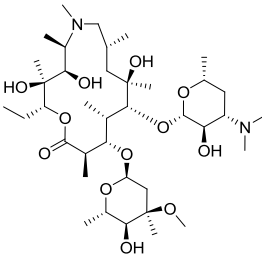
Using GOSTAR and/or literature, informations on the preferred route of administration were collected. Drugs administered orally and that require systemic absorption to exert their effect were considered as oral; drugs delivered by all the other routes were classified as parenteral, and drugs delivered orally but not absorbed systemically (i.e., drugs that exert their pharmacological action in the gastrointestinal tract) were annotated as parenteral.

Data on the human doses were extracted from GOSTAR and/or literature and converted to an average daily dose expressed in milligrams (mg).

Where possible, oral bioavailability (F) was obtained from the literature. To facilitate analysis, human F data were also binned to three categories (low: $F < 30\%$; medium: $30\% < F < 60\%$; and high: $F > 60\%$).

A dataset of macrocycles in clinical development was obtained in a similar manner using Adis R&D Insight [165]. The human dose was not included as this either had not been set or was not publically available for most of the clinical candidates.
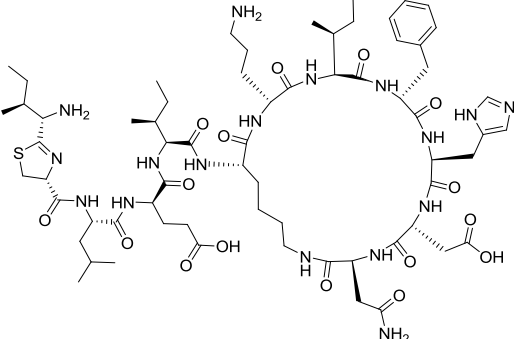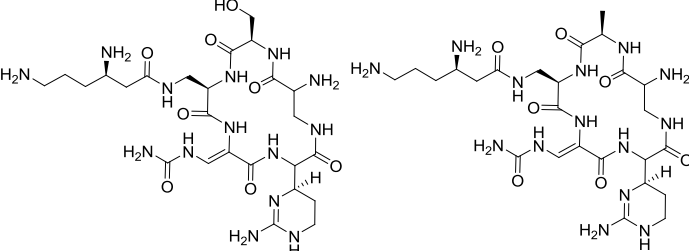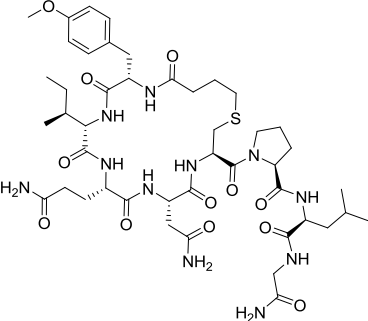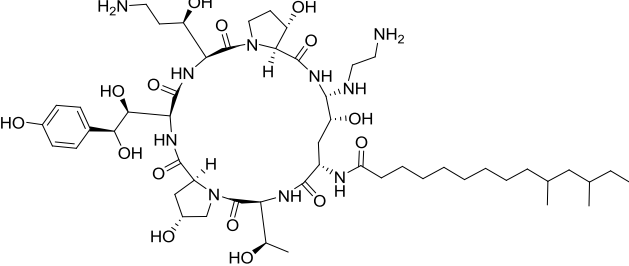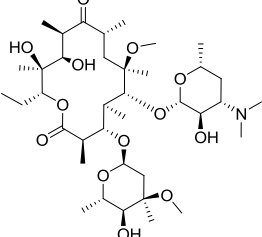
Table A.16.1 Registered macrocyclic-based drugs as of January 25, 2017.

Drug name	Structure	Class
Amphotericin b		Macrolide
Anidulafungin		Cyclic peptide
Argipressin		Cyclic peptide
Atosiban		Cyclic peptide
Azithromycin		Macrolide

Subclass	Therapeutic area	Oral	Avg dose (mg/day)	Human *F* (%)	Human *F* class	HBD	PSA	MW	*cLogP*
Polyene	Infection	No	44			13	348	924	−3.7
Echinocandin	Infection	No	200			14	416	1140	2.2
Disulfide bridge	Cardiovascular	No				20	505	1084	−3.8
Disulfide bridge	Gynecology	No				14	402	994	−0.1
Erythronolide	Infection	Yes	500	37	Med	5	186	749	2.6

(*Continued*)
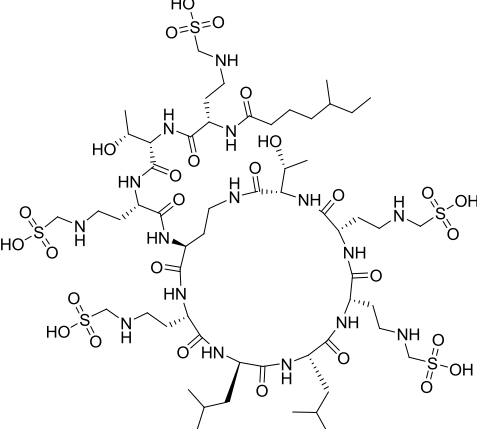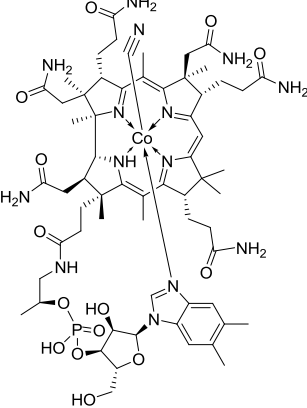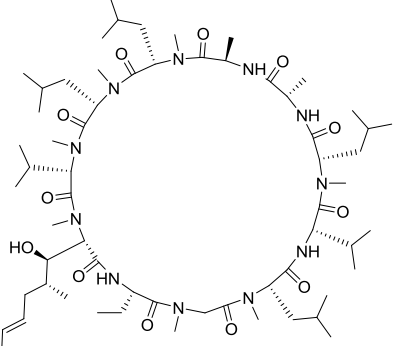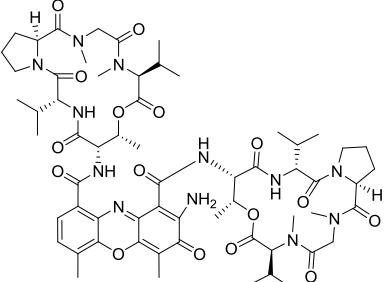
Table A.16.1 (Continued)

Drug name	Structure	Class
Bacitracin		Cyclic peptide
Capreomycin		Cyclic peptide
Carbetocin		Cyclic peptide
Caspofungin		Cyclic peptide
Clarithromycin		Macrolide

Subclass	Therapeutic area	Oral	Avg dose (mg/day)	Human F (%)	Human F class	HBD	PSA	MW	cLogP
Lactam bridge	Infection	No				20	579	1423	−2.1
Side chain modification	Infection	No	1000						
Thioether bridge	Gynecology	No	0.1			13	398	988	0
Echinocandin	Infection	No	120			18	454	1093	−2.9
Erythronolide	Infection	Yes	1000	55	Med	4	190	748	2.4

(*Continued*)
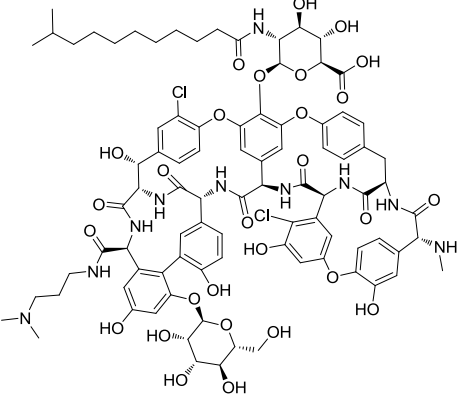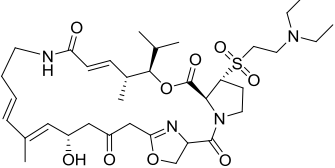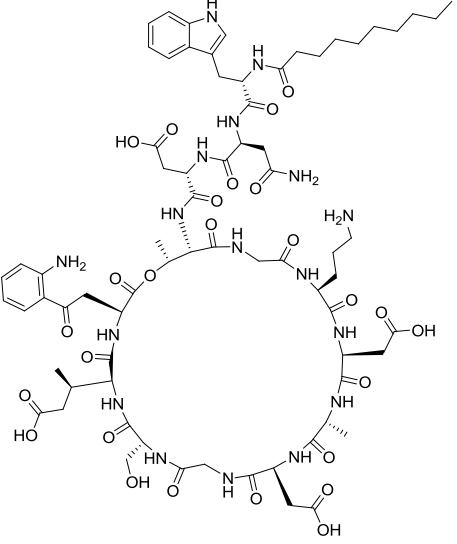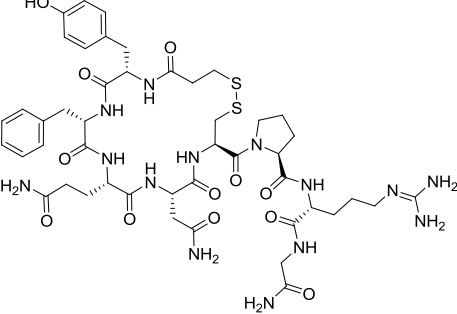
Table A.16.1 (Continued)

Drug name	Structure	Class
Colistimethate		Cyclic peptide
Cyanocobalamin		Porphyrin
Cyclosporine A		Cyclic peptide
Dactinomycin		Cyclic peptide

Subclass	Therapeutic area	Oral	Avg dose (mg/day)	Human *F* (%)	Human *F* class	HBD	PSA	MW	cLog*P*
Side chain modification	Infection	No	788			23	778	1640	−23.8
	Hematology	No	0.6			16	492	1355	−0.5
N-alkylated	Immunology	Yes	950	30	Med	5	290	1203	14.4
N-alkylated	Oncology	No	0.5			6	368	1255	8.1

(*Continued*)
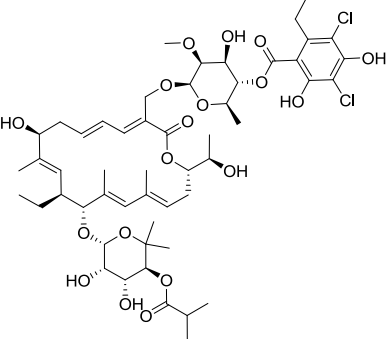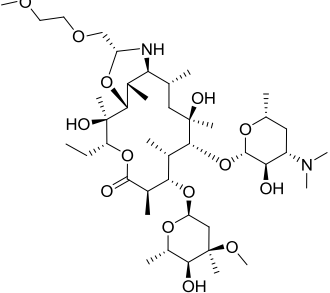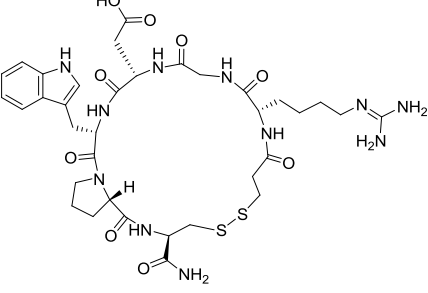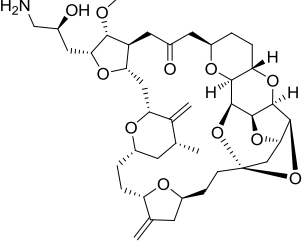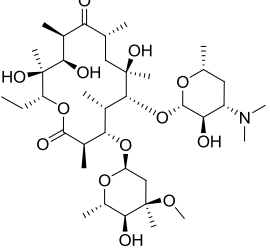
Table A.16.1 (Continued)

Drug name	Structure	Class
Dalbavancin		Cyclic peptide
Dalfopristin		Macrolide
Daptomycin		Cyclic peptide
Desmopressin		Cyclic peptide

Subclass	Therapeutic area	Oral	Avg dose (mg/day)	Human F (%)	Human F class	HBD	PSA	MW	cLogP
Glycopeptide	Infection	No	2000			21	564	1817	−1.5
Streptogramin	Infection	No	1313			2	178	691	1.4
Lipopeptide	Infection	No	280			25	774	1621	−2.4
Disulfide bridge	Cardiovascular	No	0.1			18	477	1069	−3.2

(*Continued*)

Table A.16.1 (Continued)

Drug name	Structure	Class
Difimicin		Macrolide
Dirithromycin		Macrolide
Eptifibatide		Cyclic peptide
Eribulin		Macrolide
Erythromycin		Macrolide

Subclass	Therapeutic area	Oral	Avg dose (mg/day)	Human *F* (%)	Human *F* class	HBD	PSA	MW	*cLogP*
Tiacumicin	Infection	No	400			7	284	1058	7.2
Erythronolide	Infection	Yes	500	10	Low	5	203	835	2.8
Disulfide bridge	Cardiovascular	No	13			13	350	832	−2.9
Halichondrin	Oncology	No	2.3			3	148	730	1.2
Erythronolide	Infection	Yes	2500	25	Low	5	203	734	1.6

(*Continued*)
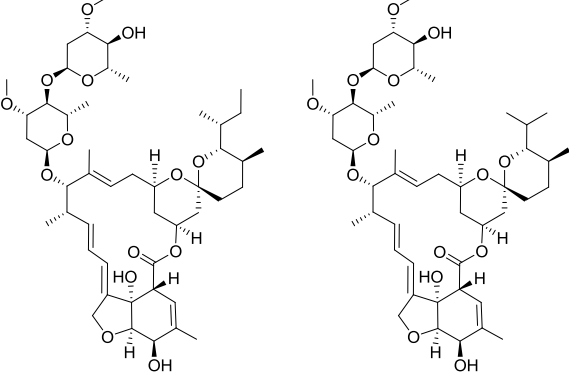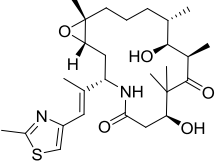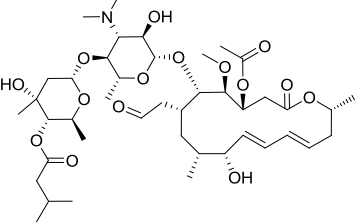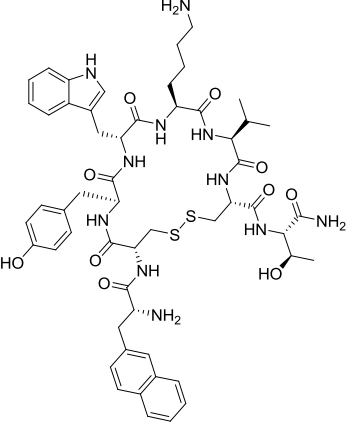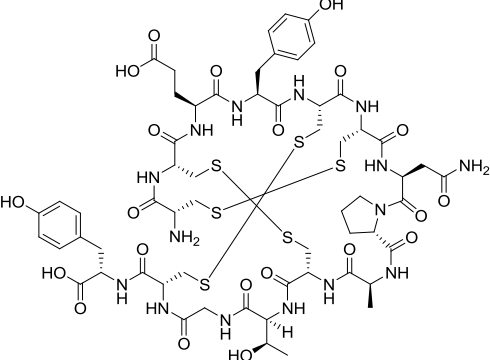
Table A.16.1 (Continued)

Drug name	Structure	Class
Erythromycin ethylsuccinate		Macrolide
Everolimus		Macrolide
Flurithromycin ethylsuccinate		Macrolide
Grazoprevir		"De *novo* designed"
Hydroxocobalamin		Porphyrin

Subclass	Therapeutic area	Oral	Avg dose (mg/day)	Human F (%)	Human F class	HBD	PSA	MW	cLog$P$
Erythronolide	Infection	Yes	500	55	Med	4	235	862	3.2
Rapamycin	Immunology	Yes	2.8	16	Low	3	213	958	7.1
Erythronolide	Infection	Yes	500			4	235	880	3.0
	Infection	Yes	100			3	203	767	6.3
	Hematology	No	0.6			17	507	1347	−1.2
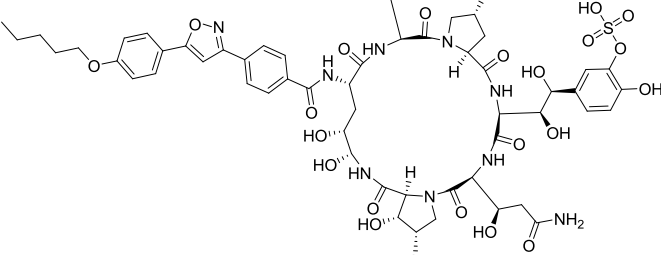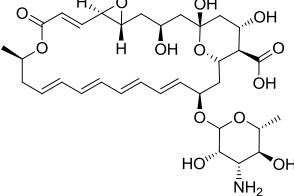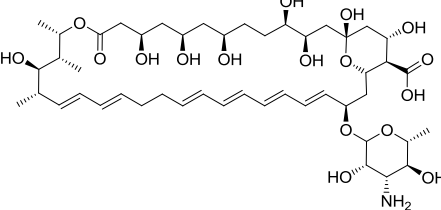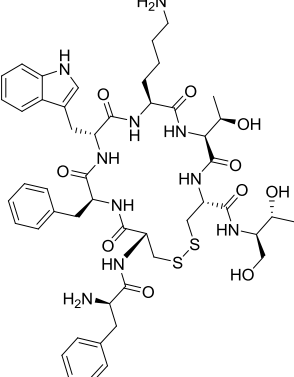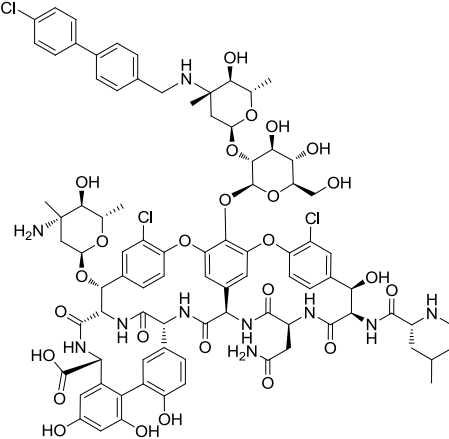
Drug name	Structure	Class
Ivermectin		Macrolide
Ixabepilone		Epothilone
Josamycin		Macrolide
Lanreotide		Cyclic peptide
Linaclotide		Cyclic peptide

Subclass	Therapeutic area	Oral	Avg dose (mg/day)	Human F (%)	Human F class	HBD	PSA	MW	cLog$P$
Avermectin	Infection	Yes	9	60	Med				
	Oncology	No	65			3	115	507	3.1
Leucomycin	Infection	Yes	1000	95	Hi	3	212	828	3.7
Disulfide bridge	Endocrinology	No				16	392	1096	3.4
Disulfide bridge	Gastrointestinal	No				19	638	1527	−3.1
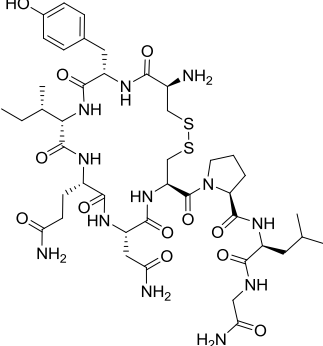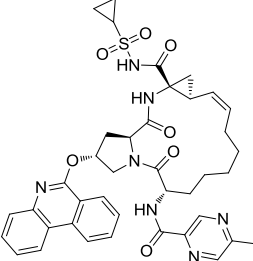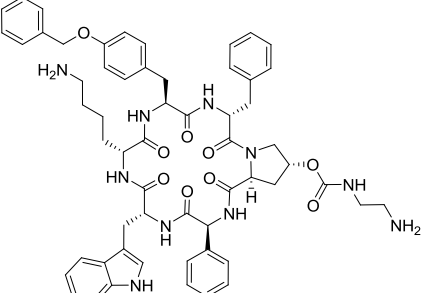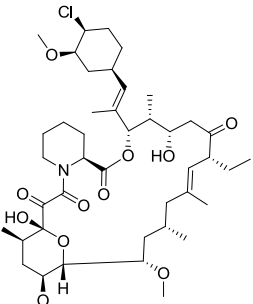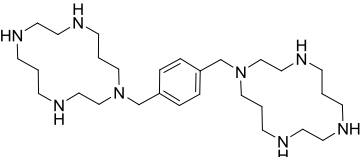
Table A.16.1 (Continued)

Drug name	Structure	Class
Micafungin		Cyclic peptide
Natamycin		Macrolide
Nystatin		Macrolide
Octreotide		Cyclic peptide
Oritavancin		Cyclic peptide

Subclass	Therapeutic area	Oral	Avg dose (mg/day)	Human *F* (%)	Human *F* class	HBD	PSA	MW	*cLogP*
Echinocandin	Infection	No	50			19	571	1272	−2.6
Polyene	Infection	No	8			8	244	666	−4.8
Polyene	Infection	No	100			12	325	924	−2.9
Disulfide bridge	Oncology	No	0.6			15	368	1019	2.5
Glycopeptide	Infection	No	1200			20	561	1793	−0.7
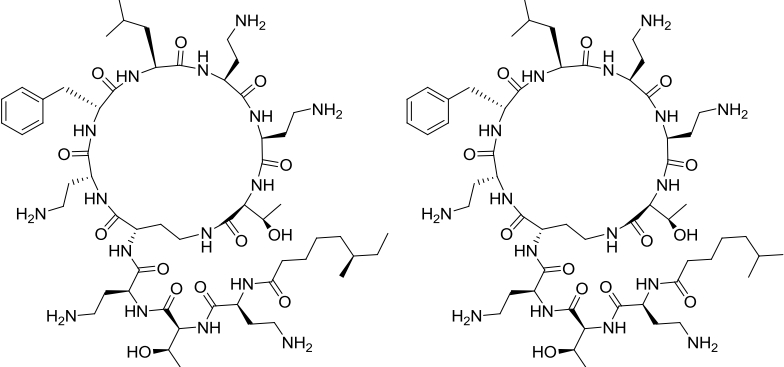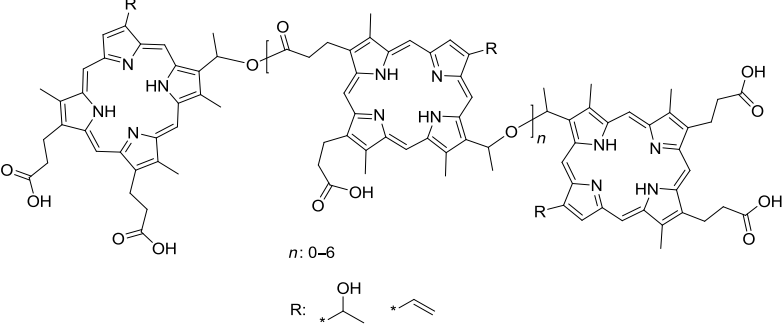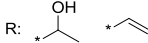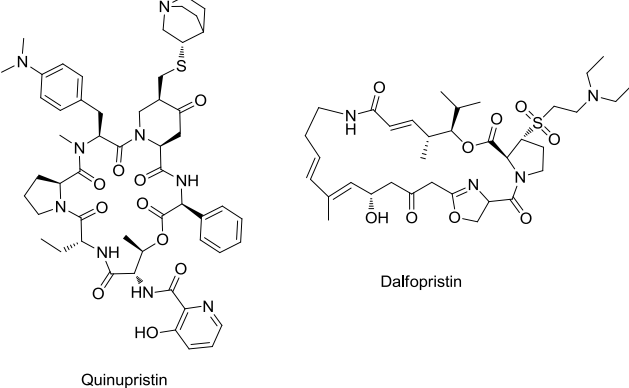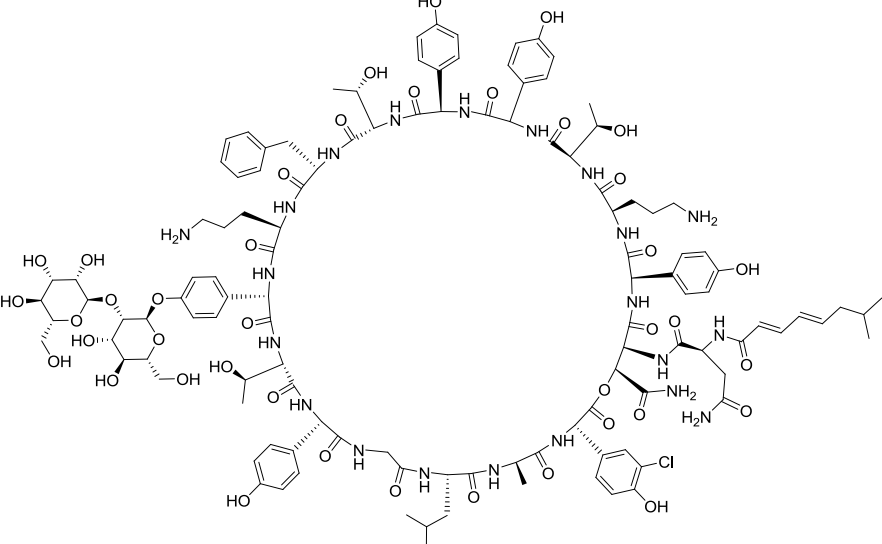
Table A.16.1 (Continued)

Drug name	Structure	Class
Oxytocin		Cyclic peptide
Paritaprevir		"*De novo* designed"
Pasireotide		Cyclic peptide
Pimecrolimus		Macrolide
Plerixafor		Bicyclam

Subclass	Therapeutic area	Oral	Avg dose (mg/day)	Human F (%)	Human F class	HBD	PSA	MW	cLogP
Disulfide bridge	Gynecology	No				16	439	1007	−0.7
	Infection	Yes	150			3	190	766	2.7
Side chain modification	Endocrinology	No	1			11	304	1047	6.7
Ascomycin	Dermatology	No				2	158	811	6.0
	Oncology	No	17			6	90	503	−0.3

(*Continued*)

Drug name	Structure	Class
Polymyxin B		Cyclic peptide
Porfimer	 *n*: 0–6 R:	Porphyrin
Quinupristin Dalfopristin (30/70 w/w)	 Dalfopristin Quinupristin	Macrolide
Ramoplanin		Cyclic peptide

Subclass	Therapeutic area	Oral	Avg dose (mg/day)	Human F (%)	Human F class	HBD	PSA	MW	cLogP
Lipopeptide	Infection	No							
	Oncology	No							
Streptogramin	Infection	No	500						
Depsipeptide	Infection	No				32	891	2144	0
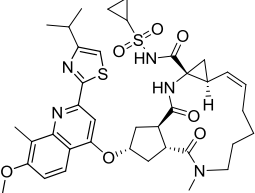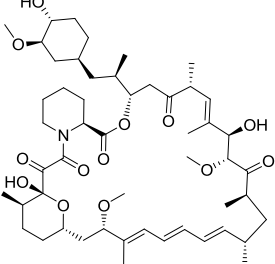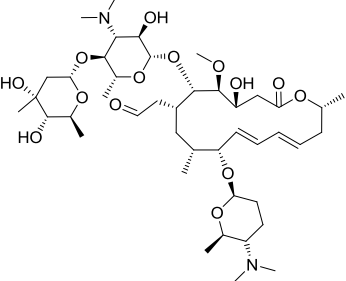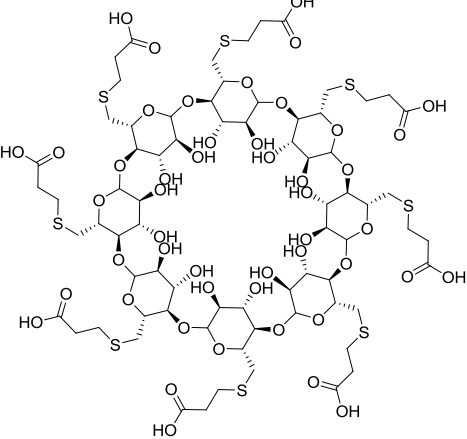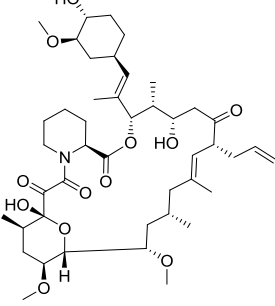
Drug name	Structure	Class
Rifabutin		Ansamycin
Rifampicin		Ansamycin
Rifapentine		Ansamycin
Rifaximin		Ansamycin
Rokitamycin		Macrolide
Romidepsin		Cyclic peptide
Roxithromycin		Macrolide

Subclass	Therapeutic area	Oral	Avg dose (mg/day)	Human F (%)	Human F class	HBD	PSA	MW	cLogP
Naphthoquinone	Infection	Yes	300	53	Med	5	217	847	4.7
Naphthoquinone	Infection	Yes	600	50	Med	6	234	823	3.7
Naphthoquinone	Infection	Yes	750	70	Hi	5	211	847	5.1
Naphthoquinone	Infection	No	600			5	206	786	7.2
Leucomycin	Infection	Yes	300			3	212	828	3.8
Depsipeptide	Oncology	No	23			4	158	541	3.4
Erythronolide	Infection	Yes	300	78	Hi	5	224	837	2.3
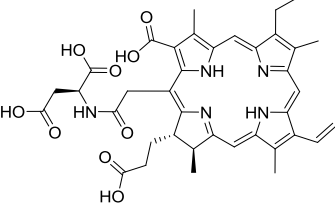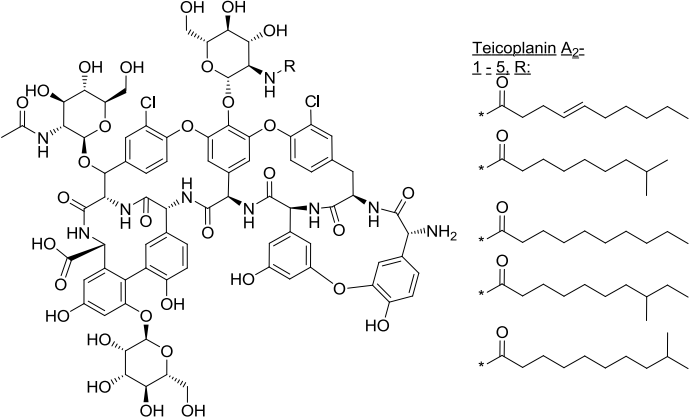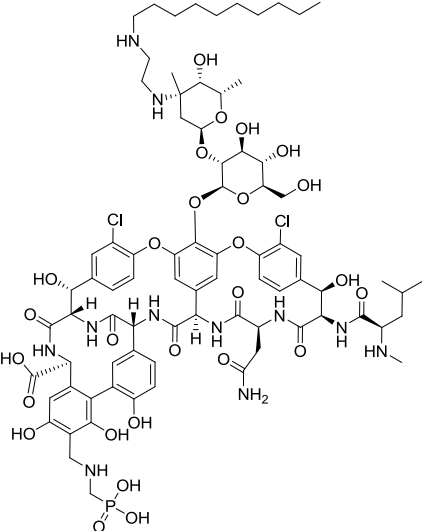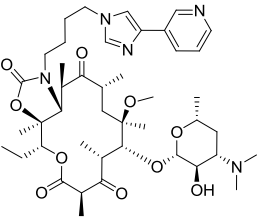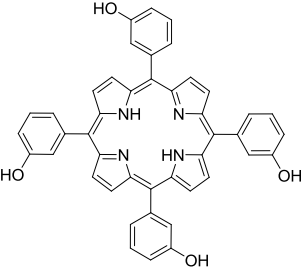
Table A.16.1 (Continued)

Drug name	Structure	Class
Simeprevir		*"De novo designed"*
Sirolimus		Macrolide
Spiramycin		Macrolide
Sugammadex		Cyclodextrin
Tacrolimus		Macrolide

Subclass	Therapeutic area	Oral	Avg dose (mg/day)	Human F (%)	Human F class	HBD	PSA	MW	cLogP
	Infection	Yes	150	62	Hi	2	157	750	5.3
Rapamycin	Immunology	Yes	2	15	Low	3	204	914	7.0
Leucomycin	Infection	Yes	1500	35	Med	4	200	843	2.0
	Anesthesiology	No				24	828	2002	−12.0
Ascomycin	Immunology	Yes	21	15	Low	3	186	804	5.8

(*Continued*)
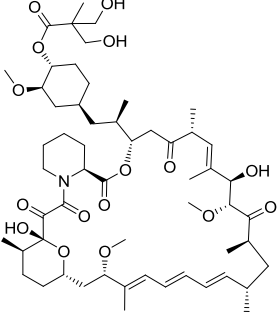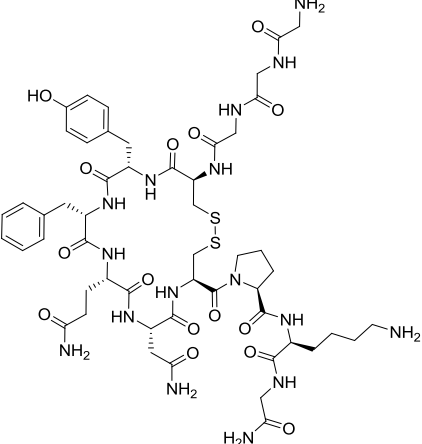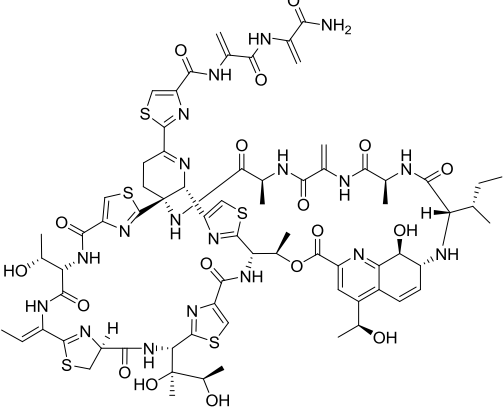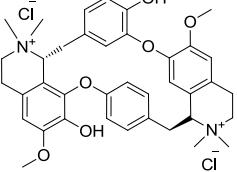
Drug name	Structure	Class
Talaporfin		Porphyrin
Teicoplanin		Cyclic peptide
Telavancin		Cyclic peptide
Telithromycin		Macrolide
Temoporfin		Porphyrin

Subclass	Therapeutic area	Oral	Avg dose (mg/day)	Human F (%)	Human F class	HBD	PSA	MW	cLogP
	Oncology	No	70			7	245	712	7.3
Glycopeptide	Infection	No							
Glycopeptide	Infection	No	700			24	665	1756	1.9
Erythronolide	Infection	Yes	800	57	Med	1	163	812	3.8
	Oncology	No				6	140	681	12.1
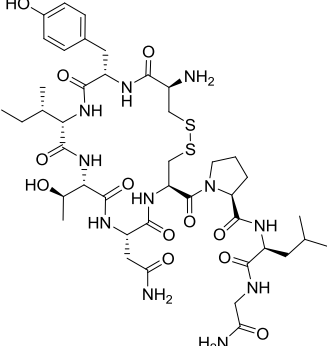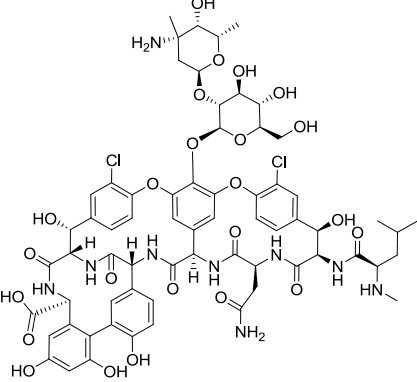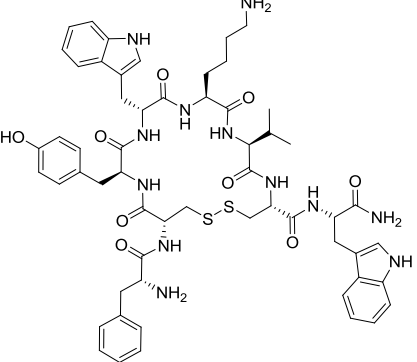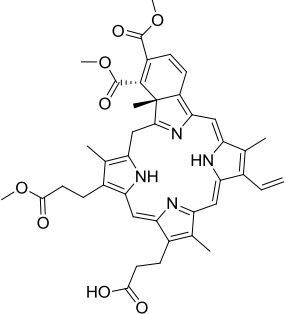
Table A.16.1 (Continued)

Drug name	Structure	Class
Temsirolimus		Macrolide
Terlipressin		Cyclic peptide
Thiostrepton		Cyclic peptide
Tubocurarine chloride		Alkaloid

Subclass	Therapeutic area	Oral	Avg dose (mg/day)	Human F (%)	Human F class	HBD	PSA	MW	cLogP
Rapamycin	Oncology	No	25			4	254	1030	7.5
Disulfide bridge	Cardiovascular	No	10			22	583	1242	−4.1
Thiazole-based	Infection	No				18	600	1665	−0.6
	Anesthesiology	No	18			2	84	610	3.6

(*Continued*)
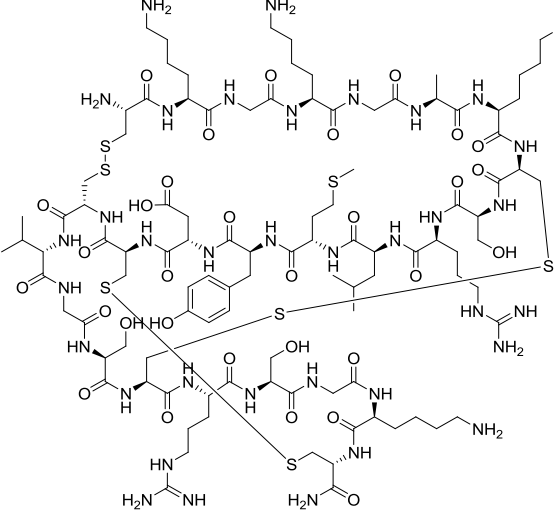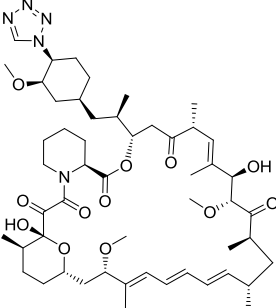
Table A.16.1 (Continued)

Drug name	Structure	Class
Urofollitropin		Cyclic peptide
Vancomycin		Cyclic peptide
Vapreotide		Cyclic peptide
Verteporfin		Porphyrin

Subclass	Therapeutic area	Oral	Avg dose (mg/day)	Human *F* (%)	Human *F* class	HBD	PSA	MW	*c*Log*P*
Disulfide bridge	Gynecology	No	0.8			15	415	980	0.4
Glycopeptide	Infection	No	2000			21	585	1449	−1.1
Disulfide bridge	Cardiovascular	No	1.2			16	383	1131	4.3
	Ophthalmology	No	10			3	170	719	6.5
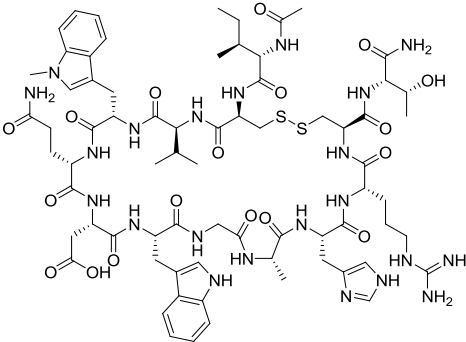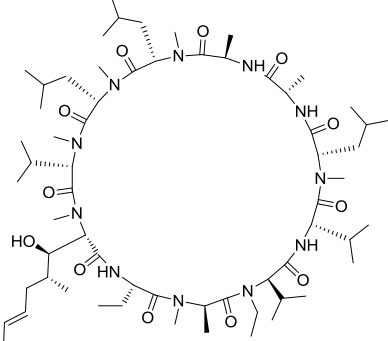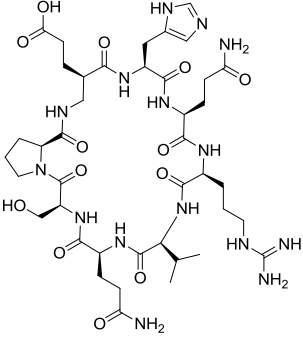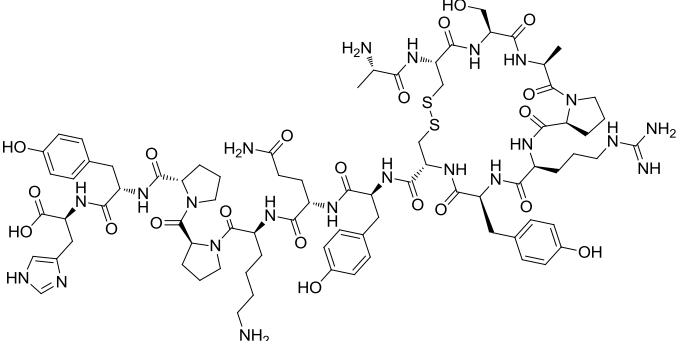
(*Continued*)

Table A.16.1 (Continued)

Drug name	Structure	Class
Ziconotide		Cyclic peptide
Zotarolimus		Macrolide

Subclass	Therapeutic area	Oral	Avg dose (mg/day)	Human *F* (%)	Human *F* class	HBD	PSA	MW	*c*Log*P*
Disulfide bridge	Pain	No	0.2			50	1259	2639	0
Rapamycin	Immunology	No	0.3			2	222	966	7.5

Table A.16.2 Macrocyclic-based compounds in clinical development as of January 25, 2017.

Drug name	Structure
AL78898A (POT-4)	
Alisporivir (UNIL025, DEB025)	
AZP 531	
Balixafortide (POL6326)	

Class	Subclass	Therapeutic area	Clinical phase	Oral	HBD	PSA	MW	cLogP
Cyclic peptide	Disulfide bridge	Ophthalmology	II	No	25	687	1628	−3.9
Cyclic peptide	N-alkylated	Infection	III	Yes	5	279	1217	4.2
Cyclic peptide	Lactam bridge	Endocrinology	I	No	18	444	990	−9.0
Cyclic peptide	Disulfide bridge	Oncology	II	Yes	27	685	1782	−10.4

(*Continued*)
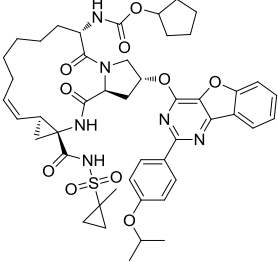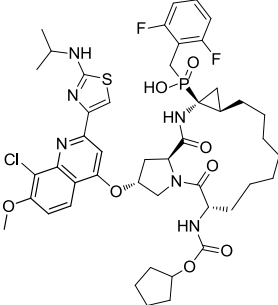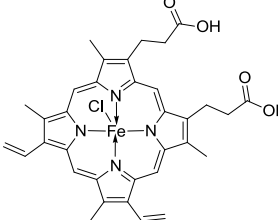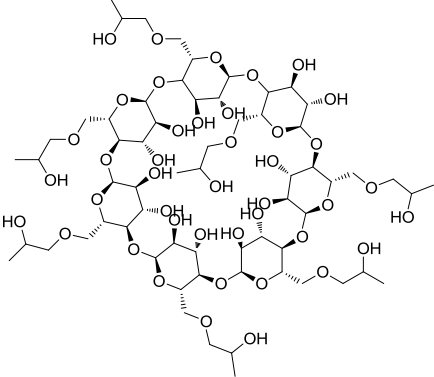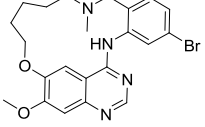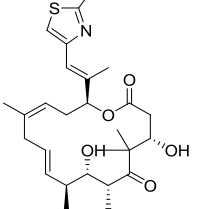
Drug name	Structure
Bremelanotide (PT-141)	
Bryostatin 1	
BQ123	
Cilengitide (EMD 121974)	
Danoprevir (R7227, ITMN-191)	
Exeporfinium chloride (XF-73)	

Class	Subclass	Therapeutic area	Clinical phase	Oral	HBD	PSA	MW	cLog$P$
Cyclic peptide	Lactam bridge	Endocrinology	III	No	15	407	1025	−1.8
Macrolide	Bryostatin	Oncology	III	No	4	243	903	3.0
Cyclic peptide	Lactam bridge	Cardiovascular	II	No	6	189	611	0.8
Cyclic peptide	N-alkylated	Oncology	III	No	9	257	589	−1.7
"*De novo* designed"		Infection	III	Yes	3	193	732	5.6
Porphyrin		Infection	I/II	No	2	67	695	2.7
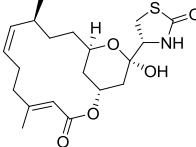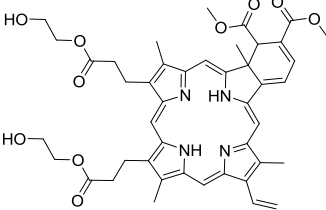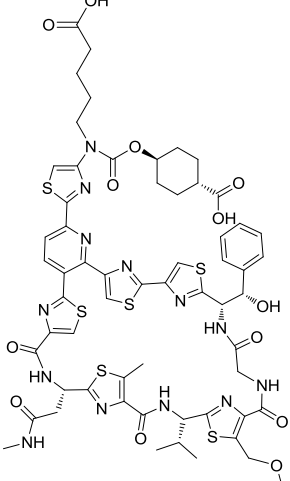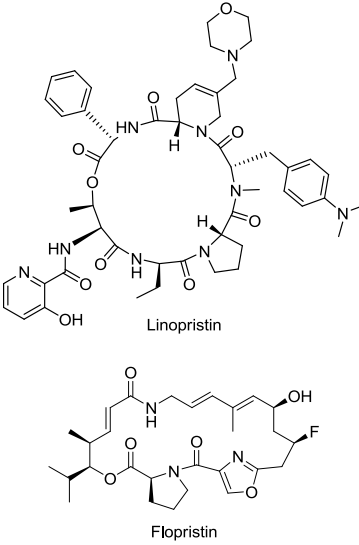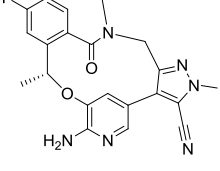
Table A.16.2 (Continued)

Drug name	Structure
Furaprevir (TG-2349)	
GS-9256	
Hemin	
Hydroxypropyl beta cyclodextrin	
JNJ 26483327	
KOS 1584	

Class	Subclass	Therapeutic area	Clinical phase	Oral	HBD	PSA	MW	cLogP
"*De novo* designed"		Infection	II	Yes	3	208	897	6.5
"*De novo* designed"		Infection	II	Yes	4	181	958	8.1
Porphyrin		Hematology	II	No	2	102	651	7.7
Cyclodextrin		Endocrinology	II/III	No	21	554	1375	−12.4
"*De novo* designed"		Oncology	I	Yes	1	54	457	6.6
Epothilone		Oncology	II	No	2	101	490	4.4

(*Continued*)

Drug name	Structure
Latrunculin B (INS115644)	
Lemuteporfin	
LFF571	
Linopristin/flopristin (NXL103)	LinopristinFlopristin
Lorlatinib (PF-06463922)	

Class	Subclass	Therapeutic area	Clinical phase	Oral	HBD	PSA	MW	cLog*P*
Macrolide	Latrunculin	Ophthalmology	I	No	2	91	396	2.6
Porphyrin		Dermatology	I/II	No	4	202	793	5.4
Cyclic peptide	Thiazolyl peptide	Infection	II	No	8	539	1366	3.5
Cyclic peptide	Depsipeptide	Infection	II	Yes				
"*De novo* designed"		Oncology	I/II	Yes	1	110	406	1.6

Table A.16.2 (Continued)

Drug name	Structure
Merotocin (FE 202767)	
MK-2748	
MK-6325	
Myolimus	
Nepadutant (MEN-11420)	

Class	Subclass	Therapeutic area	Clinical phase	Oral	HBD	PSA	MW	cLogP
Cyclic peptide	Thioether bridge	Gynecology	II	No	14	374	1042	−2.5
"*De novo* designed"		Infection	I	Yes	3	202	837	4.3
"*De novo* designed"		Infection	I	Yes	3	195	821	4.8
Macrolide	Rapamycin	Cardiovascular	I	No	3	186	900	8.9
Cyclic peptide	Lactam bridge	Gastrointestinal	II	No	13	386	947	1.1

(*Continued*)

Drug name	Structure
NIM811	
Novexatin (NP213)	
NVB302	
OTX008	
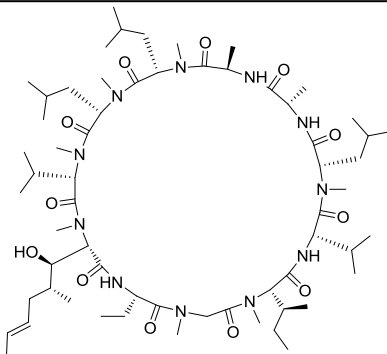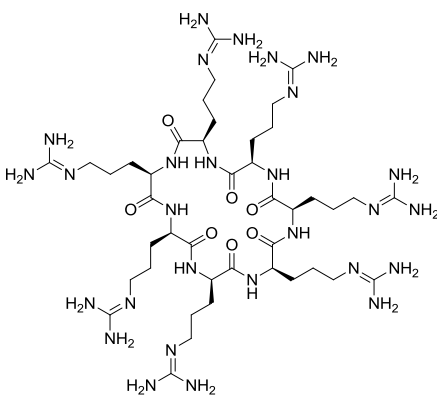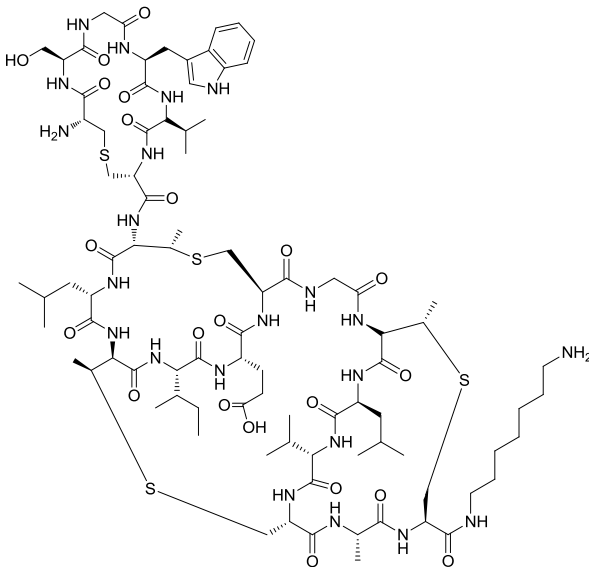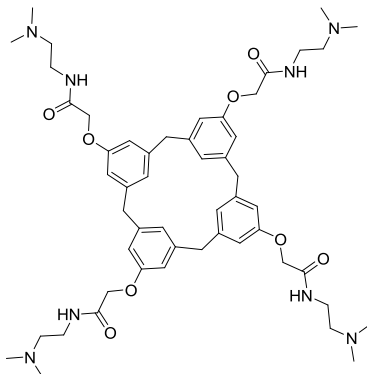
Class	Subclass	Therapeutic area	Clinical phase	Oral	HBD	PSA	MW	cLog*P*
Cyclic peptide	N-alkylated	Infection	II	Yes	5	279	1203	3.7
Cyclic peptide	Lactam bridge	Infection	II	No	35	655	1093	−10.8
Cyclic peptide	Thioether bridge	Infection	I	No	24	678	1987	−5.1
"*De novo* designed"		Oncology	I	No	4	173	937	6.1

(*Continued*)
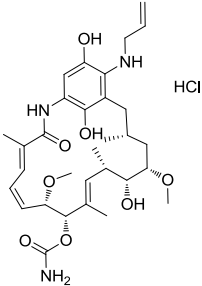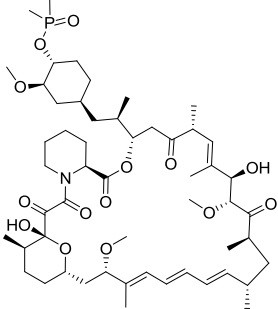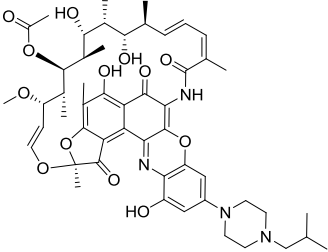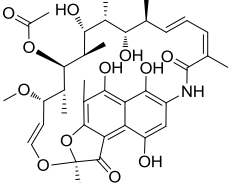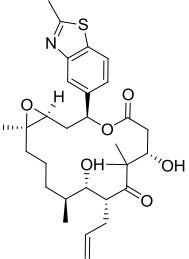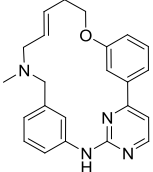
Table A.16.2 (Continued)

Drug name	Structure
Pacritinib (ONX 0803,SB1518)	
Padeliporfin (WST-11)	
Patupilone (Epothilone B, EPO906)	
PL3994	
Plitidepsin (Aplidin, dehydrodidemnin B)	

Class	Subclass	Therapeutic area	Clinical phase	Oral	HBD	PSA	MW	cLogP
"*De novo* designed"		Oncology	III	Yes	1	62	473	4.3
Porphyrin		Oncology	III	No	1	222	838	−0.3
Epothilone		Oncology	II	No	2	110	508	3.2
Cyclic peptide	Disulfide bridge	Cardiovascular	II	No	31	763	1875	−10.9
Cyclic peptide	Depsipeptide	Oncology	III	No	4	299	1110	8.0

(*Continued*)
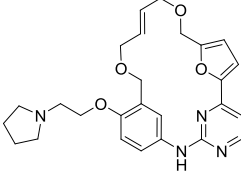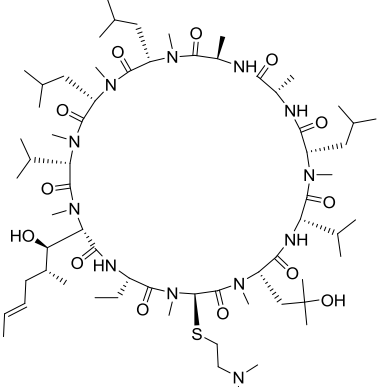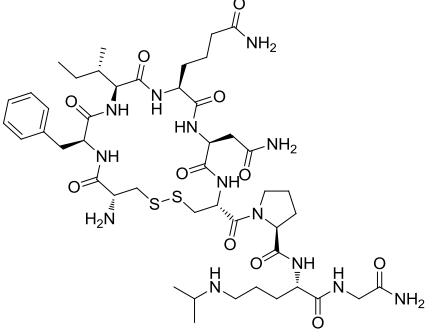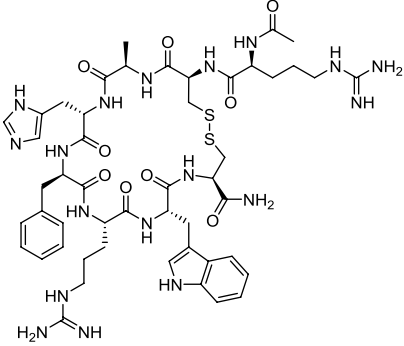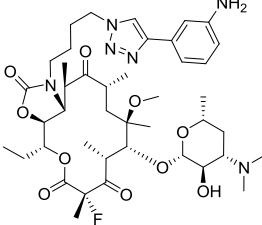
Table A.16.2 (Continued)

Drug name	Structure
Retaspimycin hydrochloride (IPI 504, MEDI 561)	
Ridaforolimus (AP23573, deforolimus, MK 8669)	
Rifalazil (ABI-1648, KRM-1648, PA-1648, AMI-1648)	
Rifamycin SV	
Sagopilone (BAY86-5302, ZK219477)	
SB1317 (TG02)	

Class	Subclass	Therapeutic area	Clinical phase	Oral	HBD	PSA	MW	*c*Log*P*
Ansamycin	Benzoquinone	Oncology	II	No	7	188	588	3.0
Macrolide	Rapamycin	Oncology	Preregistration	Yes	2	209	990	7.2
Ansamycin	Naphthoquinone	Infection	III	Yes	5	235	941	8.2
Ansamycin	Naphthoquinone	Infection	III	Yes	6	201	698	4.2
Epothilone		Oncology	II	No	2	110	544	4.2
"*De novo* designed"		Oncology	I/II	Yes	1	45	373	5.4

(*Continued*)
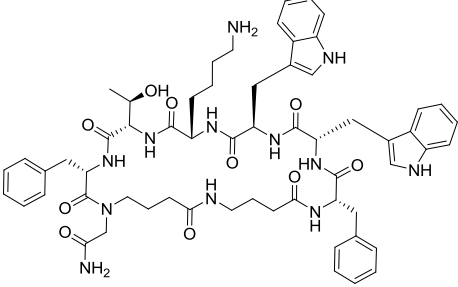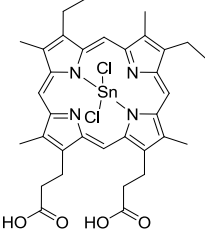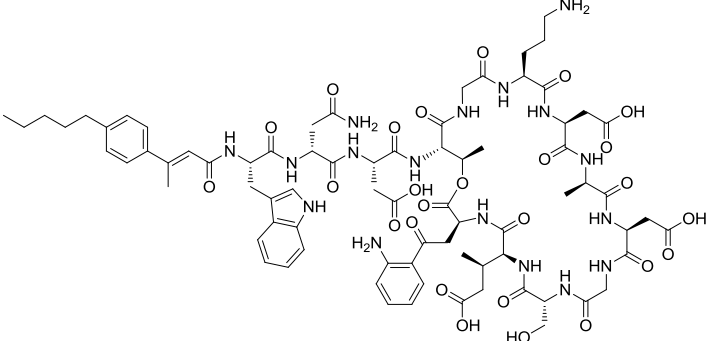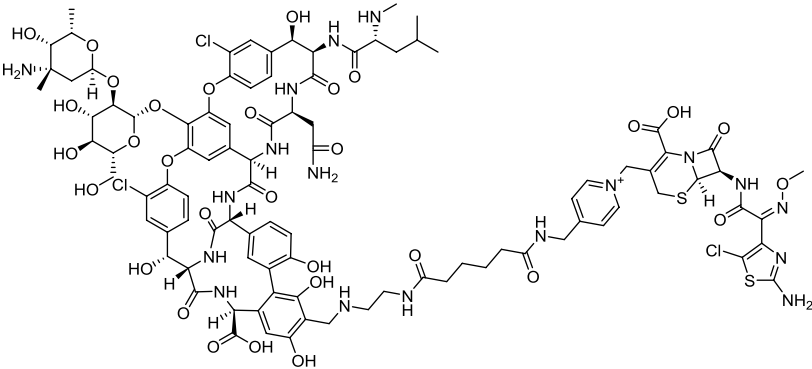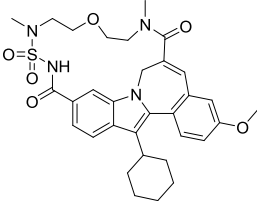
Table A.16.2 (Continued)

Drug name	Structure
SB1578 (CT1578)	
SCY 635	
Selepressin (FE-202158)	
Setmelanotide (RM493)	
Solithromycin (CEM-101, OP-1068)	

Class	Subclass	Therapeutic area	Clinical phase	Oral	HBD	PSA	MW	*c*Log*P*
"*De novo* designed"		Immunology	I	Yes	1	72	463	3.7
Cyclic peptide	N-alkylated	Infection	II	Yes	6	314	1322	13.1
Cyclic peptide	Disulfide bridge	Cardiovascular	II/III	No	16	391	1048	−4.9
Cyclic peptide	Disulfide bridge	Endocrinology	II	No	20	449	1117	−5.3
Macrolide	Erithronolide	Infection	Preregistration	Yes	3	197	831	3.2

(*Continued*)

Table A.16.2 (Continued)

Drug name	Structure
Somatoprim (DG3173, PTR3173, veldoreotide)	
Stannsoporfin (Sn-mesoporphyrin)	
Surotomycin (CB-183, 315)	
TD 1607	
TMC647055	

Class	Subclass	Therapeutic area	Clinical phase	Oral	HBD	PSA	MW	*c*Log*P*
Cyclic peptide	Lactam bridge	Endocrinology	II	No	14	374	1123	2.9
Porphyrin		Gastrointestinal	III	No	2	123	754	9.1
Cyclic peptide	Lipopeptide	Infection	III	No	22	702	1681	−5.7
Cyclic peptide	Lipopeptide	Infection	I	No	27	767	2184	−5.8
"*De novo* designed"		Infection	II	Yes	1	110	607	6.5

(*Continued*)

Table A.16.2 (Continued)
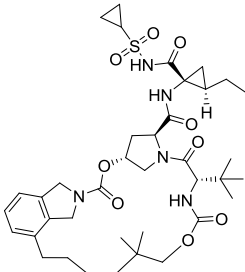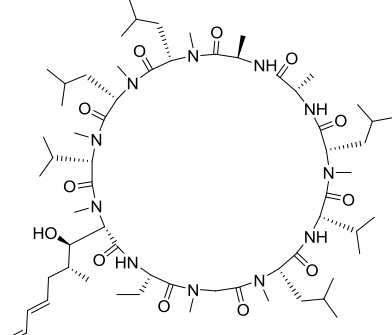
Drug name	Structure
Vaniprevir (MK-7009)	
Voclosporin (ISA 247)	

Table A.16.3 Examples of macrocyclic-based compounds with undisclosed chemical structure.

Drug name	Structure	Class	Subclass	Therapeutic area	Clinical phase	Oral	HBD	PSA	MW	cLog*P*
POL6014	NA	NA	NA	Respiratory	I	No	NA	NA	NA	NA
POL7080	NA	NA	NA	Infection	II	No	NA	NA	NA	NA
CYT1010	NA	NA	NA	Pain	I	No	NA	NA	NA	NA

References

1 Hann, M. M.; Keserü, G. M. Finding the Sweet Spot: The Role of Nature and Nurture in Medicinal Chemistry. *Nat. Rev. Drug Discov.* **2012**, *11* (5), 355–365.

2 Lipinski, C. A.; Lombardo, F.; Dominy, B. W.; Feeney, P. J. Experimental and Computational Approaches to Estimate Solubility and Permeability in Drug Discovery and Development Settings. *Adv. Drug Deliv. Rev.* **2001**, *46* (1–3), 3–26.

3 Leeson, P. D.; Springthorpe, B. The Influence of Drug-like Concepts on Decision-Making in Medicinal Chemistry. *Nat. Rev. Drug Discov.* **2007**, *6* (11), 881–890.

4 Rozek, R. P. Economic Aspects of Small and Large Molecule Pharmaceutical Technologies. *Adv. Econ. Bus.* **2013**, *1* (3), 258–269.

5 Surade, S.; Blundell, T. L. Structural Biology and Drug Discovery of Difficult Targets: The Limits of Ligandability. *Chem. Biol.* **2012**, *19* (1), 42–50.

6 Driggers, E. M.; Hale, S. P.; Lee, J.; Terrett, N. K. The Exploration of Macrocycles for Drug Discovery—An Underexploited Structural Class. *Nat. Rev. Drug Discov.* **2008**, *7* (7), 608–624.

7 Mallinson, J.; Collins, I. Macrocycles in New Drug Discovery. *Future Med. Chem.* **2012**, *4* (11), 1409–1438.

8 DeLorbe, J. E.; Clements, J. H.; Whiddon, B. B.; Martin, S. F. Thermodynamic and Structural Effects of Macrocyclic Constraints in Protein–Ligand Interactions. *ACS Med. Chem. Lett.* **2010**, *1* (8), 448–452.

9 Bogdan, A. R.; Davies, N. L.; James, K. Comparison of Diffusion Coefficients for Matched Pairs of Macrocyclic and Linear Molecules over a Drug-Like Molecular Weight Range. *Org. Biomol. Chem.* **2011**, *9* (22), 7727–7733.

10 Hewitt, W. M.; Leung, S. S. F.; Pye, C. R.; Ponkey, A. R.; Bednarek, M.; Jacobson, M. P.; Lokey, R. S. Cell-Permeable

Class	Subclass	Therapeutic area	Clinical phase	Oral	HBD	PSA	MW	*c*Log*P*
"De novo designed"		Infection	III	Yes	3	193	758	7.2
Cyclic peptide	N-alkylated	Immunology	III	Yes	5	290	1215	14.5

Cyclic Peptides from Synthetic Libraries Inspired by Natural Products. *J. Am. Chem. Soc.* **2015**, *137* (2), 715–721.

11 Traboulsi, H.; Larkin, H.; Bonin, M.-A.; Volkov, L.; Lavoie, C. L.; Marsault, É. Macrocyclic Cell Penetrating Peptides: A Study of Structure-Penetration Properties. *Bioconjug. Chem.* **2015**, *26* (3), 405–411.

12 Rand, A. C.; Leung, S. S. F.; Eng, H.; Rotter, C. J.; Sharma, R.; Kalgutkar, A. S.; Zhang, Y.; Varma, M. V.; Farley, K. A.; Khunte, B.; Limberakis, C.; Price, D. A.; Liras, S.; Mathiowetz, A. M.; Jacobson, M. P.; Lokey, R. S. Optimizing PK Properties of Cyclic Peptides: The Effect of Side Chain Substitutions on Permeability and Clearance(). *MedChemComm* **2012**, *3* (10), 1282–1289.

13 Bockus, A. T.; Lexa, K. W.; Pye, C. R.; Kalgutkar, A. S.; Gardner, J. W.; Hund, K. C. R.; Hewitt, W. M.; Schwochert, J. A.; Glassey, E.; Price, D. A.; Mathiowetz, A. M.; Liras, S.; Jacobson, M. P.; Lokey, R. S. Probing the Physicochemical Boundaries of Cell Permeability and Oral Bioavailability in Lipophilic Macrocycles Inspired by Natural Products. *J. Med. Chem.* **2015**, *58* (11), 4581–4589.

14 Molinari, G. Natural Products in Drug Discovery: Present Status and Perspectives. *Adv. Exp. Med. Biol.* **2009**, *655*, 13–27.

15 Harvey, A. L.; Edrada-Ebel, R.; Quinn, R. J. The Re-Emergence of Natural Products for Drug Discovery in the Genomics Era. *Nat. Rev. Drug Discov.* **2015**, *14* (2), 111–129.

16 Koehn, F. E.; Carter, G. T. The Evolving Role of Natural Products in Drug Discovery. *Nat. Rev. Drug Discov.* **2005**, *4* (3), 206–220.

17 Mishra, B. B.; Tiwari, V. K. Natural Products: An Evolving Role in Future Drug Discovery. *Eur. J. Med. Chem.* **2011**, *46* (10), 4769–4807.

18 Li, J. W.-H.; Vederas, J. C. Drug Discovery and Natural Products: End of an Era or an Endless Frontier? *Science* **2009**, *325* (5937), 161–165.

19 Giordanetto, F.; Kihlberg, J. Macrocyclic Drugs and Clinical Candidates: What Can Medicinal Chemists Learn from Their Properties? *J. Med. Chem.* **2014**, *57* (2), 278–295.

20 Bockus, A. T.; Schwochert, J. A.; Pye, C. R.; Townsend, C. E.; Sok, V.; Bednarek, M. A.; Lokey, R. S. Going Out on a Limb: Delineating the Effects of β-Branching, N-Methylation, and Side Chain Size on the Passive Permeability, Solubility, and Flexibility of Sanguinamide A Analogues. *J. Med. Chem.* **2015**, *58* (18), 7409–7418.

21 Kotz, J. Bringing Macrocycles Full Circle. *SciBX Sci.-Bus. Exch.* **2012**, *5* (45), 1–7.

22 Terrett, N. K. Methods for the Synthesis of Macrocycle Libraries for Drug Discovery. *Drug Discov. Today Technol.* **2010**, *7* (2), e97–e104.

23 Marsault, E.; Peterson, M. L. Macrocycles Are Great Cycles: Applications, Opportunities, and Challenges of Synthetic Macrocycles in Drug Discovery. *J. Med. Chem.* **2011**, *54* (7), 1961–2004.

24 Yu, X.; Sun, D. Macrocyclic Drugs and Synthetic Methodologies toward Macrocycles. *Mol. Basel Switz.* **2013**, *18* (6), 6230–6268.

25 GOSTAR: Databases, https://gostardb.com/gostar/databases.jsp#onlinedb (accessed February 20, 2017).

26 Adis Insight Databases, http://www.springer.com/gp/adis/products-services/adisinsight-databases (accessed February 20, 2017).

27 Obrecht, D.; Chevalier, E.; Moehle, K.; Robinson, J. A. β-Hairpin Protein Epitope Mimetic Technology in Drug Discovery. *Drug Discov. Today Technol.* **2012**, *9* (1), e63–e69.

28 Over, B.; McCarren, P.; Artursson, P.; Foley, M.; Giordanetto, F.; Grönberg, G.; Hilgendorf, C.; Lee, M. D.; Matsson, P.; Muncipinto, G.; Pellisson, M.; Perry, M. W. D.; Svensson, R.; Duvall, J. R.; Kihlberg, J. Impact of Stereospecific Intramolecular Hydrogen Bonding on Cell Permeability and Physicochemical Properties. *J. Med. Chem.* **2014**, *57* (6), 2746–2754.

29 el Tayar, N.; Mark, A. E.; Vallat, P.; Brunne, R. M.; Testa, B.; van Gunsteren, W. F. Solvent-Dependent Conformation and Hydrogen-Bonding Capacity of Cyclosporin A: Evidence from Partition Coefficients and Molecular Dynamics Simulations. *J. Med. Chem.* **1993**, *36* (24), 3757–3764.

30 Alex, A.; Millan, D. S.; Perez, M.; Wakenhut, F.; Whitlock, G. A. Intramolecular Hydrogen Bonding to Improve Membrane Permeability and Absorption in beyond Rule of Five Chemical Space. *MedChemComm* **2011**, *2* (7), 669–674.

31 Ptachcinski, R. J.; Burckart, G. J.; Venkataramanan, R. Cyclosporine. *Drug Intell. Clin. Pharm.* **1985**, *19* (2), 90–100.

32 Fahr, A. Cyclosporin Clinical Pharmacokinetics. *Clin. Pharmacokinet.* **1993**, *24* (6), 472–495.

33 Fricker, G.; Drewe, J.; Huwyler, J.; Gutmann, H.; Beglinger, C. Relevance of P-Glycoprotein for the Enteral Absorption of Cyclosporin A: In Vitro-In Vivo Correlation. *Br. J. Pharmacol.* **1996**, *118* (7), 1841–1847.

34 Fatouros, D. G.; Karpf, D. M.; Nielsen, F. S.; Mullertz, A. Clinical Studies with Oral Lipid Based Formulations of Poorly Soluble Compounds. *Ther. Clin. Risk Manag.* **2007**, *3* (4), 591–604.

35 Gibaud, S.; Attivi, D. Microemulsions for Oral Administration and Their Therapeutic Applications. *Expert Opin. Drug Deliv.* **2012**, *9* (8), 937–951.

36 Economou, N. J.; Nahoum, V.; Weeks, S. D.; Grasty, K. C.; Zentner, I. J.; Townsend, T. M.; Bhuiya, M. W.; Cocklin, S.; Loll, P. J. A Carrier Protein Strategy Yields the Structure of Dalbavancin. *J. Am. Chem. Soc.* **2012**, *134* (10), 4637–4645.

37 Goldman, R. C.; Baizman, E. R.; Longley, C. B.; Branstrom, A. A. Chlorobiphenyl-Desleucyl-Vancomycin Inhibits the Transglycosylation Process

Required for Peptidoglycan Synthesis in Bacteria in the Absence of Dipeptide Binding. *FEMS Microbiol. Lett.* **2000**, *183* (2), 209–214.

38 Okano, A.; Nakayama, A.; Wu, K.; Lindsey, E. A.; Schammel, A. W.; Feng, Y.; Collins, K. C.; Boger, D. L. Total Syntheses and Initial Evaluation of [Ψ[C(=S)NH]Tpg4]vancomycin, [Ψ[C(=NH)NH]Tpg4]vancomycin, [Ψ[CH2NH]Tpg4]vancomycin, and Their (4-Chlorobiphenyl)methyl Derivatives: Synergistic Binding Pocket and Peripheral Modifications for the Glycopeptide Antibiotics. *J. Am. Chem. Soc.* **2015**, *137* (10), 3693–3704.

39 Yarlagadda, V.; Akkapeddi, P.; Manjunath, G. B.; Haldar, J. Membrane Active Vancomycin Analogues: A Strategy to Combat Bacterial Resistance. *J. Med. Chem.* **2014**, *57* (11), 4558–4568.

40 Leighton, A.; Gottlieb, A. B.; Dorr, M. B.; Jabes, D.; Mosconi, G.; VanSaders, C.; Mroszczak, E. J.; Campbell, K. C. M.; Kelly, E. Tolerability, Pharmacokinetics, and Serum Bactericidal Activity of Intravenous Dalbavancin in Healthy Volunteers. *Antimicrob. Agents Chemother.* **2004**, *48* (3), 940–945.

41 Dorr, M. B.; Jabes, D.; Cavaleri, M.; Dowell, J.; Mosconi, G.; Malabarba, A.; White, R. J.; Henkel, T. J. Human Pharmacokinetics and Rationale for Once-Weekly Dosing of Dalbavancin, a Semi-Synthetic Glycopeptide. *J. Antimicrob. Chemother.* **2005**, *55* (Suppl 2), ii25–30.

42 http://www.pbm.va.gov/PBM/clinicalguidance/drugmonographs/Dalbavancin_Dalvance_Monograph.pdf (accessed February 20, 2017).

43 http://www.pbm.va.gov/PBM/clinicalguidance/drugmonographs/Oritavancin_Orbactiv_Monograph.pdf (accessed February 20, 2017).

44 Vibativ (Telavancin for Injection) Drug Information: Description, User Reviews, Drug Side Effects, Interactions—Prescribing Information at RxList, http://www.rxlist.com/vibativ-drug.htm (accessed February 20, 2017).

45 Vancomycin Hydrochloride (Vancomycin Hydrochloride Injection) Drug Information: Description, User Reviews, Drug Side Effects, Interactions—Prescribing Information at RxList. http://www.rxlist.com/vancomycin-injection-drug.htm (accessed February 20, 2017).

46 Boone, B.; Ongenae, K.; Van Geel, N.; Vernijns, S.; De Keyser, S.; Naeyaert, J.-M. Topical Pimecrolimus in the Treatment of Vitiligo. *Eur. J. Dermatol. EJD* **2007**, *17* (1), 55–61.

47 Jacobi, A.; Braeutigam, M.; Mahler, V.; Schultz, E.; Hertl, M. Pimecrolimus 1% Cream in the Treatment of Facial Psoriasis: A 16-Week Open-Label Study. *Dermatol. Basel Switz.* **2008**, *216* (2), 133–136.

48 Kreuter, A.; Sommer, A.; Hyun, J.; Bräutigam, M.; Brockmeyer, N. H.; Altmeyer, P.; Gambichler, T. 1%

Pimecrolimus, 0.005% Calcipotriol, and 0.1% Betamethasone in the Treatment of Intertriginous Psoriasis: A Double-Blind, Randomized Controlled Study. *Arch. Dermatol.* **2006**, *142* (9), 1138–1143.

49 Firooz, A.; Solhpour, A.; Gorouhi, F.; Daneshpazhooh, M.; Balighi, K.; Farsinejad, K.; Rashighi-Firoozabadi, M.; Dowlati, Y. Pimecrolimus Cream, 1%, vs Hydrocortisone Acetate Cream, 1%, in the Treatment of Facial Seborrheic Dermatitis: A Randomized, Investigator-Blind, Clinical Trial. *Arch. Dermatol.* **2006**, *142* (8), 1066–1067.

50 Gottlieb, A. B.; Griffiths, C. E. M.; Ho, V. C.; Lahfa, M.; Mrowietz, U.; Murrell, D. F.; Ortonne, J.-P.; Todd, G.; Cherill, R.; Marks, I.; Emady-Azar, S.; Paul, C. F.; the Multi-Centre Investigator Group. Oral Pimecrolimus in the Treatment of Moderate to Severe Chronic Plaque-Type Psoriasis: A Double-Blind, Multicentre, Randomized, Dose-Finding Trial. *Br. J. Dermatol.* **2005**, *152* (6), 1219–1227.

51 Weiss, H. M.; Fresneau, M.; Moenius, T.; Stuetz, A.; Billich, A. Binding of Pimecrolimus and Tacrolimus to Skin and Plasma Proteins: Implications for Systemic Exposure after Topical Application. *Drug Metab. Dispos.* **2008**, *36* (9), 1812–1818.

52 Billich, A.; Aschauer, H.; Aszódi, A.; Stuetz, A. Percutaneous Absorption of Drugs Used in Atopic Eczema: Pimecrolimus Permeates Less through Skin than Corticosteroids and Tacrolimus. *Int. J. Pharm.* **2004**, *269* (1), 29–35.

53 Kirsner, R. S.; Heffernan, M. P.; Antaya, R. Safety and Efficacy of Tacrolimus Ointment versus Pimecrolimus Cream in the Treatment of Patients with Atopic Dermatitis Previously Treated with Corticosteroids. *Acta Derm. Venereol.* **2010**, *90* (1), 58–64.

54 Ashcroft, D. M.; Dimmock, P.; Garside, R.; Stein, K.; Williams, H. C. Efficacy and Tolerability of Topical Pimecrolimus and Tacrolimus in the Treatment of Atopic Dermatitis: Meta-Analysis of Randomised Controlled Trials. *BMJ* **2005**, *330* (7490), 516.

55 Brufani, M.; Cellai, L.; Cerrini, S.; Fedeli, W.; Marchi, E.; Segre, A.; Vaciago, A. X-Ray Crystal Structure of 4-Deoxy-3′-bromopyrido[1′,2′-1,2]imidazo[5,4-C] rifamycin S. *J. Antibiot. (Tokyo)* **1984**, *37* (12), 1623–1627.

56 Marchi, E.; Mascellani, G.; Montecchi, L.; Venturini, A. P.; Brufani, M.; Cellai, L. 4-Deoxypyrido[1′,2′:1,2] imidazo[5,4-C]rifamycin SV Derivatives. A New Series of Semisynthetic Rifamycins with High Antibacterial Activity and Low Gastroenteric Absorption. *J. Med. Chem.* **1985**, *28* (7), 960–963.

57 http://www.accessdata.fda.gov/drugsatfda_docs/ nda/2010/022554Orig1s000SumR.pdf (accessed February 20, 2017).

58 Press Announcements—FDA approves Rapamune to treat LAM, a very rare lung disease, http://www.fda. gov/newsevents/newsroom/pressannouncements/ ucm448523.htm (accessed February 20, 2017).

59 Mahalati, K.; Kahan, D. B. D. Clinical Pharmacokinetics of Sirolimus. *Clin. Pharmacokinet.* **2012**, *40* (8), 573–585.

60 Hudes, G. R. Targeting mTOR in Renal Cell Carcinoma. *Cancer* **2009**, *115* (S10), 2313–2320.

61 Hudes, G. R.; Berkenblit, A.; Feingold, J.; Atkins, M. B.; Rini, B. I.; Dutcher, J. Clinical Trial Experience with Temsirolimus in Patients with Advanced Renal Cell Carcinoma. *Semin. Oncol.* **2009**, *36* (Suppl 3), S26–36.

62 Buckner, J. C.; Forouzesh, B.; Erlichman, C.; Hidalgo, M.; Boni, J. P.; Dukart, G.; Berkenblit, A.; Rowinsky, E. K. Phase I, Pharmacokinetic Study of Temsirolimus Administered Orally to Patients with Advanced Cancer. *Invest. New Drugs* **2010**, *28* (3), 334–342.

63 Chan, F.; Samlowski, E. E.; Samlowski, W. E. Temsirolimus: A Review of Its Use in the Treatment of Advanced Renal Cell Carcinoma. *Clin. Med. Insights Ther.* **2009**, *2009* (1), 167–174.

64 Faivre, S.; Kroemer, G.; Raymond, E. Current Development of mTOR Inhibitors as Anticancer Agents. *Nat. Rev. Drug Discov.* **2006**, *5* (8), 671–688.

65 Atkins, M. B.; Yasothan, U.; Kirkpatrick, P. Everolimus. *Nat. Rev. Drug Discov.* **2009**, *8* (7), 535–536.

66 Kirchner, G. I.; Meier-Wiedenbach, I.; Manns, M. P. Clinical Pharmacokinetics of Everolimus. *Clin. Pharmacokinet.* **2004**, *43* (2), 83–95.

67 Burke, S. E.; Kuntz, R. E.; Schwartz, L. B. Zotarolimus (ABT-578) Eluting Stents. *Adv. Drug Deliv. Rev.* **2006**, *58* (3), 437–446.

68 http://www.accessdata.fda.gov/drugsatfda_docs/ label/2014/206255lbl.pdf (accessed February 20, 2017).

69 González Canga, A.; Sahagún Prieto, A. M.; Diez Liébana, M. J.; Fernández Martínez, N.; Sierra Vega, M.; García Vieitez, J. J. The Pharmacokinetics and Interactions of Ivermectin in Humans—A Mini-Review. *AAPS J.* **2008**, *10* (1), 42–46.

70 Edwards, G.; Dingsdale, A.; Helsby, N.; Orme, M. L. E.; Breckenridge, A. M. The Relative Systemic Availability of Ivermectin after Administration as Capsule, Tablet, and Oral Solution. *Eur. J. Clin. Pharmacol.* **1988**, *35* (6), 681–684.

71 Palatin Technologies, Inc. Announces Dosing of Subcutaneous Bremelanotide Trial in Men, http://www. prnewswire.com/news-releases/palatin-technologies-inc-announces-dosing-of-subcutaneous-bremelanotide-trial-in-men-83875672.html (accessed July 1, 2016).

72 Palatin Technologies Reports Positive Bremelanotide Study Improved Safety Profile with Subcutaneous

Administration, http://www.biospace.com/News/palatin-technologies-reports-positive/152975 (accessed July 1, 2016).

73 A Phase 3, Randomized, Double-Blind, Placebo-Controlled, Parallel-Group Trial with an Open-Label Extension—Full Text View—ClinicalTrials.gov. https://clinicaltrials.gov/ct2/show/NCT02338960?term=bremelanotide&rank=2 (accessed July 1, 2016).

74 Naoumov, N. V. Cyclophilin Inhibition as Potential Therapy for Liver Diseases. *J. Hepatol.* **2014**, *61* (5), 1166–1174.

75 Membreno, F. E.; Espinales, J. C.; Lawitz, E. J. Cyclophilin Inhibitors for Hepatitis C Therapy. *Clin. Liver Dis.* **2013**, *17* (1), 129–139.

76 Hopkins, S.; Gallay, P. Cyclophilin Inhibitors: An Emerging Class of Therapeutics for the Treatment of Chronic Hepatitis C Infection. *Viruses* **2012**, *4* (11), 2558–2577.

77 Steinkasserer, A.; Harrison, R.; Billich, A.; Hammerschmid, F.; Werner, G.; Wolff, B.; Peichl, P.; Palfi, G.; Schnitzel, W.; Mlynar, E. Mode of Action of SDZ NIM 811, a Nonimmunosuppressive Cyclosporin A Analog with Activity against Human Immunodeficiency Virus Type 1 (HIV-1): Interference with Early and Late Events in HIV-1 Replication. *J. Virol.* **1995**, *69* (2), 814–824.

78 Lawitz, E.; Godofsky, E.; Rouzier, R.; Marbury, T.; Nguyen, T.; Ke, J.; Huang, M.; Praestgaard, J.; Serra, D.; Evans, T. G. Safety, Pharmacokinetics, and Antiviral Activity of the Cyclophilin Inhibitor NIM811 Alone or in Combination with Pegylated Interferon in HCV-Infected Patients Receiving 14 Days of Therapy. *Antiviral Res.* **2011**, *89* (3), 238–245.

79 Hopkins, S.; Scorneaux, B.; Huang, Z.; Murray, M. G.; Wring, S.; Smitley, C.; Harris, R.; Erdmann, F.; Fischer, G.; Ribeill, Y. SCY-635, a Novel Nonimmunosuppressive Analog of Cyclosporine That Exhibits Potent Inhibition of Hepatitis C Virus RNA Replication In Vitro. *Antimicrob. Agents Chemother.* **2010**, *54* (2), 660–672.

80 Hopkins, S.; Bobardt, M.; Chatterji, U.; Garcia-Rivera, J. A.; Lim, P.; Gallay, P. A. The Cyclophilin Inhibitor SCY-635 Disrupts Hepatitis C Virus NS5A-Cyclophilin A Complexes. *Antimicrob. Agents Chemother.* **2012**, *56* (7), 3888–3897.

81 Flisiak, R.; Horban, A.; Gallay, P.; Bobardt, M.; Selvarajah, S.; Wiercinska-Drapalo, A.; Siwak, E.; Cielniak, I.; Higersberger, J.; Kierkus, J.; Aeschlimann, C.; Grosgurin, P.; Nicolas-Métral, V.; Dumont, J.-M.; Porchet, H.; Crabbé, R.; Scalfaro, P. The Cyclophilin Inhibitor Debio-025 Shows Potent Anti-Hepatitis C Effect in Patients Coinfected with Hepatitis C and Human Immunodeficiency Virus. *Hepatology* **2008**, *47* (3), 817–826.

82 Paeshuyse, J.; Kaul, A.; De Clercq, E.; Rosenwirth, B.; Dumont, J.-M.; Scalfaro, P.; Bartenschlager, R.; Neyts, J. The Non-Immunosuppressive Cyclosporin DEBIO-025 Is a Potent Inhibitor of Hepatitis C Virus Replication in Vitro. *Hepatol. Baltim. MD* **2006**, *43* (4), 761–770.

83 Gallay, P. A.; Lin, K. Profile of Alisporivir and Its Potential in the Treatment of Hepatitis C. *Drug Des. Devel. Ther.* **2013**, *7*, 105–115.

84 Coelmont, L.; Kaptein, S.; Paeshuyse, J.; Vliegen, I.; Dumont, J.-M.; Vuagniaux, G.; Neyts, J. Debio 025, a Cyclophilin Binding Molecule, Is Highly Efficient in Clearing Hepatitis C Virus (HCV) Replicon-Containing Cells When Used Alone or in Combination with Specifically Targeted Antiviral Therapy for HCV (STAT-C) Inhibitors. *Antimicrob. Agents Chemother.* **2009**, *53* (3), 967–976.

85 Xia, B.; Barve, A.; Heimbach, T.; Zhang, T.; Gu, H.; Wang, L.; Einolf, H.; Alexander, N.; Hanna, I.; Ke, J.; Mangold, J. B.; He, H.; Sunkara, G. Physiologically Based Pharmacokinetic Modeling for Assessing the Clinical Drug-Drug Interaction of Alisporivir. *Eur. J. Pharm. Sci. Off. J. Eur. Fed. Pharm. Sci.* **2014**, *63*, 103–112.

86 Herrmann, E.; Käfer, A.; Flisiak, R.; Nicolas-Métral, V.; Zeuzem, S.; Crabbe, R. 946 PK-PD Modeling of Viral Kinetics during Treatment with Debio-025 Plus Pegylated Interferon Alpha-2a in Treatment-Naive HCV Patients. *J. Hepatol.* **2009**, *50*, S344.

87 Ling, S. Y.; Huizinga, R. B.; Mayo, P. R.; Freitag, D. G.; Aspeslet, L. J.; Foster, R. T. Pharmacokinetics of Voclosporin in Renal Impairment and Hepatic Impairment. *J. Clin. Pharmacol.* **2013**, *53* (12), 1303–1312.

88 Mayo, P. R.; Huizinga, R. B.; Ling, S. Y.; Freitag, D. G.; Aspeslet, L. J.; Foster, R. T. Voclosporin Food Effect and Single Oral Ascending Dose Pharmacokinetic and Pharmacodynamic Studies in Healthy Human Subjects. *J. Clin. Pharmacol.* **2013**, *53* (8), 819–826.

89 Vardakas, K. Z.; Polyzos, K. A.; Patouni, K.; Rafailidis, P. I.; Samonis, G.; Falagas, M. E. Treatment Failure and Recurrence of *Clostridium difficile* Infection Following Treatment with Vancomycin or Metronidazole: A Systematic Review of the Evidence. *Int. J. Antimicrob. Agents* **2012**, *40* (1), 1–8.

90 LaMarche, M. J.; Leeds, J. A.; Amaral, A.; Brewer, J. T.; Bushell, S. M.; Deng, G.; Dewhurst, J. M.; Ding, J.; Dzink-Fox, J.; Gamber, G.; Jain, A.; Lee, K.; Lee, L.; Lister, T.; McKenney, D.; Mullin, S.; Osborne, C.; Palestrant, D.; Patane, M. A.; Rann, E. M.; Sachdeva, M.; Shao, J.; Tiamfook, S.; Trzasko, A.; Whitehead, L.; Yifru, A.; Yu, D.; Yan, W.; Zhu, Q. Discovery of LFF571: An Investigational Agent for *Clostridium difficile* Infection. *J. Med. Chem.* **2012**, *55* (5), 2376–2387.

91 Mullane, K.; Lee, C.; Bressler, A.; Buitrago, M.; Weiss, K.; Dabovic, K.; Praestgaard, J.; Leeds, J. A.; Blais, J.; Pertel, P. Multicenter, Randomized Clinical Trial to Compare the Safety and Efficacy of LFF571 and Vancomycin for *Clostridium difficile* Infections. *Antimicrob. Agents Chemother.* **2015**, *59* (3), 1435–1440.

92 Crowther, G. S.; Baines, S. D.; Todhunter, S. L.; Freeman, J.; Chilton, C. H.; Wilcox, M. H. Evaluation of NVB302 versus Vancomycin Activity in an In Vitro Human Gut Model of *Clostridium difficile* Infection. *J. Antimicrob. Chemother.* **2013**, *68* (1), 168–176.

93 Bouillaut, L.; McBride, S.; Sorg, J. A.; Schmidt, D. J.; Suarez, J. M.; Tzipori, S.; Mascio, C.; Chesnel, L.; Sonenshein, A. L. Effects of Surotomycin on *Clostridium difficile* Viability and Toxin Production In Vitro. *Antimicrob. Agents Chemother.* **2015**, *59* (7), 4199–4205.

94 Mascio, C. T. M.; Chesnel, L.; Thorne, G.; Silverman, J. A. Surotomycin Demonstrates Low In Vitro Frequency of Resistance and Rapid Bactericidal Activity in *Clostridium difficile*, *Enterococcus faecalis*, and *Enterococcus faecium*. *Antimicrob. Agents Chemother.* **2014**, *58* (7), 3976–3982.

95 Mascio, C. T. M.; Mortin, L. I.; Howland, K. T.; Van Praagh, A. D. G.; Zhang, S.; Arya, A.; Chuong, C. L.; Kang, C.; Li, T.; Silverman, J. A. In Vitro and In Vivo Characterization of CB-183,315, a Novel Lipopeptide Antibiotic for Treatment of *Clostridium difficile*. *Antimicrob. Agents Chemother.* **2012**, *56* (10), 5023–5030.

96 Snydman, D. R.; Jacobus, N. V.; McDermott, L. A. Activity of a Novel Cyclic Lipopeptide, CB-183,315, against Resistant *Clostridium difficile* and Other Gram-Positive Aerobic and Anaerobic Intestinal Pathogens. *Antimicrob. Agents Chemother.* **2012**, *56* (6), 3448–3452.

97 Mita, M. M.; Mita, A. C.; Chu, Q. S.; Rowinsky, E. K.; Fetterly, G. J.; Goldston, M.; Patnaik, A.; Mathews, L.; Ricart, A. D.; Mays, T.; Knowles, H.; Rivera, V. M.; Kreisberg, J.; Bedrosian, C. L.; Tolcher, A. W. Phase I Trial of the Novel Mammalian Target of Rapamycin Inhibitor Deforolimus (AP23573; MK-8669) Administered Intravenously Daily for 5 Days Every 2 Weeks to Patients with Advanced Malignancies. *J. Clin. Oncol.* **2008**, *26* (3), 361–367.

98 Fetterly, G. J.; Mita, M. M.; Britten, C. D.; Poplin, E.; Tap, W. D.; Carmona, A.; Yonemoto, L.; Bedrosian, C. L.; Rubin, E. H.; Tolcher, A. W. Pharmacokinetics of Oral Deforolimus (AP23573, MK-8669). *ASCO Meet. Abstr.* **2008**, *26* (15_suppl), 14555.

99 Still, J. G.; Schranz, J.; Degenhardt, T. P.; Scott, D.; Fernandes, P.; Gutierrez, M. J.; Clark, K. Pharmacokinetics of Solithromycin (CEM-101) after Single or Multiple Oral Doses and Effects of Food on Single-Dose Bioavailability in Healthy Adult Subjects. *Antimicrob. Agents Chemother.* **2011**, *55* (5), 1997–2003.

100 Bertrand, D.; Bertrand, S.; Neveu, E.; Fernandes, P. Molecular Characterization of Off-Target Activities of Telithromycin: A Potential Role for Nicotinic Acetylcholine Receptors. *Antimicrob. Agents Chemother.* **2010**, *54* (12), 5399–5402.

101 Ross, D. B. The FDA and the Case of Ketek. *N. Engl. J. Med.* **2007**, *356* (16), 1601–1604.

102 Stefano, A. F. D. D.; Rusca, A.; Loprete, L.; Dröge, M. J.; Moro, L.; Assandri, A. Systemic Absorption of Rifamycin SV MMX Administered as Modified-Release Tablets in Healthy Volunteers. *Antimicrob. Agents Chemother.* **2011**, *55* (5), 2122–2128.

103 Hosoe, K.; Mae, T.; Konishi, E.; Fujii, K.; Yamashita, K.; Yamane, T.; Hidaka, T.; Ohashi, T. Pharmacokinetics of KRM-1648, a New Benzoxazinorifamycin, in Rats and Dogs. *Antimicrob. Agents Chemother.* **1996**, *40* (12), 2749–2755.

104 Chen, Y.-X.; Cabana, B.; Kivel, N.; Michaelis, A. Effect of Food on the Pharmacokinetics of Rifalazil, a Novel Antibacterial, in Healthy Male Volunteers. *J. Clin. Pharmacol.* **2007**, *47* (7), 841–849.

105 Bacon, B. R.; Gordon, S. C.; Lawitz, E.; Marcellin, P.; Vierling, J. M.; Zeuzem, S.; Poordad, F.; Goodman, Z. D.; Sings, H. L.; Boparai, N.; Burroughs, M.; Brass, C. A.; Albrecht, J. K.; Esteban, R. Boceprevir for Previously Treated Chronic HCV Genotype 1 Infection. *N. Engl. J. Med.* **2011**, *364* (13), 1207–1217.

106 Poordad, F.; McCone, J.; Bacon, B. R.; Bruno, S.; Manns, M. P.; Sulkowski, M. S.; Jacobson, I. M.; Reddy, K. R.; Goodman, Z. D.; Boparai, N.; DiNubile, M. J.; Sniukiene, V.; Brass, C. A.; Albrecht, J. K.; Bronowicki, J.-P. Boceprevir for Untreated Chronic HCV Genotype 1 Infection. *N. Engl. J. Med.* **2011**, *364* (13), 1195–1206.

107 Perni, R. B.; Almquist, S. J.; Byrn, R. A.; Chandorkar, G.; Chaturvedi, P. R.; Courtney, L. F.; Decker, C. J.; Dinehart, K.; Gates, C. A.; Harbeson, S. L.; Heiser, A.; Kalkeri, G.; Kolaczkowski, E.; Lin, K.; Luong, Y.-P.; Rao, B. G.; Taylor, W. P.; Thomson, J. A.; Tung, R. D.; Wei, Y.; Kwong, A. D.; Lin, C. Preclinical Profile of VX-950, a Potent, Selective, and Orally Bioavailable Inhibitor of Hepatitis C Virus NS3-4A Serine Protease. *Antimicrob. Agents Chemother.* **2006**, *50* (3), 899–909.

108 Kwong, A. D.; Kauffman, R. S.; Hurter, P.; Mueller, P. Discovery and Development of Telaprevir: An NS3-4A Protease Inhibitor for Treating Genotype 1 Chronic Hepatitis C Virus. *Nat. Biotechnol.* **2011**, *29* (11), 993–1003.

109 Hézode, C.; Forestier, N.; Dusheiko, G.; Ferenci, P.; Pol, S.; Goeser, T.; Bronowicki, J.-P.; Bourlière, M.; Gharakhanian, S.; Bengtsson, L.; McNair, L.; George, S.; Kieffer, T.; Kwong, A.; Kauffman, R. S.; Alam, J.; Pawlotsky, J.-M.; Zeuzem, S. Telaprevir and Peginterferon with or without Ribavirin for Chronic HCV Infection. *N. Engl. J. Med.* **2009**, *360* (18), 1839–1850.

110 Fried, M. W. Side Effects of Therapy of Hepatitis C and Their Management. *Hepatol. Baltim. Md* **2002**, *36* (5 Suppl 1), S237–S244.

111 McPhee, F.; Sheaffer, A. K.; Friborg, J.; Hernandez, D.; Falk, P.; Zhai, G.; Levine, S.; Chaniewski, S.; Yu, F.; Barry, D.; Chen, C.; Lee, M. S.; Mosure, K.; Sun, L.-Q.; Sinz, M.; Meanwell, N. A.; Colonno, R. J.; Knipe, J.; Scola, P. Preclinical Profile and Characterization of the Hepatitis C Virus NS3 Protease Inhibitor Asunaprevir (BMS-650032). *Antimicrob. Agents Chemother.* **2012**, *56* (10), 5387–5396.

112 White, P. W.; Llinàs-Brunet, M.; Amad, M.; Bethell, R. C.; Bolger, G.; Cordingley, M. G.; Duan, J.; Garneau, M.; Lagacé, L.; Thibeault, D.; Kukolj, G. Preclinical Characterization of BI 201335, a C-Terminal Carboxylic Acid Inhibitor of the Hepatitis C Virus NS3-NS4A Protease. *Antimicrob. Agents Chemother.* **2010**, *54* (11), 4611–4618.

113 Harper, S.; McCauley, J. A.; Rudd, M. T.; Ferrara, M.; DiFilippo, M.; Crescenzi, B.; Koch, U.; Petrocchi, A.; Holloway, M. K.; Butcher, J. W.; Romano, J. J.; Bush, K. J.; Gilbert, K. F.; McIntyre, C. J.; Nguyen, K. T.; Nizi, E.; Carroll, S. S.; Ludmerer, S. W.; Burlein, C.; DiMuzio, J. M.; Graham, D. J.; McHale, C. M.; Stahlhut, M. W.; Olsen, D. B.; Monteagudo, E.; Cianetti, S.; Giuliano, C.; Pucci, V.; Trainor, N.; Fandozzi, C. M.; Rowley, M.; Coleman, P. J.; Vacca, J. P.; Summa, V.; Liverton, N. J. Discovery of MK-5172, a Macrocyclic Hepatitis C Virus NS3/4a Protease Inhibitor. *ACS Med. Chem. Lett.* **2012**, *3* (4), 332–336.

114 Rosenquist, Å.; Samuelsson, B.; Johansson, P.-O.; Cummings, M. D.; Lenz, O.; Raboisson, P.; Simmen, K.; Vendeville, S.; de Kock, H.; Nilsson, M.; Horvath, A.; Kalmeijer, R.; de la Rosa, G.; Beumont-Mauviel, M. Discovery and Development of Simeprevir (TMC435), a HCV NS3/4A Protease Inhibitor. *J. Med. Chem.* **2014**, *57* (5), 1673–1693.

115 Carrion, A. F.; Gutierrez, J.; Martin, P. New Antiviral Agents for the Treatment of Hepatitis C: ABT-450. *Expert Opin. Pharmacother.* **2014**, *15* (5), 711–716.

116 Sheng, X. C.; Casarez, A.; Cai, R.; Clarke, M. O.; Chen, X.; Cho, A.; Delaney, W. E.; Doerffler, E.; Ji, M.; Mertzman, M.; Pakdaman, R.; Pyun, H.-J.; Rowe, T.; Wu, Q.; Xu, J.; Kim, C. U. Discovery of GS-9256: A Novel Phosphinic Acid Derived Inhibitor of the Hepatitis C Virus NS3/4A Protease with Potent Clinical Activity. *Bioorg. Med. Chem. Lett.* **2012**, *22* (3), 1394–1396.

117 Liverton, N. J.; Carroll, S. S.; DiMuzio, J.; Fandozzi, C.; Graham, D. J.; Hazuda, D.; Holloway, M. K.; Ludmerer, S. W.; McCauley, J. A.; McIntyre, C. J.; Olsen, D. B.; Rudd, M. T.; Stahlhut, M.; Vacca, J. P. MK-7009, a Potent and Selective Inhibitor of Hepatitis C Virus NS3/4A Protease. *Antimicrob. Agents Chemother.* **2010**, *54* (1), 305–311.

118 Seiwert, S. D.; Andrews, S. W.; Jiang, Y.; Serebryany, V.; Tan, H.; Kossen, K.; Rajagopalan, P. T. R.; Misialek, S.; Stevens, S. K.; Stoycheva, A.; Hong, J.; Lim, S. R.; Qin, X.; Rieger, R.; Condroski, K. R.; Zhang, H.; Do, M. G.; Lemieux, C.; Hingorani, G. P.; Hartley, D. P.; Josey, J. A.; Pan, L.; Beigelman, L.; Blatt, L. M. Preclinical Characteristics of the Hepatitis C Virus NS3/4A Protease Inhibitor ITMN-191 (R7227). *Antimicrob. Agents Chemother.* **2008**, *52* (12), 4432–4441.

119 Strait Biotech Medical Yakuhin situation: to View TG-2349, Furaprevir: Rapid virologic response 92% (combined therapy of interferon and Leiba Wei), http://alveice.blogspot.de/2016/04/tg-2349-furaprevir-rapid-virologic.html (accessed July 1, 2016).

120 Rudd, M. T.; Butcher, J. W.; Nguyen, K. T.; McIntyre, C. J.; Romano, J. J.; Gilbert, K. F.; Bush, K. J.; Liverton, N. J.; Holloway, M. K.; Harper, S.; Ferrara, M.; DiFilippo, M.; Summa, V.; Swestock, J.; Fritzen, J.; Carroll, S. S.; Burlein, C.; DiMuzio, J. M.; Gates, A.; Graham, D. J.; Huang, Q.; McClain, S.; McHale, C.; Stahlhut, M. W.; Black, S.; Chase, R.; Soriano, A.; Fandozzi, C. M.; Taylor, A.; Trainor, N.; Olsen, D. B.; Coleman, P. J.; Ludmerer, S. W.; McCauley, J. A. P2-Quinazolinones and Bis-Macrocycles as New Templates for Next-Generation Hepatitis C Virus NS3/4a Protease Inhibitors: Discovery of MK-2748 and MK-6325. *ChemMedChem* **2015**, *10* (4), 727–735.

121 Llinàs-Brunet, M.; Bailey, M.; Fazal, G.; Goulet, S.; Halmos, T.; Laplante, S.; Maurice, R.; Poirier, M.; Poupart, M. A.; Thibeault, D.; Wernic, D.; Lamarre, D. Peptide-Based Inhibitors of the Hepatitis C Virus Serine Protease. *Bioorg. Med. Chem. Lett.* **1998**, *8* (13), 1713–1718.

122 Lamarre, D.; Anderson, P. C.; Bailey, M.; Beaulieu, P.; Bolger, G.; Bonneau, P.; Bös, M.; Cameron, D. R.; Cartier, M.; Cordingley, M. G.; Faucher, A.-M.; Goudreau, N.; Kawai, S. H.; Kukolj, G.; Lagacé, L.; LaPlante, S. R.; Narjes, H.; Poupart, M.-A.; Rancourt, J.; Sentjens, R. E.; St George, R.; Simoneau, B.; Steinmann, G.; Thibeault, D.; Tsantrizos, Y. S.; Weldon, S. M.; Yong, C.-L.; Llinàs-Brunet, M. An NS3 Protease Inhibitor with Antiviral Effects in Humans

Infected with Hepatitis C Virus. *Nature* **2003**, *426* (6963), 186–189.

123 Tsantrizos, Y. S.; Bolger, G.; Bonneau, P.; Cameron, D. R.; Goudreau, N.; Kukolj, G.; LaPlante, S. R.; Llinàs-Brunet, M.; Nar, H.; Lamarre, D. Macrocyclic Inhibitors of the NS3 Protease as Potential Therapeutic Agents of Hepatitis C Virus Infection. *Angew. Chem. Int. Ed.* **2003**, *42* (12), 1356–1360.

124 Llinàs-Brunet, M.; Bailey, M. D.; Ghiro, E.; Gorys, V.; Halmos, T.; Poirier, M.; Rancourt, J.; Goudreau, N. A Systematic Approach to the Optimization of Substrate-Based Inhibitors of the Hepatitis C Virus NS3 Protease: Discovery of Potent and Specific Tripeptide Inhibitors. *J. Med. Chem.* **2004**, *47* (26), 6584–6594.

125 Llinàs-Brunet, M.; Bailey, M. D.; Bolger, G.; Brochu, C.; Faucher, A.-M.; Ferland, J. M.; Garneau, M.; Ghiro, E.; Gorys, V.; Grand-Maître, C.; Halmos, T.; Lapeyre-Paquette, N.; Liard, F.; Poirier, M.; Rhéaume, M.; Tsantrizos, Y. S.; Lamarre, D. Structure–Activity Study on a Novel Series of Macrocyclic Inhibitors of the Hepatitis C Virus NS3 Protease Leading to the Discovery of BILN 2061. *J. Med. Chem.* **2004**, *47* (7), 1605–1608.

126 Hinrichsen, H.; Benhamou, Y.; Wedemeyer, H.; Reiser, M.; Sentjens, R. E.; Calleja, J. L.; Forns, X.; Erhardt, A.; Crönlein, J.; Chaves, R. L.; Yong, C.-L.; Nehmiz, G.; Steinmann, G. G. Short-Term Antiviral Efficacy of BILN 2061, a Hepatitis C Virus Serine Protease Inhibitor, in Hepatitis C Genotype 1 Patients. *Gastroenterology* **2004**, *127* (5), 1347–1355.

127 Reiser, M.; Hinrichsen, H.; Benhamou, Y.; Reesink, H. W.; Wedemeyer, H.; Avendano, C.; Riba, N.; Yong, C.-L.; Nehmiz, G.; Steinmann, G. G. Antiviral Efficacy of NS3-Serine Protease Inhibitor BILN-2061 in Patients with Chronic Genotype 2 and 3 Hepatitis C. *Hepatol. Baltim. Md* **2005**, *41* (4), 832–835.

128 LaPlante, S. R.; Llinàs-Brunet, M. Dynamics and Structure-Based Design of Drugs Targeting the Critical Serine Protease of the Hepatitis C Virus—From a Peptidic Substrate to BILN 2061. *Curr. Med. Chem. Anti-Infect. Agents* **2005**, *4* (2), 111–132.

129 De Luca, A.; Bianco, C.; Rossetti, B. Treatment of HCV Infection with the Novel NS3/4A Protease Inhibitors. *Curr. Opin. Pharmacol.* **2014**, *18*, 9–17.

130 LaPlante, S. R.; Nar, H.; Lemke, C. T.; Jakalian, A.; Aubry, N.; Kawai, S. H. Ligand Bioactive Conformation Plays a Critical Role in the Design of Drugs that Target the Hepatitis C Virus NS3 Protease. *J. Med. Chem.* **2014**, *57* (5), 1777–1789.

131 ZEPATIER Grazoprevir/Elbasvir—Hepatitis C New Drug Research and Liver Health, http://www.fda.gov/NewsEvents/Newsroom/PressAnnouncements/ucm483828.htm (accessed January 29, 2016).

132 http://www.ema.europa.eu/docs/en_GB/document_library/EPAR_-_Public_assessment_report/human/002777/WC500167870.pdf (accessed February 21, 2017).

133 Http://ec.europa.eu/health/documents/community-register/2015/20150115130406/anx_130406_en.pdf (accessed February 21, 2017).

134 Lin, T.-I.; Lenz, O.; Fanning, G.; Verbinnen, T.; Delouvroy, F.; Scholliers, A.; Vermeiren, K.; Rosenquist, Å.; Edlund, M.; Samuelsson, B.; Vrang, L.; de Kock, H.; Wigerinck, P.; Raboisson, P.; Simmen, K. In Vitro Activity and Preclinical Profile of TMC435350, a Potent Hepatitis C Virus Protease Inhibitor. *Antimicrob. Agents Chemother.* **2009**, *53* (4), 1377–1385.

135 https://www.drugs.com/sfx/viekira-pak-side-effects.html (accessed February 21, 2017).

136 Deeks, E. D. Ombitasvir/Paritaprevir/Ritonavir Plus Dasabuvir: A Review in Chronic HCV Genotype 1 Infection. *Drugs* **2015**, *75* (9), 1027–1038.

137 Khatri, A.; Menon, R. M.; Marbury, T. C.; Lawitz, E. J.; Podsadecki, T. J.; Mullally, V. M.; Ding, B.; Awni, W. M.; Bernstein, B. M.; Dutta, S. Pharmacokinetics and Safety of Co-Administered Paritaprevir Plus Ritonavir, Ombitasvir, and Dasabuvir in Hepatic Impairment. *J. Hepatol.* **2015**, *63* (4), 805–812.

138 Summa, V.; Ludmerer, S. W.; McCauley, J. A.; Fandozzi, C.; Burlein, C.; Claudio, G.; Coleman, P. J.; DiMuzio, J. M.; Ferrara, M.; Filippo, M. D.; Gates, A. T.; Graham, D. J.; Harper, S.; Hazuda, D. J.; McHale, C.; Monteagudo, E.; Pucci, V.; Rowley, M.; Rudd, M. T.; Soriano, A.; Stahlhut, M. W.; Vacca, J. P.; Olsen, D. B.; Liverton, N. J.; Carroll, S. S. MK-5172, a Selective Inhibitor of Hepatitis C Virus NS3/4a Protease with Broad Activity across Genotypes and Resistant Variants. *Antimicrob. Agents Chemother.* **2012**, *56* (8), 4161–4167.

139 Gentile, I.; Buonomo, A. R.; Borgia, F.; Zappulo, E.; Castaldo, G.; Borgia, G. MK-5172: A Second-Generation Protease Inhibitor for the Treatment of Hepatitis C Virus Infection. *Expert Opin. Investig. Drugs* **2014**, *23* (5), 719–728.

140 AASLD Liver Meeting, Boston, MA, Hynes Convention Center October 30–November 3, **2009**, http://www.natap.org/2010/AASLD/AASLD.htm (accessed February 21, 2017).

141 Barauskas, O.; Corsa, A. C.; Wang, R.; Hluhanich, S.; Jin, D.; Hung, M.; Yang, H.; Delaney IV, W. E.; Schultz, B. E. Binding Kinetics, Potency, and Selectivity of the Hepatitis C Virus NS3 Protease Inhibitors GS-9256 and Vedroprevir. *Biochim. Biophys. Acta* **2014**, *1840* (12), 3292–3298.

142 A Phase 1 Study of the Safety, Tolerability, and Pharmacokinetics of Single Ascending Oral Doses of

the NS3/4A Protease Inhibitor ITMN_191 in Healthy Subjects, http://www.natap.org/2008/AASLD/ AASLD_49.htm (accessed February 21, 2017).

143 Jiang, Y.; Andrews, S. W.; Condroski, K. R.; Buckman, B.; Serebryany, V.; Wenglowsky, S.; Kennedy, A. L.; Madduru, M. R.; Wang, B.; Lyon, M.; Doherty, G. A.; Woodard, B. T.; Lemieux, C.; Do, M. G.; Zhang, H.; Ballard, J.; Vigers, G.; Brandhuber, B. J.; Stengel, P.; Josey, J. A.; Beigelman, L.; Blatt, L.; Seiwert, S. D. Discovery of Danoprevir (ITMN-191/R7227), a Highly Selective and Potent Inhibitor of Hepatitis C Virus (HCV) NS3/4A Protease. *J. Med. Chem.* **2014**, *57* (5), 1753–1769.

144 Reddy, M. B.; Chen, Y.; Haznedar, J. O.; Fretland, J.; Blotner, S.; Smith, P.; Tran, J. Q. Impact of Low-Dose Ritonavir on Danoprevir Pharmacokinetics: Results of Computer-Based Simulations and a Clinical Drug-Drug Interaction Study. *Clin. Pharmacokinet.* **2012**, *51* (7), 457–465.

145 Liverton, N. J.; Holloway, M. K.; McCauley, J. A.; Rudd, M. T.; Butcher, J. W.; Carroll, S. S.; DiMuzio, J.; Fandozzi, C.; Gilbert, K. F.; Mao, S.-S.; McIntyre, C. J.; Nguyen, K. T.; Romano, J. J.; Stahlhut, M.; Wan, B.-L.; Olsen, D. B.; Vacca, J. P. Molecular Modeling Based Approach to Potent P2–P4 Macrocyclic Inhibitors of Hepatitis C NS3/4A Protease. *J. Am. Chem. Soc.* **2008**, *130* (14), 4607–4609.

146 McCauley, J. A.; McIntyre, C. J.; Rudd, M. T.; Nguyen, K. T.; Romano, J. J.; Butcher, J. W.; Gilbert, K. F.; Bush, K. J.; Holloway, M. K.; Swestock, J.; Wan, B.-L.; Carroll, S. S.; DiMuzio, J. M.; Graham, D. J.; Ludmerer, S. W.; Mao, S.-S.; Stahlhut, M. W.; Fandozzi, C. M.; Trainor, N.; Olsen, D. B.; Vacca, J. P.; Liverton, N. J. Discovery of Vaniprevir (MK-7009), a Macrocyclic Hepatitis C Virus NS3/4a Protease Inhibitor. *J. Med. Chem.* **2010**, *53* (6), 2443–2463.

147 Inc, M. G. The Antiviral Profile of TG-2349, a novel HCV Protease Inhibitor with Pan-Genotypic Activity, http://liverlearning.aasld.org/aasld/2014/ thelivermeeting/62040/chih-ming.chen.the.antiviral. profile.of.tg-2349.a.novel.hcv.protease.inhibitor. html?f=p16m2t1370l1343 (accessed June 30, 2016).

148 New HCV Protease Inhibitor: A Phase 1/2a Study of Safety, Tolerability and Pharmacokinetic Profiles of TG-2349, a Pan-Genotypic HCV Protease Inhibitor, in Healthy East Asian and Caucasian Subjects, and Its Antiviral Activity in Chronic Hepatitis C patients, http://www.natap.org/2013/AASLD/AASLD_118.htm (accessed July 1, 2016).

149 Vendeville, S.; Lin, T.-I.; Hu, L.; Tahri, A.; McGowan, D.; Cummings, M. D.; Amssoms, K.; Canard, M.; Last, S.; Van den Steen, I.; Devogelaere, B.; Rouan, M.-C.; Vijgen, L.; Berke, J. M.; Dehertogh, P.; Fransen, E.; Cleiren, E.; van der Helm, L.; Fanning, G.; Van

Emelen, K.; Nyanguile, O.; Simmen, K.; Raboisson, P. Finger Loop Inhibitors of the HCV NS5b Polymerase. Part II. Optimization of Tetracyclic Indole-Based Macrocycle Leading to the Discovery of TMC647055. *Bioorg. Med. Chem. Lett.* **2012**, *22* (13), 4437–4443.

150 Devogelaere, B.; Berke, J. M.; Vijgen, L.; Dehertogh, P.; Fransen, E.; Cleiren, E.; Helm, L. van der; Nyanguile, O.; Tahri, A.; Amssoms, K.; Lenz, O.; Cummings, M. D.; Clayton, R. F.; Vendeville, S.; Raboisson, P.; Simmen, K. A.; Fanning, G. C.; Lin, T.-I. TMC647055, a Potent Nonnucleoside Hepatitis C Virus NS5B Polymerase Inhibitor with Cross-Genotypic Coverage. *Antimicrob. Agents Chemother.* **2012**, *56* (9), 4676–4684.

151 William, A. D.; Lee, A. C.-H.; Blanchard, S.; Poulsen, A.; Teo, E. L.; Nagaraj, H.; Tan, E.; Chen, D.; Williams, M.; Sun, E. T.; Goh, K. C.; Ong, W. C.; Goh, S. K.; Hart, S.; Jayaraman, R.; Pasha, M. K.; Ethirajulu, K.; Wood, J. M.; Dymock, B. W. Discovery of the Macrocycle 11-(2-Pyrrolidin-1-Yl-Ethoxy)-14,19-Dioxa-5,7,26-Triaza-tetracyclo[19.3.1.1(2,6).1(8,12)] heptacosa-1(25),2(26),3,5,8,10,12(27),16,21,23-Decaene (SB1518), a Potent Janus Kinase 2/fms-Like Tyrosine Kinase-3 (JAK2/FLT3) Inhibitor for the Treatment of Myelofibrosis and Lymphoma. *J. Med. Chem.* **2011**, *54* (13), 4638–4658.

152 Hart, S.; Goh, K. C.; Novotny-Diermayr, V.; Tan, Y. C.; Madan, B.; Amalini, C.; Ong, L. C.; Kheng, B.; Cheong, A.; Zhou, J.; Chng, W. J.; Wood, J. M. Pacritinib (SB1518), a JAK2/FLT3 Inhibitor for the Treatment of Acute Myeloid Leukemia. *Blood Cancer J.* **2011**, *1* (11), e44.

153 Younes, A.; Romaguera, J.; Fanale, M.; McLaughlin, P.; Hagemeister, F.; Copeland, A.; Neelapu, S.; Kwak, L.; Shah, J.; de Castro Faria, S.; Hart, S.; Wood, J.; Jayaraman, R.; Ethirajulu, K.; Zhu, J. Phase I Study of a Novel Oral Janus Kinase 2 Inhibitor, SB1518, in Patients with Relapsed Lymphoma: Evidence of Clinical and Biologic Activity in Multiple Lymphoma Subtypes. *J. Clin. Oncol. Off. J. Am. Soc. Clin. Oncol.* **2012**, *30* (33), 4161–4167.

154 Wang, L.; Li, H.; Wada, R.; Dean, J. P. Exposure-Response Analysis for Pacritinib (SB1518), a Novel Oral JAK2/FLT3 Inhibitor, in Patients with Myelofibrosis. *Blood* **2013**, *122* (21), 4080–4080.

155 Hatzimichael, E.; Tsolas, E.; Briasoulis, E. Profile of Pacritinib and Its Potential in the Treatment of Hematologic Disorders. *J. Blood Med.* **2014**, *5*, 143–152.

156 FDA Places Full Clinical Hold on Myelofibrosis Drug Pacritinib, http://www.curetoday.com/articles/ pacritinib-for-myelofibrosis-placed-on-full-clinical-hold (accessed June 30, 2016).

157 William, A. D.; Lee, A. C.-H.; Poulsen, A.; Goh, K. C.; Madan, B.; Hart, S.; Tan, E.; Wang, H.; Nagaraj, H.;

Chen, D.; Lee, C. P.; Sun, E. T.; Jayaraman, R.; Pasha, M. K.; Ethirajulu, K.; Wood, J. M.; Dymock, B. W. Discovery of the Macrocycle (9E)-15-(2-(Pyrrolidin-1-Yl)ethoxy)-7,12,25-Trioxa-19,21,24-Triaza-tetracyclo[18.3.1.1(2,5).1(14,18)] hexacosa-1(24),2,4,9,14(26),15,17,20,22-Nonaene (SB1578), a Potent Inhibitor of Janus Kinase 2/fms-Like Tyrosine Kinase-3 (JAK2/FLT3) for the Treatment of Rheumatoid Arthritis. *J. Med. Chem.* **2012**, *55* (6), 2623–2640.

158 Madan, B.; Goh, K. C.; Hart, S.; William, A. D.; Jayaraman, R.; Ethirajulu, K.; Dymock, B. W.; Wood, J. M. SB1578, a Novel Inhibitor of JAK2, FLT3, and c-Fms for the Treatment of Rheumatoid Arthritis. *J. Immunol.* **2012**, *189* (8), 4123–4134.

159 Poulsen, A.; William, A.; Blanchard, S.; Nagaraj, H.; Williams, M.; Wang, H.; Lee, A.; Sun, E.; Teo, E.-L.; Tan, E.; Goh, K. C.; Dymock, B. Structure-Based Design of Nitrogen-Linked Macrocyclic Kinase Inhibitors Leading to the Clinical Candidate SB1317/ TG02, a Potent Inhibitor of Cyclin Dependant Kinases (CDKs), Janus Kinase 2 (JAK2), and Fms-Like Tyrosine Kinase-3 (FLT3). *J. Mol. Model.* **2013**, *19* (1), 119–130.

160 Pasha, M. K.; Jayaraman, R.; Reddy, V. P.; Yeo, P.; Goh, E.; Williams, A.; Goh, K. C.; Kantharaj, E. Preclinical Metabolism and Pharmacokinetics of SB1317 (TG02), a Potent CDK/JAK2/FLT3 Inhibitor. *Drug Metab. Lett.* **2012**, *6* (1), 33–42.

161 Konings, I. R. H. M.; de Jonge, M. J. A.; Burger, H.; van der Gaast, A.; van Beijsterveldt, L. E. C.; Winkler, H.; Verweij, J.; Yuan, Z.; Hellemans, P.; Eskens, F. A. L. M. Phase I and Pharmacological Study of the Broad-Spectrum Tyrosine Kinase Inhibitor JNJ-26483327 in Patients with Advanced Solid Tumours. *Br. J. Cancer* **2010**, *103* (7), 987–992.

162 Johnson, T. W.; Richardson, P. F.; Bailey, S.; Brooun, A.; Burke, B. J.; Collins, M. R.; Cui, J. J.; Deal, J. G.; Deng, Y.-L.; Dinh, D.; Engstrom, L. D.; He, M.; Hoffman, J.; Hoffman, R. L.; Huang, Q.; Kania, R. S.; Kath, J. C.; Lam, H.; Lam, J. L.; Le, P. T.; Lingardo, L.; Liu, W.; McTigue, M.; Palmer, C. L.; Sach, N. W.; Smeal, T.; Smith, G. L.; Stewart, A. E.; Timofeevski, S.; Zhu, H.; Zhu, J.; Zou, H. Y.; Edwards, M. P. Discovery of (10R)-7-Amino-12-Fluoro-2,10,16-Trimethyl-15-Oxo-10,15,16,17-Tetrahydro-2H-8,4-(metheno) pyrazolo[4,3-h][2,5,11]-Benzoxadiazacyclotetradecine-3-Carbonitrile (PF-06463922), a Macrocyclic Inhibitor of Anaplastic Lymphoma Kinase (ALK) and c-Ros Oncogene 1 (ROS1) with Preclinical Brain Exposure and Broad-Spectrum Potency against ALK-Resistant Mutations. *J. Med. Chem.* **2014**, *57* (11), 4720–4744.

163 GOSTAR: Databases, https://gostardb.com/gostar/databases.jsp#onlinedb (accessed February 21, 2017).

164 MarvinSketch—Advanced Chemical Drawing Software « ChemAxon—Cheminformatics Platforms and Desktop Applications, https://www.chemaxon.com/products/marvin/marvinsketch/ (accessed February 21, 2017).

165 AdisInsight Databases, http://www.springer.com/gp/adis/products-services/adisinsight-databases (accessed February 21, 2017).

17

The Discovery of Macrocyclic IAP Inhibitors for the Treatment of Cancer

Nicholas K. Terrett[*]

Ensemble Therapeutics Corporation, Cambridge, MA, USA

[*]Current address: Merck Sharp & Dohme Research GmbH, Kriens, Switzerland

17.1 Introduction

Tumor cells can invoke a range of mechanisms that allow them to evade the process of apoptosis, or programmed cell death, and their consequential persistence is the fundamental attribute of human cancer cells [1]. In addition to cancer cell survival, defects in apoptotic pathways— whether they are extrinsic (activated through death receptors such as the TNF receptor) or intrinsic (characterized by the release of cytochrome c from the mitochondria as a response to cell damage)—may also contribute to tumor progression and chemoresistance.

A group of endogenous proteins have been identified that inhibit apoptosis. Appropriately named "inhibitor of apoptosis proteins" (IAPs), they include the X-linked inhibitor of apoptosis protein (XIAP) and two cellular inhibitors of apoptosis proteins (cIAP-1 and cIAP-2). These proteins have distinct pro-oncogenic properties and work by regulating caspases—the enzymes that ultimately cause the breakdown of cellular proteins [2, 3]. In particular, XIAP directly binds to and inhibits caspases-3, -7, and -9 through distinct functional regions named baculovirus IAP repeat (BIR2 and BIR3) domains, resulting in the blockade of the apoptotic process [4–6]. In contrast, although cIAPs do not directly inhibit caspases, they are involved in intracellular NF-κB signaling and play significant roles in regulating the activation of caspase-8 [7]. Elevated expression of endogenous IAPs has been observed in numerous cancers and is an indicator of poor disease prognosis [8–12].

The antiapoptotic activities of IAP proteins can be counteracted by other endogenous cellular components. The mitochondrial protein Smac/Diablo (second mitochondrial activator of caspases/direct IAP-binding protein with low isoelectric point) has affinity for, and interacts with, the IAP BIR domains through its N-terminal tetrapeptide sequence [13, 14]. The amino acid sequence in the N-terminal epitope is AVPI, and importantly for novel drug design, the AVPI peptide itself, or small molecule mimetics, has been shown to potently antagonize IAPs and deliver antitumor activity *in vivo* [15–19]. In addition, molecules that contain two independent AVPI mimetic epitopes can bind simultaneously to both BIR2 and BIR3 domains and consequently attain enhanced binding affinity for the IAPs. Such agents are considerably more potent in stimulating apoptosis in various cancer cell lines [15–19]. Following this strategy, several Smac mimetics with selective binding to the IAP BIR domains have entered clinical trials and are showing encouraging results [20–23].

We have initiated a search for potent cIAP/XIAP antagonists based on macrocycles as a consequence of the clinical relevance of the target and the opportunity to exploit our library technology for novel lead discovery. Several studies have pointed to the benefits of macrocycles as unique binding motifs for disrupting protein–protein interactions [24]. This class of molecule demonstrates several advantages not commonly found in traditional small molecule drugs, including controlled conformational flexibility, propensity for reducing polar surface area through intramolecular hydrogen bonding, extended interaction motifs, and resistance to metabolic degradation. Ultimately, our goal was to find potent IAP antagonists that demonstrate cellular penetration and a proven ability to prevent tumor growth.

17.2 DNA-Programmed Chemistry Macrocycle Libraries

It has been shown that complex library mixtures of small molecules can be created in which every compound is uniquely tagged with a covalently attached DNA chain. Such library mixtures can be interrogated through affinity-based selection assays to identify compounds with binding affinity for specific target proteins [25, 26]. Our own particular brand of this technology, *DNA-programmed chemistry* (DPC), is a synthetic method for directly translating the base sequences of a designed DNA parent template strand into small molecules. Furthermore, this transformation can be applied in parallel within mixtures to generate large compound libraries for drug discovery [27, 28]. Specificity in DNA codon–anticodon base pairing ensures that the structures of the final macrocycles reflect the base sequences of the attached DNA templates. Consequently, compounds that bind to a target protein can be identified unequivocally by amplifying and sequencing the DNA in library components that are enriched through the affinity selection process. As outlined in the succeeding text, in the search for novel IAP binders, DPC methods permitted the identification of novel lead macrocycles that led subsequently to analogues with high affinity for both the BIR2 and BIR3 domains of XIAP and cIAP.

We initiated the program with the design of a DNA-programmed library (codename ELC) of 160 000 macrocyclic peptidomimetics (Figure 17.1) containing a basic *N*-terminal P1 amino acid in direct mimicry of the *N*-terminal alanine residue in Smac. The library synthesis employed a range of diverse amino acid residues in each of the positions P1, P3, and P4 that included, but were not restricted to, natural α-amino acids. The library also incorporated five "linker" azido-substituted amino acids in the P5 position that provided the covalent attachment position for the DNA encoding template. The macrocyclic ring was then derived by Huisgen 1,3-dipolar cycloaddition between the P5 azide and an alkyne side chain of the P2 amino acid, to give P2–P5-linked macrocycles containing a 1,2,3-triazole ring. Four different alkynes were selected for the P2 position,
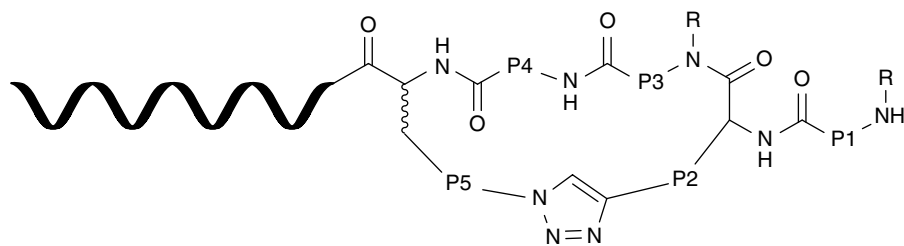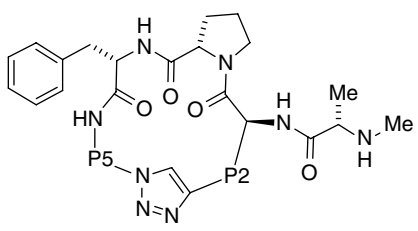
one chosen to be incorporated uniquely in each of the four library mixtures (named ELC1 through ELC4), generating 40 000 products in a total library size of 160 000 ($20 \times 20 \times 20 \times 5 \times 4$) macrocycles [29].

The open-chain peptidomimetics were synthesized on DNA using the DPC method as described by Gartner *et al.* [26] with the Huisgen cyclization giving the macrocyclic products. Unlike traditional high-throughput screening methods, DPC-derived library compounds can be screened in high-order mixtures, removing the need for intensive compound handling and screening automation. Thus, each of the four library mixtures was screened independently against isolated immobilized human XIAP BIR2 and BIR3 domains. Following incubation with the target protein immobilized on solid-support (biotinylated BIR2 on streptavidin resin and His-tagged BIR3 on nickel resin), non-binding conjugated macrocycles that remained in solution were readily washed away from the resin-bound protein. Macrocyclic library components that had any appreciable affinity for the protein target were subsequently collected following denaturation of the protein by washing the resin with TBST buffer at 70°C.

To identify the structures of hit macrocycles, DNA template sequences were amplified by PCR and identified using next-generation sequencing methods. Analysis of the sequence data indicated which DNA templates were present in high abundance. Due to synthetic variation in the preparation of each of the macrocycle compounds, rather than relying on the absolute quantity of each DNA template sequence, selection results were interpreted based on the ratio of the post-selection frequency of an individual DNA sequence, compared with its abundance in the preselection DNA library population. This ratio, described as an "enrichment" factor, has been demonstrated in our laboratories to provide a reliable indication of the intrinsic affinity of individual macrocycle library components for the target protein.

17.2.1 Initial IAP Screening Macrocycle Hits

Following an analysis of the affinity selection assay data, a number of highly enriched DNA template sequences were observed, albeit only from selections undertaken against the XIAP BIR3 domain target. Library compounds showed

Figure 17.1 Generic structure of macrocyclic compounds in the DPC-generated ELC library.

Table 17.1 Binding affinities (IC_{50} values) of P2–P5-linked macrocyclic compounds for XIAP BIR2 and BIR3.

Cpd	P2	P5	XIAP BIR2 IC_{50} (µM)	XIAP BIR3 IC_{50} (µM)
1	CH_2	L-$CH(COOH)CH_2(C_6H_4)O(CH_2)_2$	>18.8	1.32
2	$(CH_2)_4NHCO(CH_2)_2$	L-$CH(COOH)CH_2(C_6H_4)O(CH_2)_2$	>18.8	1.49
3	$(CH_2)_4NHCO(CH_2)_2$	L-$CH(COOH)(CH_2)_4$	>18.8	1.36
4	$(CH_2)_4NHCO(CH_2)_2$	$(CH_2)_2N(CH_2COOH)(CH_2)_2$	>18.8	0.900
5	$CH_2(C_6H_4)OCH_2$	L-$CH(COOH)CH_2(C_6H_4)O(CH_2)_3$	4.87	0.366
6	$CH_2(C_6H_4)OCH_2$	D-$CH(COOH)CH_2(C_6H_4)O(CH_2)_2$	7.99	2.88

IC_{50} values are an average of three independent experiments unless otherwise noted.

minimal enrichment when screened against the BIR2 domain, as overall they demonstrated stronger binding for the BIR3 domain. DNA template sequences translated directly to the structure of specific P2–P5-linked macrocycles, with the most enriched sequences observed from libraries ELC1 and ELC2 corresponding to compounds prepared from L-propynylglycine (ELC1) or L-*N*-(pent-4-ynoyl)lysine (ELC2) in the P2 position (Table 17.1). Furthermore, there was an overwhelming preference for L-*N*-methylalanine in the P1 position, with L-alanine observed in a few less strongly enriched DNA sequences. L-Proline was unequivocally the most preferred P3 residue, and L-phenylalanine was highly preferred in the P4 position. These amino acid preferences were unsurprising, bearing in mind that the *N*-terminal sequence of Smac is Ala-Val-Pro-Ile. The P5 residue, which provided the azide for macrocyclic closure by click chemistry onto the P2 alkyne, revealed no particular building block preference, although a tertiary amine-containing glycine derivative as found in compound **4** was preferred, as evidenced by the greater enrichment of DNA template sequences representing these compounds.

The activity and SAR of the newly discovered macrocyclic XIAP BIR3 binders were confirmed by individually synthesizing and screening macrocycles without any DNA template attached. For each compound, linear precursors were prepared on solid phase and cyclized by Huisgen 1,3-dipolar cycloaddition reactions, and, as the molecules no longer required a linker to DNA, the P5 building block instead presented a carboxylic acid substituent.

Some of the P2–P5 macrocyclic compounds and their binding data are listed in Table 17.1 (**1–4**). Compounds

were screened in a fluorescence polarization assay (FPA) for XIAP BIR3 and an alpha screen assay for XIAP BIR2, and these four examples revealed IC_{50} values in the low micromolar range against BIR3 but greater than 18.8 µM (the highest concentration tested) against BIR2. Compounds reveal a strong preference for P1 L-*N*-methylalanine, P3 L-proline, and P4 L-Phe, but variation in the P2 and P5 residues suggests there is flexibility in macrocycle ring size and conformation.

17.2.2 A Follow-Up DPC Macrocycle Library

To improve on the micromolar hits from the initial library, and with the intention of finding compounds with activity against both BIR domains, an iterative follow-up DPC macrocycle library was designed and synthesized. Structural variation among the 1760 compounds prepared in this library was limited, as the aim was to explore SAR close to the initial hits. The new library mixture, combined with the 40 000 ELC1 compounds, was screened against both XIAP domains in the affinity selection assay format. Combining libraries is a useful process in competition assays as the parent library can "dilute" a potentially large number of new binding compounds, providing more meaningful DNA sequence enrichment values. In addition, active compounds from ELC1 would provide a benchmark level of activity against which new hits could be compared.

Following analysis of enriched DNA sequences identified from this affinity selection assay, we were pleased to observe that the follow-up library contained hits with affinity for both BIR2 and BIR3 domains. Several

compounds were selected for resynthesis, and inhibitory activity against both XIAP domains was assessed. The presence of a P2 tyrosine derivative in the backbone of the macrocycle (Table 17.1 compounds **5** and **6**) appeared to be a key feature in compounds that bound to both targets. These results also indicated that the stereochemistry of the P5 residue had no significant influence on inhibitory activity against either domain.

17.3 A New Macrocycle Ring Structure

Co-crystal structures of key compounds bound to the isolated XIAP BIR2 domain were highly revealing of the bound conformation of these macrocycles. When in complex with BIR2, the peptide backbone of compound **5**

made numerous hydrogen-bonding interactions with the protein (Figure 17.2a). There are several lipophilic pockets on the protein surface, occupied primarily by the P1 methyl and P4 phenylalanine side chains, but it is noteworthy that the P2 and P5 groups constituting the macrocycle backbone were oriented largely into solvent.

For comparison, we examined the binding of an open-chain peptidomimetic analogue **7** (Figure 17.2b), with a P2 propynyl side chain and an L-*O*-(2-azidoethyl)tyrosine in P5, the synthetic precursor to the macrocyclic compound **1**. It was found to interact with the BIR2 protein domain in a very similar manner to compound **5**. The linear precursor had good affinity for both BIR2 and BIR3 domains (IC_{50} values of 0.54 and 0.18 μM, respectively), demonstrating affinity that far exceeded that of macrocycle **1**. More revealing was the observation that the 4-substituent on the tyrosine side chain was in close

(a)

(b)

7

BIR2 $IC_{50} = 0.54$ μM
BIR3 $IC_{50} = 0.18$ μM

(c)

Figure 17.2 X-ray co-crystal structural information indicated a superior macrocyclic ring closure, resulting in a series of compounds with greater binding affinity for the XIAP BIR2 binding site (a) X-ray co-crystal structure of the P2–P5-linked macrocyclic compound **5** (yellow) bound to the BIR2 domain (PDB accession number 4WVT). The compound makes a number of hydrogen-bond interactions (indicated as yellow broken lines) and lipophilic interactions from the P1, P3, and P4 side chains. (b) Structure of compound **7**, linear precursor to macrocycle **1**, a P2–P5-linked macrocycle. (c) Overlap of the co-crystal structures of the BIR2 domain with the linear compound **7** (green) (PDB accession number 4WVS) and P3–P5-linked macrocyclic compound **8** (orange) (PDB accession number 4WVU), showing that the backbone of the open chain overlaps almost exactly with the P3–P5-linked macrocyclic compound **8**. (*See insert for color representation of the figure.*)
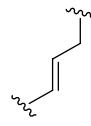
proximity through space to the P3 proline group, rather than being adjacent to the P2 side chain. This suggested that macrocycles linked between the P3 and P5 side chains might take up a conformation similar to the optimal bound conformation indicated by **7** and in consequence could be superior binders, at least to the XIAP BIR2 domain. A similar consideration of the co-crystal structure of an open-chain peptidomimetic was successfully used in the design of macrocycle inhibitors of hepatitis C virus NS3 protease [30].

Following this insight, a number of macrocycles (**8–12**) were prepared by the reaction of a P5 alkyne side chain with L-4-(S)-azidoproline to give P3–P5 cyclized macrocycles. These examples revealed superior binding affinity for BIR2 and BIR3 compared with P2–P5 macrocyclic compounds (Table 17.2). For example, a P3–P5-linked macrocycle **8** with L-valine in the P2 position and L-phenylalanine in the P4 position gave micromolar affinity for BIR2 and had an IC$_{50}$ of 0.11 μM for BIR3. This compound was co-crystallized with the XIAP BIR2

Table 17.2 Chemical structures of P3–P5 linked macrocyclic compounds and their competitive binding affinities (IC$_{50}$ values) for XIAP BIR2 and BIR3 domains and cIAP-1 BIR3 domain and activity in a cell-free caspase-3 rescue assay.

Cpd	P2	P4	P5	XIAP BIR2 IC$_{50}$ (μM)	XIAP BIR3 IC$_{50}$ (μM)	cIAP-1 BIR3 IC$_{50}$ (μM)	Caspase-3 rescue EC$_{50}$ (μM)
8	L-Val	Phenyl		1.97	0.110	0.036	6.70
9	L-Val	Phenyl		>18.8	0.232	–	–
10	L-Val	Phenyl		0.139	0.160	0.020	1.40
11	L-Chg	2-Naphthyl		2.27	0.235	–	–
12	L-^{t}BuGly	2-Naphthyl		0.827	0.214	–	–

IC$_{50}$ values are an average of three independent experiments unless otherwise noted.

domain and, when superimposed on the open-chain analogue **7**, showed remarkable overlap of the binding epitopes, supporting our decision to investigate the modified P3–P5 macrocycle design (Figure 17.2c).

Compound **8** was prepared *via* a click reaction between a P3 4-azidoproline and the acetylene from a pent-4-ynoyl derivative of L-4-aminophenylalanine at P5. Inverting P5 stereochemistry (effective inversion of the carboxylic acid configuration—compound **9**) had marginal effect on BIR3 affinity but gave a significant reduction in BIR2 affinity, suggesting the importance of a suitably oriented carboxylic acid. Other macrocycles, such as that derived from the Huisgen cyclization with *O*-propargyl-L-tyrosine **10**, revealed nicely balanced affinity against XIAP BIR2 and BIR3 with IC_{50} values of 0.139 and 0.16 μM, respectively. Although we had used the XIAP BIR domains in our primary assays, we were also very interested in the affinity for cIAP, and both **8** and **10** were shown in FPA assays to potently bind cIAP-1 BIR3 with IC_{50} values three to eightfold lower than XIAP BIR3. As previously mentioned, although cIAPs do not directly inhibit caspases, they are involved in extrinsically mediated apoptotic signaling and can regulate caspase-8 activity.

17.3.1 Functional Caspase-3 Rescue Assay

These new macrocyclic antagonists demonstrated promising activity against XIAP BIR2 and BIR3 domains in our primary screen. However, it was essential to show that the compounds were also functionally active. Specifically, by binding to the BIR2 and BIR3 domains, activated caspase-3 should be rescued from XIAP sequestration. Undertaking this assay in a tumor cell lysate in the presence of recombinant XIAP BIR2-3 protein, P3–P5-linked macrocycles **8** and **10** were assessed and exhibited EC_{50} values of 6.7 and 1.4 μM, respectively (Table 17.2). Unfortunately, this functional activity was considerably weaker than the binding affinity for the BIR domains and revealed a need for considerable improvement in the activity of the macrocycles before we could proceed to animal pharmacokinetic and efficacy studies. In particular, we speculated that there was an opportunity to find an inhibitor that could engage simultaneously with both BIR domains.

17.4 Design and Profiling of Bivalent Macrocycles

The BIR2 and BIR3 binding domains are known to reside in close proximity within the XIAP protein structure. As our objective was to develop a compound with affinity for both binding sites, we examined the possibility of introducing two binding epitopes into our macrocyclic inhibitors. Although a range of dimeric topologies might be envisioned, we focused exclusively on making macrocycles that constituted a head-to-tail dimerization of the P3–P5-linked monomeric macrocycles. Indeed, bivalent non-macrocyclic XIAP inhibitors have been previously described and their enhanced potency and efficacy have been attributed to hypervalency, possibly making concurrent interactions with both binding domains (compounds **13** and **14**, Figure 17.3) [15, 23, 31–34]. There are also reports of bivalent macrocyclic inhibitors [35, 36], although these examples, **15** and **16**, are structurally distinct from our series by being dimerized between the P2 and P4 side chains. They show very different binding activities for the BIR2 and BIR3 domains, with affinity for BIR2 being generally weak and in the micromolar range. In contrast, our goal was to find compounds with equivalent inhibitory affinity for both BIR domains in the nanomolar potency range.

Our strategy was to prepare the bivalent macrocycles for several of the best P3–P5 monomeric macrocycles (e.g., see Table 17.3). Generally, the dimeric material was synthesized as a by-product of the solid-supported synthesis of the monomeric macrocycle, but yields of the dimer could be enhanced by employing a higher substitution density during solid-phase synthesis, resulting in enhanced intermolecular reaction at the expense of intramolecular cyclization. On screening the dimeric macrocycles for binding affinity to XIAP BIR2 and BIR3 domains, we observed a significant enhancement in activity against both domains with, in many cases, similar affinities for each domain. For example, the dimeric macrocyclic compound **18** had IC_{50} values of 3 nM against BIR2 and 68 nM against BIR3, a 46-fold (BIR2) and 2.4-fold (BIR3) improvement over the corresponding monomeric macrocycle **10**, representing a ligand with unprecedented affinity for each domain. As seen previously with the monomeric macrocycles, these dimers were shown also to be potent cIAP-1 BIR3 binders.

17.4.1 *In Vitro* Antiproliferative Activity

The objective in designing and preparing potent inhibitors of the BIR2 and BIR3 domains was to find compounds that can significantly decrease proliferation of cancer cells. Compounds proven to be functionally active in the caspase-3 rescue assay were progressed to whole-cell antiproliferative assays to determine their ability to inhibit cell growth in XIAP-independent (type I), MDA-MB-231 (human triple negative breast cancer) and XIAP-dependent (type II) A875 melanoma cell lines.

The caspase-3 rescue assay and tumor cell line antiproliferative data for key P3–P5-linked macrocycles, both monomeric and dimeric, are given in Table 17.4.
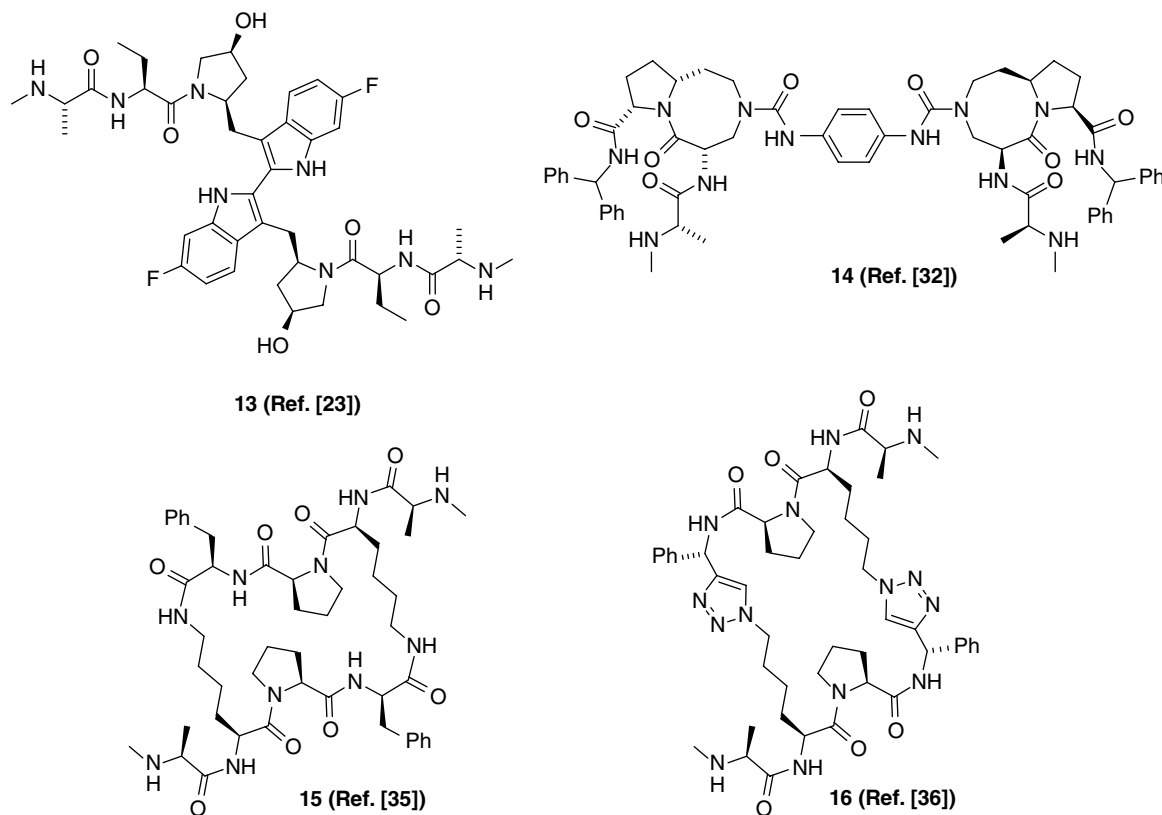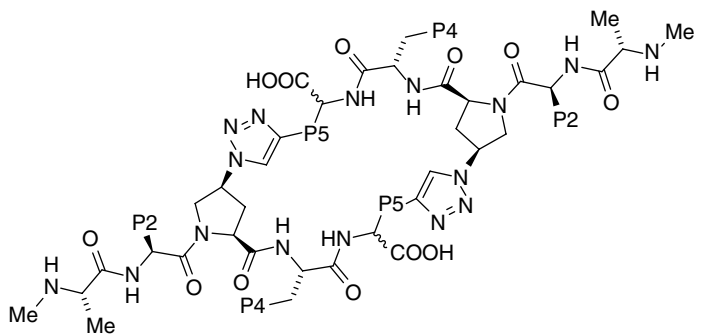
Figure 17.3 Examples of bivalent IAP antagonists **13** (birinapant), **14**, **15**, and **16**.
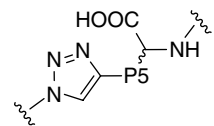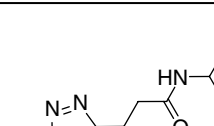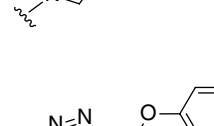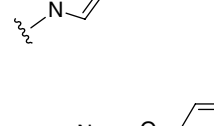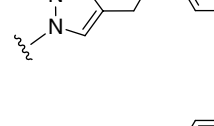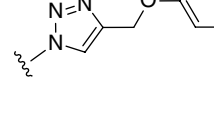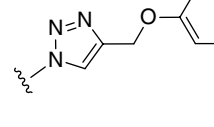
The monomeric macrocycle **10** with potent cIAP-1 BIR3 activity, but moderate XIAP BIR2 and BIR3 domain affinity and weak activity in the caspase-3 rescue assay, showed weak antiproliferative effects in the type I MDA-MB-231 cell line and no measurable effect on the proliferation of the A875 type II cell line. The corresponding dimeric macrocycle **18** had significantly enhanced affinity for the XIAP BIR2 domain, and this translated into good caspase-3 rescue activity and measurable but weak antiproliferative activity in both types I and II cell lines despite potent cIAP-1 BIR3 activity. Related dimeric macrocycles (e.g., **17**) were similarly disappointing in their antiproliferative activities despite (in some cases) good BIR domain binding and caspase-3 rescue activity. Overall, we attributed the weak antiproliferative activity to poor cell penetration for these large molecules.

There has been considerable research into the cell membrane permeability of macrocyclic peptides and peptidomimetics that fall outside of the Lipinski space [37, 38]. As our compounds might be considered too polar for good passive permeability, we synthesized analogues expected to have higher lipophilicity, within the SAR constraints as we understood them, for the BIR2 and BIR3 domains. In particular, we had observed that the IAP BIR domains would tolerate lipophilic groups in

the P2 and P4 side chain positions. Consequently, we introduced a *tert*-butyl group onto the P2 side chain and naphthyl moiety onto P4.

Dimeric macrocycles that resulted from these modifications had interesting activities. For example, compounds **19** and **20** retain L-valine in the P2 position but have L-1- and L-2-naphthylalanine, respectively, at P4. Compared with compound **18**, this structural change has little effect on caspase-3 rescue efficacy (despite a significant reduction in BIR2 inhibitory affinity) but a profound effect on antiproliferative activity. Both compounds **19** and **20** have good activity against the type I cancer cell lines, and we also observed sub-μM IC$_{50}$ values against type II A875 cells. Additional benefit was observed introducing L-cyclohexylglycine **21** or L-*tert*-butylglycine **22** into P2 while retaining L-2-naphthylalanine in P4. Potent binding affinity of these compounds for BIR2 and BIR3 domains translated into inhibition of both XIAP and cIAP-1 BIR2-3 protein constructs tested in an FPA format (Table 17.4). Further, caspase-3 rescue potency again was maintained, but antiproliferative activity was found with sub-100 nM IC$_{50}$ values against both type I and type II cancer cell lines. Screening of these compounds in an antiproliferative assay with A549 cells (insensitive to a panel of known IAP antagonists)

Table 17.3 Chemical structures of P3–P5 linked symmetric dimeric macrocyclic compounds and binding affinities (IC$_{50}$ values) for XIAP BIR2, BIR3 domains, and cIAP-1 BIR3 domain.

Cpd	P2	P4	P5	XIAP BIR2 IC$_{50}$ (µM)	XIAP BIR3 IC$_{50}$ (µM)	cIAP-1 BIR3 IC$_{50}$ (µM)
17	L-Val	Phenyl		0.006	0.047	0.008
18	L-Val	Phenyl		0.003	0.068	0.011
19	L-Val	1-Naphthyl		0.219	0.029	0.017
20	L-Val	2-Naphthyl		0.333	0.040	0.017
21	L-CyclohexylGly	2-Naphthyl		0.740	0.054	0.024
22	L-^{t}BuGly	2-Naphthyl		0.097	0.036	0.016
23	L-Val	2-Naphthyl		0.300	0.065	0.010

IC$_{50}$ values are an average of three independent experiments unless otherwise noted.

Table 17.4 Activity of key compounds in caspase-3 rescue and antiproliferative assays.

Cpd	XIAP BIR2-3 IC$_{50}$ (µM)	cIAP-1 BIR2-3 IC$_{50}$ (µM)	Caspase-3 rescue EC$_{50}$ (µM)	MDA-MB-231 cells IC$_{50}$ (µM)	A875 cells IC$_{50}$ (µM)
10	—	—	1.40	12.5	>10
17	—	—	0.070	7.90	—
18	—	—	0.045	2.94	4.22
19	—	—	0.034	0.197	0.422
20	—	—	0.059	0.082	0.218
21	0.024	0.007	0.054	0.014	0.084
22	0.022	0.005	0.030	0.026	0.077
23	0.009	0.003	0.049	2.01	6.14

Figure 17.4 Plasma levels and pharmacokinetic parameters for macrocycles **21–23** following intravenous administration to mice (**21** at 0.2 mg/kg, **22–23** both at 1 mg/kg).
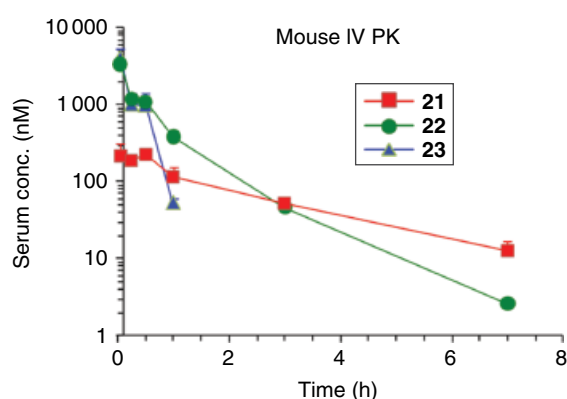
Cpd	Dose (mg/kg)	T_{half} (h)	MRT (h)	Cl (ml/min/kg)	V_{ss} (l/kg)	AUC$_{last}$ (mg/l·h)
21	0.2	1.9	2.5	4.4	0.7	457.2
22	1.0	0.85	0.79	7.1	0.34	1551.9
23	1.0	0.16	0.25	12.2	0.18	1072.3

revealed IC$_{50}$ values above 25 µM, indicating that this is a specific cytotoxic effect. Assessment in the parallel artificial membrane permeability assay (PAMPA) confirmed moderate values for passive permeability (e.g., compound **22**, $P_{app} = 1.3 \times 10^{-6}$ cm/s).

17.4.2 Pharmacokinetic Profiling

As our intention was to demonstrate *in vivo* efficacy of the best macrocycles, selecting among the more potent P3–P5-linked dimeric macrocycle IAP inhibitors, the pharmacokinetic profiles of key compounds following intravenous (i.v.) administration in mice were investigated. Three potent macrocycles **21–23** were administered intravenously to mice, and blood levels of the parent compounds were monitored. Plasma levels

and pharmacokinetic parameters for these compounds are given in Figure 17.4. The results indicate that, in general, these macrocycles have low clearance and low volumes of distribution, resulting in modest half-lives and mean residence times.

17.4.3 *In Vivo* Efficacy in a Xenograft Model

Due to its higher initial plasma concentrations and significant overall exposure as determined by the AUC, compound **22** was selected for antitumor efficacy evaluation in the MDA-MB-231 human breast cancer (Figure 17.5a) and A875 human melanoma (Figure 17.5b) xenograft models. A positive result in these studies is defined as greater than 50% tumor growth inhibition (TGI) over at least one tumor volume doubling time.

(a)

(b)
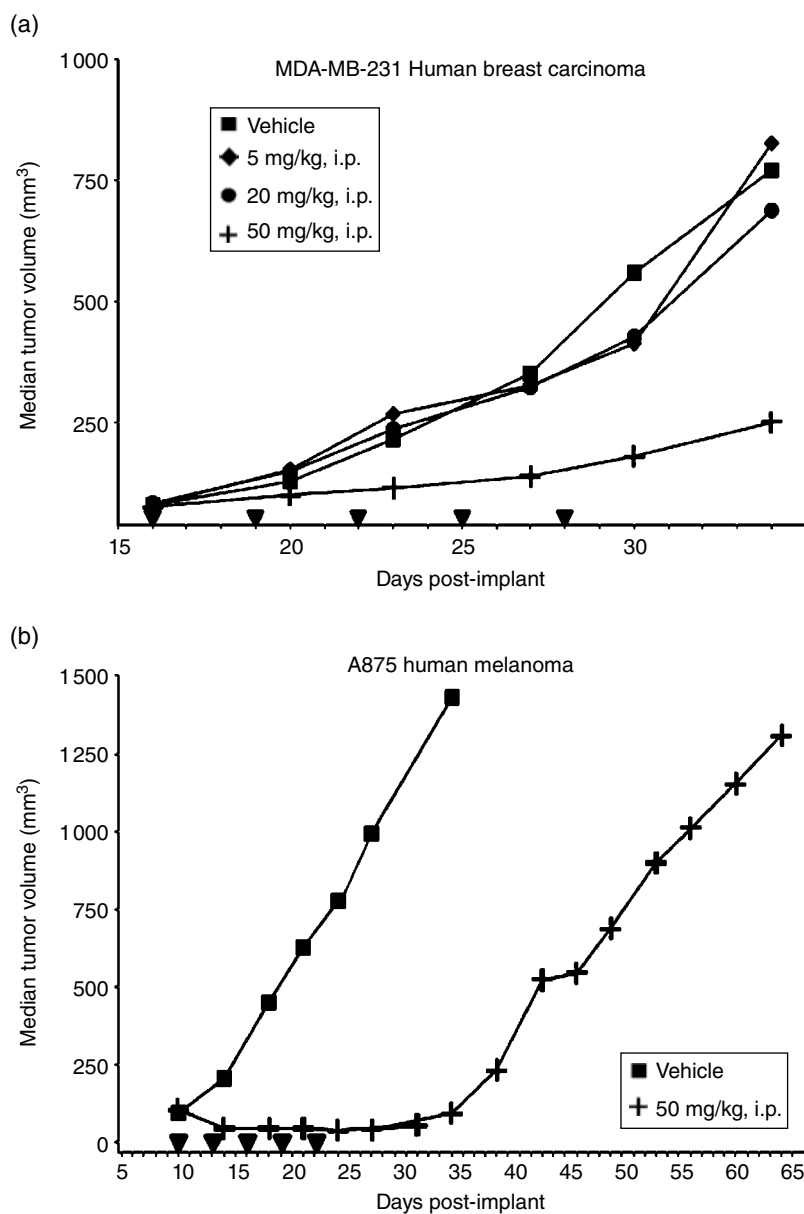
Figure 17.5 (a) Antitumor activity of compound **22** against established MDA-MB-231 human breast carcinoma xenografts implanted subcutaneously in athymic mice. (Arrowheads indicate time of dosing (q3d × 5)). (b) Antitumor activity of compound **22** against established A875 human melanoma xenografts implanted subcutaneously in athymic mice. (Arrowheads indicate time of dosing (q3d × 5)).
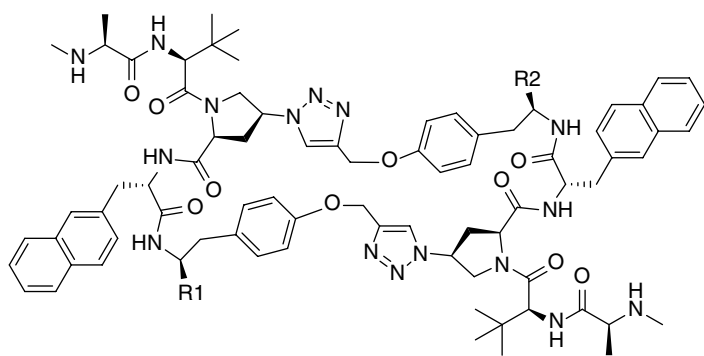
Macrocycle **22** was administered by intraperitoneal (i.p.) injection every 3 days for a total of five administrations (q3d × 5) to nude mice bearing tumors staged to 100–150 mm^3.
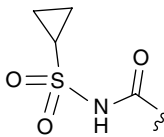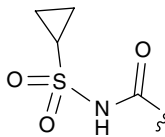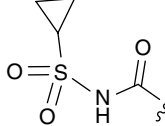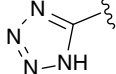
As shown in Figure 17.5a, compound **22** was inactive in the MDA-MB-231 model at doses of 5 and 20 mg/kg. However, administration at 50 mg/kg resulted in a TGI value of 78%. No overt toxicity, as indicated by morbidity or weight loss, was observed with this macrocycle at any dose level. Robust *in vivo* efficacy (148% TGI) was observed with the same macrocycle **22** when tested at 50 mg/kg in the A875 model. Figure 17.5b

illustrates the tumor regressions obtained during the dosing regimen, and TGI lasted for 12 days beyond the final dose (until day 34).

17.5 Improving the Profile of the Bivalent Macrocycles

The initial profile of compound **22** was promising, but we had concerns about the relative lack of activity in cell-based proliferation assays and that high doses were required to achieve reasonable levels of efficacy in the

Table 17.5 Biological activities of P3–P5 linked asymmetric dimeric IAP antagonists.

Cpd	R1	R2	XIAP BIR2-3 IC$_{50}$ (nM)	A875 IC$_{50}$ (nM)[a]
22	COOH	COOH	1.4	73
24	COOH	COOMe	3.7	310
25	COOMe	COOMe	32	690
26			1.8	79
27	COOH		1.8	39
28[b]	COOH		1.1	83

IC$_{50}$ values are an average of three independent experiments unless otherwise noted.
[a] Inhibition of cell growth in A875 cancer cell line in the presence of TNF.
[b] $N = 1$.

mouse tumor xenograft models. We therefore embarked on the design, synthesis, and *in vivo* evaluation of a series of macrocyclic bivalent IAP antagonists with improved potency and pharmacokinetic properties [39].

17.5.1 Replacing Carboxylic Acids

Based on our binding model and previous SAR, we hypothesized that compound **22** occupies the same binding pocket as the AVPI peptide on the surface of the BIR2-3 protein. The model suggests that both the C-terminal carboxylic acids are exposed to solvent and, as a result, are unlikely to contribute significantly to binding potency. Furthermore, carboxylic acid-containing compounds are known to typically have low cellular permeability, as well as being susceptible to phase II metabolism such as glucuronidation [40, 41]. Thus, we investigated

less polar carboxylic acid surrogates in an effort to identify compounds with improved membrane permeability and whole-cell activities. Capping the carboxylic acids as either mono- or bis-methyl esters provided compounds **24** and **25**, which were approximately 2.5- and 20-fold weaker than **22** in the XIAP BIR2-3 FRET binding assay (Table 17.5). These decreases in binding affinity were consistent with results obtained in the A875 antiproliferative assay (IC$_{50}$ = 310 and 690 nM, respectively). Several additional analogues of **22**, in which the carboxylic acids were replaced with non-acidic primary or secondary amide groups, also gave poor biochemical and cellular activities (data not shown). In contrast, replacing one or both of the carboxylic acid groups with acidic isosteres, such as a cyclopropyl acylsulfonamide or a tetrazole, appeared to be well tolerated. The bis-cyclopropyl acylsulfonamide **26** is equipotent to **22**

Table 17.6 Pharmacokinetic parameters of dimeric macrocyclic compounds in mice following a 1 mg/kg i.v. dose.

Cpd	$T_{1/2}$ (h)	CL (ml/min/kg)	V_{ss} (l/kg)	AUC_{0-7} (nM*h)
22	0.85	7.1	0.3	1550
26	0.90	3.6	0.3	2350
27	1.0	1.5	0.1	5850

in both biochemical (XIAP BIR2-3 $IC_{50} = 1.8$ nM) and cellular antiproliferative assays (A875 $IC_{50} = 79$ nM), whereas the mono-cyclopropyl acylsulfonamide analogue **27** gave similar biochemical potency but improved cellular potency (A875 $IC_{50} = 39$ nM). The mono-tetrazole isostere **28** similarly showed activity in close alignment with the parent bis-carboxylic acid **22**.

We next studied whether the acid isosteres influenced the pharmacokinetic properties of the series. Following a 1 mg/kg i.v. bolus injection, bis-cyclopropyl acylsulfonamide **26** demonstrated reduced clearance and enhanced exposure ($AUC_{0-7} = 2350$ nM*h) relative to compound **22** (Table 17.6). The mono-cyclopropyl acylsulfonamide **27** provided lower clearance and steady state volume of distribution, as well as higher exposure ($AUC_{0-\infty} = 5850$ nM*h) than **22** and **26** at the same dose. Thus, in addition to maintaining an optimal level of cellular potency, the acylsulfonamide acid isostere also conferred superior pharmacokinetic properties compared with the earlier lead macrocycle **22**.

17.5.2 Replacing Triazole Linkers

We then evaluated the impact of triazole linkers on cellular potency, using mono-acylsulfonamide **27** as a reference. Previous investigations of dimeric IAP antagonists revealed that linker length, rigidity, and polarity can have a profound effect on target binding and cellular permeability [42, 43]. The relatively polar and rigid triazole linker was selected for the initial series so as to take advantage of the efficiency of azide–alkyne click chemistry in forming the macrocycles. Our binding model suggested that both triazole groups in **22** occupy hydrophobic pockets on the XIAP BIR2-3 protein surface (Figure 17.6), suggesting that a less polar and nonaromatic linker may be tolerated. We therefore explored ring-closing metathesis (RCM), which is compatible with acylsulfonamide-containing peptide substrates, to generate analogues **29** and **30**, where one or both triazoles were replaced with less polar but similarly rigid propenyl groups. Both **29** and **30** displayed comparable biochemical and cellular activities to bis-triazole analogue **27**, indicating that the triazole linker was inessential for binding or cell permeability (Table 17.7). Macrocyclization was shown to be
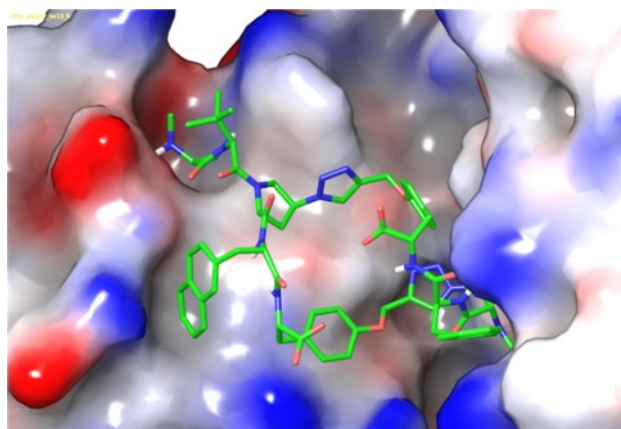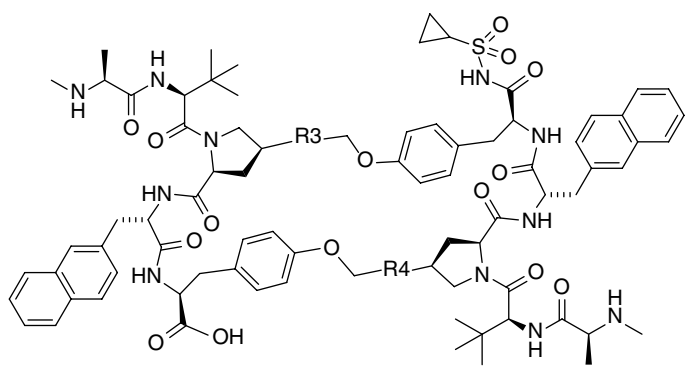
Figure 17.6 Model of compound **22** bound to the BIR2-3 domains of XIAP protein. Carbon atoms of **22** are shown in green, and oxygen and nitrogen atoms are highlighted in red and blue, respectively. The protein surface is colored by electrostatic potential, with regions of negative potential shown in red hues, positive potential in blue, and neutral (hydrophobic) regions in white. Source: Adapted from Ahlbach *et al.* [38]. Reproduced with permission of American Chemical Society. (*See insert for color representation of the figure.*)
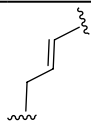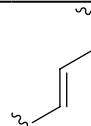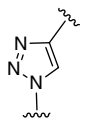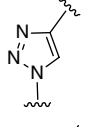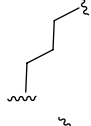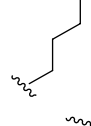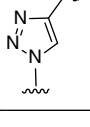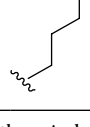
essential for potent *in vitro* activity, as macrocycle **30** was greater than 20-fold more potent than the corresponding uncyclized compound **31** in both the binding and antiproliferative assays.

To avoid any issues associated with the potentially labile allyl ether functionality, reduction of the alkene groups provided bis- or mono-propyl-linked analogues **32** and **33**. Despite increased conformational flexibility, both **32** and **33** bind to XIAP BIR2-3 proteins with IC_{50} values in the single-digit nanomolar range. Both compounds also displayed approximately a fivefold improvement in cellular potency relative to compound **22**.

17.6 Selection of the Optimal Bivalent Macrocyclic IAP Antagonist

Encouraged by the outstanding cellular potency of compounds **32** and **33**, their physiochemical properties were evaluated to select a compound for full *in vitro* and *in vivo* characterization. In particular, we aimed to identify a compound with sufficient aqueous solubility compatible with i.v. administration. We found that in this series, aqueous solubility correlates well with lipophilicity and overall charge of the peptide; compounds that are more lipophilic and net neutral are in general less soluble. Accordingly, the most lipophilic compound **32**, while among the most potent compounds tested in biochemical and cellular assays, had greatly reduced aqueous solubility (<0.01 mg/ml at pH 7.4) relative to compounds

Table 17.7 Biological activities of dimeric IAP antagonists.

Cpd	R3	R4	XIAP BIR2-3 IC$_{50}$ (nM)	A875 IC$_{50}$ (nM)[a]
29[b]			1.7	23
30			1.1	51
31			24	>1000
32			1.3	15
33			0.8	19

IC$_{50}$ values are an average of three independent experiments unless otherwise noted.
[a] Inhibition of cell growth in A875 cancer cell line in the presence of TNF.
[b] $N = 1$.

22 and 31 (0.13 and 0.05 mg/ml, respectively, at pH 7.4). On the combined basis of its *in vitro* potency and aqueous solubility, 33 was selected as the advanced lead compound for further characterization in additional biological and pharmacokinetic assays.

17.6.1 Synthesis of the Optimal Bivalent Macrocycle

Compound 22 was prepared by solid-phase peptide synthesis (SPPS) using an on-resin cyclization promoted by a Cu-mediated azide–alkyne click reaction. Synthesis of these new compounds was significantly more challenging on solid support, especially at scale, since the key RCM reaction could only be performed in solution and, thus, a solution approach was developed to prepare compound 33 (see Scheme 17.1). Starting from commercially available 2-naphthyl alanine 34, coupling to the commercially available 4-substituted prolines 35 and 36 gave compounds 37 and 38, respectively. Successive incorporation of *tert*-leucine and *N*-methylalanine building blocks using EDC–HOAt as the coupling reagents produced 39 and 40 after hydrolysis. HATU-mediated amide bond coupling of 39 and 40 with
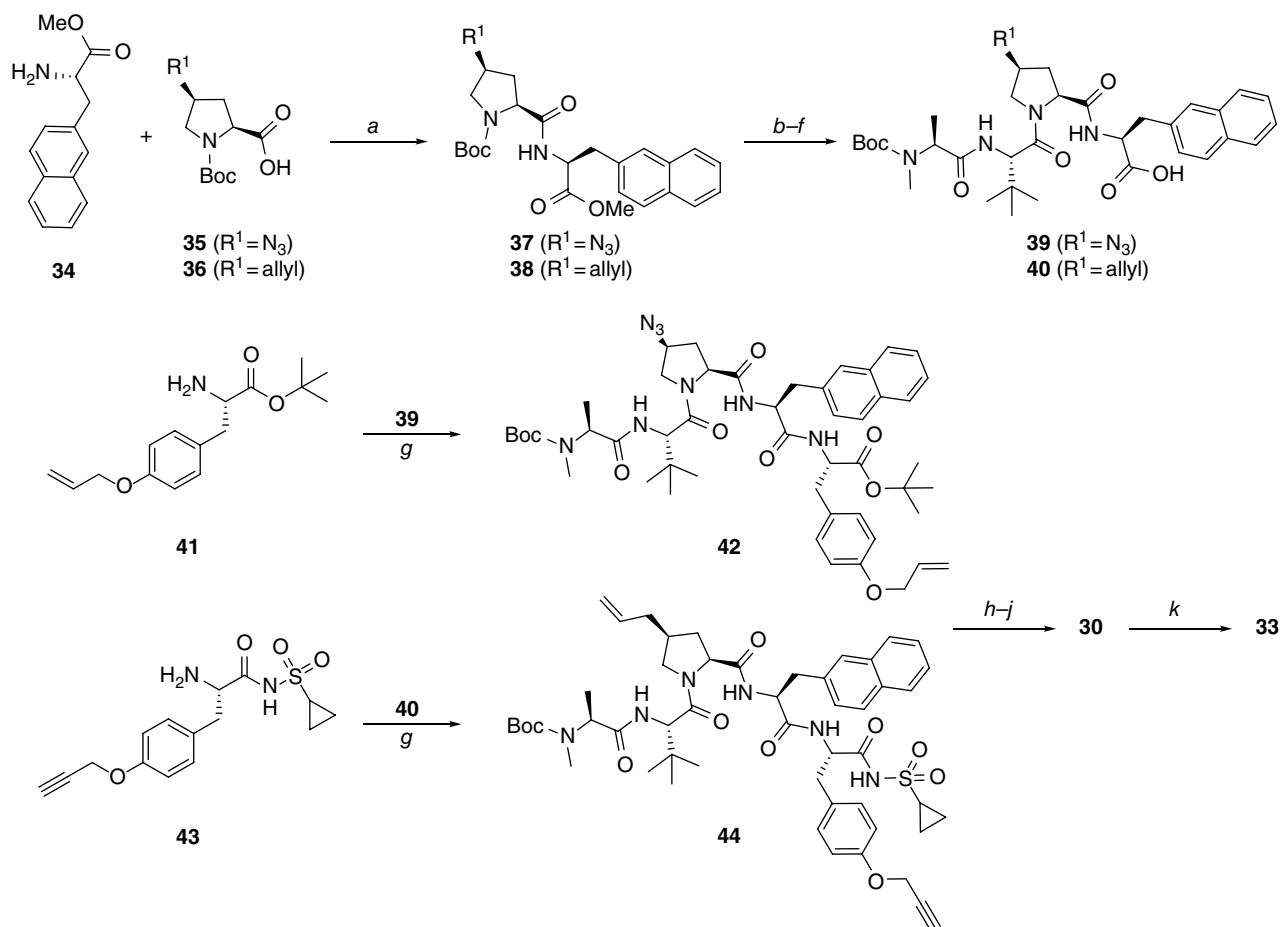
Scheme 17.1 (a) EDCI, HOAt, NMM, DMF; (b) TFA, DCM; (c) Boc-L-Leu, EDCI, HOAt, *N*-methylmorpholine, DMF; (d) TFA, DCM; (e) Boc-*N*-Me-L-Ala, EDCI, HOAt, *N*-methylmorpholine, DMF; (f) aq. LiOH, THF; (g) **39** or **40**, HATU, *N*-methylmorpholine, DMF; (h) CuSO₄, sodium ascorbic acid, THF/ᵗBuOH/H₂O; (i) Hoveyda–Grubbs II catalyst, DCE, 70°C; (j) TFA, DCM; (k) Pd/C, H₂, MeOH.

Table 17.8 Summary of IAP biological data and ADME properties for compound **33**.

Assay	Results[a]
XIAP BIR3 IC₅₀	3.5 nM
cIAP-1 BIR 2-3 IC₅₀	3.0 nM
Caspase-3 rescue EC₅₀	9.4 nM
Human CYP 1A2, 2B6, 2C8, 2C9, 2D6, 3A4 IC₅₀	>20 μM
PXR-TA EC₅₀	>50 μM
hERG inhibition at 30 μM	9.0%
Protein binding (% free): mouse, rat, dog, human	5.8, 1.9, 2.4, 7.5
IV PK: $T_{1/2}$ (h), CL (ml/min/kg), AUC₀₋₇ (nM*h)	
Mouse (1 mg/kg)	1.7, 2.1, 4490
Rat (1 mg/kg)	1.0, 6.2, 1710
Dog (0.3 mg/kg)	4.7, 0.4, 8430

[a] IC₅₀ and EC₅₀ values are an average of three experiments.

substituted tyrosine derivatives **41** and **43** provided pentapeptides **42** and **44**, respectively. Connection of **42** to **44** by cycloaddition in the presence of CuSO₄, followed by RCM and TFA deprotection, produced intermediate **30**, which was then converted to **33** *via* a straightforward hydrogenation reaction. Multiple batches of compound **33** have been synthesized on a 400–500 mg scale using this approach.

17.6.2   *In Vitro* Profiling

Lead compound **33** was further profiled in additional FRET-based binding assays and a cell-free caspase-3 rescue assay (Table 17.8). The data confirmed that **33** binds to the isolated BIR3 domain of the XIAP protein as well as the BIR2-3 domain of cIAP-1 protein with IC₅₀ values in the single-digit nanomolar range. Consistent with the mechanism of action of antagonizing XIAP to relieve inhibition of effector caspases, **33** was found to increase caspase-3 activity in a dose-dependent manner, with an IC₅₀ of 9.4 nM.
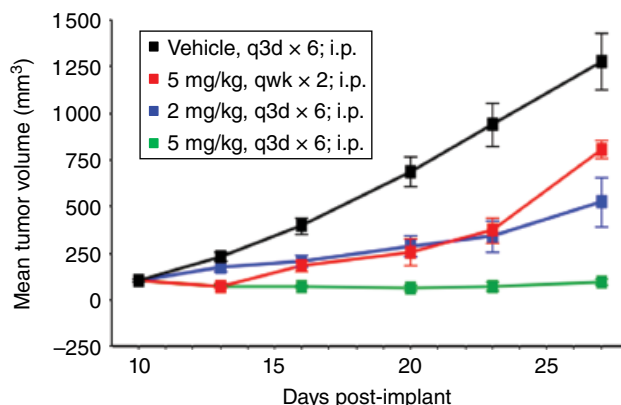
Figure 17.7 Antitumor activity of **33** in the A875 xenograft model in mice. Compounds were administered intraperitoneally (i.p.) every 3 days for six doses or weekly for two doses beginning on day 10. (*See insert for color representation of the figure.*)

17.6.3 Pharmacokinetic Profiling

The *in vitro* safety and ADME properties of compound **33** were also investigated (Table 17.8). Despite the greater lipophilicity of the acylsulfonamide substituent and alkyl linker compared with **22**, compound **33** possesses a favorable human cytochrome P450 (CYP) inhibitory profile that has very low potential for CYP induction based on the human PXR transactivation assay and showed minimal effects on hERG. No significant difference in plasma protein binding as measured by equilibrium dialysis was observed in mouse, rat, dog, or human plasma. Additionally, lead compound **33** demonstrated excellent metabolic stability ($t_{1/2} = 84$ min in rat, and $t_{1/2} > 120$ min in mouse, dog, and human liver microsomes). Finally, PK properties of compound **33** were assessed in mouse, rat, and dog following a single i.v. dose and indicated short to moderate half-lives and very low clearance across species.

17.6.4 *In Vivo* Efficacy in a Xenograft Model

Finally, we conducted *in vivo* efficacy studies with **33** against A875 tumor xenografts implanted in athymic mice. We were pleased to observe robust antitumor activity (Figure 17.7). For example, i.p. administration of **33** at 2 mg/kg every three days for six doses resulted in 67% TGI. Complete tumor stasis (>100% TGI) was observed throughout the duration of the study (when dosing at 5 mg/kg), and the macrocycle was also efficacious when administered twice on a weekly schedule at 5 mg/kg (TGI = 80%). Most importantly, compound **33** was well tolerated in all animals with no overt toxicity (weight loss or morbidity) being observed. These results compare favorably with those of **22**, where a 50 mg/kg

dose on a more frequent q3d schedule was required to achieve similar efficacy.

Macrocycle **33** was also profiled against a panel of human colorectal cancer cell lines, including those that harbor the multidrug-resistant (MDR) phenotype, and the compound displayed robust activities in all tumor cell lines regardless of their MDR status. For example, **33** was highly potent at inhibiting cell growth in both the HCT116 cell line and its MDR-positive variant HCT116/VM46 [44] ($IC_{50} = 92$ and 11 nM, respectively) and confirmed *in vivo* [45]. This result contrasts with the previously reported non-macrocyclic IAP antagonists, which were shown to be susceptible to the MDR phenotype [16].

17.7 Summary

In conclusion, DPC has been employed to generate a library of macrocycles targeted for the BIR domains of intracellular IAP proteins. Screening the library in affinity-based selections against immobilized BIR domains led to the identification of novel IAP antagonists, and information from co-crystal protein structures was critical in a redesign of the macrocycle that led to antagonists with improved and balanced affinity. The investigation of bivalent macrocycles and optimization of their permeability led to the initial lead compound **22**. This compound was active in an antiproliferative cancer cell assay and also was able to prevent growth of a human cancer xenograft in mice. However, the activity was modest, and systematic optimization of the carboxylic acid and linker regions in the macrocycle structure provided an advanced lead macrocycle **33** with improved *in vitro* and *in vivo* activities. Despite high molecular weight and a large number of lipophilic aromatic rings, this macrocycle has demonstrated desirable *in vitro* pharmacology, safety, and pharmacokinetic profiles and was efficacious at a much lower dose compared with compound **22** when evaluated in the A875 xenograft model. Furthermore, given the large number of tumors that are susceptible to the MDR phenotype, the intriguing potency in MDR-positive cell lines may provide a distinct advantage for these macrocyclic IAP antagonists.

Acknowledgments

References

1 Hanahan, D.; Weinberg, R. A. Hallmarks of cancer: The next generation. *Cell* **2011**, *144*, 646–674.

2 Fulda, S.; Vucic, D. Targeting IAP proteins for therapeutic intervention in cancer. *Nat. Rev. Drug Discov.* **2012**, *11*, 109–124.

3 Mannhold, R.; Fulda, S.; Carosati, E. IAP antagonists: Promising candidates for cancer therapy. *Drug Discov. Today* **2010**, *15*, 210–219.

4 Riedl, S. J.; Renatus, M.; Schwarzenbacher, R.; Zhou, Q.; Sun, C.; Fesik, S. W.; Liddington, R. C.; Salvesen, G. S. Structural basis for the inhibition of caspase-3 by XIAP. *Cell* **2001**, *104*, 791–800.

5 Chai, J.; Shiozaki, E.; Scrinivasula, S. M.; Wu, Q.; Datta, P.; Alnemri, E. S.; Shi, Y. Structural basis of caspase-7 inhibition by XIAP. *Cell* **2001**, *104*, 769–780.

6 Shiozaki, E. N.; Chai, J.; Rigotti, D. J.; Riedl, S. J.; Li, P.; Srinivasula, S. M.; Alnemri, E. S.; Fairman, R.; Shi, Y. Mechanism of XIAP-mediated inhibition of caspase-9. *Mol. Cell* **2003**, *2*, 519–527.

7 Varfolomeev, E.; Blankenship, J. W.; Wayson, S. M.; Federova, A. V.; Kayagaki, N.; Garg, P.; Zobel, K.; Dynek, J. N.; Elliott, L. O.; Wallweber, H. J. A.; Flygare, J. A.; Fairbrother, W. J.; Deshayes, K.; Dixit, V. M.; Vucic, D. IAP antagonists induce autoubiquitination of c-IAPs, NF-κB activation, and TNFα-dependent apoptosis. *Cell* **2007**, *131*, 669–681.

8 Tamm, I.; Kornblau, S. M.; Segall, H.; Krajewski, S.; Welsh, K.; Kitada, S.; Scudiero, D. A.; Tudor, G.; Qui, Y. H.; Monks, A.; Andreeff, M.; Reed, J. C. Expression and prognostic significance of IAP-family genes in human cancers and myeloid leukemias. *Clin. Cancer Res.* **2000**, *6*, 1796–1803.

9 Mizutani, Y.; Nakanishi, H.; Li, Y. N.; Matsubara, H.; Yamamoto, K.; Sato, N.; Shiraishi, T.; Nakamura, T.; Mikami, K.; Okihara, K.; Takaha, N.; Ukimura, O.; Kawauchi, A.; Nonomura, N.; Bonavida, B.; Miki, T. Overexpression of XIAP expression in renal cell carcinoma predicts a worse prognosis. *Int. J. Oncol.* **2007**, *30*, 919–925.

10 Lopes, R. B.; Gangeswaran, R.; McNeish, I. A.; Wang, Y.; Lemoine, N. R. Expression of the IAP protein family is dysregulated in pancreatic cancer cells and is important for resistance to chemotherapy. *Int. J. Cancer* **2007**, *120*, 2344–2352.

11 Nakagawa, Y.; Abe, S.; Kurata, M.; Hasegawa, M.; Yamamoto, K.; Inoue, M.; Takemura, T.; Suzuki, K.; Kitagawa, M. IAP family protein expression correlates with poor outcome of multiple myeloma patients in association with chemotherapy-induced overexpression of multidrug resistance genes. *Am. J. Hematol.* **2006**, *81*, 824–831.

12 Yang, L.; Cao, Z.; Yan, H.; Wood, W. C. Coexistence of high levels of apoptotic signaling and inhibitor of apoptosis proteins in human tumor cells: Implication for cancer specific therapy. *Cancer Res.* **2003**, *63*, 6815–6824.

13 Liu, Z.; Sun, C.; Olejniczak, E. T.; Meadows, R. P.; Betz, S. F.; Oost, T.; Herrmann, J.; Wu, J. C.; Fesik, S. W. Structural basis for binding of Smac/DIABLO to the XIAP BIR3 domain. *Nature* **2000**, *408*, 1004–1008.

14 Wu, G.; Chai, J.; Suber, T. L.; Wu, J.-W.; Du, C.; Wang, X.; Shi, Y. Structural basis of IAP recognition by Smac/DIABLO. *Nature* **2000**, *408*, 1008–1012.

15 Li, L.; Thomas, R. M.; Suzuki, H.; De Brabander, J. K.; Wang, X.; Harran, P. G. A small molecule Smac mimic potentiates TRAIL and TNFα-mediated cell death. *Science* **2004**, *305*, 1471–1474.

16 Oost, T. K.; Sun, C.; Armstrong, R. C.; Al-Assaad, A. S.; Betz, S. F.; Deckwerth, T. L.; Ding, H.; Elmore, S. W.; Meadows, R. P.; Olejniczak, E. T. Discovery of potent antagonists of the antiapoptotic protein XIAP for the treatment of cancer. *J. Med. Chem.* **2004**, *47*, 4417–4426.

17 Sun, H.; Nikolovska-Coleska, Z.; Yang, C.-Y.; Qian, D.; Lu, J.; Qiu, S.; Bai, L.; Peng, Y.; Cai, Q.; Wang, S. Design of small-molecule peptidic and nonpeptidic Smac mimetics. *Acc. Chem. Res.* **2008**, *41*, 1264–1277.

18 Flygare, J.; Fairbrother, W. Small-molecule pan-IAP antagonists: A patent review. *Expert Opin. Ther. Pat.* **2010**, *20*, 251–267.

19 Condon, S. M. The discovery and development of Smac-mimetics-small-molecule antagonists of the inhibitor of apoptosis proteins. *Annu. Rep. Med. Chem.* **2011**, *46*, 211–226.

20 Ramakrishnan, V.; Painuly, U.; Kimlinger, T.; Haug, J.; Rajkumar, S. V.; Kumar, S. Inhibitor of apoptosis proteins as therapeutic targets in multiple myeloma. *Leukemia* **2014**, *28*, 1519–1528.

21 Cai, Q.; Sun, H.; Peng, Y.; Lu, J.; Nikolovska-Coleska, Z.; McEachern, D.; Liu, L.; Qiu, S.; Yang, C. Y.; Miller, R.; Yi, H.; Zhang, T.; Sun, D.; Kang, S.; Guo, M.; Leopold, L.; Yang, D.; Wang, S. A potent and orally active antagonist (SM-406/AT-406) of multiple inhibitor of apoptosis proteins (IAPs) in clinical development for cancer treatment. *J. Med. Chem.* **2011**, *54*, 2714–2726.

22 Flygare, J. A.; Beresini, M.; Budha, N.; Chan, H.; Chan, I. T.; Cheeti, S.; Cohen, F.; Deshayes, K.; Doerner, K.; Eckhardt, S. G.; Elliott, L. O.; Feng, B.; Franklin, M. C.; Reisner, S. F.; Gazzard, L.; Halladay, J.; Hymowitz, S. G.; La, H.; LoRusso, P.; Maurer, B.; Murray, L.; Plise, E.; Quan, C.; Stephan, J. P.; Young, S. G.; Tom, J.; Tsui, V.; Um, J.; Varfolomeev, E.; Vucic, D.; Wagner, A. J.;

Wallweber, H. J.; Wang, L.; Ware, J.; Wen, Z.; Wong, H.; Wong, J. M.; Wong, M.; Wong, S.; Yu, R.; Zobel, K.; Fairbrother, W. J. Discovery of a potent small-molecule antagonist of inhibitor of apoptosis (IAP) proteins and clinical candidate for the treatment of cancer (GDC-0152). *J. Med. Chem.* **2012**, *55*, 4101–4113.

23 Condon, S. M.; Mitsuuchi, Y.; Deng, Y.; Laporte, M. G.; Rippin, S. R.; Haimowitz, T.; Alexander, M. D.; Kumar, P. T.; Hendi, M. S.; Lee, Y.; Benetatos, C. A.; Yu, G.; Kapoor, G. S.; Neiman, E.; Seipel, M. E.; Burns, J. M.; Graham, M. A.; McKinlay, M. A.; Li, X.; Wang, J.; Shi, Y.; Feltham, R.; Bettjeman, B.; Cumming, M. H.; Vince, J. E.; Khan, N.; Silke, J.; Day, C. L.; Chunduru, S. K. Birinapant, a Smac-mimetic with improved tolerability for the treatment of solid tumors and hematological malignancies. *J. Med. Chem.* **2014**, *57*, 3666–3677.

24 Driggers, E. M.; Hale, S. P.; Lee, J.; Terrett, N. K. The exploration of macrocycles for drug discovery – an underexploited structural class. *Nat. Rev. Drug Discov.* **2008**, *7*, 608–624.

25 Gartner, Z. J.; Liu, D. R. The generality of DNA-templated synthesis as a basis for evolving non-natural small molecules. *J. Am. Chem. Soc.* **2001**, *123*, 6961–6963.

26 Gartner, Z. J.; Kanan, M. W.; Liu, D. R. Multistep small-molecule synthesis programmed by DNA templates. *J. Am. Chem. Soc.* **2002**, *124*, 10304–10306.

27 Gartner, Z. J.; Tse, B. N.; Grubina, R.; Doyon, J. B.; Snyder, T. M.; Liu, D. R. DNA-templated organic synthesis and selection of a library of macrocycles. *Science* **2004**, *305*, 1601–1605.

28 Kleiner, R. E.; Dumelin, C. E.; Liu, D. R. Small-molecule discovery from DNA-encoded chemical libraries. *Chem. Soc. Rev.* **2011**, *40*, 5707–5717.

29 Seigal, B. A.; Connors, W. H.; Fraley, A.; Borzilleri, R. M.; Carter, P. H.; Emanuel, S. L.; Fargnoli, J.; Kim, K.; Lei, M.; Naglich, J. G.; Pokross, M. E.; Posy, S. L.; Shen, H.; Surti, N.; Talbott, R.; Zhang, Y.; Terrett, N. K. The discovery of macrocyclic XIAP antagonists from a DNA-programmed chemistry library, and their optimization to give lead compounds with in vivo antitumor activity. *J. Med. Chem.* **2015**, *58*, 2855–2861.

30 Tsantrizos, Y. S.; Bolger, G.; Bonneau, P.; Cameron, D. R.; Goudreau, N.; Kukolj, G.; LaPlante, S. R.; Llinàs-Brunet, M.; Nar, H.; Lamarre, D. Macrocyclic inhibitors of the NS3 protease as potential therapeutic agents of hepatitis C virus infection. *Angew. Chem. Int. Ed. Engl.* **2003**, *42*, 1356–1360.

31 Deveraux, Q. L.; Reed, J. C. IAP family proteins-suppressors of apoptosis. *Genes Dev.* **1999**, *13*, 239–252.

32 Sheng, R.; Sun, H.; Liu, L.; Lu, J.; McEachern, D.; Wang, G.; Wen, J.; Min, P.; Du, Z.; Lu, H.; Kang, S.; Guo, M.; Yang, D.; Wang, S. A potent bivalent Smac mimetic (SM-1200) achieving rapid, complete, and durable tumor regression in mice. *J. Med. Chem.* **2013**, *56*, 3969–3979.

33 Sun, H.; Nikolovska-Coleska, Z.; Lu, J.; Meagher, J. L.; Yang, C. Y.; Qiu, S.; Tomita, Y.; Ueda, Y.; Jiang, S.; Krajewski, K.; Roller, P. P.; Stuckey, J. A.; Wang, S. Design, synthesis, and characterization of a potent, nonpeptide, cell-permeable, bivalent Smac mimetic that concurrently targets both the BIR2 and BIR3 domains in XIAP. *J. Am. Chem. Soc.* **2007**, *129*, 15279–15294.

34 Nikolovska-Coleska, Z.; Meagher, J. L.; Jiang, S.; Kawamoto, S. A.; Gao, W.; Yi, H.; Qin, D.; Roller, P. P.; Stuckey, J. A.; Wang, S. Design and characterization of bivalent Smac-based peptides as antagonists of XIAP and development and validation of a fluorescence polarization assay for XIAP containing both BIR2 and BIR3 domains. *Anal. Biochem.* **2008**, *374*, 87–98.

35 Nikolovska-Coleska, Z.; Meagher, J. L.; Jiang, S.; Yang, C. Y.; Qiu, S.; Roller, P. P.; Stuckey, J. A.; Wang, S. Interaction of a cyclic, bivalent Smac mimetic with the X-linked inhibitor of apoptosis protein. *Biochemistry* **2008**, *47*, 9811–9824.

36 Sun, H.; Liu, L.; Lu, J.; Qiu, S.; Yang, C. Y.; Yi, H.; Wang, S. Cyclopeptide Smac mimetics as antagonists of IAP proteins. *Bioorg. Med. Chem. Lett.* **2010**, *20*, 3043–3046.

37 Rezai, T.; Yu, B.; Millhauser, G. L.; Jacobson, M. P.; Lokey, R. S. Testing the conformational hypothesis of passive membrane permeability using synthetic cyclic peptide diastereomers. *J. Am. Chem. Soc.* **2006**, *128*, 2510–2511.

38 Ahlbach, C. L.; Lexa, K. W.; Bockus, A. T.; Chen, V.; Crews, P.; Jacobson, M. P.; Lokey, R. S. Beyond cyclosporine A: Conformation dependent passive membrane permeabilities of cyclic peptide natural products. *Future Med. Chem.* **2015**, *7*, 2121–2130.

39 Zhang, Y.; Seigal, B. A.; Terrett, N. K.; Talbott, R. L.; Fargnoli, J.; Naglich, J. G.; Chaudhry, C.; Posy, S. L.; Vuppugalla, R.; Cornelius, G.; Lei, M.; Wang, C.; Zhang, Y.; Schmidt, R. J.; Wei, D. D.; Miller, M. M.; Allen, M. P.; Li, L.; Carter, P. H.; Vite, G. D.; Borzilleri, R. M. Dimeric macrocyclic antagonists of inhibitor of apoptosis proteins for the treatment of cancer. *ACS Med. Chem. Lett.* **2015**, *6*, 770–775.

40 Backer, A.; Bonnie, P. R.; Hocked, O.; Jakalian, A.; Edwards, P. J. Development of specific "drug-like property" rules for carboxylate-containing oral candidates. *ChemMedChem* **2010**, *5*, 2102–2113.

41 Meanwell, N. A. Synopsis of some recent tactical application of bioisosteres in drug design. *J. Med. Chem.* **2011**, *54*, 2529–2591.

42 Sun, H.; Liu, L.; Lu, J.; Bai, L.; Li, X.; Nikolovska-Coleska, Z.; McEachern, D.; Yan, C.; Qiu, S.; Yi, H.; Sun, D.; Wang, S. Potent bivalent Smac mimetics: Effect of the linker on binding to inhibitor of apoptosis protein (IAPs) and anticancer activity. *J. Med. Chem.* **2011**, *54*, 3306–3318.

43 Hennessy, E. J.; Adam, A.; Aquila, B. M.; Castriotta, L. M.; Cook, D.; Hattersley, M.; Hird, A. W.; Huntington, C.; Kamhi, V. M.; Laing, N. M.; Li, D.; MacIntyre, T.; Omer, C. A.; Oza, V.; Patterson, T.; Repik, G.; Rooney, M. T.; Saeh, J. C.; Sha, L.; Vasbinder, M. M.; Wang, H.; Whitston, D. Discovery of a novel class of dimeric Smac mimetics as potent IAP antagonists resulting in a clinical candidate for the treatment of cancer (AZD5582). *J. Med. Chem.* **2013**, *56*, 9897–9919.

44 Long, B. H.; Wang, L.; Lorico, A.; Wang, R. R. C.; Brattain, M. G.; Casazza, A. M. Mechanisms of resistance to etoposide and teniposide in acquired resistant human colon and lung carcinoma cell lines. *Cancer Res.* **1991**, *51*, 5275–5284.

45 Talbott, R. L.; Borzilleri, R. M.; Chaudhry, C.; Fargnoli, J.; Shen, H.; Fairchild, C.; Barnhart, B.; Ortega, M.; McDonagh, T. E.; Vuppugalla, R.; Vite, G. D.; Hunt, J. T.; Gottardis, M.; Naglich, J. G. Pharmacology of Smac mimetics; chemotype differentiation based on physical association with caspase regulators and cellular transport. *Exp. Cell Res.* **2015**, *338*, 251.

18

Discovery and Pharmacokinetic–Pharmacodynamic Evaluation of an Orally Available Novel Macrocyclic Inhibitor of Anaplastic Lymphoma Kinase and c-Ros Oncogene 1

Shinji Yamazaki, Justine L. Lam and Ted W. Johnson

Pfizer Worldwide Research & Development, San Diego, CA, USA
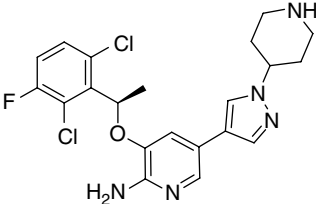
18.1   Introduction

One of the most common and lethal malignancies worldwide has long been lung cancer with 1.8 million new cases and 1.6 million deaths annually. These represent 13 and 19% of new cancers and cancer mortality yearly, respectively, as estimated in 2012 by the International Agency for Research on Cancer of the World Health Organization (http://globocan.iarc.fr/Default.aspx). The majority of lung cancers (approximately 90%) are non-small cell lung cancers (NSCLC), consisting of a number of subtypes driven by various activated oncogenes [1, 2]. Recent advances in molecular profiling technologies have made great progress in developing personalized cancer therapies, with molecularly targeted agents (MTAs) based on individual genetic or protein profiles [3, 4]. One of these successful agents for personalized cancer therapies is small-molecule tyrosine kinase inhibitors (TKIs) of activating epidermal growth factor receptor (EGFR), gefitinib and erlotinib, in NSCLC patients [5–7]. However, clinical efficacy responses to these first-generation EGFR inhibitors are not durable in most cancer patients because of drug resistance, which appears to be readily acquired by tumors. Drug resistance involves multiple mechanisms such as the secondary mutations in EGFR (e.g., T790M), the amplification of mesenchymal–epithelial transition factor (MET), and the increased activation of the receptor tyrosine kinase, AXL [8, 9]. The identification of drug resistance mechanisms toward the first-generation EGFR inhibitors has rapidly led to the development of next-generation inhibitors, with the goal to overcome acquired and/or adaptive drug resistances [10, 11]. The principles and practices on personalized cancer therapy with EGFR inhibitors highly influenced the accelerated approval of the first-generation anaplastic lymphoma kinase (ALK) inhibitor,

crizotinib[1] (Xalkori; **PF-02341066**), by the Food and Drug Administration (FDA) in 2011, which was followed by worldwide approvals [12–14]. Remarkably, FDA approval occurred less than 4 years since its molecular targets, ALK gene rearrangements (e.g., echinoderm microtubule-associated protein-like 4 (EML4)-ALK), were first reported in a handful of NSCLC patients [15, 16]. To select a specific subset of NSCLC patients with ALK gene rearrangements as personalized cancer medicine, crizotinib-prescribing information in the United States states that "Xalkori is a kinase inhibitor indicated for the treatment of patients with metastatic NSCLC whose tumors are ALK-positive as detected by an FDA-approved test" [17]. Thus, FDA approval was accompanied by the simultaneous approval of the break-apart fluorescence *in situ* hybridization (FISH) test as the companion diagnostic kit, Vysis (Abbott Molecular, Abbott Park, IL). Patients with ALK-positive NSCLC have been highly responsive to crizotinib with an objective response rate (ORR) of approximately 60% and a median progression-free survival (PFS) of 8–10 months [14, 18]. Unfortunately, as seen with other target therapies such as the first-generation EGFR inhibitors, crizotinib resistance mechanisms have been reported even before its approval [19]. Among the 69 reported cases of crizotinib-resistant ALK-positive NSCLC patients, detected crizotinib-resistant mechanisms were secondary mutations in the ALK kinase domain in 20 patients (approximately 30%), most commonly "gatekeeper" (GK) mutation L1196M, followed by amplification of the rearranged ALK locus in six patients (9%) and activation of alternative receptor tyrosine kinases (e.g., EGFR) in a few patients [20]. These crizotinib-resistant mechanisms

---

1 **PF-02341066** (crizotinib, catalog # PZ0191) is commercially available via Sigma–Aldrich (St. Louis, MO, USA).

Table 18.1 Potency and *in vitro* ADME properties of crizotinib (**1**).

Compound	Structure	ALK K_i (nM)	ALK cell IC$_{50}$ (nM)^a	Log D^b	HLM Cl (ml/min/kg)^c	MDR BA/AB (ratio)^d
1 (crizotinib)		0.74	80	2.0	44	12.5/0.28 (44.5)

^{a} NIH3T3-engineered cell line.

^{b} Log D was measured at pH 7.4.

^{c} Cl$_{int,app}$ refers to the total intrinsic clearance obtained from scaling *in vitro* half-lives in human liver microsomes (HLM).

^{d} MDCK-MDR1 BA/AB efflux at 2 μM substrate concentration and pH 7.4.

in patients with NSCLC led to the rapid development of next-generation ALK inhibitors such as **PF-06463922**[2] (lorlatinib), described herein [20–22].

18.2 Discovery and Synthesis

18.2.1 Background—Macrocyclic Kinase Inhibitors

Macrocycles are defined as ring structures consisting of at least 12 atoms [23]. There are reported ATP-competitive macrocyclic inhibitors targeting kinases such as ALK [24], JAK2, CDKs, and FLT3 [25–27], among others. In addition, reviews and perspectives have also been published describing a broad range of macrocycles spanning different therapeutic areas and targets, including kinases [23, 28]. One of the earlier ATP-competitive macrocyclic kinase inhibitors was reported by Hart and coworkers [26]. Exemplified by SB1518, an aminopyrimidine hinge-binding motif was cyclized to an 18-membered ring utilizing a ring-closing metathesis (RCM) reaction. The inhibitor showed potent biochemical-based inhibitory activity against JAK2 and FLT3 kinases, among others. A similar example from Breslin *et al.* uses the 2,4-diaminopyrimidine hinge-binding scaffold to form 14-membered rings, also via RCM reactions, that showed favorable potency for ALK [25]. The linkers are generally all carbon, aliphatic groups, and flexible, allowing the formerly acyclic-binding portion of the ligand the ability to adopt a conformation similar to that of the acyclic (usually optimized) analogue. However, improvements in potency are mostly

driven by bulk increase in lipophilicity in these cases, leaving the macrocycles with no ligand or lipophilic efficiency advantages.

18.2.2 Crizotinib Discovery and SAR

Table 18.1 highlights some of the key properties of crizotinib **1**. Since crizotinib was not originally designed as an ALK inhibitor, activity was modest in both biochemical and cell-based engineered assays. *In vitro* clearance was also not optimal, although **1** performed better *in vivo* due to time-dependent CYP inhibition [29]. In addition, crizotinib was a substrate of P-glycoprotein (P-gp), displaying high efflux ratios. This was also not surprising since crizotinib was not designed to be brain penetrant.

18.2.3 Resistance Mechanisms to Crizotinib

Although crizotinib demonstrated initial robust efficacy in ALK-positive tumors, patients eventually developed resistance. There are multiple mechanisms of acquired resistance that may occur or be enhanced during treatment with ALK inhibitors, including upregulation of ALK, bypass mechanisms, and sequence modifications to the enzyme. Initial reports focused on missense mutations in the kinase domain that were both distal and proximal to the crizotinib binding site in the ATP pocket. Generally speaking, those distal to the inhibitor increase kinase activity without interrupting crizotinib binding affinity, while those more proximal *may* reduce binding affinity [30]. To date, many NSCLC EML4-ALK patient-derived missense, insertion, and deletion mutants are reported in the literature, including F1174L, C1156Y, G1269A, S1206Y, L1196M, L1152R, G1202R, 1151Tins (threonine insertion at 1151), I1171T, and V1180L. In addition to the acquired resistance mutations, patients

---

2 **PF-06463922** (lorlatinib, catalog # PZ0271) is commercially available via Sigma–Aldrich (St. Louis, MO, USA).

Table 18.2 Potency and efficiency of crizotinib in ALK-L1196M.

Compound	ALK-L1196M K_i (nM)	ALK-L1196M cell IC_{50} (nM)[a]	Log D[b]	LipE[c]
1 (crizotinib)	8.2	843	2.0	4.1

[a] NIH3T3-engineered cell line.
[b] Log D was measured at pH 7.4.
[c] LipE = $-$log ALK L1196M cell $IC_{50} - \log D$.

experience progression during therapy due to uncontrolled brain metastases, since many of the marketed inhibitors, including crizotinib, do not adequately pass the blood–brain barrier (BBB). Interestingly, Shaw *et al.* recently reported the re-sensitization of a patient to crizotinib therapy. The patient experienced disease progression on initial treatment with crizotinib followed by other ALK inhibitor therapies before a successful retreatment with crizotinib [31].

18.2.4 Program Goals and Lab Objectives

Due to the development of resistance to crizotinib, we aimed to implement improvements in several key areas, including broad spectrum ALK potency and reasonable absorption, distribution, metabolism, and excretion (ADME) properties, including penetration into the central nervous system (CNS) to treat brain metastases. In addition, we required high levels of selectivity given the increased distribution of low efflux compounds. Early in the program, the ALK gatekeeper (GK) mutant, L1196M, was the most prevalent and resistant crizotinib reported

mutant and was used as a surrogate mutation to determine sensitivity, with testing against other reported mutants later in the screening cascade as they were identified.

The potency and efficacy of crizotinib in the GK mutant kinase is shown in Table 18.2. Both the biochemical ALK-L1196M K_i and cell IC_{50} are shifted to considerably weaker potencies relative to wild-type ALK (approximate 10-fold loss in potency). The lipophilic efficiency (LipE or LLE) of crizotinib against the GK mutant ALK-L1196M value was modest at 4.1. LipE ($-$log $IC_{50} - \log D$) is a measure of lipophilicity-corrected potency and can be useful in optimizing multiple properties simultaneously, including potency, clearance, permeability, and selectivity [32, 33]. Lipophilic molecules tend to bind nonspecifically to proteins. Hence, a focus on improving LipE values also helps avoid the trap of improving potency by increasing lipophilicity through nonspecific binding, leading to issues with off-target activities and clearance, for example. The presence of the bulk-solvent-exposed piperidine group helps raise the LipE value for crizotinib. This is generally true since bound ligands with polarity directed to solvent can substantially lower log D but do not negatively impact affinity because desolvation penalties are minimal.

18.2.5 Structural Data, Potency, ADME— Crizotinib and PF-06439015

Figure 18.1 (left panel) shows crizotinib bound to the GK mutant of ALK. Crizotinib is a type I kinase inhibitor occupying the ATP-binding pocket and protein solvent
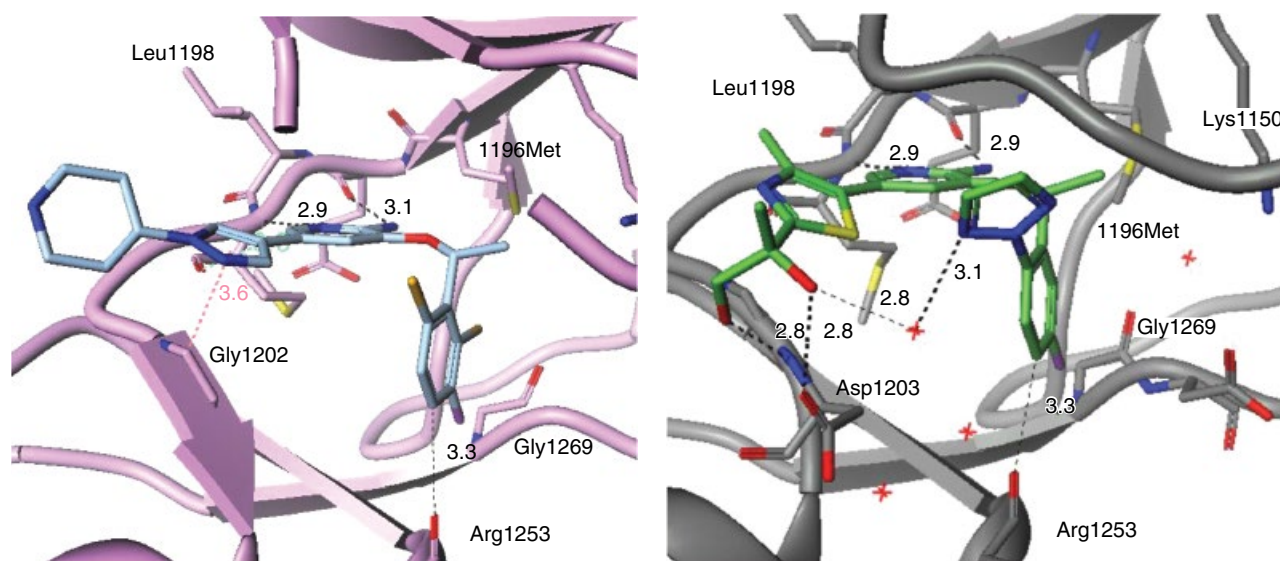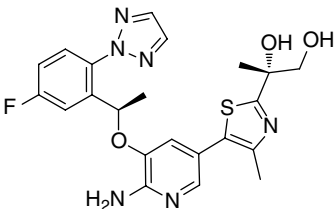
Figure 18.1 Left panel: Crizotinib (**1**) co-crystal structure in ALK-L1196M kinase domain (PDB 2YFX, 1.7 Å). Right panel: PF-06439015 (**2**) bound to ALK-L1196M KD (PDB 4CD0, 2.2 Å). (*See insert for color representation of the figure.*)

Table 18.3 Potency and *in vitro* ADME properties of PF-06439015.

Compound	Structure	ALK-L1196M K_i (nM)	ALK-L1196M cell IC_{50} (nM)[a]	Log D[b]	LipE[c]	HLM Cl (ml/min/kg)[d]	MDR BA/AB (ratio)[e]
2 (PF-06439015)		0.2	6.6	2.9	5.3	13	30.6/2.8 (10.9)

[a] NIH3T3-engineered cell line.
[b] Log D was measured at pH 7.4.
[c] LipE = −log ALK L1196M cell IC_{50} − log D.
[d] $Cl_{int,app}$ refers to the total intrinsic clearance obtained from scaling *in vitro* half-lives in human liver microsomes (HLM).
[e] MDCK-MDR1 BA/AB efflux at 2 μM substrate concentration and pH 7.4.

front, without occupying the back pocket of the protein (past the GK residue toward the DFG Phe and c-alpha helix). It is interesting to note that the glycine-rich loop (G-loop) of the protein is disordered, which implies that ligand affinity may not be optimal especially in the region of the ligand closest to the G-loop.

Since crizotinib was optimized for cMET, efforts were directed at improving affinity of analogues for ALK. A recent publication highlights the design of potent acyclic ALK inhibitors from crizotinib [34], resulting in an optimized ALK inhibitor, PF-06439015 (**2**; Table 18.3). **2** makes several noteworthy interactions with the ALK protein (Figure 18.1, right panel). The chlorophenyl head group was modified to improve overall binding for ALK. The chlorine atom was removed to allow the Gly1269 backbone carbonyl to relax toward the inhibitor, better resembling the apo conformation. The diol interacts with Asp1203, while an internal water molecule bridges the triazole nitrogen acceptor and the internal alcohol. Interestingly, this interaction creates a pseudo-macrocycle by a water-bridged intramolecular hydrogen bond. In addition, The G-loop (above the triazole) is resolved, unlike crizotinib (Figure 18.1, left panel).

Although PF-06439015 was extremely potent in ALK biochemical and cell-based assays and generally displayed good *in vitro* ADME properties, it was designed to be excluded from the CNS. The diol moiety added molecular weight, reduced lipophilicity, and added two hydrogen bond donors, all of which resulted in P-gp efflux and CNS exclusion.

18.2.6 Acyclic ALK Inhibitors

According to Table 18.4, other acyclic analogues were pursued that lacked excess hydrogen bond donors and polarity. Compounds **3a** and **3b** both had improved *in vitro* clearance and permeability relative to crizotinib.

The MDR efflux ratios for both compounds are less than or equal to 2.5 and consistent with good predicted brain availability in humans. Unfortunately, both wild-type and L1196M ALK cellular IC_{50} values suffered. Compound **3c** also displayed a desirable, low MDR efflux ratio but lacked the required potency and *in vitro* clearance.
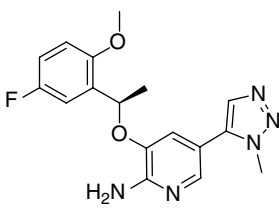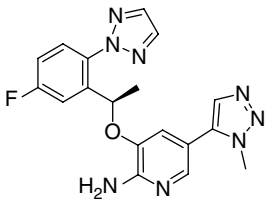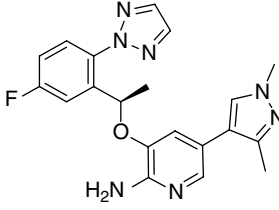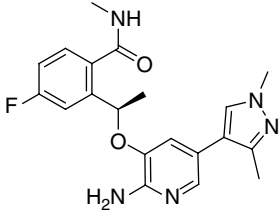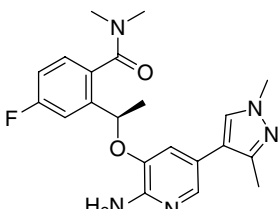
The amide substituents on the phenyl ring of compounds **3d** and **3e** were designed to lower lipophilicity and improve efficiency. Indeed, the amide group in **3d** and **3e** lowered lipophilicity significantly relative to the triazole **3c**. Insights into the impact of the amide on potency and efficiency were gained by highlighting matched molecular pairs. The secondary amide **3d** showed roughly a 10-fold reduction in cellular potencies against both wild-type and mutant ALK yet a slight improvement in LipE compared with the aminopyridine 1,2,3-triazole **3c**. Addition of a methyl group provided the tertiary amide analogue **3e**, which lost greater than 100-fold potency relative to the triazole analogue **3c**, presumably due to steric clash of the pyrazole and *N,N*-dimethylamide in the preferred bound conformation.

These acyclic compounds highlighted the difficulty in overlapping potency (L1196M $IC_{50} < 25$ nM) and low MDR BA/AB ratios (less than 2.5) to afford the highest probability of reaching efficacious exposures in the CNS. To overlap the required properties, new design efforts targeted neutral inhibitors with improved lipophilic efficiency that fell within property space commensurate with low efflux.

18.2.7 Design from Acyclic Structural Data

The U-shaped ligand structures of acyclic compounds exemplified by **1** and **2** (Figure 18.1), among others, inspired the design of linkers that connect head and tail regions of the ligands. We desired a linker that (i)

Table 18.4 Acyclic ALK inhibitors—potency, efficiency, and *in vitro* ADME.

Cpd #	Structure	ALK-L1196M K_i (nM)	pALK-L1196M cell IC$_{50}$ (nM)[a]	Log D[b]	LipE[c]	HLM Cl (ml/min/kg)[d]	MDR BA/AB (ratio)[e]
3a	*(structure)*	38	3200	2.4	3.1	25	16.3/20.0 (0.82)
3b	*(structure)*	70	2650	2.4	3.2	8.0	27.5/11.0 (2.5)
3c	*(structure)*	2.6	176	3.4	3.4	66	16.5/10.9 (1.5)
3d	*(structure)*	35	1665	2.1	3.7	28	12.6/0.74 (17.0)
3e	*(structure)*	310	ND	2.1	ND	58	18.8/2.5 (7.6)

ND, not determined.

[a] NIH3T3-engineered cell line.

[b] Log D was measured at pH 7.4.

[c] LipE = −log ALK L1196M cell IC$_{50}$ − log D.

[d] Cl$_{int,app}$ refers to the total intrinsic clearance obtained from scaling *in vitro* half-lives in human liver microsomes (HLM).

[e] MDCK-MDR1 BA/AB efflux at 2 μM substrate concentration and pH 7.4.

reinforced binding conformation without additional binding strain and (ii) provided additional, enhanced specific protein–ligand interactions, thus improving LipE.

Prior to embarking on the macrocycle synthetic journey, we reviewed the advantages and disadvantages of macrocycles in the context of our program objectives.

We thought that cyclization might improve passive permeability through rigidification, reduction in rotatable bonds and size, making the inhibitor smaller and more compact. In addition, we desired to improve potency by reinforcing the bound conformation and providing additional protein–ligand interactions, including in the linker
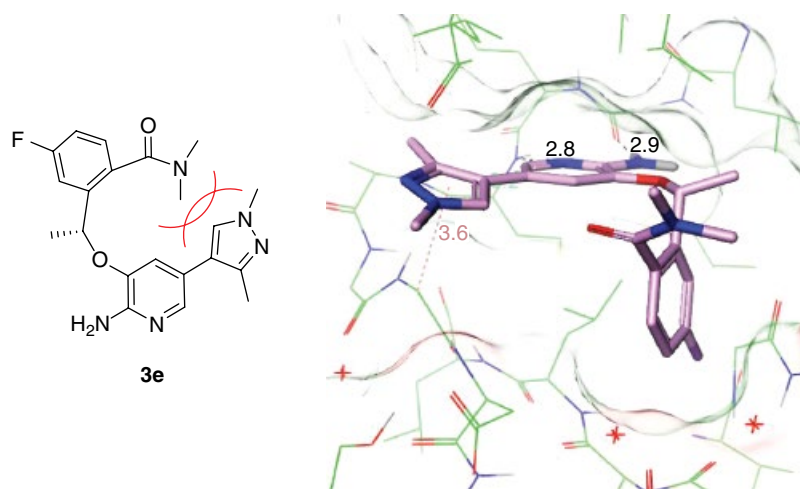
Figure 18.2 Internal clash of amide and pyrazole in preferred conformation of **3e** causes rotation of the amide into a less productive binding conformation. **3e** co-crystallized with ALK KD (PDB 5KZ0). (*See insert for color representation of the figure.*)

portion of the macrocycle. Making a macrocycle, especially a rigid macrocycle, required that we get the conformation just right to avoid locking the inhibitor in an unproductive binding conformation. Although ring-forming strategies are thought of as improving potency through the removal of entropic barriers, it is likely that conformational entropy is a minor factor, while enthalpy considerations are more substantial [35]. Enthalpic impact more often outweighs any entropy contributions in both make-a-ring and break-a-ring strategies to improve binding efficiency. For this reason, eventually building additional interactions of the linker was desired to increase potency and potency efficiency.

18.2.8 Macrocyclic ALK Inhibitors

To evaluate the macrocycle design concept, a variety of 12- to 14-membered ether-linked macrocycles were prepared based on the acyclic co-crystal structure analyses, as summarized in Table 18.5. According to matched molecular pairs, the smaller ring sizes consistently provided the most lipophilic efficient macrocycles. For example, cyclic ethers **4a**, **4c**, and **4e** had higher LipE than their corresponding larger-ring matched molecular pairs **4b**, **4d**, and **4f**. The 12-membered macrocycle **4e** displayed the highest LipE (4.4) with pM binding affinities and good cellular potencies (ALK IC$_{50}$ 1.0 nM; ALK-L1196M IC$_{50}$ 20 nM). Although some of the more efficient analogues provided improved potency and LipE relatively to the acyclic analogue **3a**, the macrocyclic ethers were generally too lipophilic and still lacked the required efficacy for more facile overlap of potency and CNS ADME.

We moved to optimize the acyclic amides in Table 18.4 that showed the highest LipE values (**3d** and **3e**). Internal clash of the amide in **3e** (Figure 18.2) causes amide rotation to an unproductive conformation for interactions

with the G-loop and conserved lysine, providing an opportunity for optimization. To reinforce the binding conformation, modeling (Figure 18.3, left panel) suggested a single covalent linkage of the amide carbon with the proximal pyrazole moiety leading to a proposed 12-membered lactam that would have minimal binding strain. In addition, the *N*-methyl group may provide close contact with Val1130, Leu1122, and Gly1123 of the G-loop, and the lactam carbonyl oxygen may act through a structural water to stabilize Lys1150 (Figure 18.3, left panel). Importantly, the amide macrocycles would significantly lower lipophilicity, placing them in an optimal log*D* space.

A set of amide-linked macrocycles was prepared to test the hypothesis. The co-crystal structure of the ALK kinase domain with the cyclic amide **4g** supported the design hypothesis and molecular modeling, superimposing well with the original docking result (Figure 18.3, right panel). As expected, the *N*-methyl group in **4g** was pulled tighter toward the G-loop by 1.2 Å from the open amide position and therefore had a closer contact with the carbonyl group of Leu1122 (3.4 Å) and nearby side chains of Leu1122 (4.1 Å), Gly1123 (4.7 Å), and Val1130 (4.7 Å). The amide carbonyl of macrocycle **4g** formed a water bridge with Lys1150 and a second water bridge to His1124. It was expected that interaction of the lactam carbonyl oxygen with waters in the bound state may effectively lower binding desolvation penalties.

Improvement in key parameters was realized upon cyclization to the amide macrocycle **4g** (Table 18.5) from acyclic analogues **3d–e** (Table 18.4). Relative to acyclic amide **3d**, macrocycle **4g** improved cellular potency against the GK mutant protein by 119-fold while maintaining log*D*, which also translated to a two-unit increase in LipE. In addition, molecular weight was low. Improvements in potency and efficiency were even more pronounced relative to the closest matched pair, acyclic

Table 18.5 Early macrocyclic ALK inhibitors—potency, efficiency, and *in vitro* ADME.

Cpd #	Structure	ALK-L1196M K_i (nM)	ALK-L1196M cell IC$_{50}$ (nM)[a]	Log D[b]	LipE[c]	HLM Cl (ml/min/kg)[d]	MDR BA/AB (ratio)[e]
4a		1.6	101	3.0	4.0	19.3	26.5/4.38 (6.06)
4b		<0.1	112	3.6	3.4	47	14.4/0.89 (16.2)
4c		29	654	3.4	2.8	103	17.3/11.6 (1.50)
4d		36	3655	3.1	2.3	55	ND
4e		0.57	20	3.3	4.4	ND	ND
4f		0.62	21	3.8	3.9	ND	ND
4g		0.29	14	2.2	5.7	8.6	28.3/8.1 (4.2)

ND, not determined.

[a] NIH3T3-engineered cell line.

[b] Log D was measured at pH 7.4.

[c] LipE = −log ALK L1196M cell IC$_{50}$ − log D.

[d] Cl$_{int,app}$ refers to the total intrinsic clearance obtained from scaling *in vitro* half-lives in human liver microsomes.

[e] MDCK-MDR1 BA/AB efflux at 2 μM substrate concentration and pH 7.4.
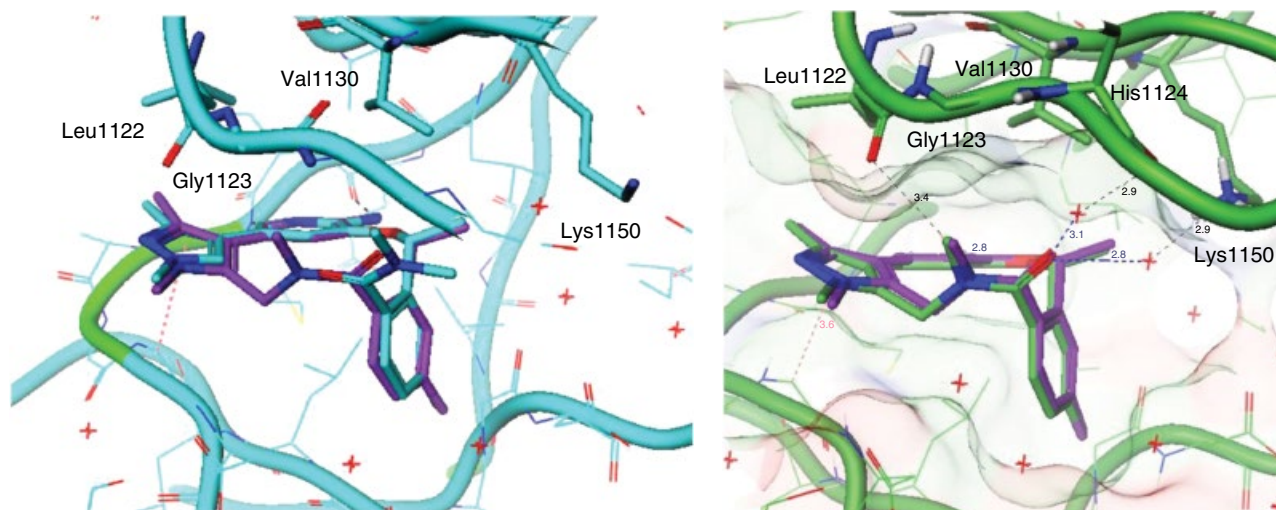
Figure 18.3 Left panel: Acyclic amide **3e** co-crystal structure in ALK (cyan, PDB 5KZ0) overlaid with modeled macrocycle **4g** (purple) in ALK. Right panel: **4g** co-crystal structure in ALK-kinase domain (green, PDB 4CMU) overlaid with modeled ligand (purple). (*See insert for color representation of the figure.*)

N,N-dimethyl amide **3e**. A reduction of the *in vitro* clearance from 56 ml/min/kg (high) to the lower limit of detection for this assay demonstrated the inherent metabolic stability of the cyclic structure. The permeability of **4g**, measured by P-gp efflux potential, was superior to the acyclic analogue **3e**. Overall, there was a dramatic and compelling improvement in overall properties for **4g** relative to **3e**. These results clearly positioned the macrocyclic amides as an attractive series for the generation of ALK inhibitors capable of brain penetration. The higher LipE and lower MW allowed navigation to desired CNS-ADME space without sacrificing potency and safety.

Table 18.6 highlights the important ALK protein sensitivities to subtle structural changes within the amide macrocycle series. The stereochemical sensitivity was determined by the eutomer–distomer ratio. Both **4g** and **4j** improved potency relative to their enantiomeric pairs **4h** and **4k** by 210- and 610-fold, respectively, based on GK mutant biochemical potencies. The desmethyl analogue **4i** lost potency and LipE relative to the more potent methyl analogue **4g**. Three matched molecular pairs highlighted the tolerance of the aminopyrazine core. Several examples (**4g/4j** and **4l/4m** and **4n/4o**) showed an improvement in potency for the aminopyrazine analogues, but the LipE improvement was attenuated as this change was accompanied by an increase, rather than a decrease, in lipophilicity. The additional buried nitrogen atom was not well solvated and also decreased the basicity of the aminopyrazine, leading to an increase in lipophilicity. Table 18.6 also highlights the tolerability of both substituted 5- and 6-membered aromatics adjacent to the aminopyridine or aminopyrazine

cores. The methanesulfonyl–benzene substituent on the aminopyrazine inhibitor **4o** was one of the most lipophilic efficient analogues (L1196M cell IC_{50} LipE 6.5). A comparison of sulfones **4n** and **4o** with the dimethylpyrazoles **4g** and **4j** revealed that both inhibitors possess almost identical potencies. The increased LipE of the sulfone is partly due to the polarity of the sulfone exposed to solvent, which maintained potency and lowered log *D* without incurring additional desolvation penalties.
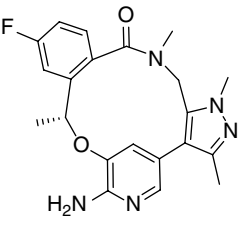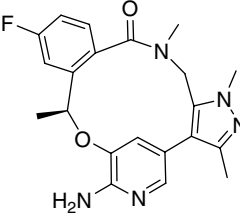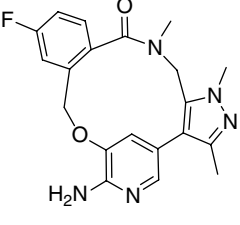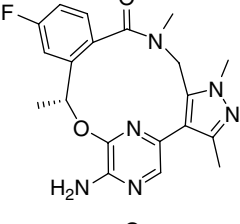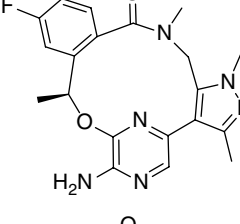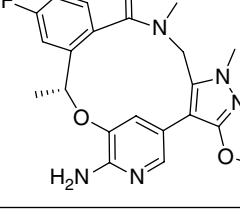
In addition to providing potent inhibitors of ALK within the desired range of log *D* (2–3), the amide macrocycles generally displayed low clearance and low MDR BA/AB efflux ratios. With the initial encouraging results, lead optimization on the macrocyclic amide 2-aminopyridine/pyrazine series was carried out to achieve the best overall balance of potency, CNS-ADME, *and* selectivity in a *single* compound.

18.2.9 Selectivity Strategy

The distribution of residues in the kinome can lead to selectivity strategies and clues about mutational proclivity. The residue at position 1198 in ALK is leucine, a relatively small aliphatic amino acid. Approximately 60% of the protein kinome contains a larger aromatic phenylalanine or tyrosine at this site. Targeting this available space created by the smaller ALK leucine residue formed the basis of the medicinal chemistry selectivity strategy. Indeed, broad spectrum selectivity was vital given the CNS and systemic distribution.

As a surrogate for kinases containing a Phe/Tyr residue at the position corresponding to ALK Leu1198,

Table 18.6 Amide macrocyclic ALK inhibitors—potency, efficiency, and *in vitro* ADME.

Cpd #	Structure	ALK-L1196M K_i (nM)	pALK-L1196M cell IC$_{50}$ (nM)[a]	Log D[b]	LipE[c]	HLM Cl (ml/min/kg)[d]	MDR BA/AB (ratio)[e]
4g		0.29	14	2.2	5.7	8.6	28.3/8.1 (4.2)
4h		61	—	2.2	—	8.0	34.6/5.8 (6.0)
4i		1.9	97	2.0	5.0	8.4	25.4/4.6 (5.5)
4j		0.10	1.4	2.5	6.4	8.0	26.5/11.9 (2.2)
4k		61	1230	2.5	3.4	9.7	29.6/9.6 (3.1)
4l		0.10	2.1	2.4	6.3	8.3	19.9/7.2 (2.8)

(*Continued*)

Table 18.6 (Continued)

Cpd #	Structure	ALK-L1196M K_i (nM)	pALK-L1196M cell IC_{50} (nM)[a]	Log D^b	LipE^c	HLM Cl (ml/min/kg)^d	MDR BA/AB (ratio)^e
4m		<0.02	0.75	2.7	6.4	23.5	40.3/20.1 (2.0)
4n		0.40	21	1.8	5.9	9.1	22.1/2.4 (9.2)
4o		0.12	1.9	2.2	6.5	8.0	8.0/1.2 (6.7)

[a] NIH3T3-engineered cell line.
[b] Log D was measured at pH 7.4.
[c] LipE = –log ALK L1196M cell IC_{50} – log D.
[d] $Cl_{int,app}$ refers to the total intrinsic clearance obtained from scaling *in vitro* half-lives in human liver microsomes.
[e] MDCK-MDR1 BA/AB efflux at 2 μM substrate concentration and pH 7.4.

TrkB (PDB 4AT3) [34] and ALK proteins were aligned by superposition based on a set of residues in the active site (Figure 18.4). Compound **4g** showed a 3.1 Å distance from the pyrazole methyl to the closest TrkB Tyr635 carbon atom, which may provide selectivity with further substitution.

Macrocyclic amides **4g** and **4p–s** were tested against TrkB (Table 18.7). Both the pyrazoles substituted at C3 with methyl and cyclopropyl (**4g** and **4p**, respectively) retained pM enzymatic potencies against TrkB and provided little to no selectivity based on ALK-L1196M K_i (approximately fourfold). However, the cyanopyrazole **4q** (**PF-06463922**) and the methyl-substituted imidazo-pyrimidine **4r** displayed significantly attenuated potency in TrkB and provided reasonable selectivity ratios (approximately 40-fold). Finally, the cyanoimidazo-pyridine **4s** afforded the most robust selectivity ratio (116-fold). These selectivities were consistent with our previous modeling analysis.
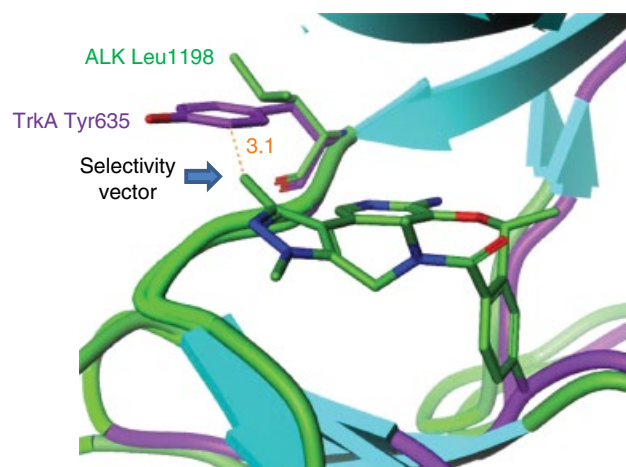
Figure 18.4 Structure of **4g** bound in ALK (green, PDB 4CMU) and TrkB (purple, PDB 4AT3) with selectivity residues and vector highlighted. (*See insert for color representation of the figure.*)

Table 18.7 Potency, ADME, and selectivity of macrocyclic analogues.

Cpd #	Structure	ALK-L1196M K_i (nM)	pALK-L1196M cell IC$_{50}$ (nM)[a]	Log D^b	HLM Cl$_{int,app}{}^c$	MDR BA/AB (ratio)^d	TrkB K_i (nM) (selectivity)^e
4g		0.29	14	2.2	8.6	28.3/8.1 (4.2)	0.5 (1.7×)
4p		<0.1	5.8	2.9	14.6	16.3/8.0 (2.0)	0.4 (4.0×)
4q (PF-06463922)		0.70	21	2.3	<8	28.0/19.3 (1.5)^f	23 (33×)
4r		2.0	365	1.7	<8	32.4/1.74 (20.2)	77 (39×)
4s		0.56	45	2.4	<8	22.1/3.8 (5.8)	65 (116×)

[a] NIH3T3-engineered cell line.
[b] Log D was measured at pH 7.4.
[c] Cl$_{int,app}$ refers to the total intrinsic clearance obtained from scaling *in vitro* half-lives in human liver microsomes.
[d] MDCK-MDR1 BA/AB efflux at 2 μM substrate concentration and pH 7.4.
[e] TrkB K_i and ratio relative to ALK-L1196M K_i.
[f] *RRCK-BCRP* BA/AB is 37/28 (1.8); determined at 2 μM substrate concentration and pH 7.4.

The pyrazole cyano moiety in **PF-06463922** was conducive of selectivity because the cyano contains only one more heavy atom than the nonselective methyl analogue (**4g**) and gains >35× selectivity, similar to the bulkier methyl-substituted imidazopyridine (**4r**). It is hypothesized that the nitrile makes an unfavorable contact with the closest carbon atom of the Tyr635 in TrkB (Figure 18.4). Unfavorable desolvation penalties or electrostatics due to the proximity of the electron-rich nitrile nitrogen atom and tyrosine may further enhance selectivity.

18.2.10 Structural Analysis of PF-06463922 (4q)

Not surprisingly, the amide macrocycles overlay well with the structure of crizotinib in crystallographic studies, but there are also some significant differences that provide enhanced binding of **PF-06463922** relative to crizotinib (Figure 18.5). Addition of the amide allows interaction of the carbonyl with several key structural water molecules that form interactions to both the conserved Lys1150 and the backbone carbonyl of residue Gly1123 in the G-loop and Gly1269 at the start of the activation loop. The N-Me group also interacts with the backbone carbonyl groups of G-loop residues (Gly1123 and Leu1122). Additionally, the *cis* amide of the cyclic ligand near the G-loop pays a lower desolvation penalty, while the carbonyl oxygen interacts with structural waters, thereby avoiding any desolvation energies. These interactions likely help stabilize the G-loop and render it ordered in the **PF-06463922** structure in contrast to the crizotinib-bound structure.

The matched molecular pair, 12-membered macrocyclic ether **4e** and **PF-06463922**, highlight the importance of the amide linker. While the two inhibitors have similar ALK-L1196M cell IC50 potencies (approximately 20 nM), the LipE of the amide macrocycle **PF-06463922** is approximately 1.0 unit higher due to the reduction in lipophilicity (log D 3.3–2.3). Importantly, the amide is positioned to interact with structural waters and surrounding protein (G-loop) without inducing addition strain and reinforces the role of enthalpy over entropy contributions to binding affinity.

18.2.11 Overlapping Potency and Selectivity

Since **4q** displayed good overall *in vitro* properties, including low efflux and excellent overall selectivity, it was tested in a panel of crizotinib-resistant patient-reported ALK mutations (Figure 18.6). **PF-06463922** performed well across the panel of mutants with cellular phospho-ALK IC_{50} values ranging from 0.2 to 77 nM, corresponding to a 40- to 825-fold improvement in cellular potency relative to crizotinib. Since most mutations simply increase kinase activity, the increase in binding affinity translates into a reduction in cellular IC_{50} values.

18.2.12 Synthesis of PF-06463922 (4q)

The synthesis of **PF-06463922** begins with the elaborated aminopyridine intermediate **5** [36] (Scheme 18.1). Palladium-catalyzed carbonylation followed by trapping with pyrazole amine **6** provided the coupling product **7**, which was brominated with *N*-bromosuccinimide to provide the 5-bromo-aminopyridine **8**. To prepare the acyclic precursor for macrocyclization, the amine was exhaustively protected as the acetyl derivative **9** in good yield. The cyclization precursor was then treated under catalytic Pd(0)/cataCXium conditions to provide the
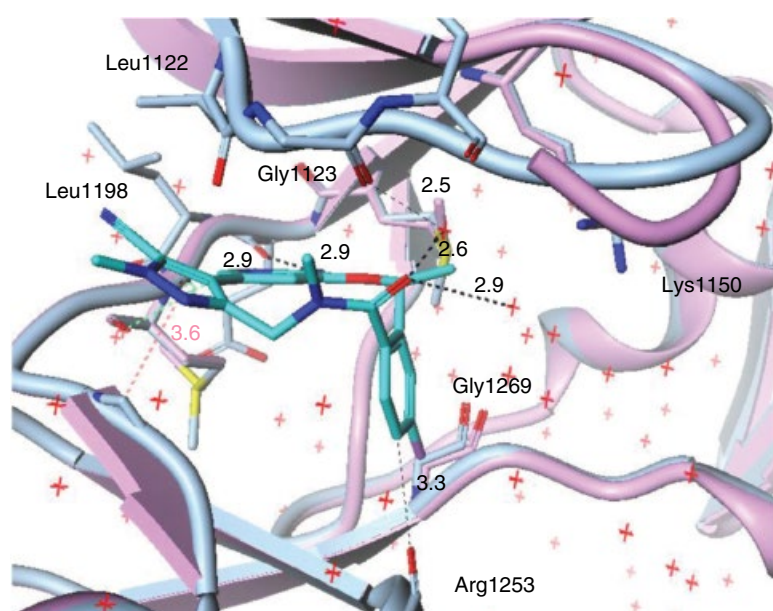
Figure 18.5 PF-06463922 (**4q**) co-crystal structure in ALK-L1196M kinase domain (PDB 4CLJ, 1.7 Å) overlaid with crizotinib (**1**) in complex with ALK-L1196M from Figure 18.1, left panel. (*See insert for color representation of the figure.*)

direct arylated macrocycle, which was deprotected under acidic conditions to provide **PF-06463922** in good yield (42% over two steps) [37].

18.2.13 Summary of Discovery and Synthesis

The successful design of macrocycles, including **PF-06463922**, relied heavily on structure-based design, efficiency metrics, and property space analysis.
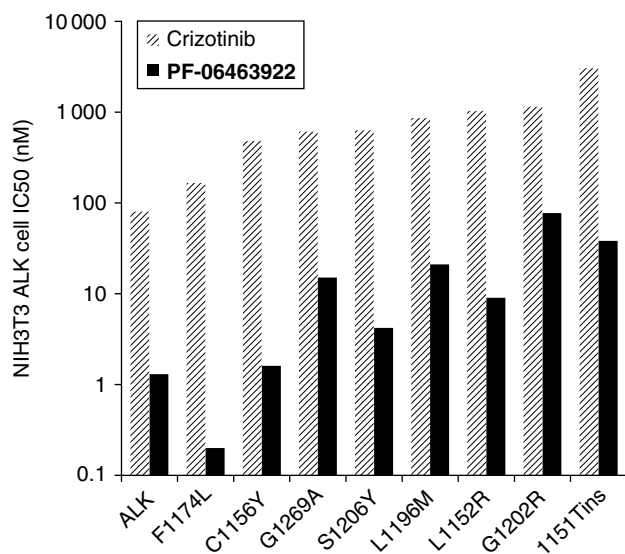
Figure 18.6 Crizotinib (**1**) and **PF-06463922** (**4q**) NIH3T3 phospho-ALK IC$_{50}$ values across an engineered panel of patient-reported crizotinib-resistant mutations.

Improvements in LipE were tracked and rationalized with analysis of co-crystal structure data and computational data. Moderation of log D and reduction of molecular weight and hydrogen bond donors aided design into a highly permeable chemical space, reducing efflux in P-gp and BCRP overexpressing cell lines. As previously mentioned, structure-guided design was paramount in the generation of a successful selectivity strategy [36]. Although our approach utilized structural data to guide the inception and optimization of macrocyclic inhibitors of ALK, it could be envisioned that library chemistry, or another more modular approach to building macrocycles, could be adopted using limited or no structural data as guidance.

18.3 Evaluation of Pharmacokinetic Properties Including CNS Penetration

18.3.1 Background

Despite the recent dramatic advances in treating malignancies with MTAs, the continuing challenge in cancer therapy has been to penetrate the BBB into the CNS, a sanctuary site for both primary and metastatic tumors. In lung cancer, brain metastases occur with a 5-year cumulative incident rate of approximately 16%. Autopsy studies show that up to 25% of lung cancer patients develop brain metastases [38]. Furthermore, the
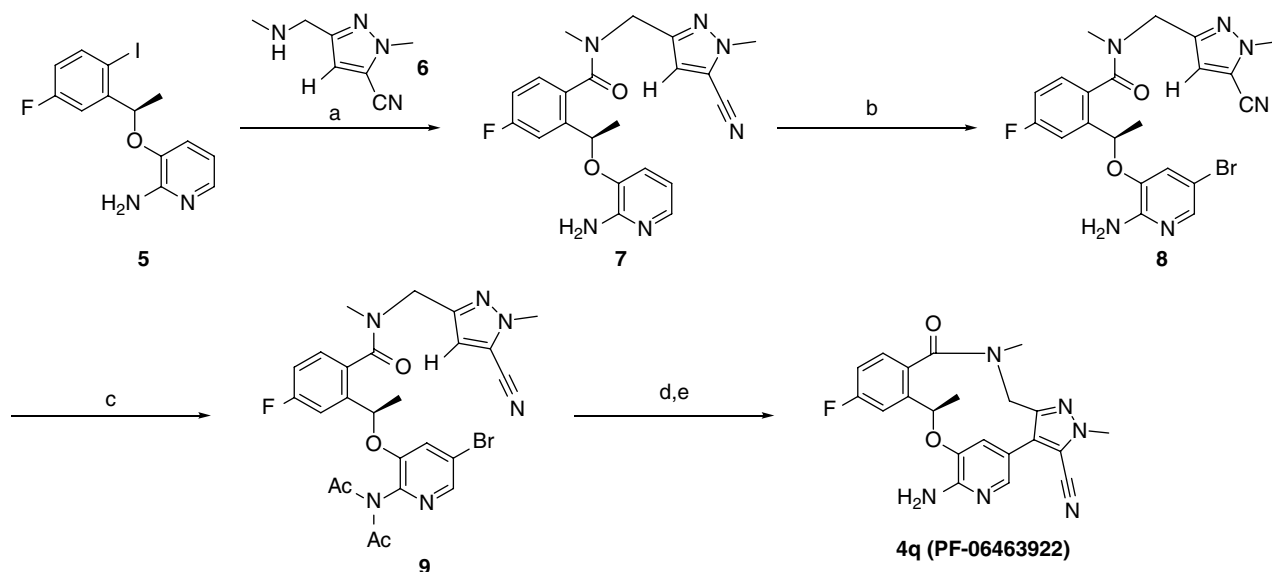
Scheme 18.1 Synthesis of **PF-06463922** (**4q**) by an unprecedented directed arylation. *Reagents and conditions*: (a) 5 mol% Pd(P^{t}Bu$_3$)$_2$, 3 eq DIPEA, 1.1 eq **6**, toluene, 80°C, 4 bar CO, 18 h, 70%; (b) 1.1 eq NBS, THF, −10°C, 2 h, 86%; (c) acetic anhydride, 100°C, 8 h, quant.; (d) 20 mol% cataCXium A, 10 mol% Pd(OAc)$_2$, 5 eq KOAc, *t*-AmOH, 130°C, 14 h; (e) 10 eq 4N HCl in dioxane, MeOH, 60°C, 14 h, 42% over two steps.

incidence of brain metastases is on the rise, primarily due to two factors: (i) early detection of CNS disease with improved imaging technologies and (ii) improved systemic therapies prolonging survival, which increases the risk for brain metastases. Needless to say, the unmet medical need to treat brain malignancies is now at an all-time high. The major barrier to an effective treatment is the BBB. The unique properties of the BBB, including continuous tight junctions with no fenestrations of the endothelial cells and expression of high levels of efflux transporters, contribute to poor CNS penetration. Among the efflux transporters that pump drugs out of CNS into circulation, P-gp is the best studied and is responsible for extruding most cancer drugs [39].

18.3.2 Lab Objectives and *In Vitro* Screening for CNS Penetration

In addition to broad spectrum potency against mutations from resistance to crizotinib and reasonable ADME properties, the next-generation ALK inhibitor required CNS penetration to treat brain metastases. Based on the unique properties of the BBB, *in vitro* screening of new compounds for brain penetration focused on two assays: (i) MDCK-MDR1 and (ii) RRCK [40]. Madin-Darby canine kidney (MDCK)-MDR1 cells are canine kidney cells overexpressing human P-gp cultured as a monolayer in a transwell system. Compounds are added to either the apical or the basolateral donor chamber and measured from the corresponding basolateral or apical receiver chamber. The concentration ratio of B → A (basolateral to apical) and A → B (apical to basolateral) indicates whether a compound is a P-gp substrate. Most CNS drugs have B → A/A → B ratio < 3. RRCK, on the other hand, is a subclone of the MDCK parental cell line, displaying low expression of endogenous P-gp. In the RRCK transwell assay, only A → B values are measured. Compounds with good permeability usually have A → B values $>10 \times 10^{-6}$ cm/s. Most of the ALK macrocycles possessed RRCK values $>10 \times 10^{-6}$ cm/s, indicating high permeability. The RRCK value of **PF-06463922** was 38×10^{-6} cm/s, and its MDCK-MDR1 B → A/A → B ratio was 1.8, suggesting that it is not a substrate for P-gp.

18.3.3 ADME Evaluation

Pharmacokinetics (PK) of **PF-06463922** was evaluated *in vivo* in nonclinical species, rats and dogs. Intravenous (IV) and oral studies were conducted to assess PK parameters such as clearance, volume of distribution, and oral bioavailability. The plasma concentration–time profiles are shown in Figure 18.7a and b for rats and dogs, respectively. **PF-06463922** exhibited low clearance and moderate
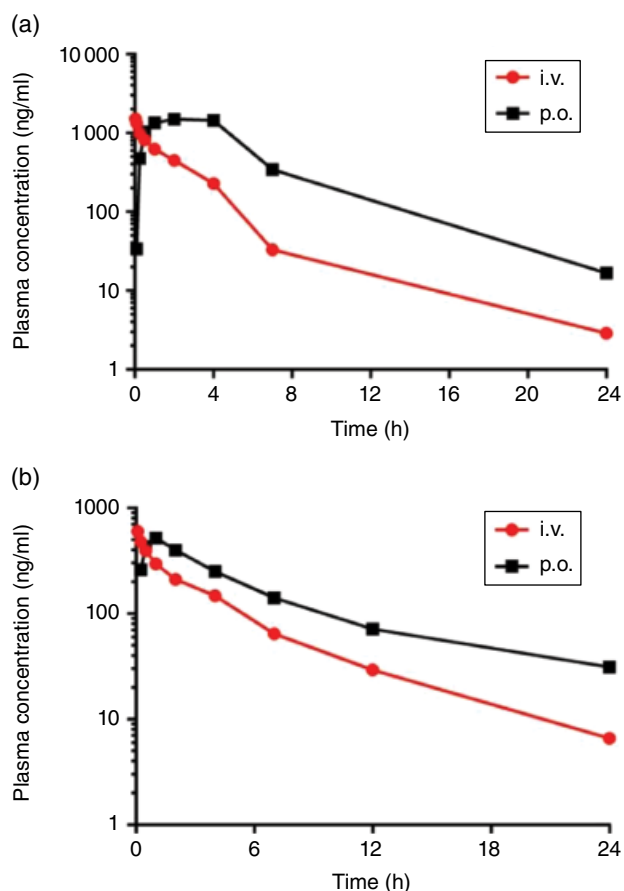
Figure 18.7 Concentration–time profile of **PF-06463922** in rats (a) and dogs (b), $n = 2$. Rats were administered 1 mg/kg (i.v.) and 5 mg/kg (oral gavage) in solution formulation. Dogs were administered 1 mg/kg (i.v.) and 2 mg/kg (oral gavage) in solution formulation.

Table 18.8 PK parameters of **PF-06463922** in rats and dogs.

PK parameters	Rats	Dogs
Dose i.v./oral (mg/kg)	1/5	1/2
Clearance (ml/min/kg)	15.5	9.1
Steady-state volume of distribution (l/kg)	2.6	2.8
Terminal half-life (h)	2.7	4.6
Oral absorption (%F)	~100	97

volume of distribution in both rats and dogs with near complete absorption (Table 18.8). Oral bioavailability of **PF-06463922** was near 100% in rats and dogs.

18.3.4 *In Vivo* Assessment of Brain Penetration in Rats Measuring Brain Homogenate and CSF

Wistar-Han rats were administered oral doses of **PF-06463922**. Brain, plasma, and CSF were sampled at 1, 4, 7, 12, and 24 h posts dose, and concentrations of
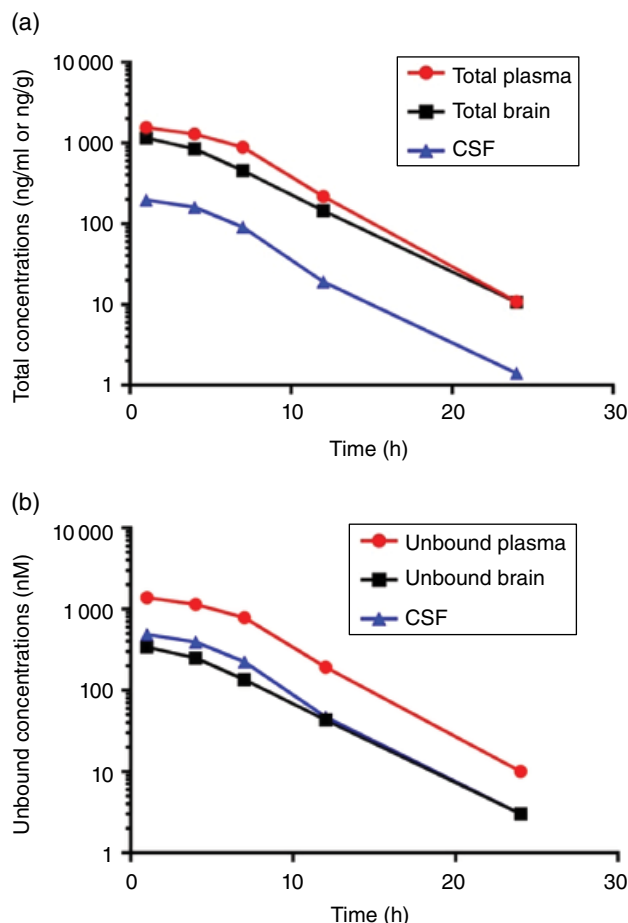
Figure 18.8 Total (a) and unbound (b) concentrations of **PF-06463922** in brain homogenate, CSF, and plasma ($n=2$).

PF-06463922 in brain homogenate, plasma, and CSF were determined (Figure 18.8a). Plasma and brain tissue binding results were used to obtain unbound brain ($C_{u,brain}$) and unbound plasma ($C_{u,plasma}$) concentrations of **PF-06463922** (Figure 18.8b).

Since CSF contains very low levels of protein, it was assumed that free concentrations of drug are measured in CSF. The unbound level of drugs enable comparison of free concentrations in plasma, brain, and CSF to elucidate whether there is any impairment in brain penetration [41]. The area under the time–concentration (unbound) curves (AUC) of each matrix were calculated and compared. With no impairment in brain penetration, the ratio of $C_{u,brain}$ to $C_{u,plasma}$ (also known as $K_{p,uu,brain}$) and/or the ratio of CSF to $C_{u,plasma}$ (also known as $K_{p,uu,csf}$) should be approximately 1, indicating free drug is at equilibrium between both sides of the BBB. When a drug is not brain penetrant, the $K_{p,uu,brain}$ is approximately 0.04 accounting for compound trapped in the vasculature during sampling of the brain tissue. For **PF-06463922**, the $K_{p,uu,brain}$ and $K_{p,uu,csf}$ were 0.23

and 0.33, respectively. These values suggest that approximately 30% of the free drug in plasma is able to cross the BBB. While unable to reach complete equilibrium across BBB, 30% brain penetration is quite impressive for a cancer drug compared with other drugs in the same class. A major disadvantage of this *in vivo* model involves removal of the brain and homogenization; therefore, it is not possible to distinguish between vascular and parenchymal compartments.

18.3.5 *In Vivo* Assessment of Brain Penetration in Rats Using Quantitative Autoradiography

Tissue distribution of total radioactivity was evaluated by quantitative whole-body autoradiography (QWBA) in Long–Evans rats after an oral dose of [^{14}C]**PF-06463922** [42]. Following a single oral dose, one rat per time point was prepared for QWBA at 0.25, 1, 2, 4, 8, 24, 48, 96, 168, 336, and 672 h. Concentrations of radioactivity were determined in tissues and biological fluids (Figure 18.9).

The exposure and tissue distribution data from the QWBA study suggest that [^{14}C]**PF-06463922**-derived radioactivity partitioned more extensively into tissue than blood and distributed across the BBB into noncircumventricular CNS tissue (cerebellum and cerebrum) for up to 24 h post-dose. The distribution of [^{14}C]**PF-06463922**-derived radioactivity appears to be uniform in cerebellum and cerebrum. The AUC ratio of noncircumventricular CNS tissue to blood is 0.26, suggesting 26% of **PF-06463922** in the blood partitioned into the CNS tissue, which is consistent with the *in vivo* brain PK results (Section 18.3.4). The limitation of the QWBA method is that the radioactivity measured cannot distinguish between the parent drug and its metabolites or between bound and free drug.

18.3.6 *In Vivo* Assessment of Spatial Brain Distribution in Mice Using Matrix-Assisted Laser Desorption Ionization-Mass Spectrometry (MALDI-MS)

In larger brain tumor lesions, the vasculature of the BBB tends to be more fenestrated; thus certain cancer drugs can penetrate through and lead to temporary tumor shrinkage. However, smaller lesions or tumor (stem) cells tend to be protected by the BBB with normal structural vasculature, which can eventually progress into large tumors. Therefore, it is important to examine spatial distribution of a compound in a brain tumor pharmacology model to ensure that tumor growth inhibition was caused by a brain penetrant drug and not by a fenestrated vasculature. While being quantitative, measuring brain homogenate/CSF or radioactivity in the brain region provided no or low resolution on spatial distribution of
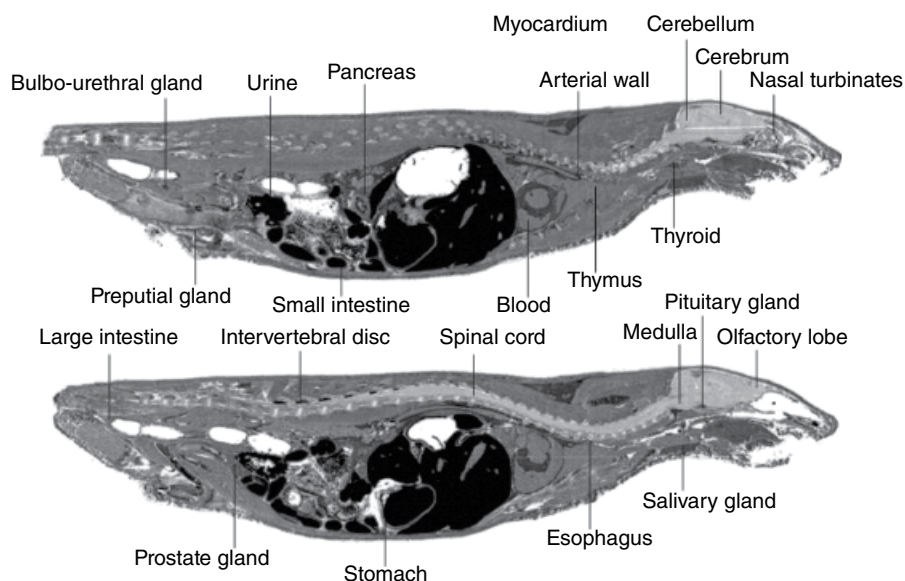
Figure 18.9 Quantitative whole-body autoradiograph of a male animal 1 h following a single oral dose of [^{14}C]**PF-06463922**.

PF-06463922. In addition, with respect to drug safety, if a compound preferentially localizes to a particular region of the brain with high enough concentrations, unexpected adverse events can occur. For **PF-06463922**, MALDI imaging technology was used to assess brain and brain tumor spatial distribution in a preclinical pharmacology model [43]. A patient-derived orthotopic brain tumor model was developed in mice via intracranial injection of patient cells containing the ALK mutation for non-small cell lung carcinoma. Tumors were allowed to grow for 1–2 weeks then treated orally with **PF-06463922** at select dose and time ranges. Post-dose craniotomies were performed to remove tumor-bearing and naïve brains for MALDI imaging. Since this is an MS-based technology, only **PF-06463922** was monitored.

Figure 18.10a shows the hematoxylin and eosin (H&E) stains of an adjacent section of Figure 18.10b, indicating substructures of the brain. Figure 18.10b shows a ubiquitous distribution of **PF-06463922** in a tumor-naïve brain, which is consistent with QWBA image. Figure 18.10c–f are from tumor-bearing mouse brain slices where tumors were indicated with dashed lines. Brain slices from 200 and 100 mg/kg are shown in Figure 18.10d and f, respectively. **PF-06463922** in Figure 18.10d and f was evenly distributed in the brain tissue in a dose-dependent manner; it does not appear to partition to the tumor to a much greater extent compared with the adjacent brain tissue. The ubiquitous distribution of **PF-06463922** observed in the MALDI images is consistent with a good brain-penetrant compound, thus the tumor growth inhibition effect observed (next section) was due to on-target effect with minimum CNS toxic effects.

18.3.7 *In Vivo* Efficacy Assessment of Orthotopic Brain Tumor Model Using Magnetic Resonance Imaging

Whether the extent of **PF-06463922** brain penetration (20–30%) was sufficient would depend on its ability to elicit a response at a reasonable dose, that is, a dose that is pharmaceutically plausible (not exceeding formulation capacities), pharmacologically efficacious, and devoid of toxic effects to the CNS or the rest of the body. Therefore, antitumor efficacy of **PF-06463922** in an EML4-ALK-positive brain metastasis model was evaluated [44]. Tumor cells were engineered to express either firefly luciferase or Gaussia luciferase in order to allow noninvasive growth monitoring by whole-body *in vivo* imaging system. Tumor cells were intracranially injected into the left hemisphere of the brain and allowed to grow for 1–2 weeks, followed by twice daily oral treatment of either vehicle (14 days treatment) or **PF-06463922** (28 day treatment). As shown in MRI images (Figure 18.11a, 5 mg/kg data not shown), **PF-06463922** demonstrated significant antitumor activity against EML4-ALK brain metastases. Tumor sizes were quantitatively determined and shown in Figure 18.11b.

Vehicle control-treated mice were euthanized, on average, 11 days after treatment initiation because of declining health attributed to tumor burden. In contrast, **PF-06463922** treatment suppressed tumor growth in all mice for the duration of the experiment (28 days) in a dose-dependent manner, indicating that sufficient **PF-06463922** amounts crossed the BBB and exerted ALK inhibitory effect. In subcutaneous xenograft
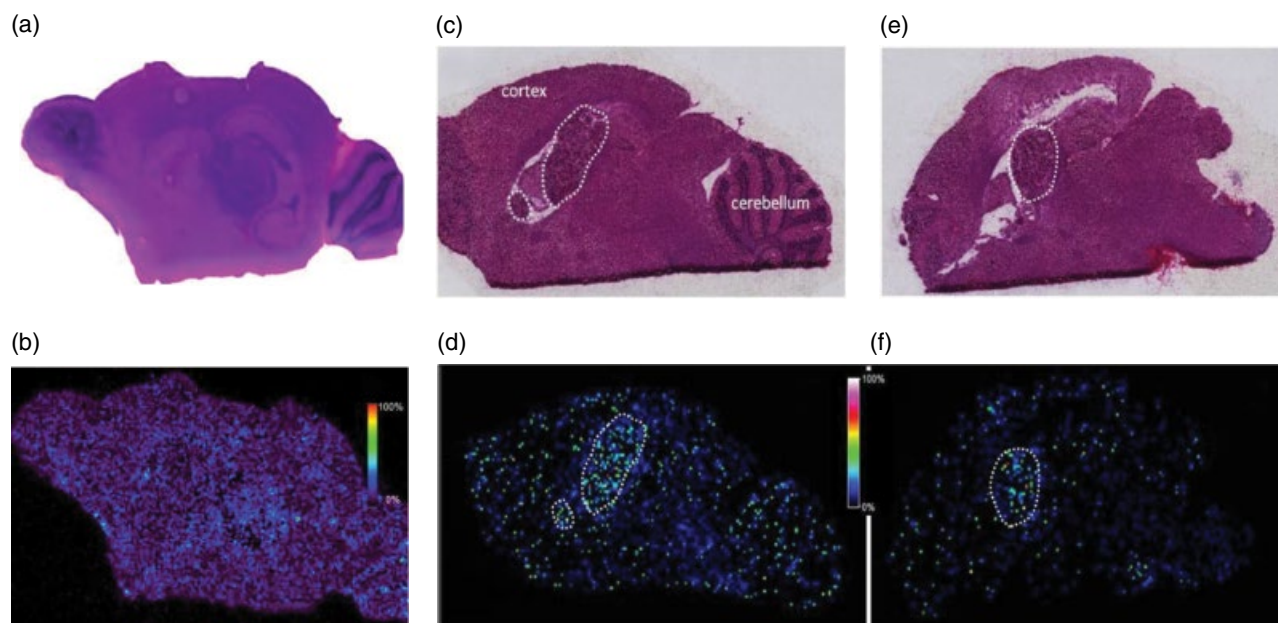
Figure 18.10 H&E stains (a, c, and e) and MALDI-MS images (b, d and f) of mouse brain slices. (a) and (b) are from a tumor-naïve mouse dosed at 400 mg/kg. (c) and (d) are from a tumor-bearing mouse dosed at 200 mg/kg. (e) and (f) are from a tumor-bearing mouse dosed at 100 mg/kg. All animals were orally dosed once. MS images were acquired at 75 × 75 μm pixel resolution. (*See insert for color representation of the figure.*)
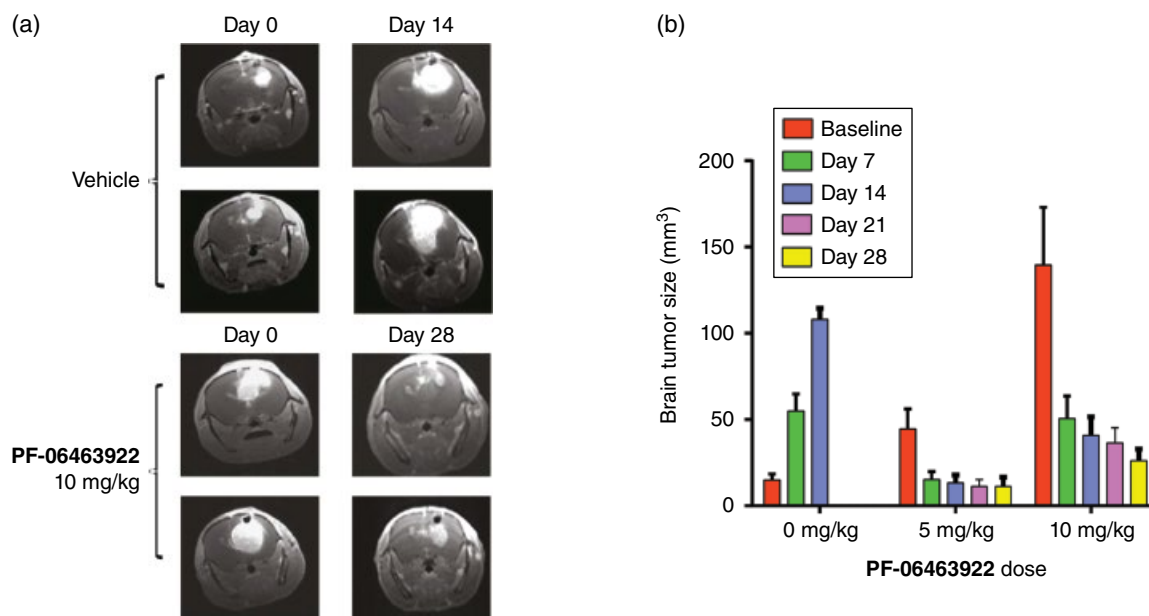
Figure 18.11 **PF-06463922** antitumor efficacy in ALK fusion-driven intracranial tumor models. (a) Representative magnetic resonance images showing regression of large established H3122 EML4-ALKWT intracranial tumors in mice following **PF-06463922** infusion. (b) Quantitation of brain tumor sizes following **PF-06463922** treatment in the H3122 EML4-ALKWT intracranial model shown in (a). Values are presented as mean ± SEM. (*See insert for color representation of the figure.*)

studies, EML4-ALK wild-type and mutant tumors displayed similar sensitivity to **PF-06463922** (Section 18.4).

18.3.8 PK and Brain Penetration Summary

Several preclinical methods were used to profile the brain penetration and antitumor effect of **PF-06463922**. The extent of brain penetration (20–30%) was consistent between the *in vivo* rat brain PK and QWBA studies. The distribution of **PF-06463922** appears to be uniform as shown from the QWBA and the MALDI images. Finally, the extent of **PF-06463922** brain penetration was sufficient to elicit an antitumor response with no adverse events. Adequate brain penetration and other favorable ADME properties deemed **PF-06463922** suitable for further clinical development.

18.4 Evaluation of Pharmacokinetic–Pharmacodynamic (PKPD) Profiles

18.4.1 Background

The transition probability in each clinical development stage from first in human to registration is the lowest in phase II in all therapeutic areas including oncology [45]. Thus, despite an increased understanding of translational pharmacology from bench to bedside, one of the major reasons for clinical failures of new molecular entities (NMEs) is the attrition risk related to efficacy evaluated in phase II trials as proof of concept [46, 47]. Dynamic modeling and simulation (M&S) is a mathematical approach linking drug exposures to pharmacological responses (e.g., target modulation and antitumor efficacy) as a function of time, providing a quantitative estimation of *in vivo* drug potency with mechanistic

insights [48–51]. Dynamic M&S approaches are increasingly being applied to every phase of drug discovery and development as well as regulatory decisions including labeling [52, 53]. Furthermore, M&S can be a valuable asset in the field of translational pharmacology to establish quantitative exposure–response relationships of NMEs in nonclinical models, in order to extrapolate the relationships to the clinic with mechanistic insights. Accordingly, a growing emphasis is being placed upon mechanistic M&S to estimate quantitative *in vivo* exposure–response relationships of NMEs, particularly MTAs such as TKIs in oncology [48–50, 54]. The application of M&S for MTAs in nonclinical tumor models is typically divided into three main tiers to understand *in vivo* drug exposure–response relationships between (i) drug exposures and pharmacodynamic (PD) responses such as target modulation, that is, PKPD relationships; (ii) drug exposures and disease (DZ) such as antitumor efficacy, that is, pharmacokinetic-disease (PKDZ) relationships; and (iii) biomarker responses and antitumor efficacy, that is, pharmacodynamic-disease (PDDZ) relationships, which are generally based on a two-step approach in parallel via the comparison between PKPD and PKDZ relationships, as summarized in Figure 18.12.

18.4.2 *In Vivo* Nonclinical Studies

The PKPD relationships of **PF-06463922** between its systemic exposures, target modulation in tumors, and antitumor efficacy were characterized in mice implanted with tumor cells. The experimental designs and methods of the *in vitro* and *in vivo* PKPD studies were previously reported [44, 54, 55]. Briefly, three separate multiple oral dose studies were conducted with **PF-06463922** in female athymic nu/nu mice implanted subcutaneously with H3122 NSCLC cells expressing the EML4-ALK^{L1196M} (studies 1 and 2) or NIH3T3 cells expressing
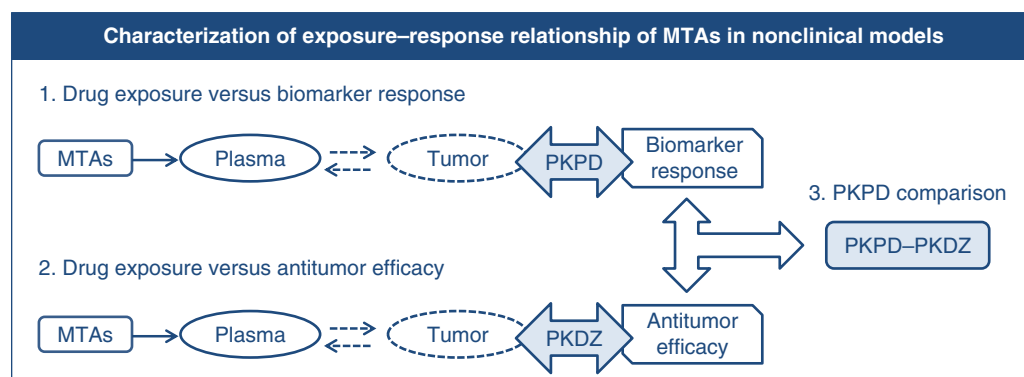
Figure 18.12 Main workstream of a two-step approach to characterize *in vivo* exposure–response relationships of MTAs between drug exposures, biomarker response, and antitumor efficacy. MTAs, molecularly targeted agents; PKDZ, pharmacokinetics-disease; PKPD, pharmacokinetics–pharmacodynamics.
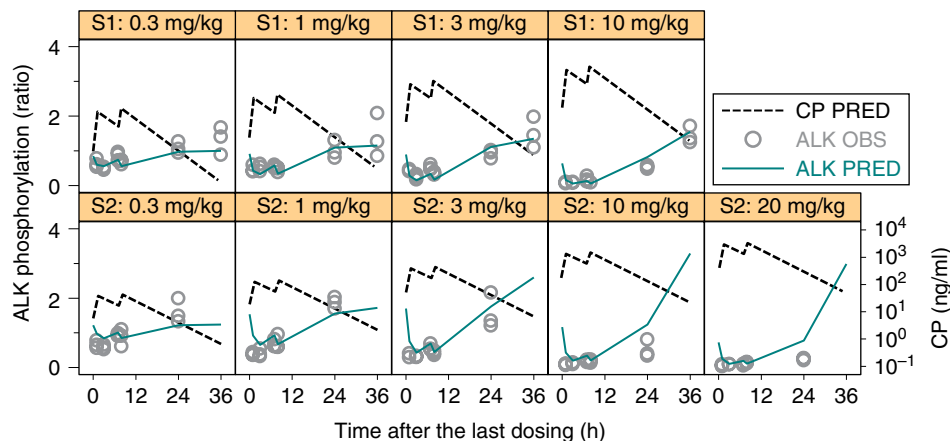
Figure 18.13 PKPD model-fitted and observed ALK inhibition by **PF-06463922** in athymic mice implanted with H3122 non-small cell lung cancer (NSCLC) cells expressing the EML4-ALKL1196M following repeated oral administration. ALK OBS, the observed ALK response (ratio to the vehicle control animal data); ALK PRED, the model-fitted ALK responses; CP PRED, the one-compartment-fitted plasma concentrations of **PF-06463922**, S1, study 1; S2, study 2. Source: Yamazaki *et al*. [54]. Reproduced with permission of American Society for Pharmacology and Experimental Therapeutics.

CD74-ROS1 (study 3); these nonclinical models are henceforth referred to as the ALK- and ROS1-tumor models, respectively. Animals received **PF-06463922** twice daily, 7 h apart, at the oral doses of 0.3–10 mg/kg/dose for 4 days (study 1), 0.3–20 mg/kg/dose for 13 days (study 2), and 0.01–3 mg/kg/dose for 9 days (study 3).

18.4.3 PK Modeling

Following multiple oral dose administrations, **PF-06463922** was rapidly absorbed with t_{max} of approximately 1 h post-dose. Thereafter, the plasma concentrations of **PF-06463922** near-mono-exponentially declined to the last time points, for example, 24 or 36 h post-dose. A standard one-compartment PK model was applied to determine pharmacokinetic parameters of **PF-06463922**. The plasma concentrations of **PF-06463922** in both ALK- and ROS1-tumor models were reasonably described by the one-compartment model. Typical PK parameter estimates for oral clearance (*CL/F*, l/h/kg), volume of distribution (*V/F*, l/kg), and absorption rate constant (k_a, h^{-1}) were, respectively, 1.2 l/h/kg, 5.3 l/kg, and 2.0 h^{-1} in study 1; 1.1 l/h/kg, 7.0 l/kg, and 1.3 h^{-1} in study 2; and 1.7 l/h/kg, 11 l/kg, and 4.0 h^{-1} in study 3.

18.4.4 PKPD Modeling for Target Modulation

The inhibition of ALK phosphorylation in ALK-tumor models was sustained after the first and second daily doses, whereas the plasma concentrations of **PF-06463922** reached the maximal levels at 1 h post-dose and then rapidly declined. Unexpectedly, the

dose-dependent rebound of ALK phosphorylation was observed. That is, the responses of ALK phosphorylation in tumor (expressed as the ratio to the vehicle control group) were partially back to near or above the baseline around 24 h post-dose, resulting in ALK phosphorylation ratios that were greater than unity in the treatment groups relative to the vehicle control group. Accordingly, the response of ALK phosphorylation in tumor to plasma concentrations of **PF-06463922** was modeled by an indirect response model with a modulator, which was required to take accounts of the observed rebound [56–58]. The PKPD model sufficiently fit the time courses of ALK phosphorylation, including the rebound (Figure 18.13). The EC$_{50}$ for ALK inhibition was estimated to be 58 ng/ml as total plasma concentration (bound plus unbound), which corresponded to the unbound concentration of 36 nM with the correction for an unbound fraction of 0.25 in mouse plasma.

18.4.5 PKDZ Modeling for Antitumor Efficacy

PF-06463922 dose-dependently inhibited tumor growth in both ALK and ROS1 tumor models. A two-step M&S approach was used to estimate the *in vivo* antitumor efficacy of **PF-06463922** in ALK and ROS1 tumor models [54]. First, tumor growth models with a first-order growth rate with and without a logistic function were established to characterize individual tumor growth curves of the vehicle control groups in ALK and ROS1 tumor models, respectively. Subsequently, the tumor growth inhibition by **PF-06463922** was modeled by a modified indirect response model (i.e., PKDZ model) with the assumption that **PF-06463922** stimulated the

(a)

(b)
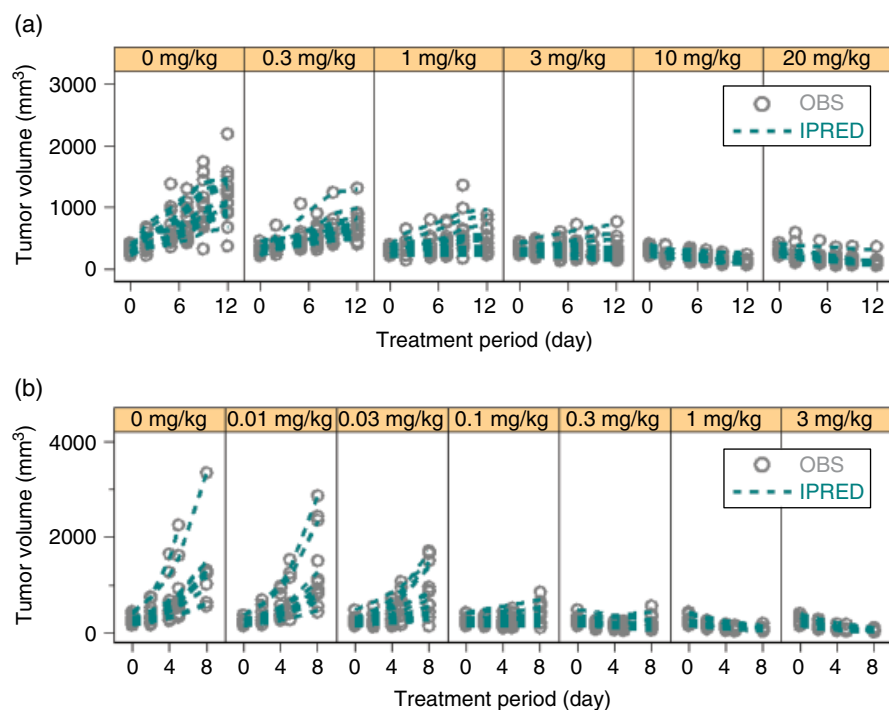
Figure 18.14 Observed tumor volumes and model-fitted tumor growth inhibition curves in athymic mice implanted with H3122 NSCLC cells expressing the EML4-ALKL1196M (a) or NIH3T3 cells expressing the CD74-ROS1 (b) following repeated oral administration of **PF-06463922**. IPRED, the model-fitted individual tumor growth curves; OBS, the observed individual tumor volumes. Source: Yamazaki *et al*. [54]. Reproduced with permission of American Society for Pharmacology and Experimental Therapeutics.

tumor killing rate, thus ultimately inhibiting tumor growth rate, which is characterized by the tumor growth models. The PKDZ model reasonably fit the observed individual tumor growth curves in all groups of ALK tumor models (Figure 18.14a). The plasma concentration of **PF-06463922** required for 100% tumor growth inhibition, that is, tumor stasis concentration (*Tsc*), was estimated to be 83 ng/ml as total plasma concentration (51 nM as unbound concentration). The PKDZ model also adequately fit the observed tumor volumes in all groups of ROS1 tumor models (Figure 18.14b). The *Tsc* of **PF-06463922** was estimated to be 10 ng/ml as total plasma concentration (6.2 nM as unbound concentration). Thus, the estimated *Tsc* of **PF-06463922** was eightfold lower in ROS1 tumor models than ALK-tumor models.

18.4.6 Quantitative Comparison of Exposure–Response Relationships

To understand the relationship between ALK phosphorylation and antitumor efficacy, the exposure–response curves of **PF-06463922** for ALK inhibition and tumor growth inhibition were simulated at plasma concentration range of 0.01–10000 ng/ml using the parameters estimated from ALK and ROS1 tumor models (Figure 18.15). It is worth noting that the tumor growth

inhibition ranges from 0 to 120% (including tumor regression), while the range of ALK inhibition is 0–100%.

In ALK tumor models, the unbound EC_{50} (36 nM) for ALK inhibition was 1.4-fold lower than the unbound *Tsc* (51 nM), resulting in that the *Tsc* estimate was roughly comparable with the EC_{60} (52 nM) for ALK inhibition. In ROS1 tumor model, the estimated unbound Tsc of 6.2 nM is approximately 10-fold lower than that (51 nM) in ALK tumor models.

18.4.7 PKPD Summary

The relationships among systemic exposures of **PF-06463922**, target modulation, and antitumor efficacy in nonclinical tumor models (PK-PDDZ relationships) were characterized well in a quantitative manner using a mathematical M&S approach (Figure 18.16).

The PK-PDDZ relationships suggest that >60% ALK inhibition is required for tumor stasis in ALK tumor models and **PF-06463922**-mediated antitumor efficacy is more potent in ROS1 tumor models relative to ALK tumor models. Accordingly, we proposed that the unbound EC_{60} for ALK inhibition (approximately 50 nM) could be considered a pharmacologically active concentration of **PF-06463922** in NSCLC patients with EML4-ALK rearrangements (with and without ALK mutations).
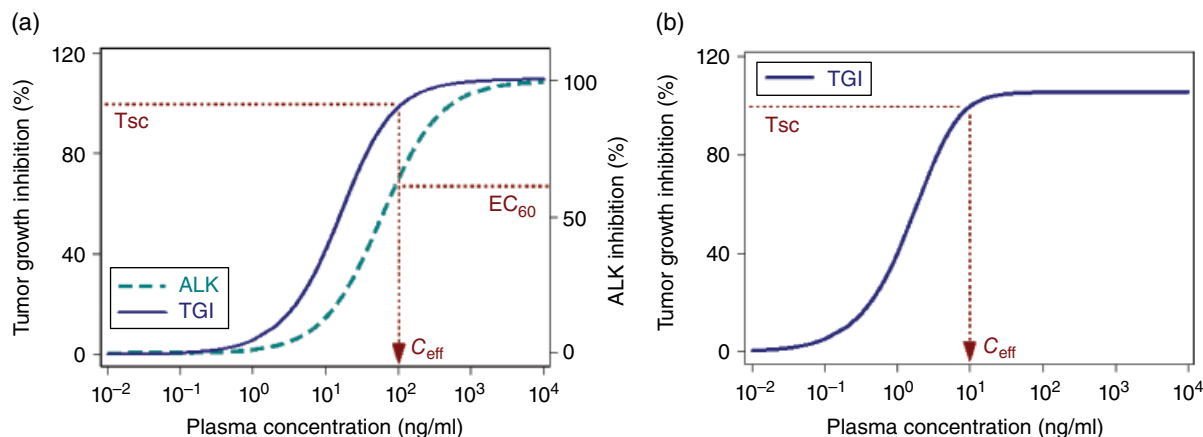
Figure 18.15 Comparison of **PF-06463922** concentration–response curves for target modulation and tumor growth inhibition in nonclinical tumor models. Concentration–response curves for ALK inhibition and tumor growth inhibition were simulated at the concentration range of 0.01–10 000 ng/ml using the parameters estimated from nonclinical tumor models with H3122 NSCLC cells expressing the EML4-ALK^{L1196M} (a) and NIH3T3 cells expressing the CD74-ROS1 (b). The dotted lines to the axes indicate the estimated tumor stasis concentration (Tsc), the EC$_{60}$ estimate for ALK inhibition (EC$_{60}$), and the proposed minimum target efficacious concentration (C$_{eff}$). Source: Yamazaki *et al.* [54]. Reproduced with permission of American Society for Pharmacology and Experimental Therapeutics.
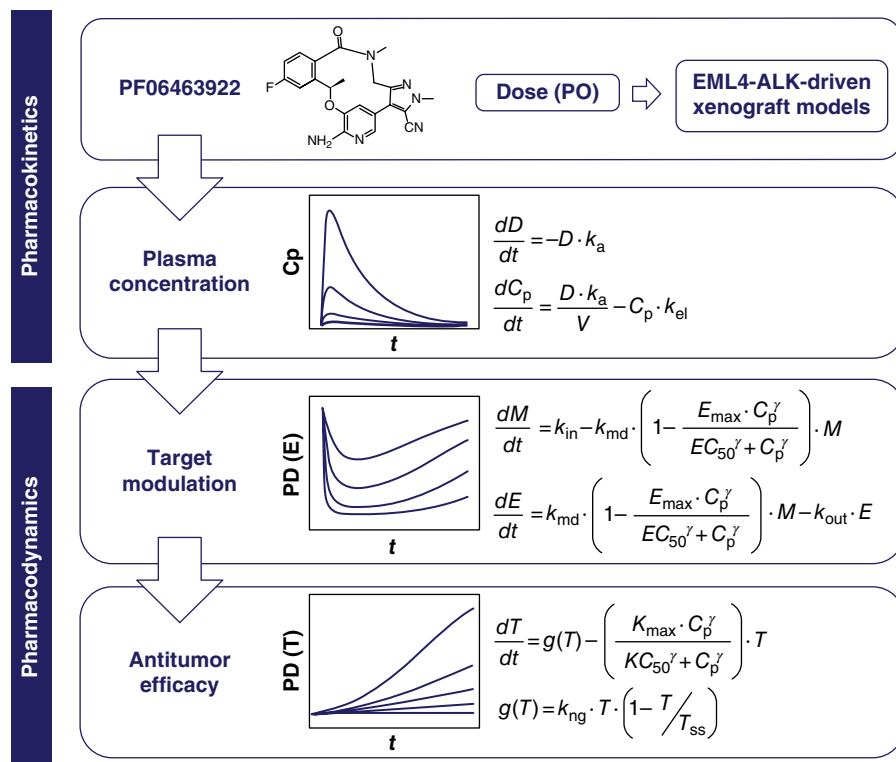
Figure 18.16 M&S summary for evaluation of pharmacokinetic-pharmacodynamic-disease (PK-PDDZ) relationships of **PF-06463922** in nonclinical tumor models. Source: Yamazaki *et al.* [54]. Reproduced with permission of American Society for Pharmacology and Experimental Therapeutics.

The proposed pharmacologically active concentration could also be sufficient for patients with ROS1 rearrangements. Overall, we believe that the quantitative mathematical modeling efforts in nonclinical tumor models would be helpful in understanding clinical exposure–response relationships and also in guiding dose escalation or de-escalation to maintain efficacious exposure of **PF-06463922** in the clinic.

18.5 Conclusion

The discovery of a novel macrocyclic ALK inhibitor, **PF-06463922**, was aided by structure-based drug design and physical property-based optimization to increase broad spectrum potency and permeability, including brain penetration. **PF-06463922** showed desirable metabolic stability *in vitro* and *in vivo*. In nonclinical species, **PF-06463922** showed low systemic clearance, high oral bioavailability, and sufficient brain penetration. Dynamic M&S results suggest that 60% ALK inhibition would be required for tumor stasis in mouse xenograft models with NSCLC expressing ALK mutation. Accordingly, the EC_{60} for ALK inhibition has been proposed to be a minimum target concentration of **PF-06463922** in clinical trials to maintain the efficacious exposures. **PF-06463922** is currently being evaluated in phase I/II clinical trials.

References

1 Ettinger, D. S.; Akerley, W.; Bepler, G.; Blum, M. G.; Chang, A.; Cheney, R. T.; Chirieac, L. R.; D'Amico, T. A.; Demmy, T. L.; Ganti, A. K.; Govindan, R.; Grannis, F. W., Jr.; Jahan, T.; Jahanzeb, M.; Johnson, D. H.; Kessinger, A.; Komaki, R.; Kong, F. M.; Kris, M. G.; Krug, L. M.; Le, Q. T.; Lennes, I. T.; Martins, R.; O'Malley, J.; Osarogiagbon, R. U.; Otterson, G. A.; Patel, J. D.; Pisters, K. M.; Reckamp, K.; Riely, G. J.; Rohren, E.; Simon, G. R.; Swanson, S. J.; Wood, D. E.; Yang, S. C. Non-small cell lung cancer. *J. Natl. Compr. Canc. Netw.* **2010**, *8*, 740–801.

2 Larsen, J. E.; Cascone, T.; Gerber, D. E.; Heymach, J. V.; Minna, J. D. Targeted therapies for lung cancer: clinical experience and novel agents. *Cancer J.* **2011**, *17*, 512–527.

3 Arnedos, M.; Vielh, P.; Soria, J. C.; Andre, F. The genetic complexity of common cancers and the promise of personalized medicine: is there any hope? *J. Pathol.* **2014**, *232*, 274–282.

4 Meric-Bernstam, F.; Farhangfar, C.; Mendelsohn, J.; Mills, G. B. Building a personalized medicine infrastructure at a major cancer center. *J. Clin. Oncol.* **2013**, *31*, 1849–1857.

5 Cardarella, S.; Johnson, B. E. The impact of genomic changes on treatment of lung cancer. *Am. J. Respir. Crit. Care Med.* **2013**, *188*, 770–775.

6 Moreira, A. L.; Thornton, R. H. Personalized medicine for non-small-cell lung cancer: implications of recent advances in tissue acquisition for molecular and histologic testing. *Clin. Lung Cancer* **2012**, *13*, 334–339.

7 Li, T.; Kung, H. J.; Mack, P. C.; Gandara, D. R. Genotyping and genomic profiling of non-small-cell lung cancer: implications for current and future therapies. *J. Clin. Oncol.* **2013**, *31*, 1039–1049.

8 Chong, C. R.; Janne, P. A. The quest to overcome resistance to EGFR-targeted therapies in cancer. *Nat. Med.* **2013**, *19*, 1389–1400.

9 Remon, J.; Moran, T.; Majem, M.; Reguart, N.; Dalmau, E.; Marquez-Medina, D.; Lianes, P. Acquired resistance to epidermal growth factor receptor tyrosine kinase inhibitors in EGFR-mutant non-small cell lung cancer: a new era begins. *Cancer Treat. Rev.* **2014**, *40*, 93–101.

10 Robinson, K. W.; Sandler, A. B. EGFR tyrosine kinase inhibitors: difference in efficacy and resistance. *Curr. Oncol. Rep.* **2013**, *15*, 396–404.

11 Yu, H. A.; Riely, G. J. Second-generation epidermal growth factor receptor tyrosine kinase inhibitors in lung cancers. *J. Natl. Compr. Canc. Netw.* **2013**, *11*, 161–169.

12 Gerber, D. E.; Minna, J. D. ALK inhibition for non-small cell lung cancer: from discovery to therapy in record time. *Cancer Cell* **2010**, *18*, 548–551.

13 Ou, S. H. Crizotinib: a drug that crystallizes a unique molecular subset of non-small-cell lung cancer. *Expert Rev. Anticancer Ther.* **2012**, *12*, 151–162.

14 Shaw, A. T.; Kim, D. W.; Nakagawa, K.; Seto, T.; Crino, L.; Ahn, M. J.; De Pas, T.; Besse, B.; Solomon, B. J.; Blackhall, F.; Wu, Y. L.; Thomas, M.; O'Byrne, K. J.; Moro-Sibilot, D.; Camidge, D. R.; Mok, T.; Hirsh, V.; Riely, G. J.; Iyer, S.; Tassell, V.; Polli, A.; Wilner, K. D.; Janne, P. A. Crizotinib versus chemotherapy in advanced ALK-positive lung cancer. *N. Engl. J. Med.* **2013**, *368*, 2385–2394.

15 Rikova, K.; Guo, A.; Zeng, Q.; Possemato, A.; Yu, J.; Haack, H.; Nardone, J.; Lee, K.; Reeves, C.; Li, Y.; Hu, Y.; Tan, Z.; Stokes, M.; Sullivan, L.; Mitchell, J.; Wetzel, R.; Macneill, J.; Ren, J. M.; Yuan, J.; Bakalarski, C. E.; Villen, J.; Kornhauser, J. M.; Smith, B.; Li, D.; Zhou, X.; Gygi, S. P.; Gu, T. L.; Polakiewicz, R. D.; Rush, J.; Comb, M. J. Global survey of phosphotyrosine signaling identifies oncogenic kinases in lung cancer. *Cell* **2007**, *131*, 1190–1203.

16 Soda, M.; Choi, Y. L.; Enomoto, M.; Takada, S.; Yamashita, Y.; Ishikawa, S.; Fujiwara, S.; Watanabe, H.; Kurashina, K.; Hatanaka, H.; Bando, M.; Ohno, S.; Ishikawa, Y.; Aburatani, H.; Niki, T.; Sohara, Y.; Sugiyama, Y.; Mano, H. Identification of the transforming EML4-ALK fusion gene in non-small-cell lung cancer. *Nature* **2007**, *448*, 561–566.

17 FDA. XALKORI® (crizotinib) prescribing information. Available at http://www.accessdata.fda.gov/drugsatfda_docs/label/2016/202570s017lbl.pdf **2016** (accessed February 21, 2016).

18 Kwak, E. L.; Bang, Y. J.; Camidge, D. R.; Shaw, A. T.; Solomon, B.; Maki, R. G.; Ou, S. H.; Dezube, B. J.; Janne, P. A.; Costa, D. B.; Varella-Garcia, M.; Kim, W. H.; Lynch, T. J.; Fidias, P.; Stubbs, H.; Engelman, J. A.; Sequist, L. V.; Tan, W.; Gandhi, L.; Mino-Kenudson, M.; Wei, G. C.; Shreeve, S. M.; Ratain, M. J.; Settleman, J.; Christensen, J. G.; Haber, D. A.; Wilner, K.; Salgia, R.; Shapiro, G. I.; Clark, J. W.; Iafrate, A. J. Anaplastic lymphoma kinase inhibition in non-small-cell lung cancer. *N. Engl. J. Med.* **2010**, *363*, 1693–1703.

19 Choi, Y. L.; Soda, M.; Yamashita, Y.; Ueno, T.; Takashima, J.; Nakajima, T.; Yatabe, Y.; Takeuchi, K.; Hamada, T.; Haruta, H.; Ishikawa, Y.; Kimura, H.; Mitsudomi, T.; Tanio, Y.; Mano, H.; ALK Lung Cancer Study Group. EML4-ALK mutations in lung cancer that confer resistance to ALK inhibitors. *N. Engl. J. Med.* **2010**, *363*, 1734–1739.

20 Awad, M. M.; Shaw, A. T. ALK inhibitors in non-small cell lung cancer: crizotinib and beyond. *Clin. Adv. Hematol. Oncol.* **2014**, *12*, 429–439.

21 Gridelli, C.; Peters, S.; Sgambato, A.; Casaluce, F.; Adjei, A. A.; Ciardiello, F. ALK inhibitors in the treatment of advanced NSCLC. *Cancer Treat. Rev.* **2014**, *40*, 300–306.

22 Casaluce, F.; Sgambato, A.; Maione, P.; Rossi, A.; Ferrara, C.; Napolitano, A.; Palazzolo, G.; Ciardiello, F.; Gridelli, C. ALK inhibitors: a new targeted therapy in the treatment of advanced NSCLC. *Target. Oncol.* **2013**, *8*, 55–67.

23 Driggers, E. M.; Hale, S. P.; Lee, J.; Terrett, N. K. The exploration of macrocycles for drug discovery—an underexploited structural class. *Nat. Rev. Drug Discov.* **2008**, *7*, 608–624.

24 Breslin, H. J.; Lane, B. M.; Ott, G. R.; Ghose, A. K.; Angeles, T. S.; Albom, M. S.; Cheng, M.; Wan, W.; Haltiwanger, R. C.; Wells-Knecht, K. J.; Dorsey, B. D. Design, synthesis, and anaplastic lymphoma kinase (ALK) inhibitory activity for a novel series of 2,4,8,22-tetraazatetracyclo[14.3.1.1(3),(7).1(9),(1)(3)] docosa-1(20),3(22),4,6,9(21),10,12,16,18-nonaene macrocycles. *J. Med. Chem.* **2012**, *55*, 449–464.

25 Hart, S.; Goh, K. C.; Novotny-Diermayr, V.; Hu, C. Y.; Hentze, H.; Tan, Y. C.; Madan, B.; Amalini, C.; Loh, Y. K.; Ong, L. C.; William, A. D.; Lee, A.; Poulsen, A.; Jayaraman, R.; Ong, K. H.; Ethirajulu, K.; Dymock, B. W.; Wood, J. W. SB1518, a novel macrocyclic pyrimidine-based JAK2 inhibitor for the treatment of myeloid and lymphoid malignancies. *Leukemia* **2011**, *25*, 1751–1759.

26 Poulsen, A.; William, A.; Blanchard, S.; Nagaraj, H.; Williams, M.; Wang, H.; Lee, A.; Sun, E.; Teo, E. L.; Tan, E.; Goh, K. C.; Dymock, B. Structure-based design of nitrogen-linked macrocyclic kinase inhibitors leading to the clinical candidate SB1317/TG02, a potent

inhibitor of cyclin dependant kinases (CDKs), Janus kinase 2 (JAK2), and Fms-like tyrosine kinase-3 (FLT3). *J. Mol. Model.* **2013**, *19*, 119–130.

27 William, A. D.; Lee, A. C.; Blanchard, S.; Poulsen, A.; Teo, E. L.; Nagaraj, H.; Tan, E.; Chen, D.; Williams, M.; Sun, E. T.; Goh, K. C.; Ong, W. C.; Goh, S. K.; Hart, S.; Jayaraman, R.; Pasha, M. K.; Ethirajulu, K.; Wood, J. M.; Dymock, B. W. Discovery of the macrocycle 11-(2-pyrrolidin-1-yl-ethoxy)-14,19-dioxa-5,7,26-triaza-tetracyclo[19.3.1.1(2,6). 1(8,12)] heptacosa-1(25),2(26),3,5,8,10,12(27),16,21,23-decaene (SB1518), a potent Janus kinase 2/fms-like tyrosine kinase-3 (JAK2/FLT3) inhibitor for the treatment of myelofibrosis and lymphoma. *J. Med. Chem.* **2011**, *54*, 4638–4658.

28 Giordanetto, F.; Kihlberg, J. Macrocyclic drugs and clinical candidates: what can medicinal chemists learn from their properties? *J. Med. Chem.* **2014**, *57*, 278–295.

29 Mao, J.; Johnson, T. R.; Shen, Z.; Yamazaki, S. Prediction of crizotinib-midazolam interaction using the Simcyp population-based simulator: comparison of CYP3A time-dependent inhibition between human liver microsomes versus hepatocytes. *Drug Metab. Dispos.* **2013**, *41*, 343–352.

30 Katayama, R.; Friboulet, L.; Koike, S.; Lockerman, E. L.; Khan, T. M.; Gainor, J. F.; Iafrate, A. J.; Takeuchi, K.; Taiji, M.; Okuno, Y.; Fujita, N.; Engelman, J. A.; Shaw, A. T. Two novel ALK mutations mediate acquired resistance to the next-generation ALK inhibitor alectinib. *Clin. Cancer Res.* **2014**, *20*, 5686–5696.

31 Shaw, A. T.; Friboulet, L.; Leshchiner, I.; Gainor, J. F.; Bergqvist, S.; Brooun, A.; Burke, B. J.; Deng, Y. L.; Liu, W.; Dardaei, L.; Frias, R. L.; Schultz, K. R.; Logan, J.; James, L. P.; Smeal, T.; Timofeevski, S.; Katayama, R.; Iafrate, A. J.; Le, L.; McTigue, M.; Getz, G.; Johnson, T. W.; Engelman, J. A. Resensitization to crizotinib by the lorlatinib ALK resistance mutation L1198F. *N. Engl. J. Med.* **2016**, *374*, 54–61.

32 Edwards, M. P.; Price, D. A. Role of physicochemical properties and lipophilic ligand efficiency (LipE or LLE) in addressing drug safety risks. *Annu. Rep. Med. Chem.* **2010**, *45*, 381–391.

33 Freeman-Cook, K. D.; Hoffman, R. L.; Johnson, T. W. Lipophilic efficiency: the most important efficiency metric in medicinal chemistry. *Future Med. Chem.* **2013**, *5*, 113–115.

34 Huang, Q.; Johnson, T. W.; Bailey, S.; Brooun, A.; Bunker, K. D.; Burke, B. J.; Collins, M. R.; Cook, A. S.; Cui, J. J.; Dack, K. N.; Deal, J. G.; Deng, Y. L.; Dinh, D.; Engstrom, L. D.; He, M.; Hoffman, J.; Hoffman, R. L.; Johnson, P. S.; Kania, R. S.; Lam, H.; Lam, J. L.; Le, P. T.; Li, Q.; Lingardo, L.; Liu, W.; Lu, M. W.; McTigue, M.; Palmer, C. L.; Richardson, P. F.; Sach, N. W.; Shen, H.;

Smeal, T.; Smith, G. L.; Stewart, A. E.; Timofeevski, S.; Tsaparikos, K.; Wang, H.; Zhu, H.; Zhu, J.; Zou, H. Y.; Edwards, M. P. Design of potent and selective inhibitors to overcome clinical anaplastic lymphoma kinase mutations resistant to crizotinib. *J. Med. Chem.* **2014**, *57*, 1170–1187.

35 Chang, C. E.; Chen, W.; Gilson, M. K. Ligand configurational entropy and protein binding. *Proc. Natl. Acad. Sci. U. S. A.* **2007**, *104*, 1534–1539.

36 Johnson, T. W.; Richardson, P. F.; Bailey, S.; Brooun, A.; Burke, B. J.; Collins, M. R.; Cui, J. J.; Deal, J. G.; Deng, Y. L.; Dinh, D.; Engstrom, L. D.; He, M.; Hoffman, J.; Hoffman, R. L.; Huang, Q.; Kania, R. S.; Kath, J. C.; Lam, H.; Lam, J. L.; Le, P. T.; Lingardo, L.; Liu, W.; McTigue, M.; Palmer, C. L.; Sach, N. W.; Smeal, T.; Smith, G. L.; Stewart, A. E.; Timofeevski, S.; Zhu, H.; Zhu, J.; Zou, H. Y.; Edwards, M. P. Discovery of (10R)-7-amino-12-fluoro-2,10,16-trimethyl-15-oxo-10,15,16,17-tetrahydro-2H-8,4-(m etheno) pyrazolo[4,3-h][2,5,11]-benzoxadiazacyclotetradecine-3-carbonitrile (PF-06463922), a macrocyclic inhibitor of anaplastic lymphoma kinase (ALK) and c-ros oncogene 1 (ROS1) with preclinical brain exposure and broad-spectrum potency against ALK-resistant mutations. *J. Med. Chem.* **2014**, *57*, 4720–4744.

37 Zapf, A.; Ehrentraut, A.; Beller, M. A new highly efficient catalyst system for the coupling of nonactivated and deactivated aryl chlorides with arylboronic acids. *Angew. Chem. Int. Ed. Engl.* **2000**, *39*, 4153–4155.

38 Deeken, J. F.; Loscher, W. The blood-brain barrier and cancer: transporters, treatment, and Trojan horses. *Clin. Cancer Res.* **2007**, *13*, 1663–1674.

39 Pan, S. T.; Li, Z. L.; He, Z. X.; Qiu, J. X.; Zhou, S. F. Molecular mechanisms for tumour resistance to chemotherapy. *Clin. Exp. Pharmacol. Physiol.* **2016**, *43*, 723–737.

40 Callegari, E.; Malhotra, B.; Bungay, P. J.; Webster, R.; Fenner, K. S.; Kempshall, S.; LaPerle, J. L.; Michel, M. C.; Kay, G. G. A comprehensive non-clinical evaluation of the CNS penetration potential of antimuscarinic agents for the treatment of overactive bladder. *Br. J. Clin. Pharmacol.* **2011**, *72*, 235–246.

41 Di, L.; Rong, H.; Feng, B. Demystifying brain penetration in central nervous system drug discovery. Miniperspective. *J. Med. Chem.* **2013**, *56*, 2–12.

42 Harrell, A. W.; Sychterz, C.; Ho, M. Y.; Weber, A.; Valko, K.; Negash, K. Interrogating the relationship between rat in vivo tissue distribution and drug property data for >200 structurally unrelated molecules. *Pharmacol. Res. Perspect.* **2015**, *3*, e00173.

43 Oppenheimer, S.; Teague, M.; Lam, J. L.; Wang, J.; Tsaparikos, K.; Wang, H.; Stroh, J.; Zou, H. Y.; Li, Q. T.;

Smeal, T.; Levkoff, T.; Johnson, T. W.; Song, W.; Miller, E. Drug Distribution and Pharmacokinetics in an Orthotopic Brain Tumor Model by MS Imaging and LC-MS. American Society for Mass Spectrometry Annual Conference, Baltimore Convention Center, Baltimore, MD, June 15–19, **2014**.

44 Zou, H. Y.; Friboulet, L.; Kodack, D. P.; Engstrom, L. D.; Li, Q.; West, M.; Tang, R. W.; Wang, H.; Tsaparikos, K.; Wang, J.; Timofeevski, S.; Katayama, R.; Dinh, D. M.; Lam, H.; Lam, J. L.; Yamazaki, S.; Hu, W.; Patel, B.; Bezwada, D.; Frias, R. L.; Lifshits, E.; Mahmood, S.; Gainor, J. F.; Affolter, T.; Lappin, P. B.; Gukasyan, H.; Lee, N.; Deng, S.; Jain, R. K.; Johnson, T. W.; Shaw, A. T.; Fantin, V. R.; Smeal, T. PF-06463922, an ALK/ROS1 inhibitor, overcomes resistance to first and second generation ALK inhibitors in preclinical models. *Cancer Cell* **2015**, *28*, 70–81.

45 Kola, I.; Landis, J. Can the pharmaceutical industry reduce attrition rates? *Nat. Rev. Drug Discov.* **2004**, *3*, 711–715.

46 Liederer, B. M.; Berezhkovskiy, L. M.; Dean, B. J.; Dinkel, V.; Peng, J.; Merchant, M.; Plise, E. G.; Wong, H.; Liu, X. Preclinical absorption, distribution, metabolism, excretion, and pharmacokinetic-pharmacodynamic modelling of N-(4-(3-((3S,4R)-1-ethyl-3-fluoropiperidine-4-ylamino)-1H-pyrazolo[3,4-b] pyridin- 4-yloxy)-3-fluorophenyl)-2-(4-fluorophenyl)-3-oxo-2,3-dihydropyridazine-4-carboxa mide, a novel MET kinase inhibitor. *Xenobiotica* **2011**, *41*, 327–339.

47 Schuster, D.; Laggner, C.; Langer, T. Why drugs fail—a study on side effects in new chemical entities. *Curr. Pharm. Des.* **2005**, *11*, 3545–3559.

48 Chien, J. Y.; Friedrich, S.; Heathman, M. A.; de Alwis, D. P.; Sinha, V. Pharmacokinetics/pharmacodynamics and the stages of drug development: role of modeling and simulation. *AAPS J.* **2005**, *7*, E544–E559.

49 Cohen, A. Pharmacokinetic and pharmacodynamic data to be derived from early-phase drug development: designing informative human pharmacology studies. *Clin. Pharmacokinet.* **2008**, *47*, 373–381.

50 Derendorf, H.; Lesko, L. J.; Chaikin, P.; Colburn, W. A.; Lee, P.; Miller, R.; Powell, R.; Rhodes, G.; Stanski, D.; Venitz, J. Pharmacokinetic/pharmacodynamic modeling in drug research and development. *J. Clin. Pharmacol.* **2000**, *40*, 1399–1418.

51 Lesko, L. J.; Rowland, M.; Peck, C. C.; Blaschke, T. F. Optimizing the science of drug development: opportunities for better candidate selection and accelerated evaluation in humans. *Pharm. Res.* **2000**, *17*, 1335–1344.

52 Lalonde, R. L.; Kowalski, K. G.; Hutmacher, M. M.; Ewy, W.; Nichols, D. J.; Milligan, P. A.; Corrigan, B. W.; Lockwood, P. A.; Marshall, S. A.; Benincosa, L. J.; Tensfeldt, T. G.; Parivar, K.; Amantea, M.; Glue, P.;

Koide, H.; Miller, R. Model-based drug development. *Clin. Pharmacol. Ther.* **2007**, *82*, 21–32.

53 Huang, S. M.; Abernethy, D. R.; Wang, Y.; Zhao, P.; Zineh, I. The utility of modeling and simulation in drug development and regulatory review. *J. Pharm. Sci.* **2013**, *102*, 2912–2923.

54 Yamazaki, S.; Lam, J. L.; Zou, H. Y.; Wang, H.; Smeal, T.; Vicini, P. Translational pharmacokinetic-pharmacodynamic modeling for an orally available novel inhibitor of anaplastic lymphoma kinase and c-Ros oncogene 1. *J. Pharmacol. Exp. Ther.* **2014**, *351*, 67–76.

55 Yamazaki, S.; Lam, J. L.; Zou, H. Y.; Wang, H.; Smeal, T.; Vicini, P. Mechanistic understanding of translational pharmacokinetic-pharmacodynamic relationships in nonclinical tumor models: a case study of orally available novel inhibitors of anaplastic lymphoma kinase. *Drug Metab. Dispos.* **2015**, *43*, 54–62.

56 Sharma, A.; Ebling, W. F.; Jusko, W. J. Precursor-dependent indirect pharmacodynamic response model for tolerance and rebound phenomena. *J. Pharm. Sci.* **1998**, *87*, 1577–1584.

57 Jusko, W. J.; Ko, H. C. Physiologic indirect response models characterize diverse types of pharmacodynamic effects. *Clin. Pharmacol. Ther.* **1994**, *56*, 406–419.

58 Dayneka, N. L.; Garg, V.; Jusko, W. J. Comparison of four basic models of indirect pharmacodynamic responses. *J. Pharmacokinet. Biopharm.* **1993**, *21*, 457–478.

19

Optimization of a Macrocyclic Ghrelin Receptor Agonist (Part II): Development of TZP-102

Hamid R. Hoveyda[1], Graeme L. Fraser[1], Eric Marsault[2], René Gagnon[3] and Mark L. Peterson[4]

[1] *Ogeda SA, Gosselies, Belgium*
[2] *Department of Pharmacology, University of Sherbrooke, Sherbrooke, Quebec, Canada*
[3] *Department of Chemistry, University of Sherbrooke, Sherbrooke, Quebec, Canada*
[4] *Cyclenium Pharma Inc., Montreal, Quebec, Canada*

19.1   Introduction

Ghrelin is an octanoylated 28-mer peptide[1] discovered by Kojima and coworkers in 1999 [1] as the endogenous ligand to the human ghrelin receptor GRLN, previously referred to as the growth hormone (GH) secretagogue receptor, hGHS-R1a [2]. The short-lived ghrelin peptide (plasma $T_{1/2} \leq 15\,min$) is unique among mammalian polypeptides by virtue of the posttranscriptional modification in which the serine-3 residue is covalently linked through an ester bond to a medium-chain fatty acid, that is, octanoic acid. Acylated ghrelin is required for activation of GRLN and consequent endocrine and gastrointestinal (GI) effects. The generation of this active form of ghrelin peptide (heretofore meaning "acyl-ghrelin") is mediated by the enzyme ghrelin *O*-acyltransferase (GOAT) [3]. The tetrapeptide at the N-terminus of ghrelin peptide, that is, GSS(octanoyl)F, has been known through the work of Bednarek *et al.* to be the minimal necessary sequence for activation of the receptor or the "active core" of this peptide (EC$_{50}$, Ca^{2+} = 72 nM vs. 2 nM for the full length peptide) [4]. The ghrelin peptide is principally produced in the gastric mucosa of the stomach and has been labeled as the "hunger hormone" since its circulating levels are higher preprandially [5]. GRLN is a class A G protein-coupled receptor (GPCR) that was discovered by Merck researchers in 1996 [6] and is closely related to motilin, neurotensin, and GPR39 receptors [7]. The key signal transduction pathway for GRLN is via Gα$_q$/PLCβ signaling that renders a Ca^{2+} bioluminescence functional assay relevant for tracking the bioactivity structure–activity relationship (SAR). The *in vitro* SAR in this project was followed through both radioligand binding (reversible competitive displacement of ^{125}I-ghrelin peptide) and Ca^{2+} functional aequorin assays for confirmation of full agonism.

In contrast to the early recognition of its GH-releasing properties [5], the gastroprokinetic effects of ghrelin peptide have only been more recently appreciated [8–10]. The phase II clinical trial data with ulimorelin (**2**; Figure 19.1) [11–14] demonstrated the GI stimulatory property of this synthetic macrocyclic ghrelin agonist relevant to the treatment of such GI motility disorders as postoperative ileus (POI) and diabetic gastroparesis. Also noteworthy was the observation that ulimorelin displayed more profound effects on GI activity than on GH release in rats [15] and humans, unlike other full agonists of GRLN, thus demarcating the *in vivo* pharmacology of GRLN in terms of GH vis-à-vis GI prokinetic effects for the first time, which compared favorably to such effects for other GRLN agonists in development [16–22]. The work by Holst and coworkers demonstrating that ligand-specific bias and/or agonist-allosteric signaling can be relevant for peptide and non-peptide GRLN agonists is worthy of mention in this context [23].

The initial lead optimization efforts on the foregoing macrocyclic ghrelin agonists from the high-throughput screening (HTS) hit (**1**; Figure 19.1), from a diverse library of macrocyclic peptidomimetics encompassing a tripeptide connected head to tail by a non-peptidic tether [24], to the initial clinical candidate (**2**; Figure 19.1), in terms of potency and pharmacokinetic (PK) properties, were reported previously [25]. Although TZP-101, which was primarily intended for acute intravenous applications such as treatment of POI, was well tolerated in phase I safety studies and found to be efficacious in phase II studies for POI, its cytochrome P450 (CYP) 3A4 profile (IC$_{50}$ = 0.6 μM) was considered a disadvantage for

---

1 Ghrelin (human) amino acid sequence is as follows: GSS(*n*-octanoyl)FLSPEHQRVQQRKESKKPPAKLQPR. The octanoylated ghrelin was used throughout the work herein.
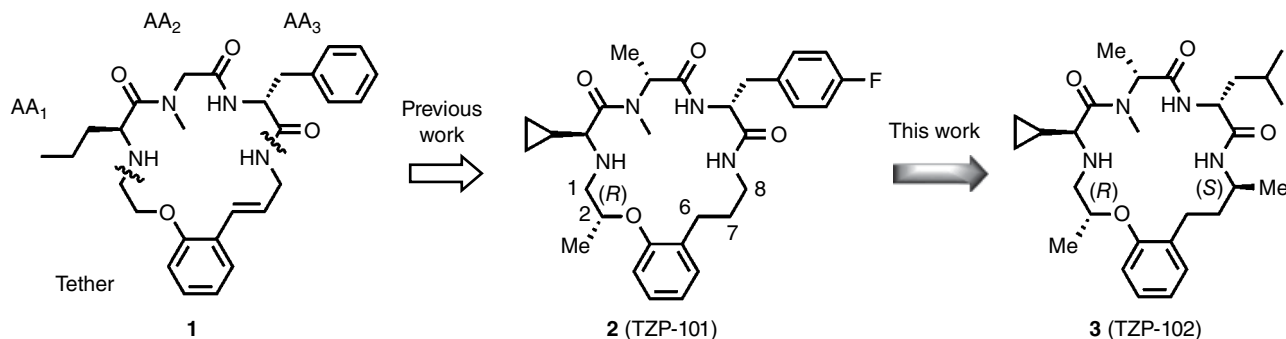
Figure 19.1 Lead progression: HTS hit structure (**1**), initial clinical candidate (**2**, TZP-101 or ulimorelin), and optimized oral clinical candidate (**3**, TZP-102). (The nomenclature and the tether backbone numbering shown are used throughout the text.)

chronic therapeutic applications due to the increased risk of potential drug–drug interactions. Thus, additional optimization was undertaken to attempt to improve the CYP 3A4 profile while maintaining, or ameliorating, the bioactivity and oral exposure to enhance oral efficacy for chronic applications such as treatment for diabetic gastroparesis. A summary of these efforts that culminated in the nomination of TZP-102 (**3**; Figure 19.1) as the second clinical candidate from the ghrelin agonist program is provided here.

The guiding principles for lead optimization of macrocyclic compounds are no different than those applied in medicinal chemistry projects involving non-macrocyclic structures. However, given the potential for greater conformational flexibility with macrocyclic ligand design versus traditional small-molecule lead structures, more emphasis on conformational restriction as a means of lead optimization is generally warranted. That said, the well-recognized notion of improving ligand lipophilic efficiency (LLE)[2]—a metric that helps capture the risk–reward balance of improved bioactivity against lipophilicity [26, 27]—as part of the lead optimization strategy also applies to this class of compounds, as was noted before [25]. The emphasis on LLE improvement is primarily based on the minimization of toxicological risks [28, 29] rather than Lipinski rule-of-five [30] concerns pertaining to limited oral availability. The concerns with conformational restriction and combined potency and LLE improvements governed the selections made throughout the course of the previously described lead optimization, as well as the subsequent optimization efforts described here. For example, the choice of cyclopropylglycine (Cpg) as the amino acid at the so-called AA$_1$ position (Figure 19.1) against even more potent variants, in spite of the higher cost and potential large-scale sourcing issues, was predicated not only on the greater conformational restriction of the cyclopropyl

ring (in Cpg) versus *sec*-butyl (in Ile) but also the greater lipophilic efficiency of the cyclopropyl ring, as evident in the superior aqueous solubility of Cpg-containing analogues versus congeners with Ile or Nva at the AA$_1$ position [25].

As shown in our earlier work [25], strategically positioned methyl substitutions proved a particularly efficient means of introducing local conformational constraints without adding to the rotatable bond count. In the initial lead optimization efforts, leading to the discovery of ulimorelin, this strategy was pursued in particular in the so-called "ethylene bridge" segment of the tether (see Figure 19.1). The so-called PK cooperativity effect between (*R*)-Me substitution at the C-2 position (in the "ethylene bridge" segment of the tether) and the Cpg at AA$_1$ greatly helped improve clearance and thus overall bioavailability of ulimorelin, as previously described [25]. A hydrophobic collapse, resulting in the "closed" macrocyclic conformation (Figure 19.2b), together with improved side-chain lipophilicity at AA$_1$ (i.e., with cyclopropyl in Cpg), was suggested as a possible rationale for this PK cooperativity effect. An intramolecular hydrogen bond (IHB) [31] was observed in the solid state (single crystal X-ray), as well as solution nuclear magnetic resonance (NMR) structures (Figure 19.2c–e), consistent with the β-turn present in ulimorelin. The β-turn motif has also been suggested as the active conformation in other ghrelin receptor agonists and GPCRs in general [32, 33]; the D-N-Me-Ala residue at AA$_2$ plays a key role as turn inducer in the foregoing structures [25]. In the collapsed conformation, the cyclopropyl ring AA$_1$ shields one face of the macrocycle with the (*R*)-Me tether substituent and the AA$_3$ phenyl ring side chain covering the opposite face. The polar fields mainly associated with the amide moieties are thus pushed away from the central macrocyclic cavity in the collapsed conformation (Figure 19.2b), helping to shield the IHB network that in turn helps maintain the macrocyclic core conformation.

2 LLE = pK_i − cLog$P$ (or log$D_{7.4}$).
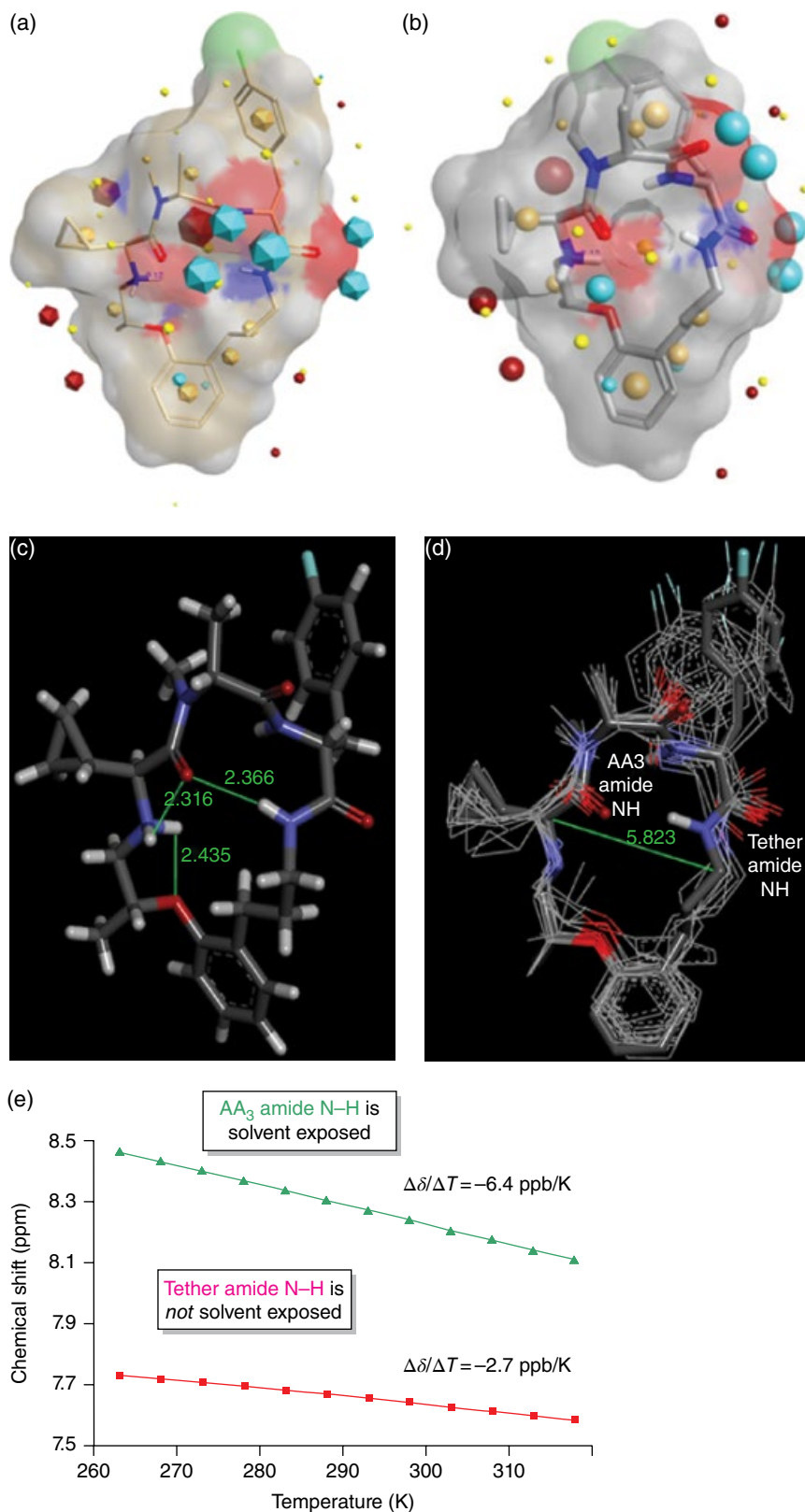
Figure 19.2 Panels a and b: The open (a) and closed (b) conformation of TZP-101 macrocyclic structure showing the molecular fields and solvent-accessible molecular surface using Forge™ software (v10, Cresset, United Kingdom). Panel c: X-ray crystal structure of TZP-101 showing the IHB network (solvent and counterion omitted for clarity). Panel d: Solution NMR consensus structure and molecular dynamics simulation also demonstrating hydrophobic collapse possibility. Panel e: Variable temperature NMR data indicating that the tether amide N–H (cf. Figure 19.1) is not solvent exposed, likely due to IHB. (*See insert for color representation of the figure.*)

TZP-101

Strategy 1:
(a) Reduce aromatic content
(b) Introduce polar heteroatom(s)

Strategy 2:
Introduce conformational bias (Me substitution) in the unexplored tether regions
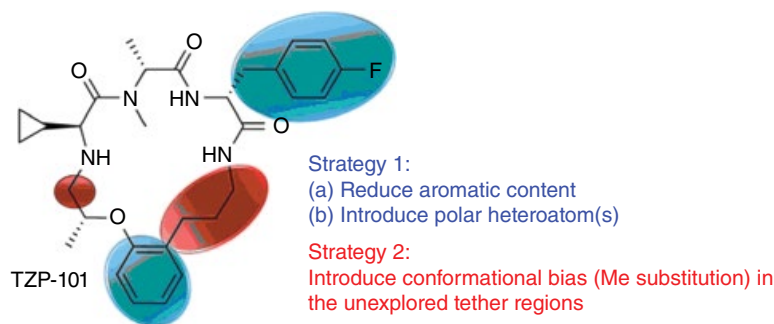
Figure 19.3 Lead optimization strategies discussed herein. (*See insert for color representation of the figure.*)

Improving CYP 3A4 off-target profile in ulimorelin ($IC_{50} = 0.6\,\mu M$) was one of the key goals in the second round of advanced lead optimization described herein. Several approaches to tackle this were envisaged as summarized in Figure 19.3. Conformational restriction can help "lock out" conformations that fall prey to metabolic enzymes, as well as those that give rise to off-target interactions, thereby improving the overall PD–PK profile. Introduction of polarity in the lead structure could be beneficial given the general tendency of CYP 3A4 toward binding more lipophilic substrates. The third strategy was inspired by the CYP 3A4 X-ray structure that was published around the time we were conducting the second round of lead optimization in 2004 [34]. Among the distinctive structural features of CYP 3A4 versus other CYP isoforms, Williams and coworkers noted that in addition to two phenylalanine residues pointing toward the active site, another five phenylalanine residues form a "Phe cluster." The said Phe cluster lies above the active site with the aromatic side chains stacked against each other to form a hydrophobic aromatic core. These novel observations at the time prompted us to explore the potential impact aromaticity reduction may bring about in terms of CYP 3A4 binding. As such, reduction of aromaticity through either the tether section of the lead structure or the AA_3 side chain was pursued as a further strategy as summarized in Section 19.2. It should be noted in passing that since the time this work was carried out, many reports have appeared in the literature extolling the virtues of aromatic content reduction in successful lead optimization [35–37].

As already mentioned, in the work that led to the discovery of ulimorelin (Figure 19.1, **2**) [25], a so-called cooperative effect was observed in structures such as **2** wherein *both* stereospecific (*R*)-Me in the C-2 tether position (cf. Figure 19.1) *and* the cyclopropyl AA_1 side chain proved critical to the improved PK profile including reduced clearance and prolonged elimination half-life. Moreover, the role of D-N-Me-Ala at the AA_2 position as an important β-turn-inducing element was made clear through the earlier investigations. Thus, in the lead optimization beyond ulimorelin that culminated

in the discovery of TZP-102 (Figures 19.1 and 19.3), these key features were generally retained, and the main focus was directed to additional optimization through the AA_3 side chain (more tolerant in terms of bioactivity SAR), as well as the less explored tether regions in the lead structure (Figure 19.3). A summary of the key findings is provided herein.

19.2 Advanced AA_3 and Tether SAR

19.2.1 AA_3 Options for Improved CYP3A4 Profile

The impact of AA_3 side chains other than the 4-fluorophenylalanine present in ulimorelin (**2**) was explored initially in combination with various tethers developed in our lab up until that time. A summary of these results is provided in Table 19.1. It was gratifying to observe that addition of a polar heteroatom (e.g., phenol oxygen in AA_3 = D-Tyr analogues such as **4**) or reduction of aromaticity (e.g., isobutyl side chain in AA_3 = D-Leu analogues such as **5**) helped improve CYP3A4 IC_{50} by three- to five-fold versus ulimorelin while providing equipotent leads (cf. Table 19.1; **4–5** vs. **2**). Alternatively, introduction of a heteroatom by converting the tether phenyl ring in structures **4** and **5** to the pyridine tether congeners, that is, **6** and **7** (Table 19.1), respectively, also resulted in a 10-fold CYP 3A4 IC_{50} amelioration. However, compound **6** displayed extremely poor passive permeability in the Caco-2 assay and was accordingly not orally bioavailable in rats (%*F* = 0) in keeping with its rather high topological polar surface area (TPSA) = $132\,\text{Å}^2$. In addition, the higher clearance rates with the foregoing pyridine tether analogues **6** and **7** (CL = 40 and 49 ml/min/kg, respectively), in spite of the presence of Cpg and C-2 tether (*R*)-Me that helped improve clearance in ulimorelin (**2**: CL = 23 ml/min/kg), suggested that the pyridine ring acts as a soft spot for the elimination of such analogues.

The chiral benzopyran tether design developed during the ulimorelin lead optimization (**8**: K_i = 0.9 nM) proved effective in terms of bioactivity with D-Tyr (**9**) and D-Leu

Table 19.1 PK–ADME and CYP 3A4 impact of D-Tyr and D-Leu at the AA$_3$ position together with initial tether variations.

Cpd	R at AA$_3$	Tether	RLB K_i (nM)	3A4 IC$_{50}$ (µM)	Caco-2 P_{app} (nm/s)			TPSA	rat PK	%F
					AB	BA	ER		iv CL$_T$ (ml/min/kg)	
2			22	0.6	140	150	1	100	23	16
4			12	3.3	—	—	—	120	—	—
5			31	2.1	—	—	—	100	—	—
6			61	30	<LLOQ	<LLOQ	—	132	40	0
7			400	>20	—	—	—	112	49	9
8			0.9	<1	—	—	—	100	13	
9			8	29	12	67	6	120	12	9
10			10	5	86	142	2	100	14	27

(*Continued*)

Table 19.1 (Continued)

| Cpd | R at AA$_3$ | Tether | RLB K_i (nM) | 3A4 IC$_{50}$ (µM) | Caco-2 P_{app} (nm/s) | | | TPSA | rat PK | |
					AB	BA	ER		iv CL$_T$ (ml/min/kg)	%F
11			431	—	—	—	—	100	—	—
12			19	>20	<LLOQ	<LLOQ	—	132	37	0
13			69	>20	12	16	1	112	42	nd

For reference: propranolol 300/320 ER = 1.
LLOQ, lower limit of quantification.
nd, not determined.

(**10**) AA$_3$ variants as well (K_i = 8–10 nM). Once again, with the more polar AA$_3$ side chain (**9**) or through aromatic content reduction with D-Leu at AA$_3$ (**10**), improved CYP 3A4 profile was observed (IC$_{50}$ = 29 and 5 µM, respectively) as compared with that of the ulimorelin congener, that is, analogue **8** (CYP 3A4 IC$_{50}$ < 1 µM) bearing the D-4-fluorophenyl AA$_3$ side chain. In contrast, the dihydrobenzofuran tether design was much less effective in terms of potency (cf. **11** vs. **10**; Table 19.1), and hence it was discarded from further consideration. Attempts to introduce the heteroaryl pyridine ring in the benzopyran tether design (**12–13**), while rather successful in terms of CYP 3A4 improvement (IC$_{50}$ > 20 µM), were far less so in terms of passive permeability and also led to elevated clearance rates (cf. Table 19.1), consistent with the similar results noted for the related pyridinyl tether analogues **6** and **7** discussed previously. Also noteworthy was the observation that with the leads carrying D-Tyr at the AA$_3$ position, P-gp efflux was apparent through the high efflux ratios (ER) obtained, for example, ER = 6 in **9** versus ER = 2 in **10**, the corresponding AA$_3$ = D-Leu counterpart. The trend of low permeability and high efflux observed systematically with D-Tyr containing analogues, such as compounds **6**, **9**, and **12**, is consistent with their high TPSA (≥120 Å^2). The impact of TPSA in affecting permeability, and thus oral availability, in the foregoing series was also evident by comparing the congeneric D-Leu analogues **10** and **13** that differ

only by virtue of the phenyl versus pyridinyl ring in the tether moiety, respectively. Although **13** displayed a superior CYP 3A4 IC$_{50}$ against **10**, a high clearance rate (pyridine ring) as well as very low passive permeability (TPSA > 100 Å^2) was also abundantly clear. These results clarified the point that while lipophilicity reduction/ introduction of polar heteroatoms is a successful strategy to improve CYP 3A4 IC$_{50}$ profile, a balanced approach in terms of hydrogen bond donor/acceptor count is required to maintain TPSA ≤ 100 Å^2 and thus obtain good passive permeability and moderate clearance rates in order to generate agonists with oral efficacy (see plots in Figure 19.4). Based on this perspective, D-Leu appeared to be more promising as compared with D-Tyr as the AA$_3$ of choice. In addition, pyridine-containing tether designs were discarded from further consideration[3] Instead, we turned our attention to other hitherto unexplored aspects of tether design as detailed in the following section.

---

3 We also investigated the possibility of introducing D-pyridyl-alanine (D-Pal) in the AA$_3$ position. The best potency was obtained with D-2-Pal at AA$_3$. However, such macrocycles proved particularly prone to epimerization at AA$_3$ (during the coupling stage). This factor, as well as a tendency toward partial agonism in the subseries (particularly evident with meta- and para-congeners), dissuaded us from further consideration of this AA$_3$ variant.

Figure 19.4 top plot box: TPSA > 110Å²: low P_{app} but improved CYP 3A4

P_{app} (nm/s) vs TPSA; legend 3A4 IC₅₀: 0.6, 15.3, 30

CYP 3A4 IC₅₀ ↓ correlates to clog*P* ↑

3A4 IC50 (µM) vs *c*Log*P*; $r^2 = 0.70$; legend P_{app} AB: 0, 70, 140
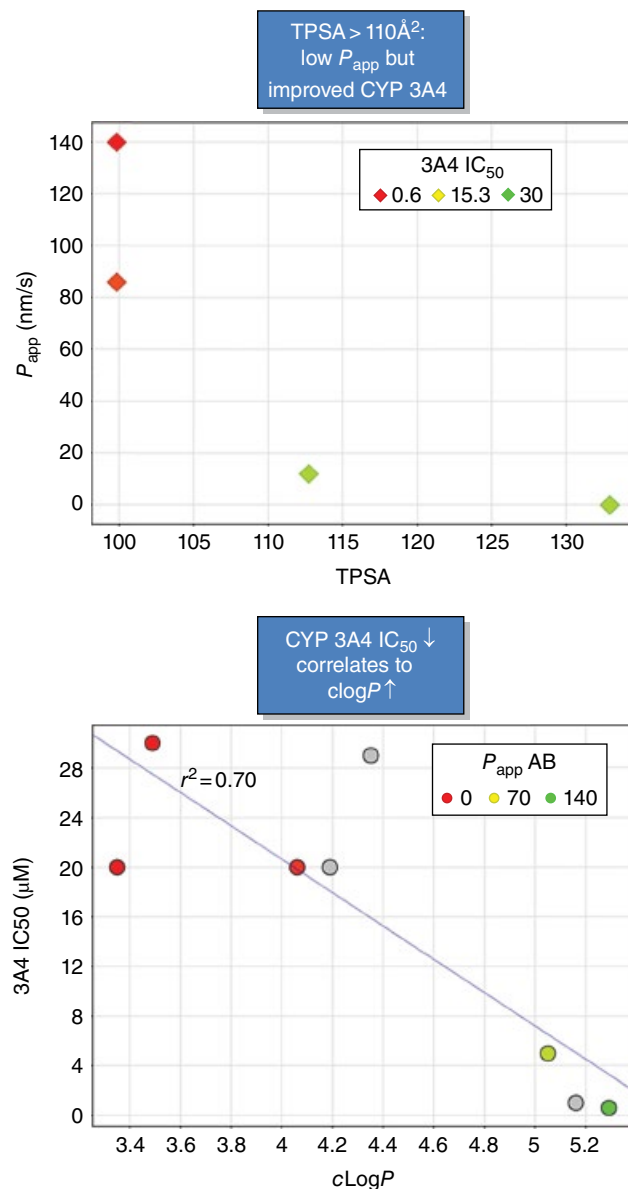
Figure 19.4 Correlation plots based on data presented in Table 19.1. (*See insert for color representation of the figure.*)

19.2.2 Additional Tether SAR Explorations: Reduction of the Aromatic Content and Additional Conformational Constraints through Methyl Substitution

As indicated in Figure 19.3, a significant component of this round of lead optimization consisted of exploration of tether SAR that included both aromatic content reduction and introduction of additional conformational constraints through methyl substitutions. A selection of these results is provided in Table 19.2.

One notable discovery was that the aromatic ring in the tether moiety in ulimorelin (Figure 19.1) is not indispensable for potency. Thus, structure **14** (Table 19.2;

$K_i = 2.4$ nM) bearing the chiral cyclohexyl tether proved fivefold more potent than the congeneric aryl tether structure **4** (Table 19.1; $K_i = 12$ nM). Likewise, a comparison of AA₃ = D-Leu congeners **15** (Table 19.2; $K_i = 9$ nM) versus **5** (Table 19.1; $K_i = 31$ nM) supported the same conclusion, that is, the reduced phenyl ring tether structures furnished more potent ghrelin agonists. Interestingly, an improved CYP 3A4 IC₅₀ profile in cyclohexyl tether analogues vis-à-vis the aryl tether congeners was also observed, in line with the conjecture aforementioned in terms of impact of aromatic ring content on CYP 3A4 affinity. This was particularly evident when comparing the congeneric D-Leu analogue **15** (Table 19.2, IC₅₀ = 6.7 µM) against **5** (Table 19.1, IC₅₀ = 2.1 µM), that is, greater than threefold improvement upon reducing aromatic content through both AA₃ and tether modifications. Also noteworthy was the observation that cyclohexyl tether analogues **14** and **15** displayed comparable clearance rates to ulimorelin, with somewhat superior oral bioavailability even with D-Tyr at AA₃. In the final analysis, however, the synthetic complexity of the chiral cyclohexyl tether outweighed the benefits provided through these analogues when measured against the other easier-to-access improved tether designs discussed in the succeeding text.

The (*R,R*)-1,2-diMe-substituted tether design exemplified through lead structures **16** and **17** (Table 19.2) constituted another important finding. Like the case of chiral cyclohexyl tether analogues (**14** and **15**) mentioned previously, this tether design also demonstrated clear improvement in terms of agonist potency and CYP 3A4 IC₅₀ against the congeners with the ulimorelin tether design. For example, D-Tyr analogue **16** (Table 19.2; $K_i = 17$ nM, 3A4 IC₅₀ = 14 µM) was nominally more potent in terms of GRLN receptor binding and fourfold superior in CYP 3A4 versus congener **4** (Table 19.1; $K_i = 12$ nM, 3A4 IC₅₀ = 3.3 µM). Similarly, D-Leu analogue **17** (Table 19.2; $K_i = 4$ nM, 3A4 IC₅₀ = 8.2 µM) was both significantly more potent and improved in CYP 3A4 versus congener **5** (Table 19.1; $K_i = 31$ nM, 3A4 IC₅₀ = 2.1 µM). Additionally, **16** and **17** were comparable in terms of their rat PK profiles against that of ulimorelin. However, the steric encumbrance due to the additional methyl substitution at the *C*-1 position in the (*R,R*)-1,2-diMe-substituted tether rendered the tether-AA₁ coupling reaction, whether through a Fukuyama–Mitsunobu or a direct alkylation approach, rather arduous and low yielding. The latter factors were weighted against further consideration of this tether design considering other options that become available (see succeeding text).

The aforementioned cases contrasted with those of the cyclopropanated (Table 19.2; **18–19**) and 2,7-diMe-substituted (**20**) tether designs that were generally

Table 19.2 Additional tether SAR explorations: Reduction of aromatic content and additional conformational constraints through methyl substitution.
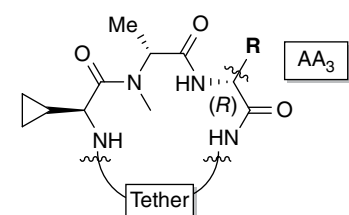
Cpd	R at AA$_3$	Tether	RLB K_i (nM)	3A4 IC$_{50}$ (µM)	rat PK	
					iv CL$_T$ (ml/min/kg)	%*F*
14			2.4	4.5	19	29
15			9	6.7	28	37
16			17	14	15	18
17			4	8.2	19	12
18			201	—	—	—
19			90	—	—	—
20			61, 117	—	—	—
21			19	—	—	—

Table 19.2 (Continued)

Cpd	R at AA₃	Tether	RLB K_i (nM)	3A4 IC$_{50}$ (μM)	rat PK iv CL$_T$ (ml/min/kg)	%F
22	(4-F-benzyl)	2,8-diMe ether tether	22	—	—	—
23	(4-F-benzyl)	(R),(R)-2,9-diMe ether tether	8	—	—	—
24	(4-F-benzyl)	(R),(S)-2,9-diMe ether tether	4	—	—	—
3	(isobutyl)	(R),(S)-2,9-diMe ether tether	6	8.5	5.3 (7.7)[a]	23 (29)[a]
25	(isobutyl)	(R),(S)-2,9-diMe pyridine tether	305	>20	20	—
26	(isobutyl)	Me, F-aryl ether tether	31	4.2	21	51

[a] Monkey PK data in parenthesis.

unsuccessful due to right-shifted bioactivity. The 2,8-diMe tether design was more successful in that it afforded equipotent leads to the ulimorelin congener, regardless of the stereochemistry of the substituted methyl at the C-8 position (cf. **21** and **22**). However, with the (R,S)-2,9-diMe tether design (e.g., **23** and **24**), a greater than fivefold improvement in potency was evident when compared against the (R)-2-Me tether congener, that is, **24** versus **2**. The congener (R,R)-2,9-diMe was twofold less effective in terms of bioactivity than its (R,S)-epimer (**23** vs. **24**). Combining D-Leu at AA₃ position with the said (R,S)-2,9-diMe tether design provided a compound (**3**) with improved potency both versus ulimorelin and vis-à-vis its D-Leu congeners **15** and **5**. Analogue **3** also showed a superior CYP 3A4 result, IC$_{50}$ = 8.5 μM

(vs. 0.6 μM in ulimorelin), as well as a low clearance rate and good oral bioavailability both in rat and monkey PK experiments (Table 19.2). Based on these findings, compound **3** was advanced into further preclinical safety profiling (e.g., hERG, AMES, and Cerep broad selectivity profile) from which it emerged successfully.[4]

The improved oral efficacy of this analogue was established through the gastric emptying studies after oral dosing shown in Figure 19.5. As can be seen, **3** (TZP-102)

4 The safety data are as follows: hERG IC$_{50}$ > 500 μM (patch-clamp assay); Ames test negative at all concentrations tested up to 180 μM; Cerep panel of 85 pharmacologically relevant receptors, transporters, and ion channels at 10 μM only showed a weak affinity (K_i 6.3–7.8 μM) for the 5-HT$_{1\alpha}$ receptor, which was not associated with any functional activity.
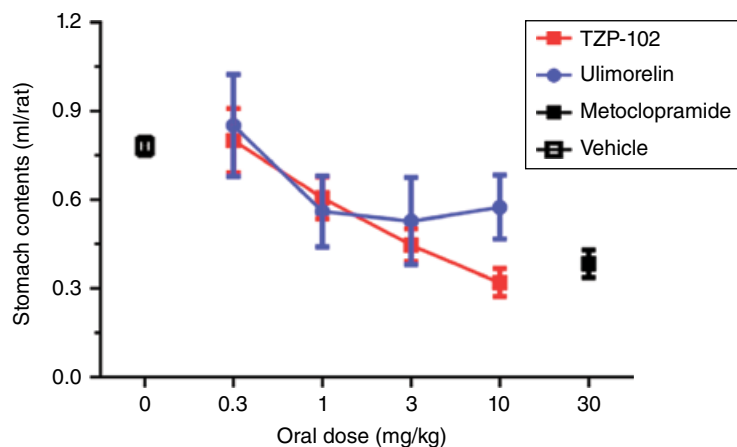
Figure 19.5 Rat gastric emptying data (oral administration, metoclopramide as positive control). (*See insert for color representation of the figure.*)

attained greater maximal efficacy in these studies demonstrating a >60% dose-dependent acceleration of gastric emptying as compared with ulimorelin where maximal efficacy on gastric emptying was <30%. The superior efficacy of TZP-102 is consistent with the improved agonist potency and PK–ADME (Absorption-Distribution-Metabolism-Excretion) profiles already discussed.

Overall, ulimorelin and TZP-102 demonstrated efficacy in phase II trials for the treatment of POI and diabetic gastroparesis, respectively [13, 14, 38]. In all cases, these compounds were well tolerated and no major adverse effects were reported. It is also noteworthy that no special formulations were necessary for these macrocyclic molecules and standard preparations were able to be utilized in the clinic for each. Although development of these compounds eventually was halted[5] for these indications [39, 40], the pioneering research with ulimorelin and TZP-102 provided initial clinical proof-of-concept data validating GRLN as a viable therapeutic target for GI disorders and spurning development of subsequent GRLN agonists in the field [18, 41–46].

19.3 Structural Studies

The conformation of the peptide backbone can be described by the three torsion angles,[6] that is, ϕ, ψ, and ω [47, 48]. Shown in Table 19.3 are the torsion angles for TZP-102 based on its X-ray crystal structure.

As was the case with TZP-101, a (nonideal) type I′ β-turn structure is evident in TZP-102 as well (Figure 19.6).

Table 19.3 Amide torsion angles in the X-ray structure of TZP-102 salt.

	i	$i+1$	$i+2$
Angle	**$AA_1 = Cpg$**	**$AA_2 = $D-N-Me-Ala**	**$AA_3 = $D-Leu**
ϕ	—	85.56°	72.13°
ψ	−70.48	2.59°	13.71°
ω	—	168.04°	−173.49°

Type I′ β-turn defined as $(\phi, \psi)_{i+1} = (60°, 30°)$ and $(\phi, \psi)_{i+2} = (90°, 0°)$.

19.4 Conclusions

Nature often employs stereospecific methyl substitutions as local conformation constraint elements to modulate biological properties as elegantly exemplified in polyketides [49]. Such so-called "magic" methyl groups [50] are particularly advantageous as they introduce conformational bias *without adding to the rotatable bond count*. As was noted by Veber and coworkers in their landmark paper in 2002 [51], the definition of rotatable bond count (nRot) of zero is incorrect for larger rings, that is, macrocycles. As such, macrocycles, as well as noncyclic lead structures, can benefit from such magic methyl group effects for optimization of biological properties, whether in terms of potency or PK–ADME properties. Thus, even though the initial hit structure **1** (Figure 19.1) has apparently a quite low nRot = 4, it would be misleading to consider such macrocyclic structures as conformationally completely rigid. Indeed, the consensus on NMR structures and MD simulations performed on the initial clinical candidate indicated that ulimorelin (**2**; cf. Figure 19.2d) illustrates conformational flexibility present in the foregoing structures, in particular in the tether region. Application of additional conformational rigidification as well as enhancement of LLE helped progress the hit (**1**) to the initial clinical candidate,
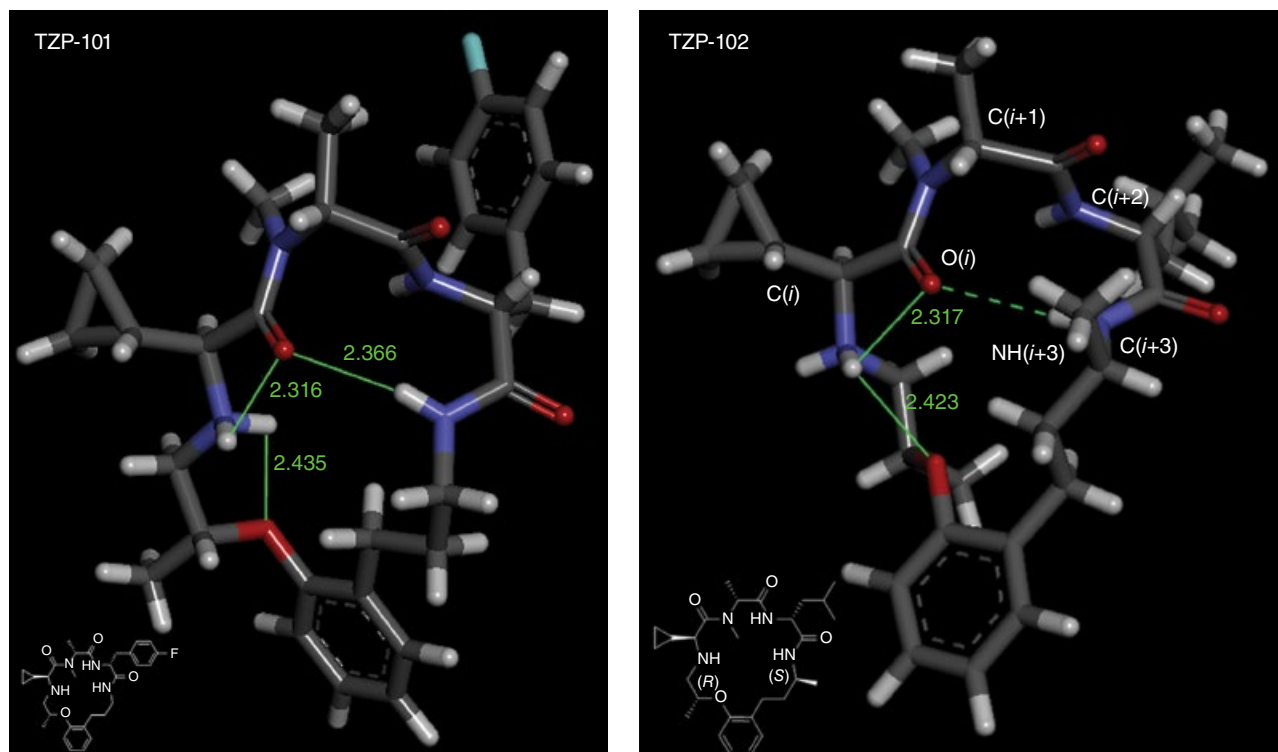
5 In both instances, significant placebo responses resulted in insufficient differentiation for the treatment arms; see references 39 and 40 for more detail.

6 Torsion angles (ϕ, ψ, ω) define peptide conformation through angle definitions as follows: ϕ is the angle formed by C(O)-N-Cα-C(O); ψ by N-Cα-C(O)-N; and ω, or the "amide torsion angle," by Cα-C(O)-N-Cα (thus $\omega = 180°$ for *trans*-amide and 0° for *cis*-amide bonds). See Refs. 47 and 48.

Figure 19.6 X-ray crystal structures of **2** (TZP-101) and **3** (TZP-102) (counterions omitted for clarity). (*See insert for color representation of the figure.*)

ulimorelin (**2**; Figure 19.1), as previously reported [25]. The strategies of introducing polar heteroatoms and reduction of aromatic content were effective in improving the CYP 3A4 profile compared with ulimorelin. However, introduction of polar atoms (HBA/D count increase) needs to be balanced against the adverse impact of increased TPSA and the attendant deterioration in passive permeability, as well as an increased potential for P-gp efflux. These findings underscore the fact that although the initial scaffold is nontraditional in terms of lead optimization considerations, macrocyclic structures are no different than the more conventional small molecules in that the same medicinal chemistry tenets apply. Overall, the principles of conformational rigidification, optimization of LLE, and reduction of aromatic content proved quite useful to generate optimized clinical candidates with excellent safety profile.

Back in the early 2000s, we were confronted with a good deal of skepticism by many scions of the pharmaceutical industry who generally considered such macrocyclic lead structures undevelopable due to the strictures of the Lipinski rule of five, lack of evidence for oral bioavailability, anticipated difficulties in scale-up, and other unchartered territories in the macrocyclic drug discovery landscape of the time. Clearly such skepticism was unfounded as the work discussed herein, and within this volume, shows that macrocyclic lead structures can be as optimizable in terms of PK–ADME or off-target aspects as any other "classical" small molecule in traditional medicinal chemistry projects. The significant shift in perspective in the industry today in terms of acceptance of macrocyclic ligand design bodes well for interesting future discoveries as it helps expand the traditional chemical space for the discovery of novel drugs [52–56].

Acknowledgments

References

1 Kojima, M.; Hosoda, H.; Date, Y.; Nakazato, M.; Matsuo, H.; Kangawa, K. Ghrelin is a growth-hormone-releasing acylated peptide from stomach. *Nature* **1999**, *402*, 656–660.

2 Davenport, A. P.; Bonner, T. I.; Foord, S. M.; Harmar, A. J.; Neubig, R. R.; Pin, J. P.; Spedding, M.; Kojima, M.; Kangawa, K. International Union of Pharmacology. LVI. Ghrelin receptor nomenclature, distribution, and function. *Pharmacol. Rev.* **2005**, *57*, 541–546.

3 For a recent review on GOAT: Khatib, M. N.; Gaidhane, S.; Gaidhane, A. M.; Simkhada, P.; Zahiruddin, Q. S. Ghrelin O acyl transferase (GOAT) as a novel metabolic regulatory enzyme. *J. Clin. Diagn. Res.* **2015**, *9*, LE01–LE05.

4 Bednarek, M. A.; Feighner, S. D.; Pong, S. S.; McKee, K. K.; Hreniuk, D. L.; Silva, M. V.; Warren, V. A.; Howard, A. D.; Van Der Ploeg, L. H.; Heck, J. V. Structure-function studies on the new growth hormone-releasing peptide, ghrelin: minimal sequence of ghrelin necessary for activation of growth hormone secretagogue receptor 1a. *J. Med. Chem.* **2000**, *43*, 4370–4376.

5 Perello, M.; Dickson, S. L. Ghrelin signalling on food reward: a salient link between the gut and the mesolimbic system. *J. Neuroendocrinol.* **2015**, *27*, 424–434.

6 Howard, A. D.; Feighner, S. D.; Cully, D. F.; Arena, J. P.; Liberator, P. A.; Rosenblum, C. I.; Hamelin, M.; Hreniuk, D. L.; Palyha, O. C.; Anderson, J.; Paress, P. S.; Diaz, C.; Chou, M.; Liu, K. K.; McKee, K. K.; Pong, S. S.; Chaung, L. Y.; Elbrecht, A.; Dashkevicz, M.; Heavens, R.; Rigby, M.; Sirinathsinghji, D. J.; Dean, D. C.; Melillo, D. G.; Patchett, A. A.; Nargund, R.; Griffin, P. R.; DeMartino, J. A.; Gupta, S. K.; Schaeffer, J. M.; Smith, R. G.; Van der Ploeg, L. H. A receptor in pituitary and hypothalamus that functions in growth hormone release. *Science* **1996**, *273*, 974–977.

7 For a general review: Kojima, M.; Kangawa, K. Ghrelin: structure and function. *Physiol. Rev.* **2005**, *85*, 495–522.

8 Peeters, T. L. Ghrelin: a new player in the control of gastrointestinal functions. *Gut* **2005**, *54*, 1638–1649 and references therein.

9 Murray, C. D.; Martin, N. M.; Patterson, M.; Taylor, S. A.; Ghatei, M. A.; Kamm, M. A.; Johnston, C.; Bloom, S. R.; Emmanuel, A. V. Ghrelin enhances gastric emptying in diabetic gastroparesis: a double blind, placebo controlled, crossover study. *Gut* **2005**, *54*, 1693–1698.

10 Greenwood-Van Meerveld, B.; Kriegsman, M.; Nelson, R. Ghrelin as a target for gastrointestinal motility disorders. *Peptides* **2011**, *32*, 2352–2356.

11 Ejskjaer, N.; Vestergaard, E. T.; Hellstrom, P. M.; Gormsen, L. C.; Madsbad, S.; Madsen, J. L.; Jensen, T. A.; Pezzullo, J. C.; Christiansen, J. S.; Shaughnessy, L.; Kosutic, G. Ghrelin receptor agonist (TZP-101) accelerates gastric emptying in adults with diabetes and symptomatic gastroparesis. *Aliment. Pharmacol. Ther.* **2009**, *29*, 1179–1187.

12 Wo, J. M.; Ejskjaer, N.; Hellstrom, P. M.; Malik, R. A.; Pezzullo, J. C.; Shaughnessy, L.; Charlton, P.; Kosutic, G.; McCallum, R. W. Randomised clinical trial: ghrelin agonist TZP-101 relieves gastroparesis associated with severe nausea and vomiting—randomised clinical study subset data. *Aliment. Pharmacol. Ther.* **2011**, *33*, 679–688.

13 Popescu, I.; Fleshner, P. R.; Pezzullo, J. C.; Charlton, P. A.; Kosutic, G.; Senagore, A. J. The ghrelin agonist TZP-101 for management of postoperative ileus after partial colectomy: a randomized, dose-ranging, placebo-controlled clinical trial. *Dis. Colon Rectum* **2010**, *53*, 126–134.

14 Bochicchio, G.; Charlton, P.; Pezzullo, J. C.; Kosutic, G.; Senagore, A. Ghrelin agonist TZP-101/ulimorelin accelerates gastrointestinal recovery independently of opioid use and surgery type: covariate analysis of phase 2 data. *World J. Surg.* **2012**, *36*, 39–45.

15 Fraser, G. L.; Hoveyda, H. R.; Tannenbaum, G. S. Pharmacological demarcation of the growth hormone, gut motility and feeding effects of ghrelin using a novel ghrelin receptor agonist. *Endocrinology* **2008**, *149*, 6280–6288.

16 Moulin, A.; Ryan, J.; Martinez, J.; Fehrentz, J. A. Recent developments in ghrelin receptor ligands. *ChemMedChem* **2007**, *2*, 1242–1259.

17 Costantino, L.; Barlocco, D. Ghrelin receptor modulators and their therapeutic potential. *Future Med. Chem.* **2009**, *1*, 157–177.

18 Charoenthongtrakul, S.; Giuliana, D.; Longo, K. A.; Govek, E. K.; Nolan, A.; Gagne, S.; Morgan, K.; Hixon, J.; Flynn, N.; Murphy, B. J.; Hernandez, A. S.; Li, J.; Tino, J. A.; Gordon, D. A.; DiStefano, P. S.; Geddes, B. J. Enhanced gastrointestinal motility with orally active ghrelin receptor agonists. *J. Pharmacol. Exp. Ther.* **2009**, *329*, 1178–1186.

19 Garcia, J. M.; Polvino, W. J. Pharmacodynamic hormonal effects of anamorelin, a novel oral ghrelin mimetic and growth hormone secretagogue in healthy volunteers. *Growth Horm. IGF Res.* **2009**, *19*, 267–273.

20 Venkova, K.; Mann, W.; Nelson, R.; Greenwood-Van Meerveld, B. Efficacy of ipamorelin, a novel ghrelin mimetic, in a rodent model of postoperative ileus. *J. Pharmacol. Exp. Ther.* **2009**, *329*, 1110–1116.

21 Greenwood-Van Meerveld, B.; Tyler, K.; Mohammadi, E.; Pietra, C. Efficacy of ipamorelin, a ghrelin mimetic,

on gastric dysmotility in a rodent model of postoperative ileus. *J. Exp. Pharmacol.* **2012**, *4*, 149–155.

22 Camilleri, M.; Acosta, A. Emerging treatments in Neurogastroenterology: relamorelin: a novel gastrocolokinetic synthetic ghrelin agonist. *Neurogastroenterol. Motil.* **2015**, *27*, 324–332.

23 Holst, B.; Brandt, E.; Bach, A.; Heding, A.; Schwartz, T. W. Nonpeptide and peptide growth hormone secretagogues act both as ghrelin receptor agonist and as positive or negative allosteric modulators of ghrelin signaling. *Mol. Endocrinol.* **2005**, *19*, 2400–2411.

24 Marsault, E.; Hoveyda, H. R.; Peterson, M. L.; Gagnon, R.; Vezina, M.; Pinault, J. F.; Landry, A.; Saint-Louis, C.; Ouellet, L. G.; Beauchemin, S.; Benakli, K.; Beaubien, S.; Brassard, M.; Wang, Z.; Champagne, M.; Galaud, F.; Fortin, N.; Fortin, D.; Plourde, V.; Ramaseshan, M.; Bhat, S.; Bilodeau, F.; Lonergan, D.; Lan, R.; Li, S.; Berthiaume, G.; Foucher, L.; Peng, X.; Dory, Y.; Deslongchamps, P. High throughput solid phase parallel synthesis of macrocyclic peptidomimetics. *Adv. Exp. Med. Biol.* **2009**, *611*, 15–16.

25 Hoveyda, H. R.; Marsault, E.; Gagnon, R.; Mathieu, A. P.; Vezina, M.; Landry, A.; Wang, Z.; Benakli, K.; Beaubien, S.; Saint-Louis, C.; Brassard, M.; Pinault, J. F.; Ouellet, L.; Bhat, S.; Ramaseshan, M.; Peng, X.; Foucher, L.; Beauchemin, S.; Bherer, P.; Veber, D. F.; Peterson, M. L.; Fraser, G. L. Optimization of the potency and pharmacokinetic properties of a macrocyclic ghrelin receptor agonist (part I): development of ulimorelin (TZP-101) from hit to clinic. *J. Med. Chem.* **2011**, *54*, 8305–8320.

26 Hopkins, A. L.; Keseru, G. M.; Leeson, P. D.; Rees, D. C.; Reynolds, C. H. The role of ligand efficiency metrics in drug discovery. *Nat. Rev. Drug Discov.* **2014**, *13*, 105–121.

27 Leeson, P. D.; Springthorpe, B. The influence of drug-like concepts on decision-making in medicinal chemistry. *Nat. Rev. Drug Discov.* **2007**, *6*, 881–890.

28 Leeson, P. D.; Empfield, J. R., Chapter 24—Reducing the Risk of Drug Attrition Associated with Physicochemical Properties. In *Annual Reports in Medicinal Chemistry*, John, E. M., Ed. Academic Press, New York: **2010**; Vol. *45*, pp 393–407.

29 Gleeson, M. P.; Hersey, A.; Montanari, D.; Overington, J. Probing the links between in vitro potency, ADMET and physicochemical parameters. *Nat. Rev. Drug Discov.* **2011**, *10*, 197–208.

30 Lipinski, C. A.; Lombardo, F.; Dominy, B. W.; Feeney, P. J. Experimental and computational approaches to estimate solubility and permeability in drug discovery and development settings. *Adv. Drug Deliv. Rev.* **2001**, *46*, 3–26.

31 For a recent review on the importance of IHB on molecular structures and properties: Kuhn, B.; Mohr, P.; Stahl, M. Intramolecular hydrogen bonding in medicinal chemistry. *J. Med. Chem.* **2010**, *53*, 2601–2611.

32 Tyndall, J. D.; Pfeiffer, B.; Abbenante, G.; Fairlie, D. P. Over one hundred peptide-activated G protein-coupled receptors recognize ligands with turn structure. *Chem. Rev.* **2005**, *105*, 793–826.

33 Loughlin, W. A.; Tyndall, J. D.; Glenn, M. P.; Hill, T. A.; Fairlie, D. P. Update 1 of: beta-strand mimetics. *Chem. Rev.* **2010**, *110*, PR32–PR69.

34 Williams, P. A.; Cosme, J.; Vinkovic, D. M.; Ward, A.; Angove, H. C.; Day, P. J.; Vonrhein, C.; Tickle, I. J.; Jhoti, H. Crystal structures of human cytochrome P450 3A4 bound to metyrapone and progesterone. *Science* **2004**, *305*, 683–686.

35 Lovering, F.; Bikker, J.; Humblet, C. Escape from flatland: increasing saturation as an approach to improving clinical success. *J. Med. Chem.* **2009**, *52*, 6752–6756.

36 Ritchie, T. J.; Macdonald, S. J. The impact of aromatic ring count on compound developability—are too many aromatic rings a liability in drug design? *Drug Discov. Today* **2009**, *14*, 1011–1020.

37 Luker, T.; Alcaraz, L.; Chohan, K. K.; Blomberg, N.; Brown, D. S.; Butlin, R. J.; Elebring, T.; Griffin, A. M.; Guile, S.; St-Gallay, S.; Swahn, B. M.; Swallow, S.; Waring, M. J.; Wenlock, M. C.; Leeson, P. D. Strategies to improve in vivo toxicology outcomes for basic candidate drug molecules. *Bioorg. Med. Chem. Lett.* **2011**, *21*, 5673–5679.

38 Ejskjaer, N.; Wo, J. M.; Esfandyari, T.; Mazen Jamal, M.; Dimcevski, G.; Tarnow, L.; Malik, R. A.; Hellstrom, P. M.; Mondou, E.; Quinn, J.; Rousseau, F.; McCallum, R. W. A phase 2a, randomized, double-blind 28-day study of TZP-102 a ghrelin receptor agonist for diabetic gastroparesis. *Neurogastroenterol. Motil.* **2013**, *25*, e140–e150.

39 Shaw, M.; Pediconi, C.; McVey, D.; Mondou, E.; Quinn, J.; Chamblin, B.; Rousseau, F. Safety and efficacy of ulimorelin administered postoperatively to accelerate recovery of gastrointestinal motility following partial bowel resection: results of two randomized, placebo-controlled phase 3 trials. *Dis. Colon Rectum* **2013**, *56*, 888–897.

40 McCallum, R. W.; Lembo, A.; Esfandyari, T.; Bhandari, B. R.; Ejskjaer, N.; Cosentino, C.; Helton, N.; Mondou, E.; Quinn, J.; Rousseau, F. Phase 2b, randomized, double-blind 12-week studies of TZP-102, a ghrelin receptor agonist for diabetic gastroparesis. *Neurogastroenterol. Motil.* **2013**, *25*, e705–e717.

41 Costantino, L.; Barlocco, D. Ghrelin receptor modulators: a patent review (2011–2014). *Expert Opin. Ther. Pat.* **2014**, *24*, 1007–1019.

42 Tack, J.; Corsetti, M. Ghrelin agonists as emerging prokinetic agents. *Clin. Gastroenterol. Hepatol.* **2015**, *13*, 2320–2322.

43 Naitou, K.; Mamerto, T. P.; Pustovit, R. V.; Callaghan, B.; Rivera, L. R.; Chan, A. J.; Ringuet, M. T.; Pietra, C.; Furness, J. B. Site and mechanism of the colokinetic action of the ghrelin receptor agonist, HM01. *Neurogastroenterol. Motil.* **2015**, *27*, 1764–1771.

44 Ellis, A. G.; Zeglinski, P. T.; Brown, D. J.; Frauman, A. G.; Millard, M.; Furness, J. B. Pharmacokinetics of the ghrelin agonist capromorelin in a single ascending dose phase-I safety trial in spinal cord-injured and able-bodied volunteers. *Spinal Cord* **2015**, *53*, 103–108.

45 Shin, A.; Camilleri, M.; Busciglio, I.; Burton, D.; Smith, S. A.; Vella, A.; Ryks, M.; Rhoten, D.; Zinsmeister, A. R. The ghrelin agonist RM-131 accelerates gastric emptying of solids and reduces symptoms in patients with type 1 diabetes mellitus. *Clin. Gastroenterol. Hepatol.* **2013**, *11*, 1453–1459.e4.

46 Shin, A.; Camilleri, M.; Busciglio, I.; Burton, D.; Stoner, E.; Noonan, P.; Gottesdiener, K.; Smith, S. A.; Vella, A.; Zinsmeister, A. R. Randomized controlled phase Ib study of ghrelin agonist, RM-131, in type 2 diabetic women with delayed gastric emptying: pharmacokinetics and pharmacodynamics. *Diabetes Care* **2013**, *36*, 41–48.

47 Chou, P. Y.; Fasman, G. D. Prediction of the secondary structure of proteins from their amino acid sequence. *Adv. Enzymol. Relat. Areas Mol. Biol.* **1978**, *47*, 45–148.

48 Ramachandran, G. N.; Sasisekharan, V. Conformation of polypeptides and proteins. *Adv. Protein Chem.* **1968**, *23*, 283–438.

49 Hoffmann, R. W. Conformation design of open-chain compounds. *Angew. Chem. Int. Ed. Engl.* **2000**, *39*, 2054–2070.

50 Barreiro, E. J.; Kummerle, A. E.; Fraga, C. A. The methylation effect in medicinal chemistry. *Chem. Rev.* **2011**, *111*, 5215–5246.

51 Veber, D. F.; Johnson, S. R.; Cheng, H. Y.; Smith, B. R.; Ward, K. W.; Kopple, K. D. Molecular properties that influence the oral bioavailability of drug candidates. *J. Med. Chem.* **2002**, *45*, 2615–2623.

52 Driggers, E. M.; Hale, S. P.; Lee, J.; Terrett, N. K. The exploration of macrocycles for drug discovery—an underexploited structural class. *Nat. Rev. Drug Discov.* **2008**, *7*, 608–624.

53 Marsault, E.; Peterson, M. L. Macrocycles are great cycles: applications, opportunities, and challenges of synthetic macrocycles in drug discovery. *J. Med. Chem.* **2011**, *54*, 1961–2004.

54 Giordanetto, F.; Kihlberg, J. Macrocyclic drugs and clinical candidates: what can medicinal chemists learn from their properties? *J. Med. Chem.* **2014**, *57*, 278–295.

55 Mallinson, J.; Collins, I. Macrocycles in new drug discovery. *Future Med. Chem.* **2012**, *4*, 1409–1438.

56 You, L.; An, R.; Liang, K.; Cui, B.; Wang, X. Macrocyclic compounds: emerging opportunities for current drug discovery. *Curr. Pharm. Des.* **2016**, *22*, 4086–4093.

20

Solithromycin: Fourth-Generation Macrolide Antibiotic

David Pereira, Sara Wu, Shingai Majuru, Stephen E. Schneider and Lovy Pradeep

Cempra, Inc., Chapel Hill, NC, USA

20.1   Introduction

In the United States, 5–10 million cases of community-acquired bacterial pneumonia (CABP) are reported yearly, and CABP is a leading cause of death from infections [1–4]. The current treatment options are limited to either a cephalosporin (e.g., ceftriaxone) plus a macrolide (e.g., azithromycin) or a fluoroquinolone (e.g., levofloxacin or moxifloxacin) [5]. Both of these options have drawbacks. Third-generation cephalosporins are only delivered intravenously, and, thus, an oral step-down is unavailable. Fluoroquinolones can lead to tendon rupture, increased frequency of *Clostridium difficile* colitis, and peripheral neuritis and, additionally, have not been approved for pediatric populations [6, 7].

The widespread use of these and other antibiotics has led to increased risk from antibiotic-resistant bacteria [8–10]. This growing public health concern led the US Congress to pass the Generating Antibiotic Incentives Now (GAIN) Act to spur the development of new antibiotics. President Obama signed the bill into law on July 9, 2012 [11].

Cempra, Inc. was founded in 2006 to develop novel antibiotics to address the need for new and safe pharmaceuticals effective against resistant bacteria. Macrolides, such as erythromycin, clarithromycin, and azithromycin, have been considered safe and effective antibiotics for all age groups. Thus, Cempra licensed a library of over 500 macrolides from Optimer Pharmaceuticals (now part of Cubist/Merck) for further investigation and development. The currently approved antibiotic macrolides share three key structural features (Figure 20.1): the macrolide ring (circle A), the desosamine sugar (circle B), and the cladinose sugar (circle C) as depicted on the erythromycin structure. The ketolide subclass of macrolides, such as telithromycin, consists of the macrolide ring and the desosamine sugar of the earlier generation of macrolides, with the cladinose sugar replaced by a keto group at position C3 (hence, the ketolide moniker) and the C11,12-carbamate substituted with an aryl–alkyl side chain.

20.2   Structure–Activity Relationship (SAR) of Ketolides and Selection of Solithromycin

20.2.1   MIC Testing of Triazole Analogues

Many of the macrolides in the original Optimer library incorporated the chemically robust, substituted [1,2,3]-triazole group as a key structural component of the aryl–alkyl side chain [12]. The minimum inhibitory concentration (MIC) against a number of test bacterial strains for selected compounds in this series is presented in Table 20.1. Although analogues **1–4** had good activity against erythromycin-susceptible strains, they exhibited poor activity against resistant strains. Hence, further investigation of the SAR in the series was undertaken in order to identify analogues with broader antibiotic profile.

20.2.2   Importance of 2-Fluorine for Activity

Telithromycin, the first approved member of the ketolide subclass of macrolides, is effective against penicillin and erythromycin-resistant *Streptococcus pneumoniae* and, further, is a non-inducer of macrolide–lincosamide–streptogramin B (MLSB) resistance [13]. To probe the optimum length of the chain required for maximum activity, a series of compounds with three to four carbon side chains were synthesized. The data indicated that a chain of four carbons provided the greatest activity as indicated by MIC in Table 20.2.

The 2-position of the macrolactone is amenable for electrophilic substitution. However, groups larger than
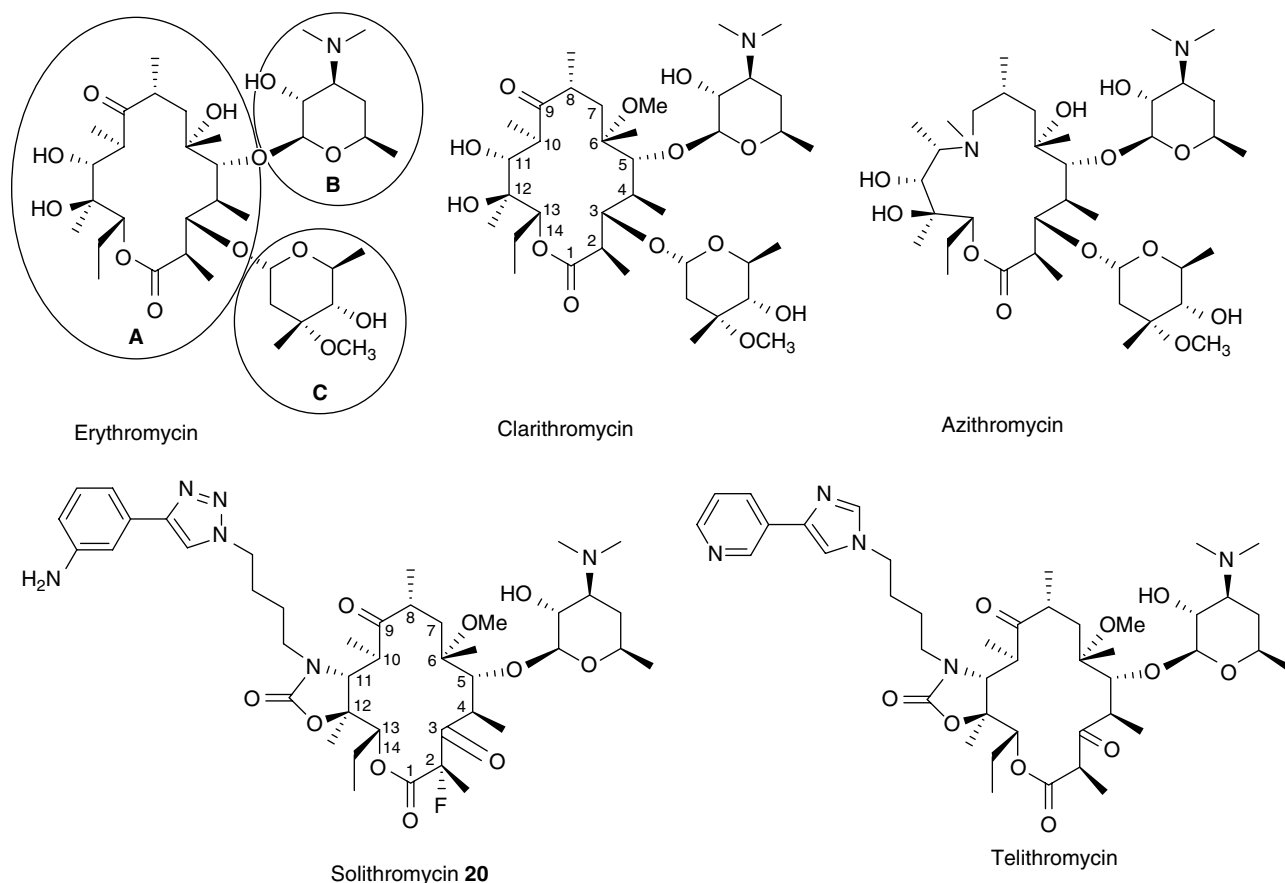
Figure 20.1 Structures of macrolides and ketolides.
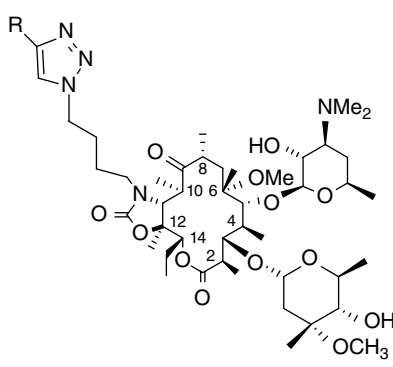
a fluorine led to a loss of activity [14]. A number of C2-fluoroketolide analogues were part of the licensed macrolide library and were tested against the bacterial test panel. These compounds had enhanced activity over the corresponding des-fluoro analogues as shown in Table 20.3. Importantly, it was also noted that the C2-fluoroketolides retained high activity against organisms possessing resistance-imparting genes *ermA*, *ermB*, and *mefA*, including the highly resistant *ermB*/*mefA* strains.
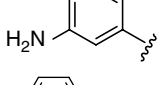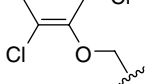
Thus, the key structural features necessary for enhanced antibacterial activity are (i) lack of C3-*O*-cladinose, (ii) presence of C3-keto group, (iii) a C2-fluorine atom, and (iv) presence of an optimal 4-carbon length side chain containing an aromatic functionality to interact with domain II of the bacterial ribosome. Compound **20** incorporated all of these features and demonstrated superior antibacterial property among all the compounds tested in the macrolide library. Therefore, **20** was selected for preclinical development as CEM-101 and was later named solithromycin, which has subsequently been approved as the unique nonproprietary name by the USAN Council.

20.2.3 *In Vitro* Genotoxicity Studies on Solithromycin

The side chain of solithromycin (**20**) possesses several structural features uncommon in drug candidates. The first is the 1,4-substituted 1,2,3-triazole. Stereochemical control of the substitution pattern was not possible until the advent of copper-catalyzed azide–alkyne cycloaddition (CuAAC); therefore, this heterocycle was not previously employed in drug discovery [15, 16]. The aromatic amine found in solithromycin is the second structural component that is typically not utilized in pharmaceutical discovery due to the potential toxicity of anilines [17]. Gratifyingly, for **20**, no toxicity was observed despite the presence of the aromatic amine.

Compound **20** was tested in a number of *in vitro* and *in vivo* assays to determine its potential mutagenic toxicity. It was found to be negative in the *Salmonella–Escherichia coli* (Ames test)/mammalian microsome reverse mutation assay [18]. The latter assay was conducted in the presence and absence of an exogenous metabolic activation system (S9). Additionally, **20** was evaluated in a

Table 20.1 MIC data of clarithromycin analogues.

Entry	R	Minimum inhibitory concentration (µg/ml)[a]					
		Staphylococcus aureus		Streptococcus pneumoniae			Haemophilus influenzae
		25923		49619	163	303	49247
		Ery-S	RN220[b]	Ery-S	Ery-R (MefA)[b]	Ery-R (ermB)[b]	Ery-S
Telithromycin	N/A	≤0.25	2	≤0.125	≤0.125	≤0.125	4
1		0.25	8	≤0.0625	0.125	2	Not tested
2		0.25	8	≤0.0625	≤0.06	1	Not tested
3		1	8	≤0.0625	0.5	2	Not tested
4		≤0.25	8	≤0.0625	0.5	2	Not tested

[a] MIC determined per Clinical and Laboratory Standards Institute (CLSI) guidelines.
[b] Strains carrying resistant genes.

third assay to determine potential mutagenic toxicity, chromosomal aberrations in cultured human peripheral blood lymphocytes, with and without an exogenous metabolic activation system [19]. Compound **20** was negative in this assay as well. The rat bone marrow micronucleus assay is used to determine *in vivo* clastogenic activity and/or disruption of the mitotic apparatus of a test article by detecting micronuclei in polychromatic erythrocytes (PCE) in CD°(SD)IGS BR rat bone marrow [20]. Due to its superior antibacterial property and because it was negative in all mutagenicity/toxicity
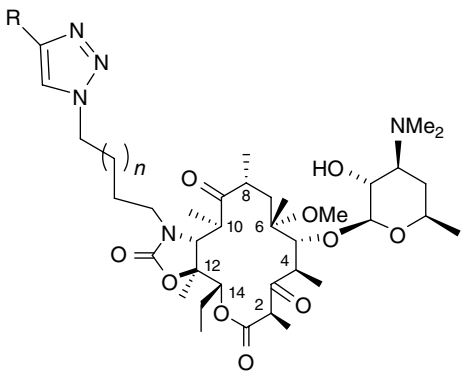
assays, **20** was advanced for further nonclinical development, followed by clinical development.
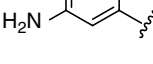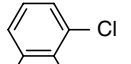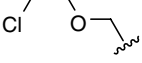
20.2.4 Mouse PK and Protection Studies

The oral bioavailability of **20** was evaluated in mice. At doses of 2.5 and 10 mg/kg, **20** had promising oral pharmacokinetic (PK) properties with an extended plasma half-life (Table 20.4) [21].

Since **20** was orally bioavailable, the *in vivo* antibacterial activity of **20** was studied in a number of different

Table 20.2 MIC data of ketolides.

			Minimum inhibitory concentration (μg/ml)[a]					
			Staphylococcus aureus		*Streptococcus pneumoniae*			*Haemophilus influenzae*
			29213	96:11480	49619	163	303	49247
Entry	n	R	Ery-S	Ery-R (*MLSb*)[b]	Ery-S	Ery-R (*MefA*)[b]	Ery-R (*ermB*)[b]	Ery-S
Azithromycin	—	N/A	≤0.125	>64	≤0.125	>64	>64	2
Telithromycin	—	N/A	≤0.125	≤0.125	≤0.125	≤0.125	≤0.125	4
5	3		1	1	≤0.125	≤0.125	>64	64
6	4		≤0.125	0.25	≤0.125	≤0.125	2	8
7	5		≤0.125	≤0.125	≤0.125	≤0.125	0.25	16
8	3		2	2	≤0.125	1	>64	>64
9	4		≤0.125	4	≤0.125	2	64	64
10	5		≤0.125	0.25	≤0.125	0.25	4	16
11	3		0.5	Not tested	≤0.125	≤0.125	>64	16
12	4		≤0.125	≤0.125	≤0.125	≤0.125	≤0.125	2
13	5		≤0.125	≤0.125	≤0.125	≤0.125	0.25	8
14	3		1	1	≤0.125	≤0.125	>64	>64
15	4		≤0.125	≤0.125	≤0.125	≤0.125	1	16
16	5		0.25	0.5	≤0.125	≤0.125	2	32
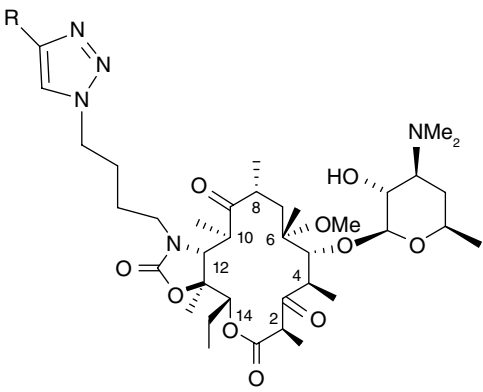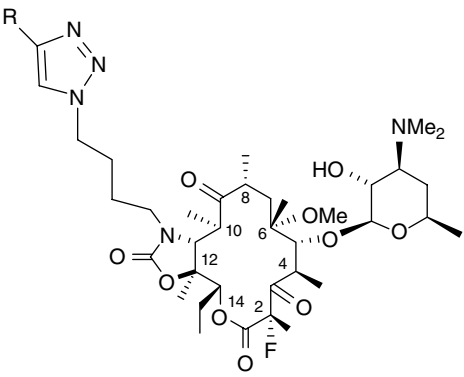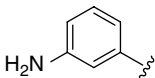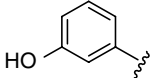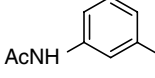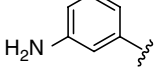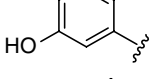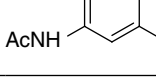
[a] MIC determined per Clinical and Laboratory Standards Institute (CLSI) guidelines.
[b] Strains carrying resistant genes.

mice infection models. To test the efficacy of **20** against *in vivo* infections, a murine systemic infection model was tested using both susceptible and macrolide-resistant bacterial strains including the resistant isolates MRSA, MRSA 300, *mef* R *S. pneumoniae*, *Streptococcus pyogenes*, and a serotype 19A *S. pneumoniae* isolate. Compound **20** had either equivalent or greater activity in this infection model when compared to telithromycin or clarithromycin [21].

Further *in vivo* antimicrobial evaluations of **20** were conducted in mouse subcutaneous abscess, lung infection, and neutropenic thigh infection (*S. pneumoniae* 1629) models to measure the microbial load reductions in these infections. In mouse subcutaneous abscess model, a 10 mg/kg QD dose of **20** led to a 4.2 $\log_{10}$ reduction in microbial load, while clarithromycin only achieved a 1.5 $\log_{10}$ reduction compared to the control group [21]. Compound **20** exhibited bactericidal activity

Table 20.3 Comparison of MIC data of ketolides and fluoroketolides.

17–19

20–22

		Minimum inhibitory concentration (µg/ml)[a]						
		Streptococcus pneumoniae		*Staphylococcus aureus*		*Streptococcus pyogenes*		
Entry	R	ATCC 49619	120-1037B *ermB/mefA*[b]	024-11A WT	BAA-977 *ermA*[b]	ATCC 19615	129-7129A *ermA*[b]	089-14217A *ermB*[b]
Clarithromycin		≤0.06	>64	0.25	>64	≤0.06	>64	>64
Azithromycin		≤0.06	>64	0.5	>64	≤0.06	>64	>64
17	H₂N–(3-aminophenyl)	≤0.015	0.5	0.12	0.12	≤0.015	≤0.015	0.12
18	HO–(3-hydroxyphenyl)	≤0.015	8	0.12	0.25	≤0.015	≤0.015	16
19	AcNH–(3-acetamidophenyl)	≤0.015	16	0.06	0.06	≤0.015	≤0.015	16
20	H₂N–(3-aminophenyl)	≤0.015	0.12	≤0.06	≤0.06	≤0.015	≤0.015	0.25
21	HO–(3-hydroxyphenyl)	≤0.015	1	0.06	0.06	≤0.015	≤0.015	2
22	AcNH–(3-acetamidophenyl)	≤0.015	16	0.06	0.06	≤0.015	≤0.015	16

[a] MIC determined per Clinical and Laboratory Standards Institute (CLSI) guidelines.
[b] Strains carrying resistant genes.

Table 20.4 Mouse pharmacokinetics of compound **20**.

Dose (mg/kg)	Route	T_{max} (h)	C_{max} (ng/ml)	AUC_{0-24} (ng·h/ml)	Half-life (h)
2.5	PO	1	359.15	1172.63	2.85
10.0	PO	0.5	1436.60	4757.93	2.85

in the lung infection study 48-h posttreatment, whereas clarithromycin was bacteriostatic. In the neutropenic thigh infection model, 8.0 mg/kg of **20** achieved a 3 $\log_{10}$ bacterial load reduction compared with untreated mice. In contrast, to reach the same bacterial load reduction, telithromycin and clarithromycin required 15.5 and 13.5 mg/kg of dosing, respectively [21].

The favorable PK results and *in vivo* antimicrobial activity supported the further drug development of **20** as the first member of the fluoroketolide class.

20.3 Mechanism of Action

20.3.1 Ribosome Binding of Antibiotics

The bacterial 70S ribosome, which constitutes the protein synthesis machinery, has two rRNA subunits: the 30S and 50S subunits (Figure 20.2) [22]. Protein synthesis is accomplished in three phases: initiation, elongation, and termination–release. During the initiation phase, the 30S and 50S subunits, mRNA, formyl-methioninyl tRNA (the initiator tRNA), and initiation factors assemble to form the ribosome complex. The elongation phase occurs at three specific regions of the ribosome: the A-site (aminoacyl site), P-site (peptidyl site), and E-site (exit site). The A-site is the acceptor of the amino acid brought in by the tRNA based on the mRNA triplet sequence (codon). The P-site is occupied by the peptidyl–tRNA, which carries on it the growing polypeptide chain. The E-site harbors the deacylated tRNA in transit as it exits the ribosome. Protein elongation continues as dictated by the mRNA sequence and,

upon termination, exits via the nascent peptide exit tunnel (NPET) with the simultaneous dissociation of the ribosome complex [22–24].

Classes of antibiotics that inhibit protein synthesis exert their inhibition by interacting with one of the major ribosome subunits in a 1 : 1 molar ratio [25]. Since different antibiotics bind to different sites, protein synthesis disruption can occur by interfering with any of the three phases of protein synthesis (Figure 20.2). Aminoglycoside antibiotics, such as neomycin B, gentamicin, paromomycin, kanamycin, and tetracyclines, bind to the 30S subunit and interfere with the translation of the mRNA [26–28]. A diverse group of antibiotics bind to the 50S subunit at the peptide exit tunnel or at the peptidyl transferase center. The MLSB group, chloramphenicol, puromycins, pleuromutilins (tiamulin), oxazolidinones (linezolid), and sparsomycin inhibit peptide chain elongation [23, 25, 29]. The erythromycin macrolide class of antibiotics (erythromycin, clarithromycin, and azithromycin) are known to interfere with protein synthesis by binding to the bacterial ribosome in the peptide exit tunnel, but without inhibiting peptidyltransferase activity, thereby arresting the complete translation of the polypeptide chain [27, 30–32]. The macrocyclic ring of these antibiotics forms hydrophobic interactions with the floor of the peptide tunnel. The cladinose sugar aligns within the peptide tunnel and points toward the peptidyltransferase tunnel [32]. Additionally, the 2′-OH group of the desosamine sugar appears to form hydrogen bonds with N1 of A2041 (A2058 Ec numbering), N6 of A2040 (A2057 Ec). The dimethylamino group of the desosamine sugar interacts with G2484 (G2505 Ec) through either ionic or hydrogen bonding interactions
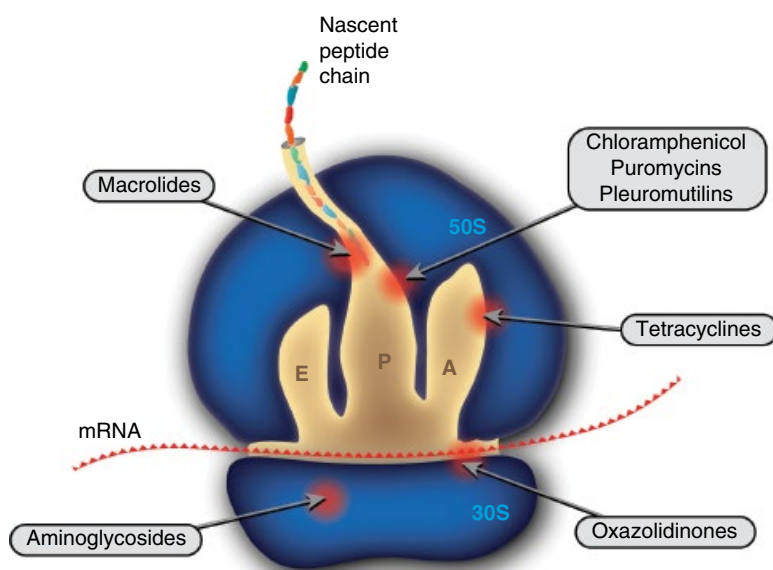
Figure 20.2 Schematic representation of bacterial ribosome and antibiotic sites of interaction. (*See insert for color representation of the figure.*)
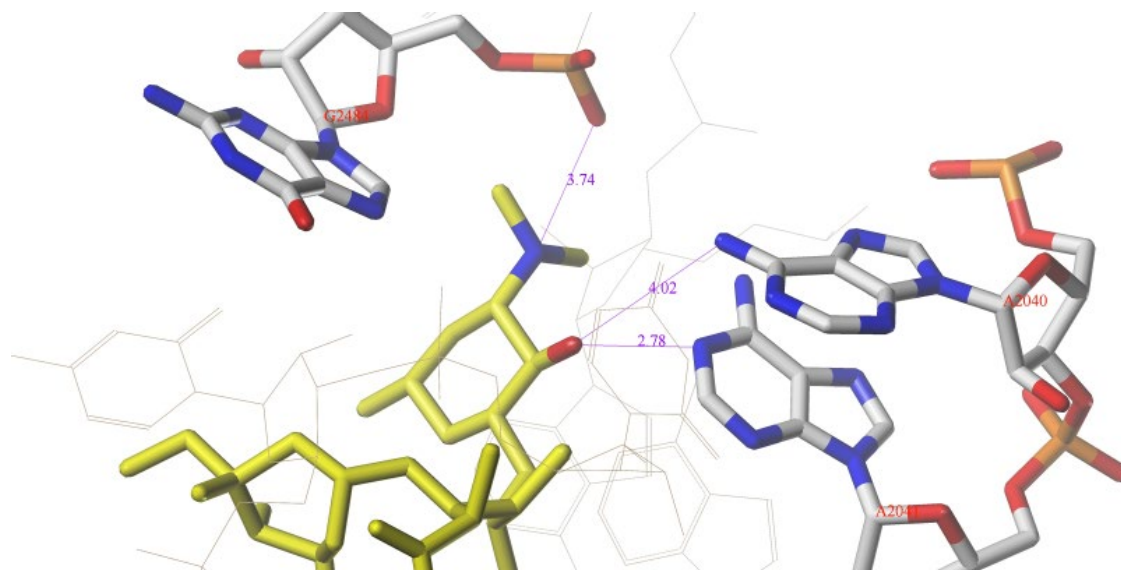
Figure 20.3 Crystallographic structure of clarithromycin bound to the *Deinococcus radiodurans* ribosome from PDB code 1J5A. The purple-colored lines and numbers are the interaction distances (values are in angstroms) between clarithromycin (yellow) and ribosome in the active site. The interacting residues and clarithromycin are presented in capped sticks with their atom types. Remaining residues are presented as stick model in beige color. All residues are labeled with their residue names in red color. Hydrogen atoms are omitted. (*See insert for color representation of the figure.*)

(Figure 20.3). These hydrogen bonds anchor the macrolide to the ribosome and are required for activity [27, 30, 32–34].

A common mechanism that leads to macrolide resistance involves *erm*-mediated methylation of the bacterial ribosomal nucleotide (N^6 of A2058), leading to interference with the binding of the desosamine sugar of the macrolide, thereby reducing the binding affinity of the macrolide to the bacterial ribosome [35, 36]. This loss of binding affinity leads to a decrease in antibacterial activity. However, solithromycin has excellent activity against bacteria carrying the *erm* gene as described in the SAR data and has been shown to be so in additional studies [12]. This activity against resistant bacteria can be explained by its mode of binding to the bacterial ribosome.

20.3.2 Ribosome Binding of Solithromycin

Insights into the binding of macrolides to ribosomes were first gained through crystallographic studies of macrolides bound to bacterial (*Deinococcus radiodurans*) or archaeal (*Haloarcula marismortui*) ribosomes [37]. Differences were noted in the binding orientation of the side chain of telithromycin between the two ribosomes, raising doubts as to the true binding mode of ketolides to pathogenic bacterial ribosomes [37, 38]. In the crystal structure of telithromycin bound to the *E. coli* ribosome, the aryl–alkyl side chain of telithromycin was observed to interact with the ribosome A752-

U2609 base pair. This base pair is found in many pathogenic bacterial ribosomes but is absent in the usually studied *D. radiodurans* and *H. marismortui* ribosomes; therefore, the macrolide-pathogenic bacterial ribosome interactions are impossible in these ribosomes. Macrolide–*E. coli* ribosome complexes are, therefore, thought to be better models to study interactions between macrolides and pathogenic bacterial ribosomes in order to more fully understand the antibacterial activity of new analogues such as solithromycin [37].

A high resolution crystal structure of the solithromycin bound to the *E. coli* ribosome complex was obtained as shown in Figure 20.4a [37, 39]. The macrolactone ring of solithromycin binds to Domain V of the 23S rRNA by hydrophobic interactions in the same manner as telithromycin [38, 40]. As noted previously, the desosamine sugar plays a key role in the binding of macrolides to bacterial ribosomes; these interactions were also observed with solithromycin wherein the *N,N*-dimethylamine group of the desosamine sugar of solithromycin likely forms ionic association with the rRNA residue G2505 (Figure 20.4b) and the desosamine hydroxyl group forms hydrogen bonds with residues A2058 and A2059 of the ribosomal rRNA.

Unlike erythromycin, clarithromycin, and azithromycin, solithromycin has a C11,12 side chain capped with a 3-aminophenyl-1,2,3-triazole moiety, which interacts with Domain II of the 23S rRNA (Figure 20.4c). Specifically, this moiety forms a stacking interaction with the A752-U2609 base pair of the bacterial ribosome.
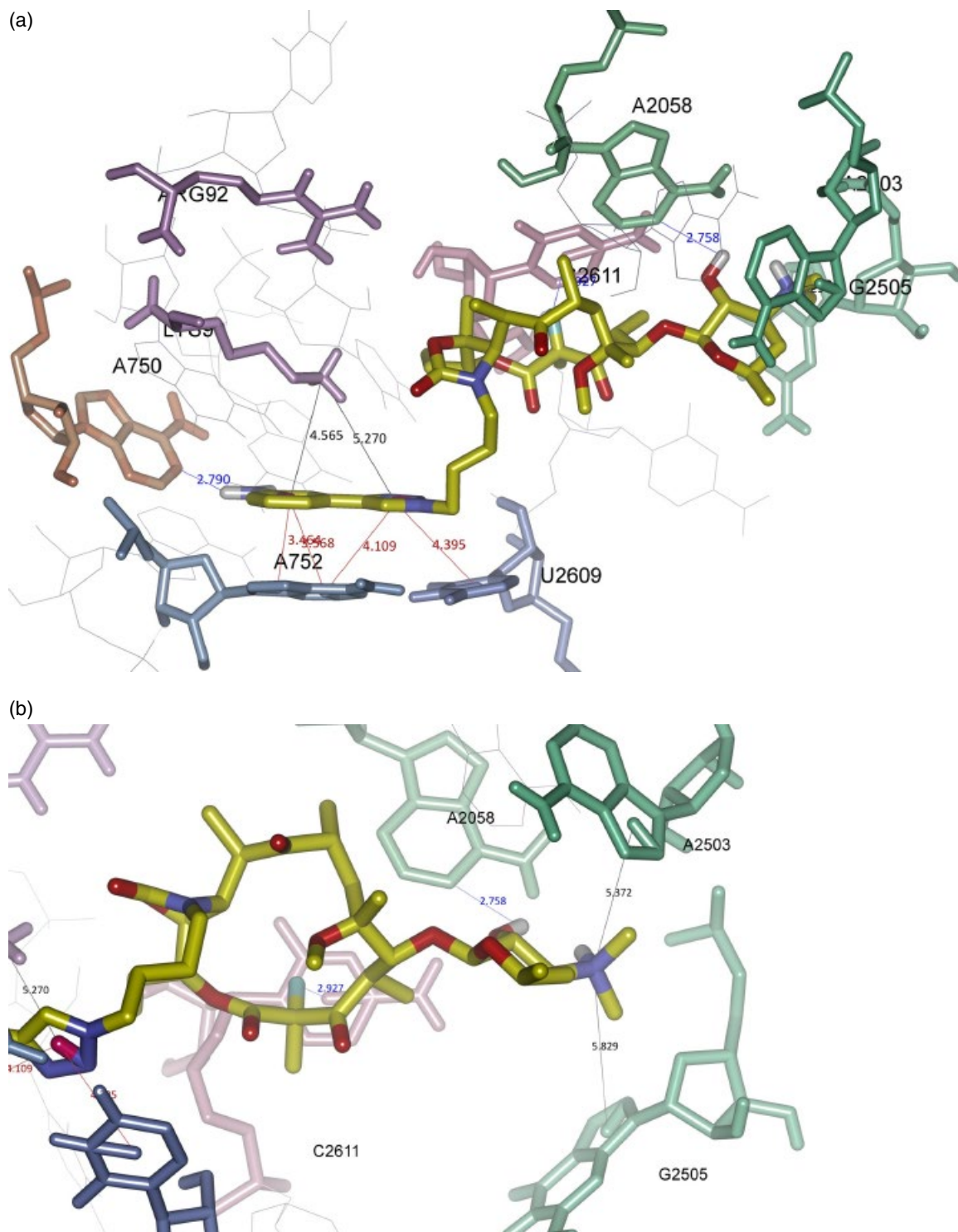
(a)

(b)

Figure 20.4 Crystallographic structure of solithromycin bound to the *Escherichia coli* ribosome from PDB code 4WWW. (a) Position of solithromycin (yellow) within the ribosomal binding site. The neighboring 23S rRNA residues and amino acid residues of protein L22 are labeled. Only polar hydrogens are shown. Interacting residues and solithromycin are shown in capped sticks. (b) Interactions involving the triazolyl-aminophenyl side chain of solithromycin. (c) Interactions of 2-fluorine of solithromycin and desosamine to 23S rRNA in the drug binding site. (*See insert for color representation of the figure.*)

(c)
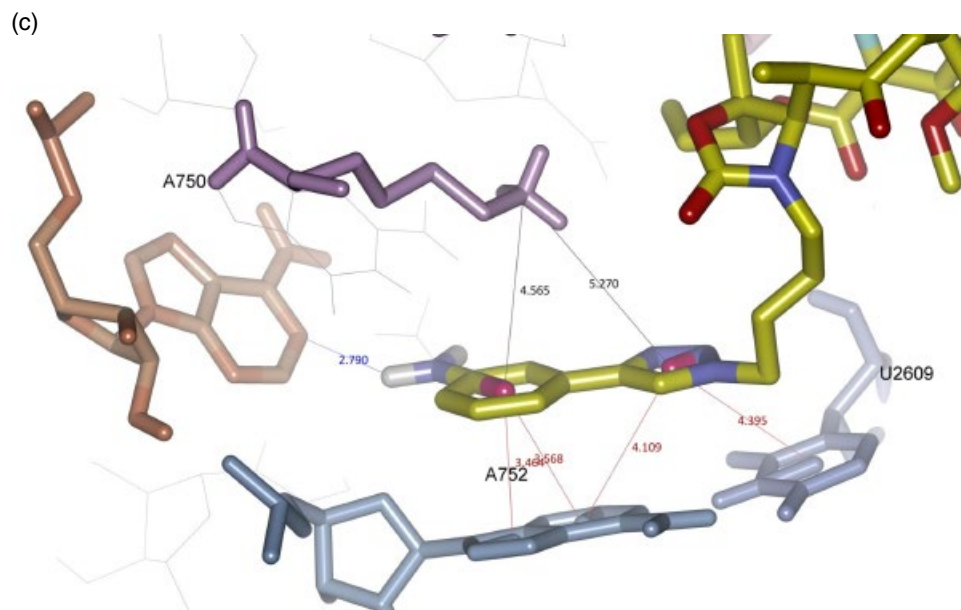
Figure 20.4 (Continued)

The amine of the aminophenyl group likely acts as a hydrogen donor to O-4 of A752 and O-6 of G748 and a hydrogen acceptor from N-1 of G748 [37]. These additional interactions with the ribosome result in better anchoring of the solithromycin side chain than is observed with telithromycin, which lacks a group to participate in such hydrogen bond formation [37]. The ε-amino group of Lys[90] of protein L22 (a ribosomal protein) is >4 Å away from the aminophenyl group. This distance is probably too large for direct interaction between these groups and, therefore, does not significantly contribute to solithromycin binding to the ribosome.

Solithromycin is active against bacteria carrying the *erm* resistance gene, perhaps due to the lack of the cladinose sugar, thereby providing additional room for solithromycin to bind to the methylated ribosome by forming a hydrogen bond between the desosamine hydroxyl group and the N-1 atom of residue A2058 in the presence of the methylated N-6 group of A2058. Solithromycin has yet another unique feature, a fluorine atom at position C-2, seen in close proximity to N-1 of C2611 of the 23S rRNA (Figure 20.4c) and may therefore contribute to ribosome binding [39]. Solithromycin's C-2 fluorine atom generally confers greater activity against organisms carrying the *erm* resistance gene (Table 20.3) as shown from the SAR experiments using ketolide analogues containing a C-2 fluoro substitution and shows higher activity than telithromycin's activity against telithromycin-resistant organisms [37, 41].

20.3.3 Solithromycin Protein Inhibition

Macrolides exert their bacteriostatic properties by inhibition of protein synthesis. It was long thought that macrolides, by blocking the NPET, prevented the synthesis of all nascent peptides [42]. Besides providing a route for the synthesized peptide for exiting the ribosome, the NPET also has a functional role in the regulation of protein synthesis. The regulation of protein synthesis occurs via interaction of certain nascent peptide chains with the NPET, while the peptide is being synthesized. This interaction can result in peptide stalling or in the arrest of peptide synthesis. Only short conserved portions of the N-terminus of nascent peptides, named ribosome arrest peptides (RAPs), with specific residues can cause peptide arrest. RAPs, by stalling protein synthesis, regulate gene expression in organisms due to changes in the amount of protein translocation factors or in the concentration of small-molecule metabolites [43–46].

It has been shown, however, that macrolides do not stop all bacterial protein synthesis but only inhibit the synthesis of certain proteins [47]. Analysis of macrolide–ribosome complexes reveals that macrolides do not completely block the NPET, which could allow for some translation of polypeptides in the macrolide–ribosome complexes. Slight movement of the highly flexible rRNA residue A2062 at the constriction point of the NPET in the area of the macrolide binding site would result in sufficient room for the nascent peptide to bypass the bound macrolide. The ability to shift the position of A2062 by certain nascent peptides is directly related to the amino

acid sequence of the N-terminus of the nascent peptide. Peptide sequences having this bypass N-terminus sequence can move past the macrolide-blocked NPET, allowing the synthesis of long peptide chains. The bypass sequence can be as short as 12 amino acids in length [47]. It was also observed that synthesis of some polypeptides is not arrested in the early phase of translation but rather in the elongation phase of translation by the macrolide–ribosome complex. As with the specific N-terminus bypass peptide sequence, the elongation–stalling of peptide synthesis is dependent upon the sequence of the polypeptide chain. Thus, macrolides bound to a ribosome can cause both early phase and late phase translation arrest of the polypeptide chain [47].

Interestingly, although more potent than the earlier generation macrolides (erythromycin, clarithromycin, and azithromycin), solithromycin (and telithromycin) inhibited overall protein synthesis to a lesser extent [41, 47]. The lack of the cladinose in the ketolide class may allow for more space or more flexibility at the constriction point of the NPET, allowing for a greater number of nascent peptides to slip around the macrolide blockade. A greater flexibility at the constriction point of the NPET allows for a partial translation of the bacterial proteome, as is seen with solithromycin, and this actually may be more lethal to the cell than a complete arrest of protein synthesis. An incomplete proteome will result in the disruption of biochemical pathways, leading to either the accumulation of toxic metabolic intermediates or depletion of cofactors [42, 47].

20.4 Overcoming the Ketek Effect

The approved ketolide telithromycin (Ketek®) was found to be associated with several adverse events [48, 49]. These adverse events, collectively referred to as "Ketek effects," include exacerbation of myasthenia gravis symptoms, visual disturbance or blurred vision, and liver failure [49]. Research to understand the side effects caused by telithromycin implicates a preferential inhibition of the nicotinic acetylcholine receptors (nAChRs) by telithromycin and its metabolites and is specifically attributable to the pyridine moiety in its side chain. A comparison of the structures of telithromycin and solithromycin shows the absence of the pyridine moiety in the aromatic side chain of the latter (Figure 20.1).

Macrolides, in general, inhibit the nAChRs, and the extent of their inhibition is investigated via *in vitro* experiments using electrophysiology techniques. In cells overexpressing a given nAChR subtype currents evoked by acetylcholine (due to the opening of the nAChR channels) are recorded in the presence and absence of different macrolides in a dose-dependent manner. In all

experiments, a clinically relevant concentration of $2\,\mu M$ for all macrolides was used to understand their interaction with the nAChR subtypes evaluated [50, 51].

At $2\,\mu M$ concentration, human $\alpha_3\beta_4$ subtype nAChRs (in the ciliary ganglion of the eye) were inhibited by clarithromycin, azithromycin, and solithromycin to the extents of $38\pm5\%$, $56\pm7\%$, and $61\pm4\%$, respectively, whereas telithromycin showed a $90\pm1\%$ inhibition of these receptors [50, 51]. Likewise, when the α_7 subtype of the nAChRs (present in the ciliary ganglion and in the vagus nerve innervating the liver) was investigated, telithromycin showed $88\pm2\%$ inhibition as opposed to $49\pm3\%$, $51\pm12\%$, and $<6\pm3\%$ inhibition by clarithromycin, azithromycin, and solithromycin, respectively, at $2\,\mu M$ concentrations [50, 51]. From the dose–response curves for the $\alpha_3\beta_4$ and the α_7 nAChRs, it is evident that telithromycin inhibition is achieved at lower concentration compared to the other macrolides, and this effect can be deemed as the possible reason for the greater frequency and severity of liver damage (hepatotoxicity) that it causes.

However, when telithromycin was tested against the $\alpha_4\beta_2$ nAChR subtype (present in the brain) and the $\alpha_1\beta_1\delta\varepsilon$ nAChR subtype (at neuromuscular junctions), the extent of inhibition was similar to the other macrolides at $2\,\mu M$ concentrations [50]. Hence, this inhibitory effect alone was not sufficient to explain the curare-like effect of telithromycin at the neuromuscular junctions of myasthenia gravis patients. Further investigation revealed that the metabolites of telithromycin, namely, telithromycin *N*-oxide, pyridine/imidazole, and pyridine-*N*-oxide–imidazole markedly inhibit the $\alpha_1\beta_1\delta\varepsilon$ nAChR subtype (at neuromuscular junctions) to extents of $21\pm18\%$, $51\pm5\%$, and $56\pm11\%$, respectively; pyridine-*N*-oxide-imidazole additionally inhibits the $\alpha_3\beta_2$ nAChRs subtype (at presynaptic endings of neuromuscular junctions) by 25% [50, 51]. These findings led to the conclusion that dual collective inhibitory action of telithromycin and its metabolites together exacerbate myasthenia gravis symptoms in these patients.

Likewise, telithromycin's metabolites exhibit inhibition of the α_7 nAChRs by large extents of up to $72\pm5\%$. The severe hepatotoxicity seen in telithromycin-treated patients, therefore, may be caused via the combined inhibitory effects of telithromycin and its metabolites on the α_7 nAChRs [50, 51].

Compounds that contain pyridine and pyrimidine moieties, in general, are known to interact with nAChRs causing inhibition [52, 53]. Telithromycin and its metabolites contain the pyridine moiety that is lacking in the other macrolides, and its pronounced inhibitory effect due to the pyridine moiety can be further substantiated by another experiment conducted using the antifungal compounds voriconazole and fluconazole. Voriconazole contains the pyrimidine moiety and inhibits the ganglionic

$\alpha_3\beta_4$ nAChRs, whereas fluconazole lacks the pyrimidine moiety and does not inhibit the ganglionic receptors. Voriconazole-treated patients do show adverse events of visual disturbances, while fluconazole-treated patients do not, thus endorsing the inhibitory effects of pyridine and pyrimidine-containing compounds on nAChRs [54].

In conclusion, the profound inhibitory effect of telithromycin on the various subtypes of nAChRs is attributable to the pyridine moiety in its aromatic side chain, and the inhibition appears to be further compounded by its pyridine moiety-containing metabolites. Solithromycin, on the other hand, lacks a pyridine moiety in its aromatic side chain. Due to this key structural difference, the extent of inhibition of the nAChRs by solithromycin is much lower than those of telithromycin [50].

20.5 Manufacture of Solithromycin

Clarithromycin is a convenient and readily available starting material for the synthesis of next-generation macrolides and was chosen as the starting point for the synthesis of solithromycin. As shown in Figure 20.5, solithromycin is prepared in nine steps from clarithromycin [55]. The current batch size of these stages ranges from 250 to 400 kg depending on the particular step. As with many macrolide syntheses, the cladinose and desosamine sugar hydroxyls are first selectively protected. Though the acetate group is often used, benzoyl protection with benzoic anhydride in the presence of triethylamine and DMAP was selected for solithromycin since the UV absorption of the aromatic rings simplified analytical method development [56, 57]. Selective activation of the C12 hydroxyl with concomitant elimination of the C11 hydroxyl is achieved by treating the resulting 2′,4″-di-*O*-benzoyl-6-*O*-methyl-erythromycin A (**23**) with 1,8 diazabicyclo[5.4.0] undec-7-ene (DBU), followed by 1,1-carbonyldiimidazole (CDI) to yield 10,11-anhydro-2′,4″-di-*O*-benzoyl-12-*O*-imidazolylcarbonyl-6-*O*-methylerythromycin A (**24**) [58].

The first half of solithromycin's side chain is then introduced by treatment of **24** with 4-azidobutylamine and DBU to form 2′,4″-di-*O*-benzoyl-11-*N*-(4-azidobutyl)-6-*O*-methylerythromycin A 11,12-cyclic carbamate (**25**) [59]. The more labile cladinose sugar is then cleaved from azide **25** by hydrolysis with 1 N HCl to provide 11-*N*-(4-azidobutyl)-5-(2′-benzoyldesosaminyl)-3-hydroxy-6-*O*-methylerythronolide A 11,12-cyclic carbamate (**26**) [55, 58]. Alcohol **26** is then efficiently oxidized to 1-*N*-(4-azidobutyl)-5-(2′-benzoyldesosaminyl)-3-oxo-6-*O*-methylerythronolide A 11,12-cyclic carbamate (**27**) with Dess–Martin periodinane (DMP), eliminating the need

for cryogenic conditions and the malodorous sulfide byproducts of the more common Swern oxidation [58].

In the step that makes solithromycin first in class, fluorination of ketolide **27** is accomplished with *N*-fluorobenzenesulfonimide (NFSI) under basic conditions to afford fluoroketolide **28**, exclusively in the (*S*)-configuration, as confirmed by single crystal X-ray structure analysis (data not shown). The triazole intermediate (**29**) is prepared by copper-catalyzed azide–alkyne cycloaddition reaction between **28** and 3-ethynylaniline (see also Chapter 11). The benzoyl protecting group is then cleaved from triazole intermediate (**29**) by refluxing in methanol to yield crude solithromycin, which is converted to the desired polymorph by crystallization in the final step [59].

20.6 Polymorphism

Four unique crystalline solithromycin patterns have been identified by XRPD, termed Forms I to IV. Form I is an anhydrous, slightly hygroscopic crystal, while Form II is an anhydrous, nonhygroscopic crystal. Form III is an unstable intermediate solvated crystal that was isolated under a variety of conditions. Form III converts to Form II on heating. Form IV is a metastable methanol solvate that also readily converts to Form II. Five additional crystalline XRPD patterns were observed via automated polymorph screening, but could not be reproduced for characterization, indicating that they are also metastable (Figure 20.6).

Form II is typically isolated from organic solvents and retains residual solvent levels above ICH Q3C residual solvent limits [60]. In contrast, Form I can be isolated from a purely aqueous process. Form I is a monoclinic crystal system with a P21 space group and a crystallite size of 50–80 nm. Of the two stable polymorphs, Form I was selected for clinical and subsequent commercial development since it was demonstrated to be stable during manufacturing and during long-term storage, did not retain residual solvents, and demonstrated good bioavailability. Form I active pharmaceutical ingredient (API) in the solid oral dosage form has not been observed to convert to Form II under accelerated or long-term stability conditions.

20.7 Pharmaceutical Development

The oral route of drug administration is generally the most preferred route comprising tablets and capsules for adults and solutions or suspensions for the pediatric population [61]. For extremely ill patients, however, an intravenous (IV) formulation may be required.
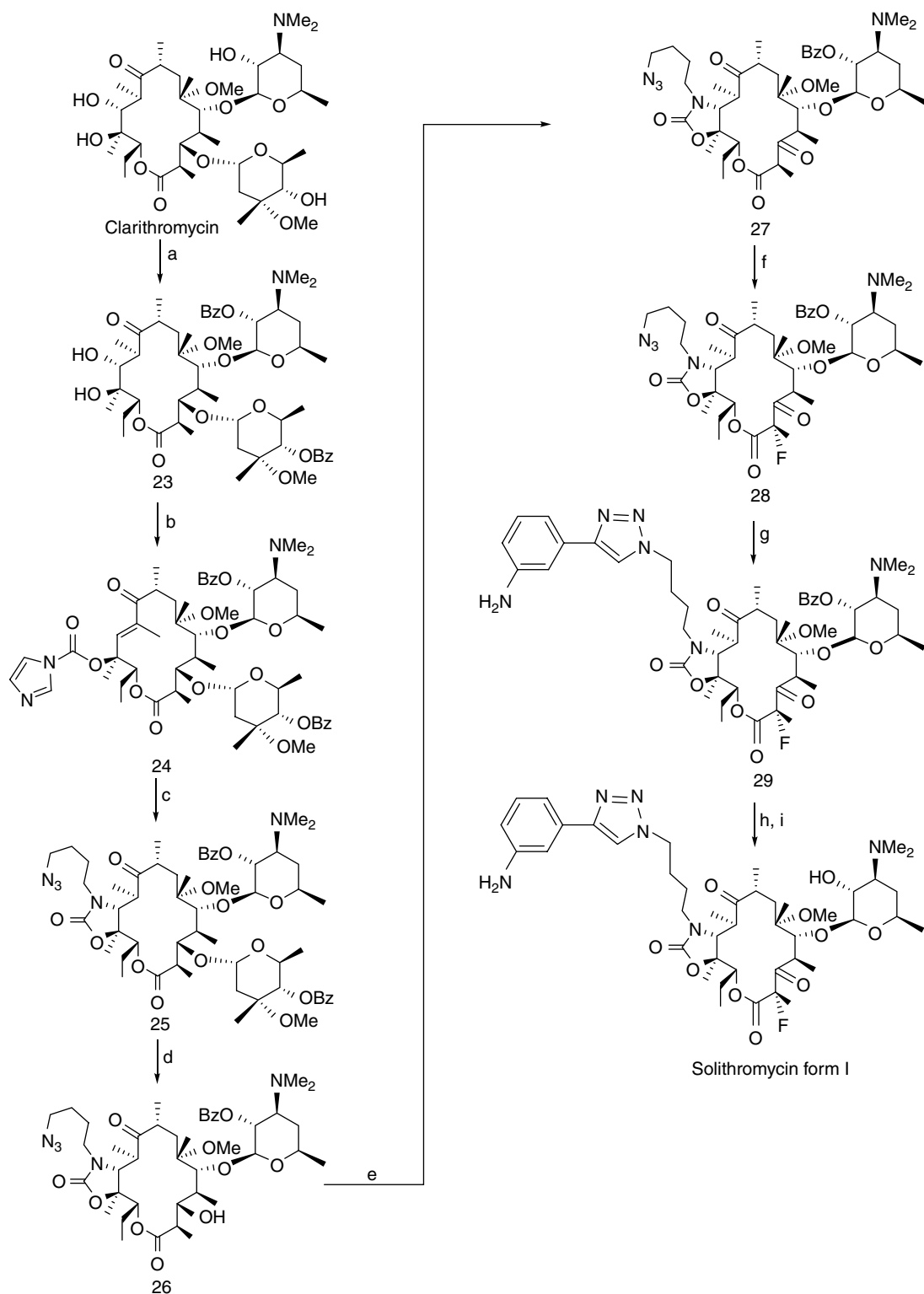
Figure 20.5 Large-scale synthesis of solithromycin. (a) Bz₂O, TEA, DMAP, ethyl acetate, 30–40°C; (b) CDI, DBU, DMF, 40–50°C; (c) 4-azidobutylamine, DBU; DMF, 30–35°C; (d) 4 N HCl, acetone/water, 30–40°C; (e) DMP; methylene chloride, 20–35°C; (f) NFSI, DBU, DMF/isopropyl acetate, −20 to −25°C; (g) 3-ethynylaniline, copper (II) acetate, sodium ascorbate, DMF/water, 50–65°C; (h) Methanol/water, 65–75°C; and (i) HCl aqueous/ammonium hydroxide/water, 10–20°C.
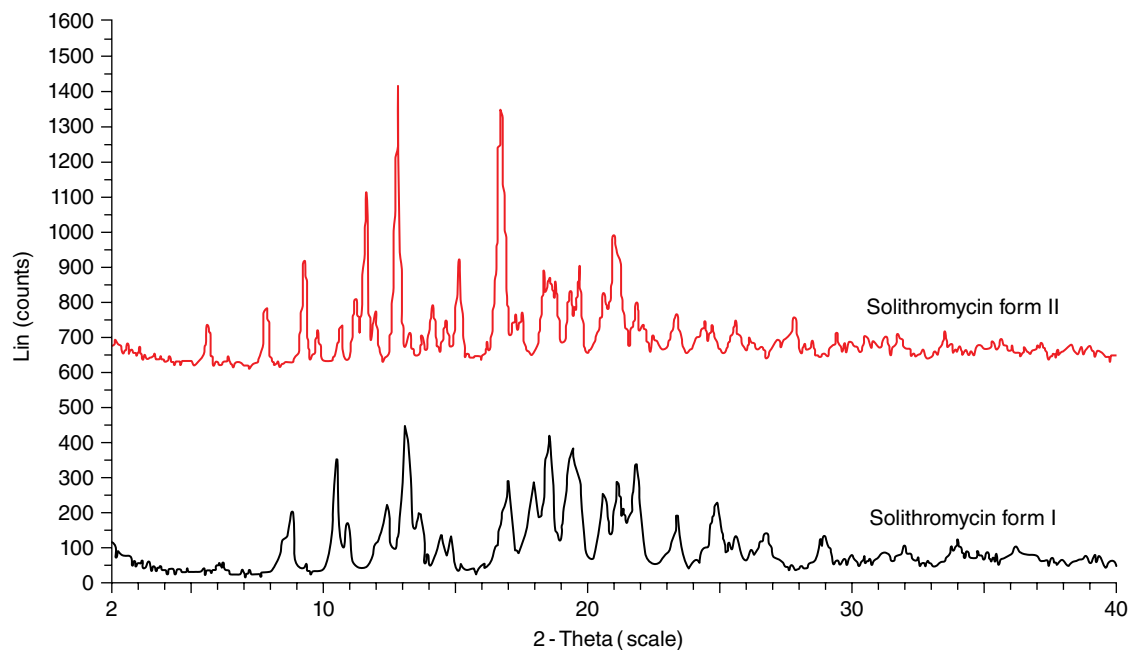
Figure 20.6 Representative XRPD diffractogram of solithromycin Forms I and II.

Having both oral and IV formulations empowers the physician with flexibility to switch a patient from the IV formulation to the oral dosage form during the course of treatment, which could allow for the patient to be discharged from the hospital more rapidly, resulting in cost savings to the healthcare system. Therefore, capsule, IV, and powder for oral suspension (POS) formulations were prepared for solithromycin and evaluated in the clinic. Solithromycin is the first antibiotic in many years to be developed with oral, IV, and pediatric formulations.

20.7.1 Capsule Development

20.7.1.1 Capsule Formulation Development

The results of the PK and tolerability studies of solithromycin after single or multiple oral doses, as well as the effects of food on oral bioavailability in healthy adult subjects, have been reported [62]. These studies supported the development of solithromycin once-daily oral regimens in the clinical management of respiratory tract infections and other infectious disorders. An immediate release, hard gelatin capsule formulation was used for these preliminary studies and was later selected as the dosage form for further development, clinical studies, and initial commercialization [62].

Capsule development began with preformulation characterization of the physical and chemical properties of solithromycin alone and in combination with pharmaceutically acceptable excipients. Generally, in pharmaceutical product development, the goal of preformulation studies is to apply biopharmaceutical principles to drug substance properties in order to design an optimal drug delivery system [63]. For solithromycin, the API properties evaluated included aqueous solubility, partition coefficient, and polymorphism, in addition to stability and compatibility with pharmaceutically acceptable excipients. These properties were taken into consideration for the design of the dosage form.

Preformulation studies on solithromycin API demonstrated that the API exhibits high aqueous solubility in acidic conditions and its solubility decreased with increasing pH, consistent with the pKa (3.9) of the aniline amine. As noted Section 20.6, solithromycin exists in two stable polymorphic forms; Form I was selected for development. Solithromycin is stable at room temperature conditions and adsorbs <5% w/w water even at relative humidity (RH) levels as high as 90%.

The selection of excipients in formulation development was guided by the drug–excipient compatibility studies. The proper selection of dosage form composition using API-excipient compatibility studies at the outset of a pharmaceutical development program leads to reduction of "surprises" during long-term stability testing of drug products [64]. Excipient selection for API compatibility was based on the knowledge of excipients typically used in immediate release capsules and institutional experience with these dosage forms. The excipients were selected from the following functional groups: diluents, binders, disintegrants, wetting agents, and lubricants.

For the excipient–API compatibility studies, binary and ternary blends of solithromycin and the common
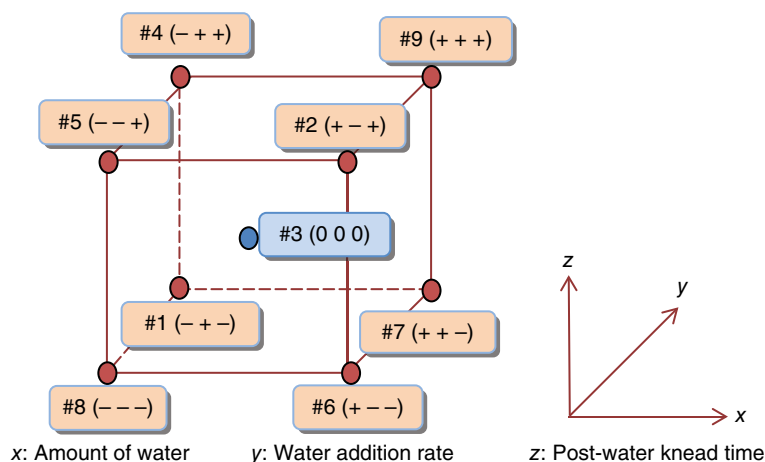
Figure 20.7 Solithromycin granulation DOE design.

x: Amount of water y: Water addition rate z: Post-water knead time

excipients for the desired form (microcrystalline cellulose, croscarmellose sodium, sodium lauryl sulfate, povidone, and magnesium stearate) were prepared. These compositions were stored in open and closed vials at $40 \pm 2°C/75 \pm 5\%$ RH for 1 month and at $60°C$/ambient humidity for 2 weeks. No significant changes in either the assay values or the related substances profiles were observed compared to control samples of API alone under the same conditions. These excipients were determined to be compatible with solithromycin and incorporated into the drug product formulation.

20.7.1.2 Capsule Manufacturing Process

The capsule manufacturing process includes high-shear wet granulation of solithromycin with all excipients, except the lubricant, magnesium stearate. Povidone dissolved in water is used as the granulation solution, and water is used to complete the granulation as required. The wet granules are dried using a fluidized bed dryer followed by sizing of the dried granules. The sized granules are then blended with magnesium stearate in a diffusion-type blender followed by encapsulation into size 0 hard gelation capsules. Each capsule contains a target of 200 mg active ingredient.

After formulation was selected, it was necessary to conduct manufacturing process development and optimization to ensure that manufactured capsules consistently met preestablished acceptance criteria. To guide the manufacturing process development and optimization, all processing steps were evaluated so that a robust manufacturing process could be defined. Accordingly, prior to manufacturing the registration batches required for submission of the new drug application (NDA), the manufacturing process was optimized using a design-of-experiment (DOE) approach [65]. This approach allows evaluation of all manufacturing factors in a systematic manner, resulting in a robust manufacturing process. The granulation process was the main focus of the DOE

because a quality risk assessment had indicated that it had the greatest potential to impact the critical quality attributes of assay, uniformity of dosage units, and dissolution. The DOE was a 3-factorial, 2-level, 1-center design as illustrated in Figure 20.7.

The DOE study identified the design space for the granulation process [66]. A scale-up batch followed by three registration batches was manufactured based on the process parameters determined from the DOE [67]. The in-process granulation and encapsulation data indicated that predetermined critical product attributes were met. Process capability analysis indicated that the process used to manufacture registration batches was capable of meeting specifications (C_p (process capability) > 1.33) and was centered with a C_{pk} (process capability index) > 1.33, indicating that the process has potential for Six Sigma performance [68].

20.7.1.3 Capsule Dissolution

The dissolution of the scale-up and registration batch capsules was evaluated in comparison with solithromycin batches utilized in clinical trials. The dissolution test was conducted in 900 ml of pH 4.0 acetate buffer at $37 \pm 0.5°C$ using USP Apparatus I (baskets) at 50 RPM. Dissolution profiles of capsule batches used in clinical batches and registration batches are shown in Figure 20.8. The data show that all capsule batches evaluated were immediate release with more than 80% of solithromycin released by the 30-min time point. The data demonstrate that the clinical and the registration batches exhibited comparable dissolution profiles.

20.7.2 Powder for Oral Suspension

In order to treat children with CABP, a solithromycin powder for oral suspension (POS) dosage form is in development. The formulation is designed for reconstitution with water prior to dispensing to the patient. This

Figure 20.8 Dissolution profiles for solithromycin capsules. (*See insert for color representation of the figure.*)
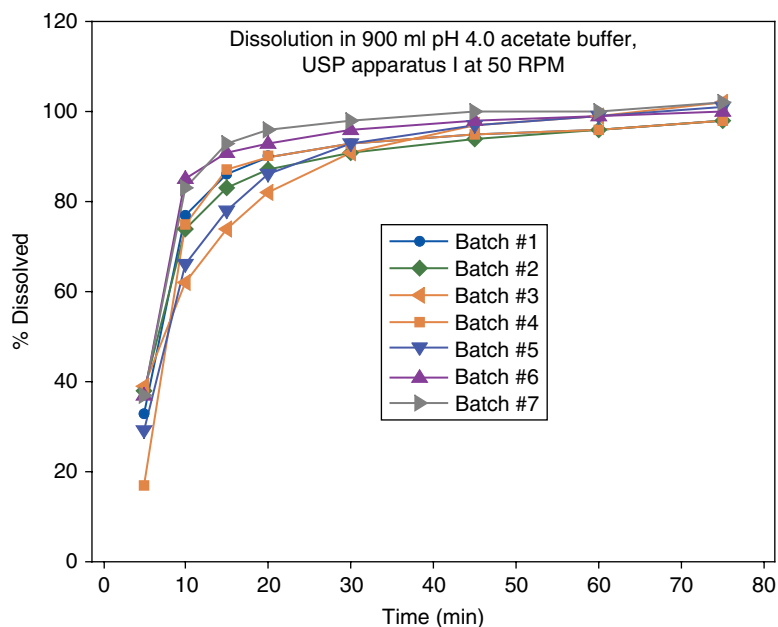
dosage form was selected for development as it provides dosing flexibility and is appropriate across all pediatric age groups. All macrolide antibiotics, including azithromycin and clarithromycin, have a bitter taste that must be taste-masked for use in pediatric oral suspensions [69, 70]. Although solithromycin was less bitter than clarithromycin in an initial taste evaluation, taste-masking was included in solithromycin oral suspension formulation development to ensure better patient compliance. A POS formulation with acceptable taste was developed and composed of a number of sweeteners, excipients, a buffer, a flavoring, and a coloring agent [71]. The formulation is currently undergoing clinical evaluation.

20.7.3 Solithromycin for Injection

20.7.3.1 The Challenge of Solithromycin IV Formulation Development

Solithromycin contains a tertiary amino group on the desosamine sugar moiety and an aromatic amino group on the phenyl ring of the side chain. The pK_a values of the two amino groups are 9.4 and 3.9, respectively. Due to protonation of the two amino groups, solithromycin is more soluble at acidic pHs and less soluble at higher pHs. As solution pH approaches neutrality, the aqueous solubility decreases to <0.4 mg/ml. A target concentration of 1.6 mg/ml was established as a formulation development goal in order to deliver up to a 1000 mg single dose in a reasonable infusion volume.

In order to achieve this target concentration at a pH suitable for infusion, a variety of approaches to enhance the aqueous solubility of solithromycin, including organic cosolvents, cyclodextrins, surfactants, and pH

adjustment, were studied. Although organic solvents, cyclodextrins, surfactants, and lipids improved solubility, the concentration of these agents required to achieve a usable formulation may have exceeded the precedent daily doses in approved drug products for these excipients. Therefore, formulation development focused on a pH adjustment approach using aqueous buffers. The first-generation solithromycin lyophilized formulation was 50 mg/ml API in 38.5 mM tartaric acid at a pH of 3.8. This formulation was reasonably well tolerated in preclinical studies [72].

The tartaric acid-based formulation was evaluated in a phase 1 clinical study. The lyophilized tartaric acid formulation was reconstituted with 5 ml water for injection (WFI) and then diluted into 0.45% sodium chloride to a concentration in the range of 0.1–1.6 mg/ml solithromycin. The drug was infused as single doses of 25–800 mg and as multiple doses of 50–100 mg. At higher single doses and with multiple doses of 100 mg, several subjects experienced infusion site-related pain and/or phlebitis. The cause of the infusion site reactions was considered to be related, at least in part, to precipitation of solithromycin upon encountering the blood stream due to a pH increase in the vicinity of the infusion site. For drugs with low aqueous solubility at neutral pH, precipitation upon infusion is a function of both drug concentration and the rate of infusion [73, 74]. Hence, a highly buffered amino acids based IV formulation was developed to slow pH increase upon injection to minimize precipitation of solithromycin until protein binding and drug dilution occurs down steam from the injection site [75]. A sterile lyophilized formulation was developed that contained the API, L-histidine, L-glutamic acid, and L-aspartic acid.

The lyophilized cake is reconstituted with WFI and diluted into 250 ml of 0.9% sodium chloride injection. This formulation was used in phase 1 clinical trial to evaluate patient safety and in the pivotal IV-to-Oral phase 3 clinical trial to evaluate efficacy.

20.8 Clinical Data

20.8.1 Phase 1 PK and Bioavailability

An escalating single oral dose (50–1600 mg) clinical trial and a repeat oral dose for 7 days (200–600 mg) clinical trial were conducted to gain knowledge on the PK and tolerability of solithromycin in healthy volunteers. All single doses were well tolerated. On day 7 in the repeat dose study, a 400 mg daily dose on day 7 gave a mean C_{max} of 1.09 μg/ml, $t_{1/2}$ of 7.47 h and AUCτ of 13.27 μg·h/ml, which provided confidence that once-a-day dosing with solithromycin would be effective in the treatment of CABP [62]. Solithromycin is ~70% orally bioavailable [62, 76]. A PK/PD analysis concluded that a single 800 mg loading oral dose on day 1 followed by 4 days of a single dose of 400 mg would be effective [77]. This dosing regimen was used in the pivotal oral phase 3 clinical trial.

20.8.2 Phases 2 and 3 Trials

Efficacy and safety of solithromycin was evaluated against levofloxacin in a randomized phase 2 trial in 132 adults diagnosed with moderate to moderately severe CABP. The efficacy, safety, and tolerability of solithromycin were comparable to levofloxacin, justifying continued clinical development [78].

Two double-blind phase 3 trials have been completed to date in adults diagnosed with moderate to severe CABP. In the first phase 3 global trial (Solitaire-Oral), 860 patients were randomized 1:1 to receive oral solithromycin (5 days) or oral moxifloxacin (7 days). For this trial, the treatment regimen for patients randomized to solithromycin was 2 days shorter than the treatment regimen for patients randomized to moxifloxacin; patients randomized to the solithromycin arm were given placebo on days 6 and 7. Nonetheless, this trial met the primary objective of statistical non-inferiority (10% non-inferiority margin) of solithromycin at the early clinical response (ECR) time after initiation of therapy [79, 80].

In the second phase 3 global trial (Solitaire-IV), 863 patients with moderate to severe CABP were randomized 1:1 to receive solithromycin or moxifloxacin for 7 days. All patients were initially dosed IV, with the option to be switched to oral dosing of their assigned drug based on the assessment of their clinical stability. This trial also met the primary objective of statistical non-inferiority (10% non-inferiority margin) of the ECR [81].

20.9 Summary

Solithromycin is a novel 14-member macrolide in the fluoroketolide subclass. The drug exhibits superior antibacterial activity against pathogenic bacteria, including those carrying the *mef* and *erm* resistance genes. This activity is the result of a disruption of the bacterial proteome through binding of solithromycin to the bacterial ribosome near the constriction point of the NPET.

A polymorph screen found that solithromycin exists in two stable polymorphic forms and Form I was chosen for clinical and commercial development. The specific polymorph form is established in the final step of the nine-step manufacture of solithromycin. The process begins with clarithromycin and encompasses C11,12-carbamate formation, cladinose removal, oxidation, fluorination, and 1,2,3-triazole formation followed by deprotection, before isolation of Form I in the final step.

Three drug product formulations have been developed and taken into clinical development. A 200 mg capsule formulation composition using traditional excipients was used in all clinical phases. An IV formulation was also developed in order to infuse 400 mg of solithromycin over 60 minutes. For pediatric patients, a POS was developed and is currently being evaluated in a phase 2/3 clinical study.

References

1 Mandell, L. A.; Wunderink, R. G.; Anzueto, A.; Bartlett, J. G.; Campbell, G. D.; Dean, N. C.; Dowell, S. F.; File, T. M.; Musher, D. M.; Niederman, M. S.; Torres, A.; Whitney, C. G. Infectious Diseases Society of America/American Thoracic Society Consensus Guidelines on the Management of Community-Acquired Pneumonia in Adults. *Clin. Infect. Dis.* **2007**, *44*(Supplement 2), S27–S72.

2 Xu, J.; Kochanek, K. D.; Murphy, S. L.; Tejada-Vera, B. Deaths: Final Data for 2007. *Natl. Vital Stat. Rep. 2010*, 58, 1–19.

3 Magill, S. S.; Edwards, J. R.; Bamberg, W.; Beldavs, Z. G.; Dumyati, G.; Kainer, M. A.; Lynfield, R.; Maloney, M.; McAllister-Hollod, L.; Nadle, J.; Ray, S. M.; Thompson, D. L.; Wilson, M. D.; Fridkin, S. K. Multistate Point-

Prevalence Survey of Health Care–Associated Infections. *N. Engl. J. Med.* **2014**, *370*(13), 1198–1208.

4 Broulette, J.; Yu, H.; Pyenson, B.; Iwasaki, K.; Sato, R. The Incidence Rate and Economic Burden of Community-Acquired Pneumonia in a Working-Age Population. *Am. Health Drug Benefits* **2013**, *6*(8), 494.

5 Bartlett, J. G.; Dowell, S. F.; Mandell, L. A.; File, T. M.; Musher, D. M.; Fine, M. J. Practice Guidelines for the Management of Community-Acquired Pneumonia in Adults. *Clin. Infect. Dis.* **2000**, *31*(2), 347–382.

6 Liu, H. H. Safety Profile of the Fluoroquinolones. *Drug Saf.* **2010**, *33*(5), 353–369.

7 Mehlhorn, A. J.; Brown, D. A. Safety Concerns with Fluoroquinolones. *Ann. Pharmacother.* **2007**, *41*(11), 1859–1866.

8 Grundmann, H.; Aires-de-Sousa, M.; Boyce, J.; Tiemersma, E. Emergence and Resurgence of Methicillin-Resistant *Staphylococcus aureus* as a Public-Health Threat. *Lancet* **2006**, *368*(9538), 874–885.

9 Arias, C. A.; Murray, B. E. Antibiotic-Resistant Bugs in the 21st Century—A Clinical Super-Challenge. *N. Engl. J. Med.* **2009**, *360*(5), 439–443.

10 Davidson, R.; Cavalcanti, R.; Brunton, J. L.; Bast, D. J.; de Azavedo, J.; Kibsey, P.; Fleming, C.; Low, D. E. Resistance to Levofloxacin and Failure of Treatment of Pneumococcal Pneumonia. *N. Engl. J. Med.* **2002**, *346*(10), 747–750.

11 Forsyth, C. Repairing the Antibiotic Pipeline: Can the Gain Act Do It? *Wash. J. Law Tech. Arts* **2013**, *9*(1), 1–18.

12 Hwang, C.-K.; Duffield, J.; Chiu, Y.-H.; Liang, C.-H.; Yao, S.; Roberts, N.; Babakhani, F.; Sears, P.; Shue, Y.-K.; Ichikawa, Y.; Fernandes, P.; Pereira, D.; Romero, A. 48th Interscience Conference on Antimicrobial Agents and Chemotherapy (ICAAC), Washington, D.C., USA, October 25–28, **2008**, Abstr. F1–3973.

13 Zhanel, G. G.; Walters, M.; Noreddin, A.; Vercaigne, L. M.; Wierzbowski, A.; Embil, J. M.; Gin, A. S.; Douthwaite, S.; Hoban, D. J. The Ketolides. *Drugs* **2002**, *62*(12), 1771–1804.

14 Denis, A.; Bretin, F.; Fromentin, C.; Bonnet, A.; Bonnefoy, A.; Agouridas, C.; Piltan, G. β-Keto-Ester Chemistry and Ketolides. Synthesis and Antibacterial Activity of 2-Halogeno, 2-Methyl and 2, 3-Enol-Ether Ketolides. *Bioorg. Med. Chem. Lett.* **2000**, *10*(17), 2019–2022.

15 Tornøe, C. W.; Christensen, C.; Meldal, M. Peptidotriazoles on Solid Phase: [1, 2, 3]-Triazoles by Regiospecific Copper (I)-Catalyzed 1, 3-Dipolar Cycloadditions of Terminal Alkynes to Azides. *J. Org. Chem.* **2002**, *67*(9), 3057–3064.

16 Rostovtsev, V. V.; Green, L. G.; Fokin, V. V.; Sharpless, K. B. A Stepwise Huisgen Cycloaddition Process: Copper (I)-Catalyzed Regioselective "Ligation" of Azides and Terminal Alkynes. *Angew. Chem. Int. Ed.* **2002**, *41*(14), 2596–2599.

17 Ambs, S.; Neumann, H. G. Acute and Chronic Toxicity of Aromatic Amines Studied in the Isolated Perfused Rat Liver. *Toxicol. Appl. Pharmacol.* **1996**, *139*(1), 186–194.

18 Organisation for Economic Co-operation and Development Guideline (OECD). Bacterial Reverse Mutation Test. **1997**, Test 471. From https://www.oecd.org/chemicalsafety/risk-assessment/1948418.pdf (accessed March 27, 2017).

19 Organisation for Economic Co-operation and Development Guideline (OECD). In Vitro Mammalian Chromosomal Aberration. **2014**, Test 473. From http://www.oecd-ilibrary.org/docserver/download/9716391e.pdf (accessed March 27, 2017).

20 Organisation for Economic Co-operation and Development Guideline (OECD). Mammalian Erythrocyte Micronucleus Test. **1997**, Test 474. From http://www.oecd.org/chemicalsafety/risk-assessment/1948442.pdf (accessed March 27, 2017).

21 Murphy, T. M.; Gaffney, M.; Little, S.; Wu, R.; Slee, A. M.; Ong, C.; Fernandes, P. 19th European Congress of Clinical Microbiology and Infectious Diseases, Helsinki, Finland, May 16–19, **2009** Abstr. F1–3985.

22 Madigan, M. T.; Martinko, J. M.; Parker, J. *Brock Biology of Microbiology.* Prentice Hall, Upper Saddle River, NJ, **1997**, pp. 199–201.

23 Poehlsgaard, J.; Douthwaite, S. The Bacterial Ribosome as a Target for Antibiotics. *Nat. Rev. Microbiol.* **2005**, *3*(11), 870–881.

24 Korostelev, A.; Trakhanov, S.; Laurberg, M.; Noller, H. F. Crystal Structure of a 70S Ribosome-tRNA Complex Reveals Functional Interactions and Rearrangements. *Cell* **2006**, *126*(6), 1065–1077.

25 Champney, W. Bacterial Ribosomal Subunit Assembly Is an Antibiotic Target. *Curr. Top. Med. Chem.* **2003**, *3*(9), 929–947.

26 Ryu, D. H.; Rando, R. R. Aminoglycoside Binding to Human and Bacterial A-Site rRNA Decoding Region Constructs: In Vitro Selected Nucleic Acids. *Bioorg. Med. Chem.* **2001**, *9*(10), 2601–2608.

27 Sutcliffe, J. A. Improving on Nature: Antibiotics That Target the Ribosome. *Curr. Opin. Microbiol.* **2005**, *8*(5), 534–542.

28 Foster, C.; Champney, W. S. Characterization of a 30S Ribosomal Subunit Assembly Intermediate Found in *Escherichia coli* Cells Growing with Neomycin or Paromomycin. *Arch. Microbiol.* **2008**, *189*(5), 441–449.

29 Wilson, D. N. On the Specificity of Antibiotics Targeting the Large Ribosomal Subunit. *Ann. N. Y. Acad. Sci.* **2011**, *1241*(1), 1–16.

30 Asaka, T.; Manaka, A.; Sugiyama, H. Recent Developments in Macrolide Antimicrobial Research. *Curr. Top. Med. Chem.* **2003**, *3*(9), 961–989.

31 Schlünzen, F.; Zarivach, R.; Harms, J.; Bashan, A.; Tocilj, A.; Albrecht, R.; Yonath, A.; Franceschi, F. Structural Basis for the Interaction of Antibiotics with the Peptidyl Transferase Centre in Eubacteria. *Nature* **2001**, *413*(6858), 814–821.

32 Katz, L.; Ashley, G. W. Translation and Protein Synthesis: Macrolides. *Chem. Rev.* **2005**, *105*(2), 499–528.

33 Takashima, H. Structural Consideration of Macrolide Antibiotics in Relation to the Ribosomal Interaction and Drug Design. *Curr. Top. Med. Chem.* **2003**, *3*(9), 991–999.

34 Hansen, J. L.; Ippolito, J. A.; Ban, N.; Nissen, P.; Moore, P. B.; Steitz, T. A. The Structures of Four Macrolide Antibiotics Bound to the Large Ribosomal Subunit. *Mol. Cell* **2002**, *10*(1), 117–128.

35 Fernandes, P. *Antibiotics: Current Innovations and Future Trends*. Caister Academic Press, Norfolk, UK, **2015**, pp. 375–393.

36 Canu, A.; Malbruny, B.; Coquemont, M.; Davies, T. A.; Appelbaum, P. C.; Leclercq, R. Diversity of Ribosomal Mutations Conferring Resistance to Macrolides, Clindamycin, Streptogramin, and Telithromycin in *Streptococcus pneumoniae*. *Antimicrob. Agents Chemother.* **2002**, *46*(1), 125–131.

37 Llano-Sotelo, B.; Dunkle, J.; Klepacki, D.; Zhang, W.; Fernandes, P.; Cate, J. H.; Mankin, A. S. Binding and Action of CEM-101, a New Fluoroketolide Antibiotic That Inhibits Protein Synthesis. *Antimicrob. Agents Chemother.* **2010**, *54*(12), 4961–4970.

38 Dunkle, J. A.; Xiong, L.; Mankin, A. S.; Cate, J. H. Structures of the *Escherichia coli* Ribosome with Antibiotics Bound Near the Peptidyl Transferase Center Explain Spectra of Drug Action. *Proc. Natl. Acad. Sci. U. S. A.* **2010**, *107*(40), 17152–17157.

39 Images of 4WWW (Ref. 37) were created with Sybyl-X version 2.1.1 (Certara USA, Inc., Princeton, NJ).

40 Berisio, R.; Harms, J.; Schluenzen, F.; Zarivach, R.; Hansen, H. A.; Fucini, P.; Yonath, A. Structural Insight into the Antibiotic Action of Telithromycin Against Resistant Mutants. *J. Bacteriol.* **2003**, *185*(14), 4276–4279.

41 Rodgers, W.; Frazier, A. D.; Champney, W. S. Solithromycin Inhibition of Protein Synthesis and Ribosome Biogenesis in *Staphylococcus aureus*, *Streptococcus pneumoniae*, and *Haemophilus influenzae*. *Antimicrob. Agents Chemother.* **2013**, *57*(4), 1632–1637.

42 Gamerdinger, M.; Deuerling, E. Macrolides: The Plug Is Out. *Cell* **2012**, *151*(3), 469–471.

43 Nakatogawa, H.; Ito, K. The Ribosomal Exit Tunnel Functions as a Discriminating Gate. *Cell* **2002**, *108*(5), 629–636.

44 Woolhead, C. A.; Johnson, A. E.; Bernstein, H. D. Translation Arrest Requires Two-Way Communication between a Nascent Polypeptide and the Ribosome. *Mol. Cell* **2006**, *22*(5), 587–598.

45 Woolstenhulme, C. J.; Parajuli, S.; Healey, D. W.; Valverde, D. P.; Petersen, E. N.; Starosta, A. L.; Guydosh, N. R.; Johnson, W. E.; Wilson, D. N.; Buskirk, A. R. Nascent Peptides That Block Protein Synthesis in Bacteria. *Proc. Natl. Acad. Sci. U. S. A.* **2013**, *110*(10), E878–E887.

46 Martínez, A. K.; Gordon, E., Sengupta, A.; Shirole, N.; Klepacki, D.; Martinez-Garriga, B.; Brown, L. M.; Benedik, M. J.; Yanofsky, C.; Mankin, A. M.; Vazquez-Laslop, N.; Sachs, M. S.; Cruz-Vera, L. R. Interactions of the TnaC Nascent Peptide with rRNA in the Exit Tunnel Enable the Ribosome to Respond to Free Tryptophan. *Nucleic Acids Res.* **2014**, *42*(2), 1245–1256.

47 Kannan, K.; Vázquez-Laslop, N.; Mankin, A. S. Selective Protein Synthesis by Ribosomes with a Drug-Obstructed Exit Tunnel. *Cell* **2012**, *151*(3), 508–520.

48 Ross, D. B. The FDA and the Case of Ketek. *N. Engl. J. Med.* **2007**, *356*(16), 1601–1604.

49 Jarvis, L. M. The Ketek Effect. *Chem. Eng. News* **2008**, *86*(15), 861–862.

50 Bertrand, D.; Bertrand, S.; Neveu, E.; Fernandes, P. Molecular Characterization of Off-Target Activities of Telithromycin: A Potential Role for Nicotinic Acetylcholine Receptors. *Antimicrob. Agents Chemother.* **2010**, *54*(12), 5399–5402.

51 Bertrand, D.; Bertrand, S.; Fernandes, P. 49th Interscience Conference on Antimicrobial Agents and Chemotherapy (ICAAC), San Francisco, CA, USA, September 12–15, **2009**, Abstr. A1–580.

52 Blum, A. P.; Lester, H. A.; Dougherty, D. A. Nicotinic Pharmacophore: The Pyridine N of Nicotine and Carbonyl of Acetylcholine Hydrogen Bond Across a Subunit Interface to a Backbone NH. *Proc. Natl. Acad. Sci. U. S. A.* **2010**, *107*(30), 13206–13211.

53 Kuhnen-Clausen, D.; Hagedorn, I.; Gross, G.; Bayer, H.; Hucho, F. Interactions of Bisquaternary Pyridine Salts (H-Oximes) with Cholinergic Receptors. *Arch. Toxicol.* **1983**, *54*(3), 171–179.

54 Bertrand, D.; Bertrand, S.; Pereira, D.; Fernandes, P. 51st Interscience Conference on Antimicrobial Agents and Chemotherapy (ICAAC), Chicago, IL, USA, September 17–20, **2011**, Abstr. A2–588.

55 Fernandes, P.; Pereira, D.; Jamieson, B.; Keedy, K. Solithromycin. *Drugs Future* **2011**, *36*(10), 751–758.

56 Li, B.; Magee, T. V.; Buzon, R. A.; Widlicka, D. W.; Bill, D. R.; Brandt, T.; Cao, X; Coutant, M.; Dou, H.; Granskog, K.; Flanagan, M. E.; Hayward, C. M.; Li, B.; Liu, F.; Liu, W.; Nguyen, T.; Raggon, J. W.; Rose, P.;

Rainville, J.; Reilly, U. D.; Shen, Y.; Sun, J.; Wilcox, G. E. Process Development of a Novel Azetidinyl Ketolide Antibiotic. *Org. Process Res. Dev.* **2012**, *16*(5), 788–797.

57 Wu, Y.; Su, W. Recent Developments on Ketolides and Macrolides. *Curr. Med. Chem.* **2001**, *8*(14), 1727–1758.

58 Pereira, D.; Kanchanbhai, M.; Deo, K., Process for the Preparation of Macrolide Antibacterial Agents, PCT International Publication No. WO2009/055557, **2009**.

59 Pereira, D., Crystalline Forms of a Macrolide, and Uses Therefor, US Patent 8,759,500, June 24, **2014**.

60 International Conference on Harmonisation of Technical Requirements for Registration of Pharmaceuticals for Human Use. Impurities: Guideline for Residual Solvents Q3C(R3). February **2011**.

61 Marsault, E.; Peterson, M. L. Macrocycles Are Great Cycles: Applications, Opportunities, and Challenges of Synthetic Macrocycles in Drug Discovery. *J. Med. Chem.* **2011**, *54*(7), 1961–2004.

62 Still, J. G.; Schranz, J.; Degenhardt, T. P.; Scott, D.; Fernandes, P.; Gutierrez, M. J.; Clark, K. Pharmacokinetics of Solithromycin (CEM-101) After Single or Multiple Oral Doses and Effects of Food on Single-Dose Bioavailability in Healthy Adult Subjects. *Antimicrob. Agents Chemother.* **2011**, *55*(5), 1997–2003.

63 Vilegava, K.; Vidyasagar, G.; ChandarKar, P. Preformulation Studies of Pharmaceutical New Drug Molecule & Products: An Overview. *Am. J. Pharm. Health Res.* **2013**, *1*(3), 2321–3647.

64 Serajuddin, A. T. M.; Thakur, A. B.; Ghoshal, R. N.; Fakes, M. G.; Ranadive, S. A.; Morris, K. R.; Varia, S. A. Selection of Solid Dosage Form Composition Through Drug–Excipient Compatibility Testing. *J. Pharm. Sci.* **1999**, *88*(7), 696–704.

65 Hwang, R. C.; Kowalski, D. L. Design of Experiments for Formulation Development. *Pharm. Technol.* **2005**, (1), 1–5.

66 Pradeep, L.; Hollis, C.; Majuru, S.; Cocolas, H.; Pereira, D. 2014 AAPS Annual Meeting and Exposition, San Diego, CA, USA, November 2–6, **2014**. Abstr. W4310.

67 Pradeep, L.; Hollis, C.; Majuru, S.; Cocolas, H.; Pereira, D. 2014 AAPS Annual Meeting and Exposition, San Diego, CA, USA, November 2–6, **2014**. Abstr W4344.

68 Majuru, S.; Pradeep, L.; Pereira, D.; Hollis, C.; Cocolas, H.; Thomas, R.; Schlee, J. 2014 AAPS Annual Meeting and Exposition, San Diego, CA, USA, November 2–6, **2014**. Abstr W4305.

69 Ishizaka, T.; Miyanaga, Y.; Mukai, J.; Asaka, K., Nakai, Y.; Tsuji, E.; Uchida, T. Bitterness Evaluation of Medicines for Pediatric Use by a Taste Sensor. *Chem. Pharm. Bull.* **2004**, *52*(8), 943–948.

70 Tanigake, A.; Miyanaga, Y.; Nakamura, T.; Tsuji, E.; Matsuyama, K.; Kunitomo, M.; Uchida, T. The Bitterness Intensity of Clarithromycin Evaluated by a Taste Sensor. *Chem. Pharm. Bull.* **2003**, *51*(11), 1241–1245.

71 Pereira, D.; Shingai, M.; Fernandes, P., Powder Oral Suspension Formulations of Antibacterial Agents, PCT International Application No. WO 2016/022658, **2016**.

72 Fernandes, P.; Degenhardt, T.; Pereira, D. 50th Interscience Conference on Antimicrobial Agents and Chemotherapy (ICAAC), Boston, MA, USA, September 12–15, **2010**, Abstr. F1–2151.

73 Yalkowsky, S. H.; Krzyzaniak, J. F.; Ward, G. H. Formulation-Related Problems Associated with Intravenous Drug Delivery. *J. Pharm. Sci.* **1998**, *87*(7), 787–796.

74 Johnson, J. L.; He, Y.; Yalkowsky, S. H. Prediction of Precipitation-Induced Phlebitis: A Statistical Validation of an In Vitro Model. *J. Pharm. Sci.* **2003**, *92*(8), 1574–1581.

75 Pereira, D.; Fernandes, P. Wu, S. U. S. Patent Application US 2013/034179.

76 Keelan, J. A.; Payne, M. S.; Kemp, M. W.; Ireland, D. J.; Newnham, J. P. A New, Potent, and Placenta-Permeable Macrolide Antibiotic, Solithromycin, for the Prevention and Treatment of Bacterial infections in Pregnancy. *Front. Immunol.* **2016**, *7*, 1–11.

77 Okusanya, O. O.; Bhavnani, S. M.; Forrest, A.; Bulik, C.C.; Oldach, D.; Fernandes, P.; Ambrose, P. G. 53th Interscience Conference on Antimicrobial Agents and Chemotherapy (ICAAC), San Francisco, CA, USA, September 9–12, **2012**, Abstr. A–1269.

78 Oldach, D.; Clark, K.; Schranz, J.; Das, A.; Craft, J. C.; Scott, D.; Jamieson, B. D.; Fernandes, P. Randomized, Double-Blind, Multicenter Phase 2 Study Comparing the Efficacy and Safety of Oral Solithromycin (CEM-101) to Those of Oral Levofloxacin in the Treatment of Patients with Community-Acquired Bacterial Pneumonia. *Antimicrob. Agents Chemother.* **2013**, *57*(6), 2526–2534.

79 Oldach, D. W.; Barrera, C. M.; Luna, C.; Szabo, P.; Mitha, I.; Tanaseanu, C. M.; Doreski, A.; Clark, K.; Jamieson, B.; Das, A.; Keedy, K.; Fernandes, P. 25th Annual Congress European Respiratory Society, Amsterdam, the Netherlands, September 26–30, **2015**. Abstr. PA2655.

80 Barrera, C. M.; Mykietiuk, A.; Metev, H.; Nitu, M.; Karimjee, N.; Doreski, P.A.; Mitha, I.; Tanaseanu, C. M.; Molina, J. M.; Antonovsky, Y.; Van Rensburg, D. J.; Rowe, B. H.; Flores-Figueroa, J.; Rewerska, B.; Clark, K.; Keedy, K.; Sheets, A.; Scott, D.; Horwith, G.; Das, A.F.; Jamieson, B.; Fernandes, P.; Oldach, D. Efficacy and

Safety of Oral Solithromycin Versus Oral Moxifloxacin for Treatment of Community-Acquired Bacterial Pneumonia: A Global, Double-Blind, Multicentre, Randomised, Active-Controlled, Non-Inferiority Trial (SOLITAIRE-ORAL). *Lancet Infect. Dis.* **2016**, *16*(4), 421–430.

81 File Jr., T. M.; Rewerska, B.; Tanaseanu, C. M.; Mihailovic-Vucinic, V.; Gonong, J. R.; Jamieson, B.D.; Taylor, D.; Sheets, A.; Keedy, K.; Oldach D. W.; Fernandes, P. American Thoracic Society International Conference, San Francisco, CA, USA, May 13–18, **2016**. Abstr. P840.

Index

Figure 2.1 Pharmaceutical, agricultural, and industrial applications of cyclotides. The range of potential applications of cyclotides is illustrated schematically by showing the relevant target organisms.

Scheme 4.1 Principal of polyketide synthesis with subsequent macrocyclization. During its biosynthesis the linear precursor is connected via a thioester bond to acyl carrier proteins (ACP, bound to the sulfur – only the bond is shown in the scheme). Modifications and transfer to the next monomer are catalyzed by additional domains of the respective module. The starter unit is gray.

Valinomycin (**9**)

Octane crystal   K⁺ complex
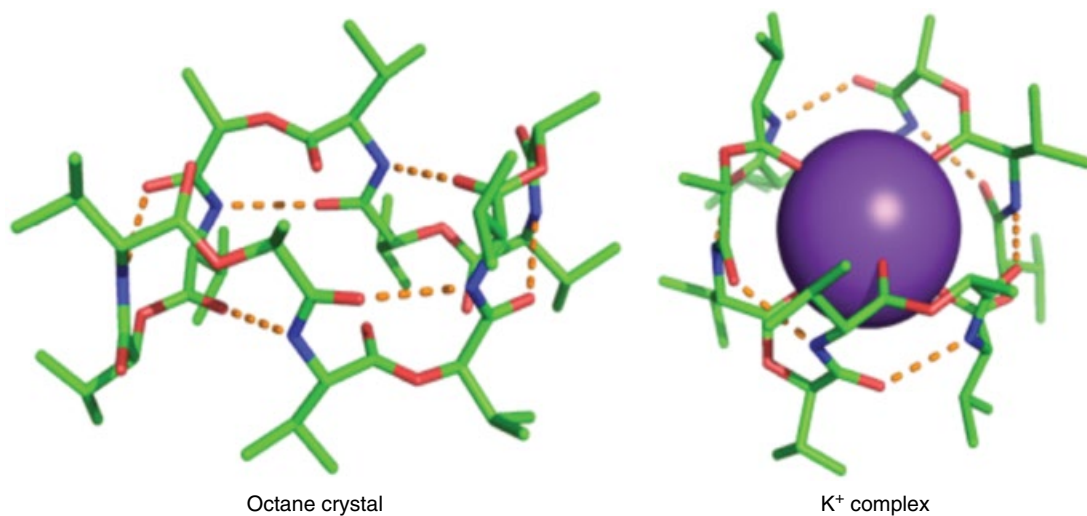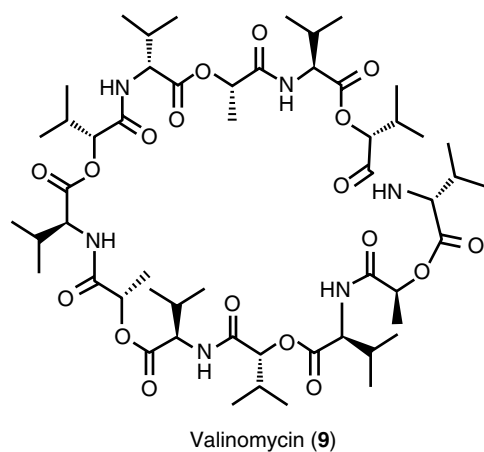
Figure 5.5 Conformations of valinomycin.
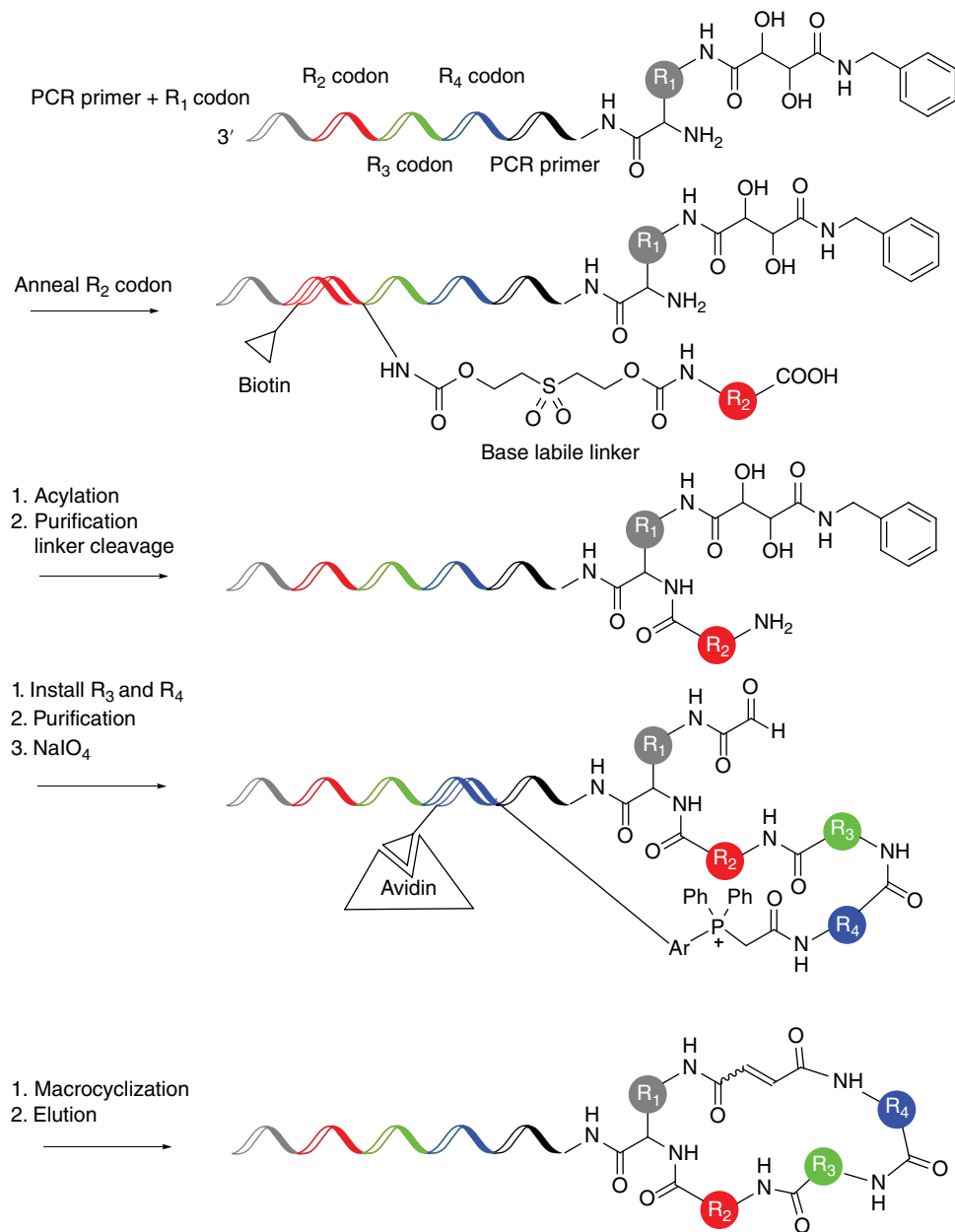
Figure 6.8 Steps involved in the synthesis of DNA-encoded macrocyclic libraries.
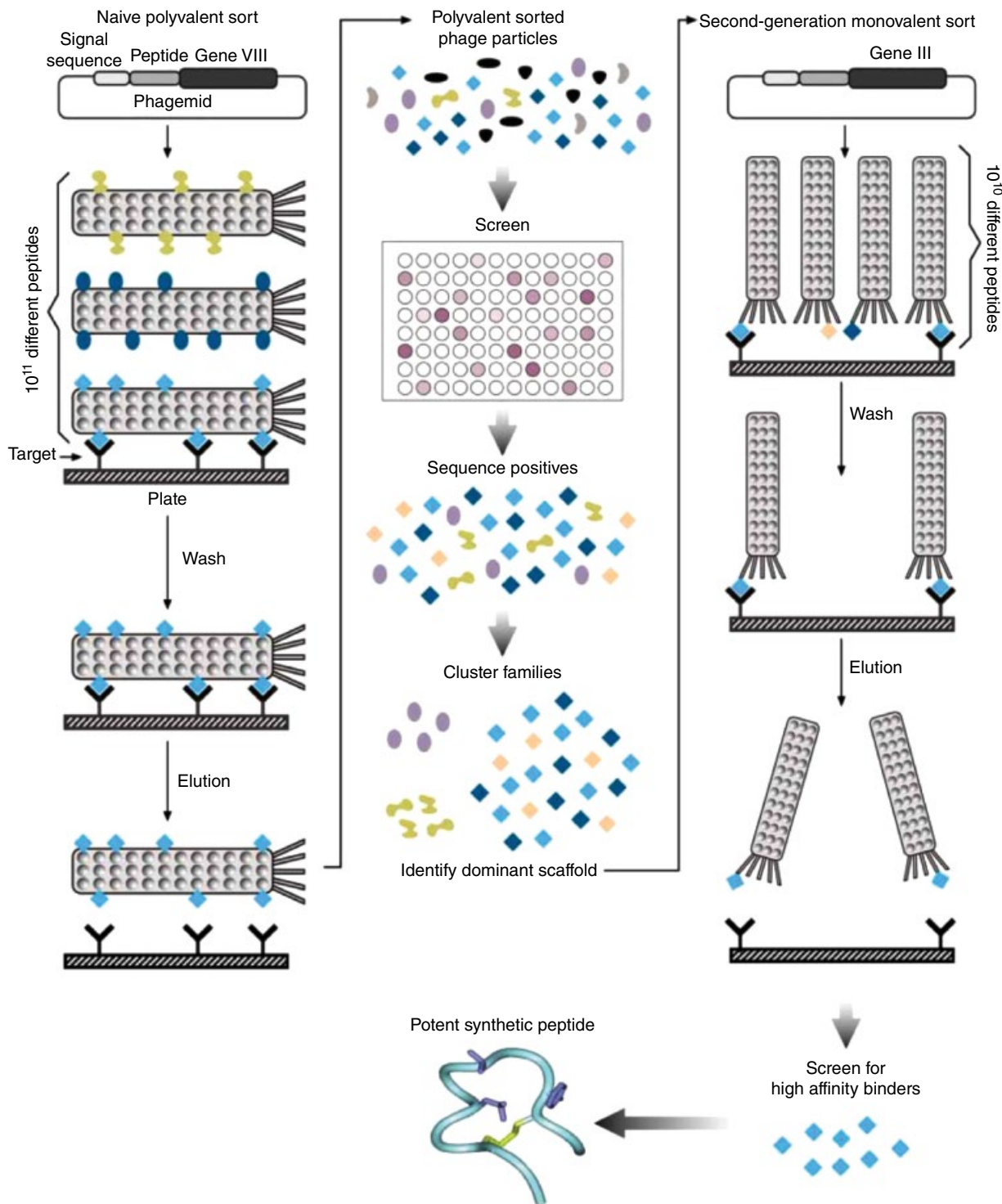
Figure 7.1 Schematic diagram for naïve selection and affinity maturation of disulfide-bridged cyclic peptide ligands via M13 phage display. A naïve library is first displayed on a high-valency format through fusion to the pVIII coat protein. Positive hits are validated via a phage ELISA assay and sequenced to identify consensus motifs. Affinity maturation of the ligand is achieved via a second-generation library designed based on the consensus motifs, followed by display on a low-valency format (pIII fusion) and affinity selection. Source: Adapted from Deshayes *et al*. [17]. Reproduced with permission of Elsevier.

Figure 7.4 Macrocyclic peptide binders of human IgG Fc fragment. (a) View of **Fc-III** peptide (DCAWHLGELVWCT; green; stick models) bound to the surface of human IgG Fc domain (pdb 1DN2); (b) Computer models of **FcBP-1** and **FcBP-2** mimetics as prepared by transplanting 9 or 13 residues, respectively, from **Fc-III** onto the ^{D}Pro-^{L}Pro template.

Figure 7.6 Crystal structure of human uPA in complex with monocyclic and bicyclic peptide inhibitors. (a) Disulfide-bridged peptide upain-1 (pdb 2NWN); (b) TBMB-linked bicyclic peptide UK18 (pdb 3QN7); (c) TBAB-linked bicyclic peptide UK903 (pdb 4MNY); and (d) bicyclic disulfide-bridged peptide UK504 (pdb 4GLY). The TBMB and TBAB linkers are colored in magenta. Key amino acid residues involved in the interaction with uPA are showed as sphere models. For each complex, a schematic representation of the corresponding peptide ligand is provided.

Figure 7.7 Overview of mRNA display system for the selection of functional peptides. A template DNA library is first transcribed *in vitro* to generate a randomized mRNA library (i). After conjugation with puromycin (ii) and translation of the mRNA-encoded polypeptide (iii), a peptide–mRNA conjugate is formed. A double-stranded DNA/RNA hybrid is then generated via reverse transcription, followed by panning of the RNA/DNA-conjugated peptide library against an immobilized target protein. The protein-bound peptide–RNA/DNA molecules are then recovered and amplified by polymerase chain reaction (PCR), followed by transcription and translation. Iterative rounds of affinity selection and amplification enrich the library with peptide with high affinity for the target protein, whose sequence can be determined by DNA sequencing.

(a)

Flexizyme (eFx)

ClAc^DW-tRNA_{CAU}

Flexizyme
(eFx or dFx)

N-Me-Xaa-tRNA_{CAU}

X = various side chains

R = CME

R = DNB

(b)

1st	2nd				3rd
	U	C	A	G	
U	^{Me}F	Ser	Tyr	Cys	U C A G
C	^{Me}S	Pro	His	Arg	U C A G
A	^{Me}G / ClAc^DW	Thr	Asn	Ser	U C A G
G	Val	^{Me}A	Asp	Gly	U C A G

(c)

cDNA library
ATG (NNT)_{8–15} TGC

1. Transcription
2. Ligation with puromycin

mRNA library
AUG (NNU)_{8–15} UGC

Pu

6. PCR

E6AP
HECT

SAvB

AUG (NNU)_{8–15} UGC

5. Selection

ClAc^DW-tRNA^{fMet}

CAU

N-^{Me}X-tRNA^{Asn-E2}

GNN

FIT system
(flexible *in vitro*
translation)

• Ribosome
• Translation factors
• Designated
  proteinogenic aa
• Designated ARSs
• tRNAs, NTPs, etc.

3. Translation

AUG (NNU)_{8–15} UGC

AUG (NNU)_{8–15} UGC

4. Reverse transcription

Cyclic *N*-methylated peptide library

Figure 7.9 Screening of *in vitro* translated cyclic peptide libraries via the FIT and RaPID system. (a) Flexizyme-catalyzed tRNA aminoacylation. Initiator tRNA_{CAU} is loaded with *N*-chloroacetyl-^DTrp, and other selected tRNAs are loaded with N-methylated amino acids (MeF, MeS, MeG, MeA). (b) Reprogrammed genetic code used for mRNA display peptide library against the HECT domain of ubiquitin ligase E6AP. Selected codons are made "vacant" via removal of the corresponding tRNA and AARS from the *in vitro* translation system. These codons are reprogrammed using the aminoacylated tRNAs prepared in (a). (c) Overview of the RaPID system for the selection of macrocyclic *N*-methylated peptides against E6AP. Messenger RNA libraries containing a randomized sequence, (NNU)_{8–15}, are transcribed from the corresponding cDNA library and conjugated with an oligonucleotide bearing a puromycin residue. The resulting mRNAs are translated by the FIT system in the presence of the appropriate aminoacylated tRNAs as in (a). The mRNA-displayed linear peptides are cyclized via a reaction between the cysteine residue and the N-terminal α-chloroacetyl group. After affinity selection against immobilized E6AP, the cDNAs of the protein-bound mRNA–peptide fusions are recovered and amplified by PCR. After multiple rounds of affinity selection/amplification (typically 6–10), the identity of the "hits" is determined by DNA sequencing. Source: Hipolito *et al*. [109] and Yamagishi *et al*. [101]. Reproduced with permission of Elsevier & American Chemical Society.

Figure 8.1 Split-intein circular ligation of peptides and proteins (SICLOPPS) and the reverse two-hybrid system (RTHS). (a) The expressed SICLOPPS intein (I_C : target peptide : I_N) folds to form an active intein. An *N*-to-*S* acyl shift occurs at the target N-terminal intein junction to produce a thioester, which upon transesterification with a side chain nucleophile (serine or cysteine, X = O or S, respectively) at the C-terminal intein junction forms a lariat intermediate. An asparagine side chain liberates the cyclic peptide as a lactone, which then undergoes rearrangement to generate the desired cyclic peptide as a lactam. (b) RTHS: Interacting proteins X and Y are expressed as N-terminal fusions with the 434 and p22 repressor proteins, respectively, under the control of the IPTG promoter. Dimerization of X and Y forms an active repressor construct, with 434 and p22 binding to their respective deoxyribonucleic acid (DNA) response elements and inhibiting downstream expression of the reporter cassette. When a cyclic peptide inhibits the interaction between X and Y, the repressor construct is not formed, therefore allowing for cell survival on selective media. For identification of inhibitors of homodimeric PPIs, a homodimeric system composed of only the 434 repressors can be used.

Figure 8.3 Random nonstandard peptide integrated discovery (RaPID) system. A complementary deoxyribonucleic acid (cDNA) library is generated via polymerase chain reaction (PCR), containing random sequences, which is transcribed to form an mRNA library (1). A puromycin linker is ligated to the 3′-end of each mRNA species (2). The mRNA is translated to a nonstandard peptide using the flexible *in vitro* translation (FIT) system, (3) forming a library of peptide–puromycin linker–mRNA species. These undergo reverse transcription (4) to prevent nonspecific binding during selection. The target protein is immobilized with a magnetic bead and the resultant peptide–mRNA–cDNA library is then screened for target binding (5). Library enrichment is performed through PCR amplification of those sequences found to contain target binders (6).

Figure 8.7 Interaction of PERM-1 with the surface of ERα. The surface of ERα (yellow) provides a good fit for the residues of PERM-1 (cyan). The N-terminal Lys and C-terminal Gln residues of PERM-1 are labeled. Protein data bank (PDB) code: 1PCG.

(a)

(b)

Compound	Sequence $* = R_8 * = S_5$	Charge at pH 7.4	α helicity (%)	K_d (nM)	Cell permeable	Cell death
WT	Ac-LSQETFSDLWKLLPEN-NH$_2$	−2	11	410 ± 19	No	−
SAH-p53-1	Ac-LSQETFSD*WKLLPE*-NH$_2$	−2	25	100 ± 8	No	−
SAH-p53-2	Ac-LSQE*FSDLWK*LPEN-NH$_2$	−2	10	400 ± 50	No	−
SAH-p53-3	Ac-LSQ*TFSDLW*LLPEN-NH$_2$	−2	12	1200 ± 89	No	−
SAH-p53-4	Ac-LSQETF*DLWKLL*EN-NH$_2$	−2	59	0.92 ± 0.11	No	−
SAH-p53-5	Ac-LSQETF*NLWKLL*QN-NH$_2$	0	20	0.80 ± 0.05	Yes	−
SAH-p53-6	Ac-LSQQTE*NLWRLL*QN-NH$_2$	+1	14	56 ± 11	Yes	−
SAH-p53-7	Ac-QSQQTF*NLWKLL*QN-NH$_2$	+1	36	50 ± 10	Yes	−
SAH-p53-8	Ac-QSQQTF*NLWRLL*QN-NH$_2$	+1	85	55 ± 11	Yes	+
SAH-p53-8$_{F19A}$	Ac-QSQQTA*NLWRLL*QN-NH$_2$	+1	39	>4000	Yes	−
UAH-p53-8	Ac-QSQQTF*NLWRKK*QN-NH$_2$	+1	36	100 ± 10	Yes	−

Figure 8.8 Synthesis and sequences of SAH-p53 peptides. (a) Nonnatural olefinic amino acid derivatives were incorporated into the sequence at positions avoiding critical HDM2-binding residues and cross-linked at the *i*, *i* + 7 positions by ruthenium catalyzed ring-closing olefin metathesis. (b) The series of SAH-p53 peptides were generated by stapling the p53$_{14–29}$ sequence at the indicated positions within the sequences shown. Charge, α-helicity, HDM2 binding affinity, cell permeability, and impact on cell viability are all indicated. Source: Reprinted with permission from Bernal et al. [75]. © 2007 American Chemical Society.

Figure 8.11 Hot loops are defined by meeting one or more of the following three criteria: (i) the average $\Delta\Delta G_{residue}$ over the entire loop must be greater than 1 kcal mol^{-1}, (ii) the loop contains greater than or equal to three hot spot residues ($\Delta\Delta G_{residue} > 1$ kcal mol^{-1}), and (iii) the loop contains greater than or equal to two consecutive hot spot residues. Loops representing each category are represented in the yellow, blue, and red circles. Some hot loops satisfy two of these criteria, and representative loops in green, purple, and boxes. There are 67 hot loops that fulfill all three criteria with one example depicted in the gray box. All structures, rendered in PyMOL (PDB codes depicted in boxes), show the interfacial chain in blue, binding partner in gray, hot loop in green, and hot spot residues in orange ($\Delta\Delta G_{residue} > 1$ kcal mol^{-1}) and yellow ($\Delta\Delta G_{residue} > 2$ kcal mol^{-1}). Source: Reprinted with permission from Gavenonis *et al.* [79]. © 2014 Macmillan Publishers Ltd.

Figure 10.1 (a) An illustration of a small-molecule binding to an enzyme active site. (b) Small-molecule modulators of protein–protein interactions via interface or an allosteric site.
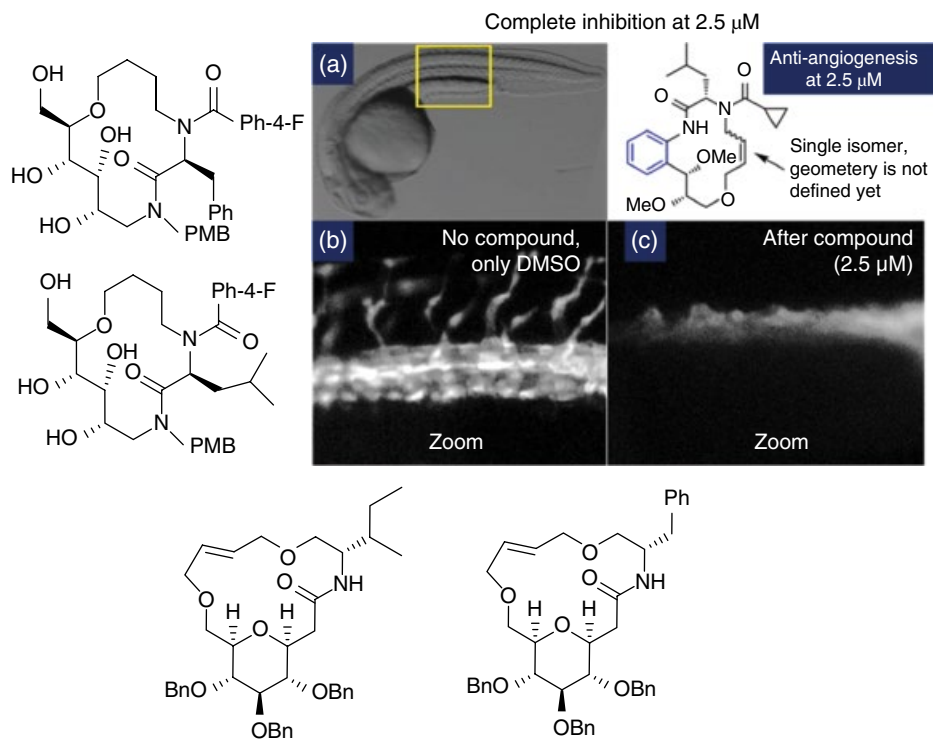
Figure 10.25 The discovery of several macrocyclic compounds functioning as anti-angiogenesis agents in an embryonic zebrafish study; (a) zoom section; (b) with DMSO as a control; and (c) the effect of a small molecule.

Figure 10.26 The discovery of macrocyclic small molecules functioning as correctors of the damage induced in the pore formation caused by thapsigargin, resulting in the rescue of cell death in pancreatic β-cells: (a) our proposed working model for the dynamic regulation of protein–protein interactions; (b) mitochondrial images with thapsigargin-induced damage and subsequent reorganization of mitochondria in the presence of **139**; (c) two sets of macrocyclic compounds and their acyclic precursors.

Figure 11.5 Macrocyclic XIAP antagonists with X-ray structure bound to the isolated XIAP-BIR2 domain depicted right.

Figure 11.7 (a) A view of the intermolecular hydrogen bonding observed between two macrocycles of **41** with the hydrogen atoms of the side chains omitted for clarity. Peptide backbone hydrogen bonds are shown as yellow dashed bonds and the triazole hydrogen bonds as dashed red lines. (b) A representation of the structure of **41** showing the nanotubular structure. The structure of **41** showing extended β-sheet conformation, with the triazole-containing macrocyclic linkage omitted for clarity. Side view of the dimerization of the nanotubular structures in the crystal. Top view of the dimerized nanotubes in a space-filling representation. (c) ESI spectrum of compound **41** showing the formation of oligomeric assemblies in the gas phase [M + Na] and an SEM image of the rod-like assemblies of **41**. (d) Superimposition of the crystallographic structure of **41** (green) with **43** (black) docked into cathepsin S.

Scheme 11.8 Additional macrocyclic protease inhibitors.

Figure 14.2 (a) Schematic sketch of solvated cyclosporine A conformation in polar medium (water), highlighting possible hydrogen interactions with the solvent. (b) Schematic sketch of cyclosporine A conformation in nonpolar medium (chloroform), showing the macrocycle "hiding" some of its hydrogen donors and acceptors through intramolecular interactions.

Scheme 14.2 (a) The Passerini three-component reaction (P3CR). (b) The Ugi four-component reaction (U4CR). (c) General scheme of a multicomponent macrocyclization approach (MiB). The macrocycle carries the diversity delivered by the additional component FG³ [22]. (d) Multicomponent reaction-based macrocyclization of a hypothetical peptide highlighting the atom economy of the entire process.

Scheme 14.4 Ugi-4CR-based macrocyclizations of single bifunctional building blocks. The monofunctional building blocks define the side chain functionality.

Scheme 14.7 Ugi-4CR-based macrocyclizations of peptides involving amphoteric aziridine carboxaldehydes (a) Proposed mechanism. (b) Examples of synthesized macrocycles **8–10**. (c) Application in the macrocyclization of rigid homochiral oligoprolines and comparison with standard procedures. (d) On-resin Ugi-4CR macrocyclization of peptides with aziridine carboxaldehyde and *tert*-butyl isonitrile.

Scheme 14.23 Synthesis of three-dimensional multi-macrocycles by threefold Ugi-4CR-based macrocyclizations, including trifunctional building blocks.

Labels in scheme:

66

67, 47%

Cryptands

68, 41%

65

69, 44%

Hemicryptophanes

70, 42%

Steroid-based cages

Cryptand	R^1	R^2	R^3
71a	Bn	Bn	Bn
71b	Bn	Bn	i-Pr
71c	Bn	Bn	CH$_2$CO$_2$Me
71d	Bn	i-Pr	CH$_2$CO$_2$Me
71e	Bn	CH$_2$CO$_2$Me	CH$_2$CO$_2$Me
71f	Bn	i-Pr	i-Pr
71g	i-Pr	i-Pr	i-Pr
71h	i-Pr	i-Pr	CH$_2$CO$_2$Me
71i	i-Pr	CH$_2$CO$_2$Me	CH$_2$CO$_2$Me
71j	CH$_2$CO$_2$Me	CH$_2$CO$_2$Me	CH$_2$CO$_2$Me

Scheme 14.24 Synthesis of a mixed library of cryptands by a threefold combinatorial MiB.

Scheme 14.25 Sequential MiBs applied to the synthesis of multi-macrocycles. (a) Clam-shaped macrobicycles and (b) igloo-shaped macrotetracycles.

(a)

(b)

7

BIR2 $IC_{50} = 0.54$ μM
BIR3 $IC_{50} = 0.18$ μM

(c)

Figure 17.2 X-ray co-crystal structural information indicated a superior macrocyclic ring closure, resulting in a series of compounds with greater binding affinity for the XIAP BIR2 binding site (a) X-ray co-crystal structure of the P2–P5-linked macrocyclic compound **5** (yellow) bound to the BIR2 domain (PDB accession number 4WVT). The compound makes a number of hydrogen-bond interactions (indicated as yellow broken lines) and lipophilic interactions from the P1, P3, and P4 side chains. (b) Structure of compound **7**, linear precursor to macrocycle **1**, a P2–P5-linked macrocycle. (c) Overlap of the co-crystal structures of the BIR2 domain with the linear compound **7** (green) (PDB accession number 4WVS) and P3–P5-linked macrocyclic compound **8** (orange) (PDB accession number 4WVU), showing that the backbone of the open chain overlaps almost exactly with the P3–P5-linked macrocyclic compound **8**.

Figure 17.6 Model of compound **22** bound to the BIR2-3 domains of XIAP protein. Carbon atoms of **22** are shown in green, and oxygen and nitrogen atoms are highlighted in red and blue, respectively. The protein surface is colored by electrostatic potential, with regions of negative potential shown in red hues, positive potential in blue, and neutral (hydrophobic) regions in white. Source: Adapted from Ahlbach *et al.* [38]. Reproduced with permission of American Chemical Society.

Figure 17.7 Antitumor activity of **33** in the A875 xenograft model in mice. Compounds were administered intraperitoneally (i.p.) every 3 days for six doses or weekly for two doses beginning on day 10.

Figure 18.1 Left panel: Crizotinib (**1**) co-crystal structure in ALK-L1196M kinase domain (PDB 2YFX, 1.7 Å). Right panel: PF-06439015 (**2**) bound to ALK-L1196M KD (PDB 4CD0, 2.2 Å).
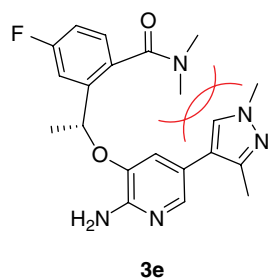
3e
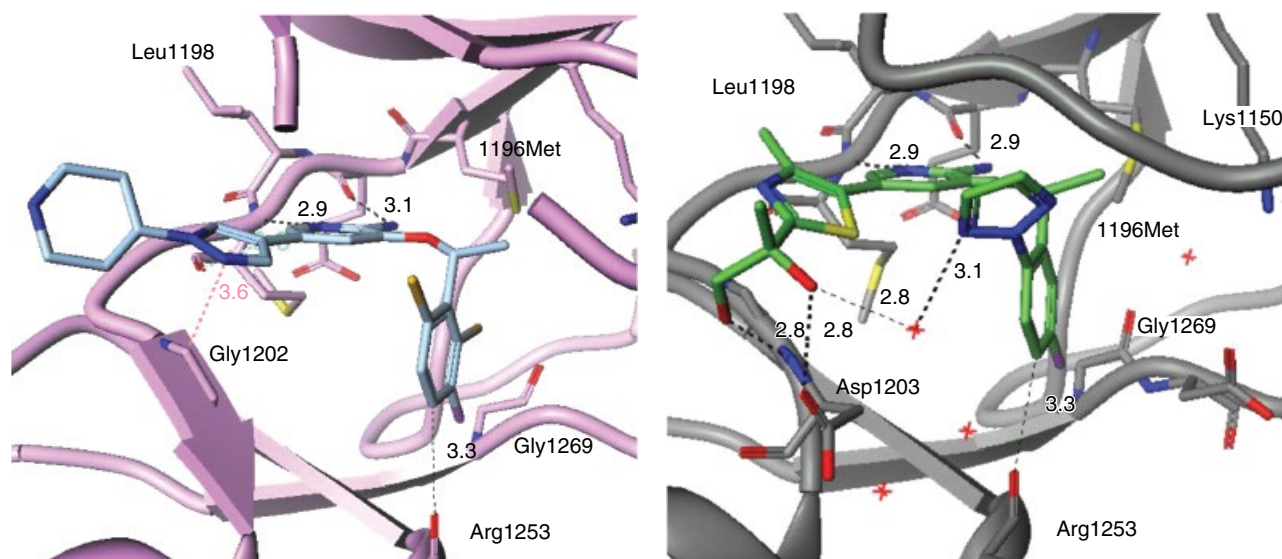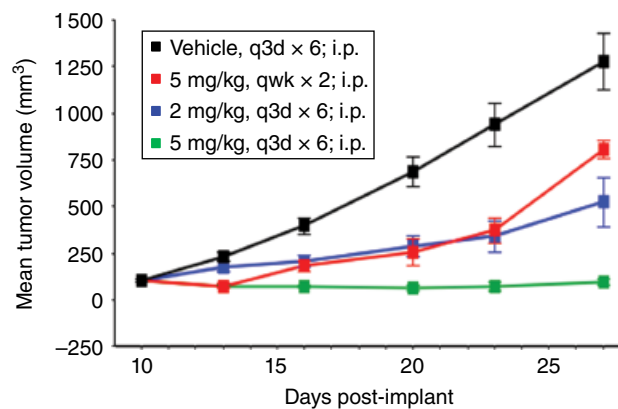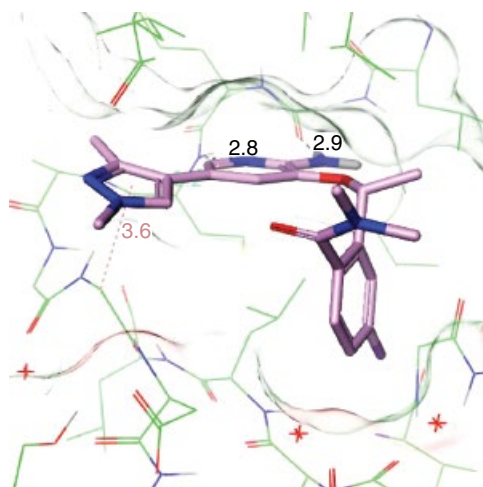
Figure 18.2 Internal clash of amide and pyrazole in preferred conformation of **3e** causes rotation of the amide into a less productive binding conformation. **3e** co-crystallized with ALK KD (PDB 5KZ0).
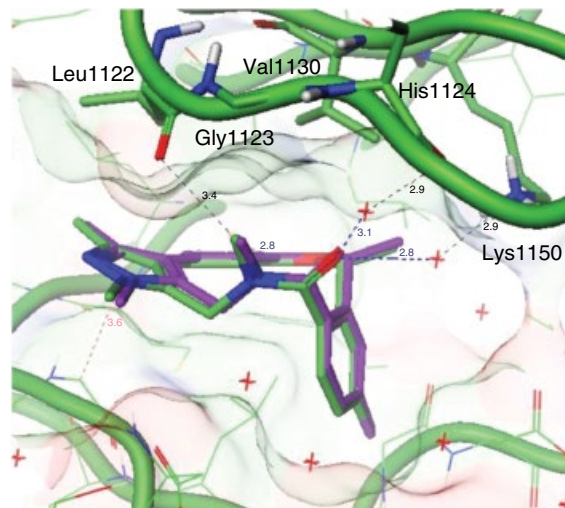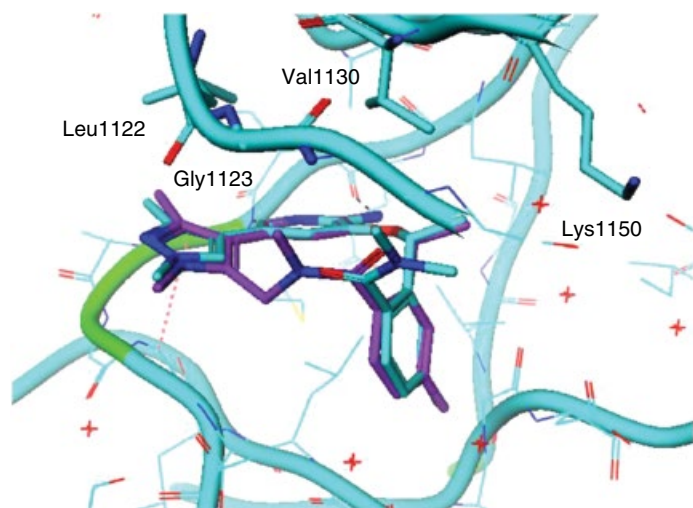
Figure 18.3 Left panel: Acyclic amide **3e** co-crystal structure in ALK (cyan, PDB 5KZ0) overlaid with modeled macrocycle **4g** (purple) in ALK. Right panel: **4g** co-crystal structure in ALK-kinase domain (green, PDB 4CMU) overlaid with modeled ligand (purple).

Figure 18.4 Structure of **4g** bound in ALK (green, PDB 4CMU) and TrkB (purple, PDB 4AT3) with selectivity residues and vector highlighted.
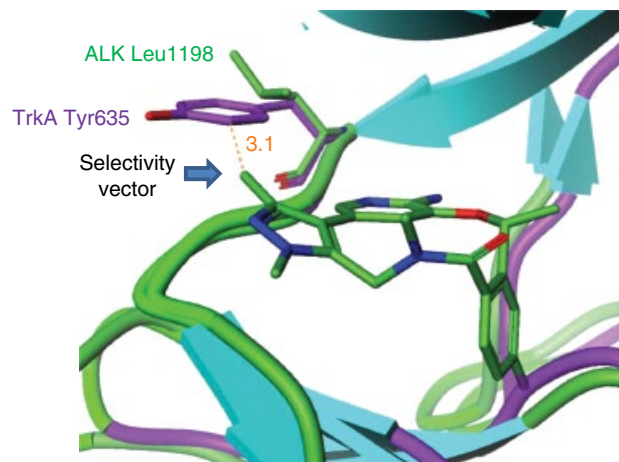
Figure 18.5 PF-06463922 (**4q**) co-crystal structure in ALK-L1196M kinase domain (PDB 4CLJ, 1.7 Å) overlaid with crizotinib (**1**) in complex with ALK-L1196M from Figure 18.1, left panel.
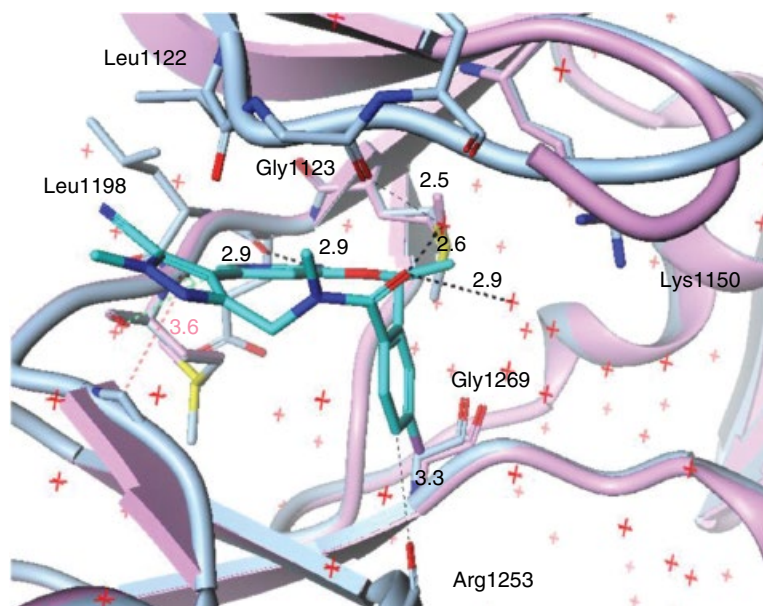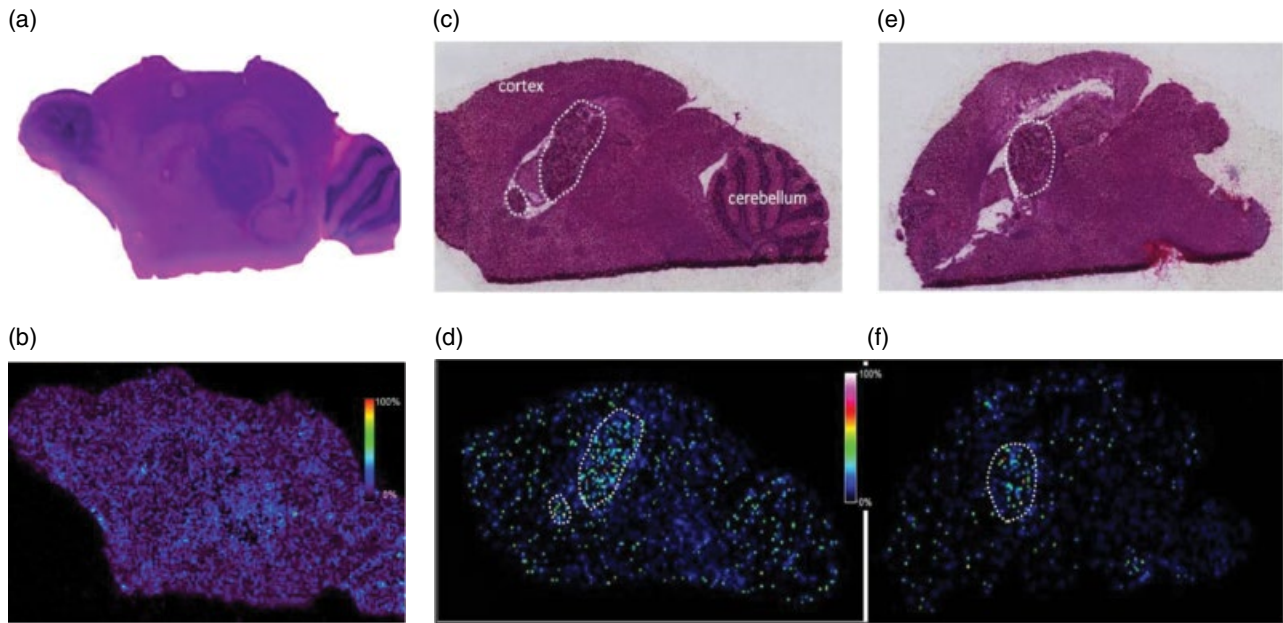
Figure 18.10 H&E stains (a, c, and e) and MALDI-MS images (b, d and f) of mouse brain slices. (a) and (b) are from a tumor-naïve mouse dosed at 400 mg/kg. (c) and (d) are from a tumor-bearing mouse dosed at 200 mg/kg. (e) and (f) are from a tumor-bearing mouse dosed at 100 mg/kg. All animals were orally dosed once. MS images were acquired at 75 × 75 µm pixel resolution.

Figure 18.11 **PF-06463922** antitumor efficacy in ALK fusion-driven intracranial tumor models. (a) Representative magnetic resonance images showing regression of large established H3122 EML4-ALKWT intracranial tumors in mice following **PF-06463922** infusion. (b) Quantitation of brain tumor sizes following **PF-06463922** treatment in the H3122 EML4-ALKWT intracranial model shown in (a). Values are presented as mean ± SEM.
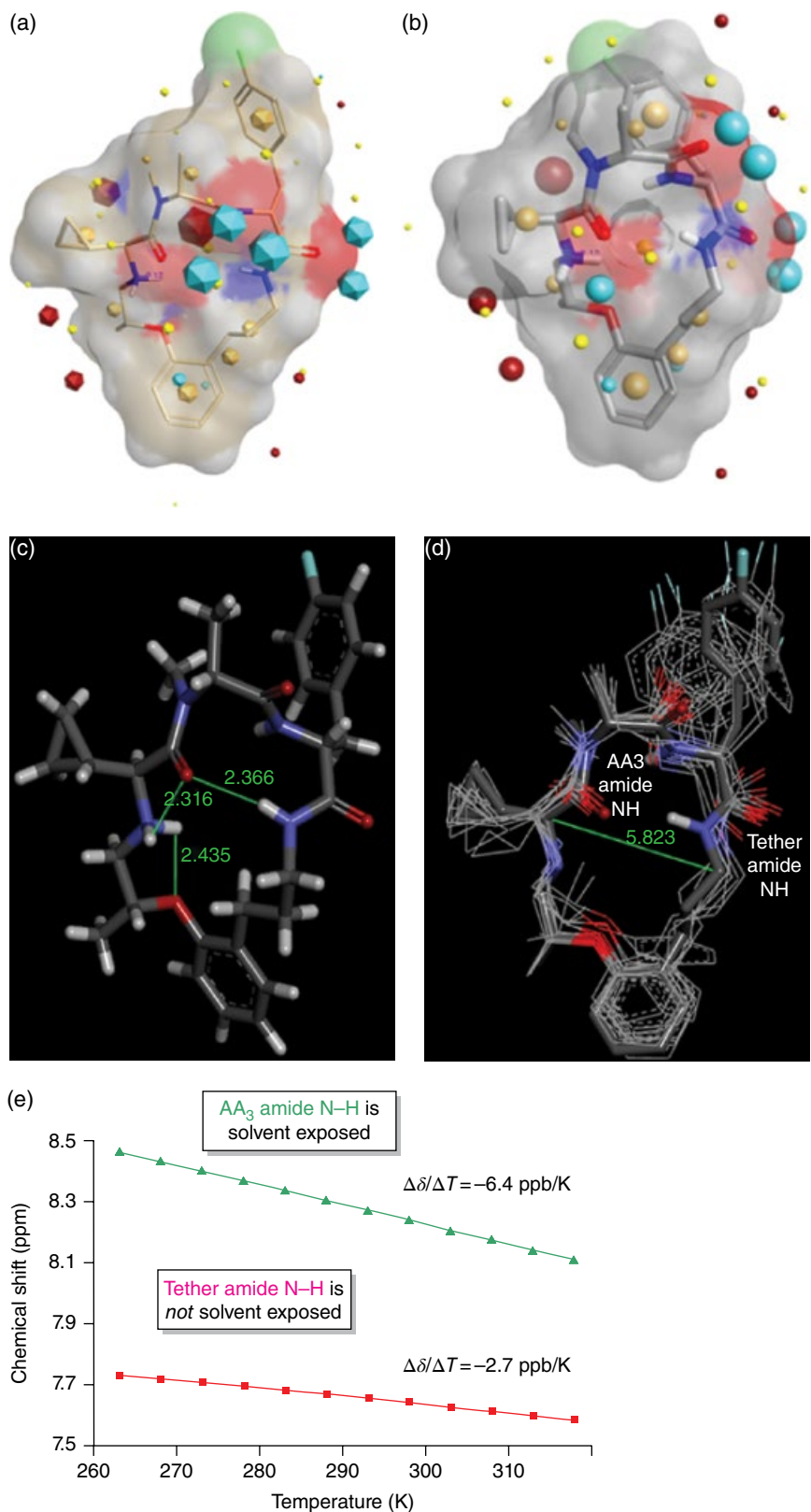
Figure 19.2 Panels a and b: The open (a) and closed (b) conformation of TZP-101 macrocyclic structure showing the molecular fields and solvent-accessible molecular surface using Forge™ software (v10, Cresset, United Kingdom). Panel c: X-ray crystal structure of TZP-101 showing the IHB network (solvent and counterion omitted for clarity). Panel d: Solution NMR consensus structure and molecular dynamics simulation also demonstrating hydrophobic collapse possibility. Panel e: Variable temperature NMR data indicating that the tether amide N–H (cf. Figure 19.1) is not solvent exposed, likely due to IHB.
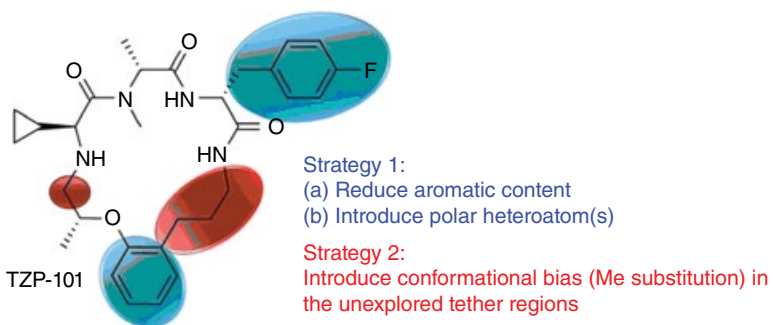
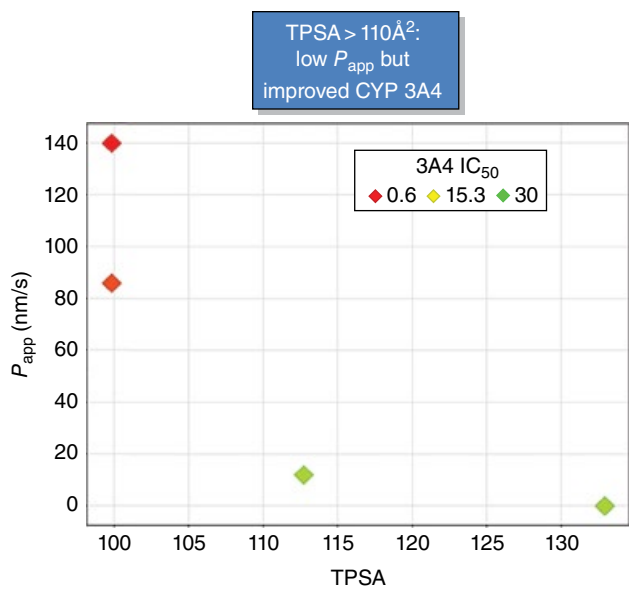**Figure 19.3** Lead optimization strategies discussed herein.

TZP-101

Strategy 1:
(a) Reduce aromatic content
(b) Introduce polar heteroatom(s)

Strategy 2:
Introduce conformational bias (Me substitution) in the unexplored tether regions

Figure 19.4 Correlation plots based on data presented in Table 19.1.

TPSA > 110Å^2: low P_{app} but improved CYP 3A4

3A4 IC$_{50}$
◆ 0.6 ◆ 15.3 ◆ 30

P_{app} (nm/s)

TPSA

CYP 3A4 IC$_{50}$ ↓ correlates to $clogP$ ↑

$r^2 = 0.70$

P_{app} AB
● 0 ● 70 ● 140

3A4 IC50 (µM)

$cLogP$
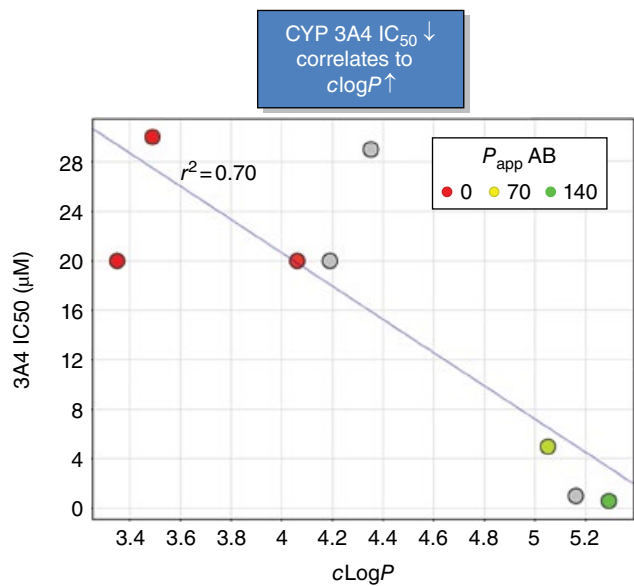
Figure 19.5 Rat gastric emptying data (oral administration, metoclopramide as positive control).

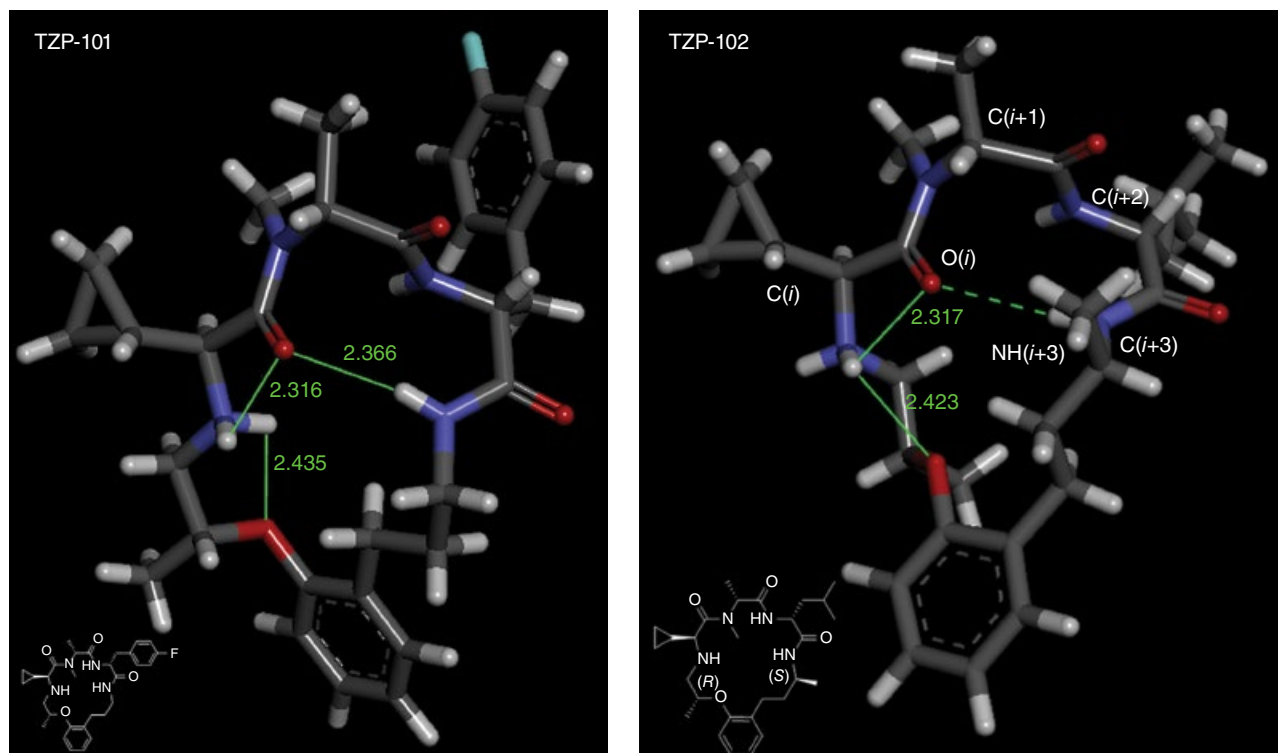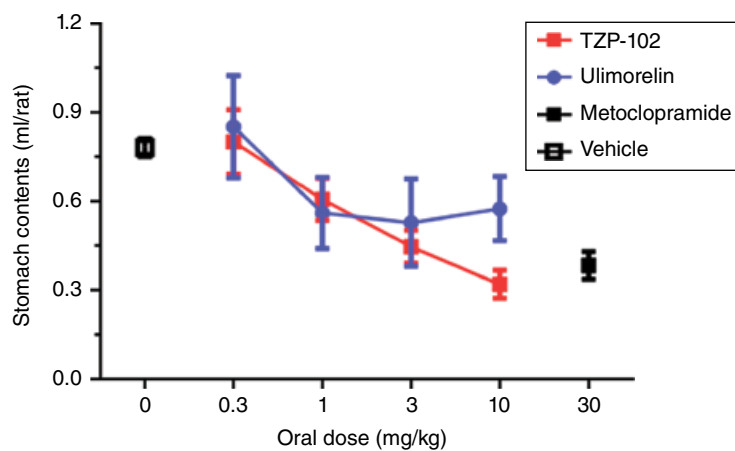**Figure 19.6** X-ray crystal structures of **2** (TZP-101) and **3** (TZP-102) (counterions omitted for clarity).
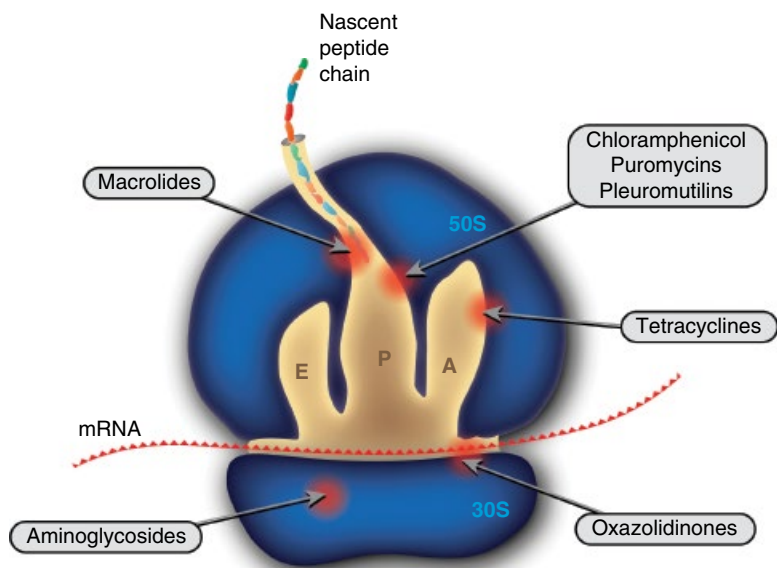
Nascent peptide chain

Macrolides

Chloramphenicol
Puromycins
Pleuromutilins

50S

E   P   A

Tetracyclines

mRNA

Aminoglycosides

30S

Oxazolidinones

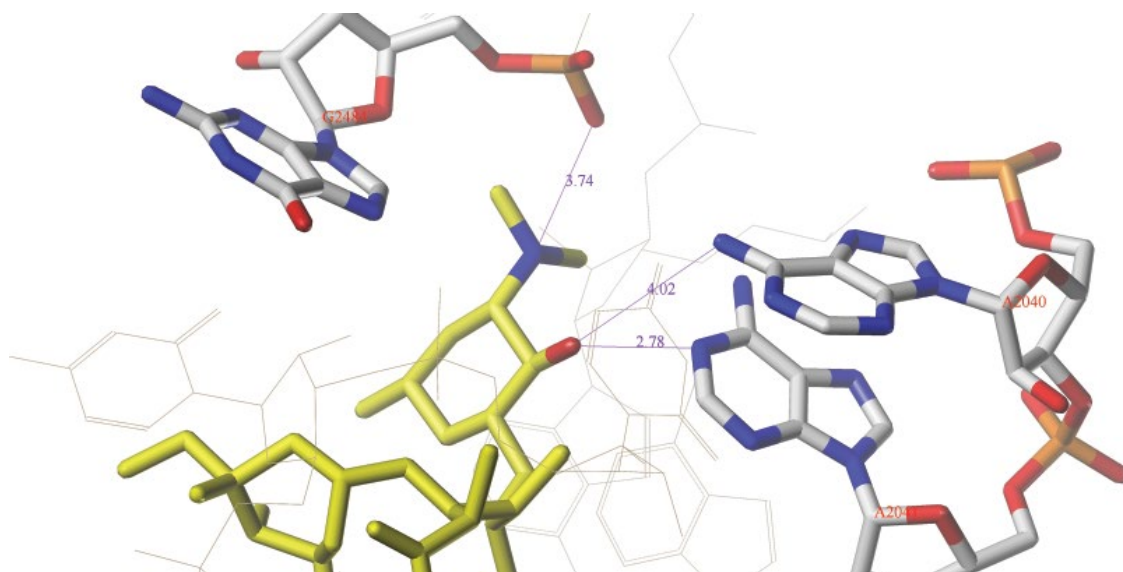**Figure 20.2** Schematic representation of bacterial ribosome and antibiotic sites of interaction.

Figure 20.3 Crystallographic structure of clarithromycin bound to the *Deinococcus radiodurans* ribosome from PDB code 1J5A. The purple-colored lines and numbers are the interaction distances (values are in angstroms) between clarithromycin (yellow) and ribosome in the active site. The interacting residues and clarithromycin are presented in capped sticks with their atom types. Remaining residues are presented as stick model in beige color. All residues are labeled with their residue names in red color. Hydrogen atoms are omitted.
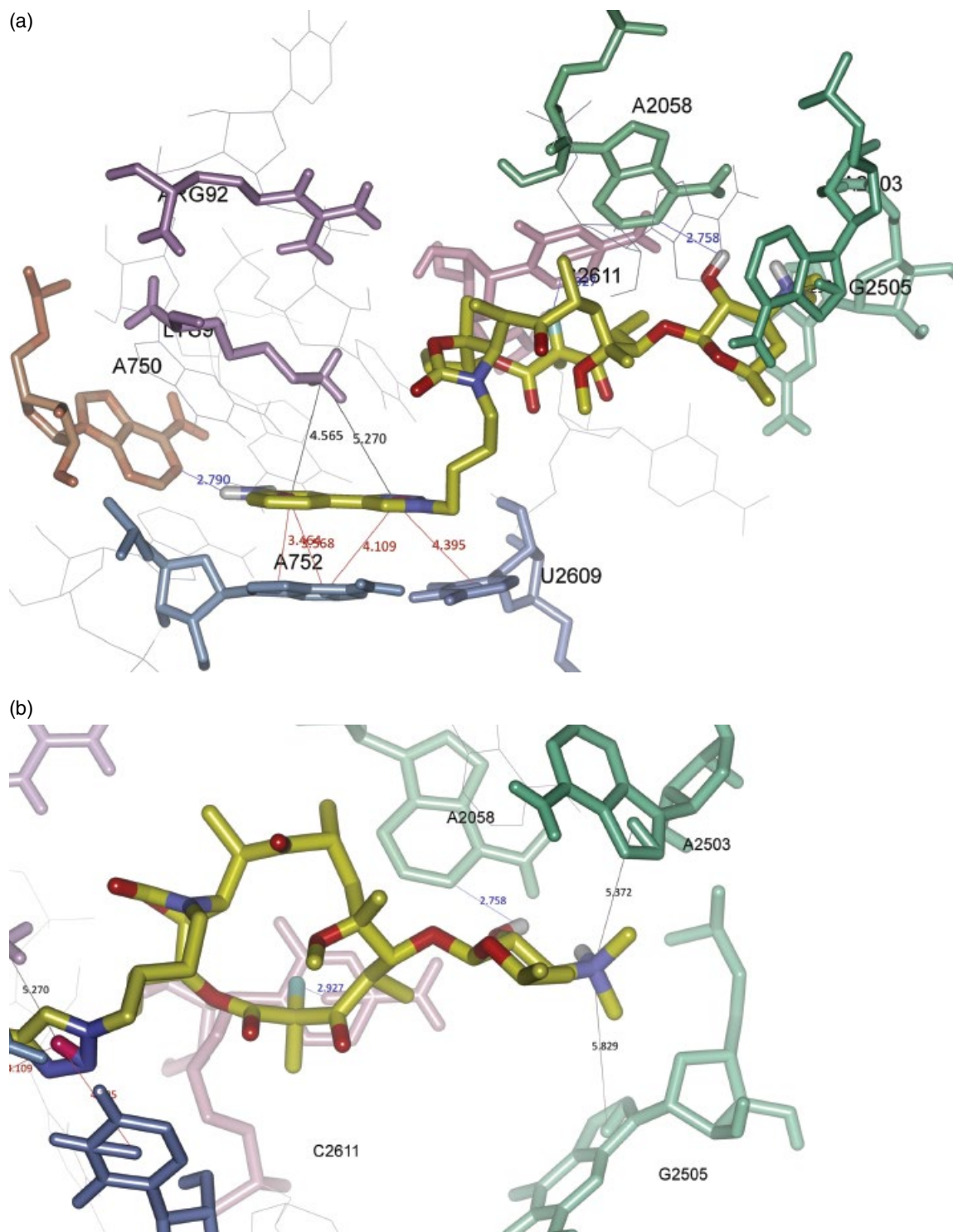
(a)

A2058

03

2.758

2611

G2505

ARG92

LYS9

A750

4.565 5.270

2.790

3.468 4.109 4.395

A752

U2609

(b)

A2058

A2503

2.758

5.372

5.270

2.927

5.829

109

C2611

G2505

Figure 20.4 Crystallographic structure of solithromycin bound to the *Escherichia coli* ribosome from PDB code 4WWW. (a) Position of solithromycin (yellow) within the ribosomal binding site. The neighboring 23S rRNA residues and amino acid residues of protein L22 are labeled. Only polar hydrogens are shown. Interacting residues and solithromycin are shown in capped sticks. (b) Interactions involving the triazolyl-aminophenyl side chain of solithromycin. (c) Interactions of 2-fluorine of solithromycin and desosamine to 23S rRNA in the drug binding site.
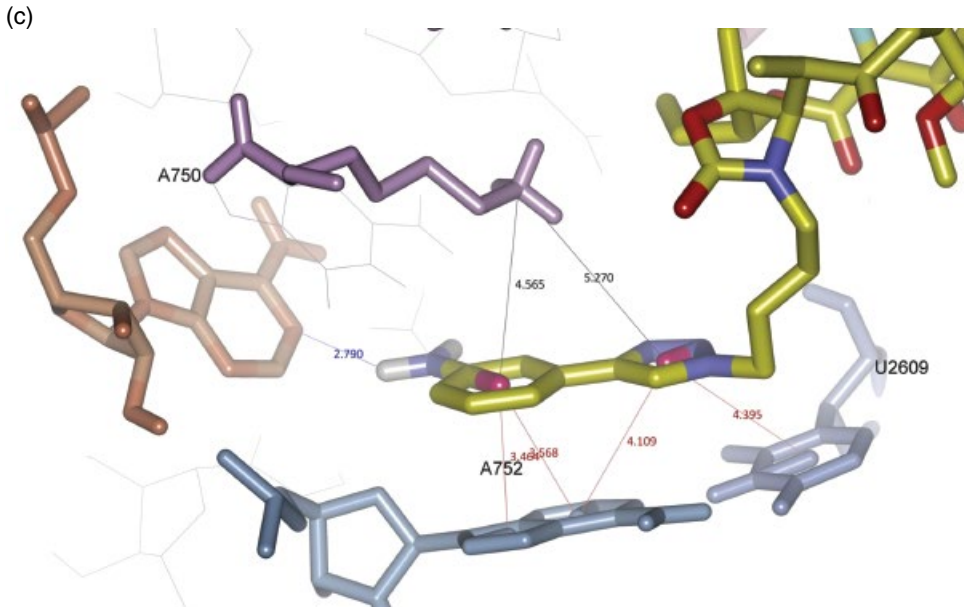
(c)

Figure 20.4 (Continued)

Dissolution in 900 ml pH 4.0 acetate buffer,
USP apparatus I at 50 RPM

Batch #1
Batch #2
Batch #3
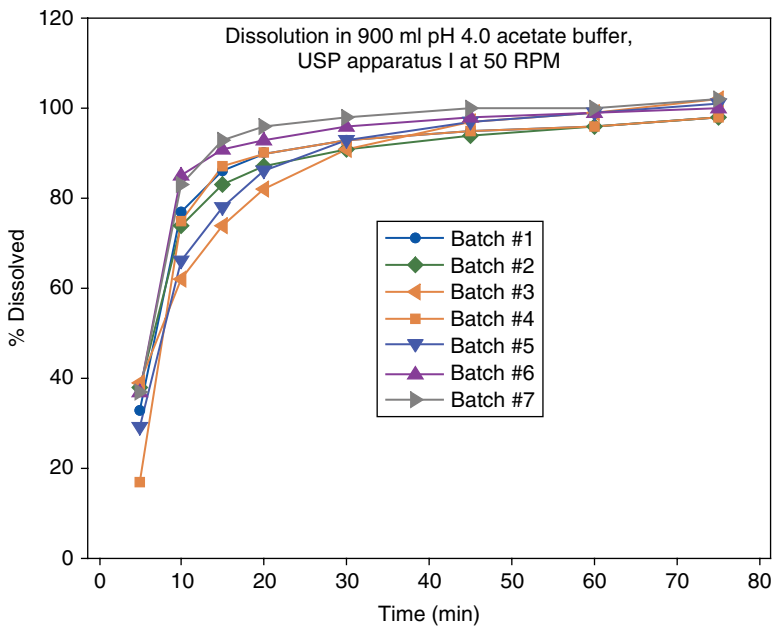Batch #4
Batch #5
Batch #6
Batch #7

% Dissolved

Time (min)

Figure 20.8 Dissolution profiles for solithromycin capsules.